BULLETIN OF THE EARTHQUAKE RESEARCH INSTITUTE,
UNIVERSITY OF TOKYO. Vol. XXXV, Part 1. March, 1957.

東京大學
地震研究所彙報

第35號　第1册

昭和32年3月

目　次

論文及報告

頁

1. 表面波の研究 XIII. 二つの表面層をもつ媒質内を伝わるラブ波の位相速度を求める計算図表（英文）……佐藤泰夫 1
2. 1936年6月18日～19日の磁気嵐の D_{st} 場（英文）……力武常次, 佐藤節子 7
3. ウォルドン重力計による伊豆大島の重力測量（英文）……横山泉, 田島広一 23
4. 瀬戸内地質区を中心とした西南日本の新生代火山活動（英文）……森本良平, 藤田和夫, 笠間太郎 35
5. 山形盆地西縁の新第三紀堆積岩に関する地質学的考察（英文）……市村毅, 青木和子 47
6. 火山活動のエネルギー（第2報）I. 大島三原山の1950～52年間の活動について II. 日本及びインドネシヤの諸火山の活動例について（英文）……横山泉 75
7. 火山活動のエネルギー（第3報）（英文）……横山泉 99
8. 常時微動の測定結果　第2報（東京都内 III）（邦文）……金井清, 田中貞二, 長田甲斐男 109
9. 常時微動の測定結果　第3報（横浜市内）（邦文）……金井清, 田中貞二, 長田甲斐男 135
10. 常時微動の測定結果　第4報（庄内地方）（邦文）……金井清, 那須信治, 田中貞二, 長田甲斐男 149
11. 常時微動の測定結果　第5報（大阪市内）（邦文）……金井清, 河角広, 田中貞二, 長田甲斐男 163
12. 常時微動の測定結果　第6報（一宮市内）（邦文）……金井清, 田中貞二, 森下利三, 中川恭次 181
13. 常時微動の測定結果　第7報（川崎市内）（邦文）……金井清, 田中貞二, 長田甲斐男 191
14. 1944年12月7日東南海地震に見られた遠江地方の家屋被害分布と地盤との関係（邦文）……大庭正八 201

(The titles in occidental languages are given on the back cover.)

本彙報ハ年4回（但シ第1號ヨリ第6號マデハ不定期ニ，第7號ハ3冊トシテ發行セリ），彙報別冊ハ不定期ニ發行ス．

本彙報掲載ノ論文及ビ報告ノ內容ニ關シテハ著者ノミニ其責任アルモノトス．

本彙報ニ關スル照會通信ハ東京大學地震研究所長ヘ宛テラレタシ．

The Bulletin is published quarterly. (Vols. I–VI were published at irregular intervals and Vol. VII consisted of three parts.)
Supplementary Volume is published at irregular interval.

The authors of the papers alone are responsible for the statements and opinions contained in their respective papers.

All communications relating to this Bulletin should be addressed to the Director of the Earthquake Research Institute, University of Tokyo.

1. *Study on Surface Waves XIII.* *Nomograph for the Phase Velocity of Love-Waves in Doubly Stratified Medium.*

By Yasuo SATÔ,

Earthquake Research Institute.

(Read May 24, 1955.—Received Nov. 27, 1956.)

1. Introduction

It is more than forty years ago that A. E. H. Love discovered the possibility of the existense of surface waves which are constituted by the *SH* waves and are propagated in a stratified medium[1]. This sort of surface wave is now called by his name, and a number of modified forms have been discovered by later authors. One of the most prominent is the same kind of surface waves propagated in a medium with double superficial layer, which is especially important because the practical structure of the crust is today believed to be such in the larger part of the world. These waves, which we will call "Love waves in a doubly stratified medium," were theoretically discovered by R. Stoneley and T. Matuzawa[2] independently, and are now used for the analysis of the seismogram and for the estimation of the thickness of the crust[3].

Thirty years ago, the proof of the existence and the calculation of dispersion curves of these waves deserved to be an independent paper, but today we must calculate many cases giving various values of parameters in the characteristic equation and search for a structure giving a dispersion curve that fits well with the observed one. This is, however, a fairly troublesome task, for the calculation of a dispersion curve requires many hours of numerical calculation work, and we are apt to be satisfied by not a large number of the combination of parameters such as density ratio, velocity ratio, thickness ratio and so on. As a result the progress of investigation in this branch of seismometry is obliged to be slow, and it is desirable to establish a method by which

---

1) A. E. H. LOVE, "Some Problems of Geodynamics," 1911 (Cambridge).
2) R. STONELEY and E. TILOTSON, *M.N.R.A.S., Geo. Sup.*, **1** (1927), 521.
T. MATUZAWA, *Proc. Phys. Math. Soc. Japan*, [iii] **10** (1928), 25.
3) Papers refered in 2) and Y. SATÔ, *Bull. Earthq. Res. Inst.*, **29** (1951), 435.

we can easily calculate the velocity. The present author has already published several nomographs for the case of a single layer[4], but the ones for the doubly stratified medium have remained undone.

The nomograph presented here is made urged by the above request. Because of the complicated form of the characteristic equation, we cannot make a complete nomograph, but must be satisfied by finding an approximate value of frequency corresponding to some given value of velocity by the method of trial and error. The precision, nevertheless, seems to be satisfactory for our practical work, and the time required to obtain dispersion curves is reduced to about one tenth or one fifth that of the ordinary method.

2. Fundamental equation

As the form of the fundamental characteristic equation was often presented in various papers[5], it will not be necessary to describe here the process of deriving this equation. We will only give the final form

$$D \equiv D^c + D^s = 0 \,,$$

$$\begin{cases} D^c = \mu_2 s_2 \cos s_1 H_1 (\mu_3' s_3 \cos s_2 H_2 + \mu_2 s_2 \sin s_2 H_2) \,, \\ D^s = \mu_1 s_1 \sin s_1 H_1 (-\mu_3' s_3 \sin s_2 H_2 + \mu_2 s_2 \cos s_2 H_2) \,, \end{cases} \tag{2.1}$$

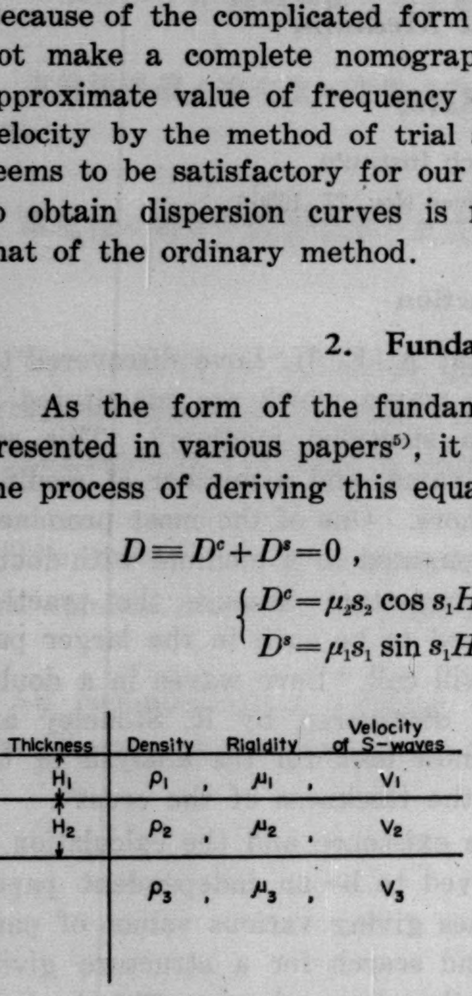

Fig. 1.

where

$$s_k = f\sqrt{(V^2/V_k^2 - 1)} = i\sigma_k \,,$$

$$\mu_3' = i\mu_3 \,,$$

V; the phase velocity of Love-waves ,

f; $2\pi/$(wave length of Love-waves) ,

and other notations are illustrated on Fig. 1.

We modify the above expression for convenience sake, namely dividing the expression (2.1) by $(\mu_2 s_2)^2 \cos s_1 H_1 \cos s_2 H_2$, we have

$$-\frac{\mu_3}{\mu_2}\frac{\sigma_3}{s_2} + \tan s_2 H_2 + \frac{\mu_1}{\mu_2}\frac{s_1}{s_2} \tan s_1 H_1 \left(\frac{\mu_3}{\mu_2}\frac{\sigma_3}{s_2} \tan s_2 H_2 + 1\right) = 0 \,. \tag{2.2}$$

4) Y. SATÔ, *Bull. Earthq. Res. Inst.*, **31** (1953), 81 and 255. *Journal of Physics of the Earth*, **4** (1956), 41.

5) *e.g.*, Y. SATÔ, *Bull. Earthq. Res. Inst.*, **29** (1951), 435.

Or, introducing new notations the next equation is obtained.

$$XR=\frac{Y-S}{YS+1}\ , \tag{2.3}$$

where

$$X\equiv\frac{\mu_1}{\mu_2}\frac{s_1}{s_2}\ ,\qquad R\equiv\tan s_1H_1\ ,$$

and

$$Y\equiv\frac{\mu_3}{\mu_2}\frac{\sigma_3}{s_2}\ ,\qquad S\equiv\tan s_2H_2\ .$$

When the velocity of Love-waves is smaller than that of the intermediate layer ($V<V_2$), we put

$$s_2=i\sigma_2\ , \tag{2.4}$$

into (2.2) and obtain

$$\frac{\mu_3}{\mu_2}\frac{\sigma_3}{\sigma_2}+\tanh\sigma_2H_2-\frac{\mu_1}{\mu_2}\frac{s_1}{\sigma_2}\tan s_1H_1\left(\frac{\mu_3}{\mu_2}\frac{\sigma_3}{\sigma_2}\tanh\sigma_2H_2+1\right)=0\ . \tag{2.5}$$

As before, introducing new notations

$$X'\equiv\frac{\mu_1}{\mu_2}\frac{s_1}{\sigma_2}\ ,$$

and

$$Y'\equiv\frac{\mu_3}{\mu_2}\frac{\sigma_3}{\sigma_2}\ ,\qquad S'\equiv\tanh\sigma_2H_2\ ,$$

we have

$$X'R=\frac{Y'+S'}{Y'S'+1}\ . \tag{2.6}$$

Using the equations (2.3) and (2.6) we obtain the relation between the velocity and the period. The details will be described in the next section.

3. Explanation of the figure and directions for use[6)]

Case I. $V>V_2$. (Fig. 6.)

1) In Fig. 2, [1] is the axis of V_1/V_2. When some structure[7)] of

6) In this section $A(V_1/V_2)$, for example, represents a point A whose ordinate is V_1/V_2.

the crust is given we can at once calculate the value of V_1/V_2, so we can take a point A on this axis corresponding to this value.

2) Next we choose some value of V/V_2 and find a curve α which has the value given above. (Usually we give several values of V/V_2 at once.) α is the curve of s_2/s_1 and we can find this value on the axis-[2] following the arrow line. (Point C.)

3) By the right half of the same figure we can easily obtain $X \equiv \frac{\mu_1}{\mu_2}\frac{s_1}{s_2}$ on the axis-[4] taking the value of μ_1/μ_2 calculated from the given structure. We must remember this value X and use it at the last stage of this calculation. As is clear in the above procedure, X is independent with the value of ω.

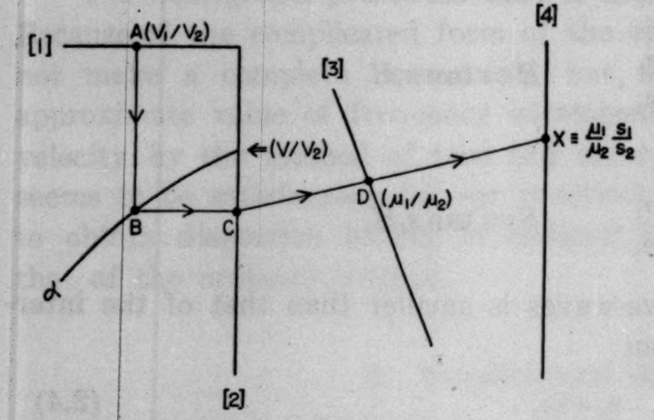

Fig. 2. $A(V_1/V_2)$, for example, means a point A with an ordinate V_1/V_2.[6)]
$A(V_1/V_2)$ and $D(\mu_1/\mu_2)$ can be directly obtained from the structure[7)] of the medium.
⇨ means to find a curve with a parameter of assigned value.

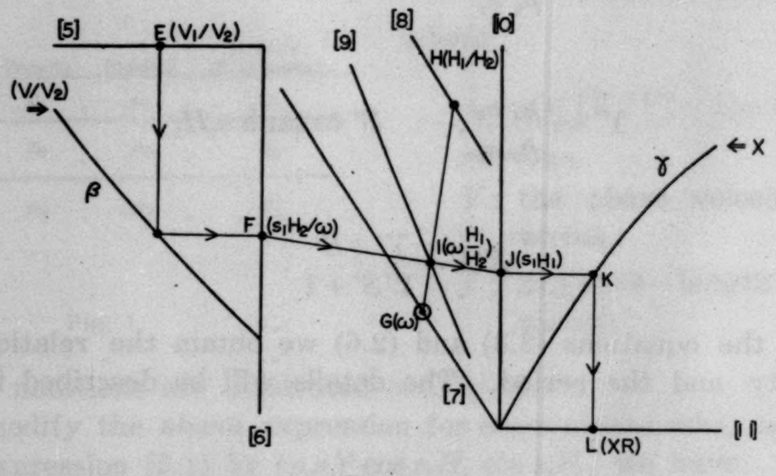

Fig. 3.
$E(V_1/V_2)$ and $H(H_1/H_2)$ can be directly obtained from the structure[7)] of the mediunm.
⇨ means to find a curve with a parameter of assigned value.
⊙ is a point tentatively given.

7) In this section the word "structure" means the doubly stratified structure and the material constants as shown in Fig. 1.

4) Just as in 1) we find a point $E(V_1/V_2)$ on [5], and as in 2) we take a curve β. V_1/V_2 and V/V_2 must be equal to those used in the previous stages. (See Fig. 3.)

5) Since β is the curve of s_1H_2/ω[8] we can get this value shown by the point F on the axis-[6]. (We are using H_2 as the unit of length.)

6) We assume some value of ω tentatively and take it on [7]-axis. (Point $G(\omega)$.) On the other hand, $H(H_1/H_2)$ is given by the structure, therefore we can easily determine $I(\omega H_1/H_2)$ on the axis [9].

7) From $F(s_1H_2/\omega)$ and $I(\omega H_1/H_2)$ we get $J(s_1H_1)$ on the axis-[10]. This is simple multiplication.

8) Using a curve having a parameter X, which we have obtained in 3), we can find a point L on the axis-[11], which gives the value XR. The expression (2.3) requires that XR is equal to $Z\equiv(Y-S)/(YS+1)$, which must be calculated in the next steps. The nomographs necessary for them are given just below those which were used for the above calculations.

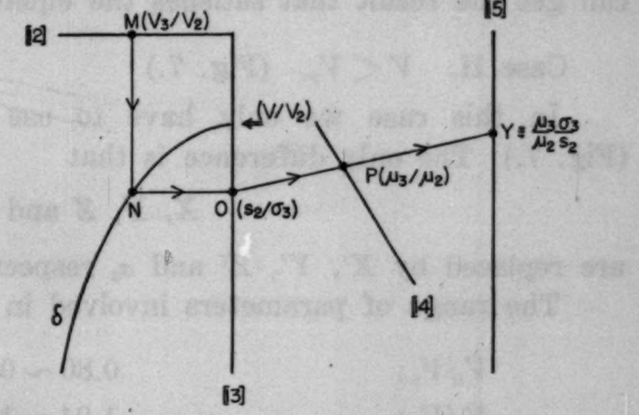

Fig. 4. $M(V_3/V_2)$, for example, means a point M with an ordinate V_3/V_2.

$M(V_3/V_2)$ and $P(\mu_3/\mu_2)$ can be directly obtained from the structure[7] of the medium.

$\Rightarrow$ means to find a curve with a parameter of assigned value.

9) By exactly the same way as in 1)$\sim$3) we can obtain Y on the axis-[15]. (See Fig. 4.) We only have to notice that the value of V/V_2 used in this step should be the same as the one used before.

10) Next, on the axis-[16] we take a point Q. Since s_2H_2/ω is a function of V/V_2 only, we only have to find a point with an assigned value of V/V_2 on this axis. (See Fig. 5.)

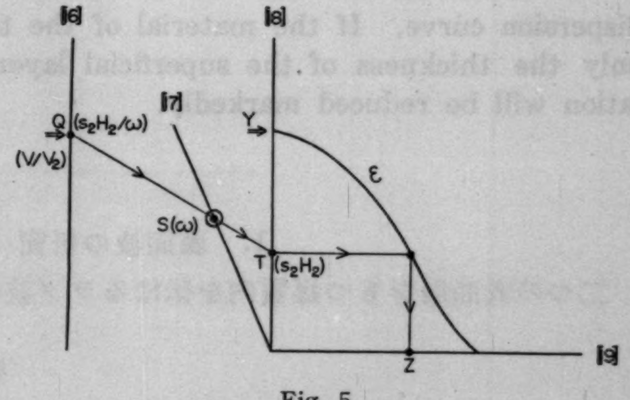

Fig. 5.

$\odot$ is a point tentatively given.

8) $\omega=(2\pi/T)(H_2/V_2)$ gives the frequency without a dimension.

11) The following processes are very simple. Assuming $S(\omega)$ on the axis-[17], in which ω must be equal to the value used before in $G(\omega)$, we get $T(s_2H_2)$ on the axis-[18].

12) Using Y, which was already obtained in 9), we can get $Z = (Y-S)/(YS+1)$ on the axis-[19] following the arrow line.

If the obtained values of XR and Z are equal, assumed value $\omega=\frac{2\pi}{T}\frac{1}{V_2}H_2$ is the frequency which gives the phase velocity V/V_2. Usually, however, such a circumstance does not occur, and we must assume another value of ω and again try the same procedure until we can get the result that satisfies the equation $XR=Z$.

Case II. $V<V_2$. (Fig. 7.)

In this case we only have to use another sheet of nomograph. (Fig. 7.) The only difference is that

$$X,\ Y,\ Z \text{ and } s_2$$

are replaced by X', Y', Z' and σ_2 respectively.

The range of parameters involved in our nomographs is:

V_1/V_2; $0.80 \sim 0.96$,

V_3/V_2; $1.04 \sim 1.25$,

V/V_2; $0.82 \sim 0.98$ $(V<V_2)$, $1.02 \sim 1.20$ $(V>V_2)$,

μ_1/μ_2; $0.30 \sim 1.00$,

μ_3/μ_2; $1.00 \sim 3.40$ $(V<V_2)$, $1.00 \sim 4.00$ $(V>V_2)$.

It takes an hour or less to find several points lying on the same dispersion curve. If the material of the three media are unaltered and only the thickness of the superficial layer changes, time for the calculation will be reduced markedly.

---

1. 表面波の研究 XIII.

二つの表面層をもつ媒質内を伝はるラブ波の位相速度を求める計算図表

地震研究所 佐藤泰夫

一つの表面層がある媒質を伝はるラブ波については，位相速度及び群速度を求める計算図表を数回にわたつて発表したが，[4] 今回は二重の表面層をもつ媒質を伝はるラブ波についての図表を作つた．計算に必要な時間は数値計算の 1/5 乃至 1/10 にすることができる．精度は実用上十分である．

PHASE VELOCITY OF LOVE-WAVES IN DOUBLY STRATIFIED MEDIUM

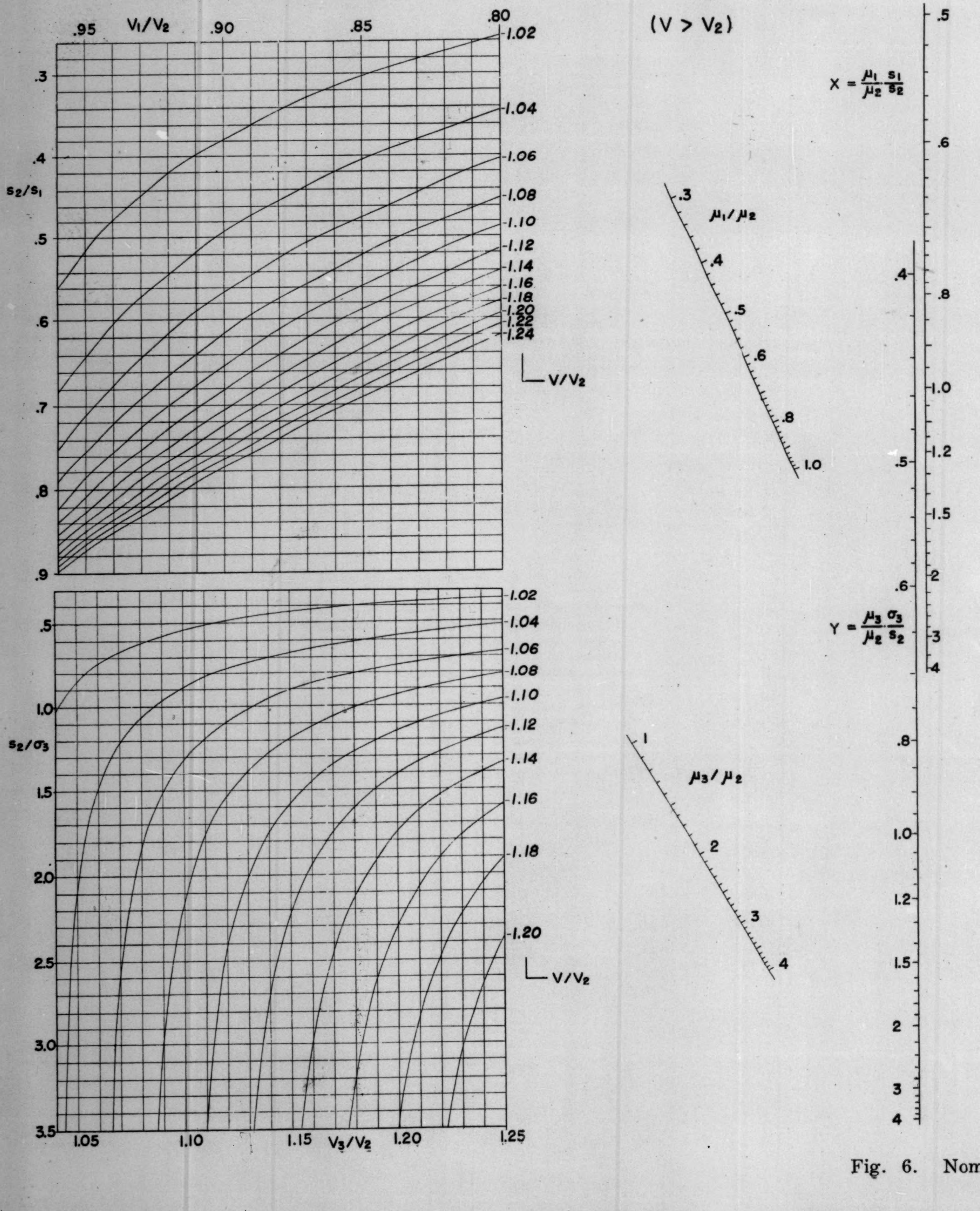

Fig. 6. Nom

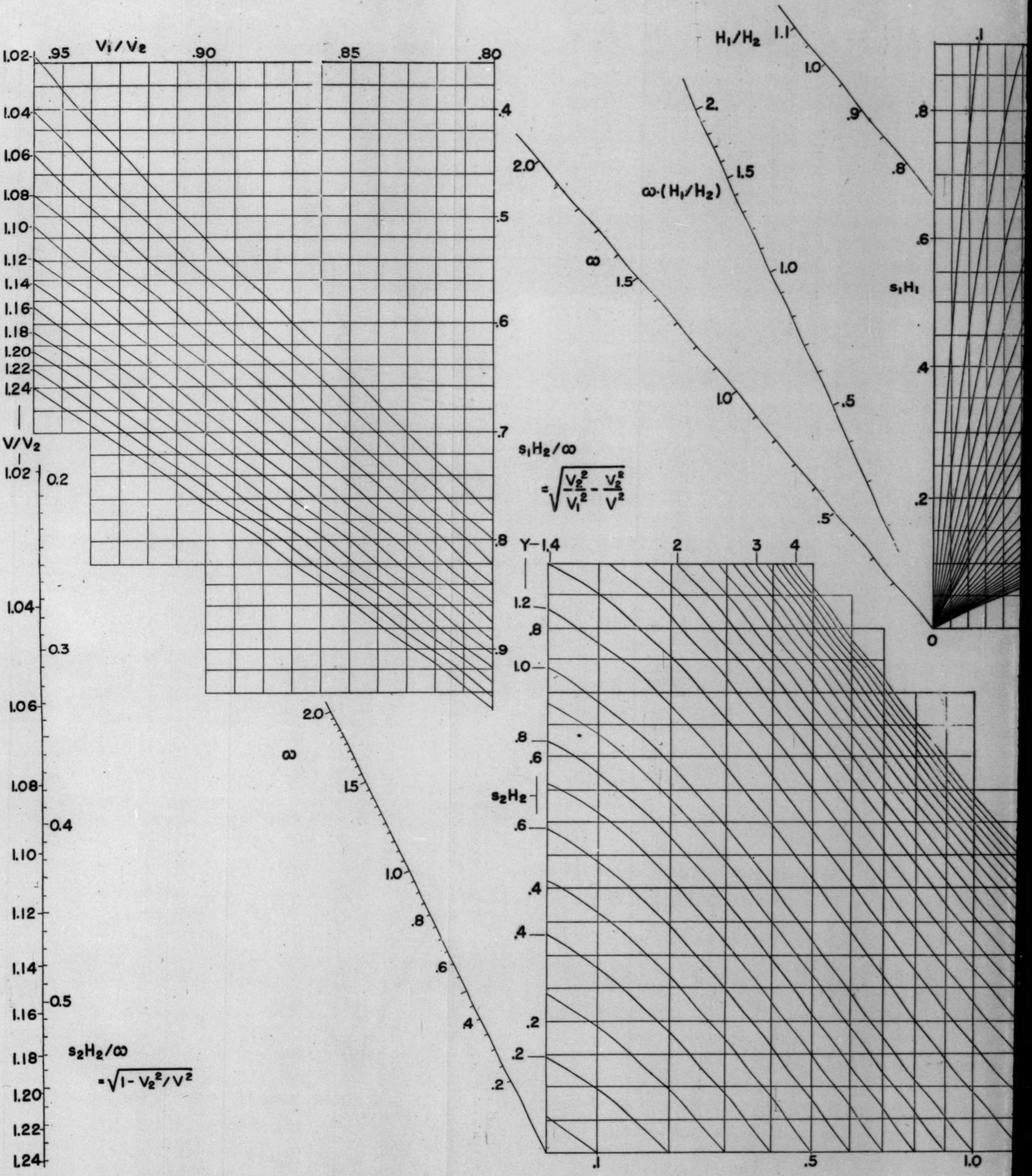

Nomograph for the Phase Velocity of Love-Waves in Doubly Stratified Medium ($V > V_2$).

MEDIUM

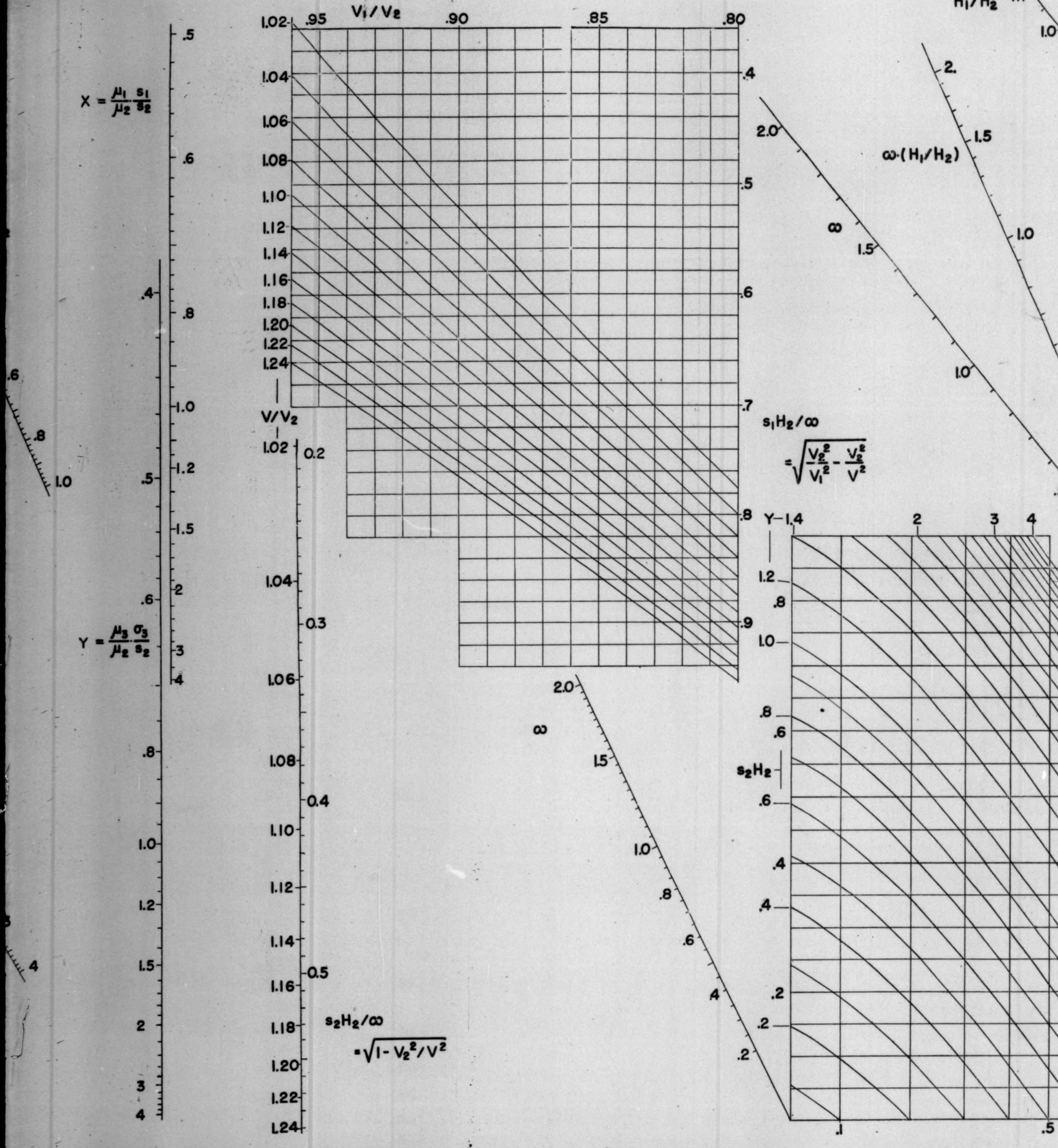

Fig. 6. Nomograph for the Phase Velocity of Love-Waves in Doubly Stratified Medium ($V > V_2$).

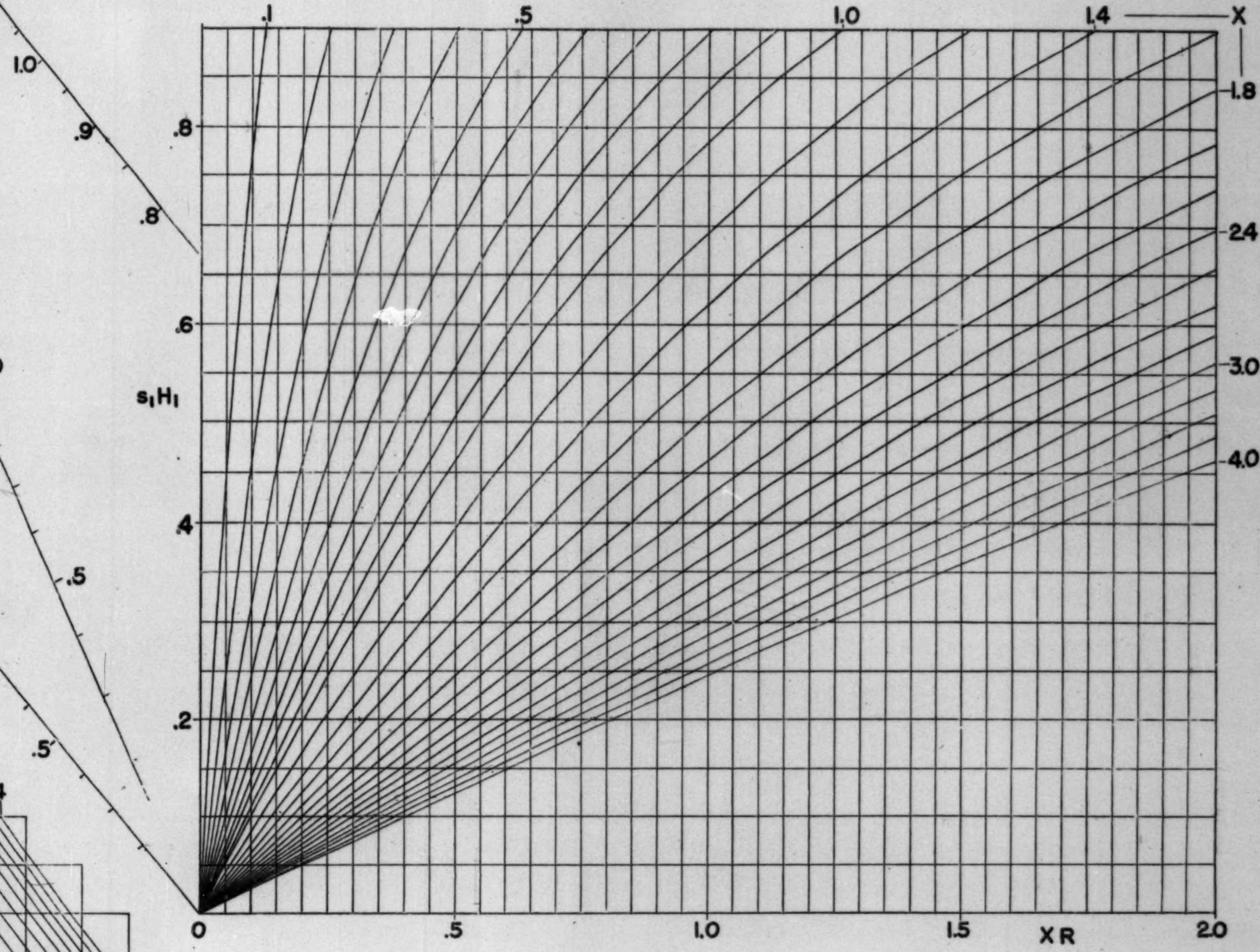

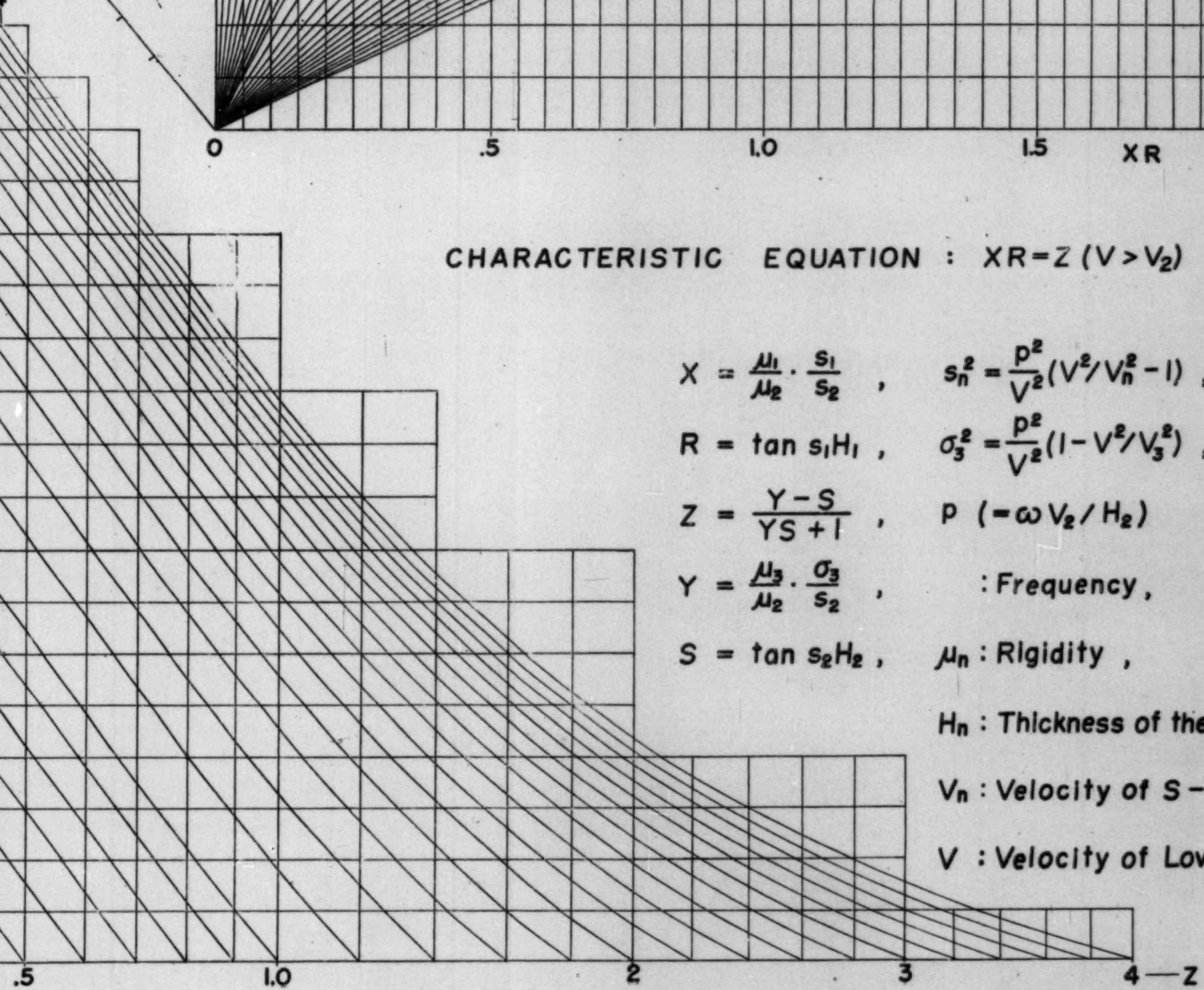

CHARACTERISTIC EQUATION : $XR = Z \; (V > V_2)$

$X = \dfrac{\mu_1}{\mu_2} \cdot \dfrac{s_1}{s_2}$, $s_n^2 = \dfrac{p^2}{V^2}(V^2/V_n^2 - 1)$,

$R = \tan s_1H_1$, $\sigma_3^2 = \dfrac{p^2}{V^2}(1 - V^2/V_3^2)$,

$Z = \dfrac{Y - S}{YS + 1}$, $p \; (= \omega V_2 / H_2)$

$Y = \dfrac{\mu_3}{\mu_2} \cdot \dfrac{\sigma_3}{s_2}$, : Frequency ,

$S = \tan s_2H_2$, μ_n : Rigidity ,

H_n : Thickness of the Layer ,

V_n : Velocity of S-waves ,

V : Velocity of Love-waves .

PHASE VELOCITY OF LOVE-WAVES IN DOUBLY STRATIFIED MEDIUM

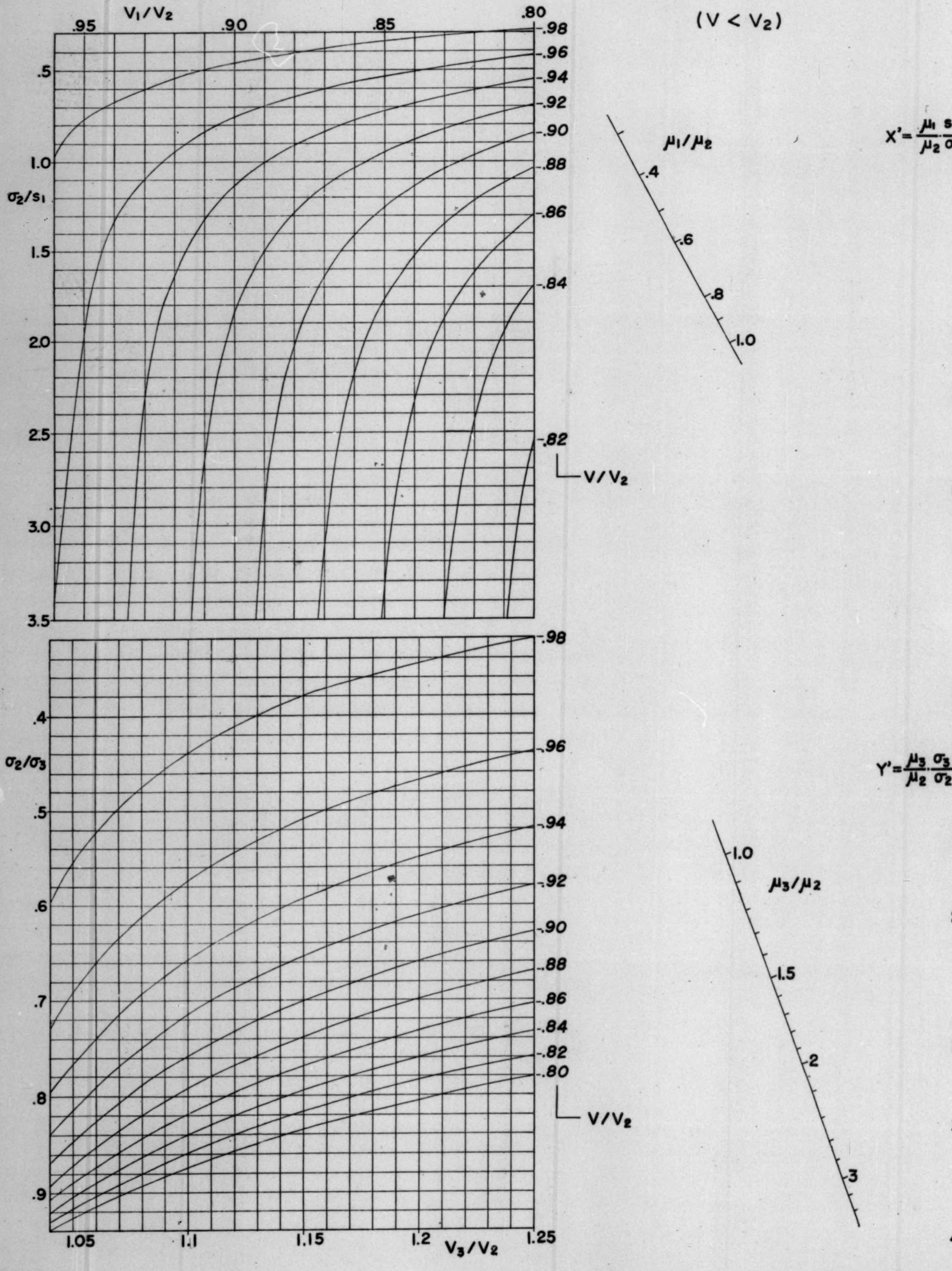

Fig. 7.

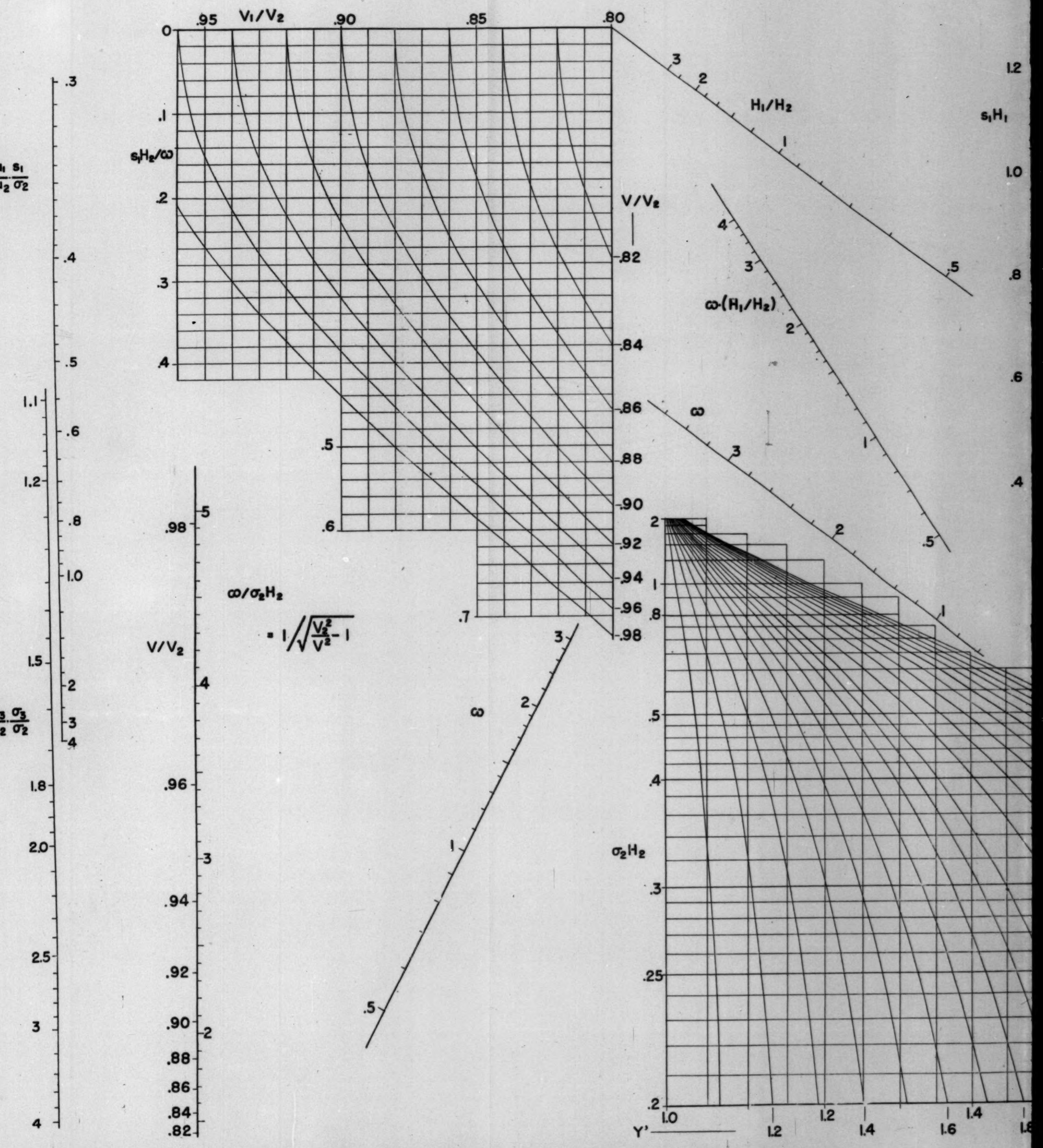

7. Nomograph for the Phase Velocity of Love-Waves in Doubly Stratified Medium ($V < V_2$).

RATIFIED MEDIUM

$V < V_2$)

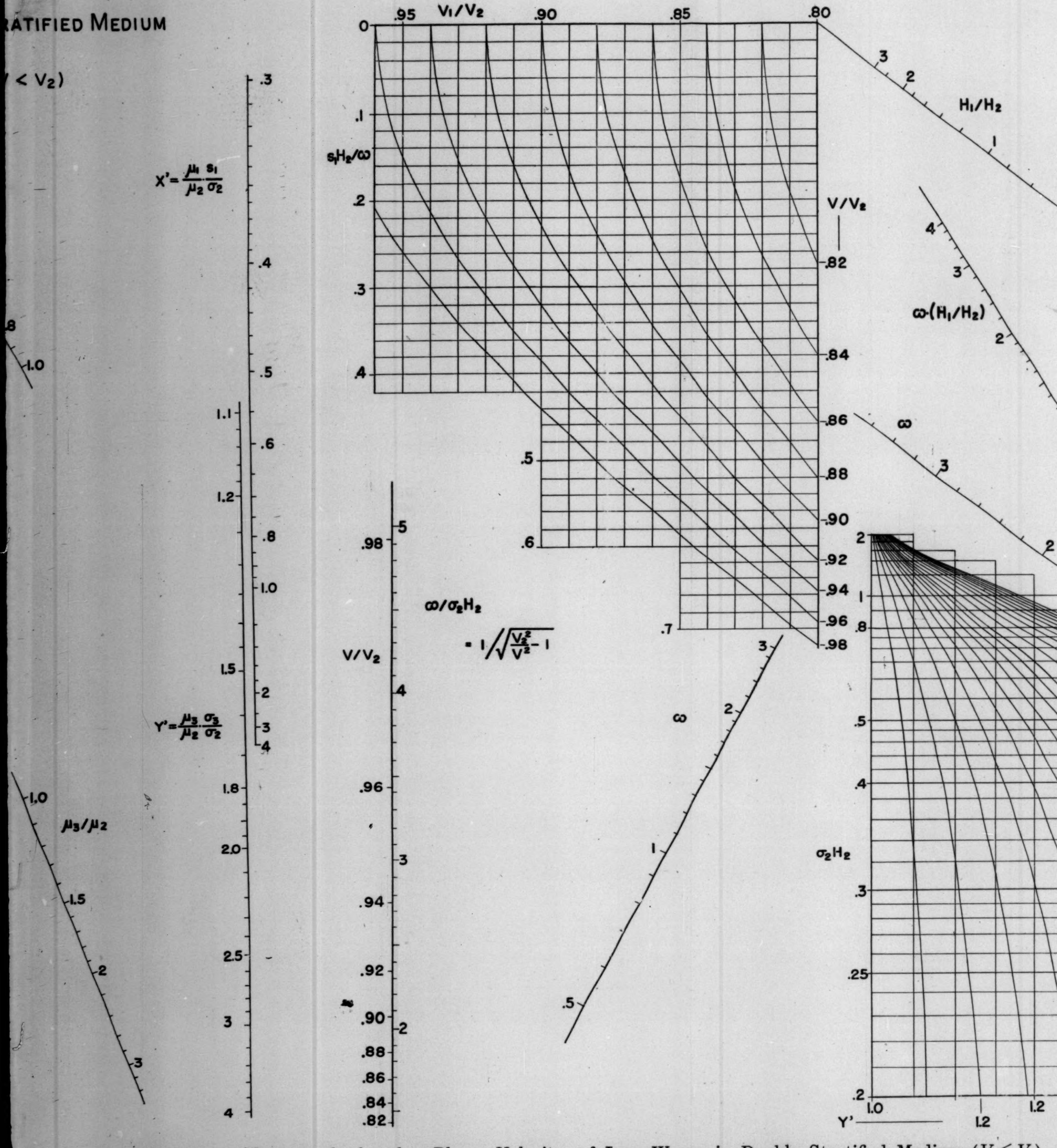

Fig. 7. Nomograph for the Phase Velocity of Love-Waves in Doubly Stratified Medium ($V < V_2$).

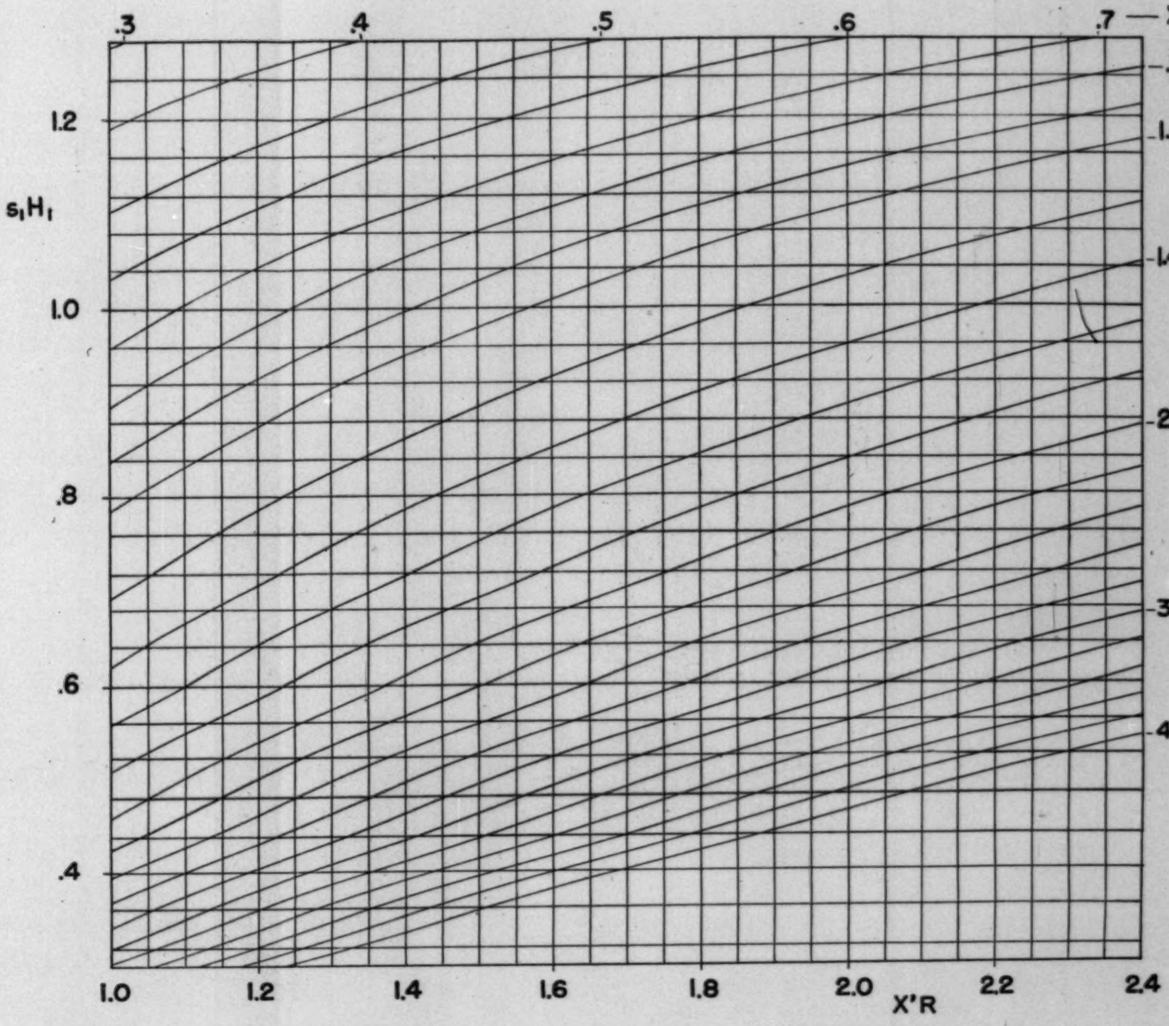

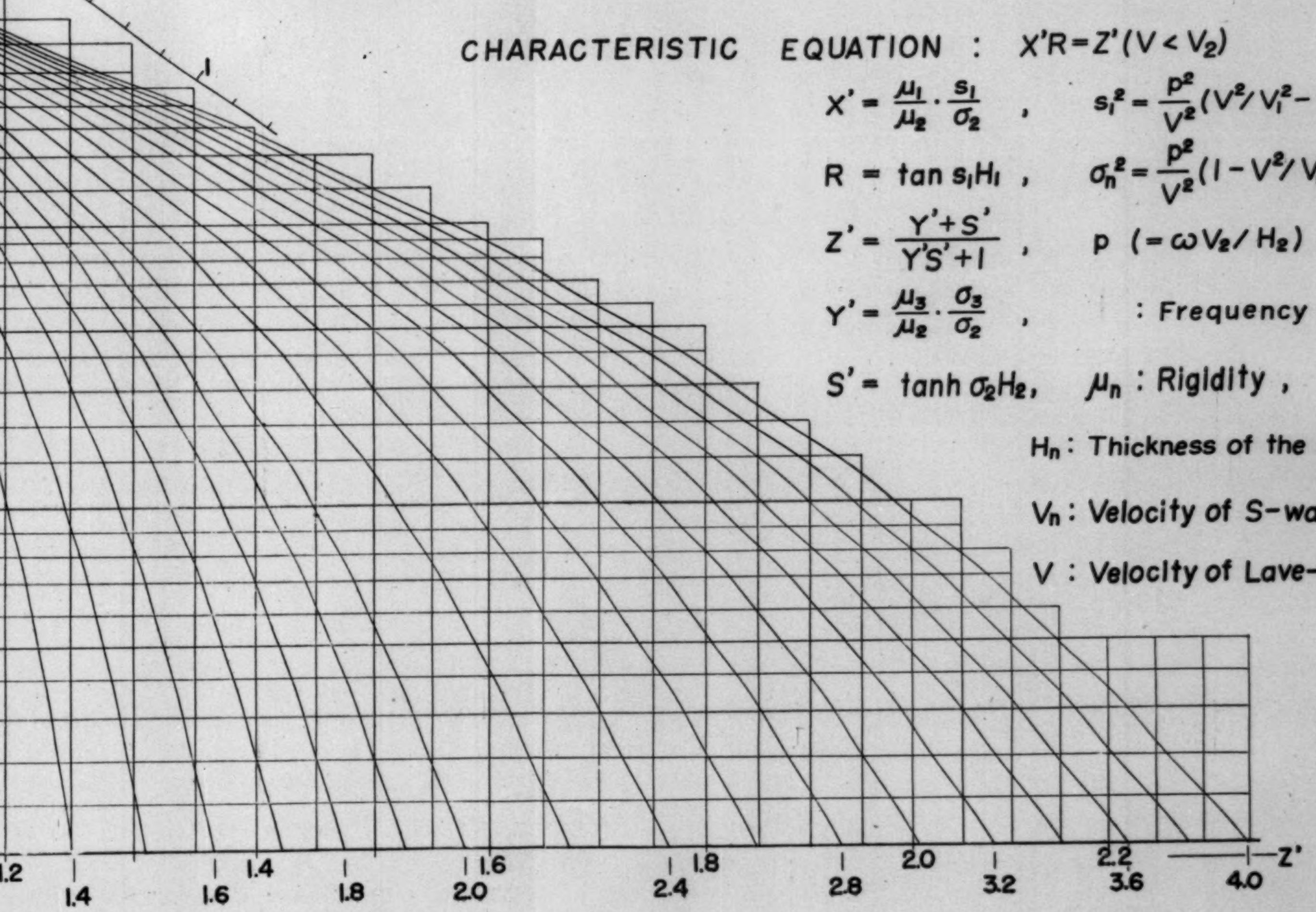

CHARACTERISTIC EQUATION : $X'R = Z'(V < V_2)$

$$X' = \frac{\mu_1}{\mu_2} \cdot \frac{s_1}{\sigma_2}, \quad s_1^2 = \frac{p^2}{V^2}(V^2/V_1^2 - 1),$$

$$R = \tan s_1 H_1, \quad \sigma_n^2 = \frac{p^2}{V^2}(1 - V^2/V_n^2),$$

$$Z' = \frac{Y' + S'}{Y'S' + 1}, \quad p \; (= \omega V_2 / H_2)$$

$$Y' = \frac{\mu_3}{\mu_2} \cdot \frac{\sigma_3}{\sigma_2}, \quad : \text{Frequency},$$

$S' = \tanh \sigma_2 H_2$, μ_n : Rigidity ,

H_n : Thickness of the Layer ,

V_n : Velocity of S-waves ,

V : Velocity of Lave-waves .

$_2$).

2. *The Geomagnetic D_{st} Field of the Magnetic Storm on June 18–19, 1936.*

By Tsuneji RIKITAKE and Setsuko SATO,

Earthquake Research Institute.

(Read Nov. 27, 1956.—Received Dec. 31, 1956.)

Summary

The D_{st} part of the magnetic storm on June 18–19, 1936 is examined with the aid of many copies of magnetograms sent from well-distributed observatories. It is found that the relation between the external origin and internal origin parts of the D_{st} field is well explained by the electromagnetic induction within the earth, of which the distribution of the electrical conductivity is taken as the one obtained by one of the writers.

1. Introduction

S. Chapman and A. T. Price[1] analysed the storm-time variation or D_{st} field of magnetic storms. The relation between the external origin and internal origin parts was obtained by them by use of spherical harmonic analysis. It was made clear that the magnetic potential of the D_{st} field in the low and middle latitude can be expressed as a combination of a few zonal harmonics of low degree, because the field does not depend on longitude. Among these harmonics, however, the term including $P_1(\cos\theta)$ is so large that the other ones such as $P_3(\cos\theta)$ and $P_5(\cos\theta)$ can be almost ignored.

The physical interpretation, which is based on the theory of electromagnetic induction within the earth, of the relation between both the parts led to an important conclusion that the electrical conductivity of the deeper part of the earth is to be larger than that of the shallow region whose conductivity has been estimated from analyses of the S_q variation. Chapman and Prices' study was followed by others concerning the electromagnetic induction within a non-uniform earth[2),3)]. As a result of these studies, the distribution of the electrical conductivity is

1) S. CHAPMAN and A. T. PRICE, *Phil. Trans. Roy. Soc. London A*, **229** (1930), 427.
2) B. N. LAHIRI and A. T. PRICE, *Phil. Trans. Roy. Soc. London A*, **237** (1939), 509.
3) T. RIKITAKE, *Bull. Earthq. Res. Inst.*, **28** (1950), 45, 219, 263; **29** (1951), 61.

Table I. List of the observatories.

Observatory	Abbreviation	Geographic latitude	Geographic longitude	Geomagnetic latitude	Geomagnetic longitude
Godhavn	GO	69.°2	306.°5	79.°8	32.°5
Tromsö	TR	69.7	18.9	67.1	116.7
Sodankylä	SO	67.4	26.6	63.8	120.0
Lerwick	LE	60.1	358.8	62.5	88.6
Eskdalemuir	ES	55.3	356.8	58.5	82.9
Lovö	LO	59.4	17.8	58.1	105.8
Rude Skov	RS	55.8	12.4	55.8	98.5
Wilhelmshaven	WL	53.5	8.2	54.5	92.9
Abinger	AB	51.2	359.6	54.0	83.3
De Bilt	DB	52.1	5.2	53.8	89.6
Val Joyeux	VJ	48.8	2.0	51.3	84.5
Wien	VI	48.2	16.2	47.9	98.1
San Miguel	SM	36.6	101.4	45.6	334.4
Ebro	EB	40.8	0.5	43.9	79.7
San Fernando	SF	36.5	353.8	41.0	71.3
Helwan	HE	29.9	31.3	27.2	106.4
Cape Town	CT	−33.9	18.5	32.7	79.9
Sitka	SI	57.0	224.7	−60.0	275.4
Cheltenham	CH	38.7	283.2	50.1	350.5
Tucson	TU	32.2	249.2	40.4	312.2
San Juan	SJ	18.4	293.9	29.9	3.2
Teoloyucan	TE	19.7	260.8	29.6	327.1
Honolulu	HO	21.3	201.9	21.1	266.5
Huancayo	HU	−12.0	284.7	− 0.6	353.8
Pilar	PI	−31.7	296.1	−20.2	4.6
Toyohara	TY	47.0	142.8	36.9	203.5
Kakioka	KA	36.2	140.2	26.0	206.0
Dehra Dun	DD	30.3	78.0	20.5	149.9
Alibag	AL	18.6	72.9	9.5	143.6
Apia	AP	−13.8	188.2	−16.0	260.2
Kuyper	KU	− 6.0	106.7	−17.5	175.5
Watheroo	WA	−30.3	115.9	−41.8	185.6
Toolangi	TO	−37.5	145.5	−46.7	220.8
Christchurch	CR	−43.5	172.7	−47.7	252.5

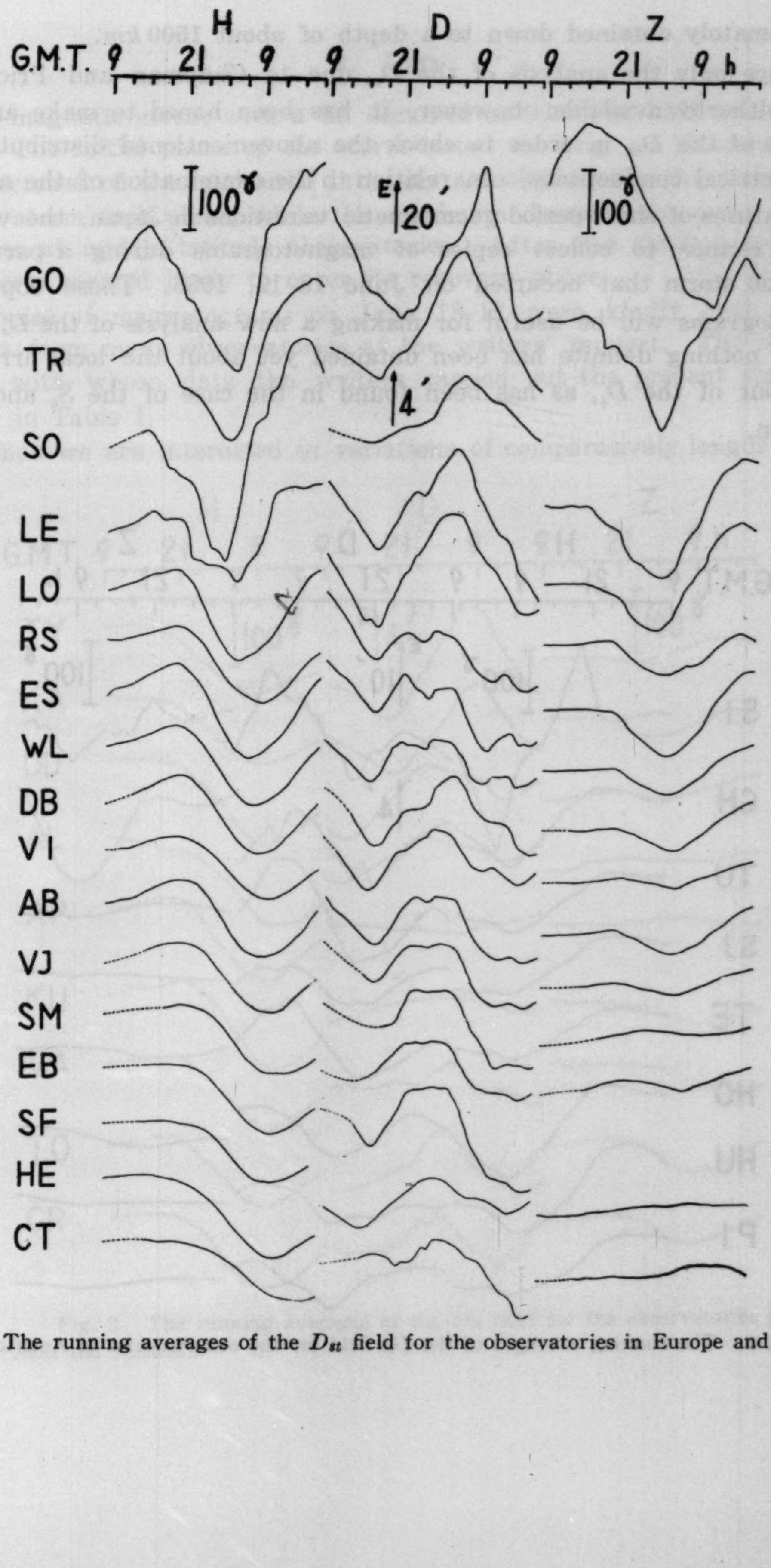

Fig. 1. The running averages of the D_{st} field for the observatories in Europe and Africa.

approximately obtained down to a depth of about 1500 *km*.

Since only the analysis of the D_{st} due to Chapman and Price has been hitherto available, however, it has been hoped to make another analysis of the D_{st} in order to check the abovementioned distribution of the electrical conductivity. In relation to the examination of the anomalous features of short-period geomagnetic variations in Japan, the writers had a chance to collect copies of magnetograms during a particular magnetic storm that occurred on June 18–19, 1936. These copies of magnetograms will be useful for making a new analysis of the D_{st} field, though nothing definite has been obtained yet about the local irregular behaviour of the D_{st} as has been found in the case of the S_q and bays n Japan.

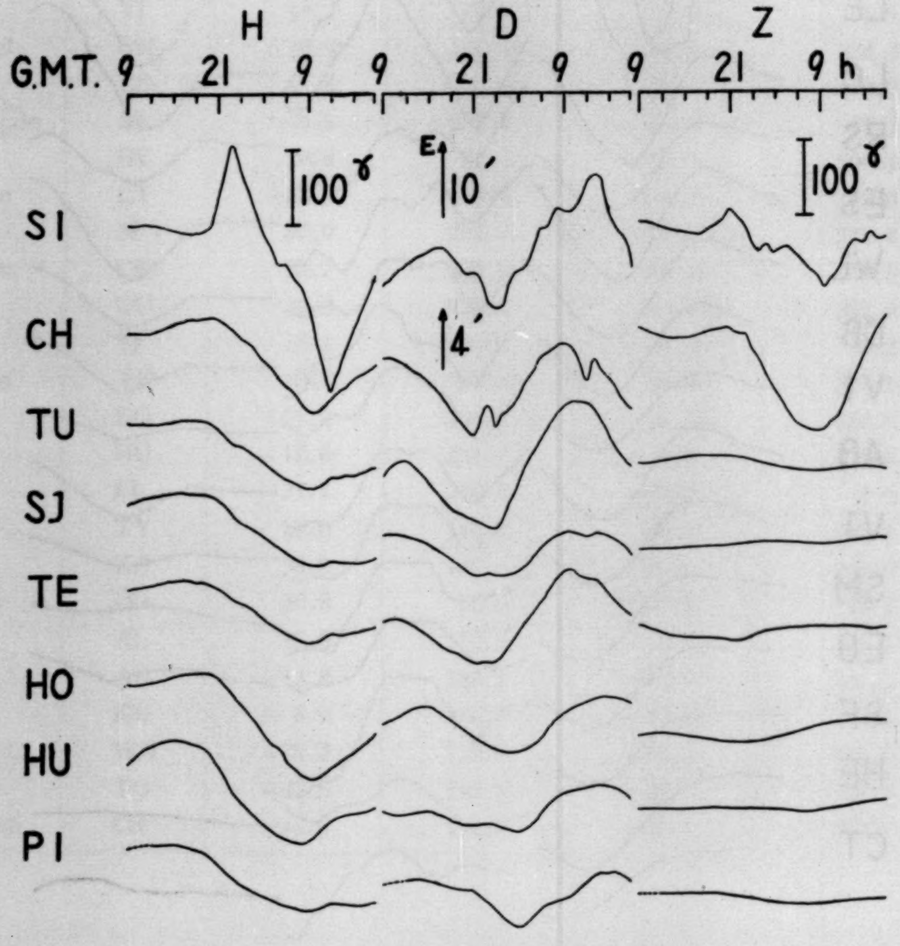

Fig. 2. The running averages of the D_{st} field for the observatories in America.

2. Data

A magnetic storm with a SC occurred at $9h$ $41m$ GMT on June 18, 1936. The initial phase of the storm lasted as long as 10 *hours* when the decrease of the horizontal intensity associated with the main phase of the storm took place, while the maximum decrease amounted to 200 *gammas* at middle latitude observatories. After $10h$ GMT on June 19, the storm seemed likely to enter its recovery phase.

Copies of magnetograms on June 18-19 were kindly sent to the writers from many observatories at the writers' request. The observatories with whose data the writers carried out the present study are shown in Table I.

Since we are interested in variations of comparatively longer period,

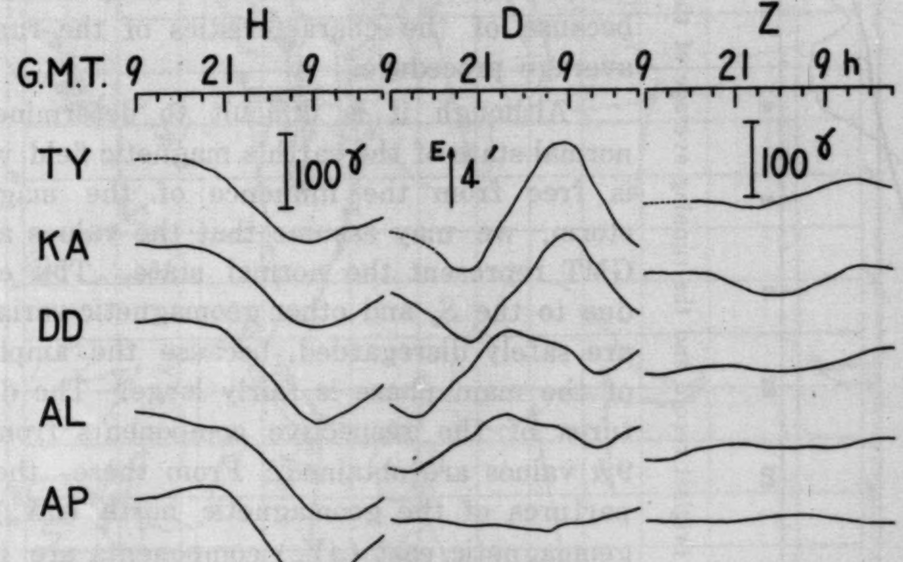

Fig. 3. The running averages of the D_{st} field for the observatories in Asia and Australia.

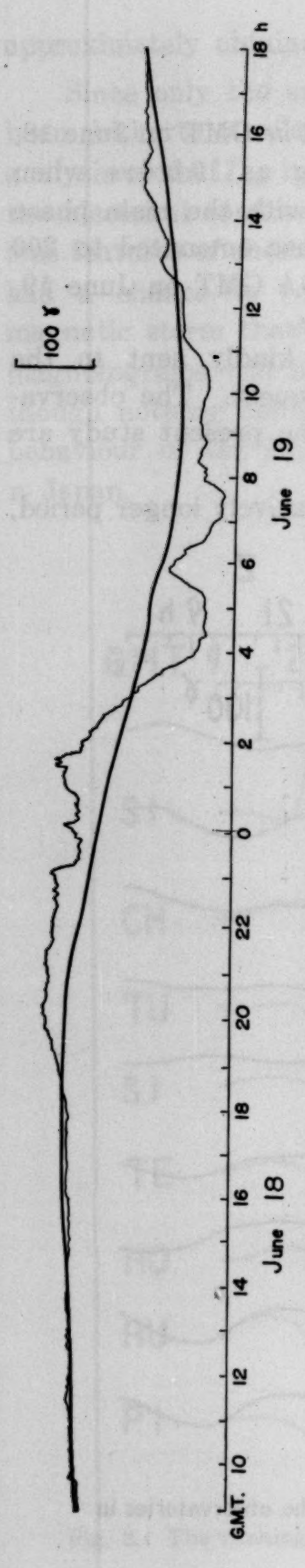

Fig. 4. The original record and the running average of the H-curve at Honolulu.

running averages of H (horizontal intensity), D (declination) and Z (vertical component) are made at all the observatories. From the readings of hourly values of the respective components, the averages of 13 readings are calculated. The values thus obtained are regarded as the values at the centred time of the averaged interval. The results are shown in Figs. 1, 2 and 3 respectively at the observatories in Europe and Africa, America, and Asia and Australia. A comparison of the original record to the running average is shown in Fig. 4 in which we see that short-duration changes having periods of a few *hours* are nearly eliminated because of the characteristics of the running average procedure.

Although it is difficult to determine the normal state of the earth's magnetic field which is free from the influence of the magnetic storm, we may assume that the values at $9\,h$ GMT represent the normal state. The errors due to the S_q and other geomagnetic variations are safely disregarded, because the amplitude of the main phase is fairly large. The departures of the respective components from the $9\,h$ values are obtained. From these, the departures of the geomagnetic north (ΔX_m) and geomagnetic east (ΔY_m) components are calculated. ΔX_m is shown in Table II for every 4 *hours* after $9\,h$ GMT on June 18. The departures of the vertical component (ΔZ) are also shown in Table III in the same way.

As can be seen in Figs. 1, 2 and 3, the variations of the horizontal intensity show a typical course of magnetic storms which has been studied in detail in the morphology of magnetic storms. Although it is beyond the scope of the present paper to study various features of the storm, the overhead equivalent

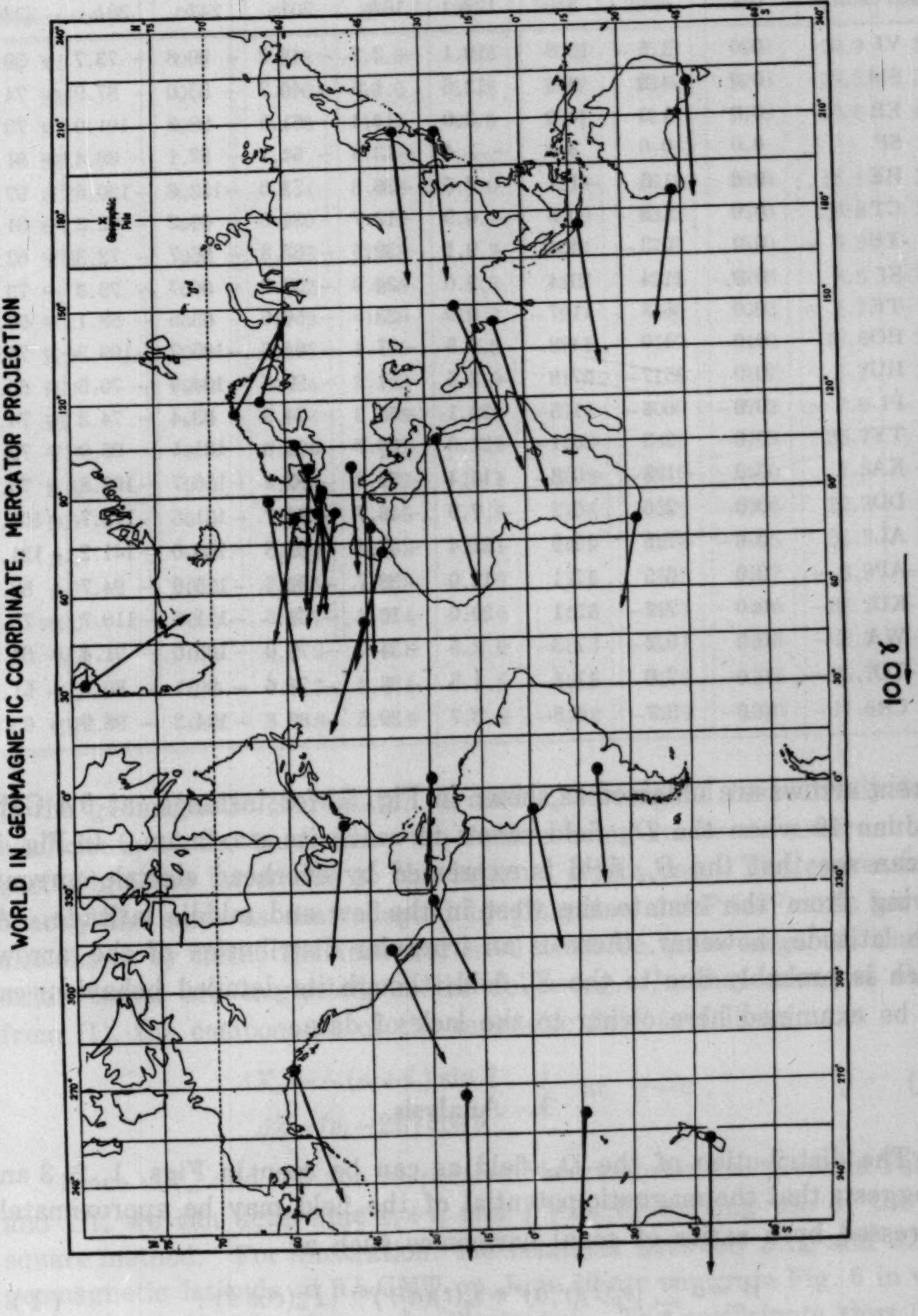

Fig. 5. The disturbance field at 9*h* GMT on June 19 as expressed by the equivalent current arrows.

Table II. ΔX_m in *gamma*.

Observatory	0h	4h	8h	12h	16h	20h	24h	28h	32h
VI	0.0	1.5	12.3	19.1	− 2.7	− 47.2	− 79.8	− 73.7	− 39.2
SM	0.0	4.9	9.4	13.6	1.5	− 40.7	− 83.0	− 87.9	− 74.9
EB	0.0	1.5	4.0	3.0	−14.4	− 61.5	− 98.8	−101.0	− 73.8
SF	0.0	0.0	3.4	− 1.4	−13.8	− 54.1	− 87.1	− 88.4	− 91.2
HE	0.0	−1.5	−1.1	− 7.6	−30.3	− 73.0	−112.8	−120.6	− 97.0
CT	0.0	1.8	0.8	− 0.9	−12.7	− 34.6	− 69.2	− 82.2	− 81.2
TU	0.0	0.3	4.4	− 9.1	−39.5	− 67.8	− 86.7	− 72.3	− 62.3
SJ	0.0	11.4	15.4	7.0	−24.9	− 53.8	− 80.7	− 76.3	− 73.4
TE	0.0	6.8	11.7	0.9	−23.5	− 50.6	− 65.5	− 58.1	− 50.4
HO	0.0	4.0	14.8	9.5	−37.4	− 84.6	−125.2	−109.3	− 76.8
HU	0.0	25.7	27.8	− 3.5	−61.9	− 97.5	−104.9	− 70.5	− 60.5
PI	0.0	6.8	1.5	−21.1	−54.3	− 74.9	− 83.4	− 74.2	− 74.5
TY	0.0	3.3	0.1	−21.3	−66.7	−106.8	−121.1	− 95.9	− 79.3
KA	0.0	−1.8	−0.8	−14.4	−52.2	− 97.8	−116.7	−102.8	− 75.0
DD	0.0	2.0	0.2	− 7.9	−46.7	− 94.7	−131.5	−118.7	−106.7
AL	0.0	−7.6	16.9	−21.4	−47.4	− 92.5	−136.0	−141.2	−121.0
AP	0.0	6.5	17.1	12.0	−38.7	− 92.5	−115.9	− 94.7	− 58.5
KU	0.0	7.2	13.1	20.0	−10.4	− 62.6	−111.6	−110.7	− 78.4
WA	0.0	5.2	7.3	2.5	−34.0	− 75.0	−106.6	− 91.4	− 64.5
TO	0.0	7.0	11.4	1.5	−35.4	− 78.6	− 90.1	− 80.3	− 51.9
CR	0.0	5.7	6.3	− 3.7	−39.5	− 89.8	−104.3	− 98.9	− 63.5

current arrows are obtained as shown in Fig. 5, for instance, at 9*h* GMT on June 19 when the D_{st} field seems to reach its maximum. In Fig. 5, we can see that the D_{st} field is expressed by overhead electric currents flowing from the east to the west in the low and middle latitude. At high latitude, however, there is an irregular distribution of the arrows which is probably due to the S_D field, though its detailed behaviour can not be examined here owing to the lack of data.

3. Analysis

The distribution of the D_{st} field as can be seen in Figs. 1, 2, 3 and 5 suggests that the magnetic potential of the field may be approximately expressed by a series of zonal harmonics such as

$$W=a\sum_n \{e_n(t)(r/a)^n+i_n(t)(a/r)^{n+1}\}P_n(\cos\theta)\,, \qquad (1)$$

where a and θ denote respectively the earth's radius and the colatitude

Table III. ΔZ in *gamma*.

Observatory	0*h*	4*h*	8*h*	12*h*	16*h*	20*h*	24*h*	28*h*	32*h*
VI	0.0	0.3	− 1.8	6.3	0.5	− 5.3	6.0	19.9	33.0
SM	0.0	6.0	10.0	17.8	24.7	23.1	19.0	19.5	28.3
EB	0.0	4.8	10.4	21.8	20.1	11.9	10.0	28.0	41.6
SF	—	—	—	—	—	—	—	—	—
HE	0.0	− 1.4	4.0	9.0	14.5	16.1	20.9	18.1	19.9
CT	0.0	3.0	6.9	9.2	5.9	13.5	25.0	26.8	19.3
TU	0.0	5.3	10.3	8.2	0.4	− 7.7	18.0	− 6.5	− 7.5
SJ	0.0	0.2	2.6	5.3	8.2	7.7	−12.8	8.5	−11.6
TE	0.0	−11.3	−15.0	−18.7	− 9.7	4.0	10.2	− 1.7	− 3.4
HO	0.0	1.5	− 4.0	− 8.5	− 8.5	1.7	14.0	18.6	20.0
HU	0.0	− 0.4	1.3	0.9	1.0	− 1.6	1.7	5.7	10.8
PI	0.0	0.4	0.9	− 0.8	− 7.3	−10.9	−37.2	− 7.9	− 6.5
TY	0.0	2.0	− 0.7	− 7.2	− 8.3	4.1	−37.9	26.7	18.5
KA	0.0	− 0.4	− 1.8	−16.1	−30.3	−28.5	−39.0	5.5	4.1
DD	0.0	3.8	8.5	7.5	1.6	3.5	−29.6	22.3	29.7
AL	0.0	7.0	16.8	21.1	14.9	15.6	−10.5	31.3	25.0
AP	0.0	− 2.4	− 3.8	− 1.9	2.5	5.2	5.7	− 3.9	− 6.6
KU	0.0	− 5.7	− 7.4	− 8.6	16.6	−29.7	4.0	−32.2	−21.6
WA	0.0	− 2.9	− 2.8	− 2.9	− 6.3	−20.1	12.6	−42.3	−40.9
TO	0.0	3.7	6.1	5.6	−12.5	−36.6	− 1.2	−25.7	− 1.9
CR	0.0	3.8	8.9	7.2	−12.2	−32.9	−12.0	−17.6	2.3

in the geomagnetic coordinate. e_n and i_n correspond respectively to the coefficients of the harmonics, the former being due to the external origin part while the latter due to the internal origin one. The expression is exactly the same as that adopted by Chapman and Price[1)]. As has been also shown by them, the term for $n=1$ is to be quite large, so that the other terms are neglected in the following. In that case, we obtain, from (1), the components of the magnetic field as follows:

$$\left.\begin{aligned} \Delta X_m &= -(e_1+i_1)\sin\theta\,, \\ \Delta Z &= (e_1-2i_1)\cos\theta\,. \end{aligned}\right\} \quad \text{at} \quad r=a\,. \qquad (2)$$

Since ΔX_m and ΔZ for respective observatories are given in Table II and III, we can determine e_1+i_1 and e_1-2i_1 by making use of the least square method. For illustration, the relations between ΔX_m and ΔZ and geomagnetic latitude at $9\,h$ GMT on June 19 are shown in Fig. 6 in which the curves defined by (2) are also illustrated. The coefficients thus determined are shown in Table IV for respective times, so that we can

calculate e_1 and i_1 separately as are also shown in the table together with their probable errors. In these analyses, only the observatories situated between 50°N and 50°S are taken into consideration in order to avoid the influence of S_D that predominates at high latitude. The time variations of e_1 and i_1 are illustrated in Fig. 7. At a glance, we

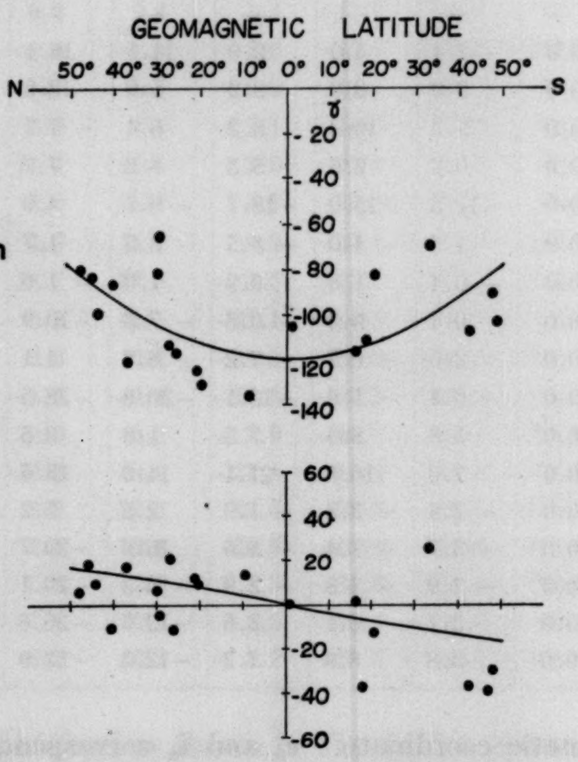

Fig. 6. The distribution of ΔX_m and ΔZ at 9*h* GMT on June 19.

Table IV. The coefficients at every 4 *hours* and their probable errors. (Unit: *gammas*)

Storm time	e_1+i_1	e_1-2i_1	e_1	i_1
0^h	0.0	0.0	0.0	0.0
4	− 5.3± 4.2	1.1± 3.0	−3.2±3.0	−2.1±1.7
8	−10.2± 5.0	1.8± 5.3	−6.2±3.8	−4.0±2.4
12	1.7± 8.3	3.2± 7.6	2.2±6.1	−0.5±3.8
16	39.6±11.7	6.4± 8.7	28.5±8.3	11.1±4.7
20	86.8±13.0	16.4±10.7	63.3±9.4	23.5±5.6
24	119.4±12.6	21.8±11.3	86.9±9.2	32.5±5.6
28	110.0±13.4	27.3±11.0	82.4±9.7	27.6±5.8
32	88.1±11.6	23.6±12.1	66.6±8.7	21.5±5.6

see that the relation between e_1 and i_1 closely resembles the one obtained by Chapman and Price[1)].

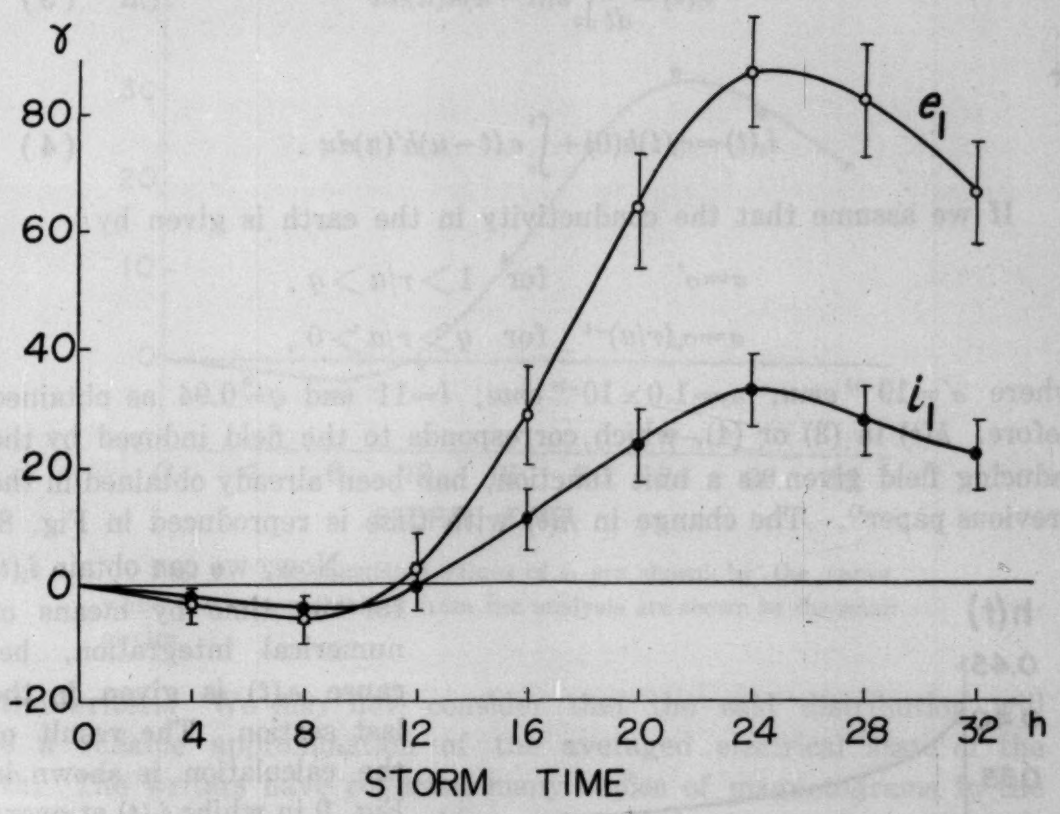

Fig. 7. The most probable values of e_1 and i_1 at every 4 *hours*. The probable errors are also shown.

4. Physical interpretation of the relation between e_1 and i_1

The theory of the electromagnetic induction in the earth has been successful in interpreting the relation between the external origin and the internal origin parts of geomagnetic variations. By applying the theory to the results of analyses of various variations, slow and rapid, the distribution of the electrical conductivity in the earth has been approximately obtained by the senior writer of the present paper. In this section, the writers would like to examine how well the conductivity distribution can explain the relation between e_1 and i_1 obtained in the previous section. Since no such analysis of the D_{st} field has been published since Chapman and Prices' study, this sort of check of the conductivity distribution will be desirable.

In so far as we take the standpoint that the internal origin part is induced by the inducing field of external origin, the relation between

the inducing and induced fields is given as

$$i_1(t) = \frac{d}{dt}\int_0^t e_1(t-u)h(u)du \tag{3}$$

or

$$i_1(t) = e_1(t)h(0) + \int_0^t e_1(t-u)h'(u)du\ . \tag{4}$$

If we assume that the conductivity in the earth is given by

$$\sigma = \sigma' \quad \text{for} \quad 1 > r/a > q\ ,$$

$$\sigma = \sigma_0(r/a)^{-l} \quad \text{for} \quad q > r/a > 0\ ,$$

where $\sigma' = 10^{-15}$ *emu*, $\sigma_0 = 1.0 \times 10^{-12}$ *emu*, $l = 11$ and $q = 0.94$ as obtained before. $h(t)$ in (3) or (4), which corresponds to the field induced by the inducing field given as a unit function, has been already obtained in the previous paper[3]. The change in $h(t)$ with time is reproduced in Fig. 8.

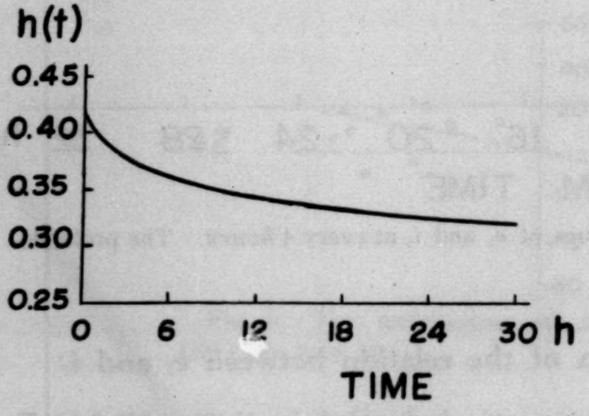

Fig. 8. The change in $h(t)$.

Now, we can obtain $i_1(t)$ for any time by means of numerical integration, because $e_1(t)$ is given in the last section. The result of the calculation is shown in Fig. 9 in whihc $i_1(t)$ at every 4 *hours*, which is obtained by the analysis, is also plotted. The agreement between the calculated curve and the values obtained from the analysis is striking, so that we may say that the distribution of the electrical conductivity obtained before is in good harmony with the present analysis of the D_{st} field.

5. Concluding remarks

It is made clear that the relation between the external origin and the internal origin parts of the D_{st} field of a magnetic storm that occurred on June 18–19, 1936 is well explained by the theory of electromagnetic induction within the earth, provided we assume the electrical conductivity distribution in the earth which has been obtained by one

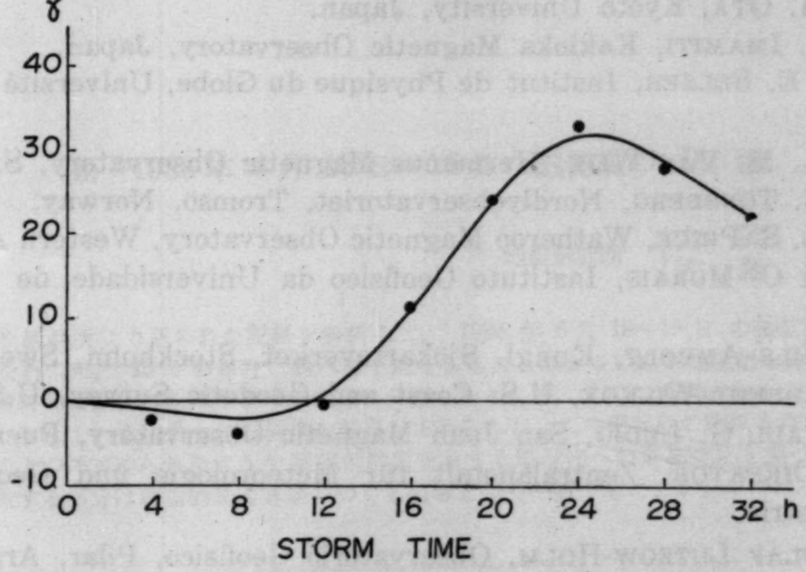

Fig. 9. The calculated values of i_1 are shown by the curve, while the values obtained from the analysis are shown by the small circles.

of the writers. We may now consider that the said distribution will give a reliable approximation of the averaged electrical state of the earth. The writers have collected many copies of magnetograms in the hope of investigating the local anomalous behaviours of geomagnetic variations in Japan. The investigations have been successful for short-period variations. An interesting result concerning the distribution of the electrical conductivity underneath Japan has been derived from the investigations. It is highly desirable to make the same sort of investigation on the D_{st} field, because there would be a possibility to infer the electrical state deeper than the one examined by short-period variations. However, the writers have not been able to accomplish such an investigation because magnetograms for the whole period of the storm have been supplied from very few observatories in and around Japan. Investigations on local anomalous feature of the D_{st} field, therefore, will be left to the future though a plausible approximation is obtained for the averaged distribution of the electrical conductivity in the earth.

In conclusion, the writers are grateful to Mr. I. Yokoyama who has constantly helped them in the course of the study. The present study was done with many copies of magnetograms which were sent to the writers from many observatories at the writers' request. The writers wish to express their cordial thanks to the following persons:

Dr. M. ÔTA, Kyoto University, Japan.

Dr. S. IMAMITI, Kakioka Magnetic Observatory, Japan.

Prof. E. SELZER, Institut de Physique du Globe, Université de Paris, France.

Dr. A. M. VAN WIJK, Hermanus Magnetic Observatory, S. A.

Dr. E. TÖNSBERG, Nordlyobservatoriet, Tromsö, Norway.

Mr. L. S. PRICE, Watheroo Magnetic Observatory, Western Australia.

Dr. J. C. MORAIS, Instituto Geofisico da Universidade de Coimbra, Portugal.

Dr. NILS AMBOLT, Kungl. Sjökarteverket, Stockholm, Sweden.

Dr. ROBERT WILKOX, U.S. Coast and Geodetic Survey, U.S.A.

Dr. PAUL G. LEDIG, San Juan Magnetic Observatory, Puerto Rico.

Der DIREKTOR, Zentralanstalt für Meteorologie und Geodynamik, Wien, Austria.

Dr. OLAF LUTZOW-HOLM, Observatorio Geofisico, Pilar, Argentina.

Dr. HELGE PETERSEN, Det Danske Meteorologiske Institut, København, Denmark.

Dr. M. DOPORTO, Meteorological Service, Dublin, Ireland.

Prof. Dr. J. J. M. REESINCK, Meteorological and Geophysical Service, Djakarta, Indonesia.

Dr. J. VELDKAMP, Koninklijk Nederlands Meteorologisch Institut, De Bilt, Netherlands.

Dr. S. L. MALURKAR, Colaba and Alibag Observatories, India.

Dr. ROSENDO OCTAVIO SANDOVAL, Instituto de Geofisica, Mexico.

Dr. RICARD MONGES LOPEZ, Instituto de Geofisica, Mexico.

The SUPERINTENDENT, Eskdalemuir Magnetic Observatory, Scotland.

Dr. J. ORIOL CARDUS, Observatorio del Ebro, Spain.

Dr. WENCESLAO BENITEZ, Instituto y Observatorio de Marina, San Fernando, Spain.

Dr. R. F. THYER, Bureau of Mineral Resources, Melbourne, Australia.

Prof. H. AMARIM FFRREIA, Servico Meteorologico Nacional, Portugal.

Dr. H. F. BAIRD, Amberley Magnetic Observatory, New Zealand.

The DIRECTOR GENERAL, Royal Observatory, Helwan, Egypt.

Dr. M. M. GILL, Apia Magnetic Observatory, Western Samoa.

Dr. JOHANNES OLSEN, Det Danske Meteorologiske Institut, København, Denmark.

Mr. B. L. GULATEE, Geodetic and Training Circle, Dehra Dun, India.

Mr. A. A. GIESECKE, JR., Instituto Geofisico de Huancayo, Peru.

Dr. EERO KATAJA, Sodankylä Magnetic Observatory, Finland.

---

2. 1936年6月18日～19日の磁気嵐の D_{st} 場

地震研究所 力武常次 佐藤節子

世界各地の観測所より送られた記録を解析して，1936年6月18～19日の磁気嵐の D_{st} 場について解析を行つた，13ヶの毎時の読みの平均をとることによつて短周期変動を除去した結果について，地球外および内に原因を有する部分に分離したところ，すでに Chapman および Price 等によつて求められている結果とほぼ同様な結果が求められた．この両部分の関係を理解するために，筆者の一人によつて求められたような電気的性質を有する地球内への電磁感応を調べてみると，地球内より発生する部分は理論的誘導電流のつくる磁場と全く一致することがわかつた．

Dr. M. Ota, Kyoto University, Japan.

Dr. S. Imamiti, Kakioka Magnetic Observatory, Japan.

Prof. E. Selzer, Institut de Physique du Globe, Université de Paris, France.

Dr. A. [illegible] Observatory, S. A.

Dr. E. Tønsberg, Nordlysobservatoriet, Tromsø, Norway.

Mr. [illegible], Watheroo Magnetic Observatory, Western Australia.

Dr. [illegible], Instituto Geofísico da Universidade de Coimbra, Portugal.

[illegible]

The Director, Zentralanstalt für Meteorologie und Geodynamik, Wien, Austria.

Dr. Olaf Lutzow-Holm, Observatorio Geofísico, Pilar, Argentina.

Dr. Helge Petersen, Det Danske Meteorologiske Institut, København, Denmark.

Dr. M. Doporto, Meteorological Service, Dublin, Ireland.

Prof. Dr. J. J. M. [illegible], Meteorological and Geophysical Service, Djakarta, Indonesia.

Dr. J. Veldkamp, Koninklijk Nederlands Meteorologisch Instituut De Bilt, Netherlands.

Dr. S. L. Malurkar, Colaba and Alibag Observatories, India.

Dr. [illegible], Instituto de Geofísica, Mexico.

Dr. [illegible], Instituto de Geofísica, Mexico.

The Superintendent, Eskdalemuir Magnetic Observatory, Scotland.

Dr. J. [illegible], Observatorio del Ebro, Spain.

Dr. [illegible], Instituto y Observatorio de Marina, San Fernando, Spain.

Dr. [illegible], Bureau of Mineral Resources, Melbourne, Australia.

Prof. H. Amorim Ferreira, Serviço Meteorológico Nacional, Portugal.

Dr. H. F. Baird, Amberley Magnetic Observatory, New Zealand.

The Director General, Royal Observatory, Helwan, Egypt.

Dr. [illegible] M. Gill, Apia Magnetic Observatory, Western Samoa.

Dr. Johannes Olsen, Det Danske Meteorologiske Institut, København, Denmark.

Mr. B. L. Gulatee, Geodetic and Training Circle, Dehra Dun, India.

Mr. A. A. Giesecke, Jr., Instituto Geofísico de Huancayo, Perú.

3. *A Gravity Survey on Volcano Mihara, Ooshima Island by Means of a Worden Gravimeter.*

By Izumi YOKOYAMA and Hirokazu TAJIMA,

Earthquake Research Institute.

(Read Dec. 18, 1956.—Received Dec. 31, 1956.)

1. Introduction

The Earthquake Research Institute has long been much interested in the geophysical and geological phenomena on Volcano Mihara, Ooshima Island, one of the most active volcanoes in Japan. Seismometrical, geomagnetic and geodetic observations have been repeatedly carried out in connection with the recent activities of the volcano.

As regards gravity measurements, T. Nagata[1] swung pendulums at three stations and also observed the second derivatives of the gravity potential at 18 stations on Ooshima Island in 1938. In 1950 and 1951, during which period the volcano displayed very active eruptions, K. Iida, M. Hayakawa and K. Katayose[2] made gravity surveys by a North American gravimeter with the chief intention of finding, if any, the relation between eventual changes in gravity with time and those in subsurface physical conditions associated with volcanic activities. Although the observations in that survey were made at numerous points with precisions high enough for the purpose, the points were unfortunately localized in too small area to obtain the general picture of gravity anomaly distribution around the volcano.

In order to find the distribution of gravity anomaly all over Ooshima Island and to get clues for figuring out the subterranean structure of the volcano together with other geomagnetic and geological information, the writers carried out a gravity survey by means of a Worden gravimeter in August, 1956.

2. Observations and reductions

The instrument used in the present survey was a Worden gravi-

1) T. NAGATA, *Bull. Earthq. Res. Inst.*, **17** (1939), 93.

2) K. IIDA, M. HAYAKAWA and K. KATAYOSE, *Geological Survey of Japan, Report* No. 152 (1952).

Table I. Observation points.

No. 1	Dormitory of E.R.I. at Nomashi, M.S. No. 37	野増震研宿舎
3	Yunohama T.P.	湯の浜三角点
4	Motomachi Primary School, M.S. No. 47	元町小学校
5	Motomachi town office	元町役場
6	Old road to Okata	元町から測候所の間
7	Weather Station (seismo. room)	測候所（地震計室）
8	〃 〃 (wind tower)	〃 （風向塔）
9	〃 〃 (bench mark)	〃 （水準点）
10	Crossing N.E. of Weather Station	測候所の北東三叉路
11	Bus stop at Kitanoyama	北の山バス停留場
12	Ogawa Farm, Zinooka	地岡小川農園前
13	Top of Mt. Atago, T.P.	愛宕山頂三角点
14	Atago shrine	愛宕神社
17	Habu wharf	波浮港荷揚場
18	Ryuoozaki lighthouse	龍王岬灯台
20	Beach of Otainohama	オタイの浜
21	Uenoyama, Habu	波浮上の山
25	Habu Fisheries Station (bench mark)	波浮水産試験場
26	Kuddachi B.M. 0–7	クダッチ水準点
27	Sashikizi Primary School	差木地小学校
28	Foot of Mt. Takenohira	岳平山麓
29	Top of Mt. Takenohira, T.P.	岳平山頂三角点
30	Radio Beacon Station, Sashikizi, M.B. 0–6	差木地送信所前水準点
33	Nomashi climbing path	野増登山道中腹
35	Outer somma, M.S. No. 39	御神火茶屋地磁気測点
37	Gojinka-chaya B.M. 0–10	御神火茶屋水準点
36	Anei-lava at atrio, B.M. 0–11	沙漠安永熔岩水準点
38	Kakoo-chaya B.M.	火口茶屋水準点
39	Peak of Kengamine	劍ケ峯
40	Foot of Mt. Shiraishi	木星号遭難地
41	Outer somma, Suberidai	滑り台上，鳥居
42	Suberidai path	滑り台登山道中腹
47	Ooshima Park, B.M. 0–1	大島公園水準点
48	〃 〃 , magnetic station, M.S. No. 43	大島公園地磁気観測所
49	Ooshima Park, path	大島公園登山道中腹
50	Eastern atrio, M.S. No. 44	裏沙漠
51	Boundary between Senzu and Sashikizi	泉津，差木地境界線
52	Tsuruoka-game	鶴岡ガメ
53	Crossing N. of Habu	波浮北方三叉路
57	Path N. of Radio Beacon Station	送信所北方山道
58	Beach of Mabushi, M.S. No. 26	間伏海岸

(to be continued.)

Table I.—(continued.)

No. 59	Path N. of Mabushi	間伏北方登山道
60	Sembazaki, B.M. 0–5	千波崎水準点
63	Naganehama, Motomachi T.P.	長根浜三角点
65	Motomachi Kindergarten, B.M. 0–4	元町保育園水準点
66	Miharashi-chaya	見望茶屋
67	Utano-chaya	歌の茶屋
68	Motomachi climbing path	六合目の上
70	Observatory at outer somma	山頂火山観測所
73	Kagamihata T.P.	鏡端三角点
74	Crater-Okata path at atrio	沙漠の火口，岡田道
75	Odori-chaya, outer somma	おどり茶屋
76	Yuba, B.M. 0–9	湯場水準点
77	Hachinowo, M.S. No. 45	蜂の尾
78	Senzu climbing path	泉津登山道中腹
79	Senzu	泉津村入口
80	Senzu Primary School	泉津小学校
83	Oomiya Park, Nomashi, M.S. No. 24	大宮公園
84	Tatsunokuchi, Nomashi	龍の口入口
85	Cross road, W.S., B.M. 0–3	測候所下水準点
86	Daimaru, B.M. 0–4	大丸水準点
87	Kazahaya lighthouse	風早灯台
90	Cross road, Mitsumine	三峯三叉路
92	Okata, B.M. 0–2	岡田入口水準点
93	Okata climbing path, M.S. No. 46	岡田登山道
94	Ooshima High School, Motomachi	大島高等学校昇降口

M.S.: magnetic station
T.P.: triangulation point
B.M.: bench mark of precise levels

meter No. 60. The methods of measurements are the same as those described by C. Tsuboi and his colleagues[3] in this Bulletin. The observed gravity value at the very site of a bench mark is relatively accurate within a few hundredths of a *milligal*. The readings of the gravimeter were corrected for the drift of the gravimeter spring and for the effect of the earth tides. All the gravity values have been deduced relative to the value at the Tokyo Fundamental Station which has been taken to be exactly 979.80100 relative to Potsdam. Thus, the results in this survey are comparable with those in the survey along the lines of precise levels throughout Japan by C. Tsuboi and his colleagues.

3) C. Tsuboi, A. Jitsukawa, H. Tajima and A. Okada, *Bull. Earthq. Res. Inst., Suppl. Vol.*, **4** (1953).

Our observations reached 66 in number, 15 of which are bench marks laid by the Institute and 4 are triangulation points. Observation points are listed in Table I and shown in Fig. 1.

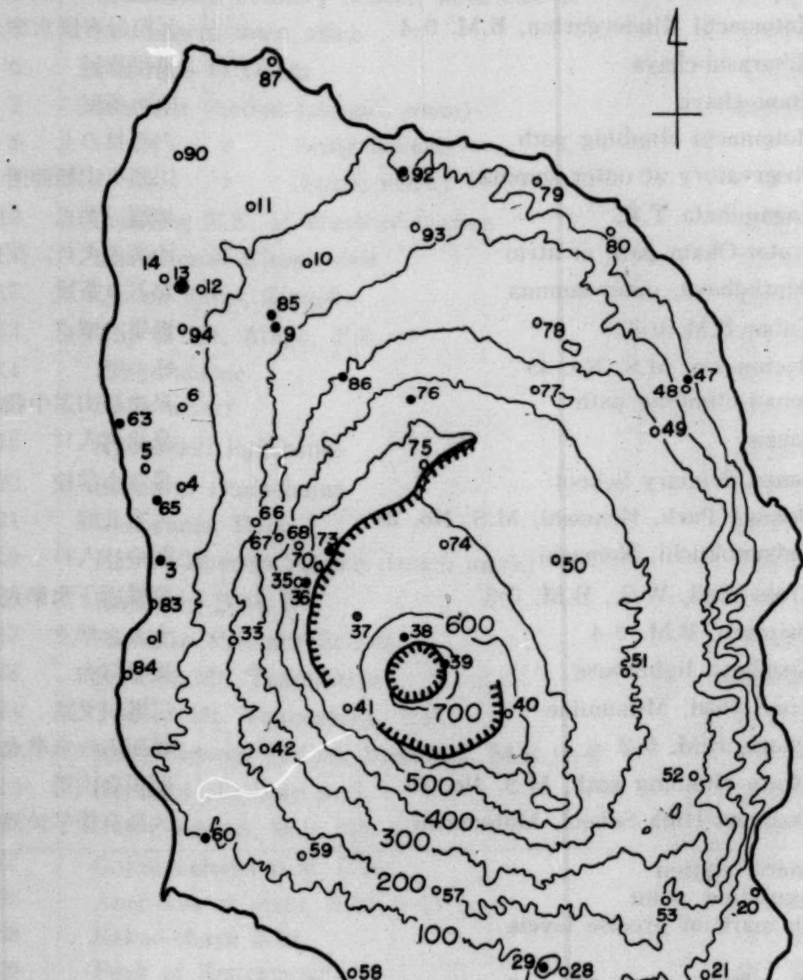

Fig. 1. Distribution of observation points and topographic contours in *meter* (full circles show the triangulation points and bench marks of precise levels)

The accuracy of gravity anomalies in our survey depends upon that of the heights of the observation points. In order to determine the heights of the observation points, we used a pair of Askania's microbarometers which enable to measure atmospheric pressure difference

of 0.01 *mm Hg*. One of the pair was placed at the Ooshima Weather Station during the observation period and the other was carried along together with the gravimeter throughout the course of the survey. Calculation of the heights of the points was made by the Laplace's barometric formula and the accuracy of the results depends on atmospheric conditions in general. The height of the base-point at the Ooshima Weather Station which was deduced from barometric observations in relation to the points where the true heights had been already known by triangular and levelling surveys, is shown in Table II. The accuracy

Table II. Height of the base-point deduced from barometric observations (true height is 191.93 *m*).

Date (1956)	Time	No.	Point	Deduced Height (*m*)	Remarks
Aug. 20	09*h*15*m*	17	Habu-ko B.M.	190.65	
〃	14 15	26	B.M. 0-7	191.78	
〃	16 25	29	Takenohira T.P.	190.41	
〃	17 25	30	B.M. 0-6	192.08	
21	11 25	36	B.M. 0-10	189.93	Windy
〃	13 25	37	B.M. 0-11	192.41	
23	14 40	17	Habu-ko B.M.	192.73	
24	09 00	65	B.M. 0-4	192.62	
〃	11 25	36	B.M. 0-10	193.69	Windy
〃	12 05	73	Kagamihata T.P.	189.92	
〃	15 30	76	B.M. 0-9	190.93	
25	10 25	86	B.M. 0-8	191.80	
〃	14 00	92	B.M. 0-2	193.19	Disturbed by motors
〃	18 10	60	B.M. 0-5	190.98	

proved itself to be higher than 3 *meters* at the worst. Thus, the writers succeeded in obtaining the accuracy of determining of gravity anomaly within 1 *mgal*.

In calculating gravity anomalies, the free air reduction was first made by the formula

$$0.3086 \times h(m) \qquad \text{in } mgal$$

although the coefficient 0.3086 is known to vary according to gravity anomalies. The values of $\partial g/\partial z$ which were calculated from the gravity values observed at the bottoms and tops of high towers etc. at several places, are shown in Table III, without topographical corrections. In

Table III. Observed values of $\partial g/\partial z$.

No.	Date (1956)	Δg (*mgal*)	Δz (*m*)	$\partial g/\partial z$ (*mgal/m*)
5	Aug. 19	3.35	10.45	0.321
8	〃 19	4.05	12.16	0.333
〃	〃 19	7.27	21.87	0.332
18	〃 20	2.81	7.68	0.366
25	〃 20	3.90	12.70	0.307
70	〃 24	2.37	6.40	0.370
87	〃 25	4.39	11.16	0.393

fact, the values vary notably from a place to another. Here, the writers take the vertical gradient to be 0.3086 *mgal/m* throughout only for the sake of simplicity.

In order to calculate the Bouguer and topographical corrections, it is necessary to know the density of the mountain-mass which, strictly speaking, varies from place to place. In this respect, Iida and his colleagues minutely examined the density of ejecta from the volcano and obtained the result that the average density of volcanic ash and lava is 1.6 and 2.6 *gr./cc* respectively. The volcano is actually a composite of such ejecta and its overall mean density will lie between the above-mentioned values. On the other hand, we may deduce the effective density of the mountain-mass from the results of gravity survey as follows: Neglecting the topographical effects and assuming the uniform density, the gravity value at the height *h m* is expressed as

$$g_h = g_0 - 0.3086\,h + 2\pi k^2 \rho h \text{ in } mgal\,,$$

where ρ is the mean density. The relation between the observed gravity values and heights is beautifully linear as shown in Fig. 2. By the least square method, the density was found to be 2.08 *gr./cc*. In the follow-

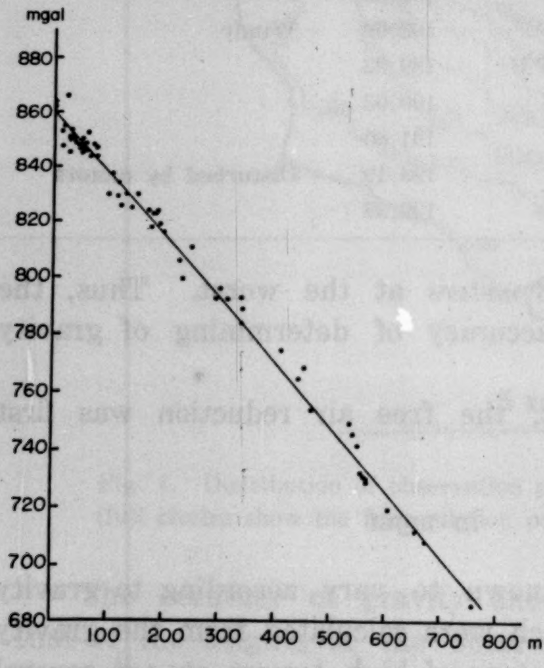

Fig. 2. Relation between observed gravity values and height

Table IV. Observed values, corrections and the Bouguer anomalies.

No.	Height (*m*)	Normal value (*mgal*)	Observed value (*mgal*)	Free-air correction (*mgal*)	Bouguer correction (*mgal*)		Topographical correction (*mgal*)	Bouguer anomaly (*mgal*)	
					$\rho=2.1$	$\rho=2.0$ or 2.4		$\rho=2.1$	$\rho=2.0$ or 2.4
1	45.6	722.6	848.5	14.1	4.0	3.8	3.4	139.4	139.6
3	51.0	723.3	847.0	15.7	4.5	4.3	3.6	138.6	138.7
4	58.0	724.0	847.5	17.9	5.1	4.9	3.5	139.8	140.0
5	30.2	724.1	852.4	9.3	2.7	2.5	3.2	138.2	138.3
6	47.7	725.0	848.2	14.7	4.2	4.0	3.9	137.6	137.8
7	191.9	725.6	822.4	59.2	16.9	16.1	5.5	144.6	145.4
8	191.4	725.6	822.0	59.1	16.8	16.0	5.5	144.1	145.0
9	190.5	725.6	822.4	58.8	16.8	16.0	5.5	144.3	145.1
10	149.7	726.1	834.6	46.2	13.2	12.5	4.6	146.1	146.8
11	76.5	726.7	848.2	23.6	6.7	6.4	3.5	141.9	142.2
12	65.1	726.0	847.0	20.1	5.7	5.4	3.4	138.8	139.1
13	119.5	726.0	829.4	36.9	10.5	10.0	4.7	134.5	135.0
14	38.7	726.1	852.6	11.9	3.4	3.2	3.5	138.5	138.7
17	1.2	718.9	860.2	0.4	0.1	0.1	4.3	145.9	145.9
18	57.6	718.7	844.6	17.8	5.1	4.8	3.7	142.3	142.6
20	48.4	720.1	863.5	14.9	4.3	4.9	7.1	161.2	160.5
21	60.2	719.2	849.3	18.6	5.3	5.0	3.6	147.0	147.3
25	2.8	718.8	858.2	0.9	0.2	0.2	4.3	144.3	144.4
26	29.7	718.4	849.4	9.2	2.6	2.5	3.2	140.8	140.9
27	44.1	718.7	842.6	13.6	3.9	3.7	3.1	136.7	136.9
28	128.0	719.2	826.6	39.5	11.3	10.7	3.7	139.3	139.9
29	231.9	719.2	796.2	71.6	20.4	19.4	3.5	131.7	132.7
30	26.0	718.8	841.4	8.0	2.3	2.2	3.1	131.4	131.5
33	226.3	722.5	806.1	69.8	19.9	19.0	7.3	140.8	141.7
35	553.3	723.0	732.8	170.8	48.7	46.3	11.3	143.2	145.6
36	558.5	723.0	731.4	172.4	49.1	46.8	11.3	142.9	145.3
37	539.1	722.9	746.5	166.4	47.4	54.2	10.1	152.6	145.9
38	672.6	722.7	709.4	207.6	59.2	56.4	11.6	146.7	149.5
39	755.8	722.3	686.4	233.2	66.5	63.3	14.3	145.1	148.3
40	653.8	721.8	711.4	201.8	57.5	54.8	11.7	145.5	148.3
41	562.2	721.9	728.4	173.5	49.5	47.1	11.5	142.0	144.4
42	291.7	721.5	791.8	90.0	25.7	24.4	7.0	141.6	142.9
47	103.9	725.0	840.3	32.1	9.1	8.7	9.1	147.3	147.8
48	113.4	725.0	836.4	35.0	10.0	9.5	9.1	145.5	146.0
49	313.9	724.4	794.4	96.9	27.6	26.3	8.4	147.6	149.0
50	450.8	723.3	769.4	139.1	39.7	45.3	8.5	154.0	148.4
51	410.3	722.2	774.5	126.6	36.1	41.2	8.6	151.4	146.3
52	337.2	721.2	791.7	104.1	29.7	33.9	8.1	153.0	148.8
53	179.6	719.9	820.3	55.4	15.8	18.1	5.3	145.3	143.0
57	174.9	720.1	815.4	54.0	15.4	14.6	6.7	140.0	141.4
58	13.5	719.2	844.2	4.2	1.2	1.1	3.1	131.1	131.2
59	136.5	720.5	822.6	42.1	12.0	11.4	3.7	135.9	136.5
60	111.9	720.6	827.3	34.5	9.8	9.4	3.6	135.0	135.4
63	13.8	724.6	855.3	4.3	1.2	1.2	3.2	136.9	137.0
65	32.8	723.9	851.8	10.1	2.9	2.8	3.3	138.4	138.5
66	196.7	723.7	817.2	60.7	17.3	16.5	6.1	143.0	143.8
67	338.7	723.4	784.7	104.5	29.8	28.4	8.3	144.3	145.7
68	463.6	723.4	755.0	143.1	40.8	38.8	8.9	142.8	144.8
70	565.4	723.2	730.6	174.5	49.7	47.4	11.3	143.4	145.8
73	604.0	723.3	720.4	186.4	53.1	50.6	12.6	142.9	145.5

(to be continued.)

Table IV.—(continued.)

No.	Height (m)	Normal value ($mgal$)	Observed value ($mgal$)	Free-air correction ($mgal$)	Bouguer correction ($mgal$)		Topographical correction ($mgal$)	Bouguer anomaly ($mgal$)	
					$\rho=2.1$	$\rho=2.0$ or 2.4		$\rho=2.1$	$\rho=2.0$ or 2.4
74	534.1	723.3	750.5	164.8	47.0	53.7	9.7	154.7	148.0
75	548.6	724.3	743.6	169.3	48.3	46.0	8.3	148.6	150.9
76	441.0	724.8	767.3	136.1	38.8	37.0	7.5	147.3	149.1
77	337.6	724.8	791.3	104.2	29.7	28.3	7.0	148.0	149.4
78	246.9	725.6	813.8	76.2	21.7	24.8	6.7	149.4	146.3
79	69.6	727.0	852.4	21.5	6.1	7.0	7.6	148.4	147.5
80	49.9	726.5	854.5	15.4	4.4	5.0	7.5	146.5	145.9
83	17.2	722.7	855.0	5.3	1.5	1.4	3.4	139.5	139.6
84	26.3	722.2	850.4	8.1	2.3	2.2	3.4	137.4	137.5
85	169.1	725.7	827.3	52.2	14.9	14.2	5.5	144.4	145.1
86	300.5	725.1	798.4	92.7	26.4	25.2	6.0	145.6	146.8
87	98.5	728.1	835.3	30.4	8.7	8.2	7.2	136.1	136.6
90	28.3	727.2	854.5	8.7	2.5	2.4	4.1	137.6	137.7
92	76.0	727.1	851.5	23.4	6.7	7.6	5.2	146.4	145.4
93	185.2	726.5	827.8	57.2	16.3	18.6	4.1	146.3	144.0
94	46.8	725.6	850.1	14.4	4.1	3.9	3.5	138.3	138.5

ing calculation, we take the effective density of the whole mountain-mass to be 2.10 *gr./cc.*

Topographical corrections were computed by using topographic maps on a scale of 1/5,000 up to 1.3 *km* and on a scale of 1/50,000 to 13 *km* and bathymetric charts on a scale of 1/100,000 to 33 *km*. Here, the densities of land and sea-water were taken to be 2.10 and 1.03 *gr./cc* respectively.

The normal gravity value was calculated according to

$$\gamma=978.04900(1+0.00528840\,\sin^2\varphi-0.00000590\,\sin^2 2\varphi)$$

where φ is latitude of the gravity point determined by using topographic maps on a scale of 1/5,000. The Bouguer anomalies are listed in Table IV and are shown in Fig. 3.

In the above discussion, we assumed the uniform density of the mountain-mass as the first approximation and obtained the Bouguer anomalies shown in Fig. 3 where relatively high anomalies are seen in the eastern and northern parts of the island. If we adopt different values for density in each part of the island as the second approximation, we may get picture of more deep structure of the volcano. Tentatively, the writers have adopted modified values for density for the above two parts, namely, observation points Nos. 37, 50, 51, 52, 53; 78, 79, 80, 92 and 93. By the same method as beforementioned, the effective

density was obtained as 2.32 and 2.44 *gr./cc* respectively while 2.00 *gr./cc* for the remainder. Adopting the value of 2.40 *gr./cc* for the high anomaly parts and 2.00 *gr./cc* for the rest, the Bouguer anomaly is

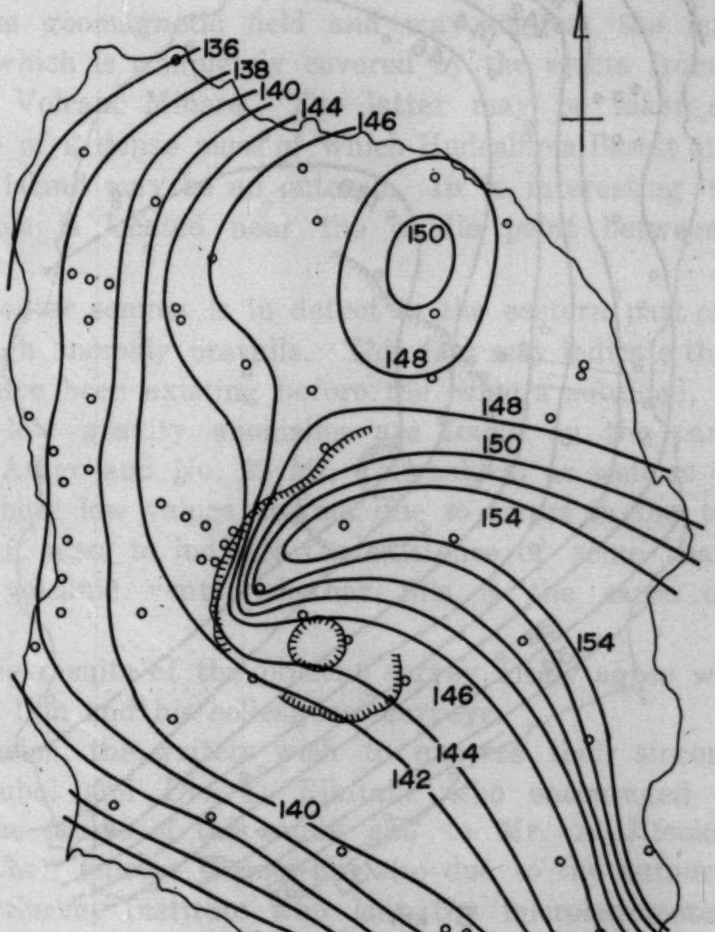

Fig. 3. Distribution of the Bouguer anomaly in *mgal*

obtained as shown in Table IV and Fig. 4 where the topographical corrections are left as before because the effect of density on them is rather small. The distribution of the Bouguer anomalies represented in the figure may be deemed to roughly suggest the density distribution under the sea level.

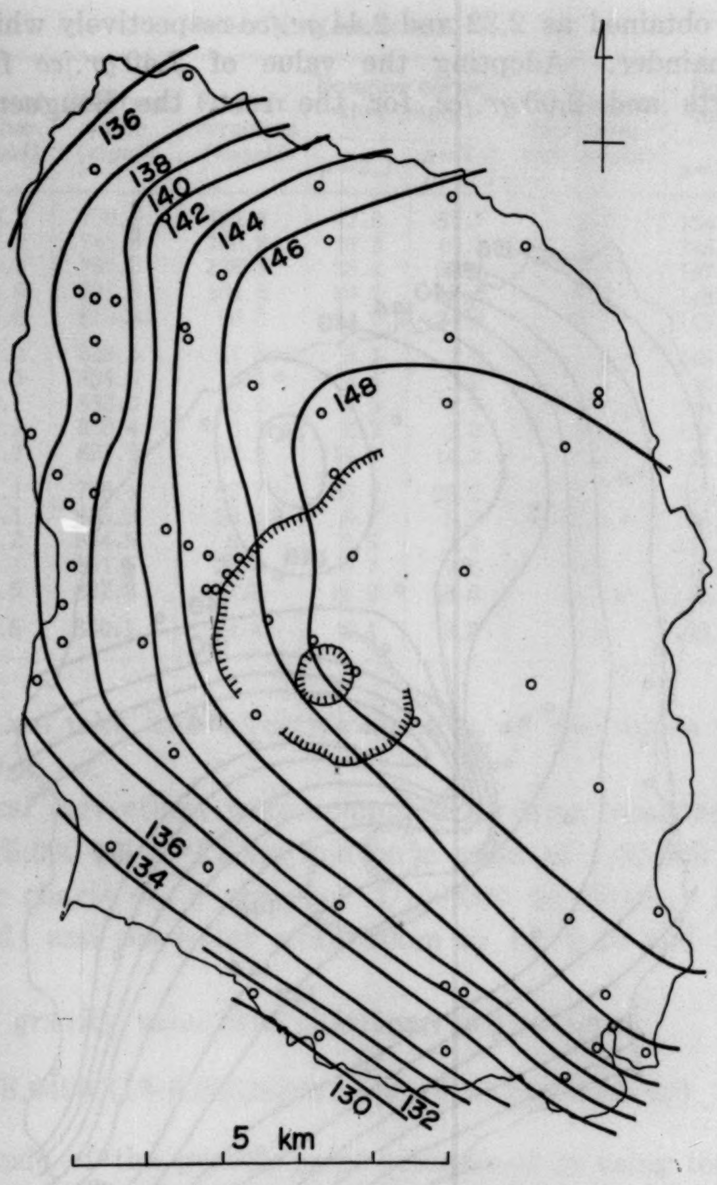

Fig. 4. Distribution of the Bouguer anomaly in *mgal* (adopting the modified Bouguer corrections)

3. Discussion and conclusions

Reserving the detailed and quantitative geophysical interpretations of the distribution of the Bouguer anomalies for future studies, the writers will mention the notable facts as seen in Figs. 3 and 4.

1) Generally speaking, the Bouguer anomaly contours are more or less similar to the shape of the island and this fact is not attributable to the coast effect of the Japan Trench which is situated about 200 *km*

distant eastward from Ooshima Island although we have not numerous observations on the sea in this area.

2) There are two areas of high gravity anomaly in the northern and eastern parts of the island as was stated before. The former gravity high corresponds to the positive anomaly of the vertical component in the geomagnetic field and may suggest the existence of a dense mass which is completely covered by the ejecta from the present central cone, Volcano Mihara. The latter may be taken as indicating the existence of a dense mass of which Hudeshima-Basalt at the eastern coast of the island may be an outcrop. It is interesting to note that Yuba fumarole is located near the saddle point between these two areas.

3) The outer somma is in defect in the eastern part of the caldera where the high anomaly prevails. This fact may indicate that the dense mass must have been existing before the caldera subsided.

4) The low gravity anomalies are found on the parasitic cones (No. 13 Mt. Atago and No. 29 Mt. Takenohira) as well as on the central cone. These low values are not due to errors in the topographical corrections but seem to indicate the existence of some coarse material around the volcanic vents whether this is the cause or effect of eruptions.

The above results of the present survey nicely agree with those of Nagata's and Iida and his colleagues' surveys.

In conclusion, the writers wish to express their sincere thanks to Prof. C. Tsuboi and Dr. T. Rikitake who encouraged the writers throughout the course of this study and to Mr. A. Jitsukawa for his kind help. Their sincere thanks are also due to the authorities of the Geographical Survey Institute who lent the microbarometers to them and to the members of the Ooshima Weather Station who assisted the writers in field observations.

---

3. ウォルドン重力計による伊豆大島の重力測量

地震研究所 横山　泉
田島広一

伊豆大島三原火山の構造を解明する手掛りを得る目的で，ウォルドン重力計による重力測量を行つた．大島全体に普遍的に測点を設けるように努め，高さの決定には一対のアスカニヤ微気圧計を用いてその精度を最悪 3 *m* 以内に止めた．地形補正は 33 *km* の範囲まで計算した，山体の密度を二様に仮定して，それぞれに対するブーゲー異常を求めた，その結果は現在までの地質調査の結果を裏付けするものであり，又磁気測量の結果ともよく調和するものである．

distant eastward from Oshima Island although we have not numerous observations on the sea in this area.

2) There are two areas of high gravity anomaly in the northern and eastern parts of the island as was stated before. The former gravity high corresponds to the positive anomaly of the vertical component in the geomagnetic field and may suggest the existence of a dense mass which is completely covered by the ejecta from the present central cone, Volcano Mihara. The latter may be taken as indicating the existence of a dense mass of which Fudeshima Basalt at the eastern coast of the island may be an outcrop. It is interesting to note that Yuba fumarole is located near the saddle point between these two areas.

3) The outer somma is in defect in the eastern part of the caldera where the high anomaly prevails. This fact may indicate that the dense mass must have been existing before the caldera subsided.

4) The low gravity anomalies are found on the parasitic cones (No. 18 Mt. Atago and No. 29 Mt. Takoshiyama) as well as on the central cone. These low values are not due to errors in the topographical corrections but seem to indicate the existence of some coarse material around the volcanic vents whether this is the cause or effect of eruptions.

The above results of the present survey nearly agree with those of Nagata's and Iida and his colleagues' surveys.

In conclusion, the writers wish to express their sincere thanks to Prof. C. Tsuboi and Dr. T. Hagiwara who encouraged the writers throughout the course of this study and to Mr. A. Hitsukawa for his kind help. Their sincere thanks are also due to the authorities of the Geographical Survey Institute who lent the microbarometers to them and to the members of the Oshima Weather Station who assisted the writers in field observations.

3. [illegible]

[illegible]

4. *Cenozoic Volcanism in Southwestern Japan with Special Reference to the History of the Setouchi (Inland Sea) Geologic Province.*

By Ryôhei MORIMOTO,
Earthquake Research Institute,
Kazuo HUZITA and Tarô KASAMA,
Osaka City University.

(Read June 17, 1952 and Jan. 25, 1955.—Received Dec. 28, 1956.)

Introduction

The Cenozoic in Southwestern Japan may be divided into three geologic provinces, namely the Inside Geologic Province on the Japan Sea side, the Setouchi (Inland Sea) Province in the middle, and the Outside one on the Pacific side. The Setouchi Geologic Province roughly occupies the middle zone between the present mountain ridge of Chûgoku District and the Median Dislocation Line. It includes Central Kyûshû, the Inland Sea (Seto-naikai) and its environs, and central Kinki District, extending eastwards to the Shidara basin in Aichi Prefecture. In the Setouchi Province, occurrence of "sanukitoid", an aphanitic lava characterized with minute equigranular hypersthene crystals has been noted by some petrologists in relation to the problems of foreign contamination in these sanukitoid lavas. The type of sedimentation in the area was quite different from those of the Inside and Outside geosynclines. This fact has made it difficult to correlate stratigraphically the strata deposited in the area. Most of them were deposited in the inland sea or in fresh water lakes formed during Neogene on the basement mostly composed of granitic rocks. This paper includes an outline of the history of Cenozoic volcanism in the Setouchi Geologic Province with those in the Inside and Outside provinces in Southwestern Japan (Table I and Fig. 1).

1) K. SUGI, *Bull. Volc. Soc. Japan*, **4** (1938), 17-33 (in Japanese).
R. MORIMOTO, *Proc. 7th Pacific Sci. Cong.*, **2** (1953), 302-307.

Table I. Correlation table of the Cenozoic formations in Southwestern Japan.

	OUTSIDE		SETOUCHI (INLAND SEA)			INSIDE		AREA / AGE	
	SOUTH KYŪSHŪ	SOUTH KINKI	CENTRAL KYŪSHŪ	SETOUCHI	CENTRAL KINKI	SAN'IN	HOKURIKU		
K	SAKURAJIMA ∇.▲		ASO CENTRAL CONE ∇.▲			GENBUDO ∇.■		K	RECENT
J	SHIRASU F.△		ASO CALDERA ∇.△ YUFU ∇.△ FUTAGO ∇.△		SHINODA-YAMA F. MACHIDANI F.	DAISEN ∇.△ SANBE ∇.△		J	PLEISTOCENE
I	KOKUBU F.		ŌITA GROUP ▲	KANKAKEI F.▲	ŌSAKA GROUP ▲		KUREHAYAMA F.	I	PLIO-PLEISTOCENE
H		(KUMANO ∇.)□ ↑↓?			MUROO ∇.□	OKI ∇.□■□■ MATSUE F.	HIMI GROUP	H	PLIOCENE
G	MIYAZAKI GROUP		NOZUHARU GROUP ▲▲△	UCHINOMI GROUP ▲△△	NIJO KOBE GROUP ▲▲△△	KIMACHI ŌMORI GROUP ▲▲	OTOKAWA GROUP	G	UPPER MIOCENE
F_3		MIYAI GROUP		SHIKAI GROUP	FUJIWARA GROUP	TAMATSUKURI GROUP △△	YATSUO GROUP △△	F_3	MIDDLE MIOCENE
F_2			USA GROUP ▲▲			KIMITANI GROUP ▲▲▲	(YATSUO GROUP) ▲▲▲	F_2	MIDDLE MIOCENE
F_1						PRE-KIMITANI □□	FUTOMIYAMA GROUP □□	F_1	LOWER MIOCENE

F : FORMATION
∇ : VOLCANOES or VOLCANIC ROCKS
△ : CALC-ALKALINE ACID VOLCANIC ROCKS
▲ : CALC-ALKALINE BASIC VOLCANIC ROCKS
□ : ALKALINE ACID VOLCANIC ROCKS
■ : ALKALINE BASIC VOLCANIC ROCKS

I. Late Palaeogene crustal movements and the beginning of the Cenozoic volcanism in Southwestern Japan —Oligocene (E)[2] to the early Miocene (F_1)—

The rocks representing the volcanism of this period are a little alkaline acid volcanic rocks recently reported from many localities; such as lithoidite-nevadite association belonging to Futomiyama group[3] in Toyama Prefecture, most of the liparites and quartz-porphyries distributed on the ridge of Chûgoku District, the anorthite-liparites found from the base of the green tuff in Tôhoku District, etc. From Oligocene (E) to early Miocene (F_1), Japan had been a theatre of crustal movements: the Japan Sea and Fossa Magna were formed; the difference between structural features of Southwestern Japan and those of North-

2) N. IKEBE, *Jour. Polytechnics, Osaka City Univ. Ser. G*, **1** (1954), 73-86.

3) Oral Communication from Prof. N. Ikebe and Mr. T. Matsumoto of the Division of Geoscience, Institute of Polytechnics, Osaka City University.

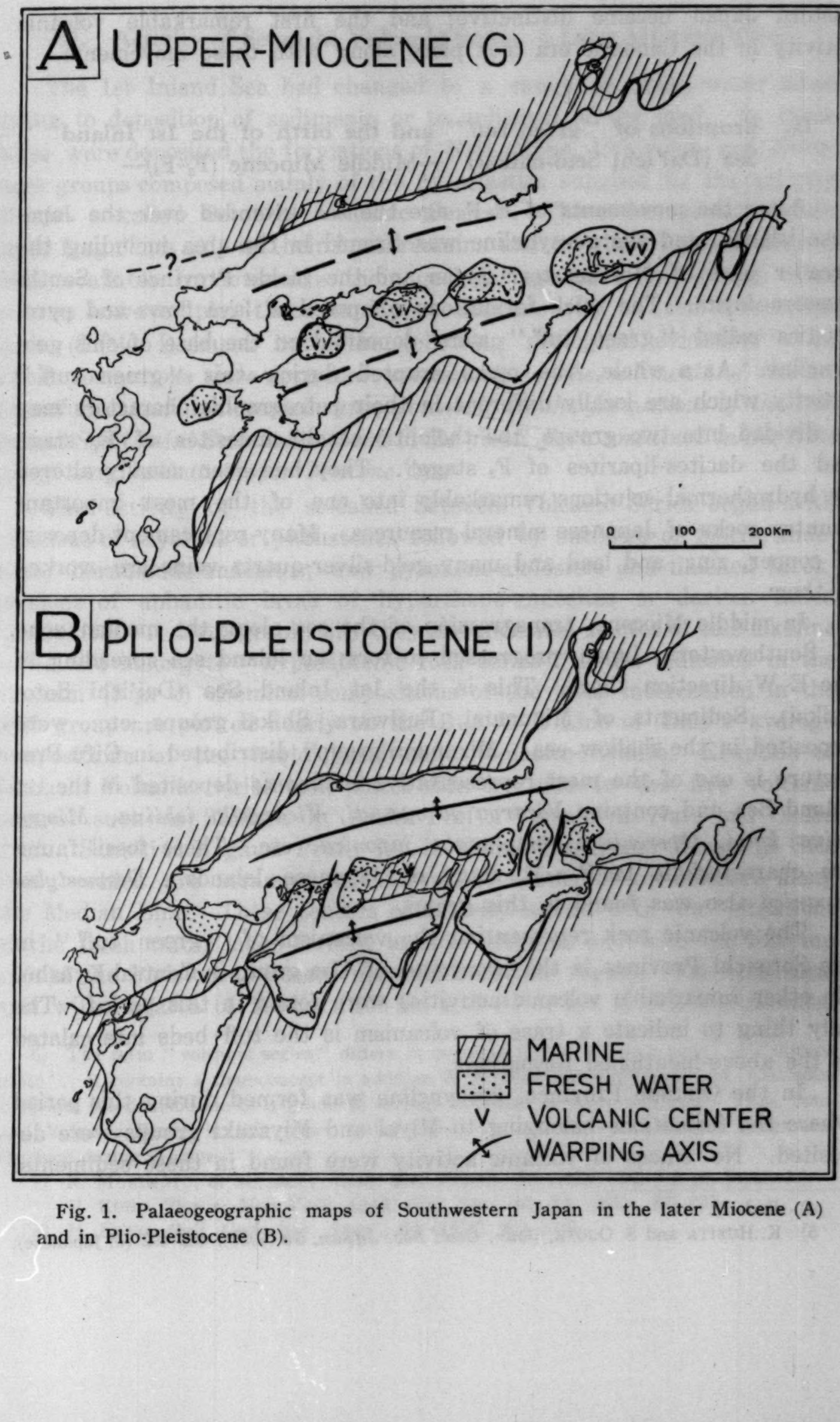

Fig. 1. Palaeogeographic maps of Southwestern Japan in the later Miocene (A) and in Plio-Pleistocene (B).

eastern Japan became distinctive; and the first remarkable volcanic activity in the Cenozoic era took place along with these movements.

II. Eruptions of "green tuff" and the birth of the 1st Inland Sea (Dai'ichi Seto-naikai) —Middle Miocene (F_2–F_3)—

After the movements of E–F_1 age the sea extended over the Japanese islands, and the geosyncline was formed in the area including the greater part of Northeastern Japan and the Inside Province of Southwestern Japan. The thick formations composed of lava flows and pyroclastics called "green tuff" were deposited on the base of this geosyncline. As a whole, the rocks erupted during this "green tuff" activity which are locally different in their petrographic characters may be divided into two groups, the tholeiitic basalts-andesites of F_2 stage and the dacites-liparites of F_3 stage[4]. They had been usually altered by hydrothermal solutions remarkably into one of the most important country rocks of Japanese mineral resources. Many replacement deposits of copper, zinc, and lead and many gold-silver-quartz veins are worked in them.

In middle Miocene, transgression of the sea along the median zone of Southwestern Japan progressed to form an inland sea spreading in the E–W direction there. This is the 1st Inland Sea (Dai'ichi Setonaikai). Sediments of Mizunami, Fujiwara, Shikai groups, etc., were deposited in the shallow sea. Mizunami group[5] distributed in Gifu Prefecture is one of the most representative sediments deposited in the 1st Inland Sea and contains *Vicarya yokoyamai*, *Vicaryella ishiina*, *Miogypsina kotoi*, *Operculina complanata japonica*, etc. These fossil fauna are characteristic to $F_2 \sim F_3$ stage of Japanese Islands. *Desmostylus japanica* also was found in this group.

The volcanic rock representing the volcanism of "green tuff" in the Setouchi Province is the propyrites of Usa group in Central Kyûshû. No other remarkable volcanic activities were found in this period. The only thing to indicate a trace of volcanism is the tuff beds intercalated in the above-mentioned formations.

In the Outside Province, geosyncline was formed during this period where the formations belonging to Miyai and Miyazaki groups were deposited. No traces of volcanic activity were found in these sediments.

4) *Ibid*. 3).
5) K. HUZITA and S. OGOSE, *Jour. Geol. Soc. Japan*, **56** (1950), 482-492 (in Japanese).

III. Activity of Setouchi Volcanic Series —Later Miocene (G)—

The 1st Inland Sea had changed to a range of fresh water lakes owing to deposition of sediments or to upheaval of the land. In these lakes were deposited the formations of Nijô, Kôbe, Uchinomi, and Nozuharu groups composed mainly of the pyroclastics supplied by the activity of the so-called Setouchi Volcanic Series[6]. These formations contain plant fragments only as their fossil remains and no other palaeontological data available to determine their geologic age have been found. The writers however plot them to Upper Miocene (G) on the correlation table (Table I) based upon the following geological evidences[7]: *a) These formations were deposited successively on the sediments of the 1st Inland Sea and are overlain unconformably by the formations of the 2nd Inland Sea (Daini Seto-naikai) and b) the fossil flora contained in the Kôbe group may indicate upper Miocene age.*

The activity of the so-called Setouchi Volcanic Series began with effusions of rhyolites or pitchstones followed by outflows of biotite-andesites, hornblende-andesites, and pyroxene-andesites and finished in extrusions of aphanitic lavas of hyperthene-andesites or dacites called " sanukites ". Petrographically they are andesites-dacites of calc-alkaline series and belong to " hypersthenic rock series "[8]. As indicated in the diagram (Fig. 2) chemical compositions of the lavas intercalated in the Nijô group are plotted nearly on the B–A–D–R Line of Daly's average compositions of the world basalt-andesite-dacite-rhyolite. Eruption of Setouchi Volcanic Series took places side by side in the five volcanic centres such as Shidara in Aichi Pref., Yamato in Nara and Osaka Prefs., Sanuki in Kagawa Pref., Iyo in Ehimé Pref., and Bungo in Oita Pref., which are arranged at intervals of about 100 km distance along the Median Line. These centres of activity accord with the situations of the fresh water lakes formed in later Miocene and with the warping axes of the Pleistocene-Recent movement in this region. The structural unit with an area of 100 km × 100 km and 30–50 km in depth is revealed

6) The term " volcanic series " differs in meaning from " volcanic zone " or " magma series ". It contains a time-concept in addition to geographical distribution of volcanoes. It means the distribution of a group of certain volcanoes in space and time. Thus, Setouchi Volcanic Series in this paper includes only the volcanic rocks erupted in Setouchi Province during G-stage.

7) R. MORIMOTO, et al., *Jour. Geol. Soc. Japan*, **58** (1952), 342–343 (in Japanese).
H. KUNO, *Trans. New York Acad. Sci., Ser.*, [ii], **14** (1952), 225-231.

8) H. KUNO, *Bull. Geol. Soc. Amer.*, **61** (1950), 957–1020.

Table II. Chemical composition of the lavas erupted from Nijô volcano near Osaka in G-stage.*

Constituents	N_1	N_2	N_3	N_4	N_5	N_6	N_7
SiO_2	61.50	61.72	60.19	61.67	64.55	64.58	70.52
Al_2O_3	17.52	19.18	17.29	17.92	16.73	18.05	13.48
Fe_2O_3	0.77	0.53	1.47	0.41	3.04	2.34	1.36
FeO	4.70	4.11	3.77	3.91	1.37	0.73	0.94
MgO	2.74	2.12	2.00	1.52	1.37	0.87	0.58
CaO	5.31	5.59	5.49	4.77	3.88	5.02	2.63
Na_2O	2.22	2.65	3.41	3.00	3.78	2.60	2.08
K_2O	1.88	1.99	1.85	2.42	2.52	2.23	2.94
H_2O (+)	1.96	0.45	2.86	0.87	1.33	0.58	4.27
H_2O (−)	0.37	0.23	0.49	0.53	0.96	1.69	0.98
TiO_2	0.81	0.62	0.70	0.60	0.58	0.53	0.16
P_2O_5	0.20	0.18	0.12	0.18	0.12	0.25	0.18
MnO	0.13	0.10	0.07	0.11	0.08	0.03	0.02
CO_2				1.66			
Total	100.11	99.47	99.71	99.57	100.31	99.50	100.14

* Garnet crystals are spersely contained in all of these lavas.

N_1: Hata-lava, porphyritic hypersthene-andesite.**

N_2: Kasugayama-lava, sanukite, an aphanitic hypersthene-andesite**.

N_3: Kôtoku-lava, sanukite, aphanitic hornblende bearing hypersthene-andesite, Anal. J. Ossaka, Earthquake Research Institute.

N_4: Ishikiriba (quarry)-lava, garnet-biotite-dacite, Anal. S. Tanaka, Earthquake Research Institute.

N_5: Odake-lava, aphanitic hornblende bearing hypersthene-dacite, Anal. J. Ossaka, Earthquake Research Institute.

N_6: Myôjinyama-lava, hornblende bearing hypersthene-plagioliparite**

N_7: Rokuyaji-lava, biotite-pitchstone (Y. KAWANO, *Rep. Geol. Surv. Japan* **134** (1950), 1–29 (in Japanese).)

** The anylyses were performed by Tama Kushida of the Geological Survey of Japan under the auspices of the Earthquake Research Institute for one of the writers (R. Morimoto). He expresses his sincere thanks to Dr. Yoshinori Kawano, Chief of the Geological Department of the Geological Survey of Japan for his kind instructions throughout these analyses by T. Kushida. His sincere thanks are also due to Mr. Joyo Ossaka and Mrs. Tama K. Suyama for their elaborate chemical analyses.

in the recent crustal deformation and seismic activities in this region[9].

The Inside Zone subsided greatly in the later Miocene to deposit thick strata of black shale in its basin and was in a comparatively calm state, though there occurred eruptions of andesites and deposition of

9) H. KAWASUMI and Y. SATÔ, *Spec. Bull. Earthq. Res. Inst.*, **5** (1947), 1–36 (in Japapese).

Table III. Chemical composition of some lavas from Muroo volcano, Mt. Mikasa, Central Kinki District, and from minor volcanic bodies near Osaka.

Constituents	M_1	M_2	M_3	S_1	S_2	S_3	S_4
SiO_2	72.55	71.15	57.42	51.72	52.40	57.24	64.02
Al_2O_3	13.17	13.03	16.79	15.71	16.94	15.31	15.42
Fe_2O_3	1.84	1.15	2.10	2.15	2.23	1.82	1.78
FeO	0.88	1.43	5.22	5.65	5.55	4.81	2.43
MgO	0.61	0.53	4.49	9.89	7.65	7.52	4.45
CaO	1.19	1.28	6.39	7.86	7.69	5.71	2.93
Na_2O	2.87	3.28	2.96	2.74	2.45	2.91	3.45
K_2O	3.97	4.23	2.18	0.79	1.15	1.46	2.57
H_2O (+)	1.48	2.63	1.65	2.30	1.06	1.76	2.32
H_2O (−)	0.97	0.32	0.36	0.85	1.05	0.39	0.38
TiO_2	0.24	0.27	0.73	0.58	1.01	0.54	0.42
P_2O_5	0.10	0.17	0.04	0.07	0.16	0.18	0.04
MnO	0.05	0.05	0.11	0.14	0.15	0.11	0.09
Total	99.92	99.52	100.44	100.45	99.49	99.76	100.30

M_1: Hypersthene-biotite-liparite from Kôchikei, Muroo, Mie Pref., Anal. J. Ossaka, Earthquake Research Institute.

M_2: Hypersthene-biotite-liparite from Hayama, Tsugeno, Nara Pref., Anal. J. Ossaka, Earthquake Research Institute.

M_3: Augite-hypersthene-andesite from Mt. Mikasa, Nara, Anal. J. Ossaka, Earthquake Research Institute.

S_1: Augite-olinine-basalt from Mt. Shigi, Nara Pref., Anal. J. Ossaka, Earthquake Research Institute.

S_2: Olivine-augite-basaltic andesite, Shibayama, Kokubu, Osaka Pref., Anal. T. Kushida, Geological Survey of Japan**.

S_3: Olivine augite-hypersthene-andesite from Shionomiya near Nagano, Osaka Pref., Anal. J. Ossaka, Earthquake Research Institute.

S_4: Biotite-quartz-hypersthene-andesite, a hybrid rock, from Terayama, Minamikawachi, Osaka Pref., Anal. J. Ossaka, Earthquake Research Institute.

the pyroclastic sediments such as Omori group[10]. These volcanic rocks also are of hypersthenic rock series as those of Setouchi Volcanic Series.

IV. Period of peneplanation —Pliocene (H)—

The Miocene sea had regressed from the Inside and Outside provinces in Pliocene age and left there local sedimentary basins. The 1st Inland Sea also had quite disappeared; deposits of the 1st Inland Sea were eroded with the basal granitic rocks to form peneplains. An event

10) T. TOMITA and E. SAKAI, *Jour. Geol. Soc. Japan*, **45** (1938), 529-531 (in Japanese).

of this age were the eruptions of Muroo welded tuff that took place on the Central Kinki District and covered an area of about 28 *km* in EW and 15 *km* in NS. The Muroo volcanic rocks are a little alkaline plagioliparite sometimes containing anorthoclasses (Table II).

In the Outside Province, Kumano Acidic Rocks intruding into Miyai group (F_2–F_3) are notifiable. The liparites containing potash felspar played an important rôle in its activity and formed welded tuff locally. Eruptions of the acidic rocks may be considered to have taken places probably in late Miocene or in Pliocene.

In the Inside Province, sediments of Pliocene are locally distributed such as Himi group in Toyama Pref., Matsue formation in Shimané Pref., etc. Eruptions of alkaline olivine-basalts, trachytes, alkaline rhyolites took places on Oki island in this age[11]. Trachyandesites and a little alkaline liparites extruded from the coast of San'in District[12].

V. Appearance of the 2nd Inland Sea —Plio-Pleistocene (I)—

Present shape of Japanese islands were formed in this stage. In the Setouchi Province, the 2nd Inland Sea (Daini-Seto-naikai) was widely extensive including the present Inland Sea, Central Kinki, and Central Kyûshû. Formations of Osaka, Akashi, Oita groups, etc., are the deposits in the Sea. *Metasequoia*, *Glyptostrobus*, *Liquidambar*, etc.,[13] are found in the lower portion of these formations (I_1) with *Stegodon akashiensis*. *Stegodon orientalis*, *Elephas naumanni*, etc., are found in the upper portion (I_2). As the volcanic rocks related to this stage, some of the Tsukushi lavas in Central Kyûshû[14], Kankakei lavas of Shôdo island, Kagawa Pref.[15], and pyroxene-andesites of Mt. Mikasa, Nara Pref.[16], may be pointed out. In association with these andesites, olivine-basalts or dolerites are found. The basalts and its derivatives are distinctive in composition from those of upper Miocene (Fig. 2 and Table III).

VI. Volcanoe of San'in and Ryûkyû Volcanic Zones —Pleistocene (J) to Recent (K)—

The present Inland Sea had retired from the drama of volcanism and Central Kyûshû appeared on the stage instead the former. In Pleisto-

11) T. TOMITA, *Jour. Shanghai Sci. Inst.*, **11** (1933), 37–146.
12) M. MUKAE, *Jour. Sci. Hiroshima Univ., Series C.*, **1** (1954), 51–60.
13) K. HUZITA, *Jour. Polytechnics Osaka City Univ., Ser. G*, **2** (1954), 75-85.
14) GEOLOGICAL SURVEY OF JAPAN, 1:500,000 Geological Map "Fukuoka" (1951).
15) GEOLOGICAL SURVEY OF JAPAN, 1:75,000 Geological Map "Saidaiji" (1934).
16) S. KOKAWA, *Jour. Geol. Soc. Japan*, **60** (1954), 487–493 (in Japanese).

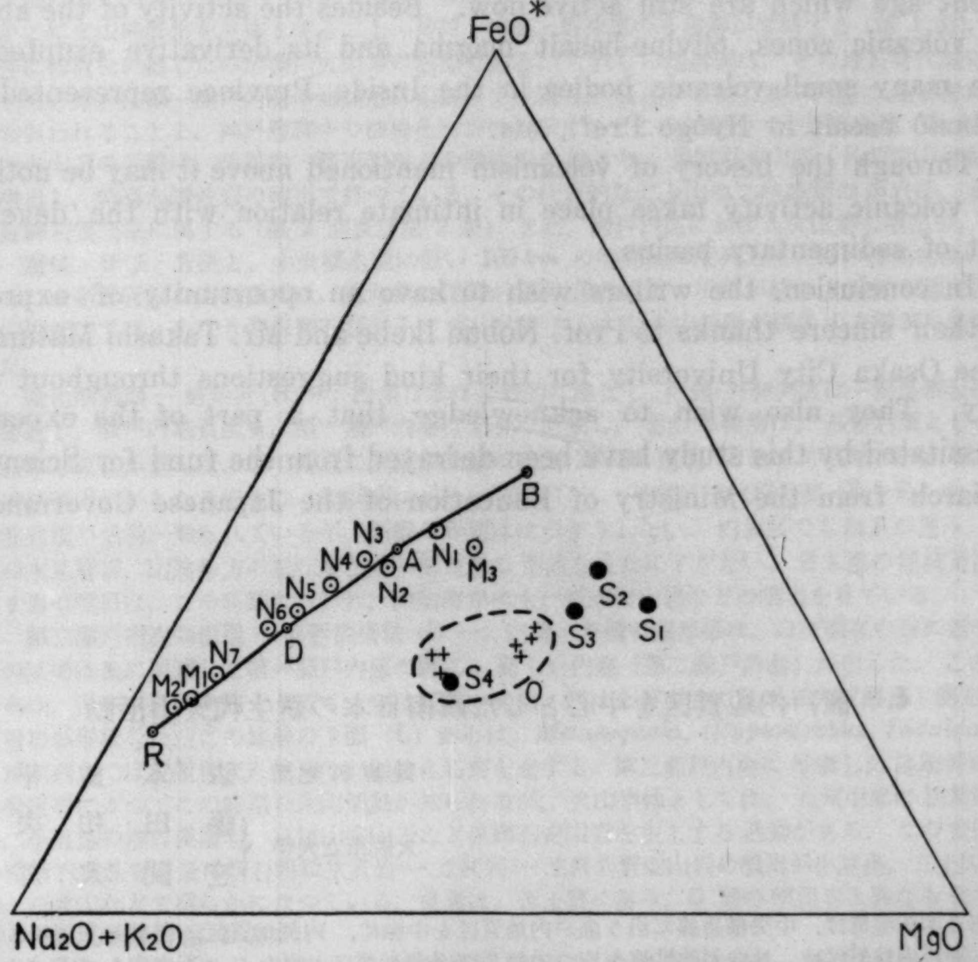

Fig. 2. FeO-MgO-Alkalis ratio of some lavas from the Setouchi Geologic Province. N_1–N_7: Lavas erupted from Nijô volcano in G-stage, M_1–M_2: Liparites from Muroo volcano, M_3: Pyroxene-andesite from Mt. Mikasa, S_1–S_4: Basalts and andesites erupted from the minor volcanic bodies near Osaka in I-stage, +plotted in the area O surrounded by a broken line: Andesites from Otozan, Shôdoshima, Kagawa Pref. (M. YAMAGUCHI, *Sci. Rep. Geol. Inst. Kyushu Univ.* **3** (1951), 105–126 (in Japanese).), FeO*: Total iron oxides, sesquioxide being recalculated as ferrous oxide and added.

cene, Futagoyama, Unzen, Yufu, etc., in Central Kyûshû and Daisen, Sanbe, Aonoyama, etc., in the Chûgoku District were formed. Main activity of these volcanoes belonging to San'in or Daisen Volcanic Series[17)] was following by the activity of the volcanoes of the Ryûkyû Zone; somma volcanoes of the great calderas began to outbreak[18)]. After remarkable collapse-calderas formation characterized by extensive welded tuff distribution around them, central cones were formed in them in

17) T. KASAMA, *Jour. Polytech. Osaka City Univ.*, **1** (1954), 59-67.
18) T. MATSUMOTO, *Jap. Jour. Geol. Geogr.*, **19** (1943), Special Number.

Recent age which are still active now. Besides the activity of the above two volcanic zones, olivine-basalt magma and its derivative erupted to form many small volcanic bodies in the Inside Province represented by Genbudô basalt in Hyôgo Pref., etc.

Through the history of volcanism mentioned above it may be noticed that volcanic activity takes place in intimate relation with the development of sedimentary basins.

In conclusion, the writers wish to have an opportunity of expressing their sincere thanks to Prof. Nobuo Ikebe and Mr. Takashi Matumoto of the Osaka City University for their kind suggestions throughout this study. They also wish to acknowledge that a part of the expenses necessitated by this study have been defrayed from the fund for Scientific Research from the Ministry of Education of the Japanese Government.

---

4. 瀬戸内地質区を中心とした西南日本の新生代火山活動

地震研究所　森 本 良 平
大阪市立大学 { 藤 田 和 夫
　　　　　　　 笠 間 太 郎

西南日本新生界は，中央構造線に沿う瀬戸内地質区を中軸に，内側地質区，外側地質区に三分される．瀬戸内地質区は，地向斜的性格を持つ内側及び外側地質区と異なり．不安定な内海または淡水湖に形成された堆積区で，地層の不連続と岩相変化の著しいこととにより，これまで地層の対比が充分に行われなかつた．筆者らは 1950 年以来，瀬戸内地域の火山層序学的研究を進め，堆積盆地の形成発達の経過と新生代火山活動の時代的変遷を調べたので，ここに瀬戸内区の火山活動と地史を中心に西南日本新生代火山活動史の概略を述べることにする．

1. 古第三紀末の地殻変動と初期の火山活動 — 漸新世 (E) ～ 中新世期 (F_1) —： 日本列島全域が著しい変動を受け，日本海・フォッサ・マグナが形成され，東北日本・西南日本の構造区分が明らかになつた．最近，北陸地方の Lithoidite-nevadaite-association からなる太美山層群がこの時期のものであることが明らかにされた．西南日本では中国脊梁山地の石英粗面岩・石英斑岩の大部分，東北日本ではグリン・タフの基底をなす anorthoclase-liparite などがこの期のもので，酸性岩で特徴づけられる．太美山期の火山岩類・火山砕屑岩は，構造上，以後の新第三系の基盤をなしている．

2. グリン・タフ期と第一瀬戸内海の形成 —中新世中期 (F_2-F_3)—：大変動後の広汎な海侵により東北日本の大半と西南日本の内側に形成された一連の地向斜に，グリン・タフといわれる熔岩流及び砕屑物からなる厚層が累積する．西南日本中軸には東西に伸びた内海「第一瀬戸内海」が形成され，瑞浪・藤原・四海層群など浅海性の地層群が堆積する．瀬戸内区のグリン・タフ期の火山活動としては，九州中部の変朽安山岩からなる宇佐層群がある以外に，顕著な活動はなく，前記の地層群に含まれる凝灰岩に，わづかに火山活動の余波が窺われるだけである．第一瀬戸内海を代表する瑞浪層群に産する *Vicarya yokoyamai, Vicaryella ishiiana, Miogypsina kotoi, Opeculina complanata japonica* などのが，この時期の特徴的な化石群である．外側区では，この時期に地向斜性の宮井層群・宮崎層群が沈積し，火山活動は知られていない．

3. 瀬戸内火山系の活動 — 中新世後期 (G) —: 第一瀬戸内海は，東西に配列する淡水湖列となり，そこに火山砕屑物を主体とする二上・神戸・内海・野津原の各層群が堆積する (第 1 図). この地層群に物質を供給したのが瀬戸火山系の活動である. これらの地層群は，その地質時代論に問題を残していたが，第一瀬戸内海の海成層に引続いて堆積し，後述する第二瀬戸内海の地層群に不整合におおわれることと，神戸層群中の植物化石群の指示するところに従つて中新世後期 (G) とした. 瀬戸内火山系の活動は，流紋岩・瀝青岩などの酸性岩に始まり，黒雲母安山岩・角閃安山岩を引続いて噴出し，特異な讃岐岩の噴出で終つている. その代表的な二上山のこの時期の熔岩は，典型的な紫蘇輝石質岩系に属する (第 2 図及び第 2 表). また，瀬戸内区における火山群の噴出が，設楽・大和・讃岐・伊予・豊後と，中央構造線に沿い 100 *km* の等間隔に配列しているのは興味深い点である. 中新世後期の内側区では，地向斜の沈降が進み黒色頁岩の堆積が続き比較的平穏であつたが，山陰地方では，やはり紫蘇輝石質岩系の安山岩を主とする火山活動が続き大森層群に物質を供給した.

4. 陸化削剥期 — 鮮新世 (H) —: 西南日本は全般的に陸化し，内側・外側両区は一部堆積盆地を残して海退し，瀬戸内地質区も，第一瀬戸内海は完全に消滅し，その堆積物は，基盤岩類とともに削剥され準平原化が進んだ. この時期に近畿中央部に東西 28 km 南北 15 km の広域にわたる，大部分が熔結凝灰岩からなる室生の **plagioliparite** が噴出した. 外側区では宮井層 (F_2-F_3) を貫く熊野酸性岩類の活動が知られているが，活動の時期ははつきりしない. 内側区でも海退が進み，北陸地方の氷見層群，山陰地方の松江層など一部地層の形成を見たにすぎない. 日本海の隠岐道後のアルカリ岩の噴出は，この時期に行われ，山陰海岸にも，粗面安山岩などの噴出を見ている.

5. 第二瀬戸内海の出現 — 鮮新洪積世 (I) —: 内側・外側の海岸線は，ほぼ現在の形に近づき，瀬戸内区では先に消滅した第一瀬戸内海の跡に，新しい内海「第二瀬戸内海」が生じた. この内海の分布は，現在の瀬戸内海より広く，東は近畿中央部，西は九州にまで及び，大阪層群・明石層群・大分層群が堆積した. この地層の下部 (I_1) からは，***Metasequoia, Glyptostrobus, Liquidambar*** など日本列島では鮮新世末に絶滅した植物化石群を産する. 第二瀬戸内海に堆積した地層群に夾在する凝灰岩によつてこの時期の火山活動が知られるが，火山岩体としては，九州中部の筑紫熔岩の一部，小豆島の寒霞渓熔岩，三笠山安山岩など複輝石安山岩を主とする活動がある. この安山岩に伴い橄欖石斑晶を多量に含む粗粒玄武岩 — 玄武岩 — 玄武岩質安山岩の噴出が小豆島，二上山近傍，鍋山，三笠山などで明らかになつている. 後者は，苦土質に富み，G 期の噴出岩と異なる化学成分を示す (第 2 図及び第 3 表).

6. そのごの火山活動 — 洪積世 (J) ～沖積世 (K) —: 洪積世に入つて，瀬戸内区の西端に当る九州中部に，両子・由布・雲仙などの諸火山が噴出し，角閃安山岩からなる円頂丘を形成した. この火山列の延長は，本州を縦走して山陰に至り，三瓶・青野・大山など「山陰 (大山) 火山系」に属する一連の火山を噴出している. ついで九州中部では，山陰系火山の活動に引続き，阿蘇・恰良・阿多・鬼介の大規模なカルデラの形成，それにつぐ現在の中央火口丘群の噴出，琉球弧北側に分布する活火山群の活動を見るに至る. 山陰・琉球の二つの火山系のほかに，西南日本内側では玄武洞を典型とする玄武岩質岩石の小火山丘が，山陰から北九州にかけて形成されている. 以上の西南日本における新生代火山活動の推移を見れば，堆積盆地の形成と密接な関連を以つて火山活動が行われていることが知られる.

---

5. *Some Geological Considerations of the Neogene Sediments Exposed at the Western Margin of the Yamagata Basin.*

By Takeshi ICHIMURA and Kazuko AOKI,

Yamagata University.

(Read Nov. 27, 1956.—Received Nov. 27, 1956.)

Introduction

Neogene sediments are largely exposed on the hilly land adjacent to the western margin of the Yamagata Basin, extending northwards or southwards to other districts and disappearing beneath the lava flows, agglomerates and mud flows of the Hayama Volcano and Shirataka Volcano.

These sediments have very complicated features in stratigraphy and geological structure. They have already been investigated by Y. Funayama[1] and others[2] in connection with the possibilities of oil resources in this area.

The sediments exposed here, however, have been almost entirely neglected as regards the determination of mineral compositions and rock-fragments contained in them, although it is very necessary from such various geological standpoints as sedimentation, source, igneous activity, etc. For this purpose, the field and laboratory works of sedimentary petrology on these sediments were recently started by the writers[3].

To examine mineral components, many speciments were collected from different horizons of the sediments distributed at the area interposed between the Yamagata Basin and the Mogami-gawa. Such specimens are mostly represented by tuffaceous and pumiceous sediments. They were mechanically analysed respectively, and their thin sections were closely examined. The results of this investigation indicate that they

1) Y. FUNAYAMA and S. TAKAHASHI, *Bull. Geol. Surv. Japan*, **3** (1952), 1–9.

2) T. ICHIMURA, S. MINAKAWA and O. YAMAGATA, *Jour. Geol. Soc. Japan*, **61** (1955), 357.

3) T. ICHIMURA, *Jour. Geol. Soc. Japan*, **61** (1955), 354.
K. AOKI, Graduation Theisis, *Inst. Earth Sc. Fac. Educ. Yamagata Univ.*, (*M.S.*), (1956).

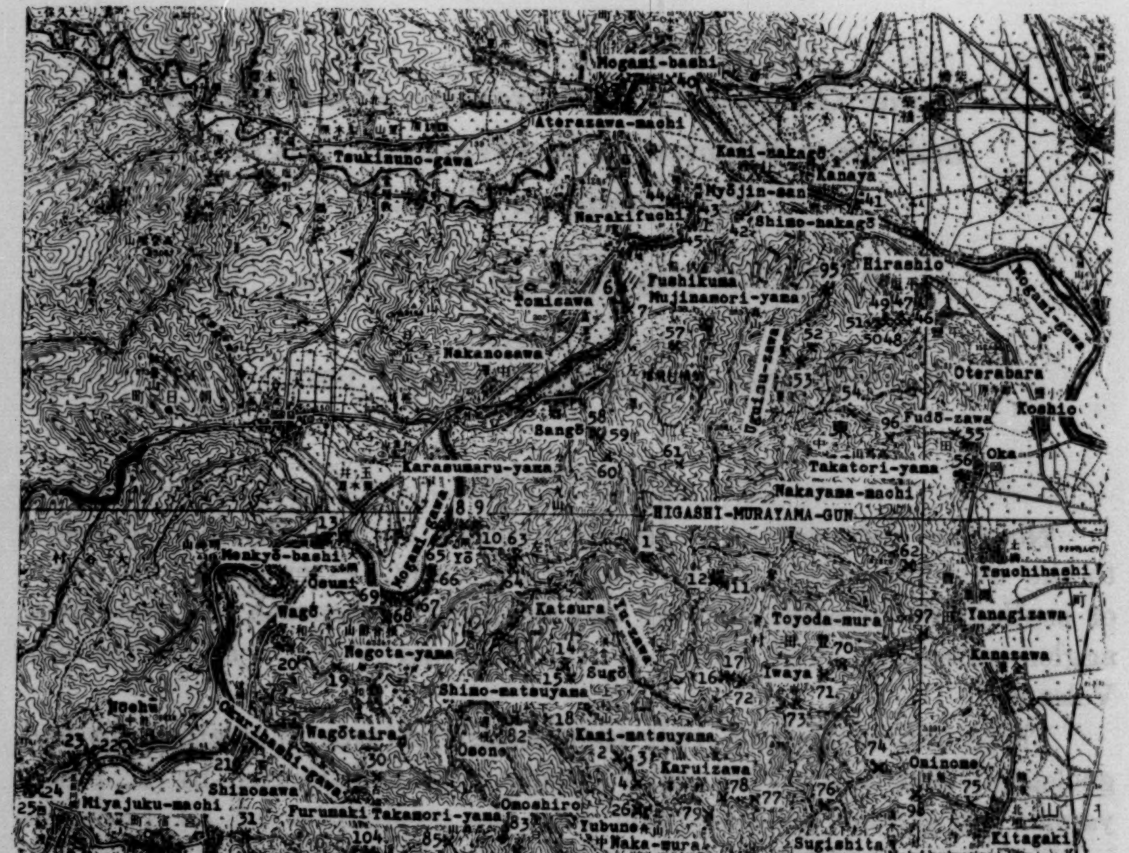

Fig. 1. Map showing the location where the specimens of sandy or tuffaceous rocks were collected.

are rich in the minerals and rock-fragments supplied from various sources, particularly from the intrusive and extrusive rocks, suggesting that igneous activities took place repeatedly during and prior to the deposition of Neogene sediments.

General Features of Topography and Geology

The area is situated between the Yamagata Basin and the Mogami-gawa, including the hilly land which extends from Aterazawa to Yamanobe and Miyajuku. It is easy of access from Yamagata through several bus roads and the Aterazawa Railway Line.

The hilly land here is more or less elevated at its central part, but is gradually descends towards the Yamagata Basin and the Mogami-gawa, being complicatedly dissected by the Uguisu-zawa, Yu-zawa, Okurihashi-gawa, etc. It is generally 300–400 meters high above sea-level and is frequently fringed by terraces along the Mogami-gawa. The southern end of this area is, on the other hand, bordered by the Shirataka Volcano which rises up to 922 meters above sea-level at the highest point (Fig. 1).

The hilly land under consideration is built up of Neogene sediments and overlying volcanics as well as Quaternary fluvial deposits (Figs. 2–3). Among them, Neogene sediments are mainly composed of tuff, tuffaceous sandstone, shale, mudstone, siltstone and conglomerate. Such

Table I. Succession of Neogene sediments exposed near the Yamagata Basin.

Groups	Formations	Thickness	Shinjō Basin Katō & Taguchi (1950)
Sagae Group	Omi Formation	45 m.	Yamuke Formation
	Inazawa Formation	200–300 m.	Sakekawa Formation
	Ōya Formation	200–250 m. +	
Murayama Group	Hongō Formation	100–240 m.	Mitsumori Formation
	Hashigami Formation	130–220 m.	
	Mazawa Formation	30–150 m.	Furukuchi Formation
	Tsunatori Formation	25–130 m.	
	Mizusawa Formation	250–520 m. +	Kusanagi Formation
	Tsukioka Formation	600 m.	
Yamagata Group	Hodōji Formation	50–300 m. +	Kaneyama Formation
	Ōisawa Formation	180 m. +	

(in descending order)

sediments laterally pass into one another, resulting in the different facies even in the same formation. Stratigraphically, they can be correlated with the upper half of the Neogene sediments in the adjoining district where the preceeding classification has been tried by S. Minakawa and O. Yamagata[4] in 1955 (Table I).

So far as is known at present, the sediments exposed in the field of the writers are represented by the Inazawa Formation (100 m. −), Nakanosawa Formation (50–200 m. +), Hashigami Formation (170–200 m. +), Mazawa Formation (150 m. +) and Tsunatori Formation (30–60 m. +). These formations gradually pass into one another and indicate different lithological characters changing from place to place. Moreover, the sediments here are usually tuffaceous and frequently pumiceous, although there are some formations rich in shale or mudstone.

The oldest sediments of this area are dark grey shale, tuffaceous sandstone and tuff of the Tsunatori Formation exposed mainly on the cutting near the Yoshizawa Bridge connecting Jōmyōji and Yoshizawa. The shale bed here is frequently intercalated with a coarse tuffaceous sandstone and contains many concretions at its lower horizon. It passes downwards into tuff or tuffaceous sandstone mottled with green spots. Such sediments are also to be seen along the Uguisu-zawa or elsewhere.

The Mazawa Formation is traceable from north to south at the eastern periphery and western half of this area, being extensively exposed in connection with the Tsunatori Formation and Hashigami Formation. It is characterized by the predominance of shale and siltstone of a dark grey color, but there is a gradual increase of tuff or tuffaceous sandstone as it approaches the Tsunatori Formation. In these cases, the formation of the eastern periphery extends from Hirashio to Tsubuteishi southwards, passing Oterabara, Takatori-yama, Yanagizawa, Oninome, Makibukuro, Sugishita, Shirasaka, Takinohira and Uwadaira.

One of the remarkable features indicated by the lower half of this formation is the frequent occurrence of fairly indurated shale of a dark grey color. This kind of shale is well exposed along the truck road between Jōmyōji and Yoshizawa or Takinohira, where it is found together with coarse sandstone. The similar shale is also seen at Yanagizawa and Shirasaka as well as at the lower course of the Uguisu-zawa.

The upper half is, on the other hand, composed of common black shale or siltstone and grades to the Hashigami Formation with an increase of tuff or tuffaceous sandstone.

4) T. ICHIMURA, S. MINAKAWA and O. YAMAGATA, *op*. cit., (1955), 357.

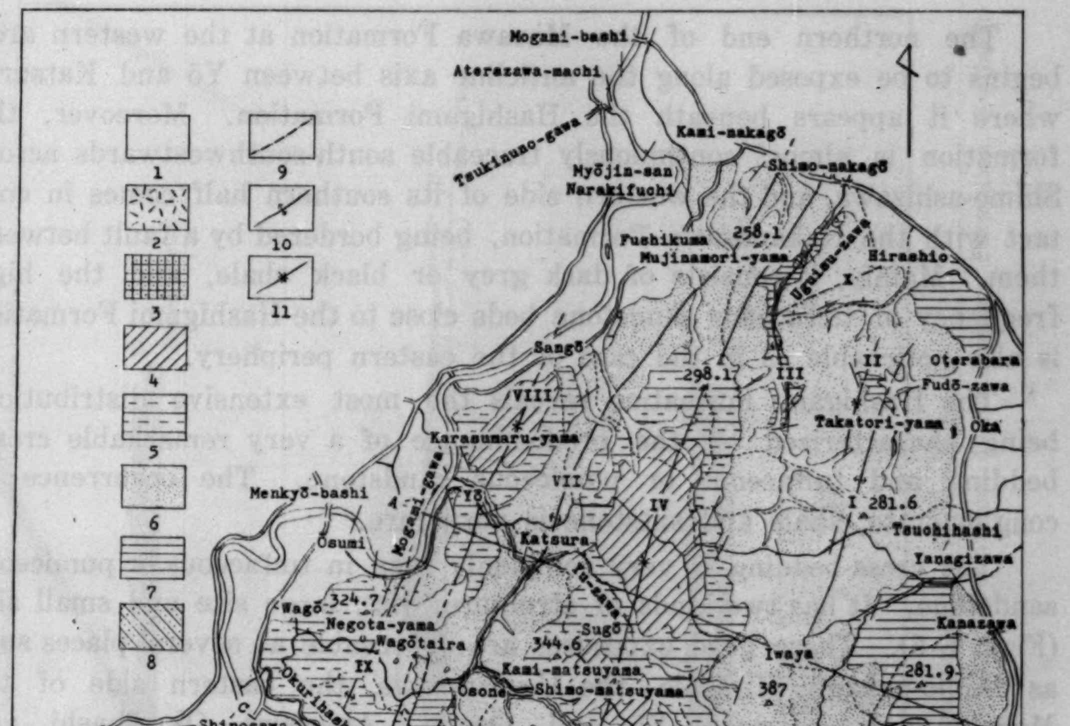

Fig. 2. Geological map of the hilly land adjacent to the western margin of the Yamagata Basin.

1=Quaternary sediments, 2=Mud flows of the Shirataka Volcano, 3=Lava flows of the Shirataka Volcano, 4=Inazawa Formation, 5=Nakanosawa Formation, 6=Hashigami Formation, 7=Mazawa Formation, 8=Tsunatori Formation, 9=Fault, 10=Anticlinal axes, 11=Synclinal axes, I=Takatori-yama anticline, II=Takatori-yama syncline, III=Uguisu-zawa anticline, IV=Kami-matsuyama syncline, V=Omoshiro anticline, VI=Takamori-yama syncline, VII=Okurihashi anticline, VIII=Karasumaru-yama syncline, IX=Negota-yama anticline, X=Hirashio fault, XI=Yoshizawa fault, XII=Shimo-ashizawa fault.

The northern end of the Mazawa Formation at the western area begins to be exposed along the anticline axis between Yō and Katsura, where it appears beneath the Hashigami Formation. Moreover, the formation is almost continuously traceable south-southwestwards across Shimo-ashizawa, and the western side of its southern half comes in contact with the Nakanosawa Formation, being bordered by a fault between them. Mainly, it consists of dark grey or black shale, and the high frequency of tuffaceous sandstone beds close to the Hashigami Formation is also noticeable as in the case of the eastern periphery.

The Hashigami Formation reveals the most extensive distribution, being characterized by the predominance of a very remarkable cross-bedding and tuffaceous or pumiceous sandstone. The occurrence of conglomerate, shale and siltstone is very rare.

The cross-bedding is very commonly seen in tuffaceous or pumiceous sandstone. It has two kinds of structure, viz., large size and small size (Figs. 5–6). These good exposures are observable at several places such as Shimo-nakagō, Hirashio—the Uguisu-zawa, the eastern side of the Mogami-gawa between Yō and Ōsumi, Ainosawa—Okurihashi and Yubune—Omoshiro or elsewhere.

The most remarkable cross-bedding is always found at the transition stage to the Nakanosawa Formation. It is coarsely and distinctly bedded with an alternation of hard and soft bands, being exposed at Mogami-bashi, Myōjin-yama, Narakifuchi, Iwaya, Ainosawa, Ōwarabi and Shimo-ashizawa—Tateno (Fig. 5).

The Hashigami Formation mentioned above indicates some anomalies at the area surrounding Hirashio, where it is occasionally tuffaceous and massive conspicuously without any noticeable cross-bedding. This formation was formerly named "Hirashio Formation"[5] in which tuff and tuffaceous sandstone is rich in angular fragments, large or small, of hard shale, black shale and siliceous liparite as well as in such minerals as hypersthene and augite. It is also noteworthy that some violent disturbance due to a submarine eruption seems to have taken place during the deposition of these sediments.

In the Hashigami Formation, conglomerate or conglomeratic sandstone is found close to the Nakanosawa Formation and contains such kinds of pebbles as liparite, felsophyre, felsite, dolerite, basalt, green tuff, shale, etc.

5) Y. FUNAYAMA and S. TAKAHASHI, *op. cit.*, 5.

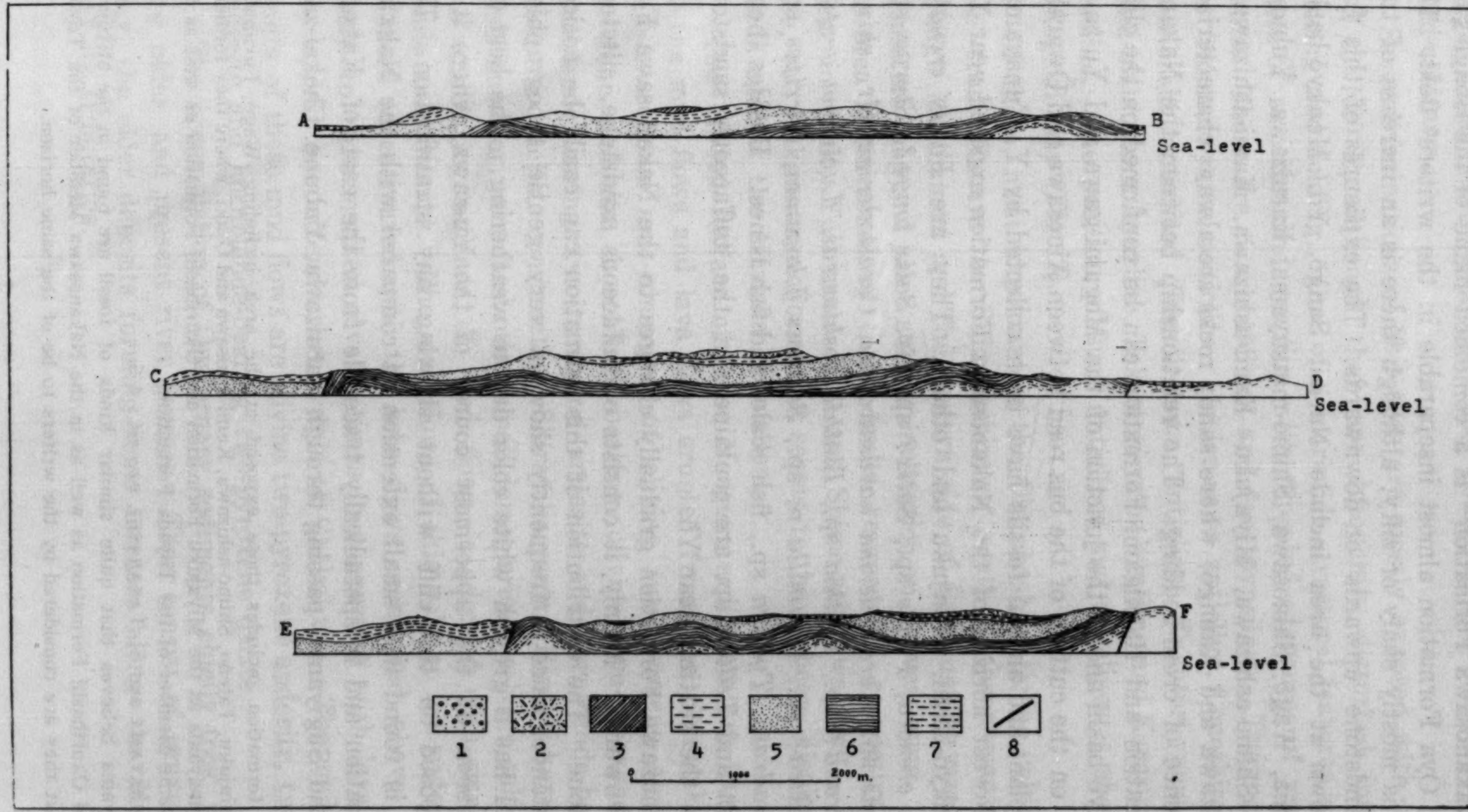

Fig. 3. Geological profile of the hilly land adjacent to the western margin of the Yamagata Basin.
1=Quaternary sediments, 2=Mud flows of the Shirataka Volcano, 3=Inazawa Formation, 4=Nakanosawa Formation, 5=Hashigami Formation, 6=Mazawa Formation, 7=Tsunatori Formation, 8=Fault.

The Nakanosawa Formation[6] is a combined name of the Hongō Formation and Ōya Formation almost inseparable in the writers' field. The formation is mostly shaly or silty, although there is an increase of tuffaceous sandstone upwards or downwards. The exposures of this formation known at the area include Nariai, Sangō, Yō, Menkyō-bashi, Negota-yama, Wagō, Shinosawa, Shimo-matsuyama, Karuizawa, Yubune, Miyajuku—Shimo-ashizawa, Miyajuku—Kami-ashizawa, Kami-ashizawa—Shimo-ashizawa and Kamigō, where sandy rocks are always characterized by the absence of cross-bedding. The relationship between the Nakanosawa Formation and Hashigami Formation can be confirmed on the cliffs near Menkyō-bashi and at the junction of the Mogami-gawa and Yu-zawa as well as on the cutting of the bus road between Ainosawa and Ōwarabi.

Some plant and animal fossils have been collected by Y. Funayama[7] from the lowest horizon of the Nakanosawa Formation exposed near Yō, Sugō, Menkyō-bashi, Shinjuku and others. They are *Fagus crenata*, *Fagus* cfr. *crenata*, *Fagus* sp., *Salix?* sp. cfr. *Salix longa?*, *Styrax* sp., *Ancistrolepis* sp., *Cerastoderma narusawaense*, *Cerastoderma* cfr. *shinjiense*, *Gastrana?* sp., *Linthia* sp., *Linthia yoshiwarai*, *Lucinoma acutiliformis*, *Natica?* sp., *Potamilla* n. sp., *Serripes yokoyamai*, *Serripes* sp., *Tyasira quadrata*, *Tyasira* sp., fish scales and fish bones. Besides these, *Calcharodon* and *Tellina* sp. are contained in the tuffaceous sandstone exposed on the cutting near Yō.

The Inazawa Formation gradually changes to the Nakanosawa Formation downwards. Mainly, it consists of tuffaceous sandstone, siltstone and mudstone. The distribution of this formation can easily be noticed from a distance, since it frequently shows a very gentle topographical feature and has a greyish white color due to weathering. The best exposure is seen at the uppermost course of the Yu-zawa, where it is largely exposed on the cliff without showing any stratification. The formation is found in a small extension as compared with the Nakanosawa Formation and is sporadically traceable from the east of Katsura to Ōtaki and Sugiyama, passing through Karuizawa, Yubune, Chōkai-zan,

6) This formation includes those exposed at the area including Wagō, Furumaki, Shinosawa, Shinjuku, Tateno, Shimo-ashizawa, Kami-ashisawa and Ōtaki, where they formerly mapped by Funayama as the Miyajuku Formation and Okurihashi Formation as well as the Shimo-matsuyama Member of the Toyoda Formation.

7) Y. FUNAYAMA and S. TAKAHASHI, *op. cit.*, 4–5.

Funayama believes that quite similar kinds of fossil are found in the Miyajuku Formation and Okurihashi Formation as well as in the Nakanosawa Member of the Toyoda Formation, but they are considered by the writers to be of the same horizon.

Sangō, Karasumaru-yama, the upper course of the Okurihashi-gawa and Kami-ashizawa.

Several formations of this area are mostly exposed with a strike of N–S to N30°E, although they are frequently disturbed intensely by faulting and folding. One of remarkable structural features is the abundance of anticline and syncline with repeated exposures of various sediments. There are five anticlines and four synclines. They are named the Takatori-yama anticline, Uguisu-zawa anticline, Omoshiro anticline, Okurihashi anticline, Negota-yama anticline, Takatori-yama syncline, Kami-matsuyama syncline, Takamori-yama syncline and Karasumaru-yama syncline. The position of such anticlines and synclines is shown in the geological map (Fig. 2).

Of these, most important is the Okurihashi anticline, which is traceable from Kanaya to Shimo-ashizawa south-southwestwards, passing through Mujinamori and the eastern side of Karasumaru-yama. It is 10 kilometers long and has a steeper inclination on its west-wing. Moreover, the area is traversed by three faults represented respectively by the Hirashio fault, Yoshizawa fault and Shimo-ashizawa fault. In the last case, the Nakanosawa Formation seems to have been displaced downwards against the Mazawa Formation.

The eroded surface of these Neogene sediments are partly covered by the mud flows and lava flows erupted from the Shirataka Volcano. The lava flows are composed of olivine two-pyroxene andesite, two-pyroxene andesite, hornblende-bearing olivine·two-pyroxene andesite, hornblende-bearing two-pyroxene andesite and hornblende-bearing two-pyroxene dacite, constructing Shirataka-yama, Higashi-kuromori-yama, Nishi-kuromori-yama and other small domes around a large caldera, where the undulating surface of mud flows is adorned with small beautiful ponds and swamps. The mud flows of this volcano are extensively distributed as compared with the lava flows mentioned above. They are likely to have erupted several times in connection with lava flows, and the largest one extends northwards to Chōkai-zan. The andesite fragments of these mud flows are olivine two-pyroxene andesite, two-pyroxene andesite and hornblende-bearing two-pyroxene dacite.

The accumulation of Quaternary sediments chiefly took place along the older and present river courses. They consist of gravel, sand and clay, the older deposits forming some terraces along the Mogami-gawa and its tributaries.

Lithological Characters of Neogene Sediments

As has already been stated, Neogene sediments of this area include several formations ranging from the Tsunatori Formation up to the Inazawa Formation. Most of these formations are characterized by the high frequency of tuffaceous rocks, although such formations as the Mazawa Formation and Nakanosawa Formation are partly composed of shale, mudstone and siltstone. It, therefore, suggests that there were repeated igneous activities during and prior to the deposition of Neogene sediments. In this case, the tuffaceous rock is mostly represented by tuff and tuffaceous sandstone associated closesely with non-tuffaceous sandstone, conglomeratic sandstone and conglomerate, being sometimes intercalated with shale, mudstone and siltstone.

Of these, tuff, tuffaceous sandstone and non-tuffaceous sandstone have been selected for sedimentary petrography, because they contain mineral components and rock-fragments that can be easily examined under the microscope. Exclusive of some heavy components, nearly the same kinds of minerals are found in each formation together with angular or subangular pieces of granite, plagioliparite (rhyolite), perlite, granophyre, felsite, felsophyre, dacite, andesite, propylite, basalt, green tuff, pumice and shale. They are summarized as follows.

(1) Tsunatori Formation:—The mineral components in the tuff and tuffaceous sandstone of this formation are quartz, orthoclase, plagioclase, biotite, glauconite, allanite, cordierite, garnet, actinolite, green hornblende, hypersthene, ilmenite, limonite, magnetite, tourmaline and pink zircon. Green hornblende is, however, very scarce as compared with the tuffaceous or non-tuffaceous sandstone of the Hashigami Formation. These minerals are intermixed with minute fragments of plagioliparite, andesite, propylite, basalt, shale and green tuff, being cemented by tuffaceous matrix.

(2) Mazawa Formation:—The frequency of tuffaceous or non-tuffaceous sandstone gradually increases towards the Hashigami Formation. In such a case, they are composed of quartz, microcline, orthoclase, plagioclase, biotite, glauconite, actinolite, bluish green hornblende, brown hornblende, green hornblende, tremolite, augite, hypersthene, olivine (?), ilmenite, limonite, magnetite (hematite), pyrite, pyrrhotite, allanite, epidote, anatase, garnet, rutile, titanite, tourmaline, colorless zircon, pink zircon and angular fragments of granite, plagioliparite (rhyolite), andesite, basalt, propylite, green tuff, shale, pumice as well as of tuf-

faceous matrix. Of these, green hornblende is usually abundant in the sandstone close to the Hashigami Formation, but is absent or almost absent in other cases. Such a tendency can be seen in the specimens collected on the cutting near Ainosawa and Suwa. The same may be said of actinolite, brown hornblende and hypersthene. The occurrence of the last mineral is, however, known only in the sandstones exposed along the bus road between Takinohira and Yanazawa as well as near Suwa.

(3) Hashigami Formation:—The most important feature of the Hashigami Formation is the high frequency of tuffaceous or non-taffaceous sandstone with a grey or dark grey color in association with pumiceous sandstone. The mineral components of these rocks have some similarities to those of the Mazawa Formation and Nakanosawa Formation, consisting of quartz, microcline, orthoclase, plagioclase, biotite, muscovite, calcite, chlorite, glauconite, actinolite, bluish green hornblende, brown hornblende, green hornblende, tremolite, augite, hypersthene, olivine (?), ilmenite, limonite, magnetite (hematite), pyrite, allanite, epidote, zoisite, anatase, apatite, garnet, rutile, spinel, staurolite, titanite, topaz (?), tourmaline, colorless zircon and pink zircon. Among them, green hornblende is abundantly present as compared with other heavy minerals. This may be one of characteristic features in the Hashigami Formarion. The tuffaceous sandstone exposed near Hirashio is, however, rich in hypersthene and augite. The frequent occurrence of these minerals is also known at the area including Kami-nakagō, Karuizawa—Ōninome, Iwaya—Yanagizawa, Sangō and Yō.

The light and heavy minerals mentioned above are embedded in the tuffaceous or pumiceous matrix together with such minute rock-fragments as granite, andesite, basalt, felsophyre, plagioliparite (rhyolite), propylite, pumice, green tuff and shale.

(4) Nakanosawa Formation:—It is lithologically distinguishable from the Hashigami Formation in the standpoint of the occasional occurrence of shale beds, although there are many mineralogical similarities between them.

The mechanical analyses and microscopical investigations indicate that the tuffaceous or non-tuffaceous sandstone of this formation contain quartz, microcline, orthoclase, plagioclase, biotite, muscovite, calcite, chlorite, glauconite, actinolite, bluish green hornblende, brown hornblende, green hornblende, tremolite, augite, hypersthene, ilmenite, limonite, magnetite (hematite), pyrite, allanite, epidote, zoisite, anatase, apatite,

garnet, rutile, titanite, tourmaline, colorless zircon and pink zircon, andesite, basalt, felsophyre, plagioliparite (rhyolite), perlite (?), propylite, pumice, green tuff and shale. They are cemented with a tuffaceous or pumiceous matrix.

(5) Inazawa Formation:—A gradual transition can be seen between the Inazawa Formation and Nakanosawa Formation, with an upward decrease in the frequency of tuffaceous or non-tuffaceous sandstone, in which quartz, microcline, othoclase, plagioclase, biotite, chlorite, bluish green hornblende, brown hornblende, green hornblende, tremolite, hypersthene, olivine (?), ilmenite, limonite, magnetite (hematite), allanite, epidote, zoisite, garnet, rutile, staurolite (?), tourmaline, colorless zircon and pink zircon are found together with the rock-fragments derived from andesite and plagioliparite. They are embedded in the tuffaceous or pumiceous matrix. In this case, it is noteworthy that hornblende and hypersthene or augite are nearly or entirely absent. Other heavy minerals are also present in low frequency.

The mineral components and rock-fragments in many specimens obtained from each formation are summarized in the following table (Table II).

Microscopical Characters of Mineral Components and Rock-fragments

Exclusive of such fine-grained sediments as shale or mudstone, mechanical analyses and microscopical investigations of thin sections were carried out on 115 specimens to examine the mineral components and rock-fragments contained in tuffaceous or non-tuffaceous sandstone and siltstone. They are listed in the preceeding table (Table II).

Of these, quartz is the commonest component in most specimens and generally takes an angular or subangular form. The crystal is usually rich in liquid inclusions and occasionally reveals a wavy extinction. There are also many crystals subjected to magmatic corrosion, suggesting that they were supplied from plagioliparite, rhyolite or dacite.

In contrast with the abundance of quartz, microcline is scarcely present as minute fragments, 1.3 mm. across in the largest crystal. Similarly, orthoclase is an unimportant component and is lacking in some specimens. It is characterized by the frequency of perthite.

Plagioclase is, however, widely distributed, and it is richly contained in different kinds of sandstone exposed at this area. It ranges from albite to labradorite or bytownite and has a fresh appearance as in the

Table II. Mineral components and rock-fragments contained in the sandy o

	(1)	(2)	(3)*	(4)	(5)*	(6)	(7)	(8)	(9)	(10)	(11)	(12)*	(13)*	(14)*	(15)	(16)	(17)	(18)*	(19)	(20)	(21)*	(22)*	(23)*	(24)	(25)	(26)
Quartz	×	×	—	×	—	×	×	×	×	×	×	—	—	—	×	×	×	—	—	×	—	—	—	×	×	×
Microcline	×	—	—	×	—	×	—	—	—	—	—	—	—	—	—	—	—	—	—	—	—	—	—	×	×	×
Orthoclase	×	—	—	×	—	—	—	×	—	×	—	—	—	—	×	—	×	—	×	—	—	—	—	—	×	—
Plagioclase	×	×	—	×	—	×	×	×	×	×	×	—	—	—	×	×	×	—	×	—	—	—	—	×	×	×
Biotite	×	×	—	×	—	×	×	×	×	×	—	—	×	×	×	×	—	×	×	×	×	—	—	×	×	×
Muscovite (sericite)	—	—	—	—	—	—	×	×	—	—	—	—	—	—	—	—	—	—	—	—	—	—	—	—	—	—
Calcite	—	—	—	—	—	—	—	—	—	—	—	—	—	—	—	—	—	—	—	—	—	—	—	—	—	—
Chlorite	×	—	—	—	—	—	—	×	×	—	×	—	—	—	×	×	—	—	—	—	×	—	—	×	—	×
Glauconite	—	—	—	—	—	×	×	×	×	—	—	—	—	—	×	×	—	—	—	—	×	—	—	×	×	—
Actinolite	×	—	×	—	—	×	—	×	×	—	—	—	×	×	×	—	—	—	×	×	—	—	—	—	×	—
Bluish green hornblende	×	—	—	—	—	×	—	—	—	—	—	—	—	—	×	—	—	—	×	—	—	—	—	—	—	×
Brown hornblende	×	—	—	—	—	×	—	—	—	—	—	—	×	—	—	—	—	×	—	—	—	—	—	—	—	×
Green hornblende	×	—	—	×	×	×	×	×	×	×	×	×	×	×	×	—	×	×	×	×	×	—	—	—	×	×
Tremolite	×	—	×	—	—	×	—	×	—	—	—	—	×	—	—	—	—	×	×	—	—	—	—	—	×	×
Augite	—	—	—	—	—	—	—	—	—	—	—	×	—	—	—	—	—	—	—	—	—	—	—	×	—	×
Hypersthene	—	—	—	×	—	—	—	—	—	—	—	×	—	—	—	—	—	×	×	—	—	×	—	×	—	×
Olivine	?	—	—	—	—	—	—	?	—	—	—	—	—	—	—	—	—	—	?	—	—	—	—	—	—	?
Limonite	—	—	—	—	—	×	×	—	×	×	—	—	—	—	—	×	×	—	—	—	—	—	—	×	×	—
Magnetite (ilmenite, hematite)	×	×	×	×	×	×	×	×	×	×	×	×	×	×	×	×	×	×	×	×	×	×	×	×	×	×
Pyrite	—	—	—	—	—	—	—	—	×	—	—	—	—	—	—	—	—	—	—	—	—	—	—	—	—	—
Pyrrhotite	—	—	—	—	—	—	—	—	—	—	—	—	—	—	—	—	—	—	—	—	—	—	—	—	—	—
Allanite	×	—	×	×	×	—	—	×	×	×	—	—	×	—	×	×	—	×	×	×	×	—	×	—	—	×
Epidote	×	—	×	×	×	×	×	×	—	×	—	×	×	×	×	×	—	×	×	×	×	—	×	×	×	×
Zoisite	—	—	—	—	×	—	—	—	—	—	—	—	—	—	—	—	—	—	—	—	—	—	—	—	—	—
Anatase	—	—	—	—	—	—	—	×	—	—	—	—	—	—	—	—	—	×	—	—	×	—	—	—	—	—
Apatite	—	—	—	—	—	—	—	—	—	—	—	—	—	—	—	—	—	—	—	—	—	—	—	—	—	—
Cordierite	—	—	—	—	—	—	—	—	—	—	—	—	—	—	—	—	—	—	—	—	—	—	—	—	—	—
Garnet	×	—	×	×	×	×	×	×	×	×	—	×	×	—	×	×	×	×	×	×	×	×	×	×	×	×
Rutile	×	—	×	—	—	—	—	×	—	—	—	—	—	—	—	×	—	—	×	—	—	×	—	×	×	—
Spinel	—	—	—	—	—	—	—	—	—	—	—	—	—	—	—	—	—	—	—	—	—	—	—	—	—	—
Staurolite	—	—	?	—	—	—	—	—	—	—	—	—	—	—	—	—	—	—	—	—	—	—	—	—	—	—
Titanite	—	—	—	—	—	—	?	—	×	×	—	—	—	—	—	—	—	—	×	—	—	×	×	—	×	×
Topaz	—	—	—	—	—	—	—	—	—	—	—	—	—	—	—	—	—	—	—	—	—	—	—	—	—	—
Tourmaline	×	—	×	—	×	×	×	×	×	—	—	×	×	—	×	×	—	×	×	×	×	×	×	—	×	×
Colorless zircon	—	—	×	—	×	×	—	—	—	—	—	—	—	—	—	—	—	×	×	×	—	—	—	—	—	—
Pink zircon	×	—	×	×	×	×	×	×	×	×	×	×	×	×	×	×	×	×	×	×	×	×	×	×	×	×
Granite	—	—	—	—	—	—	—	—	—	—	—	—	—	—	—	—	—	—	—	—	—	—	—	—	—	—
Andesite	×	—	—	—	—	—	—	—	—	×	×	—	—	—	—	—	×	—	×	—	—	—	—	—	—	×
Basalt	—	—	—	—	—	—	—	—	?	×	×	—	—	—	×	—	—	—	—	—	—	—	—	—	—	—
Felsophyre & plagioliparite	×	—	—	—	—	—	—	×	×	×	×	—	—	—	—	×	×	—	×	—	—	—	—	—	×	×
Perlite	—	—	—	—	—	—	—	—	—	—	×	—	—	—	—	—	—	—	—	—	—	—	—	—	—	—
propylite	—	—	—	—	—	—	—	—	—	×	—	—	—	—	—	—	—	—	—	—	—	—	—	—	—	—
Green tuff	—	—	—	—	—	—	—	×	×	—	—	—	—	—	—	—	×	—	×	—	—	—	—	—	—	—
Shale	—	—	—	—	—	—	—	—	—	×	—	—	—	—	×	—	—	—	×	—	—	—	—	—	—	—
Pumice & tuffaceous substance	×	×	—	—	—	×	×	×	×	×	×	—	—	—	×	×	×	—	×	—	—	—	—	×	×	×
Foraminifera fossils	—	—	—	—	—	—	—	—	—	—	—	—	—	—	×	×	—	—	—	—	—	—	—	—	—	—

	(59)*	(60)	(61)	(62)*	(63)	(64)	(65)*	(66)	(67)	(68)	(69)*	(70)	(71)*	(72)	(73)*	(74)	(75)	(76)	(77)*	(78)	(79)	(80)	(81)*	(82)*	(83)	(84)
Quartz	—	×	×	—	×	×	—	×	×	×	—	×	—	×	—	×	×	×	—	×	×	×	—	—	×	×
Microcline	—	—	—	—	×	×	—	—	—	×	—	×	—	—	—	×	—	×	—	×	×	×	—	—	×	×
Orthoclase	—	—	—	—	?	×	—	×	×	×	—	×	—	—	—	×	—	×	—	×	—	—	—	—	—	×
Plagioclase	—	×	×	—	×	×	—	×	×	×	—	×	—	×	—	×	×	×	—	×	×	×	—	—	×	×
Biotite	—	×	—	—	×	×	×	×	×	×	—	×	×	×	×	×	×	×	×	×	×	×	—	×	×	×
Muscovite (sericite)	—	—	—	—	—	—	—	×	—	—	—	—	—	—	—	—	—	—	—	—	—	—	—	—	—	—
Calcite	—	—	—	—	—	×	—	—	—	—	—	—	—	×	—	—	—	—	—	—	—	—	—	—	—	×
Chlorite	—	×	—	—	×	—	—	×	×	×	—	—	—	—	—	—	×	—	—	×	—	×	—	—	×	—
Glauconite	—	×	—	—	×	×	—	—	—	×	—	—	—	×	—	×	—	×	—	×	—	—	—	—	×	—
Actinolite	—	—	—	—	—	—	×	—	—	×	—	×	—	—	×	—	—	—	—	×	—	×	×	—	×	—
Bluish green hornblende	×	×	—	—	—	—	—	—	—	—	—	—	—	—	×	—	×	—	—	—	×	—	—	×	—	—
Brown hornblende	—	—	×	—	×	—	×	—	—	×	—	×	—	×	×	—	—	—	×	—	—	—	—	—	×	—
Green hornblende	×	×	×	×	×	×	×	×	×	×	—	×	×	×	×	×	×	×	×	×	×	×	×	×	×	×
Tremolite	—	—	×	×	—	×	×	—	×	×	—	—	×	×	—	?	—	—	—	×	×	?	—	×	—	—
Augite	×	—	×	—	—	×	×	—	—	×	—	×	—	×	×	—	×	×	×	×	×	—	—	—	—	—
Hypersthene	—	×	×	—	—	×	×	—	—	×	—	—	×	—	—	×	×	×	×	×	×	—	—	—	—	—
Olivine	—	—	—	—	?	—	—	—	—	—	—	—	—	?	—	—	?	?	×	—	—	—	—	—	—	—
Limonite	—	—	—	—	×	—	—	×	×	—	—	×	—	×	—	—	—	—	—	×	—	—	—	—	×	—
Magnetite (ilmenite, hematite)	×	×	×	×	×	×	×	×	×	×	×	×	×	×	×	×	×	×	×	×	×	×	×	×	×	×
Pyrite	—	×	×	—	—	×	×	—	—	×	×	—	—	—	—	—	—	—	—	×	—	—	—	—	—	—
Pyrrhotite	—	—	—	—	—	—	—	—	—	—	—	—	—	—	—	—	—	—	—	—	—	—	—	—	—	—
Allanite	×	×	×	×	×	×	×	×	—	×	×	×	×	×	?	×	×	×	×	×	×	×	×	×	×	×
Epidote	—	×	×	×	—	×	×	×	—	×	—	×	×	×	×	×	×	×	×	×	×	×	×	×	×	—
Zoisite	—	—	—	—	—	—	—	—	—	—	—	—	—	—	—	—	—	—	—	—	—	—	—	—	—	—
Anatase	—	—	—	—	—	—	×	—	—	×	—	—	—	—	—	—	—	—	—	—	—	—	—	×	—	—
Apatite	—	—	—	—	—	×	×	—	—	×	—	—	—	×	—	—	—	—	—	—	—	—	—	—	—	—
Cordierite	—	—	—	—	—	—	—	—	—	—	—	—	—	—	—	—	—	—	—	—	—	—	—	—	—	—
Garnet	—	×	×	—	—	×	×	×	×	×	—	×	—	×	×	×	×	×	—	×	×	×	×	×	×	—
Rutile	—	—	—	—	—	—	—	—	—	—	—	—	—	—	×	—	—	—	—	—	×	—	—	—	×	—
Spinel	—	—	—	—	—	—	—	—	—	—	—	—	—	—	—	—	—	—	—	—	—	—	—	—	—	—
Staurolite	—	—	—	—	—	—	—	—	—	—	—	—	—	—	—	—	—	—	—	—	—	×	—	—	—	—
Titanite	—	—	×	—	—	—	×	—	×	×	—	×	—	—	—	—	×	×	—	—	×	?	?	—	—	—
Topaz	—	—	—	—	—	—	—	—	—	—	—	—	—	?	—	—	—	—	—	—	—	—	—	—	—	—
Tourmaline	—	×	×	—	×	—	—	—	—	×	—	—	×	×	×	×	×	×	—	—	×	—	×	×	×	—
Colorless zircon	—	—	—	—	—	—	—	—	—	—	—	—	—	—	—	×	—	—	—	×	×	—	—	—	—	—
Pink zircon	×	×	×	×	×	×	×	×	×	×	×	×	×	×	×	×	×	×	×	×	×	×	×	×	×	×
Granite	—	—	—	—	—	—	—	—	—	—	—	—	—	—	—	—	—	×	—	—	—	×	—	—	—	—
Andesite	—	—	×	—	×	×	—	×	×	—	—	×	—	×	—	×	×	×	—	—	×	×	—	—	×	—
Basalt	—	—	—	—	—	—	—	—	—	—	—	—	—	—	—	—	×	×	—	—	×	—	—	—	—	×
Felsophyre & plagioliparite	—	—	×	—	×	×	—	×	×	×	—	×	—	×	—	×	×	×	—	×	—	×	—	—	×	×
Perlite	—	—	—	—	—	—	—	—	—	—	—	—	—	—	—	—	—	—	—	—	—	—	—	—	—	—
Propylite	—	×	—	—	×	—	—	—	×	×	—	—	—	×	—	—	—	×	—	—	—	×	—	—	×	×
Green tuff	—	×	—	×	—	—	—	—	×	×	—	—	—	—	—	—	×	—	—	—	×	×	—	—	—	×
Shale	—	—	—	—	—	—	—	—	—	—	—	—	—	—	—	—	—	—	—	—	×	—	—	—	—	—
Pumice & tuffaceous substance	—	×	×	—	×	×	—	×	×	×	—	×	—	×	—	×	—	—	—	—	×	—	—	—	×	×
Foraminifera fossils	—	—	—	—	—	—	—	—	—	—	—	—	—	—	—	—	—	—	—	—	—	—	—	—	—	—

(1)–(5)=Inazawa Formation, (6)–(39)=Nakanosawa Formation, (40)–(94)=Hashigami Formation, (95)–(111)=Mazawa Formation, (112)–(115)=Tsunatori Formation

* Light minerals are partly undetermined.

y or tuffaceous rocks.

(26)	(27)	(28)*	(29)	(30)*	(31)	(32)*	(33)	(34)	(35)*	(36)	(37)	(38)*	(39)*	(40)	(41)	(42)*	(43)*	(44)	(45)	(46)	(47)*	(48)	(49)	(50)	(51)	(52)*	(53)	(54)	(55)	(56)*	(57)*	(58)*
×	×	—	×	—	×	—	×	×	—	×	×	—	—	×	×	—	—	?	×	×	—	×	×	×	×	—	×	×	×	×	—	—
×	×	—	—	—	×	—	×	—	—	—	×	—	—	—	—	—	—	×	—	×	—	—	×	×	—	—	×	×	×	—	—	—
—	×	—	×	—	×	—	—	—	—	—	—	—	—	—	—	—	—	×	×	×	—	×	×	—	—	—	×	×	×	—	—	—
×	×	—	×	—	×	—	×	×	—	×	×	—	—	×	×	—	—	×	×	×	—	×	×	×	×	—	×	×	×	×	—	—
×	×	×	×	×	×	—	×	—	×	×	×	×	×	×	×	—	×	×	×	×	—	×	×	×	—	×	×	×	×	—	—	—
—	—	—	—	—	—	—	—	—	—	×	—	—	—	—	—	—	—	—	—	—	—	—	×	—	—	—	—	—	—	—	—	—
—	—	—	—	—	—	—	—	—	—	—	—	—	—	—	—	—	—	—	×	—	—	—	—	—	—	—	—	—	—	—	—	—
×	×	—	×	×	×	—	—	—	—	—	—	—	×	—	—	—	—	—	—	×	—	—	×	×	—	—	×	—	—	—	—	—
—	—	—	—	—	—	—	×	—	—	×	—	—	—	—	×	—	—	×	—	—	—	×	—	—	—	—	—	×	×	—	—	—
—	—	×	×	—	×	×	×	×	×	×	×	×	×	×	×	—	×	—	—	×	—	—	×	—	×	—	—	—	×	×	×	×
×	—	—	—	—	—	—	×	—	×	×	—	—	—	—	×	—	—	×	×	—	—	—	—	—	—	—	—	—	—	—	—	—
×	×	—	—	—	—	×	—	—	—	—	—	×	—	—	—	—	×	—	—	—	—	—	×	×	—	—	—	—	—	—	—	×
×	×	×	×	×	×	×	×	×	×	×	×	×	×	×	×	×	×	×	×	×	×	×	×	×	×	×	—	×	×	×	×	×
×	—	×	?	—	×	×	—	—	×	—	—	×	×	—	×	—	—	×	×	—	—	—	×	—	×	×	—	×	—	×	×	×
×	×	×	—	—	?	—	—	—	—	—	—	—	×	×	—	×	×	—	×	—	—	×	×	—	×	×	—	—	—	—	—	×
×	×	—	—	×	×	×	—	—	×	—	—	—	×	×	—	×	×	—	—	—	×	×	×	×	×	×	—	—	—	—	—	—
?	—	—	—	—	×	?	—	—	—	—	—	—	—	—	—	—	—	—	—	—	—	—	×	—	—	—	—	—	—	—	—	—
—	—	—	—	—	—	—	×	×	—	×	—	—	—	—	×	—	—	—	—	—	—	×	—	—	×	—	—	×	×	×	—	—
×	×	×	×	×	×	×	×	×	×	×	×	×	×	×	×	×	×	×	×	×	×	×	×	×	×	×	×	×	×	×	×	×
—	—	—	—	—	×	—	—	—	—	—	—	—	—	—	—	—	—	—	—	—	—	—	—	—	—	—	—	—	—	—	—	—
—	—	—	—	—	—	—	—	—	—	—	—	—	—	—	—	—	—	—	—	—	—	—	—	—	—	—	—	—	—	—	—	—
×	×	×	×	×	?	×	×	—	×	×	×	×	×	—	—	—	×	×	—	×	—	×	×	×	—	×	×	×	×	?	—	×
×	×	×	×	—	×	×	×	×	×	—	×	×	×	×	×	—	×	—	—	×	×	×	×	×	×	—	×	×	×	×	×	×
—	—	—	—	—	×	—	—	—	—	—	×	—	—	—	—	—	—	—	—	—	—	—	×	—	—	—	—	—	?	—	—	—
—	—	—	—	—	—	—	—	—	×	—	—	×	×	—	×	—	—	—	—	—	—	×	—	×	—	—	—	—	×	—	—	—
—	—	—	—	—	—	×	—	—	—	—	—	—	—	—	—	—	—	—	—	—	—	—	—	—	—	—	—	—	—	—	—	—
—	—	—	—	—	—	—	—	—	—	—	—	—	—	—	—	—	—	—	—	—	—	—	—	—	—	—	—	—	—	—	—	—
×	×	?	×	—	×	×	×	—	×	×	—	×	×	—	×	—	×	—	—	×	×	×	×	×	—	×	—	—	—	—	×	×
—	×	×	—	—	×	×	—	×	—	—	—	—	—	—	—	—	—	—	—	—	—	—	×	—	—	—	—	—	—	×	—	—
—	—	—	—	—	—	—	—	—	—	—	—	—	—	—	—	—	—	—	—	—	—	—	—	—	—	—	—	—	—	—	—	—
—	—	—	—	—	—	—	—	—	—	—	—	—	—	—	—	—	—	—	—	—	—	—	—	—	—	—	—	—	—	—	—	—
×	—	?	×	—	×	×	×	—	—	—	—	—	—	—	—	—	—	—	—	—	—	×	×	×	—	—	—	—	—	—	—	—
—	—	—	—	—	—	—	—	—	—	—	—	—	—	—	—	—	—	—	—	—	—	—	—	—	—	—	—	—	—	—	—	—
×	×	×	×	—	×	×	×	—	×	×	×	×	×	—	—	—	×	×	—	×	×	—	×	—	×	—	×	—	×	—	×	×
—	—	×	—	—	×	×	—	—	—	—	×	—	—	—	—	—	—	—	—	—	—	—	—	—	—	—	—	—	—	—	—	—
×	×	×	×	×	×	×	×	×	×	×	×	×	×	×	×	—	×	×	×	×	×	×	×	×	×	×	×	×	×	×	×	×
—	—	—	—	—	—	—	—	—	—	—	—	—	—	—	—	—	—	—	—	—	—	—	—	—	—	—	—	—	—	—	—	—
×	×	—	—	—	×	—	—	—	—	—	×	—	—	×	—	—	—	—	×	×	—	—	—	—	×	—	×	—	—	—	—	—
—	—	—	—	—	—	—	—	—	—	—	—	—	—	—	—	—	—	—	—	—	—	—	—	—	×	—	—	—	—	—	—	—
×	×	—	×	—	×	×	×	—	—	—	×	—	—	×	—	—	—	×	×	×	—	—	×	×	—	—	×	×	—	—	—	—
—	—	—	—	—	—	—	—	?	—	—	—	—	—	—	—	—	—	—	—	—	—	—	—	—	—	—	—	—	—	—	—	—
—	—	—	—	—	—	—	—	—	—	—	—	—	—	—	—	—	—	—	×	—	—	—	—	—	—	—	—	—	—	—	—	—
—	—	—	—	—	—	—	—	—	—	—	—	—	—	—	—	—	—	—	×	—	—	—	—	—	—	—	—	—	—	—	—	—
—	—	—	—	—	×	—	—	—	—	×	—	—	—	—	—	—	—	—	—	—	—	—	—	×	—	—	—	—	—	—	—	—
×	×	—	×	—	×	×	×	×	—	×	×	—	—	×	—	—	—	×	—	×	—	×	×	×	×	—	×	×	×	×	—	—
—	—	—	—	—	—	—	—	—	—	—	—	—	—	—	×	—	—	—	—	—	—	—	—	—	—	—	—	—	—	—	—	—

(84)	(85)	(86)	(87)	(88)*	(89)	(90)	(91)	(92)*	(93)*	(94)*	(95)*	(96)	(97)	(98)*	(99)	(100)	(101)	(102)	(103)	(104)*	(105)	(106)*	(107)	(108)	(109)	(110)	(111)	(112)	(113)	(114)	(115)*
×	×	×	×	—	×	×	×	—	—	—	—	×	×	—	×	×	×	×	×	—	×	—	×	×	×	×	×	×	×	×	—
×	—	×	—	—	×	×	×	—	—	—	—	—	×	—	×	—	×	×	×	—	×	—	—	—	×	—	×	—	—	—	—
×	—	×	—	—	×	×	×	—	—	—	—	×	×	—	×	—	×	×	—	—	×	—	×	—	—	×	×	—	×	—	—
×	×	×	×	—	×	×	×	—	—	—	—	×	×	—	×	×	×	×	×	—	×	—	×	×	×	×	×	×	×	×	—
×	×	×	—	—	×	—	×	—	—	—	—	×	×	×	×	—	×	×	×	×	×	×	—	×	×	—	×	×	×	—	—
—	—	—	—	—	—	—	×	—	—	—	—	—	—	—	—	—	—	—	—	—	—	—	—	—	—	—	—	—	—	—	—
×	—	×	—	—	—	—	—	—	—	—	—	—	—	—	—	—	—	—	—	—	—	—	—	—	—	—	—	—	—	—	—
—	—	×	—	—	×	×	—	—	—	—	—	—	×	—	—	—	—	—	—	—	×	—	—	—	—	—	—	—	—	—	—
—	×	×	—	—	×	×	×	—	—	—	—	—	—	—	×	×	—	×	×	—	×	—	×	—	—	×	×	—	×	—	—
—	×	—	—	—	—	×	—	—	×	—	—	×	×	×	—	—	×	×	×	—	—	—	—	—	—	—	×	—	×	—	—
—	—	—	—	—	—	—	—	—	×	×	—	—	×	×	—	—	—	—	—	—	—	—	—	—	—	—	—	—	—	—	—
—	—	—	—	—	—	×	×	—	×	—	—	—	—	×	—	—	—	×	×	—	—	—	—	—	—	—	—	—	—	—	—
×	×	×	×	×	×	×	×	×	×	×	—	×	×	×	×	×	×	×	×	×	×	—	?	×	×	×	×	—	—	×	×
—	×	—	—	—	—	—	—	—	×	—	—	—	×	—	—	—	—	×	×	—	—	—	—	—	—	—	—	—	—	—	—
—	—	—	×	—	×	×	×	—	—	—	—	×	—	—	—	—	—	—	—	—	—	—	×	—	—	—	—	—	—	—	—
—	—	×	—	×	—	—	—	—	—	×	×	×	—	—	×	—	—	—	—	×	×	—	×	—	—	—	×	×	×	×	—
—	—	—	—	—	?	—	—	—	—	—	—	—	—	—	—	—	?	—	—	—	—	—	—	—	—	—	—	—	—	—	—
—	×	×	—	—	×	—	×	—	—	—	—	×	×	—	×	×	—	—	×	—	×	—	×	×	×	×	×	×	×	×	—
×	×	×	×	×	×	×	×	×	×	×	×	×	×	×	×	×	×	×	×	×	×	×	×	×	×	×	×	×	×	×	×
—	—	—	—	×	—	—	—	—	—	—	—	—	—	×	—	×	—	—	—	—	×	—	—	—	—	—	—	—	—	—	—
—	—	—	—	—	—	—	—	—	—	—	—	—	—	×	—	—	—	—	—	—	×	—	—	—	—	—	—	—	—	—	—
×	×	×	×	×	×	×	×	×	×	×	—	×	×	×	×	—	×	×	×	×	—	—	×	×	×	—	×	×	×	—	×
—	×	—	×	×	×	×	×	×	×	×	—	×	×	×	×	×	×	×	×	—	—	—	×	—	—	—	—	—	—	—	—
—	—	—	—	—	—	—	—	—	—	—	—	—	—	—	—	—	—	—	—	—	—	—	—	—	—	—	—	—	—	—	—
—	—	—	—	—	—	—	—	—	—	—	—	—	×	—	—	—	—	×	×	—	—	—	—	—	—	—	×	—	—	—	—
—	—	—	—	—	—	—	—	—	—	—	—	—	—	—	—	—	—	—	—	—	—	—	—	—	—	—	—	—	—	—	—
—	—	—	—	—	—	—	—	—	—	—	—	—	—	—	—	—	—	—	—	—	—	—	—	—	—	—	—	—	—	×	—
—	—	×	×	×	×	—	—	×	×	×	×	—	×	—	×	—	×	×	×	—	×	—	—	×	×	×	×	—	×	×	×
—	—	—	—	—	—	—	—	—	—	—	—	—	×	—	—	—	×	—	×	—	—	—	—	—	—	—	—	—	—	—	—
—	—	—	—	—	—	×	—	—	—	—	—	—	—	—	—	—	—	—	—	—	—	—	—	—	—	—	—	—	—	—	—
—	—	—	—	—	—	—	—	—	—	—	—	—	—	—	—	—	—	—	—	—	—	—	—	—	—	—	—	—	—	—	—
—	—	—	×	—	×	×	—	—	—	—	—	—	—	×	×	×	—	—	×	—	×	—	—	—	—	—	—	—	—	—	—
—	—	—	—	—	—	—	—	—	—	—	—	—	—	—	—	—	—	—	—	—	—	—	—	—	—	—	—	—	—	—	—
—	×	×	—	×	—	—	?	×	—	—	—	—	—	—	—	—	—	—	×	×	—	—	—	—	—	—	×	—	—	×	—
—	—	—	—	—	—	—	—	—	—	—	—	—	—	—	—	×	×	—	—	—	—	×	—	—	—	—	×	—	—	—	—
×	×	×	×	×	×	×	×	×	×	×	—	×	×	×	×	×	×	×	×	×	×	×	×	×	×	×	×	×	×	×	×
—	—	—	—	—	—	—	—	—	—	—	—	—	—	—	—	—	—	—	?	—	—	—	—	×	—	—	—	—	—	—	—
—	×	—	×	—	×	×	×	—	—	—	—	×	×	—	×	×	?	×	×	—	×	—	×	×	×	×	×	×	—	—	—
×	—	—	—	—	—	—	—	—	—	—	—	—	—	—	—	×	—	—	—	—	×	—	—	—	—	—	—	—	—	—	—
×	×	×	×	—	×	×	×	—	—	—	—	×	?	—	×	×	×	×	×	—	×	—	×	×	×	×	×	×	—	×	—
—	—	—	—	—	—	—	—	—	—	—	—	—	—	—	—	—	—	—	—	—	—	—	—	—	—	—	—	—	—	—	—
×	×	×	—	—	—	—	—	—	—	—	—	×	—	—	—	×	—	—	×	—	—	—	—	×	×	—	—	×	—	—	—
×	×	?	—	—	×	—	—	—	—	—	—	—	—	—	—	—	—	—	—	—	—	—	—	?	×	—	×	×	—	×	—
—	—	—	—	—	×	—	×	—	—	—	—	×	—	—	—	×	—	—	×	—	×	—	×	—	—	—	—	—	—	×	—
×	×	×	×	—	×	?	×	—	—	—	—	×	—	—	×	×	×	×	×	—	×	—	—	×	×	×	×	×	×	×	—
—	×	×	—	—	—	—	—	—	—	—	—	—	—	—	—	—	—	—	—	—	—	—	—	—	—	×	—	—	—	—	—

ation.

Table III. Localities of sandy rocks in the preceeding table.

		Village or town	District or city
(1)	Yō-Iwaya (Tuffaceous sandstone)	Aterazawa-machi	W. Murayama-gun.
(2)	Kami-matsuyama-Yubune (〃)	Yamanobe-machi	E. Murayama-gun.
(3)	〃 (Siltstone)	〃	〃 .
(4)	〃 (〃)	〃	〃 .
(5)	Shinjuku-Kami-ashizawa (Fine sandstone)	Asahi-machi	W. Murayama-gun.
(6)	Nariai (Fine sandstone)	Aterazawa-machi	〃 .
(7)	〃 (〃 〃)	〃	〃 .
(8)	Yō (Tuffaceous sandstone)	〃	〃 .
(9)	〃 (Siltstone)	〃	〃 .
(10)	〃 (Coarse sandstone)	〃	〃 .
(11)	The Uguisu-zawa (Coarse sandstone)	Nakayama-machi	E. Murayama-gun.
(12)	〃 (〃 〃)	〃	〃 .
(13)	Menkyō-bashi (Tuffaceous sandstone)	Asahi-machi,	W. Murayama-gun.
(14)	Kami-matsuyama (〃 〃)	Yamanobe-machi	E. Murayama-gun.
(15)	〃 (〃 〃)	〃	〃 .
(16)	Iwaya (Nodule in siltstone)	Nakayama-machi	〃 .
(17)	〃 (Tuffaceous sandstone)	〃	〃 .
(18)	Shimo-matsuyama (〃 〃)	Yamanobe-machi	〃 .
(19)	Wagōtaira-Wagō (〃 〃)	Asahi-machi	W. Murayama-gun.
(20)	Wagō (〃 〃)	〃	〃 .
(21)	Nōchū (Sandstone)	〃	〃 .
(22)	Nōchū-Yatsunuma (Siltstone)	〃	〃 .
(23)	〃 (Coarse sandstone)	〃	〃 .
(24)	Yatsunuma (Siltstone)	〃	〃 .
(25)	〃 (Sandstone)	〃	〃 .
(26)	Yubune (Sandstone)	Yamanobe-machi	E. Murayama-gun.
(27)	Yubune-Chōkai-zan (Coarse sandstone)	〃	〃 .
(28)	〃 (Sandstone)	〃	〃 .
(29)	Omoshiro-Ōwarabi (Fine tuffaceous sandstone)	〃	〃 .
(30)	Furumaki (Sandstone)	Asahi-machi	W. Murayama-gun.
(31)	Miyajuku (Tuffaceous sandstone)	〃	〃 .
(32)	Shinjuku-Shimo-ashizawa (Sandstone)	〃	〃 .
(33)	Shinjuku-Tateyama (Siltstone)	〃	〃 .
(34)	Shimo-ashizawa (Fine tuffaceous sandstone)	〃	〃 .
(35)	〃 (Fine sandstone)	〃	〃 .
(36)	Shinjuku-Kami-ashizawa (Siltstone)	〃	〃 .
(37)	〃 (Tuffaceous sandstone)	〃	〃 .
(38)	Ōtaki (Fine sandstone)	〃	〃 .
(39)	Shimo-ashizawa-Kami-ashizawa (Tuffaceous sandstone)	〃	〃 .
(40)	Mogami-bashi (〃 〃)	Aterazawa-machi	E. Murayama-gun.
(41)	Kanaya (Fine sandstone)		Sagae-shi
(42)	Kami-nakagō (〃 〃)		〃 .
(43)	Myōjin-yama (Tuffaceous sandstone)		〃 .
(44)	Narakifuchi (〃 〃)		〃 .
(45)	〃 (Sandstone)		〃 .
(46)	Hirashio (Fine sandstone)		〃 .
(47)	〃 (〃 〃)		〃 .
(48)	〃 (〃 〃)		〃 .
(49)	〃 (〃 〃)		〃 .
(50)	〃 (〃 〃)		〃 .
(51)	〃 (〃 〃)		〃 .
(52)	The Uguisu-zawa-Hirashio (Tuffaceous sandstone)		〃 .
(53)	The Uguisu-zawa (Fine sandstone)		〃 .
(54)	The Fudō-zawa (〃 〃)	Nakayama-machi	E. Murayama-gun.
(55)	Oka (〃 〃)	〃	〃 .
(56)	〃 (〃 〃)	〃	〃 .

(to be continued.)

(continued.)

		Village or Town	District or city
(57)	Fushikuma (Fine tuffceous sandstone)	Aterazawa-machi	W. Murayama-gun,
(58)	Sangō (Sandstone)	〃	〃 .
(59)	〃 (〃)	〃	〃 .
(60)	〃 (Coarse sandstone)	〃	〃 .
(61)	〃 (〃)	〃	〃 .
(62)	Tsuchihashi (〃)	Nakayama-machi	E. Murayama-gun.
(63)	Yō (Tuffaceous sandstone)	Aterazawa-machi	W. Murayama-gun,
(64)	〃 (Coarse sandstone)	〃	〃 .
(65)	〃 (Tuffaceous sandstone)	〃	〃 .
(66)	〃 (〃)	〃	〃 .
(67)	〃 (Coarse tuffceous sandstone)	〃	〃 .
(68)	Ōsumi (Fine tuffaceous sandstone)	Asahi-machi	〃 .
(69)	〃 (〃)	〃	〃 .
(70)	Iwaya-Yanagizawa (Tuffaceous sandstone)	Nakayama-machi	E. Murayama-gun.
(71)	〃 (〃)	〃	〃 .
(72)	〃 (〃)	〃	〃 .
(73)	〃 (Conglomeratic sandstone)	〃	〃 .
(74)	Oninome (Tuffaceous sandstone)	Yamanobe-machi	〃 .
(75)	Kitagaki-Oninome (〃)	〃	〃 .
(76)	Oninome-Karuizawa (〃)	〃	〃 .
(77)	Iwaya (Conglomeratic sandstone)	Nakayama-machi	〃 .
(78)	Karuizawa (Tuffaceous sandstone)	Yamanobe-machi	〃 .
(79)	〃 (Conglomeratic sandstone)	〃	〃 .
(80)	Karuizawa-Ōtera (Tuffaceous sandstone)	〃	〃 .
(81)	Yamanobe-Ainosawa (〃)	〃	〃 .
(82)	Osone-bashi (〃)	〃	〃 .
(83)	Takamori-yama-Omoshiro (Tuffaceous sandstone)	〃	〃 .
(84)	Omoshiro (Conglomeratic sandstone)	〃	〃 .
(85)	Okurihashi-Takamoriyama (Tuffaceous sandstone)	Asahi-machi	W. Murayama-gun.
(86)	Okurihashi-Ōwarabi (〃)	〃	〃 .
(87)	〃 (〃)	〃	〃 .
(88)	〃 (〃)	〃	〃 .
(89)	Ōwarabi (〃)	〃	〃 .
(90)	Ainosawa-Ōwarabi (〃)	Yamanobe-machi	E. Murayama-gun.
(91)	〃 (〃)	〃	〃 .
(92)	Tamamushi-numa-Shinden (〃)	〃	〃 .
(93)	〃 (Sandstone)	〃	〃 .
(94)	Shimo-ashizawa-Tateno (Tuffaceous sandstone)	〃	〃 .
(95)	The Uguisu-zawa (Sandstone)		Sagae-shi .
(96)	The Fudō-zawa (Coarse sandstone)	Nakayama-machi	E. Murayama-gun.
(97)	Yanagizawa (Tuffaceous sandstone)	〃	〃 .
(98)	Oninome (〃)	Yamanobe-machi	〃 .
(99)	Suwa (〃)	〃	〃 .
(100)	〃 (Sandstone)	〃	〃 .
(101)	Yamanobe-Ainosawa (Sandstone)	〃	〃 .
(102)	〃 (Tuffaceous sandstone)	〃	〃 .
(103)	Ainosawa (〃)	〃	〃 .
(104)	Okurihashi (〃)	Asahi-machi	W. Murayama-gun.
(105)	Shimo-ashizawa (〃)	〃	〃 .
(106)	Takinohira (〃)	Yamanobe-machi	E. Murayama-gun.
(107)	Takinohira-Yanazawa (Sandstone)	〃	〃 .
(103)	Yoshizawa (Tuffaceous sandstone)	〃	〃 .
(109)	Ideshio (Sandstone)	Murakizawa	Yamagata-shi .
(110)	〃 (〃)	〃	〃 .
(111)	〃 (Tuffaceous sandstone)	〃	〃 .
(112)	Shimobara (〃)	Yamanobe-machi	E. Murayama-gun.
(113)	Ideshio (Tuff)	Murakizawa	Yamagata-shi .
(114)	〃 (Brecciated tuff)	〃	〃 .
(115)	〃 (〃)	〃	〃 .

case of microcline.

The occurrence of biotite is not so remarkable as compared with quartz and plagioclase, although it is commonly found in several specimens. Some of its crystal is twisted and irregularly outlined. This mineral is strongly pleochroic from light yellow (X) to dark reddish brown or dark brown (Y, Z), being partly altered to chlorite.

Muscovite is, on the other hand, very rare, and is observed only in several thin sections, whereas sericite forms a scaly aggregate in feldspar crystals.

In fossiliferous specimens, calcite is extremely abundant and constructs the matrix of other components. Such examples can be seen in tuffaceous sandstone collected from the Hashigami Formation of Iwaya—Omoshiro and the Yu-zawa.

Chlorite seems to be a secondary mineral derived chiefly from biotite and partly from other ferro-magnesian minerals. The frequent occurrence of this mineral is known in the tuffaceous sandstone exposed at Hirashio (Hashigami Formation).

Besides it, the light mineral with a green color is represented by glauconite which occurs in some tuffaceous or non-tuffaceous fine sandstone and siltstone of the Mazawa Formation, Hashigami Formation and Nakanosawa Formation. The mineral is noticeably contained in the tuffaceous sandstone obtained at the opposite side of Yoshizawa village (Tsunatori Formation), at the upper course of the Yoshi-zawa (Mazawa Formation), Takinohira—Yanazawa (Mazawa Formation) and Takamoriyama—Omoshiro (Hashigami Formation) as well as in the siltstone of Hirashio (Hashigami Formation). It has a rounded from and beautiful aggregate polarization color. Moreover, a micaceous crystal resembling mica is found in the sandstone from the cutting between Karuizawa and Ōdera.

Several kinds of amphibole determined under the microscope are actinolite, bluish green hornblende, brown hornblende, green hornblende and tremolite. Among them, actinolite is to be seen in various formations, but is low in its frequency, showing a weak pleochroism between colorless (X, Y) and faint green (Z). In other amphiboles, green hornblende (Fig. 7) is most predominant, whereas bluish green hornblende and brown hornblende are almost same in frequency. All of these hornblendes are distinctly pleochroic, viz., light yellow (X), light green (Y), bluish green (Z); light brown (X), brown (Y), reddish brown (Z); light yellow (X), yellowish green (Y), green (Z). The extinction angle, $Z \wedge c$,

is 17°–19°. These kinds of hornblende are particularly abundant in the tuffaceous or non-tuffaceous sandstone of the Mazawa Formation, Hashigami Formation and Nakanosawa Formation from which other formations are distinguishable with scarcity of hornblende crystals. Some of the green hornblende is remarkable for the presence of "hacksaw structure"[8]. The largest crystal is 0.44 mm. long in green hornblende. Tremolite is distributed to a small extent, and its frequency is nearly same as actinolite.

The occurrence of augite (Fig. 8) and hypersthene (Fig. 9) is also a characteristic feature of the Hashigami Formation and Nakanosawa Formation. Of these minerals, augite is very commonly seen in the tuffaceous sandstone obtained from Narakifuchi, Mogami-bashi of Aterazawa, Iwaya—Yanagizawa, Hirashio, Ōwarabi—Ainosawa, Ōwarabi—Okurihashi, Oninome—Karuizawa, Kitagaki—Oninome and Sangō (Hashigami Formation) as well as in the similar kinds of sandstone exposed at the Uguisu-zawa, Yubune and Chōkai-zan—Yubune (Nakanosawa Formation). It has a faint green color and is 0.73 mm. long and 0.34 mm. across in the largest crystal. Its extinction angle, $Z \wedge c$, is 40–41°. Moreover, there is a hacksaw structure in some crystals. Hypersthene is often assocsated with augite in almost the same frequency. In this case, the hacksaw termination of hypersthene srystals (Fig. 9) is more striking than that of augite (Fig. 8). Such examples can be seen in the tuffaceous sandstone exposed at Mogami-bashi, Hirashio, Oninome—Karuizawa, Yō—Iwaya, Kami-nakagō, Kitagaki—Oninome, Hirashio—the Uguisu-zawa and Fudō-zawa (Hashigami Formation) as well as in the similar sediments distributed along the Uguisu-zawa (Nakanosawa Formation). This mineral is very abundant in the tuffaceous sandstone obtained on the cutting between the Uguisu-zawa and Hirashio (Hashigami Formation) and along the Uguisu-zawa (Nakanosawa Formation). Sometimes, there are well-defined crystals. The largest crystal is 1.1 mm. is long and 0.37 mm. across.

The occurrence of a colorless mineral identified with olivine is known in the tuffaceous sandstone from the Yu-zawa, Kami-matsuyama—Shimomatsuyama and Yō (Nakanosawa Formation). The same mineral is also contained very scarcely in the non-tuffaceous sandstone from Oninome—Karuizawa (Hashigami Formation).

8) C. H. EDELMAN, *Fort. Min. Krist. Pet.*, **16** (1931), 67–68.
C. H. EDELMAN u. D. J. DOEGLAS, *Min. Pet. Mitt.*, **42** (1931), 482–490.
F. J. PETTIJOHN, *Sedimentary Rocks*, (1948), 490–491.

In most specimens, allanite (Fig. 10) is a characteristic mineral with a strong absorption from dark brown (X) to dark reddish brown (Y) or light brown (Z). Its frequency is, however, very low except in the tuffaceous sandstone from near Jōmyōji (Tsunatori Formation) and the non-tuffaceous sandstone found at Kitagaki—Oninome and Karuizawa—Oninome (Hashigami Formation) as well as in the tuffaceous sandstone of Chōkai-zan—Yubune (Nakanosawa Formation). The mineral has a wide distribution in all formations, and well-defined prismatic crystals are to be seen in the sandstone from Karuizawa—Oninome (Hashigami Formation) and the tuffaceous sandstone from Chōkai-zan—Yubune, Shimo-ashizawa and near Menkyō-bashi (Nakanosawa Formation). Its largest crystal is 0.44 mm. in length. Epidote is commonly found in most sandy rocks except those of the Tsunatori Formation, being abundant in the tuffaceous sandstone of Chōkai-zan—Yubune (Nakanosawa Formation). In the epidote group, zoisite is a rare mineral whose occurrence seems to be confined to only the tuffaceous or non-tuffaceous sandstone of the Inazawa Formation, Nakanosawa Formation and Hashigami Formation.

The frequency of anatase (Fig. 11) is exceedingly low, when compared with that of allanite and epidote which are seen in almost all specimens collected by the writers. The crystal takes a sharp pyramidal form with striations parallel to the intersection of (111) and (110), being 0.15 mm. long and 0.07 mm. across in the largest one. It has an indigo-blue or dark brown color, and some of it is weakly pleochroic. The occurrence of this mineral is restricted to the specimens of tuffaceous sandstone gained from Yanagizawa, Yamanobe—Ainosawa, Yoshizawa—Hayasaka (Mazawa Formation), Mogami-bashi, Hirashio, Oka, Yō, the northern foot of Negota-yama, Osone-bashi (Hashigami Formation), Kami-matsuyama—Shimo-matsuyama, the opposite side of Shinosawa, Shimo-ashizawa and near Ōtaki (Nakanosawa Formation).

The similar frequency is also shown by apatite (Fig. 12). This mineral is found scarcely in the tuffaceous sandstone exposed widely at the eastern foot of Tate-yama (Nakanosawa Formation), the Yu-zawa, Iwaya and the northern foot of Negota-yama as well as near Yō (Hashigami Formation), where it mostly reveals a remarkable cross-bedding. Such apatite has a stout prismatic habit, being 0.29 mm. long in the largest crystal. Its crystal generally occurs in a fresh appearance, but on rare occasions exhibits a dark core due to decomposition.

Garnet is a scanty but characteristic mineral contained as rounded

crystals or angular pieces with varying ranges of color, viz., pink, light brown, reddish brown, red and colorless. Among them, pink garnet is in high frequency as compared with others, and the reddish brown variety is commonly present in the tuffaceous sandstone of the Yu-zawa (Hashigami Formation) and non-tuffaceous sandstone of Nōchū and Hachibe (Nakanosawa Formation). Red or light brown garnet is, however, almost absent in the specimens from this area.

Magnetite, ilmenite, hematite and limonite are very extensively distributed in all kinds of sandy rocks, although the frequency of these minerals is much variable from place to place. In many specimens, ilmenite is a noticeable mineral with a hexagonal platy form and jet-black color. Hence, it is easily distinguishable from magnetite and hematite. In general, the decomposed sandstone and siltstone are rich in limonite. Mostly, it has a very irregular form and seems to have partly been derived from pyrite.

Pyrite is a common mineral in the tuffaceous or non-tuffaceous sandstone from Jōmyōji—Yoshizawa (Tsunatori Formation), Oninome—Fudō-bashi (Mazawa Formation), Sangō, the Yu-zawa, Yō, Oninome—Karuizawa, Ōwarabi—Okurihashi, the northern foot of Negota-yama (Hashigami Formation) and Shinjuku—Shimo-ashizawa (Nakanosawa Formation). The crystal is represented by cube and pentagonal dodecahedron. There are also some granular aggregates resembling marcasite. Moreover, the specimens from Takinohira (Mazawa Formation) and Kitagaki (Tsunatori Formation) contain pyrrhotite in a negligible amount.

In some specimens, tourmaline (Fig. 13) and rutile occur as minor components. Usually, the former has a granular or fragmental form, although there are well-defined crystals with a stout prismatic habit in the tuffaceous rocks from Menkyō-bashi, near Nariai, Shinjuku—Kami-ashizawa and Shimo-ashizawa (Nakanosawa Formation). It is strongly pleochroic with following absorption colors, viz., (i) X=light blue, Z=blue, (ii) X=light brown, Z=brown, (iii) X=yellowish brown, Z=dark yellowish brown, (iv) X=grey, Z=dark grey, (v) X=greyish brown, Z=dark brown, (vi) X=greyish brown, Z=blue, (vii) X=greyish blue, Z=dark greyish blue. The latter is, on the other hand, slightly pleochroic from reddish brown to yellowish brown, and tuffaceous sandstones of Yō and Chōkai-zan—Yubune (Nakanosawa Formation) indicate a rare occurrence of minute knee-shaped twin.

The specimens collected from many places are free of cordierite, spinel and staurolite except the sandstones of Yoshizawa (Tsunatori

	(1)	(2)	(3)	(4)	(5)	(6)	(7)	(8)	(9)	(10)	(11)	(12)	(13)	(14)	(15)	(16)
....	①		①			①		①	①				①	①	I	
e	①					①							①			
green hornblende...	Ⅲ		I	Ⅶ	①	Ⅳ	Ⅱ	I	Ⅳ	Ⅱ	Ⅲ	I	I	Ⅵ	Ⅱ	
....	I		①			①		①					①			
....												Ⅱ				
....				①								V				
....	?							?								
te, hematite)......	Ⅵ	X	Ⅸ	Ⅳ	Ⅸ	Ⅵ	Ⅶ	Ⅸ	Ⅶ	Ⅸ	Ⅷ	Ⅳ	Ⅷ	V	Ⅷ	Ⅸ
....																
....	①		①	①	①			①	①	①			①		①	①
....					I											
....								①								
....																
....																
....	①		①	①	①	①	①	①	①	①		①	I		①	①
....	①		①					①								①
....																
....			?													
....							?		①	①						
....																
....	①		①	①		①	①	①	①			①	①		①	①
zircon	Ⅱ		Ⅱ	①	Ⅱ	I	I	Ⅱ	I	I	I	①	Ⅱ	I	I	Ⅱ

	(59)	(60)	(61)	(62)	(63)	(64)	(65)	(66)	(67)	(68)	(69)	(70)	(71)	(72)	(73)	(74)
....							①			①		①			①	
e			①		①		①			①		①		①	①	
reen hornblende...	Ⅳ	Ⅳ	Ⅱ	Ⅱ	Ⅱ	V	Ⅲ	Ⅷ	Ⅳ	Ⅵ		Ⅳ	Ⅳ	Ⅲ	Ⅵ	Ⅲ
....			①	①		①	①		①	①			①	①		
....	Ⅱ		Ⅲ			①	①			①		Ⅱ		I	①	
....		①	I	V		①	①			①			①			①
....					?									?		
te, hematite)	V	Ⅵ	Ⅵ	Ⅳ	Ⅸ	V	Ⅶ	Ⅲ	Ⅶ	Ⅳ	X	V	Ⅶ	Ⅶ	V	Ⅶ
....																
....	①	①	①	①	①	①	①	①		①	①	?	①	①	①	①
....																
....							①			①						
....						①	①			①				I		
....																
....		①	①	①		I	①	①	①	①		①		①	①	①
....															①	
....																
....																
....			①				①		①	①		①				
....														?		
....		?		①	①							?	①	①	①	①
zircon	I	Ⅱ	①	I	I	I	I	I	I	I	I	I	I	I	I	I

①<1%, I=1-10%, Ⅱ=11-20%, Ⅲ=21-30%, Ⅳ=31-40%, V=41-50%, Ⅵ=51-60%, Ⅶ=61-70%,

Table IV. Frequency of some heavy minerals.

(17)	(18)	(19)	(20)	(21)	(22)	(23)	(24)	(25)	(26)	(27)	(28)	(29)	(30)	(31)	(32)	(33)	(34)	(35)	(3
		①	①					①			①	①		①	①	①	①	①	①
	①								①	①					①				
①	IV	I	①	①				①	V	II	II	I	①	①	V	I	①	V	II
	①	①						①	①		①			①	①			①	
							I		II	II	①			?					
	①	①			①		I		①	①			①	①	I			III	
		?							?					①	?				
X	VII	X	IX	VIII	VIII	IX	IX	IX	IV	VIII	VIII	VII	IX	IX	V	IX	X	IV	VI
	①	①	①	①		①			①	①	①	①	①	?	①	①		①	①
														①					
	①			①														①	
															①				
①	①	①	①	①	I	I	①	①	①	①		①		①	①	①		①	①
		①			①		①	I		①	①			①	①		①		
		①			①	①		①	①		?	①		①	①	①			
	①	①	①	①	①	①		①		①	①	①		①	①	①		①	①
I	I	I	II	III	III	I	I	I	I	I	I	II	II	II	I	I	I	I	I

(75)	(76)	(77)	(78)	(79)	(80)	(81)	(82)	(83)	(84)	(85)	(86)	(87)	(88)	(89)	(90)	(91)	(92)	(93)	(9
			①			①		①		①					①			①	
		①						①							①	①		①	
III	II	I	IV	I	II	II	I	III	X	①	①	①	V	II	V	I	①	V	VI
			①	①			①			①								①	
I	II	III	I	①								①		III	①	IV			
I	I	II	①	V							①		①						①
	?	①												?					
VII	VII	VI	IV	V	IX	IX	VIII	VIII	I	X	X	IX	VI	V	V	VI	X	VI	V
I	I	①	①	①	①	①	①	①	①	①	①	I	①	①	①	①	①	①	①
							①												
①	①		①	①	①	①	①	①			①	①	①	①			①	①	①
				①				①											
															①				
					①														
①	①			①		?						①		①	①				
①	①			①		①	①	①		①	①		①			?	①		
I	I	I	II	I	I	I	I	I	①	I	I	I	I	I	I	I	I	I	I

0%, VIII=71-80%, IX=81-90%, X=91-100%.

Table IV. Frequency of some heavy minerals.

(19)	(20)	(21)	(22)	(23)	(24)	(25)	(26)	(27)	(28)	(29)	(30)	(31)	(32)	(33)	(34)	(35)	(36)	(37)	(38)
①	①					①			①	①		①	①	①	①	①	①	①	①
							①	①					①						①
I	①	①				①	V	II	II	I	①	①	V	I	①	V	III	①	V
①						①	①		①			①	①			①			①
					I		II	II	①			?							
①			①		I		①	①			①	①	I			III			
?							?					①	?						
X	IX	VIII	VIII	IX	IX	IX	IV	VIII	VIII	VII	IX	IX	V	IX	X	IV	VII	IX	V
①	①	①		①			①	①	①	①	①	?	①	①		①	①	①	①
												①						I	
		①														①			①
													①						
①	①	①	I	I	①	①	①	①		①		①	①	①		①	①		①
①			①		①	I		①	①			①	①		①				
①			①	①		①	①		?	①		①	①	①					
①	①	①	①	①		①		①	①	①		①	①	①		①	①	①	①
I	II	III	III	I	I	I	I	I	I	II	II	II	I	I	I	I	I	II	I

(77)	(78)	(79)	(80)	(81)	(82)	(83)	(84)	(85)	(86)	(87)	(88)	(89)	(90)	(91)	(92)	(93)	(94)	(95)	(96)
	①			①		①		①					①			①			①
①						①							①	①		①			
I	IV	I	II	II	I	III	X	①	①	①	V	II	V	I	①	V	VI		III
	①	①			①			①								①			
III	I	①								①		III	①	IV					①
II	①	V							①		①						①	I	①
①												?							
VI	IV	V	IX	IX	VIII	VIII	I	X	X	IX	VI	V	V	VI	X	VI	V	IX	VIII
①	①	①	①	①	①	①	①	①	①	I	①	①	①	①	①	①	①		①
					①														
	①	①	①	①	①	①			①	①	①	①			①	①	①	I	
		①				①													
													①						
			①																
		①		?						①		①	①						
		①		①	①	①		①	①		①			?	①				
I	II	I	I	I	I	I	①	I	I	I	I	I	I	I	I	I	I	I	II

0%, IX=81-90%, X=91-100%.

(38)	(39)	(40)	(41)	(42)	(43)	(44)	(45)	(46)	(47)	(48)	(49)	(50)	(51)	(52)	(53)	(54)	(55)	(56)	(57
①	①	①	①		①			①			①		①				①	①	①
①					①						①	①							
V	Ⅲ	I	I	I	Ⅲ	VI	VI	I	①	I	Ⅳ	Ⅲ	II	II		I	I	Ⅲ	Ⅲ
①	①		I			①	①				①		①	①		①		①	①
	①	I		I	①		I			①	I		II	I					
	II	Ⅷ		IX	①				①	①	I	I	I	Ⅷ					
											①								
V	VI	II	IX	I	Ⅷ	Ⅳ	Ⅳ	IX	Ⅷ	IX	VI	Ⅶ	Ⅶ	II	IX	IX	IX	Ⅶ	VI
①	①				①	①		①		①	①	①		①	①	①	①	①	
											①						?		
①	①		①							①		①					①		
①	①		①		①			①	①	①	①	①		①					①
											①							①	
										①	①	①							
①	①				①	①		①	①		①		①		①		①		①
I	I	①	II		I	I	①	II	Ⅲ	II	I	I	①	①	I	I	II	I	I

(96)	(97)	(98)	(99)	(100)	(101)	(102)	(103)	(104)	(105)	(106)	(107)	(108)	(109)	(110)	(111)	(112)	(113)	(114)	(115
①	①				①	①	①								①		①		
		①				①	①												
Ⅲ	I	V	II	①	II	II	V	①	①		?	①	①	①	①			①	I
	①					①	①												
①											①								
①			①					①	①		I				①	①	①	①	
					?														
Ⅷ	Ⅷ	VI	IX	IX	IX	IX	V	X	IX	Ⅲ	Ⅷ	Ⅳ	IX	V	IX	II	IX	Ⅷ	VI
									①										
①	①	①	①		①	①	①	①			①	II	I		①	Ⅳ	①		I
	①					①	①								①				
																		①	
	①		①		①		①		①			①	①	①	①		①	①	I
	①				①		①												
			①				①		①										
							①	①							①			①	
II	II	I	I	II	I	I	I	I	II	Ⅷ	Ⅲ	VI	I	VI	II	VI	II	II	V

Formation), Ainosawa—Ōwarabi (Hashigami Formation) and Kami-matsuyama (Inazawa Formation) respectively, but contain zircon in almost all cases.

So far as has been examined by the writers, zircon (Fig. 14) is composed of two varieties, pink and colorless, the former being more predominant. The crystals are combinations of (100), (110); (110), (111) and (110), (111), (100), (311). They have a prismatic or granular form, and the pink variety is sometimes characterized by a long prismatic crystal with an etched surface. Such crystals are commonly rich in prismatic or granular enclosures with unknown characters.

Besides the mineral components mentioned above, it is worth noting that various kinds of rock-fragments are contained in almost all specimens. They are granite, plagioliparite (rhyolite) (Figs. 15～16), perlite, granophyre (Fig. 17), felsophyre (Fig. 18), felsite, dacite, andesite (Fig. 19), propylite (Fig. 20), basalt (Figs. 21～22), green tuff (Fig. 23), shale and pumice (Fig. 24) embedded in the tuffaceous or pumiceous or sandy matrix. Most predominant are plagioliparite, felsophyre or felsite and represent the main rock-fragments in each formation, taking a rounded or angular form and indicating a microgranitic or spherulitic groundmass with corroded quartz phenocrysts.

Other noticeable rocks are andesite and propylite with a pilotaxitic groundmass. The occurrence of fragmental perlite is, however, restricted to the tuffaceous sandstone from the Uguisu-zawa and Shimo-ashizawa (Nakanosawa Formation), and green tuff is found in nearly same frequency as propylite. Basalt and shale are, on the other hand, very rare as in the case of granite. Moreover, the specimens from Yō, the Uguisu-zawa, Mogami-bashi, Hirashio, the northern foot of Negota-yama (Hashigami Formation) are always characterized by the abundance of pumice. There are also many specimens with large amounts of tuffaceous or glassy substance.

In association with them, the remains of foraminifera are sometimes seen in the tuffaceous sandstones of Okurihashi—Owarabi, Yamanobe, the upper course of the Yoshi-zawa (Mazawa Formation), Narakifuchi, Omoshiro (Hashigami Formation), Katsura—Kami-matsuyama, Okurihashi—Takamori-yama (Nakanosawa Formation).

The frequency of some heavy minerals is shown in Table IV.

Some Geologidal Considerations on the Environment of Sedimentation

One of the characteristic features confirmed from the investigations of sediments distributed extensively in this district is the abundance of such rock rich in tuffaceous substance except for formations almost completely composed of argillaceous rocks. The mineral components of these sediments mostly have an angular form and reveal a fresh appearance, although there are sometimes sericitized orthoclase and plagioclase as well as chloritized biotite. It is also noticeable that apatite and cordierite are still preserved in some specimens, since these minerals are very easily decomposable. Such facts, therefore, suggest that the sediments exposed here were not transported from a distance. Moreover, glauconite is contained in several formations ranging from the Tsunatori Formation up to the Nakanosawa Formation, indicating the sedimentation to have possibly taken place in rather shallow water[9]. This may be similarly inferred from the high frequency of cross-bedding shown by the sandy rocks of the Hashigami Formation and others which are supposed to have been accumulated under a deltaic condition. In such cases, most of the Hashigami Formation probably correspond to the topset or foreset bed, whereas the Nakanosawa Formation may pass from the topset bed to bottomset bed by going westwards.

The deposition of these sediments seems to have taken place in the basin built up largely of granitic masses. It can be guessed from the extensive distribution of granitic rocks in the surrounding area, as is indicated by those of Yamadera, Gando-san, Ryū-zan, Fubira-san, Banjō-zan, Takato-yama, Kamanohata, Isazawa, Asahi-dake, Shōjiga-take, Ōhibara-yama, Akamidō-dake, Ishimidō-dake and others which are not included in the writers' map. At that time, the basin was probably opened northwards, and the accumulation of Neogene sediments was preceeded by that of green tuff in association with repeated igneous activities. Such kinds of green tuff are well exposed on the hilly land behind and at the eastern side of the Shirataka Volcano, being intercalated and traversed by plagioliparite (rhyolite), perlite, felsophyre, andesite, propylite and basalt. These volcanics are represented by sill,

9) W. H. TWENHOFEL, *Treatise on Sedimentation*, (1926), 339.
J. TAKAHASHI and T. YAGI, *Econ. Geol.*, **24** (1929), 838-851.
A. HADDING, *Lunds Univ. Arsskrift, N. F. Avd. 2*, **23** (1932), 153.
T. ICHIMURA, *Mem. Fac. Sc. and Agr. Taihoku Imp. Univ.*, **22** (1940), 61.

dyke and lava flow. Among them, the large exposures of rhyolite and felsophyre flows associated closely with perlite, plagioliparite and andesite are known at the neighbouring area which includes Togami-yama, Omori-yama, Hasedō, Sukarita, Kakumaba, Takatori-yama and Kyōzuka-yama. It is, however, noticed that the occurrence of these volcanics is quite unknown at the area investigated by the writers, notwithstanding that their minute fragments are commonly contained in almost all sandy rocks collected from various formations under consideration. The fragments are frequently found together with those of green tuff and shale. Besides, there are conglomeratic sandstones with many pebbles of volcanics mentioned above. From such evidences, it can be say that green tuff beds already deposited within the basin were locally upheaved and subjected to contemporaneous erosion during the sedimentation of younger formations. This erosion possibly began with the accumulation of the Tsunatori Formation, and the sediments are likely to have been supplied from the area where green tuff and associated volcanics had been exposed together with the granitic rocks and old sedimentary rocks. The green tuff beds exposed here were probably eroded down to the lower horizon characterized by the presence of propylite.

Igneous Activities during and prior to the Deposition of Neogene Sediments

There is much evidence of igneous activities at the mountainous or hilly area adjacent to the Yamagata Basin, where Neogene sediments are extensively exposed. Such activities are now believed to have taken place during and prior to the accumulation of these sediments including large granitic intrusions.

So far as is known from the geological features in surrounding districts, these activities are inferred to have started with the intrusions of granitic or dioritic rocks, and such geological events are supposed to to have been repeated several times.

The granitic or dioritic rocks here are composed of granite (granodiorite), quartz diorite, diorite, aplite, pegmatite and quartz veins. They are mostly pre-Miocene intrusives except some small bodies considered to have been injected into green tuff and associated sediments.

The next activity is represented by the eruption of andesite lavas which rest upon the eroded surface of granitic rocks and are unconformably overlain frequently by Neogene sediments. This type of andesite

is not found on the hilly land near the Yamagata Basin, but is to be seen near Funabiki-yama rising up at the boundary between Miyagi and and Yamagata Prefectures. It was then followed by other kinds of andesite exposed now on Ryūga-take and at the uppermost course of the Tsukinuno-gawa.

Intense activities are also indicated by the remarkable distribution of green tuffs in the adjacent area. Moreover, these activities resulted in the repeated injections or extrusions of plagioliparite (rhyolite), perlite, felsophyre, granophyre, felsite, dacite, andesite, propylite, basalt (dolerite), etc. during the deposition of green tuff beds. At this area, however, the occurrence of Neogene holocrystalline intrusives has not yet been confirmed, although some plutonics ranging quartz diorite to gabbro were found by I. Katō[10] at the northeastern margin of the Shinjō Basin.

Besides, tuffaceous or pumiceous sediments are extremely abundant in the upper horizon of Neogene formations distributed on the hilly land between the Yamagata Basin and the Mogami-gawa, suggesting that the activity was repeated even after the sedimentation of green tuff. They are strikingly abundant in the Tsunatori Formation, Hashigami Formation and Nakanosawa Formation. Mineralogically speaking, the tuffaceous rock of the Hashigami Formation and Nakanosawa Formation occasionally reveal the high frequency of hypersthene or augite crystals at the area covering Hirashio, Mogami-bashi, Karuizawa, Oninome, Iwaya, Yanagi-zawa, Kami-nakagō, Sangō, Yō, Kami-ashizawa and Shimo-ashizawa. This evidence seems to suggest that the submarine eruption repeatedly happened and supplied two minerals mentioned above during the deposition of the Hashigami Formation and Nakanosawa Formation. It is furthermore proved by the abundance of fragmental hard shale, black shale and siliceous liparite embedded in the tuff or tuffaceous sandstone beds exposed near Hirashio. Tertiary lava flows or intrusive bodies are, however, entirely lacking at the area occupied by the sediments ranging from the Tsunatori Formation up to the Inazawa Formation.

Sources of Mineral Components

As has already been stated, the Neogene sediments of the hilly land under consideration contain various kinds of light and heavy minerals supplied from the sources of the surrounding area, where intrusives and extrusives as well as older sedimentaries have been subjected to the intense erosion.

10) KATŌ, *Sc. Rep. Tōhoku Univ., III*, **5** (1955), 76–84.

Of these, some quartz crystals are supposed to have been derived from plagioliparite (rhyolite) or dacite, being embedded in most of tuffaceous or non-tuffaceous sandstones exposed here. Other quartz crystals are, however, believed to have had their sources in granite (granodiorite) and quartz diorite.

Microcline and orthoclase are found in very low frequency as compared with quartz. In these cases, orthoclase occasionally reveals a microperthetic structure, suggesting that such a type of orthoclase was supplied from granite or pegmatite together with microcline. The orthoclase crystals free of this structure were, on the other hand, brought from the area, where granite, plagioliparite, felsophyre, etc. had been exposed. Generally, the phenocrystic orthoclase is rather scarce in plagioliparite (rhyolite) or felsophyre of the surrounding districts. The main source of orthoclase is, therefore, attributed to granitic rocks.

The most important mineral next to quartz is plagioclase which is always characterized by a very fresh appearance. The geological features of the neighbouring area indicate that it came from such plutonics and volcanics as granite (granodiorite), quartz diorite, diorite, gabbro, plagioliparite (rhyolite), felsophyre, dacite, andesite, propylite and basalt (dolerite).

The occurrence of biotite is, however, not so remarkable as quartz and plagioclase. So far as is known at present, biotite granite or hornblende biotite granite, pegmatite, plagioliparite (rhyolite) and other sediments metamorphosed by granitic intrusions are likely to have supplied this mineral during their erosion. It is somewhat different from muscovite whose source was probably pegmatite.

Hornblende is noticeably present in some specimens, as is shown by its bluish green or green variety. They have different sources. For instance, the bluish green hornblende is considered to have originally been a component mineral of metamorphic rocks, whereas the green variety was undoubtedly supplied by the erosion of hornblende biotite granite, hornblende granite, quartz diorite, diorite, hornblende plagioliparite, etc. In contrast with them, the occurrence of the brown hornblende is restricted to a small extent, and its distribution depends upon the exposures of gabbro, gabbro pegmatite and lamprophyre. Besides these, actinolite and tremolite are respectively the erosion products of some actinolite schist and impure limestone recrystallized by the granitic intrusion.

Augite and hypersthene are not so largely distributed as green

hornblende. They are locally found in high frequency, but are occasionally absent even in the beds of the same horizon. Such a mode of occurrence seems to suggest that the submarine eruption took place intermittently during the sedimentation and led these two minerals to the local concentration. They are furthermore characterized by the frequency of well-defined crystals derived from the andesitic lavas and ejecta.

Iron ores are also important components in some specimens, and several sources are inferred for each case. The most noticeable occurrence is shown by ilmenite with a jet-like color and six-sided platy form. It is not infrequently contained in the Neogene andesite exposed here and there at the area behind the Shirataka Volcano.

As to allanite, it is already known that this mineral occasionally occurs in granite or granodiorite forming the foundation of the Zaō and Gando Volcanoes as well as in those of Asahi-dake[11]. Similar plutonics may be the sources of apatite, titanite and pink garnet, but epidote is likely to have had its origin in epidotized granite or granodiorite and propylite.

Tourmaline is usually seen in granite, pegmatite, aplite and also in metamorphosed sediments (for example, hornfels). In these rocks, the tourmaline crystals of pegmatite and aplite have some different pleochroic scheme, viz., light blue (X) or light brown (X) to blue (Z) and greyish blue (Z). Those of hornfels or other metamorphosed sediments are, however, pleochroic from light yellowish brown (X) to dark brown (Z), taking a well-deffned crystal form in most cases. Most of tourmaline crystals in the Neogene sediments are, therefore, supposed to have been brought from the contact aureole as in the case of staurolite and cordierite.

Rutile is not rare in granite and such a green rock as amphibolite or hornblende schist, and anatase is apt to occur in granite and quartz-porphyry, but their mother rocks have not yet been confirmed in the surrounding districts. Similarly, it is still obscure from where spinel was supplied. Oliving is hardly preserved in sediments, since it is easily subjected to decomposition, and its possible source may be olivine basalt associated closely with green tuff beds.

Zircon is, on the other hand, a common accessory mineral in granite, granodiorite and plagioliparite. It is worth noting that the zircon crystals from granitic rocks of adjacent area are mostly represented by pink or

11) Personal Communication by T. OGURA.

colorless varieties with a stout prismatic habit and well-defined form.

Those of plagioliparite are, however, frequently elongated and always have a pink color, being sometimes corroded to a crub-like form with an irregular outline. The crystals from such different sources are found together in the Neogene sandy rocks exposed here and on the adjacent hilly land. Moreover, there are glauconite, pyrite, chlorite, calcite and limonite which are diagenetic or secondary minerals indifferent from the sources of sediments.

Summary

(i) Neogene sediments free of green tuff are largely exposed on the hilly land between the Mogami-gawa and Yamagata Basin. They are represented by the Tsunatori Formation, Mazawa Formation, Hashigami Formation, Nakanosawa Formation and Inazawa Formation, being composed of conglomeratic sandstone, tuffaceous or non-tuffaceous sandstone, siltstone, shale, mudstone, tuff, etc.

(ii) These Neogene sediments were intensely folded and faulted, but they have a general strike of N–S to N30°E, showing anticlinal or synclinal structures.

(iii) Many specimens represented mostly by the tuffaceous or non-tuffaceous sandstones were collected from various parts of each formation to examine mineral components and rock-fragments contained in them. For this purpose, the microscopical investigations of their thin sections and isolated minerals separated by mechanical analyses were carried out on these specimens. The minerals determined in this way are quartz, microcline, orthoclase, plagioclase, biotite, muscovite (sericite), calcite, chlorite, glauconite, bluish green hornblende, brown hornblende, green hornblende, actinolite, tremolite, augite, hypersthene, olivine, hematite, ilmenite, limonite, magnetite, pyrite, pyrrhotite, allanite, epidote, zoisite, anatase, cordierite, garnet, spinel, staurolite, titanite, topaz (?), colorless zircon and pink zircon. Moreover, they are found in association with such rock-fragments as granite (granodiorite), plagioliparite (rhyolite), felsophyre, felsite, granophyre, perlite, dacite, andesite, propylite, basalt (dolerite), pumice, green tuff and shale.

(iv) Various kinds of mineral components and rock-fragments as well as the pebbles of conglomeratic sandstone suggest that their sources were granite (granodiorite), quartz diorite, diorite, gabbro, pegmatite, aplite, lamprophyre, plagioliparite (rhyolite), felsophyre, felsite, perlite,

granophyre, dacite, andesite, propylite, basalt (dolerite), amphibolite, hornblende schist, actinolite schist, biotite schist, hornfels, green tuff and associated sandy or shaly rocks.

In the surrounding districts, important intrusives and extrusives are granite or granodiorite, plagioliparite (rhyolite), felsophyre, andesite, propylite and basalt. Among them, granite or granodiorite constructs a base rock overlain by Neogene sediments, whereas plagioliparite and other kinds of volcanics are closely associated with green tuff beds intercalted by siltstone, mudstone, shale and sandstone.

(v) The Neogene sediments exposed here and at the adjacent area are likely to have been deposited in the basin surrounded partly by the exposures of granite (granodiorite) and other plutonic rocks as well as of some metamorphosed sediments. It is also inferable that green tuff beds were locally upheaved during the accumulation of still younger Neogene sediments and were subjected to the contemporaneous erosion. The mineral components and rock-fragments of Neogene sediments younger than green tuff are, therefore, supposed to have been supplied from the surrounding area, where green tuff and associated volcanics had extensively been exposed together with granitic rocks.

(vi) Volcanic substances are abundantly present in the Neogene sediments of the hilly land bordered by the Mogami-gawa, Yamagata Basin and Shirataka Volcano. They are remarkably tuffaceous and sometimes pumiceous, excluding the tuff intercalated between them. Such a lithological character may partly depend upon the erosion of green tuff beds already deposited, but it can also be said that volcanic eruptions took place repeatedly on the sea bottom and its adjacent land during the continuous accumulation of sediments. The possibilities of submarine eruption are indicated by the abnormal features which are not infrequently found in the beds of tuff and tuffaceous sandstone exposed near Hirashio or elsewhere.

Acknowledgement

The writers wish to express their cordial thanks to the staff of the Teikoku Oil Company who gave them an opportunity to start their field works. They are also indepted deeply to Dr. H. Tsuya and Mr. T. Watanabe of the Earthquake Research Institute whose kindness largely facilitated their laboratory investigations. A part of this investigation

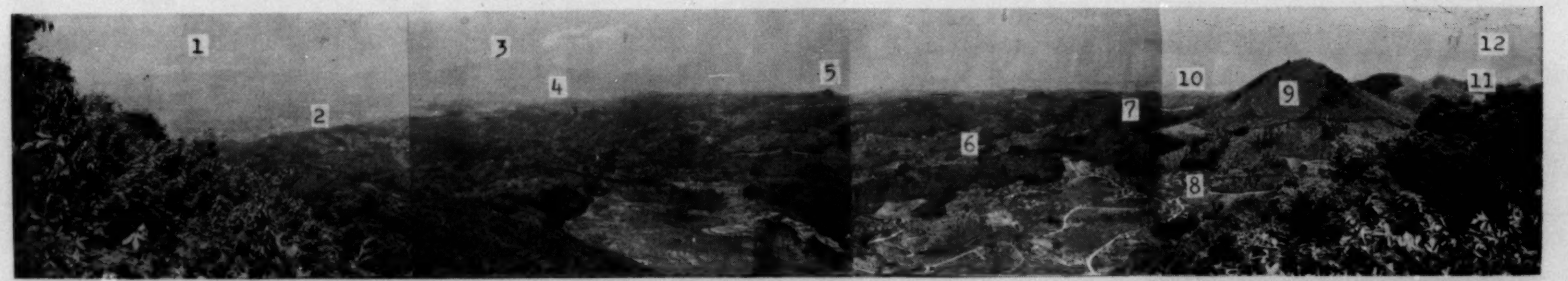

Fig. 4. A panoramic view of the hilly land adjacent to the western margin of the Yamagata Basin. This picture was taken from the summit of Nishi-kuromori-yama.

1=Gassan, 2=The Mogami-gawa, 3=Ha-yama, 4=Aterazawa, 5=Chōkai-zan between Yubune and Araya, 6=Yanazawa, 7=Rai-zan, 8=Hataya, 9=Higashi-kuromori-yama, 10=Yamagata Basin, 11=Ō-numa, 12=Gando-san.

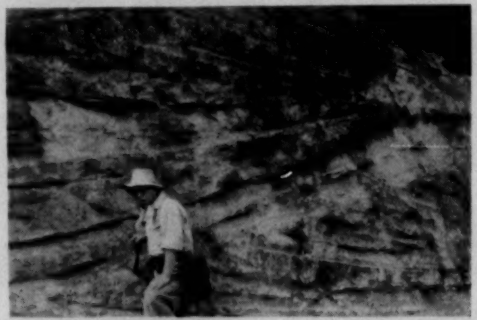

Fig. 5. Cross-bedding of tuffaceous sandstone exposed on the cutting of bus road between Aino-sawa and Ōwarabi.

Fig. 6. Cross-bedding of tuffaceous sandstone exposed along the trail between Hirashio and the Uguisu-zawa.

(震研彙報 第三十五号 図版 市村・青木)

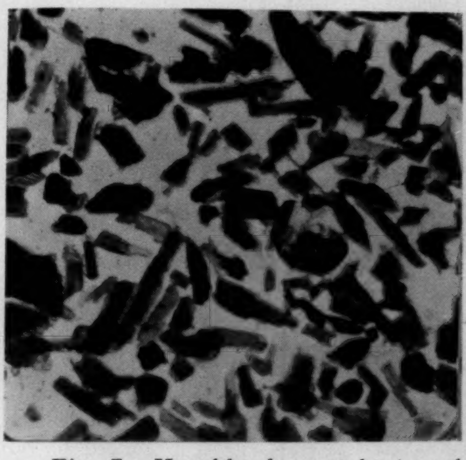

Fig. 7. Hornblend crystals (conglomeratic ss., Hashigami Formation, Omoshiro). ×40.

Fig. 8. Augite crystals with a hacksaw structure (tuffaceous ss., Hashigami Formation, Oninome-Karuizawa). ×100.

Fig. 9. Hypersthene crystals with a hacksaw structure (tuffaceous ss., Hashigami Form., Oninome-Karuizawa). ×100.

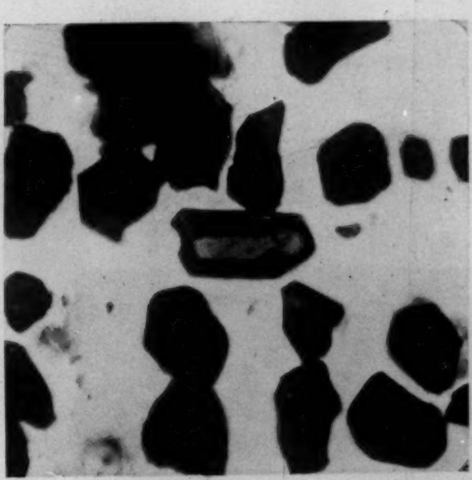

Fig. 10. Allanite, prismatic crystal (tuffaceous ss., Nakanosawa Formation, Wagōtaira-Wagō). ×100.

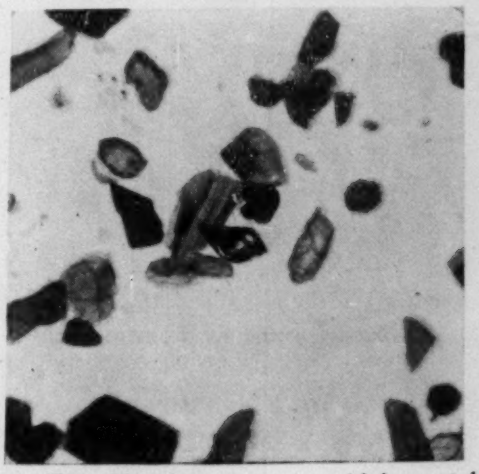

Fig. 11. Anatase, pyramidal crystal (taffaceous ss., Hashigami Formation, Oka). ×100.

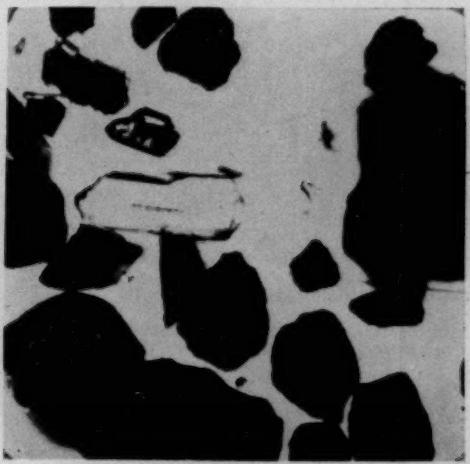

Fig. 12. Apatite, prismatic crystal (tuffaceous ss., Hashigami Formation, Iwaya). ×100.

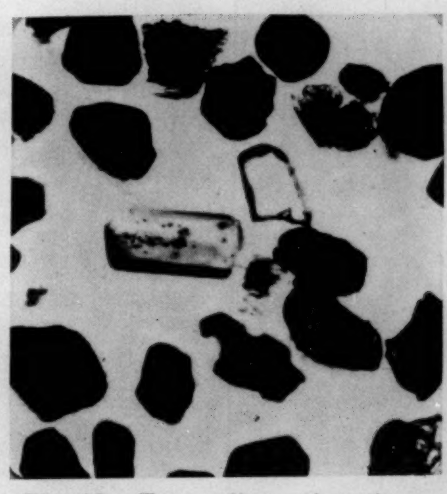

Fig. 13. Tourmaline, prismatic crystal (tuffaceous ss., Nakanosawa Formation, Wagōtaira-Wagō). ×100.

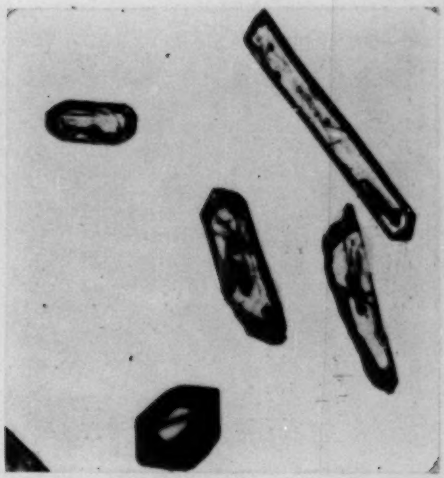

Fig. 14. Zircon crystals (siltstone, Inazawa Formation, Kami-matsuyama). ×100.

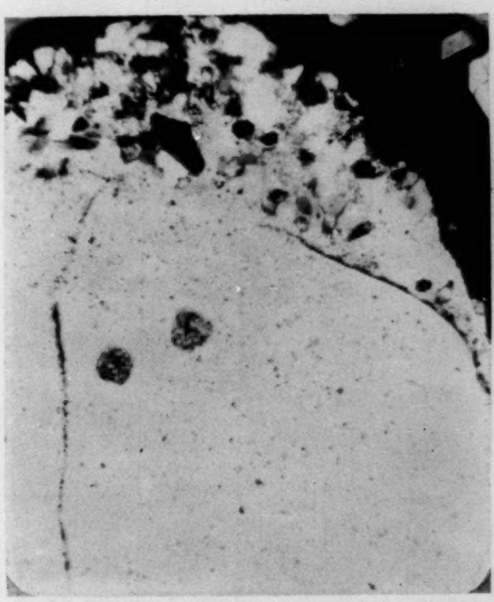

Fig. 15. Plagioliparite-fragment (tuffaceous ss., Hashigami Formation, Iwaya). ×100.

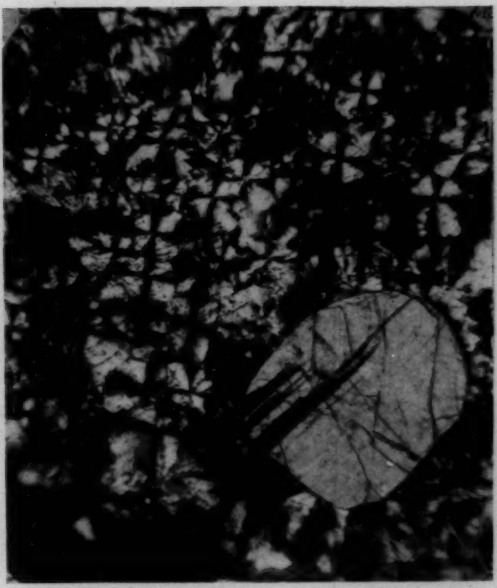

Fig. 16. Spherulitic rhyolite-fragment (ss., Mazawa Formation, Suwa). ×100.

Fig. 17. Granophyre-fragment (brecciated tuff, Tsunatori Formation, Deshio). ×100.

Fig. 18. Felsophyre-fragment (tuffaceous ss., Hashigami Formation, Ainosawa-Ōwarabi). ×100.

Fig. 19. Andesite-fragment (ss., Nakanosawa Formation, Yubune). ×100.

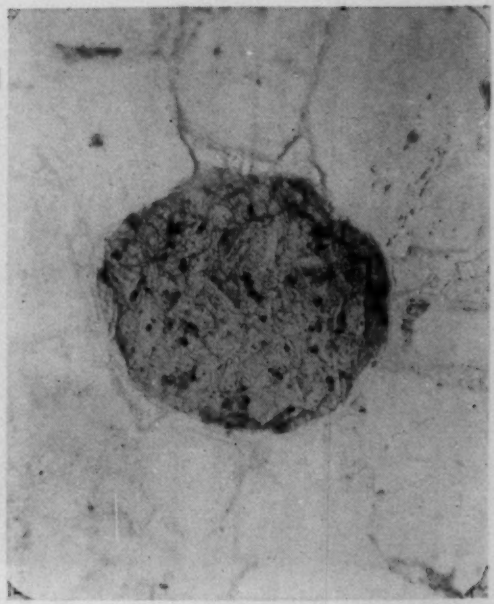

Fig. 20. Propylite-fragment (tuffaceous ss., Hashigami Formation, Ainosawa-Ōwarabi). ×100.

Fig. 21. Basalt-fragment (ss., Hashigami Formation, Hirashio . ×100.

Fig. 22. Dolerite-pebble (conglomeratic ss., Ma awa Formation, Oninome). ×100.

Fig. 23. Green tuff-fragment (ss., Nakanosawa Formation, Yubune-Chōkai-zan). ×100.

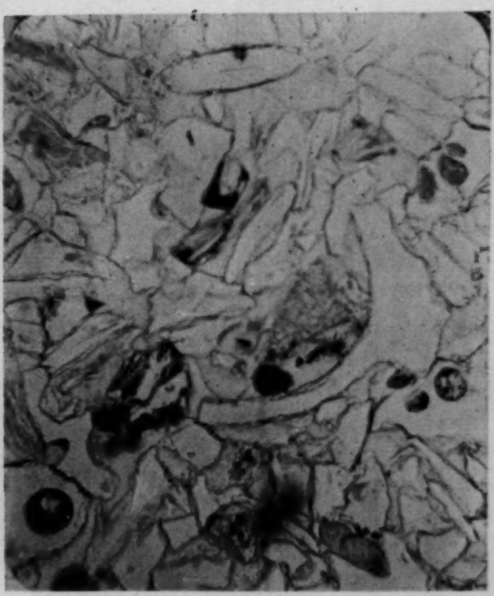

Fig. 24. Pumice-fragments (tuffaceous ss., Nakanosawa Formation, Shinjuku-Kamiashizawa). ×100.

was carried out with the aid of an Education Ministry Grant for Natural Science.

---

5. 山形盆地西縁の新第三紀堆積岩に関する地質学的考察

山形大学 {市村　毅 / 青木和子}

山形盆地と最上川との間を占める丘陵地帯には，新第三系が広く露出している．この新第三系を形成する堆積岩は，凝灰岩，凝灰質砂岩，非凝灰質砂岩，頁岩，泥岩，シルト岩，礫岩などであり，それ等の中でも凝灰質の岩石が特に多い．凝灰質砂岩，非凝灰質砂岩，シルト岩には，石英（蝕融されたもの多し)，正長石（屢々微ペルト構造を示す）微斜長石，斜長石，黒雲母，白雲母，方解石，海緑石，緑泥石，帯青緑色角閃石，[透角閃石，陽起石，普通輝石，紫蘇輝石，橄欖石，褐簾石，緑簾石，黝簾石，鋭錐石，燐灰石，柘榴石，菫青石，スピネル，十字石，電気石，金紅石，クサビ石，磁鉄鉱，赤鉄鉱，褐鉄鉱，チタン鉄鉱，黄鉄鉱，磁硫鉄鉱，トパツ(?)，ジルコンなどと共に，花崗岩，文象岩，斜長石石英粗面岩，真珠岩，珪長斑岩，珪長岩，石英安山岩，安山岩，変朽安山岩，玄武岩，緑色凝灰岩，頁岩の微小片，浮石片および凝灰質物を含有する．これ等の内容から分る様に，この地域の堆積岩は，主として斜長石石英粗面岩，安山岩，玄武岩，変朽安山岩などと共に花崗岩花崗閃緑岩およびその関係岩類，古期の堆積岩，変成岩，緑色凝灰岩などよりなる地域からその各種材料が供給され，然も浮石とか凝灰質物が上下の地層を通じて多い点は，各地層の堆積当時，火山活動(陸上海底共)が非常に劇しかつたことを物語つている．更に各種の鉱物は，角立ち，且つ新鮮なる外観を有するものが多い．従つてこの地域の堆積岩を形成する材料は決して遠方から運ばれたものでなく，現在の周縁地域における地質が示す通り，恐らく材料の根源が，白鷹火山以南の最上川最上流地域，山形盆地以東および寒河江川の上流地域あたりにあつたものと想像される．

---

6. *Energetics in Active Volcanoes. 2nd Paper.*

By Izumi YOKOYAMA,

Earthquake Research Institute.

(Read Oct. 23, 1956.--Received Dec. 31, 1956.)

Summary

Energetics related to the 1950~52 activities of Volcano Mihara, Ooshima Island are analysed in Part I of this paper in a way similar to the writer's previous paper. In Part II, the study of energetics of volcanic action is extended to many volcanoes in Japan and foreign countries, the discussion being made on the basis of the results obtained by the analyses of activities of Volcano Mihara during the period from 1950 to 1954.

PART I.

Activities of Volcano Mihara, Ooshima Island during the Period 1950 ~ 1952.

Volcano Mihara, Ooshima Island commenced an eruption at the crater on July 16, 1950 after 10 years' quiescence. The eruption continued until Sept. 23, 1950 displaying progressive activities of the *Strombolian* type. Next year, from Feb. 4 to June 28, the volcano resumed its activity on a larger scale. We name these two years' activities the 1950–51 eruption, which seems to be one of the most violent eruptions in historical times ranking with the 1777–78 eruption.

As a continuation of the previous paper[1], the writer is going to summarize here all the data related to energetics of volcanic action observed on Volcano Mihara during the period from 1950 to 1952, the method of the analysis being based upon the same principle as the one in the previous analyses.

1. Energy of volcanic tremors.

In estimating the energy of volcanic tremors on Volcano Mihara during the period, the writer investigates the seismometrical records obtained by the Ooshima Weather Station which is situated at a dis-

1) I. YOKOYAMA, *Bull. Earthq. Res. Inst.*, **34** (1956), 185.

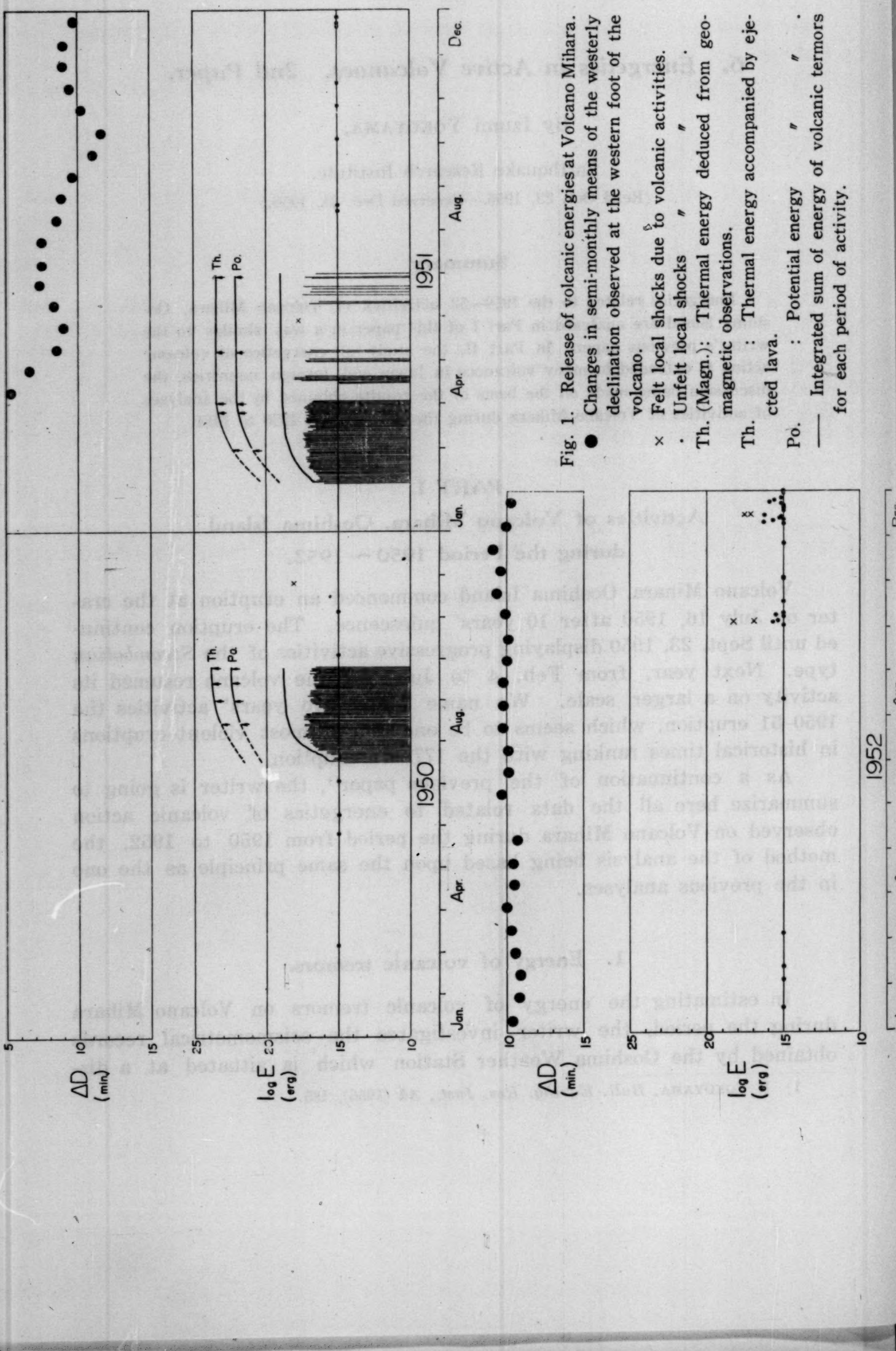

Fig. 1 Release of volcanic energies at Volcano Mihara.

● Changes in semi-monthly means of the westerly declination observed at the western foot of the volcano.

× Felt local shocks due to volcanic activities.

· Unfelt local shocks 〃 〃.

Th. (Magn.): Thermal energy deduced from geomagnetic observations.

Th. Thermal energy accompanied by ejected lava. 〃 〃

Po. : Potential energy 〃 〃

—— Integrated sum of energy of volcanic tremors for each period of activity.

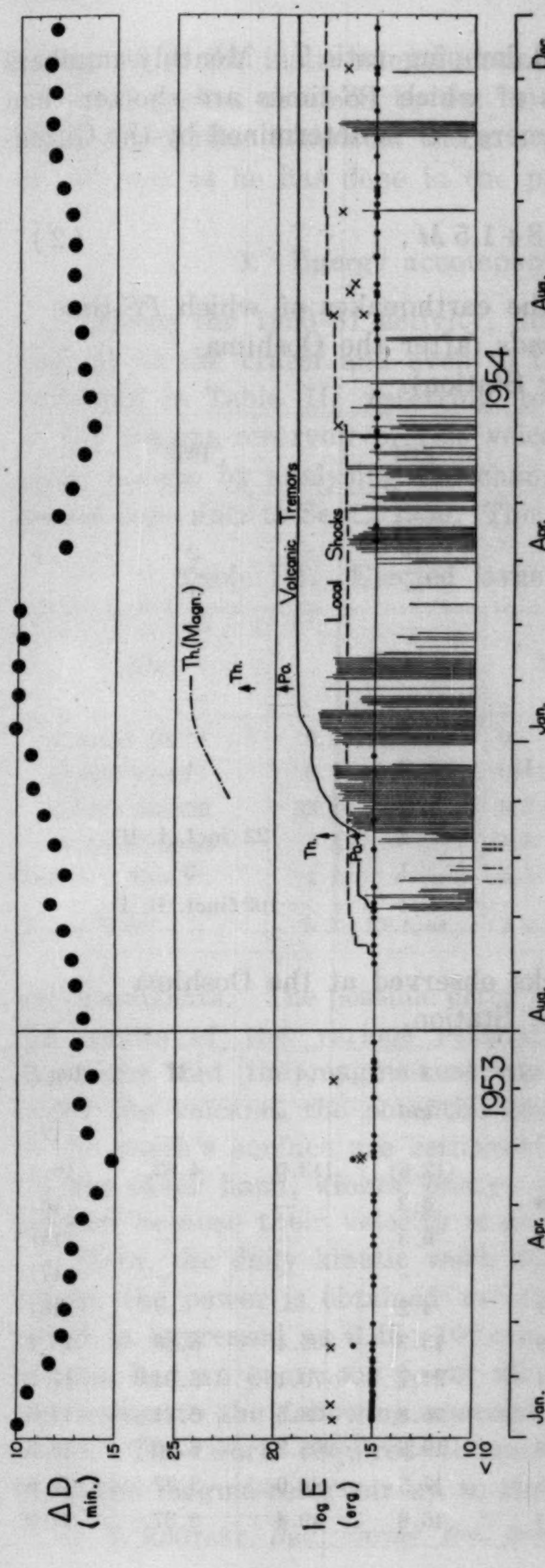

tance of 4.8 *km* from the crater. Some investigations of these records had already been carried out by Y. Kizawa[2] who kindly placed his data at the writer's disposal. Kizawa has given the maximum amplitude of the three components of volcanic termors at 08 and 20 *h* every day. By K. E. Bullen's method as was adopted in the previous paper, the daily energy which is emitted as tremors is approximately given by

$$E = 2.68 \times 10^{10} \sum_{1}^{2} A^2 \frac{\Delta T}{\tau} (erg), \quad (1)$$

where A is the amplitude of the horizontal component measured in *micron* and τ is the period of vibration which varies from 0.6 to 0.8 *sec*. For the sake of convenience, we assume the duration time ΔT as 6 *hours*. The results thus obtained are shown by the columns for each day in Fig. 1.

2. Energy of volcanic earthquakes.

The energy of local shocks of volcanic origin is estimated from the seismometrical data obtained by the Ooshima Weather Station. The seismometers are Wiehert-type ones usually having

2) Y. KIZAWA, *Jour. Geogra.* (Tokyo), **60** (1951),128.

magnification 100, period 5.0 *sec.* and damping ratio 7. Monthly numbers of the felt and unfelt earthquakes of which *PS*-times are shorter than 5 *sec.* are shown in Table I. The energy E is determined by the Gutenberg and Richter's formula:

$$\log E = 11.8 + 1.5\,M\,, \qquad (2)$$

Table I. Monthly numbers of the earthquakes of which *PS*-time is shorter than 5 *seconds* (after the Ooshima Weather Station).

Month \ Year	1950	1951	1952
Jan.	—	—	1
Feb.	—	—	2
Mar.	1	—	1
Apr.	—	—	—
May	1	1 (I)	—
June	1	—	—
July	1	—	—
Aug.	6 (II, II, I, I, II, I)	3	1
Sept.	—	—	—
Oct.	1	2	22 (incl. I, II)
Nov.	2 (incl. II)	1	3
Dec.	—	4	102 (incl. II, I)

Table II. Felt local shocks observed at the Ooshima Weather Station.

P (J. S. T.)			Intensity	$P \sim S$	Δ	A	M	$\log E$
		d h m		*sec.*	*km*	μ		
1950	Jan.	4 03 40	II	—	—	—	—	(17)
		5 01 41	II	—	(12.6)	113.0	4.63	16.4
		5 04 48	I	0.9	6.3	—	—	(16)
		5 11 08	I	0.9	6.3	—	—	(16)
		5 18 55	II	—	—	—	—	(17)
		25 21 13	I	0.7	4.2	—	—	(16)
	Nov.	25 10 26	II	1.9	13.3	305.4	6.26	18.1
1951	May	28 17 32	I	3.1	21.7	70.1	5.94	17.7
1952	Oct.	4 04 45	I	2.4	16.8	38.5	5.21	17.0
		4 19 41	II	2.8	19.6	205.2	6.50	18.3
	Dec.	15 00 55	II	2.5	17.5	84.0	5.77	17.6
		15 06 44	I	2.4	16.8	49.4	5.37	17.2

where M is the instrumental magnitude. The energy of the felt volcanic earthquakes obtained by eq. (2) is also shown in Table II and Fig. 1 while the writer estimates the energy of the unfelt shock at the order of 10^{15} *ergs* as he has done in the previous paper.

3. Energy accompanied by the lava-flows.

During the 1950–51 activity, fluidal lavas over-flowed from the central pit to the crater and even to the caldera. Their distributions are tabulated in Table III referring to various reports. As for the depth of the magma-reservoir of this volcano, T. Rikitake[3] presumed it to be about 5.5 *km* by analysing the changes in geomagnetic dip during the period from July to Sept., 1950. This value is also acceptable from geological standpoints. The possible error in this value would not seriously affect the results of the various estimations which will be made hereafter. Assuming that the magma-reservoir is situated at a depth of 5.5 *km* under the volcano, the potential energies required to push up the lavas to the earth's surface are estimated as shown in Table IV and Fig. 1. On the other hand, kinetic energy of the fluidal motion of lava-flows is ignored because their velocity is small enough in the crater-vent.

Table III. Ejected lavas in the 1950–51 eruption.

Site	1950	1951	Total		
			Volume	Density	Mass
Central pit	9.8×10^6 *tons*	0	$3.66\times10^6 m^3$	2.7	9.8×10^6 *tons*
Cinder cone	6.2 〃	0	3.62 〃	1.7	6.2 〃
Crater bottom	33.4 〃	8.3×10^6 *tons*	15.44 〃	2.7	41.7 〃
Nomashi flows	1.3 〃	11.3 〃	5.05 〃	2.5	12.6 〃
Senzu flow	1.1 〃	4.5 〃	2.25 〃	2.5	5.6 〃
Total	5.2×10^7 *tons*	2.4×10^7 *tons*	3.0×10^7 m^3		7.6×10^7 *tons*

Here, the daily kinetic work done by lifting the lava, or in other words, the power is obtained as shown in Table IV, where 1 *horse-power* is expressed as 6.45×10^{11} *erg./day*. As seen from the table, the volcano had an enormous power all through the period. The fact leads the writer to the following speculation on the beginning stage of eruptions: The work required to carry the fluidal lava through the pit from the magma-reservoir up to the crater vent will be easily obtained

3) T. RIKITAKE, *Bull. Earthq. Res. Inst.*, **29** (1951), 161.

Table IV. Mass and energies of ejecta.

Period	Ejected Mass Integrated Sum	Potential Energy Integrated Sum	Potential Energy Power	Thermal Energy Integrated Sum
1951 July 16 ~Aug. 14	1.4×10^{7} *tons*	7.5×10^{21} *ergs*	2.5×10^{20} *ergs/day*	1.8×10^{23} *ergs*
~Aug. 31	3.5 〃	1.9×10^{22}	7.1 〃	4.5 〃
~Sept. 13	5.0 〃	2.7 〃	6.0 〃	6.3 〃
~Sept. 24	5.2 〃	2.8 〃	1.3 〃	6.6 〃
1951 Feb. 4 ~Feb. 27	1.7×10^{6}	9.2×10^{20}	3.8×10^{19}	2.1×10^{22}
~Mar. 25	1.5×10^{7}	8.1×10^{21}	2.7×10^{20}	2.0 〃
~Mar. 31	2.0 〃	1.1×10^{22}	5.0 〃	2.6 〃
~May 6	2.2 〃	1.2 〃	2.8×10^{19}	2.7 〃
June 5 ~June 28	2.4×10^{7}	1.3×10^{22}	4.1×10^{19}	3.0×10^{23}
1954 Jan. 27	$8\ \times10^{5}$	1.6×10^{20}	7.7×10^{20}	6.7×10^{21}

in the following, provided the friction in the pit is neglected. Assuming that the density of lava is 2.3 *gr./cc* and the sectional area of the pit is 100 m^2 (the diameter of the vent observed in Sept. 1950 was about 5 *m*), the potential energy required to fill up the pit with lavas is estimated at 4.0×10^{20} *ergs*. If we assume a value of the power such as is obtained in Table IV, it is probably possible that activity of magma-reservoir reaches the earth's surface in only a day or less. Although no definite value of the power of volcanic action is known at the beginning stage of eruption, it seems of interest and importance that the activity that takes place in the reservoir may come up with a fairly large speed such as a few *kilometers* a day as far as the resistance in the pit is disregarded. In fact, no forerunning phenomena were apparent previous to the 1950 eruption, while the volcanic tremors whose origins are deemed to be situated near the surface began to occur only 8 *minutes* before the eruption. These facts would suggest that the lava came up quickly without causing any marked effects such as forerunning earthquakes.

Next, we must take into account the thermal energy transported by the lavas which plays the most important role in energetics of the volcanic activities as discussed in the previous paper. If we take the specific heat of the basaltic lava as 0.25 *cal./gr.°C* the temperature of the lava as 1,000°*C* and the heat of fusion as 50 *cal./gr.*, the thermal

energy carried away through the vent of the volcano is to ordinary temperature estimated as follows:

$$E_{th} = M(1000°C \times 0.25\, cal./gr.°C + 50\, cal./gr.)J \quad (ergs) \qquad (3)$$

where M is the mass of ejected lava and J is the equivalent work of heat. The sums of the thermal energy integrated for each period are also shown in Table IV and Fig. 1.

4. Energy released in other forms.

In the previous sections, the writer has been estimating the amount of the energies which are released in various ways in connection with volcanic activity, all of which can be estimated quantitatively provided we can conduct proper observations. But there may be energies released in other forms which are really difficult to observe, as they are lost by heat-conduction and gas-expansion from the reservoir to the vent of the volcano. The only way to estimate this sort of energy would be to subtract the known energies such as have been examined in the preceding sections from the energy supplied to the reservoir.

Fortunately, the order of the energy which is supplied to the reservoir in the course of an activity of the volcano can be approximately inferred from geomagnetic studies: During the early period of the 1950 eruption, from July to September, T. Rikitake observed anomalous changes in geomagnetic dip-angle associated with the activity. He concluded that the changes are likely to be caused by an apparent magnetic dipole situated just beneath the volcano at a depth of 5.5 km with a magnetic moment amounting to 6.3×10^{14} *emu*, the direction of the polarization of the dipole being nearly opposite to that of the earth's magnetic field there. The demagnetization, which is suggested by the occurrence of such a dipole, seems to be due to the rise in temperature in the said region associated with the eruption. As is the case of the 1953–54 eruption, the amount of heat that is necessary for the demagnetization observed by Rikitake in 1950 is estimated at about 2.6×10^{18} *cal.* (1.1×10^{26} *ergs*), though thermal processes relating to these changes can't be discussed in detail because no continuous observation of geomagnetism was available in Ooshima at that time.

Here, it may be reasonably assumed that the energy supplied to the magma-reservoir in the case of the 1950 eruption is at least of the same order of magnitude as the above figures. As fully discussed in

the last section, the energy released from the volcano in such a form that we could observe and estimate quantitatively was estimated at 4.4×10^{23} *ergs*. The residue must be dissipated by thermal conduction, convection and radiation and expansion of gases from the reservoir as discussed previously.

On the other hand, S. Murauchi[4] made a few observations of the amount of the gases (almost composed of water vapour) emitted from Volcano Mihara in the 1950-51 eruption. He has given the following figures, though not so accurately.

	Emitted water vapour	Ejected lava
Sept. 1, 1950	2.1 *tons/sec.*	15.9 *tons/sec.*
〃 17, 1950	1.8 〃	12.6 〃
Feb. 11, 1951	0.055 〃	0.50 〃

According to this result, it may be said that water vapour amounting to more than 10^4 *tons* per day was emitted in the active stage of the eruption. If we take the temperature of water vapour at the vent of the volcano as $500°C$, thermal energy carried away by the vapour is estimated at about 10^{13} *cal.* ($\approx 10^{20}$ *ergs*) per day. Thus, the emission of gases from the volcano would certainly play a rather important role in its energetics though we have never had continuous observation of emitted gases on the volcano. This sort of observation would be difficult to carry out on an actual volcano, because we usually find there many vents or cracks which are emitting gases all the time. In order to complete energetics of active volcanoes, however, we should put much stress to the observation of this kind though many difficulties are to be overcome.

5. Discussion.

On examining the results shown in Fig. 1, the writer reaches the following conclusions which are almost the same as those of 1st Paper.

1) The total energy emitted as volcanic tremors was almost the same order in magnitude as that of local shocks which occured during the period.

2) Local shocks, either felt or unfelt, scarcely occured when volcanic tremors are prevailing. This fact would suggest that an activity in

4) S. MURAUCHI, *Bull. Natur. Sci. Mus.*, **20** (1953), 70.

the deeper interior of the volcano does not occur simultaneously with that near the surface.

3) It is made clear that the thermal energy such as the heat carried away by lavas and gases occupies the main part of the energy which comes out from the volcano, while the amount of the other energies of tremors and local shocks and potential energy, is definitely smaller than the thermal one.

PART II.

Activities of a Number of Volcanoes in Japan and Indonesia in the Past.

A number of geophysicists have hitherto discussed magnitude or energy of particular explosions especially those of the *Vulcanian*-type volcanoes. For example, T. Minakami[5] studied in great detail the explosions and related phenomena on Volcano Asama. Meanwhile, T. Matuzawa[6] estimated various energies released by the great 1914 eruption of Volcano Sakurazima and pointed out that the thermal energy accompanied by the lava-flows was the largest.

Recently, H. Tsuya[7] proposed an intensity scale of volcanic eruption which classifies intensity of volcanic activity into ten grades, 0–IX, assuming that the intensity is proportional to the potentiality of volcanic gases to drive their container, either fluent or fragmentary, hence proportional to the total volume of ejecta. Then he divided the volcanic ejecta into three types, essential lava-flow (A-type), fragmentary ejecta only (B-type) and essentially old detritus ejected in the past (D-type).

On taking into account the results obtained in Part I of this paper, the writer would like to extend Tsuya's classification by volume of ejecta to one by energy sent out by volcanic activities. As a consequence of this investigation, several examples of volcanic activities in Japan and Indonesia will be illustrated in the following.

1. Classification and estimate of volcanic energies.

Generally speaking, the energy of volcanic activities is spent in the following ways:

5) T. MINAKAMI, *Bull. Earthq. Res. Inst.*, **20** (1942), 431.
6) T. MATUZAWA, *Zisin-gaku* (in Japanese) (1950), 363.
7) H. TSUYA, *Bull. Earthq. Res. Inst.*, **33** (1955), 341.

1). In producing volcanic tremors;
2). In producing local earthquakes;
3). In breaking the material of the mountain-mass;
4). In ejecting the material from the interior of volcano such as lava-flows, fragmentary ejecta and gases;
5). In producing disturbances in the air or sea.

The first two energies released as volcanic tremors and local shocks were already discussed in detail for the case of Volcano Mihara.

The energy spent in the third way is, at the lowest, equal to elastic strain energy which may be contained in the rock-mass before it ultimately breaks down, namely,

$$E_e = \frac{1}{2} Y e^2 V, \qquad (4)$$

where Y, e and V represent Young's modulus, ultimate strain of the rock and volume of the destroyed mountain-mass respectively. Y may be supposed to be $5 \times 10^{11}\,dyne/cm^2$ on referring to F. Birch's[8)] paper. According to C. Tsuboi's[9)] studies on the crustal movemnts in Japan and experimental studies on rocks, e may be safely assumed to be 10^{-4}.

The fourth energy is accompanied by materials including fluidal lavas, solid ejecta and gases and classified into three subgroups;

Potential energy, kinetic energy and thermal energy.

Potential energy will be estimated if the depth of the magma-reservoir is given. The depth is generally believed to amount to several *kilometers* beneath the volcano. It has been demonstrated by the writer that geomagnetic methods are useful for presuming the depth of the reservoir, especially on the volcano composed of basaltic rocks.

Kinetic energy consumed by eruptions is determined by the initial velocity of ejecta at the vent of the volcano which was closely studied by T. Matuzawa. On Volcano Asama, T. Minakami established the relation between the explosion energy and the amplitude of the volcanic earthquakes observed at a station on the foot of the volcano.

The higher the temperature of ejecta is, the more important is the thermal energy. And ejecta composed of old detritus is almost unrelated with thermal energy. If the ejected lava has a temperature of almost $1{,}000°C$ and is fluidal, the total heat lost by lava crystallizing and cooling to ordinary temperature is approximately estimated by

8) F. BIRCH, *Handbook of Physical Constants* (1942), 73.
9) C. TSUBOI, *Bull. Earthq. Res. Inst.*, **11** (1933), 275.

$$E_{th}=M(1000°C\times 0.25\,cal./gr.°C+50\,cal./gr.)J \qquad (ergs), \qquad (5)$$

where the specific heat and the latent heat of lava is assumed to be 0.25 $cal./gr.°C$ and 50 $cal./gr.$ respectively. And if the ejecta has a temperature of 500°C, the heat-loss by it is given by

$$E_{th}=M(500°C\times 0.20\,cal./gr.°C)J \qquad (ergs). \qquad (6)$$

In the following discussion, the writer assumes that the temperatures of A- and B-type ejecta is 1,000°C and 500°C respectively.

As for gases, thermal energy accompanied by them was discussed for the case of the eruption of Volcano Mihara in Part I. In short, it is not possible to estimate accurately this sort of energy.

Lastly, the energy of producing distrubances in the air or sea is found to be so small that we can neglect it completely compared with the other energies.

2. Examples of the estimation of volcanic energies.

During these scores of years, early pioneers in geophysics and geology have made quantitative and reliable observations of various volcanic activities in Japan. The writer's analyses of energetics of Japanese volcanoes are altogether due to their work. In discussing the eruptions of Indonesian volcanoes the writer refers to "Catalogue of the Active Volcanoes of the World" which is the standard authority concerning active volcanoes.

The following examples of estimation of the volcanic energies will be based upon the principles obtained by the previous studies. It turns out, however, that we may take into account, for order-of-magnitude estimates, only thermal energy because energies of other kinds do not contribute very much to the total sum of the energy.

Tambora, Sumbawa 1815

On April 5, 1815 thundering explosions were heard even at distances of 1250 and 1400 km. The paroxysmal eruptions lasted from April 10 to 12. Detonations were heard at distances of 1500 and 1750 km. Rock fragments of 2 cm in diameter and a few of 15 cm have fallen at a distance of 40 km from the crater.

Verbeek estimated the amount of ejecta at 150 km^3, Petroeschevsky at 100 km^3, while Pannekoek van Rheden calculated it at only 30 km^3.

Here, the writer adopts 100 km^3 as the amount of ejecta and estimates its thermal energy which is clearly the largest one of the various energies:

$$E_{th}=10^2\times 10^{15}\,cc\times 2.0\,gr./cc\times 0.20\,cal./gr.{}^\circ C\times 500^\circ C\times J=8.4\times 10^{26}\ ergs.$$

Krakatoa, Sunda Str. 1883

According to the Report of the Krakatoa Committee (1886), a part of the mountain amounting to at least 5.6×10^{15} *cc* in volume disappeared in the great 1883 eruption. The writer also made a rough estimation

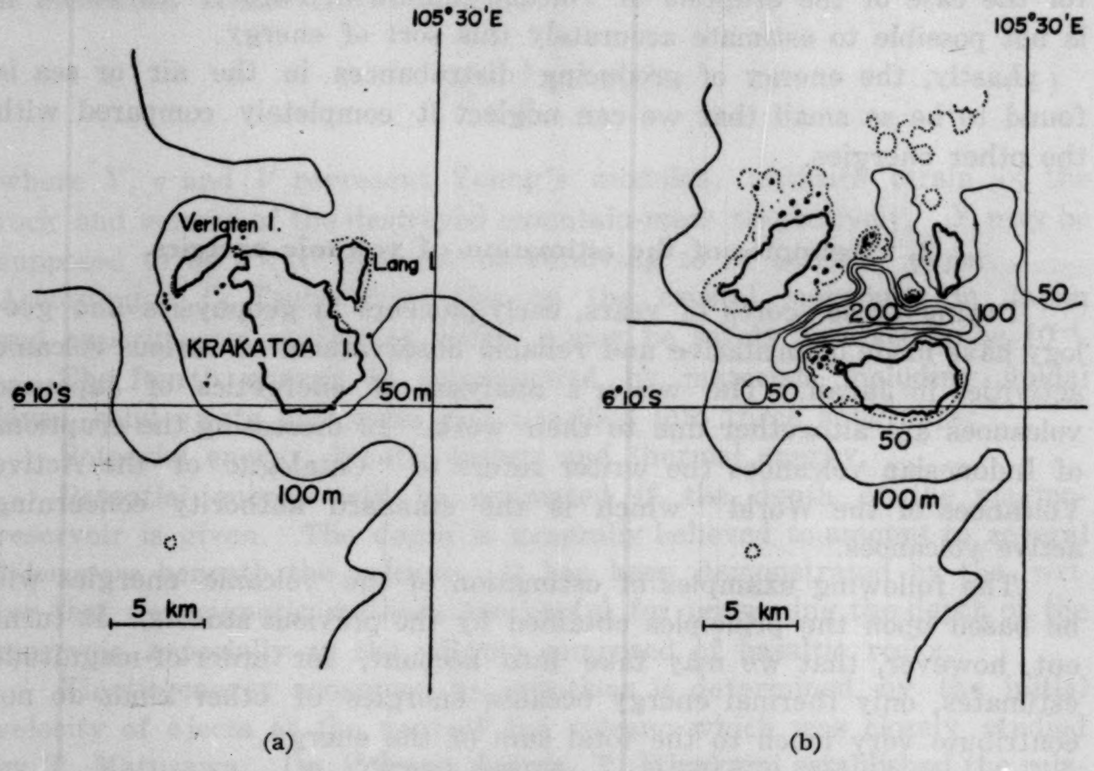

Fig. 2. Bathygraphic charts around Krakatoa Island.
a) before the 1883 eruption
b) after the 1883 eruption

of the volumes of Krakatoa before and after the eruption with the aid of the two sheets of bathygraphic chart in the Report;

Before the eruption: volume above sea-level 5.9×10^{15} *cc*,

After the eruption: ,, ,, 3.6×10^{15} *cc*

And the volume under the sea-level blown off by the eruption was about 7.7×10^{14} *cc*. Therefore, total volume of the devastated mountain-

mass would be about 3.1×10^{15} *cc*. Here, we may adopt the figure 5×10^{15} *cc* as the ejected volume.

After F. Von Wolf, the maximum pressure of the explosion was 425 *atm*. Initial velocity of ejecta is to be obtained by the following assumed relation

$$p=\frac{1}{2}\rho v_0^2$$

where ρ is the mean density of ejecta. If ρ is taken as 2.3 *gr./cc*, v_0 becomes 193 *m/sec*. Thus, the kinetic energy of the eruption is obtained as

$$E_k=\frac{1}{2}\times2.3\,gr./cc\times5\times10^{15}\,cc\times(1.93\times10^4\,cm/sec.)^2=2.1\times10^{24}\,ergs$$

at most.

Assuming that only the temperature of the missing mass under the sea-level was 500°*C*, the thermal energy accompanied by it is estimated as

$$E_{th}=7.7\times10^{14}\,cc\times2.3\,gr./cc\times500°C\times0.20\,cal./gr.°C\times J=8.4\times10^{24}\,ergs,$$

so that we see that the total energy sent out at the time of the eruption was as much as 10^{25} *ergs*.

Sakurazima, Japan

a) 1914

The volume of the overflowed lavas was estimated at 1.5 km^3 and that of the ejected ash and pumice at 0.62 km^3, while the volume of the land-depression around the volcano was proved to be 1.4 km^3 by the repeated levelling-surveys.

T. Matuzawa evaluated the various energies associated with eruption as follows:

Potential energy accompanied by lava	1.9×10^{22} *ergs*
Thermal ,, ,,	4.6×10^{25} 〃
Kinetic energy of ash and pumice (v_0=100 *m/sec.*)	7.5×10^{22} 〃
Thermal ,, ,,	6.2×10^{24} 〃

He concluded that the total energy sent out by this eruption was of the order of 10^{25} *ergs*.

b) 1946

After T. Nagata, S. Sakuma and N. Fukushima[10], the fluidal lava ejected in this eruption totaled to 8.3×10^{13} *cc* in volume.

The amount of the thermal energy accompanied by the lava-flows was about 2.1×10^{21} *ergs*.

Huzi (san), Japan 1707

H. Tsuya[11] estimated the volume of the ejecta which was B-type in his classification, at 8.5×10^{14} *cc*.

The thermal energy released by the eruption was roughly given as

$$E_{th}=8.5\times10^{14}\,cc\times2.0\,gr./cc\times500°C\times0.20\,cal./gr.°C\times J=7.1\times10^{21}\,ergs$$

Asama (yama), Japan

a) 1783

The volumes of the ejecta by the eruption were estimated as follows;

Oni-oshidashi lava-flow	1.7×10^{14} *cc*	(after S. Aramaki)
Kambara nuée ardente	$0.1\text{–}0.01\times10^{14}$ *cc*	,, ,,
Agatsuma ,, ,,	1.0×10^{14} *cc*	,, ,,
Pumice	1.7×10^{14} *cc*	(after T. Minakami)

The thermal energies accompanied by the ejecta of each kind are

Lava-flow	$1.7\times10^{14}\times2.5\times(1000\times0.25+50)\times J=5.4\times10^{21}$ *ergs*
Nuée ardente	$1.1\times10^{14}\times2.0\times(1000\times0.25+50)\times J=2.8\times10^{21}$ *ergs*
Pumice	$1.7\times10^{14}\times0.8\times500\times0.2\times J=5.9\times10^{23}$ *ergs*

The total thermal energy becomes about 8.8×10^{21} *ergs*, while T. Minakami[12] estimated the kinetic energy of the explosion as

$$E_k=\frac{1}{2}\times1.7\times10^{14}\,cc\times0.8\,gr./cc\times(2.5\times10^{1}\,cm/sec.)^2=4.4\times10^{22}\,ergs.$$

b) 1935

After T. Minakami[13], the total mass of the lava ejected in this ex-

10) T. NAGATA, S. SAKUMA and N. FUKUSHIMA, *Bull. Earthq. Res. Inst.*, **24** (1946), 162.

11) H. TSUYA, *loc. cit.*, 7).

12) T. MINAKAMI, *Bull. Earthq. Res. Inst.*, **20** (1942), 93.

13) T. MINAKAMI, *Bull. Earthq. Res. Inst.*, **20** (1942), 82.

plosion amounted to 4.5×10^{12} *gr.*, so that the thermal energy is obtained as

$$E_{th} = 4.5 \times 10^{12}\ gr. \times 1000°C \times 0.25\ cal./gr.°C \times J = 4.8 \times 10^{22}\ ergs.$$

c) 1938

According to T. Minakami's[14] study, the total mass of the ejecta which was B-type, was 3.8×10^{11} *gr.* and the initial velocity of the ejecta at the vent was 212 *m/sec.* From these data he obtained the kinetic energy of explosion as 1.7×10^{21} *ergs.*

On taking into account Minakami's statement that the temperature of a volcanic bomb was about 800°*C* at the time of its landing, the total thermal energy accompanied by all the ejecta is estimated roughly at

$$E_{th} = 3.8 \times 10^{11}\ gr. \times 1000°C \times 0.25\ cal./gr.°C \times J = 4.0 \times 10^{21}\ ergs.$$

Mihara (yama), Ooshima, Japan

Volcano Mihara is a typical *Strombolian* volcano as discussed in the previous part of this paper. The thermal energy released by the essential lava flows in the cases of several eruptions is estimated as follows;

a) 1777–78 $3.4 \times 10^{13}\ cc \times 2.5\ gr./cc \times (1000°C \times 0.25\ cal./gr.°C + 50\ cal./gr.)J = 1.0 \times 10^{24}\ ergs.$

b) 1912 $2 \times 10^{10}\ cc \times 2.5\ gr./cc \times 1000°C \times 0.2\ cal./gr.°C \times J = 6.3 \times 10^{20}\ ergs.$

c) 1950–51 $3.0 \times 10^{13}\ cc \times 2.5\ gr./cc \times (1000°C \times 0.25\ cal./gr.°C + 50\ cal./gr.)J = 9.4 \times 10^{23}\ ergs.$

d) 1954 $4 \times 10^{11}\ cc \times 2.5\ gr./cc \times (1000°C \times 0.25\ cal./gr.°C + 50\ cal./gr.)J = 1.3 \times 10^{22}\ ergs.$*

Torishima, Japan 1939

The writer estimates the volume of the ejected lava in the 1939

14) T. MINAKAMI, *Bull. Earthq. Res. Inst.*, **20** (1942), 86.

* *Corrigenda* to 1st Paper, *Bull Earthq. Res. Inst.*, **34** (1956). Page 193, line 20. Read 6.7×10^{21} for 6.7×10^{22}. In 1st Paper, the writer adopted 0.20 *cal./gr.°C* as the specific heat of lava and neglected the latent heat.

eruption at 3.1×10^{13} *cc*. The thermal energy accompanied by the fluidal lava is obtained as

$$E_{th} = 3.1 \times 10^{13} cc \times 2.5\, gr./cc \times (1000°C \times 0.25\, cal./gr.°C + 50\, cal./gr.)J$$
$$= 9.7 \times 10^{23}\, ergs.$$

Komagatake, Japan 1928

According to S. Tsuboi and H. Tsuya[15], the initial temperature of pumice ejecta was presumed to be not conspicuously higher than 730°*C*. On referring to their result of the observation of the ejecta, the writer estimates its volume at 5.1×10^{13} *cc*. The thermal energy released by the ejecta is obtained as

$$E_{th} = 5.1 \times 10^{13}\, cc \times 1.5\, gr./cc \times 800°C \times 0.25\, cal./gr.°C \times J = 5.6 \times 10^{23}\, ergs.$$

Miyakeshima, Japan 1940

According to S. Omote[16], the area of the parasitic cones was $2.7 \times 10^5\, m^2$ and that of the lava-flow was $2.9 \times 10^5\, m^2$. The volumes of the parasitic cones and the lava-flow respectively 11.6×10^6 and $7.5 \times 10^6\, m^3$. The total volume of erupted lava amounted to $19.1 \times 10^6\, m^3$, the same order of magnitudes as that of lava erupted in the activities of 1874, as calculated by H. Tsuya[17]. Assuming the bulk density of the new ejecta to be 2.0 *gr./cc*, the total weight of the new ejecta was estimated, without serious error, at 3.8×10^7 *tons*.

The thermal energy accompanied by the new ejecta is obtained as

$$E_{th} = 3.8 \times 10^{13} gr. \times (1000°C \times 0.25 cal./gr.°C + 50 cal./gr.)J = 4.8 \times 10^{13}\, ergs.$$

Bandaisan, Japan 1888

According to S. Sekiya aud Y. Kikuchi[18], *the most striking feature in the whole of this eruption was the deluge of rock and earth. Notwithstanding the violence of the phenomena, and the completeness with which the mountain was destroyed, the nature of the eruption was comparatively simple. The destructive agency was merely the sudden expansion of imprisoned steam, unaccompanied by lava flows or pumice ejection. By far the greater volume was comparatively in a dry state, being moistened only by condensing steam, and must have derived its fluid or*

15) S. TSUBOI and H. TSUYA, *Bull. Earthq. Res. Inst.*, **8** (1930), 317.
16) S. OMOTE, *Bull. Earthq. Res. Inst.*, **19** (1941), 388.
17) H. TSUYA, *Zisin* (in Japanese), **12** (1940), 473.
18) S. SEKIYA and Y. KIKUCHI, *Trans. Seism. Soc. Japan*, **8** (1890), Part II, 153.

semi-fluid properties from a rapid process of pulverization. They estimated the volume of the mountain destroyed at $1.2\times10^{15}\,cc$ and deemed the density of the mountain as $2.33\,gr./cc$. On the other hand, T. Matuzawa[19] obtained the initial vertical velocity of ejecta at the creater as $172\,m/sec.$

Except the energy necessary for projecting the ejecta, the energy necessary for breaking down the mountain-mass is equal to the elastic strain energy which is shown by equation (4):

$$E_e=1/2\times5\times10^{11}\,dyne/cm^2\times(10^{-4})^2\times1.2\times10^{15}\,cc=3.0\times10^{18}\,ergs.$$

If we assume the initial velocity of all ejecta as $170\,m/sec.$, the kinetic energy will be obtained as

$$E_k=1/2\times1.2\times10^{15}\,cc\times2.33\,gr./cc\times(1.7\times10^4\,cm/sec.)^2=4.1\times10^{23}\,ergs.$$

Assuming the sliding down of the collapsed material by gravity, we get the vertical and horizontal displacements of the mass as 300 and 2,500 m respectively in Fig. 3. Then we obtain the velocity at the low-

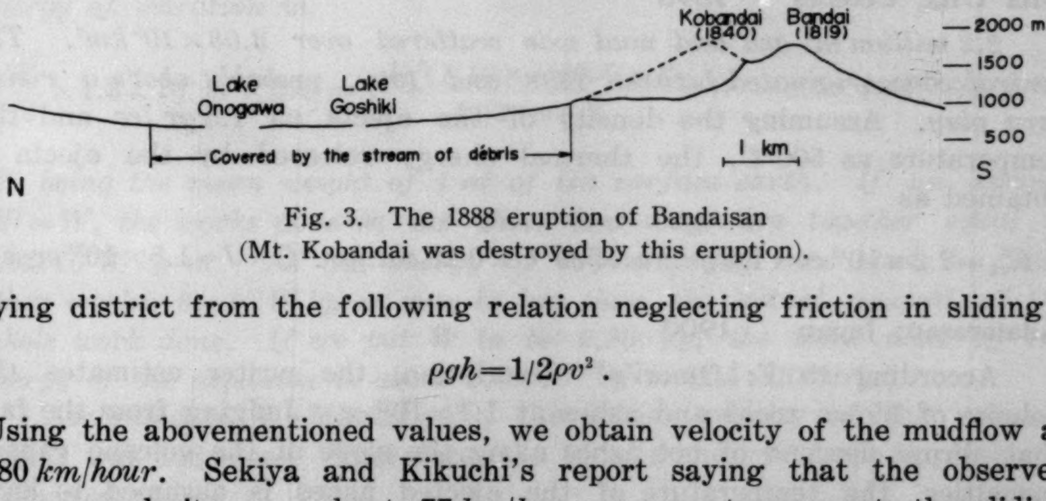

Fig. 3. The 1888 eruption of Bandaisan
(Mt. Kobandai was destroyed by this eruption).

lying district from the following relation neglecting friction in sliding;

$$\rho gh=1/2\rho v^2\ .$$

Using the abovementioned values, we obtain velocity of the mudflow as $280\,km/hour$. Sekiya and Kikuchi's report saying that the observed average velocity was about $77\,km/hour$, seems to suggest the sliding down of the meterial by gravity but there must have been the driving agency in the initial motion.

After all, the order of magnitude of the total energy associated with the eruption might be $10^{23}\,ergs$.

Guntur, Java 1843

The eruptions were generally of short duration, throwing out ashes

19) T. MATUZAWA, *Bull. Earthq. Res. Inst.*, **11** (1933), 343.

and glowing stones. Sometimes however enormous quantities were emitted (7.8 million m³ in 1843). The thermal energy accompanied by the ejecta is estimated at

$$E_{th}=7.8\times10^{12}\,cc\times2.0\,gr./cc\times500°C\times0.20\,cal./gr.°C\times J=6.5\times10^{22}\,ergs.$$

Pematang Bata, Sumatra 1933

Only old material was thrown up, maximal 1100 m high, while the the steam clouds rose to more than 2,000 m height. In total 0.210 km³ of mud was thrown out. The initial vertical velocity of thrown up mud is obtained from the following formula,

$$v_0=\sqrt{2gh}=\sqrt{2\times980\times1.1\times10^5}=1.47\times10^4\,cm/sec.$$

The kinetic energy of this steam eruption is estimated as

$$E_k=\frac{1}{2}\times2.1\times10^{14}\,cc\times2.0\,gr./cc\times(1.4\times10^4\,cm/sec.)^2=4.5\times10^{22}\,ergs.$$

Una Una, Celebes 1898

2.2 million m³ ash and mud was scattered over 3.03×10^5 km². The central cone originated between 1898 and 1900, probably above a rising lava plug. Assuming the density of the ejecta as 1.5 *gr./cc* and the temperature as 500°*C*, the thermal energy released by the ejecta is obtained as

$$E_{th}=2.2\times10^{12}\,cc\times1.5\,gr./cc\times500°C\times0.20\,cal./gr.°C\times J=1.8\times10^{22}\,ergs.$$

Adatarasan, Japan 1900

According to F. Omori's[20] description, the writer estimates the volume of blown rocks and ashes at 1.1×10^{12} *cc*. Judging from the fact that abrupt descend of hot ashes along the slope of the volcano caused casualties, the temperature of the ejected ashes is assumed to have been about 300°*C* at the lowest. Then, the thermal energy released by the eruption is obtained as

$$E_{th}=1.1\times10^{12}\,cc\times2.3\,gr./cc\times300°C\times0.20\,cal./gr.°C\times J=6.4\times10^{21}\,ergs.$$

Azumasan, Japan 1893

F. Omori's[21] estimation of the volcanic energy in the 1893 eruption

20) F. OMORI, *Rep. Imp. Earthq. Inv. Comm.*, No. 35 (in Japanese).
21) F. OMORI, *Seism. Journ. Japan*, **19** (1894), 1.

was as follows: *The mud and ashes seemed to have been projected upwards to a height of about 1 km. We have no means of finding the height to which the centre of gravity of the whole projected mass was raised. Let us assume this height to be 100 m, which probably would not be much greater than the actual value. Then, since the total volume of rock and mud projected is* $5\times10^5\ m^3$, *the work done would be*

$$100\ m\times5\times10^5\ m^3\times W=5\times10^7\times W\ kg\cdot m,$$

W being the weight of $1\ m^3$ *of rock and mud.*

The energy of an earthquake vibration is, when the motion is of simple harmonic type, given by the formula $1/2\,mv^2$ *in which v is the maximum velocity of the earth particle, and m is the whole of the disturbed mass. In the case of the earthquake caused by the explosion under consideration, we may probably, without much mistake, put the mean amplitude of motion at 1/10 mm, and the period at 1/10 sec. If we further suppose the whole area of disturbance,* $1{,}300\ km^2$ *extent, to have been at any instant of time disturbed to a uniform depth of 1/4 km, the energy of vibration is*

$$\frac{1}{2}\times1.3\times10^9\ m^2\times250\ m\times\frac{4\pi^2(1/10\times1/1000\ m)^2}{(1/10\ sec.)^2}\times W'=6.4\times10^6 W'\ kg\cdot m$$

W′ being the mean weight of $1\ m^3$ *of the surface earth. If we assume* $W'=W$, *the works done in the above two ways are together equal to* $5.6\times10^7 W\ kg\cdot m$. *As the energy of explosion has been spent in doing other works,* $6\times10^7 W\ kg\cdot m$ *may be less than the actual amount of the whole work done. If we put W to be 2,300 kg, the work done by the energy of the explosion is about* $1.4\times10^{11}\ kg\cdot m$ $(1.4\times10^{19}\ ergs)$.

According to T. Matuzawa[22], the initial velocity of the volcanic bombs was 148 *m/sec*. Therefore, the kinetic energy of the explosion is estimated as

$$E_k=\frac{1}{2}\times5\times10^{11}\ cc\times2.3\ gr./cc\times(1.48\times10^4\ cm/sec.)^2=1.3\times10^{20}\ ergs.$$

Assuming the temperature of the ejecta to be 100°*C*, the thermal energy released by the ejecta is estimated at

$$E_{th}=5\times10^{11}\ cc\times2.3\ gr./cc\times100°C\times0.20\ cal./gr.°C\times J=1.0\times10^{21}\ ergs$$

22) T. Matuzawa, *loc. cit.*, 15).

Total energy of the eruption is deemed to be order of magnitude 10^{21} *ergs*.

Tokachidake, Japan

According to F. Tada and H. Tsuya's[23] report, volume of ejected material (old detritus and new volcanic bombs) was $1.3\times10^{10}\,cc$ and volume of the destructed part of the old central cone which descended along the slope of the mountain as the mudflow, was about $2.7\times10^{12}\,cc$. S.T. Nakamura[24] calculated the initial velocity of the mud-flow as $80\,m/sec$. On referring to the above observations, the thermal energy accompanied by the ejecta is estimated at

$$E_{th}=1.3\times10^{10}\,cc\times2.0\,gr./cc\times500C^{\circ}\times0.20\,cal./gr.{}^{\circ}C\times J=1.1\times10^{20}ergs.$$

And elastic strain energy stored in the destructed mountain-mass is obtained as

$$E_e=\frac{1}{2}\times5\times10^{11}\,dyne/cm^2\times(10^{-4})^2\times2.7\times10^{12}\,cc=6.8\times10^{15}\,ergs.$$

The kinetic energy of the mud-flow is estimated at

$$E_k=\frac{1}{2}\times2.7\times10^{12}\,cc\times2.0\,gr./cc\times(8\times10^3\,cm/sec.)^2=1.7\times10^{20}\,ergs.$$

Thus, the total energy of the eruption is regarded as 2.8×10^{20} *ergs*.

Myoozin Reef near the Bayonnaise Rocks, Japan 1952

S. Murauchi[25] observed the sea-waves which had been caused by the eruption of the submarine volcano at Myoozin Reef on Sept. 23 and obtained the wave-height as $2\,m$ at the distance at about $1,500\,m$ from the centre of the explosion. He estimated the energy of the one submarine explosion to be about 10^{18} *ergs* after the analogy of the results obtained by the experiments of the underwater explosion of atomic bombs in the Pacific. The total energy of this submarine eruption may be regarded as the order of magnitude 10^{19} *ergs* at the least.

Kusatsu-Shiranesan, Japan 1932

After H. Tsuya[26], volcanic ash fell more than $3\,cm$ in thickness

23) F. TADA and H. TSUYA, *Bull. Earthq. Res. Inst.*, **2** (1927), 49 (in Japanese).
24) S.T. NAKAMURA, *Chikyu* (in Japanese), **6** (1926), 79.
25) S. MURAUCHI, *Zisin* (in Japanese), [ii], **5** (1952), 158.
26) H. TSUYA, *Bull. Earthq. Res. Inst.*, **11** (1933), 82.

over a radius of 410 m around the crater and the solid ejecta consisted wholly of non-incandescent detritus, all coming under the title "accessory ejecta". The volume of the ejecta is roughly estimated at

$$\pi(4.1\times10^4\ cm)^2\times3\ cm=1.6\times10^{10}\ cc.$$

The initial velocity of the volcanic bombs was presumed as 128 $m/sec.$ by T. Matuzawa[27]. Then the kinetic energy of the ejecta is obtained as follows assuming the density of the volcanic ash to be 1.2 $gr./cc.$

$$E_k=\frac{1}{2}\times1.6\times10^{10}\ cc\times1.2\ gr./cc\times(1.28\times10^4\ cm/sec.)^2=1.6\times10^{18}\ ergs.$$

3. Conclusion.

All the examples of volcanic eruptions discussed in the previous section are summarized in Table V where the Tsuya's intensity scale is considered together. As seen in Table V, it is true that the amount of the released energy by volcanic activities depends on the volume of ejecta, but physical (especially thermal) conditions of the ejecta play more important role in energetics in active volcanoes. For an example, the volume of ejecta in the 1888 eruption of Volcano Bandai (san) was very enormous while its total volcanic energy is estimated at rather low value. In fact, the ejecta in this eruption, strictly speaking, was almost the collapsed mountain-mass unaccompanied by the high temperature lava or pumice.

Total energy of a present "large" eruption proved to reach something around $10^{24}\sim10^{25}$ $ergs$. This magnitude of energy is comparable to that of a large earthquake. And the lower limit of the total energy in a "eruption" may be speculated to be about $10^{16}\sim10^{17}$ $ergs$ while fumarole activities are releasing more minor quantity of the energy.

Discussion concerning the relation between energies of vlocanism and earthquake occurrences will be tried in the next paper.

In concluding, the writer wishes to express his hearty thanks to Dr. T. Rikitake who has given him helpful suggestions in course of the present study. He is also indebted to many senior investigators whose valuable papers he quoted in this report.

27) T. MATUZAWA, *loc. cit.*, 19).

Table V. Estimation of volcanic energies on Japanese and Indonesian volcanoes.

Volcano	Year	Ejecta		Total Energy		Tsuya's Intensity scale		Activity
		Volume (*cc*)	Type	(*erg*)	Log.	Vol. of Ejecta (*cc*)	Grade	
Tambora	1815	1×10^{17}	B	8.4×10^{26}	**27**	10^{17}	VIII	○↑⊠†
Sakurazima	1914	2.1×10^{15}	AB	4.6×10^{25}	**26**	$10^{16}\sim10^{15}$	VII	○-↑≋>⊠
Krakatoa	1883	5×10^{15}	B	$\sim10^{25}$	**25**	〃	VII	○○∘↑⊼
Asama	1783	4.5×10^{14}	AB	8.8×10^{24}	**25**	$10^{15}\sim10^{14}$	VI	○↑≋>→⊠†
Huzisan	1707	8.5×10^{14}	B	7.1×10^{24}	**25**	〃	VI	○∘↑⊠
Sakurazima	1946	8.3×10^{13}	A	2.1×10^{24}	**24**	$10^{14}\sim10^{13}$	V	○-↑≋>
Mihara	1777–8	3.4×10^{13}	A	1.0×10^{24}	**24**	〃	V	○↑≋>
Torishima	1939	3.1×10^{13}	AB	9.7×10^{23}	**24**	〃	V	○↑≋>⊠
Mihara	1950–1	3.0×10^{13}	A	9.4×10^{23}	**24**	〃	V	○↑≋>
Komagatake	1929	5.1×10^{13}	B	5.6×10^{23}	**24**	〃	V	○↑
Miyakeshima	1940	1.9×10^{13}	AB	4.8×10^{23}	**24**	〃	V	○-≋>↑○
Bandaisan	1888	1.2×10^{15}	D	$\sim10^{23}$	**23**	$10^{16}\sim10^{15}$	VII	○⇡⤳⊠†
Guntur	1843	7.8×10^{12}	B	6.5×10^{22}	**23**	$10^{13}\sim10^{12}$	IV	○↑⊠
Asama	1935	2.2×10^{12}	B	4.8×10^{22}	**23**	〃	IV	○↑
Pematang Bata	1933	2.1×10^{14}	D	4.5×10^{22}	**23**	$10^{15}\sim10^{14}$	VI	⇡
Una Una	1898	2.2×10^{12}	B	1.8×10^{22}	**22**	$10^{13}\sim10^{12}$	IV	↑⤳⊠
Mihara	1954	4×10^{11}	A	1.3×10^{22}	**22**	$10^{12}\sim10^{11}$	III	○↑≋>
Adatarasan	1900	1.1×10^{12}	B	6.4×10^{21}	**22**	$10^{13}\sim10^{12}$	IV	○↑⇡
Asama	1938	1.5×10^{11}	B	4.0×10^{21}	**22**	$10^{12}\sim10^{11}$	III	○↑
Azumasan	1893	5×10^{11}	B	$\sim10^{21}$	**21**	〃	III	○↑⇡
Mihara	1912	2×10^{10}	A	6.3×10^{20}	**21**	$10^{11}\sim10^{10}$	II	○↑≋>
Tokachidake	1926	2.7×10^{12}	DB	2.8×10^{20}	**20**	$10^{13}\sim10^{12}$	IV	○↑⤳⊠†
Myoozin Reef	1952	?	B	$\sim10^{19}$	**19**	?	?	⊼↑⇡
Kusatsu-Shiranesan	1932	1.6×10^{10}	D	1.6×10^{18}	**18**	$10^{11}\sim10^{10}$	II	○↑

Types of ejecta
- A: essential lava-flow,
- B: fragmentary ejecta only,
- D: essentially ejected old detritus.

List of symbols for volcanic activities (after Catalogue of the Active Volcanoes of the World, 1951)

Symbol	Meaning	Symbol	Meaning
○	Eruption in the central crater	≋>	Lava flow
○∘	Eruption in a parasitic crater	⇡	Phreatic explosions
○-	Eruption in a radial fissure	⤳	Mud flow
=	Eruption in a regional fissure	⊼	Submarine eruption
↑	Normal explosions	⊠	Destruction of arable land
→	Eruption producing nuées ardentes	†	Casualities

6. 火山活動のエネルギー (第2報)

I. 大島三原山の1950～52年間の活動について
II. 日本及びインドネシヤの諸火山の活動例について

地震研究所 横 山 泉

第1報に続いて，順序は逆であるが，大島三原山の1950～52年間の活動について，エネルギー論的に調べた．結果は第1報のそれと全く同じである．これらの結果を基にして，他の諸火山の活動エネルギーを吟味した．既に先年津屋教授は噴火強度階なるものを提唱したが，これに準じて，信頼性あり且つ定量的な調査報告の存在する日本及びインドネシヤの諸火山の活動について，エネルギーを検討した．尚，稀少文献の報文は煩を厭わず，そのまま引用した．

7. *Energetics in Active Volcanoes. 3rd Paper.*

By Izumi YOKOYAMA,

Earthquake Research Institute.

(Read Nov. 27, 1956.—Received Dec. 31, 1956.)

Summary

The method of estimating energy related to volcanic activity, which has been applied to Volcano Mihara and other volcanoes in the previous papers, is extended to an estimate of total energy required to form a particular volcanic zone such as the Seven Izu Islands. The energy thus obtained is discussed in relation to theories of volcanism and seismicity which have been developed by Verhoogen, Gutenberg, Tsuboi, Bullard and Matuzawa.

1. Introduction.

Energy-problems of earthquakes have been fully studied by many geophysicists. The mutual relation between earthquake occurrences and volcanism is generally conceived by tacit understanding in many respects, but there seems no clue to verify it quantitatively. Energetics of the active volcanoes discussed in the previous papers makes it possible to trace back the volcanic energy to past times. Here, the writer will discuss the meaning of a "volcanic zone" from the standpoint of energetics.

A seismic zone and a volcanic zone generally coexist at limited areas on the earth and these two zones are distributed side by side not intermingling with each other. This fact may be taken as indicating that both are derivatives of the same origin energized from the deep. Reserving the discussion on the mechanism of earthquake occurrences and volcanism, the writer will consider their energy-release as heat-flow from the deep to the earth-surface.

2. Review of energetics related to volcanic and seismic zones.

Before the writer[1] obtained some conclusions regarding energetics in volcanic activity by the analyses of the recent activities of Volcano

1) I. YOKOYAMA, *Bull. Earthq. Res. Inst.*, **34** (1956), 185; **35** (1957), 75.

Mihara, J. Verhoogen[2] already formed his opinions on the igneous activities since the Precambrian: He considered volcanic phenomena in their true proportion as compared to the earth as a whole. He estimated the total volume of lava erupted since the close of the Precambrian at $3\times10^{22}\,cm^3$. A present day "large" eruption would amount to something around $10^{15}\,cm^3$ on the average as shown in Table V of 2nd Paper. As regards heat, he pointed out that total amount of the heat required to account for all volcanic activities since that time would be of the order of $4\times10^{25}\,cal.$ taking the total heat carried away by one *gram* of lava crystallizing and cooling from $1000°C$ to ordinary temperature to be 400 *cal.* (the writer deemed it 300 *cal.* in the previous papers). From his estimation, the heat flow radiated by volcanic activities all over the earth-surface during the period will be obtained as

$$\frac{4\times10^{25}\,cal.}{5.08\times10^{18}\,cm^2\times15\times10^{15}\,sec.}=5.2\times10^{-10}\,cal./cm^2\cdot sec. \qquad (1)$$

Volcanic heat represents only a very small fraction of the heat radiated by the earth considering that the average value of the heat flow near the earth-surface is $1.23\times10^{-6}\,cal./cm^2\cdot sec.$ His conclusion is as follows: *These facts suggest that the real problem of volcanoes is not so much to find a suitable source of energy as to provide ways and means by which rather insignificant amounts of heat can be focussed on relatively insignificant volumes of the crust. The orders of magnitude suggest that volcanic activity may result from a coincidence of various factors which may themselves have a small probability by usual standards. In other words, volcanic activity may be something exceptional, and there may be no need to wonder if its manifestations occasionally show somewhat unexpected deviations from the behavior that purely petrological thinking has accustomed us to consider as normal.*

C. Tsuboi[3], who discussed Japanese seismic data including conspicuous and rather conspicuous earthquakes during the period 1912 ~ 40 statistically in time and space, remarked that the earthquakes of which the magnitude is about 6.7 ($10^{22}\,ergs$ in energy estimated by the formula $\log E=11.8+1.5\,M$), occur 10 or 15 times a year in the region $150\times150\times50\,km^3$ of the Japan Islands. Substituting the heat flow for energy of the above earthquakes, we get

2) J. VERHOOGEN, *Am. Journ. Sci.*, **244** (1946), 745.

3) C. TSUBOI, *Geophys. Notes* (*Geophys. Inst., Tokyo Univ.*), **3** (1949), No. 4; *Journ. Phys. Earth*, **5** (1957), 1.

$$\frac{10^{23}\ erg.}{150\times 150\ km^2 \times 1\ yr.} = 3.3\times 10^{-7}\ cal./cm^2\cdot sec. \qquad (2)$$

Recently, B. Gutenberg[4)] discussed the energy of earthquake and stated as follows: *The average annual energy release of about 10^{25} ergs may be compared with an annual energy loss of the earth of nearly 10^{28} ergs by heat flowing out of the interior across the earth's surface. Thus, for the whole earth, the average heat developed during earthquakes is roughly one-thousandth of the heat flow through the surface; however, in earthquake zones locally both quantities may be of the same order of magnitude. Assuming a width of 250 km for the Japanese and Solomon Islands earthquake zones, the most active on earth, an average annual energy release of the order of magnitude 10^8 ergs/cm² ($\approx 10^{-7}$ cal./cm²·sec.) results for these zones, which is roughly one-tenth of the average energy released in radioactive heat in the earth. However, it has to be considered that the processes which produce the strain resulting ultimately in earthquakes may receive their energy from areas far beyond the earthquake belts. Thus, the energy of earthquakes could well result ultimately from radioactive processes in the earth's interior.*

E. C. Bullard[5)], who deems the volcanic heat to be derived from the dissipation of mechanical energy associated with earthquakes, mentioned the following figures: Smoothed curve involving the epicenters of the shallow earthquakes in the Japan-Kamchatka area is found to have an area of $2.0\times 10^6\ km^2$ and the average energy sent out as seismic waves from this area is 1.7×10^{26} *ergs/year* (this value may be converted to about 10^{25} *ergs/year* by the new energy formula) both according to Gutenberg and Richter's book. Using the abovementioned figures, heat flow substituted for earthquakes is estimated as follows;

$$\frac{10^{25}\ erg./yr.}{2.0\times 10^6\ km^2} \approx 10^{-7}\ cal./cm^2\cdot sec. \qquad (3)$$

According to his assumption, the remainder of the elastic energy that gave rise to the earthquake is dissipated as heat near the focus and this energy may be at least as great as that appearing as seismic waves. Thus, energy that has been stored as elastic energy should be double the above figure.

Recently T. Matuzawa[6)] formed a theory of earthquake field from

4) B. GUTENBERG, *Quart. Journ. Geol. Soc. London*, **112** (1956), 1.
5) E. C. BULLARD, in G. P. Kuiper (ed.), *The Earth as a Planet* (1954), 120.
6) T. MATUZAWA, *Bull. Earthq. Res. Inst.*, **31** (1953), 179.

the point of view that a solid-liquid phase transformation at the bottom of the crust may supply strain energy to the crust and cause a great earthquake to occur. Statistical studies show that a great earthquake having an energy of 10^{25} *ergs* occurs once a hundred *years* in the circular region of radius 50 *km* in the Japanese seismic zone. Matuzawa pointed out that heat of fusion amounting to about 9×10^{27} *ergs* should be supplied gradually from the deep into the bottom of the crust to give rise to the abovementioned earthquake as a result of the phase transformation. This supply of thermal energy for heat of fusion from the deep is equivalent to the following heat flow

$$\frac{9\times10^{27}\,erg}{100\,yr.\times\pi\times50^2\,km^2}=8.5\times10^{-4}\,cal./cm^2\cdot sec. \qquad (4)$$

3. Dissipation of energy in earthquake occurrences and volcanism.

As mentioned in the previous section, Tsuboi, Gutenberg and Bullard estimated the energy of seismic waves per unit area and unit time, while Matuzawa discussed quantitatively the mechanism and the supplied energy which should cause the great earthquakes to occur and concluded that the supply of thermal energy to the earthquake zone is about 800 times the normal heat flow observed at the earth-surface. Remainder of the elastic energy should be dissipated as heat.

If we use the term "Squander factor (S factor)" as the ratio of the dissipated energy to the various energies which we could observe, this factor amounts to about 10^2 in the case of the great earthquakes according to Matuzawa's analyses mentioned above.*

As regards volcanic activities, their occurrence is rare and their quantitative observations are rather difficult compared to those of earthquakes. Therefore, we have scarcely the statistical and quantitative methods by which we might estimate the supplied energy from the deep to the magma-reservoir except the geomagnetic method for basaltic volcanoes as discussed in the previous papers. By this method, the writer estimated the lowest amount of thermal energy supposed to be supplied to the magma-reservoir assuming that the changes in the geomagnetic field on the volcano should be caused by the rise of temperature in the reservoir. The order of magnitude of the squander factor for the two cases of activities on Volcano Mihara, 1950 and 1953 ~ 54

*) The effective fuel efficiency of the usual steam locomotive is about 10%, namely, its S factor equals 90/10=9.

are shown as follows;

for the 1950 eruption:

$$\frac{1.1\times10^{26}\ ergs}{9.4\times10^{23}\ ergs}=120\ ,$$

for the 1953 ∼ 54 eruption:

$$\frac{1.9\times10^{24}\ ergs}{1.3\times10^{22}\ ergs}=150\ .$$

4. Volcanic heat associated with the Seven Izu Islands.

Repetitions of volcanic eruption during long periods should have composed the mountain-mass of a volcano, especially of a stratified one. The largest part of the energy released from a volcano is the thermal energy accompanied by the essential lava flows (the A-type ejecta). Here, we may make a rough estimation of the total energy consumed by the formation of volcanoes assuming that their ejecta were all of the A-type.

The Seven Izu Islands are one branch of the festoon islands and run southward perpendicularly to Japan Proper (Honshu). This archipelago extends about 700 *km* and continues to Mariana Islands via Bonin (Ogasawara) Islands and Sulphur (Iwoo) Islands. All the islands are volcanic ones including active,

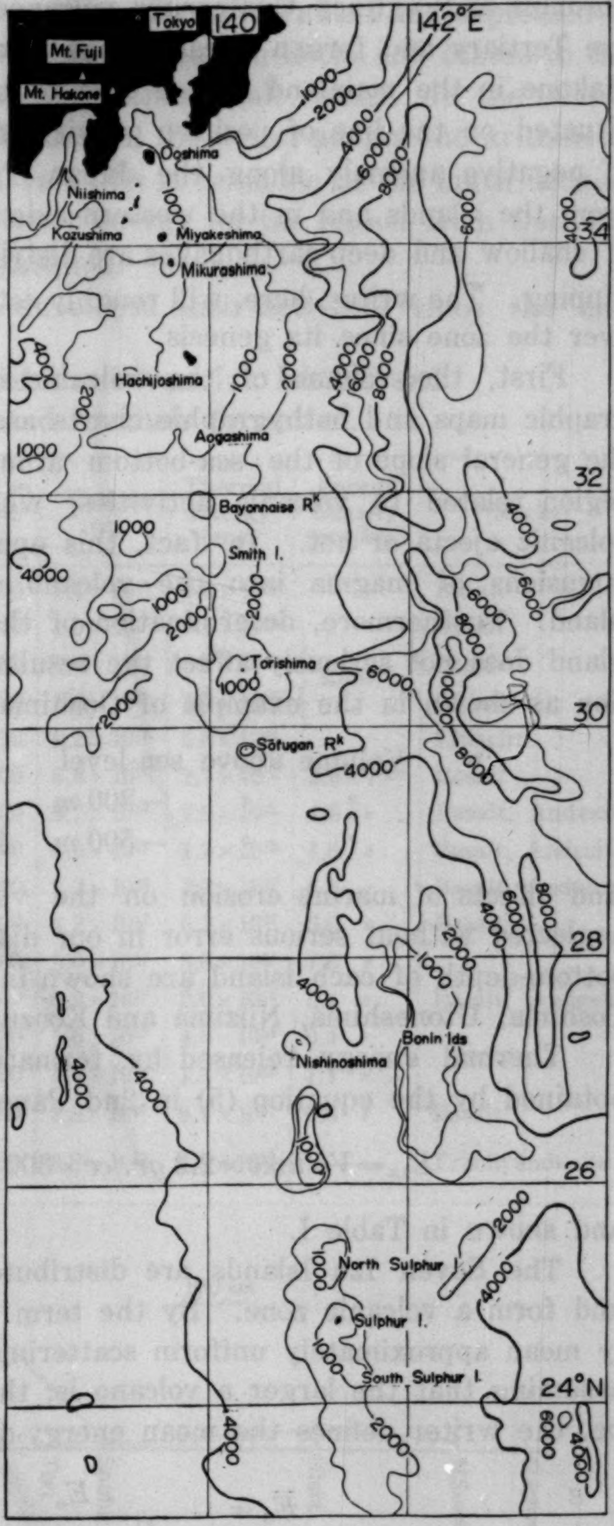

Fig. 1. The Seven Izu Islands (numerals show the depth of the sea in *meter*).

dormant and extinct Quaternary volcanoes except Bonin Islands which are Tertiary and form a volcanic zone together with Mts. Huji (Fuji) and Hakone in the mainland. It is remarkable that this volcanic zone is situated on the line of positive gravity-anomaly, while there is the line of negative anomaly along the Japan Trench eastward about 200 *km* from the islands and in the western side of the volcanic zone, epicentres of shallow and deep earthquakes are distributed on the plane westwardly dipping. The writer, here, will roughly estimate the total volcanic energy over the zone since its genesis.

First, the volume of the volcanic island is obtained by the topographic maps and bathygraphic charts assuming that the upheaval from the general slope of the sea-bottom around the island represents the region related to volcanic activities, whether the bottom meterial is volcanic ejecta or not. In fact, this upheaval would be caused by the intrusions of magma into the volcano which usually centres at the island. Furthermore, determination of the bottom-depth of the volcanic island does not seriously affect the results of the following order-estimation as shown in the example of Ooshima Island:

Volume above sea-level		$20\,km^3$
〃 〃	$-300\,m$	71 〃
〃 〃	$-500\,m$	140 〃

And effects of marine erosion on the volume of the islands may be neglected without serious error in our discussion. Volume and adopted bottom-depth of each island are shown in Table I where the four islands Toshima, Utoneshima, Niizima and Koozushima are remarkably small.

Thermal energy released by formation of the volcanic island is obtained by the equation (5) in 2nd Paper as

$$E_{th} = Volume \times 2.3\, gr./cc \times 300\, cal./gr. \times J \quad (ergs), \qquad (5)$$

and shown in Table I.

The Seven Izu Islands are distributed on a belt about 50 *km* wide and form a volcanic zone. By the term " volcanic zone ", we generally mean approximately uniform scattering of volcanoes on a belt. So, assuming that the larger a volcano is, the wider its energy-source will be, the writer defines the mean energy-density of one volcanic island as

$$\overline{E}_n = \frac{E_n}{\Delta x_n \dfrac{E_n}{E_{n-1}} + \Delta x_{n+1} \dfrac{E_n}{E_{n+1}}} . \qquad (6)$$

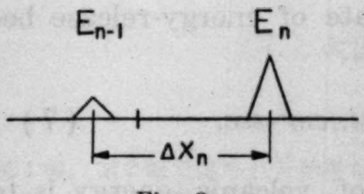

Fig. 2.

They are also shown in Table I and expressed in Fig. 3 where Soofu-gan Rocks and others to the south take rather small values. In the following discussion, the writer adopts the arithmetic mean value 4×10^{25} *ergs/km* as the linear density of volcanic energy for the region from Ooshima to Torishima.

The volcanoes in this zone developed their activities since the end

Table I. Volume of the Seven Izu Islands and Energy released by their formation.

Island	Latitude (North)	Bottom Depth (*m*)	Volume (*cc*)	Thermal Energy (*erg*)	Energy Density (*erg/km*)	Rocks
Ooshima	34° 45′	− 300	7.1×10^{16}	2.0×10^{27}	—	Basalt
Toshima	34 30	− 100	1.9×10^{15}	5.5×10^{25}		Basalt
Utoneshima	34 28	− 100	0.4×10^{15}	1.2×10^{25}	small	Basalt
Niizima (incl. Shikine I.)	34 22	− 100	1.0×10^{16}	3.0×10^{26}		Liparite
Koozushima	34 12	− 100	9.2×10^{15}	2.6×10^{26}		Liparite
Miyakeshima	34 05	− 300	5.8×10^{16}	1.7×10^{27}	3.6×10^{25}	Basalt
Mikurashima	33 52	−1000	9.7×10^{16}	2.8×10^{27}	4.6 〃	Basalt, Andesite
Hachizyoshima	33 05	− 500	4.0×10^{17}	1.2×10^{28}	1.6 〃	Basalt, Andesite
Aogashima	32 28	− 800	7.7×10^{16}	2.2×10^{27}	6.5 〃	Basalt, Andesite
Bayonese Rocks	31 55	−1200	2.2×10^{17}	6.3×10^{27}	3.0 〃	Basalt
Smith Island	31 24	−1200	3.0×10^{17}	8.6×10^{27}	7.6 〃	
Torishima	30 28	−1600	6.9×10^{17}	2.0×10^{28}	3.4 〃	Basalt, Andesite
Soofu-gan Rocks	29 50	−2000	1.6×10^{17}	4.6×10^{27}	0.4 〃	
Nishinoshima	27 14	−1000	4.4×10^{16}	1.3×10^{27}	1.1 〃	
North Sulphur Island	25 25	−1000	2.8×10^{17}	8.1×10^{27}	0.6 〃	Basalt
Sulphur I. (incl. South Sulphur I.)	24 45	−1000	8.8×10^{17}	2.5×10^{28}	—	Trachyandesite

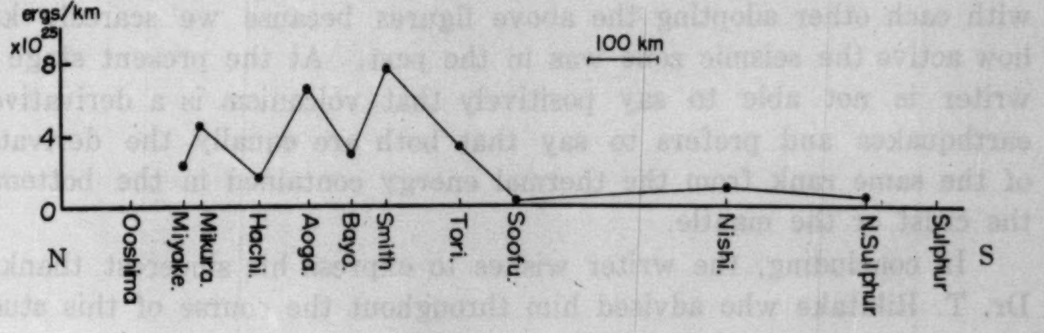

Fig. 3. Mean energy-density of the Seven Izu Islands.

of Tertiary or later period. Therefore, the rate of energy-release becomes as

$$\frac{4\times10^{25}\,erg./km}{10^6\,yr.\times50\,km}=6.0\times10^{-8}\,cal./cm^2\cdot sec. \qquad (7)$$

The writer would rather say that real release of volcanic energy is to be obtained by multiplying the above value by an "*S* factor" which is estimated at 150 as has been discussed in the previous section. Then, we get the heat flow substituted for the total volcanic energy in the Seven Izu Islands as

$$9.0\times10^{-6}\,cal./cm^2\cdot sec.$$

5. Conclusion.

Three investigators (Tsuboi, Gutenberg and Bullard) estimated the energy-release by earthquake-waves in Japan and the surrounding region as the order of 10^{-7} *cal./cm²·sec.* coincided with each other. Verhoogen discussed the igneous activities on the earth as a whole and obtained the value 10^{-10} *cal./cm²·sec.* In this paper volcanic energy released in "the volcanic zone" the Seven Izu Islands is estimated at 10^{-7} *cal./cm²·sec.* in net amount. It is clear and very plausible that the heat-flow has been more concentrated in the volcanic zone than in the other regions though the example is the only one for a volcanic zone in the ocean.

Matuzawa deduced theoretically the all-inclusive energy-release of earthquakes as the order of 10^{-3} *cal./cm²·sec.*, while the volcanic one was obtained as the order of 10^{-5} *cal./cm²·sec.* in this paper. The former is conspicuously larger than the latter and both two are larger than the normal heat flow at the earth-surface, namely 10^{-6} *cal./cm²·sec.* This estimate may be taken as suggesting that the terrestrial heat flow is more or less focused in the seismic and volcanic zones. Regarding the general association of both two zones we can not compare them with each other adopting the above figures because we scarcely know how active the seismic zone was in the past. At the present stage the writer is not able to say positively that volcanism is a derivative of earthquakes and prefers to say that both are equally the derivatives of the same rank from the thermal energy contained in the bottom of the crust or the mantle.

In concluding, the writer wishes to express his sincerest thanks to Dr. T. Rikitake who advised him throughout the course of this study.

7. 火山活動のエネルギー (第3報)

地震研究所 横 山 泉

第1報，第2報で得られた結果を基として，いわゆる火山帯なるものの意義をエネルギー論から検討した．既に地震帯なるものについては，諸学者がいろいろな算定を行い，これからいろいろな説を立てているので，一応これを概観した．火山帯の例として，伊豆七島をとり，これが形成されるまでに放出されたであろう熱エネルギーの量を概算して，地震帯のエネルギーと比較吟味した．

of Tertiary or later period. Therefore, the rate of energy release becomes as

$$10^{[illegible]}\ cal/cm^2/sec. \qquad (17)$$

The writer [illegible] that total release of volcanic energy is [illegible] [illegible], the above value summed [illegible] factors which are estimated as [illegible] has been discussed in the previous chapter. [illegible] we get the [illegible] [illegible] estimation for the total volcanic energy in the [illegible] [illegible] [illegible] as

$$[illegible]\ cal/cm^2/sec.$$

5. Conclusion

Then [illegible] (Gutenberg and Bullard) estimated the energy release by earthquake-waves in Japan and the surrounding region on the order of [illegible] which agreed with each other. Verhoogen discussed the thermal [illegible] on the earth as a whole and obtained the value [illegible] cal/cm²/sec. In this paper volcanic energy released in " the volcanic zone " the Seven Izu Islands is estimated at [illegible] cal/cm²/sec. in net amount. It is clear and very plausible that the heat-flow has been more concentrated in the volcanic zone than in the other regions though the example is the only one for a volcanic zone in the ocean.

Matuzawa deduced theoretically the all-inclusive energy-release of earthquakes as the order of [illegible] cal/cm²/sec., while the volcanic one was obtained as the order of [illegible] cal/cm²/sec. in this paper. The former is conspicuously larger than the latter and both two are larger than the normal heat-flow at the earth-surface, namely [illegible] cal/cm²/sec. This estimate may be taken as suggesting that the terrestrial heat flow is more or less focused in the seismic and volcanic zones. Regarding the general association of both two zones we can not compare them with each other adopting the above figures because we scarcely know how extent the seismic zone was in the past. At the present stage the writer is not able to say positively that volcanism is a derivative of earthquakes and prefers to say that both are equally the derivatives of the same rank from the thermal energy contained in the bottom of the crust or the mantle.

In concluding, the writer wishes to express his sincerest thanks to Dr. T. Hagiwara who advised him throughout the course of this study.

8. 常時微動の測定結果 第2報

(東京都内 III)

地震研究所 { 金井　清
田中貞二
長田甲斐男

(昭和29年1月26日, 3月23日, 昭和30年6月28日,
10月25日発表——昭和31年12月31日受理)

1. まえがき

常時微動は各場所特有の波形を示し，その波形は地盤の構造に密接な関係があることがこれまでの調査で相当はつきり認められた．しかも，常時微動の頻度曲線は同じ場所における地震動の頻度曲線に非常によく似ている．

従つて，地盤には固有の震動特性があり，この特性が地震動にも常時微動にも現われるものと考えられる．

常時微動は振幅がミクロン位以下の非常に小さいものなので，交通機関，機械振動等の人工的震動源から直接計器にとどく震動の影響を受けて，地盤特有の震動性状を示す筈の波形が大なり小なり乱される．従つて，常時微動の波形から地盤特有の震動性状を求めるために，近接地点で数多くの測定を行わねばならなかつた．その点，本測定は何時でも簡単に行えるから便利である．

本報告の測定結果は昭和27年以来，耐震工学上の地盤係数を求める研究の1つとして行つたものの外，建物の震動試験等の機会をできるだけ利用したものである．

2. 測定方法

常時微動の測定方法は既報[1),2)]の通りで，電磁式煤書微動計（換振器は固有周期1秒の動線輪型倒立振子）によつて5分間の測定を行い，その中の2分間について解析を行つた．

測定場所を第1図並びに第I表に示す．記録の解釈にあたつて，主として交通機関などの人工的震動源からの直接の影響の有無大小を推定するための目安にするという意味で，測定場所の環境条件を第I表に詳細に記しておいた．

1) 金井　清・田中貞二・長田甲斐男　地震研究所彙報 **32** (1954), 199.
2) 地震研究所地盤研究会　同上 **33** (1955), 492～495.

3. 測定結果

(i) 頻度曲線

2 分間の波形についての周期の頻度を求めたものを第 2〜24 図に示す．既に報告ずみの場所については頻度曲線は省略して，前論文で使つた測定点番号と本報告で使う番号とを対比させて第 II 表に示しておいた．

日中と夜間（午前2時頃）の頻度曲線はよく似ている場合が多いが，一般に，日中のものは 0.1 秒附近の頻度が比較的に多い．これは，交通機関等の人工的震動源からの直接の影響によるものと考えられる．大きな建物の地階などで常時微動の測定を行うと，建物固有の震動性状の影響を受けて，地盤特有の震動性状を知る上に邪魔になるが，この不利よりも，人工的震動源から直接換振器にとどく短周期の震動が建物の重量によつて抑制されるための有利さの方が大きい．それで，繁華な地域とか，工場の近くでの測定では，なるべく地面に直接換振器をおくことを避けるようにした．

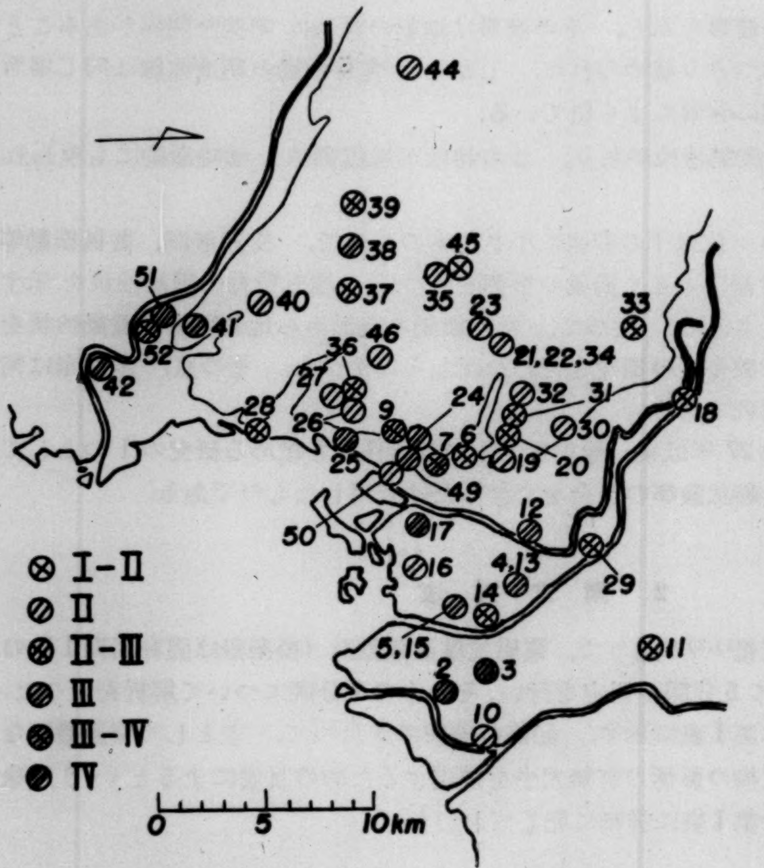

第 1 図　常時微動の測定場所（I〜IV の記号は建築基準法関係の地盤種別）

頻度曲線の極大になる周期を卓越周期，2 分間の波数で時間を割つた値を平均周期と名づけ，又，この計器で記録した波形の中での最も長い周期を最大周期と名づけて第 III 表に示した，第 III 表に書き込んである最大振幅は，2 分間の記録の中で，大振幅が 2,3 波つづくものの中での最大値である．頻度曲線が非常に平坦な場所と頻度の山が 2 つ以上ある場所については，卓越周期の意味が曖昧になるので，読取は行わなかつた．即ち測定点 2（江東区西瑞江 4 丁目），3（江東区東小松川 5 丁目），7（千代田区大手町），12（台東区隅田公園），49（中央区東銀座）は頻度曲線が平坦なため，測定点 5（江東区大島町）は頻度曲線に山が 2 つ以上あるため，第 III 表に卓越周期の値が記入してない．

第I表 常時微動の測定場所

番号	場所
2	江東区西瑞江4丁目 今井トロリーバス車庫（大通り脇，木造建コンクリート床）
3	江東区東小松川5丁目大杉公園附近（田圃の中の農家の土間）
4	江東区吾嬬東5丁目吾嬬中学校（運動場の表土）
5	江東区大島町東京ガス会社敷地（大通りより約 100 m 奥，木造平家内土間）
6	千代田区神田電機大学（電車通りより 150 m，鉄筋コンクリート4階建地下室床）
7	千代田区大手町富士銀行（電車通り脇，鉄筋コンクリート6階建物の地下室床）
9	港区芝明舟町専売公社（電車通り脇，鉄筋コンクリート5階建物の地下室床）
10	江戸川区東篠崎町みよし化学（工場内倉庫コンクリート床上，周囲は田圃）
11	葛飾区金町東北毛織（省線より約 300 m 煉瓦造配電室コンクリート床）
12	台東区聖天町隅田公園プール事務所（隅田川畔，鉄筋コンクリート1階建床）
13	墨田区吾嬬町5丁目吾嬬ポンプ場（鉄筋コンクリート1階，ポンプ室床）
14	江戸川区逆井1丁目小松川高校（運動場隅の平家物置内，コンクリート床）
15	江東区大島町5丁目小名木川変電所（大通より 50 m 鉄筋コンクリート変電室床）
16	江東区豊住町木場ポンプ場（大通より 150 m，木造平屋内コンクリート床上）
17	江東区深川富岡町数矢小学校（大通より 200 m 鉄筋コンクリート構堂内）
18	北区志茂町土木研究所赤羽分室（小路脇の鉄筋コンクリート1階床上）
19	文京区本富士町東大地震研究所（鉄骨鉄筋コンクリート2階建地下2階床上）
20	文京区柳町保坂氏宅（大通脇の木造2階建1階玄関コンクリート床上）
21	新宿区戸塚町高田馬場駅（小路脇，南口事務室内のコンクリート床上）
22	新宿区戸塚町日本電話工業（小路脇，高台，モルタル塗2階建玄関コンクリート床上）
23	新宿区百人町建築研究所（小路より 20 m 鉄筋コンクリート2階建地下1階床上）
24	千代田区霞ケ関厚生省（大通り脇，鉄筋コンクリート建物地下1階床上）

（つづく）

第I表（つづき）

番号	場所
25	港区芝海岸通り鉄道技術研究所（鉄筋コンクリート建物1階床上）
26	港区麻布本村町パピリオ（大通より30m モルタル塗2階建1階床上）
27	港区麻布田島町東栄電気（小路脇の鉄筋コンクリート建1階床上）
28	品川区東品川明石製作所（大通り脇，本造平屋コンクリート床上，機械振動あり）
29	足立区千住橋戸町千住アパート（小路脇の鉄筋コンクリート建物入口）
30	豊島区駒込駒込アパート（鉄筋コンクリート建物入口）
31	文京区第六天町第六天アパート（大通より30m，高台，鉄筋コンクリート建入口）
32	文京区関口町鈴木氏宅（大通より50m，モルタル塗2階建入口）
33	板橋区志村前野町志村アパート（小路脇の鉄筋コンクリート建物入口）
34	新宿区戸塚町高田馬場アパート（鉄筋コンクリート建入口，省線より100m）
35	中野区栄町2丁目中野アパート（大通より100m，鉄筋コンクリート建入口）
36	港区麻布本村町麻布アパート（大通より150m 鉄筋コンクリート建入口）
37	世田ケ谷区太子堂町太子堂アパート（小路より100m，鉄筋コンクリート建入口）
38	世田谷区世田谷豪徳寺アパート（大通より100m，鉄筋コンクリート建入口）
39	世田谷区経堂町経堂アパート（大通脇，鉄筋コンクリート建入口，交通少なし）
40	大田区石川町石川町アパート（鉄筋コンクリート建入口，周囲は静か）
41	大田区久ケ原久ケ原アパート（大通より50m，鉄筋コンクリート建入口）
42	大田区中六郷六郷アパート（鉄筋コンクリート建入口，鉄道より60m）
44	北多摩郡神代町運輸技術研究所（構内の空地表土上，周囲は極く静か）
45	杉並区和田本町鈴木氏宅（小路より100m，木造平屋建玄関コンクリート上）
46	渋谷区緑岡町青山学院（小路脇校門入口の石の上）
49	中央区東銀座北海道新聞社（大通り脇の鉄筋コンクリート建地下1階床上）

（つづく）

第 I 表 (つづき)

番号	場所
50	中央区東銀座中央計量検定所(大通り脇鉄筋コンクリート建物1階床上)
51	大田区下丸子町キヤノンカメラ株式会社(鉄筋コンクリート建物1階床上)
52	大田区原町昭電グラウンド場内(小路より 150 m, 周囲は空地至極静か)

卓越周期と平均周期の関係を第 25 図に示す. 一般に, 卓越周期と平均周期の値は非常に近い事が第 25 図からよくわかる. 地盤の震動性状を平均周期から解釈する事は容易でないが, 前に述べたように, 卓越周期は頻度曲線の形によつては決めにくい場合があるが, 平均周期はどんな場合にでも機械的に決められるので, 統計的には卓越周期と平均周期の値が近い事実を利用して, 平均周期を卓越周期の代りの意味で使う事にする.

一般に, 平均周期は卓越周期よりも僅かに大きい傾向がある. その原因は, 主として, 交通機関等の人工的震動源から直接換振器にくる 0.1 秒前後の短周期の震動が頻度曲線の形に及ぼす影響, 即ち卓越周期を短目にする度合は平均周期に対するものよりも大きいためと考えられる.

測定点 4(江東区吾嬬東5丁目), 17 (江東区深川富岡町) のように, 平均周期の方が卓越周期よりも小さい場所の頻度曲線は第2図及び第3図で見られるように, 特別な形をしている. その中で測定点 4 の頻度曲線には 0.7 秒附近の比較的長周期のところに山があるにかかわらず, 最大周期は大きくない. この特性については, 軟弱な厚い層があり, その層の中は弾性的に余り変化がないという 1 つの解釈ができる. (軟弱な厚い層がある場合には, 層の中が弾性的に多層から成つていると考えられる場合が多いので, 頻度曲線は平坦になるのが普通である.)

第 II 表 本報告と前報告の測定点番号の対比

本報告番号	前報告番号	
	脚註 1)	脚註 2)
2	25	8
3	22	7
5	17	—
6	9	—
7	24	—
9	21	—
10	—	1
11	—	3
12	—	6
13	—	4
14	—	2
15	—	5
16	18	—
18	15	—
19	8	—
20	16	—
23	2	—
24	14	—
25	23	—
26	5	—
27	3	—
28	11	—
29	12	—
30	6	—

(ii) 日中と夜間の常時微動の周期の比較

日中と夜間(午前2時頃)の平均周期の比較を第 26 図に示す. 前にも述べたように, 日中は交通機関等の影響のために周期が短目に出る可能性が多い事が第 26 図によく現われている. 測定点 28 (品川区東品川)で, 夜間に比べて日中の平均周期が特に短いのは,

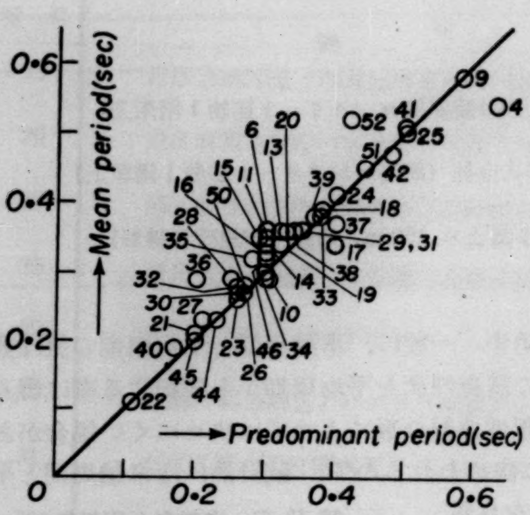

第 25 図　常時微動の卓越周期と平均周期の関係

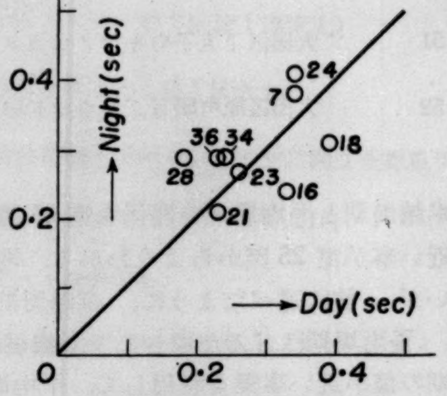

第 26 図　日中と夜間の常時微動の平均周期の比較

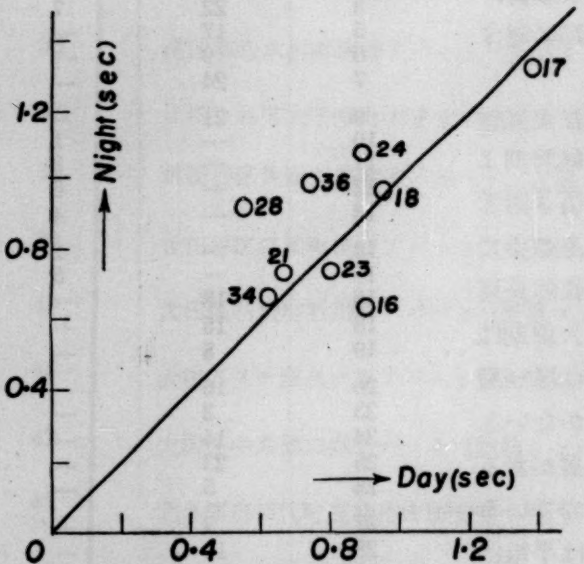

第 27 図　日中と夜間の常時微動の最大周期の比較

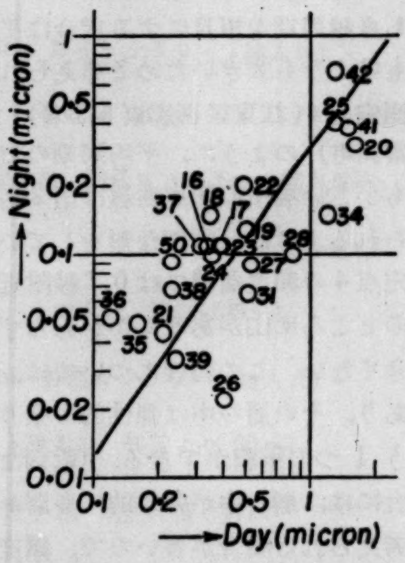

第 28 図　日中と夜間の常時微動の最大振巾の比較

第 III 表 常時微動の周期と最大振幅

No.	Period (sec)						Largest Amplitude (μ)		Alluvium Thickness (m)
	Dominant		Mean		Largest				
	Day	Night	Day	Night	Day	Night	Day	Night	
2	—	—	—	0.59	—	1.46	—	—	—
3	—	—	—	0.46	—	1.38	—	—	—
4	0.63	—	0.54	—	1.04	—	—	—	30~40
5	—	—	—	0.39	—	0.94	—	—	30~40
6	—	0.30	—	0.36	—	0.95	—	—	0~10
7	—	—	—	0.56	—	1.25	—	—	0~10
9	0.58	—	0.58	—	1.30	—	—	—	10~20
10	0.30	—	0.29	—	0.70	—	—	0.5	—
11	0.30	—	0.35	—	0.88	—	—	0.3	—
12	—	—	—	0.46	—	1.13	—	—	30~40
13	0.32	—	0.36	—	0.96	—	—	—	30~40
14	0.30	—	0.34	—	0.96	—	—	1.0	—
15	0.29	—	0.35	—	1.04	—	—	—	30~40
16	0.29	0.23	0.33	0.24	0.90	0.63	0.3	0.1	30~40
17	0.40	0.30	0.34	0.38	1.38	1.32	0.3	0.1	30~40
18	0.38	—	0.39	0.31	0.95	0.96	0.3	0.2	—
19	—	0.32	—	0.34	—	0.84	0.5	0.1	0
20	—	0.33	—	0.36	—	0.85	1.5	0.3	0~10
21	0.20	0.20	0.23	0.21	0.66	0.73	0.2	0.05	0
22	—	0.11	—	0.11	—	0.39	0.5	0.2	0
23	0.26	0.26	0.26	0.27	0.80	0.73	0.3	0.1	0
24	0.40	0.40	0.34	0.41	0.89	1.07	0.3	0.1	10~20
25	0.50	—	0.50	—	1.52	—	1.5	0.5	20~30
26	—	0.27	—	0.27	—	0.74	0.5	0.2	0~10
27	—	0.21	—	0.23	—	0.89	0.5	0.1	0~10
28	0.20	0.26	0.18	0.29	0.55	0.92	1.0	0.1	—
29	—	0.35	—	0.36	—	0.92	—	—	30~40
30	—	0.26	—	0.27	—	0.78	—	—	0
31	—	0.35	—	0.36	—	0.70	0.5	0.05	0
32	—	0.26	—	0.28	—	0.90	—	—	0~10
33	0.38	—	0.38	—	0.58	—	0.3	—	—
34	0.24	0.30	0.24	0.29	0.62	0.66	1.0	0.2	0
35	—	0.28	—	0.32	—	0.92	0.2	0.05	0
36	0.20	0.20	0.23	0.29	0.74	0.98	0.1	0.05	0
37	—	0.40	—	0.37	—	0.93	0.3	0.1	0
38	—	0.34	—	0.36	—	1.06	0.2	0.05	0
39	—	0.37	—	0.38	—	0.98	0.2	0.03	0
40	0.17	—	0.19	—	0.76	—	0.2	—	0
41	0.50	—	0.51	—	1.02	—	1.5	0.3	—
42	—	0.48	—	—	—	1.06	1.5	0.5	—
44	0.23	—	0.23	—	0.40	—	0.2	—	0
45	0.20	—	0.20	—	0.66	—	—	—	0
46	0.30	—	0.32	—	0.80	—	0.3	—	0
49	—	—	0.50	—	1.13	—	—	—	0~10
50	—	0.27	—	0.28	—	0.90	0.2	0.1	0
51	—	0.44	—	0.45	—	1.40	—	0.3	—
52	0.42	—	0.52	—	1.20	—	—	0.5	—

この附近に工場の多い影響であろう．測定点 16 (江東区豊住町)，18 (北区志茂町)では，逆に，夜間の方が日中よりも平均周期が短く出ている．前論文[3]の第6図及び第5図を見ると，これらの場所の昼と夜の頻度曲線は非常に異り，日中のものは比較的に複雑であるが，夜間のものは卓越周期が読取れる位に単純である．この性質に対する1つの解釈は，日中は震動勢力が大きくて地中深い所までの震動性状に関係するが，夜間は勢力が，小さくて，地表面近いところの性質だけに関係する．しかも，地表面近くの層と次の層との弾性比は相当に大きい．言い換えると，地表面近くに特に軟弱な層があると考えるものである．尚，江東区豊住町の同じ場所では以前に地震観測から求めた頻度曲線があり，近地地震の頻度曲線と夜の常時微動のものとが類似し遠地地震と昼とが類似している事については前論文で報告してある．

日中と夜間(午前2時頃)の最大周期関係は第27図に示すように，平均周期の関係と大体同じ傾向である．平均周期，最大周期共に日中と夜間の差違が余りない場合の方が多く，特別な場合でも，その差違は最大 50% 位である．

(iii)　日中と夜間の常時微動の最大振幅の比較

日中と夜間(午前2時頃)の最大振幅の比較を第28図に示す．第28図からわかる事は，日中の振幅は夜間よりも2倍から10倍大きく，その比は，絶対振幅の小さい場所程大きい傾向にある．言い換えると静かな場所程，日中に比べて夜間の静けさの度合が大きい．

測定点 26 と 36 は共に港区麻布本村町で，その距離も近いのに，26 は比率の大きい方の例外，36 は小さい方の例外となつているから，極く局所的な原因によるものと推察される．何れにしても，常時微動の振幅の昼夜の差違は，周期のそれとは比較にならない位に大きい．

(常時微動の振幅や周期の時間的分布に関しては詳しい調査結果があり，別の論文として出す予定である.)

(iv)　常時微動の周期と最大振幅との関係

常時微動の平均周期と最大振幅との関係を昼と夜に分けて第29図及び第30図に示す．第29,30図から，平均周期は大体 0.2 秒から 0.5 秒の間にあるのに対して，振幅は日中で 0.1 ミクロンから 2 ミクロン，夜間で 0.03 ミクロンから 1 ミクロンの間にあり，振幅は場所による差違が大きいことがわかる．又，平均周期と振幅との間には相関性はほとんど見られない．

常時微動の周期は，地盤の震動性状とかなり密接な関係がありそうであるが，振幅は測定場所の環境条件に支配される度合が大きいため，地盤固有の震動的性質を比較法によつて求めるのには不適当と考えられる．

(v)　常時微動の平均周期と最大周期の関係

常時微動の平均周期と最大周期の関係を第31図に示す．測定点 2 (江東区西瑞江 4

3)　前出 1), 203, 204.

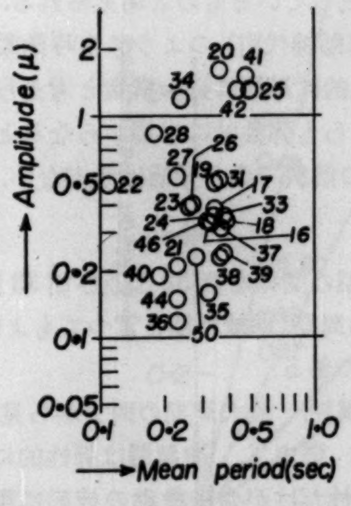

第 29 図　日中の常時微動の平均周期と最大振巾との関係

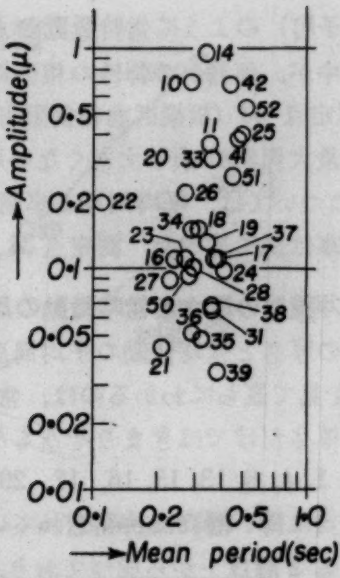

第 30 図　夜間の常時微動の平均周期と最大振巾との関係

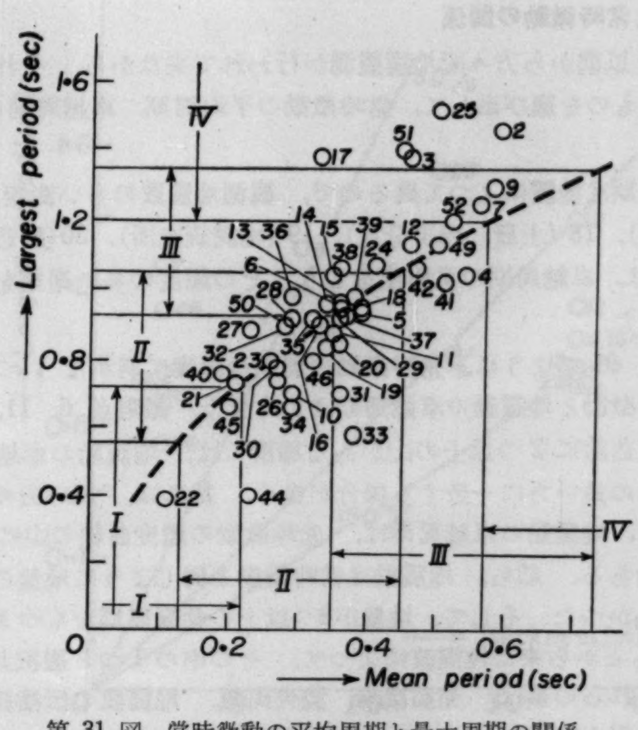

第 31 図　常時微動の平均周期と最大周期の関係
(I～IV の 記号は建築基準法関係の地盤種別)

丁目) 3 (江東区東小松川5丁目), 17 (江東区深川富岡町), 25 (港区芝海岸通), 51(大田区下丸子町) のように常時微動の最大周期が平均周期に比べて特に長い地盤は, 厚い軟弱層の中が, 何層かの弾性の相当異る土層から成つているものと考えられる.

又, 測定点 33 (板橋区志村前野町), 44(北多摩郡神代町) のように常時微動の平均周期に比べ最大周期が余り大きくない地盤は, 弾性的に単層に近い構造と考えられる. 測定点40については, 平均周期と卓越周期の比較からも弾性的に単層からなるという解釈ができる事は既に述べた. 測定点 31,34 等も, この解釈で余り矛盾は生じない.

(vi) 冲積層の厚さと常時微動の周期の関係

冲積層の厚さと常時微動の平均周期及び最大周期の関係を第32図及び第33図に示す. 第32図を見て直ちにわかるのは, 常時微動の平均周期(卓越周期と言つてもよい)は冲積層全体の厚さだけではきまりそうもないという事である.

測定点 1, 4, 5, 13, 15, 16, 17, 29 では, 平均周期, 最大周期の両方から見て, 常時微動は相当に薄い層内で誘発されている事になる. 従つて, 冲積層は弾性的にはつきり差違のある2層以上から成つており, 第1層の特性だけが常時微動の波形に現われるものと考えられる. 測定点 17, 25 等は平均周期は小さいが最大周期が普通であるから, 深い所の影響が現われていると解釈される.

(vii) 地震動と常時微動の関係

東京都内では, 以前から方々で地震観測が行われて来たから, それらの報告の中から卓越周期に関するものを選び出して, 常時微動の平均周期, 卓越周期と並べて第IV表に示した.

地震動の卓越周期は地震によつて異るので, 観測地震数の多い測定点 6 (電機大学), 11 (金町東北毛織), 18 (土研, 赤羽分室), 19 (地震研究所), 30(駒込アパート), 46(青山学院)については, 卓越周期の又頻度をとり, その頻度の多い周期を, その場所の卓越周期として採用した.

測定点 19, 30, 46 のように, 常時微動の周期の頻度に明かな 1 つの山ができる場所においては, 常時微動と地震動の卓越周期はよく合う. 測定点 6, 11, 18 のように, 常時微動の周期頻度曲線に2つ以上の山がある場所では, 地震動の卓越周期は, 常時微動の頻度の山のうちの長い方に一致する場合が多く, 稀には, 短い方の山と同じ場合がある. 言い換えると, 地震動の卓越周期は, 常時微動の頻度曲線の山になる周期の中のどれかに当るわけである. 即ち, 地震動は常時微動と同じように地盤の震動特性に大きく支配される事がわかつた. そして, 地盤が2つ以上の共振周期をもつような構成になつている場所では, もとから来た地震波によつて, その中の1つと選択共振する場合が多い事もわかつた. これらの事は, 発震機構, 震央距離, 地震波の伝播経路等に関係する筈であり, 詳細な検討を現在行いつつある.

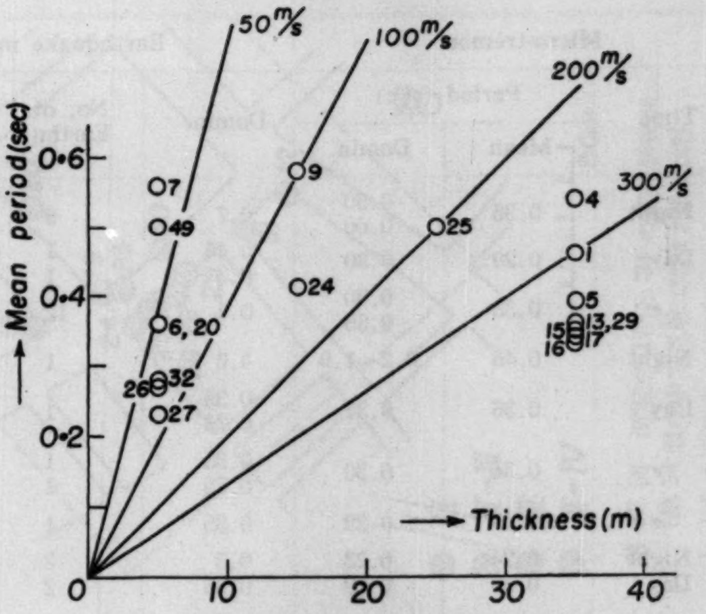

第 32 図 冲積層の厚さと常時微動の平均周期との関係

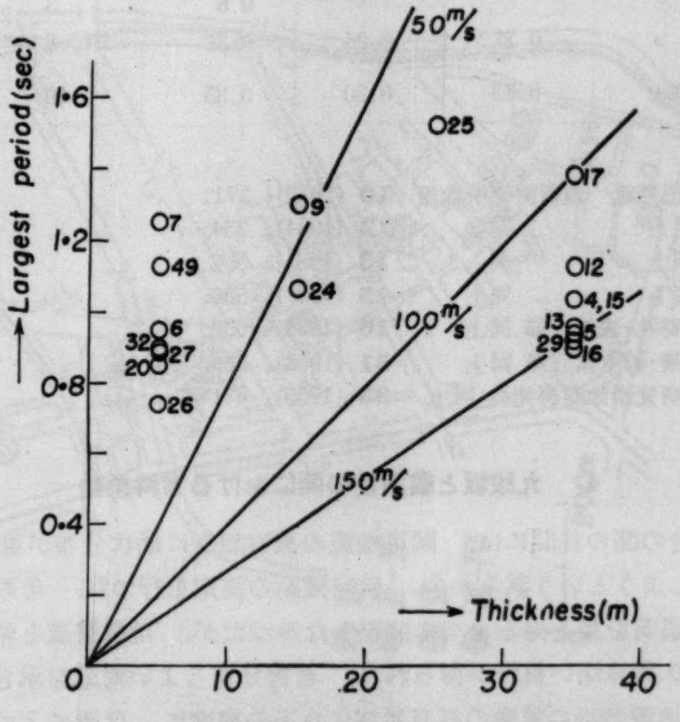

第 33 図 冲積層の厚さと常時微動の最大周期との関係

第 IV 表　地震動と常時微動の周期特性の比較

No.	Micro-tremor			Earthquake motion		
	Time	Period (sec)		Domin.	No. of Earthq.	Bibli.
		Mean	Domin.			
6	Night	0.36	0.30 0.60	0.7	9	2, 3, 4
10	Day	0.29	0.30	0.45 0.3	1 1	7
11	〃	0.35	0.30 0.55	0.5	12	7
12	Night	0.46	0.2～1.0	0.6	1	7
13	Day	0.36	0.32	0.35 0.75	1	7
14	〃	0.34	0.30	0.35 0.75	1 1	7
15	〃	0.35	0.29	0.35	1	7
16	Night Day	0.24 0.33	0.23 0.29	0.3 0.35	2 2	2, 4
18	Day	0.39	0.38	0.4 0.9	10	2, 3, 4
19	Night	0.34	0.32	0.3～0.4	29	1, 2, 3, 4, 5, 7
29	〃	0.36	0.35	0.35 0.6	2 3	6
30	〃	0.27	0.26	0.35	8	6
46	Day	0.32	0.30	0.35	10	2, 3, 4

備　考

文献 (1) 石本巳四雄　地震研究所彙報 **10** (1932), 171.
(2) 同上　同上 **12** (1934), 234.
(3) 同上　同上 **13** (1935), 592.
(4) 同上　同上 **15** (1937), 536.
(5) 萩原尊礼・表俊一郎 同上 **16** (1938), 632.
(6) 金井清・鈴木富三郎 同上 **31** (1953), 305.
(7) 地震研究所地盤研究会 同上 **33** (1955), 471.

4.　九段坂と駿河台の間における常時微動

九段坂と駿河台の間の谷間には，関東地震の被害程度に縞状分布が現われたので，振動学的な解釈をしようという試みから，常時微動の測定を行つた．その結果，被害分布にはつきりした説明を加え得るまでには至らなかつたが，地質構造と常時微動の性質との関係についての興味深い資料が得られた．被害分布とよい対応を示さない1つの理由としては，関東地震当時の家屋の新旧並びに良否の程度に，区画によつて相当の差違があつたらしい事があげられる．

九段坂と駿河台との間で，常時微動の測定を行つた場所を第 34, 35 図及び第 V 表に示

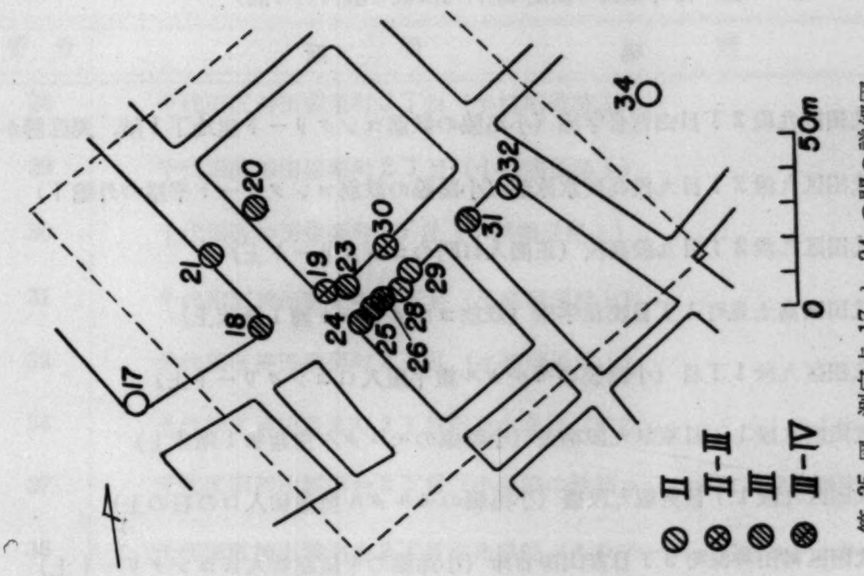

第 35 図 測定点 17 と 34 の間の詳細図
(第 34 図の中で点線で囲まれた地域)
(I〜IV の記号は建築基準法関係の地盤種別)

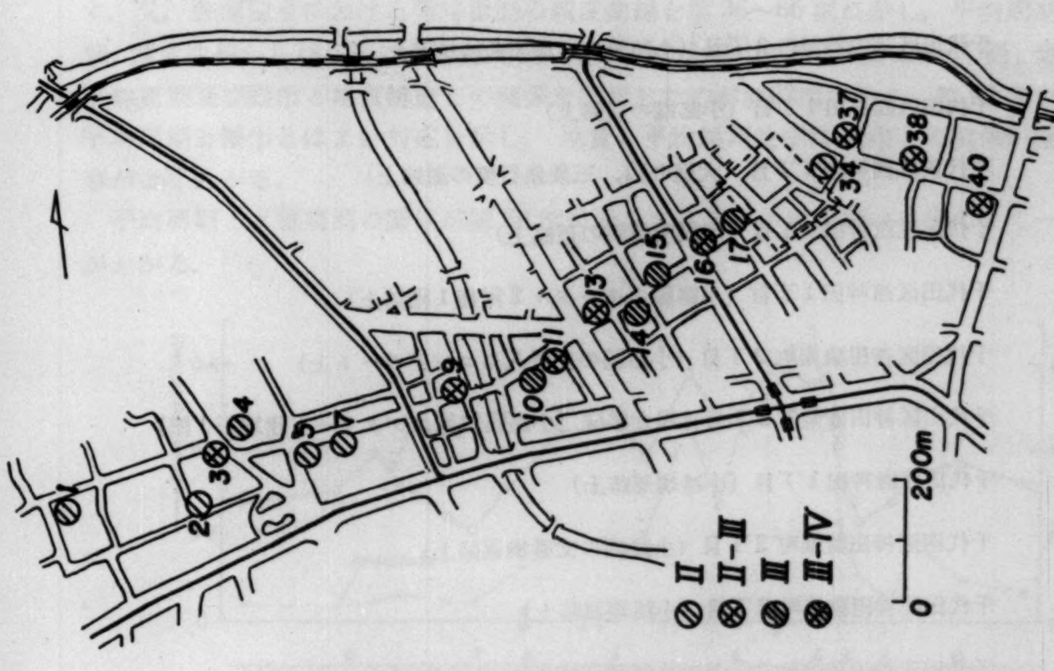

第 34 図 九段坂と駿河台の間における常時微動の測定場所(I〜IV の記号は建築基準法関係の地盤種別)

第 V 表 常時微動の測定場所(九段坂と駿河台の間)

番号	場所
1	千代田区九段2丁目白百合学園 (小路脇の鉄筋コンクリート建地下1階, 周囲静か)
2	千代田区九段2丁目九段高校水泳部 (小路脇の鉄筋コンクリート平屋の外壁下)
3	千代田区九段2丁目九段高校 (正面入口門のコンクリート上)
4	千代田区富士見町1丁目暁星学園 (鉄筋コンクリート建1階床上)
5	千代田区九段1丁目 (小路脇のモルタル塗平屋入口コンクリート上)
7	千代田区九段1丁目東鉄九段宿舎 (小路脇のモルタル塗建物1階床上)
9	千代田区九段1丁目東販九段寮 (小路脇のモルタル塗建物入口の石の上)
10	千代田区神田神保町3丁目富山房倉庫 (小路脇の平屋建物入口コンクリート上)
11	千代田区神田神保町3丁目高陽書院 (モルタル塗2階建1階入口の床上)
13	千代田区西神田2丁目日中友好協会 (大通り脇の鉄筋コンクリート建1階入口)
14	千代田区神田神保町2丁目 (小路脇の印刷所前の焼跡)
15	千代田区西神田1丁目 (小路端の道路上)
16	千代田区西神田1丁目 (大通り脇, 三菱銀行横の道路上)
17	千代田区西神田1丁目 (印刷所前隣の道路上)
18	千代田区西神田1丁目 (小路脇のモルタル2階建1階床上)
19	千代田区神田猿楽町2丁目 (小路脇の交番入口コンクリート上)
20	千代田区神田猿楽町2丁目神田女学園 (小路脇鉄筋コンクリート建地下1階)
21	千代田区西神田1丁目 (小路端道路上)
23	千代田区神田猿楽町2丁目 (小路端の交番横道路上)
24	千代田区神田猿楽町2丁目 (小路端道路上)
25	千代田区神田猿楽町2丁目 (小路端道路上)
26	千代田区神田猿楽町2丁目(小路端道路上)

(つづく)

第 V 表（つづき）

番号	場所
28	千代田区神田猿楽町2丁目（小路端道路上）
29	千代田区神田猿楽町2丁目（小路端道路上）
30	千代田区神田猿楽町2丁目（小路端道路上）
31	千代田区神田猿楽町2丁目（小路端道路上）
32	千代田区神田猿楽町2丁目（小路端道路上）
34	千代田区神田猿楽町2丁目明治中学校（鉄筋コンクリート建1階入口床上）
37	千代区田神田駿河台2丁目（小路脇の鉄筋コンクリート建1階床上）
38	千代田区神田駿河台2丁目文化学院（入口アーケード内コンクリート上）
40	千代田区神田駿河台1丁目明治大学文学部（大通り脇，鉄筋コンクリート建1階）

す．又，各測定点における常時微動の頻度曲線を第36～66図に示し，平均周期，最大周期，頻度曲線から読み取つた卓越周期，並びに最大振巾を第VI表に示す．尚，常時微動の平均周期及び振巾と地質構造との関係を図示したのが第67図である．第67図を見ると，平均周期と振巾とはよい対応を示し，地質と平均周期並びに振巾との関係が極めて深い事がよくわかる．

平均周期と卓越周期の関係が第68図に示してあるが，両周期は非常によく一致する事がわかる．

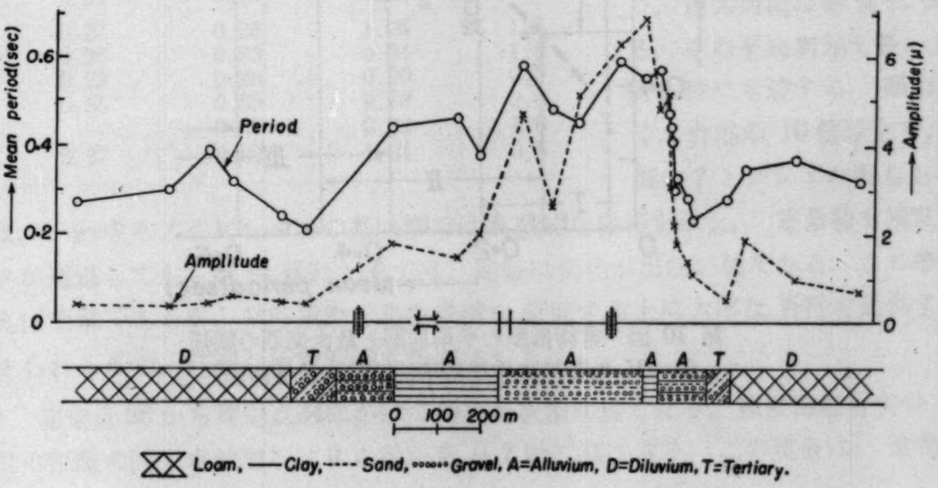

第 67 図　九段坂と駿河台の間における地質と常時微動との関係

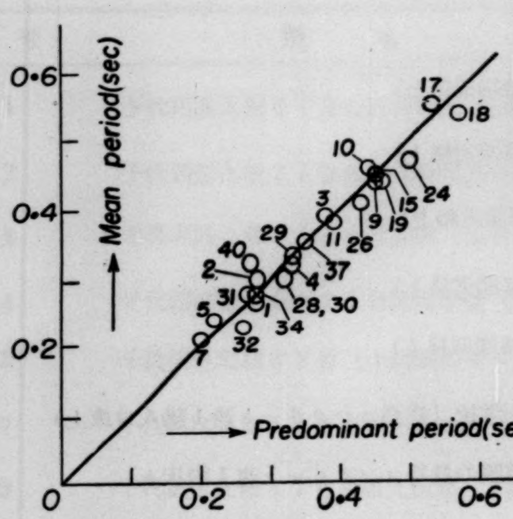

第 68 図 常時微動の卓越周期と平均周期の関係

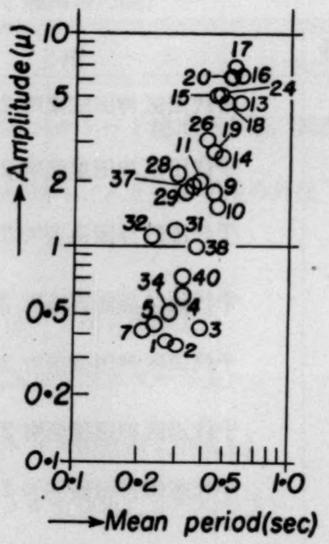

第 69 図 常時微動の平均周期と最大振巾の関係

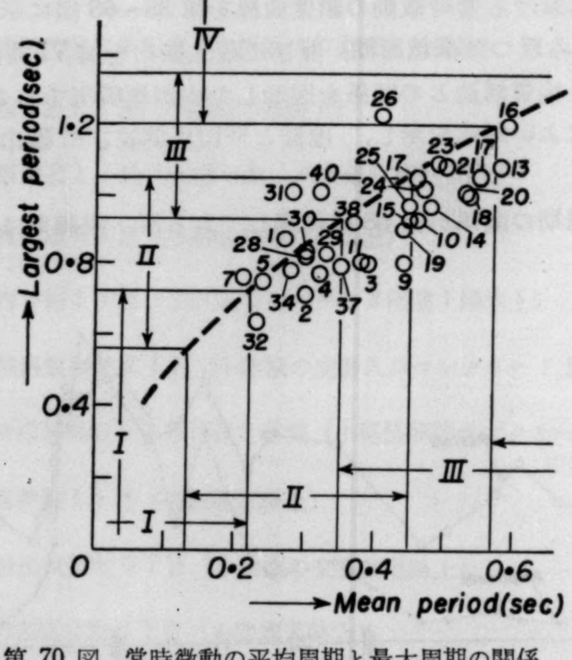

第 70 図 常時微動の平均周期と最大周期の関係
(I~IV の記号は建築基準法関係の地盤種別)

平均周期と最大振巾の関係を第 69 図に示す．第 69 図から，平均周期が長くなると，最大振巾が大きくなる傾向のある事がわかる．狭い地域についての測定結果を集めたものなので，地盤震動を誘発する，もとの勢力が大体似ており，従つて，振巾の方にも地盤震動特性が比較的によく現われたものと考えられる．

第 VI 表　九段坂と駿河台の間における常時微動の測定結果

No.	Period (sec)			Largest Amplitude (μ)
	Dominant	Mean	Largest	
1	0.28	0.27	0.87	0.3
2	0.27	0.30	0.71	0.3
3	0.38	0.39	0.80	0.5
4	0.33	0.32	0.77	0.5
5	0.22	0.24	0.75	0.5
7	0.20	0.21	0.76	0.5
9	0.45	0.44	0.80	2.0
10	0.44	0.46	0.93	1.5
11	0.39	0.38	0.80	2.0
13	—	0.58	1.08	4.5
14	—	0.48	0.97	2.5
15	0.45	0.45	0.93	5.0
16	—	0.59	1.20	6.5
17	0.53	0.55	1.05	7.0
18	0.57	0.57	1.00	4.5
19	0.46	0.44	0.90	2.5
20	—	0.53	0.96	6.0
21	—	0.50	1.08	—
23	—	0,49	1.09	—
24	0.50	0,47	1.02	5.0
25	—	0.44	0.96	—
26	0.43	0.41	1.23	3.0
28	0.32	0.30	0.82	2.0
29	0.33	0.33	0.83	2.0
30	0.32	0.30	0.82	—
31	0.27	0.28	1.05	1.5
32	0.26	0.23	0.64	1.0
34	0.28	0.28	0.90	0.5
37	0.35	0.35	0.79	2.0
38	—	0.37	0.92	1.0
40	0.27	0.32	1.01	0.5

平均周期と最大周期の関係を示したのが第 70 図である．

次に，この地域の解析結果を九段坂の方から順次列挙する．

(1)　九段の台地（測定点 1～4）の卓越周期は 0.3～0.4 秒で，東京都内の山手で一般に見られる性質である．

(2)　中坂の途中（測定点5, 7）の頻度曲線は非常に尖り，その卓越周期は約 0.2 秒である．第 3 紀の粘土砂礫層が出ているためであろう．

(3)　中坂を降り切ると，急に周期の長い波形となり，頻度曲線は平坦になる．台地に近い測定点 9, 10, 11 では 0.4～0.45 秒で頻度が卓越する．

(4)　谷間の測定点 13～25 では，頻度曲線が非常に平坦になり，最大周期は非常に長くなる．その平均周期も長い所では 0.6 秒にも達する．振巾も大きく，台地の 10 倍以上で，最大振巾 7 ミクロンの所もある．この辺は，いわゆるノイズレベルの高い事では典型的な様相を示し，重量物を満載したトラックが通過しても，数 m 離れた所では，記録に変化が出ない位である．この事は当然と言えば当然であるが，常時微動の発生機構を研究する上に大事な資料を提供するものと考えられるので，詳細な検討を行う予定である．

(5)　測定点 26 から測定点34にかけて周期が次第に短くなり，頻度曲線も尖つてくる．50m位の距離の間で卓越周期は 0.4 秒から 0.2 秒に順次変る．この現象は，常時微動を波動として研究する上で極めて大切な事である．

(6) 駿河台(測定点 37, 38, 39) では，頻度曲線に鋭い卓越性は見られないが，卓越周期は，0.3秒～0.4 秒で東京都内の山手で多く見られる値である．

台地の振巾は 0.3～1 ミクロンであるが，谷間の振巾は，1～7 ミクロンで，最大と最小の振巾比は約 20 倍にも達する．

5. む す び

本研究でわかつた常時微動の性質を次に列記する．

(I) 常時微動の卓越周期と平均周期は略一致する．頻度曲線が平坦な場合，2つ以上の山のできる場合には卓越周期の読取は困難であるから，地盤の震動特性を示す係数の1つとしては平均周期を使う方が便利である．

(II) 一般に厚い軟弱層では，頻度曲線が平坦である．特別な場合として，弾性的に均一に近いと考えられる場所では，0.6 秒以上の長周期で頻度が卓越する．

(III) 日中と夜間の周期(卓越，平均，最大)の差違は一般に小さく，特別な場合でも勢々 50% 位の差違である．従つて，常時微動の周期は，地盤固有の震動係数として使うのに適している．

(IV) 日中と夜間の振巾は非常に異り，昼は夜の2倍から10倍に達する．一般に，いわゆる静かな場所程，この比が大きいのは，常時微動の発生機構から考えて当然であろう．振巾は測定場所の環境条件に支配されるから，地盤固有の震動係数としては不適当である．

(V) 地盤の震動性状は冲積層の厚さだけではきまらない．冲積層が何層かの土層から成つている場合は第1層の性質が出やすい．

(VI) 常時微動の頻度曲線の山が 1 つの場合は地震動の卓越周期に一致する．山が 2 つ以上ある場所では，地震によつて，そのどれかの周期が卓越周期になる．

(VII) 地質が順次変化している場所では，僅か 50 m 位の距離の間で，地質の変化に従つて卓越周期が2倍も変る．

終りに臨み，本調査に当り多大の御援助を賜つた東京都建築局並びに調査地の方々に深い謝意を表する．又，懇ろな御援助と御議論を賜つた地震研究所地盤研究会の方々に厚く御礼を申し述べる．

附 記

常時微動が地盤の震動性状に密接な関係がありそうな事に眼をつけ，常時微動の平均周期と最大周期とを使つて，建築基準法関係の地盤種別を推定する試案を作つてみた．(筆者 常時微動による地盤種別判定法試案，地震研究所，1956年5月)第1図，第31図第34図，第35図及び第70図中の I～IV の記号は，その試案によつたものである．

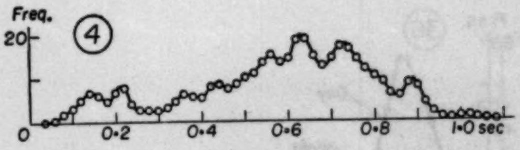

第 2 図　江東区吾嬬東5丁目吾嬬中学校

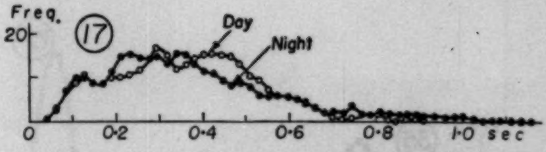

第 3 図　江東区深川富岡町数矢小学校

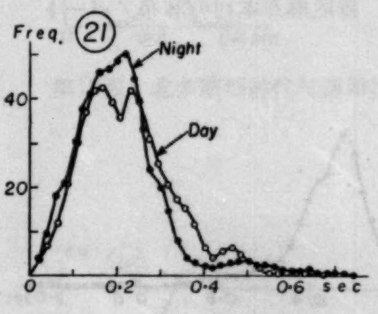

第 4 図　新宿区戸塚町高田馬場駅

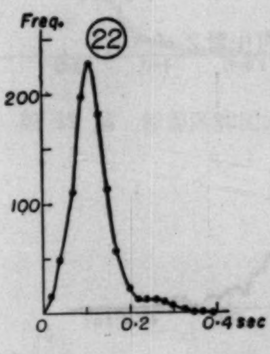

第 5 図　新宿区戸塚町日本電話工業

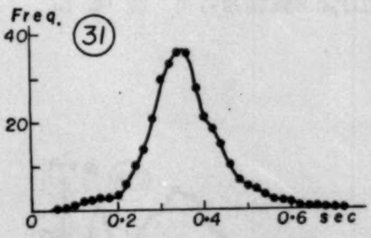

第 6 図　文京区第六天町第六天アパート

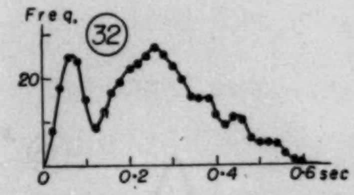

第 7 図　文京区関口町鈴木氏宅

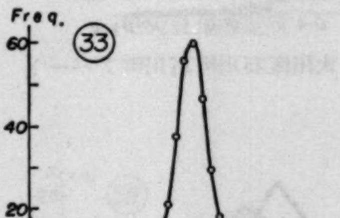

第 8 図　板橋区志村前野町志村アパート

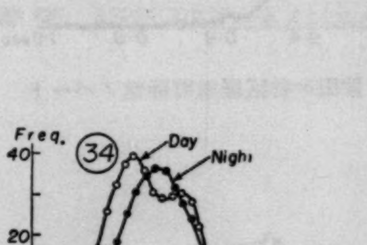

第 9 図　新宿区戸塚町高田馬場アパート

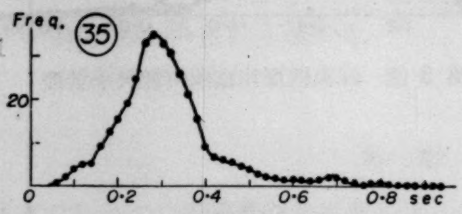

第 10 図 中野区栄町中野アパート

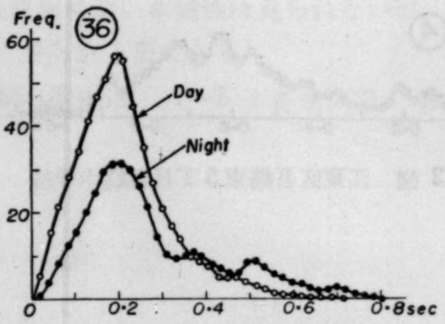

第 11 図 港区麻布本村町麻布アパート

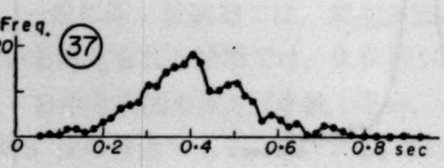

第 12 図 世田ケ谷区太子堂町
太子堂アパート

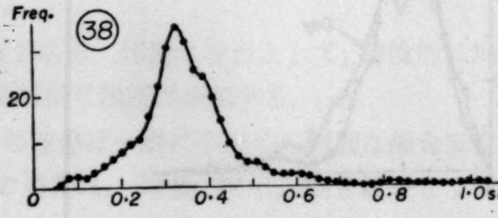

第 13 図 世田ケ谷区世田ケ谷
豪徳寺アパート

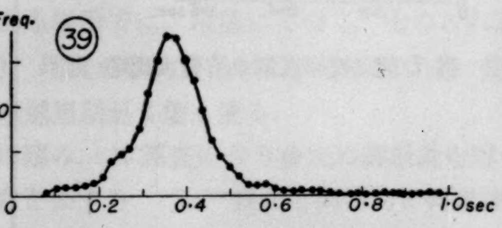

第 14 図 世田ケ谷区経堂町経堂アパート

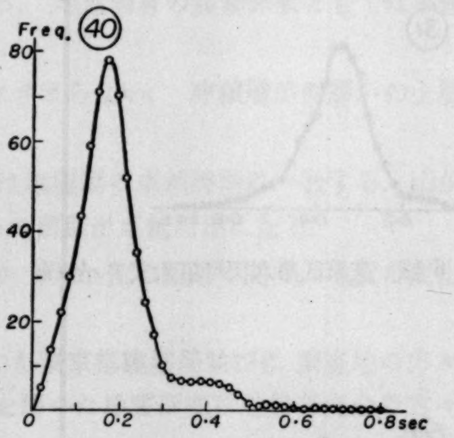

第 15 図 大田区石川町石川町アパート

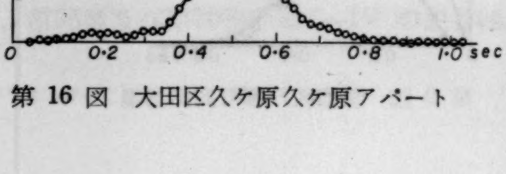

第 16 図 大田区久ケ原久ケ原アパート

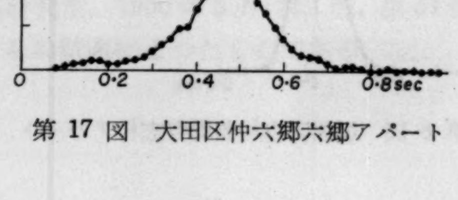

第 17 図 大田区仲六郷六郷アパート

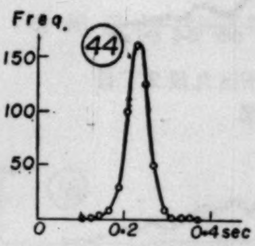

第18図　北多摩郡神代町運輸技術研究所

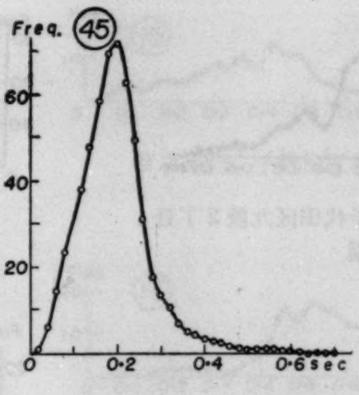

第 19 図　杉並区和田本町鈴木氏宅

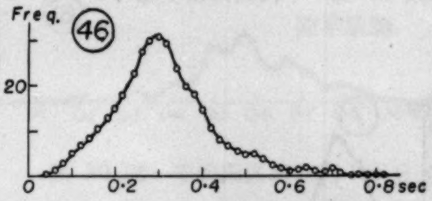

第 20 図　渋谷区緑岡町青山学院

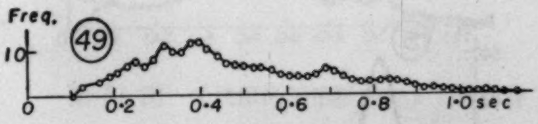

第 21 図　中央区東銀座北海道新聞社

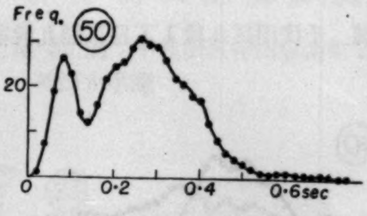

第 22 図　中央区東銀座
中央計量検定所

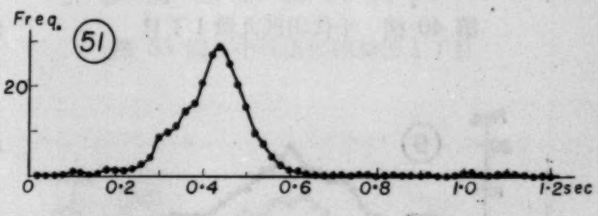

第 23 図　大田区下丸子キャノンカメラ株式会社

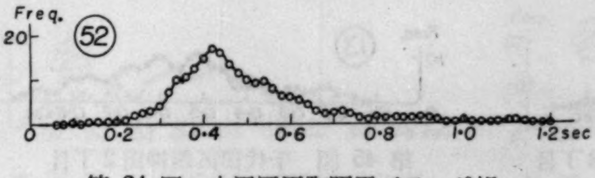

第 24 図　大田区原町昭電グランド場

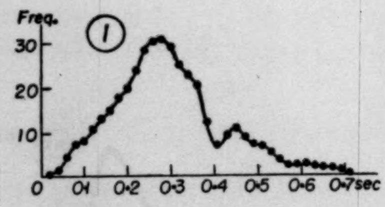

第 36 図 千代田区九段２丁目
白百合学園

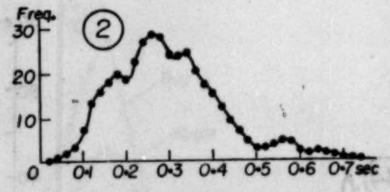

第 37 図 千代田区九段２丁目
九段高校水泳部

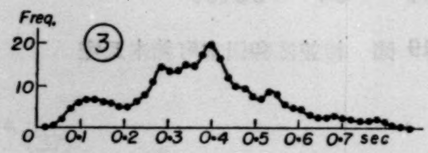

第 38 図 千代田区九段2丁目九段
高校

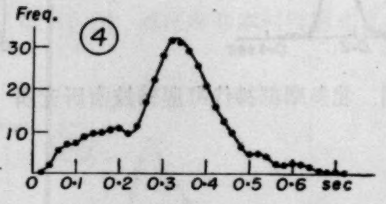

第 39 図 千代田区富士見町１丁目
暁星学園

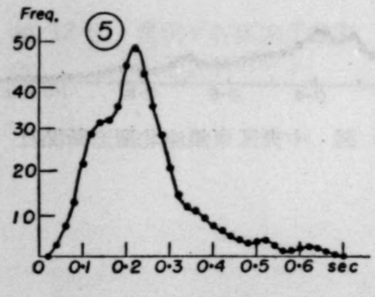

第 40 図 千代田区九段１丁目

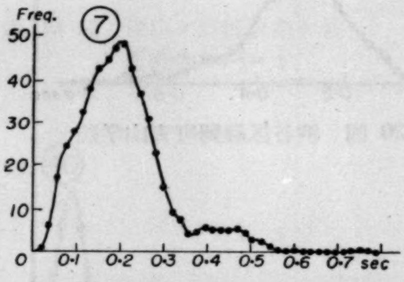

第 41 図 千代田区九段１丁目東鉄九段宿舎

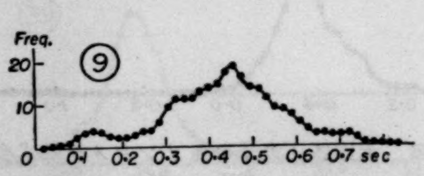

第 42 図 千代田区九段１丁目
東販九段寮

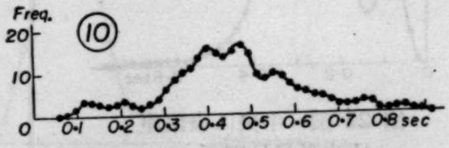

第 43 図 千代田区神田神保町２丁目
富山房倉庫

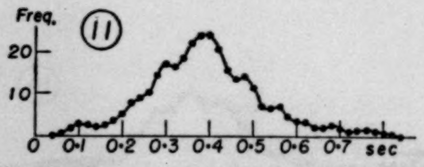

第 44 図 千代田区神田神保町３丁目
高陽書院

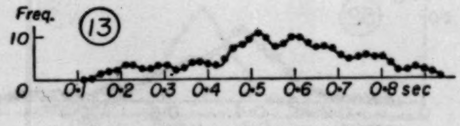

第 45 図 千代田区西神田２丁目
日中友好協会

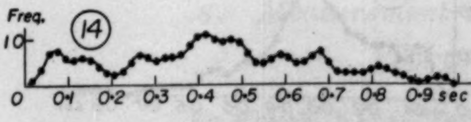

第 46 図　千代田区神田神保町2丁目

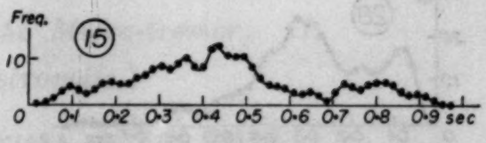

第 47 図　千代田区西神田1丁目

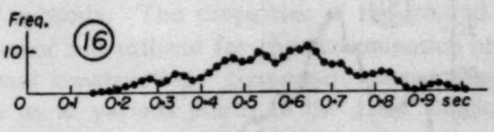

第 48 図　千代田区西神田1丁目三菱銀行横

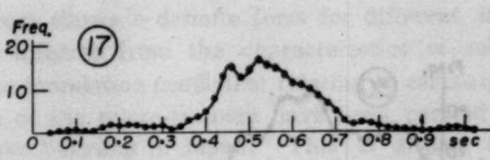

第 49 図　千代田区西神田1丁目

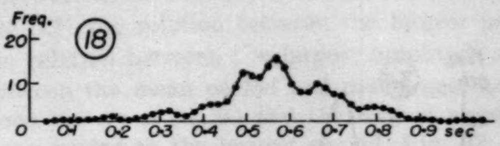

第 50 図　千代田区西神田1丁目

第 51 図　千代田区神田猿楽町2丁目交番

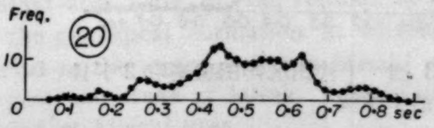

第 52 図　千代田区神田猿楽町2丁目
神田女学園

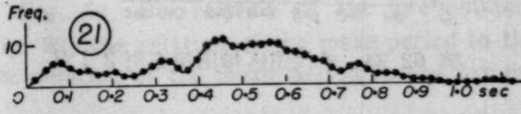

第 53 図　千代田区西神田1丁目

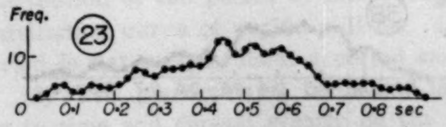

第 54 図　千代田区神田猿楽町2丁目

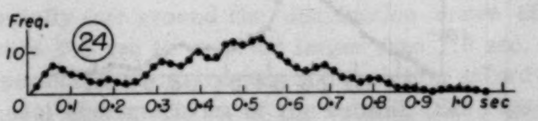

第 55 図　千代田区神田猿楽町2丁目

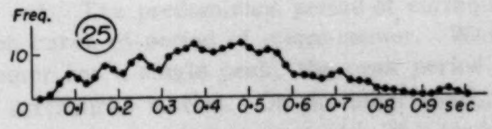

第 56 図　千代田区神田猿楽町2丁目

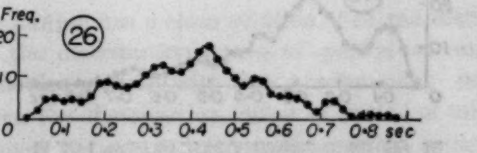

第 57 図　千代田区神田猿楽町2丁目

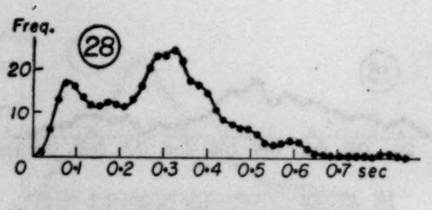

第 58 図　千代田区神田猿楽町 2 丁目

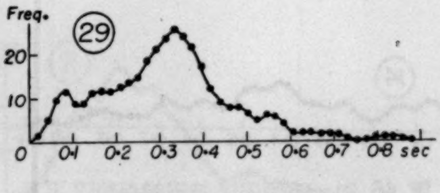

第 59 図　千代田区神田猿楽町 2 丁目

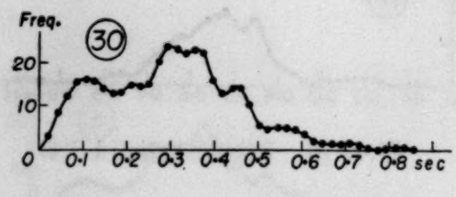

第 60 図　千代田区神田猿楽町 2 丁目

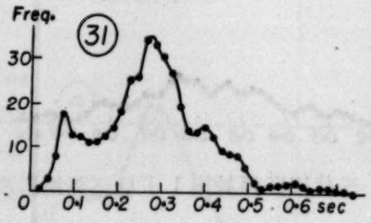

第 61 図　千代田区神田猿楽町 2 丁目

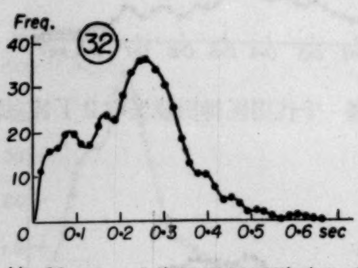

第 62 図　千代田区神田猿楽町 2 丁目

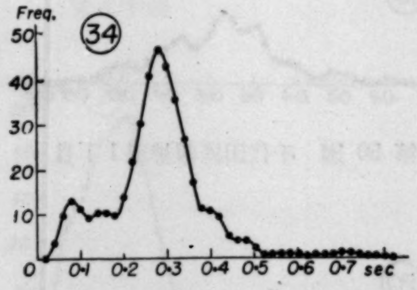

第 63 図　千代田区神田猿楽町 2 丁目
明治中学校

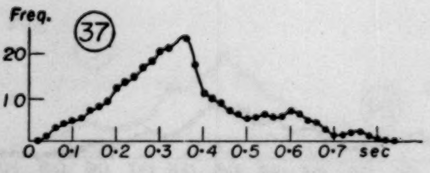

第 64 図　千代田区神田駿河台 2 丁目

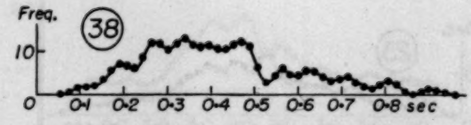

第 65 第　千代田区神田駿河台 2 丁目文化学院

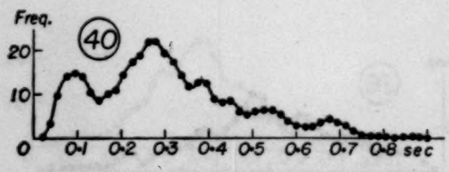

第 66 図　千代田区神田駿河台 1 丁目
明治大学文学部

8. *Measurement of the Micro-tremor. II.* *(Tokyo Metropolis.)*

By Kiyoshi KANAI, Teiji TANAKA and Kaio OSADA,

Earthquake Research Institute.

The distribution of periods of micro-tremors shows a definite form for different kinds of subsoils. The properties of the ground as inferred from the characteristics of micro-tremor are utilized for the determination of the foundation coefficient relating to earthquake-proof construction. Systematic measurements of the micro-tremors have been carried out by us at various places in the great earthquake districts in Japan. This is a part of a series of our investigations.

Fig. 1 shows the measurement places. Figs. 2-24; distribution of the period of micro-tremors. Fig. 25; the relation between the predominant period and the mean period of micro-tremors. Fig. 26; the relation between the mean period at day time and at midnight. Fig. 27; the relation between the largest period at day time and at midnight. Fig. 28; the relation between the largest amplitude at day time and at midnight. Fig. 29; the relation between the mean period and the largest amplitude at day time. Fig. 30; the relation between the mean period and the largest amplitude at midnight. Fig. 31; the relation of the mean period to the largest period. Fig. 32; the relation of the mean period to the thickness of alluvium. Fig. 33; the relation of the largest period to the thickness of alluvium.

Figs. 34, 35; the measurement places along the lines of Kudan to Surugadai in Tokyo (Misaki area.) Figs. 36-66; the frequency distribution of the period of micro-tremor at Misaki area. Fig. 67; the relation of the mean period as well as the largest amplitude to the geological formation at Misaki area. Fig. 68; the relation of the predominant period to the mean period at Misaki area. Fig. 69; the relation of the mean period to the largest amplitude at Misaki area. Fig. 70; the relation of the mean period to the largest period at Misaki area.

From systematic measurements, we found many micro-tremor characteristics, which we shall now summarize as follows.

(1) The harder the rigidity of the subsoil is, the sharper the shape of the frequency distribution of the period of micro-tremors and the shorter the predominant period of the distribution curve of period will be. On especially soft ground the distribution curve of period is flat ranging from a period smaller than 0.2 sec to a period larger than 1.0 sec.

(2) The predominant, mean and largest periods of micro-tremors differ slightly according to time and depend greatly on the vibrational characteristics of the subsoil. (See Figs. 26, 27, 28.) But, the largest amplitude of micro-tremor in the daytime is much larger than that at midnight, that is to say, the ratios are 2-10 times, because the amplitudes of micro-tremor depend greatly on the activity of the artificial vibration source surrounding the measureing place. (See Figs. 29, 30.)

(3) The predominant period of earthquake motion has a close relation with the distribution curve of period of micro-tremor. While, the distribution curve of period of micro-tremor has a single peak, the peak period coincides clearly with the predominant period of earthqurke motion. On the other hand, when the distribution curve of period of micro-tremor has more than two peaks, the predominant period of earthquake motion coincides with either of them. (See Table IV.)

8. Measurement of the Micro-tremor II. (Tokyo Metropolis.)

By Kiyoshi KANAI, Teiji TANAKA and Kazo OSADA

Earthquake Research Institute.

The distribution of periods of micro-tremors shows a definite form for different kinds of subsoils. The properties of the ground as inferred from the characteristics of micro-tremor are utilized for the determination of the foundation coefficient relating to earthquake-proof construction. Systematic measurements of the micro-tremors have been carried out by us at various places in the great earthquake districts in Japan. This is a part of a series of our investigations.

Fig. 1 shows the measurement places. Figs. 2-23; distribution of the period of micro-tremors. Fig. 25; the relation between the predominant period and the mean period of micro-tremors. Fig. 26; the relation between the mean period at day time and at midnight. Fig. 27; the relation between the largest period at day time and at midnight. Fig. 28; the relation between the largest amplitude at day time and at midnight. Fig. 29; the relation betwen the mean period and the largest amplitude at day time. Fig. 30; the relation between the mean period and the largest amplitude at midnight. Fig. 31; the relation of the mean period to the largest period. Fig. 32; the relation of the mean period to the thickness of alluvium. Fig. 33; the relation of the largest period to the thickness of alluvium.

Figs. 34, 35; the measurement places along the lines of Roden to Suzugaoka in Tokyo (Misaki area.) Figs. 36-66; the frequency distribution of the period of micro-tremor at Misaki area. Fig. 67; the relation of the mean period as well as the largest amplitude to the geological formation at Misaki area. Fig. 68; the relation of the predominant period to the mean period at Misaki area. Fig. 69; the relation of the mean period to the largest amplitude at Misaki area. Fig. 70; the relation of the mean period to the largest period at Mizaki area.

From systematic measurements, we found many micro-tremor characteristics, which we shall now summarize as follows.

(1) The harder the rigidity of the subsoil is, the sharper the shape of the frequency distribution of the period of micro-tremors and the shorter the predominant period of the distribution curve of period will be. On especially soft ground the distribution curve of period is flat ranging from a period smaller than 0.2 sec to a period larger than 1.0 sec.

(2) The predominant, mean and largest periods of micro-tremors differ slightly according to time and depend greatly on the vibrational characteristics of the subsoil. (See Figs. 26, 27, 28.) But, the largest amplitude of micro-tremor in the daytime is much larger than that at midnight, that is to say, the ratios are 2-10 times, because the amplitudes of micro-tremor depend greatly on the activity of the artificial vibration source surrounding the measuring place. (See Figs. 29, 30.)

(3) The predominant period of earthquake motion has a close relation with the distribution curve of period of micro-tremor. While, the distribution curve of period of micro-tremor has a single peak, the peak period coincides clearly with the predominant period of earthquake motion. On the other hand, when the distribution curve of period of micro-tremor has more than two peaks, the predominant period of earthquake motion coincides with either of them. (See Table IV.)

9. 常時微動の測定結果第3報
(横浜市内)

地震研究所 金井　清　田中貞二　長田甲斐男

(昭和31年4月24日，9月25日発表——昭和31年12月31日受理)

1. まえがき

常時微動の波形は地盤の震動性状と密接な関係があることがわかつたので，その性質を耐震工学上の地盤係数を求める方面に利用する方法の研究に必要な資料を得るための調査を各地で行つている．

現在までにわかつた常時微動の性質のうちの主なものは；

(1) 頻度曲線は堅い地盤では鋭く，その卓越周期は短い．軟い地盤になるほど，卓越周期が長くなり曲線は平になる．

(2) 常時微動の周期(卓越，平均，最大)の時刻による差違は小さいが，振幅は2倍から10倍の差違がある．周期関係は地盤特性に関係が深いが，振幅は環境条件の影響の受け方が大きい．

(3) 常時微動の波形は冲積層の厚さだけではきまらなく，土層の構成に大いに関係する．第1層の性質が最も出やすい．

(4) 常時微動の頻度曲線の山が1つの場所では，その周期は地震動の卓越周期に一致する．2つ以上の山がある場所では，地震動の卓越周期は，そのうちの何れかの山の周期となる．

2. 測定方法

常時微動の測定方法は既報[1),2)]の通りで，電磁型煤書微動計(換振器は固有周期1秒の動線輪型倒立振子)によつて5分間の測定を行い，その中の2分間について解析を行つた．

本報告の測定は，昭和29年4月，7月，昭和31年2月，6月の4回行つたものである．測定場所を第1図並びに第I表に示す．記録の解釈にあたつて，主として交通機関な

1) 金井　清・田中貞二・長田甲斐男　地震研究所彙報 **32** (1954), 199.
2) 地震研究所地盤研究会　同上 **33** (1955), 492～495.

どの人工的震動源からの直接の影響の有無大小を推定するのに役立てる意味で，測定場所の環境条件を第I表に詳細に記しておいた．

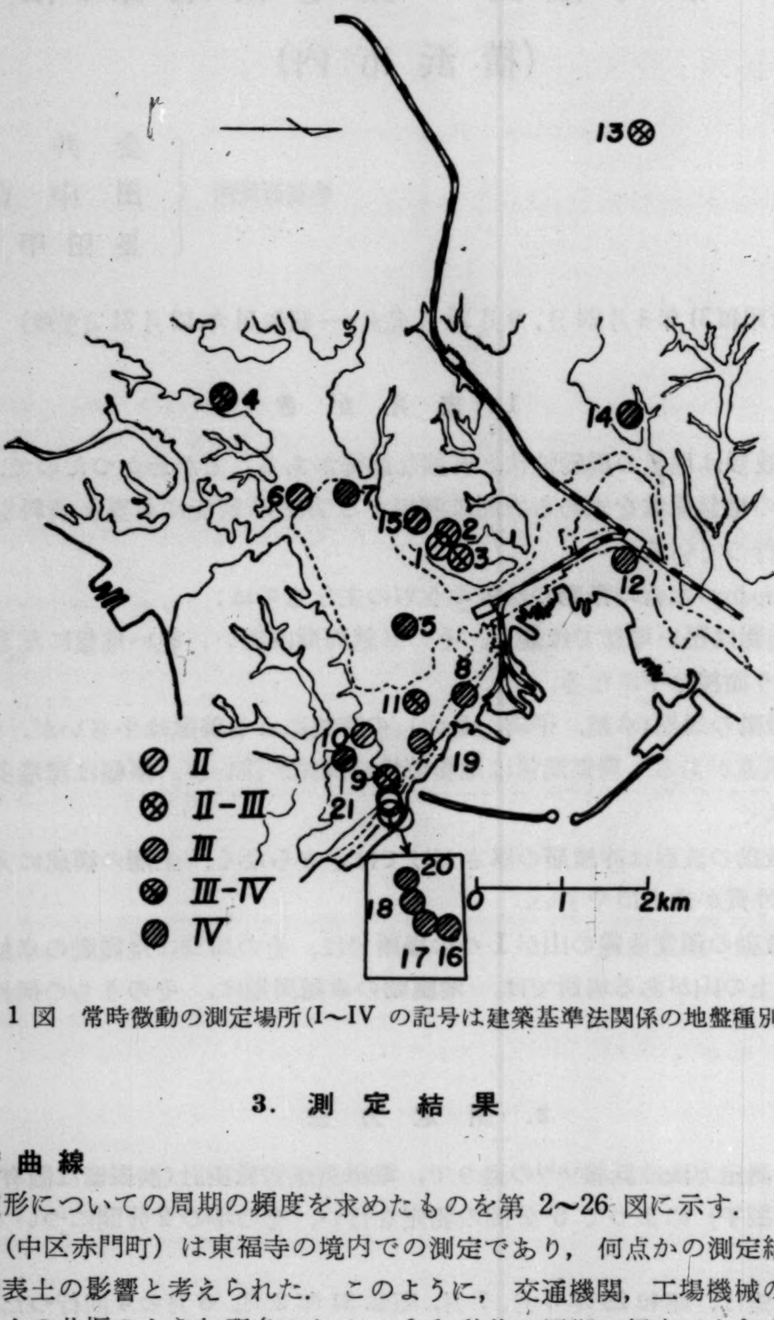

第 1 図　常時微動の測定場所(I～IV の記号は建築基準法関係の地盤種別)

3. 測 定 結 果

(i) 頻 度 曲 線

2 分間の波形についての周期の頻度を求めたものを第 2～26 図に示す．

測定点 15 (中区赤門町) は東福寺の境内での測定であり，何点かの測定結果から 0.1 秒の山は砂の表土の影響と考えられた．このように，交通機関，工場機械の直接の影響だけでなく表土の共振のような現象のために 0.1 秒位の周期の頻度が大きくなることが時々ある．

測定点 1 (野毛山プール)，3 (震災記念館)，6 (共進中学校)，9 (横浜測候所) においては日中及び深夜(午前 2 時) の測定を行つた．測定点 1，6，9 の昼夜の頻度曲線は大

第I表 常時微動の測定場所

番号	場所
1	中区老松町野毛山プール内（鉄筋コンクリート建物床上）
2	中区野毛山遊園地（休憩所地下室コンクリート床上）
3	中区老松町震災記念館（大通り脇鉄筋コンクリート建物1階床上）
4	南区大岡町国立大学工学部（電車通りより約 100 m 奥の平屋建物コンクリート床上）
5	中区羽衣町吉田中学校（電車通り脇鉄筋コンクリート建物1階床上）
6	南区蒔田町共進中学校（電車通りより約 150 m 奥の鉄筋コンクリート建物1階床上）
7	南区山王町日枝小学校（電車通り脇鉄筋コンクリート建物1階床上）
8	中区日本大通り県庁（大通り脇鉄筋コンクリート建物地下1階床上）
9	中区山手町横浜測候所（大通り脇鉄筋コンクリート建物地下1階地震計室床上）
10	中区山手町フエリス女学院（大通り脇鉄筋コンクリート建物1階床上）
11	中区中消防署（大通り脇鉄筋コンクリート建物1階床上）
12	西区内田町横浜市警察署（大通りより約 300 m 奥，鉄筋コンクリート建物1階床上）
13	保土ケ谷区西谷浄水場（大通り脇木造建物土間の上，交通に敏感）
14	西区宮ケ谷町（小路脇中庭を約 30 cm 掘る）
15	中区赤門町東福寺（大通りより約 100 m 奥，木造平屋建物コンクリート床上）
16	中区新山下町山下埠頭（岸壁より約 1 m 離れたコンクリート道路上）
17	中区山下町山下アパート（小路脇鉄筋コンクリート建物1階床上）
18	中区山下町信号所の崖下（小路より約 40 m 奥の建物跡石段上）
19	中区山下町ニューグランドホテル（大通り脇鉄筋コンクリート建物1階床上）
20	中区信号所（大通りより約 30 m 離れた信号所の玄関，周囲は至極静か）
21	中区山手町山手病院（大通り脇鉄筋コンクリート建物ドライエリヤ）
22	港北区日吉町慶応義塾附属高校（鉄筋コンクリート建物1階床上，周囲は至極静か）

（つづく）

第 I 表（つづき）

番　号	場　　　　所
23	鶴見区下末吉町　森永製菓株式会社鶴見工場（構内車庫コンクリート上）
24	鶴見区生麦　キリンビール株式会社横浜工場（構内鉄筋コンクリート建物 1 階床上）
25	神奈川区恵比須町　別子建設横浜出張所（木造小屋土の上）

体類似している．昼の頻度曲線にだけ 0.1 秒附近に僅かな山ができるのは，換振器のごく附近で起る交通機関等の人工的震動の影響と考えられる．測定点 3 の夜の頻度曲線は非常に異形であり，その解釈はまだついていない．頻度曲線の極大になる周期を卓越周期，2 分間の波数で時間を割つた値を平均周期，この計器で記録した波形の中で最も長い周期を最大周期と名づけて第 II 表に示した．又，同表中の最大振幅とは，2 分間の記録中で，大振幅が 2, 3 波続くものの中での最大値である．

第 II 表　常時微動の周期と最大振巾

No.	Period (sec)						Largest Amplitude (μ)	Alluvium Thickness (m)
	Dominant		Mean		Largest			
	Day	Night	Day	Night	Day	Night		
1	0.28	0.28	0.27	0.29	0.79	0.82	—	—
2	—	0.48	—	0.48	—	0.72	—	—
3	0.26	0.39	0.28	0.42	0.85	0.78	—	—
4	—	0.28	—	0.34	—	1.26	—	10～20
5	—	—	—	0.37	—	1.40	—	30～40
6	—	—	0.37	0.39	1.11	1.06	—	10～20
7	—	—	0.53	—	1.63	—	—	20～30
8	—	—	—	0.53	—	1.61	—	40～50
9	—	—	0.52	0.46	1.22	0.92	—	—
10	—	0.48	—	0.47	—	0.64	—	—
11	—	—	—	0.42	—	1.30	—	30～40
12	—	—	—	0.57	—	1.65	—	30～40
13	0.24	—	0.30	—	0.98	—	—	—
14	—	0.25	—	0.26	—	0.88	—	—
15	—	0.48	—	0.48	—	1.09	—	—
16	—	—	0.81	—	1.60	—	2.0	—
17	0.33	—	0.38	—	1.66	—	1.5	—
18	—	—	0.48	—	1.52	—	1.0	—
19	0.40	—	0.78	—	1.61	—	2.5	30～40
20	—	—	0.45	—	1.39	—	1.0	—
21	0.53	—	0.54	—	1.37	—	1.0	—
22	0.32	—	0.34	—	0.90	—	0.5	0
23	—	—	0.46	—	1.26	—	0.5	30～40
24	0.25	—	0.25	—	0.65	—	1.5	0～10
25	—	—	0.53	—	1.26	—	1.5	30～40

頻度曲線が非常に平坦なものと，頻度の山が2つ以上あるものについては，卓越周期の意味が曖昧なので読取らなかつた．即ち，測定点6(共進中学校)，7(日枝小学校)，8(県庁)，11(中消防署)，12(横浜市警察署)，23（森永製菓)，25(別子建設）は頻度曲線が平坦なため，測定点 5（吉田中学校)，19（横浜測候所）は頻度曲線の山が2つ以上あるため，第II表の中に卓越周期の値が記入してない．

卓越周期と平均周期の関係を第27図に示す．第27図から卓越周期と平均周期の値は非常に近いことがわかる．

平均周期が卓越周期よりも僅かに大きい原因は第2報で述べたように，人工的震動の影響のきゝ方の差違によるものと考えられる．

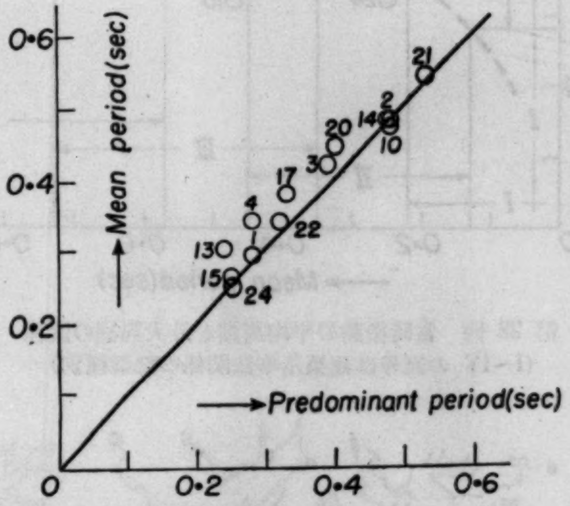

第 27 図　常時微動の卓越周期と平均周期の関係

(ii)　日中と夜間の常時微動の周期の関係

日中と夜間の測定のある場所は測定点 1, 3, 6, 9 であるが，第II表で見られる通り，測定点3を除いては，昼夜の平均周期の値は非常に近い．(測定点3の夜の頻度曲線が異形な事は既に述べた)．昼夜の最大周期は各測定点共に大差はない．

(iii)　常時微動の平均周期と最大周期の関係

常時微動の平均周期と最大周期の関係を第28図に示す．第28図で平均周期と最大周期の関係が特に飛び離れている測定点には 7, 8, 12 及び 5 の群と，2, 10 の群とがある．測定点 7（日枝小学校)，8(県庁)，12（横浜市警察署)，5（吉田中学校）の頻度曲線は特に平坦であり，軟弱な冲積層が特に厚いためと考えられる．測定点 2（野毛山遊園地)，10（フェリス女学院）の頻度曲線は非常に単純であり，その卓越周期は比較的に長い．横浜の台地には，かなり均一で厚い表面層（25 m 位）の場所があるという事で1つの解釈はできる．

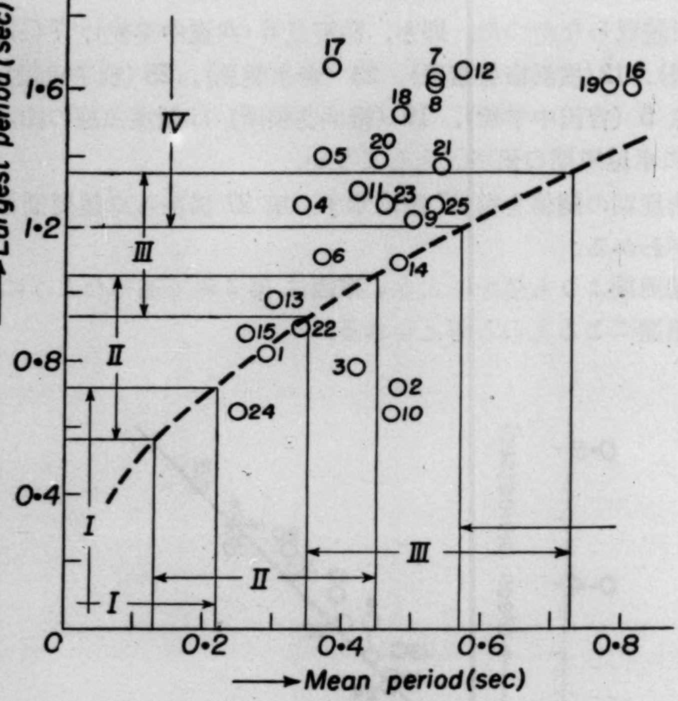

第 28 図　常時微動の平均周期と最大周期の関係
(I～IV の記号は建築基準法関係の地盤種別)

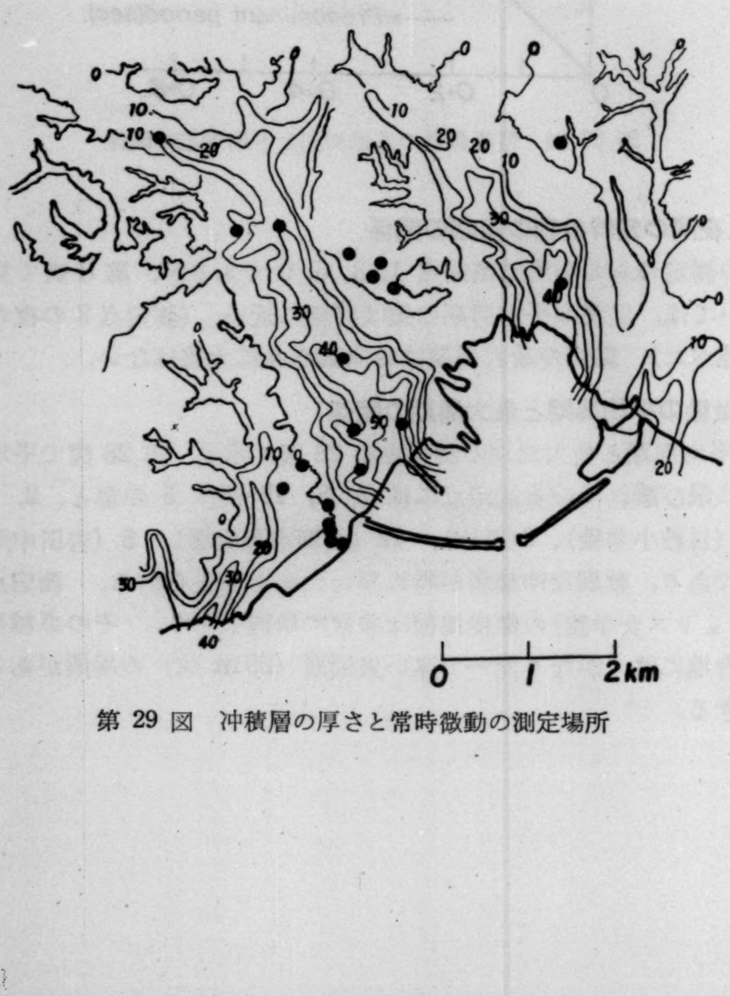

第 29 図　冲積層の厚さと常時微動の測定場所

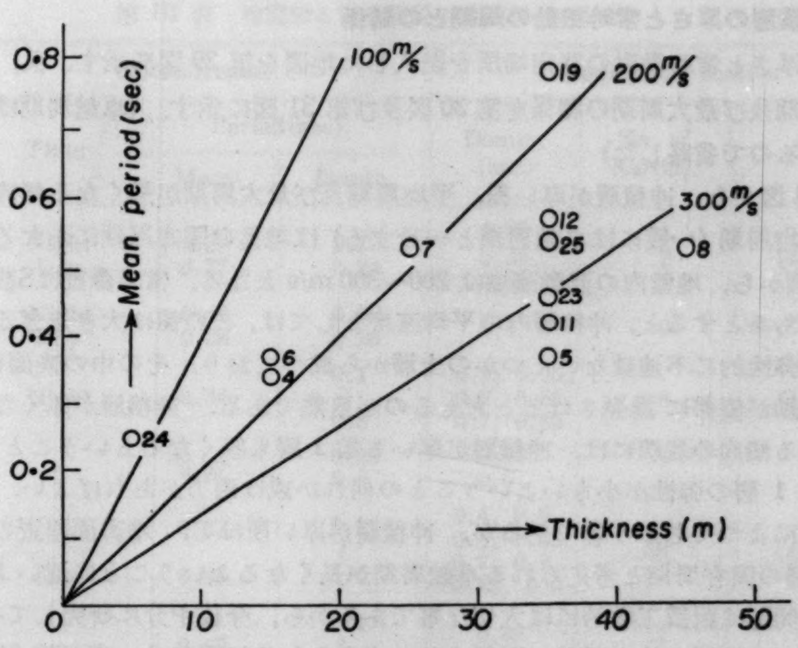

第 30 図 沖積層の厚さと常時微動の平均周期との関係

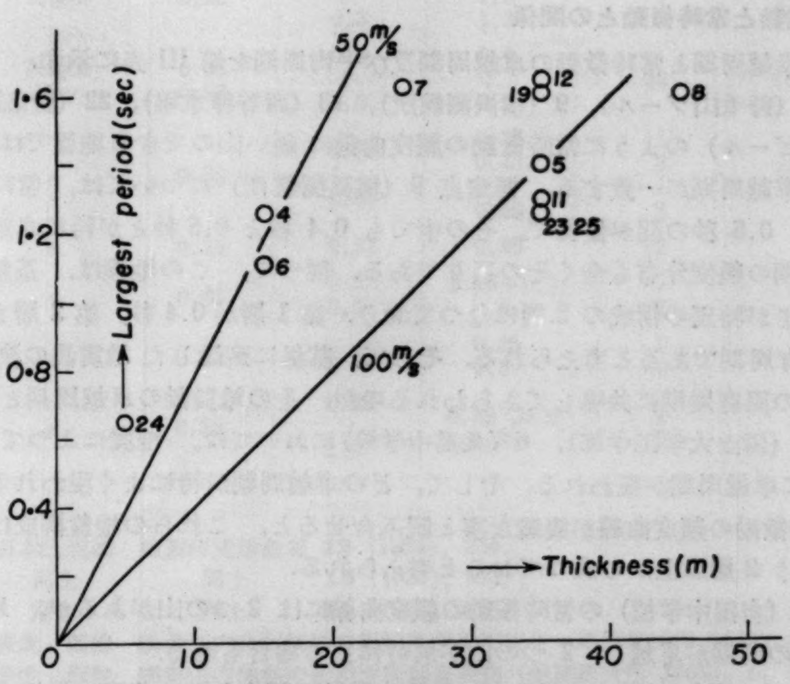

第 31 図 沖積層の厚さと常時微動の最大周期との関係

(iv)　冲積層の厚さと常時微動の周期との関係

冲積層の厚さと常時微動の測定場所を記入した地図を第 29 図に示す．又，冲積層の厚さと平均周期及び最大周期の関係を第 30 図及び第 31 図に示す．(卓越周期はきめにくい測定点もあるので省略した)

第 30，31 図から，冲積層が厚い程，平均周期及び最大周期が長くなる傾向にある事がわかる．平均周期 (一般には卓越周期と一致する) は地盤の固有周期にあたると仮定すると，第 30 図から，地盤内の波動速度は 200～300 m/s となる．常時微動はS波に属するものが優勢であるとすると，冲積層内の平均速度としては，この値は大き過ぎる．従つて，冲積層内が弾性的に不連続ないくつかの土層から成つており，その中の表面に近い第 1 層の固有震動が優勢に誘発されると考えるのが自然である．冲積層が厚くなると平均周期が長くなる傾向の説明には，冲積層が厚いと第 1 層も厚くなるということと，冲積層が厚いと第 1 層の弾性が小さいということの何れか或は両方があればよい．この両者の関係は場所によつてちがう筈であるが，冲積層が厚い所ほど，地表面附近の弾性が小さく，第 1 層の固有周期と考えられる卓越周期が長くなるということに近いように考えられる．この問題は耐震工学的には大切な事であるから，今後十分に研究してゆきたい．

最大周期は冲積層全体の震動に関係すると考えられる場所が多い事が第 31 図からわかる．

(v)　地震動と常時微動との関係

地震動の卓越周期と常時微動の卓越周期及び平均周期を第 III 表に示す．

測定点 1 (野毛山プール)，9 (横浜測候所)，13 (西谷浄水場)，22 (慶応附属高校)，24 (キリンビール) のように常時微動の頻度曲線に鋭い山のできる地盤では，常時微動と地震動の卓越周期が一致する．測定点 9 (横浜測候所) については，常時微動の頻度は 0.4 秒と 0.5 秒の間が優勢で，その中でも 0.4 秒と 0.5 秒とが特に卓越する．地震動の卓越周期の頻度分布も全くその通りである．従つて，この地盤は，基盤の上が弾性比，層の厚さが特別の構成の 2 層になつており，第 1 層が 0.4 秒，第 2 層まで含めると 0.5 秒の固有周期であると考えられる．そして，基盤に到達した地震波の波形によつて，その何れかの固有周期に共鳴してあらわれるのが，その地震動の卓越周期と考えられる．

測定点 4 (国立大学工学部)，6 (共進中学校) においては，地震によつて 0.3 秒から 1.0 秒の間に卓越周期が現われる．そして，どの卓越周期が特によく現われるという事はない．常時微動の頻度曲線が複雑な事と睨み合せると，これらの地盤構成は比較的に弾性比のちがう 2 層以上から成つておると考えられる．

測定点 5 (吉田中学校) の常時微動の頻度曲線には 2 つの山があるが，地震動では，その何れかの周期が卓越し，2 つの山が同時に出る場合もある．

測定点 7 (日枝小学校)，8 (県庁) の常時微動の頻度曲線は非常に平坦であり，卓越周期が 1 秒に近い長周期となる地震が多い．厚い軟弱な冲積層のためと考えられる．

測定点 23 (森永製菓) では，0.3 秒附近で常時微動の頻度も大きく，地震動も卓越する

第 III 表　地震動と常時微動の周期特性の比較

No.	Micro-tremor			Earthquake motion		
	Time	Period (sec)		Domin. (sec)	No. of Earthq.	Bibli.
		Mean	Domin.			
1	Night Day	0.29 0.27	0.27 0.28	0.25 0.35 0.55	1 2 2	(4), (5)
3	Night Day	0.42 0.28	0.39 0.26	0.3	9	(1), (2), (3)
4	Night	0.34	0.1 ≀ 0.8	0.3, 0.35, 0.5, 0.65, 0.7, 0.85	6	(4), (5)
5	〃	0.37	0.25 0.6	0.25 0.5	1 2	(4)
6	〃 Day	0.37 0.39	0.2 ≀ 1.0	0.4, 0.5, 0.6, 0.65, 0.7, 0.8, 0.85, 0.9	33	(4), (5)
7	〃	0.53	0.1 ≀ 0.5	0.45 0.85	1 3	(5)
8	Night	0.53	0.1 ≀ 0.3	0.8 1.0 1.2	3 1 1	(4), (5)
9	Night Day	0.46 0.52	0.4 ≀ 0.5	0.4 ≀ 0.5	46	(4), (5)
13	〃	0.30	0.25 0.55	0.35 0.45 0.5 0.55	1 2 1 2	(4), (5)
22	〃	0.34	0.32	0.35	12	(6)
23	〃	0.46	0.3 0.6	0.25～0.3 0.6	5 2	(6)
24	〃	0.25	0.25	0.25 0.3	1 4	(6)
25	〃	0.53	0.35 ≀ 1.0	0.35 ,0.9 0.35	4 1	(6)

備　考

文献　(1) 石本巳四雄　地震研究所彙報 **12** (1934), 234.

(2) 同上　同上 **13** (1935), 592.

(3) 同上　同上 **15** (1937), 536.

(4) 表俊一郎他　横浜市内軟弱地盤の振動性能調査報告（地震研究所 1954), 1.

(5) 表俊一郎他　横浜市内地盤の振動性能調査報告（地震研究所 1955), 1.

(6) 表俊一郎他　京浜工業地帯の地盤基本調査結果概報（地震研究所 1956), 1.

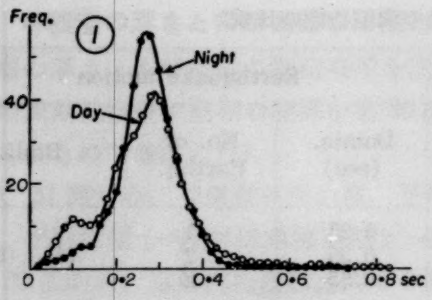

第 2 図 野毛山プール

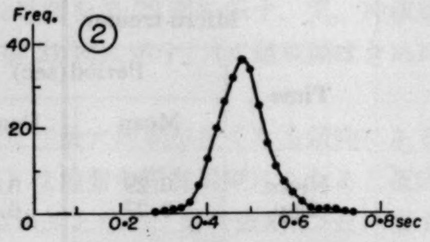

第 3 図 野毛山遊園地

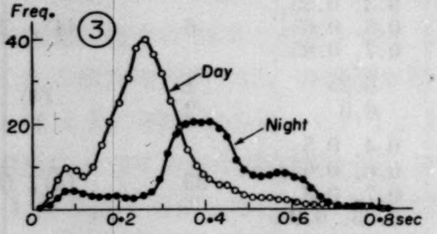

第 4 図 震災記念館

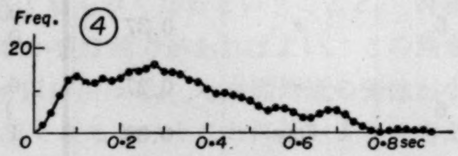

第 5 図 横浜国立大学

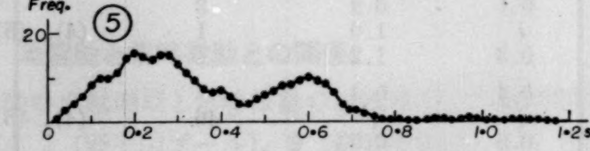

第 6 図 吉田中学校

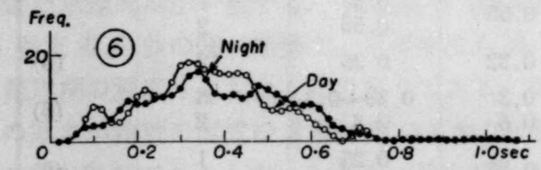

第 7 図 共進中学校

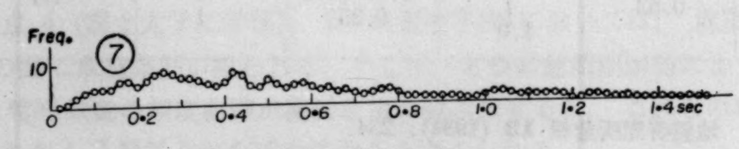

第 8 図 日枝小学校

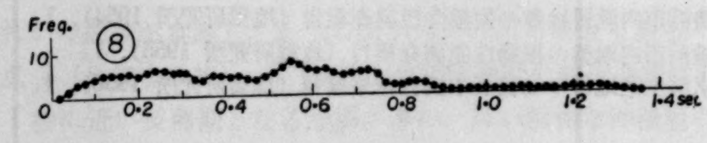

第 9 図 神奈川県庁

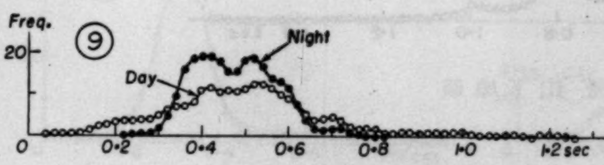

第 10 図　横浜測候所

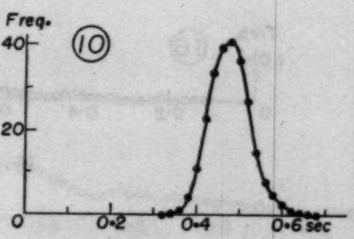

第 11 図　フエリス女学院

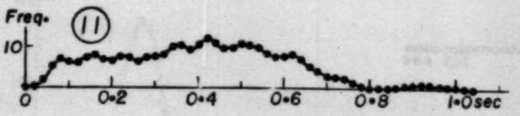

第 12 図　中 消 防 署

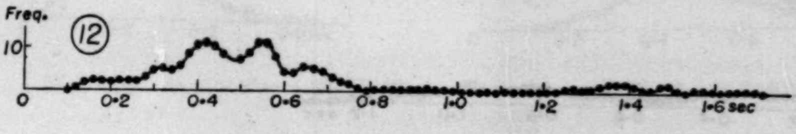

第 13 図　横浜市警察署

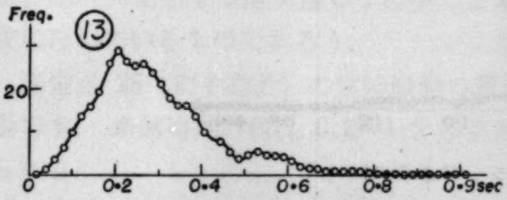

第 14 図　西谷浄水所

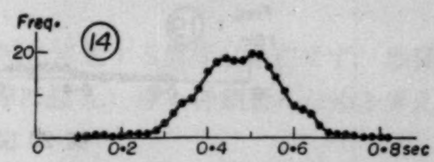

第 15 図　宮 ケ 谷 町

第 16 図　東　福　寺

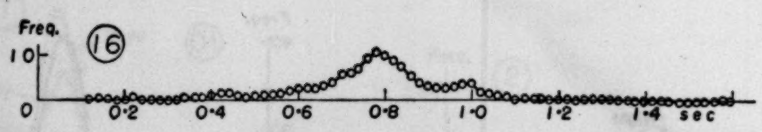

第 17 図 山下埠頭

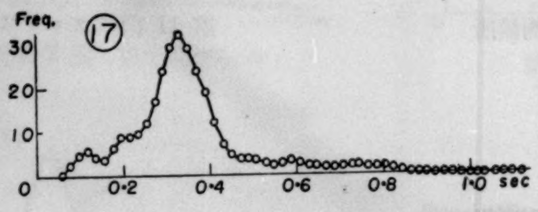

第 18 図 新山下アパート

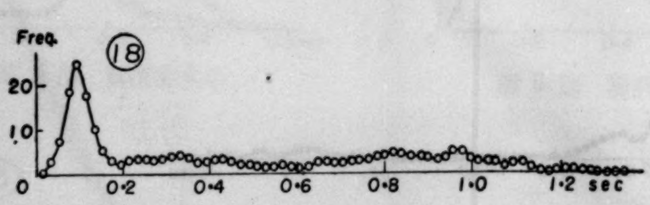

第 19 図 信号所崖下

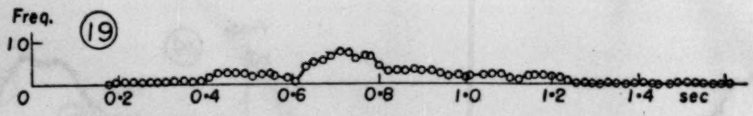

第 20 図 ニューグランドホテル

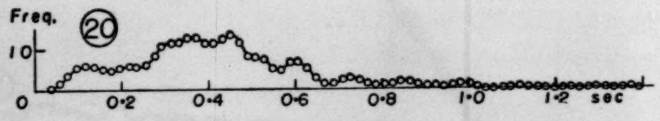

第 21 図 信 号 所

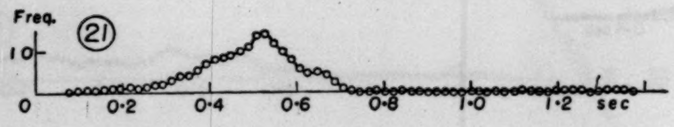

第 22 図 山手病院

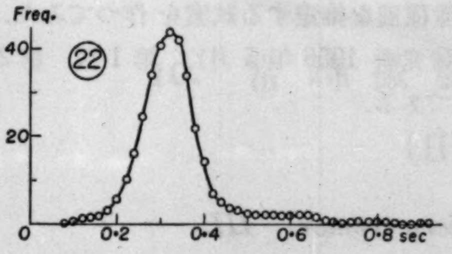

第 23 図　慶応義塾附属高校(日吉)

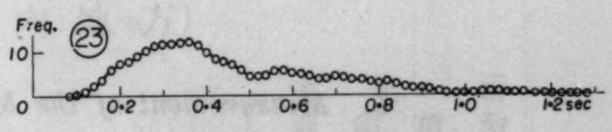

第 24 図　森永製菓川崎工場

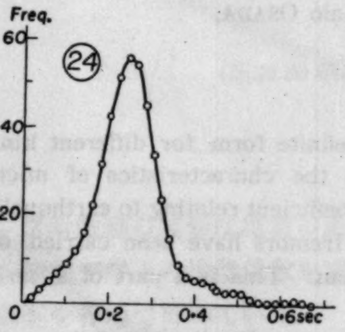

第 25 図　キリンビール横浜工場

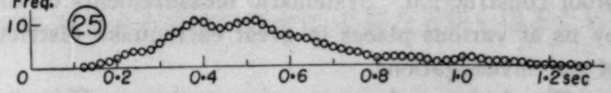

第 26 図　別子建設横浜出張所

ものが多い．常時微動の頻度は 0.6 秒附近でも僅かに大きいが， 0.3 秒附近が特に卓越しないような地震動は 0.2～1.0 秒にわたつて略一様な頻度である．この地盤は，0.3秒位の固有周期をもつ第 1 層の下に少くとももう1層あり，第 1 層の固有震動が起り易い構成になつているものであろう．

測定点 25 (別子建設) の常時微動の頻度曲線には特に卓越する周期が存在せず， 地震動でも， 卓越周期の値は 0.2～1.0 秒にわたつて同等に起る． 厚い冲積層のためと考えられる．

4. む す び

横浜市内の常時微動の測定で，新たにわかつた事を次に列記する．

(I)　横浜の台地は，かなり厚い(東京よりも)表面層から成る．

(II)　卓越周期は冲積層の中の第1層の固有周期にあたるものが多いと考えられる．

(III)　最大周期は冲積層全体の震動に関係すると考えられる場所が多い．

(IV)　地盤が厚い軟弱層の常時微動の頻度曲線は平坦であり， 地震動は短周期から長周期にわたつて同等の頻度を示す場所と，地震によつて卓越周期がちがう場所とがある．

終りに臨み， 多大の御援助を頂いた横浜市当局に深く感謝の意を表する． また， 懇ろな御援助と御議論を賜つた地震研究所地盤研究会の方々に厚く御礼を申し述べる．

附 記

常時微動が地盤の震動性状に 密接な関係がありそうなことに眼をつけ 常時微動の平均

周期と最大周期とを使つて，建築基準法関係の地盤種別を推定する試案を作つてみた.（筆者 常時微動による地盤種別判定法試案 地震研究所 1956年5月）. 第1図，第28図の中の I~IV の記号は，その試案によつたものである.

9. *Measurement of the Micro-tremor. III.*

(*Yokohama City.*)

By Kiyoshi KANAI, Teiji TANAKA and Kaio OSADA,

Earthquake Research Institute.

The distribution of periods of micro-tremors shows a definite form for different kinds of subsoils. The properties of the ground as inferred from the characteristics of micro-tremor are utilized for the determination of the foundation coefficient relating to earthquake-proof construction. Systematic measurements of the micro-tremors have been carried out by us at various places in great earthquake districts in Japan. This is a part of a series of our investigations.

Fig. 1 shows the measurement places. Figs. 2-26; frequency distribution of the period of micro-tremors. Fig. 27; the relation between the predominant period and the mean period of micro-tremors. Fig. 28; the relation of the mean period to the largest period. Fig. 29; contour of the thickness of the alluvium. Fig. 30; the relation of the mean period to the thickness of alluvium. Fig. 31; the relation of the largest period to the thickness of alluvium.

From systematic measurements, we found many micro-tremor of characteristics, which we shall now summarize as follows.

(1) The harder the rigidity of the subsoil is, the sharper the shape of the freqnency distribution of the period of micro-tremors and the shorter the predominant period of the distribution curve of period will be. On especially soft ground the distribution curve of period is flat ranging from a period smaller than 0.2 sec to a period larger than 1.0 sec.

(2) The predominant, mean and largest periods of micro-tremors differ slightly according to time and depend greatly on the vibrational characteristics of the subsoil. But, the largest amplitudes of micro-tremor in the daytime is much larger than that at midnight, that is to say, the ratio is 2~10 times, because the amplitudes of micro-tremor depend greatly on the activities of the artificial vibration source surrounding the measuring place.

(3) The wave form of micro-tremor can be decided not only from the thickness of alluvium but also from the physical condition of each stratum, that is to say, vibrational impedance ratio of neighbouring layer and the thickness of each layer.

(4) The predominant period of earthquake motion has a close relation with the distribution curve of period of micro-tremor. While when the distribution curve of period of micro-tremor has a single peak, the peak period coincides clearly with the predominant period of earthquake motion. On the other hand, in a distribution curve of period of micro-tremor has more than two peaks, the predominant period of earthquake motion coincides with either of them. (See Table III.)

10. 常時微動の測定結果 第4報
(庄内地方)

地震研究所 { 金井 清 / 那須信治 / 田中貞二 / 長田甲斐男

(昭和30年10月25日発表——昭和31年12月31日受理)

1. まえがき

常時微動の波形は地盤の震動性状と密接な関係があることがわかつたので，その性質を耐震工学上の地盤係数を求める方面に利用する方法の研究に必要な資料を得るための調査を各地で行つている.

現在までにわかつた常時微動の性質のうちの主なものを次に列記する.

(1) 地盤が堅い程頻度曲線は鋭く卓越周期は短い. 非常に厚い軟弱地盤の頻度曲線は広い周期の範囲にわたつて平で卓越周期は存在しない.

(2) 頻度—周期関係は地盤特性に関係が深いが，振巾はむしろ環境条件に大きく支配される.

(3) 波形は冲積層の厚さだけではきまらない. 卓越周期としては第1層の固有周期が出る場合が多い.

(4) 最大周期は冲積層全体の震動に関係する.

(5) 頻度曲線の山が1つの場所では，その山は地震動の卓越周期に一致する. 2つ以上の山がある場所の地震動の卓越周期は，地震によつて，その何れかの山の周期となる. 頻度曲線が非常に平な場所における地震動は，いつも平な頻度曲線を示す場所と，地震によつて異る卓越周期が出る場所とがある.

2. 測定方法

本報告の測定は昭和30年8月に行つたものである. 測定方法は電磁式煤書微動計（換振器は固有周期1秒の動線輪型倒立振子）[1),2)]によつて5分間の測定を行い，その中の2分間について解析を行つた.

測定場所を第1，2図並びに第I表に示す. 記録の解釈に役立てる意味で，測定場所

---

1) 金井 清・田中貞二・長田甲斐男 地震研究所彙報 **32** (1954), 199.
2) 地震研究所地盤研究会 同上 **33** (1955), 492～495.

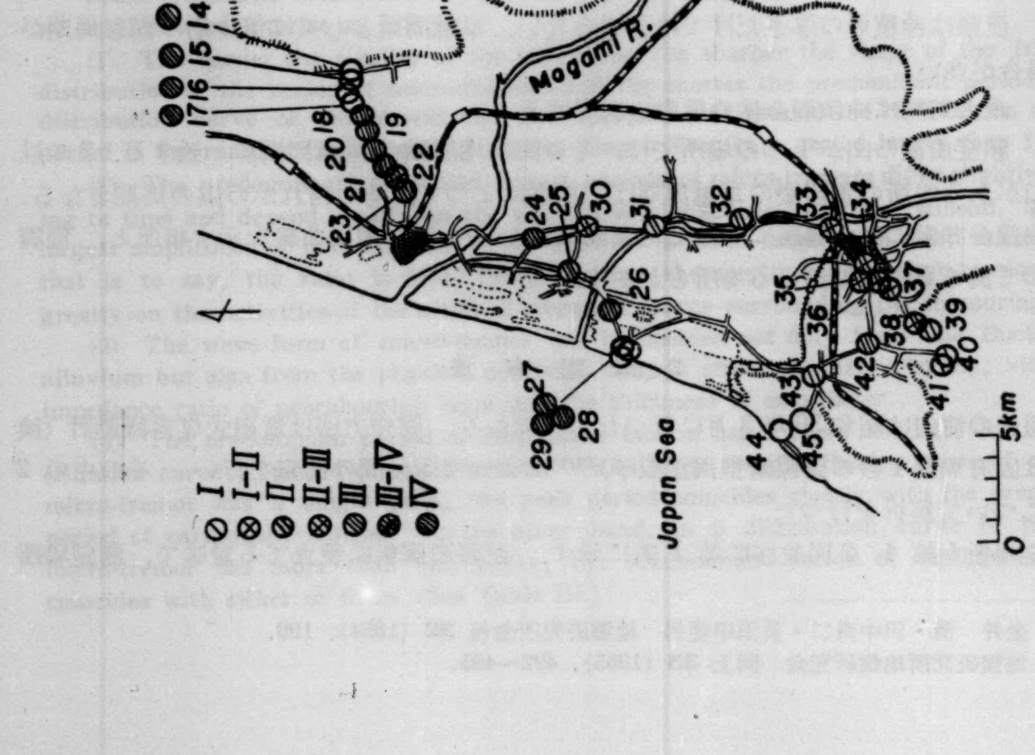

第1図 庄内地方全域の常時微動の測定場所
(I~IV の記号は建築基準法関係の地盤種別)

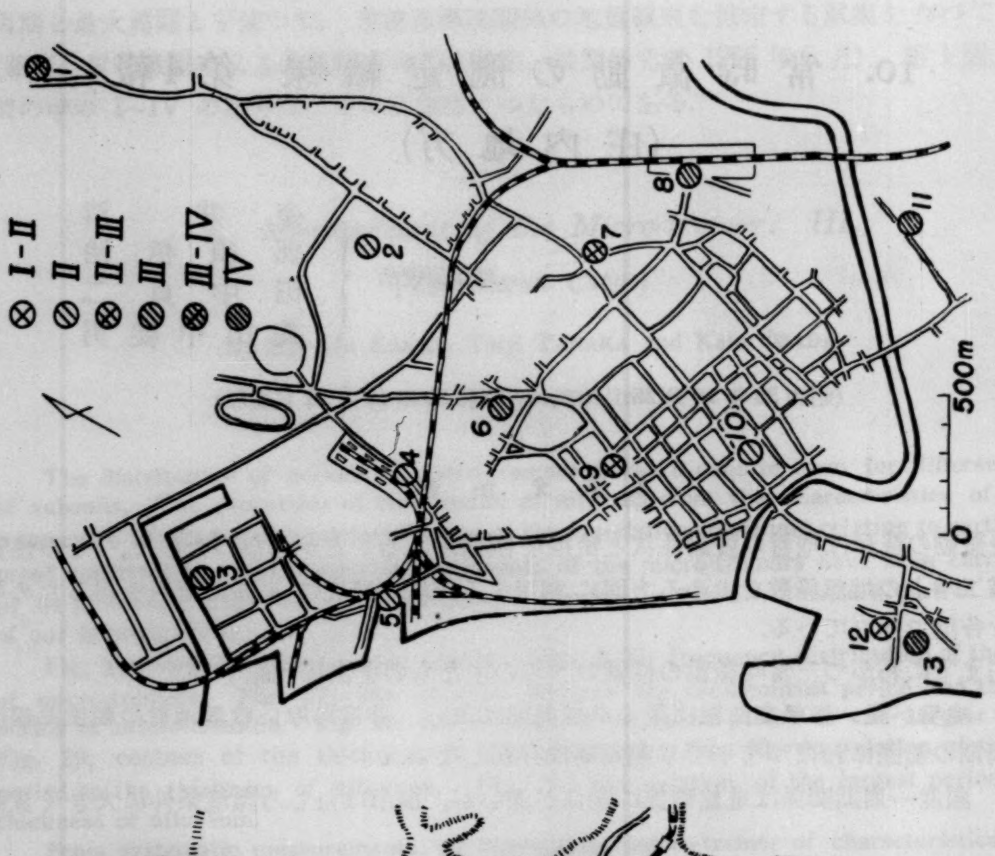

第2図 酒田市内の常時微動の測定場所
(I~IV の記号は建築基準法関係の地盤種別)

第 I 表　常時微動の測定場所

番　号	場　　　　所
1	酒田市豊里酒田公立病院（大通より約 60 m 入つた木造家屋コンクリート廊下）
2	酒田市北千松境酒田第1中学校（木造2階建玄関コンクリート床）
3	酒田市新町光ケ丘国立食糧倉庫（倉庫中央の廊下コンクリート床）
4	酒田市新町鉄興社（大通より約 30 m，鉄筋コンクリート建1階床）
5	酒田市新町建設省港湾事務所（事務所入口際のコンクリート床）
6	酒田市今町酒田西高等学校（正面玄関入口のコンクリート上）
7	酒田市浜畑町本間美術館（小路より 30 m，木造家屋の玄関タタキ）
8	酒田市酒田駅前（駅前コンクリート道路上）
9	酒田市伝馬町酒田ホテル（大通り脇の木造建物玄関コンクリート床）
10	酒田市本町酒田市役所（大通り脇の木造2階建正面玄関入口コンクリート床）
11	酒田市苗代堰酒田第2中学校（玄関前の広場の地表 5 cm 位掘る）
12	酒田市小中島酒田第3中学校（木造2階建玄関コンクリート床）
13	酒田市小中島酒田測候所（鉄筋コンクリート建物玄関）
14	酒田市東平田北境（小路道路上，交通機関の影響あり）
15	酒田市東平田北境（小路道路上）
16	酒田市東平田北境（小路より 3 m，周囲は田圃）
17	酒田市東平田境興野（小路道路上）
18	酒田市東平田中興野（小路より 6 m，周囲は田圃）
19	酒田市北平田布目（小路より 5 m，周囲は田圃）
20	酒田市北平田漆曾根（小路より 5 m，周囲は田圃）
21	酒田市北平田漆曾根（小路より 5 m，周囲は田圃）
22	酒田市北平田慈鈴観音（小路脇の石の上）

（つづく）

第 I 表 (つづき)

番号	場所
23	酒田市北平田大多新田 (小路道路上)
24	酒田市広田 (大通より 10 m, 小路道路上)
25	酒田市黒森酒田市役所袖浦支所 (大通より 20 m, 木造建物玄関タタキ)
26	酒田市広岡新田 (大通脇の松林の中, 土の上)
27	酒田市袖浦浜中 (部落内道路上, 土の上)
28	酒田市袖浦浜中, 浜中海岸砂丘上 (波打際より 300 m, 土手の上)
29	酒田市袖浦浜中, 浜中海岸砂丘上 (波打際より 200 m, 砂浜を約 30 cm 掘る)
30	酒田市広野新田 (大通り部落内道路上)
31	鶴岡市押切 (大通りより少し奥の表土上)
32	鶴岡市横山 (大通り端の道路上)
33	鶴岡市道形 (大通り端の道路上)
34	鶴岡市馬場町鶴岡市役所 (大通り脇の鉄筋コンクリート建物正面玄関)
35	鶴岡市新町禅竜寺 (小路道路上のふみ石の上)
36	鶴岡市八日町朝陽第 4 小学校 (正面玄関タタキ)
37	鶴岡市番田 (大通り脇道路上)
38	鶴岡市二ツ屋療養所 (正門の際)
39	鶴岡市二ツ屋 (自動車々庫のコンクリート床)
40	鶴岡市湯田川役場 (大通り脇木造建物入口コンクリート床)
41	鶴岡市湯田川琴平神社 (小路脇の石段上)
42	鶴岡市大泉白山林小学校 (木造建物玄関)
43	大山町大山町役場 (役場前の石の上)
44	鶴岡市加茂港 (大通り脇の岩盤に建つ石塔の上)
45	鶴岡市加茂町加茂トンネル (トンネル内道路端)

の環境条件はできるだけ詳細に記入してある．第 1 図は庄内地方の測定全域であり，第 2 図は酒田市内の測定場所である．

3. 測 定 結 果

(i) 頻 度 曲 線

2 分間の波形について，周期の頻度を求めたものを第 3～47 図に示す．

測定点 4 (鉄興社)，5 (港湾事務所)，6 (酒田西高校)，9 (酒田ホテル)，31 (鶴岡市押切)，43 (大山町役場) において比較的短周期に頻度の山が出るのは交通機関等の人工的震動源からの直接波の影響であろう．

測定点 12 (酒田第 3 中学校) における短周期の卓越震動は砂の薄い表土の固有震動が誘発されたものと考えられる．

頻度曲線の極大になる周期を卓越周期，2 分間の波数で時間を割つた値を平均周期，この計器で記録した最も長い周期を最大周期，2 分間の記録の中で大振巾が 2, 3 波続くものの中での最大値を最大振巾と名づけ，それらの値を第 II 表に示した．

頻度曲線が平坦な測定点 8, 11, 14, 15, 16, 17, 18, 19, 20, 21, 22, 24, 26, 27, 28, 29, 42, 44, 45 と頻度曲線に 2 つ以上の山のできる測定点 3, 4, 9, 10, 23, 25, 43 については，卓越周期の意味が曖昧なので読取らなかつた．

卓越周期と平均周期の関係を示すと第48図になる．第48図から卓越周期と平均周期が非常によく一致し，都会地のように平均周期が卓越周期よりも僅かに大きいという傾向は余り見られない．交通機関等の人工的震動源からの直接の影響を受ける度合が少いためであろう．

第 II 表　常時微動の周期と最大振巾

No.	Period (sec)			Largest Ampli. (μ)
	Domin.	Mean	Largest	
1	0.33	0.42	1.35	0.2
2	0.33	0.32	0.90	0.2
3	—	0.33	1.09	0.2
4	—	0.23	0.48	—
5	0.30	0.27	0.70	0.5
6	0.36	0.33	1.18	0.3
7	0.35	0.36	0.98	0.5
8	—	0.53	1.10	0.5
9	—	0.25	1.03	0.3
10	—	0.32	0.85	—
11	—	0.51	1.48	1.0
12	0.14	0.17	0.66	0.2
13	0.30	0.27	0.88	0.3
	0.33	0.42	1.68	0.05
14	—	0.40	1.58	—
15	—	0.56	1.68	—
16	—	0.44	1.48	—
17	—	0.57	1.98	—
18	—	0.57	1.65	—
19	—	0.67	1.87	—
20	—	0.60	1.62	—
21	—	0.70	1.79	—
22	—	0.59	1.27	0.2
23	—	0.48	1.67	—
24	—	0.42	1.48	0.3
25	—	0.38	1.23	0.2
26	—	0.55	1.68	—
27	—	0.51	1.65	—
28	—	0.52	1.59	—
29	—	0.53	1.72	0.2
30	0.39	0.40	1.04	0.1
31	0.25	0.26	0.75	0.3
32	0.25	0.27	0.74	0.2
33	0.35	0.33	0.96	0.3
34	0.39	0.38	0.71	0.3
35	0.38	0.35	0.67	0.5
36	0.37	0.35	0.87	0.3
37	0.40	0.41	0.81	0.5
38	0.30	0.31	1.01	0.1
39	0.32	0.34	0.74	0.2
40	0.12	0.12	0.37	0.03
41	0.10	0.098	0.28	0.01
42	—	0.46	1.21	—
43	—	0.23	0.61	0.5
44	—	0.55	1.57	—
45	—	0.55	1.71	—

(ii) 常時微動の周期と最大振幅の関係

常時微動の平均周期(卓越周期と考えてもよい)と最大振巾の関係を第 49 図に示す．第

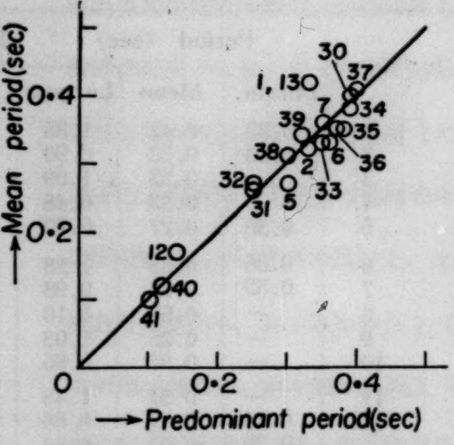

第 48 図　常時微動の卓越周期と平均周期の関係

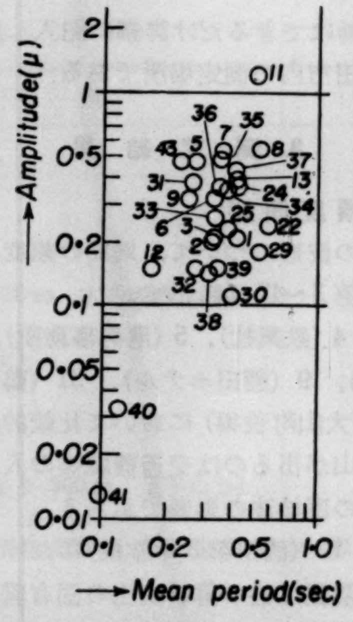

第 49 図　常時微動の平均周期と最大振巾の関係

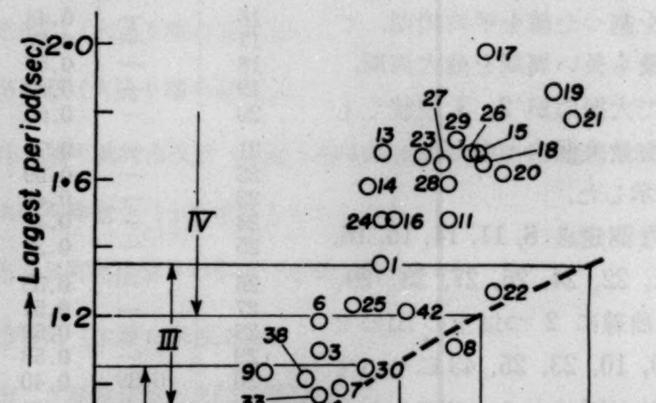

第 50 図　常時微動の平均周期と最大周期の関係
(I～IV の記号は建築基準法関係の地盤種別)

49図を見ると，平均周期と最大振巾との関係は，相当にばらつくが，平均周期が長いほど，振巾が大きいという傾向は出ている．詳しく見ると測定点22(北平田慈鮀観音)，29(浜中海岸)，30(広野新田)のような人里離れた場所の振巾は平均周期の割合にして小さいことがわかる．

(iii) 日中と夜間の常時微動の比較

測定点 13（酒田測候所）では日中と深夜(午前2時)の測定を行つた．第 15 図を見ると，昼夜共に 0.3 秒附近に頻度の山ができる．昼のものには 0.1 秒附近の頻度が多少大きく，0.3秒附近の山が夜のものよりも少し短かく，長周期が現われにくいのは，測定点のごく近くの工場の影響の多少によるものであろう．なお，振巾は昼が 0.3 ミクロンに対し夜は 0.05 ミクロンで，その比は 6 倍である．

(iv) 常時微動の平均周期と最大周期

常時微動の平均周期と最大周期の関係を第 50 図に示す．

長周期の波が多く現われ，頻度曲線が平坦な場所は，測定点 14～23（東平田村，北平田村の田圃地域），測定点 11（酒田第2中学校），測定点 13（酒田測候所），測定点 26～29（袖浦浜中附近），測定点 44（加茂港の岩盤上），測定点 45（加茂トンネル内）であり，第 50 図の平均周期と最大周期の関係でも飛び離れている．

(14)～(23)，(11)，(13) の場所で長周期の波の出るのは，地盤が特に厚い軟弱層から成つているということで了解される．(26)～(29) の場所は砂丘であるから，その解釈は今後に残される．

ここで先づ不思議に感じられたのは (44)，(45) の場所での常時微動の性質である．岩盤上における震動は短周期が卓越するという従来の常識を全く裏切る現象が出たわけである．この事は次のように考えれば，一応の答にはなる．即ち，岩盤上で短周期が卓越するのは岩盤の表面近くの風化の進んだ部分が震動的な1つの層を形成し，その層の固有震動が誘発されると考えるものである．常時微動は色々な原因で発生した色々の周期と振巾とをもつた波が四方八方から集つたものと考えれば，新鮮な岩盤では，もとから来た波がそのままの形で記録されるのでいわゆるホワイト，ノイズに近い性質を示すと考えるわけである．

4. む　す　び

庄内地方の常時微動の測定で，新たにわかつた性質を次に列記する．

(I) 環境条件に大きな差違のない場所の間では，平均周期(卓越周期と同等) が大きい所ほど，振巾が大きい傾向にある．

(II) 新鮮な岩盤上の常時微動の頻度曲線は広い範囲にわたつて平坦である．

終りに臨み，本調査に多大の御援助を受けた庄内地方地盤調査会に深い謝意を表する．また調査上に一方ならぬ御協力を戴いた酒田市建設課長菅原士郎氏その他の方々並びに

種々の御援助と御議論を賜つた地震研究所地盤研究会の方々に厚く御礼を申し述べる.

附 記

常時微動の平均周期と最大周期を使つて，建築基準法関係の地盤種別を推定する試案を作つてみた.（筆者 常時微動による地盤種別判定法試案 地震研究所 1956年5月）. 第1図，第2図及び第50図の中の I～IV の記号は，その試案によつたものである.

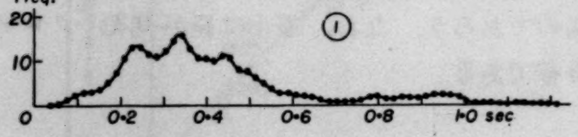

第 3 図 酒田市豊里酒田公立病院

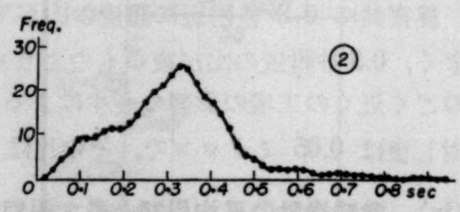

第 4 図 酒田市北千松境酒田第1中学校

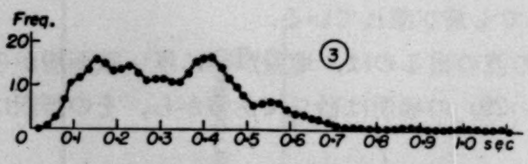

第 5 図 酒田市新町光ケ丘国立食糧倉庫

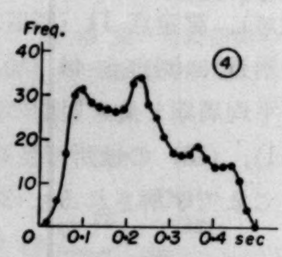

第 6 図 酒田市新町鉄興社

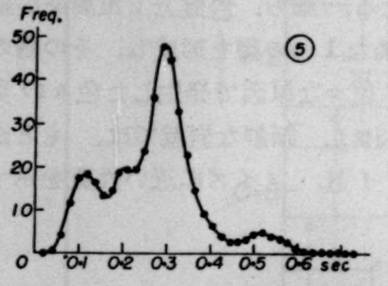

第 7 図 酒田市新町建設省港湾事務所

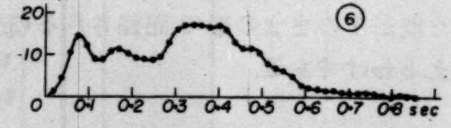

第 8 図 酒田市今町酒田西高等学校

第 9 図 酒田市浜畑町本間美術館

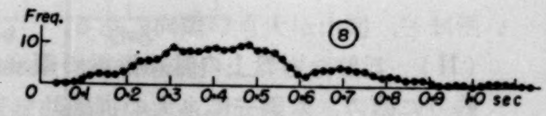

第 10 図 酒田市酒田駅前

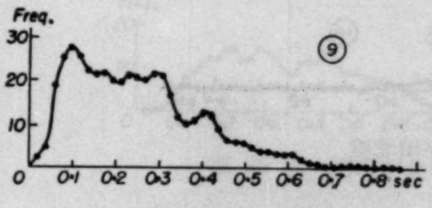

第 11 図　酒田市伝馬町酒田ホテル

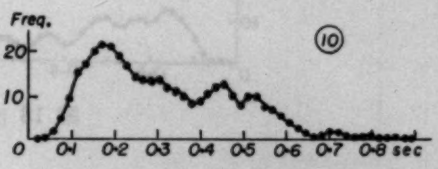

第 12 図　酒田市本町酒田市役所

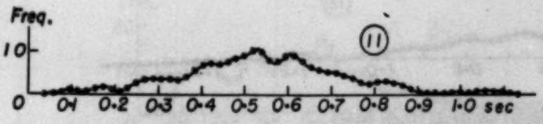

第 13 図　酒田市苗代堰酒田第 2 中学校

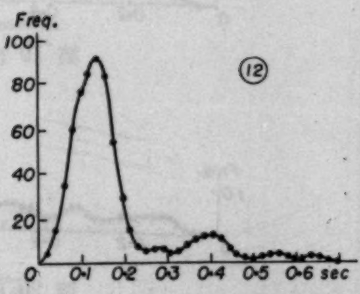

第 14 図　酒田市小中島酒田第 3 中学校

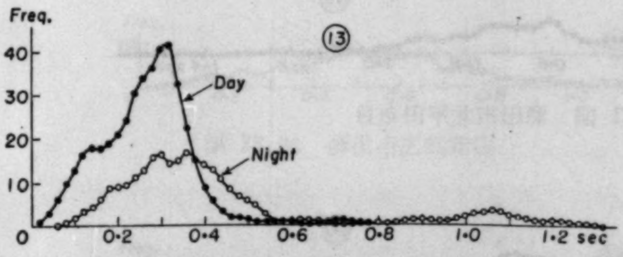

第 15 図　酒田市小中島酒田測候所

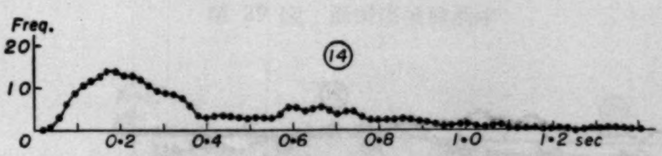

第 16 図　酒田市東平田北境

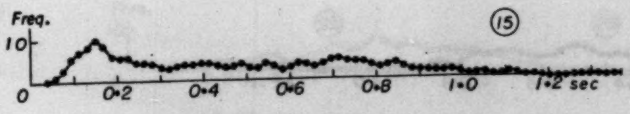

第 17 図　酒田市東平田北境

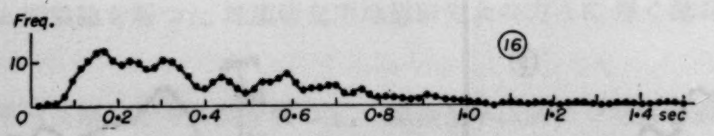

第 18 図　酒田市東平田北境

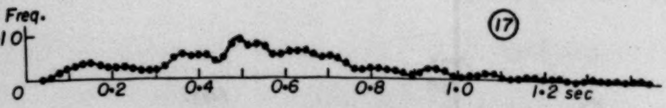

第 19 図　酒田市東平田境興野

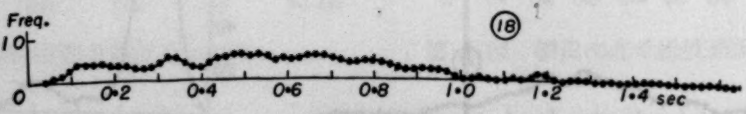

第 20 図　酒田市東平田中興野

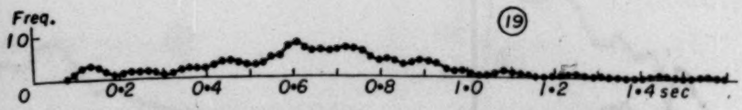

第 21 図　酒田市北平田布目

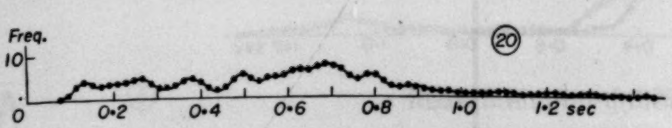

第 22 図　酒田市北平田漆曾根

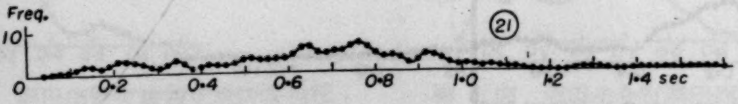

第 23 図　酒田市北平田漆曾根

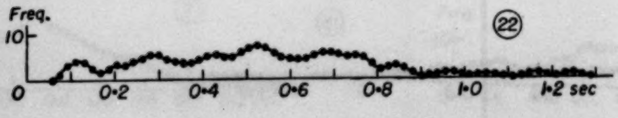

第 24 図　酒田市北平田慈鮎観音

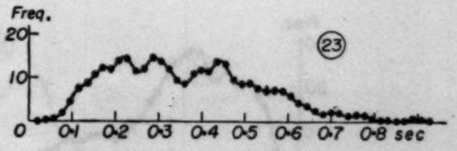

第 25 図　酒田市北平田大多新田

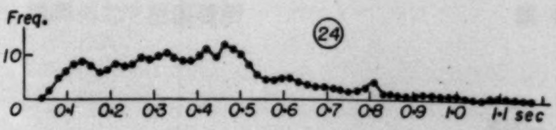

第 26 図　酒田市広田

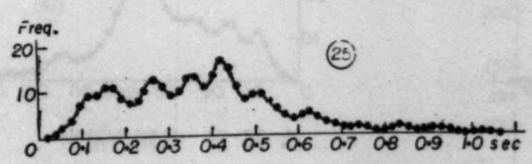

第 27 図　酒田市黒森酒田市役所袖浦支所

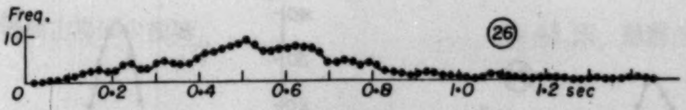

第 28 図　酒田市広岡新田

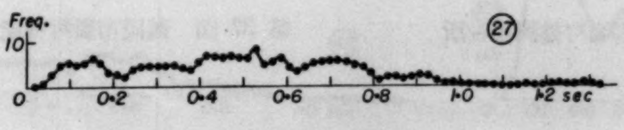

第 29 図　酒田市袖浦浜中

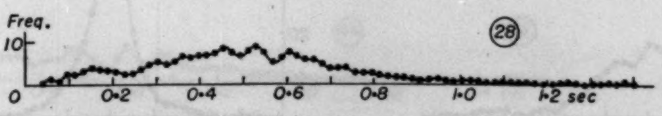

第 30 図　酒田市袖浦浜中

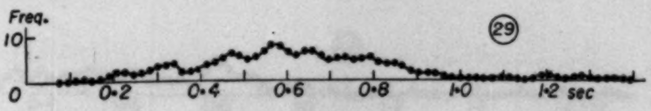

第 31 図　酒田市袖浦浜中

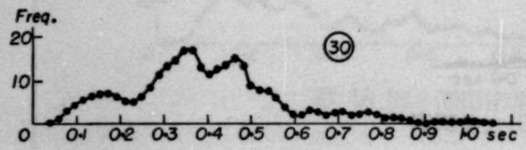

第 32 図　酒田市広野新田

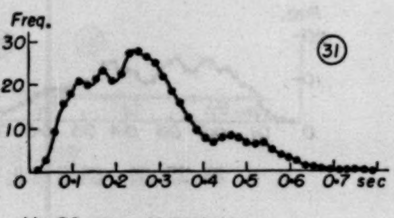

第 33 図　鶴岡市押切

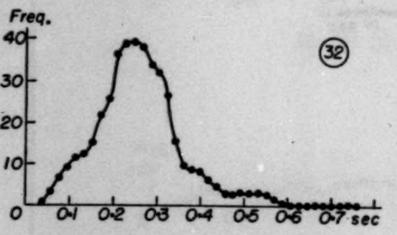

第 34 図　鶴岡市横山

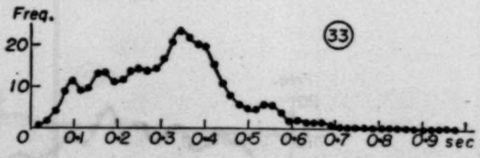

第 35 図　鶴岡市道形

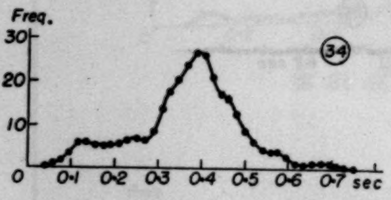

第 36 図　鶴岡市馬場町鶴岡市役所

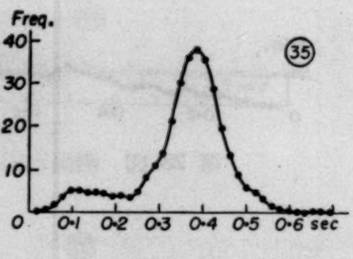

第 37 図　鶴岡市新町禅竜寺

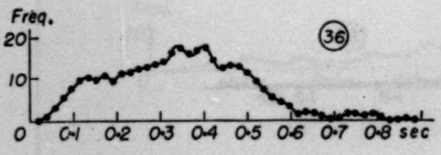

第 38 図　鶴岡市八日町朝陽第 4 小学校

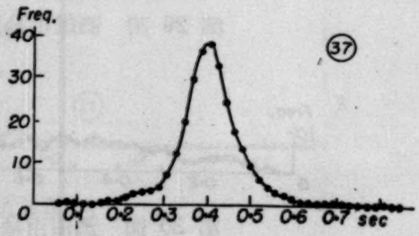

第 39 図　鶴岡市番田

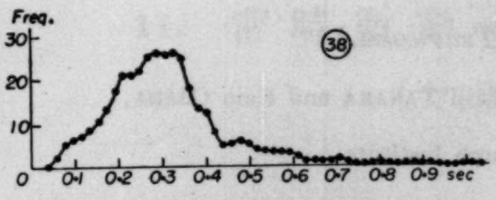

第 40 図　鶴岡市ニツ屋療養所

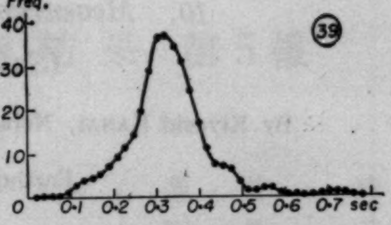

第 41 図　鶴岡ニツ屋

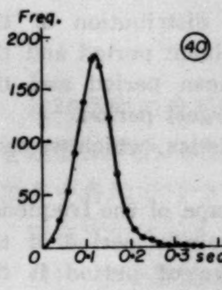

第 42 図　鶴岡市湯田川役場

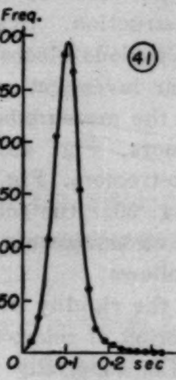

第 43 図　鶴岡市湯田川琴平神社

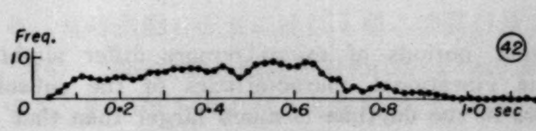

第 44 図　鶴岡市大泉白山林小学校

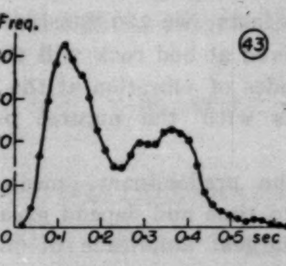

第 45 図　大山町大山町役場

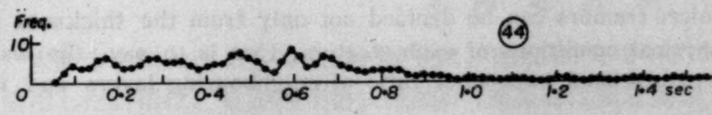

第 46 図　鶴岡市加茂港

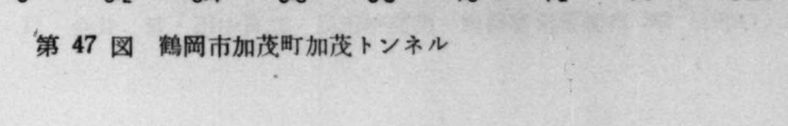

第 47 図　鶴岡市加茂町加茂トンネル

10. *Measurement of the Micro-tremor. IV.*
(Sakata and Tsuruoka.)

By Kiyoshi KANAI, Nobuji NASU, Teiji TANAKA and Kaio OSADA,

Earthquake Research Institute.

The distribution of periods of micro-tremors shows a definite form for different kinds of subsoils. The properties of the ground as inferred from the characteristic of micro-tremor are utilized for the determination of the foundation coefficient relating to earthquake-proof construction. Systematic measurements of the micro-tremors have been carried out by us at various places in the great earthquake districts in Japan. This is a part of a series of our investigations.

Figs. 1, 2 shows the measurement places. Figs. 3–47; frequency distribution of the period of micro-tremors, Fig. 48; the relation between the predominant period and the mean period of micro-tremors, Fig. 49; the relation between the mean period and the largest amplitude, Fig. 50; the relation of the mean period to the largest period.

From systematic measurements, we found micro-tremor characteristics, which we shall now summarize as follows:

(1) The harder the rigidity of the subsoil is, the sharper the shape of the frequency distribution of the period of micro-tremors and the shorter the predominant period of the distribution curve. On especially soft ground the distribution curve of period is flat ranging from a period smaller than 0.2 sec to a period larger than 1.0 sec.

(2) The frequency distribution curve of the period of micro-tremor on fresh rock is flat at periods ranging from less than 0.2 sec to larger than 1.0 sec. (See Figs. 46 and 47). From these facts, we can consider that the distribution curve of the period of micro-tremor arrived at bed rock will flat in form. Then, we can reach the conclusion that the amplitudes of vibration at the surface become relatively large at such periods as are synchronous with the natural period of the stratum from the feature of selective resonance.

(3) The predominant, mean and largest periods of micro-tremors differ slightly according to time and depend greatly on the vibrational characteristics of the subsoil. But, the largest amplitude of micro-tremors in the daytime is much larger than that at midnight, that is to say, the ratio is 2-10 times, because the amplitudes of micro-tremor depend greatly on the activity of the artificial vibration source surrounding the measuring place.

(4) The wave form of micro-tremors can be decided not only from the thickness of alluvium but also from the physical conditions of each stratum, that is to say, the wave form depends mainly on the vibrational impedance ratio of neighbouring layers and the thickness of each layer.

(5) The predominant period of earthquake motion has a close relation with the distribution curve of period of micro-tremor. In a place in which the distribution curve of period of micro-tremor has a single peak, the peak period coincides clearly with the predominant period of earthquake motion. On the other hand, in a place in which the distribution curve of mirco-tremor has more than two peaks, the predominant period of earthquake motion coincides with either of them.

11. 常時微動の測定結果 第5報
(大阪市内)

地震研究所 金井　清
河角　広
田中貞二
長田甲斐男

(昭和30年5月24日，昭和31年4月24日発表——昭和31年12月31日受理)

1. ま え が き

常時微動の波形は地盤の震動性状と密接な関係があることがわかつたので，その性質を耐震工学上の地盤係数を求める方面に利用する方法の研究に必要な資料を得るための調査を各地で行つている．

現在までにわかつた常時微動の性質を綜合すると次のようになる．

(1) 常時微動の頻度曲線は，堅い地盤では鋭くその卓越周期は短い．軟い地盤になる程卓越周期が長くなり曲線は平になる．

(2) 常時微動の周期(卓越，平均，最大)の時刻による差違は小さいが，振巾は時刻によつて2倍から10倍の差違がある．周期関係は地盤特性に関係が深いが，振巾は環境条件の影響の受け方が大きい．

(3) 常時微動の波形は冲積層の厚さだけではきまらなく，土層の構成に大いに関係する．常時微動の波形には第1層の性質が最も出やすい．

(4) 常時微動の頻度曲線の山が1つの場所では，その周期は地震動の卓越周期に一致する．2つ以上の山がある場所では，地震動の卓越周期は，地震によつて，そのうちのいづれかの山の周期となる．

2. 測 定 方 法

大阪市内における常時微動の測定は，昭和30年2月，同年9月の2回行つた．測定に使用した計器は，電磁型煤書式微動計(換振器は固有周期1.0秒の動線輪型倒立振子)である[1]．

測定場所を第1図に示し，測定場所の状況を第I表に示す．常時微動の測定にあたつては交通機関等の人工的震動源からの直接の影響を，できるだけ避けたいところであるが，都会地での測定ではどうしても多少の影響は受けることになる．第I表は波形の解析

1) 金井　清・田中貞二・長田甲斐男　地震研究所彙報 **32** (1954)，199.

にあたつて，人工的震動源からの直接の影響の大小を推定するのに役立つものである．

大阪市内には非常に数多くのボーリングの結果があるが，今回は，地盤の硬度[2)]と常時微動の性質との関係を一通り調べた．

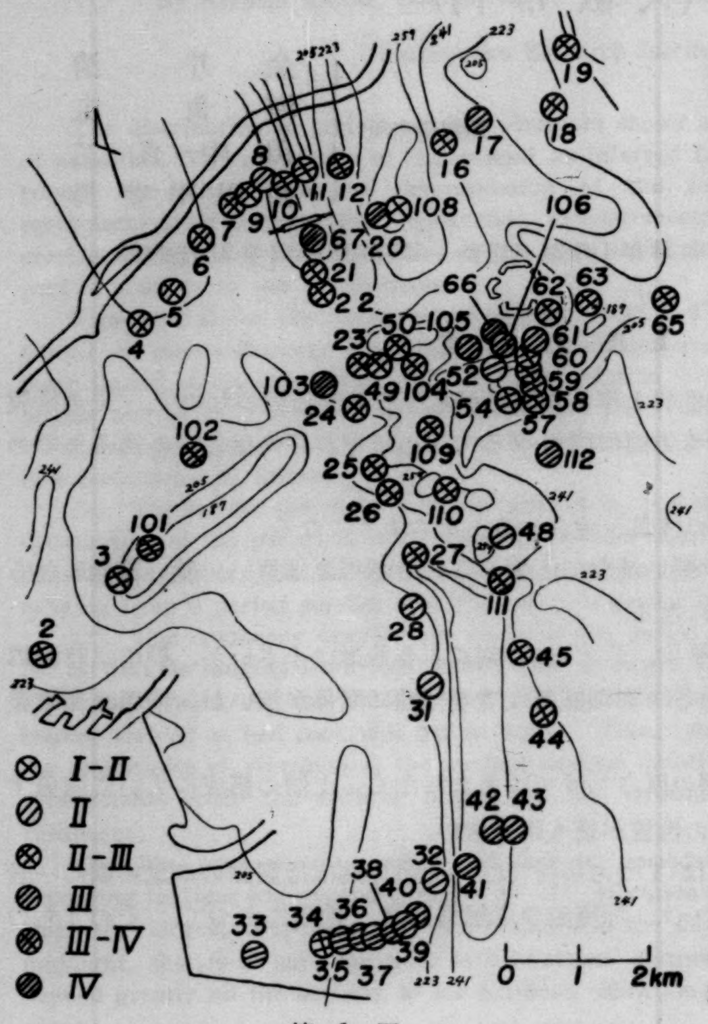

第 1 図

なお，大阪市内では地震観測が行われており，2 ケ所の比較観測の結果が既に公表されているので，同じ場所における常時微動の測定結果と睨み合せての検討を試みた．

3. 測定結果とその検討

a. 頻度曲線

2 分間の記録についての周期の頻度を第 2～68 図に示す．測定点 20, 67 以外は全部昼間の測定である．測定点 20(北区大阪市立大学) 及び測定点 67 (北区梅田町第 1 生命ビル) で，昼間と深夜 (午前 2 時頃) の 2 回測定を行つた結果は第 29 図と第68図に示してある．両図の中で黒丸が日中，白丸が夜間である．両図を見ると，日中と夜間の頻度曲線が非常によく似ている事がわかる．測定点 20, 67 における日中の頻度曲線で 0.1 秒附近が高いのは交通機関の影響と考えられる．測定点 31(西成区東皿池町)，105 (南大江小学校)，107 (東陽中学)，110 (日本橋小学校) の頻度曲線で 0.1 秒附近が高いのも皆同じ原因であろう．

頻度曲線の山になる周期を卓越周期，2 分間の波数で時間を割つた値を平均周期，読取つた周期の中での最も長い周期を最大周期と名づけ，また，5 分間の記録の中で同程度の振巾が 2, 3 波つづくものの中の最大値を最大振巾として採用し，各測定点におけるこれらの値と，地表から10 m, 20 m, 30 m までの地盤の硬度指数とを第 II 表に示した．

2) 河角 広 災害危険度の分布 (資源調査会 1952)，18.

第 I 表　測定場所の状況

測定点	場所
101	港区市立市岡中学校　(鉄筋コンクリート建物入口)
102	西区市立九条東小学校　(鉄筋コンクリート建物入口)
103	西区市立大学 (鉄筋コンクリート建物入口)
104	東区東商業高等学校　(鉄筋コンクリート建物入口)
105	東区南大江小学校　(鉄筋コンクリート建物入口)
106	東区日本赤十字社　(中庭表土上)
107	東成区東陽中学校　(鉄筋コンクリート建物入口)
108	北区扇町公園　(あずま屋内)
109	南区上町道仁小学校　(鉄筋コンクリート建物ドライエリヤ内)
110	浪速区市立日本橋小学校　(鉄筋コンクリート建物入口)
111	天王寺区大阪市立図書館　(鉄筋コンクリート建物入口)
112	天王寺区天王寺　(鉄筋コンクリート建物入口)
2	港区三条通り 1 の 10 市港湾局　(鉄筋コンクリート建物床上)
3	港区夕凪町 2 の 36　(電車通りより約 15 m 入つた小路道路上, 電車の影響なし)
4	福島区海老江下 2 の 40 (大通り脇の道路上, トラツクの影響あり)
5	福島区海老江上 2 の 61 (大通り脇の道路上, トラツクの影響あり)
6	大淀区浦江北 4 の 19 (木造建物コンクリート床上)
7	大淀区大仁本町 3 丁目　(小路脇コンクリート上)
8	大淀区中津南通り 3 の 100 (電車通り脇の空地石の上)
9	大淀区大仁本町 3 の 37(電車通りより約 50 m奥の自動車々庫内のコンクリート床上)
10	北区芝田町 36 (電車通りより約 30 m 奥の建物脇コンクリート上)
11	大淀区豊崎西通り 3 の 28 (電車通りより約 80 m 奥の小路上)
12	北区豊島町 20 (電車通りより約 30 m 奥の小路脇の民家入口)
16	都島区都島本通 1 の 1 (電車道路, 橋のたもと)
17	都島区都島工業高校内　(鉄筋コンクリート建物地下ドライエリヤ内)
18	城東区野江西之町大和銀行　(大通り脇の銀行入口)
19	旭区市立高殿小学校　(小路脇木造建物入口コンクリート上)
20	北区大阪市立大学久保研究室の実験室　(鉄筋コンクリート建物内床上)
21	北区堂島中通り勧銀支店　(鉄筋コンクリート 2 階建物入口)
22	西区土佐堀船町 1 丁目　(小路端の道路上)
23	西区阿波堀通り 1 丁目　(鉄筋コンクリート建物入口)
24	西区長堀北通り 1 丁目　(小路脇の鉄筋コンクリート建物入口)
25	浪速区国鉄湊町駅前　(大通り駅前鉄筋コンクリート建物入口)
26	浪速区府立体育館　(小路脇の建物入口コンクリート床上)
27	浪速区敷津町 3 丁目市立敷津小学校　(小路脇の校舎入口)

(つづく)

第I表 (つづき)

測定点	場所
28	西成区長橋通り1の4 (小路脇の鉄筋コンクリート2階建物倉庫入口)
31	西成区東皿池町 (電車通り脇の鉄筋コンクリート建物入口，交通機関の影響大)
32	住吉区粉浜中之町4丁目 (住吉公園内鉄筋コンクリート建物入口)
33	住吉区釜口町 (大通り端の道路上)
24	住吉区北島町 (大通り端の道路上)
35	住吉区南加賀屋町 (大通り端の道路上)
36	住吉区南加賀屋町 (大通り脇の競輪場入口石の上)
37	住吉区御崎町2丁目 (大通り脇の鉄筋コンクリート建物入口)
38	住吉区御崎町2丁目 (大通り端の道路上)
39	住吉区御崎町2丁目 (大通り端の道路上)
40	住吉区浜口西2丁目 (大通り端の道路上)
41	住吉区住吉町大海神社内 (小路端の道路上)
42	住吉区万代西5丁目 (小路端の道路上)
43	住吉区万代東5丁目 (小路端の道路上)
44	阿倍野区大阪大学南校内 (大通り脇建物入口)
45	阿倍野区阿倍野警察署内 (電車通り脇の鉄筋コンクリート建物入口)
48	天王寺区逢坂上之町 (大通り脇の鉄筋コンクリート2階建物入口)
49	東区南本町5丁目 (小路端の道路上)
50	東区本町2丁目呉羽紡ビル (電車通り脇の鉄筋コンクリート3階建物入口)
52	東区谷町6丁目 (小路脇の鉄筋コンクリート3階建物入口)
54	東区谷町8丁目 (小路脇の道路上)
57	天王寺区東高津北之町貯金局 (大通り脇の鉄筋コンクリート4階建物入口)
58	天王寺区清堀町10高津中学校 (小路脇の木造建物入口)
59	天王寺区清水谷東之町 (電車通りを約50m入つた鉄筋コンクリート建物内)
60	東区仁右衛門町大阪女子学院 (鉄筋コンクリート3階建物入口)
61	東区元伊勢町79 (小路脇の木造モルタル塗建物入口)
62	東区森之宮西之町 (小路脇の木造モルタル塗建物入口)
63	城東区森町南市バス車庫(電車通りを約20m入つた鉄筋コンクリート2階建車庫内)
64	東成区深江西2丁目宝来小学校 (鉄筋コンクリート建物入口)
65	東成区西今里町2の13東中本小学校 (鉄筋コンクリート建物入口)
66	東区法円坂町国立大阪病院内 (木造観測小屋内，周囲は至極静か)
67	北区梅田町第1生命ビル (大通り脇の鉄筋コンクリート建物地下1階床上)

第 II 表　各種地盤の周期並びに最大振巾の値

No.	Period (sec)			Ampl.	Hardness coeff.		
	Domin.	Mean	Larg.	(μ)	10 m	20 m	30 m
101	0.29	0.34	1.32	—	95~104	187~205	306
102	—	0.31	1.27	—	95~104	205~223	360
103	0.36	0.38	1.55	—	104	223~241	333
104	0.28	0.32	0.95	—	131~140	241~259	333~360
105	0.29	0.26	1.07	—	113~122	241	333~360
106	—	0.33	1.18	—	104	241	360
107	0.25	0.24	1.26	—	—	—	—
108	0.11	0.13	0.46	—	122~131	>277	414
109	0.35	0.36	0.85	—	122~131	259	360
110	0.25	0.26	1.00	—	131	259	387~414
111	—	0.33	1.24	—	104~113	241~259	387~414
112	0.45	0.48	0.90	—	104	241	360
2	—	0.38	0.90	—	95	241	333
3	0.35	0.39	0.94	0.5	104~113	205	333
4	0.35	0.38	0.83	1.5	113	205	360
5	0.35	0.38	0.88	1.5	104	223	360
6	0.35	0.39	0.90	0.5	104~113	223	360
7	0.40	0.42	0.90	0.5	113	241	360
8	0.33	0.34	0.92	1.5	113	241	333~360
9	0.36	0.38	0.86	1.0	113	241	360
10	0.37	0.42	0.88	0.5	104	223	306~333
11	0.33	0.37	1.03	1.0	104	205	306~333
12	0.39	0.41	1.29	0.5	131	241	387
16	0.27	0.34	0.97	1.0	113	241	387~414
17	0.43	0.47	1.19	0.5	104	241	333
18	0.30	0.37	0.92	0.5	95~104	223	—
19	0.32	0.34	1.02	0.5	95~104	205	—
20	—	0.32	0.98	0.3	131	>277	387~414
		0.35	1.17	—			
21	0.39	0.40	0.92	1.5	113	223~241	360~387
22	0.35	0.39	1.04	0.5	113	241	360
23	0.33	0.37	0.95	1.0	113~122	241	333~360
24	0.40	0.41	0.94	0.5	104	241	333
25	0.29	0.32	0.96	1.5	104~113	259~277	360
26	0.40	0.40	0.81	0.5	104	259	360
27	0.42	0.40	0.88	1.0	131	241~259	360
28	—	0.34	0.86	—	104~113	223	360
31	0.25	0.28	0.89	—	131	241	333
32	0.28	0.31	0.76	—	122~131	223	360
33	0.47	0.45	0.97	1.0	—	—	—
34	0.30	0.35	1.00	1.0	—	205	—
35	0.46	0.47	0.68	1.5	—	223	—
36	0.45	0.48	0.67	1.5	—	223	—
37	0.46	0.47	0.63	1.5	—	223	333
38	0.47	0.48	0.86	1.0	113	223	360
39	0.46	0.47	0.82	1.0	113	223	360
40	0.28	0.40	1.03	—	113	223	360
41	0.45	0.47	0.73	0.5	122	277	360
42	0.42	0.45	1.13	—	—	277	387
43	0.46	0.48	0.86	0.5	—	259	—
44	0.45	0.44	0.92	—	122	259	387

（つづく）

第 II 表 (つづき)

No.	Period (sec)			Ampl.	Hardness coeff.		
	Domin.	Mean	Larg.	(μ)	10 m	20 m	30 m
45	0.39	0.40	0.86	1.0	—	259	387
48	0.28	0.30	0.78	1.0	122	259	387
49	0.45	0.40	0.88	1.0	122～131	259～277	360
50	0.35	0.39	1.04	—	131	259	360
52	0.25	0.31	0.90	1.0	95	205～223	360
54	—	0.40	0.89	0.5	104	223	360
57	0.34	0.41	1.03	0.5	104	223	360
58	0.36	0.40	1.03	—	104	205	360
59	—	0.36	0.90	—	104	187	360
60	—	0.35	0.90	—	95	205～223	360
61	—	0.39	1.13	—	95	223～241	360
62	0.32	0.35	0.87	—	95	241	360
63	0.34	0.40	1.05	—	104	205	360
64	0.26	0.33	0.94	—	—	—	—
65	0.32	0.38	0.82	—	—	—	—
66	—	0.45	1.15	—	122	241	360
67	—	0.51 0.49	1.83 1.29	—	104	187	333

頻度曲線が非常に平坦なものと，頻度曲線に 2 つ以上の山のできるものについては，卓越周期の意味が曖昧になるので第 II 表に記入しなかつた．平坦な頻度曲線の測定点は 67, 101, 102, 103 であり，2 つ以上の山のある頻度曲線の測定点は 2, 59, 66 である．

平均周期と卓越周期の関係を示したのが第 69 図である．第 69 図から，両者の値が非常に近い事がわかる．平均周期の方が卓越周期よりも少しづつ大き目の点が多いのは，都会地のため，交通機関の直接の影響を受ける場所が多いためと解釈される．(工場機械交通機関等から直接伝わつて来る短周期の震動は，卓越周期の値に最も大きな影響を与える．)

平均周期と卓越周期とは近い値であり，卓越周期の方が人工的震動源の影響を受ける度合が大きく，又，頻度曲線によつては卓越周期が決めにくい場合がある事などから，地盤の震動特性を示す指数の 1 つとしては平均周期を使う事が便利である．

平均周期と最大周期の関係を示すと第70図になる．測定点 67 (第一生命ビル)，103 (市立大学) のように最大周期が特別に大きい地盤の頻度曲線は，第 68 図及び第 4 図で見られる通り非常に平坦である．このような震動特性を示す地盤は，何層かの土層から成る厚い冲積層と解釈される．測定点 35～39 (住吉区南加賀町，御崎町) 等のように平均周期 (卓越周期に近い) が比較的に大きいのに，最大周期がそれ程大きくない地盤の頻度曲線は第 42～46 図でわかるように非常に単純である．このような地盤の震動特性は，固い基盤の上に，弾性的に均一に近く，軟くて厚い層があるとして，1 つの解釈ができる．

平均周期と振巾との関係を示したのが第 71 図であるが，両者の間の関係はかなり浅い

事がわかる．振巾は，測定点の環境の影響を大きく受けるから，地盤本来の震動性状を調べる目的には不向である．

b. 常時微動の性質と地盤の硬度との関係

表面から 10 m, 20 m, 30 m までの硬度指数と常時微動の平均周期，最大周期の関係を第 72～77 図に示す．これらの図から，硬度指数が大きくなると平均周期も最大周期も短くなる傾向が見られ，特に，20 m までの硬度指数と最大周期の間に密接な関係のある事がわかる．

c. 常時微動と地震動との関係

常時微動の測定点 103（西区市立大学）と測定点 2（市港湾局）では自然地震の比較観測が行われたので，その解析結果と常時微動の測定結果を並べて第 III 表に示す．

第 III 表　常時微動と自然地震の比較

No.	Micro-tremor			Earthquake Motion		
	Time	Period (sec)		Dominant Period (sec)	No. of Earthq.	Bibli.
		Mean	Domin.			
103	Day	0.38	0.1～1.0	0.3	1	3)
				0.3, 0.6	1	
2	〃	0.38	0.2～0.8	0.3～0.8	4	3)
				0.8	1	
				0.3	1	

測定点 103 のように，常時微動の頻度曲線に凹凸のできる地盤では，地震動の卓越周期が 2, 3 種類あり，地震によつて，その中の 1 つ或は 2 つが卓越するという関係がある．冲積層の地盤では，この震動性状のものが多く見られる．

4. む　す　び

大阪市内の常時微動の測定で，はつきりした事柄を次に列挙する．

(I)　地盤の硬度指数と常時微動の周期特性との間には，或関係が見られる．

(II)　常時微動の頻度曲線に 2 つ以上の山のできる地盤における地震動は，その中の1つ或は 2 つの山に当る周期の波が卓越する[3),4)]．

(III)　比較的に長い卓越周期をもち，しかも頻度曲線の形が単純な地盤は，固い基盤の上に比較的に軟くて均一で，しかも厚い土層があると解釈される．

終りに臨み，本調査に当つて多大の御援助を戴いた大阪市建築部指導課長 稗田治氏，同課指導係長椚座正信氏その他の方々に深い謝意を申し述べる．又，本研究に当り，多大の御援助と有益な御議論を賜つた地震研究所地盤研究会の方々に厚く御礼申し述べる．

3) 高橋竜太郎他　大阪市内の地盤基本調査結果　第 1 報（地震研究所 1956），1.
4) 那須信治・萩原尊礼　地震研究所彙報 **14** (1936), 290.

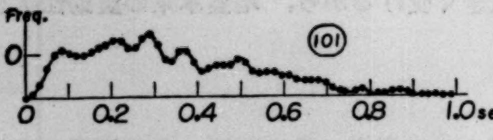

第 2 図 港区市立市岡中学校

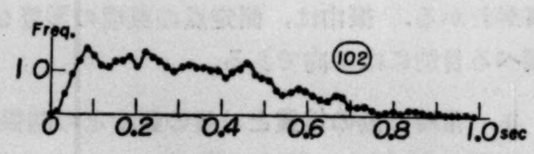

第 3 図 西区市立九条東小学校

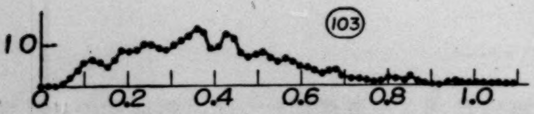

第 4 図 西区市立大学

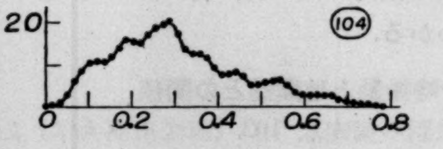

第 5 図 東区東商業高等学校

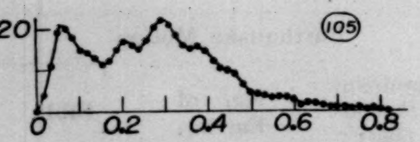

第 6 図 東区南大江小学校

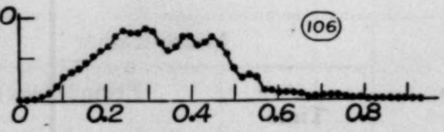

第 7 図 東区日本赤十字社

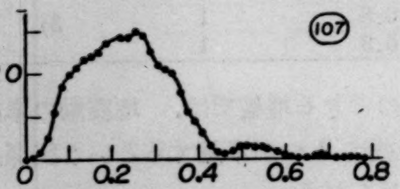

第 8 図 東成区東陽中学校

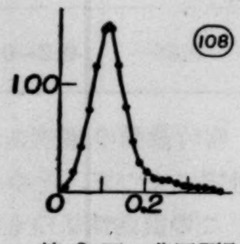

第 9 図 北区扇町公園

第 10 図 南区上町道仁小学校

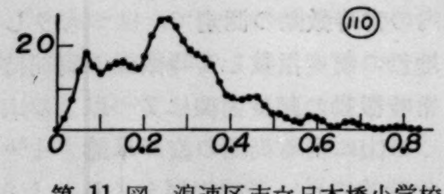

第 11 図 浪速区市立日本橋小学校

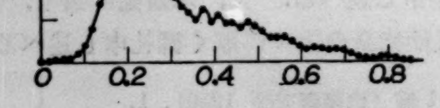

第 12 図 天王寺区大阪市立図書館

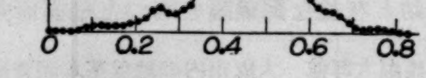

第 13 図 天王寺区天王寺

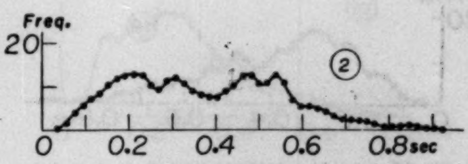

第 14 図　港区三条通り市港湾局

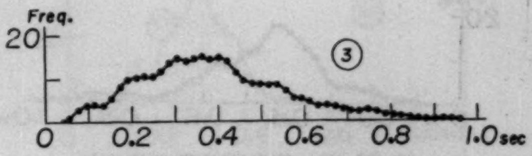

第 15 図　港区夕凪町 2 丁目

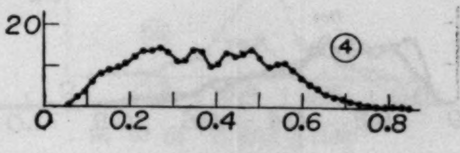

第 16 図　福島区海老江下 2 丁目

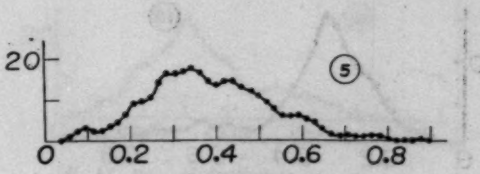

第 17 図　福島区海老江上 2 丁目

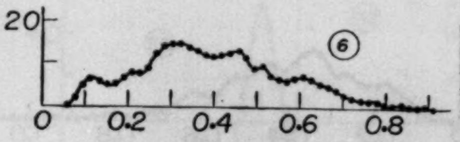

第 18 図　大淀区浦江北 4 丁目

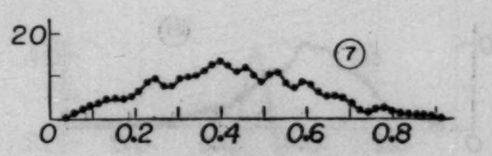

第 19 図　大淀区大仁本町 3 丁目

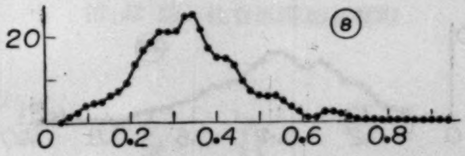

第 20 図　大淀区中津南通り 3 丁目

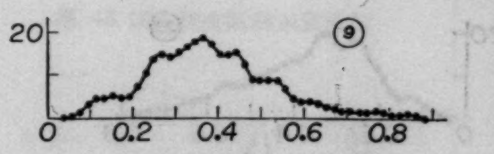

第 21 図　大淀区大仁本町 3 丁目

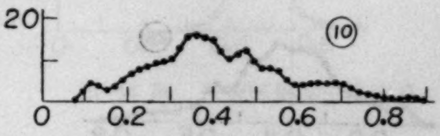

第 22 図　北区芝田町 36

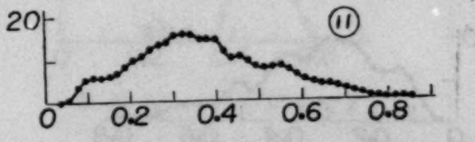

第 23 図　大淀区豊崎西通り 3 丁目

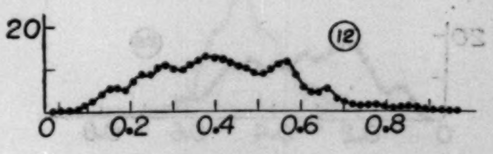

第 24 図　北区豊島町 20

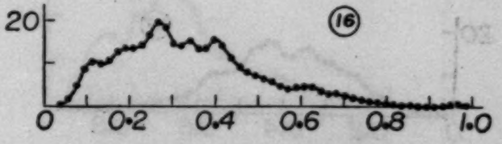

第 25 図　都島区都島本通り 1 丁目

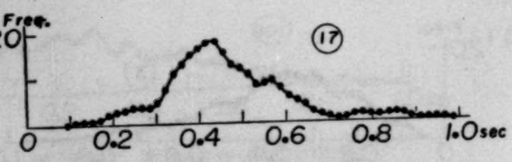

第 26 図　都島区都島工業高校

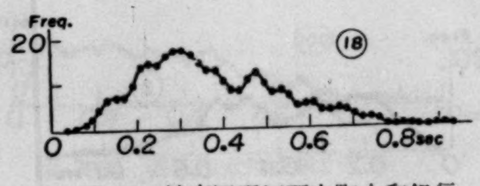

第 27 図　城東区野江西之町大和銀行

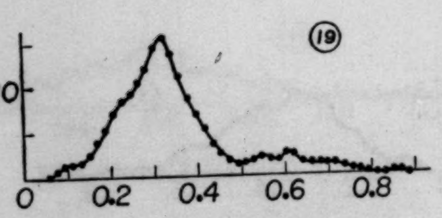

第 28 図　旭区市立高殿小学校

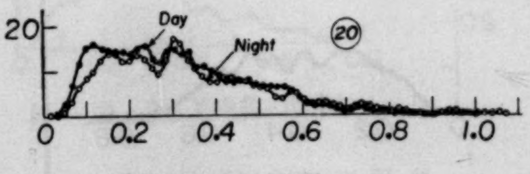

第 29 図　北区大阪市立大学

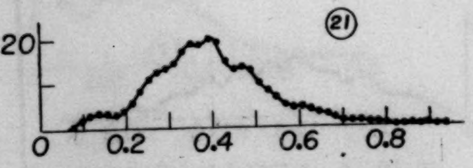

第 30 図　北区堂島中通り勧銀支店

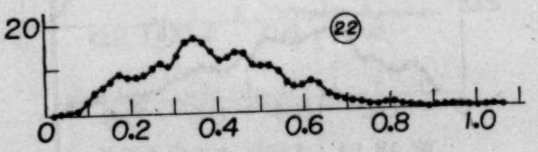

第 31 図　西区土佐堀船町 1 丁目

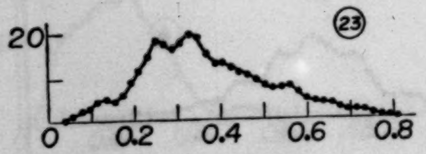

第 32 図　西区阿波堀通り 1 丁目

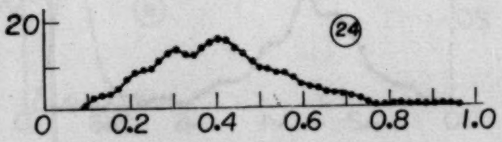

第 33 図　西区長堀北通り 1 丁目

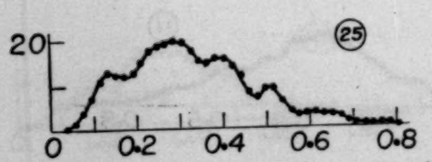

第 34 図　浪速区国鉄湊駅前

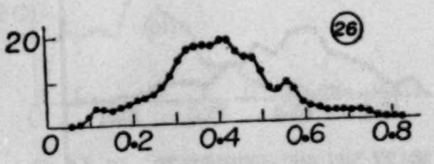

第 35 図　浪速区府立体育館

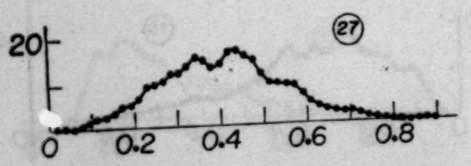

第 36 図　浪速区敷津町市立敷津小学校

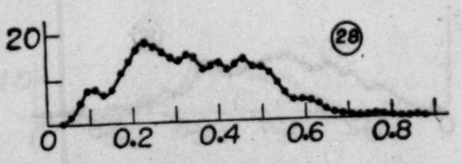

第 37 図　西成区長橋通り 1 丁目

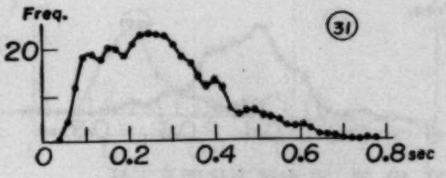

第 38 図　西成区東皿池町

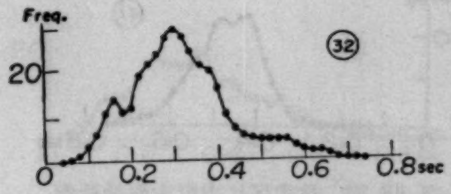

第 39 図　住吉区粉浜中之町 4 丁目

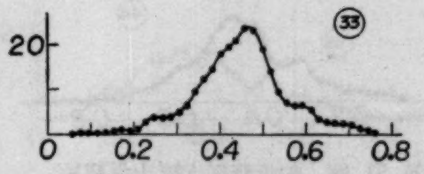

第 40 図　住吉区釜口町

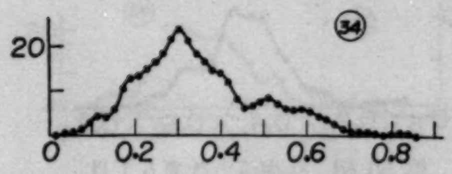

第 41 図　住吉区北島町

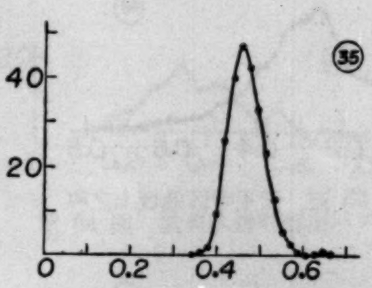

第 42 図　住吉区南加賀屋町

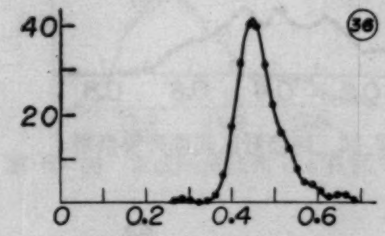

第 43 図　住吉区南加賀屋町

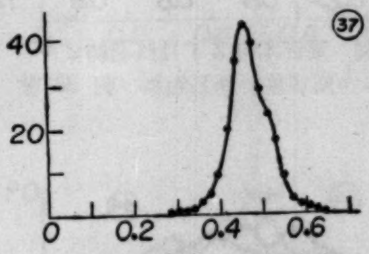

第 44 図　住吉区御崎町 2 丁目

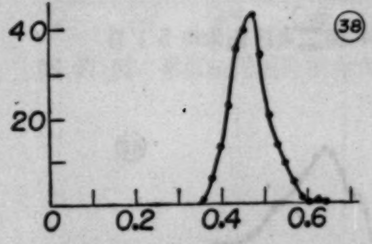

第 45 図　住吉区御崎町 2 丁目

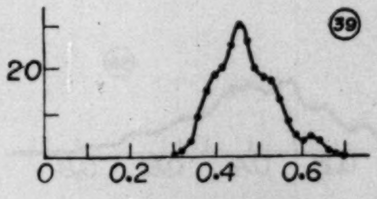

第 46 図　住吉区御崎町 2 丁目

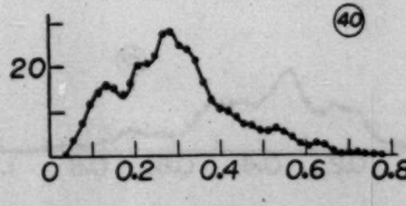

第 47 図　住吉区浜口西 2 丁目

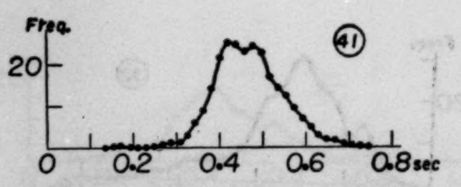

第 48 図 住吉区住吉町大海神社内

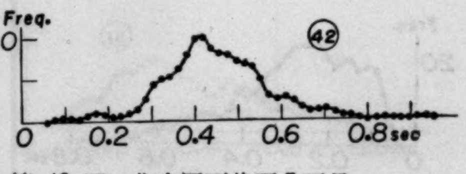

第 49 図 住吉区万代西 5 丁目

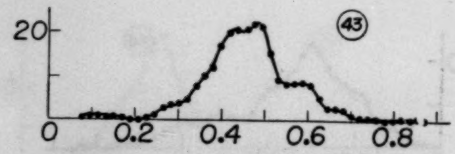

第 50 図 住吉区万代東 5 丁目

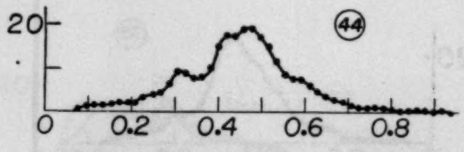

第 51 図 阿倍野区大阪大学南校

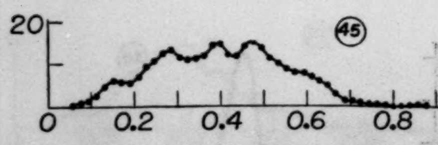

第 52 図 阿倍野区阿部野警察署

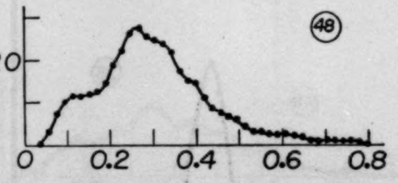

第 53 図 天王寺区逢坂上之町

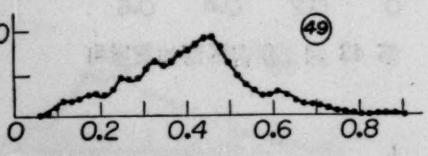

第 54 図 東区南本町 5 丁目

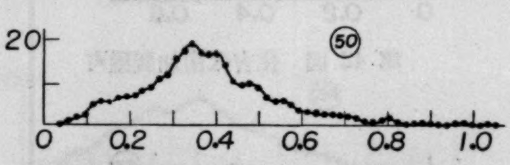

第 55 図 東区本町 2 丁目呉羽紡ビル

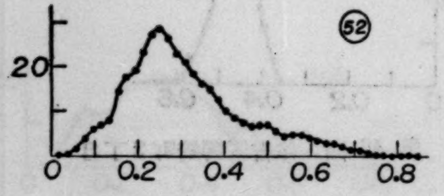

第 56 図 東区谷町 6 丁目

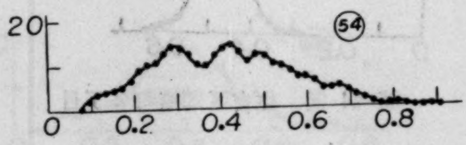

第 57 図 東区谷町 8 丁目

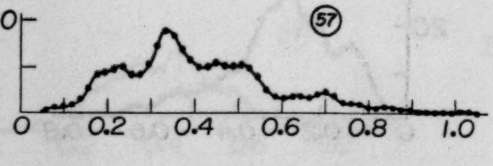

第 58 図 天王寺区東高津北之町貯金局

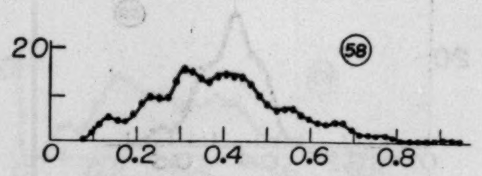

第 59 図 天王寺区清堀町高津中学校

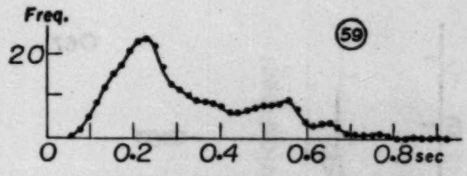

第 60 図　天王寺区清水谷東之町

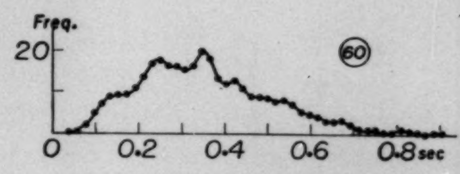

第 61 図　東区仁右衛門町大阪女子学院

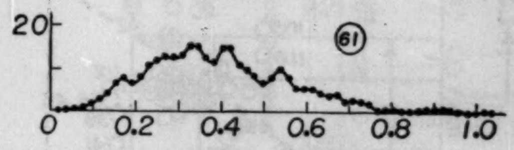

第 62 図　東区元伊勢町 79

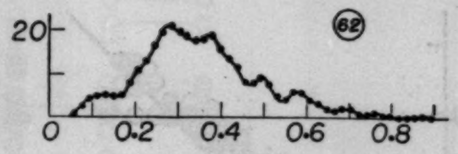

第 63 図　東区森之宮西之町

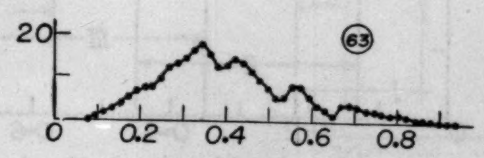

第 64 図　城東区森町南市バス車庫

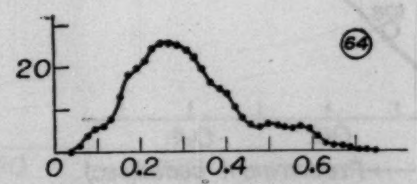

第 65 図　東成区深江西 2 丁目宝来小学校

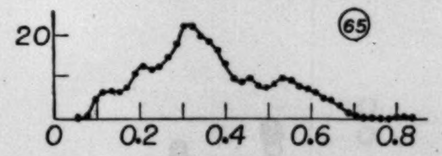

第 66 図　東成区西今里町東中本小学校

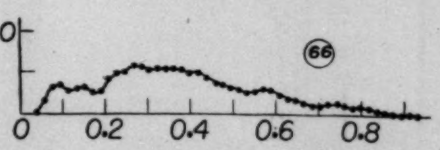

第 67 図　東区法円坂町国立大阪病院

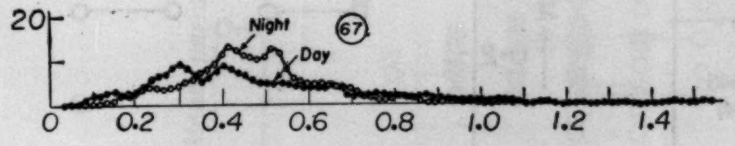

第 68 図　北区梅田町第 1 生命ビル

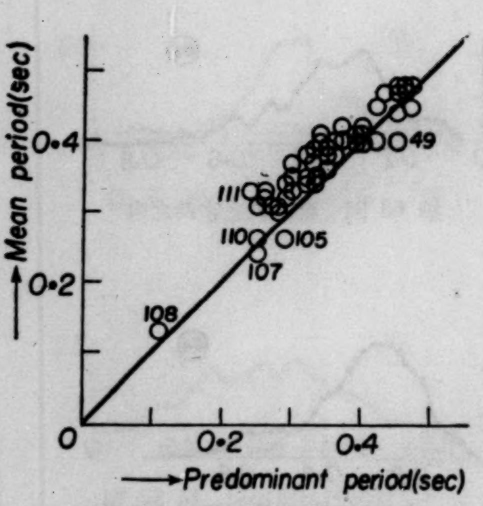

第 69 図　常時微動の卓越周期と平均周期の関係

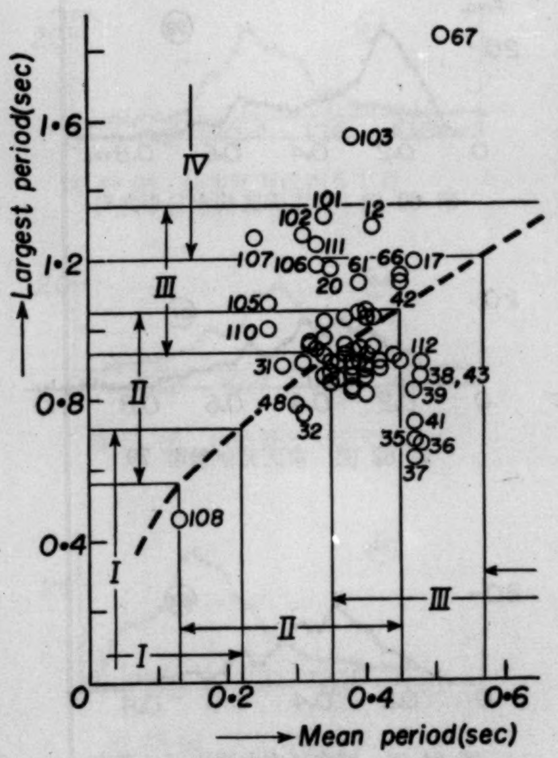

第 70 図　常時微動の平均周期と最大周期の関係
(I～IV の記号は建築基準法関係の地盤種別)

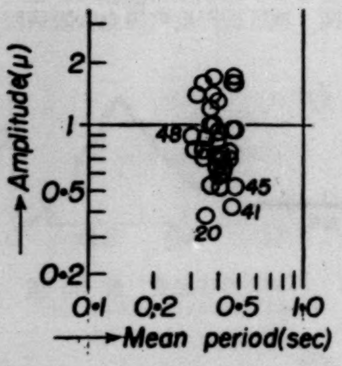

第 71 図　常時微動の平均周期と最大振巾の関係

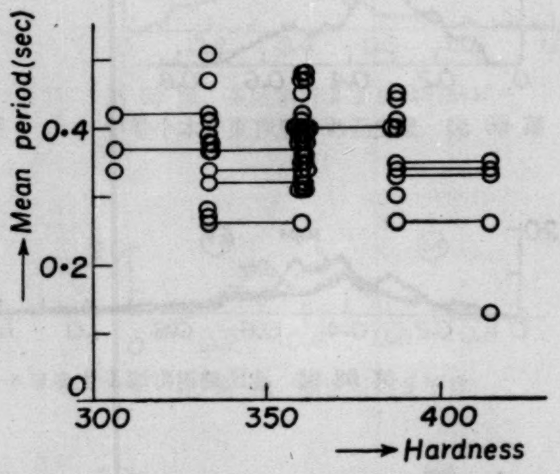

第 72 図　地下 30 m 迄の地盤の硬度と常時微動の平均周期の関係

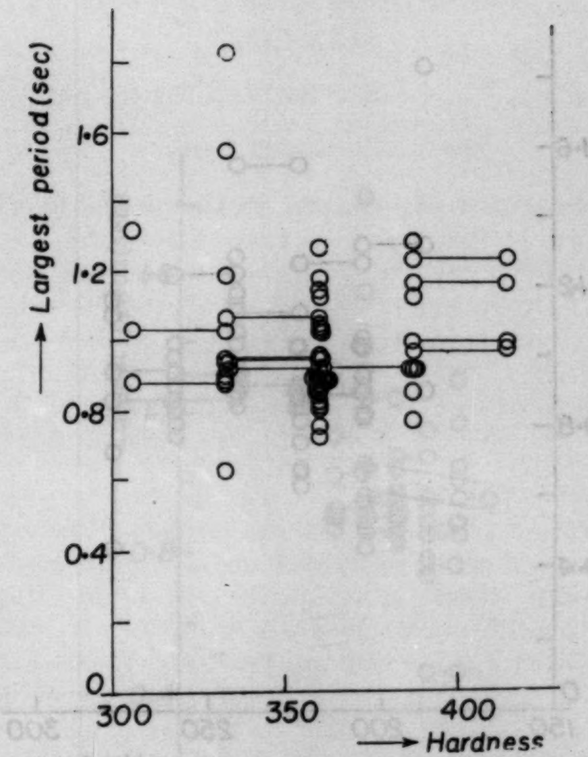

第 73 図　地下 30 m 迄の地盤の硬度と常時微動の最大周期との関係

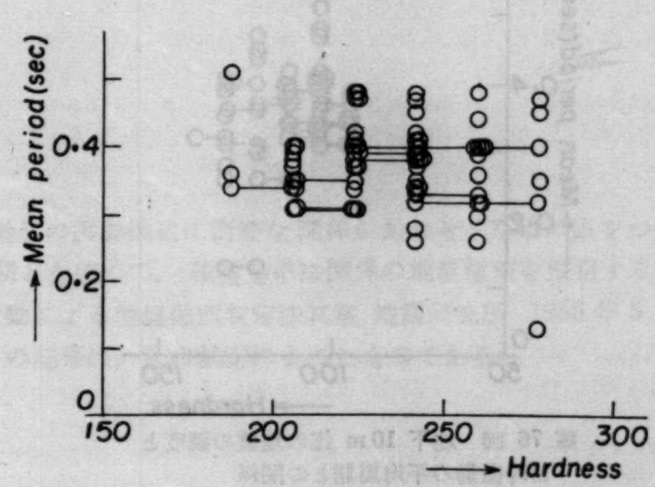

第 74 図　地下 20 m 迄の地盤の硬度と常時微動の平均周期との関係

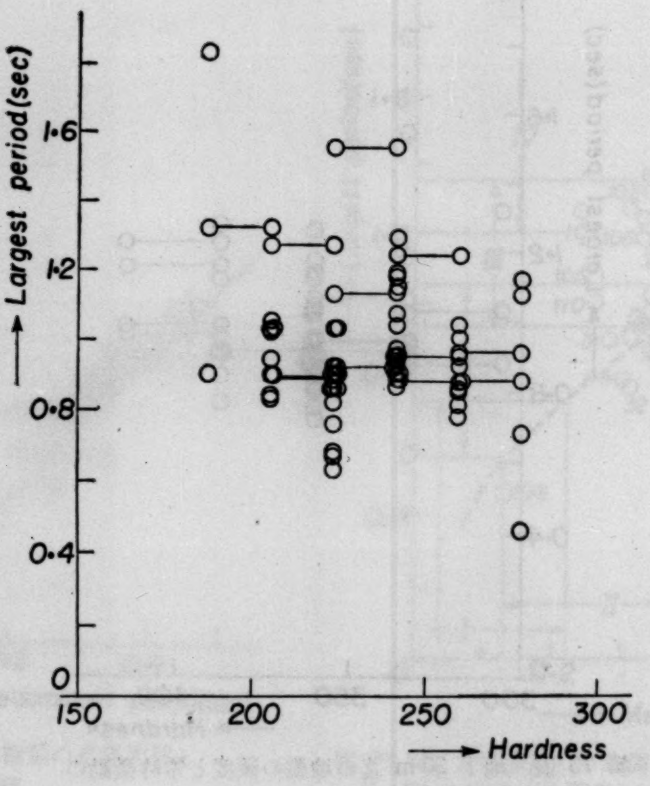

第 75 図 地下 20 m 迄の地盤の硬度と常時微動の最大周期との関係

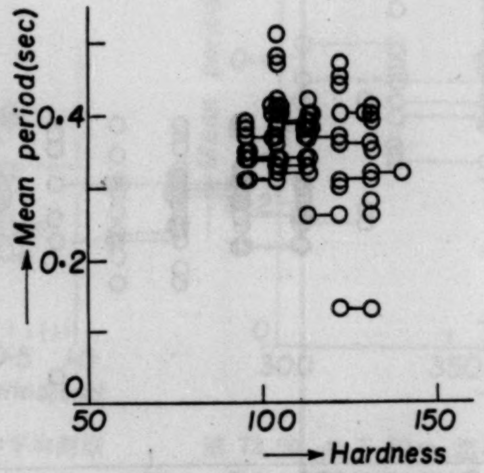

第 76 図 地下 10 m 迄の地盤の硬度と
常時微動の平均周期との関係

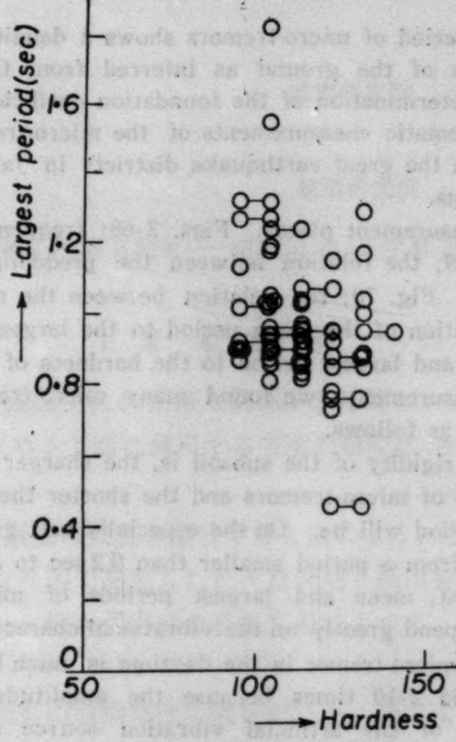

第 77 図 地下 10 m 迄の地盤の硬度と常時微動の最大周期との関係

附 記

常時微動が地盤の震動性状に密接な関係がありそうな事に眼をつけ，常時微動の平均周期と最大周期とを使つて，建築基準法関係の地盤種別を推定する試案を作つてみた.（筆者 常時微動による地盤種別判定法試案 地震研究所 1956 年 5 月.）第 1 図及び第 70図の I〜IV の記号は，その試案によつたものである.

11. *Measurement of Micro-tremor. V.* *(Osaka City.)*

By Kiyoshi KANAI, Hirosi KAWASUMI, Teiji TANAKA and Kaio OSADA,

Earthquake Resarch Institute.

The distribution of period of micro-tremors shows a definite form for different kinds of subsos. Thile properties of the ground as inferred from the characteristics of micro-tremor are utilized for determination of the foundation coefficient relating to earthquake-proof construction. Systematic measurements of the micro-tremor have been carried out by us at various places in the great earthquake districts in Japan. This is a part of a series of our investigations.

Fig. 1 shows the measurement places. Figs. 2-68; frequency distribution of the period of micro-tremo s. Fig. 69; the relation between the predominant period and the mean period of micro-tremors. Fig. 70; the relation between the mean period and the largest period. Fig. 71; the relation of the mean period to the largest amplitude. Figs. 72~77; the relation of the mean and largest period to the hardness of the ground.

From systematic measurements, we found many micro-tremor characteristics, which we shall now summarize as follows.

(1) The harder the rigidity of the subsoil is, the sharper the shape of the frequency distribution of the period of micro-tremors and the shorter the predominant period of the distribution curve of period will be. On the especially soft ground the distribution curve of period is flat ranging from a period smaller than 0.2 sec to a period larger than 1.0 sec.

(2) The predominant, mean and largest periods of micro-tremors differ slightly according to time and depend greatly on the vibrational characteristics of the subsoil. But, the largest amplitude of micro-tremor in the daytime is much larger than that at midnight, that is to say, the ratio is 2-10 times, because the amplitudes of micro-tremor depend greatly on the activity of the artificial vibration source surrounding the measuring place.

(3) The wave form of micro-tremor can be decided not only from the thickness of alluvium but also from the conditions of each stratum, that is to say, the wave form depends mainly on the vibrational impedance ratio of neighbouring layers and the thickness of each layer.

(4) The predominat period of earthquake motion has a close relation with the distribution curve of period of micro-tremors. In a place in which the distribution curve of period of micro-tremor has a single peak, the peak period coincides clearly with the predominant period of earthquake motion. On the other hand, in a place in which the distribution curve of period of micro-tremor has more than two peaks, the predominant period of earthquake motion coincides with either of them.

(5) The predominant period of micro-tremors is in many cases influenced by the properties of the first layer. All the properties between the free surface and the bed rock seem to play an important part in deciding the largest period of micro-tremors.

(6) The frequency distribution curve of the period of micro-tremor on fresh rock is flat at periods ranging from less than 0.2 sec to larger than 1.0 sec. From these facts, we can consider that the distribution curve of the period of micro-tremor arrived at bed rock will be flat in form. Then we can reach the conclusion that the amplitudes of vibration at the surface become relatively large at such periods as are synchronous with the natural period of the stratum from the feature of selective resonance.

12. 常時微動の測定結果 第6報
(一宮市内)

地震研究所 金井　清
田中貞二
森下利三
建築研究所 中川恭次

(昭和31年2月28日発表——昭和31年12月31日受理)

1. まえがき

常時微動の波形は地盤の震動性状と密接な関係がある事がわかつたので，その性質を耐震工学上の地盤係数を求める方面に利用する方法の研究に必要な資料を得るための調査を各地で行つている．

現在までにわかつた常時微動の性質を綜合すると次のようになる．

(1) 常時微動は，色々な原因で発生した色々な周期と振巾をもつた波が，四方八方から来たものの集りであつて，地表層内での重複反射によつて，地盤固有の震動性状を呈するものである．

(2) 常時微動の周期は地盤の震動特性に関係深いが，振巾は人工的震動源の遠近大小等の環境条件に大きく支配される．

(3) 常時微動の波形は冲積層の厚さだけではきまらない．卓越周期には第1層の固有周期が出る場合が多く，最大周期は冲積層全体の厚さに関係が深い．

(4) 常時微動の頻度曲線は地震動の周期特性に密接な関係がある．

2. 測定方法

本報告の測定は，昭和30年9月に行つたものである．測定方法は電磁式煤書微動計(換振器は固有周期1秒の動線輪型倒立振子)[1,2]によつて5分間の測定を行い，その中の2分間について解析を行つた．

測定場所を第1図並びに第I表に示す．記録の解釈に役立てる意味で，測定場所の環境条件はできるだけ詳細に記入してある．

---

1) 金井　清・田中貞二・長田甲斐男　地震研究所彙報 **32** (1954), 199.
2) 地震研究所地盤研究会　同上 **33** (1955), 492～495.

第 I 表 常時微動の測定場所

番号	場所
1	宮西通り，体育館（木造2階建物入口）
2	宮西通り，宮西小学校(木造2階建物入口)
5	葉栗，葉栗中学（校庭表土上）
7	杉山，神明社（境内）
9	奥町，奥中学校(木造2階建物コンクリート廊下)
10	奥町，奥小学校（木造建物1階コンクリート床）
11	西奥，蘇東橋（コンクリート小橋）
12	奥町，野田家（門のタタキ）
15	吉田，田のあぜ（道路脇の土の上）
16	今伊勢町，今伊勢小学校（工事中の鉄筋コンクリート3階建物，1階床）
17	東八幡町，住友銀行（鉄筋コンクリート建物，入口）
18	伝馬通り，商工会議所（鉄筋コンクリート建物1階床）
20	葵町，市役所（鉄筋コンクリート建物1階床）
21	神山町，愛知県中宮綜合事務所（入口タタキ）
22	苅安賀，ブロック住宅（建物の入口コンクリート床）
23	苅安賀，県立尾張病院（建築中の3階建コンクリート建物1階床）
24	萩原，萩原中学校（木造2階建物入口，コンクリート床）
25	大和町，大和中学校（木造2階建物入口，コンクリート床）
26	北園通り，一宮高等学校（木造建物1階廊下，コンクリート床）
27	公園通り，地方裁判所（鉄筋コンクリート建物入口）
33	朝日通り，朝日保育園（道路傍の木造平家土間）
35	小赤見，バス停留所（道路上）
36	西成中学校，（木造平家，コンクリート渡り廊下）
37	印田通り，花祇アパート（鉄筋コンクリート4階建物入口）
38	川田町，大志小学校（鉄筋コンクリート建講堂内）

3. 測 定 結 果

(i) 頻度曲線

2分間の波形について，周期の頻度を求めたものを第 2～26 図に示す．

機業地のため，機械から来る短周期の震動が直接換振器に作用するため，いまの目的に到底向かない記録が少くなかつた．解析結果に欠番の多いのはそのためであり，又，短周期の頻度の大きい測定結果の数が比較的に多いのもそのためである．

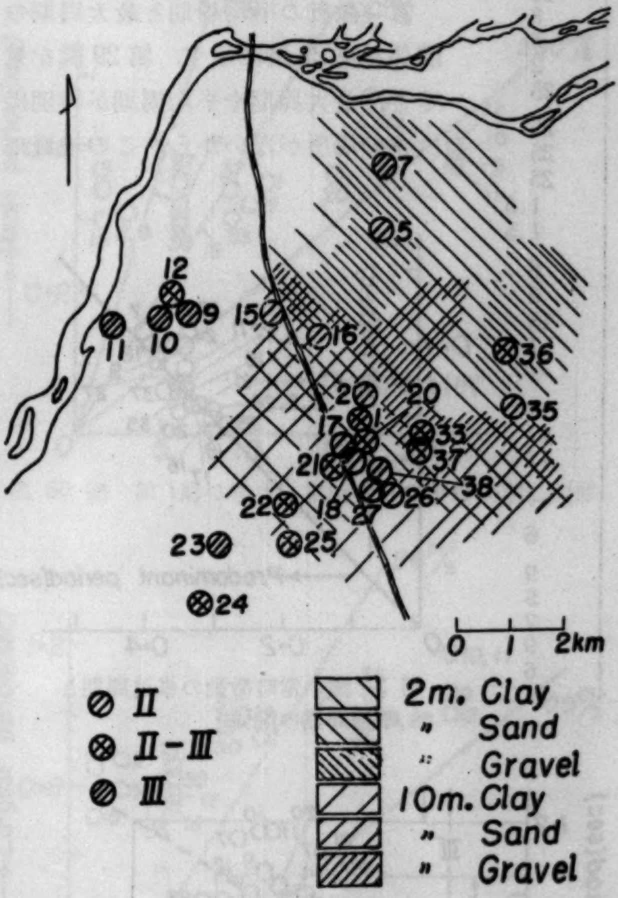

第 1 図 常時微動の測定場所
(I～IV の記号は建築基準法関係の地盤種別)

頻度曲線の極大になる周期を卓越周期，2 分間の波数で時間を割つた値を平均周期，この計器で記録した最も長い周期を最大周期，2 分間の記録の中で大振巾が 2，3 波続くものの中での最大値を最大振巾と名づけ，それらの値を第II表に示した．

卓越周期と平均周期の関係を第27図に示す．第 27 図から，この両周期の値は非常に近い事がわかる．但し，頻度曲線が非常に平坦な測定点 23(県立尾張病院)と，2 つ以上の山のできる測定点 33 (朝日保育園)，36(西成中学校)の卓越周期は意味が曖昧なので読取らなかつた．

(ii) 常時微動の周期と最大振巾との関係

第 28 図からわかるように，常時微動の平均周期と最大振巾との関係は，余り深くなく，同じ平均周期で振巾は 10 倍以上もちがう例さえある．これは，振巾は人工的震動源からの直接の影響，いい換えると，環境条件に非常に支配されるためである．即ち，測定点 9，10，11，12 のように機業の盛んな地域では振巾が大きい．測定点 7 は昼間は機械震動が激しいので午後 11 時頃に測定したので振巾が小さい．

(iii) 日中と夜間の常時微動の比較

測定点 26(一宮高校)では日中と深夜(午前 2 時頃)の測定を行つた．第20図を見ると，0.3 秒附近の頻度の山は，昼夜共一致する．昼のものだけに 0.1 秒附近の短周期に山ができる．この短周期の山は機械振動からの直接の影響と考えられる．振巾は昼が 0.5 ミク

第 II 表 常時微動の周期と最大振幅
(括弧は深夜の測定)

No.	Period (sec)			Largest Amplitude (μ)	Alluvium thick (m)
	Dominant	Mean	Largest		
1	0.34	0.35	0.93	0.5	11
2	0.30	0.31	0.87	0.5	3
5	0.30	0.31	0.79	0.1	3
7	0.40	0.42	1.15	0.05	2
9	0.38	0.38	1.06	1.5	25
10	0.38	0.39	1.17	1.0	25
11	0.34	0.37	1.17	1.5	25
12	0.39	0.40	1.00	3.0	25
15	0.34	0.34	0.85	1.0	1.5
16	0.30	0.30	0.71	1.0	1.5
17	0.33	0.32	0.77	1.0	6
18	0.28	0.30	0.75	1.0	6
20	0.35	0.36	1.02	0.5	15
21	0.32	0.32	1.00	0.5	1
22	0.34	0.35	0.94	0.5	—
23	—	0.47	0.98	0.3	17
24	0.34	0.40	0.96	0.5	17
25	0.38	0.44	0.98	0.5	17
26	0.30 (0.30)	0.27 (0.31)	0.79 (0.78)	0.5 (0.2)	—
27	0.35	0.35	0.85	1.5	6
33	—	0.30	0.96	0.2	9
35	0.35	0.34	0.72	0.1	5
36	—	0.27	1.06	0.1	2
37	0.37	0.34	0.98	0.2	9
38	0.28	0.29	0.82	0.3	6

ロンに対して夜は 0.2 ミクロンであり，その比は約3倍である．

(iv) 常時微動の平均周期と最大周期

常時微動の平均周期と最大周期の関係を第29図に示す．第29図を見ると，最大周期や平均周期が特別に大きい場所がないから，この地域に

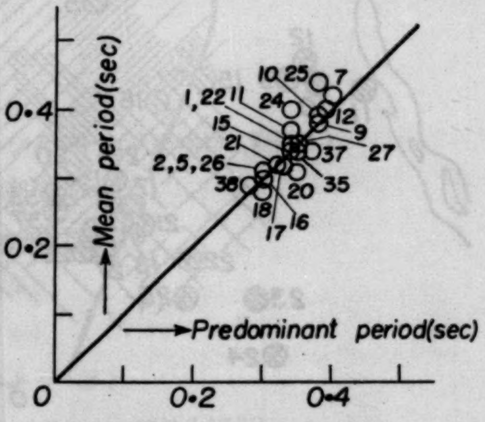

第 27 図 常時微動の卓越周期と平均周期の関係

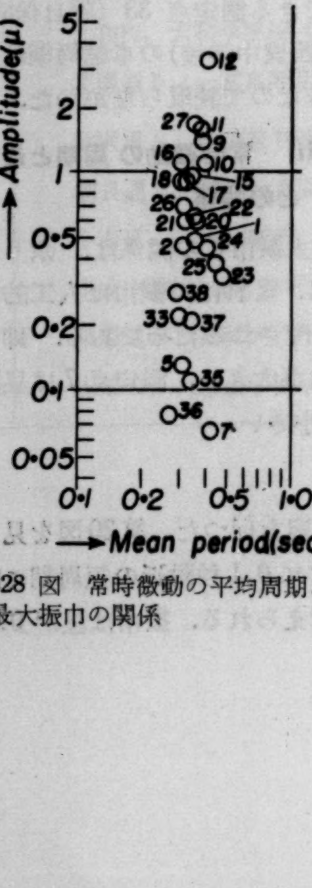

第 28 図 常時微動の平均周期と最大振巾の関係

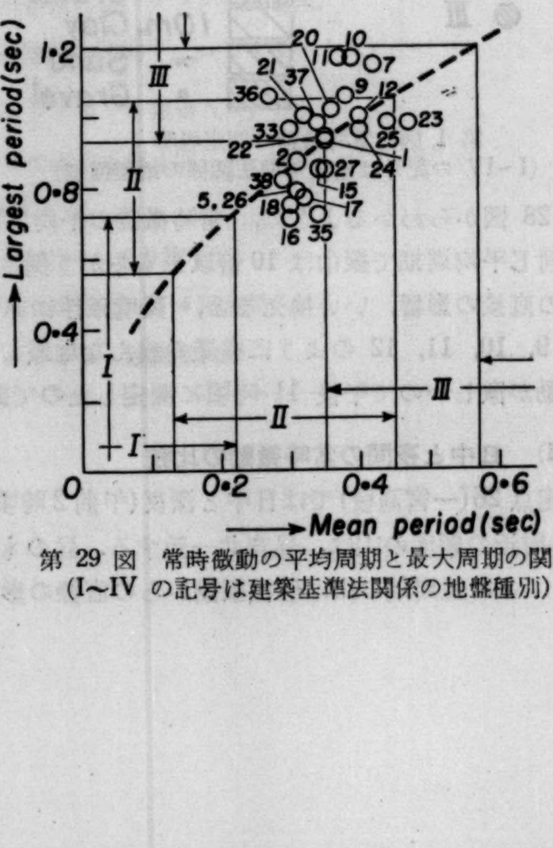

第 29 図 常時微動の平均周期と最大周期の関係
(I～IV の記号は建築基準法関係の地盤種別)

は震動的に厚い軟弱層がない事を意味するものであろう.

(v)　表土層の深さと常時微動の周期との関係

一宮地域は木曽川流域の，いわゆる底なしの冲積層である．この冲積層は表土層，粘土層，砂層，砂礫層，礫層から成つている．そこで，弾性波地下探査結果[3]を参考にして，表土層，粘土層，砂層を最軟弱層と考え，これらの層と砂礫層，礫層との境が弾性的な境界面と仮定し，この境界面と地表との間を第1層という事にする．測定点21及び36は地表近くが礫層で下が粘土層及び砂層という特別の場合である．

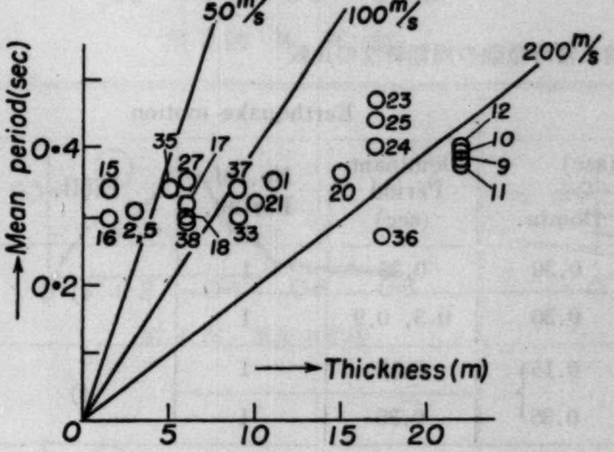

第 30 図　第1層の厚さと常時微動の平均周期の関係

この第1層の厚さと常時微動の平均周期及び最大周期の関係を第30図及び第31図に示す．第30, 31図から，第1層の厚さが大きくなる程，平均周期，最大周期が長くなる傾向が見られる．しかし，速度関係から見て，固有震動を誘発される層は，この第1層よりも深い場合と浅い場合がある事があると考えられる．又，最大周期に関係する層は第1層よりも浅いものはなさそうである．

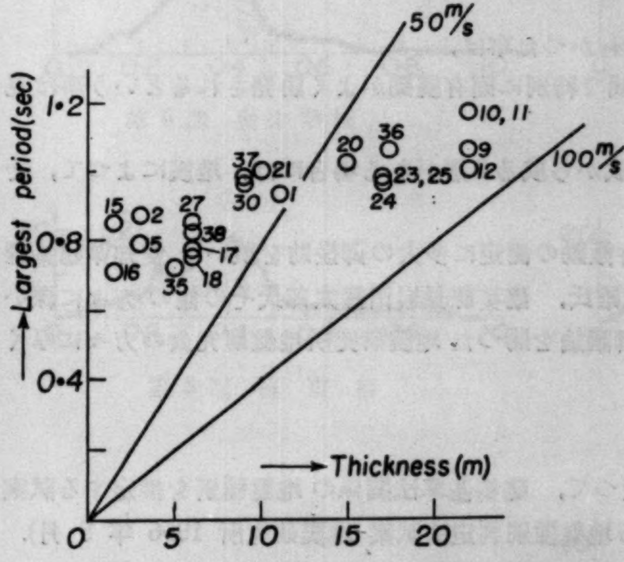

第 31 図　第1層の厚さと常時微動の最大周期の関係

(vi)　地震動と常時微動の関係

地震動と常時微動の周期特性の比較を第III表に示す．

測定点26（一宮高校）における常時微動の頻度曲線（第20図参照）には，0.3秒附近に1つの顕著な山ができるが，曲線全体に凹凸があり，単純な1層でない事を示している．2つの自然地震でも，0.3秒附近にはつきりした山ができ，その内の1つの地震では0.3秒の他に0.9秒附近にも僅かな山ができる．この長周期の山は，地下深い所に第2の境界面がある事を意味し，そのために常時微動の頻度曲線が複雑になるものと考えられる．

---

3)　岩津　潤・林田精郎・中川恭次　一ノ宮市地盤調査報告（昭和29年5月）．

測定点 36(西成中学校)における常時微動の頻度曲線(第24図参照)には 0.15 秒と 0.35 秒の2つのはつきりした山ができる. この事から, 基盤の上が2層に分れており, それらの弾性比と層の厚さとが特別な関係になつていると考えるのが自然である. そのため, もとから来た地震波の波形によつて, 或地震では 0.15 秒が卓越し,或地震では 0.35 秒が優勢に出るものであろう.

第 III 表 地震動と常時微動の周期特性の比較

No.	Micro-tremor			Earthquake motion		
	Time	Period (sec)		Dominant Period (sec)	No. of Earthq.	Bibli.
		Mean	Domin.			
26	Night	0.31	0.30	0.25	1	4)
	Day	0.27	0.30	0.3, 0.9	1	
36	Day	0.27	0.15, 0.35	0.15	1	4)
				0.35	1	

4. む す び

一宮市内の常時微動の測定で新たにわかつた事は,

(I) 礫層との境界面と地表面との間で特別に固有震動がよく誘発されるという事は見出せない.

(II) 弾性比と層の厚さが特別な構成から成る2層がある場合には, 地震によつて, そのうちの1つの固有周期が卓越する.

終りに臨み, 一宮市内における常時微動の測定に多大の御援助を頂いた愛知県建築課長水野金市氏, 一宮市土木部長加藤徳雄氏, 建築課長岩田鋑太郎氏その他の方々に深い謝意を表する. 又, 色々と御援助と御議論を賜つた地震研究所地盤研究会の方々に厚く御礼を申し述べる.

追 記

常時微動の平均周期と最大周期を使つて, 建築基準法関係の地盤種別を推定する試案を作つてみた. (筆者 常時微動による地盤種別判定法試案 地震研究所 1956 年 5 月). 第1 図及び第 29 図の中の I〜IV の記号は, その試案によつたものである.

4) 金井 清・他 常時微動と地震観測による一宮市の地盤調査並に地盤震度図案 (地震研究所, 建設省建築研究所 1956).

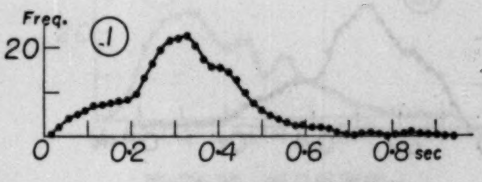

第 2 図 体 育 館

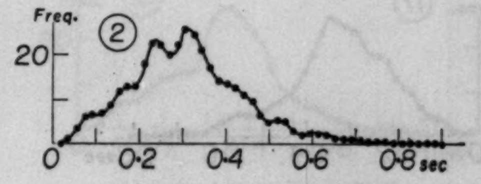

第 3 図 宮西小学校

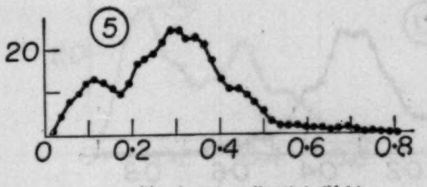

第 4 図 葉栗中学校

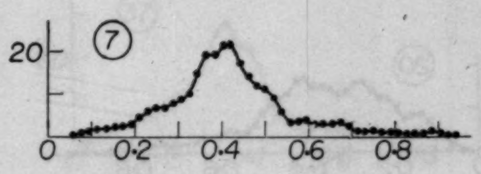

第 5 図 神 明 社

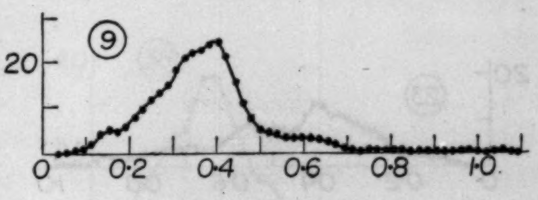

第 6 図 奥中学校

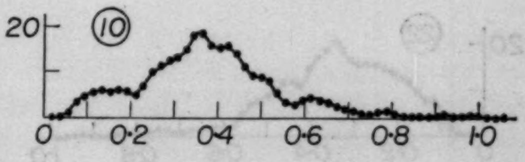

第 7 図 奥小学校

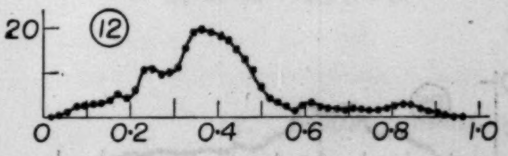

第 8 図 蘇 東 橋

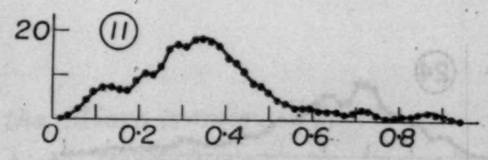

第 9 図 野 田 家

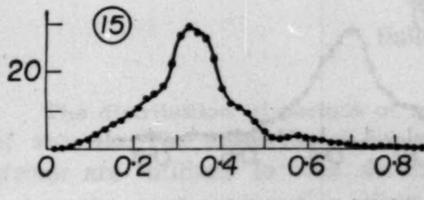

第 10 図 吉田，田のあぜ

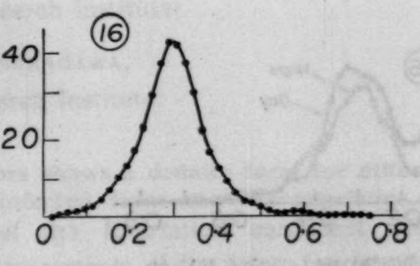

第 11 図 今伊勢小学校

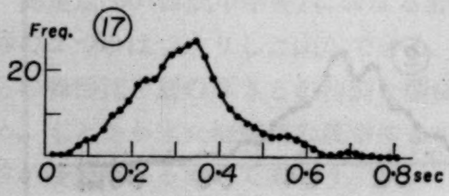

第 12 図　住 友 銀 行

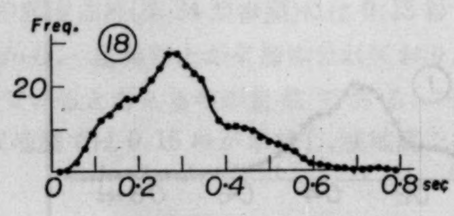

第 13 図　商工会議所

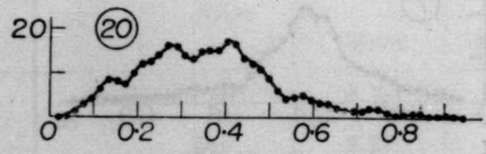

第 14 図　市 役 所

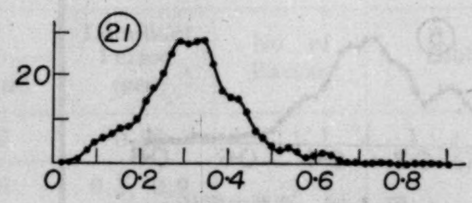

第 15 図　愛知県中宮綜合事務所

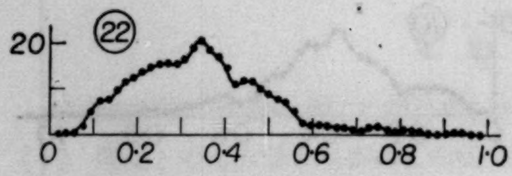

第 16 図　刈安賀ブロック住宅

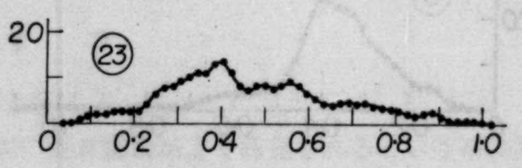

第 17 図　県立尾張病院

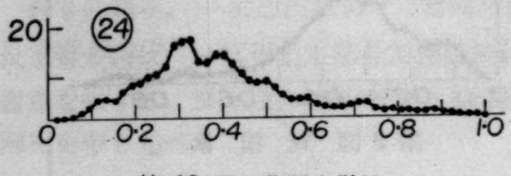

第 18 図　萩原中学校

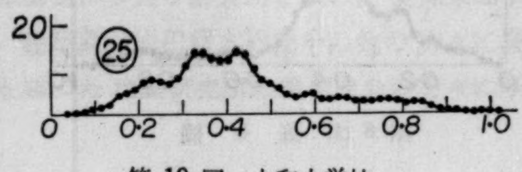

第 19 図　大和中学校

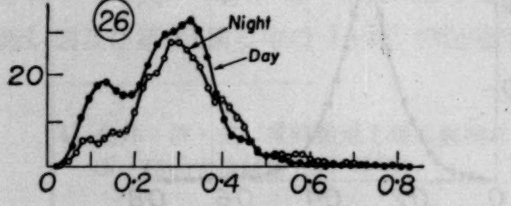

第 20 図　一宮高等学校

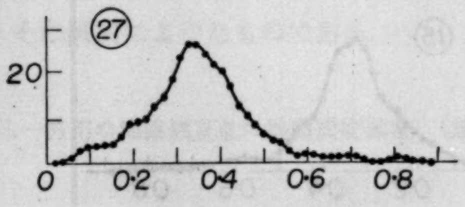

第 21 図　地方裁判所

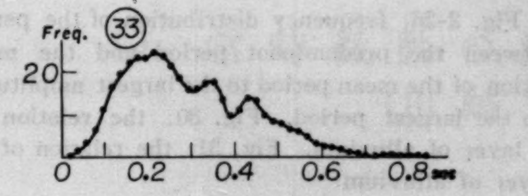

第 22 図 朝日保育園

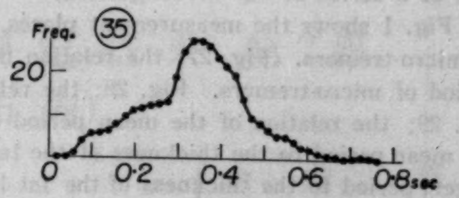

第 23 図 小赤見バス停留所

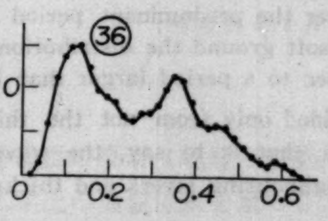

第 24 図 西成中学校

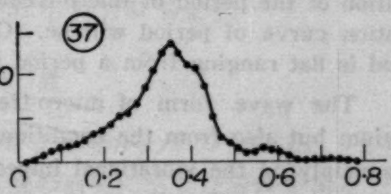

第 25 図 花祇アパート

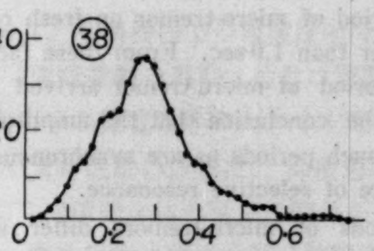

第 26 図 大志小学校

12. Measurement of the Micro-tremor. VI. (Ichinomiya City, Aichi Prefecture.)

By Kiyoshi KANAI, Teiji TANAKA, Tosizo MORISHITA.
Earthquake Research Institute;

and Kyoji NAKAGAWA,
Building Research Institute.

The distribution of periods of micro-tremors shows a definite form for different kinds of subsoils. The properties of the ground as inferred from the characteristics of micro-tremor are utilized for the determination of the foundation coefficient relating to earthquake proof construction. Systematic measurements of the micro-tremors have been carried out by us at various places in the great earthquake districts in Japan. This is a

part of a series of our investigations.

Fig. 1 shows the measurement places. Fig. 2–26; frequency distribution of the period of micro-tremors. Fig. 27; the relation between the predominant period and the mean period of micro-tremors. Fig. 28; the relation of the mean period to the largest amplitude. Fig. 29; the relation of the mean period to the largest period. Fig. 30; the relation of the mean period to the thickness of the 1st layer of alluvium. Fig. 31; the relation of the largest period to the thickness of the 1st layer of alluvium.

From systematic measurements, we found many micro-tremor characteristics, which we shall now summarize as follows.

(1) The harder the rigidity of the subsoil is, the sharper the shape of the frequency distribution of the period of micro-tremors and the shorter the predominant period of the distribution curve of period will be. On the especially soft ground the distribution curve of period is flat ranging from a period smaller than 0.2 sec to a period larger than 1.0 sec.

(2) The wave form of micro-tremor can be decided only from not the thickness of alluvium but also from the conditions of each stratum, that is to say, the wave form depends mainly on the vibrational impedance ratio of neighbouring layers and thickness of each layer.

(3) The predominant period of micro-tremor is in many cases influenced by the properties of the first layer. All the properties between the free surface and the bed rock seem to play an important part in deciding the largest period of micro-tremors.

(4) The frequency distribution curve of the period of micro-tremor on fresh rock is flat at periods ranging from less than 0.2 sec to larger than 1.0 sec. From these facts, we can consider that the distribution curve of the period of micro-tremor arrived at bed rock will be flat in form. Then, we can reach the conclusion that the amplitudes of vibration at the surface become relatively large at such periods as are synchronous with the natural period of the stratum from the feature of selective resonance.

(5) The predominant, mean and largest periods of micro-tremors differ slightly according to time and depend greatly on the vibrational characteristics of the subsoil. But, the largest amplitudes of micro-tremor in the daytime is much larger than that at midnight, that is to say, the ratio is 2–10 times, because the amplitudes of micro-tremor depend greatly on the activity of the artificial vibration source surrounding the measuring place.

(6) The predominant period of earthquake motion has a close relation with the distribution curve of period of micro-tremor. In a place in which the distribution curve of period of micro-tremor has a single peak, the peak period coincides clearly with the predominant period of earthquake motion. On the other hand, in a place in which the distribution curve of period of micro-tremor has more than two peaks, the predominant period of earthquake motion coincides with either of them. (See Table III).

13. 常時微動の測定結果 第7報
(川崎市内)

地震研究所 金井 清 / 田中貞二 / 長田甲斐男

(昭和31年4月24日発表——昭和31年12月31日受理)

1. まえがき

常時微動の波形は地盤の震動性状と密接な関係がある事がわかつたので，その性質を耐震工学上の地盤係数を求める方面に利用する方法の研究に必要な資料を得るための調査を各地で行つている．

現在までにわかつた常時微動の性質を綜合すると次のようになる．

(1) 常時微動は色々な原因で発生した色々な周期と振巾の波が四方から来たものの集りであり，地表層内での重複反射で地盤固有の震動性状を呈するものである．

(2) 常時微動の周期は地盤の震動特性に関係が深いが，振巾は人口的震動源の遠近，大小等の環境条件に大きく支配される．

(3) 常時微動の波形は，冲積層の厚さ或は礫層までの深さだけではきまらない．最大周期は冲積層全体の厚さに関係が深い．

(4) 常時微動の頻度曲線は地震動の周期特性に密接な関係がある．

2. 測定方法

本報告の測定は，昭和31年2月に行つたものである．測定方法は電磁式煤書微動計(換振器は固有周期1秒の動線輪型倒立振子)[1),2)]によつて5分間の測定を行い，その中の2分間について解析を行つた．

測定場所を第1図並びに第I表に示す．記録の解釈に役立てる意味で，測定場所の環境条件はできるだけ詳細に記入しておいた．

3. 測定結果

(i) 頻度曲線

2分間の波形について，周期の頻度を求めたものを第2～16図に示す．

---

1) 金井清・田中貞二・長田甲斐男 地震研究所彙報 **32** (1954), 199.
2) 地震研究所地盤研究会 同上 **33** (1955), 492～495.

測定点 10(三菱石油)における常時微動は，第 7 図の頻度曲線でわかるように，0.5秒位に非常にはつきりした頻度の山があり，しかも周期 1 秒以上の波も含まれている．非常に珍らしい震動特性である．その解釈は，相当に厚い冲積層が何層かの土層から成つており，その第 1 層の震動インピーダンスが非常に小さいという事でもできる．又，第 1 層と第 2 層以下の層との厚さ関係，並びにインピーダンス関係が，第 1 層の固有震動を誘発し易いような構成[3]になつているという事でも解釈できる．何れにしても，測定点10の地盤は，相当に厚くて 2 層以上の土層から成る冲積層と推定され，ボーリングの結果とも定性的には合う．

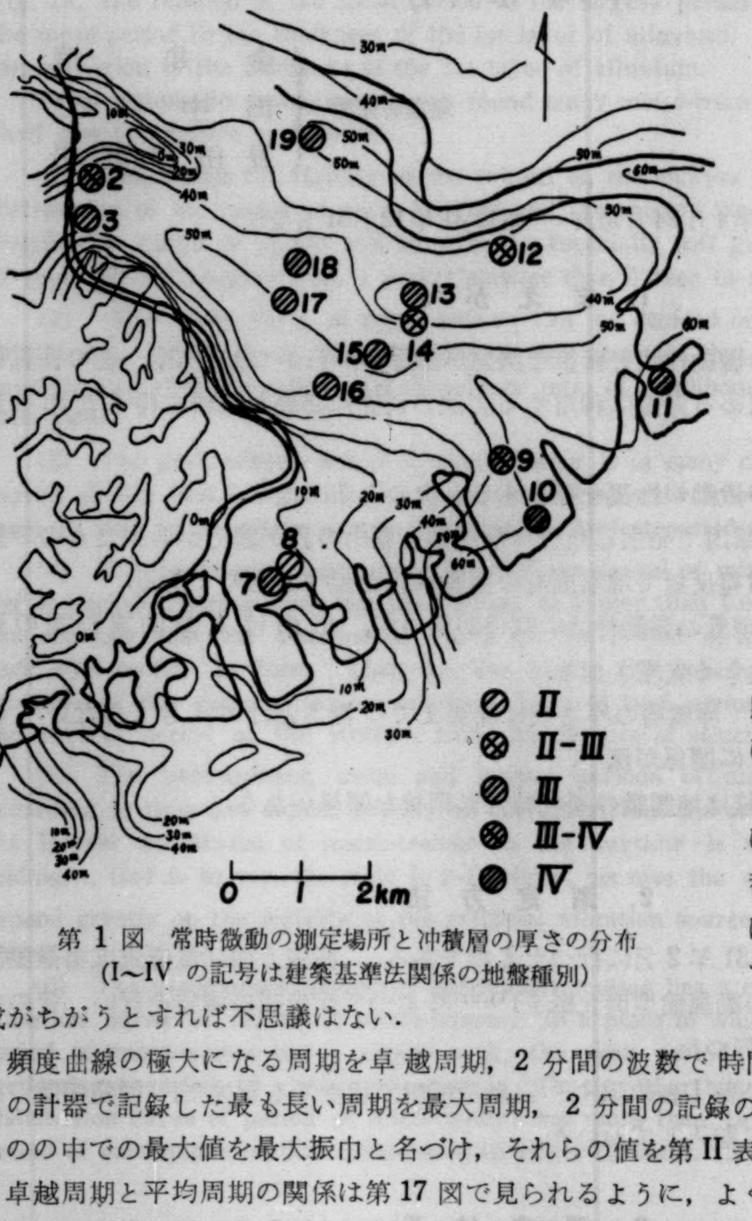

第 1 図　常時微動の測定場所と冲積層の厚さの分布
(I～IV の記号は建築基準法関係の地盤種別)

測定点 7 と 8 は共に旭ガラス株式会社構内で，その距離は 100 m 前後であるのに，第 4 図と第 5 図の頻度曲線でわかるように，非常に震動特性がちがう．東京都内九段坂，駿河台間における測定結果[4]から考えて，測定点 7 と 8 で地盤構成がちがうとすれば不思議はない．

頻度曲線の極大になる周期を卓越周期，2 分間の波数で時間を割つた値を平均周期，この計器で記録した最も長い周期を最大周期，2 分間の記録の中で大振巾が 2，3 波続くものの中での最大値を最大振巾と名づけ，それらの値を第 II 表に示した．

卓越周期と平均周期の関係は第 17 図で見られるように，よく一致する．但し，頻度曲線が特に平坦な測定点 2 (南加瀬)，9 (日本鋼管) 及び頻度曲線の山が 2 つ以上ある測定点 7 (旭ガラス)，11 (港湾事務所)，12 (味の素)，14 (新川眼科) については，卓越周期の意味が曖昧なので読取を省いた．

---

3)　金井清・吉沢静代　地震研究所彙報 **34** (1956)，167～184.
4)　金井清・田中貞二・長田甲斐男　地震研究所彙報 **35** (1957)，120～126.

第 I 表　常時微動の測定場所

番号	場所
2	南加瀬（大通りより約 100 m 奥の小路脇，周囲は田圃，交通機関に敏感）
3	建設省京浜港工事々務所（大通より約 15 m 奥の木造平屋建物コンクリート床上）
7	潮田町，旭ガラス株式会社（大通り脇正門のコンクリート上）
8	潮田町，旭ガラス株式会社 （大通より約 100 m 奥の鉄筋コンクリート建物 1 階床上）
9	南渡田 2730 番地，日本鋼管株式会社川崎製鉄所（鉄筋コンクリート建物内）
10	安善町，三菱石油（構内自動車々庫コンクリート床上）
11	千鳥町，川崎港湾部川崎港湾工事々務所（木造車庫コンクリート床上）
12	鈴木町 2964 番地，味の素株式会社川崎工場附近 （小路脇の民家入口門のコンクリート上，鉄道線路に近く交通機関に敏感）
13	砂子，川崎市役所（大通脇，鉄筋コンクリート建物 1 階床上）
14	南町，新川眼科医院（大通脇，鉄筋コンクリート建物の玄関）
15	南町，川崎運送修理工場（大通より約 60 m 入つた木造平屋建物コンクリート床上）
16	東京電機株式会社（大通脇木造モルタル塗建物の玄関）
17	尻手，尻手駅（大通より約 50 m 奥，駅構内のコンクリート上）
18	南幸町3の149番地，川崎中央市場 （大通より約 150 m 奥の鉄筋コンクリート建物 1 階床上）
19	小向東芝町 1，東京芝浦電気株式会社小向工場（鉄筋コンクリート建物 1 階床上）

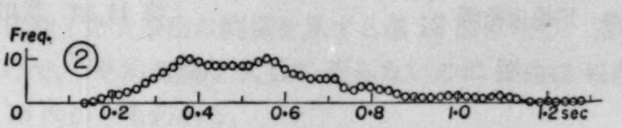

第 2 図　南　加　瀬

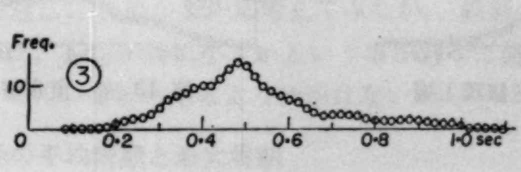

第 3 図　建設省京浜港工事々務所

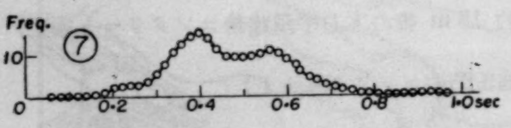

第 4 図　旭ガラス

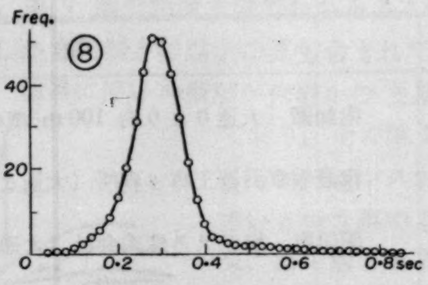

第 5 図　旭ガラス

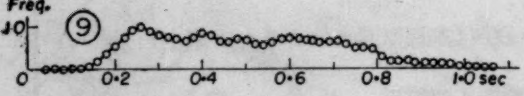

第 6 図　日本鋼管

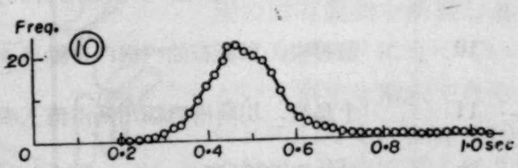

第 7 図　三菱石油

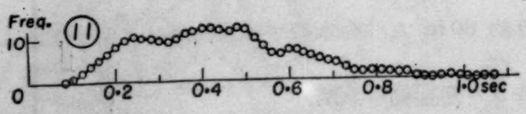

第 8 図　川崎市港湾事務所

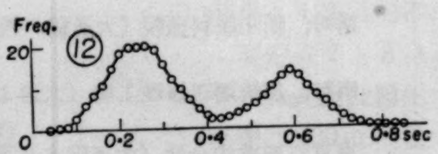

第 9 図　味の素川崎工場附近

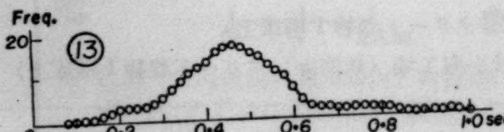

第 10 図　川崎市役所

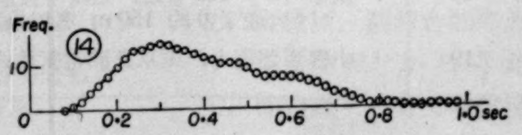

第 11 図　新川眼科医院

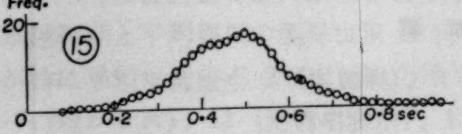

第 12 図　川崎運送修理工場

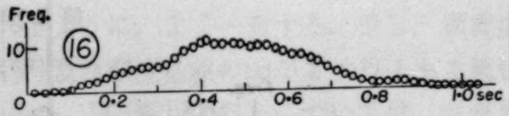

第 13 図　東京電機株式会社

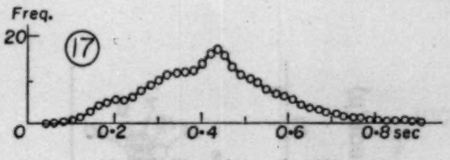

第 14 図　尻　手　駅

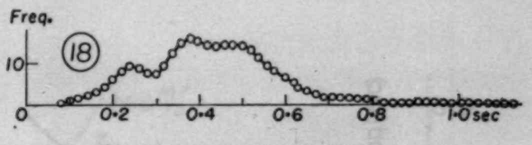

第 15 図　川崎中央市場

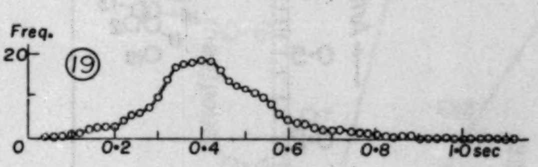

第 16 図　東芝小向工場

第 II 表　常時微動の周期と最大振幅

No.	Period (sec) Dominant	Mean	Largest	Largest Amplitude (μ)	Alluvium Thickness (m)
2	—	0.53	1.36	0.5	40～50
3	0.48	0.52	1.08	1.0	40～50
7	—	0.47	0.93	1.5	0～10
8	0.29	0.30	0.83	0.1	0～10
9	—	0.50	1.23	1.5	50～60
10	0.49	0.50	1.41	1.5	60～
11	—	0.43	1.05	0.5	60～
12	—	0.38	1.02	1.0	30～40
13	0.46	0.48	1.10	1.0	20～30
14	—	0.39	0.96	1.5	30～40
15	0.47	0.48	0.93	1.5	40～50
16	0.50	0.48	1.12	1.5	50～60
17	0.41	0.43	1.16	1.0	40～50
18	0.44	0.43	1.11	1.0	40～50
19	0.40	0.43	1.10	0.5	50～60

(ii)　常時微動の周期と最大振幅の関係

常時微動の平均周期と最大振巾の関係を示すと第 18 図になる．常時微動の振巾は環境条件に支配されるので，平均周期は大して変らないのに振巾は場所によつて相当な差違がある事が，第 18 図からもわかる．

それにしても，測定点 8 (旭ガラス)の振巾が特に小さい事が目立つ．鉄筋コンクリート建物の地階で測定したためかと一応考えてみたが，鉄筋コンクリート建物の地階で測定した実例は多いが，振巾が特に小さいという事があつた例はない．結局，建物の基礎が特別な条件になつていると考えるよりほかはない．

(iii)　常時微動の平均周期と最大周期

常時微動の平均周期と最大周期の関係を第 19 図に示す．測定点 10 (三菱石油) の最大周期は特に大きく，冲積層が非常に厚いと解釈される．この解釈はボーリングの結果と

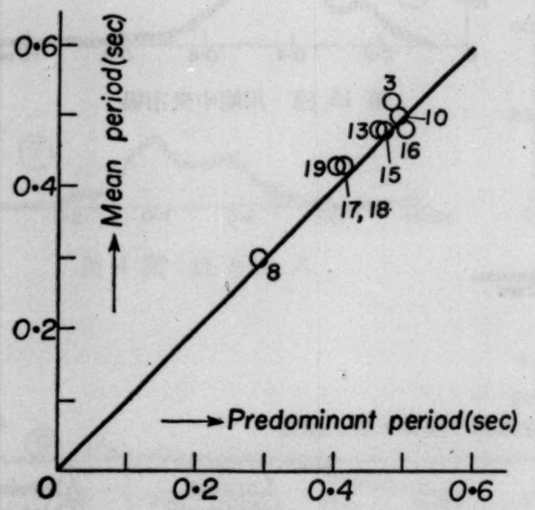

第 17 図　常時微動の卓越周期と平均周期の関係

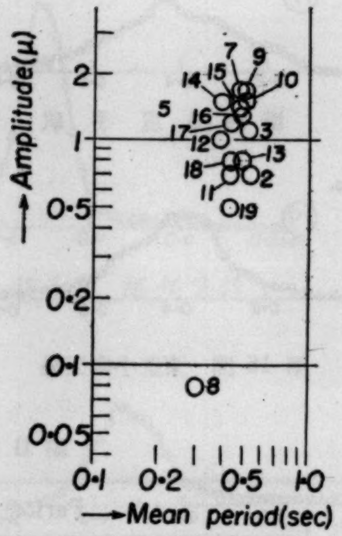

第 18 図　常時微動の平均周期と最大振幅の関係

も一致する．

(iv)　常時微動の周期と冲積層の厚さとの関係

冲積層の厚さと常時微動の平均周期及び最大周期の関係を第 20 図及び第 21 図に示す．第 20，21 図から冲積層の厚さが大きくなると，常時微動の平均周期，最大周期が長くなる傾向のある事がわかる．しかし，速度関係からして，平均周期（卓越周期と同等）は冲積層全体の固有震動の誘発によつて現われたものではないと考えられる．即ち，冲積層の中に震動インピーダンス比の顕著な不連続面があり，その面と地表面との間の固有震動が誘発され易いと考えるのが自然である．

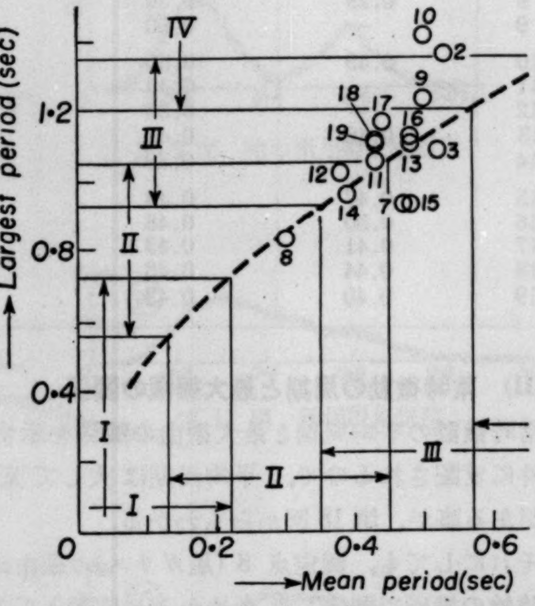

第 19 図　常時微動の平均周期と最大周期の関係
(I～IV の記号は建築基準法関係の地盤種別)

最大周期は大体，冲積層全体の震動に関係していると考えられる．

測定点 7，8 の旭ガラス株式会社附近の冲積層は 20～30 m はありそうに考えられる．

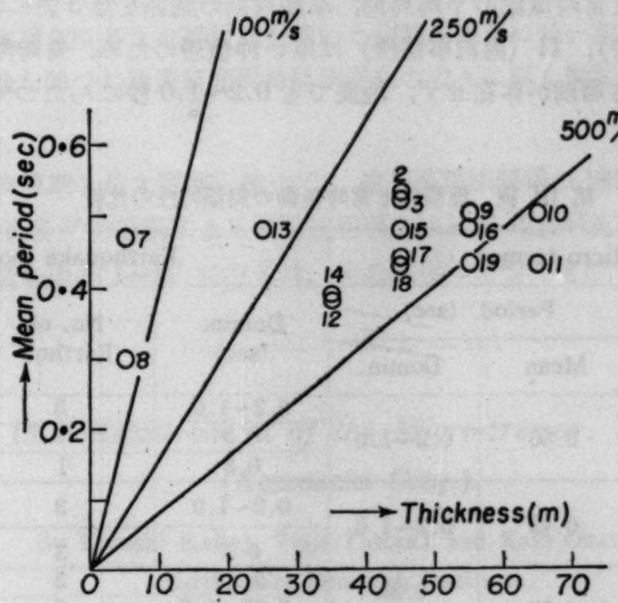

第 20 図　冲積層の厚さと常時微動の平均周期の関係

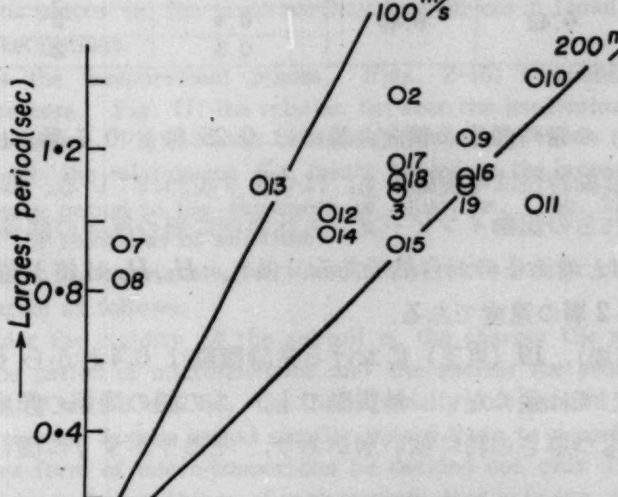

第 21 図　冲積層の厚さと常時微動の最大周期の関係

(v)　**地震動と常時微動**

地震動の卓越周期と常時微動の平均周期，卓越周期の関係を第3表に示す．

測定点 9（日本鋼管），11（港湾事務所）は厚い冲積層のため，常時微動の頻度曲線には特に頻度の卓越する周期が存在せず，地震でも 0.2～1.0 秒にわたつて同等の頻度のものが多い．

第 III 表　地震動と常時微動の周期特性の比較

No.	Micro-tremor			Earthquake motion		
	Time	Period (sec)		Domin. (sec)	No. of Earthq.	Bibli.
		Mean	Domin.			
9	Day	0.50	0.2～1.0	0.2～1.0	3	5)
				0.3	2	
				0.6	1	
11	Day	0.43	0.2～1.0	0.2～1.0	3	5)
				0.3	3	
12	Day	0.38	0.25 0.6	0.25	3	5)
				0.25～0.6	2	
				0.6	2	
18	Day	0.43	0.4～0.5	0.5	3	5)
				0.1～0.7	1	
19	Day	0.43	0.40	0.25	1	5)
				0.4	2	
				0.5	2	

測定点 12（味の素）の常時微動の頻度曲線には 0.25 秒と 0.6 秒にはつきりした頻度の山ができる．この震動特性は地震動にも，はつきり現われている．即ち，基盤の上が2層に分れており，それらの震動インピーダンス比並びに層の厚さの関係が $H_1/V_1=H_2/V_2$ の関係[6]になつていると考えるのが自然である．但し，H_1, H_2 は第1層，第2層の厚さ，V_1, V_2 は第1層，第2層の速度である．

測定点 18（中央市場），19（東芝）における常時微動は 0.4 秒から 0.5 秒の間の頻度が大きいが，曲線としては鋭くない．地震動でも，この間の周期の頻度が卓越するから，この位の周期をもつ厚さの特に軟い層があり，その下がすぐに固い基盤になつていると解釈される．

4. むすび

川崎市内での常時微動の測定結果から特に目立つた性質としては，

(I)　常時微動の卓越周期は冲積層全体の固有震動の誘発によるものではない．最大周

5) 表　俊一郎・小牧昭三・小林直吉　地震研究所彙報 **34** (1956), 335.

6) 前出 3)

期は冲積層全体の震動に関係が深い.

(II)　常時微動の頻度曲線は地震動の周期特性に密接な関係がある.

終りに臨み，本調査に多大の御援助を頂いた川崎市当局に深い謝意を表する．又，種々御援助と御議論を賜つた地震研究所地盤研究会の方々に厚く御礼を申し述べる.

附　記

常時微動の平均周期と最大周期を使つて，建築基準法関係の地盤種別を推定する試案を作つてみた.（筆者 常時微動による地盤種別判定法試案 地震研究所 1956 年 5 月）. 第 1 図及び第 19 図の中の I～IV の記号は，その試案によつたものである.

---

13. Measurement of the Micro-tremor. VII.
(Kawasaki City.)

By Kiyoshi KANAI, Teiji TANAKA and Kaio OSADA,
Earthquake Research Institute.

The distribution of periods of micro-tremors shows a definite form for different kinds of subsoils. The properties of the ground as inferred from the characteristics of micro-tremor are utilized for the determination of the foundation coefficient relating to earthquake-proof construction. Systematic measurements of the micro-tremors have been carried out by us at various places in the great earthquake districts in Japan. This is a part of a series of our investigations.

Fig. 1 shows the measurement places. Figs. 2-16; frequency distribution of the period of micro-tremors. Fig. 17; the relation between the predominant period and the mean period of micro-tremors. Fig. 18; the relation between the mean period and the largest amplitude. Fig. 19; the relation of the mean period to the largest period. Fig. 20; the relation of the mean period to the thickness of alluvium. Fig. 21; the relation of the largest period to the thickness of alluvium.

From systematic measurements, we found many micro-tremor characteristis, which we shall now summarize as follows.

(1) The harder the rigidity of the subsoil is, the sharper the shape of the frequency distribution of the period of micro-tremors and the shorter the predominant period of the distribution curve of period will be. On the especially soft ground the distribution curve of period is flat ranging from a period smaller than 0.2 sec to a period larger than 1.0 sec.

(2) The wave form of micro-tremor can be decided not only from the thickness of alluvium but also from the conditions of each stratum, that is to say, the wave form depends mainly on the vibrational impedance ratio of neighbouring layers and the thickness of each layer.

(3) The predominant period of micro-tremor is in many cases influenced by the properties of the first layer. All the properties between the free surface and the bed rock seem to play an important part in deciding the largest period of micro-tremor.

(4) The frequency distribution curve of the period of micro-tremor on fresh rock is flat at periods ranging from less than 0.2 sec to larger than 1.0 sec. From these facts,

we can consider that the distribution curve of the period of micro-tremor arrived at bed rock will be flat in form. Then we can reach the conclusion that the amplitudes of vibration at the surface become relatively large at such periods as are synchronous with the natural period of the stratum from the feature of selective resonance.

(5) The predominant, mean and largest periods of micro-tremors differ slightly according to time and depend greatly of the vibrational characteristics of subsoil. But, the largest amplitude of mirco-tremor at day time is greatly larger than that at midnight, that is to say, the ratio is 2-10 times, because the amplitudes of micro-tremor depend greatly on the activity of the artificial vibration source surrounding the measuring place.

(6) The predominant period of earthquake motion has a close relation with the distribution curve of period of micro-tremor. When the place in which the distribution curve of period of micro-tremor has a single peak, the peak period coincides clearly with the predominant period of earthquake motion. On the other hand, when the place in which the distribution curve of period of micro-tremor has more than two peaks, the predominant period of earthquake motion usually takes either of them.

14. 1944年12月7日東南海地震に見られた遠江地方の家屋被害分布と地盤との関係*

静岡県小笠郡菊川北中学校　大庭正八

(昭和31年11月27日発表—昭和31年12月28日受理)

(目　次)

I　はしがき……201
II　被害分布の研究方法……202
III　地盤の研究方法とその区分……204
IV　家屋被害分布の概況……207
V　各地域毎の家屋被害と地盤の状態……209
(1) 太田川低地 (Co, Go)……209
(2) 菊川低地 (Ck)……214
(3) 牧の原山麓小沖積地 (Cm)……216
(4) 浜名湖附近小沖積地 (Ch, Sh)……217
(5) 天竜川平野 (Gt)……219
(6) 大井川扇状地 (Gi)……221
(7) 小笠山砂礫地 (Gg)……222
(8) 海岸砂丘地帯 (Sc)……222
(9) 洪積台地 (D)……226
(10) 岩石地盤 (R)……227
VI　遠江地方大地震の歴史的考察……228
VII　被害家屋の特徴……230
VIII　結　論……236
IX　資　料……237

I. はしがき

この東南海地震とは，1944年(昭和19年)12月7日午後1時36分頃，熊野灘から発震し，静岡・愛知・三重その他の府県に被害を与えた大地震で，そのあらましは中央気象台東南海大地震調査報告(1945年2月)及び東京大学地震研究所彙報第24号1～4冊(1946)によつて知ることができる．この報告では最激震地の一つである静岡県遠江地方の家屋被害分布について記載し，あわせて立地地盤との関係を考察する．多くの例で見ら

---

* 河角所員紹介．

れる通り，この地震でも家屋の被害分布が地盤の状態に著しく影響されている．家屋密度の高い当地方ではいずれの地盤にも家屋が多く分布しているので地盤と震害の関係をくまなく調べることができる．それ故特にえらんで上記のテーマを取上げたのであり，今後の防災上の一助ともなれば幸である．

この研究の資料のうち，被害関係は主として当時の市町村当局から得られた報告や現地調査の結果によるものであり，また地盤関係は二，三の文献を基とし現地調査の結果も採用したが，地盤研究は十分とはいいかねるので今後の精査が要望される．

この研究に当つて，東京大学地震研究所河角広教授より，終始懇切な御指導と，発表上出版上の御尽力をいただいた．又種々の御教示をいただいた東京教育大学地質学鉱物学教室氏家宏氏，東京大学地震研究所宮村摂三助教授，東京大学地理学教室多田文男教授，商工省地質調査所福田理技師，静岡県立榛原高等学校栗林沢一教諭，静岡大学教育学部佐々木清治教授，同文理学部望月勝海教授，同教育学部佐々倉航三教授，同学部土井喜久一助教授，研究資料を御提供下さつた各市役所・支所，町村役場の方々，御前崎測候所増田春備氏・鈴木秀雄氏・伊部良一氏，浜松測候所の方，及び各方面の諸氏，研究上の声援と便宜を与えられた静岡県小笠郡菊川北中学校長鈴木久氏，前校長戸塚博氏，前前校長中島清市氏を始め同校歴代勤務の皆さん，特に中野市朗氏，戸塚英一氏，旧静岡県小笠地方教育事務所の皆さん，執筆中の手助けをして下さつた菊川北中学校の生徒の皆さんなどの御厚意に頼る所が絶大である．又菊川町教育委員会，菊川北中学校 PTA，静岡県教育委員会，文部省等よりは研究費の補助を支給された．ここに銘記して深甚な感謝の意を表わす次第である．

II. 被害分布の研究方法

家屋被害分布の研究方法としては，

(a) 被害家屋個々の分布状況を調べる

(b) 被害率の分布を調べる

の二つが考えられる．この中 (a) では個々の被害家屋を，全潰・半潰というような段階別に，全地域にわたつて地図に記入すれば，被害分布の細密な総覧図が完成されて，被害分布研究の最基礎資料として，特に地盤の微細な変化を調べる上に役立つが，資料入手に困難があり，この度の調査では部分的に補助的な方法として用いたに過ぎない．（第 1 図）

(b) の被害率は，或る地区の被害家屋数の全家屋数に対する比率であつて，家屋が統計的に一様に近いと見られる場合にはそれによつて震度をおしはかることができるので，地震被害と地盤との関係を調べるのに好都合である．それ故この報告では被害率分布を調べることに主力をおき，具体的には，部落毎の住家全潰率分布を調べることにした．その理由は次の通りである．

(i) 部落を単位とした理由――部落は所謂小字(こあざ)の事で区(く)とも呼び，市街地では町内(ちようない)という．普通 20～30 戸から 60～70 戸で構成されるが市街では 200～300 戸或いはそれ以上の

第 1 図
磐田郡東浅羽村被害図
(同村鈴木末吉氏による)

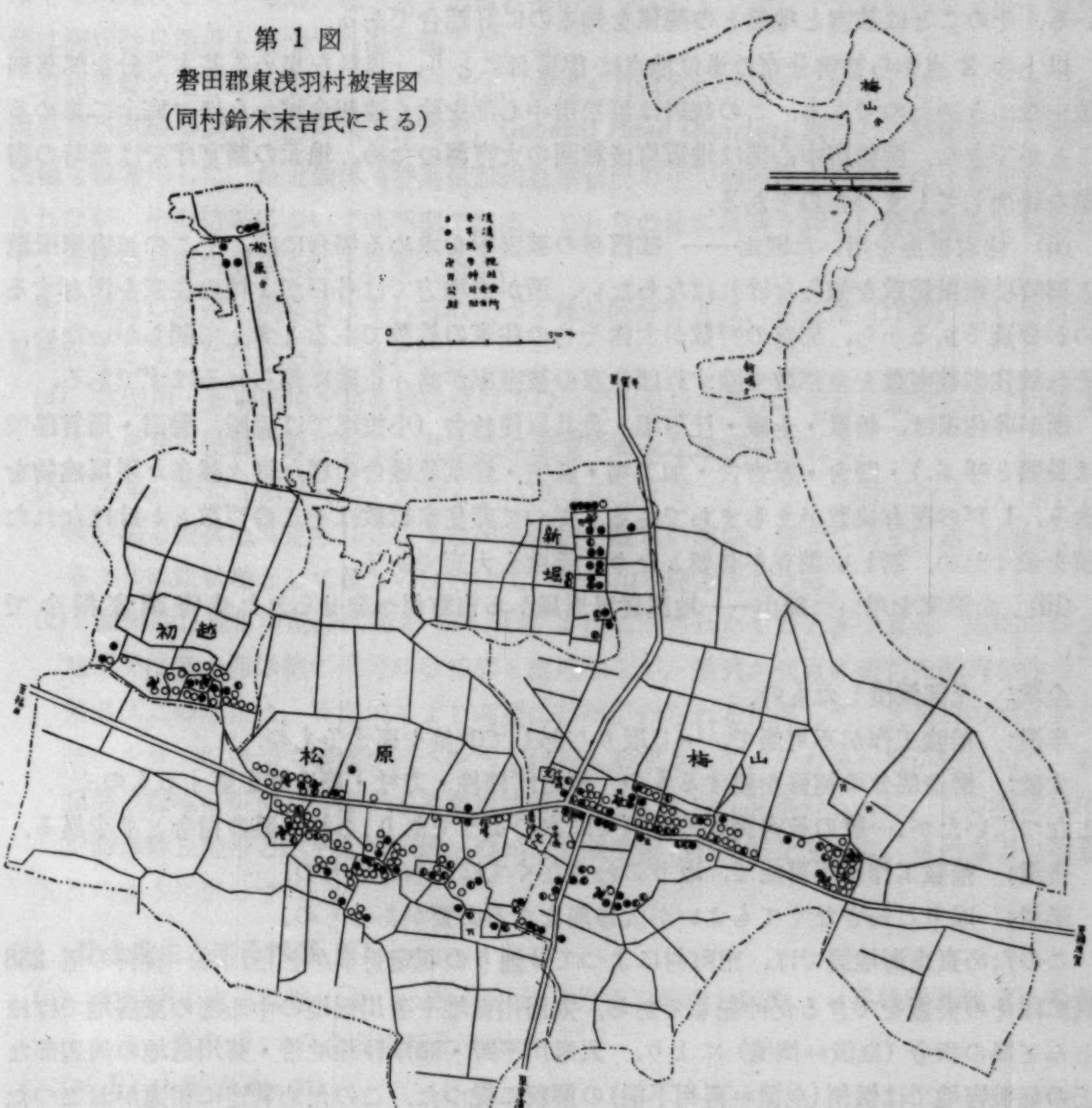

Fig. 1. Distribution of damaged houses in Higashi-Asaba Village, Iwata County. Black and half-black circles denote the totally collapsed and half collapsed dwelling houses, respectively, while circles denote undamaged ones.

こともある．部落の中には「組」又は「班」という小集団があつたが，地震直後各市町村で行われた管内の被害調査にそれを基にして被害集計をした町村はない．しかしながら部落単位に集計した被害数は，ほとんど全地域にわたつて求め得られた．

しかも 1 部落内の集落を見ると，当地方では同一地盤におさまつている所が多く，被害地 1 市[1] 116 町村内約 1,180 部落のうち凡そ 98% に当る 1,150 部落までがそうなつて

1)　浜松市　但し市役所直轄区域を除く．

いる．そのことは被害と地盤との関係を知るのに好都合である．

以上の 2 点から被害分布の単位地点は部落毎にとり，資料を集める基本方針を部落別被害数にきめたのである．この統計は浜松市中心部を除く遠州全域からほゞ完全に集めることができた．浜松市中心部は地震直後数回の大空襲のため，地元の諸官庁では当時の書類を焼失してしまつたのである．

(ii) 住家被害を用いた理由—— 部落毎の被害率を求める場合には，そこの被害家屋数と同時に家屋総数を知らなければならない．所が当地方では各戸が 1 棟の住家を所有するのが普通であるから，部落の戸数が大体そこの住家の総数であると考えて間ちがいない．それ故住家被害数を全戸数で除すれば住家の被害率が略々正確に得られるはずである．

所が非住家は，物置・土蔵・仕事場・農具収獲物舎（小笠郡では脇屋(わきや)，磐田・周智郡では長屋と呼ぶ．）・雞舎・家畜舎・加工場・温室・煙草乾燥舎の様な種々雑多な附属建物を含み，1 戸の所有棟数がまちまちである．従つて非住家総数はそこの戸数とかけはなれた値を示すため，新しい調査が必要となり，手数も大変である．

(iii) 全潰率を用いた理由——地震後県当局から市町村へ発せられた被害調査指令では，

全潰： 全部倒潰したもの．

半潰： 補強工作が不可能で，一旦取りこわして改築を要するもの．

大破： 構造部分の補修を要するもの，例えば控柱・方杖・筋違等を要するもの．

となつていたが，一般の被害調査の慣例では次のようであり，これは県の指令と多少異る．

全潰： 補強工作が不可能で，取りこわさなくてはならないもの．

半潰： 取りこわさなくてもよいが大修理をする必要があるもの．

このため東南海地震では，市町村によつて 2 通りの判定規準がとられた．資料の部 238 頁にはその実態をできるだけ記してある．太田川低地や菊川低地の中心部の激震地ではほとんど県の指令（全潰＝倒潰）により，天竜川平野・海岸砂丘地帯・菊川低地の周辺部などの軽被害地では慣例（全潰＝再用不能）の解釈に従つた．このため判定に相違がおこつたが，その程度は全潰に比べて，半潰の方が甚しく，例えば太田川低地の激震地磐田郡今井村の半潰は辛うじて立ち残つた程度のものをいうが菊川地方の或軽被害地では少しく傾斜したものや屋根瓦のつい落，ショーウインドウの破損まで半潰に含まれている．従つて町村によりまちまちの程度のひどい半潰をもとに全体の被害分布研究をするのはあまり好ましくない．また，前述のように高被害地ではどの町村でも県の指令によつており，県指令と慣例と両方が入乱れているのは，全潰率で見れば 20% 以下の低率におさまつてしまうので，大勢に影響が少くて工合がよい．以上の二点から被害率をば全潰率で表わすことにした．

III. 地盤の研究方法とその区分

遠江地方は北部の山岳・丘陵地域と南部の冲積平野地域に分けられる．南部の平野地域

はそこに起伏している第三紀丘陵や洪積台地によつていくつかの小平野に区分され，最外側は海岸砂丘地帯となつて外海に臨んでいる．

遠州平野の地盤区分をするに当つては，渡辺光(1942)の文献[2]を引用した．このほか静岡県農事試験場調査の静岡県土性図や，General Head Quarters 刊行の土質図東京・飯田図幅も参考にした．最近農林省静岡統計調査事務所の手で静岡県内の詳細な土質調査がなされたが，その結果については不明である．これらの他には余り詳しい地盤調査も見当らず，今後の研究が要望される次第である．

所で地盤の成因・状態及びそれらに基づく地盤区分などは，渡辺光 (1942) といささか見解がことなつた点がある．それは，

(a) 太田川・菊川低地を始め牧の原周辺の小河川沿岸低地は，それに述べられているような単なる侵蝕平野でなく，沈水性の埋積平野及び埋積谷である．

(b) 天竜川平野を扇状地といい切るには余りにも平坦であつて，勾配がゆるく，また，等高線も扇状地に見られるような同心弧状とは言い難い．従つて同文に述べられているように扇状地として扱うのはさけて，天竜川平野ととなえる．

(c) 海岸砂丘地帯の範囲は同著 218 頁第 2 図に示されたものと多少異る．遠江の砂丘地帯では多く海岸線に平行の砂丘部と湿地部とが，幾列か交互に帯状の配列を作る．筆者はこの地帯は，天竜川口より両翼に砂嘴が作られるに際して，天竜川のプログラデーションに伴つて砂嘴が沖へ沖へと何列も形成されて，その後一帯が陸化して，砂丘部と湿地部が交互に配列する海岸地帯ができたという見解のもとに，この地域全体を海岸砂丘地帯と総称し[3]，以上のべた文献や新しい見解をもとに，遠州地方の地盤を次のように区分する．

(1)　粘土を主とする地盤 (C)

(a) 太田川本支流低地 (Co, 一部 Go) 以下太田川低地と略称．一部砂礫質地 (G) の所もある．次の 5 つの地区に細分する．

(a-I) 中部 (Co-m)

(a-II) 南部 (Co-s)

(a-III) 北部 (Go-n)

(a-IV) 原野谷川地区 (Go-ha)

(a-V) 逆川地区 (Co-sk)

(b) 菊川低地 (Ck)

(c) 牧の原山麓小冲積地 (Cm)

(d) 浜名湖附近冲積地 (Ch, Sh) 一部砂質 (S) の所がある．

(2)　砂礫質地盤 (G)

---

2) 渡辺　光　東海地方東部沿岸地帯の地形誌　日本地誌学 (1942).

3) 氏家宏氏の教示に負う所が少くない．

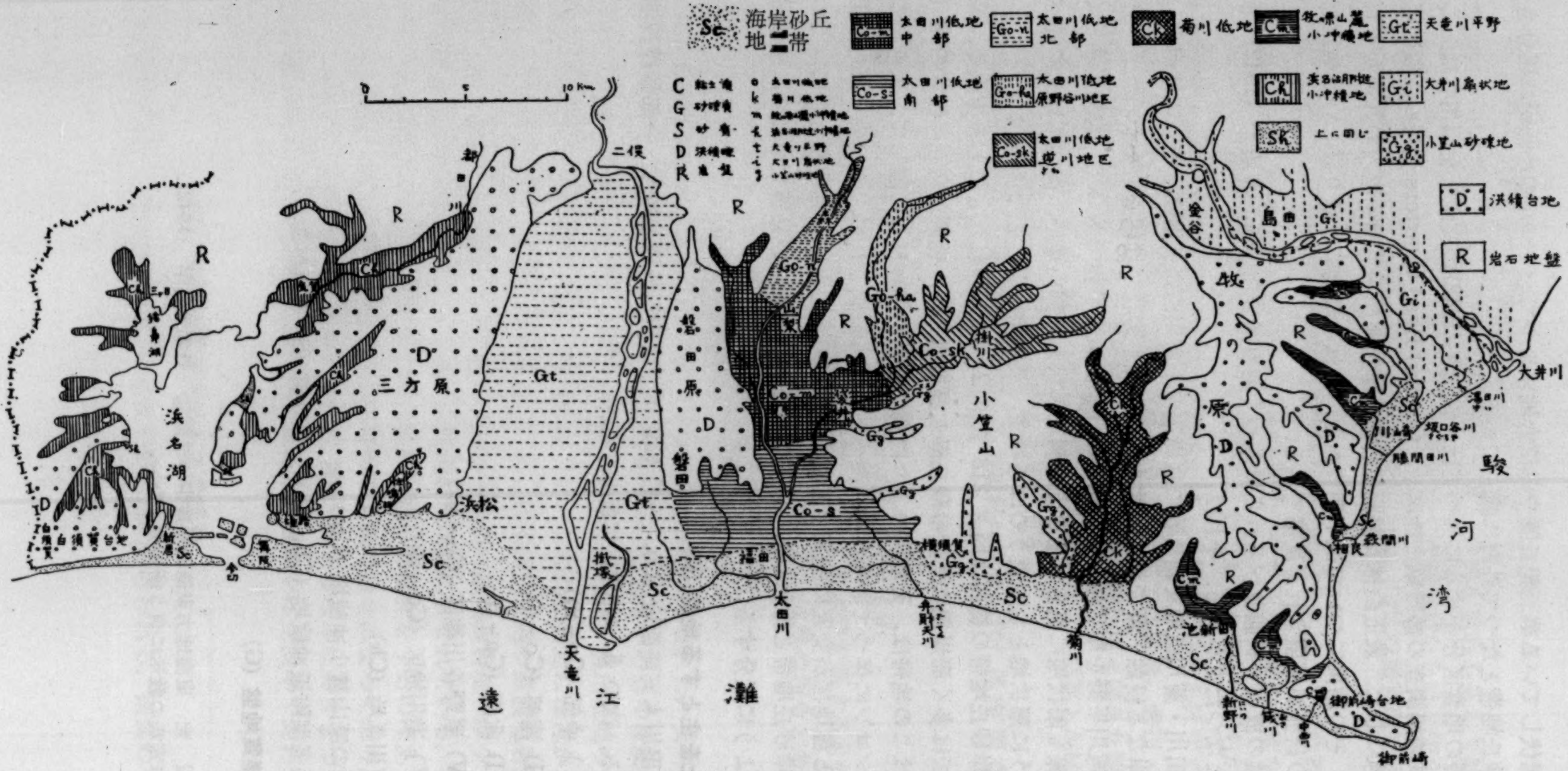

第 2 図　遠江地盤区分図

Fig. 2. Subsoil divisions in the province of Tōtōmi. C, S, G, D, and R denote the clayey, sandy, gravel, diluvial and rocky foundations respectively.

(e)　天竜川平野 (Gt)

(f)　大井川扇状地 (Gi)

(g)　小笠山附近砂礫地 (Gg)

(3)　**砂質地盤** (S)

(h)　海岸砂丘地帯 (Sc)

(4)　**固い地盤**

(i)　洪積台地 (D)

(j)　岩石地盤 (R)

以上のうち (a)～(h) はいう迄もなく冲積地である (第 2 図). また, 地盤の厚さは平地内の掘抜井戸の深さから推定した (第 3 図).

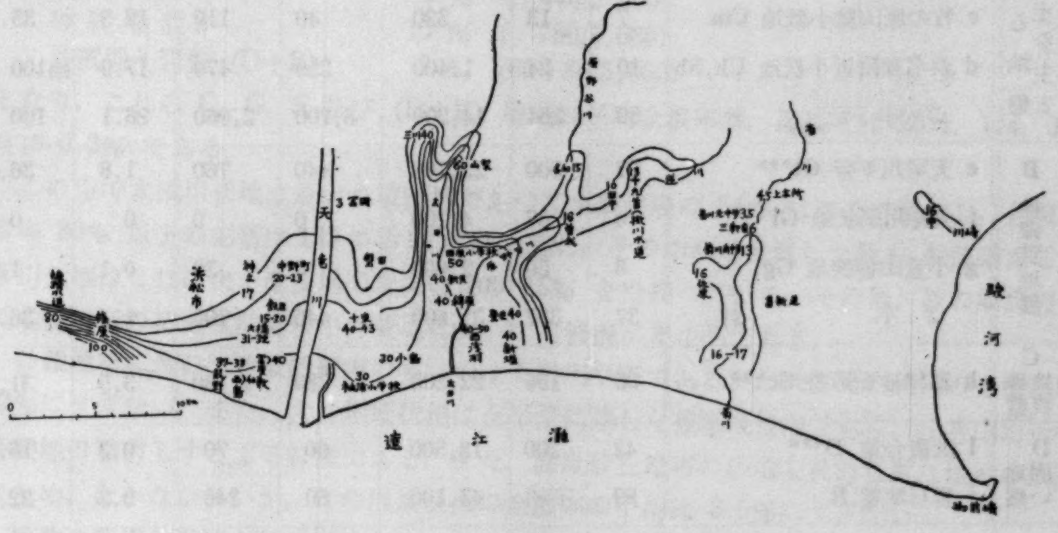

第 3 図　掘抜井戸の深度分布図 (単位＝間)

Fig. 3.　Distribution of the depth of artesian wells (unit in ken, or 1.82 m).

IV. 家屋被害分布の概況

東南海地震の全震域の家屋被害は

住家全潰	26,130	棟
同　半潰	46,950	〃
同　全焼	12	〃
同津波流出	3,059	〃

と集計されている[4]. また, 死人は 998 人であつた. 遠州地方では 当時の戸数約 166,000 戸の内, 次のような被害であり, 全域被害の 1/5 程度をうけていることがわかる.

4)　武者金吉　日本地震史料 (1951).

第I表 各地盤毎の被害集計表

Table 1. Statistics of damage to dwelling houses in different subsoil conditions.
Column 1: subsoil; 2: region; 3: total number of families; 6-i: number of totally collapsed houses; 6-ii: number of half collapsed houses;
7-i and 7-ii mean and maximum percentages of the same respectively.
Row A: clayey, B: gravel, C: sandy, D: diluvial or R: rocky foundations;
Σ: sum or total.

1 地盤	2 地域	3 市町村の数	4 部落数	5 戸数*	6 住家被害棟数** i 全潰	6 ii 半潰	7 住家全潰率 i 平均	7 ii 最高
A 粘土を主とする地盤	a 太田川低地 Co, Go	31	183	10,840	2,740	1,980	25.5%	100%
	b 菊川低地 Ck	12	44	1,700	670	400	39.4	91.7
	c 牧の原山麓小低地 Cm	7	13	320	40	110	12.5	35.4
	d 浜名湖附近小低地 Ch, Sh	10	24	1,400	250	470	17.9	殆100
	Σ 小計	59	264	14,200	3,700	2,960	26.1	100
B 砂礫質地盤	e 天竜川平野 Gt***	27	300	25,100	440	760	1.8	36.4
	f 大井川扇状地 Gi	4	37	4,100	0	0	0	0
	g 小笠山砂礫地 Gg	6	50	2,600	3	30	0.1	1.2
	Σ 小計	37	387	31,800	440	790	1.4	36.4
C 砂質地盤	h 海岸砂丘地帯 Sc***	35	196	22,200	780	1,130	3.5	31.1
D 固い地盤	i 洪積台地 D***	42	200	18,500	60	70	0.3	16.7
	j 岩石地盤 R	89	不明	43,100	80	240	0.2	22.2
	Σ 合計	154	不明	129,800	5,060	5,197	3.9	100

2 太田川低地の地区		3 市町村の数	4 部落数	5 戸数*	6 住家被害数** i 全潰	6 ii 半潰	7 住家全潰率 i 平均	7 ii 最高
a-I 太田川低地中部	Co-m	8	65	3,300	1,820	720	55.1%	100%
a-II 同南部	Co-s	10	39	1,800	770	530	42.8	90.4
a-III 同北部	So-n	3	27	1,900	40	70	2.1	16.1
a-IV 同原野谷川地区	So-ha	3	5	340	2	13	0.4	1.3
a-V 同逆川地区	Co-sk	8	47	3,500	110	650	3.1	33.3
Σ 計		31	183	10,840	2,740	1,980	25.3	100

* 1000 未満のものは 1 の位を，1000 以上のものは 10 の位までを夫々四捨五入した.
** 20 未満は実数を表わす. 21 以上は 1 の位を四捨五入した.
*** 浜松市内の浜松市役所直轄区域を除いてある.

住家全潰 5,183 棟
同 半潰 5,529 〃
同 全焼 3 〃

なお津波の被害はなく，死者は 221 人であつた．

第 1 表は遠江地方の地盤毎の被害合計を示し，また，第4図(附図)は部落単位の住家全潰率分布の状態をあらわしている．これらによつて，被害のほとんどが冲積地内に集中しており，更に太田川・菊川低地の様な粘土地盤に圧倒的に集中していることがわかる，そして同じ冲積地でありながら砂地や砂礫地にはあまり著しくない．また洪積台地や岩石地盤に至つてはすこぶる無事である．各地盤毎の全潰住家数の全潰住家合計数に対する割合は

粘土質を主とする地盤C	73 %	(3,700/5,060)
砂礫質地盤G	9 %	(440/5,060)
砂質地盤S	15 %	(780/5,060)
洪積地・岩盤 (D+R)	3 %	(60+80/5,060)

となり，これら C, G. S 及び (D+R) 地域の平均全潰率は，それぞれ 26.1, 1.4, 3.5 及び 0.2% である．

この中で太田川低地は最大の被害地であつて全潰住家の 54% はここに集結し，住家全潰率 80% 以上の部落は 183 の中 22 部落に達し，その中には全滅した所も 4 部落ある．菊川低地はこれに次ぐ激震地で全潰住家の 15% を受持つている．その他，牧の原周辺や浜名湖附近の粘土質地盤の小冲積地においても被害が集中的である．

砂礫地盤において比較的被害の多いのは天竜川平野であるが，同平野内平均の全潰率は 2%にすぎない．また，大井川扇状地は全半潰に達した被害は皆無であり，小笠山附近の砂礫地の被害もすこぶる軽微である．また，海岸砂丘地帯の砂地も被害総数は地域の広汎なため，なかなか多いが，この地域全体の全潰率の平均は 3.5%にすぎない．

地盤の堅固な洪積台地や岩盤などでは被害はまれである．

V. 各地域毎の家屋被害と地盤の状態

1. 太田川低地 (Co, Go)

太田川本流と，その支流原野谷川・逆(さか)川・敷地(しきぢ)川・仿僧(ぼうそう)川及び弁財天(べざいてん)川一帯の平地であつて，遠江第2の広さを持つ，この低地の上流部は丘陵や台地に囲まれているが，下流部は南の海岸砂丘地帯や西の天竜川平野に接続する．そして海岸砂丘地帯との境界は小笠郡横須賀町・磐田郡福田(ふくで)町・同掛塚町を結ぶ 2 号国道沿いの集落の北限を結ぶ線とし，天竜川平野へは磐田原台地西南端磐田郡磐田町天竜・上岡田・下岡田・中野等を結ぶ線で漸移する．

この低地には地震当時磐田・周智(しゆうち)・小笠 3 郡の 31 町村が存在していて，183 部落 10,800 戸の住家があり，そのうち全潰 2,740 棟，半潰 1,980 棟，従つて全潰率は 25% となり，最高の被害地である．

町村単位に被害数を見ると，磐田郡袋井町（市町村の名称と区域は地震当時のものを用いてある．）が最高で，1,920 戸中住家全潰 575 棟，同半潰 142 棟で，これは名古屋市・清水市に次いでの高被害数である．磐田郡今井村は 336 戸の住家中やつと立残つた 14 棟を残して倒れ尽した．従つて全潰率は 95.8% となり，市町村単位に見ると全地震区域第 1 の高率である．低地内の高被害率の町村を列挙すると，

町村名	住家全潰率	(住家全潰数/戸数)
1. 今井村	95.8 %	(322/336)
2. 南御厨(みくりや)村	63.8 %	(167/271)
3. 田原村	45.7 %	(167/384)
4. 山梨町	39.0 %	(244/626)
5. 上浅羽村	38.1 %	(217/575)
6. 久努西(くどにし)村	34.5 %	(182/576)
7. 向笠(むかさ)村	33.1 %	(122/369)
8. 袋井町	31.5 %	(575/1,920)
9. 西浅羽村	30.7 %	(131/391)
10. 久努(くど)村	28.3 %	(180/639)

この低地の被害分布を検討して見ると，それは各部分によつて一様ではない．それらに応じて，a. 中部(Co-m) b. 南部 (Co-s) c. 北部 (Go-n) d. 原野谷川地区 (Go-ha) e. 逆川地区 (Co-sk) に区分する．

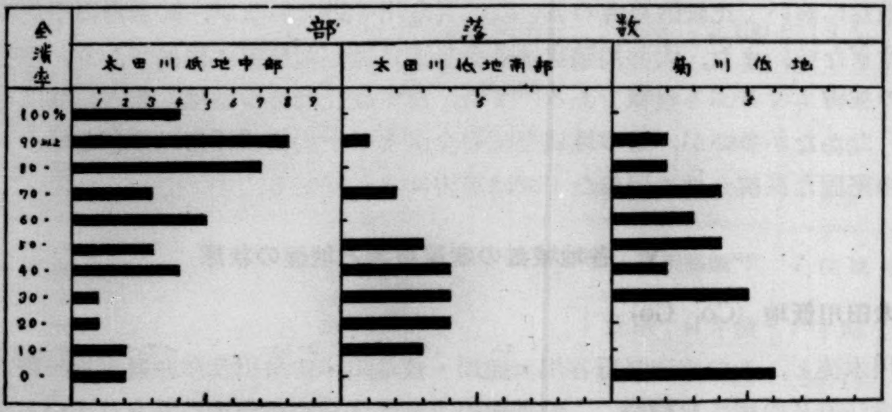

第 5 図　全潰率 10% 毎の部落数

Fig. 5. Frequency of damage percentage in the middle part of the Oota-gawa basin, southern part of the same and in the Kikugawa basin.

(a) 太田川低地中部 (Co-m)

太田川口から約 8〜18 km 上流の間で，東海道線沿いの磐田郡御厨村新貝・田原村新池を結ぶ線以北から山梨町あたりまでの本流沿いと，袋井以東 3 km ほどの磐田郡久努村久津部・貫名を結ぶ線までの原野谷川沿いと，敷地川沿いの範囲である．この地区は前記

の今井村や袋井町を含む最激震地で，8 町村 65 部落，約 3,300 戸中住家全潰 1820 棟，同半潰 720 棟の被害を出した．従つて全潰率は 55.1% で，今全潰率を 10% 毎の級別に部落数を数えると第 5 図の様になり，高率の部落の多いことがわかる．

ここでは震度がずい分大きかつたらしく，高さ約 5 m の太田川堤防は今井村地内で崩落し，やつと通れる程度の幅を残しただけとなり，また，袋井町東方の東海道線の高さ数 m の築堤はすつかり埋没してしまつた部分もある．

被害家屋の分布状況は低地のすみずみまでひろがり，特に磐田原台地に接した側では，大ていその裾ぎわまで倒されている．この方面の磐田郡向笠（むかさ）村・田原村・御厨（みくりや）村等の内で，里と呼ばれる低地側と原と呼ばれる台地上にまたがる部落の部分を比較すると，被害のコントラストが顕著である（第 6 図）．もつとも里側でも台地裾の岩盤上の家や，それに極く接近した家は無事である．同様な有様は袋井町でも見られる．ここでは低地内の大字（おおあざ）袋井・川井が平均 77% の全潰率を示しているのに反して，段丘上の高尾では 2% ほどに過ぎない（第 7 図）．

(b)　太田川低地南部 (Co-s)

大体東海道線附近の田原村彦島・松袋井以南の地区で，10ヶ町村 39 部落 1,800 戸中，住家全潰 770 棟，同半潰 530 棟の被害を出した．全潰率は 42.8% で，上流側の低地中部より軽い．全潰率 10% の段階毎の部落数を調べて見ると，（第 5 図）高率地もあるが，低率地が仲々多い．この南部地区が中部地区より軽被害の理由は不明であるが，ここが海岸に近い関係から，地下に砂層の存在する事も考えられ，この地域の地下探査が要望される次第である．

(c)　太田川低地北部 (Go-n)

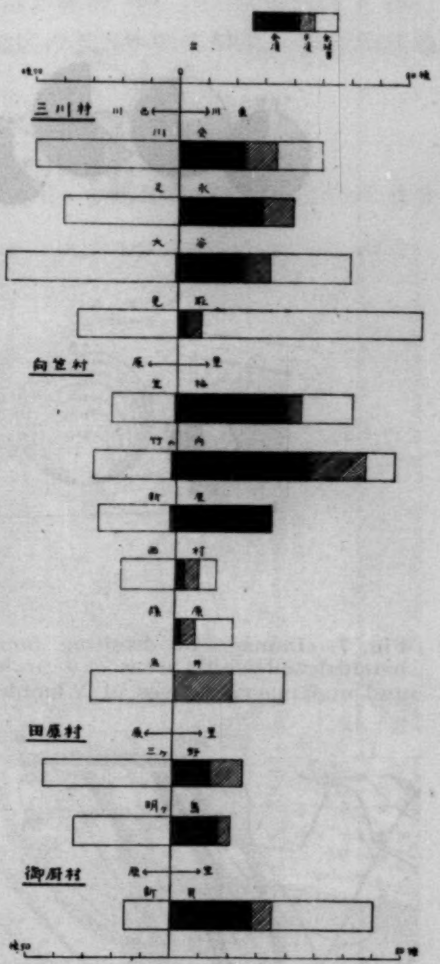

第 6 図　磐田原台地と太田川低地とにまたがる部落の住家被害

川東＝三川村内敷地川以東の低地部
川西＝　〃　以西の山麓部
里＝向笠・田原・御厨村の低地部
原＝　〃　の台地部

Fig. 6.　Contrast of damages of dwelling houses in the parts on the Iwatahara Plateau (left) and the parts in the Ootagawa basin (right) of the same hamlets. The lengths of the black, hatched and white bars, respectively, denote the numbers of totally collapsed, half collapsed and undamaged dwelling houses.

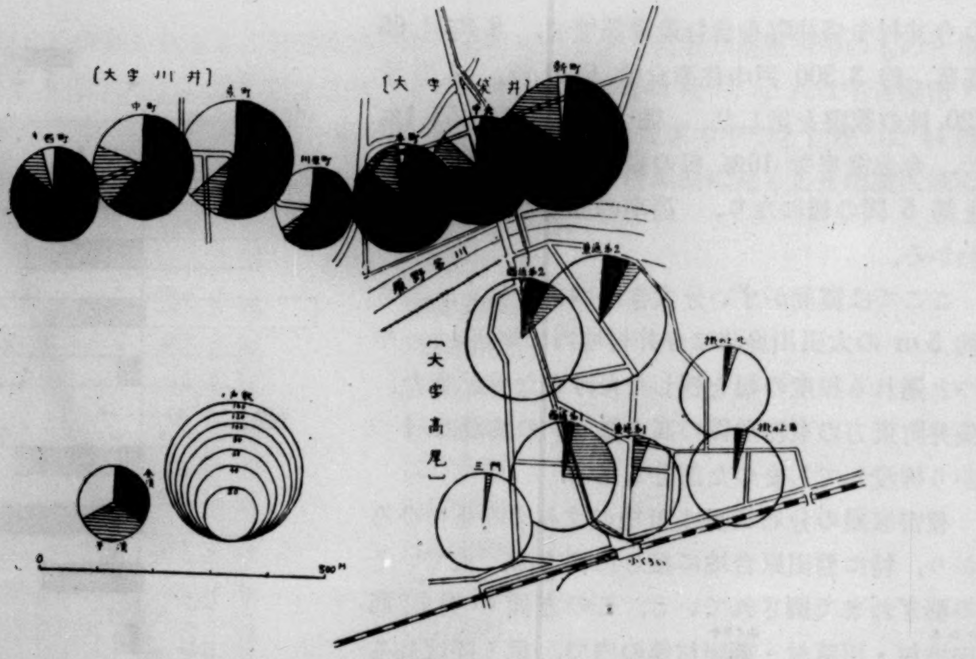

第7図 磐田郡袋井町の被害

Fig. 7. Damage of dwelling houses in the Fukuroi Town, Iwata County Black, hatched and white areas of a circle represent the numbers of collapsed, half collapsed and undamaged houses of a hamlet.

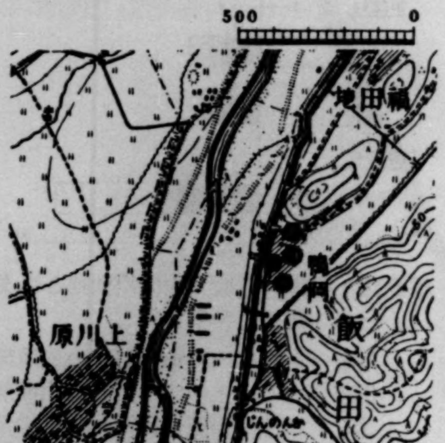

第 8 図 周智郡飯田村鴨谷（＝鴨岡）部落の全潰住家（● 印）

Fig. 8. Location of totally collapsed houses at Kamoya Hamlet, Iida Village, Shūchi County,

山梨町北端から森町までである．この地区では周智郡森町・飯田村・園田村 3 ヶ町村の部落が関係し，被害数は住家全潰 38 棟，同半潰 71 棟，全潰率は 2.1% である．この地区が中部に比べて震害が軽いのは，集落が山沿いにかたよつている事と，ここの地盤が砂礫質に変つているためであろう．少しく掘ると礫層につきあたるという部落もある．

飯田村鴨岡では 40 戸中住家全潰 4 棟，同半潰 13 棟に達し，近隣の部落に比して幾分被害が目立つ．ここの被害家屋は北東に分岐する小支谷の出口に集中しており，多分その支流が本流の堆積に閉塞されて湿地化され，細泥質の堆積を促したためであらう．(第 8 図)

園田村谷中(やなか)部落の一部分である田中では 10 戸中 8 戸倒れ，部分的に高率である．

(d) 原野谷川地区 (Go-ha)

これは太田川支流原野谷川中流の部分で，小笠

郡和田岡村・原谷(はらや)村・原田村内の5部落が関係し被害は戸数約 340 の内住家全潰 2 棟，同半潰 13 棟，全潰率は 0.4% で軽微である．この地区の被害が軽いのは，太田川低地北部と同様に，ここの冲積層が砂礫質のためであろう．

(e) 逆(さか) 川 地 区 (Co-sk)

原野谷川の支流逆川沿いの平地で，支流垂木(たるき)川・倉真(くらみ)川・初馬(はつま)川等の平地もこれに含め

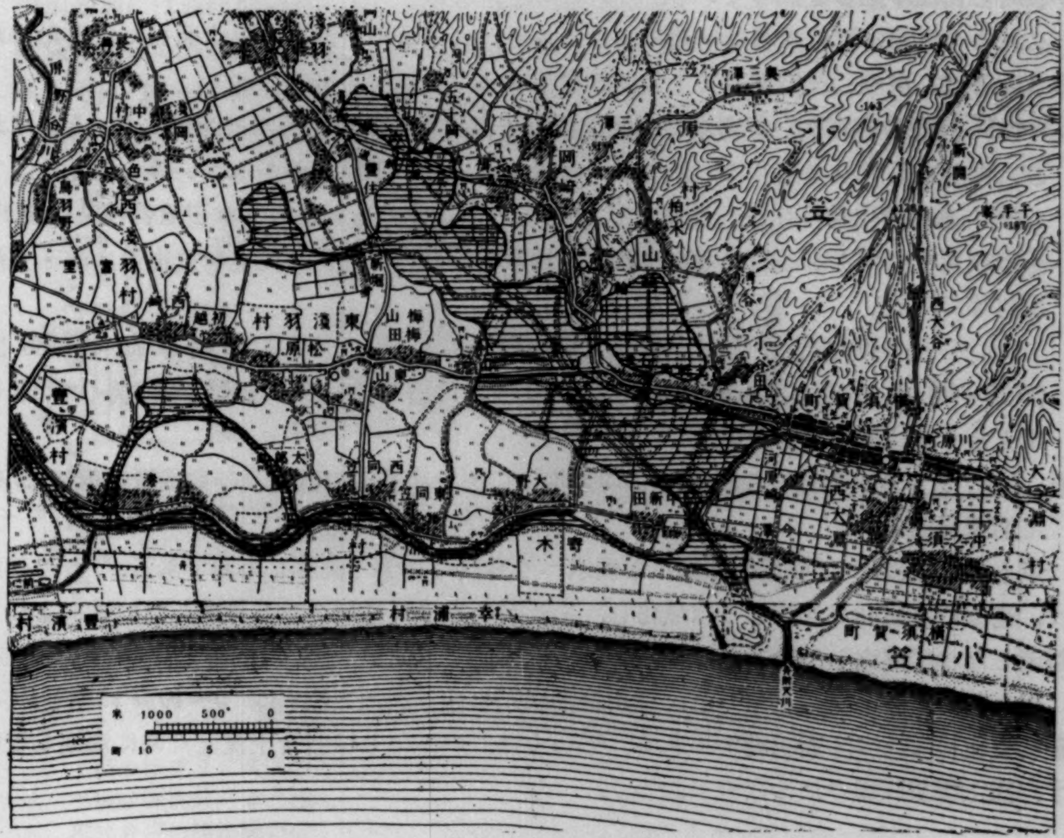

第 9 図　18 世紀中頃の横須賀浅羽地方の湛水区域　(平行線の部分)

Fig. 9. Area which was covered with water in the middle of 18th century in the Yokosuka-Asaba District.

る．ここには小笠郡掛川町を始め 8 ヶ町村部 74 落があり，3,470 戸中住家全潰 113 棟，同半潰 645 棟の被害があつた．ここで目立つことは，全潰率は 3.2% でさ程でないが，それに比べて半潰被害の多い事であり，半潰率は 15.9% にも達する．東海地震より 90 年昔の安政地震の際には，このあたりではおびただしい全潰家を出し，中でも掛川宿は全倒の上発火し，烏有に帰した．安政地震後丈夫な家が建てられたのによるか地盤及び地震の特性が違うか，興味ある問題である．

激震地太田川低地には，最近まで広い湖水を湛えていたことが文献の上からも地形・地質の上からも証明できる．第 9 図は小笠郡横須賀町及び磐田郡東浅羽村に残る古地

図[5]のスケッチや写真図に基いて画いた17世紀中葉の湛水区域である．この入江は他の多くの古図にも描かれ，その1部は1879年（明治12年）発行の地図[6]に迄残存して記入されている．

他の古図[7]には磐田郡磐田町見付(みつけ)附近の今之浦川上流にも今之浦という湖が記入されている．現在においてもここから南部一帯は広い沼田で，その一部には大池（約1,200 ha）が往時の湖面の面影を止めている．

これらの湖沼は更に大昔は一連のものであり，この低地一面に広い水面をたたえたであろうとこは，次の二三の例証で十分に推察できる．

(a) 貝塚の存在[8]．磐田原の南縁磐田町や御厨(みくりや)村には数ヶ所に貝塚があり，それはおびただしいしじみの集りで，あさり・はまぐり・はいがい・かがみがい等も混える．

(b) 水草炭化物の存在．当地方で，まこもとか，すくもとかいう水辺植物の炭化物が，土地改良や河川工事の際に掘出される．周智郡宇刈(うがり)村・磐田郡向笠(むかさ)村笠梅の大海(たいかい)・上浅羽村等である．

(c) 一連の細泥層．一帯にきわめて粘土質である．そしてこの層厚は40〜50間（=72〜90 m）に達し，かなり厚い．このような地層の成立は，沈降性の内湾の水面を考えなくては説明できない．

(d) リヤス式山麓線の地形．この低地にのぞむ小笠山の西麓及び磐田原南裾において明瞭である．

以上要するに，この低地は静かな湖水への堆積によつて成立したのである．この湖水は，過去の侵蝕面が沈降して水域化し，それが西方の天竜川口から伸展した砂嘴によつて潟湖となつて成立したのであろう．

但し被害の軽い低地北部や原野谷川地区は川の流れが急で傾斜は5〜10‰に達し，堆積物も粗粒であつて扇状地的である．恐らくはこのあたりは割合上流なために海進も受けず，陸上堆積区域のためなのであろう．

2. 菊 川 低 地 (Ck)

遠江東部の小流菊川下流には長さ12〜13 kmばかりの狭長な低地を伴うが，ここは太田川低地に次ぐ被害地である．菊川は西方川・上小笠川・佐東川・牛淵川・丹野川等の支

5) 横須賀附近は1648（正保5）年に描かれた横須賀城附近の地図．このスケッチが下記の論文中に記されている．
多田文男「遠州灘沿岸横須賀附近の海岸地形」地理学評論 **19** (1943), No. 12, 6.
浅羽地方は1686（貞享3）年に画かれた浅羽堤に関しての論争と公儀からの裁許状に附随した地図．これの写真図が下記の書の巻頭に掲げられている．
原田 和 白羽草 (1937).
6) 関川美建編 郡画改正 遠江精細全図（1879=明治12年）.
7) 五雲亭貞秀 東海道写真五十三次勝景 島田より白須賀まで（1800=万延元年）
8) 静岡県磐田市発行磐田市史編纂執委員会編纂 磐田市史上巻 (1954), 7-15.

流をもち，それぞれが谷平地を伴うのでこの低地は全体的に樹枝状を呈する．土質は皆粘土質である．なお低地の南側は海岸砂丘地帯に接する．

この低地には 12 ヶ町村 44 部落が関係し，約 1,740 戸の内，受けた震害は住家全潰 671 棟，同半潰 400 棟，全潰率は約 38.6% で，太田川低地中部には及ばず，同南部の 42.8% に匹敵する．太田川低地には全潰率 80% をこえる所が 183 部落中 22 部落もあるのに，こちらには 44 部落中 4 部落を数えるだけである．(第 5 図) 震度そのものも太田川低地には及ばないらしく，堤防や道路の崩落はない．これには粘土層の厚さが大きく関係している様に思われる．即ち太田川低地の最厚 40～50 間 (=72～90 m) に比してこちらでは 16～17 間 (=28.8～30.6 m) である．

粘土層の厚さと震害との関係を調べて見ると，前記の 16～17 間 (=28.8～30.6 m) 附

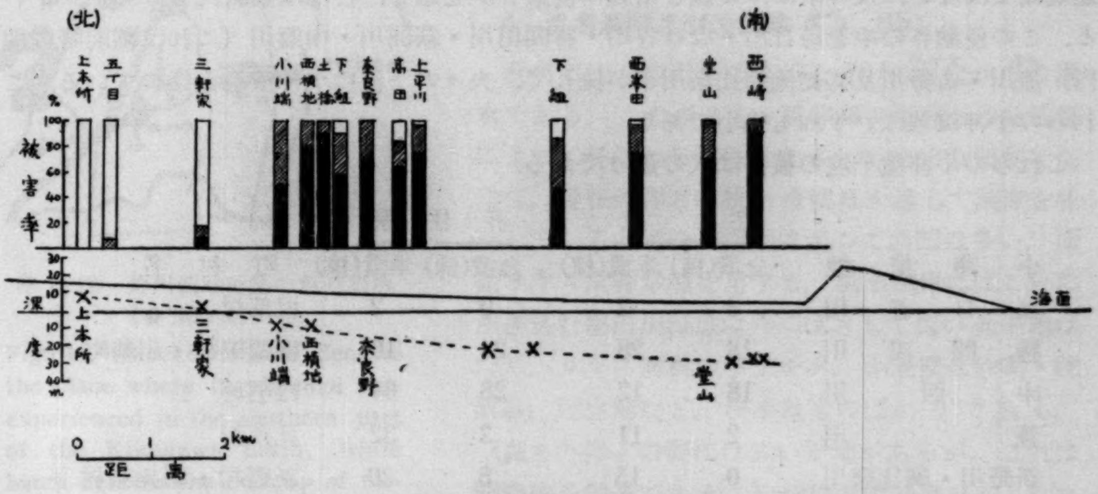

第 10 図 菊川低地の粘土層の厚さと住家被害率との関係

上段の棒グラフは低地内の部落の住家被害率を示し，黒は全潰，斜線は半潰をあらわす．下段は掘抜井戸より推定した粘土層の厚さを示し，破線が粘土層の下底をあらわす．×は掘抜井戸の採水層の高さである．(下段は三井・大谷 1950 による．)

Fig. 10. Relation between the thickness of clayey overburden and the damage percentage of dwelling houses in the Kikugawa basin. Solid line and dotted line respectively denote the surface profile and the lower boundary of the clayey overburden.

近が最甚で 93.3%，北上して地層がうすくなるにつれて震害も軽くなり，7 間 (=12.6 m) の厚さの小川端で 50 % となり，6 間 (=10.8 m) の三軒家で 8.1% に減じ，ここが全潰被害の北限である．但し途中小笠郡横地村の土橋 (91.7%)，西横地 (81.0%) は異常的に高率となつている．(第 10 図)

下流方面の激震地のまつただ中に，いささかの被害もうけない所が 4 ケ所 26 戸ある．それは小笠郡平田村東峰田の 7 戸，同堂山の 17 戸，戸同西ヶ崎の 1 戸，同郡中村高塚の 1 戸等である．これらの土地では沖積粘土層の中に，堅固な第 3 紀層の基盤が地表近

くまで高まり，その上に家屋がのつているためである事がわかつた．これ等の個所では 90 年昔の安政大地震の時も無事であつた[9]，(第 11 図)

第 2 の激震地菊川低地にも，そこに潟湖が存在していた事が知られている[10)11)]．厚い粘土層は上流の堀之内附近にまで達し，大昔には太田川低地と同様にこの盆地に広く湖水をたたえていたものであろう．

3. 牧の原山麓小沖積地 (Cm)

牧の原は小笠郡淡ケ岳 (514 m) 附近より南々東御前崎方面に向つてのびる長さ 20 km ばかりの台地で，高さは北部で 250 m，南下するにつれて低下し，池新田附近で 80 m 位にさがる．なお御前崎の半島も 30〜50 m の高さの台地であるが，これは牧の原の連続面ではない．牧の原には東麓と南麓に侵蝕谷が発達し，台地は幾脈にも分岐している．この侵蝕谷の中を湯日川・坂口谷川・勝間田川・萩間川・中西川 (これは御前崎台地内) 筬川・新野川及其支流朝比奈川等が流れて，夫々の下流に小沖積地を伴つている．これらの小沖積地はいずれも狭小である．

これらの小沖積平地の被害は次の通りである．

小沖積地	住家		非住家		町村名
	全潰(棟)	半潰(棟)	全潰(棟)	半潰(棟)	
坂口谷川	3	2	9	2	坂部村
勝間田川	18	28	24	16	勝間田村・川崎町
中西川	18	12	28	64	白羽村
筬川	2	11	2	32	比木村
新野川・朝比奈川	0	15	5	20	新野村・朝比奈村
計	41	68	68	134	

この中榛原郡川崎町庄内では 48 戸中住家全潰 12 棟，同半潰 17 棟，従つて全潰率は 35.4% で相当高率である．ここでの粘土層の厚さは約 16 間 (=28.8 m) ある．榛原郡白羽村中西では 79 戸中住家全潰 18 棟，同半潰 43 棟，全潰率は 22.8% である．この村の判定は全潰=倒伏の意で，半潰の内殆全潰を加えると全潰は 34 棟となる．この平地は一見砂地であるが，1 m 程下には青粘土層があるという事である．これらの小沖積地にも次に示す証左によりやはり過去に湖水をたたえていたものであろう．

9) 現小笠郡小笠町役場宮城正男氏による．
10) 増田又右門衛・増田 実 高天神城戦史 (1953)，68.
この書には 1571 年 (元亀元年) 武田信玄が塩買坂 (現小笠町磯部) から高天神城 (現城東村) を攻めるに当り菊川の川下を探索した所大きな池があり，その下に国安の渡し，その上に獅子ケ鼻の渡しがあつたと記してある．国安の渡しは小笠郡千浜村国安，獅子ケ鼻の渡しは同郡中村大石と考えられ，両者は約 4 km の距離がある．
11) 三井嘉都男・大谷成夫 「遠州菊川流域の地下水」 資源科学研究所彙報 **15** (1950).

(a) 古文献[12]: 勝間田川・萩間川・新野川平地等について，内山真竜著遠江風土記伝にその記載がある．

(b) 独木舟の出土
新野川沿いより出土した．

(c) 水辺植物の埋れた層
勝間田川平地に存在する．

(d) 水辺に関係ある地名
勝間田川平地勝間は加都間で，水草の意．萩間川平地の大江，海老江．新野川平地の池新田等．

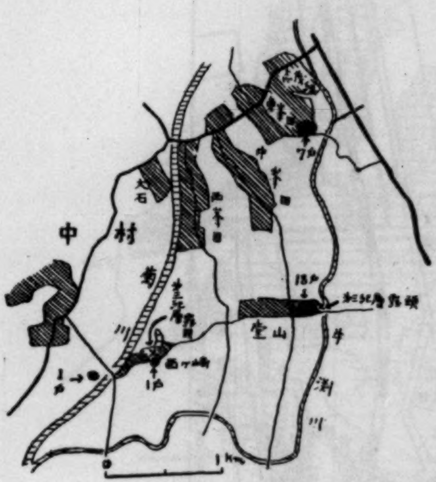

第11図　菊川低地南部の無被害地（● 印）

Fig. 11. Blackened area denotes the place where no damage was experienced in the southern part of the Kikugawa basin, while hatch denotes the outcrop of tertiary formation.

4. 浜名湖附近小沖積地 (Ch, Sh)

浜名湖は遠州西部に拡がる 70 km² ばかりの湖水である．この湖はもと遠州灘の海湾が砂丘地帯によつて外洋から切りはなされて出来た潟湖であつて，現在外洋とは狭い今切口を通じて潮流を吐呑している．湖の平面形は至つて凸凹の多い，所謂リヤス式海岸線を呈する．浜名湖岸にはこれに注ぎ込む都田川流域以外にはさして広い低平地はなく，リヤス湾奥の小デルタ，小規模な砂嘴・陸繋島，埋立地など，狭小なものばかりである．（湖と外洋との間には広い平地があるが，これは海岸砂丘地帯である．）近時湖面開発が盛んになり，各所に埋立地や干拓地が現出しつつある．

これらの小沖積地の被害棟数は次の通りである．

	住家		非住家	
地区	全潰(棟)	半潰(棟)	全潰(棟)	半潰(棟)
鷲津町	68	190	8	13
入出村	71	192	20	12
村櫛村	82	58	12	11
都田川平地	10	8	6	11
その他の平地	12	19	5	18
計	243	476	51	65

上記の統計には背後の岩盤や洪積層の被害数が含まれている疑いもある，従つて実数は

12) 栗林沢一教諭の教示による所多大である．

これより稍少いであらう．

沿岸小平地では全体的に見てこの様に被害は多い方ではない．密集被害地もたくさんはない．被害の目立たない理由として，次の様な事が考えられる．即ちここの集落を見ると，どの家屋も好地盤の山地や台地のへりに接して建てられている．また，砂嘴や陸繋島

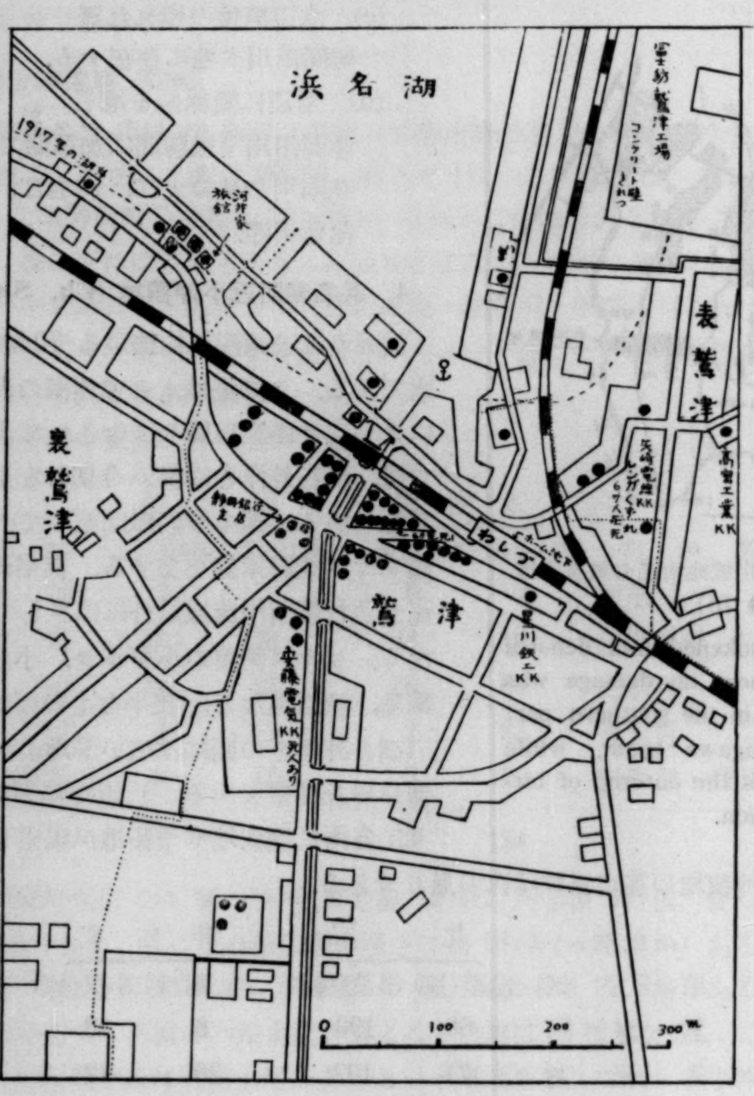

第12図 浜名郡鷲津町中心部の倒家分布図（黒丸） 柴田保司氏による．

Fig. 12. Distribution of totally collapsed houses (black dots) in the central part of the Washizu Town, Hamana County,

は砂質で地盤はよい．埋立地には家屋は少い等である．

局部的な高被害地としては，浜名郡鷲津町・入出村・次いで村櫛村等が挙げられる．鷲津町では国鉄鷲津駅前の繁華街に密集被害を出した（第12図）．また入出村でも湖に面した埋立地に密集被害を出した．村櫛村でも埋立地上の北明部落に被害が多かつた．（ここ

の仲町は旧砂嘴[13]に乗るため被害は少い.）

浜名湖に注入する都田川は，湖北の古期岩石山地から発する湖岸第一の長流である．こ

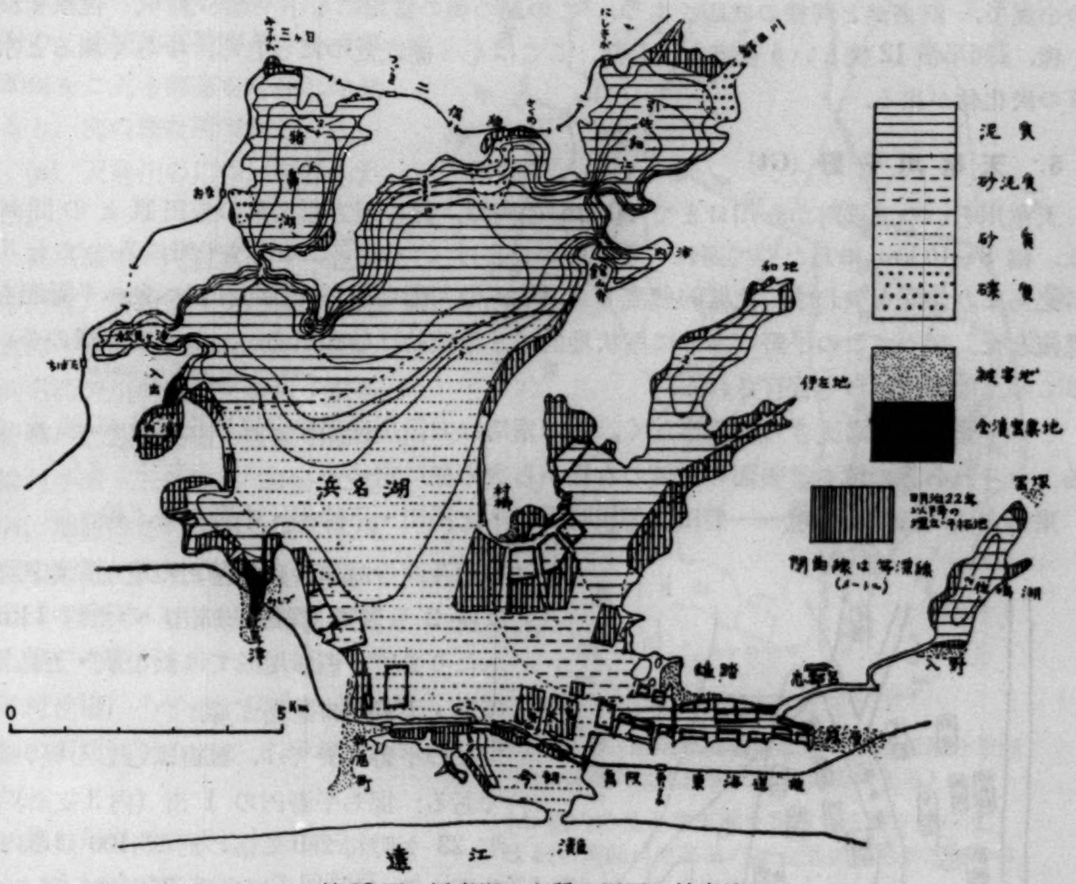

第13図　浜名湖の底質と周囲の被害地

Fig. 13. Distributions of bottom deposits in the Lake Hamana area, and heavily (solid) and lightly (dotted) damaged area in the vicinity. The hatched area with vertical thick lines denotes the land reclaimed since 1889.

の川沿いでも被害は少く，2 町村 7 部落 400 戸ばかりの中住家全潰 10 棟，同半潰 8 棟にすぎない．ここの被害の少い理由は冲積層の被覆のうすい事も関係しているのであらう．

以上のべた以外の小冲積地，即ち沿岸の伊佐見・和地(わぢ)・東浜名・三ケ日(みつかび)・知波田・太田川沿い・笠子川沿い等リヤス湾奥のもの，新所(しんじょ)・入出村内浦湾口・村櫛村仲町等の旧砂嘴，堀江の陸繋島，及び各地の埋立地等でも被害は少い．

浜名湖岸諸低地の被害分布を湖の底質[14]と比較してみると，両者は密接な関係がある．即ち鷲津・入出のような被害密集の所は，いずれも湖底が泥質水域のほとりである．村櫛の様な被害地は砂泥質である．浜名湖は今後急速に陸化させる計画といわれるが，その場

13) 村櫛小学校に掲示された明治初年の地図による．
14) 浜松測候所　浜松湖観測調査報告第 1 報　第19図底質分布図 (1937).

所へ建築するに当つて既往の底質に充分留意する必要がある．(第13図)

佐鳴湖附近小平地について．佐鳴湖は浜松市西方4kmばかりの所にある約1.5平方kmの小湖で，浜名湖と同様の成因をもつ．この湖の奥の富塚にも小平地があり，住家全潰2棟，同半潰12棟という被害を出した．ここはもと湖底だつたらしく，少しく掘ると水草の炭化物が出る．

5. 天竜川平野 (Gt)

天竜川ぞいの二俣町から川口まで20kmの両岸，西の三方原と東の磐田原との間には，幅8〜10kmにわたつて遠江一の平野がひらけている．この川は平野に入つても川口迄あまり勾配を失わず，比較的急流で1.4‰の勾配を保ち，往時は西へ東へ平野内を乱流した．従つてこの平野は多分に扇状地的で，堆積物は砂礫が多い．この事は畑の多いここの土地利用からも首肯される．

この平野は東西さえぎられる事なく，その南部は太田川低地や海岸砂丘地帯に接続する．今それらとの境を，表面の土質の有様から次の様に定める．

東の太田川低地との境——磐田郡磐田町天竜・上岡田・下岡田・中野を結ぶ線．

南及西の海岸砂丘地帯との境左岸地区では現2号国道(掛塚—福田)の北約1kmあたりまで．右岸地区では浜松駅・五島村西島・天竜川口を結ぶ線．

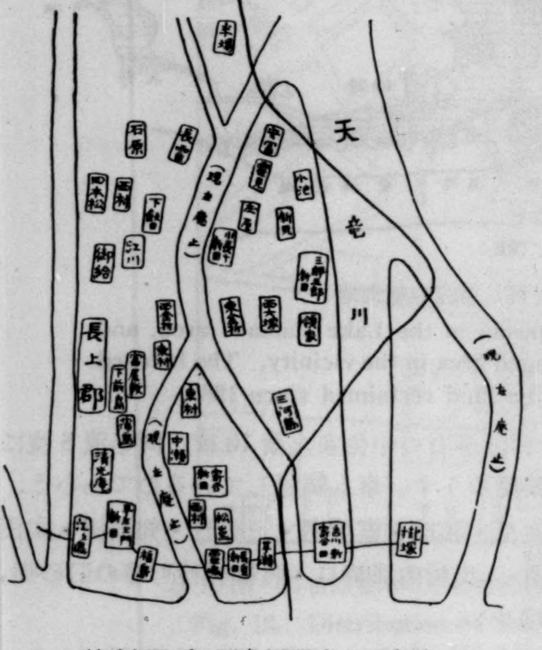

第14図 A 天竜川下流の旧水路
(浜松市 内田六郎氏所蔵 1838 (天保 8)年千尋作遠江国全図の部分的なスケッチ)

Fig. 14. A. Former course of the River Tenryū near its mouth based on the map made in 1838.

この平野に於ては，被害はむしろ軽い方である．即ち平野内の1市(内3支所)3町23ヶ町村280部落の約25,100戸の内，住家全潰440棟，同半潰760棟，従つて全潰率は1.8%となり，全潰率20%をこえる部落は13ヶ所にすぎない．なお全潰分布範囲は天竜川口より上流11kmの線以南に限られ，下流に向うに従つて漸増の傾向である．

天竜川平野に被害が軽い理由は，ここの土地が砂礫質であるためである．太田川・菊川低地等が沈水した時代にも，ここでは上流からの多量の運搬物のためにあまり海進をうけず，おびただしい陸上堆積を続けたものであろう．従つて恐らくは，表層から下底まで厚い砂礫層が続いているであろう．なおこの厚さは掘抜井戸の深さから察

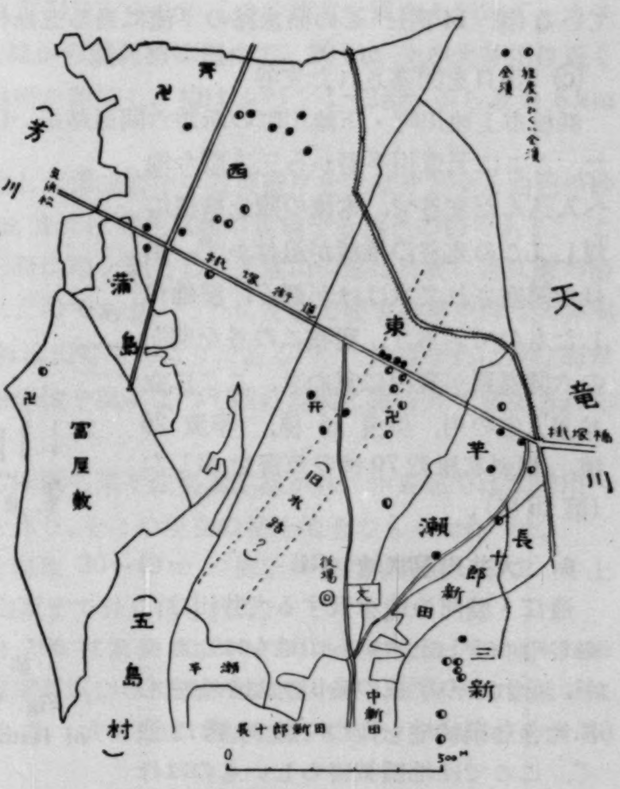

第14図 B　浜名郡河輪村北半の全潰家屋分布図
（現浜松市河輪支所石川氏による）
（A 図内の長上郡東村を貫通する廃止河川は，B 図の河輪村東部落内の全潰家屋密集部分の位置を流れていたものであろう.）

Fig. 14. B.　Distribution of damaged houses in the northern part of the Kawawa Village, Hamana County.　Dotted lines show former river course from Fig. 14. A.

して最厚 40 間 (=72 m) 以上に達すると思われる.

全般的に被害の軽いこの平野内の，比較的高被害の，全潰率 20% をこえる部落を吟味して見ると，次の様な所である.

(a)　天竜川の川岸に近接した所.

浜名郡中ノ町村富田・一色（いつしき）・中野町，磐田郡十東村高木・堀之内・平間（ひらんま），磐田郡掛塚町西堀，浜名郡芳川（ほうがわ）村老間（おいま）・金折（かなおり）・東金折等の部落である. 又浜名郡河輪村芋瀬（いもせ）・三新（さんしん）等も 20% に近い. 地震のさい川岸各地では地盤の亀裂，田畑の隆起・陥没，道路の沈下・砂まじりの水の噴出等の地変があらわれ，旧中ノ町村役場，小学校，病院等は地盤の不同沈下によつて半潰した.

然し川岸が必ずしも皆被害大というわけではない. 掛塚町部のように全戸 723 戸のうち，住家全潰 6 棟，同半潰 37 棟，全潰率 0.8% という程軽微な所もある. ここはさびれた町で，建物も古いのに大多数は壁に亀裂の程度の被害ですんだ. 東岸の池田村も同様で，全戸 357 戸中，住家全潰 11 棟，同半潰 18 棟，全潰率は 3.1% の被害である. それは全戸の 7～8 割までが木の皮やトタン屋根で，瓦屋根が少いためであろう.

(b)　天竜川の旧水路に当る所

下流西岸の河輪の全潰家は，前記の芋瀬・三新以外に西（にし）・東（ひがし）両部落に密集している. このあたりは天竜川の分流があつた事が言伝えられ，その流路は幕末の地図[15)16)]にも描かれ

(15)　遠江国全図，1828 年＝文政 11 年製作図，作者不詳.
(16)　遠江国全図，1838 年＝天保 8 年千尋作との銘がある.
　上記 2 図は浜松市内田六郎氏所蔵の古地図.

ている（第 14 図）．この旧水路の下流に当る五島（ごとう）村の鶴島・松島も被害が多い．

(c)　出口を閉塞された支谷

浜松市上池川町・下池川町の所謂六間道路沿いは最近迄深田で，蓮なども植えてあつた．ここは天竜川平野から三方原台地へ入込んだ支谷で，本流の陸上堆積に対してこの支谷の堆積が追付かず，出口を閉塞されて水はけが悪く，湿地化したものであろう．現在この谷を前記の六間道路が東西に貫ぬき，ここに立並ぶ人家の内，倒潰 16 棟，半潰 26 棟，傾斜家屋約 70 棟の被害を出した（第 15 図）．

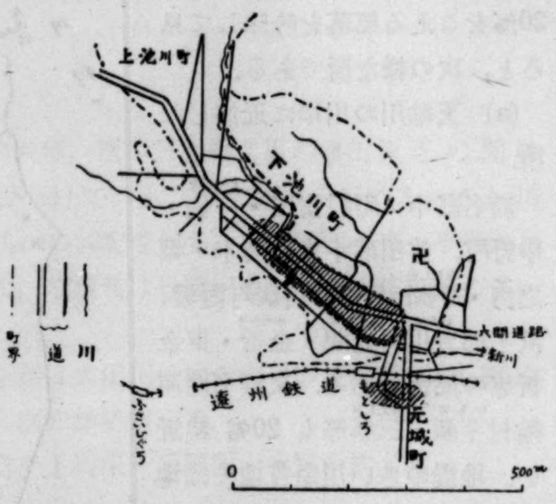

第 15 図　浜松市街北部の被災地（斜線の部）

Fig. 15. Damaged area in the nothern part of Hamamatsu City (hatched area).

6.　大井川扇状地 (Gi)

遠江・駿河の境を画する大井川は，金谷町の少し上流から山地をはなれるが，それより下流の島田あたりを中心に大きな扇状地を作つて駿河湾に注ぐ．ここでは地震被害らしいものはほとんど見当らず，遠江側ではひどい所で庇や壁が落ちた程度に止まる．

大井川は天竜川に比して更に急流で，傾斜は川口まで 5‰ を下らない．そのために運搬砂礫の粒度が天竜川のそれよりはるかに粗い．それは島田地方の地下水面が大井川の水位の上下に鋭敏に影響される程透水度の高い事からも推量される．このあたりでは 1 尺も掘れば厚い礫層につき当り，田んぼは深耕出来ない．大井川扇状地に被害が軽微だつたのは，この様な粒度の大きな砂礫層のためであろう．

7.　小笠山砂礫地 (Gg)

これは小笠山の谷平地と南麓の扇状地群の地盤である．小笠山は全山ほとんど洪積礫層から成る半独立丘陵である．平面形は南西に向けて開いた扇形で，その方向に緩斜している．東と北は急斜面である．山は壮年的に解析されて幾つかの侵蝕谷に刻まれ，その谷の中は崩れて運ばれた砂礫で幅広く埋められている．又南麓の旧海蝕崖下には小扇状地が並んでいる．

この砂丘地には 6 ケ町村 50 部落の約 2,570 戸が所属し，地震被害は住家全潰 3 棟，同半潰 30 棟，従つて全潰率は 0.1% となり，被害軽微である．

8.　海岸砂丘地帯 (Sc)

遠江の外洋遠江灘には，西は愛知県境から東は御前崎半島まで延々 60 km にわたつて

平滑な砂浜の海岸が続き，その形状は天竜川口を中心に二つの雄大な弧をえがいて，カスプ状を呈している．砂浜の延長は御前崎から駿河湾に廻つて，20 km 先の大井川口近くまで達する．この砂礫の内側には砂丘地帯が附随し，幅はふつう 1〜2 km から最大 5 km に及ぶ大規模なものである．

この長大な砂丘地帯の大部分は，風化した深成岩中の石英細片を主成分とする白色の砂から成る．但し大井川口より西約 10 km までは有色鉱物の卓越する黒色の砂である．この砂粒成分から考えて前者の白色砂は内帯山地を源とし，天竜川に運ばれ更に遠江灘の沿岸流丘卓越風によつてそこにもたらされたのであり，これに反して後者の黒色砂は大井川の営力によるものであつて，両者の境界は川崎町あたりである[17]．換言すれば遠江海岸地方は，天竜川及び一部大井川の砂が沿岸流や風によつて陸の前面に運ばれて形成された砂丘地帯である．

この砂丘地帯の背後には，西部に於ては浜名湖や佐鳴湖が抱かれ，中東部では太田川・菊川下流域を始めとし多くの旧潟湖群を作り，そこの現在の粘土地盤のもとを作つた．

冬期の強力な卓越風は，この砂丘砂を海抜 30〜40 m の御前崎台地や佐倉丘陵に吹上げ，河東（かとう）南部の河東山は 70〜80 m の山頂まで砂丘化された．

この砂丘地帯の地震被害は 35 市町村 196 部落約 22,200 戸の内住家全潰 780 棟，同半潰 790 棟，全潰率は 3.5% である．地域が広いので被害数は多いが，被害率はさ程ではなく，全潰率 20% をこえる部落はまれで，大部分は 5% 以下であり，0% の所が 60 部落もある．

海岸砂丘地帯の被害分布を細序するに当り記述の便宜上これを次の 3 地区に区分する．

(a)　天竜川以西地区——天竜川口より遠江西端まで．

(b)　天竜川以東地区——天竜川口より横須賀町まで．

(c)　小笠・榛原地区——大淵村以東の小笠・榛原両郡下の部分．

a.　天竜川以西地区

この地区の最も広い所は三方原南縁沿いの約 10 km の部分で，3〜5 km の幅をもつ．ここの部分では 3 つの砂丘列と 2 つの湿地が帯状に配列している．これらは北から，第 1 砂丘列，第 1 湿地，第 2 砂丘列，第 2 湿地，第 3 砂丘列と名付ける．第 1 砂丘列は浜松市内砂山町・竜禅寺町のものや，志都呂（しとろ）砂丘，雄踏砂丘などであり，第 2 砂丘列は国鉄高塚駅を中心とするものであり，第 3 砂丘列は海寄りのものである．第 3 砂丘列は天竜川口から今切口をまたいで西の県境に達しており，それは東の新津地区では 3 列に分岐している．これらに夾まれた二帯の湿地は，湿地といつてもかなり砂質の所が多い．なお第 2 湿地には蓮池がある．

これらの砂丘列は先述のように，天竜川のプログラデーションに伴つて沖へと順次配列形成された砂洲に由来するものである．(第 16 図)

---

17)　栗林沢一・栗林治雄　「砂丘に関する覚え書 (その 2)」——砂の移動に関する資料——

この地区の地震被害は比較的軽度で，1市（内1支所）10町村85部落の9,900戸の内，住家全潰190棟，半潰240棟，全潰率は1.6%である．比較的被害の多いのは篠原(しのはら)(810戸中住家全潰31棟，半潰55棟，全潰率3.8%)，入野（581戸中住家全潰29棟，半潰27棟，全潰率5.0%）であるが，これとても天竜川平野下流の全潰率の程度である．（第17図）

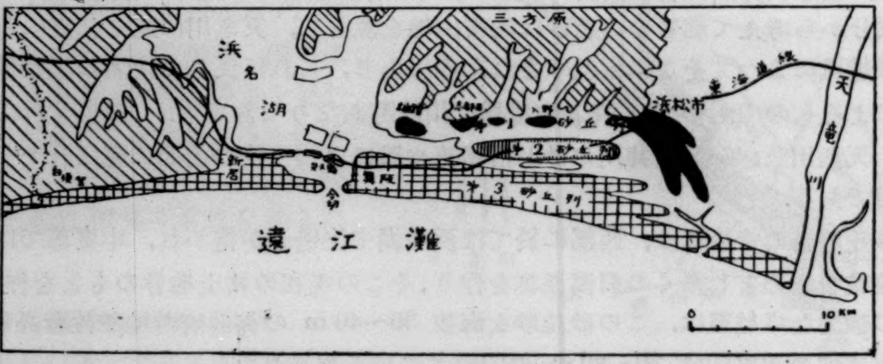

第16図　海岸砂丘地帯天竜川以西地区の3つの砂丘列
Fig. 16.　Three bands of sand-dunes along the coast west of River Tenryū.

被害個所は湿地又はそれに接した所に多い．入野について仔細に見ると，倒家は砂地の芯部に少く，佐鳴湖から出る川のへりや泥質の佐鳴湖べりや，湿地側に多い．同様な傾向は西隣の志都呂や宇布見でも見られる．志都呂は台地に接した砂丘地の部落であるが，被害家はやはり湿地寄りにある．宇布見は顕著な砂地盤の上に高さ10米程の砂丘を2列配した所であるが，砂地盤内部で倒れたのは不安定な2階家1棟だけで，他の11棟は皆旧時の浜名湖底又は旧湖畔の位置にある．浜松市内竜禅寺町では倒家5棟，半潰7棟，傾斜家屋50棟等の密集被害を出したが，これも砂丘間の低湿地に当る所である．

以上記した以外は被害はわずかである．浜名湖内の弁天島は，第3砂丘列の延長に当る砂洲と，湖底の砂をすくい上げた埋立地とから成立つているので，湖中の低平な小島であるのにかかわらず地震の損傷は少く，全半潰に至つたものはない．

この方面では工場の被害が多かつた．

b.　天竜川以東地区

天竜川以東の地区では，以西に見られる様な砂丘列や湿地の整然たる配列は見られない．これは背後の太田川低地が未だ潟の時代の潮流や，その後これを横断する河川によつて，大半は破壊し去られたものであろう．その残片がわかるのは太田川以東の部分であつて，ここでは海岸から2.5kmばかりの内陸，即ち小笠郡笠原村横砂・磐田郡東浅羽村梅山・松原・初越(はつこし)，西浅羽村富里東(とみさとひがし)の線に，砂丘や砂地盤を判然と認める事が出来る[18]．

18) 原田和著白羽草 (1937) には石津から富里東までにわたつて砂丘や砂層の露頭を20ヶ所ほど記してある，露頭のない所でも4～5尺掘れば砂層に達する事がある．

その南寄りの小笠郡横須賀町沖の須・今沢・中新田，磐田郡幸浦村大野・同笠・太郎助等一連の部落をのせる地盤も，砂丘列の千切れた残りであろう．

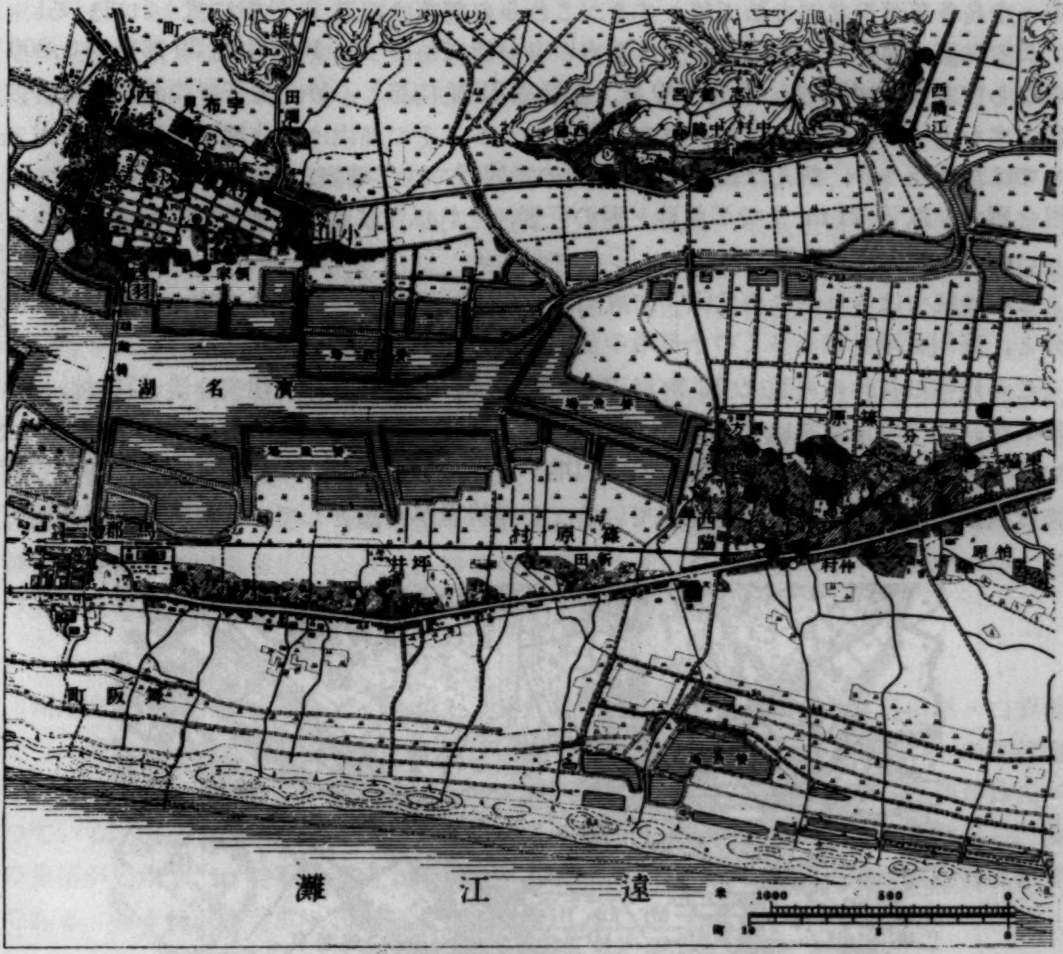

第17図　浜名郡雄踏町・篠原村及び附近の倒潰住家分布図（●印）

雄踏町は中村信作氏，渥美幸雄氏，篠原村は榊原正雄氏，神久呂村志都呂は辻村義雄氏，入野村西鴨江は入野村役場諸氏による．

Fig. 17. Distribution of collapsed houses (black dots) on the south-eastern side of Lake Hamana.

これらの砂丘列の間には，場所によつてはかなり砂質な湿田が横たわつて，最近まで湖水をたたえていた．

この意味から東浅羽の砂丘列以南をここの砂丘地帯とする．東浅羽と幸浦の両砂丘列は天竜川以西地区の第 1・第 2 砂丘列に対比できよう．

太田川以西の部分では砂丘地帯の限界が甚だあいまいで，認めるに困難である．然し長野村小島地内の長野小学校北方 300 m の路傍では海岸砂丘の白い砂地への移り変りが明

瞭である．従つてここでは小島以南を海岸砂丘地帯ときめる．

以上の結果から，天竜川以東地区の砂丘地帯の範囲を横砂・東浅羽・西ケ崎・豊浜・福田・小島各集落の北端を結ぶ線とする．これらの部落は国道 2 号線に貫かれている．

この地区は海岸砂丘地帯としては被害の多い所であつて，10ケ町村 39 部落約 3,800 戸のうち住家全潰 460 棟，半潰 370 棟，全潰率 12% に達し，砂丘地帯での最高の被害数と被害率をもつ．何故にここに被害率が高かつたか，その理由は多分地下に泥層がまじるためではなかろうか．例えば全潰率約 20% の幸浦村では，地表から 2 m までが砂と泥の混合層で，以下 21 m までが細砂と泥の互層，それ以下は細砂層となつている．

c. 小笠・榛原地区

この地区ではうしろに小笠山・河東(かとう)山・牧の原・御前崎台地等の丘陵・台地を控えた部分と，菊川低地を始め多くの小低地の前面の部分が交互している．

この地帯の被害の概数は 12 町村 73 部落約 8,700 戸の内，住家全潰 170 棟，半潰 550 棟，従つて全潰率は 2.0% で，やはり全体として軽度であるが，中には稍被害の大きい所もある．総体的に被害軽微なのは山地や台地の前面であつて，震害の目立つ所の背後には大がい潟湖由来の低地を伴つている．この状態が画然としているのは榛原郡川崎町で

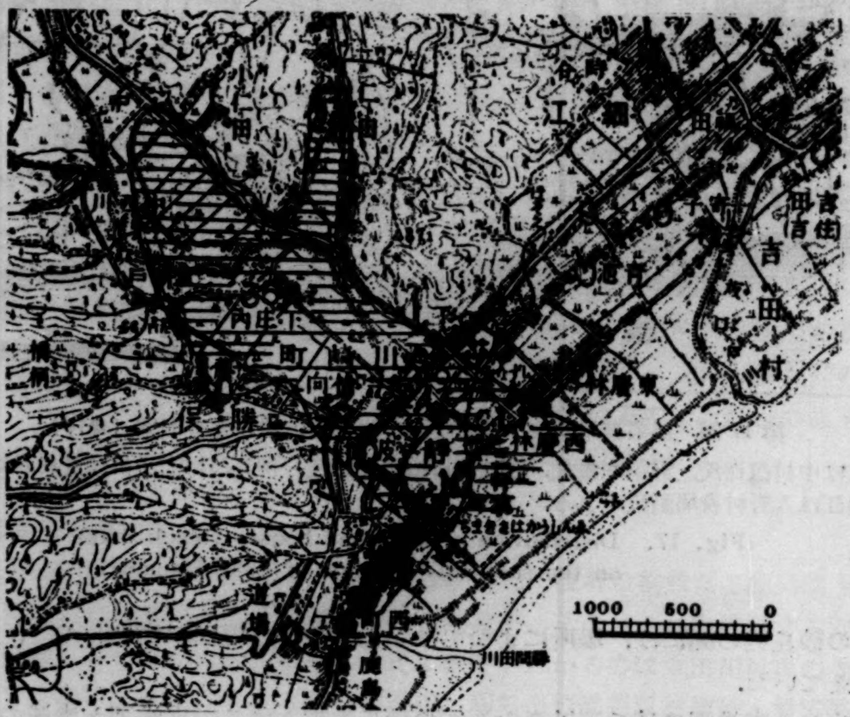

第18図　榛原郡川崎町の被害．数字は住家全潰率で，平行線内が全潰区域を示す．

Fig. 18. Area of heavy damage in Kawasaki Town, Haibara County. The numerals denote the damage percentages.

あつて[19]，ここでは幅 1 km 許りの直線状の勝間田川低地の延長部分だけに限つて住家全潰 31 棟，半潰 48 棟の被害家が分布している．背後の勝間田川低地は前述の通り潟から出来た地盤であつて，庄内のような被害地もここにある．所がこれをわずか外れた牧の原台地前面では被害ほとんど皆無である．冲積層の厚さを比べて見ると，低地の延長部では附近の深井戸から推して少くとも 16 間（=28.8 m）あるのに，台地前面ではわずか 3〜4 m にすぎない．（第 18 図）

この地区の最高被害地は激震地である菊川低地の前面であつて， 3 ケ村 8 部落 650 戸許りの中住家全潰 63 棟，半潰 212 棟，全潰率 9.8% である．最高被害地は小笠郡千浜村喜右衛門新田（きえもんしんでん）で 53 戸中住家全潰 16 棟，半潰 37 棟で全潰率は 30.2% である．ここは菊川の川岸であつて，この附近には地震のさい土地のかんぼつ，砂泥噴出などの地変[20]もあつて，地下に軟層の存在を思わせる．

低地前面の被害例は篋川（おきさ）下流や池新田でも見られる．篋川下流では 3 ケ村 4 部落約 220 戸の内，住家全潰 7 棟，半潰 9 棟で全潰率 3.0%，池新田では 800 戸の内住家全潰 6 棟，半潰 12 棟，全潰率は 0.7% である．

これと反対に背後が丘陵や台地の部分が被害が稀なのは前述の通りである．この様な所に被害が軽微なのは基盤岩石が浅く，砂層の被覆がうすいためであろう．川崎町の例は前述の通りであり，他の所でも所々岩盤が露出する程の薄さである．

9. 洪積台地 (D)

遠州地方には広い台地がいくつかある．それらは牧の原・御前崎台地・磐田原・白須賀台地（=愛知県天伯原の延長部）等である．牧の原は第三紀層の上に 10〜30 m の洪積礫層をかぶつたものであり，御前崎台地もやはり同様な構造で，表面の一部には海岸砂丘がのつている．他は皆礫層又は砂礫層台地である．最近はどこも開拓が進んで耕地化し，多くの集落が発達した．地盤の固いこれらの台地上では，特殊な数個所を除けば被害はわずかである．各々の被害概数は次表の通りである．

台地名	市町村	部落	戸数	住家全潰	同半潰	全潰率(%)
牧の原	14	25	1,340	2(棟)	0(棟)	0.1
御前崎台地	3	11	1,330	7	20	0.5
磐田原	8	57	7,600	8	20	0.1
三方原	16	74	7,650	9	13	0.1
白須賀台地	1	14	580	38	21	6.5
合計	42	181	18,500	64	74	0.3

次に洪積台地上の被害地について述べる．

19) 栗林沢一氏の教示による．
20) 現大浜町三俣岩倉次郎作氏観察

三方原台地引佐郡気賀町老ケ谷(おいがや)ではこの地震で住家114戸中全潰 4棟，同半潰 17棟の被害を出した．ここの地盤は堅固な礫層である故，被害の原因は建物自体にあると思われる：ここは開拓地のために小造りの家が多く，倒家は皆 30 年程度を経た，間口に比して奥行のつまつた構造の小さい家であり[21]，そのそまつな作り方のために早く老朽して被害を招いたものであろう．浜名郡吉野村では370戸の内，住家全潰4棟，半潰10棟であつて，原因は老朽のためである．

浜松市内安座(あんざ)（30戸）の大部分は三方原台地上のふちに乗り，一部分その斜面と佐鳴湖畔にある．ここの被害は住家全潰 3 棟，半潰 1 棟で，全部台地のふちの部分から出した．ここも砂礫の強い地盤である故，原因は地形的なもの（崖縁の振動）か弱い建て方にあるであろう．又非住家を工場に改造した非住家も倒れたという事である．

浜名郡白須賀町の中心部は海抜 70 m 許りの白須賀台地上に位する．この町は1707年(寶永4年)以来の宿場町であつて，1889（明治22）年鉄道開通に伴つて交通を奪われて以来，現在戸数の 80% は農家となり，町は徒らに古風な様式のさびれた面影だけを止めて宿場の機能を失つている．ここは堅固な砂礫台地上としては被害が多く，東町から西町に至る6町内では319戸の内，住家全潰28棟，半潰18棟，全潰率8.8%に達する．被害の理由[22]は明治以後町が発展せず，家屋が更新されなかつたことによるのであつて，特にさびれた東部に多い．尚当町では戦争疎開者がそまつな非住家を改造して住み，これらの中でも倒れたものがあつた．

10. 岩 石 地 盤

遠江地方の基盤岩石の出ている山地・丘陵の事であつて，冲積層のうすい谷間や段丘礫層の地盤もこれに含める．岩石地盤の所では家屋被害はまれで，石灯籠や鳥居・墓石の転倒，高い煙突の折損，不安定な崖や築堤の崩落等が各地から伝えられるに過ぎない．被害概数は関係89ヶ町村約43,000戸の内，住家全潰80棟，半潰240棟許りで全潰率は 0.2%となる．

ただこの中，小笠郡南山村堀之内及北の谷ではやや被害が目立つ．この両部落では62戸の内住家全潰10棟，半潰13棟，全潰率は 16.1% である．この両部落は固い第三紀層の上にのり，一部分南の河東山(かとうやま)の小笠山洪積礫層であつて地盤は大変良好である．被害の原因は不明であるが，ここで目立つ事は3間×4 間ばかりの小さい農家の建物の多い事であり，この小家屋の固有周期が短く山地の地盤振動と共振したか或はこの小さい貧弱な建て方かが多くの被害を出した原因であろう．

VI. 遠江地方大地震の歴史的考察

今後この遠江地方がいつどの程度の大地震に襲われるか，これを適確に知る事は勿論容

---

21) 同地名倉氏観察．

22) 旧白須賀町長田村橘治氏，春木氏による．

易なことではないが，この地方の歴史上の大地震の記録を基にして，これの大ざつぱな予想を立てたい．

今回の東南海地震から90年昔の 1854年12月23日（安政元年11月4日）当地方に所謂安政の大地震が起つた．この地震は余程激烈であつたらしく，武者金吉著日本地震史料に集録された文献の一つ[23]を引用すれば，

（前略）

金谷宿　瓦町より仲町迄焼失．上の方四五間通潰．

日　坂　歯ヌケ潰．

掛川宿　宿内残らず焼失．死人 140～150 人許．御城内大破．宿内何一つ之無く原の如く見ゆ．

袋井宿　残らず焼失．死人 200 人許．此宿も原の如く見ゆ．

見付宿　三分通り潰．

浜松宿　三分通り潰．

舞坂宿　此辺田畑一里余汐入，池の如く成．

荒井宿　津波にて 18 人許死．

白須賀宿　三分潰．（後略）

被害程度の表現は執筆者によつてまちまちであるが，上記を始め各地共，今次の地震よりも数等激しかつた様である．

同書には街道沿いや城下町・関所等の被害が記されているが，街道を外れた方面でもこの時のさんたんたる有様が口碑にうけつがれ，古文書に残つている．例えば原田和著白羽草（しろわぐさ）によると，東浅羽の松原では法音庵と 1，2 の民家を残して全村倒潰した．松原では今回の地震で103戸中住家25棟倒れ，24.3%の倒潰率である．(同地はほとんど砂質地盤）又菊川上流の友田では[24]住家倒伏5棟であつたのに対し，今回は49戸皆無事である．（同地は第三紀層の上にうすい段丘礫をのせた地盤）又海岸各地では津波におそわれ，例えば小笠郡千浜村では 1.5 km 内陸の海抜数 m の喜右衞門（きえもん）新田まで腰たけの津波が来た[25]．

安政地震と今回の地震との比較をすれば，

(a)　被害区域は今回と類似であつたが，その程度は安政地震の方がはるかに大きかつた．

(b)　安政地震の方が被害範囲が上流の良好地盤にまで及んだ．

(c)　安政地震の方が津波や地変が大きかつた．

上記の安政地震を始めとして，遠江と関係の深い本邦外側地震帯から発した歴史上の最大級の地震は，

---

23)　同書の 130—131 頁に記された井上伝太夫の観察記録．

24)　現菊川町友田鈴木重平氏宅に伝わる古文書による．

25)　口碑　現小笠郡菊川町堀之内在住佐藤ゆか老による．

26)　武者金吉「外側地震帯中部より発する大地震」東南海大地震調査報告　中央気象台 (1945).

(a)　1361 年（天正 16 年）畿内・東海道
(b)　1498 年（明応 7 年）東海道全般
(c)　1605 年（慶長 9 年）東海道・西海道
(d)　1707 年（宝永 4 年）全国土
(e)　1854 年（安政元年）東海道・南海道
(f)　1944 年（昭和 19 年）東海道

等である．そしてこれらの年数間隔を順次に取つて見ると，137年，107年，102年，147年，90年となり，この平均は117年である．

これらの最大級の地震にはさまつて，遠江では小規模な地震や遠方の大地震のために多少の被害を生じている．それらは，

(a)　1589 年（天文 17 年）駿河・遠江
(b)　1686 年（貞享 3 年）遠江・三河
(c)　1891 年（明治 24 年）濃尾
(d)　1945 年（昭和 20 年）三河

等である．この中 1891 年の濃尾地震では太田川低地に相当の被害があつた事が伝えられている．1954 年の三河地震のさいもやはり影響をうけた．地盤の最悪な太田川低地では，この程度の地震でもまつ先に被害をうけるのである．恐らくは上記以外の小規模地震の時にも同様な事があつたと推量される．

この様にここの歴史上の顕著地震を統計的に吟味すると，此の地方は約百年毎に今回や安政地震のような大規模地震に襲われ，両地震の結果から推して，太田川・菊川低地を始めとする冲積地に大被害を与え，又その合間にもこの地方に取つて稍軽度の地震が不定年数毎に発生して，その度毎に太田川低地では幾莫かの被害を生じて来たのである．

当地方のこの様な現象は，恐らくは今後の将来にも引続き反復されるに違いない．将来の大地震の震度分布を推量するに，やはり今回や安政地震と相似なものであろう．前述の様に被害率の大小はそのまま相対的な震度の大小を指示すると考えられるが故に，今後建築や構造物の築造に当つては，今回の震害分布状況を詳かに参照し，それから知られる各地の震度に応じて耐震設計をする必要がある．

VII. 被害家屋の特徴

次に当地方に於ける東南海地震の被害家屋の経過年数・種類・構造等について述べる．本報告のテーマからは外れるが，防災上有意義と思われるので記しておく．何分にも資料が断片的であるから，十分な記述は出来ないのを遺憾と思う．

(1)　家屋の経過年数と震害

今回の地震では一般的にいつて老齢な家屋の方が多く被害をうけた．

全潰率 25% ばかりの磐田郡東浅羽の砂地では 20 年経過以上の家が倒れその倒家の大部

分は60年以上のものである．同村松原部落の倒潰家の経過年数は次表の通りであり，同村の砂地盤上の他の部落も同様な傾向である[27]．

経過年数	倒潰棟数	記事
20 年程度	2	瓦屋根
30	1	瓦屋根
40	0	
50	1	瓦屋根
60	6	茅屋根 5，茅屋根茅改造瓦屋根 1
70	4	茅屋根
80	2	茅屋根 1，茅改造瓦屋根 1
年齢不明	5	
計	21	

40% 程の倒潰を出した太田川低地南部の粘土地盤磐田郡西浅羽村では経過年数10年以上の家が倒れ，倒家の多くは50年以上経たものである[28]．

96%倒れて殆んど全滅した太田川低地中部の磐田郡今井村では新旧の別なく倒され，立ち残りの家は特に頑丈な家である[29]．

以上の三村の例によつて，この地震ではおおむね被害率の低い所ほど老齢の家が倒され，高い所へ行くに従つて，より新しい家の方まで倒されたのだという事がわかる．

もつとも仔細に観た場合には，被害は必ずしも家の古さだけによるものではない．例えば三方原台地の引佐郡気賀町老ケ谷の様に，30 年程度の家が多く倒れて60年程度の家が半潰ですんだという例もある．前者の建て方は開拓地の小造りの家であるという事から或いは家屋の作りが粗末なために早く老朽して震害をうけたのかも知れない．

また小笠郡南山村では小学校の新しい方の校舎がほとんど倒れ，古い方の校舎や役場が残つた．ここは山際近い位置の粘土地盤である．但し粘土層は余り厚くないと思われる．この様な，古い建物より新しい建物が倒れた例は磐田郡田原村でも観察された．

総じて家の経過年数と老朽度の関係は，各々の家屋の材料・構造等による元来の強さやその後の補修の程度の差によつて一様では無いはずである．従つて上の例の様な振動週期の問題を度外視しても年令の割に早く老朽弱化したものが倒れて反対の家が立残るという事は当然考えられる．然しこの関係についての調べはなされなかつた．

(2) 構造上の欠陥から倒れた家

a．埋立ての土盛が不十分

27) 旧東浅羽村役場鈴木末吉氏による．
28) 旧西浅羽村長大石政一氏，助役鈴木彰氏による．
29) 旧今井村役場収入役鈴木利雄氏，高橋慶亘氏による．立ち残りの家の中には，後日解体されたものもある．

激震地今井村では倒潰を免れた家は土盛の高いものだという．小笠郡掛川町や磐田郡十東村では，埋立の土盛をせず低い地盤へ直接コンクリートや木の柱を立てて土台を支えた家が全半潰を見た．

b. 基礎工事の不完全な家

単に柱の根に玉石の基礎を置いた家は弱い．（磐田郡東浅羽村の例）

c. 土台を基礎へボルトじめにした家

磐田郡十東村では，比較的新しい家で土台を基礎のコンクリートへボルトじめにしたために倒れたという例がある．これは振動のために足をさらわれたのであろう．反対の例として小笠郡平田村や千浜村では，新築間もない家が振動で基礎をはなれて 1 尺も飛出して，然も余り痛まなかつたというのがある．

d. 柱数や壁の面数が少ない家

小笠郡掛川町では南北通りの栄町に半潰が多かつたが，これは南北の主要振動に対して支えになる間口の方向の壁が少いからである．磐田郡東浅羽村では東西に長い家は南北に長い家より倒れ方が少なかつたというが，これも壁の多い方向と主要振動との関係からのようである．

浜松市を始め遠江西部地方では織物工場から軍需工場に転換したものが被害が多かつたが，これは織機の代りに工作機械を設ける目的で壁や柱を切取つたためである．

e. 階下の狭い二階家

浜名郡雄踏町では道路拡張のために階下の一部を失つて不安定になつた二階家が倒れた

f. 継柱（つぎばしら）を使つた二階家

浜松市竜禅寺町や小笠郡平田村に例がある．

g. 平家（ひらや）改造の二階家

小笠郡土方（ひじかた）村に例がある．

h. 木造三階家

浜松市砂山町・小笠郡平田村に例がある．

i. 古材を用いて建替えた家

小笠郡和田岡村・磐田郡東浅羽村に例がある．

j. 草葺を瓦葺に改造した家

磐田郡東浅羽村・浜名郡白須賀町に例がある．これは施工のさい，一部の柱を継足さなくてはならないが，この継目が弱点となるのである．

k. 本間（軸部）が草葺きで庇通りが瓦葺きの構造

磐田郡東浅羽村・今井村に例がある．

l. 曲り角の家

市街地で家屋が密接している場合は相互にもたれ合う結果仲々倒れにくいが，その端部の家は片方から押されても反対側により掛る事が出来ないのでそちらへ倒れ易い．小笠郡掛川町・周智郡山梨町に例がある．（第 19 図）

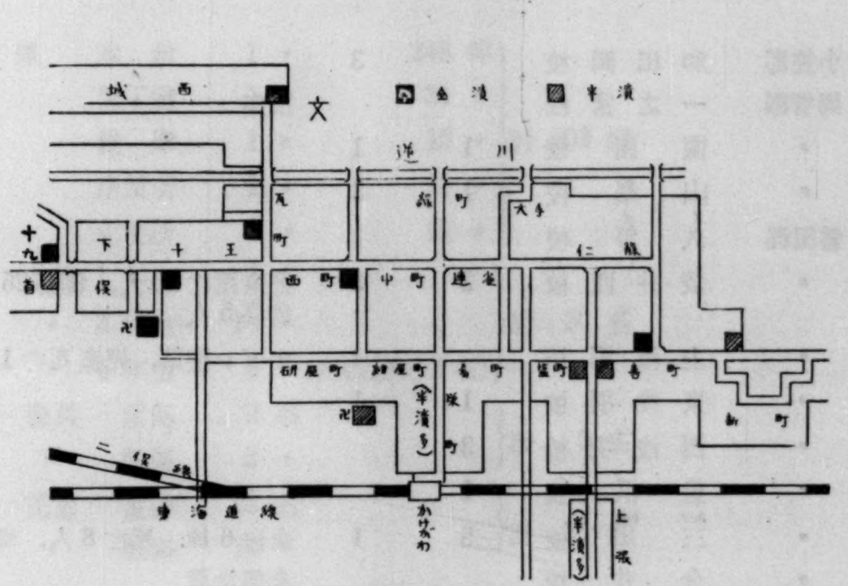

第19図　掛川町の被害

Fig. 19.　Collapsed houses in the Kakegawa Town, showing that the houses at street corners, facing both of front and side streets, were destroyed markedly.

(3)　公共建物の被害

公共建物の被害の中，小学校・寺院・神社は被害が大きく，また，西遠地方では工場被害が多かつた.

小学校(当時，国民学校と呼ばれた)の被害は次の通りである.

No.	郡市	小学校	全潰(棟)	半潰(棟)	記事
1	榛原郡	吉田校			壁落下
2	〃	勝間田校			傾斜，壁脱落
3	〃	川崎町静波校	2		他に大破 2 棟
4	〃	地頭方校	1		全潰は廊下，児童死亡
5	〃	白羽(しろわ)校			小破
6	小笠郡	六郷校			小破
7	〃	平田校	1		児童死亡 2 人
8	〃	南山校		3	約 30° 傾斜
9	〃	千浜校		4	
10	〃	佐東校			門柱全倒
11	〃	中村校	3	4	
12	〃	大淵校	1	1	
13	〃	笠原校			式場校舎破損
14	〃	西山口校		1	
15	〃	桜木南校			破損 1棟

16	小笠郡	和田岡校		3	
17	周智郡	一之宮校			損傷
18	〃	園田校	1	1	
19	〃	山梨校	1	3	
20	磐田郡	久努校		1	
21	〃	袋井西校	2	5	児童死亡20人，負傷25人，職員負傷5人
22	〃	上浅羽校		1	オダレ墜落，児童死亡1人
23	〃	東浅羽校	1	1	
24	〃	西浅羽校	3		
25	〃	豊浜校	1		
26	〃	三川校	5	1	全校6棟．死亡8人，当時2年生
27	〃	今井校			全部全潰
28	〃	田原校			大破
29	〃	南御厨校			半潰
30	〃	岩田校			損傷
31	〃	福田校	1	3	
32	〃	池田校	1		負傷2人
33	〃	井通校			被害大
34	〃	十東校	2		唱歌室20坪，物置20坪
35	引佐郡	金指校		1	
36	浜名郡	中ノ町校	1		校舎地盤不同沈下，死亡1人
37	〃	芳川校	1		廊下
38	浜名郡	篠原校	48坪	125坪	全潰は廊下，半潰は教室
39	〃	入出校	1		校舎地盤不同沈下，運動場亀烈，傷負2人
40	浜松市	富塚校			破損
41	〃	県居校			南校舎大壁崩落，柱3～4本折損屋根瓦2/3落下

小学校に被害が多かつた理由は当時戦時中で修理や改築はかえりみられず，老朽に近い校舎が多かつたためで，学校建築は建坪や高さの割に柱や壁が少いことも被害の原因となろう．特に式場校舎が被害をうけ易いのもその理由である．

この中袋井西小学校と三川小学校は多くの死傷者を出して傷ましい．袋井西校の被害の内訳は，

全潰2棟	教室	1棟	184坪	計331坪
	廊下	1〃	147坪	

半潰 5 棟	本　館	1 〃	248 坪	計 303 坪
	使丁室	1 〃	21 〃	
	雑　庫	1 〃	10 〃	
	南便所	1 〃	12 〃	
	北便所	1 〃	12 〃	
死者	初等 1 年生	2 名		計 20 名
	〃 2 年生	10 〃		
	〃 4 年生	8 〃（内疎開児 2 名）		
傷者	職員　重傷	2 名		計 5 名
	〃　軽傷	3 〃		
	児童　重傷	13 名		計 25 名
	〃　軽傷	12 〃		

袋井では小学校の外に袋井保育所 4 棟 80 坪が倒伏し，園児 19 名が圧死し，保姆 1 名が殉職した．最近，各地の危険校舎も，中学校の整備一段落と共に新様式で改築の緒についたのは喜ばしい事である．

次に寺院・神社の多く罹災した原因は，

a．総体に老齢である．

b．内部を広く，明るくするために，柱や壁が少い．

c．全形を荘重にするために屋根を大きくしてある．

などが考えられる．

浜松市を始め遠江西部では多くの中小工場や航空機工場が全半潰したが，その原因は，

a．中小工場で軍需工場に転換したものは柱や壁を切取つたため弱体化した．

b．西部の生糸工場は工程に湿気が必要のため水蒸気を立てるので，そのため各部が腐朽していた．

c．航空機の大工場がバラック式に急造されたが，総体に弱く特に柱が不足していた．

d．煉瓦造りで崩潰した物が 2～3 棟ある．

(4)　被害のなかつた家

今回の地震に被害のなかつた家は，

a．基礎の堅固な家．（各地）基礎を置石とせず，厚いコンクリートを廻した構造

b．壁の厚い家．壁にすじかいを入れた家．（各地）

c．屋根の軽い家．磐田郡池田村は全村 7～8 割まで木の皮やトタン葺の屋根であるが，それらは被害皆無で，残りの瓦屋根の家に被害を見た．

d．土蔵．（磐田郡今井村・袋井町）

e．通し柱を使つた 2 階家．（小笠郡平田村）

f．埋立のしつかりしている家．（磐田郡今井村）

VIII. 結　論

筆者は昭和19年12月7日東南海地震の際に遠江地方で見られた家屋被害分布と地盤の状態との関係を調査した．この研究の遂行には東京大学地震研究所河角広教授を始め，先輩諸賢の御指導，各行政機関からの経費補助，多くの市町村当局や研究機関並びに有志諸氏よりの資料提供，菊川北中学校始め教育関係の援助に頼る所が多かつた．

被害の研究には被害率分布即ち被害家屋数の全家屋数に対する比率の分布を調べる方法を主体とした．それは被害率からその場所の相対的な震度を推定できる筈であるからである．被害率の代表としては部落毎の住家全潰率を用いた．また，このほか個々の被害家の分布や被害数の分布，その他の調査も補助的な方法として用いた．

一方地盤の研究は在来の研究や土性図を参考にして行い，次のような地盤区分をした．

a．太田川低地（粘土質地盤，一部砂礫質．Co，Go）
b．菊川低地（粘土質地盤，Ck）
c．牧の原山麓小冲積地（粘土質地盤，Cm）
d．浜名湖附近小冲積地（粘土質地盤，一部砂質 Ch，Sh）
e．天竜川平野（砂礫質地盤，Gt）
f．大井川扇状地（砂礫質地盤，Gi）
g．小笠山砂礫地（砂礫質地盤，Gg）
h．海岸砂丘地帯（砂質地盤，Sc）
i．洪積台地（砂礫質地盤，D）
j．岩石地盤（R）

これらの中 a から h までは冲積地であることは言うまでもない．太田川低地は更に次のように細分した．

a-I．中部（Co-m）　a-II．南部（Co-s）　a-III．北部（Go-n）　a-IV．原野谷川地区（Go-ha）　a-V．逆川地区（Co-sk）

なお，地盤の厚さは掘抜井戸の深さから推定した．

遠江地方の地震被害はほとんどが冲積地に分布し，特に太田川低地，次いで菊川低地などの粘土質地盤に圧倒的で住家全潰数の 73% はここに集中している．両低地内では全潰率 80% 以上の部落が前者に 30，後者に 5 あり，前者には全滅した部落も数ケ所ある．その他，牧の原山麓小冲積地，浜名湖附近小冲積地も同様な地盤で密集被害がある．粘土層の厚さは太田川低地で最高約 90 m，菊川低地で 30 m ある．

同じ冲積地でも天竜川平野・大井川扇状地・小笠山砂礫地等の砂礫質地盤や海岸の砂質地盤では被害も軽く，就中大井川扇状地の遠江側には全半潰に達したものは皆無である．砂礫質及び砂質地盤の住家全潰数は，それぞれ住家全潰総数の 9%，15% だけである．

被害の大きい太田川低地等の粘土質地盤は，過去の静かな水域に形成されたデルタ堆積によるものであつて，この水域は天竜川口から東西にのびた砂洲によつて外海の荒波から

守られていたのである．軽被害地の天竜川平野や無被害の大井川扇状地は，過去の海進の時代にも多量に運び出される砂礫によつて水域ともならず，陸上堆積を続けたものであろう．軽被害地海岸砂丘地帯は主として前述の天竜川から発達した砂洲がもととなつてできたのである．

粘土質，砂礫質，砂質地盤及び硬い岩盤（洪積台地を含む）の地域の平均の全潰率は，それぞれ，26.1，1.4，3.5 及び 0.2%であつた．

過去の歴史時代にはこの遠江地方は本邦外側地震帯中部から発した大地震のために度々大被害を蒙つたことが知られている．武者金吉によれば，それらの大地震は 1361 年・1498 年・1605 年・1707 年・1854 年，それと今回のものである．そしてこれらの大地震相互間の年数はかなり等間隔的であつて，その平均は 117 年である．1854 年の安政地震の結果から推せば，これらの大地震では今回と相似した被害分布を呈したであろうと想像される．おそらく将来においても，東南海地震と類似な被害分布の大地震が，同様な周期で繰返されるのであろう．各被害地では今後建築その他の構造物を施工するに当つて，今回の被害分布を参考にそれ相当の耐震構造とする必要がある．

今回の地震では全般的に老朽家屋が被害をうけた．しかし構造上の欠陥から倒れたものもある．公共建物では小学校寺院神社等が多く被害をうけ，西部地方では工場被害が大きかつた．

IX. 資　　料

ここに集録した家屋震害資料は，主として地震後各市町村で行われた震害調査の記録，または沿革誌災害誌等に基ずくものである．入手の方法は各当局に記入用紙を送つて報告を依頼し，大体小笠郡下は 1945 年(昭和 20 年）と 1949 年（昭和 25 年）に，他の郡市は 1949 年(昭和 25 年）から 1951 年（昭和 27 年）にかけて行われた．なお地震当時の記録が残つていない町村からは次の方法で資料が得られた．

（Ⅰ）　役場当局による再調査（引佐郡気賀町）
（Ⅱ）　役場の人々の記憶の綜合（小笠郡比木村，浜名郡新所村）
（Ⅲ）　地元の学校に調査依頼（盤田郡南御厨村：磐田郡神明中学校鈴木哲郎教諭）
（Ⅳ）　宮村摂三：東海道地震の震害分布，東大震研彙報 24 号（1946）（浜名郡舞坂町）
（Ⅴ）　東南海大地震調査報告，中央気象台（1945　小笠郡掛川町，磐田郡田原村）

次に資料編集の留意点を述べると，

（1）　番号　郡市及び被害町村等の配列は地図の上で上から下へ右から左へ順番をとり，部落の配列は市町村からの報告書に記入された順のままとした．
（2）　郡市町村　地震当時の行政区画と名称とによつて記し，下のかつこ内に昭和 32 年 1 月 1 日現在の新市町村を併記した．
（3）　部落　地震当時の区分による．読みかたは地元に問合せて正確を期した．

(4) 地盤 用いた記号については本文に記してある.

(5) 戸数 小笠郡及び榛原郡（但し菅山村を除く）の被害町村は皆地震当時のものが得られたが磐田・周智郡以西は調査の着手が遅れた関係から地震当時より大分時日を隔てている資料もある. 昭和 22 年以後の戸数が示されている所は他の資料と共に第 II 表に示す.

(6) 住家及び非住家の被害数棟数を表わす. 本文に述べたように市町村によつて全潰の判定規準が違つている. 全潰の解釈を倒潰と修復不能に分けると, 前者を取つた町村は次の通りである.

榛原郡勝間田村・白羽村・小笠郡河城村・加茂村・平田村・新野村・佐束村・土方村・大坂村睦浜村・笠原村・桜木村・和田岡村・曾我村・周智郡一の宮村・園田村・山梨町・磐田郡久務村袋井町・上浅羽村・東浅羽村・西浅羽村・幸浦村・三川村・今井村・向笠村・田原村・御厨村・南御厨村・福田町・於保村・池田村・長野村・引佐郡気賀町・浜名郡飯田村・和地村・雄踏町・神久呂村・可美村・新所村・浜松市富塚支所.

後者を取つた町村は次の通りである.

小笠郡六郷村・小笠村・南山村・比木村・大淵村・西山口村・西郷村・掛川町・西南郷村・周智郡宇刈村・磐田郡井通村・十束村・浜名郡和田村・飯田村(此村は殆倒潰以上)・河輪村・村櫛村・入野村・新津村・篠原村・新居町・鷲津町・入出村・浜松市白脇支所.

(7) 住家被害率 住家全潰率は住家全潰数の, 全半潰率は全潰数と半潰数の合計の, それぞれ戸数に対する百分率を示した.

(8) 備考 公共物被害, 小被害, 被害理由, 出火, 死傷, 地表の変形, 掘抜井戸の深さ, 地盤の状況, 町村合併の詳細, その他の参考事項を記した.

第II表 昭和 22 年以降の戸数が示されている町村

Table II. List of the towns and villages for which the total numbers of families in them at the time of the earthquake could not be known. The data at later epochs from various sources are tabulated.

No.	(a) 町村及市支所	(b) 本 資 料	(c) 調査時期	(d) 宮 村 (1946)	(e) 中央気象台 (1945)	(f) 静岡県勢要覧 (1948)
		(戸)	(年 月)	(戸)	(戸)	
1	5 菅山村	425	1950.9	358	—	424
2	46 園田村	530	1948.3	423	—	535
3	48 宇刈村	452	1948.3	372	—	451
4	49 山梨町	810	1950	626	660	855
5	50 久努西村	576	1950.8	478	478	—
6	61 御厨村	324	1950	299	—	332
7	66 磐田町	7,024	1950.1	5,254	—	6.976
8	70 池田村	359	1950	295	—	362

(つづく)

第 II 表（つづき）

No.	(a) 町村及市支所	(b) 本資料	(c) 調査時期	(d) 宮村 (1946)	(e) 中央気象台 (1945)	(f) 静岡県勢要覧 (1948)
		(戸)	(年 月)	(戸)	(戸)	
9	71 井 通 村	690	1950	611	—	706
10	72 長 野 村	572	1950.8	495	—	578
11	74 袖 浦 村	588	1950	530	—	626
12	80 気 賀 町	2,077	1951.10	1,577	—	2,125
13	83 竜 池 村	486	1950.10	414	—	468
14	84 北 浜 村	3,417	1950.10	2,121	—	2,904
15	87 豊 西 村	730	1950	606	—	729
16	88 笠 井 町	1,299	1948	1,055	—	1,315
17	89 長 上 村	1,155	1947. 2	927	—	1,161
18	91 和 田 村	1,191	1948. 1	894	—	1,180
19	92 飯 田 村	848	1949. 2	579	—	—
20	95 五 島 村	417	1951. 7	367	—	422
21	97 吉 野 村	370	1951. 6	301	—	412
22	98 和 地 村	642	1948	476	—	639
23	103 雄 踏 町	1,888	1951. 7	1,468	—	1,886
24	107 新 津 村	858		714	—	929
25	110 新 居 町	2,346	1950.10	1,288	—	2,420
26	117 浜松市曳馬支所	2,365	1947.10	—	—	—
27	118 同蒲支所	807	1947.10	—	—	—
28	119 同白脇支所	944	1947.10	—	—	—
29	120 同富塚支所	420	1947.10	—	—	—

(a) 地震当時の町村及市支所名（数字は本報告中の番号）.
(b) 本報告採用のもの（主として地震後各市町村で行われた震害調査の記録，または沿革誌・災害誌等に基ずくものである）.
(c) (b) の戸数の調査時期.
(d) 宮村摂三： 東海道地震の震害分布(その1)震研彙報 **24**(1946)所載のもので地震当時のものを示す.
(e) 中央気象台：東南海大地震調査報告(1945)所載のもので地震当時のものを示す.
(f) 静岡県刊行の静岡県勢要覧に所載のもので，1948年3月末日現在.
—は資料を欠くもの.

第 III 表 1944 年東南海地震による部落別被害家屋統計

Table III. Statistics of the earthquake damage in each hamlet in the province of Tōtōmi.

番号	郡 市 町 村	部 落	地 盤	戸数 a	住家被害 全潰 b	住家被害 半潰 c	非住家被害 全潰	非住家被害 半潰	住家被害率 全潰率 b/a×100	住家被害率 全半潰率 (b+c)/a×100	備 考
									%	%	
I	榛原郡										
1- 1	坂部村	一部落	R, Cm	69			9				工場全潰1棟，神社の鳥居全潰1基.
2	(榛原町)	二部落	〃	79		2		2		2.5	
3		三部落	〃	83	3			10	3.6	3.6	
4		四部落	〃	71							
5		五部落	R	85							石鳥居全潰1基.
6		六部落	〃	70							
		計		457	3	2	9	12	0.7	1.1	
2- 1	勝間田村	中	Cm, R	96		8	1				非住家全潰1棟は中央公会堂で，倒潰．大正5年建てたもの.
2	(榛原町)	勝間 下	R, Cm	47						8.3	枝村藤十郎氏宅の掘抜井戸は深さ16間．小学校は壁落下し，傾斜した.
3		〃 上	R	73							
4		切山 下	〃	61							
5		〃 中	〃	46							
6		〃 上	〃	70							
7		勝田 上	〃	70							
8		〃 下	〃	65							
9		三栗	〃	68							
10		朝生	〃	85							
11		牧之原 南	D	36							
12		〃 北	〃	111							
13		海仁館住宅	〃	53							
		計		881		8	1			0.9	
3- 1	川崎町	静波一丁目	Sc	153							郵便局(旧位置)の煉瓦塀崩れ，1名下敷死亡．小学校2棟全潰2棟大破．寺院1棟破損.
2	(榛原町)	〃 二丁目	〃	163	10	8			6.1	11.0	中学校(現榛原高校)大破.

3-3	川崎町	〃 三丁目	Sc	76	17	16			22.4	43.4	
4	(榛原町)	〃 四丁目	〃	98	1	5			1.0	6.1	
5		〃 西五丁目	〃	105		15	15	108		14.3	
6		〃 東五丁目	〃	104	1	4	3		1.0	4.8	
7		〃 六丁目	〃	86				3			
8		〃 七丁目	〃	52							
9		〃 八丁目	〃	49	1				2.0	2.0	
10		〃 九丁目	〃	41							
11		〃 十丁目	〃	89							
12		〃 十一丁目	〃	90							
13		〃 十二丁目	〃	78	1				1.1	1.1	
14		細江 根松	〃	62							
15		〃 堀之内	〃	92							
16		〃 東福田	〃	90							
17		〃 西福田	〃	76							
18		〃 青池	〃	82							
19		〃 寄子	〃	48							
20		〃 東慶林	〃	89							
21		〃 道上	〃	82							
22		勝俣 橋向	〃	60	1	2		3	1.7	5.0	
23		〃 藤沢	R,Cm	33	3	1			9.1	12.1	
24		〃 庄内	Cm	48	12	17	23	11	35.4	60.4	
25		〃 仁田	R,Cm	31	2			2	2.4	2.4	
26		道場	R	20				1			
27		鹿島	Sc	42			1				
		計		2,044	49	68	51	153	2.4	5.7	
4-1	相良町	新町 西	Sc	28		5					(相良町) この町では壁のきれつ，建物の傾きが多かつた．倒家は，当時の下流側
2	(相良町)	〃 中	〃	19							
3		〃 東	〃	16		1					

番号	郡市町村	部落	地盤	戸数 a	住家被害 全潰 b	住家被害 半潰 c	非住家被害 全潰	非住家被害 半潰	住家被害率 全潰率 b/a×100	住家被害率 全半潰率 (b+c)/a×100	備考
4-4	相良町	御荒神	Sc	15							の橋のたもとにあり，老朽家で特に土台が粗末．屋根の瓦のすべり落ちた家が多かつたが被害数に含めてない．震後小津波があつたが被害はない．なお非住家も被災した．
5	(相良町)	前浜西	〃	29	1	3					
6		河岸	〃	19	1	2					
7		前浜東	〃	19		1					
8		市場西	〃	18		3					
9		〃 中	〃	20		1					
10		〃 東-1	〃	24							
11		〃 東-2	〃	15							
12		御長家東	〃	23		2					
13		〃 中	〃	21		1					
14		〃 西	〃	18		1					
15		相生町東	〃	12							
16		〃 西	〃	34		1					
17		福岡	〃	230	1	17			0.4	7.8	
18		波津	〃	634	9	110			1.4	18.5	
19		須々木	Sc,D	275	2	14			0.7	5.8	
20		鬼女新田	D	63							
21		大沢	R	85							
22		大江	〃	260	3	32			1.2	13.5	
23		片浜	Sc,D	250							
		計		2,173	17	194			0.7	9.2	
5-1	菅山村	西堀	Cm	54							
2	(相良町)	谷川	〃	51			1				全村壁きれつ．
3		高和	〃	44							
4		大向	R,D	38							

5- 5	菅山村	大知	R,D	28							
6	(相良町)	新田	R	40			1				
7		時ケ谷	〃	45							
8		西山寺	〃	36							
9		松本	R,Cm	49							
		計		425			2				
6- 1	地頭方村	地頭方	Sc	241	3	3			1.2	2.5	役場全潰 1 棟．学校廊下全潰，死 2 人，傷 10 人．
2	(相良町)	新庄	〃	206	7	12		8	3.4	9.2	
3		遠渡	D	168	5	7		2	3.0	7.1	
4		堀野新田	Sc	86	2	3	2	2	2.3	5.6	
5		笠名	R	56	2				3.6	3.6	
6		落居	Sc	111							
		計		868	19	25	2	12	2.2	5.1	
7- 1	御前崎村	女岩	Sc	140							
2	(御前崎町)	西側	D	203							郵便局の石垣倒れる．
3		大山	〃	203			1				全潰 1 棟は便所．
4		下岬	〃	106							
5		上岬	〃	102							灯台にはきれつが入り塀が倒れた．
6		広沢	〃	82							
		計		863			1				
8- 1	白羽村	中西	Cm	79	18	43	27	55	22.8	77.2	
2	(御前崎町)	砂原	D	48	1	6		4	2.1	14.6	駐在所中破，小学校小破．
3		新谷	〃	164	1	2			0.6	1.8	
4		北部	R	30		9	1	9		3.0	増船寺中破．
5		神子新田	Sc	37		1				2.7	

番号	郡市町村	部落	地盤	戸数 a	住家被害 全潰 b	住家被害 半潰 c	非住家被害 全潰	非住家被害 半潰	住家被害率 全潰率 b/a×100	住家被害率 全半潰率 (b+c)/a×100	備考
8-6	白羽村	七部	R,D	54		3	2	5		5.6	
7	(御前崎町)	薄原	D	83		2				2.4	
8		中原	〃	77		3		1		3.9	
9		神子	Sc	64							
		計		635	20	69	30	74	3.1	14.0	
II	小笠郡										
9-1	河城村	吉沢	R	81							
2	(菊川町)	上倉沢	〃	54							
3		下倉沢	〃	81							
4		友田	〃	49							
5		東冨田	〃	105							
6		西冨田	〃	86							
7		沢水加	〃	94				1			
8		和田	〃	82							
9		潮海寺	〃	166	1				0.6	0.6	瓦屋の仕事部屋(老朽).
		計		798	1			1	0.1	0.1	
10-1	六郷村	上本所	Ck	87							
2	(菊川町)	島	〃	30							
3		五丁目	〃	190		6				3.2	
4		打上	〃	52							
5		下本所	R,Ck	43		3				7.0	小学校式場校舎の仕切戸大破，窓ガラス，瓦各々数枚破損.
6		下半済	R	45	1	1			2.2	4.4	
7		小出	〃	16		3				18.8	

10-8	六郷村	牛淵	R	103							
9	(菊川町)	小沢	〃	9							
10		神尾	〃	98							
11		小沢原・牛淵原	D	61	1				1.8	1.8	
		計		734	2	13			0.3	2.4	
11-1	加茂村	長池	Ck	48		2		1		4.2	現菊川南中学校に於て冲積粘土層厚さ約 7間.
2	(菊川町)	西袋	Ck,R	46		1		1		2.2	
3		白岩下	R	71		3		2		7.2	
4		〃段	〃	45	1	2		1	2.2	6.7	
5		小川端	R,Ck	34	9	8	8	6	26.5	50.0	
6		三軒家	Ck	57	4	4	2	5	8.1	14.0	
		計		301	14	20	10	16	4.6	11.3	
12-1	横地村	土橋	Ck	30	33	3	35	11	91.7	100.0	
2	(菊川町)	西横地	〃	36	34	8	25	26	81.0	100.0	
3		奈良野	〃	40	37	14	34	28	72.5	100.0	
4		下組	〃	32	19	10	20	44	59.4	90.6	
5		東横地段	R,Ck	47	1	2		5	2.1	6.4	
6		〃奥	R	51		5		2		9.9	
7		三沢	〃	57	1	6	1	3	1.7	12.3	
		計		293	125	48	115	119	42.5	54.9	死 3人，傷 4人．
13-1	内田村	東平尾	R	45	2	3		1	4.4	11.1	
2	(菊川町)	西平尾	〃	45	2	3			4.4	11.1	
3		月岡	〃	22							
4		耳川	Ck	11	5	1			45.5	54.5	
5		杉森	R	33							

番号	郡市町村	部落	地盤	戸数 a	住家被害 全潰 b	住家被害 半潰 c	非住家被害 全潰	非住家被害 半潰	住家被害率 全潰率 b/a×100	住家被害率 全半潰率 (b+c)/a×100	備考
13-6	内田村	御門	R, Ck	53	1	2			1.9	5.7	
7	(菊川町)	森	R	57		2				3.5	
8		政所	R, Ck	48	1	4			2.2	11.1	
9		段平尾	R	64	1	5	1		1.6	9.4	
10		高田	Ck	42	27	8	13	6	63.6	83.3	太郎坊権現全潰 3棟56坪.
11		稲荷部	R	46							
		計		463	39	27	14	7	8.4	14.5	
14-1	平田村	上平川	CK	29	22	6	18	27	75.9	96.9	この部落は裕富な農家が多く家屋がしっかりしているので他に比して全潰が少い.
2	(小笠町)	池村	〃	28	10	18	3	27	37.5	100.0	
3		堤	〃	53	30	12	23	23	58.9	79.2	全焼住家 1 棟, 同非住家 2 棟.
4		東組	〃	44		2		1		4.6	
5		志味堂・瑞泉ケ谷	R	29		2		1		6.9	
6		石原	〃	16		2				12.5	
7		八幡ケ谷	〃	22							
8		奥の谷	〃	94		12	3	2		12.8	全焼住家 2 棟, 死 2 人. 掘抜井戸 8 間余り.
9		新道	Ck	115	63	15	17	47	56.5	98.3	
10		下組	〃	44	20	18	6	36	45.5	86.4	
11		東峯田	〃	51	18	19	2	7	35.3	72.5	小学校倒潰 1 棟, 半潰 2 棟. 学童死 1 人, 重傷後死 1 人.
12		中峯田	〃	85	61	23	42	92	71.8	98.8	寺全潰 1 棟, 半潰 1 棟.
13		西峯田	〃	67	51	14	38	45	76.1	97.0	新築直後の農家 1尺程とび出す.
14		堂山	Ck, R	59	28	12	11	44	47.5	67.8	岩盤上の18戸は無事.
15		西ケ崎	Ck	15	14	1	17	12	93.3	100.0	赤子死 1 人, 国防婦人会員消火のため負傷 1 人. 岩盤上の 1 戸は無事.
		計		751	317	202	180	375	42.2	68.6	全村で死 8 人, 傷11 人.

15-1	小笠村	赤土	Ck,R	114	37	55	8	75	32.5	80.7	死者2人．段丘上の釜太夫原17戸は無事．
2	(小笠町)	猿渡	R	20		2				10.0	
3		川上	R,Ck	180							
4		棚草	R	72		2		1		2.8	家の傾き，障子の破れが多い．
5		棚草原	D	82							
6		丹野	R	96							
7		古谷	〃	66							
8		目木	〃	10							
9		山東	〃	20							
10		布引原	D	62							
		計		722	37	59	8	76	5.1	13.3	
16-1	南山村	佐栗谷	R	23		1		2		4.4	
2	(小笠町)	坊の谷・川原	〃	31		1				3.2	
3		新道	Ck,R	72	10	1		3	13.9	15.3	被害は南部の川沿い．小学校は昭和10年新築の南校舎を除いて残3棟は殆全潰．
4		池ケ谷	R	18				2			
5		虚空蔵	〃	22		3		1		13.6	
6		虚空蔵新道	Ck,R	10	2	1		3	20.0	20.0	
7		前岡	R	36		1		2		2.8	
8		東谷	〃	16		1		2		6.3	
9		中西	〃	16		1				6.3	
10		堀之内	〃	44	6	9	1		13.6	34.1	
11		馬々崎	〃	16	3	4	2	4	18.8	43 8	
12		北之谷	〃	18	4	4	2	1	22.2	44.4	
13		枝善	CK,R	12	1	7	3	1	8.3	66.7	
14		西村	R	22	1		1		4.5	4.5	
15		藤井	〃	9		2	1			22.2	
16		平	〃	30		3		1		10.0	

番号	郡市町村	部落	地盤	戸数 a	住家被害 全潰 b	住家被害 半潰 c	非住家被害 全潰	非住家被害 半潰	住家被害率 全潰率 b/a×100	住家被害率 全半潰率 (b+c)/a×100	備考
16-17	南山村	松ケ谷	R	10							
18	(小笠町)	糯田	〃	12							
19		山平	〃	34							
20		磯部	〃	21							正林寺灯籠全倒.
21		原	D	28							
22		一の谷	R	21							
23		今間	〃	9							
		計		530	27	39	10	22	5.1	12.4	
17-1	千浜村	久兵衛新田	Sc	4			1				
2	(大浜町	喜右衛門新田	〃	53	16	37	4	1	30.2	100.0	(千浜村) 国包寺全潰，小学校半潰 4棟，役場壁きれつ．死 4人，傷 3人．堂山部落は村境変更によつて小笠町へ編入.
3	及小笠町)	国包	〃	56	5	30	6	15	8.9	62.5	
4		国安	〃	115	22	56	11	50	19.1	67.8	
5		西部	〃	135	10	71	15	86	7.4	76.3	
6		堂山	Ck	5	4	1	4	1	80.0	100.0	
7		東部	Sc	150		6		1		4.0	
8		坂里	〃	14		6		2		42.9	
9		北部	〃	38	1			26	2.1	2.1	
		計		570	58	207	41	182	10.2	46.3	
18-1	新野村	木ケ谷	R, Cm	43	2	3	1	4	4.7	11.6	
2	(浜岡町)	山田ケ谷	R	42		3		3		7.1	
3		中尾	R, Cm	46		3				6.5	
4		上組	〃	50		4	1	2		8.0	
5		有ケ谷	R	46							

18-6	新野村	原	D	31	1				3.2	3.2	
7	(浜岡町)	篠ヶ谷	R	64							
8		長谷	〃	43							
9		黒田	〃	27		1	1			3.7	
		計		392	3	14	3	9	0.5	4.3	
19-1	池新田町	一区	Sc	183		2	2	6		1.1	
2	(浜岡町)	二区南	〃	173	4	4	7	5	2.4	4.8	
3		二区北	〃	157	2	3	8	6	1.3	3.2	
4		三区	〃	146		1	1	3		0.7	
5		四区	〃	140		2		4		1.4	
6		五区	〃	151							
7		六区	〃	135							
8		七区	〃	185							
9		八区	R	25	1	1		3	0.4	0.8	
		計		1,292	7	13	18	27	0.5	1.5	
20-1	朝比奈村	山ヶ谷	R	33		1		1		3.0	
2	(浜岡町)	行僧原	D	35				4			
3		北原	〃	52				4			
4		西原	〃	35			2				
5		下	R	49				2			
6		南	〃	55							
7		宮ヶ谷	〃	70							
8		岩地	〃	45							
9		小泉	〃	31							
10		横舟	〃	65							壁落下の所がある.
11		中原	D	38							
		計		508		1	2	11		0.2	

番号	郡市町村	部落	地盤	戸数	住家被害		非住家被害		住家被害率		備考
				a	全潰 b	半潰 c	全潰	半潰	全潰率 b/a×100	全半潰率 (b+c)/a×100	
21-1	比木村	東原	D	29				1			
2	(浜岡町)	西原	〃	35			1	3			
3		中田原	〃	19				1			
4		中田の谷	R	23		1		4		4.4	
5		宮木ケ谷	〃	31		2		4		6.4	
6		会下の谷	〃	19		1		1		5.3	正福寺位牌堂，瓦つい落.
7		三間	〃	34		1		2		2.9	賀茂神社石鳥居の柱一本折損．石灯籠の笠石火袋ついらく潰滅(1基).
8		上比木	〃	38		1		2		2.6	
9		勝佐の谷	R,Cm	47	1	2		5		6.4	全潰(倒潰)は県道沿いの店.
10		山田の谷	R	28		1		4		3.6	
11		名波の谷	〃	31	1	1		3		6.5	
12		梶ケ谷	〃	25				2		4.0	
		計		359	2	11	1	32	0.5	3.6	
22-1	佐倉村	玄保	Sc	67		2	1	2		5.7	
2	(浜岡町)	洗井	〃	49		2		3		4,1	
3		上の原	〃	57				2			
4		法の沢	〃	47		2	3	7		4.3	
5		雨垂	〃	63	2	3	2	1	3.2	8.0	
6		郷	〃	54		1				1.9	
7		西佐倉	〃	66		2		1		3.0	
8		宮内	Sc,R	64	4	4	2	4	6.3	12.5	
		計		469	6	16	8	20	1.3	4.7	
23-1	上内田村	田島	Ck	11							

23-2	(掛川市)	桶田	R	37	1	1		2	2.7	5.4	
3		五百済	〃	52	1		1		1.9	1.9	
4		段金谷	R, Ck	39	1				2.6	2.6	
5		下板沢	R	49	1	1		1	2.0	4.1	
6		上板沢	〃	66	2	1		2	3.0	4.5	
7		和田	〃	22		1	2			4.5	
8		子隣	〃	32	1			1	3.1	3.1	
9		岩井寺	〃	30							
10		大谷	〃	23				1			
		計		361	7	4	3	7	1.9	3.0	
24-1	佐束村	高瀬	R, Ck	118	1	3			0.8	3.4	
2	(城東村)	小貫	〃	102	2	9		1	2.0	10.8	
3		中方	〃	93		1	1			1.1	
4		岩滑	R	112	1		1		0.9	0.9	
		計		425	4	13	2	1	0.9	4.0	
25-1	土方村	入山瀬	Gg, R	125		4				3.2	此の村の住家半潰欄には，非住家半潰数をも含んでいる．
2	(城東村)	今滝	〃	31		3	1			9.7	
3		落合	〃	104		3	2			2.9	
4		峯向	〃	104		2				1.9	
5		下土方北区	〃	66		4				6.1	
6		〃 中区	〃	66		4				6.1	
7		〃 南区	R, Cg	74	1	3			1.4	5.4	
8		川久保	Cg	34		8	1			23.5	
		計		604	1	31	4		0.2	5.5	

番号	郡市町村	部落	地盤	戸数 a	住家被害 全潰 b	住家被害 半潰 c	非住家被害 全潰	非住家被害 半潰	住家被害率 全潰率 b/a×100	住家被害率 全半潰率 (b+c)/a×100	備考
26-1	中村	公文	Ck	60	36	5	11	29	60.0	68.3	小学校全潰 1棟. 半潰 4棟. 公会全堂潰 1棟. 役場半潰 1棟. 死 1人.
2	(城東村)	下方	〃	56	18	9	6	7	32.1	48.3	
3		高塚	R,Ck	58	3	9	1	2	5.2	20.7	
4		海戸	Ck	39	15	15	27	9	38.5	76.5	傷 1人
5		大石	Ck,R	58	16	2	13	9	27.6	31.0	傷 1人
6		西の谷	R	37		1		1		2.7	
7		毛森	〃	60	1		3		1.7	1.7	全潰は老朽家.
8		田ケ谷	〃	49		2		1		4.1	
		計		417	89	43	65	63	21.3	31.6	この村の低地一帯 8～9 尺掘下げると泥炭層がある. 掘抜井戸は掘つても水が出ない.
27-1	大坂村	新川	Ck,Cg	124	27	19	23	11	21.8	36.3	被害家はこの部落の南西部に集る.
2	(大浜町)	中川原	R,Ck	64	2	5	3	3	3.1	11.0	
3		寺部	R	60	3	8	5	4	5.0	18.3	御寺傾斜, 小規模ながけ崩れ.
4		太田	〃	48		4	1	3		8.3	
5		報地	Sc	137	4	7	6	4	2.9	8.0	
6		南大坂	〃	72	3	5	4	2	4.2	11.1	
		計		505	39	48	42	27	7.7	17.2	
28-1	睦浜村	三俣	Sc	76	3	6	7	4	3.9	11.7	正月庵倒潰.
2	(大浜町)	浜川新田	〃	70	3	5	2	5	4.3	11.4	
3		浜野	〃	94			1	5			道路 3間にわたつて沈下.
4		浜野新田	〃	27				1			畑不同沈下.
5		浜野西区	〃	40	1	1		10	2.5	5.0	
		計		307	7	12	10	25	2.3	6.2	

29–1	大淵村	野賀	Sc	61	11	9	24	17	18.0	32.2	此の中住家倒潰 2 棟.
2	(大須賀町)	新井	〃	53	21	16	23	29	39.6	69.8	此の中住家倒潰 4棟程度. 御寺おだれ落ち, 観音堂倒れる.
3		中新井	〃	32	2	5	1	4	6.3	21.9	
4		岡原	Gg	40		1	1	3		2.5	
5		浜	Sc	75		1		2		1.3	小学校全潰 1棟, 半潰 1棟(奉安殿). 田地を1尺程掘るとマコモが出る.
6		野中	Gg	65			2	2			
7		雨垂	Sc	62				1			
8		東大谷	Gg	29							
9		藤庄	〃	26							
10		藤源	〃	28		1					
		計		471	34	33	51	58	7.2	14.2	
30–1	横須賀町	西大淵	Gg	104		4				3.8	村部の戸数は地震当時のもの.
2	(大須賀町)	西大谷	〃	47							
3		沖の須	Sc	191							
4		今沢	〃	40							
5		河原崎	Gg	23		3				13.0	
6		川原町	〃	147		1				0.7	以下町部の戸数は1950年 4 月30日現在のもの.
7		十六軒町	〃	35							
8		大谷町	〃	35							
9		新屋町	〃	70							
10		東本町	〃	48							
11		中本町	〃	59							
12		西本町	〃	62							
13		愛宕下	〃	18							
14		軍全町	〃	66							
15		寺町	〃	84							
16		東新町	〃	68		1				1.5	

番号	郡市町村	部落	地盤	戸数 a	住家被害 全潰 b	住家被害 半潰 c	非住家被害 全潰	非住家被害 半潰	住家被害率 全潰率 b/a×100	住家被害率 全半潰率 (b+c)/a×100	備考
30-17	横須賀町	西新町	Gg	65		1				1.5	
18	(大須賀町)	松尾町	〃	68							
19		西田町	〃	83							
20		東田町	〃	68							
21		大工町	〃	69		2				2.9	
22		西番町	〃	32							
23		中番町	〃	39							
24		東番町	〃	37							
25		南番町	〃	39							
		計		1,296		12				0.9	戸数の計は地震当時のもの．
31-1	笠原村	五十岡	R	34							
2	(磐田郡袋井町及	上区	Gg	62		1				1.6	(笠原村) 小学校破損 1棟(式場校舎)．小谷田で神社及寺院全潰各 1棟. 主要部は磐田郡袋井町へ，石津・横砂・小谷田・清ケ谷は小笠郡大須賀町へ合併.
3	小笠郡大須賀町)	西区	〃	56							
4		東区	〃	29							
5		下区	〃	48							
6		南区	Gg,Co-S	85	5				5.9	5.9	
7		三輪	R	79	1				1.3	1.3	
8		三沢	Gg	86	1				1.2	1.2	
9		石津	Sc	67	4	10	4		6.0	20.9	
10		横砂	〃	24	1	5			4.2	25.0	
11		小谷田	R	17							
12		清ケ谷	Gg	37							
13		柏木	R	31	1				3.2	3.2	
		計		655	13	16	5		2.0	3.8	

32-1	東山口村	宮村	R	52							
2	(掛川市)	海老名	〃	29							
3		影森	〃	36			1				
4		汐井川原	〃	41							
5		寺ケ谷	〃	22							慶雲寺石灯籠倒潰.
6		伊達方	〃	51							
7		新田	〃	15							
8		本所	〃	38							
9		原子	〃	28							
10		木割	〃	24							
11		千羽	〃	26							
12		山鼻	Co-sk	36		1		2		2.8	当部落は 9割方壁落ち，ガラス破損.
13		逆川	R	38							
		計		436		1	1	2		0.2	
33-1	西山口村	葛川	Co-sk	146	7	68	3	60	4.9	51.4	
2	(掛川市)	成滝	〃	112	2	33	13	56	1.8	31.2	小学校，役場，隔離舎等半潰.
3		宮脇	R	46				7			
4		安養寺	〃	16				4			
5		薗ケ谷	〃	40				11			
6		満水	〃	89	1	2	1	6	1.9	3.4	茶工場の煙突折損.
		計		445	10	103	17	143	2.5	25.4	
34-1	粟本村	水垂	R	140							
2	(掛川市)	初馬下	〃	87			1				
3		〃 中	R,Co-sk	84				4			
4		〃 上	R	99				4			
		計		410			1	8			

番号	郡市町村	部落	地盤	戸数 a	住家被害 全潰 b	住家被害 半潰 c	非住家被害 全潰	非住家被害 半潰	住家被害率 全潰率 b/a×100	住家被害率 全半潰率 (b+c)/a×100	備考
35-1	西郷村	北門	Co-sk	57	6	40		2	10.5	80.7	
2	(三笠村)	下西郷	〃	65	1	7		5	1.5	12.6	
3		小市	〃	47			1				
4		方の橋	〃	47							
5		構江	〃	37							
6		石畑	〃	67							
7		石ケ谷	R	33							
8		美人ケ谷	〃	47	1				2.1	2.1	
9		滝の谷	〃	72							
10		長間	〃	55							
11		五明	〃	85							
		計		612	8	47	1	7	1.3	9.0	
36-1	掛川町	新町	Co-sk	125	5	19	5	6	4.0	19.2	
2	(掛川市)	喜町	〃	44	2	9	2	6	4.5	25.0	
3		塩町	〃	107	7	9	3	3	6.5	15.0	
4		肴町	〃	100	11	14	3	4	11.0	25.0	
5		栄町	〃	54	18	11	2		33.0	53.7	
6		紺屋町	〃	75	2	14	3		2.7	21.3	
7		研屋町	〃	73	4	4	2	2	5.5	11.0	
8		仁藤	〃	135		22	2	1		16.3	
9		連雀	〃	81		19		1		23.7	
10		中町	〃	100	2	4			2.0	6.0	
11		西町	〃	120			2	6			
12		十王	〃	68							

36-13	掛川町	下俣・十九首	Co-sk	177	7	18	3	9	4.0	14.1	
14	(掛川市)	城西	〃	295	6	33	5	1	2.0	13.2	
15		瓦町	〃	50	2	10			4.0	24.0	
16		緑町	〃	94							
17		大手	〃	42	1	19		2	2.4	47.6	
18		松尾町	R	82				1			
19		城内	〃	75	1	5			1.3	8.0	
20		神明町	〃	201		5		1		2.5	
21		旭町	〃	41		2		1		4.9	
22		二瀬川	Co-sk	108		13		3		12.0	
23		上屋敷	R	35		5				14.3	
24		秋葉通	Co-sk	26		3		3		11.5	
25		鳥居	〃	85		17		10		20.0	
26		橘	〃	145	4	63	2	7	2.8	46.2	
27		末広	〃	52		9		2		17.3	
28		長谷	Gg	67		3	1	5		4.5	
29		上張	Co-sk,R	121	11	20		3	9.1	25.6	
30		杉谷	R	44		3	5			6.8	
		計		2,822	83	353	40	77	2.9	15.5	
37-1	西南郷村	南西郷	Co-sk,R	127	7	14	5		5.5	16.5	
2	(掛川市)	下俣	R	85		5				5.9	
3		結縁寺	〃	20							
		計		232	7	19	5		3.0	11.2	
38-1	桜木村	宮下・中才	R	23							
2	(北小笠村)	鰯原	〃	30							

番号	郡市町村	部落	地盤	戸数 a	住家被害 全潰 b	住家被害 半潰 c	非住家被害 全潰	非住家被害 半潰	住家被害率 全潰率 b/a×100	住家被害率 全半潰率 (b+c)/a×100	備考
38-3	桜木村	田中	Co-sk	60	1	8	1	4	1.7	15.0	桜木南小学校破損甚だしい.（現廃校）
4	(北小笠村)	蔵人	〃	44	2	10		1	4.5	27.3	被害は小津根地区に集結，全潰 1棟は商店．農協半潰 1棟．
5		新田	R	34							
6		小山平	Co-sk,R	32	2	11	1		6.3	40.6	全潰の中 1棟は非住家を改造のもの．
7		飛島	R	57							
8		上垂木	〃	179							以下大字を示す．
9		遊家	〃	67							
10		家代	R,Co-sk	136		12		1		8.8	半潰の大部分は海老田部落，一部分は南部落に集る．
11		富部	R	97		3		2		3.1	
		計		760	5	44	2	8	0.7	6.4	
39-1	原田村	寺島	Co-ha,R	85			1	2			
2	(原田村)	原 里 一 区	〃	57				2			
3		〃 二 区	R	72							
4		平島	〃	49							
5		久居島	〃	35							
6		中西の谷	〃	33							
7		上西の谷	〃	52		1				1.9	
		計		383		1				0.3	
40-1	原谷村	本郷	Go-ha,R	198		3				1.5	
2	(原谷村)	細谷	R	122		1				0.8	
3		西山	R,Go-ha	71							共同茶工場煙突，40余尺倒潰．
4		幡鎌	R	73							
		計		464		4				0.8	半潰といつても激震地のそれと比べれば軽微．全村にわたり壁きれつ．

41-1	和田岡村	吉岡	R	132		2		1		1.5	小学校半潰 3棟.
2	(北小笠村)	高田	〃	87		1		1		1.1	公会堂半潰 1棟.
3		各和	Go-ha	155	2	8	2	6	1.3	6.5	寺院半潰 1棟. 共同作業場及集乳所全潰. 掘抜井戸 15—18 間.
		計		374	2	11	2	8	0.5	3.5	
42-1	曾我村	細田	Co-sk	50		14		6		28.0	
2	(掛川市)	沢田	〃	25		9		4		36.0	
3		原川	〃	55		32		3		58.2	掘抜井戸 16—17間
4		梅橋	〃	24				4			
5		徳泉	〃	16		2		3		12.5	
6		篠場	Gg	50		1		4		2.0	家のひずみ, タイル壁落下の程度.
7		平野	〃	24				1			
8		高御所	〃	68			1	1			お宮の鳥居倒れる.
9		領家本村	Co-sk	50		2		8		4.0	
10		〃 綱川	〃	20	1	11		8	5.0	60.0	
11		〃 新家	〃	16	1	15		14	6.3	100.0	
12		岡津	R	35							
		計		433	2	86	1	56	0.2	20.3	
III	周智郡										
43-1	森町	城下	Go-n	231							
2	(森町)	赤松	R	55							
3		川向	Go-n	70							
4		本丁	〃	50							
5		川久保	〃	36							
6		開運町	〃	98							
7		大上	R	23							

番号	郡市町村	部落	地盤	戸数 a	住家被害 全潰 b	住家被害 半潰 c	非住家被害 全潰	非住家被害 半潰	住家被害率 全潰率 b/a×100	住家被害率 全半潰率 (b+c)/a×100	備考
43-8	森町	新町	Go-n	107							
9	(森町)	明治町	〃	123							
10		仲横町	〃	116							
11		本町	〃	129							
12		川原町	〃	73							
13		下宿	〃	105							
14		栄町	〃	130	1		3		0.8	0.8	
15		大門	R	50							
16		向天方	Go-n	95							
17		橘	Br	27							
		計		1,518	1		3		0.1	0.1	この他太田川沿いに，壁破損瓦のついらく等 121戸ある．
44-1	一の宮村	米倉	R, Co-m	43	2	5		6	4.7	16.3	
2	(森町)	大久保	〃	54	2	3	3	7	3.7	9.3	寺院半潰 1棟．
3		片瀬	〃	57	5	3	4	5	8.8	14.0	役場全潰，小学校破損．
4		赤根	〃	39	1	4	2	6	2.0	12.6	
5		谷崎	〃	45	1	3	1	1	2.2	8.8	
6		宮代東	〃	57	1	3		3	1.8	7.0	
7		〃 西	〃	53		2		1		3.8	
		計		384	12	23	10	29	2.3	9.1	
45-1	園田村	草ケ谷	R, Go-n	88		1		3		1.1	
2	(森町)	円田	〃	160			1				
3		谷中	〃	87	14	5	9	5	16.1	21.8	田中では10戸中住家倒潰 8戸．農業会倉庫，谷中作業場倒潰．役場駐在所半潰学校倒潰 1棟，半潰 1棟．
4		中川上	〃	94	3	2		1	3.2	5.3	

45-5	園田村	中川下	R,Go-n	56	2				3.6	3.6	
6	(森町)	牛飼	Go-n	45	6	3	2	1	13.3	20.0	倒潰住家 6棟の中 5棟は太田川橋畔.
		計		530	25	11	12	9	4.7	6.8	
46-1	飯田村	市場	Go-n	75		9	4	8		12.0	山名神社鳥居笠つい落，玉垣 2間倒潰，忠魂碑倒潰.
2	(森町)	下飯田	R,Go-n	85	3	5	11	13	3.5	9.4	
3		中飯田	Go-n,R	70	1	12	6	23	1.4	.8.6	
4		上飯田	〃	45	1	5	3	7	2.2	13.3	
5		東組	R	28							
6		鴨谷	Go-n,R	40	5	13	10	7	12.5	45.0	
7		西組	Go-n	25	1	16	6	25	4.0	68.0	
8		福田地	Go-n,R	35			3	9			
9		新町	〃	110	1		3	3	0.9	0.9	瓦工場全潰 2棟.
10		北組	R	45			2				瓦工場全潰 1棟.
11		南組	〃	46			4				
		計		604	12	60	52	101	2.0	11.9	
47-1	宇刈村	春岡	Co-m	136	20	37	52	46	14.7	41.9	公会堂，倉庫，共同作業場等一部破損，人死 2人，牛死 1匹，極楽寺山門倒潰，
2	(山梨町)	一色	R	22		1	6	5		4.5	
3		三沢	R,Co-m	82	5	4	13	18	6.1	11.0	隔離舎全潰 1棟，共同作業場全潰 1棟，農業会，三沢公会堂各々半潰.
4		馬ケ谷	〃	70	3	10		8	3.9	18.6	公会堂半潰.
5		中村	R	61		6		10		9.8	公会堂半潰.
6		大日	〃	81	1	1			1.2	2.5	以上の外全村壁のきれつしないものなく，表面に出ない被害が多い．一色(5町)春岡(1町)耕地隆起陥没いちじるしい.
		計		452	29	59	71	78	6.4	19.5	
48-1	山梨町	上町	Co-m	160	25	32	11	21	15.6	36.3	神社全潰 1 棟.
2	(山梨町)	中町	〃	61	7	12	4	5	11.5	31.1	

番号	郡市町村	部落	地盤	戸数 a	住家被害 全潰 b	住家被害 半潰 c	非住家被害 全潰	非住家被害 半潰	住家被害率 全潰率 b/a×100	住家被害率 全半潰率 (b+c)/a×100	備考
48-3	山梨町	下町	Go-m	112	12	25	10	15	10.7	33.0	神社全潰 1棟.
4	(山梨町)	入古町	〃	130	18	27	13	21	13.8	32.2	
5		金屋敷	〃	77	5	15	7	8	6.5	26.0	小学校半潰 3棟.
6		沖山梨	〃	32	7	7	8	9	21.9	43.8	神社全潰 1棟.
7		山科上	〃	86	7	17	11	17	9.3	27.4	神社全潰1棟,寺院半潰1棟,公会堂全潰
8		〃 下	〃	102	13	20	13	20	12.7	32.3	1棟,小学松全潰3棟,神社全潰1棟,寺院
9		平宇	〃	50	1	10	7	11	2.0	22.0	全潰1棟,公会堂全潰1棟,神社全潰1棟.
		計	〃	810	95	165	84	127	11.7	32.1	全町死者26名中11名は疎開児童.
49-1	久努西村	鷲巣下	R	57	2	1	4	7	1.8	5.3	
2	(磐田郡袋井町)	上久能	Co-m, R	83	18	8	9	12	21.7	31.4	
3		中久能	Co-m	62	36	4	22	15	58.1	64.5	
4		下久能	〃	33	9	1	22	3	27.5	30.3	
5		久能向	〃	30	26		29	2	86.7	86.7	
6		堀越上	〃	72	26	3	32	4	36.1	40.3	
7		〃 下	〃	77	35	14	53	12	45.5	63.7	
8		山科上	Co-m, R	54	20		21		37.0	37.0	
9		〃 下	Co-m	16	10		8		62.5	62.5	
10		鷲巣上	R	44							
11		可睡	〃	48							
		計		576	182	31	200	55	34.5	37.0	全村死8人,重傷8人,軽傷8人,牛死2匹.
IV	**磐田郡**										
50-1	久努村	上貫名	Co-m	67	7	47	2	30	10.4	80.6	寺山門全潰1棟. 庫裡半潰1棟.
2	(袋井町)	下貫名	〃	41	31	8	28	20	75.6	95.1	寺全潰1棟, 教会半潰1棟, 火葬場全潰1棟, 神社全潰1棟.
3		方丈	〃	40	34	6	40	5	85.0	100.0	神社全潰 1棟, 寺全潰 1棟.

50-4	久努村	新屋	Co-m	70	56	12	40	28	80.0	97.1	
5	(袋井町)	久津部 西・東	〃	108	48	52	40	20	44.4	92.6	学校半潰 1棟，寺全潰 1棟.
6		北原川・名栗	〃	68	1	9	1	5	1.5	14.7	
7		不入斗	R, Co-m	27		6		5		22.2	
8		菅ケ谷	R	41		8	2	5		19.5	
9		村松 上	〃	54	2	7	1	6	3.7	16.7	寺半潰 1棟.
10		〃 下	〃	71	1	3		5	1.4	5.6	
11		〃 西	〃	50		2		4		4.0	
		計	〃	637	180	160	154	133	28.7	53.4	
51-1	袋井町 (袋井町)	西通 第一	R	79	2	29		13	2.5	39.2	
2		〃 第二	〃	106	8	5		6	7.5	12.3	
3		東通 第一	〃	78		4				5.1	
4		〃 第二	〃	124	8	4			6.3	9.7	
5		掛の上 南	〃	59	1	1			1.7	3.4	
6		〃 北	〃	55				1			
7		柳原	〃	36		2	3	1		5.6	
8		下地	Co-m	32	20	8	31	15	62.5	87.5	
9		三門	R	69		1	6			1.5	
10		田端 西	R, Co-m	61	11	8	2	3	18.0	31.1	
11		〃 東	R	46							
12		大門 西	〃	54			1				
13		〃 中	〃	42			2				
14		〃 東	〃	47	1	2		7	2.5	7.5	
15		神長	Gg	40			1	5			
16		宝野	〃	58	1		1		1.4	1.4	
17		菩提	〃	70							
18		法多	Gg, R	54							

(袋井町)
〇公共物
イ，役場　被害軽少
ロ，登記所　全潰
ハ，土木出張所　被害軽少
ニ，袋井駅　被害軽少
ホ，警部補派出所　被害軽少
ヘ，袋井商業学校　被害軽少
ト，袋井女子裁縫学校　被害大
チ，袋井町立青年学校　被害軽少
リ，袋井東小学校　被害軽少
ヌ，袋井小学校　全潰2棟，半潰1棟
ル，袋井町幼稚園　被害軽少
ヲ，みかど幼稚園　全潰 2棟
ワ，袋井保育所　全潰 4棟
カ，天理教会　被害軽少
ヨ，静岡銀行袋井支店　被害軽少
タ，加藤化学研究所　全潰 4棟
レ，隔離舎　全潰 3棟
〇神社・寺院
イ，木原　美禰神社　全潰
ロ，川井　十二所神社　全潰
ハ，土橋　熊里神社　全潰
ニ，袋井　白髪神社　全潰

番号	郡市町村	部落	地盤	戸数 a	住家被害 全潰 b	住家被害 半潰 c	非住家被害 全潰	非住家被害 半潰	住家被害率 全潰率 b/a×100	住家被害率 全半潰率 (b+c)/a×100	備考
51-19	袋井町	上石野	Gg	66							ホ，西田 王子神社 全潰 ヘ，高尾 渋垂神社 被害なし ト，袋井 観音寺 全潰 チ，川井 円通寺 全潰 リ，川井 宗円寺 全潰 ヌ，木原 長命寺 全潰 ル，高尾 慈眼寺 半潰 ヲ，高尾 満願寺 半潰 ワ，愛野 能光寺 半潰. ○死傷 イ，死 男22人，女43人，計65人 ロ，傷 101人.
20	(袋井町)	ネギヤ	Co-m	22							
21		下石野	R	19		1	1			5.3	
22		山田川	〃	22			5	2			
23		小野田	Co-m	26	15	4	37	16	57.7	73.1	
24		新町	〃	115	104	19	29		83.9	100.0	
25		中央町	〃	79	62	10	18	9	78.5	91.1	
26		本町	〃	73	67	10	27	5	87.0	100.0	
27		河原町	〃	40	25	2	16		62.5	67.5	
28		東町	〃	96	53	11	25	4	55.2	66.7	
29		中町	〃	74	47	15	39	8	63.5	83.8	
30		西町	〃	56	50	6	34	3	89.3	100.0	
31		木原	〃	59	53	2	53	43	89.8	93.2	
32		土橋	〃	36	33	2	75	8	91.7	97.2	
33		西田	〃	15	12	1	15	4	80.0	86.7	
		計		1,920	575	142	422	153	29.9	37.3	
52-1	上浅羽村	諸井	Co-s, R	131	55	36	21	17	42.0	69.5	
2	(浅羽町)	浅羽	〃	233	35	38	16	34	15.0	31.3	此の中篠ヶ谷 (30戸中住家全潰2棟)貫名地(33戸中被害なし)を含む. 死3人.
3		浅名	〃	132	64	11	42	16	48.5	56.5	此の中岡山 (40戸中住家全潰2棟)を含む. 死3人，傷2人. 小学校おだれ落下.
4		豊住	Co-s	76	64	3	63	27	83.8	88.2	御寺全潰 1棟. 死3人，軽傷 1人.
		計		572	218	88	142	94	38.1	53.5	役場附近 3尺地下よりマコモが出る. 豊住で掘抜井戸 40間

53-1	東浅羽村	新堀	Co-s	24	16	6	10	15	66.7	91.7	無住寺院半潰 1. 死 1.
2	(浅羽町)	梅山	Sc	114	31	15	16	20	27.2	40.4	寺院全潰2棟,半潰2棟,公会堂全潰1棟,小学校全潰1棟,半潰1棟,青年学校小破1棟,農業会半潰1棟.
3		松原	〃	103	25	15	23	16	24.3	38.8	寺院全潰 3棟.
4		初越	〃	26	7	1	5	9	26.9	30.8	寺院全潰 2棟.
		計		267	76	38	54	60	28.5	42.7	
54-1	西浅羽村	富里上	Co-s	30	9	11	10	5	30.0	66.7	(西浅羽村) 以上の外に
2	(浅羽町)	〃 中	〃	50	20	21	15	21	40.0	82.0	イ，農業会事務所　全潰 2棟.
3		〃 下	〃	44	26	6	20	19	59.1	72.7	ロ，神社寺院　全潰 7棟，半潰 4棟.
4		〃 東	Sc	34	3	3	3	5	8.8	17.6	ハ，役所　半潰 1棟
5		浅羽一色	Co-s	26	3	16	4	6	11.5	73.1	ニ，小学校　全潰 3棟.
6		中	〃	58	15	22	20	15	25.9	64.1	ホ，公会堂　全潰 3棟.
7		長溝	〃	84	29	31	23	23	34.5	71.4	掘抜井戸は 40—50間.
8		浅岡	〃	65	29	31	25	27	44.6	92.3	
		計		391	131	141	120	121	30.7	67.6	
55-1	幸浦村	湊西	Sc	45	14	3	7	5	31.1	37.8	(幸浦村)
2	(浅羽町)	〃 中	〃	56	10	6	5	6	17.9	28.6	役場　半潰 1棟
3		〃 東	〃	62	12	2	6	4	19.4	22.6	学校　全潰 1棟，半潰 1棟.
4		太郎助	〃	35	8	1		3	22.9	25.7	農業会　全潰 1棟,半潰 1棟.
5		西同笠	〃	64	11	1	5	4	17.2	18.8	神社　半潰 1棟.
6		東同笠	〃	69	13	2	6	7	18.8	21.7	寺院　全潰 5棟.
7		大野	〃	106	26	13		15	24.5	36.1	倒家は大概 60—70 の古さのもので，安政地震直後のものもある．震害の 1 原因として，海岸の為に台風を警戒して 6—7 寸角の松の木材を棟木に用いて屋根を重くしたことが考えられる．
8		中新田	〃	68	5	4		5	7.4	13.2	学校の倒れた校舎は式場兼用のもので大正13年建立．他の校舎は大正 6年と明治時代のもの．
		計		505	99	32	48	49	18.0	25.9	

番号	郡市町村	部落	地盤	戸数	住家被害		非住家被害		住家被害率		備考
					全潰	半潰	全潰	半潰	全潰率	全半潰率	
				a	b	c			b/a×100	(b+c)/a×100	
56-1	豊浜村	中野	Sc	129	26	6	14	12	20.2	24.8	役場半潰1棟，小学校全潰1棟，半破1棟，駐在所半潰1棟，工場半潰3棟
2	(福田町)	大島	〃	190	37	14	20	8	19.5	26.8	幼稚園　全潰1.
3		雁代	〃	82	14	10	9	8	19.1	29.3	公会堂全潰1棟，共同出荷場　全潰1棟.
4		小島方	〃	63	12	12	4	11	19.0	38.1	
		計		464	89	42	47	39	28.2	28.2	
57-1	三川村	見取	Co-m, R	132	3	5	6	5	2.2	6.1	(三川村) 以上の外に小学校全潰5棟，半潰1棟，(全校6棟の中)学童死亡8人(当時の2年生)．役場全潰1棟，農協全潰4棟，見取，
2	(袋井町)	大谷	〃	121	22	10	30	10	10.2	26.4	大谷，友永，川会等の部落では西方の磐田原台地の山沿いの部分に被害がまれで，ほとんどが東方の平野の部分に
3		友永	〃	79	29	20	32	23	24.0	62.0	集結している．一谷の一集落水洗はほとんど全滅した．
4		萱間	〃	88	9	3	8	16	10.2	13.6	掘抜井戸は見取で上層24—25間，下層40間，小学校で40間，川会で13間から取水する．又他にも水層は数段あるといわれ，豊富に噴出する．
5		川会	〃	96	23	11	29	53	24.0	35.4	岩盤（多分大日砂岩層）よりの取水もあるといわれ，冲積層の厚さの推定はむづかしい
6		山田	R, D	103		1				0.9	
		計		619	86	50	105	89	13.9	22.0	
58-1	今井村	深見一部	Co-m	35	29	6	24	11	82.9	100.0	(今井村) 被害率の上から，この村は全地震村域に於て最甚．
2	(袋井町)	〃二部	〃	32	30	2	24	8	93.8	100.0	以上のほか学校，役場，隔離舎等皆全潰．神社全潰7棟，寺院全潰7棟，
3		〃三部	〃	40	37	3	33	7	92.5	100.0	死亡17人(重傷後の死を含む)．
4		太田	〃	67	67		67		100.0	100.0	
5		延久	〃	43	43		43		100.0	100.0	
6		横井	〃	20	19	1	20		95.0	100.0	
7		徳光	〃	23	23		23		100.0	100.0	
8		小山	〃	76	74	2	71	5	97.4	100.0	
		計		336	322	14	305	31	95.8	100.0	

59-1	向笠村	笠梅	里原	Co-m	61	37	6	84	60	60.7	90.2	被害は上村，中村に集中し，大海は無事.
2	(磐田市)	〃	里原	D	23	1				4.3	4.3	
3		竹之内	里原	Co-m	76	46	20	105	100	60.5	87.0	
4		〃	里原	D	29	2				6.9	6.9	
5		新屋	里原	Co-m	33	34		76	70	100.0	100.0	
6		〃	里原	D	27	1	1			3.7	7.4	
7		西村	里原	Co-m	14	3	5	5	8	21.4	57.1	
8		〃	里原	D	19							
9		篠原	里原	Co-m	20	2	5	5	3	10.0	35.0	
10			里原	D	0							
11		岩井	里原	D,Co-m	38		20		50		52.4	
12			里原	D	29							
		計			369	125	57	277	271	33.1	9.3	全村で死亡2人，重傷2人，軽傷1人.
60-1	田原村	玉	越	Co-m	21	18	3	20	28	85.7	100.0	(田原村)
2	(磐田市及	西	島	〃	67	29	32	38	43	43.2	91.0	死3人，重傷3人，軽傷2人.
3	袋井町)	三ケ	野	Co-m,D	63	13	14	10	17	20.6	42.9	太田川新堤は1日川敷を横切る所が沈下．掘抜井戸小学校で50間．王越，西島，三ケ野，明ケ島は磐田市へ彦島，松袋井，上下新池は袋井町へ合併.
4		明ケ	島	〃	50	16	4	8	9	32.0	40.0	
5		彦	島	Co-s	29	15	11	15	27	51.7	93.1	
6		松袋	井	〃	42	26	9	10	7	61.9	83.3	
7		上・下新	池	Co-m	63	61	2	47	44	96.0	100.0	
		計			384	167	75	147	175	45.7	63.0	
61-1	御厨村	鎌	田	D	168	2	2		9	1.2	2.4	被害は 80—90 年経過.
2	(磐田市)	新	貝	D,Co-s	84	28	7	7	15	33.3	41.7	台地上の馬山(15戸)，台地ぎわの山本(18戸)には被害はない.
3		東	貝	D	42							
4		稗	原	Co-s	30	19	3	5	30	63.3	66.7	この村の倒家は東西に長い家で，残ったものは南北に長い家．低地では浅井戸は 1.5間位で水質悪く，掘抜井戸は40間位で水質がよい.
		計			324	49	12	12	54	15.1	18.8	

番号	郡市町村	部落	地盤	戸数 a	住家被害 全潰 b	住家被害 半潰 c	非住家被害 全潰	非住家被害 半潰	住家被害率 全潰率 b/a×100	住家被害率 全半潰率 (b+c)/a×100	備考
62-1	南御厨村	小島	Co-s	38	15				39.5		(南御厨村) 此の村の部落別住家全潰数は磐田郡神明中学校鈴木哲郎教諭調査のもの. 役場当局回答，全村被害数は 住家全潰 167棟 〃 半潰 88〃 非住家全潰 210〃 〃 半潰 115〃 死亡 男 2人 女 2人 計 4人 負傷 男 3人 女 4人 計 7人 役場及駐在所 全潰 学校及農業会 半潰. 小島・南島は福田町へ，他は磐田市へ合併.
2	(磐田市及福田町)	南島	〃	51	35	資料なし			68.6		
3		和口	〃	46	31				67.0		
4		新出	〃	52	47				90.4		
5		東新屋	〃	27	11				40.4		
6		大立野	〃	27	21				77.8		
7		蛭池	〃	30	23				76.8		
		計		271	183				63.8		
63-1	福田町	福田	Sc	890	107	61			12.0	18.9	(福田町) 以上のほか 全潰(棟) 半潰(棟) 小学校 1 3 神社 3 0 部長派出所 0 1 郵便局 0 1 農業会 0 2 食糧営団 1 1 寺院 5 3 工場 60 42 役場 0 2 死亡 6人 負傷 24人 罹災戸数 745戸.
2	(福田町)	中島	〃	228	22	14			9.7	15.8	
3		下太	Co-s	32	6	1			18.7	21.9	
		計		1,150	136	76			11.7	18.3	
64-1	於保村	五十子	Co-s	42	9	7	8	12	21.4	38.1	寺 全潰1棟，死亡 2人.
2	(於保村)	大原	〃	187	38	42	41	45	20.3	42.8	寺 半潰1棟.
3		下大之郷	〃	41	11	10	8	7	26.8	51.2	

64-4	於保村	南田	Co-s	43	5	4	6	4	11.6	20.9
5	(於保村)	塩新田	Sc	42	5	3	5	6	11.9	18.6
6		一色	〃	36	3	4	7	8	8.3	15.2
7		清庵新田	〃	20	1	5	4	3	5.0	30.0
8		太郎馬新田	〃	16	2	4	3	2	12.5	38.8
9		浜部	〃	43	5	7	8	9	11.6	27.9
		計		470	79	86	90	96	16.8	35.1
65-1	磐田町	三本松	D	119			1			
2	(磐田市)	東坂	〃	128	3		2		2.3	2.3
3		権現	〃	108	1		1		0.9	0.9
4		住吉	〃	96						
5		宿	〃	86				1		
6		川尻	D, Co-s	112	3	6	4		2.7	8.0
7		清水	D	61		1		1		1.6
8		新通	D, Co-s	92	3	8	1		3.3	12.0
9		地蔵小路	D	152			1			
10		馬場	〃	82			1			
11		天王町	〃	105						
12		倉小路	〃	79						
13		北井上	〃	187		1	1			0.5
14		西坂	〃	167	1	1			0.6	1.2
15		西之小路	〃	131		1				0.8
16		玄妙小路	〃	201	1				0.5	0.5
17		梅屋	〃	89						
18		川原	〃	297	1		1		0.3	0.3
19		横町	〃	233						
20		西境松及東境松	〃	138		1				0.7

(磐田町)
火葬場 全潰 16坪
屠場 全潰 50坪
神社 全潰 2棟 15坪
　　 半潰 1棟 15坪
寺院 全潰 4棟 73坪
　　 半潰 1棟 15坪
工場 全潰 23棟 1,494坪
　　 半潰 6棟 277.5坪
死亡 見付新道，千牛堂，中泉各 1人，計 3人.
重傷 2人
軽傷 7人
二の宮の被害は，同町内の平担部四丁目，次いで三丁目に集る.

番号	郡市町村	部落	地盤	戸数 a	住家被害 全潰 b	住家被害 半潰 c	非住家被害 全潰	非住家被害 半潰	住家被害率 全潰率 b/a×100	住家被害率 全半潰率 (b+c)/a×100	備考
65-21	磐田町	西北浦	D	56			1				
22	(磐田市)	中北浦	〃	21							
23		東北浦	〃	63			1				
24		中町	〃	259							
25		東町	〃	286		1		1		0.4	
26		七軒町	〃	213							
27		西町	〃	299							
28		田町	〃	226							
29		久保町	〃	217							
30		坂之上	〃	263							
31		西新町	〃	388		3	1			0.8	
32		石原	〃	293	3	16			1.0	6.5	
33		栄町	〃	83	14	15			16.9	34.9	
34		御殿	D, Co-s	293							
35		二之宮	〃	542	22	13			4.1	6.5	
36		梅原	D	283	2	12	2		0.7	5.0	
37		天龍	D, Co-s	141				1			
38		豊島	〃	36	2	2		1	5.5	11.1	
39		北島	〃	19		1				5.3	
40		千手堂	Gt	65	2	4	2	1	3.1	9.2	
41		万正寺	〃	43			5				
42		中野	〃	25	9	7	2	1	36.0	64.0	
43		上大之郷	〃	33	16	10	1		48.5	78.7	
44		下岡田	Gt, Co-s	22	7	9			31.8	72.7	
45		上岡田	Gt, Co-s	40	10	6	4		25.0	40.0	
46		西貝塚	D	165	2	4	6		1.2	3.6	

65-47	磐田	町	西之島	Co-s	55	10	25	4		18.2	63.6	
48	(磐田 | 市)	上南田	〃	14	7	3			50.0	71.4	
49			安久路	D	38							
50			城之崎	〃	34							
			計		7,042	119	150	42	6	1.7	3.8	
66-1	広瀬	村	上神増	Gt	151			1				広瀬小学校壁きれつ及脱落 123.5 坪，ガラス破損22枚，煉突破損1基.
2	(豊岡 | 村)	社山	R	36							
3			壱貫地	Gt	97							
4			神増	〃	45		1				2.2	
5			惣兵衛	〃	20							
6			平松	〃	57		1				1.8	
7			掛下	〃	31							
8			松之木島上	〃	42		1				2.4	
9			〃　下	〃	57		1				1.8	
10			三家	〃	34		1				2.9	
11			下神増	〃	34							
			計		604		5	1			0.8	
67-1	岩田	村	勾坂	Gt	24							
2	(磐田 | 市)	勾坂中	〃	57			1				
3			〃　下	〃	55							学校，役場に多少の損傷があるが記載する程の事はない
4			〃　上	〃	69	1				1.5	1.5	
5			寺谷圦下	〃	47							
6			〃　上	〃	53							
7			寺谷新田	〃	17							
			計		322			1		0.3	0.3	

番号	郡市町村	部落	地盤	戸数 a	住家被害 全潰 b	住家被害 半潰 c	非住家被害 全潰	非住家被害 半潰	住家被害率 全潰率 b/a×100	住家被害率 全半潰率 (b+c)/a×100	備考
68-1	富岡村	勾坂西	Gt	61		1				1.6	(富岡村) 小学校でガラス100枚程破損．電線，電柱に相当の被害．村道破損20ケ所，橋梁2ケ所．掘抜井戸3間程度．
2	(豊田村)	〃 中之郷	〃	20							
3		七蔵新田	〃	34		1				2.9	
4		中野戸	〃	56		2				3.6	
5		気賀西	〃	18							
6		上気賀	〃	24							
7		勾坂下	〃	18							
8		気賀下	〃	43				1			
9		加茂東	〃	43	1		2	2	2.3	2.3	
10		〃 西	〃	44	1	3	2	1	2.3	9.1	
11		〃 川原	〃	24				1			
12		〃 東原	D	56							
13		東 原	〃	50							
		計		491	2	7	6	7	0.4	1.5	
69-1	池田村	龍 東	Gt	21							この村にはひはだや，トタン屋根が7—8割をしめる．被害は瓦屋根の家屋，学校，神社だけに見られる．北東部に地盤の沈下が見られた．
2	(豊田村)	新町上	〃	28	4	1			14.3	17.9	
3		〃 下	〃	31	2				6.5	6.5	
4		賀美町	〃	35	2	3			5.7	14.3	
5		宿	〃	44	2	4	2		4.5	13.6	
6		田 中	〃	37		1				2.7	
7		中町上	〃	17							
8		〃 中	〃	15							
9		〃 下	〃	19	1	2	1		5.3	16.0	
10		居楽町	〃	21		3				14.8	
11		下横町	〃	27							

69–12	池田村	下町	Gt	17		3				17.6	
13	(豊田村)	八町	〃	16		1				6.3	
14		林	〃	29			1				
		計		357	11	18	4		3.1	8.1	
70–1	井通村	一言	Gt	126	3	15			2.4	14.3	
2	(豊田村)	上万能	〃	22		3				13.6	
3		彌藤太島	〃	19		1				5.3	
4		森岡	〃	10	1				10.0	10.0	
5		上新屋	〃	29	3	6			14.4	31.0	
6		小立野	〃	24	1	5	不	不	4.2	25.0	
7		西之島	〃	57	4	8			7.0	21.0	
8		長森	〃	34	2	4			5.9	17.7	
9		源平新田	〃	10		2				20.0	
10		森本	〃	81	5	5			6.2	12.4	
11		立野	〃	54	2	9			3.7	20.4	小学校も被害甚大.
12		森下	〃	35	1	3			2.9	11.4	
13		宮一色	〃	38	3	2			7.9	13.2	
14		中之田	〃	16	1	2	明	明	6.3	18.8	
15		気子島	〃	54	6	3			11.1	16.7	
16		笹原島	〃	11		1				9.8	
17		海老塚	〃	40	3	6			7.5	22.5	
18		下万能	〃	30	3	3			10.0	20.0	{非住家の被害は記してないが，物置小屋や小さい小屋の被害が大きかつた.
		計		690	38	78			5.7	16.8	
71–1	長野村	鮫島	Sc	108	6	29	8	14	5.6	32.4	{火葬場　全潰 1棟，死亡2人.
2	(磐田市)	小島	〃	125	7	23	7	14	5.6	24.0	掘抜井戸小学校及道辻の民家で各々約
3		草崎	Gt	115	5	24	6	11	4.4	25.2	30間.

番号	郡市町村	部落	地盤	戸数 a	住家被害 全潰 b	住家被害 半潰 c	非住家被害 全潰	非住家被害 半潰	住家被害率 全潰率 b/a×100	住家被害率 全半潰率 (b+c)/a×100	備考
71-4	長野村	野箱	Gt	16	2		2	4	12.5	12.5	
5	(磐田市)	白拍子	〃	21	2			2	9.5	9.5	
6		新島	〃	35	4	7	5	9	11.4	31.4	
7		前野	〃	106	5	21	8	13	4.7	24.5	寺院 全潰 4棟，神社 半潰 2棟.
8		長須賀	〃	21	2	4	3	5	9.5	28.6	
9		刑部島	〃	25	2		2	4	8.0	8.0	
		計		572	35	108	41	76	6.1	24.9	安政地震で村は潰滅し，建物はそれ以後のもの，倒家は古い家に限る.
72-1	十束村	上本郷	Gt	20	2	1	1	5	10.0	15.0	(十束村) 以上の外
2	(龍洋町及豊田村)	下本郷	〃	33	2	10	1	10	6.1	36.4	小学校全潰2棟（唱歌室平家瓦葺20坪，物置平家瓦葺20坪）.
3		赤池	〃	35	5	1	3	4	14.3	17.1	全潰住家の中倒潰は12棟，その残りは復旧困難の破損，堀之内では田が隆起畑が沈下した所がある．道路は各所できれつ水を噴出した。掘抜井戸は40—43間，地震の時にごつて増水，余震の遠のくのに従つて平常に復す.
4		中島	〃	65	11	12	7	13	16.9	35.4	
5		宮本	〃	14	1	11	2	25	7.1	85.7	
6		高木	〃	53	11	15	6	18	20.8	49.1	
7		松本	〃	6		3	1	4		50.0	上本郷，下本郷，赤池は豊田村へ，他は龍洋町へ合併.
8		堀之内	〃	54	13	6	15	10	24.1	35.2	
9		平間	〃	36	8	20	14	18	21.9	77.8	
		計		316	53	79	50	107	16.8	41.8	
73-1	袖浦村	駒場	Sc	201	13	46	27	23	6.5	29.4	(袖浦村) 破損家屋は古い瓦屋．掘抜井戸は小学校用のもの40間，自噴する.
2	(龍洋町)	西平松	〃	94	7	9	14	15	7.4	17.0	
3		平岡	〃	49	1	5	9	8	2.0	12.2	
4		中平松	〃	58	1	4	13	11	1.7	8.6	
5		東平松	〃	52	4	1	11	9	7.7	9.6	
6		海老島	〃	63	1	3	11	12	1.6	6.4	

73–7	袖浦町	小中瀬	Sc	20	7	2	6	7	35.0	45.0	
8	(竜洋町)	大中瀬	〃	28	4	3	4	5	14.3	25.0	
9		稗原	〃	23	3		5	4	13.0	13.0	
		計		588	41	73	100	94	7.0	19.4	
74–1											
2	掛塚町	本町	Gt	143	1	7		1	0.7	5.6	(掛塚町)
3	(龍洋町)	砂町	〃	74		5				6.8	全町的に壁落下し，ガラスは破損した．古い家が罹災．
4		中町	〃	63	2	1			3.2	4.8	
5		田町	〃	34		3				8.8	
6		大当町	〃	43		5				11.6	
7		横町	〃	102		8				7.8	
8		新町	〃	95	1	3			1.1	4.2	
9		蟹町	〃	81	1	2			1.2	3.7	
10		東町	〃	53	1	3			1.9	7.5	
11		十郎島	〃	35							
12		白羽	〃	139	3	3			2.1	4.3	
13		野崎	〃	45	2	5			4.4	15.6	
14		川袋	〃	75	1	9			1.3	13.3	
15		西堀	〃	38	8	11	1	3	21.1	50.0	
16		敷地	〃	30	1	7	3	2	3.3	26.6	
17		内名	〃	24	1	4			4.2	20.8	
18		吹上	〃	17							
19		江口	〃	39	2	8			5.1	23.1	
		金洗	〃	40	1	3			2.5	10.0	
		計		1,170	25	87	7	6	2.1	9.6	

番号	郡市町村	部落	地盤	戸数	住家被害		非住家被害		住家被害率		備考
				a	全潰 b	半潰 c	全潰	半潰	全潰率 b/a×100	全半潰率 (b+c)/a×100	
V	引佐郡										
75-1	麁玉村	大屋敷	Gt	79				1			
2	(浜名郡浜北町)	町	Gt,D	112		1				0.9	
3		有隣	Gt	123		2		1		1.6	
4		野口	〃	69				1			
5		梔池	Gt,D	67							
6		譲栄	D,Gt	78		1		1		1.3	
7		東原	Gt	124				2			
8		本村	〃	126				1			
9		下善	〃	134							
10		大平	R	91				1			
11		堀谷	〃	54							
12		灰木	〃	38							
13		辺田原	D	9							
		計		1,104		5		8		4.5	
76-1	都田村	川山	R	52							
2	(浜松市)	新木	〃	47							
3		横尾	〃	56							
4		谷上	〃	41							
5		中津	〃	98		1	1			1.0	
6		一色	〃	28							
7		吉影	〃	61							
8		中野	〃	101							
9		須部		49							

76-10	都田村	滝東	R	66							
11	(浜松市)	〃 中	〃	52							
12		〃 西	〃	50							
13		鷲沢	〃	35							
		計		736		1	1			0.1	
77-1	中川村	一区	R	71							
2	(細江町)	二区	〃	86							
3		三区	Ch	68	2				2.9	2.9	
4		四区	D	94		1				1.1	
5		五区	〃	50				1			
6		六区	Ch	62			2				
7		七区	D	114	1			1	0.9	0.9	
8		八区	Ch	69	2				3.0	3.0	
9		九区	D	90				1			
10		十区	〃	122		4	1	3		3.3	
		計		826	5	5	3	6	0.6	1.2	
78-1	金指町 (引佐町)	金指	R	267	3	1	1	2	1.1	1.5	小学校 半潰.
79-1	気賀町	伊目	D	235		1				0.4	
2	(細江町)	老ケ谷	〃	114	4	7	1		3.5	9.6	
3		油田	〃	62							
4		広岡	R	75							
5		小野	〃	101							
6		清水	R,Ch	385	2		1	2	0.5	0.5	土蔵壁落下数庫，灯籠倒多い.
7		上町	〃	465				1			同 上， 同 上.
8		呉石	R	111							倉庫屋根一部落下 2庫.

番号	郡市町村	部落	地盤	戸数 a	住家被害 全潰 b	住家被害 半潰 c	非住家被害 全潰	非住家被害 半潰	住家被害率 全潰率 b/a×100	住家被害率 全半潰率 (b×c)/a×100	備考
79-9	気賀町	葭本	R	44							
10	(細江町)	小森	〃	47							
11		下村	〃	166							
12		五根山	〃	158		1				0.6	
13		寸座	〃	115							秋葉灯籠　全潰.
		計		2,077	6	9	2	3	0.3	0.7	
80-1	東浜名村	都筑	R	377							(東浜名村) 全潰1棟は工場で，腐朽が甚だしい建物であつた．家屋人畜の被害は皆無に近かつたが倒潰を免れたものでも壁のはげ落ち，きれつ，軸部の損傷は全戸数の 1/3 に及ぶ.
2	(三ケ日町)	大崎	〃	242			1				
3		大谷	〃	140							
4		佐久米	〃	104							
5		駒場	〃	48							
		計		911			1				
81-1	三ケ日町	三ケ日	R	681							柱損傷 2棟，屋根瓦緩隙 6棟.
2	(三ケ日町)	宇志	〃	99							
3		津々崎	〃	67							
4		岡本	〃	141							
5		摩訶耶	〃	33							
6		只木	〃	92							
7		福長	〃	146							
8		平山	〃	141							
9		釣	〃	53							
10		日比沢	〃	66							
11		本坂	〃	77							

81-12	三ケ日町	鵺代	R	110							
13	(三ケ日町)	下尾奈	〃	175			1				
14		上尾奈	〃	88							
		計		1,969			1				
VI	**浜名郡**										
82-1	龍池村	善地	Gt	110		1		1		0.9	(龍池村)
2	(浜北町)	上善地	〃	93							南部に震動が激しかつた.
3		永島	〃	90							
4		八幡	〃	46							
5		高薗	〃	147							
		計		486		1		1		0.2	
83	北浜村 (浜北町)	27ケ部落	Gt	3,417							村内に3—4棟の半潰があつたが詳細不明.
84-1	小野口村	小松 八幡	Gt	108							
2	(浜名町)	〃 本村	〃	98							
3		〃 東中瀬	〃	139							
4		〃 南中瀬	〃	329			1				
5		〃 西中瀬	〃	148	1				0.7	0.7	
6		〃 尾島	〃	93							
7		〃 沖	〃	40							
8		〃 西向	〃	92							
9		内野 上	〃	106							
10		〃 西	D,Gt	86							
11		〃 下	Gt	65							
12		〃 小島	〃	73							
13		平口 新田	〃	105							

番号	郡市町村	部落	地盤	戸数 a	住家被害 全潰 b	住家被害 半潰 c	非住家被害 全潰	非住家被害 半潰	住家被害率 全潰率 b/a×100	住家被害率 全半潰率 (b+c)/a×100	備考
84-14	小野口村	平口 法師軒	Gt	87							
15	(浜名町)	〃 本村	D,Gt	125							
		計		1,690	1		1		0.1	0.1	
85-1	積志村	万斛	Gt	112			1	1			
2	(積志村)	橋爪	〃	223			1				
3		西ケ崎	〃	314			1				
4		下大瀬	〃	187		3	2	3		1.6	
5		有玉	Gt,D	544	4	11	16		0.7	2.8	
6		半田	〃	180	1				0.6	0.6	
7		漆島	Gt	55							
8		上大瀬	〃	79							
9		上前島	〃	59							
		計		1,753	5	14	21	21	0.3	1.1	
86-1	豊西村	中善地	Gt	35							
2	(浜松市)	末島	〃	77							(豊西村)
3		常光	〃	100		1	1			1.0	南半にやや被害．被害家は老朽弱化のため．
4		貴平	〃	77				1			
5		恒武	〃	135	1		1		0.7	0.7	
6		石原	〃	100							
7		倉中瀬	〃	69							
8		本田	〃	42			1				
9		随国	〃	46							
10		羽鳥	〃	49							
		計		730	1	1	3	1	0.1	0.3	

87-1	笠井町	一区	Gt	410	1				0.2	0.2	
2	(浜松市)	二区	〃	282	1				0.3	0.3	
3		三区	〃	291							
4		四区	〃	138							
5		五区	〃	122							
6		六区	〃	56							
		計		1,299	2				0.2	0.2	
88-1	長上村	上石田北	Gt	79			1				東亜航空浜松工場半潰（木造瓦葺平家鋸屋根 120 坪）.
2	(浜松市)	〃 南	〃	87							
3		市野東	〃	86							
4		〃 南	〃	114		4				3.5	
5		〃 北	〃	83							
6		小池北	〃	105							
7		〃 南	〃	109		2				1.8	
8		中田	〃	53	1	3			1.9	7.5	
9		原島	〃	62							
10		天王	〃	71		3				4.2	
11		下堀	〃	59							
12		天王新田	〃	58	2	3			3.4	8.6	
13		下石田北	〃	94		1				1 1	
14		〃 南	〃	95	1	3			1.1	4.2	
		計		1,155	4	19	1		0.3	2.0	
89-1	中の町村	中里	Gt	55	7	3	11	4	12.7	18.2	（中の町）神社全潰 3棟，半潰 1棟．小学校全潰 1 棟（井戸屋形）半潰 1 棟（廊下）死 2人．被害家は古い家，屋根の重い家，かどの家，お宮等．役場，学校，病院等地盤の不同沈下によつて破損した（重みのかかつた柱の部分が沈下）各所より地震の際噴水．
2	(浜松市)	松小池	〃	65	7	5	9	7	10.8	18.5	
3		大明神	〃	41	1	4	1		2.4	12.2	
4		萱場	〃	104	4	5	2	4	3.8	8.6	

番号	郡市町村	部落	地盤	戸数 a	住家被害 全潰 a	住家被害 半潰 c	非住家被害 全潰	非住家被害 半潰	住家被害率 全潰率 b/a×100	住家被害率 全半潰率 (b+c)/a×100	備考
89–5	中の町村 (浜松市)	国吉	Gt	196	6	47	6	15	3.1	27.0	掘抜井戸は20—23間.
6		中野町	〃	603	46	64	31	9	7.6	18.2	東海道本線鉄橋はピアにきれつが入り上部が移動。天竜川原に立つ送電塔南に傾斜.
7		一色	〃	52	11	5	1	1	21.5	30.8	
8		富田	〃	22	8	2	2	2	36.4	45.5	
9		白鳥	〃	92	7	2	2	4	7.6	9.8	
		計		1,230	97	137	65	46	7.9	15.0	
90–1	和田村 (浜松市)	永田	Gt	310	1	1		1	0.3	0.6	(和田村) 天竜兵器工場倒潰し死 2 人，傷 1 人 (動員学徒).
2		橋羽	〃	205		11				5.4	全村的に家のひずみ，屋根瓦落下壁脱落等の被害.
3		篠ケ瀬	〃	85	1	1	1		1.2	2.4	東海道は橋羽東方できれつ.
4		北島	〃	68	1		1		1.5	1.5	村道薬師にて1尺程陥没.
5		薬師	〃	106	6		3	2	5.7	5.7	
6		薬師新田	〃	57	1				1.8	1.8	
7		安間新田	〃	48		3	1	1		6.3	
8		安間	〃	118		1				0.8	
9		半場	〃	116	1	1		1	0.8	1.7	
10		竜光	〃	57	1	2	1	1	1.8	5.3	
11		長鶴	〃	21	2		1		9.5	9.5	
		計		1,191	14	20	8	6	1.2	2.9	
91–1	飯田村 (浜松市)	上組	Gt	34							(飯田村)
2		西組	〃	46	1				2.2	2.2	日本楽器KK天竜工場全潰，常久寺半潰，小学校廊下崩解し，学童死 3 人.
3		田畑	〃	38							以上のほか家の傾斜，壁落下は多数.
4		開戸	〃	55		1		1		0.5	家屋のほか，田畑のきれつ甚だしく，農作に被害が多かつた.
5		新田	〃	42	1	1	1		2.4	4.8	掘抜井戸は30個内外あり，15—20間

91–6	飯田村	下飯田	Gt	63	3		1		4.8	4.8	
7	(浜松市)	西鶴見	〃	101							
8		東鶴見	〃	55							
9		青屋	〃	64							
10		新貝	〃	71	2				2.8	2.8	
11		西大塚	〃	59	1	6		8	1.8	11.9	
12		西之郷	〃	65							
13		渡瀬	〃	68							
14		小松方	〃	40							
15		日本楽器会社社宅	〃	47							
		計		848	8	8	2	9	0.9	1.9	
92–1	芳川村	石原	Gt	78	5		3		6.5	6.5	寺院全潰 2 棟，死亡 1 人.
2	(浜松市)	安松	〃	124	6		1		4.8	4.8	
3		本郷	〃	110	2	4	2		1.8	5.5	
4		頭陀寺	〃	77			6				
5		参野	〃	45	3			1	6.7	6.7	
6		大橋	〃	92	3	1	2	2	3.3	4.3	寺院　全潰 1 棟.
7		恩地	〃	45	1		2		2.2	2.2	小学校廊下全潰.
8		西恩地	〃	17	1	3		2	5.9	23.5	
9		大柳	〃	67	8	8	5	2	11.9	23.9	
10		大鼠野	〃	31	3		1	2	9.7	9.7	
11		御給	〃	25	2	1	3	4	8.0	12.0	
12		江川	〃	20	1		1	1	5.0	5.0	
13		下前島	〃	12			2	2			
14		下中島	〃	29	2	2		3	6.9	1[illegible].8	
15		四本松	〃	53		3	2	3		5.6	
16		立野	〃	57	2	2	1		3.5	7.0	

番号	郡市町村	部落	地盤	戸数 a	住家被害 全潰 b	住家被害 半潰 c	非住家被害 全潰	非住家被害 半潰	住家被害率 全潰率 b/a×100	住家被害率 全半潰率 (b+c)/a×100	備考
92-17	芳川村	古川	Gt	48	2	1	2	1	4.2	6.3	
18	(浜松市)	金折	〃	60	13	11	20	15	21.7	40.0	
19		西伝寺	〃	21			2				寺院 半潰 1 棟.
20		老間	〃	48	11	18	5	10	22.9	60.4	寺院 半潰 1 棟, 死亡 2 人.
21		東金折	〃	8	2	3		6	22.0	62.5	全村的に家がひずみ, 壁落ち, かわらガラスの被害が多かつた. 掘抜井戸は役場で31—2間, 鼠野で37—8間, 4本松で34間.
		計		1,067	67	57	60	54	6.3	11.6	
93-1	河輪村	西	Gt	83	9	29	10	9	10.9	45.8	(河輪村)
2	(浜松市)	蒲島	〃	6	1	2	2	2	16.7	50·0	神社及寺全潰 各 1 棟.
3		東	〃	108	14	30	9	14	13.0	40.7	全村的に家のひずみが多い. 江戸時代の旧天龍川流路跡に倒家.
4		芋瀬	〃	102	18	9	8	10	17.6	26.5	掘抜井戸は富屋敷で40間以上.
5		中新田	〃	16	1	3		1	6.3	25.0	
6		三新及彌助新田	〃	60	10	14	9	11	16.7	40.0	
7		長十郎新田	〃	39	2	7	3	5	5.1	23.1	
8		富屋敷	〃	25	2	3	7	6	8.0	20.0	
		計		439	57	97	46	58	13.0	35.1	
94-1	五島村	西島	Sc	149	15	24	不明		10.0	26.1	(五島村) 寺院・神社は全部半潰.
2	(浜松市)	松島	Gt	120	23	42			19.2	54.2	松島松泉寺, 福島観音寺, 西島大昌寺等被害大きく, 又松島神社は殆全潰.
3		江之島	Sc	71		4				5.6	全村的に見ると家のひずみ等の小被害が多い.
4		福島	〃	41		5				12.2	
5		鶴島	Gt	17	4	3			23.5	41.2	海岸沿いの耕地は隆起, 陥没がいちじるしい. 砂防堤は所々くぼみそこの松並木は倒れた.
6		平左衛門新田	Sc	19		8				42.1	
		計		417	42	86	21	48	10.0	30.7	

95	三方ヶ原村（浜松市）	5ヶ区	D	815				1			
96-1	吉野村（浜松市）	南区	D	45	1	2			2.2	6.7	（吉野村）被害家は老朽のため．
2		中区	〃	85	1	5			1.2	7.1	
3		北区	〃	49	1	1			2.0	4.1	
4		西区	〃	27	1	1			3.7	7.4	
5		東区	〃	31		1				3.2	
6		旭西区	〃	76							
7		〃 東区	〃	57							
		計		370	4	10			1.0	3.8	
97-1	和地村（湖東村）	中トヤ	D,Ch	83	5	2	1	1	6.0	9.6	道路面人馬の入りうる大きれつ．
2		下ノヤ	D,Ch	63				1			路面小きれつ．
3		中久保	D	82							同
4		上久保	〃	61							同
5		向	〃	95							同
6		大平山	〃	83							
8		西大山	〃	61							
9		東大山	〃	63							
		裏山	〃	51							
		計		642	5	2	1	2	0.8	1.1	
98-1	北庄内村（庄内村）	堀江	Sh	267							
2		白洲	D	241							
3		呉松	〃	169		1				0.6	
4		平松	〃	117							
5		深萩	〃	66							
		計		860		1				0.1	

番号	郡市町村	部落	地盤	戸数	住家被害		非家被任害		住家被害率		備考
				a	全潰 b	半潰 c	全潰	半潰	全潰率 b/a×100	全半潰率 (b+c) /a×100	
99-1	南庄内村	和田	D,Ch	158	2	3		4	1.3	3.2	
2	(庄内村)	脇和	〃	98		4		7		4.1	
3		庄内内山	〃	101		5		3		5.0	
		計		357	2	12		14	0.6	3.9	
100-1	村櫛村	北明	D,Ch	139	40	21	3	2	28.6	37.4	(村櫛村)
2	(庄内村)	仲町	D,Sh	247	31	22	7	4	12.6	21.5	被害は明治以後の湖面埋立の部分で，特に北明に多い．西明で死男女各1人．
3		西明	D,Ch	176	11	15	2	5	6.3	14.8	地震の時東部埋立地で赤褐色の泥水を
		計		562	82	58	12	11	14.6	24.5	吹く．
101-1	伊佐見村	伊左地	D,Ch	385	1		1		0.3	0.3	非住家全潰 1 棟は青年学校．
2	(湖東村)	佐浜	〃	213	2				0.9	0.9	
3		大人見	〃	146							
4		古人見	〃	180							
5		新田	〃	77							
6		谷上	〃	45							
		計		1,046	3		1		0.3	0.3	
102-1	雄踏町	中村	Sc	178	1	2	1	1	0.6	1.7	(雄踏町) 通称「ゆうとう町」
2	(雄踏町)	田端	〃	55	1	2	1	1	1.8	5.5	葬儀用建物倒潰 1 棟(中村)．
3		小山	〃	249	2	3	2	2	0.8	20.1	神社の水屋倒潰 1 棟(領家)．
4		領家	〃	162	2	3	1	1	1.2	3.1	山崎住家半潰 2 棟は殆全潰．
5		浅羽	〃	453	4	5	3	3	0.8	2.0	被害は砂丘地周辺の湖面開拓地に多い．養魚池の見張小屋は各所で殆全潰．
6		西ケ崎	〃	531	4	5	2	2	0.9	1.7	
7		山崎	D,Ch	278	1	2	2	2	0.4	1.1	
		計		1,888	15	22	12	12	0.8	2.0	

103-1	神久呂村	神ケ谷	D	712							(神久呂村)
2	(浜松市及入野村)	大久保	〃	266							志都呂は入野村へ編入，神ケ谷，大久保は浜松市へ合併．
3		志都呂	D,Sc	269	3	3	3	1	1.1	2.2	
		計		1,247	3	3	3	1	0.2	0.5	
104-1	入野村	田端	Sc	172	11	13	6	12	6.4	14.0	
2	(入野村及浜松市)	三村	D,Sc	146	13	8	5	9	8.9	14.4	
3		西鴨江	〃	82	4	6	1	6	4.9	12.2	
4		北脇	Sc	88	4	4	3	9	4.6	9.1	
5		道陸地	〃	82	1			2	1.2	1.2	
6		彦尾	D,Sc	80		2	1	2		2.5	
7		蜆塚	D	162	1		1	1	0.6	0.6	蜆塚は浜松市へ編入．
8		本所	Sc	93							
		計		905	34	33	17	41	3.8	7.4	
105-1	可美村	高塚	Sc	354	1		15		0.3	0.3	(可美村)
2	(可美村及浜松市)	増楽	〃	80							遠州織機KK全潰4,669.5坪死亡2,3名．鈴木織機KK全潰3,033.6坪．
3		若林	〃	345			2				高蔵寺全潰67.57坪
4		東若林	〃	203	1				0.5	0.5	工場被害の原因はバラック造りのため．雀神社，春日神社拝殿各々半潰．
5		明神野	〃	73	2		1		2.7	2.7	明神野東明神野は浜松市へ編入．
6		東明神野	〃	120			1				
		計		1,175	4		19		0.3	0.3	
106-1	新津村	新橋	Sc	200	1				0.5	0.5	
2	(浜松市)	小沢渡	〃	180							
3		倉松	〃	185							
4		堤	〃	48							

番号	郡市町村	部落	地盤	戸数 a	住家被害 全潰 b	住家被害 半潰 c	非住家被害 全潰	非住家被害 半潰	住家被害率 全潰率 b/a×100	住家被害率 全半潰率 (b+c)/a×100	備考
106-5	新津町	米津	Sc	136							
6	(浜松市)	法枝	〃	49	1				2.0	2.0	
7		田尻	〃	60							
		計		858	2				0.2	0.2	
107-1	篠原村	篠原東部	Sc	269	3	4	2	5	1.1	2.6	(篠原村) 小学校廊下全潰48坪，教室半潰125坪，寺院全潰 1棟，神社全潰 1棟，工場半潰 5棟，倒家はいずれも壁が少い．寺院は屋根が重いため倒れた．工場被害は木造の不完全な建て方による．全村砂地．篠原北部のボーリングによればずつと砂層で，20間，30間，60間の所に礫層を夾む．馬郡では地下 100 間まで砂層，所々に海藻の埋れた層がある．
2	(篠原村)	〃 中部	〃	266	11	18	6	12	4.1	10.9	
3		〃 西部	〃	275	17	33	15	20	6.2	18.2	
4		坪井	〃	200	1	8	3	6	0.5	4.5	
5		馬郡	〃	295	6	16	5	4	2.0	7.5	
6		駅前	〃	208		3	2	2		1.4	
		計		1,513	38	82	33	49	2.5	7.9	
108	舞坂町 (舞坂町)		Sc	947	1	16	6		0.1	4.5	(舞坂町) 寺院全潰 1棟，3分潰 1棟 人畜被害はない．橋はかろうじて通り得る程度の被害
109-1	新居町	栄町	Sc	246	1			3	0.4	0.4	(新居町) 町全体家がひずんだ程度．被害は源太山の舟だまり附近に多い．栄町は埋立地で微被害が目立つ．
2	(新居町)	泉町	〃	186	5			2	2.2	2.2	
3		中町	D, Sc	193	1		2	2	0.5	0.5	
4		高見	D	84		1		4		1.2	
5		西町	〃	75	2			4	2.7	2.7	
6		上田町	〃	118		3		2		2.5	
7		中田町	Sc	50	1			1	2.0	2.0	
8		俵町	〃	84		2		1		2.5	
9		船町	〃	191	2	3	1	2	1.0	2.6	
10		源太山	D, Sc	245	4	2	2	5	1.6	2.5	

109-11	新居町	柏原	Sc	58							
12	(新居町)	湊町	〃	33							
13		新居弁天	〃	41							
14		新弁天	〃	24							
15		日ヶ崎	〃	144	1	1	2	4	0.7	1.4	
16		若磯	〃	88	2			2	2.3	2.3	
17		杣山	〃	44		1				2.1	
18		高師山	〃	45							
19		松山	〃	58							
20		大倉戸	〃	60		2		3		3.3	
21		内山	D	75							
22		内之郷南	D,Sc	112	2			4	1.8	1.8	
23		〃 北	〃	110	4			2	3.6	3.6	
		計		2,364	25	15	7	41	1.1	1.7	
110-1	鷲津町	表鷲津	D,Ch	287	1	7	1	2	0.3	2.4	(表鷲津) 高密工業KK全潰，負傷13人. 富士紡鷲津工場コンクリート壁きれつの程度.
2	(湖西町)	鷲津	Ch,D	495	38	139	3	1	7.7	35.7	(鷲 津) 矢崎電工全潰，レンガ壁崩れ，6–7人圧死．安藤電気KK全潰．死亡 12人，負傷37人.
3		裏鷲津	D,Ch	270	26	30	2	3	9.6	20.7	(裏鷲津) 小工場全潰 2棟，負傷11人.
4		古見	〃	146	1	4	1		0.7	3.4	(古 見) 負傷 2 人.
5		川尻	D	127		4				3.2	
6		市場	D,Ch	143	2	4	1	1	1.4	4.2	
7		山口	D	48		2				4.2	
8		坊瀬	〃	16							
		計		1,532	68	190	8	13	4.4	16.8	
111-1	知波田村	神座	D	55							
2	(湖西町)	太田	〃	98			1	1			
3		青平	R	54	1				1.8	1.8	

番号	郡市町村	部落	地盤	戸数	住家被害		非住家被害		住家被害率		備考
					全潰	半潰	全潰	半潰	全潰率	全半潰率	
				a	b	b			b/a×100	(b+c)/a×100	
111-4	知波田村	大知波	R	182	1		1		0.5	0.5	
5	(湖西町)	利木	〃	68		1		1		1.5	
6		横山	〃	42							
		計		499	2	1	2	2	0.4	0.6	
112-1	入出村 (湖西町)	入出	R,Ch	536	71	192	20	12	13.2	49.1	小学校全潰1棟，半潰2棟，負傷2人．被害密集地は明治以後の埋立地．小学校運動場大きれつ．
113-1	新所村	新所	D,Sh	350	1				0.2	0.2	国鉄東海道本線築堤（最高20m）は北側に崩落，列車の不通2週間．
2	(湖西町)	岡崎	D	237		2				0.8	
3		梅田	〃	129							
		計		716	1	2			0.1	0.4	
114-1	白須賀町	新町	Sc	82			2				（白須賀町）古い宿場で現在はさびれて老朽家が多く，被害をうけた．地震当時疎開者が改造非住家に住込み，これも多く倒れた．
2	(湖西町)	元町第1・第2	〃	85			2	1			
3		〃第3・第4	〃	75			3				
4		東町	D	62	7	4	7	4	11.3	17.7	
5		東町橋丁	〃	63	6	4	2	1	9.5	15.9	
6		浦町	〃	36	6				16.7	16.7	
7		東中町	〃	38	5	6	3	4	13.3	29.0	
8		西中町	〃	75	2	1	5	1	2.7	4.0	
9		西町	〃	45	2	3	4	4	4.4	11.1	
10		境宿	〃	55		2	1	1		3.6	
11		境川	〃	15							
12		笠子	〃	20	2				10.0	10.0	

114-13	白須賀町	東長谷	D	45			1	1			
14	(湖西町)	中長谷	〃	90	4	1	1	4	4.4	5.6	
15		西長谷	〃	31	2			2	3.2	3.2	
		計		816	38	21	31	23	4.7	7.2	
Ⅶ	**浜松市**										
115	浜松市役所 直轄区域	81ケ町内	Gt, D, Sc	28,573	198	406	104	153	0.7	2.1	戦災のため町内別被害数は不明. 備考記事は本資料の最後部に記す.
116-1	曳馬支所	曳馬町	Gt	400							
2	(曳馬支所)	十軒町	〃	81							
3		上島町	Gt, D	287							
4		細島町	Gt	35							
5		新津町	〃	269		3				1.0	
6		助信町	〃	635		6				0.9	
7		高林町	Gt, D	409		1				0.3	
8		茄子町	Gt	70							
9		早出町	〃	143							
		計		2,365		10				0.4	
117-1	蒲支所	宮竹町	Gt	53			8				中島航空KK宮竹工場全潰(木造鋸屋根 1,600坪).
2	(蒲支所)	神立町	〃	116			4				
3		植松町	〃	225							
4		将監町	〃	49							
5		西塚町	〃	29							
6		上西町	〃	55							
7		丸塚町	〃	57							
8		上新屋町	〃	51							
9		子安町	〃	99							
10		大蒲町	〃	73							
		計		807			12				

番号	郡市町村	部落	地盤	戸数 a	住家被害 全潰 b	住家被害 半潰 c	非住家被害 全潰	非住家被害 半潰	住家被害率 全潰率 b/a×100	住家被害率 全半潰率 (b+c)/a×100	備考
118-1	白脇支所	寺脇町	Sc	167	5	5	1		3.0	6.0	高福寺全潰.
2	(白脇支所)	白羽町	〃	183	6	15	5		3.6	11.5	法蔵寺全潰.
3		中田島町	〃	125	7	8			5.6	12.0	海竜寺全潰.
4		揚子町	Gt	100		2				2.0	
5		瓜内町	Sc	138		1				0.7	
6		三島町	〃	202	5	2			2.3	3.5	
7		福塚町	〃	28							神宮寺山門全潰.
		計		944	23	33	6		2.4	5.9	{井戸によれば地下 15—6尺迄粘土，以下砂層.
119-1	富塚支所	向平	D	54							(富塚支所)
2	(富塚支所)	小薮	〃	27		1				3.7	被害の多い低地部はもとの湖底らしく
3		安座	〃	63	3	1			4.8	6.4	同地小学校地下よりコマモが出る.
4		谷田平	〃	36		1	1			2.8	
5		上の平	〃	28	1		2		3.6	3.6	
6		西脇	〃	32	1	2			3.1	9.4	
7		本村	D,ch	55	1	11			1.8	21.8	
8		東島	〃	49	1	1			2.0	4.1	
9		権現谷	D	26		1				3.8	
10		新谷	〃	50				1			
		計		420	7	18	3	1	1.7	5.9	

(浜松市役所直轄区域の備考記事)

この区域は天龍川平野，三方原台地，海岸砂丘地帯の相接する所に位置する．繁華な商店街は台地下の平野の部分で，工場地帯はその周辺を北・東・南・南西にかけてとりまく．台地上は諸官衙学校及び住宅地である．一般に下町の工場地帯に被害が多く，壁脱落，家のひずみは各所にある．特に東海道本線以南の龍禅寺町・砂山町・寺島町方面が目立ち，当時新興の軍需工場にいちじるしく多かつた．一般民家では龍禅寺町内に倒潰 5棟，半潰 7棟，傾斜 50 棟の密集被害がある．又瓦落下，壁のきれつは町内各所にある．倒家はいずれも木造二階家で，階上床の所で柱が折損して倒れた．目測によれば階上部で 2 尺程振動した． 火災はなかつた．此所一帯は元来砂地で良地盤のはずであるが，砂丘間のくぼみに当り，局部的に軟弱な泥が堆積したために被害を見たのであろう．又南駅砂山町内木造三階建旅館は倒れた．

上池川町，下池川町は新川上流が三方原を解析した谷に当る．両町では全潰 15棟，半潰 27棟，傾斜 70 棟，水道漏水（ジョイント部）600 m，鉄管切損約 100 個所．道路各所できれつを生じた．死者は 5 才の女児 1 人．被害の最もはげしいのは六間道路沿いで，従来どぶ田を埋立した個所のためであり，従つて重量建築物は 10m 近い杭打ちをしなければ危険である．

地盤のよい三方原台地やその斜面では被害はわずかである．追分町陸軍高射砲学校（現在静岡大学理工学部）では，生徒集会所（6間×30間）が倒れた．これは同建物を大ホールにする目的で壁や柱を取除いたためである．利町で五社神社石垣及び周囲の民家の土塀が崩潰した．和地山町では茶工場が 1 棟倒潰した．

砂丘地帯では浅田，森田，東伊場方面の低湿地に稍被害がある． 浅田町では 2 階造りの住家が倒れ，森田町では工場が倒れて 1 名圧死し，東伊場町では， 宇布見県道沿いに 2—3 戸倒れ， 県居小学校は 3 棟の 2 階校舎の中南校舎は大壁くずれ柱が 3－4 本損じ，屋根瓦は流れ落ちた．

元城町北部にも局部的に 14—15 戸が密集倒潰した．ここは浜松城外濠あと（妙高寺谷 と 呼ばれる）を埋立てた所で，そこの地盤は地震のさい 1 尺程沈下した．

北部の山下町でも民家が損傷し，中沢町の日本楽器会社では煉瓦造りの鋳鉄職場が崩解し， 工員 1 名が負傷した．

14. *Study of the Relation between the Subsoil Conditions and the Distribution of the Damage Percentage of Wooden Dwelling Houses in the Province of Tōtōmi in the case of the Tōnankai Earthquake of December 7th, 1944.*

By Syōhachi OOBA,
Kikugawa-Kita Middle School.

Since old times the dependence of earthquake intensity on the subsoil condition has been well-known in this country. In compliance with the national postulation to promote the building of rational and economical earthquake-resistant structures throughout our land of earthquakes, the study of the foundation coefficient for the enhancement of earthquake intensity due to the subsoil condition has been undertaken from various points of view by many scientists and engineers. Most reliable and direct data have been obtained from the observation of the earthquake intensity in actual large earthquakes in the locality. Relative intensity of an earthquake can be inferred from the difference of dynamical effect on the same kind of physical system. As Japan is very densely populated, the dwelling house is one of the most prevalent objects throughout the country, and in addition its mode of construction is almost identical within a certain area. Actually the frequency distribution of the strength of wooden dwelling houses in our country has been proved to be normal in many instances. Therefore, the percentage of houses destoryed to a certain degree in a locality may be deemed to be the best measure of the mean intensity of the earthquake in the locality. If we take, therefore, the area of a locality properly, we can obtain reliable mean intensity for a place of a given subsoil condition.

With these considerations in mind, the writer collected the statistical data on the damage of houses in each hamlet, that is the subdivision of a village or a town and consists in the mean of about 90 families (houses) in the present area. Considering the homogeneity of statistics, the percentage of totally collapsed wooden dwelling houses in each hamlet was used in this paper. It is true that some confusion was introduced by the uncommon official despatch from the prefectural government to enter only those houses perfectly levelled to the ground into the category of the totally collapsed houses, in which those houses still standing but irreparably damaged have been ordinarily included in current practice and in some reports in the present case. But the ambiguity arising from this is small in itself and much less than that seen in the classifications of half collapse and other degrees of damage. On the other hand appendage houses to a dwelling are too numerous in variety to be counted and studied statistically, while kinds of dwelling houses other than wooden houses were almost nil in these areas. These are the reasons why the writer adopted the percentage of the totally collapsed wooden dwelling houses in this study.

The writer is a native of the province of Tōtōmi, where the damage due to the Tōnankai Earthquake was severest as compared with the other provinces notwithstanding the fact that the epicentral distance was not the shortest. It was between 150 km and 220 km from the epicentre located at 33.7° of north latitude and 136.2° of east longitude by the Central Meteorological Observatory. The total number of totally collapsed houses in the whole disturbed area is reported to be 26,130, of which the province of Tōtōmi shared 5,183 amounting to almost one fifth of the total. The dwelling houses half collaps-

ed, burnt or washed away by the tsunami waves in the present area were respectively 5,529, 3 and 0 corresponding to 46,590, 12 and 3,059 suffered in the total disturbed area. Although the writer does not know the accuracy of the epicentre determination, the circumstances would not be changed so much for the true epicentre as to justify the extraordinarily high damage in our province. In fact, this extraordinary severity of intensity in the province attracted the writer's attention and compelled him to study it closely.

The statistical data, sent to the writer through the courtesy of the village and town offices or collected by the writer himself or by his friends are shown in the Table III at the end of the paper. From these data the writer calculated the percentages of totally and half collapsed dwelling houses respectively and tabulated them in the same table. The percentage of totally collapsed houses are plotted on a geographical map of scale 1:50,000 and contour (isoseismal) lines of 80, 60, 40, 20% were drawn on that map (Fig. 4). We see from the figure marked clustering of places of high damage amounting up to 100% in the drainage basins of the rivers, Ootagawa and Kikugawa, while along the river course of the Tenryū and Ooi the circumstances are entirely different. From these intensity distributions we cannot find any direct dependence of the intensity on the epicentral distance, so that we must seek other controlling factors. Since we cannot expect such a particular pattern of energy radiation from the hypocentre, and seeing the marked relation to geography and geology, we may conclude that it is mainly due to subsoil conditions.

From these points of view the area in question was divided into 10 regions as follows:

(a) Ootagawa Basin (C_o, G_o)
(b) Kikugawa Basin (C_k)
(c) Aluvial Area at the Foot of the Makinohara Plateau (C_m).
(d) Alluvium near the Lake Hamana (C_h, S_h)
(e) Tenryū Plain (G_t)
(f) Ooigawa Fan (G_i)
(g) Gravel Deposit Area around the Mt. Ogasa (G_g)
(h) Coastal Sand-dune Area (S_c)
(i) Diluvial Plateau (D)
(j) Rocky Foundation (R)

The symbols C, S, G and R indicate clay, sand, gravel and rocky foundation respectively, while the subscripts o, k, m, h, t, i and g respectively denote the region above mentioned. Some detailed descriptions of the geological conditions of these regions are given and the relation with the damage percentage of dwelling houses are discussed separately. Markedly higher damage was experienced in the basin where clayey marsh deposits extend near the low grade river courses, while on the diluvial plateau with a gravel layer or along high grade river courses with gravel beds the damage was decidedly slight, as in the Makinohara and Mikatagahara plateaus and in the Tenryū and Ooigawa regions. In the coastal sand-dune area the damage was intermediate and on the rocky fundations the damage was negligible. The statistics of the damage in these regions are tabulated in Table I.

The mean percentages for C, G, S and $(D+R)$ regions were 26.1, 1.4, 3.5 and 0.2% respectively. Some historical evidences on the development of specially weak formations are given, and the thickness of the alluvial deposits as inferred from the depth of artesian wells is also considered.

Seisimic activity in historical times in the present area and characteristic features of the damaged houses are also described in some detail.

昭和32年7月15日印刷
昭和32年7月20日發行

東京都文京區本富士町一番地
東京大學構內

編纂兼發行者　東京大學地震研究所

東京都千代田區富士見町一丁目十番地

印刷者　笠井康頼

東京都千代田區富士見町一丁目十番地

印刷所　株式會社國際文献印刷社

賣捌所

東京都中央區日本橋通二丁目六番地

丸善株式會社

Sold by

Maruzen Co., Ltd.,

Nihonbashi-dôri, Chûô-ku, Tôkyô.

Price of this copy: 1232 Yen. (Postage exclusive.)

BULLETIN OF

THE EARTHQUAKE RESEARCH INSTITUTE

UNIVERSITY OF TOKYO

Vol. XXXV, Part 1. March, 1957.

Contents.

Papers and Reports.

Page

1. Y. SATÔ, Study on Surface Waves XIII. Nomograph for the Phase Velocity of Love-Waves in Doubly Stratified Medium. (in English) 1
2. T. RIKITAKE and S. SATO, The Geomagnetic D_{st} Field of the Magnetic Storm on June 18–19, 1936. (in English) 7
3. I. YOKOYAMA and H. TAJIMA, A Gravity Survey on Volcano Mihara, Ooshima Island by Means of a Worden Gravimeter. (in English) 23
4. R. MORIMOTO, K. HUZITA and T. KASAMA, Cenozoic Volcanism in the South-western Japan with Special Reference to the History of the Setouchi (Inland Sea) Geologic Province. (in English) 35
5. T. ICHIMURA and K. AOKI, Some Geological Considerations of the Neogene Sediments Exposed at the Western Margin of the Yamagata Basin. (in English) 47
6. I. YOKOYAMA, Energetics in Active Volcanoes. 2nd Paper. (in English) 75
7. I. YOKOYAMA, Energetics in Active Volcanoes. 3rd Paper. (in English) 99
8. K. KANAI, T. TANAKA and K. OSADA, Measurement of the Micro-tremor. II. (Tokyo Metropolis.) (in Japanese) 109
9. K. KANAI, T. TANAKA and K. OSADA, Measurement of the Micro-tremor. III. (Yokohama City.) (in Japanese) 135
10. K. KANAI, N. NASU, T. TANAKA and K. OSADA, Measurement of the Micro-tremor. IV. (Sakata and Tsuruoka.) (in Japanese) 149
11. K. KANAI, H. KAWASUMI, T. TANAKA and K. OSADA, Measurement of the Micro-tremor. V. (Osaka City.) (in Japanese) 163
12. K. KANAI, T. TANAKA, T. MORISHITA and K. NAKAGAWA, Measurement of the Micro-tremor. VI. (Ichinomiya City, Aichi Prefecture.) (in Japanese) 181
13. K. KANAI, T. TANAKA and K. OSADA, Measurement of the Micro-tremor. VII. (Kawasaki City.) (in Japanese) 191
14. S. OOBA, Study of the Relation between the Subsoil Conditions and the Distribution of the Damage Percentage of Wooden Dwelling Houses in the Province of Tōtōmi in the case of the Tōnankai Earthquake of December 7th, 1944. (in Japanese) 201

(For the papers written in Japanese or in occidental languages, the abstracts are given in occidental languages or in Japanese respectively.)

東京大学地震研究所彙報　第 35 号 (1957) 第 1 冊

14.　1944 年 12 月 7 日東南海地震に見られた
遠江地方の家屋被害分布と地盤との関係

大　庭　正　八

図版　第 8 及び 9

Plates of Nos. VIII and IX of the Bulletin of the Earthquake Research Institute, Vol. 35 (1957), Part 1

14. Study of the Relation between the Subsoil Conditions and the Distribution of the Damage Percentage of Wooden Dwelling Houses in the Province of Tōtōmi in the case of the Tōnankai Earthquake of December 7th, 1944

By Syōhachi OOBA

第4図　1944年12月7日東南海地震による遠江地方の家屋被害率分布図

Fig. 4. Distribution of the damage percentage of wooden dwelling houses in the Province of Tōtōmi, due to the Tōnankai Earthquake of Dec. 7th, 1944.

[S. OOBA. Bull. Earthq. Res. Inst., Vol. XXXV, Pl. VIII.
震研彙報　第35号　図版　大庭]

[地理調査所承認済]

付

$$住家全潰率 = \frac{住家全潰数 \times 100}{全戸数}\%$$

1. 上記の式に基いて各市町村の部落毎に住家全潰率を算出する。(小数点下は4捨5入)
2. %を地図上の部落の中心部に記入する。(市町村部落図の部落番号と一致した位置)
3. 等率曲線を描入し段彩をほどこす。

灘　江

見付

住家全潰率 = $\frac{\text{住家全潰数} \times 100}{\text{全戸数}}$ %

1. 上記の式に基いて各市町村の部落毎に住家全潰率を算出する。(小数点下は4捨5入)
2. %を地図上の部落の中心部に記入する。(市町村部落図の部落番号と一致した位置)
3. 等率曲線を描入し段彩をほどこす。

(stippled)	1%
(fine horizontal lines)	20%
(vertical lines)	40%
(fine grid)	60%
(cross-hatch)	80%
(solid marks)	全潰

掛川

川

	0%
	1% — 19%
	20% — 39%
	40% — 59%
	60% — 79%
	80% — 100%
	全潰家屋密集部分

掛

浜名郡白須賀町(114) 500m

(側家) 浜名郡新居町(109) 500m

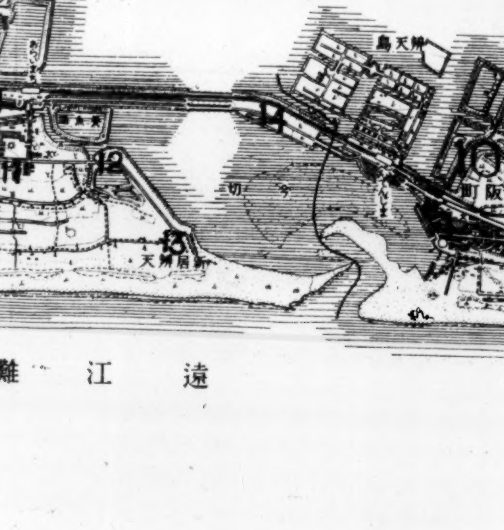

第20図 遠江地方郡市町村区劃及
小字は部落番号)

Fig. 20. Index map of the ham
boundaries of the counties, citi
denote the numbers of cities, towns a
hamlets, shown in Table III.)

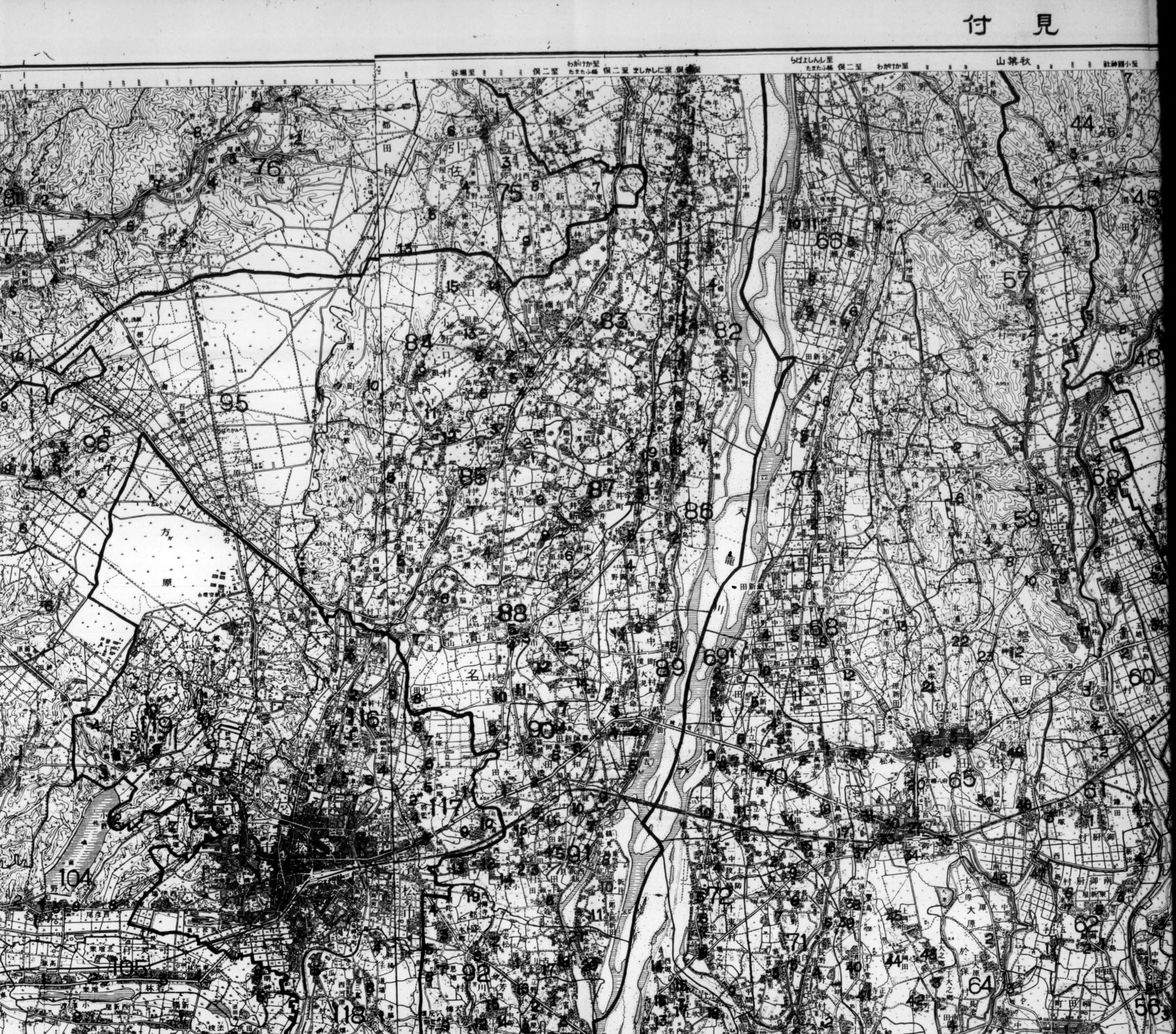

磐田郡池田村(69)

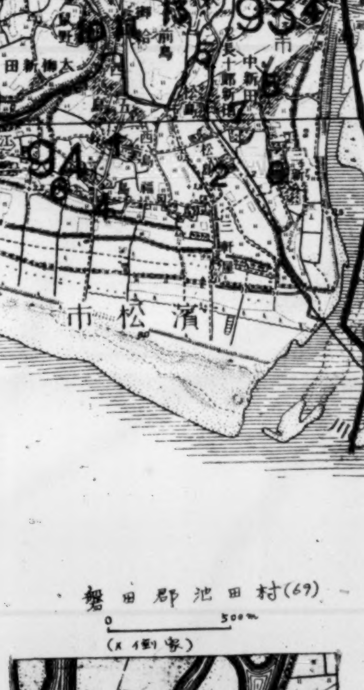

磐田郡磐田町(65)

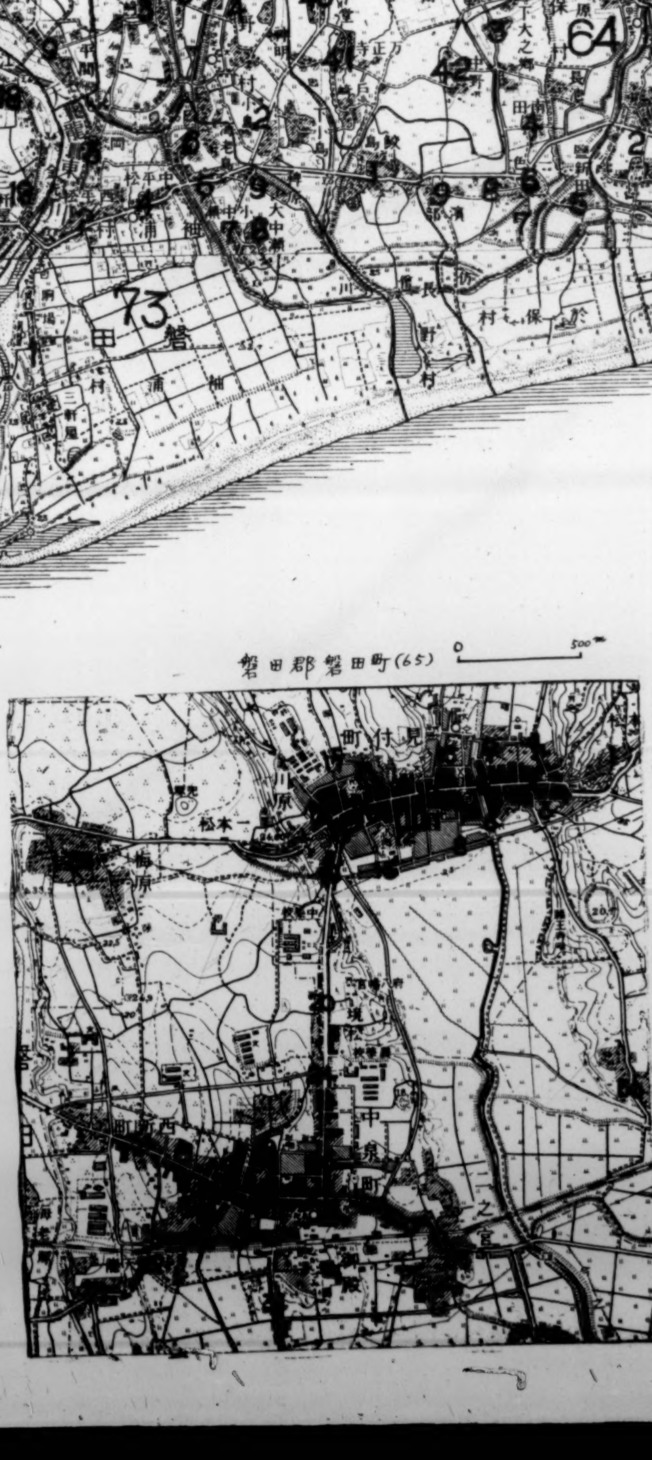

村区劃及び部落索引図 (大字は第 III 表の市, 町, 村番号,

the hamlets in the province of Tōtōmi, with
ties, cities, towns and villages. (The large numerals
s, towns and villages, while the small ones are those of the
.)

Earthq. Res. Inst., Vol. XXXV, Pl. IX.
彙報 第35号 図版 大庭

[地理調査所承認済]

付　見

遠江地方郡市町村区劃及び部落索引図（大字は第 III 表の市，町，村番号，
番号）

Index map of the hamlets in the province of Tōtōmi, with
ies of the counties, cities, towns and villages. (The large numerals
numbers of cities, towns and villages, while the small ones are those of the
hown in Table III.)

OOBA. Bull. Earthq. Res. Inst., Vol. XXXV, Pl. IX.
震研彙報　第35号　図版　大庭

[地理調査所承認済]

江

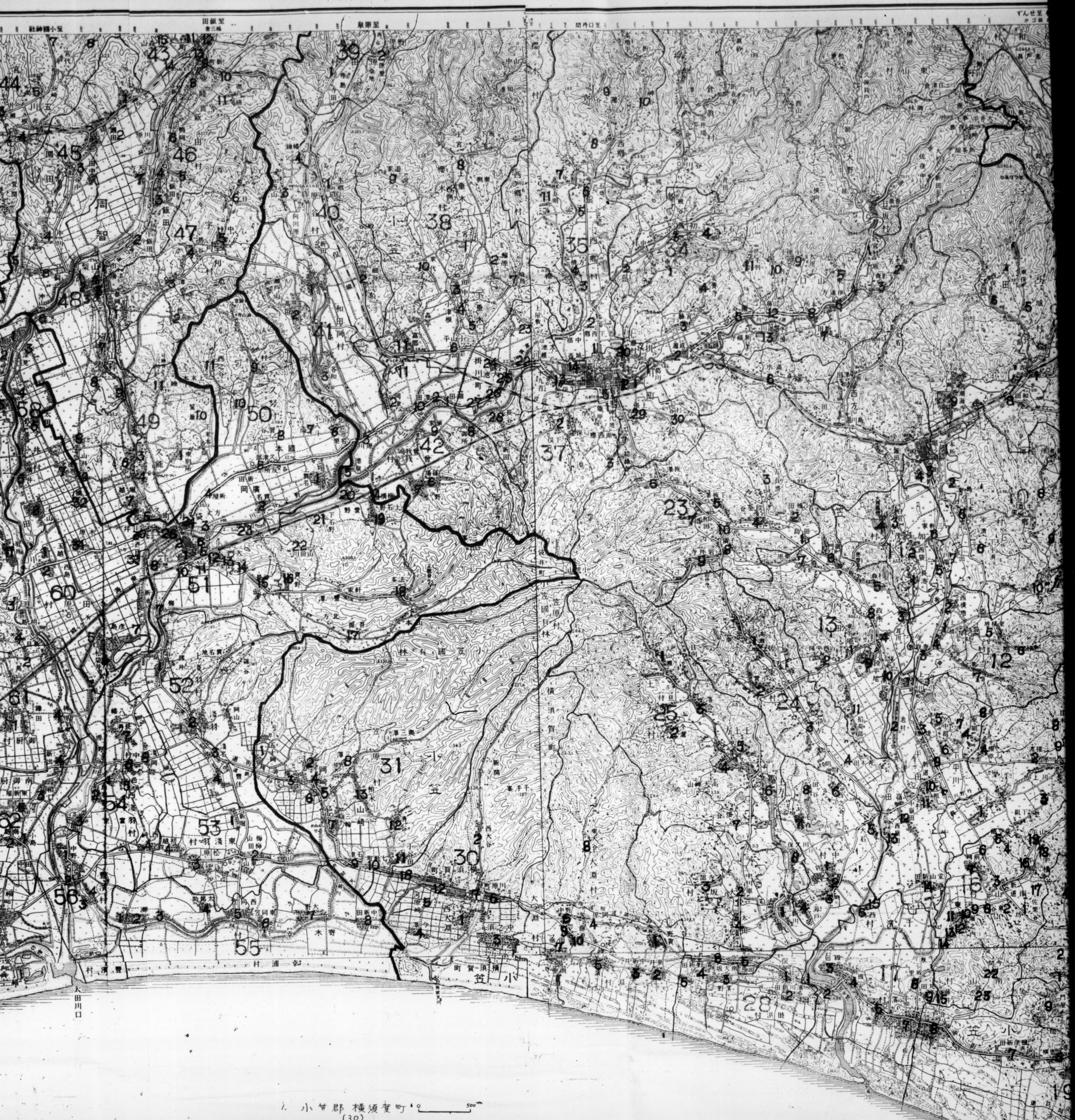

1. 小笠郡横須賀町 (30) 0 500m

小笠郡 掛川町(36) 0 500m

遠

掛川

掛

BULLETIN OF THE EARTHQUAKE RESEARCH INSTITUTE,
UNIVERSITY OF TOKYO. Vol. XXXV, Part 2. June, 1957.

東京大學
地震研究所彙報

第35號　第2册

昭和32年6月

目　次

論文及報告

			頁
15.	不均質媒質内の Rayleigh 波の分散（英文）	高橋健人	297
16.	地盤の震動特性に関する半実験式（英文）	金井清	309
17.	火山地域における地磁気異常と地下構造（英文）	横山泉	327
18.	今市地震地域の地質 (3)（英文）	森本良平 小坂丈予 福田知子	359
19.	起振機による建物の振動の位相差測定（英文）	岸上冬彦	377
20.	超短波多重遠隔記録地震計（第1報）（邦文）	宮村摂三 辻浦賢	381
21.	浅間火山及びその周辺地域の湧水並びに地下水の研究（第1報）—蛇堀川渓谷及びその附近の湧水並びに地下水の化学成分—（邦文）	小坂丈予 村井勇 南英一 津屋弘逵	395

所　報

(The titles in occidental languages are given on the back cover.)

本彙報ハ年4回（但シ第1號ヨリ第6號マデハ不定期ニ，第7號ハ3冊トシテ發行セリ），彙報別冊ハ不定期ニ發行ス．

本彙報掲載ノ論文及ビ報告ノ内容ニ關シテハ著者ノミニ其責任アルモノトス．

本彙報ニ關スル照會通信ハ東京大學地震研究所長ヘ宛テラレタシ．

The Bulletin is published quarterly. (Vols. I–VI were published at irregular intervals and Vol. VII consisted of three parts.)

Supplementary Volume is published at irregular interval.

The authors of the papers alone are responsible for the statements and opinions contained in their respective papers.

All communications relating to this Bulletin should be addressed to the Director of the Earthquake Research Institute, University of Tokyo.

15. *The Dispersion of Rayleigh Waves in Heterogeneous Media.*

By Takehito TAKAHASHI*,

Earthquake Research Institute.

(Read July 26, 1956.—Received April 6, 1957.)

1. Introduction

The dispersion of Rayleigh waves has been studied by several authors, but the calculation necessarily becomes very complicated compared with the case of Love waves. The general theory of the dispersion of Rayleigh waves propagated over heterogeneous media would be of importance in making the mechanism of the dispersion clear. For this purpose our treatment will be developed along the lines of the author's former study of Love waves[1], and the relations between Love and Rayleigh waves will also be investigated.

Our method is applicable when the medium varies slowly in the range of wave-length, so it is not suitable for long waves.

2. Approximate solutions

In the half space ($\infty > z \geqq 0$), if the density ρ and the elastic constants λ and μ are functions of z and the components of the displacement are

$$\left.\begin{aligned} u &= U(z)\exp(ipt-ifx)\,, \\ w &= W(z)\exp(ipt-ifx)\,, \\ v &= 0\,, \end{aligned}\right\} \qquad (1)$$

the equations of motion

$$\left.\begin{aligned} \rho\frac{\partial^2 u}{\partial t^2} &= \frac{\partial}{\partial x}\left\{(\lambda+2\mu)\frac{\partial u}{\partial x}+\lambda\frac{\partial w}{\partial z}\right\}+\frac{\partial}{\partial z}\left\{\mu\left(\frac{\partial w}{\partial x}+\frac{\partial u}{\partial z}\right)\right\}\,, \\ \rho\frac{\partial^2 w}{\partial t^2} &= \frac{\partial}{\partial x}\left\{\mu\left(\frac{\partial w}{\partial x}+\frac{\partial u}{\partial z}\right)\right\}+\frac{\partial}{\partial z}\left\{(\lambda+2\mu)\frac{\partial w}{\partial z}+\lambda\frac{\partial u}{\partial x}\right\}\,, \end{aligned}\right\} \qquad (2)$$

are expressed as

---

* Assistant Professor in Seizyo University, Setagaya, Tokyo.

1) T. TAKAHASHI, *Bull. Earthq. Res. Inst.*, **33** (1955), 287. Cited as I in this paper.

$$\left.\begin{aligned}&\mu\frac{\partial^2 U}{\partial z^2}+\frac{\partial\mu}{\partial z}\cdot\frac{\partial U}{\partial z}+f^2\left\{\frac{\rho p^2}{f^2}-(\lambda+2\mu)\right\}V-if\left\{(\lambda+\mu)\frac{\partial W}{\partial z}+\frac{\partial\mu}{\partial z}W\right\}=0\,,\\&(\lambda+2\mu)\frac{\partial^2 W}{\partial z^2}+\frac{\partial(\lambda+2\mu)}{\partial z}\cdot\frac{\partial W}{\partial z}+f^2\left\{\frac{\rho p^2}{f^2}-\mu\right\}W-if\left\{(\lambda+\mu)\frac{\partial U}{\partial z}+\frac{\partial\lambda}{\partial z}U\right\}=0\,.\end{aligned}\right\} \tag{3}$$

The boundary conditions are that the stresses shall vanish at $z=0$ (the surface) and $z=\infty$:

$$\left.\begin{aligned}&-ifW+\partial U/\partial z=0\,,\\&-ifU+(1+2\mu/\lambda)\partial W/\partial z=0\,.\end{aligned}\right\} \tag{4}$$

For brevity we change the variable z to

$$\zeta=fz \tag{5}$$

and put

$$\left.\begin{aligned}&\kappa(z)=(p/f)^2\cdot\rho/\mu=(v_R/v_s(z))^2\,,\\&\eta(z)=(p/f)^2\cdot\rho/(\lambda+2\mu)=(v_R/v_p(z))^2\,,\end{aligned}\right\} \tag{6}$$

in which v_R denotes the velocity of the Rayleigh wave.

Then the equations (3) and (4) become respectively

$$\left.\begin{aligned}&\ddot{U}+\left(\frac{\dot\rho}{\rho}-\frac{\dot\kappa}{\kappa}\right)\dot U+\left(\kappa-\frac{\kappa}{\eta}\right)U-i\left\{\left(\frac{\kappa}{\eta}-1\right)\dot W+\left(\frac{\dot\rho}{\rho}-\frac{\dot\kappa}{\kappa}\right)W\right\}=0\,,\\&\ddot{W}+\left(\frac{\dot\rho}{\rho}-\frac{\dot\eta}{\eta}\right)\dot W+\left(\eta-\frac{\eta}{\kappa}\right)W\\&\qquad-i\left[\left(1-\frac{\eta}{\kappa}\right)\dot U+\left\{\frac{\dot\rho}{\rho}\left(1-2\frac{\eta}{\kappa}\right)-\frac{\dot\eta}{\eta}+2\frac{\dot\kappa}{\kappa}\frac{\eta}{\kappa}\right\}U\right]=0\,,\end{aligned}\right\} \tag{7}$$

and at $\zeta=0$ and ∞

$$\left.\begin{aligned}&-iW+\dot U=0\,,\\&-iU+(1-2\eta/\kappa)^{-1}\dot W=0\,,\end{aligned}\right\} \tag{8}$$

where the dotted letters are derivatives with respect to ζ.

Now we assume that the relative variations of λ, μ and ρ are small in the range of wave-length and we can neglect the difference in the terms involving

$$(\dot\mu/\mu)^2,\ \ddot\mu/\mu\,,\ \text{etc.}$$

We further assume that $\kappa(\zeta)$ and $\eta(\zeta)$ are decreasing functions and

that η/κ or Poisson's ratio $\sigma=\lambda/2(\lambda+\mu)$ is nearly constant, i.e. $(\dot{\kappa}/\kappa-\dot{\eta}/\eta)$ is of negligible order.

Under these assumptions we can expect that the solutions will resemble those of the homogeneous medium, in which case we know that two couples of the independent solutions are obtained by putting $U=-i\dot{W}$ or $W=i\dot{U}$.

Seeing this, we want to find the solutions, accurate to the desired order, of the form

$$U_1=-im\dot{\Phi}\,,\quad W_1=m\Phi\,, \tag{9}$$

or

$$U_2=n\Psi\,,\quad W_2=in\dot{\Psi}\,, \tag{10}$$

where m and n are functions of z and only their first order derivatives will need to be taken into account.

Substituting (9) and (10) into (7), we obtain respectively

$$\frac{d}{d\zeta}\{\ddot{\Phi}+(\kappa-1)\Phi\}+\left\{\frac{\dot{m}}{m}\left(\frac{\dot{\rho}}{\rho}-\frac{\dot{\kappa}}{\kappa}\right)+\frac{\ddot{m}}{m}\right\}\dot{\Phi}$$

$$+\left(\frac{\dot{\rho}}{\rho}-\frac{\dot{\kappa}}{\kappa}+2\frac{\dot{m}}{m}\right)\ddot{\Phi}+\left\{-\dot{\kappa}+\left(\frac{\kappa}{\eta}-1\right)\frac{\dot{m}}{m}+\frac{\dot{\rho}}{\rho}-\frac{\dot{\kappa}}{\kappa}\right\}\Phi=0\,, \tag{11.1}$$

$$\{\ddot{\Phi}+(\kappa-1)\Phi\}+\frac{\kappa}{\eta}\left\{\frac{\dot{m}}{m}\left(\frac{\dot{\rho}}{\rho}-\frac{\dot{\eta}}{\eta}\right)+\frac{\ddot{m}}{m}\right\}\Phi+\left\{2\frac{\dot{\rho}}{\rho}-2\frac{\dot{\kappa}}{\kappa}+\frac{\dot{m}}{m}\left(\frac{\kappa}{\eta}+1\right)\right\}\dot{\Phi}=0\,, \tag{11.2}$$

and

$$\{\ddot{\Psi}+(\eta-1)\Psi\}+\frac{\eta}{\kappa}\left\{\frac{\dot{n}}{n}\left(\frac{\dot{\rho}}{\rho}-\frac{\dot{\kappa}}{\kappa}\right)+\frac{\ddot{n}}{n}\right\}\Psi$$

$$+\left\{\frac{\eta}{\kappa}\left(\frac{\dot{\rho}}{\rho}-\frac{\dot{\kappa}}{\kappa}+2\frac{\dot{n}}{n}\right)+\left(1-\frac{\eta}{\kappa}\right)\frac{\dot{n}}{n}+\frac{\eta}{\kappa}\left(\frac{\dot{\rho}}{\rho}-\frac{\dot{\kappa}}{\kappa}\right)\right\}\dot{\Psi}=0\,, \tag{12.1}$$

$$\frac{d}{d\zeta}\left\{\ddot{\Psi}+(\eta-1)\Psi\right\}+\left\{\left(\frac{\dot{\rho}}{\rho}-\frac{\dot{\eta}}{\eta}\right)\frac{\dot{n}}{n}+\frac{\ddot{n}}{n}\right\}\dot{\Psi}$$

$$+\left(\frac{\dot{\rho}}{\rho}-\frac{\dot{\eta}}{\eta}+2\frac{\dot{n}}{n}\right)\ddot{\Psi}-\left\{\dot{\eta}+\left(1-\frac{\eta}{\kappa}\right)\frac{\dot{n}}{n}+\frac{\dot{\rho}}{\rho}\left(1-2\frac{\eta}{\kappa}\right)-\frac{\dot{\eta}}{\eta}+2\frac{\dot{\kappa}}{\kappa}\frac{\eta}{\kappa}\right\}\Psi=0\,. \tag{12.2}$$

Now we differentiate the left side of (11.2) and compare it with

(11.1). When $\ddot{\Phi}$ is eliminated by the relation (11.2), they become respectively

$$\frac{d}{d\zeta}\{\ddot{\Phi}+(\kappa-1)\Phi\}+\left\{(1-\kappa)\left(\frac{\dot\rho}{\rho}-\frac{\dot\kappa}{\kappa}+2\frac{\dot m}{m}\right)-\dot\kappa+\left(\frac{\kappa}{\eta}-1\right)\frac{\dot m}{m}+\frac{\dot\rho}{\rho}-\frac{\dot\kappa}{\kappa}\right\}\dot\Phi=0\,, \tag{13.1}$$

and

$$\frac{d}{d\zeta}\{\ddot{\Phi}+(\kappa-1)\Phi\}+(1-\kappa)\left\{2\frac{\dot\rho}{\rho}-2\frac{\dot\kappa}{\kappa}+\frac{\dot m}{m}\left(\frac{\kappa}{\eta}+1\right)\right\}\dot\Phi=0\,, \tag{13.2}$$

in the order of our approximation.

Equating the coefficients of $\dot\Phi$ in (13.1) and (13.2), we get

$$(\dot m/m)(\kappa/\eta-1)=2\dot\kappa/\kappa-\dot\rho/\rho\,, \tag{14}$$

or

$$\dot m/m=2(1-2\sigma)\dot\kappa/\kappa-(1-2\sigma)\dot\rho/\rho\,. \tag{15}$$

If σ is constant, (15) is easily integrated to give

$$m=\kappa^{2(1-2\sigma)}\rho^{-(1-2\sigma)}\,. \tag{16}$$

Substitute (15) in the coefficient of $\dot\Phi$ in (11.2)

$$\ddot{\Phi}+(\kappa-1)\Phi+2\left\{2(1-2\sigma)\dot\kappa/\kappa+\left(2\sigma-\frac{1}{2}\right)\dot\rho/\rho\right\}\dot\Phi=0\,. \tag{17}$$

Next we define the function H_κ by the differential equation:

$$\ddot{H}_\kappa+(\kappa-1)H_\kappa=0\,. \tag{18}$$

Then it is easy to see that in our approximation (17) can be integrated and we have

$$\Phi=\kappa^{-2(1-2\sigma)}\rho^{-(2\sigma-1/2)}H_\kappa=\rho^{-1/2}m^{-1}H_\kappa\,. \tag{19}$$

Substitution of the formula (19) in (9) yields

$$\left.\begin{aligned}U_1&=-im\frac{d}{d\zeta}(\rho^{-1/2}m^{-1}H_\kappa),\\ W_1&=\rho^{-1/2}H_\kappa\,.\end{aligned}\right\} \tag{20}$$

Another couple of the solutions (U_2, W_2) is computed from equations (12.1) and (12.2) in the same way. Corresponding to the formulas (15) $\sim$ (20) we have respectively

$$\dot n/n=-2(1-2\sigma)\dot\kappa/\kappa-2\sigma\,\dot\rho/\rho\,, \tag{21}$$

$$n=\kappa^{-2(1-2\sigma)}\rho^{-2\sigma}\,, \tag{22}$$

$$\ddot{\Psi}+(\eta-1)\Psi+2\left\{-2(1-2\sigma)\dot{\kappa}/\kappa+\frac{1}{2}(1-4\sigma)\dot{\rho}/\rho\right\}\dot{\Psi}=0\,, \tag{23}$$

$$\ddot{H}_\eta+(\eta-1)H_\eta=0\,, \tag{24}$$

$$\Psi=\kappa^{2(1-2\sigma)}\rho^{(2\sigma-1/2)}H_\eta=\rho^{-1/2}n^{-1}H_\eta\,, \tag{25}$$

$$\left.\begin{aligned}&U_2=\rho^{-1/2}H_\eta\,,\\&W_2=in(d/d\zeta)(\rho^{-1/2}n^{-1}H_\eta)=im^{-1}\rho^{-1}(d/d\zeta)(\rho^{-1/2}m^{-1}H_\eta).\end{aligned}\right\} \tag{26}$$

It should be remarked that the functions H_κ and H_η are to be chosen to vanish at infinity in order to satisfy the boundary condition.

The incompressible medium yields an interesting example. In this case, as $\sigma=1/2$ and $\eta=0$, H_η is readily obtained from (24)

$$H_\eta=\exp(-\zeta)=\exp(-fz)\,. \tag{27}$$

Formulae (20) and (26) become

$$\left.\begin{aligned}&U_1=-i(d/d\zeta)(\rho^{-1/2}H_\kappa)\,, && W_1=\rho^{-1/2}H_\kappa\,,\\&U_2=\rho^{-1/2}\exp(-\zeta)\,, && W_2=i\rho^{-1}(d/d\zeta)(\rho^{1/2}\exp(-\zeta))\,.\end{aligned}\right\} \tag{28}$$

We see that these formulae include the results of R. Stoneley[2] which were obtained under the additional assumption that ρ be constant and μ be linear.

3. The functions H_κ and H_η

In treating the dispersion of Love waves, we made use of the result of R. E. Langer that the approximate solution of the differential equation

$$d^2V/dz^2+s^2V=0 \tag{29}$$

is given by Bessel functions of order 1/3 whose argument φ is defined by

$$\varphi=\int_z^H s\,dz\,, \tag{30}$$

with

$$s(H)=0\,.$$

Then it is known that the approximate solution, which vanishes at in-

2) R. Stoneley, *M. N. Geoph. Sup.* **3** (1934), 222.

finity and is valid both for negative and positive s^2, is expressed as

$$V=(-\varphi/s)^{1/2}K_{1/3}(-i\varphi)\,. \tag{31}$$

When $s^2 \leqq 0$ ($z \geqq H$), we define that $s=-i|s|$ then (31) is written as

$$V=(|\varphi|/|s|)^{1/2}K_{1/3}(|\varphi|)\,. \tag{32}$$

When $s^2 \geqq 0$ ($z \leqq H$), then $s=|s|$ and $\varphi \geqq 0$ and (31) becomes

$$\begin{aligned} V&=(\pi/2)\operatorname{cosec}(\pi/3)(\varphi/s)^{1/2}(J_{1/3}(\varphi)+J_{-1/3}(\varphi)) \\ &=(\pi/2)\operatorname{cosec}(\pi/6)(\varphi/s)^{1/2}|H^{(1)}_{1/3}(\varphi)|\cos(\pi/6+\arg H^{(1)}_{1/3}(\varphi))\,. \end{aligned} \tag{33}$$

In the present case, unlike the case of Love waves, s^2 may be negative at the surface making us unable to determine the zero point $z=H$ (s^2 is either $(\kappa-1)$ or $(\eta-1)$ then negative s^2 means either $v_R<v_s$ or $v_R<v_p$). Some device is, then, needed.

If we write

$$\varphi(z)=\varphi_0-\int_0^z s\,dz\,, \tag{34}$$

generally φ_0 means $\varphi(0)$ but, for negative $s^2(0)$, is some constant to be determined to make the errors of approximation as small as possible.

Now the accurate equation, which our approximate solution (31) satisfies, is[3]

$$V''+(s^2-r''/r)V=0\,, \tag{35}$$

in which

$$r=\varphi^{1/6}\cdot s^{-1/2}\,. \tag{36}$$

Then the order of the errors of the approximation is expressed by

$$r''/r=-5/36\cdot(s/\varphi)^2+5/16\cdot((s^2)'\cdot s^{-2})^2-1/4\cdot(s^2)''s^{-2}\,. \tag{37}$$

We shall determine φ_0 so as to make r''/r zero at the surface. The last term of the right side of (37) being small, we get

$$\varphi_0=(2/3)\cdot s_0^3/(s_0^2)'\{1+2/5\cdot s_0^2(s_0^2)''((s_0^2)^1)^{-2}\}\,, \tag{38}$$

in which

$$s_0=s(0)^{4)}.$$

Thus for H_κ, if we put

3) M. MOOSE and H. FESHBACH, *Method of Theoretical Physics* (1953), p. 1096.

4) This notation will be used for any other function.

$$\varphi=\int_{\zeta}^{\kappa=1}\sqrt{\kappa-1}\,d\zeta \qquad (\kappa_0>1), \tag{39}$$

or

$$\varphi=\varphi_0+i\int_0^{\zeta}\sqrt{1-\kappa}\,d\zeta \qquad (\kappa_0<1), \tag{40}$$

with

$$\varphi_0=-2i(1-\kappa_0)^{3/2}(3\dot{\kappa}_0)^{-1}\{1-2/5(1-\kappa_0)\ddot{\kappa}_0\dot{\kappa}_0^{-2}\}\ , \tag{41}$$

in either case $\kappa_0>1$ or $\kappa_0<1$ we can write

$$\dot{H}_\kappa/H_\kappa=\dot{\kappa}/\{4(1-\kappa)\}-(\kappa-1)^{1/2}(d/d\varphi)\log\{\varphi^{1/2}K_{1/3}(-i\varphi)\}\ . \tag{42}$$

It is convenient to express this in three ways, according to the value of κ. When $\kappa>1$ we use (33) and get

$$\dot{H}_\kappa/H_\kappa=-\dot{\kappa}/\{4(\kappa-1)\}-(\kappa-1)^{1/2}H(\varphi)\ , \tag{43}$$

in which

$$H(\varphi)=-\frac{\tan(\pi/6+\arg H_{1/3}^{(1)})}{(\pi/2)\varphi|H_{1/3}^{(1)}|^2}+\frac{1}{2\varphi}+\frac{1}{|H_{1/3}^{(1)}|}\frac{d}{d\varphi}|H_{1/3}^{(1)}|\ . \tag{44}$$

The values of $H(\varphi)$ can be calculated from the tables[5] of $H_{1/3}^{(1)}(\varphi)$. In Table I we tabulated $H(\varphi)$ and $\varphi H(\varphi)$.[6]

Table I.

φ	$H(\varphi)$	$\varphi H(\varphi)$	φ	$H(\varphi)$	$\varphi H(\varphi)$
0	∞	0.167	0.6	0.364	0.218
0.1	2.73	0.273	0.7	0.222	0.155
0.2	1.53	0.305	0.8	0.096	0.077
0.3	1.04	0.311	0.9	−0.023	−0.021
0.4	0.740	0.296	1.0	−0.139	−0.139
0.5	0.531	0.266			

The expression (43) becomes inconvenient when κ approaches to 1, in this case $|\varphi|$ being small we can use the expansion

$$J_{\pm1/3}(\varphi)=\frac{1}{\Gamma(1\pm1/3)}\left(\frac{\varphi}{2}\right)^{\pm1/3}\left\{1-\frac{\varphi^2}{4(1\pm1/3)}+\frac{\varphi^4}{32(1\pm1/3)(2\pm1/3)}+\cdots\right\}$$

5) G. N. WATSON, *Theory of Bessel Functions* (1922), p. 714.

6) The constant term 0.87 in the equation I(22) corresponds to the zero point of $H(\varphi)$, which must be nearly 0.88 from Table I. This is due to the uncorrect estimation of the first approximation value of φ_0 as 0.835 instead of the true value 0.847. Consequently the numerical calculation of the previous paper suffers a slight correction, for instance the coefficient 1.11 in I(27) and I(28) must be replaced by 1.12.

to substitute in (33) and get

$$\frac{d}{d\varphi}\log\{\sqrt{\varphi}\,(J_{1/3}+J_{-1/3})\}=\frac{1}{6\varphi}+\frac{4^{1/6}\Gamma(2/3)}{3\Gamma(4/3)\varphi^{1/3}}-\frac{3\varphi}{4}-\frac{\Gamma(2/3)\varphi^{5/3}}{4^{7/3}\Gamma(4/3)}+\cdots.$$

φ_0 is given by (39) or (41) according as $\kappa_0>1$ or $\kappa_0<1$, but it can be shown that they have the same expression in this region.

With these results we obtain after some calculation

$$\left(\frac{\dot{H}_\kappa}{H_\kappa}\right)_{\zeta=0}=-\frac{\Gamma(2/3)}{9^{1/3}\Gamma(4/3)}(-\dot{\kappa}_0)^{1/3}+\frac{\ddot{\kappa}_0+5(\kappa_0-1)^2}{10(-\dot{\kappa}_0)}+\frac{1}{8\cdot 3^{5/3}}\frac{\Gamma(2/3)(\kappa_0-1)^3}{\Gamma(4/3)(-\dot{\kappa}_0)^{5/3}}+\cdots. \tag{45}$$

When κ is far less than 1, we may use the asymptotic expansion of $K_{1/3}$:

$$K_{1/3}(\varphi)\sim(\pi\varphi/2)^{1/2}\exp(-\varphi)(1-5/72\cdot\varphi^{-2}+\cdots).$$

Then from the equation (32) we have

$$\dot{H}_\kappa/H_\kappa=\dot{\kappa}/\{4(1-\kappa)\}-(1-\kappa)^{1/2}(1-5/72\cdot|\varphi|^{-2}+\cdots),$$

from which we get, after substituting (41),

$$(\dot{H}_\kappa/H_\kappa)_{\zeta=0}=-(1-\kappa_0)^{1/2}+\dot{\kappa}_0/\{4(1-\kappa_0)\}+5/32\cdot\dot{\kappa}_0^2(1-\kappa_0)^{-5/2}+\cdots. \tag{46}$$

Similar expressions also hold for H_η. But practically it is expected that η_0 is always far less than 1. Thus we shall use only the formula similar to (46):

$$(\dot{H}_\eta/H_\eta)_{\zeta=0}=-(1-\eta_0)^{1/2}+\dot{\eta}_0/\{4(1-\eta_0)\}+5/32\cdot\dot{\eta}_0^2(1-\eta_0)^{-5/2}+\cdots. \tag{47}$$

4. The equation of dispersion

Expressing the solutions as

$$U=c_1U_1+c_2U_2,\quad W=c_1W_1+c_1W_2, \tag{48}$$

we substitute them in the boundary condition at the surface. On eliminating the constants c_1 and c_2, we have

$$(\dot{U}_1-iW_1)((1-\sigma)\sigma^{-1}\dot{W}_2-iU_2)=(\dot{U}_2-iW_2)((1-\sigma)\sigma^{-1}\dot{W}_1-iU_1), \tag{49}$$

which is the equation of dispersion.

With the results of section 2, this reduces to[7]

7) In the special case $\dot{\rho}=0$, $\sigma=1/2$ and $\dot{H}_\eta/H_\eta=-1$, this coincides with Stoneley's formula.

$$\Big\{-\dot H_\kappa/H_\kappa-2\sigma\dot\kappa/\kappa+\Big(\sigma+\frac{1}{2}\Big)\dot\rho/\rho\Big\}\Big\{-\dot H_\eta/H_\eta-(1-2\sigma)\dot\kappa/\kappa+\Big(\frac{1}{2}-\sigma\Big)\dot\rho/\rho\Big\}$$
$$=\{1-\kappa/2-((1-2\sigma)\dot\kappa/\kappa+\sigma\dot\rho/\rho)\dot H_\kappa/H_\kappa\}$$
$$\times\{1-\kappa/2+(2(1-\sigma)\dot\kappa/\kappa-(1-\sigma)\dot\rho/\rho)\dot H_\eta/H_\eta\}\,, \tag{50}$$

in the order of our approximation.

Then we solve this equation for $\dot H_\kappa/H_\kappa$ after substituting (46):

$$-\dot H_\kappa/H_\kappa=(1-\kappa/2)^2(1-\eta)^{-1/2}-(\dot\kappa/\kappa)\{-(\kappa/4)(1-\kappa/2)^2(1-\eta)^{-2}$$
$$+(2-\kappa)(1-\sigma)-2\sigma-(1-\kappa/2)^2(2-\kappa/2)(1-2\sigma)(1-\eta)^{-1}\}$$
$$-(\dot\rho/\rho)[2\sigma-1/2+\kappa(1-\sigma)/2+(1-\kappa/2)^2\{1/2-\sigma(2-\kappa/2)\}(1-\eta)^{-1}], \tag{51}$$

in which higher order terms in $\dot\kappa/\kappa$ and $\dot\rho/\rho$ are also neglected.

Corresponding to the different expressions of $\dot H_\kappa/H_\kappa$, (43)~(46), we obtain three types of the equations of dispersion:

i) $\kappa_0>1$

$$H(\varphi_0)=(1-\kappa_0/2)^2\{(\kappa_0-1)(1-\eta_0)\}^{-1/2}-(\dot\kappa_0/\kappa_0)\Delta_\sigma(\kappa_0)-(\dot\rho_0/\rho_0)\Delta_\rho(\kappa_0)(1-\kappa_0)^{-1/2}\,, \tag{52}$$

in which

$$\Delta_\sigma(\kappa)=(\kappa/4)(\kappa-1)^{-3/2}+\{(2-\kappa)(1-\sigma)-2\sigma\}(\kappa-1)^{-1/2}$$
$$-(\kappa/4)(1-\kappa/2)^2(1-\eta)^{-2}(\kappa-1)^{-1/2}$$
$$-(1-\kappa/2)^2(2-\kappa/2)(1-2\sigma)(1-\eta)^{-1}(\kappa-1)^{-1/2}\,, \tag{53}$$

and

$$\Delta_\rho(\kappa)=2\sigma-1/2+\kappa(1-\sigma)/2+(1-\kappa/2)^2\{1/2-\sigma(2-\kappa/2)\}(1-\eta)^{-1}. \tag{54}$$

ii) $\kappa_0\doteqdot 1$

$$9^{-1/3}\Gamma(2/3)\{\Gamma(4/3)\}^{-1}(-\dot\kappa_0)^{1/3}-\ddot\kappa_0(-10\dot\kappa_0)^{-1}-(\kappa_0-1)^2(-2\dot\kappa_0)^{-1}-\cdots$$
$$=(1-\kappa_0/2)^2(1-\eta_0)^{-1/2}-(\dot\kappa_0/\kappa_0)\{(\kappa_0-1)^{-1/2}\Delta_\sigma(\kappa_0)-(4\kappa_0-4)^{-1}\}$$
$$-(\dot\rho_0/\rho_0)\Delta_\rho(\kappa_0)\,. \tag{55}$$

It we put

$$-\dot\kappa_0/\kappa_0=2\dot v_s(0)/v_s(0)=\tilde L\,, \tag{56}$$

this quantity is proportional to the wave-length, and can be used as a parameter in the dispersion formula.

For the important case $\kappa_0=1$ ($v_R=v_s(0)$), if we neglect $\ddot\kappa_0$ and $\dot\rho/\rho$, (55) is written as

$$\tilde{L}^{1/3}=0.686\{(1-\sigma)/2\}^{1/2}-0.171\sigma(1+7\sigma)\tilde{L}\,. \tag{57}$$

This is solved by successive approximation; when $\sigma=1/4$ or $1/2$ the value of $\tilde{L}$ is obtained as 0.070 or 0.032.

iii) $\kappa_0 \ll 1$

$$1-(1-\kappa_0/2)^2\{(1-\kappa_0)(1-\eta_0)\}^{-1/2}$$
$$=-(\dot{\kappa}_0/\kappa_0)\sqrt{-1}\cdot\Delta_\sigma(\kappa_0)-(\dot{\rho}_0/\rho_0)\Delta_\rho(\kappa_0)\cdot(\kappa_0-1)^{-1/2}\,. \tag{58}$$

For the limiting case $\tilde{L}=0$, this becomes

$$(1-\kappa_0/2)^2=\{(1-\kappa_0)(1-\eta_0)\}^{1/2}\,, \tag{59}$$

which is the formula for the homogeneous medium. The values of κ_0 for $\tilde{L}=0$ are calculated ($\kappa_0^{1/2}=0.919$ ($\sigma=1/4$) and 0.956 ($\sigma=1/2$)). Near $\tilde{L}=0$, (58) can be solved for κ_0, if necessary, by iteration. But these microseismic waves are not practically important[8].

In the case of i), if by (52) the function $\varphi_0(\kappa_0)$ is determined, we have by the definition of φ_0

$$\int_0^{v_s(z)=v_R}\{(v_R/v_s(z))^2-1\}^{1/2}dz=f^{-1}\cdot\varphi_0(v_R)\,, \tag{60}$$

which is entirely the similar formula as the equation I(26) of the previous paper. So that the further analysis of Love waves may also be applied to our case.

5. Relations between the dispersion curves of Rayleigh waves and of Love waves

The dispersion equation of Love waves I(17) is written in our expression as

$$H(\varphi_Q)=\tilde{L}_Q\cdot\Delta_Q(\kappa_Q)-(\dot{\rho}/2\rho)(\kappa_Q-1)^{-1/2}\,, \tag{61}$$

in which

$$\tilde{L}_Q=-\dot{\kappa}_Q/\kappa_Q\,,\quad \Delta_Q(\kappa_Q)=(1/2-\kappa_Q/4)(\kappa_Q-1)^{-3/2}\,, \tag{62}$$

and the suffix Q is used to denote Love waves.

For the same velocity $v_R=v_Q$, we have from (60)

$$\tilde{L}/\tilde{L}_Q=\varphi_Q/\varphi_0\,, \tag{63}$$

8) R. STONELEY, loc. cit.

where φ_Q is near 0.88 as we have seen in I.

When φ_Q and L_Q are given as functions of κ, we can solve (52) for φ_0 with the help of Table I and get $\tilde{L}$ from (63). For this purpose, it is convenient to rewrite (52) as

$$\varphi_0 H(\varphi_0) = F_\sigma(\kappa_0)\cdot\varphi_0 + \tilde{L}_Q\varphi_Q \Delta_\sigma(\kappa_0)\,, \tag{64}$$

neglecting $\dot{\rho}/\rho$ for brevity.

The inverse problem, to determine the dispersion curves of Love waves from those of Rayleigh waves, can be solved in a similar way.

In the above procedure we assumed that σ is known. If the dispersion curves of both Love and Rayleigh waves are given, we shall be able to determine σ.

As an example we treated the case when ρ is constant and μ is linear. Dispersion curves of Love waves being investigated in the former paper, we calculated $\tilde{L}$ in two cases of $\sigma=1/2$ and 1/4. The results are shown in Fig. 1.

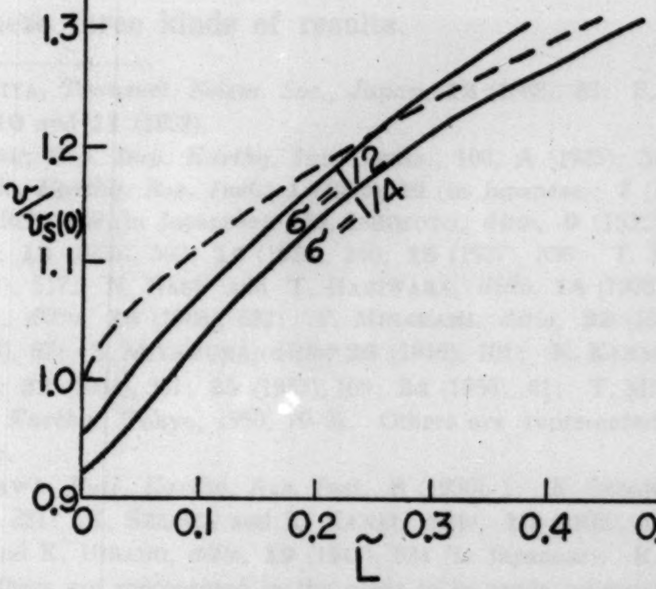

Fig. 1. Dispersion of Rayleigh waves determined from the dispersion curve of Love wave (dotted curve).

It is an essential difficulty that the phase velocity can not be uniquely determined from the observed group velocity. If we could find, by trial and error method, an appropriate structure of the medium which is fitted for both Love and Rayleigh waves, the ambiguity of

the dispersion curve would disappear.

The solutions obtained are nothing but the first terms in the asymptotic expansions for small wave-length. The further approximation will be discussed at the next opportunity.

---

15. 不均質媒質内の Rayleigh 波の分散

地震研究所 高 橋 健 人

波長が特に大きくない場合の近似式として，不均質媒質で λ, μ 及び ρ が連続的に且つゆるやかに変る場合の Rayleigh 波の分散式を求め，次に Love 波と Rayleigh 波の分散曲線の間の関係をしらべた．この両方から逆に媒質の構造を決定する方法が考えられるが，群速度から位相速度を一義的に求めることが出来ないために観測結果を直接整理するに適した形にはなつていない．

---

16. *Semi-empirical Formula for the Seismic Characteristics of the Ground.*

By Kiyoshi KANAI,

Earthquake Research Institute.

(Read July 17, 1956; Feb. 26, Mar. 26, 1957.—Received Mar. 31, 1957.)

1. Introduction

That there is usually, for each kind of ground, both a predominant period and a particular spectral response, was first determined[1] in Japan from some of the earliest seismograph records. This principle was stated near the end of the nineteenth century, shortly after the invention of the seismograph. The seismic characteristics of the ground have become clear from field observations[2], theoretical work[3], and studies of damage statistics[4] by many authors. The present paper presents a semi-empirical formula for the seismic characteristics of the ground based on these three kinds of results.

---

1) S. SEKIYA, *Transact. Seism. Soc., Japan*, **12** (1888), 83: F. OMORI, *Pub. Earthq. Inv. Comm.*, **10** and **11** (1902).

2) N. NASU, *Rep. Imp. Earthq. Inv. Comm.*, 100, A (1925), 313 (in Japanese): K. SUYEHIRO, *Bull. Earthq. Res. Inst.*, **1** (1926), 59 (in Japanese); **7** (1929), 467: A. IMAMURA, *ditto*, **7** (1929), 489 (in Japanese): M. ISHIMOTO, *ditto*, **9** (1931), 159; **10** (1932), 171; **12** (1934), 234; **13** (1935), 592; **14** (1936), 240; **15** (1937), 536: T. SAITA and M. SUZUKI, *ditto*, **12** (1934), 517: N. NASU and T. HAGIWARA, *ditto*, **14** (1936), 290: T. HAGIWARA and S. OMOTE, *ditto*, **16** (1938), 632: T. MINAKAMI, *ditto*, **22** (1944), 92: S. SAKUMA, *ditto*, **26** (1948), 67: S. MIYAMURA, *ditto*, **26** (1948), 101: K. KANAI and others, *ditto*, **31** (1953), 227, 305; **32** (1954), 361; **33** (1955), 109; **34** (1956), 61: T. MINAKAMI, *Rep. Special Comm. Fukui Earthq.*, Tokyo, 1950, 79-92. Others are represented in the cases to be made reference.

3) K. SEZAWA, *Bull. Earthq. Res. Inst.*, **8** (1930), 1: K. SEZAWA and G. NISHIMURA, *ditto*, **8** (1930), 321: K. SEZAWA and K. KANAI, *ditto*, **10** (1932), 1, 273; **13** (1935), 251; R. TAKAHASI and K. HIRANO, *ditto*, **19** (1941), 534 (in Japanese): R. TAKAHASI, *ditto*, **33** (1955), 259. Others are represented in the cases to be made reference.

4) T. MATUZAWA, *Rep. Imp. Earthq. Inv. Comm.*, 100, A (1925), 163: G. KITAZAWA, *Journ. Seism. Soci., Japan*, **3** (1950), 32 (in Japanese): H. KAWASUMI, *Journ. Architect. Inst., Japan*, 777 (1951), 10 (in Japanese): R. TANABASHI and H. ISHIZAKI, *Bull. Disast, Prev. Res. Inst.*, **5** (1953): T. SAITA, Iwanami Shoten, Tokyo, 1935, (in Japanese): S. OMOTE, *Bull. Earthq. Res. Inst.*, **24** (1946), 77; **27** (1949), 57, 63: S. MIYAMURA, *ditto*, **24** (1946), 99; S. OMOTE and S. MIYAMURA, *ditto*, **29** (1951), 183: Rep. Damage Fukui Earthq., Tokyo (1951) (in Japanese). Others are represented in the cases to be made reference.

2. Peculiarity of the ground

In most cases, the amplitude-period relation of earthquake motion is represented by a resonance type curve. The period corresponding to peak amplitude is comparatively short (0.1–0.4 sec) on hard ground and comparatively long (0.4–0.8 sec) on soft ground. From the analyses of many seismograms, we also know that the amplitude-period relation of an earthquake is quite similar to the relation between period and number of waves, with the peaks of the two curves occurring at practically the same period[5]. In this paper, we will often use the "frequency-period" relation instead of the amplitude-period relation because we have many data of the former type. Strictly speaking, the amplitude-period relation differs somewhat for different earthquakes. The "peak period" lengthens and the spectral response curve flattens as the epicentral distance or the earthquake magnitude increases. However, this variation of peak period is less than $\pm 20\%$[6].

In Figs. 1 through 7 are shown the numbers of small earthquakes and their peak periods for seven places with differing ground characteristics. Six of the places are in Tokyo: Hongo, Aoyama, Marunouti, Kanda, Komagome and Komaba. Noge-yama is in Yokohama. The

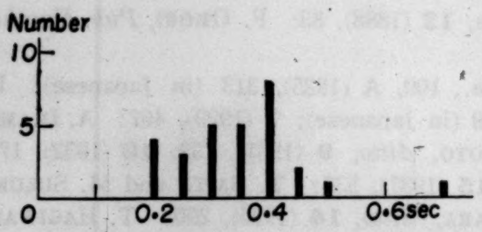

Fig. 1. The numbers of earthquakes and their peak periods at Hongo in Tokyo.

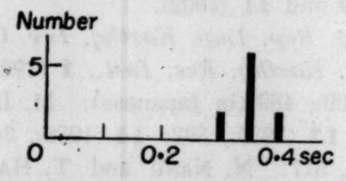

Fig. 2. The numbers of earthquakes and their peak periods at Aoyama in Tokyo.

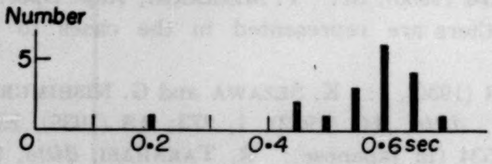

Fig. 3. The numbers of earthquakes and their peak periods at Marunouti in Tokyo.

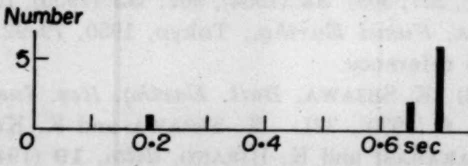

Fig. 4. The numbers of earthquakes and their peak periods at Kanda in Tokyo.

5) K. KANAI and M. SUZUKI, *Bull. Earthq. Res. Inst.*, **32** (1954), 189: Subsoil Res. Team, Earthq. Res. Inst., *ditto*, **33** (1955), 500–532. (in Japanese)

6) M. ISHIMOTO, *ditto*, **15** (1937), 536: T. MINAKAMI and S. SAKUMA, *ditto*, **26** (1948), 61.

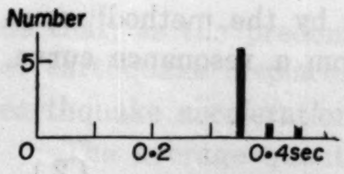

Fig. 5. The numbers of earthquakes and their peak periods at Komagome in Tokyo.

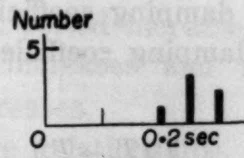

Fig. 6. The numbers of earthquakes and their peak periods at Komaba in Tokyo.

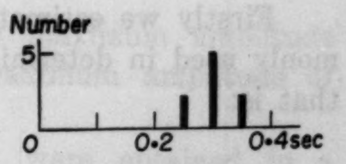

Fig. 7. The number of earthquakes and their peak periods at Nogeyama in Yokohama.

peak period in each figure may be considered the predominant period of the ground of that place. These predominant periods closely approximate the peak periods obtained from microtremor measurements at the respective places[7].

3. Empirical formula for the seismic characteristics of the ground

Since in most cases the amplitude-period relation of earthquake motion is a resonance type curve[8], we will write the following formula for the seismic characteristics of the ground:

$$U_s = \frac{c_1 U_0}{\sqrt{\left\{1-\left(\frac{T}{T_0}\right)^2\right\}^2 + \left\{\tau \frac{T}{T_0}\right\}^2}}, \tag{1}$$

where U_s = absolute amplitude of earthquake motion at free surface,
U_0 = absolute amplitude of seismic waves reaching the bottom boundary of the surface layer,
T_0 = predominant period of the ground,
T = period of seismic waves,
τ = apparent damping coefficient of the surface vibration,
c_1 = a coefficient which depends upon the impedance ratio of the two media and is independent of T_0.

Damping may be caused by both dissipation of vibration energy to the bottom medium and solid viscosity in the surface layer. The former depends on both the ratio of the impedance of the surface layer to that of the bottom medium and the natural period of the surface layer. We will now estimate the values of c_1 and τ, using data obtained by many kinds of observation.

7) K. KANAI, T. TANAKA and K. OSADA, *Bull. Earthq. Res. Inst.*, **32** (1954), 199. Subsoil Research Team, Earthq. Res. Inst., *ditto*, **33** (1955), 492–495. (in Japanese)

8) *loc. cit.*, 2), 7).

Firstly we estimate the damping coefficient τ by the method[9] commonly used in determining damping coefficient from a resonance curve, that is:

$$\tau \doteqdot \frac{T_0(T_1-T_2)}{T_1 T_2}, \qquad (2)$$

in which T_0 is the resonance period and T_1, T_2 are the periods corresponding to an amplitude of $1/\sqrt{2}$ times the resonance amplitude.

The values of τ and T_0 at many places were thus obtained from the frequency period curves of both natural earthquakes and micro-

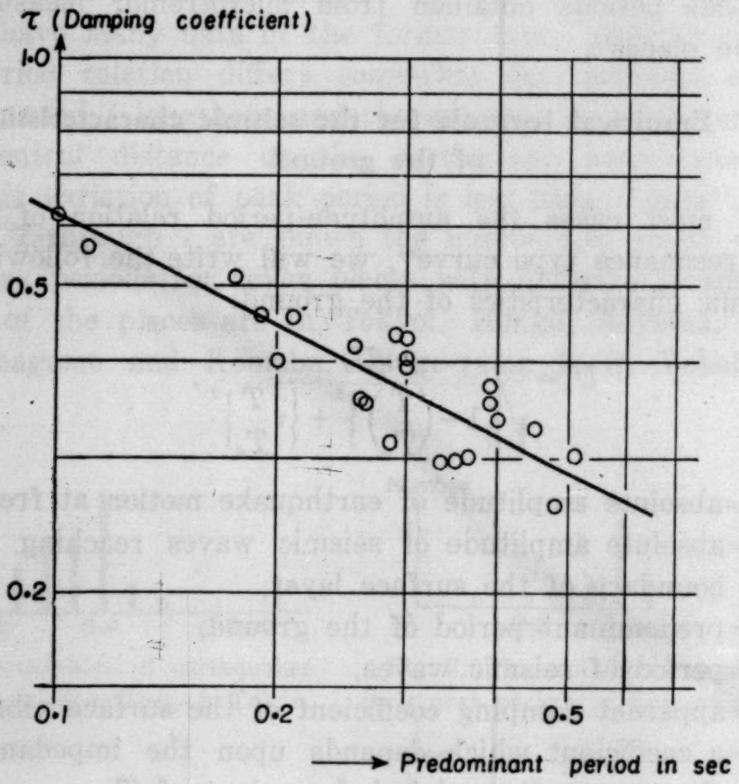

Fig. 8.

tremors[10]. These values are plotted in Fig. 8, from which we obtain an empirical formula,

$$\tau = \frac{0.2}{\sqrt{T_0}}. \qquad (3)$$

The results of many comparative observations of earthquakes tell

9) K. KANAI and S. YOSHIZAWA, *Bull. Earthq. Res. Inst.*, **30** (1952), 121.
10) *loc. cit.*, 7): K. KANAI, T. TANAKA and K. OSADA, *ditto*, **35** (1957), 10.

us that, as the predominant period increases, the maximum amplitude of earthquake displacement increases and the maximum amplitude of earthquake acceleration decreases.

The average quantitative relationships which were obtained in a previous study[11] are as follows:

$$D_{\max.} \propto T_0^{1.7\pm0.2} , \qquad (4)$$

$$A_{\max.} \propto T_0^{-0.6\pm0.1} , \qquad (5)$$

in which $D_{\max.}$ and $A_{\max.}$ are the largest amplitude of displacement and acceleration of earthquake motion respectively.

Assuming the exponents of (4) and (5) to be 1.5 and -0.5, respectively. We obtain from (4) the following empirical formula:

$$U_{s(\max.)} = c_2 T_0^{1.5} , \qquad (6)$$

where c_2 is a coefficient depending upon the nature of incident waves and the physical properties of surface layer and bed rock, but independent of T_0. Also, from (1) and (3), the amplitude in the case of resonance becomes:

$$U_{s(\text{res.})} = c_1 U_{0(\text{res.})} \frac{T_0^{0.5}}{0.2} . \qquad (7)$$

Equating (6) and (7),

$$U_{0(\text{res.})} = \frac{0.2c_2}{c_1} T_0 . \qquad (8)$$

If equipartition of energy applies to the seismic waves arriving at the bottom boundary[12], the relation of amplitude to period can be expressed as:

$$U_0 = cT , \qquad (8')$$

where c is a constant.

Thus (8) is compatible with (8′) and represents the special case of resonance. Hence (8′) will be used as a basic factor below.

Substituting (3) and (8′) in (1), we obtain the empirical formula for the spectral response of ground,

11) K. KANAI, *Bull. Earthq. Res. Inst.*, **32** (1954), 211.

12) The velocity spectra of the large number of strong motion seismograms obtained in the U.S.A.* have the form of several fluctuations superposed on a horizontal line parallel to the period axis. It appears that the reason for this flatness is that the observing places are located on thick alluvium.

* J. L. ALFORD, G. W. HOUSNER and R. R. MARTEL, 1st Tech. Rep., Office Naval Res., N6onr 244-25, Proj. Desig. Nr-081-095.

$$U_s = \frac{c_1 c T}{\sqrt{\left\{1-\left(\frac{T}{T_0}\right)^2\right\}^2 + \left\{\frac{0.2}{\sqrt{T_0}}\left(\frac{T}{T_0}\right)\right\}^2}}. \tag{9}$$

Substituting (3) only, we obtain the amplification of ground,

$$\frac{U_s}{U_0} = \frac{c_1}{\sqrt{\left\{1-\left(\frac{T}{T_0}\right)^2\right\}^2 + \left\{\frac{0.2}{\sqrt{T_0}}\left(\frac{T}{T_0}\right)\right\}^2}}. \tag{9'}$$

4. Theoretical interpretation of the empirical formula

Here we shall examine the simplest case, in which a plane distortional wave propagated vertically upward in an elastic semi-infinite medium is partly transmitted and partly reflected at the bottom boundary of the superficial visco-elastic layer and is reflected at the free surface. This is one of the multiple reflection problems of elastic waves in a superficial layer[13]. The wave amplitude at the free surface of a multi-layered ground may be expressed as:

$$U_s = \frac{2U_0}{\sqrt{\{F(T, T_{0m}, \alpha_m, \xi_m)\}^2 + \{G(T, T_{0m}, \alpha_m, \xi_m)\}^2}}, \tag{10}$$

where, m represents the layer number and α and ξ represent, respectively, the impedance ratio of neighboring layers and the viscous coefficient of a layer[14].

In the case of a simple layer, assuming that

$$\frac{p\xi}{\mu_1} \ll 1, \tag{11}$$

the wave amplitude at the free surface may be written as:

$$U_s = \frac{2U_0}{\sqrt{\{F(T, T_0, \alpha)\}^2 + \{G(T, T_0, \alpha, \xi)\}^2}}, \tag{12}$$

where

$$T_0 = \frac{4H}{v_1}, \quad \alpha = \frac{\rho_1 v_1}{\rho_2 v_2}, \quad p = \frac{2\pi}{T}, \tag{13}$$

in which subscripts 1 and 2 represent surface layer and bottom medium, respectively, and μ, ρ, v and H represent rigidity, density, velocity and

13) K. KANAI, *Bull. Earthq. Res. Inst.*, **31** (1953), 219: K. KANAI, and S. YOSHIZAWA, *ditto*, **31** (1953), 275.

14) K. KANAI, *ditto*, **28** (1950), 31.

thickness of surface layer, respectively.

Values of ξ/v^3 for various materials in the ground are always of the same order[15], i.e. approximately 10^{-6} C.G.S. Using this value and considering the range of $v_1 = 50$ to 500 m/s, $T = 0.1 - 1.0$ sec, the range of $p\xi/\mu$ becomes 0.05 to 1.5.

The relation between U_s/U_0 and $2\pi\xi/\mu_1 T_0$ in a previous paper[16] is shown in Fig. 9. The straight lines satisfactorily approximate the

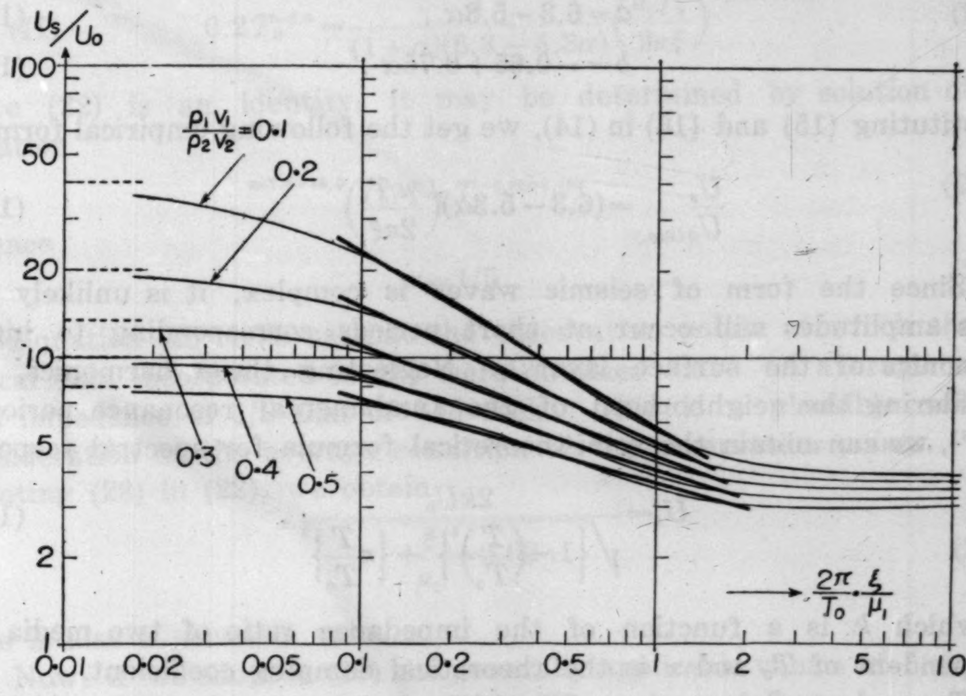

Fig. 9.

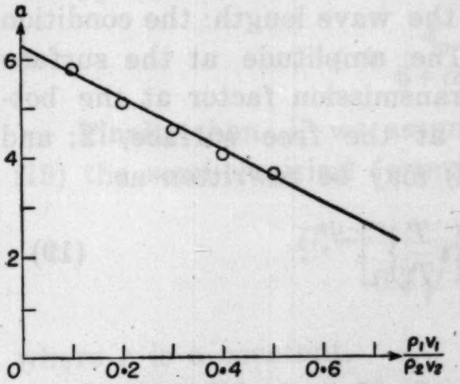

Fig. 10.

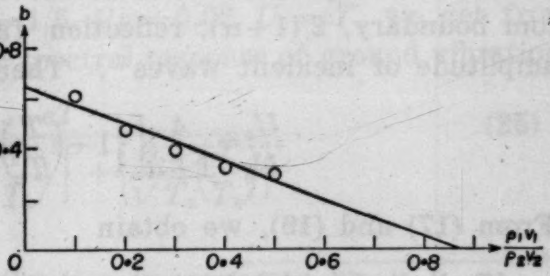

Fig. 11.

15) K. KANAI and K. OSADA, *Bull. Earthq. Res. Inst.*, **29** (1951), 514, Table II.
16) K. KANAI, *ditto*, **30** (1952), 35, Fig. 4.

curves in the range 0.05 to 1.5 of abscissa. The relation may be expressed as

$$\frac{U_s}{U_{0\,(\mathrm{Res.})}}=a\left(\frac{p_0\xi}{\mu_1}\right)^b . \tag{14}$$

By means of Figs. 10 and 11 the values of a and b are determined from Fig. 9, whence,

$$a=6.3-5.3\alpha , \tag{15}$$

$$b=-0.65+0.75\alpha . \tag{16}$$

Substituting (15) and (16) in (14), we get the following empirical formula:

$$\frac{U_s}{U_{0\,(\mathrm{Res.})}}=(6.3-5.3\alpha)\left(\frac{\mu_1 T_0}{2\pi\xi}\right)^{0.65-0.75\alpha} . \tag{17}$$

Since the form of seismic waves is complex, it is unlikely that large amplitudes will occur at short periods corresponding to higher harmonics of the surface layer[17]. Neglecting these harmonics, and considering the neighborhood of the fundamental resonance period of (12)[18], we can obtain the semi-theoretical formula for spectral response,

$$U_s=\frac{2kU_0}{\sqrt{\left\{1-\left(\frac{T}{T_0}\right)^2\right\}^2+\left\{\kappa\frac{T}{T_0}\right\}^2}} , \tag{18}$$

in which k is a function of the impedance ratio of two media and independent of T_0 and κ is the theoretical damping coefficient.

To evaluate k, we may utilize the special case where the thickness of the surface layer is much larger than the wave length: the condition $T/T_0\to 0$ may be substituted in (18). The amplitude at the surface will equal the product of three factors: transmission factor at the bottom boundary, $2/(1+\alpha)$; reflection factor at the free surface, 2; and amplitude of incident waves[19]. Then, (18) may be rewritten as

$$\frac{U_s}{U_0}=\frac{4}{1+\alpha}\left[\left\{1-\left(\frac{T}{T_0}\right)^2\right\}^2+\left\{\kappa\frac{T}{T_0}\right\}^2\right]^{-1/2} . \tag{19}$$

From (17) and (19), we obtain

17) K. KANAI and S. YOSHIZAWA, *Bull. Earthq. Res. Inst.*, **34** (1956), 167.
18) *loc. cit*, 13), 34, Figs. 2-5.
19) C. G. KNOTT, Phil. Mag., **48** (1899), 64: H. KAWASUMI and T. SUZUKI, *Journ. Seism. Soc. Japan*, **4** (1932), 277. (in Japanese)

$$\kappa=\frac{4}{(1+\alpha)(6.3-5.3\alpha)}\left(\frac{\mu_1 T_0}{2\pi\xi}\right)^{-0.65+0.75\alpha} . \tag{20}$$

To reconcile the semi-theoretical formula of (19) and the empirical formula of (9′), two conditions are necessary:

(I) $$c_1=\frac{4}{1+\alpha}, \tag{21}$$

(II) $$0.2\,T_0^{-0.5}=\frac{4}{(1+\alpha)(6.3-5.3\alpha)}\left(\frac{\mu_1 T_0}{2\pi\xi}\right)^{-0.65+0.75\alpha} . \tag{22}$$

Since (22) is an identity, it may be determined by solution of the equation

$$T_0^{-0.5}=T_0^{-0.65+0.75\alpha}, \tag{22′}$$

whence

$$\alpha=1/5 . \tag{23}$$

Equation (23) tells us that the observation points at which the empirical data incorporated in (9′) were obtained have an average vibration impedance of 1/5 that of bed rock. This is a plausible value in consideration of the average condition of the observation points. Substituting (23) in (22), we obtain

$$\frac{\xi}{\mu_1}=0.02 . \tag{24}$$

This is also a plausible value.

Now, if we adopt in (20) the generally applicable values of $\xi/v_1^2=10^{-6}$ and $\rho_1=2$, we obtain a semi-theoretical formula as follows:

$$\kappa \doteqdot \frac{4}{6+\alpha}\left(\frac{T_0}{\pi v_1}\times 10^6\right)^{-0.65+0.75\alpha} . \tag{20′}$$

Finally then, if we assume $\alpha=1/5$, $\xi/\mu_1=0.02$, $U_0=cT$, we get from (19) the semi-empirical formula for spectral response of ground vibration,

$$U_s=\frac{cT}{0.3\sqrt{\left\{1-\left(\frac{T}{T_0}\right)^2\right\}^2+\left\{\frac{0.2}{\sqrt{T_0}}\left(\frac{T}{T_0}\right)\right\}^2}}, \tag{25}$$

where c is a constant.

The amplification of ground vibration is expressed by

$$\frac{U_s}{U_0}=\frac{1}{0.3}\left[\left\{1-\left(\frac{T}{T_0}\right)^2\right\}^2+\left\{\frac{0.2}{\sqrt{T_0}}\left(\frac{T}{T_0}\right)\right\}^2\right]^{-1/2} . \tag{25′}$$

Therefore, the resonance amplitude of ground vibration becomes

$$U_{s(\text{Res.})}=\frac{50\,T_0^{1.5}}{3}\times c\,. \tag{26}$$

Comparing (25), (25′) with (9), (9′) it is seen that $c_1=10/3$.

5. Application limits of the semi-empirical formula

The semi-empirical formula, equation (25), expresses the amplitude at free surface as influenced by multiple reflection in the stratified visco-elastic layer. There are some limits of ground conditions for the application of the formula.

(I) The case of a thick stratified layer.

In the case of a thick stratified layer, the phenomenon of superposition of transmitted and reflected seismic waves will be unlikely. Therefore the amplitude at ground surface is the product of three factors as illustrated in (18) and (19). This is a special case of (25), (25′).

The Arvin-Tehachapi earthquake of July 1952 gave a good example of this case[20]. The campus of the California Institute of Technology is located on several hundred feet of alluvium and the Seismological Laboratory of the Institute rests on an outcrop of bed-rock; the ratio of maximum displacements was nearly two to one.

(II) The case of multiple stratified layers.

In the case of multiple stratified layers, since the waves reflected and refracted at various boundaries interfere with one another, the spectral response of surface amplitude is very irregular[21]. Except in the extremely special case where there are nodes both at the bottom boundary and at the first boundary below the surface, the maximum amplitudes are not as large as for a single surface layer[22]. Therefore, the empirical formula (25) is not applicable in this case.

(III) The case of exposed rock.

Usually, the predominant period observed on rock covers the range

20) G. W. HOUSNER, Geotechnique, Dec. 1954, 153.

21) *loc. cit.*, 16): K. KANAI, *Monthly Meeting, Earthq. Res. Inst.*, (July 1956).

22) The largest amplitude is nearly $2\rho_n v_n/\rho_1 v_1$ and its period is $4H_1/v_1$, in which $\rho_n v_n$ and $\rho_1 v_1$ are the vibrational impedance of the bed rock and the first layer, respectively, and H_1 is the thickness of the first layer. This phenomenon has sometimes appeared in actual earthquakes as well as in micro-tremors. This problem will be considered in a forthcoming paper.

M. ISHIMOTO, *Bull. Earthq. Res. Inst.*, **13** (1935), 592 (in Japanese): K. KANAI, *Monthly Meeting, Earthq. Res. Inst.*, (Sept. 1956).

between 1/30 and 1/5 sec. This range is explained in terms of multiple reflection in a thin weathered layer of the rock.

The semi-empirical formula (25′) may be applicable to the usual older rock outcrop.

(IV) The case of fresh exposed rock and bed rock.

On the other hand, the vibration characteristics of fresh exposed rock and bed rock are quite different[23]. The peak of the spectral response curve sometimes appears at 0.3 sec to 0.6 sec, and sometimes the curve is flat. The details of this problem will be shown in a forthcoming paper.

6. Statistical study of earthquake damage

(I) The case of wooden houses.

Recently, in Japan, in order to clarify the question of how earthquake damage varies with ground conditions, investigations have been carried out from various standpoints based on experiences in great destructive earthquakes.

Figs. 12 and 13 show the relations between damage to wooden houses and number of stories at twelve places in Tokyo in the great Kwanto earthquake of 1923.[24] Fig. 12 applies to the up-town region

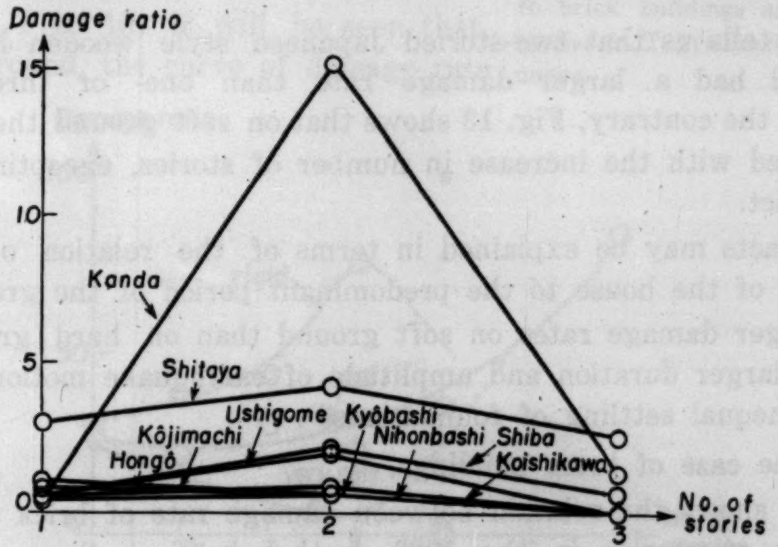

Fig. 12. Relation between damage to wooden houses and number of stories in up-town Tokyo in the 1932 earthquake.

23) K. KANAI, T. TANAKA and K. OSADA, *Monthly Meeting Earthq. Res. Inst.*, (Sept. 1956; Jan. and Feb., 1957).

24) G. KITAZAWA, *Rep. Imp. Earthq. Inv. Comm.* No. 100, Ca, 1.

where the ground consists mainly of Diluvium or Tertiary formations and the predominant period is about 0.2 to 0.4 sec, while Fig. 13 applies to the down-town region where the ground consists mainly of thick alluvium and the predominant period is about 0.5 to 0.8 sec.

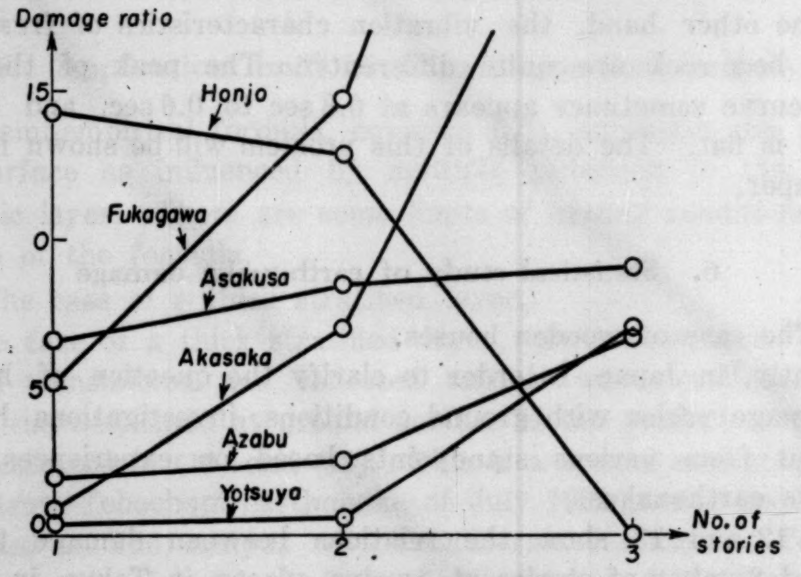

Fig. 13. Relation between damage to wooden houses and number of stories in down-town Tokyo in the 1923 earthquake.

Fig. 12 tells us that two-storied Japanese style wooden houses on firm ground had a larger damage rate than one- or three-storied houses. On the contrary, Fig. 13 shows that on soft ground the damage rate increased with the increase in number of stories, excepting in the Honjo district.

These facts may be explained in terms of the relation of the natural period of the house to the predominant period of the ground.

The larger damage rates on soft ground than on hard ground are due to the larger duration and amplitude of earthquake motion as well as to the unequal settling of foundations[25].

(II) The case of brick buildings.

Fig. 14 shows the relation between damage rate of brick buildings and number of stories in the 1923 earthquake[26] at three places in Tokyo.

The notations rigid, soft and very soft in Fig. 14 indicate that the

25) K. KANAI, *Bull. Earthq. Res. Inst.*, **29** (1951), 215. (in Japanese)
26) Y. SATO, *Rep. Imp. Earthq. Inv. Comm.* No. 100, Ca, 550.

ground consists respectively, of Diluvium or Tertiary formation, 10 to 20 m thickness of alluvium, and 30 to 50 m thickness of alluvium.

It will be seen from Fig. 14 that, the softer the ground, the less the earthquake damage of brick buildings, and that the damage rate is only slightly affected by the number of stories. These facts may be explained qualitatively as follows: (i) The natural period of one- to three-storied brick buildings is comparable to the predominant period of hard ground. (ii) The softer the ground, the larger the dissipation of earthquake vibration energy of buildings to the ground[27].

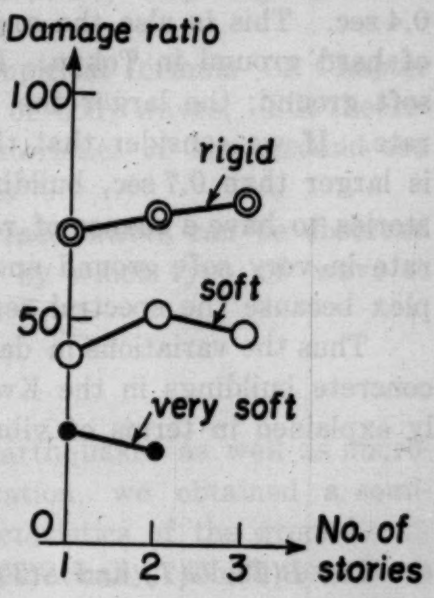

Fig. 14. Relation between damage to brick buildings and number of stories in Tokyo in the 1923 earthquake.

(III) The case of reinforced concrete buildings.

Fig. 15 shows the relation between damage rate of reinforced concrete buildings and number of stories in the 1923 earthquake[28] at three places in Tokyo. The meanings of the notations rigid, soft and very soft are the same as in Fig. 14.

From Fig. 15, it will be seen that, on rigid ground, the curve of damage rate

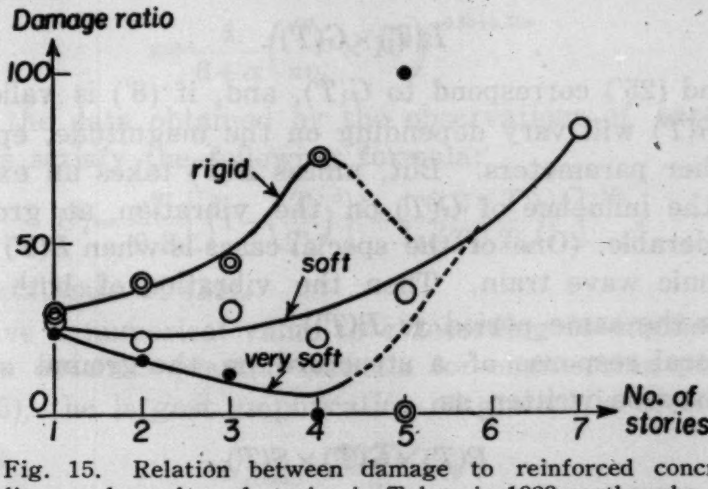

Fig. 15. Relation between damage to reinforced concrete buildings and number of stories in Tokyo in 1923 earthquake.

27) K. KANAI, *Bull. Earthq. Res. Inst.*, **27** (1949), 97: K. KANAI and S. YOSHIZAWA, *ditto*, **29** (1951), 209.

28) N. NAGATA, *Rep. Imp. Earthq. Inv. Comm.*, No. 100, Cb, 211: loc. cit., 26).

versus number of stories seems to have a peak at four-story buildings. On the other hand, the average natural period of 1923 Japanese reinforced concrete buildings may be estimated from the formula[29] $T=(0.07-0.09)\times N$, in which T is natural period in seconds and N is the number of stories; the period of four-story buildings comes out to be 0.3 to 0.4 sec. This is also the approximate range of the predominant period of hard ground in Tokyo. Paragraph Fig. 15 also shows that, in very soft ground, the larger the number of stories the larger the damage rate. If we consider that the predominant period in very soft ground is larger than 0.7 sec, buildings would have to be higher than eight-stories to have a chance of resonance. The relation between the damage rate in very soft ground and the number of stories is somewhat complex because the spectral response of such ground is complex.

Thus the variations in damage rates of wooden, brick and reinforced concrete buildings in the Kwanto earthquake of 1923 can be qualitatively explained in terms of vibrational characteristics of the ground.

7. Discussion

Let $B(T)$, $G(T)$ and $S(T)$ be respectively, the spectral response of incident waves transmitted to bed rock, the vibration characteristics of the ground, and the vibration characteristics of the structure.

The spectral response of actual earthquake motion at ground surface is expressed by

$$B(T)\times G(T)\ . \tag{27}$$

Then, (25) and (25′) correspond to $G(T)$, and, if (8′) is valid, $B(T)=cT$. In general, $B(T)$ will vary depending on the magnitude, epicentral distance and other parameters. But, unless $B(T)$ takes an extremely unusual form, the influence of $G(T)$ on the vibration at ground surface will be considerable. (One of the special cases is when $B(T)$ is an infinite simple harmonic wave train. Then the vibration of both ground and structure has the same period as $B(T)$).

The spectral response of a structure on the ground surface in an earthquake may be written as

$$B(T)\times G(T)\times S(T)\ , \tag{28}$$

is which $S(T)$ depends both on the kind of construction and the vibrational conditions between foundation and ground. Therefore, the earth-

29) C. TANIGUCHI, *Journ. Architect. Inst. Japan*, Dec. 1949. (in Japanese)

quake motion of serious consideration for earthquake-proof construction is the vibration having a period approximate to the natural period of the structure. It is needless to say that vibration with large displacement like 1 m in which the period is 10 sec, and vibration with large acceleration like 1 g in which the period is 50 c/s, only slightly affect the vibration of the structure.

The theoretical interpretation of the empirical formula in Chapter 6 was made in terms of multiple reflection of body waves. But theoretically the resonance-type vibrational characteristics of the ground can be explained also in terms of surface waves[30].

If the velocities of *S*-waves and surface waves can be observed satisfactorily, it will not be difficult to find by which type of wave to characterize the vibration of ground.

8. Conclusion

By using the observational results of earthquakes as well as micro-tremors and adding a theoretical interpretation, we obtained a semi-empirical formula for the vibrational characteristics of the ground.

The general equation obtained semi-theoretically, which expresses the spectral response of ground vibration, is

$$U_s = \frac{4U_0}{1+\alpha}\left[\left\{1-\left(\frac{T}{T_0}\right)^2\right\}^2 + \left\{\kappa\frac{T}{T_0}\right\}^2\right]^{-1/2}, \tag{19}$$

in which

$$\kappa \doteqdot \frac{4}{6+\alpha}\left(\frac{T_0}{\pi v_1}\times 10^6\right)^{-0.65+0.75\alpha}. \tag{20'}$$

Most of the data obtained by the observations of earthquakes and micro-tremors satisfy the following formula:

$$U_s = \frac{cT}{0.3}\left[\left\{1-\left(\frac{T}{T_0}\right)^2\right\}^2 + \left\{\frac{0.2}{\sqrt{T_0}}\left(\frac{T}{T_0}\right)\right\}^2\right]^{-1/2}, \tag{25}$$

(25) is a special case of (19).

If we give a numerical value to c according to engineering judgement, we can obtain a practial formula for engineering purposes.

From (25), the largest amplification of ground is as follows:

$$U_{s(\mathrm{Res.})} = \frac{50\,T_0^{1.5}}{3}\times c\,. \tag{26}$$

30) R. Stoneley, *M.N.R.A.S. Geophs. Suppl.*, **4** (1937), 39: K. Sezawa and K. Kanai, *Bull. Earthq. Res. Inst.*, **15** (1937), 577, 845: K. Tazime, *Journ. Physics of the Earth*, **5**, No. 1 (1957), 43.

It must be borne in mind that (25) explains qualitatively the damage to buildings caused by the Kwanto earthquake of 1923.

In conclusion, the author wishes to express his thanks to Prof. R. Takahasi and Prof. H. Kawasumi for their kind discussion in the course of this investigation. Also his thanks are due to Miss S. Yoshizawa who assisted him in preparing this paper.

---

16. 地盤の震動特性に関する半実験式

地震研究所 金 井 清

地震動及び常時微動の観測結果を使い，理論的な検討を加えて，地盤の震動特性に関する半実験式を作つた．即ち，地盤の増巾度を表わす式は $(U_s/U_0)_{\max}$ であり，その一般式は次式となる

$$\left(\frac{U_s}{U_0}\right)_{\max}=(6.3-5.3\alpha)\left(\frac{\mu_1 T_0}{2\pi\xi}\right)^{0.65-0.75\alpha}. \tag{17}$$

又，地震時の地盤の震動スペクトルを表わす一般式は

$$U_s=\frac{4cT}{1+\alpha}\left[\left\{1-\left(\frac{T}{T_0}\right)^2\right\}^2+\left\{\kappa\frac{T}{T_0}\right\}^2\right]^{-1/2} \tag{19}$$

で表わされる．但し

$$\kappa=\frac{4}{(1+\alpha)(6.3-5.3\alpha)}\left(\frac{\mu_1 T_0}{2\pi\xi}\right)^{-0.65+0.75\alpha}. \tag{20}$$

今日までの観測結果から κ についての平均の値を求めると $\kappa \doteqdot \frac{0.2}{\sqrt{T_0}}$ となり，地震時の地盤の震動スペクトルは次式となる．

$$U_s=\frac{cT}{0.3\sqrt{\left\{1-\left(\frac{T}{T_0}\right)^2\right\}^2+\left\{\frac{0.2}{\sqrt{T_0}}\left(\frac{T}{T_0}\right)\right\}^2}}, \tag{25}$$

c を仮定すれば工学的の実用式になる訳である．

地盤の最大増巾度は次式となる．

$$U_{s(\mathrm{Res.})}=\frac{50T_0^{1.5}}{3}\times c. \tag{26}$$

以上の半実験式は，地震観測の結果によく合うばかりでなく，関東地震の震害と地盤との関係にもこれによつて或程度の説明がつく．

基盤に到達した入射波のスペクトル・レスポンスを $B(T)$，地盤固有のスペクトル・レスポンスを $G(T)$，構造物自体のそれを $S(T)$ とすると，地震時における地表面の震動のスペクトルは実際的には次のように表わされる．

$$B(T)\times G(T), \tag{27}$$

而して，(25′) 式は $G(T)$ に当り，(25) 式は $B(T)=cT$ と仮定したときの $B(T)\times G(T)$ に当る．

地震の大きさ，震央巨離，その他の条件によつて，$B(T)$ がちがう事は想像される．しかし，$B(T)$ が余程特別なものでない限り，$G(T)$ の影響は相当に大きい筈である．(極端な場合として，入射波が無限長調和波ならば，地盤も構造物も入射波と同じ単一周期の振動をするのは無論である．)

次に，地表面上の構造物の地震時の震動のスペクトルは実際的には次のように表わせる.

$$B(T)\times G(T)\times S(T)\,, \tag{28}$$

但し，$S(T)$ は上部構造の種類並びに基礎と地面との間の震動的条件に関係する. 従つて，耐震構造上に重大な意味をもつ地震動は，構造物の周期に近い震動である. [1 m の大振巾の地震動でも周期が 10 秒のものとか，(加速度は 40 gal になる)，1 g の大加速度振巾の地震動でも，その周期が 50 c/s（変位振巾は 0.1 mm）のものとかは，実在構造物に対して破壊的作用をしないであろう.]

17. *Geomagnetic Anomaly on Volcanoes with Relation to Their Subterranean Structure.*

By Izumi YOKOYAMA,

Earthquake Research Institute.

(Read November 27, 1956.—Received March 31, 1957.)

Summary

Dip-survey on the volcanic islands of the Seven Izu Islands at the south of Japan Proper has been almost completed. These volcanic islands differ in dimension and geological structure and therefore exhibit various features of distribution of geomagnetic anomaly. The writer, in this paper, tries to interpret the anomaly in relation to the subterranean structure of the volcanoes. To attain the object, the following items are considered:

1. Representation of geomagnetic anomaly on a volcano by a dipole-field.
2. Magnetization of igneous rocks and its range.
3. Bulk-density of the mountain-mass.
4. Determination of depth of sources by analysing the vertical component in the geomagnetic field on Volcano Mihara.
5. Some knowledge obtained by a gravity survey on Volcano Mihara.
6. Some discussions on parasitic cones of Volcano Mihara.
7. Geomagnetic anomaly around the craters of volcanoes.
8. Some information obtained by aeromagnetic surveys over the volcanoes in Alaska.

Introduction

Many geophysicists have observed the geomagnetic field on volcanoes and recently even aeromagnetic surveys are carried out over volcanoes in U.S.A. It would be an endless task to cite the examples of dip-survey especially in Japan. One of the problems for a volcanologist, the writer thinks, is how to utilize significantly the analyses of the geomagnetic anomaly together with other methods in order to obtain some knowledge in relation to the subterranean structure of the volcanoes even if there is a limit to it. Here, the writer discuss this problem with reference to the geomagnetic anomalies on the Seven Izu Islands.

The Seven Izu Islands are composed of a number (more than seven) of volcanic islands including active, dormant and extinct Quaternary

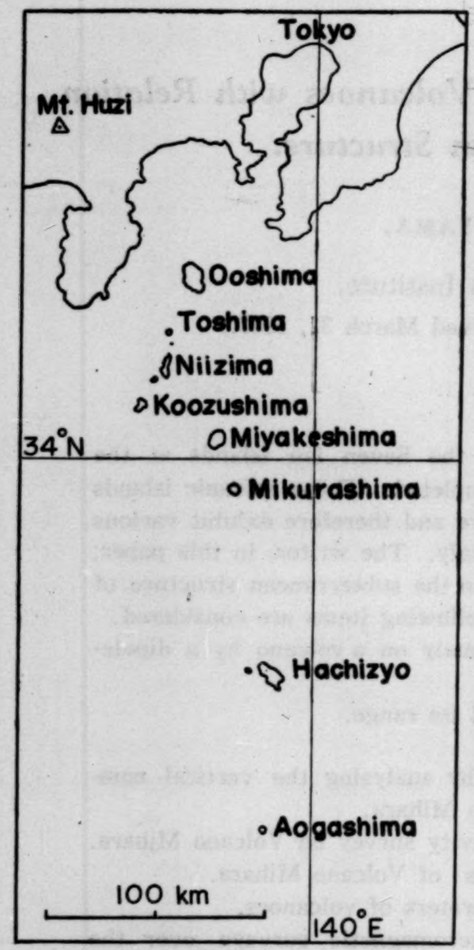

Fig. 1. The Seven Izu Islands.

volcanoes while their rocks are discriminated into basalt, andesite and liparite. This archipelago runs southward perpendicularly to Japan Proper and continues to Mariana Islands via Ogasawara (Bonin) Islands and Iwoo (Sulphur) Islands.

T. Minakami[1] carried out a dip-survey on Miyakeshima Island in 1940 and R. Takahasi and T. Nagata[2] observed the geomagnetic anomaly on Ooshima Island in 1936. T. Rikitake and the writer[3] have been increasing the observation of dip-angle and other components of geomagnetic field on Ooshima Island since 1950. The writer has almost completed dip-surveys on the other islands of the Seven Izu Islands. These results are shown in Fig. 2 and Table I. Fig. 3 shows the mean topographic profiles of each islands obtained by averaging in eight directions.

1. Representation of geomagnetic anomaly on a volcano by a dipole-field

Regarding interpretation of geomagnetic anomalies on volcanoes, there have been several opinions: Anomalous geomagnetic field was represented by uniform magnetization of the mountain-mass which was assumed to be of ellipsoidal or circular conical shape. The former approximation is called the Haalck-Koenigsberger's method and T. Minakami[4),5),6)] adopted it with the intention of interpreting the geomagnetic

1) T. MINAKAMI, *Bull. Earthq. Res. Inst.*, **19** (1940), 356.
2) R. TAKAHASI and T. NAGATA, *Bull. Earthq. Res. Inst.*, **15** (1937), 441.
3) T. RIKITAKE, *Bull. Earthq. Res. Inst.*, **29** (1951), 161.
T. RIKITAKE, I. YOKOYAMA, A. OKADA and Y. HISHIYAMA, *Bull. Earthq. Res. Inst.*, **29** (1951), 583.
4) T. MINAKAMI, *Bull. Earthq. Res. Inst.*, **18** (1940), 178.
5) H. TSUYA and T. MINAKAMI, *Bull. Earthq. Res. Inst.*, **18** (1940), 338.
6) T. MINAKAMI and S. SAKUMA, *Bull. Volcanologique*, **18** (1956), 77.

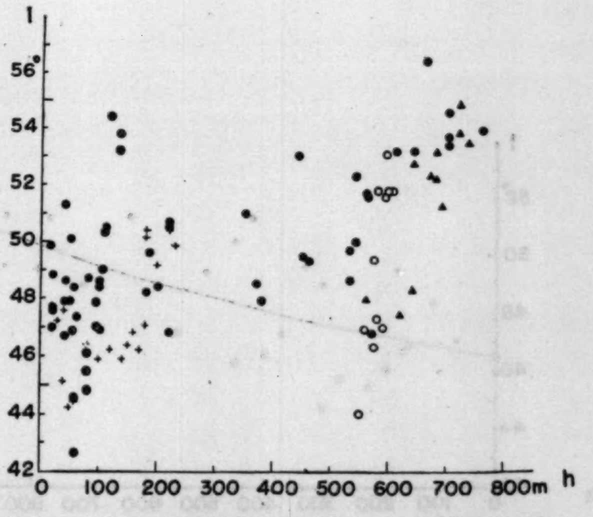

Fig. 2. a) Ooshima Island (Volcano Mihara) after T. Rikitake and I. Yokoyama.

⊙ Mt. Atago.
+ Mt. Takenohira.
○ 604*m* triangulation point on the outer somma.
▲ Mt. Shiraishi on the outer Somma.

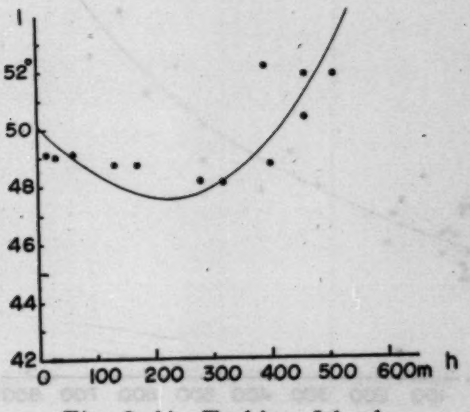

Fig. 2. b) Toshima Island.

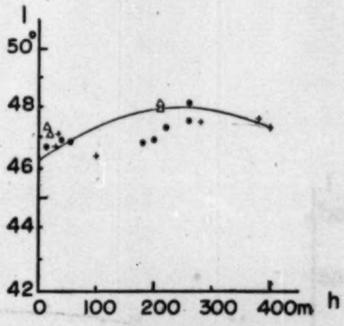

Fig. 2. c) Niizima Island.

● Mt. Mukai-yama.
+ Mt. Miyazuka.
△ Wakagoo.

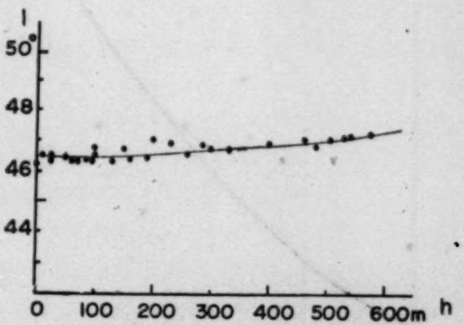

Fig. 2. d) Koozushima Island.

Fig. 2. Dip anomaly and height of the volcanoes in the Seven Izu Islands.

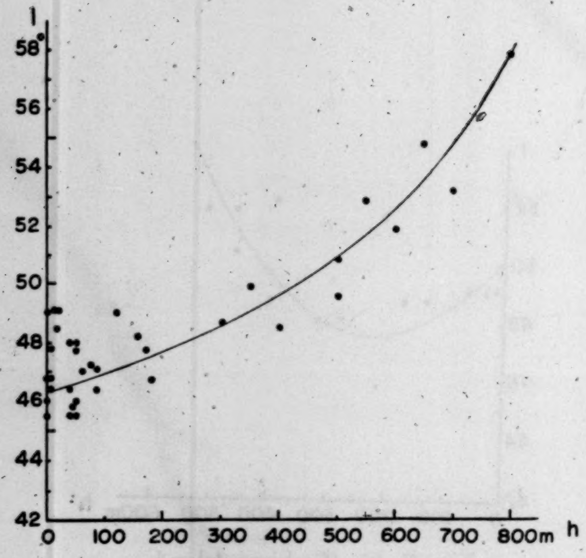

Fig. 2. e) Miyakeshima Island after T. Minakami.

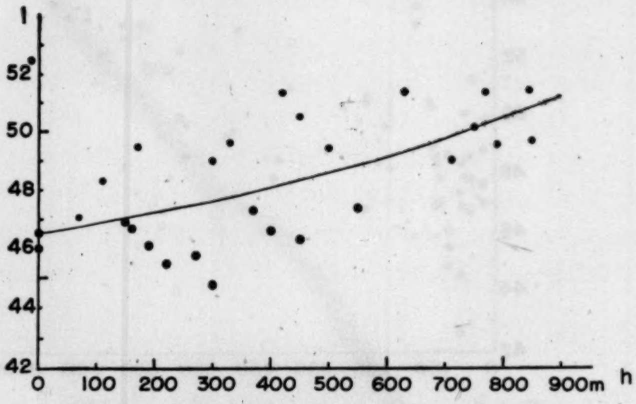

Fig. 2. f) Mikurashima Island.

● on ridge ⊙ in gorge

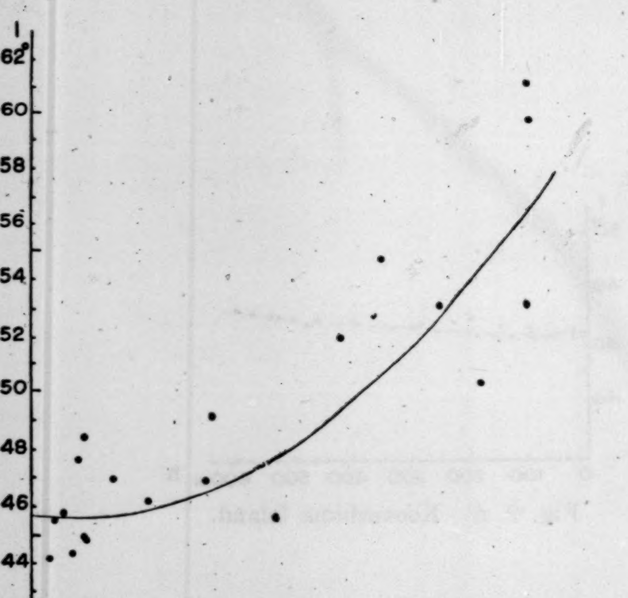

Fig. 2. g) Hachizyo Island (west).

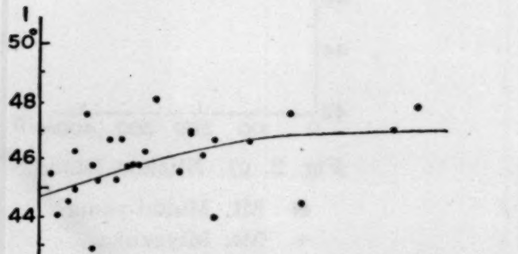

Fig. 2. h) Hachizyo Island (east).

Fig. 2. Dip anomaly and height of the volcanoes in the Seven Izu Islands. (continued)

Table I. Observation of dip on the Seven Izu Islands.

a) Toshima Island.

Time (1954)					Locality	Approximate Altitude	Dip
Aug.	11	12 *h*	30 *m*	No. 1	Village	60 *meters*	49°05′
		13	26	2	N-E slope	130	48 42
			44	3	〃	280	08
		14	07	4	〃	390	52 08
			25	5	〃	460	51 51
			44	6	Triangulation point	508	50 51
		15	16	7	N-W slope	460	20
			36	8	〃	400	48 43
			54	9	〃	320	04
		16	21	10	〃	170	42
		17	18	11	Village	30	49 00
			31	12	Coast	15	04

b) Niizima Island.

Time (1954)					Locality	Approximate Altitude	Dip
Aug.	9	14 *h*	23 *m*	No. 1	Honson Village*	17 *meters*	46°44′
		15	08	101	Mt. Mukai-yama	54	52
			45	102	〃	200	56
		16	04	103	〃	220	47 17
			44	104	〃	260	48 09
		17	20	105	〃	260	47 30
			48	106	〃	180	46 50
		18	22	8	Honson Village*	40	56
	10	10	12	107	〃	30	41
			54	108	〃	100	47 24
		11	36	109	Huzimi-pass	280	29
		12	50	110	Mt. Miyazuka	400	20
		13	56	111	〃	380	36
		14	56	112	Shrine	33	06
		15	30	113	Wakagoo Village	15	19
		16	18	114	〃	20	09
			52	115	〃	210	48 04
		17	34	116	〃	210	47 58

* T. Nagata carried out the same observation at these points in 1937. *Bull. Earthq. Res. Inst.*, **15** (1937), 497 (in Japanese).

c) Koozushima Island.

Time (1954)				Locality	Approximate Altitude	Dip
Aug. 6	15 *h*	16 *m*	No. 1	Village	50 *meters*	46°28′
		48	2	Path to Mt. Chichibu	160	22
	16	26	3	Mt. Chichibu	283	52
		58	4	Path to Mt. Chichibu	200	59
	18	22	5	Coast	10	32
7	07	54	6	Path to Mt. Tenzyo-san	85	13
	16	48	7	〃	95	18
	08	52	8	〃	190	27
	09	14	9	〃	260	34
		32	10	〃	330	42
		54	11	〃	400	53
	10	22	12	〃	480	46
	11	22	13	〃	530	47 06
	12	36	14	〃	540	08
	13	12	15	Mt. Kushiga-mine	505	00
	14	24	16	Triangulation point	574	14
	15	22	17	Shiroshima	460	02
		46	18	Path to Mt. Tenzyo-san	300	46 44
	16	19	19	〃	230	18
	17	08	20	〃	70	19
8	08	44	21	Primary School	60	23
	09	04	22	Path to Mt. Chichibu	85	24
		30	23	Middle School	25	20
	12	50	24	Shrine	25	33
	13	38	25	Foot of Mt. Tako	100	33
	14	32	26	Foot of Mt. Nachi	100	40
	15	16	27	Mt. Koodo	230	54
		54	28	〃	150	43
	16	44	29	Nagahama	2	12

d) Mikurashima Island.

Time (1956)			No.	Locality	Approximate Altitude	Dip
Apr. 5	15*h*	54*m*	No. 1	North coast	1 *meter*	46°00′
	16	12	2	〃	1	46 36
	17	10	3	Sato Village	110	48 17
6	07	24	4	Path to Mt. Oyama	160	46 42
		46	5	〃	220	45 28
	08	06	6	〃	300	44 45
		30	7	〃	400	46 36
		56	8	〃	450	46 17
	09	24	9	〃	630	51 18
		46	10	〃	710	48 58
	10	12	11	〃	750	50 06
		48	12	Summit	845	51 24
	12	03	13	Triangulation Point	851	49 35
		25	14	Path to Mt. Oyama	790	49 30
		43	15	〃	770	51 20
	15	35	16	〃	550	47 21
	16	00	17	〃	450	50 28
		24	18	〃	330	49 36
7	07	38	19	Tokkurine-uye	170	49 28
	08	28	20	North east coast	300	49 00
	10	08	21	〃	420	51 19
		57	22	Subarune-uye	500	49 24
	11	40	23	Nango Village	370	47 17
	14	42	24	Kawadagawa	270	45 45
	16	04	25	Usunango	190	46 05
9	14	53	26	Shrine	150	46 56
	15	09	27	Sato Village	70	47 03

e) Hachizyo Island.

Time (1954)			Locality		Approximate Altitude	Dip
Aug. 26	09 *h*	28 *m*	No. 1	Homei Shrine	60 *meters*	44°58′
	10	07	2	Yokomaga-hara	90	42 53
		48	3	Igona	60	46 16
	11	18	4	Kashidate Village	100	45 17
	12	56	5	〃	160	50
	13	22	6	〃	200	46 06
		46	7	Path to Mt. Higashi-yama	300	44 01
	14	09	8	〃	450	44 27
	15	05	9	Summit of Mt. Higashi-yama	650	47 46
		55	10	Path to Mt. Higashi-yama	610	02
	16	16	11	〃	430	38
		36	12	〃	360	46 34
		54	13	〃	200	48 06
	17	18	14	〃	140	46 42
	18	04	15	Shoobu-soo	50	44 37
27	08	30	16	Meiji High School	80	47 35
	09	15	17	Path to Mt. Nishi-yama	140	46 52
		33	18	〃	200	46 08
		57	19	〃	310	49 03
	10	13	20	〃	420	45 32
	11	06	21	〃	600	54 37
	12	43	22	Summit of Mt. Nishi-yama	850	61 04
	13	30	23	〃	850	53 03
	14	23	24	Triangulation Point	854	59 40
	16	01	25	Path to Mt. Nishi-yama	770	50 14
		23	26	〃	700	53 02
		43	27	〃	530	51 52
	17	26	28	〃	300	46 46
	18	07	29	〃	95	44 46
		23	30	〃	90	48 22
28	11	52	31	Nakanogoo Village	150	45 45
	12	27	32	Road to Sueyoshi Village	240	33
	13	10	33	Sueyoshi Village	180	46 15
	15	08	34	Sueyoshi Prim. School	90	45 48
		53	35	Sueyoshi Village	130	17
29	10	41	36	Ookago Village	60	42 11
	11	06	37	〃	55	45 41
		30	38	〃	70	44 16
		50	39	〃	90	56
	13	09	40	Yaene	20	45 30
	14	33	41	Ookago Village	30	44 06
30	14	08	42	Path to Mt. Higashi-yama	120	46 42
		58	43	〃	280	08
	15	26	44	〃	300	39
		54	45	〃	260	58
	16	35	46	〃	260	54
	17	27	47	Radio Relay Station	170	45 49

anomalies on Volcanoes Asama, Sakurazima and Huzi (Fuji). And the latter approximation was offered by T. Rikitake[7] who tried to interpret the geomagnetic anomalies on Volcano Mihara, Ooshima Island. The effective intensity of magnetization of these volcanoes to cause the observed geomagnetic anomalies, which was obtained by the above methods, is listed in Table II where the mountain-masses are all assumed to be uniformly magnetized.

In these methods, we must assume the uniform magnetization of the mountain-mass, namely the subterranean structure and the effective dimension of the volcano which are, the writer thinks, the

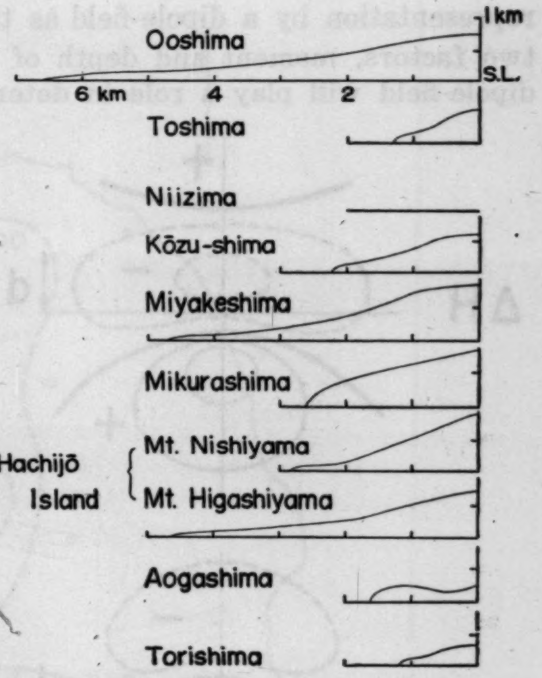

Fig. 3. Topographic profiles of the Seven Izu Islands.

Table II. Effective intensity of magnetization of the volcanoes obtained by various assumptions.

Volcano	Max. Height	Assumption	*J emu/cc*	SiO_2 %	Surveyor
Asama	2532 *m*	One ellipsoid	0.0022	62.1	T. Minakami
Sakurazima	1230	Two ellipsoids	0.0018	62.1	〃
Huzi	3776	Four 〃	0.03	51.4	〃
Ooshima	755	Circular cone	0.037	51.8	T. Rikitake

final aims for us to achieve in volcanology! And the obtained values of the effective intensity of magnetization as shown in Table II are not comparable, strictly speaking, with those of the rock-specimens near the earth-surface because the subterranean structure of the volcanoes is not always the same as their visible parts and moreover, intensity of rock-magnetization takes rather scattered values as will be discussed in a later part of this paper. Therefore, the writer regards the above-mentioned method as one of the possible second approximations, and

7) T. Rikitake, *loc. cit.* (3).

representation by a dipole-field as the first approximation which contains two factors, moment and depth of the dipole. Approximation by the dipole-field will play a role in determining the subterranean structure of volcanoes together with other methods such as gravimetric, seismometric and geological ones though it remains as the first approximation.

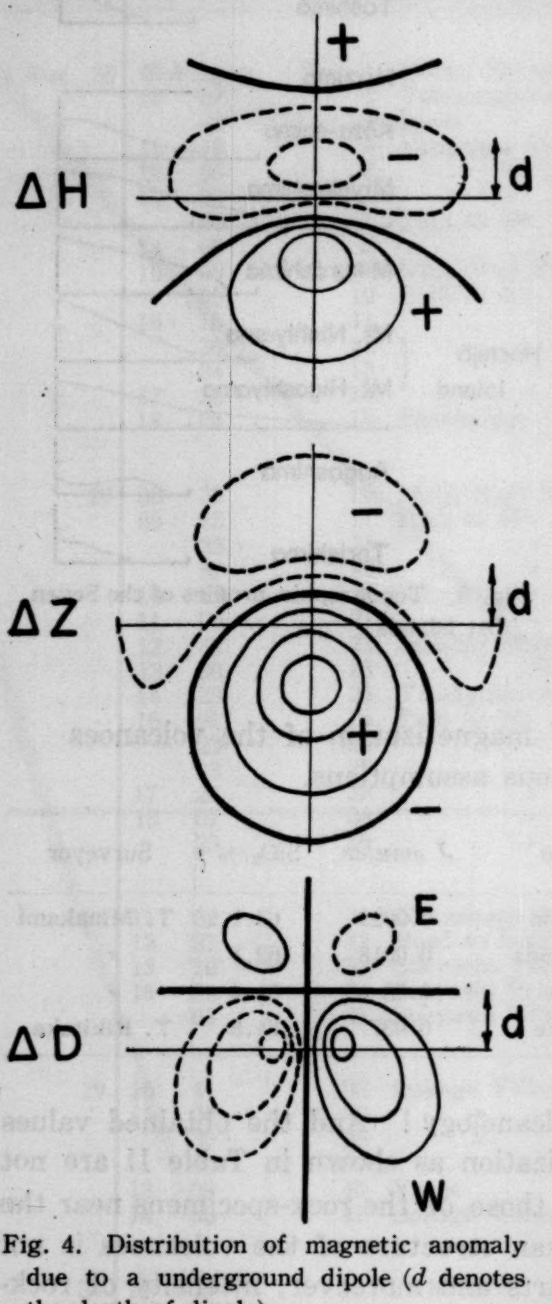

Fig. 4. Distribution of magnetic anomaly due to a underground dipole (*d* denotes the depth of dipole).

Taking the dipole as the origin of the cordinates and its depth as *d*, we get the components of geomagnetic anomaly due to the dipole after some elementary calculations,

$$\Delta H = M_z\left[\frac{1}{r^3} - \frac{3x}{r^5}\left(x + d\frac{Z_0}{H_0}\right)\right], \tag{1}$$

$$\Delta Z = 3M_z\left[\frac{-d}{r^5}\left(x - d\frac{Z_0}{H_0}\right)\frac{H_0}{Z_0} - \frac{1}{3r^3}\right], \tag{2}$$

$$\tan \Delta\delta = 3M_z\frac{y}{r^5}\left(\frac{x}{Z_0} - \frac{d}{H_0}\right), \tag{3}$$

where M and $\Delta\delta$ represent moment of the dipole and anomaly in declination respectively. The distribution of anomaly in the central part of Japan where geomagnetic inclination is approximately 45°, namely $H_0 \doteqdot Z_0$, is shown in Fig. 4. And Fig. 5 represents the distribution of three-components of the geomagnetic field observed on Volcano Mihara. In discussing geomagnetic anomaly, to consider the general mode of distribution is more plausible than the observed values at every point. For convenience, the writer, here, pays attention especially to the zero-line in the

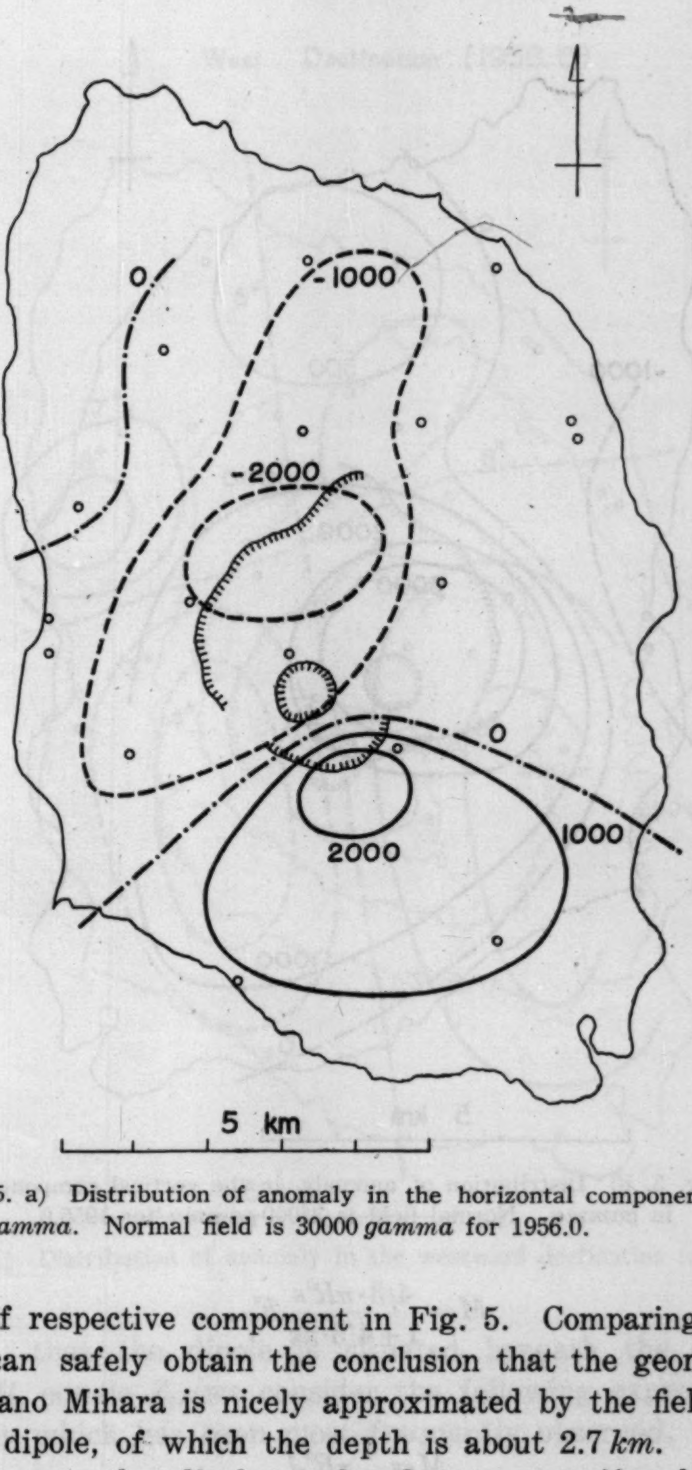

Fig. 5. a) Distribution of anomaly in the horizontal component in *gamma*. Normal field is 30000 *gamma* for 1956.0.

distribution of respective component in Fig. 5. Comparing Fig. 5 with Fig. 4, we can safely obtain the conclusion that the geomagentic anomaly on Volcano Mihara is nicely approximated by the field due to the subterranean dipole, of which the depth is about 2.7 *km*.

If we assume the dipole to be due to a uniformly magnetized sphere, its moment is expressed as follows according to its cause of magnetization whether induction by the earth-field or natural remanent magnetization (N.R.M.),

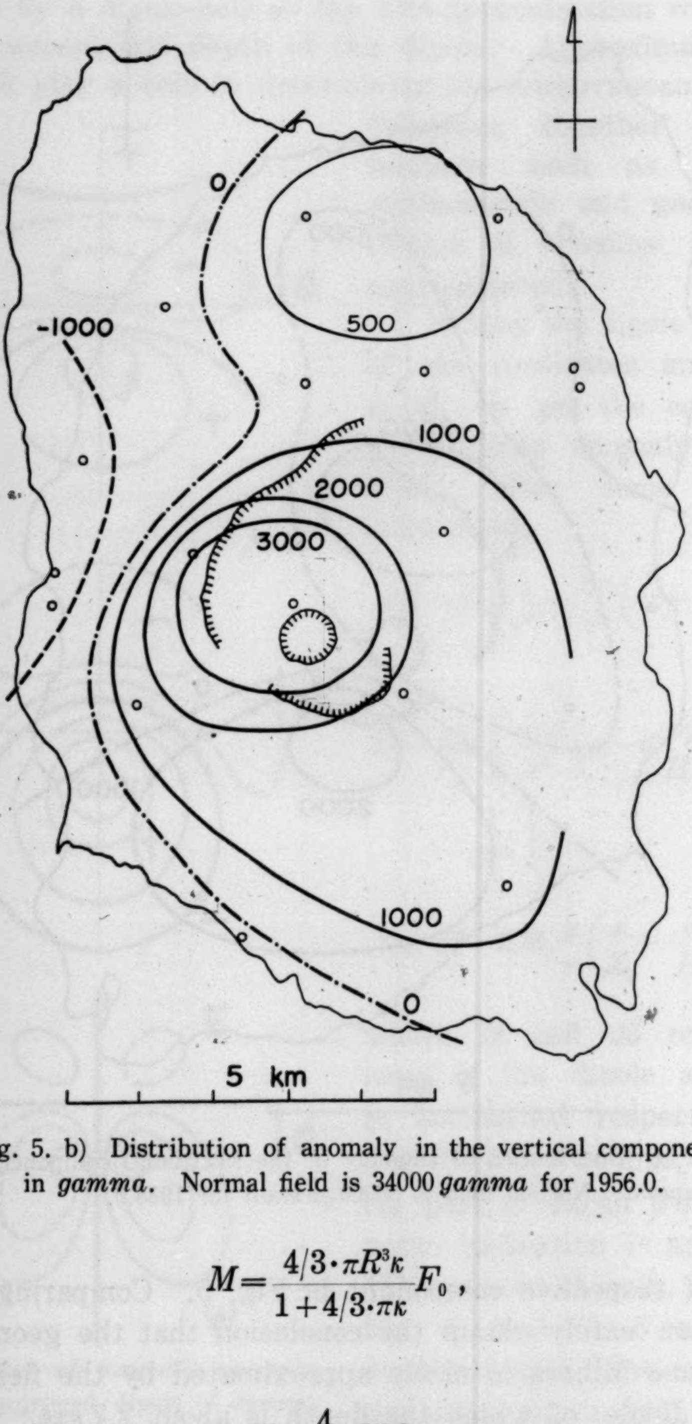

Fig. 5. b) Distribution of anomaly in the vertical component in *gamma*. Normal field is 34000 *gamma* for 1956.0.

$$M=\frac{4/3\cdot\pi R^3\kappa}{1+4/3\cdot\pi\kappa}F_0\ , \qquad (4)$$

or

$$M=\frac{4}{3}\pi R^3 J\ , \qquad (5)$$

where κ, J, R, and F_0 denote susceptibility, intensity of N.R.M., radius of the sphere and total intensity of the earth-field respectively.

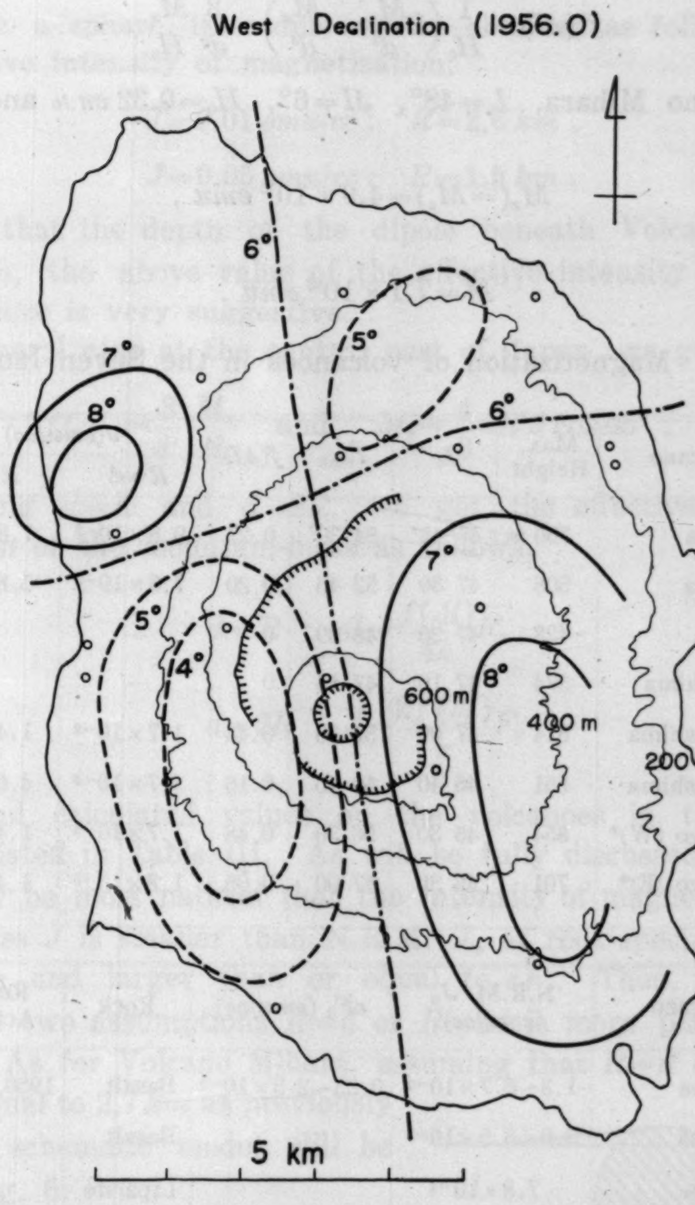

Fig. 5. (c) Distribution of anomaly in the westward declination in *degree*.

Assuming that the dipole is situated beneath the centre of the volcano and H_0 equals Z_0, we consider the following expression relating to dip-anomaly which has been most frequently observed,

$$f(\Delta I)=\frac{\tan(I_0+\Delta I)-\tan I_0}{\tan I_0}=\frac{\Delta Z}{Z_0}-\frac{\Delta H}{H_0}. \qquad (6)$$

At the top of the volcano, in other words, right above the dipole,

$$f(\Delta I)=\frac{1}{H_0}\left(2\frac{M_z}{d^3}+\frac{M_x}{d^3}\right)=\frac{3}{d^3}\frac{M_x}{H_0}. \qquad (7)$$

As for Volcano Mihara, $I_0=48°$, $\Delta I=6°$, $H_0=0.32\,emu$ and $d=2.7\,km$, we get

$$M_x(=M_z)=4.9\times10^{16}\,emu\,, \qquad (8)$$

and

$$M=7.1\times10^{16}\,emu\,. \qquad (8')$$

Table III. Magnetization of volcanoes in the Seven Izu Islands.

Volcano	Max. Height	I_0	I_{max}	$f(\Delta I)$	$J(emu/cc)$ $R=d$	$J(emu/cc)$ $R=2d$
Ooshima	755 *m*	47°45′	54°30′	0.27	9.8×10^{-3}	7.8×10^{-2}
Toshima	508	47 30	52 45	0.20	7.3×10^{-3}	5.8×10^{-2}
Niizima	428	47 20	48 09	0	—	—
Koozushima	574	47 10	47 14	0	—	—
Miyakeshima	814	47 00	57 30	0.46	1.7×10^{-2}	1.4×10^{-1}
Mikurashima	851	46 40	50 45	0.16	5.7×10^{-3}	4.6×10^{-2}
Hachizyo (W)*	854	45 30	56 30	0.48	1.7×10^{-2}	1.4×10^{-1}
Hachizyo (E)*	701	45 30	47 00	0.05	1.8×10^{-3}	1.4×10^{-2}

Volcano	N.R.M. J_n (*emu/cc*)	κF_0 (*emu/cc*)	Rock	Recent Activity
Ooshima	$1.2\sim6.7\times10^{-2}$	$0.35\sim2.5\times10^{-3}$	Basalt	1950, 51, 53
Toshima	$3.0\sim6.5\times10^{-2}$		Basalt	?
Niizima	7.8×10^{-4}		Liparite	886
Koozushima	$2.1\sim3.2\times10^{-4}$		Liparite	838
Miyakeshima	$1.2\sim5.6\times10^{-2}$	$0.43\sim1.5\times10^{-3}$	Basalt	1940
Mikurashima	$1.0\sim4.3\times10^{-3}$		Basalt & Andesite	?
Hachizyo (W)*	$1.4\sim32\times10^{-3}$		〃	1605
Hachizyo (E)*	$1.3\sim70\times10^{-3}$		〃	?

* Rock samples were offered by N. Isshiki.

If we assume the shape of the magnetic material corresponding to the

dipole to be a sphere, its radius will be obtained as follows according to its effective intensity of magnetization,

$$J=0.01\ emu/cc: \quad R=2.6\ km\ ,$$
$$J=0.05\ emu/cc: \quad R=1.5\ km\ .$$

Considering that the depth of the dipole beneath Volcano Mihara is about 2.7 *km*, the above value of the effective intensity of magnetization 0.01 *emu/cc* is very suggestive.

In a general case at the central part of Japan, we get

$$f(\Delta I)=\frac{3}{d^3}\frac{M_x}{H_0} \quad \text{and} \quad M_x=\frac{4}{3}\pi R^3 J\cos 45^\circ\ . \tag{9}$$

And assuming $d=R$ and $d=2R$, we get the effective intensity of magnetization of the mountain-mass as follows,

$$d=R\ : \quad J=\frac{f(\Delta I)}{4\pi}F_0\ ,$$

$$d=2R: \quad J=\frac{2f(\Delta I)}{\pi}F_0\ .$$

Observed and calculated values on the volcanoes in the Seven Izu Islands are listed in Table III. As will be fully discussed in later sections, it may be most natural that the intensity of magnetization of the mountain-mass J is smaller than N.R.M. J_n of rock-specimens near the earth-surface and larger than or equal to κF_0. Thus, we shall learn which of the two assumptions $R=d$ or $R=2d$ is more plausible in our estimation. As for Volcano Mihara, assuming that $R=d$ and both these values are equal to 2.7 *km* as previously obtained, a schematic model will be shown as Fig. 6.

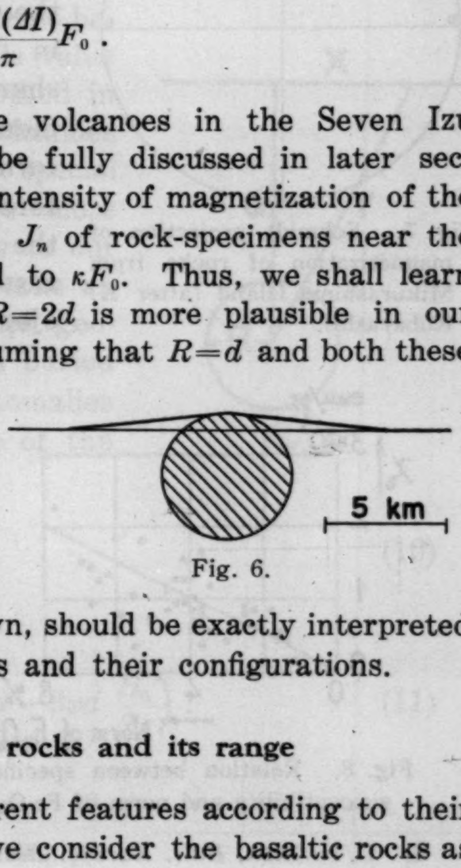

Fig. 6.

Parenthetically the writer may add that the geomagnetic anomalies on the lava-domes or volcanic necks of which the geological structures are known, should be exactly interpreted by the magnetization of the rock-samples and their configurations.

2. Magnetization of igneous rocks and its range

Magnetization of rocks presents different features according to their origin, sedimentary or igneous. Here, we consider the basaltic rocks as

an example of the igneous rocks. Order of magnitude of natural remanent magnetization (N.R.M.) and susceptibility of those rocks are

Table IV. Order of magnitude of intensity of N.R.M. and susceptibility of rocks.

Rock	Intensity of N.R.M. $J_n(emu/gr.)$	Susceptibility $\chi(emu/gr.)$	Induced magnetization by earth-field $\chi F_0(emu/gr.)$	$Q=J_n/\chi F_0$
Sedimentary	10^{-6}	10^{-4}	5×10^{-5}	0.02
Igneous	10^{-2}	10^{-3}	5×10^{-4}	20

shown in Table IV where direction of N.R.M. generally coincides with that of the earth-field as studied by T. Nagata[8)] and Fig. 7 shows, as an example, the direction of N.R.M. of the rocks from Mikurashima Island while order of their intensities are 10^{-4} *emu/gr*. Various kinds of ejecta from a volcano contribute to the magnetization of the volcano as a whole in different ways. Lava-flows have a large share in forming the N.R.M., while fragmentary ejecta and ashes share mainly in forming the induced magnetization. Therefore, it may be very important in discussing the geomagnetic anomaly on the volcano to assume the composition and distribution of ejecta in the mountain-mass.

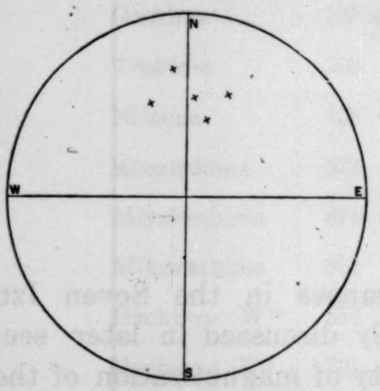

Fig. 7. Schmidt projection of magnetization of rocks from Mikurashima Island (after K. Kobayashi).

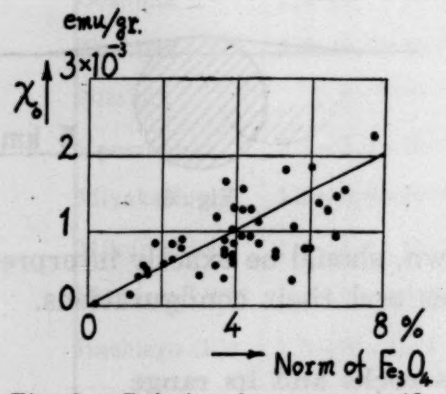

Fig. 8. Relation between specific susceptibility and norm of Fe_3O_4.

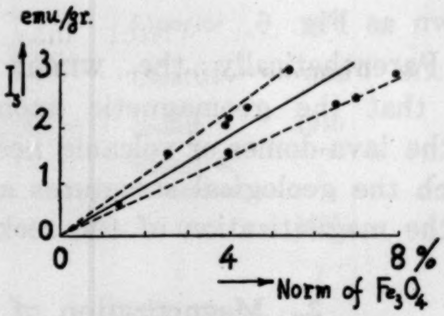

Fig. 9. Relation between saturated magnetization and norm of Fe_3O_4.

8) T. NAGATA, *Bull. Earthq. Res. Inst.*, **19** (1940), 402.

The ranges of distribution of N.R.M. and susceptibility are rather wide as shown in Table III where large values amount to twice or fifty times small ones though numbers of sampling do not always attain a high enough figure. If we assume the uniform magnetization of the mountain-mass, geomagnetic anomaly on the mountain should increase in exact proportion to the assumed intensity of magnetization. In this respect, it seems rather dangerous to attach a very high value to the intensity of magnetization of rocks.

The relation between geomagnetic anomaly on volcanoes and property of rocks composing the volcanoes is easily seen in Table I where basaltic volcanoes present large anomalies and liparitic ones almost none. This may be very natural considering T. Nagata's studies[9] shown in Figs. 8 and 9 which give the relation between magnetic susceptibility and intensity of saturation magnetization and norm of Fe_3O_4 in igneous rocks respectively, while the norm of Fe_3O_4 is inversely proportionate to the silica percentage in general.

As seen from Table IV, the *Q*-factor of igneous rocks is very large compared with sedimentary ones and a contrast between them equals $10^{-2}/5\times10^{-5}=200$. This value suggests the utility of the magnetic method in studying the subterranean structure of volcanoes which are composed of basaltic rocks. In special cases, the geomagnetic method will be more effective than the gravimetric one contrary to our common sense in potential theory. To take an ideal example, the writer will show the geomagnetic and gravity anomalies due to a buried sphere of which the radius is R. Both anomalies at the place r distant from the centre of the sphere are given as follows.

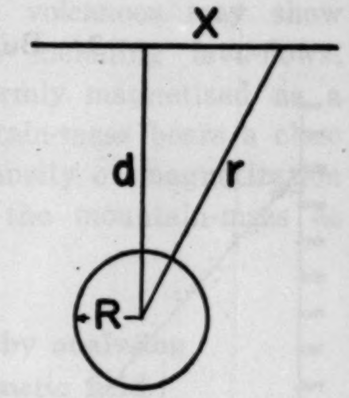

Fig. 10.

$$\Delta g=\frac{4}{3}\pi\cdot R^3k^2\Delta\rho\cdot d/r^3\ , \tag{10}$$

and

$$\Delta Z=\frac{4}{3}\pi\cdot R^3\,\Delta J\left(-x^2+2d^2-3xd\,\frac{H_0}{Z_0}\right). \tag{11}$$

At the place right above the sphere,

9) T. NAGATA, *Rock-magnetism* (1953), 89 and 106.

$$\Delta g = \frac{4}{3}\pi R^3 k^2 \cdot \Delta\rho \cdot 1/d^2 , \qquad (12)$$

and

$$\Delta Z = \frac{4}{3}\pi R^3 \cdot 2 \cdot \Delta J \cdot 1/d^3 . \qquad (13)$$

It may be safely assumed that both kinds of the contrast $\Delta\rho$ and ΔJ amount respectively 1.0 *cgs* and 0.02 *cgs emu* in a certain volcanic region. Then, the anomalies are estimated for the case where $R=1\,km$ and $d=2\,km$ as

$$\Delta g = 14\ mgal \quad \text{and} \quad \Delta Z = 1000\,\gamma .$$

Of these two quantities, geomagnetic anomaly may be more easily detected. In fact, it should be stressed that the abovementioned example is a special case. And here it may be remarked incidentally that geomagnetic anomalies on volcanoes may sometimes change accompanied by their activities as revealed by Japanese geophysicists[10].

3. Bulk-density of the mountain-mass

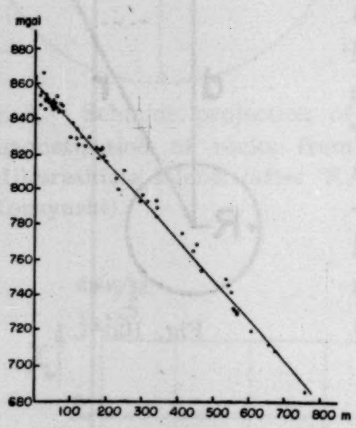

Fig. 11. Relation between observed gravity values and height.

In relation to the subterranean structure of volcanoes, the writer, here, considers the bulk-density of the mountain-mass as a whole regarding a few examples of volcanoes.

a). Volcano Mihara The writer and H. Tajima[11] carried out a gravity-survey on Volcano Mihara by means of a Worden Gravimeter and the relation between observed gravity values and height is shown in Fig. 11. Neglecting the topographical effects and assuming the uniform distribution of density, gravity at the height *h meters* is expressed as

$$g_h = g_0 - 0.3086\,h + 2\pi k^2 \rho h \ (mgal) , \qquad (14)$$

10) T. NAGATA, *Bull. Earthq. Res. Inst.*, **19** (1941), 335.
R. TAKAHASI and K. HIRANO, *Bull. Earthq. Res. Inst.*, **19** (1941), 82 and 373.
Y. KATO, *Proc. Imp. Acad. Japan*, **16** (1940), 440.
T. RIKITAKE and I. YOKOYAMA, *Journ. Geophys. Res.*, **60** (1955), 165.

11) I. YOKOYAMA and H. TAJIMA, *Bull. Earthq. Res. Inst.*, **35** (1957), 23.

where ρ is the effective density of the mountain-mass above the sea-level. By the least square method, the density was determined as 2.08 *gr./cc*. This value is rather smaller than that of the ejected lava.

b) Volcano Asama T. Minakami[12] obtained the mean density of Volcano Asama as 1.88 *gr./cc* from the observations of second derivatives of the gravity potential by a torsion balance. And his additional remarks are as follows: Borings made on the eastern slope of the volcano showed that the layers down to 50 *m* under the surface are alternations of pumice, sand, and ash, their mean bulk density being less than 1.3 *gr./cc*, so that in order to arrive at the mean density of the volcano (1.88) obtained above, it was necessary to assume, owing to increasing weight material, that deeper than 50 *m* from the surface, the density would exceed 1.88 *gr./cc*.

In addition the above examples, T. C. Mendenhall[13] and A. Tanakadate swung the pendulums on the summit of Mt. Huzi and obtained 2.08 *gr./cc* as the mean density of the mountain-mass as early as in 1881.

Taking into consideration that the bluk-density of the rocks composing the lava-flows is about 2.5 *gr./cc*, the effective density of the mountain-mass 2.0 *gr./cc* obtained at the above volcanoes may show that volcanoes are composed of various ejecta including lava-flows, pumices, bombs and ashes which are never uniformly magnetized as a whole. Thus the effective density of the mountain-mass bears a close relation to the determination of the effective intensity of magnetization in the assumption of uniform magnetization of the mountain-mass as ellipsoids or a circular cone.

4. Determination of depth of sources by analysing the vertical component in the geomagnetic field on Volcano Mihara

With the aid of E. H. Vestine and N. Davids' method[14] which has already been applied to the analysis of the local anomalous changes of geomagnetic field on Volcano Mihara during the period from 1951 to 1953 by the present author[15], an estimation of the depth of sources responsible for the local anomalous geomagnetic field on the same volcano will be made.

12) T. MINAKAMI, *Bull. Earthq. Res. Inst.*, **20** (1942), 40.
13) T. C. MENDENHALL, *Memo. Sci. Dep.*, (*Tokyo Daigaku*), **5** (1881).
14) E. H. VESTINE and N. DAVIDS, *Terr. Mag.*, **50** (1945), 1.
15) I. YOKOYAMA, *Bull. Earthq. Res. Inst.*, **32** (1954), 169.

The writer assumes the form of the volcano to be a circular cone and takes into consideration the fact that each observation point is not distributed on the same horizontal plane. Denoting the magnetic potential of the local anomalous field by $\varDelta W$ and using Fourier series and Bessel functions, the solution of Laplace's equation is expressed as

$$\varDelta W=\sum_{k=0}^{K}\sum_{n=0}^{N} e^{kz}[A_{kn}\cos n\phi+B_{kn}\sin n\phi]J_n(kr)\,, \qquad (15')$$

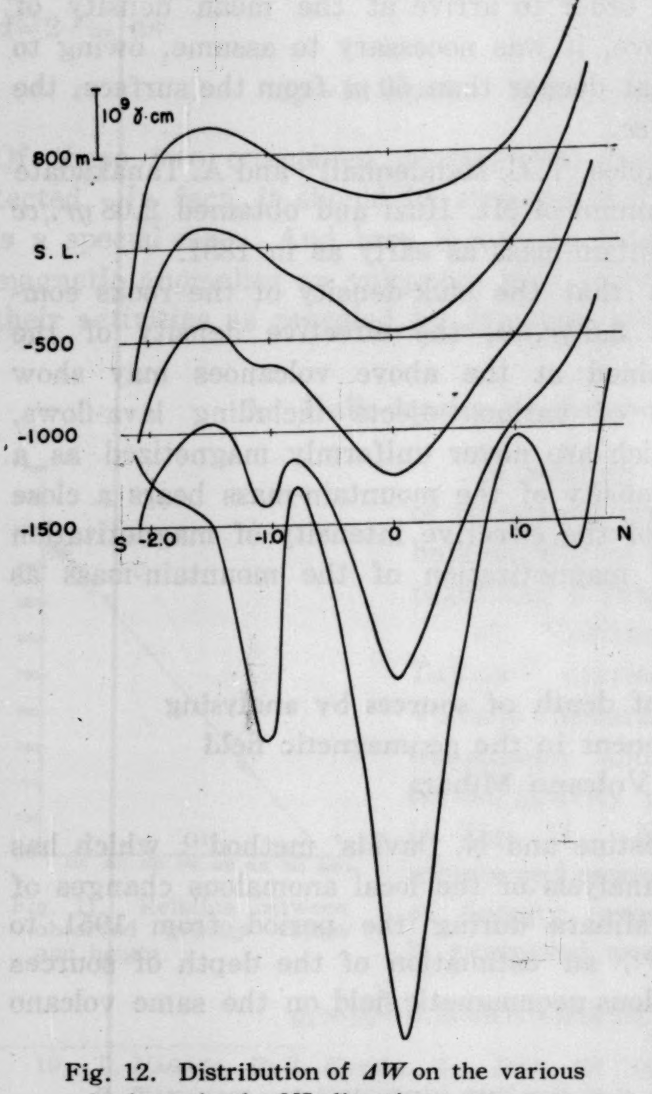

Fig. 12. Distribution of $\varDelta W$ on the various horizons in the NS direction.

where k and n are positive integers, A_{kn} and B_{kn} are constants and $J_n(kr)$ is a Bessel function of the first kind. For convenience' sake, the distribution of the vertical component $\varDelta Z$ is considered here. By differentiating (15), $\varDelta Z$ is obtained as

$$\varDelta Z=-\sum\sum ke^{kz}[A_{kn}\cos n\phi+B_{kn}\sin n\phi]J_n(kr)\,. \qquad (16)$$

Then, a set of six concentric circles is drown on Fig. 5 (b), a map of the $\varDelta Z$ distribution and the Fourier analysis for each circle affords six coefficients.

The constants A_{kn} and B_{kn} in equation (16) are determined by means of the least square method. Using these coefficients, $\varDelta W$ on the various horizons in the NS direction are calculated by eq. (15) and shown in Fig. 12. As may be seen in the figures, the distribution of $\varDelta W$ at a depth less than 1 *km* is fairly convergent, while it seems more divergent as the depth becomes greater. Hence, we may suppose that the sources

are to be found at more than 1.5 *km* depth under the sea-level. It may be possible to consider the position of the abovementioned sources as that of the magnetic dipole.

5. Some knowledge obtained by a gravity survey on Volcano Mihara

The results of the gravity survey on Ooshima Island have already been reported in this Bulletin[16]. The Bouguer anomaly is reproduced

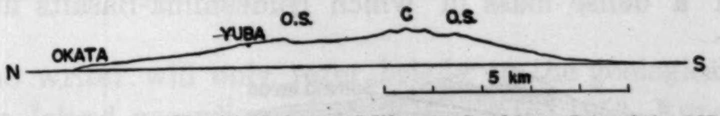

Fig. 14. Topographic profile of Volcano Mihara, Ooshima Island in NS direction.

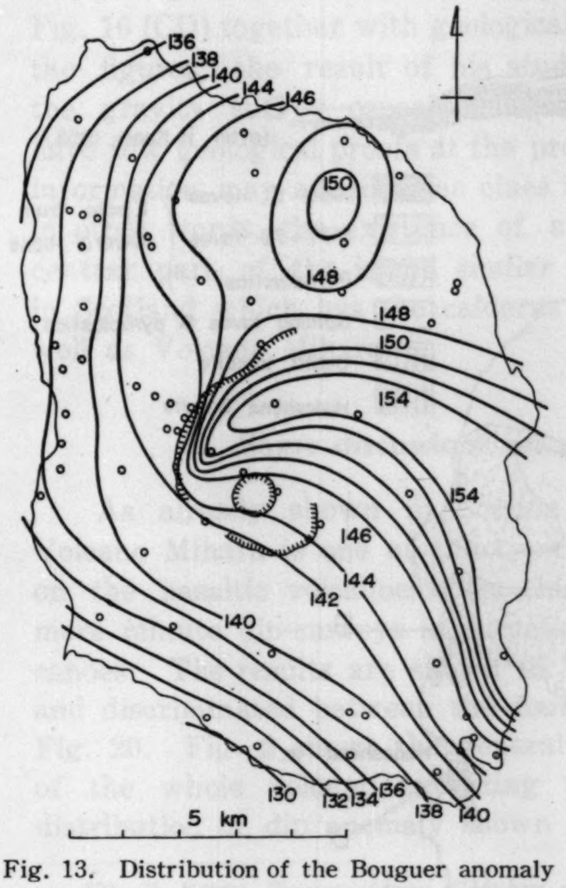

Fig. 13. Distribution of the Bouguer anomaly in *mgal*.

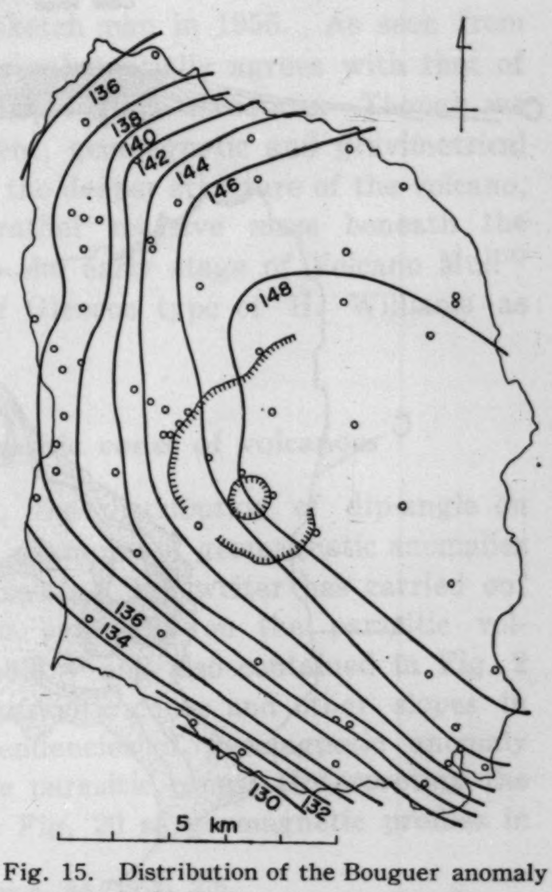

Fig. 15. Distribution of the Bouguer anomaly in *mgal*. (adopting the modified Bouguer corrections).

16) *loc. cit.* (11).

in Fig. 13 which suggests the existence of a subterranean mass of high bulk-density at two parts in the island. One of them, gravity high at the northern part corresponds to the positive anomaly in the geomagnetic vertical component and the anomalous distribution of the horizontal force and declination there. Although we have no visible evidence in geology for the anomaly, the topographical profile of this part covered by the ejecta from Volcano Mihara seems to suggest the existence of an underlying mass which is presumed to be not so large considering the amount of its anomaly. Another high, centered at the central cone and extending the south-east direction, may be taken as indicating the existence of a dense mass of which Hudeshima-Basalts at the eastern

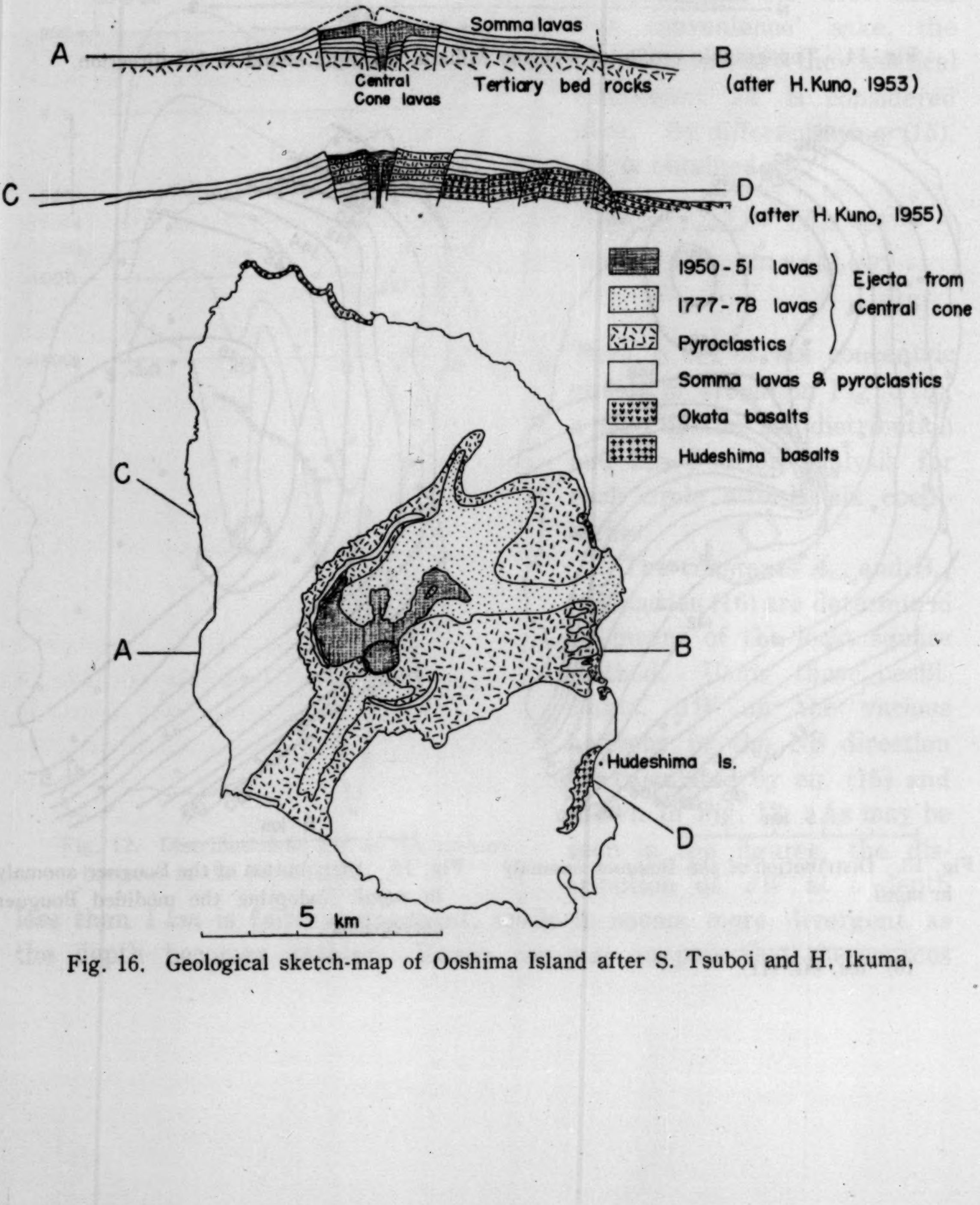

Fig. 16. Geological sketch-map of Ooshima Island after S. Tsuboi and H. Ikuma,

coast of the island may be an outcrop. The fact that the outer somma is in defect in the eastern part of the caldera where the high anomaly prevails, may indicate the existence of dense mass before the caldera subsided. Distribution of the Bouguer anomaly shown in Fig. 9 is obtained by assuming the uniform distribution of bulk-density, that is 2.08 *gr./cc*. As an approximation of higher order, density of rocks at each part of the island was determined by the relation expressed by eq. (14) as discussed in the previous report: 2.40 *gr./cc* for the highly anomalous parts and 2.00 *gr./cc* for the other parts. Using these values of density for the Bouguer correction, the gravity anomaly corresponding to the excess mass under the sea-level was obtained as shown in Fig. 15.

Here, the writer will only refer briefly to the geological perspective over Ooshima Island according to H. Kuno. In 1953 Kuno[17)] obtained the geological section as Fig. 16 (AB) and he revised it as shown in Fig. 16 (CD) together with geological sketch map in 1955. As seen from the figures, the result of his studies substantially agrees with that of the gravity survey especially in the subsurface structure. Though we have few geological proofs at the present, geomagnetic and gravimetrical information may afford some clues to the deeper structure of the volcano, in other words, the existence of a rather massive mass beneath the central part of the island similar to the early stage of Volcano Mull[18)] in Scotland which has the calderas of Glencoe type of H. Williams as well as Volcano Mihara.

6. Some discussions on parasitic cones of volcanoes

As already shown in Section 2, the distribution of dip-angle on Volcano Mihara is one of the typical examples of geomagnetic anomalies on the basaltic volcanoes. On this volcano, the writer has carried out more minute dip-surveys in succession, especially on the parasitic volcanoes. The results are shown in Table V and also contained in Fig. 2 and discriminated between the four parasitic cones and other slopes in Fig. 20. Fig. 2 shows the general tendencies of geomagnetic anomaly of the whole volcano excepting the parasitic cones. Interpreting the distribution of dip anomaly shown in Fig. 20 as geomagnetic profiles in

17) H. KUNO, *Trans. Amer. Geophys. Union*, **34** (1953), 276.

18) J. E. RICHEY, *British Regional Geology, Scotland: The Tertiary Volcanic Districts* (1948), 57 (Fig. 26).

exploration, anomaly due to a parasitic cone does not superpose itself on that due to the other parts of the mountain-mass and the general tendency of anomaly all over the volcano seems to be composed of the above respective anomalies.

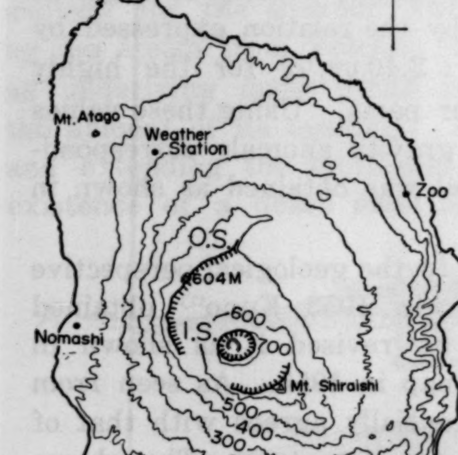

Fig. 19. Topographical map of Ooshima Island.

I.S.: Inner somma.
O.S.: Outer somma.

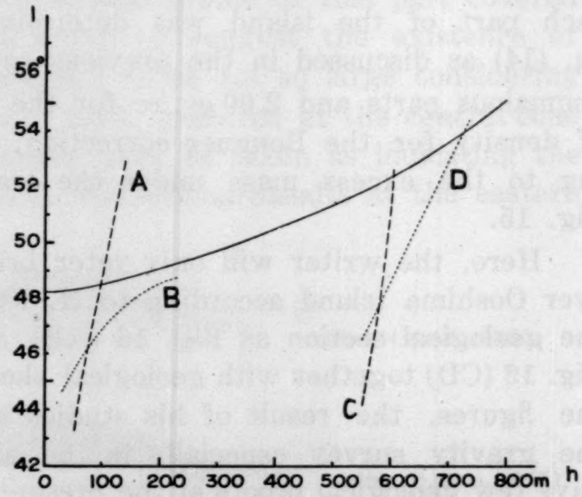

Fig. 20. Dip anomaly on Ooshima Island

A: Parasitic cone Mt. Atago.
B: Parasitic cone Mt. Takenohira.
C: 604 *m* triangulation point on the outer somma.
D: Mt. Shiraishi on the outer somma.

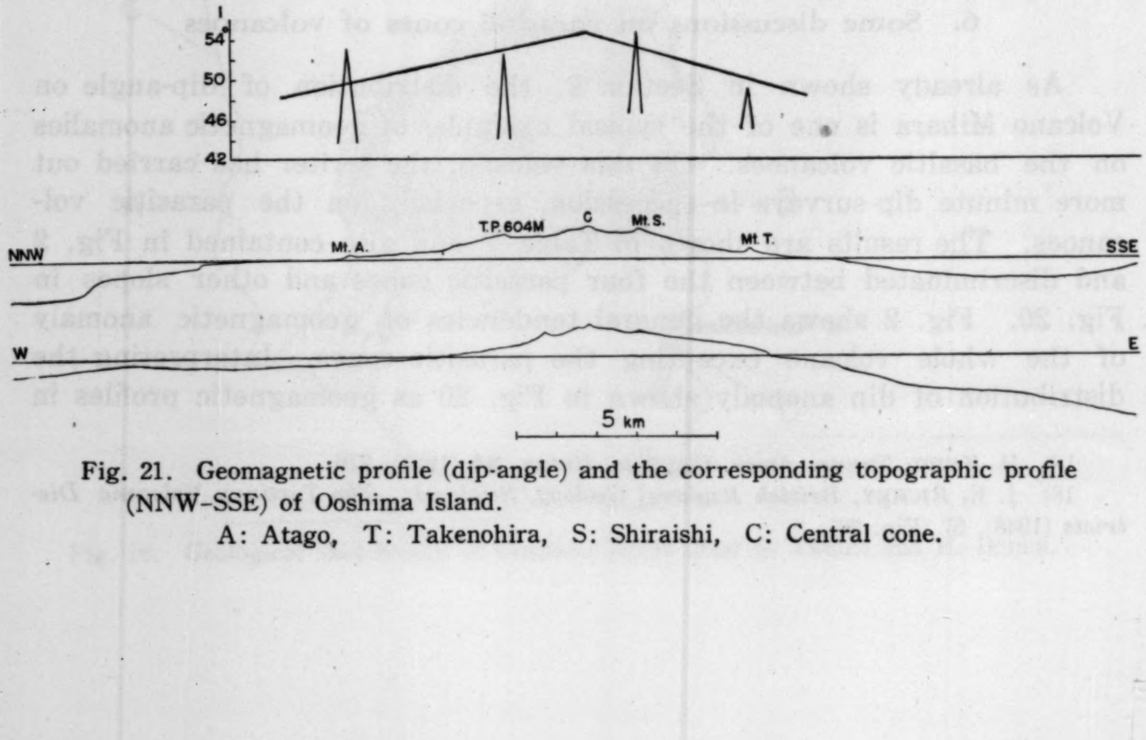

Fig. 21. Geomagnetic profile (dip-angle) and the corresponding topographic profile (NNW–SSE) of Ooshima Island.

A: Atago, T: Takenohira, S: Shiraishi, C: Central cone.

Table V. Observations of dip on the parasitic cones and the outer somma of Volcano Mihara.

a) Mt. Atago.

Time (1955)				Locality	Approximate Altitude	Dip
Apr. 12	15 *h*	49 *m*	No. 1	Southern foot	60 *meters*	44°35′
		57	2	Southern slope	70	46 06
	16	05	3	〃	80	44 51
		13	4	〃	95	47 50
		29	5	Triangulation point		53 12
					135	
		39	6	Summit	135	53 48
		45	7	Western slope	120	54 26
		52	8	〃	105	48 58
	17	01	9	〃	110	50 20
		08	10	Shrine		47 02
					95	
		15	11	Western slope	80	45 30
		23	12	Western foot	60	42 39
		33	13	Cross roads	55	46 54

b) Mt. Takenohira.

Time (1955)				Locality	Approximate Altitude	Dip
Apr. 12	09 *h*	35 *m*	No. 1	Sashikizi Prim. School	30 *meters*	47°14′
		49	2	Shrine	40	47 33
	10	01	3	Southern foot of the hill	60	44 30
		13	4	Southern slope	80	46 23
		26	5	〃	100	45 52
		39	6	Western slope	120	46 13
		53	7	Southern slope	150	46 20
	11	01	8	〃	160	47 02
		11	9	Western slope	200	49 08
		30	10	〃	220	50 26
		39	11	Triangulation point	231	49 51
		55	12	Southern slope	180	50 09
	12	06	13	〃	160	46 48
		14	14	〃	180	50 24
		21	15	〃	170	46 11
		31	16	〃	140	45 56
		48	17	Western foot of the hill	50	44 16
	13	10	18	〃	40	45 09

c) 604 *meters* triangulation point on the outer somma.

Time (1955)			Locality		Approximate Altitude	Dip
Apr. 14	13 *h*	05 *m*	No. 1	Triangulation point	604 *meters*	51°46′
		20	2	Path to Yuba	595	53 04
		28	3	〃	580	51 48
		54	4	Path to Gojinka-chaya	595	51 36
	14	04	5	〃	580	47 19
		40	6	Inner slope of outer somma	550	43 59
		50	7	〃	560	46 56
	15	03	8	〃	575	46 20
		18	9	〃	590	47 00
		48	10	〃	600	51 46
	16	09	11	Road to Yuba	575	49 24

d) Mt. Shiraishi on the outer somma.

Time (1955)			Locality		Approximate Altitude	Dip
Sept. 16	11 *h*	12 *m*	No. 1	Western foot	560 *meters*	48°01′
		26	2	Slope of the outer somma	640	48 17
		38	3	Summit of the outer somma	680	53 12
		50	4	〃	690	51 16
	12	39	5	〃	720	53 54
		54	6	Triangulation point	734	53 28
	13	12	7	Eastern slope	720	54 56
		24	8	〃	680	52 10
		34	9	〃	670	52 20
1951 Mar. 30	13	18	30	Eastern slope	640	52 48
1953 Aug. 2	17	44	42	Southern foot	620	47 30

Taking into consideration that the harmonic components of the lower orders of geomagnetic anomaly expressed in the Fourier series are generally due to the deeper origin, the geomagnetic anomaly of the general tendency of the whole volcano shown in Fig. 2 is attributable to the deeper part of the volcano and the anomaly on a parasitic cone is to be interpreted by its own magnetization or rather shallow sources.

Here, the writer will consider the effective bulk-density of the parasitic cones of Volcano Mihara by the same method as used in Section 3. Assuming the vertical gradient of gravity to be constantly 0.3086 *mgal/m*, the relation between the gravity values and the heights is given by

$$g_h = g_0 - 0.3086\,h + 2\pi k^2 \rho h - \delta_t\,, \tag{17}$$

where ρ and δ_t denote the effective density of the mountain-mass and topographical correction respectively.

On the two parasitic cones of Volcano Mihara, Mts. Atago and Takenohira, the writer observed the gravity values which are shown in Table VI. By eq. (17), the effective density are determined as 0.79 and

Table VI. Gravity values on the parasitic cones of Volcano Mihara.

		Height (*m*)	Observed Gravity (*mgal*)	Topographical Correction (*mgal*)	Bouguer Anomaly (*mgal*)
Mt. Atago	No. 12 Eastern foot	65.1	847.0	3.4	138.8
	〃 13 Top	119.5	829.4	4.7	134.5
	〃 14 Western foot	38.7	852.6	3.5	138.5
Mt. Takenohira	No. 28 Eastern foot	128.0	826.6	3.7	139.3
	〃 29 Top	231.9	796.2	3.5	131.7

0.35 *gr./cc* respectively. Though these values may contain some errors due to the above assumption, the parasitic cones are composed of rather coarse material whether this is the cause or effect of eruptions. This is the same as the region around the central cone of the volcano as mentioned in Section 5.

Next, we consider the topographical effect on geomagnetic anomaly by examples of Volcano Mihara as a whole and a parasitic cone Mt. Atago. According to T. Rikitake[19], dip-anomaly depends on intensity of magnetization J and a topographical constant G as shown by following relation,

19) T. RIKITAKE, *loc. cit.* (3).

$$f(\Delta I)=\{\tan(I_0+\Delta I)-\tan I_0\}/\tan I_0=\Delta Z/Z_0-\Delta H/H_0$$
$$=\pi JG(2\sin\theta/Z_0+\cos\theta/H_0)\,, \qquad (18)$$

where I_0 and θ denote respectively the normal value of dip and the inclination of direction of magnetization. If we fix our eyes on the centre of the top plane of a uniformly magnetized circular cone, G is given by Rikitake as follows.

$$G=\frac{m}{(m^3+1)^{3/2}}\log\frac{\alpha+m^2+1+\sqrt{m^2+1}\sqrt{(1+\alpha)^2+m^2}}{\alpha+\sqrt{m^2+1}\,\alpha}$$
$$+\frac{m}{m^2+1}\left\{\frac{m^2-1-\alpha}{\sqrt{(1+\alpha)^2+m^2}}+1\right\}, \qquad (19)$$

where

$$m=\tan\lambda\,, \qquad \alpha=c_0m/h\,,$$

and where λ, c_0 and h denote the slope of the cone, the radius of the top plane and the height of the circular cone. Using this relation, the effective value of J is obtained by knowing dip-anomaly on the top of the mountain and the topographical constant G.

Volcano Mihara as a whole:

$$I_0=\theta=48^\circ\,,\quad \Delta I=6^\circ\,,\quad \lambda=9^\circ\,,\quad c_0=500\,m\,,\quad h=700\,m \text{ and } G=0.35$$

Thus we get $J=0.033\,emu/cc$.

Mt. Atago:

$$I_0=\theta=48^\circ\,,\quad \Delta I=5^\circ\,,\quad \lambda=25^\circ\,,\quad c_0=15\,m\,,\quad h=86\,m \text{ and } G=1.16$$

Thus we get $J=0.008\,emu/cc$. As for Mt. Takenohira, the conditions are almost the same to Mt. Atago. From the above results, we may deduce that the geomagnetic anomaly on the steep mountain is interpreted even by the weak magnetization while the anomaly on the gently-sloping mountain requires the strong and uniform magnetization due to the N.R.M. which is rather unplausible as fully discussed in Section 1. In fact, the magnetizations of rock-samples from Mt. Atago and Mt. Takenohira are obtained as 1×10^{-3} and $3\times10^{-3}\,emu/gr$. respectively. Namely, the geomagnetic anomaly on Mt. Atago may be due to the magnetization of the mountain-mass mainly by induction. This agrees with the fact that the effective bulk-density of the parasitic cones proved rather small.

7. Geomagnetic anomaly around the craters of volcanoes

T. Fukutomi[20] observed the anomalous distribution of the geomagnetic declination around the crater of Volcano Asama. And T. Nagata[21] observed a similar phenomenon around the crater of Volcano Mihara and concluded that the anomaly can be interpreted as magnetic anomaly, largely due to the uniform magnetization of the central cone with its intensity of 0.0058 *emu/cc* in the direction of geomagnetic force. This magnetization is too large if the rock composing the central cone has solely induced magnetization by the present geomagnetic field, while this is too small if the rock has the natural remanent magnetization observed as $1.6\times10^{-2}\sim3.6\times10^{-2}$ *emu/cc*. Thus he concluded that the central cone of Volcano Mihara is formed not only of continuous ropy lava, but also of bombs, lapilli, ashes and other pyroclastic materials, so that by assuming that lava sheet 6 or 7 *m* thick with natural remanent magnetization $J_n = 0.025$ *emu/gr*. and specific susceptibility $\chi = 6.5\times10^{-4}$ *emu/cc* covers the body of the central cone, composed of pyroclastic ejecta, the magnetic susceptibility of which is almost the same as that of lava, but without any remanent magnetization in the sense of average character of the whole body.

Similarly Nagata presumed that the central cone of Volcano Asama is composed of 40% lava with a magnetization of $\rho(J_n+\chi F_0)$ and 60% pyroclastic ejecta with only induced magnetization $\rho\chi F_0$ where J_n and χ were assumed to be the mean of their observed values. The abovementioned discussions show that the mountain mass of the volcanoes is not always magnetized uniformly simply by N.R.M.

T. Nagata[22] made the geomagnetic measurements and torsion balance survey at eight stations on Ooshima Island in 1938 concerning the magnetization of the subterranean rocks. Assuming that the observed geomagnetic anomaly is due to uniform magnetization of the excess mass that is the cause of the observed anomaly in the second derivatives of the gravity field, he concluded that the subterranean rocks under the earth's surface of Ooshima Island ought to have fairly intense remanent magnetization which is equal to about 0.05 *emu/cc*.

20) T. FUKUTOMI, *Zisin*, **2** (1930), 641.
21) T. NAGATA, *Bull. Earthq. Res. Inst.*, **16** (1938), 288.
22) T. NAGATA. *Bull. Earthq. Res. Inst.*, **17** (1939), 93.

8. Some information obtained by the aeromagnetic surveys over the volcanoes in Alaska

It is very desirable to measure the geomagnetic field at a certain altitude from the earth's surface in order to lessen the topographical effects. In U.S.A. total-intensity aeromagnetic surveys have been carried out at several districts where volcanoes are found. The results in those surveys give some information concerning the subterranean structure of volcanoes, though each volcano may have its own structure. The profile over Mt. Adagdak in the aeromagnetic survey of Adak, Alaska by F. Keller, J. L. Meuschke and L. R. Alldredge[23] is reproduced in Fig. 24, where the computed values of the magnetic field by using the topographic profile and a susceptibility contrast of 0.005 *emu/cc*, are indicated by the small circles plotted with the profiles. The computation gives an approximate fit with the observed profile while the value of 0.005 *emu/cc* is a rather large figure for the susceptibility of a basaltic mass with reference to T. Nagata[24]'s study.

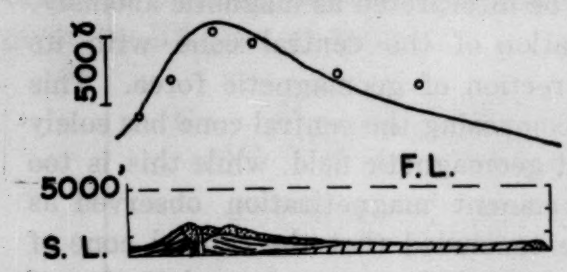

Fig. 24. Magnetic anomaly on Mt. Adagdak, Aleutian. F.L. denotes the fleight level (after F. Keller, J.L. Meuschke and L.R. Alldrege.)

An aeromagnetic map of part of northeastern Umnak, Alaska obtained by the abovementioned authors is also reproduced in Fig. 25 where the flight level is 2000 *m* above sea level. As seen in the

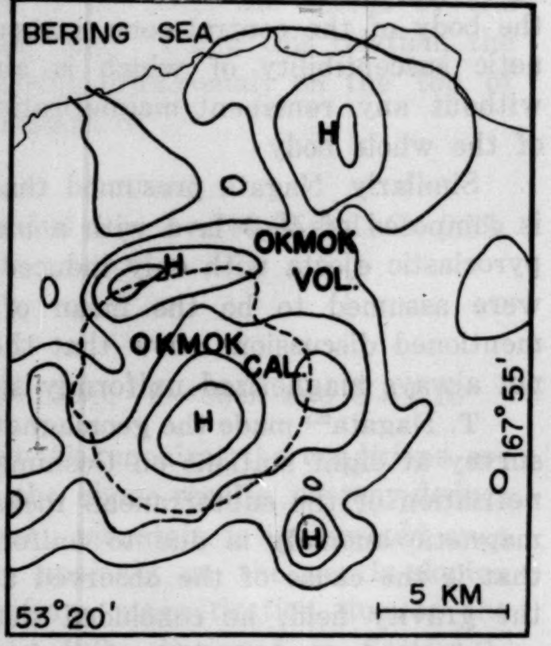

Fig. 25. Aeromagnetic map of part of northeastern Umnak, Alaska. Contour-line interval is 250γ (after F. Keller, J.L. Meuschke and L.R. Alldrege.)

23) F. KELLER, J. L. MEUSCHKE and L. R. ALLDREDGE, *Trans. Amer. Geophys. Union*, **35** (1954), 558.
24) T. NAGATA, *loc. cit.* (9), 101.

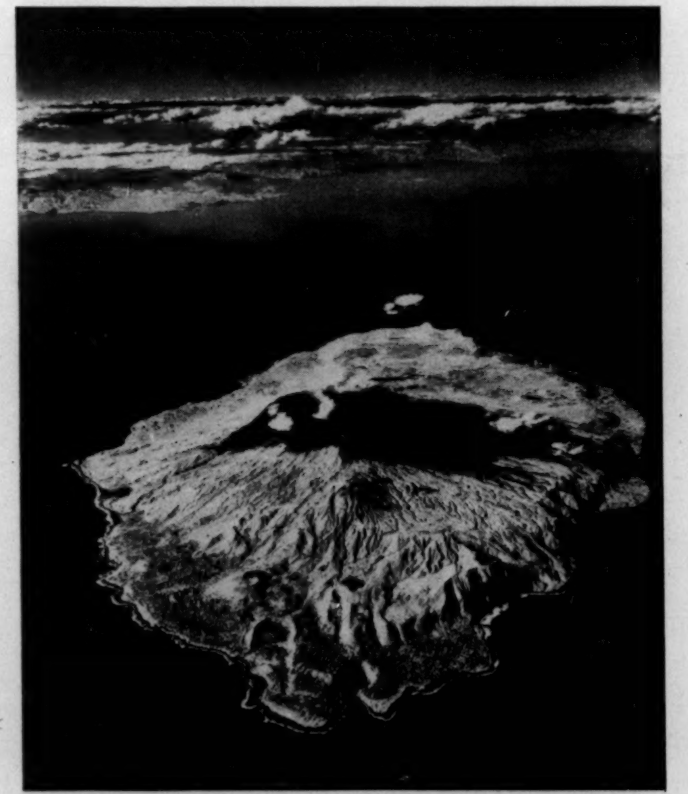

Fig. 17. Aerial view of Ooshima Island from south.
Photo. Asahi

Fig. 22. Parasitic cone Mt. Atago.

Fig. 23. Parasitic cone Mt. Takenohira.

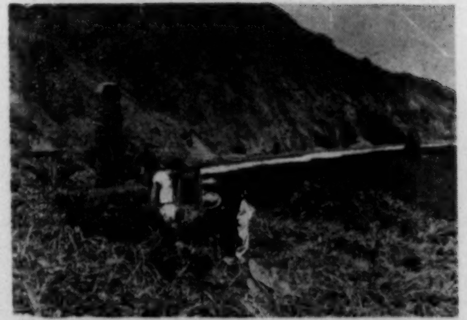

Fig. 18. Gravity survey near Hudeshima Island.

(震研彙報 第三十五号 図版 横山)

figure, the caldera rim is outlined approximately by the pattern of magnetic contours. There is no magnetic evidence, however, of any of the nine cones, but there is a large anomaly associated with the central part of the caldera. The writer is inclined to think that this is caused by a contrast of magnetization (N.R.M.) rather than by that of susceptibility of the underlying rocks because the latter contrast is not so large.

By these two examples of the aeromagnetic survey it may be said that geomagnetic anomaly related to the topographic configuration of the volcano on a large scale is due to a susceptibility contrast, and a large anomaly deviated from the profile is due to a magnetization (N.R.M.) contrast of the underlying rocks. But geomagnetic anomaly on the massive rocks which were essentially lava-flows such as lava-domes or volcanic necks is attributable to N.R.M. and associated with its topography.

Conclusion

In this paper the writer tried to figure the subterranean structure of the volcano, as an example, Volcano Mihara mainly by means of the geomagnetic methods and discussed the related phenomena to get positive proofs of the structure. As for Volcano Mihara, in fact, we have many problems to solve and many phenomena to observe in addition to the items discussed in this report but the writer made bold to figure some of the plausible subterranean structure of the volcano presumed by the existing data. Though the geomagnetic method by itself may be regarded as approximate, it will give some clues for interpreting the structure of volcanoes together with the gravimetric, seismometric and geological methods.

In concluding, the writer wishes to express his hearty thanks to Dr. T. Rikitake who advised him throughout the course of this study. His sincere thanks are also due to Prof. T. Nagata and Prof. T. Minakami whose valuable work he often referred to in this paper.

---

17. 火山地域における地磁気異常と地下構造

地震研究所 横 山 泉

日本の諸火山の帯磁に関する調査は枚挙に遑がない程，広く行われてきた．そしてこれに対する解釈も 2, 3 出されている．今や，この方法の火山学における有用性を吟味反省すべき時であると考え，若干の考察を試みた．如何なる方法と雖も，単独ではその効力を充分に発揮できないことは勿論である．地磁気異常の研究も他の方法と関連参照することにより，充分有効であると結論する．

figure, the caldera rim is outlined approximately by the pattern of magnetic contours. There is no magnetic evidence, however, of any of the nine cones, but there is a large anomaly associated with the central part of the caldera. The writer is inclined to think that this is caused by a contrast of magnetization (N.R.M.) rather than by that of susceptibility of the underlying rocks because the latter contrast is not so large.

By these two examples of the aeromagnetic survey it may be said that geomagnetic anomaly related to the topographic configuration of the volcano on a large scale is due to a susceptibility contrast, and a large anomaly deviated from the profile is due to a magnetization (N.R.M.) contrast of the underlying rocks. But geomagnetic anomaly on the massive rocks which were essentially lava flows such as lava-domes or volcanic necks is attributable to N.R.M. and associated with its topography.

Conclusion

In this paper the writer tried to figure the subterranean structure of the volcano, as an example, Volcano Mihara mainly by means of the geomagnetic methods and discussed the related phenomena to get positive proofs of the structure. As for Volcano Mihara, in fact, we have many problems to solve and many phenomena to observe in addition to the items discussed in this report but the writer made bold to figure some of the plausible subterranean structure of the volcano presumed by the existing data. Though the geomagnetic method by itself may be regarded as approximate, it will give some clues for interpreting the structure of volcanoes together with the gravimetric, seismometric and geological methods.

In concluding, the writer wishes to express his hearty thanks to Dr. T. Rikitake who advised him throughout the course of this study. His sincere thanks are also due to Prof. T. Nagata and Prof. T. Minakami whose valuable work he often referred to in this paper.

17. 火山地域に於ける地磁気異常と地下構造

地震研究所 横 山 泉

[illegible]

18. *Geology of Imaichi District with Special Reference to the Earthquake of Dec. 26, 1949 (III).*

By Ryôhei MORIMOTO, Joyo OSSAKA and Tomoko FUKUDA,

Earthquake Research Institute.

(Read Jan. 22 and Mar. 26, 1957.—Received Mar. 30, 1957.)

IV. Mineralogy of the clayey beds related to the changes of the surface

In the foregoing chapters[13),14)], were described the geology of the meizoseismic area and the changes of the surface mostly brought about by the earthquake which severely struck the town of Imaichi and its environs in Tochigi Prefecture about 100 *km* north of Tokyo on December 26, 1949. Many earth falls and landslips took place mainly on the area covered with Pleistocene clayey beds of volcanic origin. This chapter includes some results of the detailed mineralogical and chemical investigation of these clayey beds especially of the white greasy clay intercalated in "Kwantô Ash Formation or Kwantô Loam", which played an important *rôle* in breaking about the landslips.

The Pleistocene clayey beds in the meizoseismic area are enumerated as humus surface soil (O), yellow pumice bed or Kanuma soil bed (A)[15)], reddish brown pumice bed or Imaichi soil bed (B), upper Loam (C), white clay bed (D), and lower Loam (E), successively from the surface. Their geological relations in this district were schematically represented in Fig. 10 previously[16)]. Localities where each tested specimen was collected are designated as 100 (Shimo-kojiro), 101 (Azuma-cho, Imaichi town Fig. 17), 102 (Akama, Imaichi town Figs. 25, 26), 103 (Ushiro-yama Fig. 13), 104 (Yama-shita), 105 (Myôjin Fig. 28), 106

13) R. MORIMOTO, "Geology of Imaichi District with special reference to the earthquake of Dec. 26, 1949 (I)", *Bull. Earthq. Res. Inst.*, **28** (1950), 379–386.

14) R. MORIMOTO, "Ditto (II)", *Bull. Earthq. Res. Inst.*, **29** (1951), 349–358.

15) Recently Mr. Jun AKUTSU of Utsunomiya University investigated the distribution of these pumice beds in detail in relation to river terrace. The yellow pumice bed corresponds to his "Shichihon-zakura Yellow Pumice Bed". (J. AKUTSU, "The Kanto Ash Formation and the river terrace in the environs of Utsunomiya City, Tochigi Prefecture", *Bull. Utsunomiya Univ., Faculty of Liberal Arts*, No. 4 (1955), (ii), 33–46 (in Japanese).)

16) R. MORIMOTO, *op. cit.* 14), p. 354.

(Itabashi Figs. 12, 27), and 107 (Murose) on the following map (Fig. 16. Cf. Figs. 25, 27 and 28.).

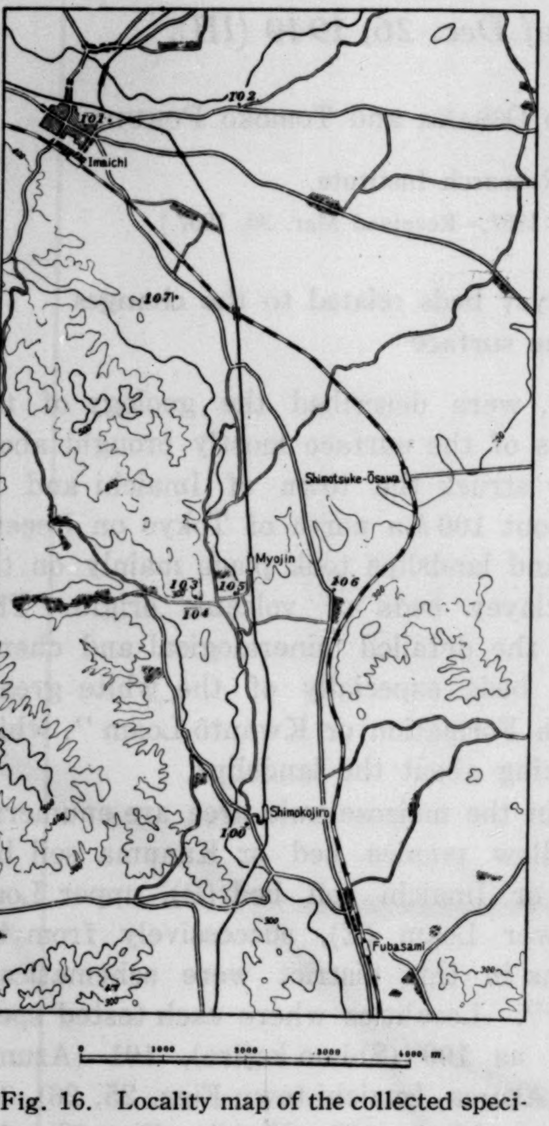

Fig. 16. Locality map of the collected specimens.

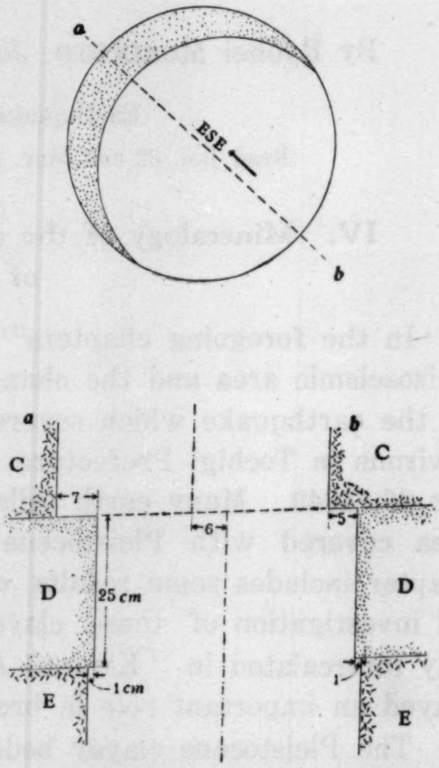

Fig. 17. Displacement of the stratum observed at the water well, Kashiwagi "Tofu" Shop, 1147, Azuma-cho, Imaichi town, Tochigi Pref..

(*1*) *Petrographic features of each clayey bed:*

These clayey beds are quite distinctive from each other in colour and in field occurrence (Fig. 29).

The black loose humus surface soil (O) is mainly composed of volcanic glass stained with dark organic matter in which minute patches of altered plagioclase, chert, and of pumice, and the broken crystals of hypersthene, augite, and plagioclase are found under the microscope.

The loose yellow pumice bed (A), 20–40 *cm* in thickness, consists of

yellow pumice grains commonly of 5–10 *mm* in diameter. Each pumice grain remains its original porous rhyolitic structure of the clean volcanic glass (Fig. 30-A), which has partly been devitrified into clay mineral. Flakes of plagioclase, hypersthene, augite, iron ore, quartz, etc., are contained.

The reddish brown pumice bed (B), 0.5–1.5 *m* in thickness, is composed of pumice grains with comparatively uniform size of 2 *cm* or more in their diameters. Lithic fragments of 3–10 *mm* in size are often found. Each pumice grain shows a uniform fluidal structure with equigranular cavities (Fig. 30-B). Under the microscope a small amount of lithic or crystal fragments such as quartz-porphyry, aggregate of pyroxene-plagioclase, hypersthene, augite, iron ore, plagioclase, etc., are observed in the vitric groundmass stained into yellowish brown. Most of the plagioclase phenocrysts are decomposed into dirty matter. An electron micrograph of the pumice collected from the cliff of Myojin (105-B, Fig. 28) indicates clearly many particles 0.03–0.05μ in their diameters (Fig. 31 above)[17], which may be identified as allophane, results of the following X-ray and differential thermal analyses being considered. Both pumice beds are said to have been derived from the adjacent Nikko volcanoes northwest of the present meizoseismic area[18].

The upper Loam (C), 2–4 *m* in thickness, as well as the lower Loam (E), 2–5 *m* or more in thickness, forms the main portion of the Pleistocene beds in this area. The former is often intercalated by pumice beds and laminae of scoriae and lappili, and the latter by normal sediments. They belong to the so-called "Kwantô Ash Formation or Kwantô Loam" extensively distributed on the Kwantô plain and its surrounding mountainlands. The two beds (C and E) are mainly composed of the vitric ash partly decomposed into clay and stained with limonitic substance. Subordinate amount of lithic or crystal ash are contained. Minute fragments of the basal rocks such as chert, quartz-porphyry, liparite or silicified slate, etc., are locally recognizable. Plagioclase, hypersthene, augite, iron ore, hornblende, and quartz are extensively found in small amount under the microscope. These fragments are commonly of 0.1–0.5 *mm* in diameter. Particles of the partly devitrified volcanic glass are arranged in equigranular mosaic aggregates in

17) The electron micrographs of the reddish brown pumice and of the white clay are kindly prepared for the present writers by Dr. Hiroshi TAKAHASHI of the Department of Chemistry, Faculty of Science, University of Tokyo, to whom the writers' sincere thanks are due.

18) J. AKUTSU, *ibid.*, 44.

thin slices (Figs. 30-C and 30-E).

The bed of white greasy clay along which the upper Loam displaced several centimetres eastwards[19] at the time of the earthquake (Fig. 17) still remains its original pumice structure though the alteration into clay is more advanced in it than in the above-mentioned pumice beds (Fig. 30-A). Each pumice grain, 2–5 *mm* in dia., with fluidal texture, contains plagioclase phenocrysts of 0.5–1 *mm* in length, most of which have been replaced by some apparently amorphous clay mineral. Hypersthene, hornblende, and iron ore are found as scanty mafic porphyritic constituents of 0.5–1 *mm* in their diameters. Lithic fragments of the basal rocks are also included in the bed among its pumice grains. The electron micrograph of the white clay indicates the particles of 0.1–0.2μ in dia. with radial spines around them[20]. These spinose particles identified as hydrated halloysite owing to analyses of the following X-ray and DTA data have been reported by T. Sudo as "chestnut shell-like particles"[21] (Fig. 31 below).

(2) *Results of the X-ray analyses:*

Each collected specimen was sifted through the sieve of 115 mesh after being let under room condition for several weeks. Fine powders thus prepared were used to be tested in the following procedures. The X-ray powder pattern was taken with filtered Cr-radiation and a camera with radius of 27.8 *mm* on each specimen (Table Ia–b). Powder photographs of the pumice or ash from A-bed and B-bed do not show any clear diffraction lines except weak lines of felspars mixtured in the prepared fine powders of Kanuma and Imaichi soils. On the cherts of the geiger counter X-ray diffractometer, however, a broad band of peaks (A in Fig. 18) was recognized at 3.4–3.5Å, which may be a weak diffraction pattern of the allophane. Diffraction patterns of hydrated halloysite are found on the powder photographs of the clay from C-, D-, and E-beds: When the Cu-anticathode is used, diffraction line at 10.2–10.3Å is weak and broad on the photographs of C and E, and strong and sharp on that of D. Diffraction patterns of quartz are always found in them. (Table Ia–b, II).

19) T. HONDA, "Land slip in the Imaichi District revealed from the breaks in the well tube", *Bull. Earthq. Res. Inst.*, **28** (1950), 449–456.

20) See foot note 17).

21) T. SUDO and H. TAKAHASHI, "Shapes of halloysite particles in Japanese clays", *Proc. 4th National Conference on Clay and Clay Minerals, National Research Council U.S.A.*, Publication No. 456 (1956), 67–79, Mineralogical Journal, **1** (1953), 66–68.

Table Ia. Lines of the X-ray powder photographs of the clays from each bed at Akama, Imaichi*.

	102–A		102–B		102–C		102–Du		102–Dl		102–E	
	d	I	d	I	d	I	d	I	d	I	d	I
H					10.0	6	10.0	10	10.2	10	10.4	4
	4.82	5b	4.79	6b								
H.Q.			4.28	10b	4.32	7	4.41	7	4.32	7	4.28	4b
	4.03	10b										
					3.66	3	3.75	1	3.71	1	3.69	1
A			3.52	4b								
A	3.45	5b										
Q					3.35	10b	3.36	4	3.35	2	3.31	10
											2.963	1
H					2.520	3b	2.548	3b	2.534	2b	2.513	2b
	2.250	1	2.228	1								
					1.810	2					1.821	1
					1.665	2b	1.671	1	1.674	1	1.665	1
					1.537	2						
					1.476	2	1.483	3	1.487	2	1.502	1
					1.376	3					1.376	3

* H: hydrated halloysite, A: allophane, Q: quartz
Cr-radiation, 30 KVP, 10 *mA*, 30–60 *minutes*, Radius of the camera being 27.8 *mm*.

Table Ib. Lines of the X-ray powder photographs of the white clays from Azuma-cho, Imaichi (101–D), Itabashi, Ochiai village (106–D), and from Murose, Imaichi (107–D)*.

	101–D		106–D		107–Dw		107–Db	
	d	I	d	I	d	I	d	I
H	9.9	10	10.1	10	10.2	10	10.2	10
	4.98	2	4.90	2	4.88	2	4.93	1
H	4.40	5	4.47	7	4.43	5	4.43	4
					4.12	2	4.13	2
			3.72	2	3.73	3	3.72	2
Q	3.34	1b	3.43	4	3.41	8	3.40	2b
H	2.58	1	2.59	3b	2.57	2b	2.58	2
					1.830	1	1.853	1
			1.698	2b			1.699	1
					1.543	2	1.547	2
			1.482	1	1.480	1	1.482	1
					1.376	2	1.370	2

* Cr-radiation, 30 KVP, 10 *mA*, 30–60 *min.*, Radius of the camera being 27.8 *mm*.

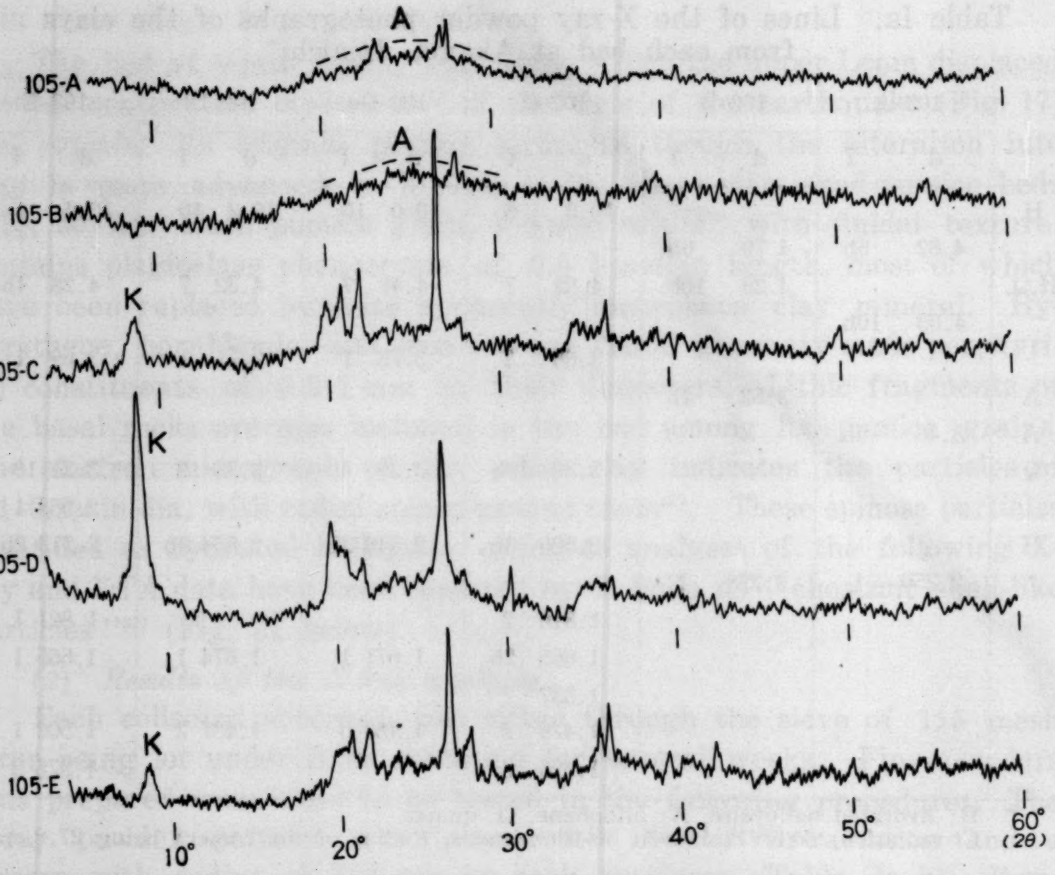

Fig. 18. X-ray powder diffraction patterns of the clays from Myojin, A: Diffraction patterns by allophane, K: Diffraction patterns at 001 of the hydrated halloysite, Cu-radiation, after T. Sudo. The patterns of the same sample of 105–D taken with Fe-radiation do not show such a distinctive sharp peak at 10Å. It appears with same intensities in every chert of 105–C, 105–D, and of 105–E.

(3) *Differential thermal analyses:*

Each specimen was filtered through a sieve of 80 mesh after being let under room temperature for several weeks. Fine powder thus prepared has been used in the following procedure results of which are represented by the differential thermal analyses curves shown in Figs. 19 and 20[22]. The thermal curves of the yellow pumice bed (105-A) and of the brown pumice bed (105-B) from the cliff exposed along the road from Myôjin station of Tôbu Line to Ushiroyama, Ochiai village indicate two peaks: one is the endothermic one between 140-150°C, another is the exothermic one near 950°C, which are identified as that

22) The equipment installed at the Geological and Mineralogical Institute, Tokyo University of Education was used by courtesy of Prof. Toshio SUDO.

Table II. X-ray powder diffraction data of the clays from Myojin*.

	105–A		105–B		105–C		105–D		105–E	
	d	I	d	I	d	I	d	I	d	I
K	Å	—	Å	—	10.3 Å	9b	10.2 Å	31	10.3 Å	7b
K	—	—	—	—	4.46	9b	4.46	15b	4.40	8b
Q	—	—	—	—	4.27	12	4.27	11	4.27	15
CF	—	—	4.06	8	4.04	14	4.08	9	4.08	20
F	3.82	9	—	—	—	—	—	—	—	—
F	3.71	8	?	?	3.71	6	3.75	7b	3.80	7b
A	3.4	7b	3.5	8b	—	—	—	—	—	—
Q	—	—	—	—	3.35	34	3.36	24	3.35	25
F	3.27	10	—	—	—	—	—	—	—	—
F	3.22	11	3.21	10	3.22	5b	3.22	6b	3.22	10
	—	—	—	—	—	—	2.93	7		
K	—	—	—	—	2.60	6b	2.57	5b	2.54	10
CQ	2.43	4	—	—	2.46	9	2.47	6b	2.50	13
Q	—	—	2.28	6b	2.29	6b	2.24	3b	2.29	5
	—	—	—	—	—	—	—	—	2.146	6
	1.191	3	—	—	—	—	—	—	1.981	4
	—	—	—	—	1.824	6	1.824	3	1.824	4
	—	—	1.658	4b	1.675	4b	1.67	3b	1.672	4

* K: hydrated halloysite, Q: quartz, C: cristobalite, F: felspar, A: allophane
Read from the cherts of a X-ray diffractometer (Fig. 18) being taken with filtered Cu-radiation by T. Sudo.

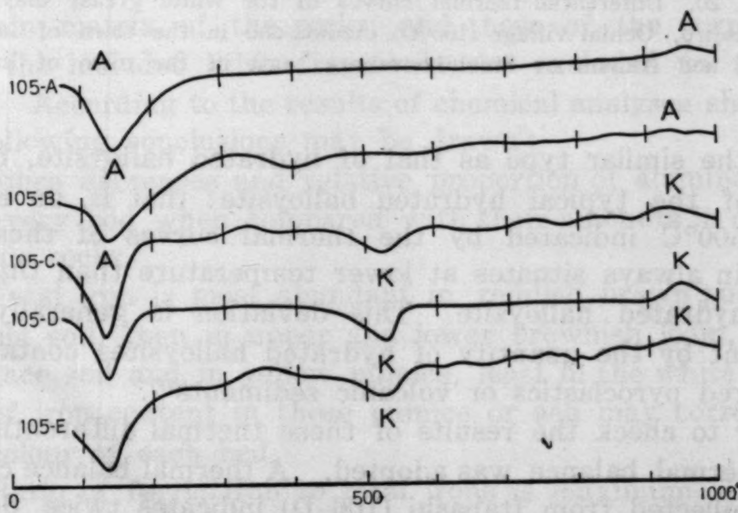

Fig. 19. Differential thermal curves of the clays from Myojin
A and K shows an endothermic or exothermic peak by allophane and hydrated halloysite respectively.

of allophane. The DTA curve of the Imaichi soil (105-B) shows an endothermic peak near 300°C slightly beside the aforementioned two peaks which may be ascribed to the existence of limonite contained in the Imaichi soil. The thermal curves of the clays from the bed of upper Loam (105-C), white clay (105-D), and lower Loam (105-E) collected at the same cliff show exclusively an exothermic reaction between 520-530°C in addition to an endothermic peak near 150°C and an endothermic one near 950°C which are of the same type as that of hydrated halloysite (Fig. 19). The curves of the white clay from Shimo-kojiro (100-D), Azuma-chô, Imaichi town (101-D), and Akama, Imaichi (102-D)

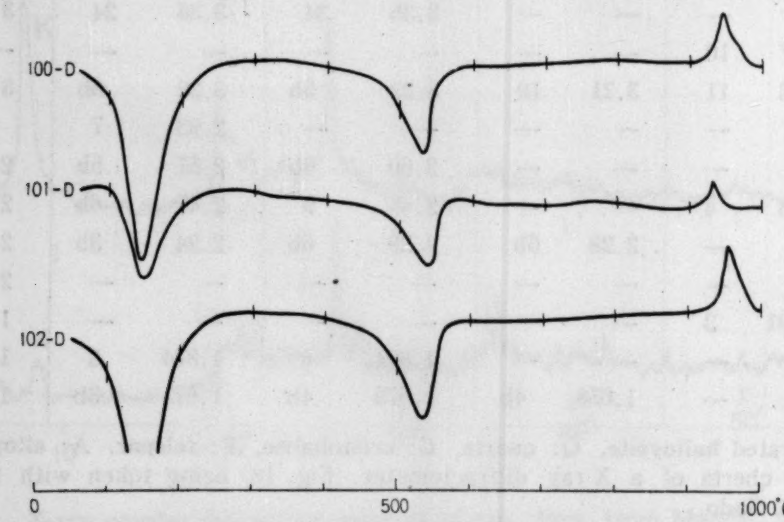

Fig. 20. Differential thermal curves of the white greasy clay from Shimo-kojiro, Ochiai village (100-D), Azuma-cho in the town of Imaichi (101-D), and Akama or Shichihonzakura, east of the town of Imaichi (102-D).

are also of the similar type as that of hydrated halloysite, but deviate from that of the typical hydrated halloysite: that is, an endothermic peak near 500°C indicated by the thermal curves of these clays of volcanic origin always situates at lower temperature than that indicated by typical hydrated halloysite. This deviation is generally shown in various extent by the quantity of hydrated halloysites contained in the slightly altered pyroclastics or volcanic sediments[23].

In order to check the results of these thermal differential analyses, test by a thermal balance was adopted. A thermal balance curve of the white clay collected from Itabashi (106-D) indicates twice dehydration:

23) T. SUDO and J. OSSAKA, "Hydrated halloysite from Japan", *Jap. Jour. Geol. Geogr.*, **22** (1952), 215-229.

the first continuously occurred towards 100°C and the second between 400–500°C. The two dehydration points correspond to the endothermic

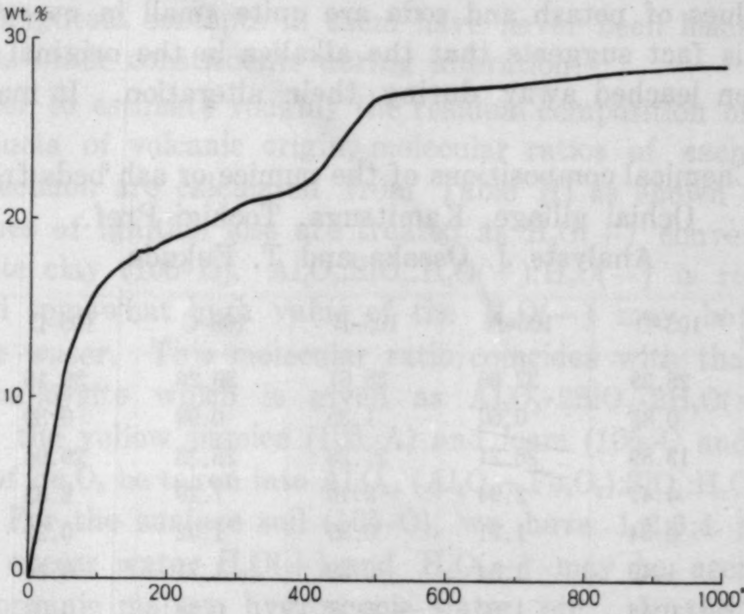

Fig. 21. Dehydration curve of the white clay from Itabashi (Fig. 27).

reactions near 150°C and near 550°C represented by the DTA curve of this white clay (Figs. 20 and 21).

(4) *Chemical analyses:*

Each specimen was filtered through a sieve of 115 mesh after natural drying under room temperature, and then treated in crucibles. Thus the results of the chemical analyses represent the compositions of the main matrix of the rocks, and those of the porphyritic minerals or of the included lithic fragments are excluded in the following discussion. According to the results of chemical analyses shown in Table III, the following conclusions may be drawn:

(a) Silica decreases and relative proportion of alumina increases in every bed when compared with their amounts in original volcanic rocks.

(b) Total iron is most abundant in reddish brown pumice of Imaichi soil, then in upper and lower brownish loam, less in surface soil and in yellow pumice, least in the white clay. Values of iron content in these pumice or ash may correspond to the colour of each bed.

(c) Ratio of ferric iron to total irons is maximum in the pumice of Imaichi soil and decreases its value in loam, surface soil, yellow pumice, and in white clay successively.

(d) Titania is comparatively rich in every specimen and changes its value corresponding to that of iron content in each sample.

(e) Values of potash and soda are quite small in every specimen. This fact suggests that the alkalies in the original rocks have been leached away during their alteration. It may be same

Table III. Chemical compositions of the pumice or ash beds from Myojin, Ochiai village, Kamitsuga, Tochigi Pref., Analysts J. Ossaka and T. Fukuda.

	105–O	105–A	105–B	105–C	105–D	105–E
SiO_2.........	28.29	37.66	25.61	39.20	39.15	38.12
TiO_2.........	0.85	0.60	1.35	0.99	0.39	1.11
Al_2O_3........	19.89	26.21	27.28	25.23	29.94	23.17
Fe_2O_3........	4.41	2.94	9.10	7.29	2.33	6.99
FeO.........	2.34	1.71	0.39	1.02	0.22	1.30
MgO........	1.49	1.54	0.39	1.71	0.24	1.76
CaO.........	0.48	1.67	0.17	0.58	0.03	0.61
Na_2O........	0.25	0.84	0.13	0.56	0.40	0.43
K_2O.........	0.33	0.56	0.05	0.51	0.15	0.51
H_2O-	16.30	15.22	24.66	12.80	15.92	15.87
H_2O+	25.23	11.13	11.08	10.27	11.41	10.05
Total.......	99.86	100.08	100.21	100.16	100.18	99.92

Table IV. Molecular ratio calculated from the chemical analyses shown in Table III.

	105–O	105–A	105–B	105–C	105–D	105–E
SiO_2.........	0.471	0.627	0.426	0.653	0.652	0.634
TiO_2.........	0.011	0.008	0.017	0.012	0.005	0.014
Al_2O_3........	0.195	0.257	0.268	0.248	0.294	0.227
Fe_2O_3........	0.028	0.018	0.056	0.046	0.015	0.044
FeO.........	0.032	0.024	0.005	0.014	0.003	0.013
MgO........	0.037	0.038	0.010	0.042	0.006	0.044
CaO.........	0.009	0.030	0.003	0.010	0.001	0.011
Na_2O........	0.004	0.014	0.002	0.009	0.006	0.007
K_2O.........	0.004	0.006	0.001	0.005	0.002	0.005
H_2O-	0.904	0.845	1.368	0.710	0.883	0.881
H_2O+	1.400	0.618	0.615	0.570	0.633	0.558
$Al_2O_3+Fe_2O_3$	0.95	0.88	1.52	0.90	0.95	0.85
SiO_2	2.00	2.00	2.00	2.00	2.00	2.00

about the lime contents, though the yellow pumice contains 1.67% lime.

(f) Magnesia contents in them have never been leached so much as other constituents during alteration.

In order to estimate roughly the residual composition of these alteration products of volcanic origin, molecular ratios of each constituent in each specimen are calculated from Table III as shown in Table IV, where values of ignition loss are treated as $H_2O(+)$ conveniently. As to the white clay (105-D), Al_2O_3:SiO_2:$H_2O(+)$:$H_2O(-)$ is roughly 2:1:2: 2.5-3.0 and somewhat high value of the $H_2O(-)$ may be ascribed to hygroscopic water. This molecular ratio coincides with that of typical hydrated halloysite which is given as $Al_2O_3 \cdot 2SiO_2 \cdot 2H_2O(+) \cdot 2H_2O(-)$. As regards the yellow pumice (105-A) and loam (105-C and E) also, if the value of Fe_2O_3 be taken into Al_2O_3, $(Al_2O_3+Fe_2O_3)$:SiO_2:$H_2O(+)$:$H_2O(-)$ =1:2:2:3. For the surface soil (105-O), we have 1:2:6:4 in the same way. The excess water $H_2O(+)$ and $H_2O(-)$ may be ascribed to the coexisting organic matter, hygroscopic water, etc.. In the Imaichi soil (105-B), we have 1.5:2:3:6. The excess Fe_2O_3 may be contained as limonite in the soil. Molecular proportions of the residual constituents in these pumice or ash thus calculated accord with the results of the afore-mentioned X-ray and thermal analyses. It is noticeable that the ratio of $Al_2O_3+Fe_2O_3$ to SiO_2 is 1:2 in the matrix of these pumice or ash except in that of Imaichi pumice (Table IV). It may be concluded therefore that the clay minerals have never been highly recrystallized, especially in the upper member of the Pleistocene clayey beds, even though these pyroclastics have already been altered into a rather advanced state chemically in spite of there still remaining their original textures.

(5) *Size distribution of the clayey beds*[24]*:*

Air-dry samples of the clayey beds from Akama (102) and Myojin (105) were sorted through sieves of various mesh such as 2,000, 840, 250, 105, and 74 mesh on the oscillation table. Data for the size distribution of the finer particles ($<$ 0.0074 *mm*) were obtained from the measurements on sedimentograph. Data thus obtained are shown by the following cumulative curves of each bed (Figs. 22 and 23) and their schematical representations are found in the Fig. 24 (Table V and VI). Besides the Imaichi reddish brown pumice (B), each bed (O, A, C, D,

24) The writers were kindly instructed by Mr. K. UCHIDA of the Kôyô Co. during these experiments.

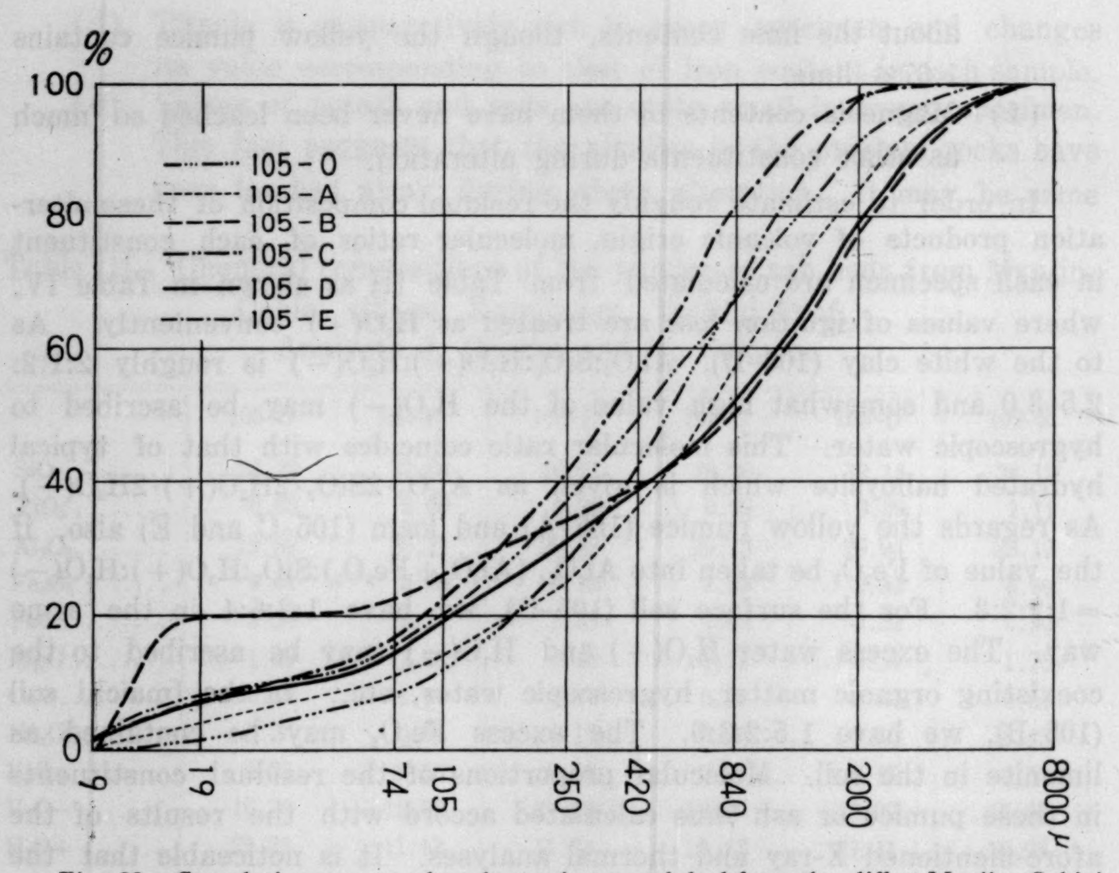

Fig. 22. Cumulative curves of each pumice or ash bed from the cliff at Myojin, Ochiai village, Kamitsuga-gun, Tochigi Pref. Notation of each bed is same in Fig. 18.

Table V. Data of the cumulative curves of the clayey beds from Akama, Imaichi town and Myojin, Ochiai village (Cf. Figs. 22 and 23).

Spec. No. \ Grain size *mm*	>2	2～0.84	0.84～0.42	0.42～0.25	0.25～0.105	0.105～0.074	0.074～0.014	0.014～0.009	<0.009
									wt%
102-A	9.55	15.94	25.25	12.28	14.45	4.90	11.81	5.55	0.26
102-B	17.88	6.34	12.85	9.81	13.80	4.77	7.26	26.95	0.34
102-C	0.16	7.36	30.83	21.26	24.61	4.42	9.44	1.71	0.22
102-D	8.51	28.34	15.76	9.21	14.68	6.01	9.97	5.60	1.92
102-E	3.24	11.75	27.26	17.89	20.02	4.94	10.44	2.23	2.24
105-O	2.73	28.38	26.31	14.52	15.94	3.71	7.82	0.59	0.00
105-A	15.28	27.02	21.23	10.57	11.31	3.02	8.89	2.68	0.00
105-B	22.27	26.76	11.42	5.19	7.83	4.29	4.89	17.34	0.00
105-C	9.56	22.31	17.70	12.80	16.64	5.25	9.29	4.25	2.20
105-D	20.48	27.30	13.10	7.54	12.06	4.68	9.20	3.86	1.78
105-E	2.13	16.43	24.52	15.34	19.44	5.55	11.12	3.48	1.99

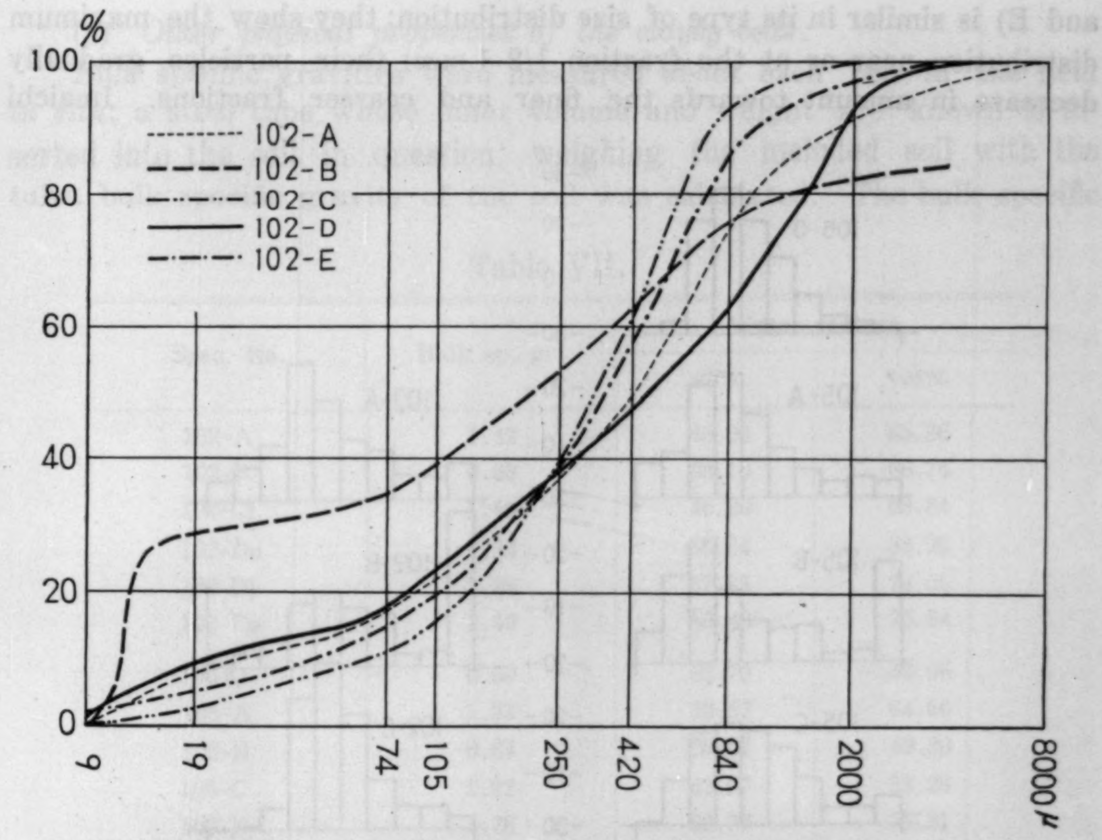

Fig. 23. Cumulative curve of each pumice or ash bed from the cliff at Akama, Imaichi town, Tochigi Pref.. Notation in the figure is the same as Fig. 18.

Table VI. Size distribution of the clayey beds from Akama, Imaichi town (102) and Myojin, Ochiai village (105) Cf. Fig. 24.

Spec. No. / Grain size *mm*	102-A	102-B	102-C	102-D	102-E	105-O	105-A	105-B	105-C	105-D	105-E
1/128 >	0.0%	0.0	0.0	1.5	2.1	0.0	0.0	0.0	2.0	1.6	1.8
1/128~1/64	7.1	28.0	2.2	6.9	2.9	1.0	3.2	18.7	5.3	4.4	4.3
1/64~1/32	4.2	2.8	4.0	4.4	3.5	2.8	3.5	1.8	3.4	4.2	4.1
1/32~1/16	4.4	2.6	4.0	3.3	4.9	3.7	3.1	1.5	3.4	3.0	4.6
1/16~1/8	9.4	9.1	9.1	10.7	9.7	7.4	5.4	6.3	8.9	8.6	11.5
1/8~1/4	11.7	10.5	21.0	11.4	16.6	13.3	9.6	6.0	14.5	9.7	15.4
1/4~1/2	18.4	13.5	30.8	12.8	25.5	21.0	15.4	7.7	17.3	10.5	21.3
1/2~1	25.1	11.5	24.4	17.5	24.0	27.1	22.6	13.2	18.6	15.2	23.0
1~2	10.3	4.3	4.0	23.0	7.6	21.0	20.7	22.6	16.9	22.3	11.8
2~4	6.2	2.2	0.5	8.0	3.2	2.7	8.9	16.5	8.7	15.5	2.2
4~8	3.2	0.5	0.0	0.5	0.0	0.0	6.6	5.7	1.0	5.0	0.0
8<	0.0	15.0	0.0	0.0	0.0	0.0	0.0	0.0	0.0	0.0	0.0

and E) is similar in its type of size distribution: they show the maximum distribution near or at the fraction 1/2–1 *mm*; their particles gradually decrease in amount towards the finer and coarser fractions. Imaichi

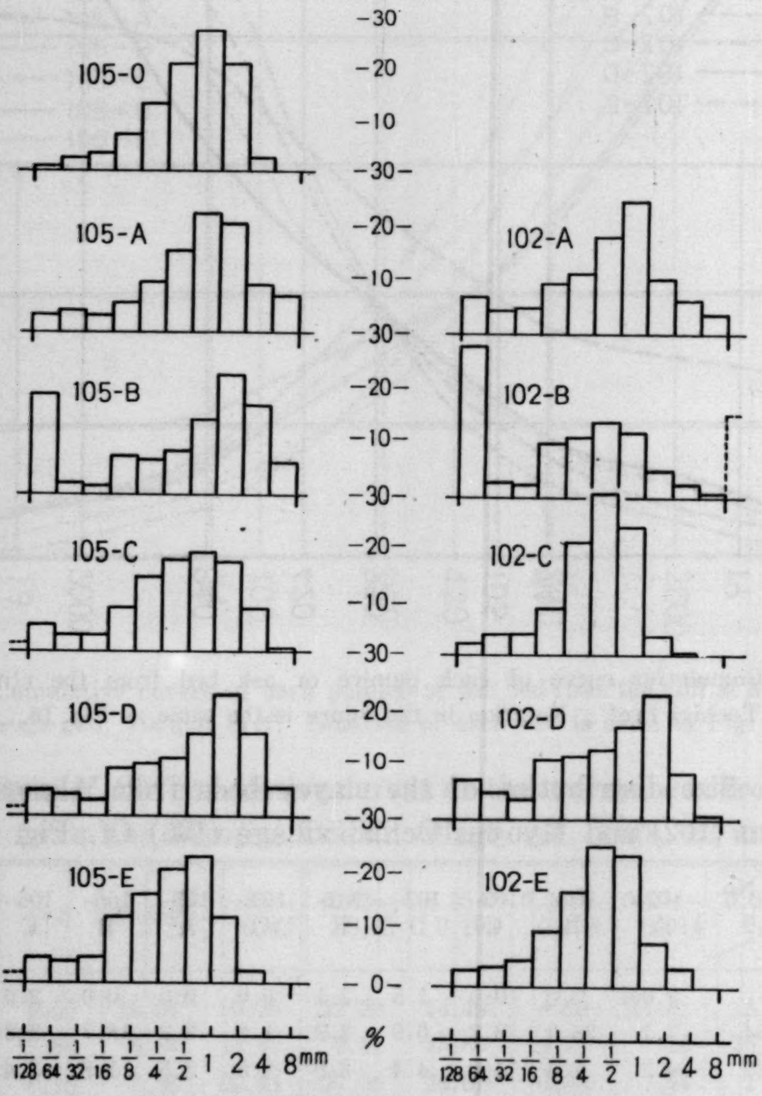

Fig. 24. Size distribution of the clayey beds from Myôjin, Ochiai village (105) and Akama, Imaichi town (102).

soil, however, is different in type of size distribution from other beds: abundance of the particles in the fraction 1/128–1/64 *mm* is conspicuous; the coarser particles (> 8 *mm*) are also abundant in the soil from Akama (102–B). The finer particles (< 1/128 *mm*) are lacking in the overlying O, A, and B beds and are contained in the underlying C, D, and E beds.

(*6*) *Other physical properties of the clayey beds:*

Bulk specific gravities were measured about each bed in the field *in situ*: a steel tube whose inner volume and weight are known is inserted into the soil in question; weighing the included soil with the tube, bulk specific gravity of the soil was calculated. The bulk specific gravities thus obtained are 0.9 for the surface humus soil and the yellow pumice and 1.2-1.4 for other beds (Table VII). The specific gravity of the white clay determined by means of pycnometer was 2.13. Weights of the specimens of these clayey beds were measured at the field soon after collection. Then their water contents were obtained in the laboratory from loss of heating at 150°C. Their values are enumerated in the same table (Table VII) with those represented by volume percentage which are calculated form the former being compared with bulk specific gravities. The white clay shows the maximum value 80%. Water absorption of the air-dryed specimens was measured in the laboratory, and the results are shown in Table VIII. The white clay of 100 *cc* may absorb 156.2 *cc* water.

Table VII.

Spec. No.	Bulk sp. gr.	Water content	
		wt%	vol%
102-A	1.42	46.03	65.36
102-B	0.98	68.10	66.74
102-Cl	1.49	46.20	68.84
102-Du	1.33	66.84	88.90
102-Dl	1.28	57.85	74.05
102-Eu	1.42	53.48	75.94
105-O	0.99	63.70	63.06
105-A	1.23	52.57	64.66
105-B	0.84	58.57	49.20
105-C	1.22	43.67	53.28
105-D	1.26	59.77	75.31
105-E	1.31	52.56	68.85

u: upper portion in a bed, l: lower portion.

Table VIII.

	wt. %	vol. %
105-A	75	92
105-B	139	117
105-C	77	94
105-D	124	156
105-E	87	114

V. Summary and conclusions

On the morning of December 26, 1949 at 08*h*18*m* and 08*h*26*m* successively, the town of Imaichi and its environs, Tochigi Prefecture, about 100 *km* north of Tokyo was struck by severe earthquakes followed by the numerous aftershocks with shallow foci. Many changes of the surface were brought about, among which the earthfalls and landslips on the area covered with thick Pleistocene formation of volcanic origin were most conspicuous. The surface humus soil, yellow pumice bed (Kanuma soil), and reddish brown pumice bed (Imaichi soil), the upper members of the Pleistocene formation in this area consist mainly of volcanic glass and allophane. Brownish loam and white clay, the lower members are composed mainly of lower crystalline hydrated halloysites and the latter is most enriched in the same clay mineral. This white greasy clay played an important *rôle* in the surface changes as a slipping plane of the landslips.

In conclusion, the writers express their cordial thanks to Prof. Toshio Sudo of the Tokyo University of Education for his kind instructions relating to this study. Their thanks are also due to Dr. Hiroshi Takahashi of the Department of Chemistry of the Tokyo University for his gift of photographs, and to Mr. Kenji Uchida of the Kôyô Co. for his kind assistance during the grain size analyses. A part of the expenses necessary for this study have been defrayed from the funds for Scientific Researches of the Ministry of Education, for which the authors here express their gratitude.

---

18. 今市地震地域の地質 (3)

地震研究所 森本良平
小坂丈予
福田知子

昭和 24 年 12 月 26 日午前 8 時 18 分と 26 分に続いて起きた地震にともなつて，栃木県上都賀郡今市町 [現在今市市] を中心とする大約 20 km 四方の地域に地変を生じたが，そのうちでも火山噴出物起源の洪積層分布地域に生じた地崩れと地辷りが，ことに著しかつた．[地震研究所彙報 28 号 (昭和 25 年)，379-386 頁，同 29 号 (昭和 26 年)，349-358 頁]．この第 3 報では，その存在が地変を生じた素因の一つとなつた洪積世の火山噴出物の各堆積層——上より (O) 表土層・(A) 黄色浮石層 (鹿沼土層)・(B) 赤褐色浮石層 (今市土層)・(C) 上部ローム層・(D) 白粘土層・(E) 下部ローム層——の主体をなす火山玻璃の風化生成物である粘土の鉱物組成，化学成分などについて研

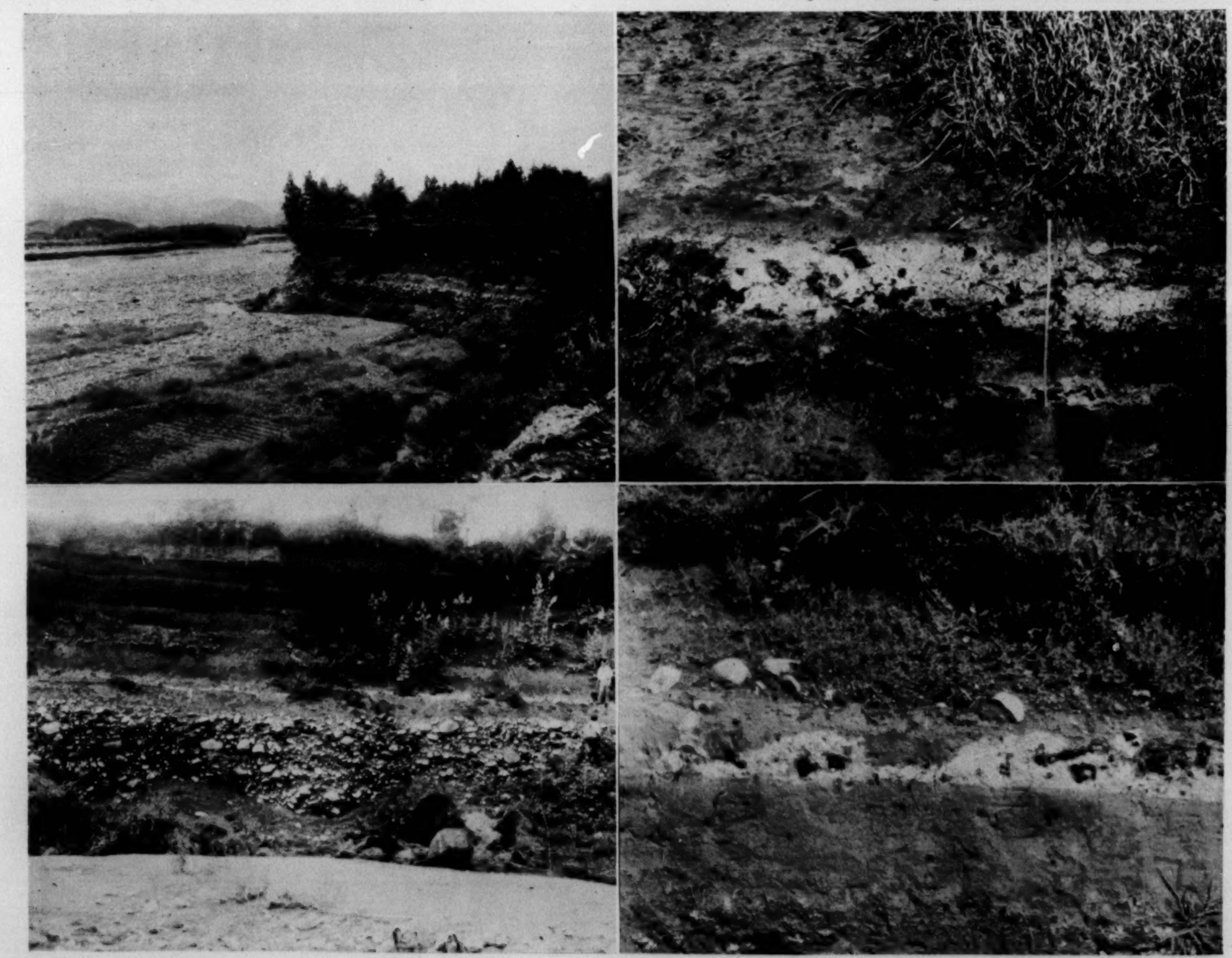

(震研彙報 第三十五号 図版 森本・小坂・福田)

Fig. 25 (Upper left). Pleistocene beds exposed along the River Daiya observed at Akama or Shichihonzakura, Imaichi, Tochigi Pref. The pumice or ash beds are underlaid by gravel and sandy beds. Fig. 26 (Lower left). Closed view of the above figure. Fig. 27 (Upper right). A bed of white clay intercalating in loamy beds, at the cliff exposed along the road from Itabashi to Osawa, Ochiai village. Fig. 28 (Lower right). Ditto at Myojin, Ochiai village.

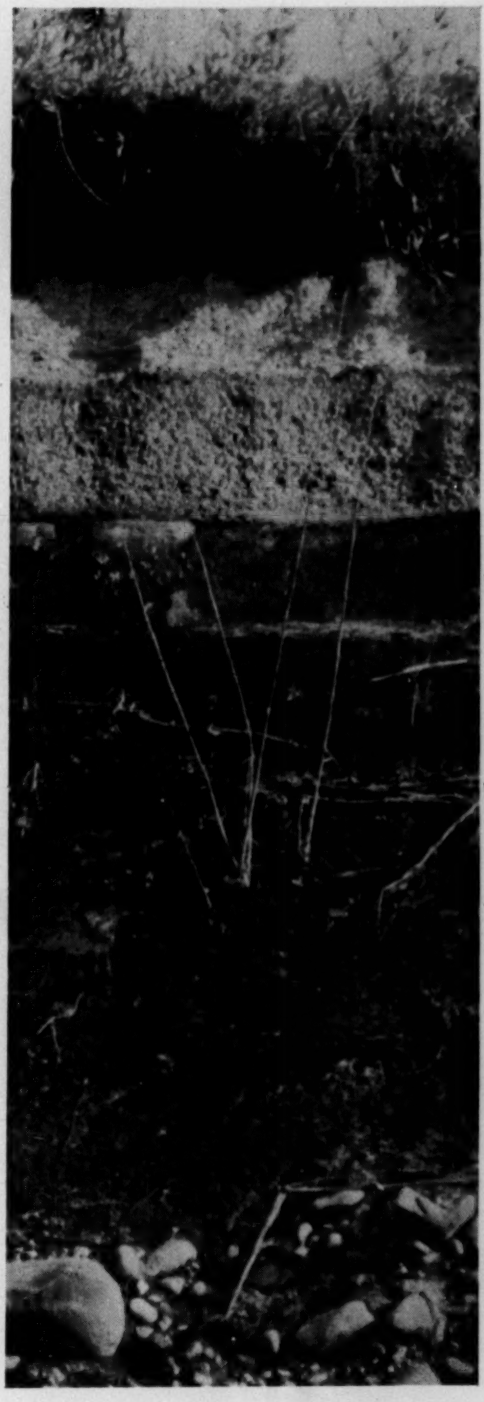

Fig. 29. Pumice or ash beds exposed at the cliff along the River Daiya, Akama, Imaichi.
O: Surface humus soil, A: Yellow pumice bed, B: Reddish brown pumice bed (Imaichi soil), C: Upper Loam, D: White clay bed, E: Lower Loam.

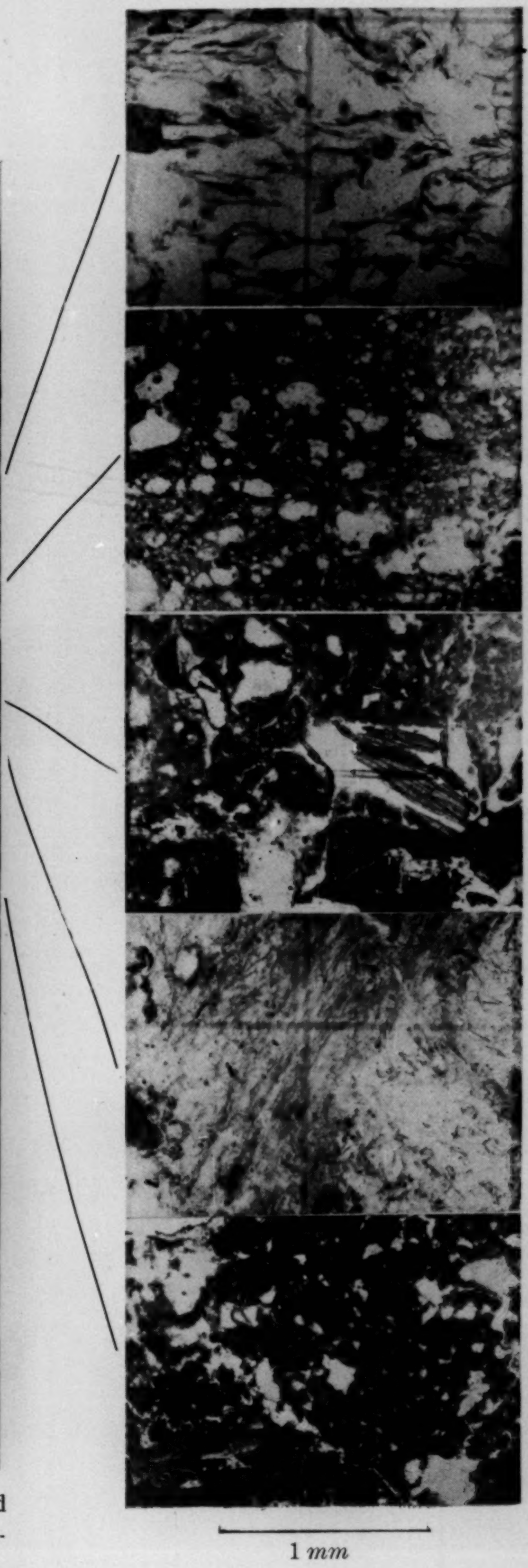

Fig. 30. Microphotographs of the specimens collected from the beds photographed in Fig. 29. Polarizer only × about 40.

(震研彙報 第三十五号 図版 森本・小坂・福田)

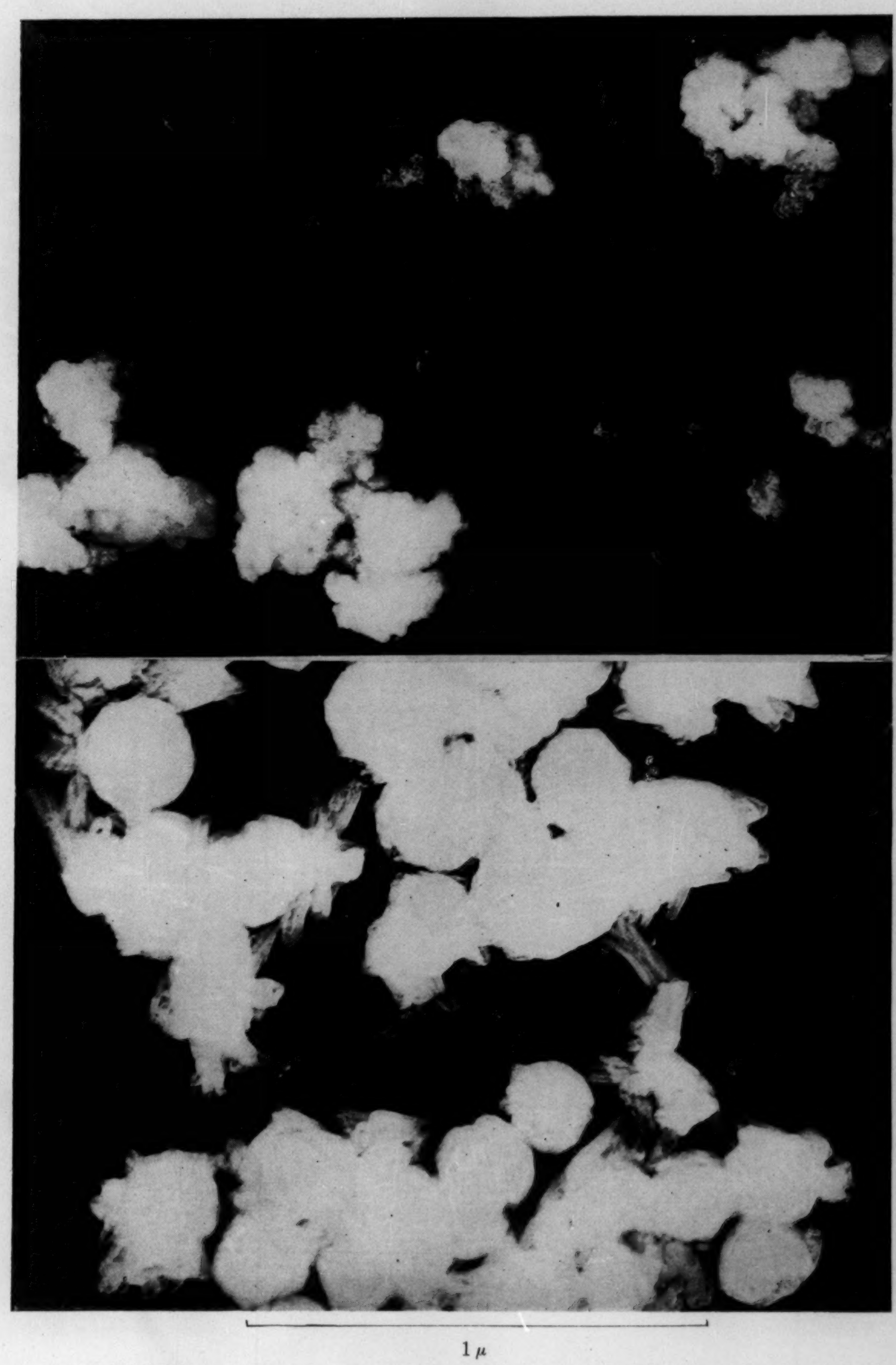

Fig. 31. Electronmicrographs of the Imaichi soil (above) and of the white clay (below) from Myojin, Ochiai village. Photo. by Dr. H. Takahashi.

究を行つた．各試料の微細な部分について X 線分析・示差熱分析・熱減量測定・化学分析を，また原土について粒度分析・比重・含水量・吸水率の測定などの結果を報告した [第 I-VIII 表]．これによると上層の表土層・鹿沼土層・今市土層はまだ再結晶の進まないアロフェンによつて，上部ローム層・白粘土層・下部ローム層などの下部層は再結晶度の低い加水ハロイサイトによつて代表されているが，そのうちでも白粘土層は，とくに多量の加水ハロイサイトを含んでいると考えられる．なおこれらの火山噴出物起源堆積層は，原岩の構造をよく残しているが，火山玻璃の部分は化学的にはきわめて変化が進んでいる．すなわち SiO_2 はいちぢるしく減少し，これに引きかえて Al_2O_3 の富む結果となり，また 1，2 の層では CaO が，いくつかの層では MgO がわづかにその一部を残して，大部分が失われ，Na_2O，K_2O はほとんど完全に溶脱していた．この結果，鉄の過剰な今市土層を除く他の各層の $Al_2O_3+Fe_2O_3$ と SiO_2 との比はいずれも 1:2 となつている．とくに加水ハロイサイトを多量に含む白粘土層は，その含水率，吸水能ともに最大の値を示し，地変に際しその地辷り面となつた．

19. *Phase Lag of Vibrations of Buildings Excited by a Vibrator.*

By Fuyuhiko KISHINOUYE,

Earthquake Research Institute.

(Read Feb. 26, 1957.—Received March 31, 1957.)

Dominant periods of building vibrations have been measured with their vibrations caused by wind gusts or by earthquakes. Recently ground vibrators have been used to excite building vibrations. The writer attained the dominant period from the phase lag of building behind the vibrator.

The ground vibrator used by the writer was reported in this journal.[1] The wheels of the vibrator were rotated by a man as fast as possible, and then allowed to rotate freely, so the forced vibration of the building was gradually prolonged, and its amplitude decreased as the rotation of the wheels grew slow. But when the dominant vibrations resonate with the rotation of the vibrator, the amplitude of building vibration becomes maximum.

We recorded vibrations of several apartment buildings in Tokyo. Instruments for the observation were vertical vibrographs of mechano-optical magnification designed by the writer. The condition of the instruments was $T=3.0$ sec., critical damping and $V=850$. Once in one

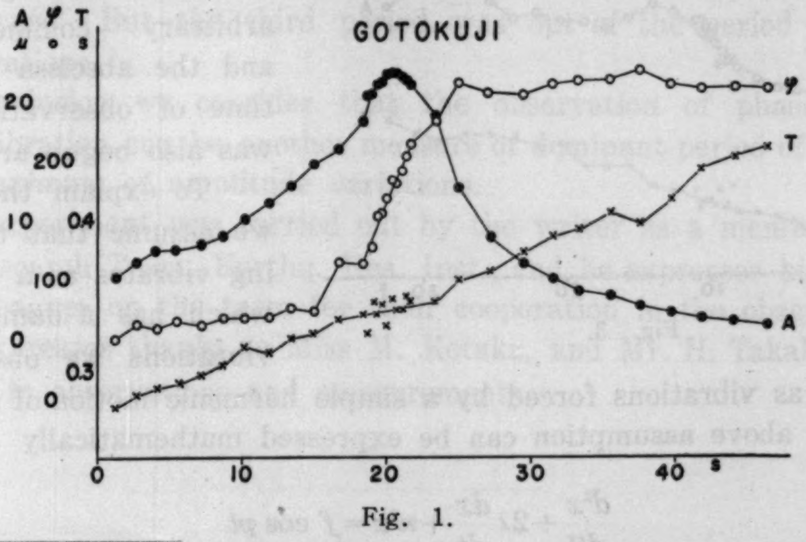

Fig. 1.

1) F. KISHINOUYE, *Bull. Earthq. Res. Inst.*, **33** (1955), 495–497.

revolution of the vibrator wheel, an electric contact was closed, and image of vibration made was interrupted by a shutter. The breaks of image showed the phase difference of the vibrator and building vibration.

Several examples of the measurement were carried out at apartment houses of similar size and shape. Three examples, observed at Gōtokuji, Kyōdō and Senjyu, are shown in Figs. 1, 2 and 3. In the graphs, *A*

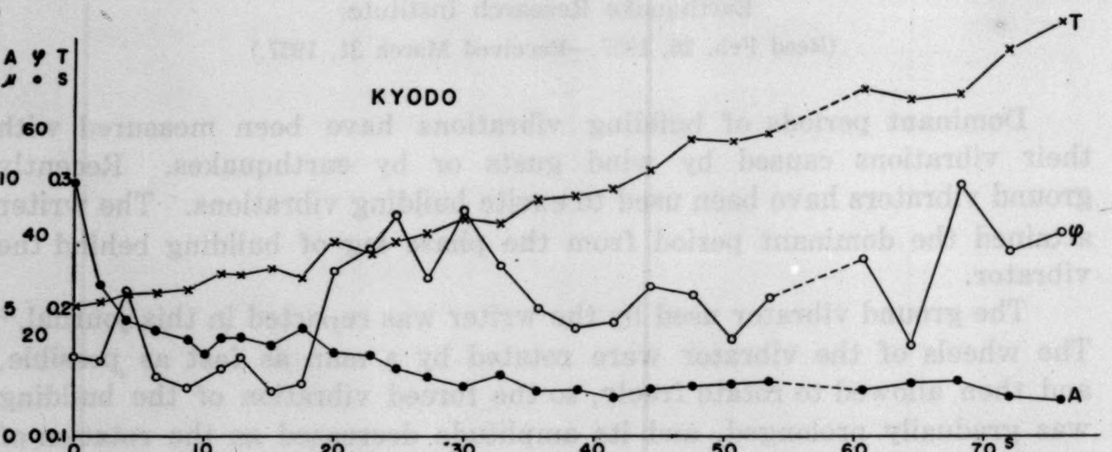

Fig. 2.

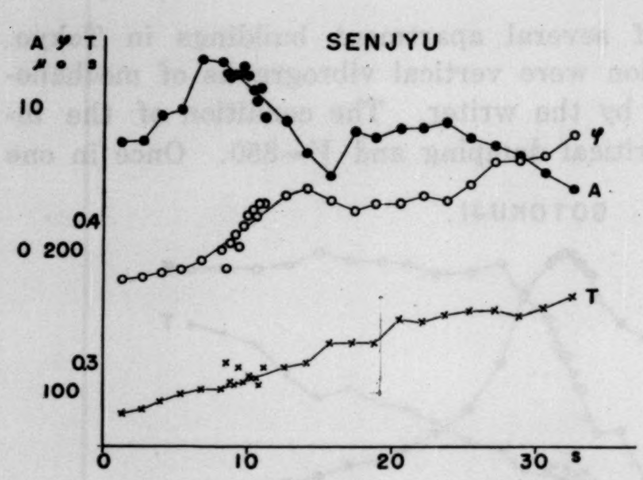

Fig. 3.

denotes the double amplitude in μ, T the period of building vibration caused by the vibrator, in sec, φ the phase difference in degree from arbitrary commencement, and the abscissa expresses time of observation which was also begun arbitrarily.

To explain the results, we assume that the building vibrates as a pendulum which has a damper. The vibrations we observe are regarded as vibrations forced by a simple harmonic motion of the vibrator. The above assumption can be expressed mathematically

$$\frac{d^2x}{dt^2}+2\lambda\frac{dx}{dt}+n^2x=f\cos pt$$

in usual notations. The right-hand term expresses the action of the vibrator. The solution of the equation is wellknown

$$x=\frac{f\cos(pt-\varepsilon)}{\sqrt{(n^2-p^2)^2+4\lambda^2p^2}},$$

where $\varepsilon=\tan^{-1}\frac{2\lambda p}{n^2-p^2}$ and gives the phase lag, and it varies according to the relation below:

$$0<\varepsilon<\frac{\pi}{2} \qquad \text{for } p<n,$$

$$\varepsilon=\frac{\pi}{4} \qquad \text{for } p=n,$$

and

$$\frac{\pi}{2}<\varepsilon<\pi \qquad \text{for } p>n.$$

This relation shows that the value of ε changes sharply as p changes near $p=n$, or resonance case.

The result obtained at Gōtokuji (Fig. 1) is a good example of the above consideration. The phase angle changed remarkably at the amplitude maximum. In the case of Kyōdō Apartment House two maximum amplitude and two corresponding phase changes are seen in Fig. 2. Similarly two dominant periods are shown in Fig. 3, although Dr. Kanai and others[2] found one more dominant period, or three dominant periods for this house. But the third period was out of the period range of our observations.

In conclusion we consider that the observation of phase lag of building vibration can be another measure of dominant period of building besides maximum of amplitude variations.

This experiment was carried out by the writer as a member of the Subsoil Research Team, Earthq. Res. Inst., and he expresses his thanks to his colleagues on the term for their cooperation in the observations. Also he expresses thanks to Miss M. Kotaka, and Mr. H. Takahashi for their help in observations and measurements.

---

2) K. KANAI and others, *Research Report* (*Ronbunshū*) *Archit. Inst. Japan*, No. 24, (1953), 185.

19. 起振機による建物の振動の位相差測定

地震研究所　岸上冬彦

建物の固有振動周期を知るのに遠心力を利用した起振機を用いる場合，起振機の車輪を速く回転させて放すとその回転が次第に遅くなり建物の振動は小さくなるが，起振機の回転が建物の固有周期と共振する所では振幅の極大が現われることはよく知られている．共振の場合には振幅ばかりでなく振動の位相も大きく変わる筈であるので，筆者は起振機と建物の振動との位相差を測定し固有周期を見出した．実例として東京都内の豪徳寺，経堂，千住の3個の大きさ，構造共に殆ど等しく，地盤の違うアパート建築について行つた実験結果を示した．

20. 超短波多重遠隔記録地震計（第 1 報）

地震研究所 { 宮村攝三
辻浦賢

（昭和 32 年 3 月 26 日発表—昭和 32 年 3 月 31 日受理）

1. はしがき

遠隔記録地震計をもちいた集中記録方式により，局地地震の精密観測網組織をつくるために，有線および無線による搬送式遠隔記録地震計の開発をくわだて，1954 年それぞれ 1 回線用の装置として LTS-I, LTS-II[1] および RTS-I[2] を完成した．その後，RTS-I は 1956 年爆破地震動研究グループにおいて実施した千葉県下における爆破地震観測[3]にももちい，VHF 無線電話装置による爆破時刻およびクロノメーター秒刻時の伝送と並用，横芝爆破点における爆破時刻および大網（△＝15 km），茂原（△＝35 km）2 地点の震動の 3 者を茂原において同一の記録紙上にとることに成功し，爆破観測においても，この方法がきわめて有用であることを立証した．

この方法の将来性については，前報告[1,2]にものべたように，普通の地震観測業務においても，余震観測その他の臨時観測においても，あるいわ各種の実験的測定においても，大いに期待できるとおもわれるので，筆者らの直接の目的としている局地地震の精密観測のためばかりでなく，ひろく一般的な地震観測法の進歩にも寄与するために，遠隔記録地震計の研究をつづけたのである．

このような遠隔記録地震計系による集中記録式地震観測法をさらに発展させるためには，さしあたり，1) 無人野外観測所に 1 成分以上の地震計をおけるようにすることと，2) 無人野外観測所の数をふやすこととが必要である．

1) については，RTS 伝送系の多重化を必要とするが，これは RTS-I においても採用していた副搬送波による 2 重変調方式をもちい，副搬送波の周波数分離によつて，容易に目的を達することができるはづである．このことは，実際の通信技術としても，ひろくおこなわれていることであり，まづ問題はすくない．

2) についても，もちろん搬送周波の周波数分離によれば問題なく，南アフリカの Wittwatersrand でおこなわれている 6 点の無人野外観測所[4]は 41 MHz から

---

1) S. MIYAMURA and H. MATUMOTO, "Line Telerecording Seismograph," *Bull. Earthq. Res. Inst.*, **33** (1955), 715–724.

2) S. MIYAMURA and M. TSUJIURA, "A VHF Radio Telerecording Seismograph," *Bull. Earthq. Res. Inst.*, **33** (1955), 725–731.

3) Res. Gr. Expl. Seism., Autumn Meeting of the Seism. Soc., Japan at Kyoto, Nov. 15, 1956.

4) P. G. GANE, H. J. LOGIE and J. H. STEPHENS, "Triggered Telerecording Equipment for Seismic Observations," *Bull. Seism. Soc. Am.*, **39** (1949), 119–143.

46 MHz のあいだに 6 つの周波数をあてがい，各点の分離をおこなつているのである．しかしながら，わがくにの電波事情あるいわ電波行政の実情からは，すくなくともいますぐ地震観測に対しこのような優先的措置はとられにくいようである．一方，地震観測所の数は 6 点にとどまらず，さらにおおくをのぞまれることは当然である．このように無線搬送式遠隔記録地震計の増設の可能性をも考慮すると，いづれにしても，できるだけすくないわりあて電波をもつて，なるべくおおくの観測所をおくことのできる方法をかんがえることが，この方法の発展のために必要なことになるのである．

周波数分離によらないで，多局の受信電波を分離するには，基地局からの別の電波をもつて各局の送信を制御して，時分割をおこなうとか，送信点に記憶装置をそなえて一時地震動信号をたくわえ，順次に送受信をおこなうとか，いろいろの方法がかんがえられるが，いづれも相当複雑な装置を要し，経費もかさむおそれがある．

そこでわれわれは，もつとも簡単な方法として，空中線による輻射電波の偏波性とその指向性とを利用し，この目的を達することができるのではないかとかんがえた．このことについては通信工学方面でもまだ充分の資料にとぼしかつたが，一応八木空中線をもちいてこれを実験してみた．のちに第 2 報で詳細に報告するように，垂直および水平偏波の電波により，同一点から同一周波数で送信された信号は，同一場所に並置した 2 つの受信装置で同時に別々に分離して受信・記録できることがわかつた．一方，これらの空中線は水平面内の指向性をもつているので，これによつて同一偏波面をもつ電波をだす 2 送信局も，受信基地からみてある程度方位角の差があれば，これもまた分離できる可能性がある．結局，以上のべた偏波性および指向性による分離を利用すれば，ただ一つの周波数の電波をもちいても，相当多数の無人野外観測所からなる観測網を構成しうることがわかつたわけである．

このような伝送の多重化および観測点増設のこころみとして，1955 年 RTS-II 型無線搬送式遠隔記録地震計 2 組の製作を計画，多重回線をもうけるためと，指向性のするどい空中線をつくるために，波長としては UHF を採用，伝送特性の向上のために，RTS-I では FM-AM 方式をとり，電波として AM 電波をもちいていたのを，RTS-II では FM-FM 方式として FM 電波を採用することとし，そのほか細部にわたり RTS-I の経験をいかして，その設計をおこなつた．1956 年 1 月 419.8 MHz, F 9 電波の実用化試験局としてこの 2 組の局の周波数認可をうけ，3 月 26 日開局をゆるされた．

その後ただちに和歌山附近の局地地震観測[5]に利用し，ついで東京都内において伝播試験その他の実験をおこない，1957 年にはいつて約 2 ヵ月間相模湾岸において地震観測をこころみ，装置の性能を試験した．

これらの実験の結果，本装置もまたさきに報告した RTS-I とともに充分われわれの地震観測に役だち，かつまた目的とした多重伝送と同一周波数送信局の分離受信とをおこ

5) S. MIYAMURA, "Seismic Activities in and near Kii Peninsula, Japan," Autumn Meeting of the Seism. Soc., Japan at Kyoto, Nov. 13, 1956.

ないうることが判明した．よつて，ここに第 1 報としてその設計，構造等の概要を報告し，第 2 報には主として本装置の性能に関する実験結果をまとめて報告することにした次第である．

2. 謝　辞

本装置 2 組の製作費は昭和 30 年度文部省科学研究費機関研究費としてあたえられた．ここに記して謝意を表したい．なお，同研究費は本装置の記録部分として，表俊一郎助教授により製作された遅延式磁気テープ多重地震記録装置[6]の経費にもあてられたことを附記しておく．

本研究に対し終始，激励後援をよせられた那須所長にふかく感謝する．また御指導をえた工学部阪本捷房教授に心からの感謝をささげる．

本装置送受信部は岩井電気株式会社，空中線部は八木アンテナ株式会社，換振器記録電流計等は地震研究所技術部の製作によつた．岩井電気株式会社八木純一氏はじめ関係会社の各位，実川部長はじめ技術部の各位にあつく感謝する．また観測および実験には技術部の後藤健一，鈴木喜吉，其他の方々，同僚堀実，松本英照の両氏らの協力をえた．しるして謝意を表したい．無線局関係事務等につき御協力をえた事務部の各位にも感謝する．

また，本装置の運用，実験に関し現地において種々御協力をえた和歌山県当局，関西電力株式会社，東京電力株式会社，網代測候所，国鉄二宮変電区，株式会社川奈ホテル，東大理学部油壷臨海実験所等にもこの場所をかりて謝意を表明しておきたい．

3. RTS-II 型遠隔記録地震計の構成

本装置は前節にのべたように，すでに製作された VHF (60.17 MHz), 1 回線無線搬送式遠隔記録地震計 RTS-I，有線搬送式遠隔記録地震計 LTS-I 乃至 LTS-II 等とともに，局地地震観測出張用の高感度集中記録式地震観測網組織の 1 環として計画され，遠隔記録観測法の発展に寄与する若干の課題の解決をはかることに成功したものである．

第 1 図はこのような観測網組織の全体をしめしたものであり，そこでは，ここに報告する RTS-II 2 組が，RTS-I 1 組，LTS 2 組とともに，基地観測所の地震計をふくめて 6 点の観測所網を構成する状況がしめされている．この図でわかるように，RTS-II もまた他の遠隔記録地震計とおなじく**無人野外観測所装置**と**基地観測所装置**の 1 対からなつている．そして，前者は地震動を受震し電気振動に変換する**地震計換振器部**と，これを増幅変換して電波として基地にむけおくりだす**送信装置部**とにわかれ，両者は有線で連絡されている．後者，基地観測所装置は，各無人野外観測所より送信される電波をたえず受信し，地震動による変化をとらえる**受信装置部**と，これらをまとめて記録する**記録**

6) S. Omote and Y. Yamazaki, "Seven Channel Triggered Magnetic Tape Recorder for Routine Seismic Observations," *Bull. Earthq. Res. Inst.*, **35** (1957). *In Press.*

装置部とからなつている.

RTS-II では多成分の地震動の伝送をおこなうのであるが，実際には経費の関係で最小必要限 3 回線の伝送路をもうけることで満足した．伝送の方式としては UHF (419.8 MHz) の FM-FM 2 重変調方式をもちい，出力 20 watts で数 10 km 程度までの伝達を目的とした．各回線の漏話 30 db 以上，綜合無歪最高感度 100 μV/40 mm，信号雑音比 40 db (10 Hz にて) であり，換振器をふくめて 10 Hz にて 10^5～10^6 程度の観測ができるものである.

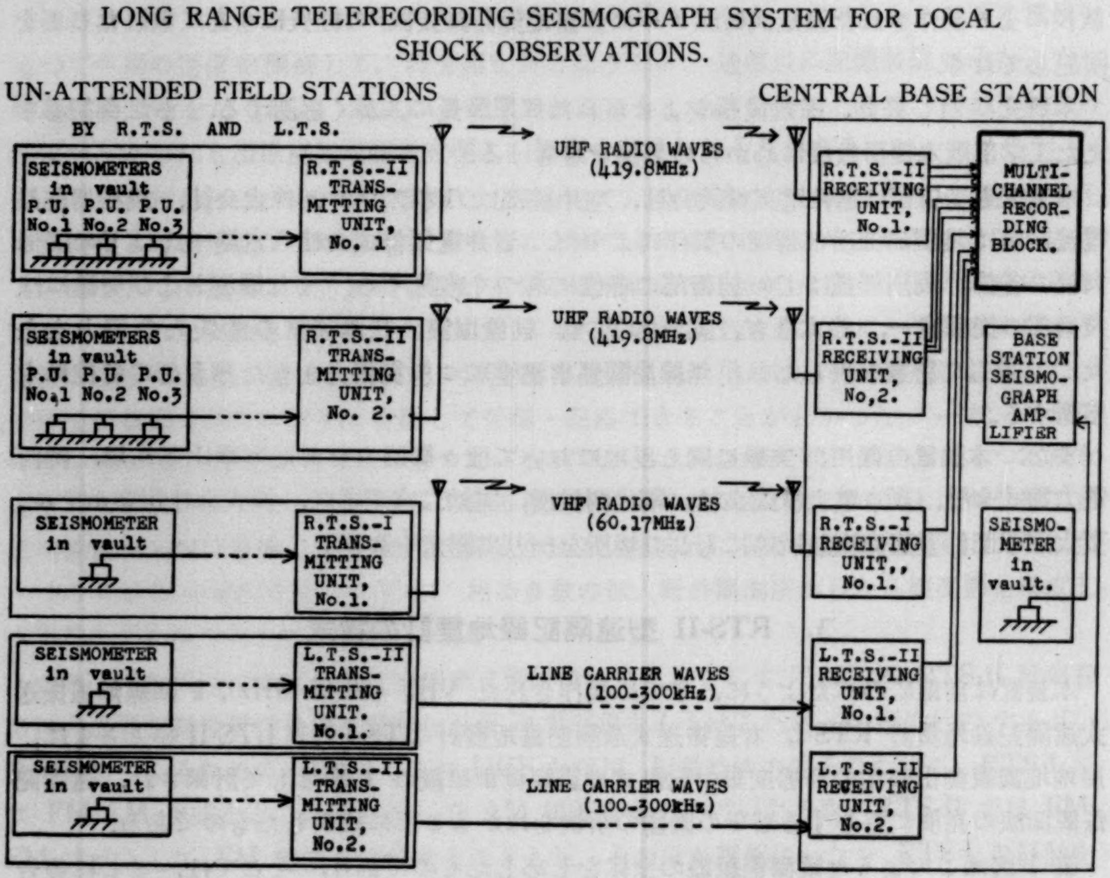

第 1 図 遠隔記録地震計による地震観測網組織図

4. RTS-II 無人野外観測所装置

4.1. 地震計換振器部 RTS-II の伝送系では現在 3 回線の伝送が可能になつているから，換振器も 3 台をおくことができる．この 3 台としては，同一場所に NS, EW, Z の 3 成分をおくか，ちがつた特性をもつ同一成分のものをおくか，あるいわ適当な距離をへだてたところに，3 角形乃至 1 直線に，同一型式の地震計をおくなど，目的によつていろいろにすることができる．いづれにしても，設置の場所は，特殊の目的をもつ場合をのぞき，できるだけ，自然的，人工的雑震動のすくないところの，堅固な岩盤のうえ，

できれば横坑のおくなどにえらぶことがのぞましい．したがつて，送信装置部のおかれる屋舎とは数 10 m 乃至数 100 m の距離ができるので，ここに当然各回線別の有線連絡をつけなければならなくなる．種々の点からこれには shielded cap-tyre cord のような完全な電気的遮蔽と，つよい力学的強度をもつ線の配線がのぞましい．

換振器としては RTS-I などの場合とおなじく，動線輪型の電磁地震計を使用するようになつている．RTS-II のために今回製作したものは，爆破地震動観測のために田望[7]により考案，製作されていた型のものを，地震研究所技術部において，いくらか改良したものである．外観は第 2 図の写真にしめした．水平動のものはまだできていないので，従来の爆破地震動グループのものを利用した．

この換振器の可動線輪は直径 43.6 mm，高さ 15 m，あつさ 0.2 mm のアクリル樹脂の環状の枠に，直径 0.07 mm のエナメル線を約 2800 回まいてあり，直流抵抗は 1.5～1.8 kΩ である．線輪は板バネを回転軸とし，つるまきばねでつるされた上下動ふりこのおもりのさきにのびたうでに固定され，MK 5 の環状同心磁石の極間にさげられている．この磁界は大約 5500 Gauss である．

ふりこの振動数は 2～10 Hz の範囲で可変であり，田望[8]の考案したように，回路に容量をつなぐことにより若干の周期のばしをすることができる．局地地震観測では大体 3 Hz くらいで使用する．減衰は送信低周波部の入力端子に並列に抵抗があり，これは 5 段きりかえになつており，送信装置のところで適当に減衰をきりかえることができる．普通は約 40 kΩ の抵抗でほぼ臨界制振にちかくしてもちいる．

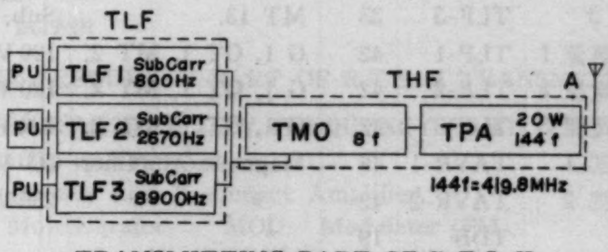

TRANSMITTING PART OF R.T.S.-II.

PU: PICK UP or TRANSDUCER.
TLF: TRANSMITTER LOW FREQUENCY PART. (ELF Amplifiers & Subcarrier Channels)
TLF 1: 1st channel. TLF 2: 2nd channel. TLF 3: 3rd channel.
THF: TRANSMITTER HIGH FREQUENCY PART. (Mixer & UHF FM Transmitter)
TMO: Transmitter Master Oscillator, etc. TPA: Transmitter Power Amplifier.
A: AERIAL.

第 3 図　RTS-II 送信装置主要部の構成

7) N. DEN, Autumn Meeting of the Seism. Soc., Japan at Kyoto, Nov. 2, 1954.
8) N. DEN, Spring Meeting of the Seism. Soc., Japan at Tokyo, May 15, 1956.

4.2. 送信装置部 RTS-II 送信装置の主要部は第 3 図にしめされるように 3 回線の送信低周波部 TLF 1～3，送信高周波部 THF および送信空中線部 TA であり，これに各部の電源および主電源安定装置，配電盤がくわわつて，全体を構成している．空中線部をのぞき，野外観測所の屋舎内に設置される送信装置の使用時の外観は第 4 図の写真でみることができる．各部の接続配線はすべて背面でなされている．

この第 4 図の写真でもわかるように，この装置は出張観測のため，可搬型として 12 個の堅固な筐体にわけられ，各部の接続線類等とともに，それぞれ別々の帆布製のふくろにおさめて運搬できるようになつている．筐体はすべて 500 mm×360 mm×230 mm の同一の形状をもち，約 1.2 mm のあつさの鉄板よりつくられ，運搬時には前面パネルに鉄板のふたをすることができる．重量は第 I 表にあるようにまちまちで，かなりおもい

第 I 表 RTS-II 送受信装置筐体一覧表
(番号 左は 1 号機 右は 2 号機のものをさす．筐体の形状はすべて同一で 50×36×23 cm である．)

番号	名称	略号	重量	真空管等	備考
1,101	送信電力部	TPA	25 kg	MT 1, Special Tube 4.	出力 20 watts 419.8±0.02 MHz
2,102	送信発振部	TMO	22	MT 10.	最大周波数偏移 ±160 kHz 逓倍数 ×144.
3,103	送信高周波部電源	THP	45	G 3.	380 VA
4,104	送信低周波部 1	TLF-1	33	MT 13.	Sub. Car. 800±160 Hz
5,105	送信低周波部 2	TLF-2	23	MT 13.	Sub. Car. 2760±550 Hz
6,106	送信低周波部 3	TLF-3	23	MT 13.	Sub. Car. 8900±1800 Hz
7,107	送信低周波部電源 1	TLP-1	42	G 1, GT 1, MT 2.	120 VA
8,108	送信低周波部電源 2	TLP-2	42	G 1, GT 1, MT 2.	120 VA
9,109	送信低周波部電源 3	TLP-3	42	G 1, GT 1, MT 2.	120 VA
10,110	送信電源安定部 1	TAVR-1	48	Magnetic Amplifier	500 VA(380+120)
11.111	送信電源安定部 2	TAVR-2	42	〃 〃	250 VA(120+120)
12,112	送信配電盤部	TDB	19		
51,151	受信高周波部	RHF	23	MT 10.	1st IF 25 MHz
52,152	受信中間周波部	RIF	22	MT 12.	2nd IF 6.55 MHz
53,153	受信高周波部電源	RHP	28	G 1.	150 VA
54,154	受信低周波部 1	RLF-1	22	MT 10.	
55,155	受信低周波部 2	RLF-2	22	MT 10.	
56,156	受信低周波部 3	RLF-3	22	MT 10.	
57,157	受信低周波部電源 1	RLP-1	37	G 1.	100 VA
58,158	受信低周波部電源 2	RLP-2	37	G 11.	100 VA
59,159	受信低周波部電源 3	RLP-3	37	G 1.	100 VA
60,160	受信電源安定部 1	RAVR-1	40	Magnetic Amplifier	250 VA(150+100)
61,161	受信電源安定部 2	RAVR-2	40	〃 〃	250 VA(100+100)
62,162	受信配電盤部	RDB	19		

ものもあるが，人力で短距離の運搬は可能である．貨車，トラック等の輸送では大体真空管等もそのままで支障ないようである．

送信装置部にはこのほか観測中一定時間ごとに数秒間地震計入力と並列に各回線に対しくわえられる一定電圧の**超低周波試験発振器**が附属している．

設置および撤収等の場合には，このほか，連絡通話用の超短波無線電話装置 (149.49 MHz)，各種測定器，工具類が使用されるが，これらについては，ここでは記述を省略する．つぎに各部別にその構造を説明しよう．

4.2.1 送信低周波部 TLF 各回線ごとにもうけられ，TLF-1, TLF-2, TLF-3 となづけられ，それぞれは，**超低周波部**と**副搬送周波部**とにわけられる．第 5 図に構成の大要をしめす．**超低周波部**は換振器部から地震動によつて生じた超低周波 ELF* 振動電圧をうけこれを増幅する部分であり，第 5 図にしめすように，6AU6 3 段，6C4, 12AU7 からなる超低周波増幅器である．6C4 には電磁オッシログラフにより記録できる端子をもうけ，必要に応じ送信点で地震動の増幅波形を監視乃至記録できるようになつている．

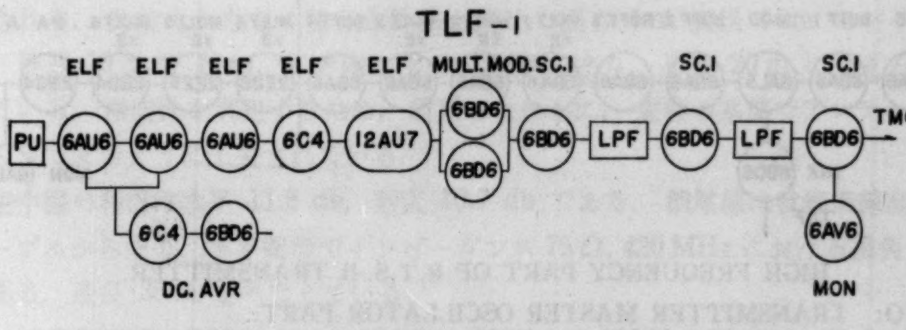

LOW FREQUENCY PART OF R.T.S.-II TRANSMITTER.

TLF-1: TRANSMITTER LOW FREQUENCY PART FOR 1st CHANNEL
PU: Pick Up or Transducer.
ELF: Extremely Low Frequency Amplifier.
MULT: Multivibrator. MOD: Modulater (FM).
SC: Subcarrier Amplifier. TMO: See Fig. 6.
LPF: Low Pass Filter. (for 1st channel) To be replaced by band pass filter, BPF, or high pass filter, HPF, for 2nd or 3rd channel respectively.

第 5 図 RTS-II 送信低周波部構成図 (第 1 回線に対応するもののみをしめす．第2，第 3 回線に対するものでは，濾波器がそれぞれ帯域濾波器，高域濾波器となる，他はまつたく同様である.)

副搬送周波部は 6BD6 2 本より構成される Multivibrator で副搬送周波矩形波を発振し，これに前段の 12AU7 の出力を cathode flower でとりだして C-R 結合でくわえ，地震動の波形に応じた周波数変調 (正確には矩形波幅変調) をおこなう．この出

* ELF (Extremely Low Frequency) とは 3～30 Hz の電気振動をさす．30～300 Hz を SLF，300～3000 Hz を ULF とすると，VLF 3～30 kHz にはじまる国際電気通信条約附属無線規則周波数呼称に接続する．前報告[1,2]で VLF としたのは ELF とすべきであつた．訂正しておく．

力は次段の 6BD6 および濾波器 2 段で正弦波になおされ，混合器（便宜上送信高周波部にいれてある）の入力となる．第 1，第 2，第 3 の各回線の副搬送波中心周波数は 800 Hz, 2670 Hz, 8900 Hz であり，各回線ごとに上記周波数変調をおこなう．濾波器は第 1，第 2，および第 3 各回線に対し，それぞれ低域，帯域および高域濾波器をもちいる．それぞれの cut off 周波数は 1000 Hz, 2670±600 Hz, 6660 Hz に設計した．副搬送波の変調特性は，第 2 報にしめすが，大体各回線とも変調指数 m=5 以上をとるように設計した．

4.2.2 送信高周波部 THF 送信低周波部各回線の副搬送波出力が混合器 MIX にくわえられ，これを第 6 図の系統にしたがつて，UHF 出力として空中線 A におくりだす部分であり，水晶制御位相変調方式超短波送信機というべきものである．筐体としては混合器，主発振器，緩衝器，変調器，逓倍器をふくむ**送信主発振部** TMO と，逓倍器，励振，出力器をふくむ**送信電力部** TPA の 2 体からなつている．

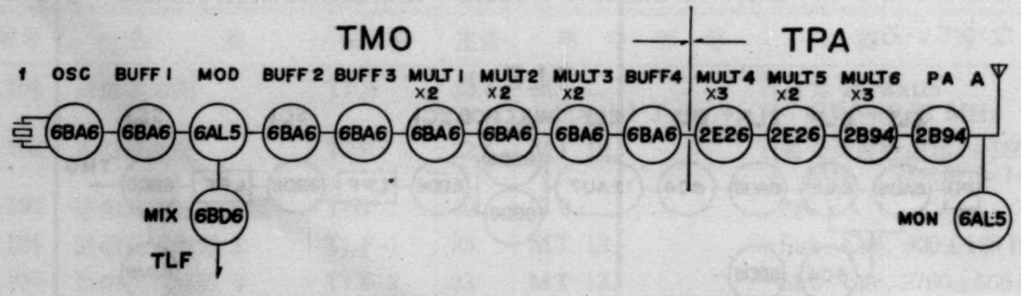

HIGH FREQUENCY PART OF R.T.S.-II TRANSMITTER.

TMO: TRANSMITTER MASTER OSCILLATOR PART.
OSC: Oscillator. (f=419.8/144 MHz) BUFF: Buffer. MIX: Mixer.
MOD: Modulator. (FM) MULT: Multiplier.
TPA: TRANSMITTER POWER AMPLIFIER PART.
MULT: Multiplier. PA: Power Amplifier. MON: Monitor.
A: AERIAL. TLF: TRANSMITTER LOW FREQUENCY PART.

第 6 図 RTS-II 送信高周波部構成図

主発振部 TMO では，まづ 6BA6 でわりあて周波数 419.8 MHz の 1/144 の基本周波数（約 2.915 MHz）をもつ主発振水晶により発振をおこない，これを緩衝増幅器をへて広帯域位相変調器にあたえる．ここで混合器からの 3 回線の副搬送波がこの主搬送波位相変調（広義の周波数変調）をおこなうことになる．こうして変調された主発振器よりの被変調波は，3 段の逓倍器によりまづ ×2×2×2=8 逓倍される．つぎに**電力部** TPA のはじめで，さらに ×3×2=6 逓倍，つまり 48 逓倍されて 2B94 にはいる．この部分で，さらに 3 逓倍して 144 逓倍を完成し，419.8 MHz の搬送波として電力増幅管 2B94 を励振し，ここで出力 20 watts として空中線にあたえられる．この終段の励振管および電力管の同調器としては平行線同調器を使用，この段の加熱防止にはシロッコ型送風器による強制空冷をおこなつている．またこの部分には B-電

圧の低下装置をつけて，必要に応じ，送信出力を 12.5 乃至 5 watts にさげて使用することもできるようにしてある．これは同一周波数の 2 局の同時受信に際し，受信電界の調整を必要とするからであり，またこれにより，過大な受信電界がえられる場合は，送信電力を低下して真空管寿命の延長をはかることもできるのである．

電気的性能についての詳細は第 2 報にゆずりたいが，設計規格の要点をのべると，周波数の許容偏差は ±0.005% 以内であり，419.8±0.02 MHz になる．変調による最大周波数偏移は ±160 kHz をとつてある．これは本装置を 3 回線にとどまらず，さらに多重回線のものに発展させる可能性を考慮したためであり，現在の偏移は副搬送波 11 kHz とみて 120 kHz 程度である．

4.2.3　送信空中線部 TA　さきにのべたように，偏波性と指向性とによる同一周波数電波の分離受信をおこなうため，今回製作された 2 組の RTS-II 装置では，第 1 号装置には水平 8 素子 1/2 波長指向性八木空中線，第 2 号装置には垂直複合 5 素子 1/2 波長指向性八木空中線を採用した．第 7 図は使用状態における送信空中線の外観をしめす写真である．可搬型とするため，軽合金製組立式になつており，携帯用カバンに格納される．支柱もおなじく軽合金製組立式で，長さ 1 m 直径 4 cm のパイプからなり，最高 10 本で 10 m，3 方向に 2 段の張綱ではり，風速 20 m にたえるようになつている．指向性を利用するため，設置したのちに，支柱の基部でアンテナを回転させ固定できるように工夫されている．

空中線の利得は水平 11.8 db，垂直 10.7 db である．饋電線は軟銅撚線高周波同軸ケーブルからなり，不平衡型でインピーダンス 75 Ω，420 MHz における損失 0.1 db/m である．最長 35 m をそなえている．

4.2.4　送信電源部　電源はすべて市用交流 50/60 c/s，100 V からとり，第 8 図にしめすように，2 個の交流定電圧装置 AVR をへて送信高周波部電源 THP，および送信低周波部電源 TLP 1～3 に供給される．

交流定電圧装置は入力一次側に周波数補償をおこなつてある磁気増幅器型定電圧装置* であり，これによつて 46～51 乃至 56～61 c/s において，75～115 V の入力を 100±1V におさえることができる．RTS-II 送信装置の総消費電力は約 800 VA であり，上述の安定装置は 500 VA および 250 VA 容量のもの各 1 個をそなえてある．

送信低周波部電源装置は各回線用低周波部それぞれに 1 つづつもうけられ，A-電源はセレン整流器と附加装置により直流を供給，B-電源の 2 次側高圧には第 8 図にしめすように真空管式定電圧装置による電圧安定化をはかつてある．各 120 VA 計 360 VA を消費する．

送信高周波部電源装置は約 400 VA を要する．

4.2.5　送信配電盤部　ここには使用時の総電流をしめすメーターと過負荷継電器を装備し，送信部のどこかに故障を生じて過大電流がながれたとき，自動的に電源スイッチ

* 電設機器株式会社製 MELS 型

を遮断し，事故の拡大をふせぐようになつている.

各部電源にも過負荷継電器を装備してあるが，特に送信管冷却用送風器の停止の場合にも電源を遮断して，真空管を保護するようにしてある.

また各部の使用真空管にはすべて check point をつけ，切換器により，メーターの指示として検出できるようになつている.

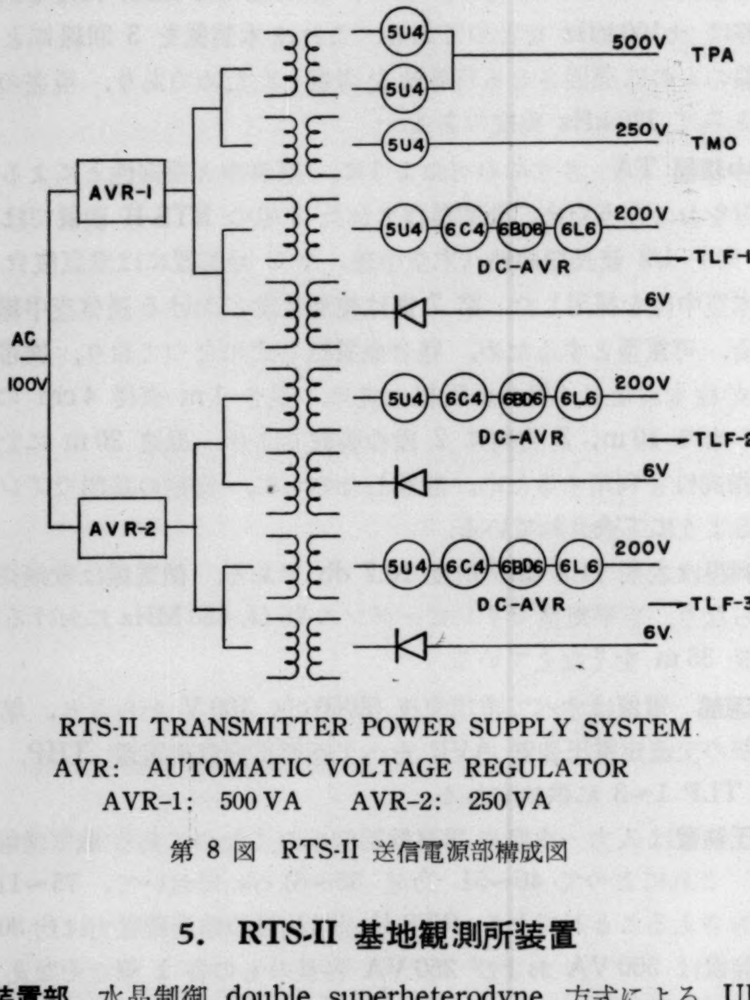

RTS-II TRANSMITTER POWER SUPPLY SYSTEM
AVR: AUTOMATIC VOLTAGE REGULATOR
AVR-1: 500 VA AVR-2: 250 VA

第 8 図 RTS-II 送信電源部構成図

5. RTS-II 基地観測所装置

5.1. 受信装置部 水晶制御 double superheterodyne 方式による UHF, FM 受信機を主体とするもので，受信空中線部 RA，受信高周波部 RHF，および受信低周波部 RLF からなる主要部と，これらに対する電源装置部および配電盤部とからなつている.

主要部構成の概要は第 9 図にしめした. 第 1 図の組織図でみたように，各無人野外観測所に対応する受信装置はすべて一ヵ所におかれるのであつて，第 10 図は基地屋舎の屋上に並置された受信空中線をしめし，第 11 図は RTS-II 受信部装置 2 組がならべられている実況をしめす写真である.

5.1.1 受信空中線部 RA 送信空中線に対応して 1 号機には水平 8 素子八木空中線，2 号機には垂直複合 5 素子八木空中線をもちいている. 構造，性能等はまつたく送信空

中線部と同様であるから，特に再説しないことにする．

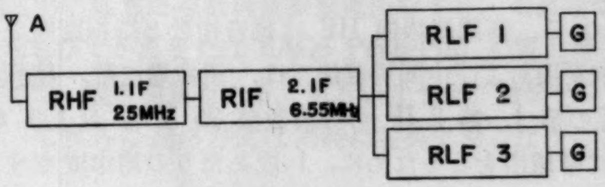

RECEIVING PART OF R.T.S.-II.

A: AERIAL.
RHF: RECEIVER HIGH FREQUENCY PART. (1st IF: 25 MHz)
RIF: RECEIVER INTERMEDIATE FREQUENCY PART. (2nd IF: 6.55 MHz)
RLF: RECEIVER LOW FREQUENCY PART. (1st, 2nd, & 3rd channel)
G: RECORDING GALVANOMETER.

第 9 図　RTS-II 受信装置主要部構成図

5.12 受信高周波部 RHF　受信部の主体をなし狭義の**受信高周波部** RHF と**受信中間周波部** RIF の 2 筐体からなつている．第 12 図にその構成をしめす．前述のごとく，水晶制御 2 重スーパーヘテロダイン方式周波数変調受信機で第 1 中間周波数 25 MHz，第 2 中間周波数 6.55 MHz にとつてある．

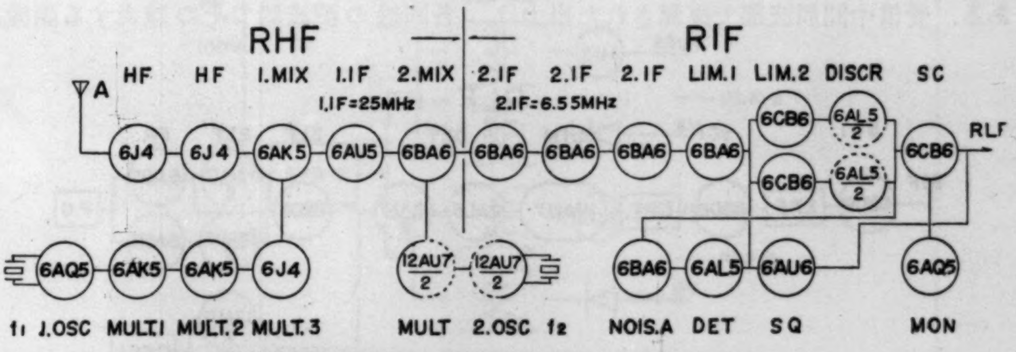

HIGH FREQUENCY PART OF R.T.S.-II RECEIVER.

RHF: RECEIVER HIGH FREQUENCY PART.　A: AERIAL.
HF: High Frequency Amplifier.
1st OSC: 1st Oscillator ($f=\overline{419.8-25}/54=7.31$ MHz)
RIF: RECEIVER INTERMEDIATE FREQUENCY PART.
IF: Intermediate Frequency Amplifier.
2nd OSC: 2nd Oscillator ($f=\overline{25-6.55}/3=6.15$ MHz)
MIX: Mixer.　LIM: Limiter.　DISCR: Discriminator.
MON: Monitor.　SC: Subcarrier Amplifier.　NOIS A: Noise Amplifier.
DET: Noise Detector.　SQ: Squelch.　RLF: see Fig. 13.

第 12 図　RTS-II 受信高周波部構成図

第 12 図にしたがつて，機能の概要を説明する．まづ，受信空中線からはいつた電波は同軸同調器をへて高周波増幅管 HF のカソードにくわえられる．入力回路は制御格

子を接地した反転型回路で，インピーダンス変換をおこなつてのち増幅するという，いわゆる Wallman circuit を採用している．この入力回路の初段真空管で 8～10 db の雑音指数がえられる．高周波増幅 HF は雑音指数と撰択度向上のため 2 段とつている．つぎに周波数変換および中間周波段では．鏡像周波数，撰択度および帯域幅の関係を考慮して上述の第 1，第 2 IF の周波数値 25 MHz および 6.55 MHz を決定した．第 2 IF では帯域巾をとるために，1 段あたりの増巾度をすくなくし，段数をふやした．これにより撰択度も向上した．

こうしてえられた中間周波振動は第 1，第 2 の振巾制限器 LIM 1, LIM 2 をへて，周波数弁別器 DISCR にあたえられ，振巾一定の中間周波からの周波数に比例した副搬送周波の振動がえられる．こうして復調された副搬送波が各回線別の低周波部にいれられるのである．

なお，この第 2 制限器と周波数弁別器の回路には雑音制御のための Squelch 回路がつけられていることは第 12 図にみるとおりである．

5.1.3 受信低周波部 RLF この部は第 10 図にしめすように各回線別に RLF 1, RLF 2, RLF 3 となつており，それぞれの構成は第 13 図にしめした第 1 回線低周波部 TLF-1 で代表される．ただ濾波器が第 1，第 2，第 3 回線でそれぞれ低域・帯域，高域沪波器となつている点がちがうだけである．濾波器の性質は送信低周波部のものと同様である．受信中間周波部で復調された出力は，各回線の沪波器でその該当する副搬送周

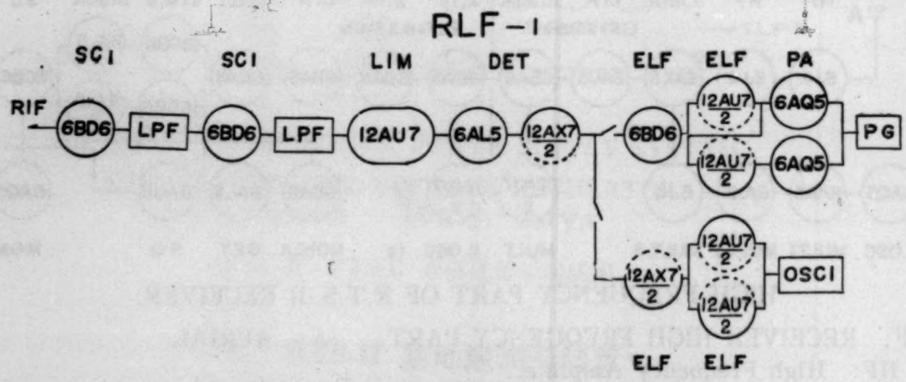

LOW FREQUENCY PART OF R.T.S.-II RECEIVER.

RLF-1: RECEIVER LOW FREQUENCY PART FOR 1-st CHANNEL.
SC 1: Subcarrier for the 1st channel.
LPF: Low Pass Filter. (for 1st channel) To be replaced by band pass filter, BPF, and high pass filter, HPF, for the 2nd and 3rd channel respectively.
LIM: Limiter. DET: Detector. ELF: ELF Amplifier.
PA: Power Amplifier. OSCI: Electro-magnetic Oscillograph.
PG: Pen-writer Galvanometer. RIF: see Fig. 12.

第 13 図 RTS-II 受信低周波部構成図（第 1 回線に対するものをしめす，第 2，第 3 回線に対するものも沪波器がちがうほかは全然同様である.）

波のものだけとなり，つぎに制限器 LIM を通じて矩形波をえ，これを復調 (FM 検波) して，地震動入力に応じた超低周波振動電圧をうる．これを電圧増巾ののち電磁オッシログラフにみちびくか，または 6AQ5 Push-Pull の電力増巾をおこない，ペンがき電流計をふらせて，地震記象をえる．あるいはまた，磁気テープ式記録装置[6]につなぐこともできる．これらの記録方式は同時に並列におこなうこともできるようになつている．

5.1.4 受信電源部 受信装置もまたすべて市用交流 100 V，50/60 c/s で使用され，送信部装置と同様の**磁気増幅器型定電圧装置**をそなえている．消費総電力は 1 局あたり 500 VA であり，250 VA のもの 2 台が装備されている．

受信高周波部電源は約 150 VA を消費し，水晶発振部の B-電圧に対し，放電管による安定化をはかつている．

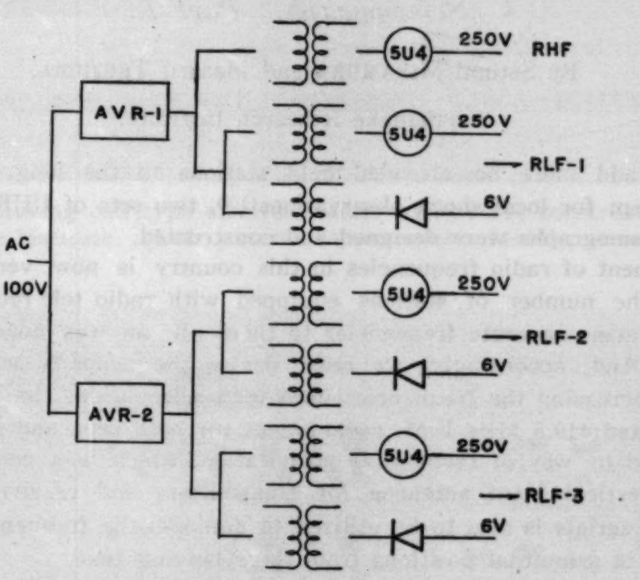

RTS-II RECEIVER POWER SUPPLY SYSTEM.
AVR: AUTOMATIC VOLTAGE REGULATOR.
AVR–1, AVR–2: 250 VA
第 14 図 RTS-II 受信電源部構成図

受信低周波部電源は各回線ごとにもうけられ，それぞれ約 100 VA を消費する．A-電源は送信低周波部電源の場合と同様である．第 14 図にはこの受信電源部構成の大要をしめした．

5.1.5 受信配電盤部 送信配電盤部と大体同様である．

5.2. 記録装置部 集中記録用多重記録装置としては，遅延式多重磁気テープ記録装置がもつともすすんだものである．これについては，別に報告されるので[6]，ここにはふれない．しかし，普通の記録円筒ですすがきまたはペンがきによつても，同一時計による秒刻時をすべての回線に重畳し，記録紙速度を相当はやくするならば，局地地震観測と

して必要な 1/50～1/100 秒程度の時間精度をえることは容易である．われわれは現在記録紙を 1 日 2 回とりかえて，4 mm/sec の記録紙速度で観測している．

記録用の電流計としては，従来使用してきた三栄測器ペンがきオッシログラフの電流計を改良したもの 6 台を本装置用として本所技術部において試作して使用した．

電流計の自己振動数 30 Hz, 線輪の直流抵抗約 2 kΩ, 電流感度約 1 mm/mA である．

記録装置部の実際の状況は第 15 図の写真でうかがえる．またえられた記録の一例は第 16 図の複写にしめしておいた．

---

20. *UHF Multi-channel Radio Tele-recording Seismograph. Part I.*

By Setumi MIYAMURA and Masaru TSUJIURA,

Earthquake Research Institute.

In order to add more non-attended field stations to the long range tele-recording seismograph system for local shock observations[1),2)], two sets of UHF multi-channel radio tele-recording seismographs were designed and constructed.

As the allotment of radio frequencies in this country is now very rigid, we cannot easily increase the number of stations equipped with radio tele-recording seismographs (RTS), assigning many separate frequencies to them all, as was done in Johannesbourg, South Africa[4)]. And, accordingly, we must devise the means to set up the RTS equipments, without increasing the frequencies used for transmission. In the new equipment, RTS-II, we adopted 419.8 MHz F.M. radio waves for both sets, and separate receiving at base was executed by way of radio wave polarization, which was accomplished by using horizontal and vertical YAGI antennae for transmitters and receivers. The directional character of the aerials is also to be utilized to diminish the frequency allotment, setting the field stations in azimuthal positions from the receiving base.

Multi-channel transmission of seismic signals, which is another necessary requirement for the tele-recording system, was effectuated by using frequency separation of F.M. subcarriers. And, at present, the writers constructed two 3-channel sets of equipment, with the subcarriers of 800, 2670 and 8900 Hz in frequencies, being modulated by three different out-puts of seismic transducers.

Construction and performance of the new apparatus, RTS-II, are described here in Part I and the experimental data showing characteristics of the equipment will be presented in Part II.

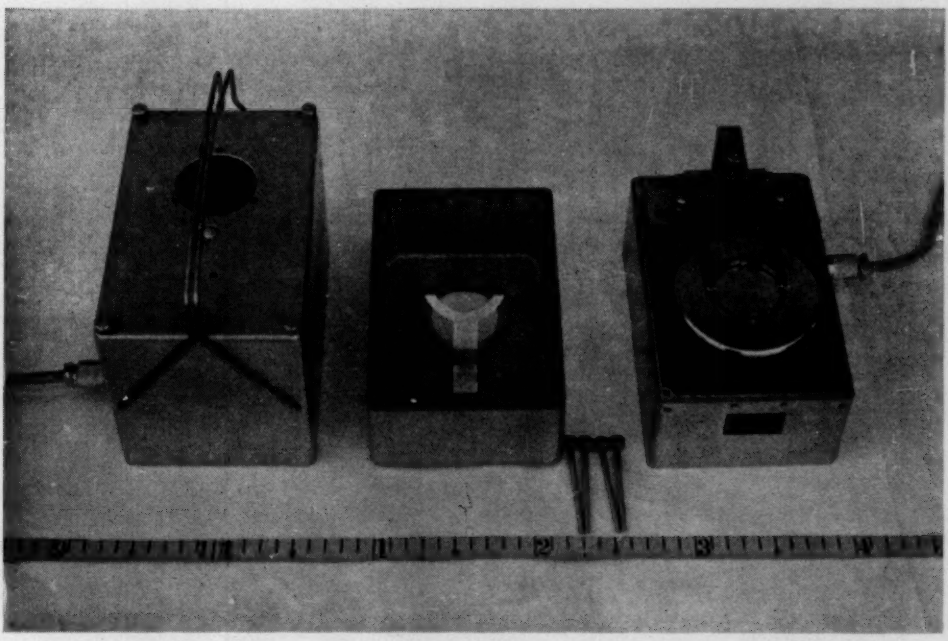

Fig. 2. Moving coil type electrodynamic transducers constructed by Technical Division of the Institute. (Left, external appearance. Middle, cover. Right, inner appearance.

C→

A→

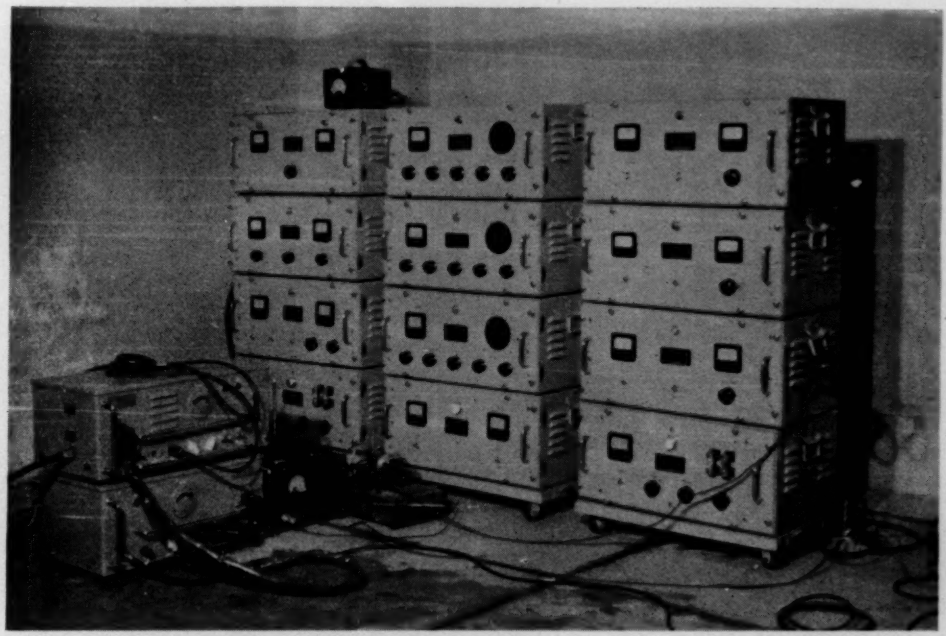

↑
B

Fig. 4. Field set-up of RTS-II transmitting unit. (In the tower of Hotel Kawana, 49 km apart from the base station at Aburatubo over the Sagami Bay.) A: VHF (149.49 MHz) Wireless Telephone. B: ELF Test-oscillator and timer. C: Antenna Dummy.

（震研彙報 第三十五号 図版 宮村・辻浦）

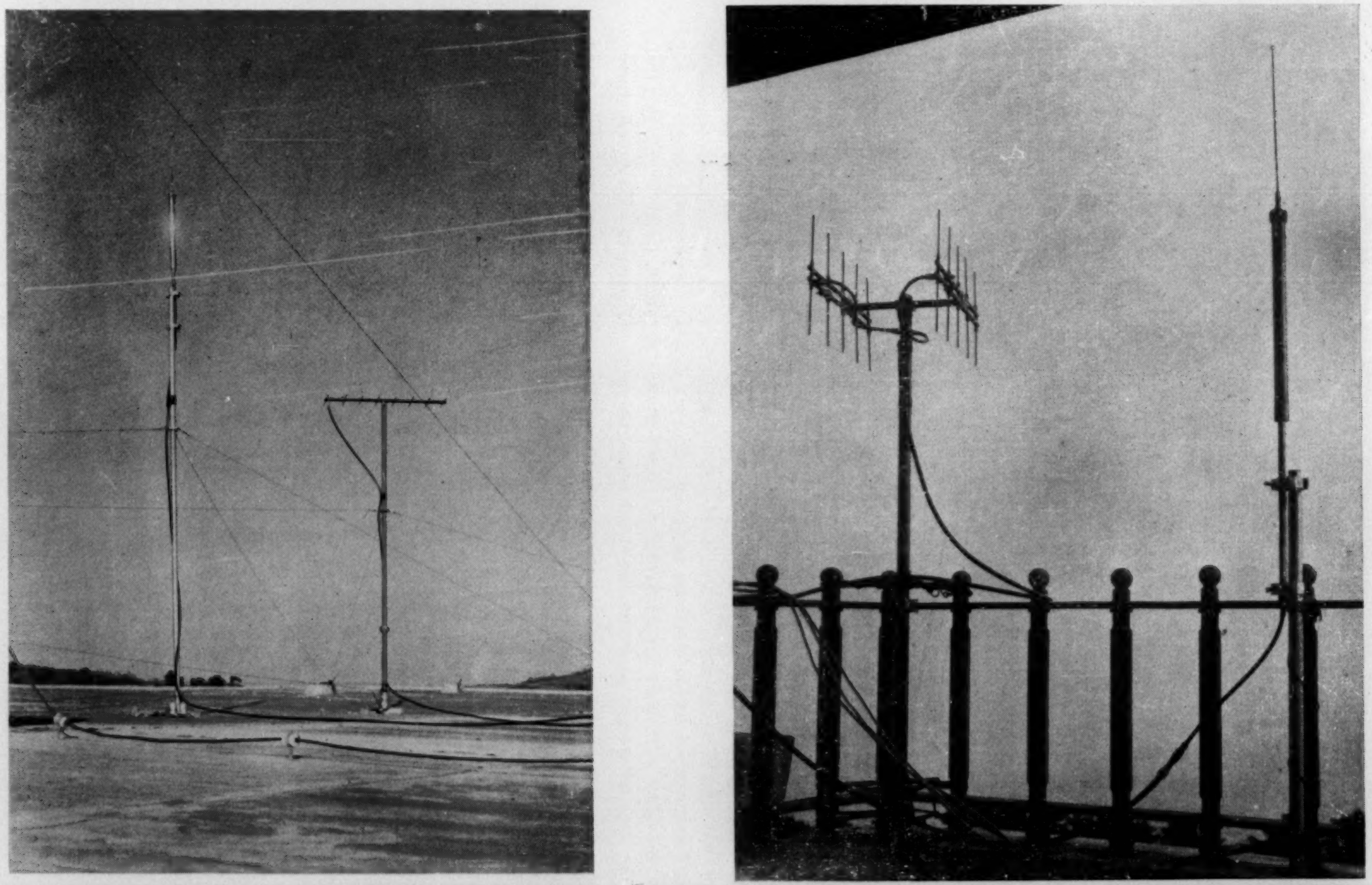

↑C ↑A ↑B ↑C

Fig. 7. Transmitting aerials of RTS-II in operation. A: Horizontal 8-elements YAGI, installed on the roof of the transformer station of Japan National Railway at Ninomiya, 35 km apart from the base at Aburatubo. B: Vertical double-stacked 5-elements YAGI, installed in the tower of Hotel Kawana, 49 km apart from Aburatubo. C: Slive antenna for VHF wireless telephone.

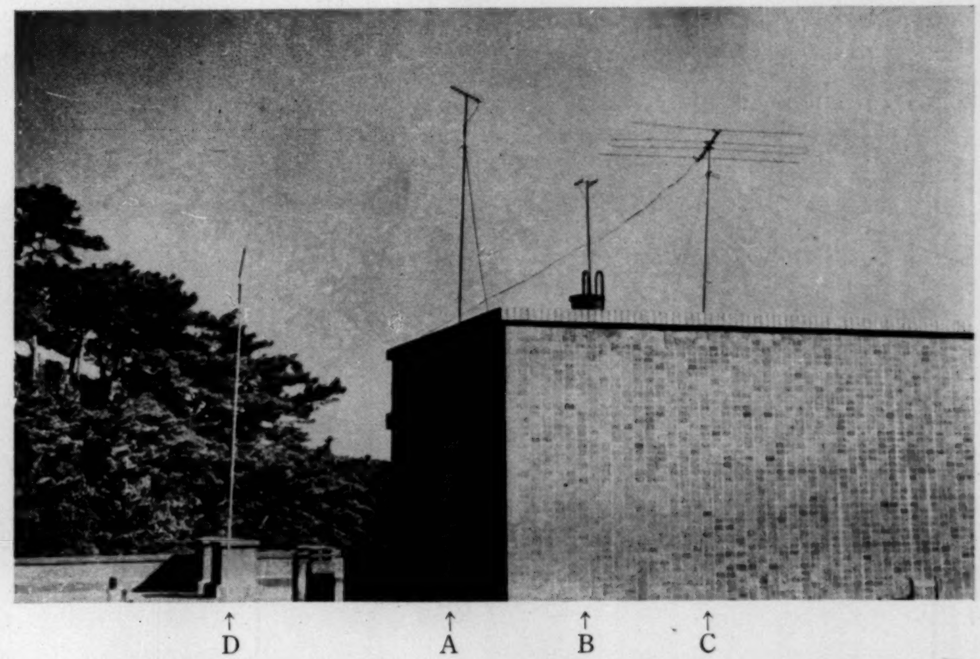

Fig. 10. Receiving aerials of R.T.S. at base. (On the roof of the Marine Biological Laboratory, Aburatubo.) A: Horizontal 8-elements YAGI for RTS-II No. 1 from Ninomiya. (D=35 km), B: Vertical double-stacked 5-elements YAGI for RTS-II No. 2 from Kawana (D=49 km), C: Horizontal 3-elements YAGI for RTS-I from Aziro (D=49 km), D: Slive antenna for VHF wireless telephone.

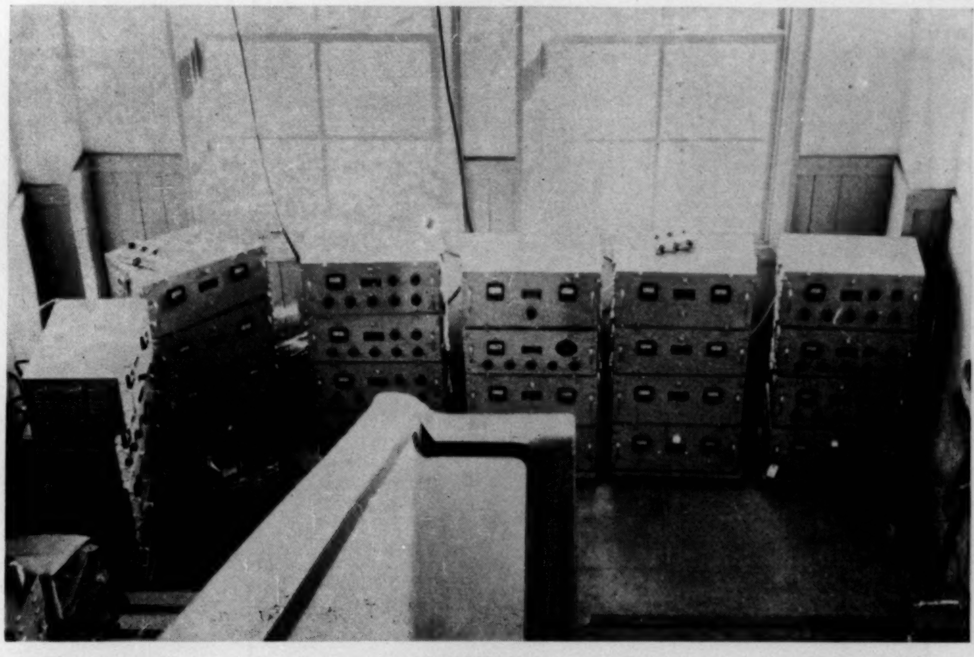

Fig. 11. Two receiving sets of RTS-II in operation at base. (In the Marine Biological Laboratory, Aburatubo.) Left half is Set No. 1 and Right half is Set No. 2.

(震研彙報 第三十五号 図版 宮村・辻浦)

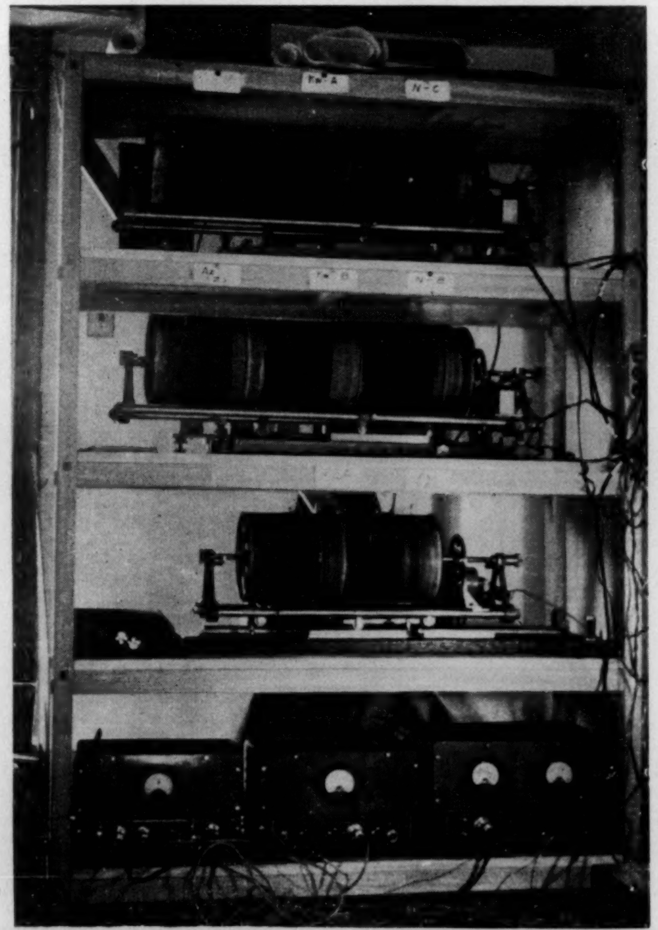

Fig. 15. Multichannel recording block in the central base station at Aburatubo. Galvanometers for visible writing are installed behind the drums. Lowest shelf contains ELF amplifiers for the base station seismometer.

I. 3 station records of a local shock near Wakayama, March 1956.

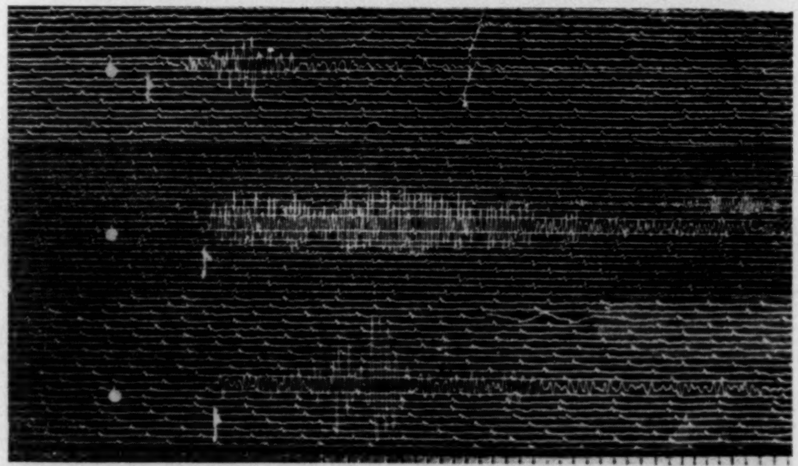

II. 3 channel records of a local shock near Sagami Bay, February 1957.

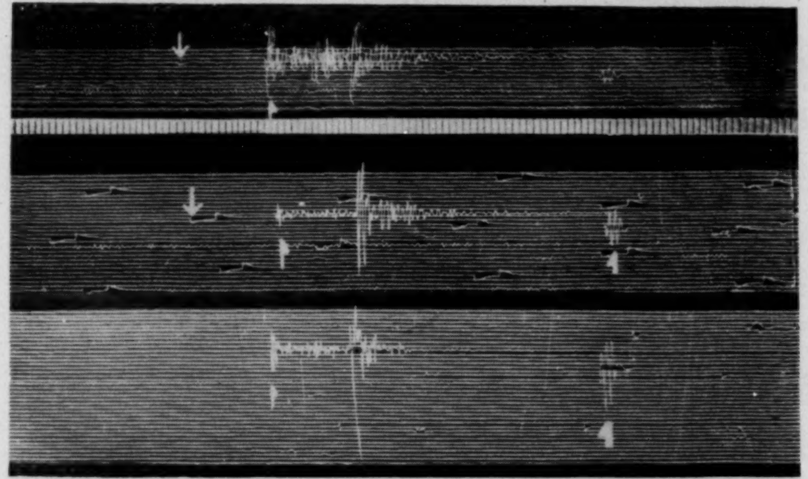

Fig. 16. Seismograms obtained by RTS-II central registrations.

I: A, by base station seismograph. B, by RTS-II No. 1 at Kada, 15 km NW from the base station at Kainan. C, by RTS-II No. 2 at Nokami, 10 km E from Kainan.

II: D, E and F are transmitted through 1st, 2nd and 3rd channels of RTS-II No. 1 from Ninomiya, 35 km NW to the base station at Aburatubo.

21. 浅間火山及びその周辺地域の湧水並びに地下水の研究（第1報）

——蛇堀川溪谷及びその附近の湧水並びに地下水の化学成分——

地震研究所 小坂丈予
村井勇
南英一
津屋弘逵

（昭和32年1月22日発表—昭和32年3月31日受理）

1. まえがき
2. 調査範囲及び測点の状況
3. 測定の順序及び分析方法
4. 分析結果
5. 分類及び総括

1. まえがき

筆者等は地震研究所小諸支所の開設にともない，1955年8月よりほぼ毎月同地に於て湧水並びに地下水の調査，測定をはじめることになつた．最初は十数点の測定を行い，それより月ごとに測定点を増加し，またそのうち数ヶ所は1〜2ヶ月ごとに観測をくりかえして今日に至つた．さらにわれわれが直接現地におもむいて調査測定を行つた資料のほか，その補助的方法として，1956年6月以降，小諸高等学校の生徒に採水を依頼して集めた試料についての分析も行つて，さらに広範囲にわたる湧水並びに地下水研究の予備的資料とした．

現在までにわれわれが現地調査によつて得た観測資料は218，そのうち全分析を行つたもの 42，採水依頼による多数点一斉調査の測点数 239，一部くりかえし調査した点を含めると延 349 資料に達した．

浅間火山の湧水の地球化学的研究としては野口喜三雄氏が1935年同地域の火山ガスの研究とともに多数の湧水，河川水についての水温，pH，湧出量の測定結果の記載を行い，また2,3の湧水の化学組成の変化についても報告したの[1]をはじめ，岩崎岩次氏は翌1936年濁川源泉の化学成分などの研究を発表し[2]，野口氏はその後も引きつづきこれらの湧水の変化の測定を継続して，その結果を発表している[3]．1940年野口氏はさらに多くの湧水，河川水についての調査結果を発表している[4]．また1948, 1949年には西条八束氏により水温，pH などのほか RpH, CO_2, Cl, O_2, SO_4, $KMnO_4$ 消費量，HCO_3, PO_4, NO_2,

1) 野口喜三雄 日化誌 **56** (1935), 1495.
2) 岩崎岩次 日化誌 **57** (1936), 265.
3) 野口喜三雄 日化誌 **57** (1936), 920, **59** (1938), 521.
4) 野口喜三雄 日化誌 **61** (1940), 432.

NH_4, Fe, SO_2, HBO_2 など多数の項目にわたる調査が行われ，その地域的分布についても種々の考察がなされた[5)]．また小平達郎氏は主として同火山の西南麓地域の地下水の水温，pH, Cl についてきわめて多くの測定を行つて，同地区の汚染の状態なども考究した[6)]．また井出義雄氏は同一地域の河川水につき多数の協力者とともに反復測定を行い，その変化状態を報告した[7)]．このほか野口氏はこの附近の火山灰の浸出実験を行い湧水の水質の起源について考察し[8)9)]，湧水中のラドン含量の研究や[10)]，柴田雄次氏らとともに重水に関する研究[11)]をも行つた．

今回は，我々の最近行つた仕事のうち，浅間火山西南側，蛇堀川渓谷沿いに分布する湧水を主とした 31 点の水の全分析の結果を報告する．しかし本地域全般にわたる湧水，地下水の本態を把握するためには，未だその踏査範囲もせまく，測定点数も十分でない．従つて今後更に多くの調査，研究を必要としている次第で，これらの結果だけから深く立ち入つた論議を行うことはさし控え，全分析結果を示して，それらの水質について若干の分類を行い，その 2～3 の特徴を挙げるにとどめることにした．

本研究を実施するにあたり，現地調査に協力を惜しまれなかつた，小諸市役所，美斉津一夫氏，小平達郎氏に深く感謝申し上げる．また地震研究所の那須信治所長，森本良平助教授，佐山守技官，細谷与七氏にも感謝の意を表するものである．

2. 調査範囲並びに測点の状況

蛇堀川は浅間火山の外側外輪山の黒斑山と内側外輪山である前掛山とにかこまれた湯ノ平火口原にその源を発し，湯ノ平南端の牙山の麓，地獄谷より外側外輪山の火口瀬を経て，外輪山西南斜面を流下し，小諸市を経て千曲川に達している（第 1 図参照）．今回の調査の対象となつた湧水及び地下水の現地の状況につき，以下に簡単に説明する．

地獄谷　湯の平南端の蛇堀川が外側外輪山を切る地点は地獄谷とよばれ，現在もなお低温の噴気活動を続けており，谷間には硫化水素ガスの悪臭が一面にたちこめている状態である．渓谷沿いに湧出する水もすべて特異の性質をもち，川底や両岸は，これらの流水中から沈澱してくる各種の物質により，赤，褐，白，黒，黄などさまざまな色を呈している．地獄谷酸性泉とわれわれが呼んでいるもののうち，下流にあるものを 1 号，上流のものを 2 号とした．いずれもその流出孔附近には白色の沈澱物を析出しており，硫化水素臭を相当強く放つている．1 号泉は特にその流出量が少く，且つ天候に左右されて変動しやすい．降雨によりその流出量が変化するばかりでなく，その成分も変化する．

5) 西条八束　東大地理学研究 **1** (1949), 73.
6) 小平達郎　北佐久郡志自然篇 (1955), 287.
7) 井出義雄　北佐久郡志自然篇 (1955), 215.
8) 野口喜三雄　日化誌 **59** (1938), 1225, 1341.
9) 野口喜三雄・川口正雄　日化誌 **61** (1940), 447.
10) 野口喜三雄　日化誌 **60** (1939), 7.
11) Y. Shibata, K. Noguchi, O. Kaneko, *Bull. Chem. Soc. Jap.*, **14** (1939), 247.

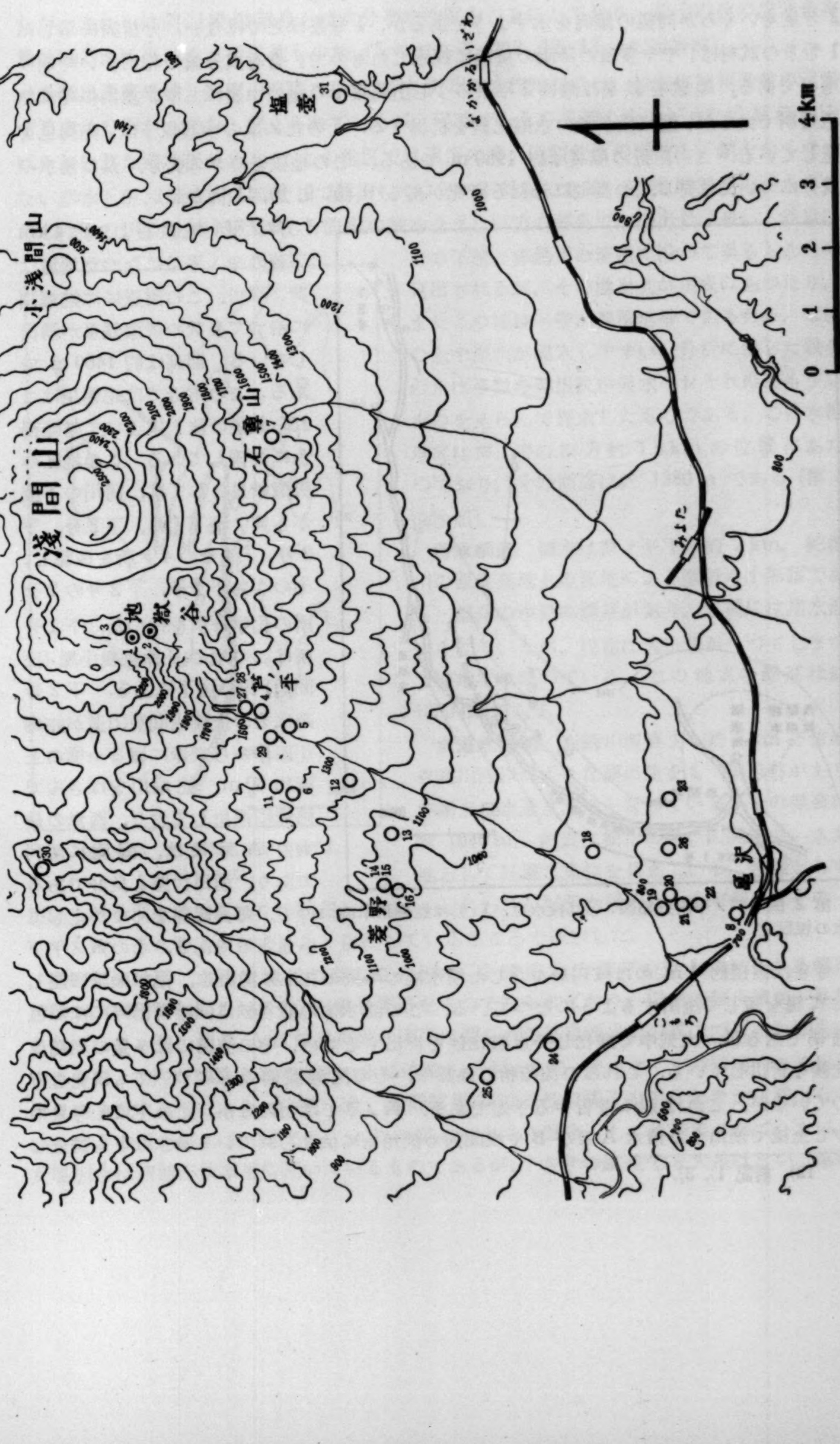

第1図 浅間火山南麓地域（番号は調査地点，第1表参照）.

2号泉もいくらか同様の傾向を示すようであるが，1号泉ほどではない．分析表に示した1号泉の試料は，やや多量の降雨の直後に採水したもので，含有成分量の相当多い時期のものである．地獄谷鉄泉は酸性2号泉の少し上流東岸の崖の中腹にあり，湧出の時は無色透明であるが，湧出後多量の水酸化鉄を析出する．そのため崖の中腹以下は，赤褐色を呈している．この附近の標高は約 1980 m である．この地獄谷のガス成分，及び湧水の成分については野口氏の長期にわたる研究がある[12] (第 9, 10, 11 図参照).

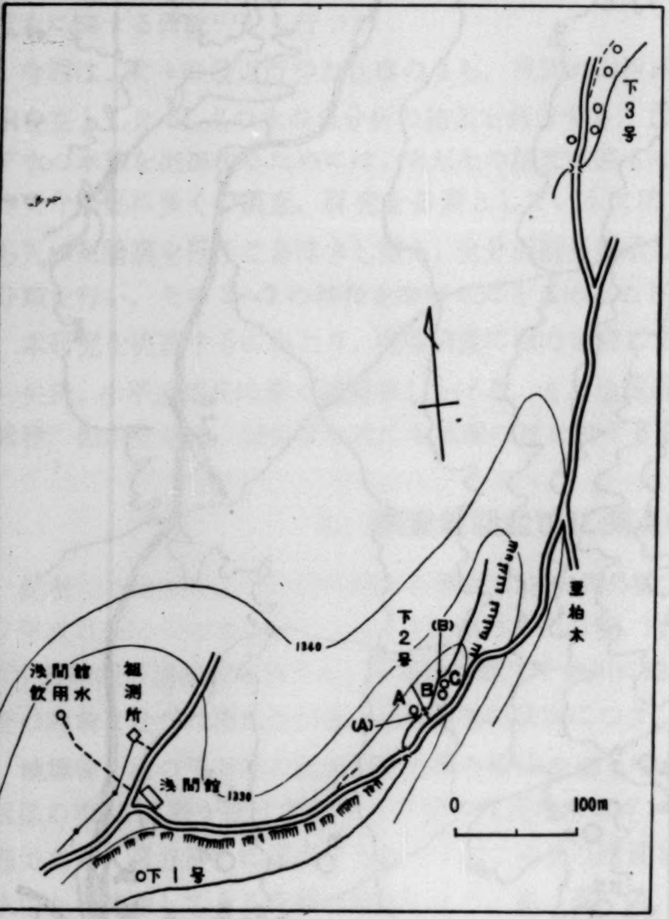

第 2 図　芦ノ平附近略図．○は採水点，（　）は蛇堀川本流水の採取点．

芦ノ平　地獄谷より約 4 km 下流のやゝ平旦になつた地域は芦ノ平で，この附近には蛇堀川に沿つて多数の炭酸鉄泉が湧出している．標高は約 1400 m である．この附近では蛇堀川はこれら鉄泉の流入によつて常時褐色に混濁している．この地区の炭酸鉄泉としては，同川の下流から芦ノ平下1号，下2号，下3号，下4号の4ヶ所を確認し，そのうち下1号，下2号の2ヶ所の化学分析を行つた．下1号泉はこの地の山林監視小屋 (浅間館) 先の崖下にある．下2号泉はその上流浅間登山道が蛇堀川西岸から東岸に渡る土橋の上流約 30 m，蛇堀川をはさんで両岸に湧出しており，西岸の最大の A 号泉は，観測に便利であり，湧出状態も良好であるので，毎月観測をくりかえしているものである．この芦ノ平下2号泉は直径約 1 m のほぼ円形をなした湧水池の中央の孔から湧出し，池の一端に附した木樋を通じて流出するようになつている．この湧水も地獄谷鉄泉同様湧出時には無色透明であるが，大気中で酸化して水酸化鉄を析出するため，その流路には多量の赤褐色沈澱を析出している．これらの沈澱物の性質や，その沈澱機構などについても研究を行つているが，これは別に報告する予定である．芦ノ平ではこのほか，この下2A 号泉の少し上流で湧出する清水 A 及び B や浅間館の飲用水に供せられている清水なども調査し

12) 前記 1), 3).

たが，これらは前記炭酸鉄泉とは大分その性質をことにしており，鉄その他の成分含有量がはるかに小さく，湧出量も少ないものである (第2, 12, 13, 14 図参照).

赤銹川源泉地域　蛇堀川西隣の小溪流赤銹川の水源地区には，以前には褐鉄鉱の沈澱する赤色の沼があつたと伝えられているが，現在でもその名残りをとどめた赤褐色泥土におおわれた湿地帯がある．この地区では濃度の高い炭酸鉄質の湧水と，鉄を全く含まない湧水とが，たがいに接近して湧出しているのが特徴である．赤銹川源泉とよんでいるのはこの川の最奥地点にある前記の鉄を含まない方の湧泉で，湧出量は多い．鉄泉はその下流，赤銹川の流路に沿つて至るところに見出されるが，その湧出孔が川底にあつたり，またこの地域一帯が泥湿地帯であるため，本流の水や泥水が混入しやすい．分析に供した鉄泉の水は多数の湧出孔中泥水のおそれの最も少いものをえらんで採水したものである．この水源地区は芦ノ平の西方約 1.5 km の位置にあたつており，その標高は約 1380 m である (第3図参照).

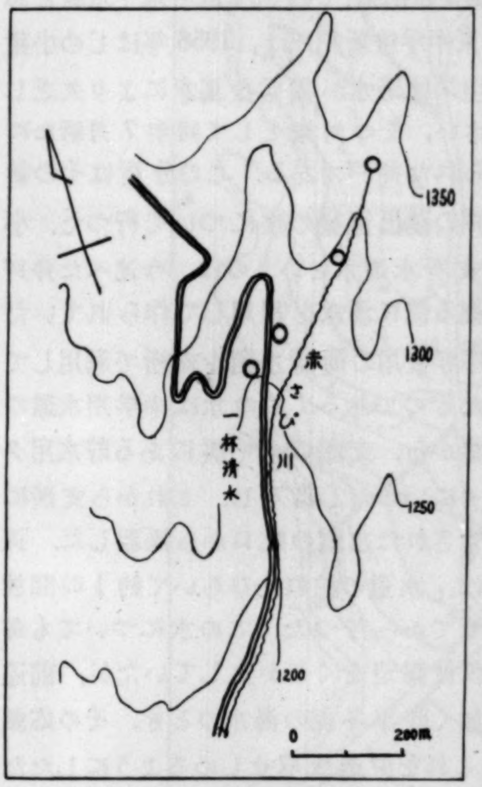

第 3 図　赤銹川源泉附近略図．
○は採水点．

清水部落　清水は芦ノ平下方約 2 km，蛇堀川の西側高地上の窪地にある数軒の小部落である．部落の中央に湧泉があり，以前には用水池になつていたが，現在は湧出量がへつてしまつて湿地状になつている．この地点の標高は約 1230 m である．

水道水源地　赤銹川源泉より約 3 km 下流の赤銹川西岸に大きな湧出量をもつ湧泉群があり小諸市の水道水源地となつている．その標高は約 1040 m，附近は樹木の多い山間部で，水源地として好適な条件を具えている．水源として用いられる湧水は，あたりに散在しており，われわれが試料を採水した本町用水はその一つである．導水管入口の勢いよく自噴しているところで採水した．

菱野鉱泉地区　水道水源地の西方約 0.8 km 小諸市北方菱平の東北隅にあたる標高 1020 m の此の地点は，古くから鉱泉湧出をもつて知られており，現在も鉱泉旅館が経営されている．菱野鉱泉 A は鉱泉旅館の床下に掘られた鉱泉湧出口の真上で採水したものであるが，井戸の構造上この場所の水は停滞しやすいので，そのすぐ下の浴場内の流出孔出口でも採水してこれを A′ とした．菱野鉱泉 B は旅館玄関下の田のわきから湧出している第2の湧水孔の水であるが，これは現在のところ鉱泉としては利用されていない．女堰引水は旅館が炊事用に用いているものであるが，さきの鉱泉水と大差はない (第4

図参照).

石峠部落 小諸市街北方の部落，標高約 850 m，近くには田や畑が多い．この地区のお鷹清水は良好な飲料水として知られ，湧水は農家の庭の半地下式貯水タンクに導入され，ここから更にパイプで附近数戸の家庭に引水されている．採水はこの貯水タンクで行つた.

坂保町震研小諸支所附近 石峠南方約 1 km 小諸市街より東に約 1.5 km，標高約750 m の位置にあたる地震研究所小諸支所附近の水質を調査した．この地域になると湧泉が少ないので一般の井戸水をも調査の対象に加えた．調査の結果，いずれも同一地下水脈と思われる相似た水質をもつていることがわかつた．東中学校新井戸は，1956 年はじめ小諸東中学校用水が異常な渇水により欠乏したさい，その対策として同年 7 月新たに掘られた井戸である．この分析はその新井戸の湧出直後の水について行つた．小諸支所水道水というのは，今述べた井戸を掘る前に湧水を利用して作られていた東中学校用の簡易水道を支所で利用していたものである．この水は中学用水道の水源から，支所のすぐ裏にある貯水用タンクにいつたん導入し，これから支所に配管された水道の蛇口から採取した．採水は，水道の蛇口をひらいて約 1 時間放流してから行つた．この水についても毎月反復測定をくりかえしていたが，前述の如く昨年冬期の渇水のとき，その応急の処置として取入口の周囲に河川水を導入して，これを沪過吸収せしめるようにしたため，1956 年 1 月以後は止むを得ずその測定を中止した．この分析結果はいうまでもなく河川水導入以前のものである (第 5, 17 図参照).

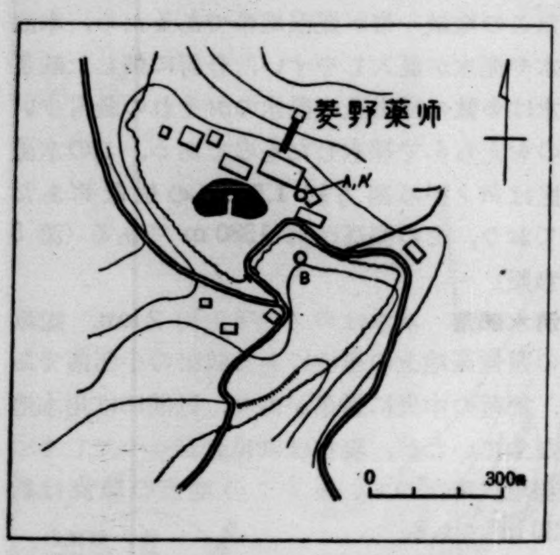

第 4 図 菱野鉱泉附近略図.
○は採水点.

坂保町の高橋氏宅は震研支所のすぐ北隣である．同家の井戸は手押しポンプ式であるので，約 5 分間汲上げた後採水や測定を行つた．支所井戸水というのは，前述の渇水現象以後，支所に於て別個の水源を求めて 1956 年 4 月，あらたに構内に掘られた井戸からその当初にポンプによらずに直接くみ上げられたものである．この井戸はその後次第に濁つてきている．現在は電動ポンプで揚水している.

北大井柏木地区 坂保町地区の東隣にあたり，標高は約 770 m，この部落のうち十数戸の家庭の井戸水は塩素が甚だ多い特異なものである．これらの井戸を各戸ごとにさらに詳細に調査しているが，その原因や理由はまだ明らかでない．これらの異常な井戸の中の 1 つが小山佐一氏方の手押ポンプ式の井戸である (第18図参照).

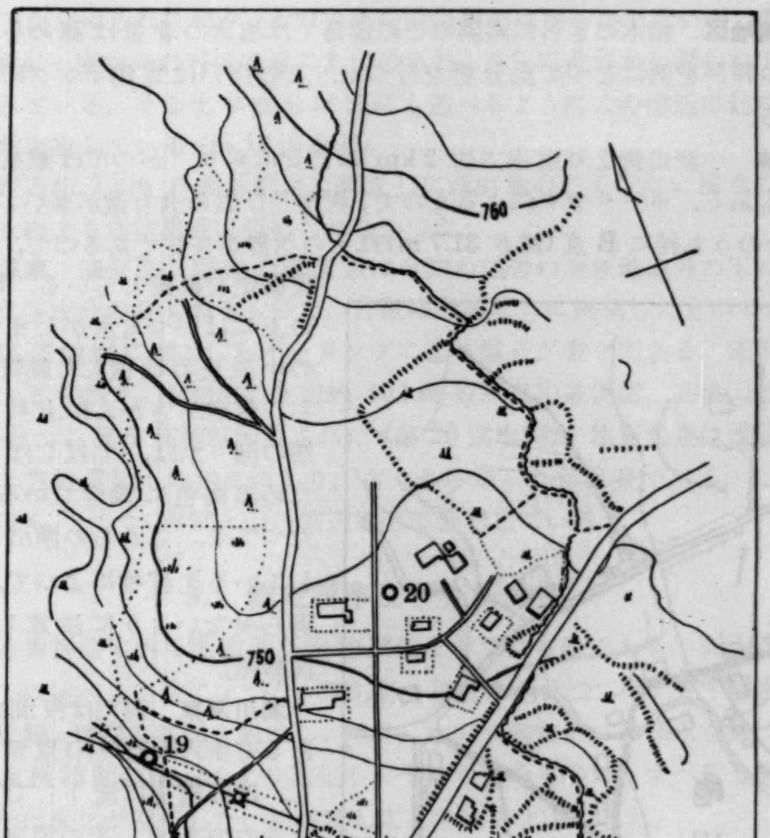

第 5 図　地震研究所小諸支所附近略図．○は採水点，番号は第 1 表参照．

北大井八満地区　柏木のさらに東隣のこの部落では塩素の著量は認められない．美斉津一夫氏方の井戸を例にとつて全分析を行つた．この井戸は電動ポンプによりくみ上げを行つている．

亀沢鉱泉跡　小諸市街より東南方約 2 km の乙女にあり，かつては鉱泉として営業していたこともある．ボーリングによるもので，炭酸及び鉄の含有量が多い．流出孔は現在 3 箇あり，そのうち特に B 点 (深さ 31.7 m) はその状態が良好であるので，ここで毎月反復測定を継続している．B 井の流出孔の上にはいつも水がたまつており，その中央底の堆積した鉄質沈澱物の間から，気泡がさかんに上昇している．上層の溜り水は，しばしば析出沈澱物のため赤褐色に濁つている．採水にあたつては，これらの湧出孔周辺に沈積している沈澱物によつて，さらに水を濁らせないように注意した (第 6, 16 図参照).

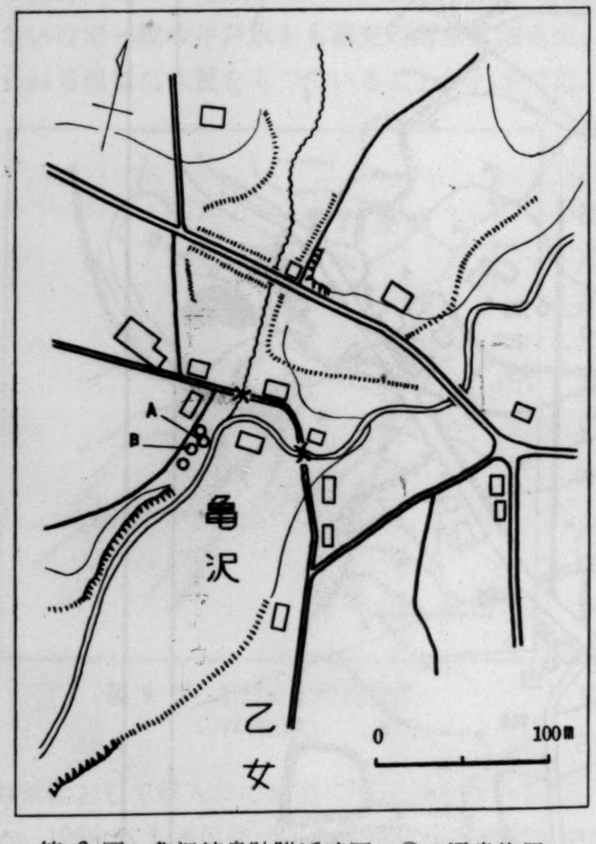

第 6 図　亀沢鉱泉跡附近略図．○は湧泉位置．

濁川源泉　濁川は浅間山火口南方にある寄生火山石尊山東側にその源を発し，ほぼ南方に流下して千曲川に合流するのである．その源泉は湧出量著大な湧泉であつて，水質は芦ノ平，赤銹川などのものと近似した炭酸鉄質泉である．この水質のために，同川はつねに濁つている．またその源泉近くには血の池などの沼や鉄質沈澱物よりなる赤褐色泥土の湿地帯が散在している．濁川源泉 A は源泉群中最大のもので，集塊岩の崖下の木柵をもうけた大きなわれ目から音をたてて大量に湧出している (第 15 図参照)．この湧泉も他の炭酸鉄質湧泉と同様流出後まもなく鉄を遊離析出してくる．この湧泉はその存在が古くから知られて居り，1783 年 (天明 3 年) 噴火の際には，その流出が一時止まつたとも伝えられている．また近年には多くの研究者により度々調査が行われた[13]．濁川の濁りは蛇掘川に比べてさらに一そう甚だしく，下流の信越本線との交叉する点に於ても，なお相当黄濁状態を呈している．

諸地区　小諸市西北方，浅間山の山すその高原丘陵地帯は，その谷合いの各地に，湧泉が存在している．小諸市街地の西北方約 1.5 km の諸弁天の清水はその一つである．湧出

13)　前掲 1), 2), 3), 5), 7).

孔周囲は石垣でかためられており，その天然の湧出状態は明らかでないが，湧出量は甚だ多く，その全量が一度中央の石垣の池にあつめられ，さらにそれから導かれて飲用並びに灌漑用に供されている．その化学成分は後にも述べるようにこの附近の他の湧泉に比較して異つた特徴を有している（第19図参照）．

さらにその西方約 1 km の滝原部落で調査した湧出量のごく少ない清水の例では，前記諸弁天の清水のような特異性は認められなかつた．

深沢，塩壺温泉 深沢及び塩壷の両温泉は今回の報告の対象地域外のものであるが，その性質及び化学成分の全く異るもので，比較のためここに掲載したものである．

浅間火山の周辺地域にはこれらボーリングによる温泉が数ケ所ある．深沢温泉はごく最近の開発によるもので，小諸市の北方約 10 km の深沢川最奥部，高峰山頂の北西に位置し，1956 年秋から温泉旅館が開設された（第 20 図参照）．塩壷温泉は浅間山東南麓，中軽井沢駅の北方約 2 km の地点にあり，古くから知られた温泉である．このほか星野，鹿沢等の温泉も，すべて浅間火山の周辺地区に分布している．

3. 測定順序及び分析方法

今回報告する資料はすべて筆者等が実地調査を行つたものである．測定及び分析については概ね以下に述べる方法によつた．即ち野外調査にあたつては，先ず採水の現地に於いて，湧水の状態，周囲の状況を観察し，気温，水温の測定並びに採水を行つた．また次の各成分は採水後時間の経過により変化のおそれのあるもので，すべてその場に於て測定するか，または変化が進行しない様固定してもち帰るようにした．

水素イオン濃度 [pH]，振盪水素イオン濃度 [RpH]，電気伝導度 [C]，振盪電気伝導度 [RC][14] の測定，第一鉄イオン [Fe^{++}] の発色固定，全炭酸 [ΣCO_2] の分析．

試料は直ちに小諸支所に持ち帰り，次の成分の分析を行つた．

第一鉄 [Fe^{++}]，第二鉄 [Fe^{+++}]，塩素 [Cl^-]，硬度（$CaCO_3$ として示す），電気伝導度 [C][15]，振盪水素イオン濃度 [RpH][15]，振盪電気伝導度 [RC][15]

以上の測定を終つた試料は東京の本所に於て，更に次の如き成分を分析した．

蒸発残渣，カリウム [K^+]，ナトリウム [Na^+]，カルシウム [Ca^{++}]，マグネシウム [Mg^{++}]，アルミニウム [Al^{+++}]，全珪酸 [H_2SiO_3]，硫酸根 [SO_4^{--}]

測定並びに分析方法

気温，水温：

1/10 度目盛普通温度計を用いた．深井戸などは 1 度目盛の留点温度計を用いた．

水素イオン濃度 [pH]

標準列比色法を用いた．

振盪水素イオン濃度 [RpH]

採水を 10～30 分振盪した後上記の方法で測定した．

---

14) 仮りにこのように称した（後に説明）．
15) 現地で測定しなかつた場合支所で行つた．

採　水

ポリエチレン瓶（またはガラス瓶）に原水のままのものと，別に沈澱防止のため濃塩酸少量を添加したものとを採水して持ち帰つた.

第一鉄 [Fe^{++}]

現地に於て α, α' ジピリジルで発色固定せしめ支所に持ち帰つて光電比色計にて測定した.

第二鉄 [Fe^{+++}]

上記第一鉄を測定した方法に更にチオグリコール酸ソーダを加えて還元せしめ総鉄量を求め，さきに出した第一鉄の価を差引いてもとめたものである.

全炭酸 [ΣCO_2]

現地に於て微量拡散分析法で行つた．即ちユニット内にて試料を硫酸で分解し，炭酸は水酸化バリウム溶液に吸収せしめ，塩酸規定液にて滴定した．滴定には水平ビュレットまたはコッホの微量ビュレットを用いた．結果は数回の測定から求めた.

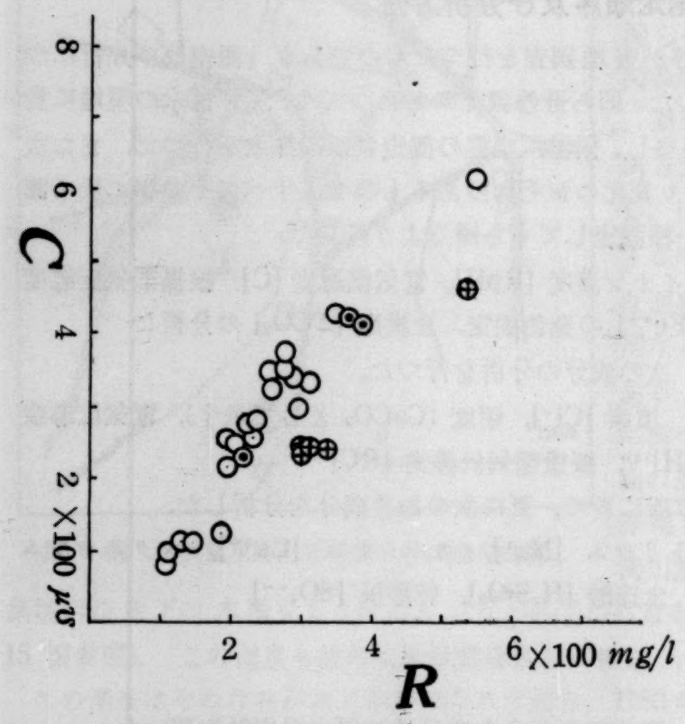

第 7 図　蒸発残渣 R と電気伝導度 C との相関図．⊙印は炭酸鉄泉を現地で測定．⊕印は炭酸鉄泉の沈澱が生じてから測定.

電気伝導度 [C]

KSK 式交流水質計により測定した．温度 20°C として補正を加えてある．なおこの値は第 7 図に示す如く，この地域に於ては蒸発残渣とほぼ比例する．しかし別に述べたように，採水後炭酸の放出により沈澱を生ずるものは，その採水直後の測定値については上の関係を満足させるが，日時を経て測定したものは，その値が小さくなつていることも認められた.

振盪電気伝導度 [RC]

振盪水素イオン濃度を測定した際と同様 10～30 分間振盪した試料につき，同一水質計をもつて測定した．大概は振盪水素イオン濃度測定の時，その振盪した検水の一部を用いて測定した．この方法によれば振盪により水素イオン濃度の変化の大きなもの，特に振盪により沈澱の生ずる試料に於て著るしい変化が認められている．振盪水素イオン濃度にならつて振盪電気伝導度と仮称している.

塩　素 [Cl^-]

ロダン水銀法により光電比色測定を行つた.

EDTA 硬度

EDTA 標準液を用い EBT を指示薬として滴定した.

蒸発残渣

試水一定量を蒸発乾涸後 105～110°C で恒量にした.

カリウム [K^+]

島津製焔光分光光度計を用い塩化カリウム標準液を用いて測定した.

ナトリウム [Na^+]

上記光度計による測定, 標準には塩化ナトリウム液を用いた.

カルシウム [Ca^{++}]

蓚酸カルシウムとして沈澱せしめ, 硫酸で溶解後過マンガン酸カリ標準液で滴定した.

マグネシウム [Mg^{++}]

燐酸アンモニウムで沈澱せしめ, 焦性燐酸マグネシウムとして重量分析を行つた.

アルミニウム [Al^{+++}]

アンモニアにより鉄, アルミニウムの水酸化物として沈澱せしめたものを焼灼して, 得られた混合酸化物から鉄の量だけ控除して求めたものである.

全珪酸 [H_2SiO_3]

重量法による全珪酸の定量を行い, メタ珪酸として表示した.

硫酸 [SO_4^{--}]

硫酸バリウムとして重量分析を行つた.

4. 分析結果

以上の如くして得られた各地区の湧水並びに地下水の全分析結果を次にかかげる. (第1表) 表には最初湧水, 地下水の略称, 採水年月日, 採水当時の気温, 水温, pH, RpH, 蒸発残渣 (検水 1l 中の mg 数), EDTA (EDTA 硬度の略, $CaCO_3$ mg/l として示す), 電気伝導度 [C] (μ℧ を以て表す), 振盪電気伝導度 [RC] (μ℧) の順で記載した. 電気伝導度の値のうち ( ) を附したものは, 現地で測定したものではなく, 実験室に持ち帰つた試水についてはかつたものであつて, 従つてこれは伝導度と振盪伝導度との中間の価を示すものである.

次ぎに陽イオンとして K^+, Na^+, Ca^{++}, Mg^{++}, Fe^{++}, Fe^{+++}, Al^{+++} の各 1l 中の mg 数を以て示した. 陰イオンとして Cl^-, SO_4^{--}, 及び炭酸を ΣCO_2 の形で同様に 1l 中の mg 数で示した. 珪酸は全珪酸を H_2SiO_3 の形で示した. 同じく 1l 中の mg 数である[16].

16) 数値はそれぞれの成分によつて, その分析法から期待し得る精度を考慮に入れて, その桁数を定めたため不ぞろいである. 特に新しく採用した分析法は, 同一試料につきくりかえした測定値から, その精度をたしかめた. 例えば本町用水の試料につき測定をくりかえした EDTA 硬度の値は $204._4 \pm 0.6$ mg/l であり, 芦ノ平下2号泉のあるときの Fe^{++} の値は 57.50 ± 0.14 mg/l, 同じく ΣCO_2 は 736 ± 2 mg/l であつた.

第 1 表

	1	2	3	4	5	6	7
湧泉名	地獄谷酸性 2	地獄谷酸性 1	地獄谷鉄泉 1	芦ノ平下 2 A	芦ノ平下 1 A	赤銹川鉄泉	濁川源泉
試料番号	A-177	A-178	A-13	A-73	A-6	A-211	A-17
採水年月日	56-VIII-24	56-VIII-24	55-VIII-4	55-XI-28	55-VIII-2	56-XI-9	55-VIII-5
気温 °C	15.7	15.7	17.8	10.9	27.0	7.8_5	21.0
水温 〃	8.4	12.2	8.2	8.7	8.9	8.7	12.8
pH	4.3	2.3	5.6	5.6	5.9	5.8	5.8
RpH	4.3	2.3	7.0	8.3	6.9	7.9	7.2
蒸発残渣 mg/l	1427.-	1862.-	336.-	$301._8$	315.-	384.-	537.-
EDTA 硬度 〃	$210._5$	$209._7$	130.-	$126._1$	127.-	$179._3$	236.-
C μ℧	1120.-	2220.-	235.-	(230.-)	(235.-)	415.-	(475.-)
RC 〃						288.-	
K^+ mg/l	4.1_4	5.8_0	3.9	2.4	2.5_3	3.4_2	5.4
Na^+ 〃	20.4	21.3	9.4	12.5	11.8	10.9_0	23.5
Ca^{++} 〃	80.6_1	84.1_1	41.7_5	35.8_9	34.0_8	56.4_2	64.7_8
Mg^{++} 〃	17.4_8	18.5_3	9.8_3	12.0_2	$13._1$	18.0_9	$20._5$
Fe^{++} 〃	56.5	65.2	58.-	55.6_0	54.-	40.9	59.-
Fe^{+++} 〃	1.2	—	—	—	10.-	1.3	12.-
Al^{+++} 〃	94.9_3	98.6_3	$4._8$	1.8_1	—	2.7_9	$6._9$
Cl^- mg/l	2.8_0	2.2_5	5.-	2.3_8	10.-	2.0_4	15.-
SO_4^{--} 〃	979.3_7	1270.7_1	$39._9$	1.3_2	tr.	tr.	20.-
$\sum CO_2$ mg/l	1134.-	$881._7$	—	$648._0$	452.-	$584._0$	949.-
H_2SiO_3 〃	69.1_0	116.8_9	$72._7$	90.9_2	$71._4$	80.0_1	$83._1$
K millival %	0.55	0.74	1.66	1.09	1.12	1.30	1.44
Na 〃	4.60	4.61	6.80	9.76	8.80	7.07	10.64
Ca 〃	20.86	20.88	34.66	32.12	29.19	41.96	33.67
Mg 〃	7.46	7.58	13.44	17.72	18.49	22.18	17.56
Fe^{II} 〃	11.42	11.61	34.56	35.71	33.18	21.83	21.99
Fe^{III} 〃	0.36	—	—	—	9.22	1.04	6.71
Al 〃	54.75	54.58	8.88	3.60	—	4.62	7.99
Ca+Mg %	30	30	52	56	53	70	58
$Fe^{II}+Fe^{III}$ 〃	12	12	38	40	47	25	33
Al 〃	58	58	10	4	0	5	9
K/(K+Na) %	10.7	13.8	19.6	10.0	11.2	15.5	11.8
Ca/(Ca+Mg) 〃	73.7	73.4	72.0	64.4	61.2	65.4	65.7
$Fe^{II}/(Fe^{II}+Fe^{III})$ 〃	96.9	—	—	—	77.9	95.5	76.6

（その 1）

8 亀沢 B A-49	9 下2本流 A(橋下) A-87	10 下2本流 B A-91	11 赤銹川 源泉 A-210	12 清水 湧水 A-141	13 水道水源 本町用水 A-169	14 菱野鉱 泉 A A-68	15 菱野鉱 泉 A′ A-39	16 菱野鉱 泉 B A-40
55-IX-21	55-XII-17	55-XII-29	56-XI-9	56-VI-14	56-VIII-2	55-X-25	55-IX-17	55-IX-17
19.1	-6.0	0.3	10.9	19.3	22.9	11.1	19.9	21.4
15.7	4.0	3.2	8.9	9.5	10.5	14.6	14.4	14.1
5.5	6.4	7.3	6.0	6.1	6.1	6.8	6.8	6.8
8.2	8.1	7.7	7.7	8.3	7.9	7.7	8.3	7.3
365.-	244.-	246.-	216.-	190.-	$293._{6}$	349.-	273.-	258.-
216.-	$114._{4}$	96.1_{3}	$131._{0}$	$110._{8}$	$202._{8}$	$154._{8}$	153.-	154.-
(430.-)	(200.-)	(190.-)	225.-	210.-	285.-	(435.-)	(370.-)	(310.-)
			201.-	210.-	285.-			
3.6	2.0	2.3	2.8_{1}	2.7	3.6_{8}	7.1	3.5	3.2
20.8	7.4_{3}	10.0	8.7_{6}	7.8	12.2	44.3	28.9	21.0
58.0_{0}	37.2_{5}	38.0_{5}	36.5_{2}	31.8_{3}	63.0_{4}	43.6_{6}	31.2_{5}	32.2_{0}
22.0_{2}	9.8_{3}	8.7_{4}	10.9_{3}	8.5_{2}	16.6_{1}	$19._{0}$	$18._{1}$	$19._{6}$
20.-	15.8	$12._{2}$	0.1_{3}	0.0_{6}	0.1_{9}	0.8_{8}	0.9_{2}	2.1_{3}
8.-	8.4	$10._{8}$	0.0_{5}	0.1_{1}	0.0_{9}	0.0_{2}	0.0_{6}	0.0_{5}
—	—	—	0.9_{2}	2.5	2.9_{6}	0.4_{2}	$2._{4}$	—
7.0_{4}	2.8_{2}	2.1_{6}	1.7_{3}	2.0	2.7_{5}	3.6_{2}	3.6_{5}	3.5_{0}
$13._{2}$	$25._{6}$	$10._{7}$	—	—	—	$11._{7}$	$6._{6}$	$14._{0}$
1711.-	40.9	75.7	$274._{8}$	$151._{4}$	$428._{9}$	238.-	374.-	215.-
$83._{1}$	$62._{4}$	$76._{6}$	61.3_{0}	$15._{6}$	73.2_{5}	$57._{1}$	$70._{1}$	$58._{4}$
1.34	1.26	1.43	2.19	2.31	1.72	3.07	1.92	1.91
13.22	7.96	10.54	11.60	11.36	9.69	32.49	26.76	21.27
42.26	45.81	45.99	55.48	53.24	57.44	36.74	33.19	37.43
26.44	19.91	17.41	27.38	23.50	24.94	26.35	31.68	37.55
10.46	13.95	10.58	0.15	0.07	0.11	0.54	0.70	1.77
6.28	11.11	14.05	0.09	0.20	0.09	0.02	0.06	0.07
—	—	—	3.11	9.32	6.01	0.79	5.69	—
80	72	72	96	89	93	98	91	98
20	28	28	0	0	0	1	1	2
0	0	0	4	11	7	1	8	0
9.2	13.6	11.9	15.9	16.9	14.9	8.6	6.6	8.2
71.0	69.7	72.5	67.0	69.4	69.7	58.2	51.1	49.9
62.4	55.6	42.9	62.5	25.0	55.0	96.9	91.6	96.2

第 1 表

湧泉名 / 試料番号	17 菱野女堰引水 A-70	18 石峠御鷹清水 A-48	19 東中学新井戸 A-171	20 支所水道水 A-47	21 高橋氏井戸 A-36	22 支所井戸水 A-116	23 美齊津氏井戸 A-21
採水年月日	55-X-25	55-IX-20	56-VIII-14	55-IX-19	55-VIII-25	56-IV-23	55-VIII-11
気温 °C	—	19.9	28.6	15.0	23.5	15.9	21.5
水温 〃	10.7	15.3	13.0	15.0	14.0	13.8	16.8
pH	6.4	6.7_5	7.0	6.8	6.9	6.9	6.8
RpH	7.8	8.0	8.4	8.3	8.3	8.5	8.3
蒸発残渣 mg/l	282.-	199.-	221.-	261.0	229.-	277.-	235.-
EDTA 硬度 〃	$197._0$	99.-	$127._0$	179.-	120.-	$173._4$	108.-
C μ℧	(335.-)	(210.-)	220.-	(335.-)	(245.-)	345.-	(270.-)
RC 〃			225.-			345.-	
K^+ mg/l	3.6	2.8	3.4_7	2.1_9	3.8	4.4	4.7
Na^+ 〃	11.6	9.5	12.2	17.3_9	14.2	15.9	22.9
Ca^{++} 〃	60.2_9	29.6_1	35.3_3	37.0_0	32.3_2	28.8_4	32.4_4
Mg^{++} 〃	$15._3$	6.0_9	10.5_8	13.7_7	$10._7$	$14._0$	7.4_2
Fe^{++} 〃	0.2_4	0.1	0.4_8	0.0_1	0.0_1	0.1_4	0.0_1
Fe^{+++} 〃	0.0_6	0.2	0.0_3	0.0_2	0.0_2	0.2_1	0.0_2
Al^{+++} 〃	—	$3._5$	1.1_0	0.6_2	$1._4$	—	$3._5$
Cl^- mg/l	1.9_0	5.1_2	5.2_8	7.1_2	12.-	13.5	28.-
SO_4^{--} 〃	$2._5$	$25._2$	—	13.5_7	$34._2$	$35._2$	$13._3$
$\sum CO_2$ mg/l	—	83.-	$152._9$	233.-	—	$180._9$	—
H_2SiO_3 〃	$53._2$	$49._4$	60.2_6	61.8_2	$51._9$	$35._1$	$44._2$
K millival %	1.89	2.51	2.62	1.45	2.88	3.31	3.21
Na 〃	10.36	14.40	15.65	19.58	18.37	20.29	26.67
Ca 〃	61.70	51.54	51.94	47.82	47.93	42.19	43.35
Mg 〃	25.81	17.47	25.63	29.33	26.15	33.74	16.33
Fe^{II} 〃	0.18	0.14	0.50	0.00	0.00	0.15	0.00
Fe^{III} 〃	0.06	0.38	0.06	0.03	0.03	0.32	0.03
Al 〃	—	13.56	3.60	1.79	4.64	—	10.41
Ca+Mg %	100	83	95	98	94	99	85
$Fe^{II}+Fe^{III}$ 〃	0	1	1	0	0	1	0
Al 〃	0	16	4	2	6	0	15
K/(K+Na) %	15.4	14.8	14.3	6.8	13.5	14.0	10.7
Ca/(Ca+Mg) 〃	70.5	74.6	67.0	61.9	64.7	55.6	72.6
$Fe^{II}/(Fe^{II}+Fe^{III})$ 〃	75.0	26.6	89.3	—	—	31.3	—

(その 2)

24 諸の清水 A-143	25 滝原の清水 A-142	26 小山氏井戸 A-118	27 芦ノ平下2上清水A A-63	28 芦ノ平下2上清水B A-92	29 浅間館飲用水 A-45	30 深沢温泉 A-81	31 塩壺温泉 A-18
56-VI-16	56-VI-16	56-V-10	55-X-23	55-XII-29	55-IX-19	55-XII-1	55-VIII-6
23.8	22.4	18.2	10.3	0.4	16.4	-4.5	23.8
13.3	11.7	9.5	9.2	7.9	12.4	27.0	34.0
7.1	6.8	6.1	7.1	6.4_5	5.7	6.9	—
8.1	8.2	7.0	7.6	7.0	7.6	8.3_5	7.5
188.-	306.-	549.-	131.-	148.-	107.-	1089.-	945.-
58.2	$126._4$	$111._3$	53.5_8	55.8_8	33.-	$604._3$	286.-
122.-	320.-	660.-	(110.-)	(110.-)	(80.-)	(1125.-)	(1230.-)
121.-	310.-	650.-					
1.4	8.9	54.7	1.9	1.9	1.1	3.9	16.8
7.2	17.8	65.7	4.3	4.8	5.0	80.3	212.4
3.9_8	37.8_0	32.6_5	$19._4$	$18._6$	10.4_2	203.0_9	50.3_5
8.9_6	$11._4$	8.5_3	3.9_3	3.9_3	$1._7$	34.7_4	$39._9$
0.0_8	0.1_0	0.1_3	0.0_8	0.0_9	$1._8$	2.3_0	0.3
0.1_6	0.1_5	0.2_7	0.0_4	0.0_8	$0._2$	0.0_3	—
3.0	1.4	3.4_1	—	—	$5._4$	4.6_0	—
2.5	$27._5$	93.0	1.7_5	1.6_3	1.5_5	3.7_9	186.-
$28._0$	$33._3$	$48._1$	$6._5$	—	$5._3$	473.2_3	154.-
$31._5$	$75._7$	$25._6$	—	88.3	120.-	$328._8$	—
$27._3$	$49._4$	$59._7$	$63._6$	$50._6$	$42._9$	57.1_4	105.-
3.57	5.71	20.03	3.20	3.23	1.77	0.58	2.78
18.94	19.38	40.91	12.21	13.79	13.73	20.33	59.70
12.04	47.22	23.32	63.18	61.21	32.91	58.99	16.24
44.58	23.48	10.03	21.08	21.31	8.86	16.63	21.21
0.18	0.10	0.07	0.20	0.20	4.05	0.48	0.07
0.48	0.20	0.21	0.13	0.26	0.70	0.01	—
20.21	3.91	5.43	—	—	37.98	2.98	—
73	95	85	100	99	49	95	100
1	0	1	0	1	6	1	0
26	5	14	0	0	45	4	0
15.8	22.8	32.9	20.7	18.9	11.4	2.7	4.4
21.3	66.8	69.9	74.9	74.1	78.7	78.0	43.3
27.3	33.3	25.0	60.0	42.8	85.3	97.6	—

以上の分析値から陽イオンの mg 当量値を計算し，その百分比を次にかかげた．さらにその値から $Ca^{++}+Mg^{++}$——$Fe^{++}+Fe^{+++}$——Al^{+++} の3成分の百分比を求めた．またこれらの値から計算した $K^{+}/K^{+}+Na^{+}$，$Ca^{++}/Ca^{++}+Mg^{++}$，$Fe^{++}/Fe^{++}+Fe^{+++}$ のそれぞれの比をとり百分率を以つて表した．第8図は $Ca^{++}+Mg^{++}$——$Fe^{++}+Fe^{+++}$——Al^{+++} の3成分を3角図表で示したものである．

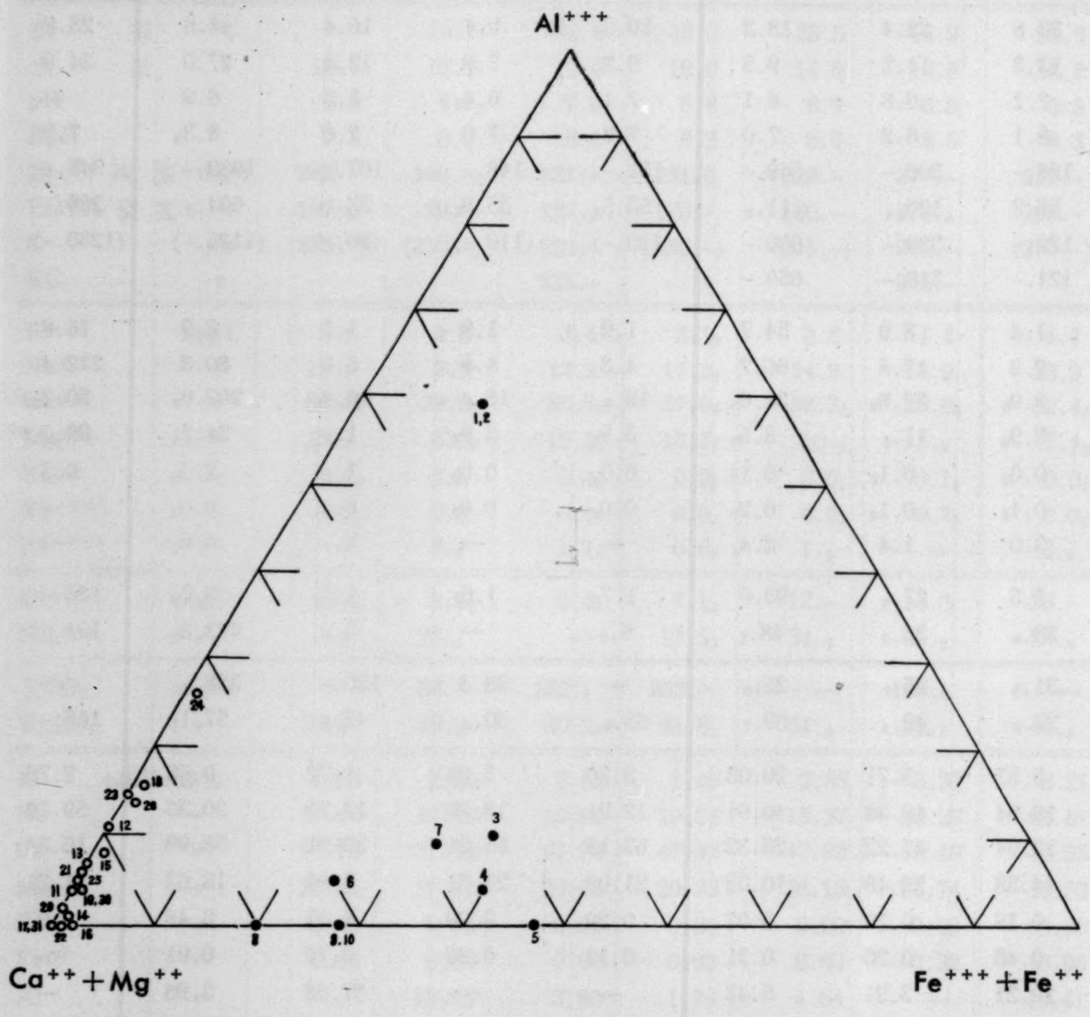

第8図 $Ca^{++}+Mg^{++}\cdot Fe^{++}+Fe^{+++}\cdot Al^{+++}$ の3成分図．⊙は第1類，●は第2類，○は第3類．

5. 分類及び総括

以上の結果を総覧して，これら湧水，地下水に共通の特徴として概ね次のような点があげられる．即ち全般に CO_2 が多く，SO_4^{--}，Cl^- が少い．(但し Cl^- は低所に於ては部分的に多いところがあるし，また SO_4^{--} は地獄谷では例外的に極めて多い)．Ca^{++}，H_2SiO_3

の値も比較的大きい. RpH, pH の差が相当に大きい. $K^+/(K^++Na^+)$ の比が概ね 5〜15 %, $Ca^{++}/(Ca^{++}+Mg^{++})$ が 60〜70 % の値を示している. 以上はこれらの湧水, 地下水の共通した性質であるがなおその他の成分の特徴から, これらの水質を次の 3 種類に大別することが出来る.

第 2 表

	第 1 類	第 2 類	第 3 類
水温 °C	10.3 (8.4〜12.2)	9.5 (8.2〜15.7)	13.1 (8.9〜16.8)
pH	3.3 (2.3〜 4.3)	5.7 (5.5〜 5.9)	6.6 (6.0〜 7.0)
RpH-pH	0.0 (0.0)	1.9 (1.0〜 2.7)	1.4 (0.5〜 2.2)
蒸発残渣 mg/l	1645 (1427〜1862)	375 (302〜 537)	253 (190〜 349)
電気伝導度 μ℧	1670 (1120〜2220)	318 (235〜 460)	292 (215〜 425)
K^+ mg/l	4.9_7 (4.1〜 5.8)	3.5 (2.4〜 5.4)	3.7 (2.2〜 7.1)
Na^+ 〃	20.9 (20.4〜21.3)	13.6 (9.4〜23.5)	17.4 (7.8〜44.3)
Ca^{++} 〃	82.4_8 (80.6〜84.1)	46.5_8 (34.1〜64.8)	38.0 (28.8〜63.3)
Mg^{++} 〃	18.0 (17.5〜18.5)	14.7 (9.8〜20.5)	13.1 (6.1〜19.6)
$Fe^{++}+Fe^{+++}$ 〃	61.5 (57.7〜65.2)	58.2 (42.2〜71.-)	0.5 (0.0〜 2.2)
Al^{+++} 〃	96.8 (94.9〜98.6)	3.3 (— 〜 6.9)	1.5 (— 〜 3.5)
陽イオン順	Al>Ca>Fe>Na >Mg>K	Fe>Ca>Mg>Na >K	Ca> Mg>Na / Na>Mg >K
Cl^- mg/l	2.5 (2.3〜 2.8)	6.9 (2.0〜15.-)	6.9 (1.7〜28.-)
SO_4^{--} 〃	1125.1 (979.4〜1270.7)	$18._6$ ($1._3$〜$39._9$)	$17._4$ ($2._5$〜$35._2$)
ΣCO_2 〃	1008 (882〜1134)	658 (452〜 949)	233 (83〜 429)
H_2SiO_3 〃	93.0 (69.1〜116.9)	79.6 (71.4〜90.9)	53.2 (15.6〜73.3)
$K^+/(K^++Na^+)$	12.3 (10.7〜13.8)	13.6 (10.0〜19.6)	12.4 (6.6〜16.9)
$Ca^+/(Ca^{++}+Mg^{++})$	73.6 (73.4〜73.7)	65.7 (61.2〜65.7)	64.0 (49.9〜74.6)

各欄にそれぞれの類の測定値の平均及び範囲 ( ) を示した.

第1類として (1) 地獄谷酸性2号泉, (2) 地獄谷酸性1号泉.

第2類として (3) 地獄谷鉄泉, (4) 芦ノ平下2号泉, (5) 芦ノ平下1号泉, (6) 赤銹川鉄泉, (7) 濁川源泉, (8) 亀沢鉱泉跡.

第3類として (11) 赤銹川源泉, (12) 清水の湧水, (13) 水道水源本町用水, (14) 菱野鉱泉A, (15) 菱野鉱泉 A′, (16) 菱野鉱泉 B, (17) 菱野女堰引水, (18) 石峠お鷹清水, (19) 東中学校新井戸, (20) 支所水道水, (21) 坂保町高橋氏方井戸, (22) 震研支所井戸水, (23) 八満美斉津一夫氏方井戸.

となる. それぞれの水の特質をその類別に説明すると,

第1類: SO_4^{--} 及び ΣCO_2 を多量に含有し, 陽イオンとしては Al^{+++}, Fe^{++} の含有量

が大きいことを特徴としている．pH は低いが振盪によつてその値が上昇することはない．

蒸発残渣は非常に多い．Ca^{++} は他の類に比較するとやや大きな値を示している．塩素は極めて少い．なお陽イオンをその量の大きな方からならべると $Al^{+++}>Ca^{++}>Fe^{++}>Na^{+}>K^{+}$ という順になる．

第 2 類：SO_4^{--} 比較的少く，CO_2 と Fe^{++} を多く含有する．Al^{+++} はほとんどない．またこの類の大きな特徴の一つは RpH と pH の差が大きいことで，最大は芦ノ平下 2 号泉の pH 5.6, RpH 8.3 その差 2.7 である．塩素もまた少い．陽イオンの値の大きな順にならべると $Fe^{++}>Ca^{++}>Mg^{++}>Na^{+}>K^{+}$ の順序となる．なお亀沢鉱泉跡は，CO_2 が著しく多く，且つそれに比して Fe^{++} が少いし，また位置的にも他の炭酸鉄質泉が，みな山腹 1300 m 以上の地点で湧出しているのに比し，標高約 700 m の麓にあり，それらの点からもこの分類項中に入れるのはやや困難な点があるが，一応比較的近い性質をもつものとしてここに加えた．

第 3 類：CO_2 は相当多量に含有するが，鉄分は非常に少ない．pH, RpH の差も相当大きいが，第 2 類ほどではなくその最高は清水の湧水の 2.2 である．陽イオンの存在量順は比較的高所の赤銹川源泉，清水の湧水などは $Ca^{++}>Mg^{++}>Na^{+}>K^{+}$ となり，それ以下の点では $Ca^{++}>Na^{+}>Mg^{++}>K^{+}$ とその順の一部が入れかわつている．

これらの特異な水質が一体如何なる原因によつてもたらされたかを知ろうとするのにはこれまでの研究の結果のみでは，未だその資料が不十分ではあるが，一応次のような考察を行つて見た．

考 察

第 1 類の地獄谷酸性泉については，この地区が本火山唯一の（現在の山頂噴火口を除く）硫気孔地帯であり，このような硫酸々性の水が全山でこの地域のみにしか湧出していないことを考えれば，その硫酸の存在は同硫気孔地帯の噴気中の硫化水素ガス，亜硫酸ガスの酸化により供給されるものであり，従つて Al もその湧泉が酸性であるために溶在しているものと考えることができる．これに芦ノ平その他に見られるような炭酸鉄質の水が混入して出来たのが地獄谷酸性泉であろう．

芦ノ平その他の第 2 類の炭酸鉄質泉については，地下高圧のもとで溶解した，炭酸を多量に含む水により，岩石中の鉄分が浸出され炭酸鉄泉として湧出したものと考えられる．またこれらが火山灰堆積層中を長く伏流して下流域で湧出するまでに．その炭酸含有量は減少し，鉄は沈澱として析出し水中より除去せられて，第 3 類の水の一部になつているものと考えられる．

しかし多量の炭酸の供給源や，鉄泉の場合の鉄の溶出機構など，さらに将来の研究を必要とする問題が多数ある．またこの地域に分布する火山灰類の抽出成分の研究も必要である．

以上の分類に入らなかつた個々の水質につき若干の説明を加える．

(9) 蛇堀川本流 A（芦ノ平下2号泉わき，丸木橋下），(10) 蛇堀川本流 B（芦ノ平下2号泉わき）．

以上の2つは蛇堀川本流の水であるが，いづれも附近の炭酸鉄質湧泉の流入により赤褐色を呈している．しかし既に急流のため充分攪拌をうけており，pH 値も高く，炭酸は少く鉄はほとんど第2鉄に移化している．下2号泉わき A の採水点はそのすぐ上流に鉄泉の流入があり，その影響をいくらかこうむつているように見うけられる．

(24) 芦ノ平下2号泉上清水 A，(25) 芦ノ平下2号泉上清水 B，(26) 浅間館飲用水．

これらの清水は根源の浅い，雨水の浸み出し水ともいえるもので，附近には濃度の高い炭酸鉄質泉が多数存在するにもかかわらず，それ自身の成分含有量は小さく，またこのような清水は外界の影響もうけやすい．浅間館飲用水については鉄分がやや多く，しかもそれが変動するので注意している．

(27) 諸の清水

水質中特に Ca の量が少いのが非常に特徴的である．このため $Ca^{++}/(Ca^{++}+Mg^{++})$ の比が崩れ，この附近の他の一般の水の 60～70 % に比して 21.3 % となつている．これは主として周囲の地質的環境の特異性によるものではないかと思われる，詳細は不明である．

(28) 滝原の清水

この地点に於ては $Ca^{++}/(Ca^{++}+Mg^{++})$ 値 66.8 % となり他の地点に対して前項の諸の清水の如き大きな変化は認められなかつた．

(29) 小山佐一氏方井戸

この附近一帯のみが，その周囲に比して著しく塩素の量の多いことは既に述べたが，その一つの例として全分析を行つたもので，特に Cl が多いほか，K が多いのが特徴である．従つて $K^+/(K^++Na^+)$ の値が附近の 6～15 に対して 32.9 となつてをり，たしかに異常である．それらの原因は目下調査中である．

(30) 深沢温泉

水温水質とも全く以上のものとは類似しないものである．深さ 135 m のボーリングにより自噴している．含有成分多く，特に Ca^{++} と SO_4^{--} が多く，その水質からは石膏泉といい得るものである．水温はボーリング当初より大分低下して調査当時 27°C であつた．

(31) 塩壺温泉

これもボーリングによる温泉であり，温度は 34°C であるが，水質は深沢温泉とも相違し Na^+, Cl^- が主要なものである．

21. *Studies on the Springs and Underground Waters in Volcano Asama and its Vicinity (1)*

—Chemical Compositions of the Springs and Underground Waters in the Zyabori River Valley and its Neighbourhood.—

By Jōyo OSSAKA, Isamu MURAI, Eiiti MINAMI and Hiromichi TSUYA.
Earthquake Research Institute.

We have carried out chemical analyses on springs and underground waters collected from 31 localities on and around the Volcano Asama. Their characteristic chemical features are as follows: (A) generally rich in $\sum CO_2$; (B) mostly poor in Cl^-; (C) generally poor in SO_4^{--} with an exception of those from Zigokudani; (D) comparatively rich in H_2SiO_3; (E) a little rich in Ca^{++}; (F) show a remarkable difference between RpH and pH; and (G) give the ratios $K/(K+Na)=5\sim15\%$ and $Ca/(Ca+Mg)=60\sim70\%$. They are classified according to their chemical contents into three groups: type (1) containing SO_4^{--}, $\sum CO_2$, Al^{+++} and Fe^{++}; type (2) $\sum CO_2$ and Fe^{++} and type (3) chiefly $\sum CO_2$.

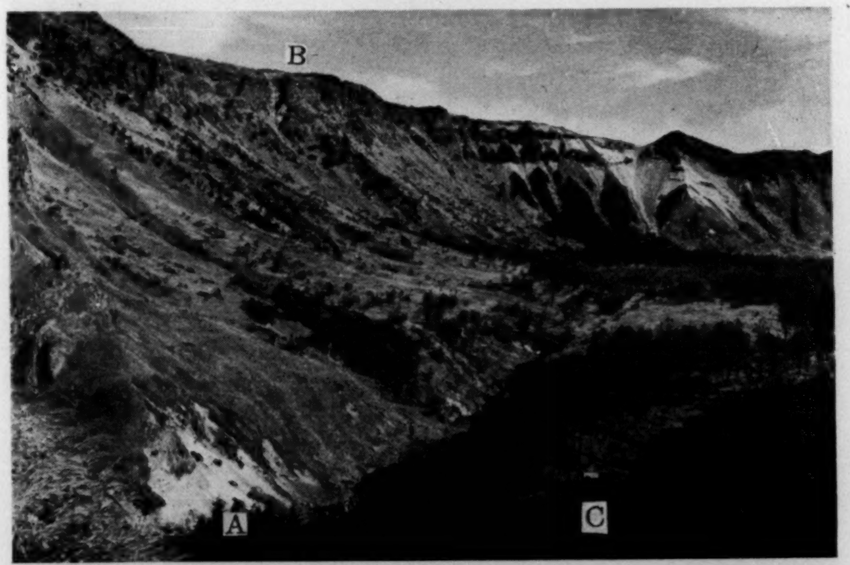

第 9 図　浅間山湯ノ平；(A) 地獄谷，(B) 黒斑山，(C) 火山館

第 11 図　地獄谷鉄泉．(A) (1955–VIII–1)

第 10 図　地獄谷酸性 1 号泉 (A) (1955–VIII–1)

第 12 図　芦ノ平下 2 号泉 A (1957–II–19)

第 13 図　芦ノ平下 1 号泉；(A) は湧出孔 (1955-VIII-2)

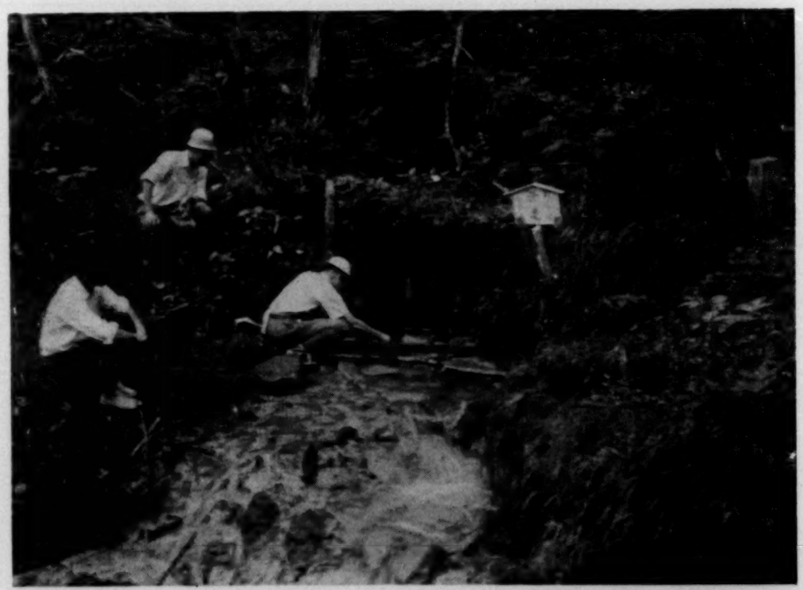
第 15 図　濁川源泉 (1955-VIII-5)

第 14 図　芦ノ平下 2 号泉上清水 B；(B) は湧出孔 (1955-XII-29)

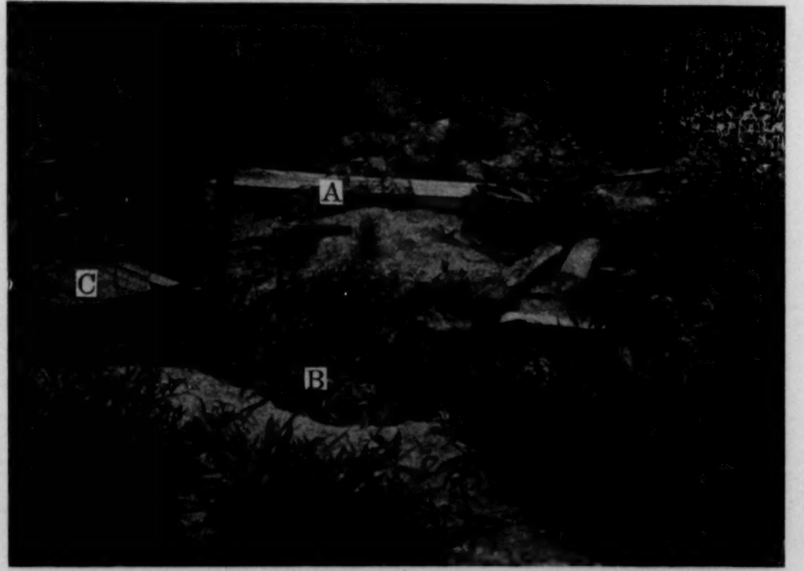

第 16 図　亀沢鉱泉跡；(A), (B), (C) はボーリング孔 (1955-IX-21)

第 17 図　東中学校及び震研小諸支所用水道貯水槽

第 19 図　諸弁天の清水 (1956-VI-16)

第 18 図　柏木小山佐一氏方井戸 (1956-V-10)

第 20 図　深沢温泉湧出孔 (1955-XII-1)

所　報

◎談話会記事

第 340 回談話会（昭和 32 年 1 月 22 日）

1. 関東地震後の地震活動について（その 1）　浅野周三
2. 円板ダイナモ系の振動　力武常次
3. 今市地震地域の地質（第 3 報）
   今市附近の地辷粘土　森本良平・小坂丈予・福田知子
4. 洞海湾の海底周辺地域における常時微動の測定結果　金井清・田中貞二・長田甲斐男
5. 浅間火山及びその周辺地域の地球化学的，地質学的研究の概要
   （スライド使用）　南英一・津屋弘逵・村井勇・小坂丈予
6. 浅間火山及びその周辺地域の湧水並びに地下水の研究（第 1 報）
   蛇堀川渓谷及びその附近の湧水並びに地下水の化学成分　小坂丈予・村井勇・南英一・津屋弘逵

第 341 回談話会　（昭和 32 年 2 月 26 日）

1. 隅田川の水質に及ぼす潮汐の性質について　野口喜三雄・岡巌
2. 横穴に於ける常時微動の測定結果　金井清・田中貞二・長田甲斐男
3. 地盤の震動特性に関する半実験式（補遺）　金井清
4. 起振機に依る建物振動の位相差の測定　岸上冬彦
5. 加速度計に関する 2, 3 の実験　河角広

追加　P 波 S 波速度の比に就いて　吉山良一

第 342 回談話会　（昭和 32 年 3 月 26 日）

1. 自然地震初動部の解析（続報）
   マグニチュードとスペクトル構造との関係について　笠原慶一
2. 超短波三回線遠隔記録地震計（第 1 報）　宮村摂三・辻浦賢
3. 地盤の震動特性に関する半実験式（続報）　金井清
4. 中国地震史の研究　明代の地震資料及び地震年表（その 1）　廖松光雄（河角所員紹介）
5. 昭和 32 年 3 月 10 日のアリューシャン津浪について　高橋竜太郎・平能金太郎

追加　今市地方の地質（第 3 報）
　　　地辷り粘土について（補遺）　森本良平・小坂丈予・福田知子

第 343 回談話会 (昭和 32 年 4 月 23 日)

1. 大地震に伴う地殻変動の特性 (第 1 報) 断層の深さと水平変動の分布 — 笠原慶一
2. 天然放射性同位元素 C^{14} の地球化学的研究 (其の 1) 火山噴出物の年代測定および泥炭の沈積速度について — 南英一, 島誠
3. 桜島の最近の噴火とその噴出物 (第 4 報) — 津屋弘逵

第 344 回談話会 (昭和 32 年 5 月 28 日)

1. 川崎, 鶴見地域で行つた地震観測 (補遺) —本郷との比較— — 表俊一郎, 小牧昭三, 小林直吉
2. 複雑な波動のスペクトル的研究 (方法及び常時微動への応用) — 安芸敬一
3. 本邦油田並びにガス田鹹水の化学成分 (続報) — 南英一, 野口喜三雄, 上野精一, 藤本昌利, 高橋保夫
4. 大爆破地震動に依る関東地方の地殻構造の研究 — 爆破地震動研究グループ 代表者 松沢武雄

第 345 回談話会 (昭和 32 年 6 月 25 日)

1. 地震時における軟弱地盤の沈下現象について — 表俊一郎, 稲葉佳
2. 地震研究所型磁力計の製作 — 横山泉, 力武常次
3. 地震研究所型磁力計に依る南極地域磁気測量 — 百瀬寛一, 小口高
4. 長野県火成岩類に依る古地磁気学的研究 — 百瀬寛一
5. 三原山の地球磁気学的研究 (第 8 報) —1955・56 年間の地磁気偏角連続観測— — 横山泉
6. 1950～1955 年の地磁気永年変化の世界分布 — 力武常次, 永田武, 中川英子
7. 大地震に伴う地殻変動の特性 (第 2 報) — 笠原慶一
8. 卓越震動が現われるための地盤の条件 (補遺) — 金井清
9. 地上と地下の地震動の周期特性 — 金井清, 吉沢静代
10. 地震の大きさと周期との関係 — 金井清
11. 浅間火山前掛山噴気孔に産する鏡鉄鉱について — 南英一, 小坂丈予

昭和32年9月20日印刷
昭和32年9月25日發行

東京都文京區本富士町一番地
東京大學構内
編集兼
發行者　東京大學地震研究所

東京都千代田區富士見町一丁目十番地
印刷者　笠井康頼

東京都千代田區富士見町一丁目十番地
印刷所　株式會社 國際文献印刷社

賣捌所
東京都中央區日本橋通二丁目六番地
丸善株式會社

Sold by
Maruzen Co., Ltd.,
Nihonbashi-dôri, Chûô-ku, Tôkyô.
Price of this copy: 380 Yen. (Postage exclusive.)

BULLETIN OF

THE EARTHQUAKE RESEARCH INSTITUTE

UNIVERSITY OF TOKYO

Vol. XXXV, Part 2. June, 1957.

Contents.

Papers and Reports.

Page

15. T. TAKAHASHI, The Dispersion of Rayleigh Waves in Heterogeneous Media. (in English) 297
16. K. KANAI, Semi-empirical Formula for the Seismic Characteristics of the Ground. (in English) 309
17. I. YOKOYAMA, Geomagnetic Anomaly on Volcanoes with Relation to Their Subterranean Structure. (in English) 327
18. R. MORIMOTO, J. OSSAKA and T. FUKUDA, Geology of Imaichi District with Special Reference to the Earthquake of Dec. 26, 1949 (III). (in English) 359
19. F. KISHINOUYE, Phase Lag of Vibrations of Buildings Excited by a Vibrator. (in English) 377
20. S. MIYAMURA and M. TSUJIURA, UHF Multi-channel Radio Tele-recording Seismograph. Part I. (in Japanese) 381
21. J. OSSAKA, I. MURAI, E. MINAMI and H. TSUYA, Studies on the Spring and Underground Waters in Volcano Asama and its Vicinity (1) —Chemical Compositions of the Spring and Underground Waters in the Zyabori River Valley and its Neighbourhood— (in Japanese) 395

Institute Notes.

(For the papers written in Japanese or in occidental languages, the abstracts are given in occidental languages or in Japanese respectively.)

BULLETIN OF THE EARTHQUAKE RESEARCH INSTITUTE,
UNIVERSITY OF TOKYO. Vol. XXXV, Part 3. September, 1957.

東京大學
地震研究所彙報

第35號　第3册

昭和32年9月

目　次

論文及報告

			頁
22.	複雜な波動のスペクトル的研究（英文）	安芸敬一	415
23.	卓越震動が現われるための地盤の条件（英文）	金井清	457
24.	震源の性状に関する地震学的及び測地学的研究（一）（英文）	笠原慶一	473
25.	観測による土地の脈動の研究（英文）	岸上冬彦	533
26.	弾性地盤上に建つ建築物の振動（英文）	佐藤泰夫 山口林造	545
27.	三原山の地球磁気学的研究 第8報（1955～56年間の偏角変化の連続観測）（英文）	横山泉	567
28.	蔵王火山の地質学的研究（第4報）（英文）	市村毅	573
29.	磁気テープ利用遅延記録方式による7素子地震動常時観測装置（英文）	表俊一郎 山崎良雄	595
30.	川崎鶴見地域9ヶ所で行つた地震観測とその場所の地盤特性（その2）（英文）	表俊一郎 小牧昭三 小林直吉	613
31.	浅間火山前掛山の鏡鉄鉱について（邦文）	南英一 小坂丈予	621

(The titles in occidental languages are given on the back cover.)

本彙報ハ年4回（但シ第1號ヨリ第6號マデハ不定期ニ，第7號ハ3冊トシテ發行セリ），彙報別冊ハ不定期ニ發行ス．

本彙報掲載ノ論文及ビ報告ノ內容ニ關シテハ著者ノミニ其責任アルモノトス．

本彙報ニ關スル照會通信ハ東京大學地震研究所長へ宛テラレタシ．

The Bulletin is published quarterly. (Vols. I–VI were published at irregular intervals and Vol. VII consisted of three parts.)

Supplementary Volume is published at irregular interval.

The authors of the papers alone are responsible for the statements and opinions contained in their respective papers.

All communications relating to this Bulletin should be addressed to the Director of the Earthquake Research Institute, University of Tokyo.

22. *Space and Time Spectra of Stationary Stochastic Waves, with Special Reference to Microtremors.*

By Keiiti AKI,

Earthquake Research Institute.

(Read May 28, 1957.—Received June 30, 1957.)

Introduction

Since the days of Wiechert and Galitzin, seismograms have chiefly been investigated from the view point that they consist of successive distinguishable phases, and the travel time curves for various phases have been essential clues in revealing the structure and state of the matter within the earth. This idea of "phase" is indeed very natural and appropriate so far as the duration of shocks at their origin is negligibly short as compared with the characteristic time of the structure, such as a crustal layer, through which the seismic waves are propagated. Here the characteristic time of a layer may be represented by the ratio of its thickness to the velocity of seismic wave propagation in the layer.

There are, however, many cases in which the above assumption of short duration of shocks does not hold. An example of such cases is the propagation of seismic waves through a complicated crust. What can be clearly identified on the records of seismic waves due to near earthquakes such as those frequently observed in Japan is the initial motion of P waves and at best that of S waves. The main remaining part of such a seismogram has not been paid due attentions, if not neglected, any information from this source regarding the nature of the medium of propagation having been scarcely expected.

Other examples are the waves due to causes other than earthquakes, such as microseismic waves closely connected with meteorological disturbances, volcanic tremors, microtremors generated by traffic, and other tremors of artificial origin. It is hardly possible to deal with those waves from the standpoint of phases and to deduce from them any useful travel time curves.

The object of the present paper is to develop a method for dealing with those complicated waves in order that the nature of the waves as

well as the nature of the medium of propagation may be revealed. Since the method is based on a statistical investigation of waves in time and in space, we need to assume that our waves are stationary in both. This assumption represents quite an opposite extremity as compared with that underlying the phase method, and is certainly an appropriate one for studying those complicated waves mentioned above.

It is true that many studies on such waves have been made by various authors from the statistical point of view. But so far as the writer is aware, those studies have been made for rather limited purposes. For example, the study of spectral distribution of seismic waves has aimed at either getting useful information for earthquake damage prevention or investigating the dependence of the spectrum on the epicentral distance, the earthquake magnitude and the nature of wave paths and so on. Similar studies have also been made about volcanic tremors as well as microtremors due to traffic origin, and the spectrum of microseismic waves has been studied in reference to that of sea waves which are believed to cause them. Also the object of the use of filters in explosion seismology has been to secure a clearer identification of phases on a seismogram.

Those studies have been primarily concerned with the spectrum of waves in time, while the spectrum in space has not yet attracted due attentions. The recent study by K. Akamatsu[1] (1956) of the autocorrelation of microtremor waves in space is among the few made on the latter subject. She has made clear the spatial character of vibration of the ground. The process for obtaining the spatial autocorrelation coefficient, however, consists of troublesome steps such as simultanous recordings of vibrations at several points, readings of the recorded amplitudes, and computations of the autocorrelation coefficient among the waves to be studied. In order to secure rapidness and efficiency of measurments in the study of this kind, K. Aki[2] (1956) built a simple automatic computer by which the computation of spatial autocorrelation coefficients can be made without following individual steps stated above.

So far as the writer knows, the study to be reported here is the first, specifically designed to elucidate the relation between the spectrum of waves in space and that in time with reference to the nature of medium of propagation. By means of the method presented in this paper, the direction distribution of propagation as well as the mode of

1) K. AKAMATU, *Zisin*, [ii], **9** (1956), 22.
2) K. AKI, *ibid*. **9** (1956), 40.

polarization of complicated waves can be learned as will be seen in later chapters. Also we can obtain the dispersion curves for those waves which are useful for deducing the structure of the medium. In addition to this, if the waves observed consist of partial waves having different velocities, the power of each waves can be found.

In Chapter 1 will be given, some results of theoretical considerations of stochastic waves which are stationary both in time and space, and it will be shown what should be measured in order to find the dispersion curves, the mode of polarization, etc. of the waves. The instruments designed specifically for this purpose will be described in Chapter 2. They consists of filters of phase shift type and an automatic computer of the correlation coefficient.

Chapter 3 will be devoted to describing the results of application of the present method to the study of microtremors due to traffic observed at Hongo, Tokyo. The results obtained are as follows; 1) those waves are propagating in every direction with almost uniform power; 2) the horizontal component of vibration is strongly polarized in the direction prependicular to the direction of propagation showing that they are of Love type; 3) the dispersion curves have been deduced, and the velocities of S waves at various depths calculated.

Chapter 1. Theory of stationary stochastic waves

The most fundamental material in the study of wave from the standpoint of phases is certainly the travel time curve which indicates the relation between the treval time and epicentral distance. It may be expected that the corresponding fundamental material in the spectral studies of waves will be a certain relation between the spectrum of the waves in space and that in time. At first we shall look for this relation in the most simplified case of one dimensional waves, and at the same time shall attempt to show the characteristics of stochastic waves which are stationary in time and space.

1. One dimensional stationary waves having one single velocity

With the assumption that our waves travel with a single and definite velocity c independent of the frequency of vibration, our waves $u(x, t)$ can be expressed for the region $x=0 \sim X$ formally

$$u(x, t)=\sum A_n \exp(i\rho_n x)\cos c\rho_n t + \sum \frac{B_n}{c\rho_n}\exp(i\rho_n x)\sin c\rho_n t \qquad (1)$$

where

$$\rho_n=2\pi\frac{n}{X} \quad (n=0, \ \pm 1, \ \pm 2, \cdots)$$

This is the solution of the one dimensional wave equation under the initial conditions that

$$\left.\begin{aligned} u(x, \ 0)&=\sum A_n \exp(i\rho_n x) \\ \dot{u}(x, \ 0)&=\sum B_n \exp(i\rho_n x) . \end{aligned}\right\} \qquad (2)$$

Since $u(x, 0)$ and $\dot{u}(x, 0)$ are both real, A_n and B_n must be the conjugate complex numbers of A_{-n} and B_{-n} respectively.

Now let us find the condition under which the waves formally given by Eq. (1) are stationary both in time and in space. At first, we notice the initial state of our waves as given by Eq. (2). Here $u(x, 0)$ and $\dot{u}(x, 0)$ should be treated as stochastic variables with a parameter x.

The Fourier coefficient A_n of a general stochastic process which is stationary with respect to a single parameter x for the region $x=0 \sim X$ is known to be written in terms of the corresponding Fourier coefficient E_n of the so called "thermal or white noise" as follows;

$$A_n=E_n^{(A)}\cdot G^{(A)}(\rho_n) , \qquad (3)$$

where $G^{(A)}(\rho_n)$ is not a stochastic variable. From the purely random character of "white noise", it follows that

$$\left.\begin{aligned} &\overline{E_n \cdot E_m}=0 , \quad n+m \neq 0 , \\ &\overline{E_n \cdot E_{-n}}=\overline{|E_n|^2}=\frac{\Delta\rho_n}{2\pi}=\frac{1}{X} , \end{aligned}\right\} \qquad (4)$$

where the bars represent the operation of average.

Using these formulas, we have

$$\left.\begin{aligned}
&\overline{A_nA_m}=0\,,\quad n+m\neq 0\,,\\
&\overline{|A_n|^2}=|G^{(A)}(\rho_n)|^2\frac{\Delta\rho_n}{2\pi}\,,\\
&\text{and in a similar way,}\\
&\overline{B_nB_m}=0\,,\quad n+m\neq 0\\
&\overline{|B_n|^2}=|G^{(B)}(\rho_n)|^2\frac{\Delta\rho_n}{2\pi}\,.
\end{aligned}\right\}\tag{5}$$

These are the statistical relations existing among the Fourier coefficients A_n's and B_n's. Moreover, if the initial distributions of displacement and that of velocity are independent of each other, we have

$$\overline{A_nB_m}=0\,,\tag{6}$$

for all n and m. From Eqs. (2) and (5), we see that $|G^{(A)}(\rho_n)|^2$ and $|G^B(\rho_n)|^2$ represent the spatial spectrum density of the initial displacement and that of the initial velocity respectively.

Defining the spatial autocorrelation function $\phi(\xi,\ t)$ of our waves for a given time t as

$$\phi(\xi,\ t)=\overline{u(x,\ t)u(x+\xi,\ t)}\tag{7}$$

and using Eqs. (5) and (6), we obtain

$$\begin{aligned}
\phi(\xi,\ t)&=\sum\frac{\Delta\rho_n}{2\pi}\left\{|G^A(\rho_n)|^2\cos^2 c\rho_n t+\frac{|G^B(\rho_n)|^2}{c^2\rho_n^2}\sin^2 c\rho_n t\right\}\exp(i\rho_n\xi)\\
&=\frac{1}{2\pi}\int\{|G^A(\rho_n)|^2\cos^2 c\rho_n t+\frac{|G^B(\rho_n)|^2}{c^2\rho_n^2}\sin^2 c\rho_n t\}\exp(i\rho_n\xi)d\rho
\end{aligned}\tag{8}$$

From Eq. (8), we see that if

$$\left.\begin{aligned}
&|G^A(\rho_n)|^2=\frac{|G^B(\rho_n)|^2}{c^2\rho_n^2}\\
&\text{or}\\
&\omega_n^2\overline{|A_n|^2}=\overline{|B_n|^2}\,,
\end{aligned}\right\}\tag{9}$$

where ω_n is the circular frequency and $\omega_n=c\rho_n$, $\phi(\xi,\ t)$ becomes independent of time. Thus we can reasonably take Eq. (9) as the condition for stationary stochastic waves. Eq. (9) can be considered as representing the law of equipartition of energy in the case of stochastic waves.

Introducing this condition into Eq. (8) and dropping the suffix A we get

$$\phi(\xi,\ t)\equiv\phi(\xi)=\frac{1}{2\pi}\int|G(\rho)|^2\exp(i\rho\xi)d\rho \tag{10}$$

We shall now proceed to investigate the relation between the spectrum in space and that in time. For this we define the spectrum density in time as

$$\Phi(\omega_n)=\frac{1}{4}\cdot\frac{\overline{\{U_c(\omega_n)\}^2+\{U_s(\omega_n)\}^2}}{\Delta\omega_n/2\pi} \tag{11}$$

where $U_c(\omega_n)$ is the Fourier cosine coefficient of $u(x,\ t)$ with respect to t and for a given x, while $U_s(\omega_n)$ is the corresponding sine coefficient. It can readily be seen from Eq. (1) that

$$\left.\begin{aligned}U_c(\omega_n)&=A_n\exp\left(i\frac{\omega_n}{c}x\right)+A_{-n}\exp\left(-i\frac{\omega_n}{c}x\right)\\U_s(\omega_n)&=\frac{B_n}{\omega_n}\exp\left(i\frac{\omega_n}{c}x\right)+\frac{B_{-n}}{\omega_n}\exp\left(-i\frac{\omega_n}{c}x\right)\end{aligned}\right\} \tag{12}$$

and

$$\Delta\omega_n=c\Delta\rho_n=\frac{2\pi c}{X}$$

Inserting Eq. (12) into Eq. (11), we get

$$\Phi(\omega_n)=\frac{\overline{\left[A_n\exp\left(i\frac{\omega_n}{c}x\right)+A_{-n}\exp\left(-i\frac{\omega_n}{c}x\right)\right]^2+\left[\frac{B_n}{\omega_n}\exp\left(i\frac{\omega_n}{c}x\right)+\frac{B_{-n}}{\omega_n}\exp\left(-i\frac{\omega_n}{c}x\right)\right]^2}}{4\Delta\omega_n/2\pi}$$

By the use of Eq. (5) this may be written as

$$\Phi(\omega_n)=\frac{2\overline{A_nA_{-n}}+2\overline{B_nB_{-n}}/\omega_n^2}{4\Delta\omega_n/2\pi}$$

Finally, inserting Eq. (9) into this, we obtain the following equation,

$$\Phi(\omega)=\frac{|G(\rho)|^2\Delta\rho/2\pi}{\Delta\omega/2\pi}=\frac{|G(\omega/c)|^2}{c} \tag{14}$$

where the suffix n is dropped. This is the relation which connects the spectrum density in space and that in time in the case of one dimensional waves.

As will be shown later, as compared with Eq. (14), the following equation which relates the spatial autocorrelation function $\phi(\xi)$ with the spectrum density $\Phi(\omega)$ in time is more convenient for the purpose of the present study,

$$\phi(\xi)=\frac{1}{2\pi}\int_{-\infty}^{\infty}\Phi(\omega)\exp\left(i\frac{\omega}{c}\xi\right)d\omega$$

or (15)

$$\phi(\xi)=\frac{1}{\pi}\int_{0}^{\infty}\Phi(\omega)\cos\left(\frac{\omega}{c}\xi\right)d\omega$$

which can readily be obtained by Eqs. (10) and (14).

2. Dispersive waves

We shall now proceed to the case of dispersive waves, and show that Eq. (15) obtained above holds also in this case without any modification except the substitution of the function $c(\omega)$ of frequency ω for the constant velocity c. For this, we notice that if we take $\Delta\rho_n$ as constant for all n, the interval $\Delta\omega_n$ between consecutive ω_n is no longer constant in the dispersive case and varies with n. Then we may write

$$\Delta\omega_n=\left(\frac{d\omega}{d\rho}\right)_n\Delta\rho_n\,. \tag{16}$$

The equation corresponding to Eq. (14) is now written as

$$\Phi(\omega)=\frac{|G(\omega/c)|^2}{d\omega/d\rho}\,. \tag{17}$$

Introducing of this into Eq. (10) yields the final formula,

$$\phi(\xi)=\frac{1}{2\pi}\int_{-\infty}^{\infty}|G(\omega/c)|^2 \exp\left(\frac{i\omega}{c(\omega)}\xi\right)\frac{d\rho}{d\omega}\,d\omega$$

$$=\frac{1}{\pi}\int_{0}^{\infty}\Phi(\omega)\cos\left(\frac{\omega}{c(\omega)}\xi\right)d\omega \qquad (18)$$

3. Spatial autocorrelations of filtered waves (1)

In this section the most essential part of our method will be illustrated in the case of one dimensional waves. Corresponding to the separation of a seismogram into successive particular phases in a study of "phases", the vibration of a seismograph is resolved into simple harmonic oscillations; in other words, a Fourier analysis is applied to the vibration in this method. For this purpose, we use electronic resonators to which we shall refer in Chapter 2. If the filtration by a resonator having frequency ω_0 is sufficiently sharp to allow us to assume the spectrum density of the filtered vibration to be

$$\Phi(\omega)=P(\omega_0)\delta(\omega-\omega_0)\,,\quad \omega>0 \qquad (19)$$

where $\delta(\omega)$ is the Dirac δ-function, then the corresponding spatial autocorrelation function (18) is written as

$$\phi(\xi,\,\omega_0)=P(\omega_0)\cos\left(\frac{\omega_0}{c(\omega_0)}\xi\right). \qquad (20)$$

Defining the autocorrelation coefficient as

$$\rho(\xi,\,\omega_0)\equiv\frac{\phi(\xi,\,\omega_0)}{\phi(0,\,\omega_0)}\,,$$

we may write it as

$$\rho(\xi,\,\omega_0)=\cos\left(\frac{\omega_0}{c(\omega_0)}\xi\right). \qquad (21)$$

The above formula shows that the dispersion curve i.e. the curve of velocity $c(\omega_0)$ as a function of frequency ω_0 can be obtained directly from the measurement of $\rho(\xi,\,\omega_0)$. The measurement of this quantity $\rho(\xi,\,\omega_0)$ for various frequencies ω_0 and for a fixed distance ξ is therefore the most fundamental in our method. But this is allowed only in the case in which the waves concerned have a single velocity corresponding

to a frequency ω.

Next, we shall consider the wave which is composed of partial waves having different velocities. In this case if we are allowed to assume that the component waves are statistically independent of one another, we can separate the composite waves into the components by measuring $\rho(\xi, \omega_0)$. Now we write the quantities related to the n'th component wave by attaching the suffix n: for instance, the displacement of the n'th component as $u_n(x, t)$ and the corresponding velocity as $c_n(\omega)$. Then from the assumption of independence among the components, it follows that

$$u(x, t)=\sum_n u_n(x, t) ,$$

$$\phi(\xi)=\sum_n \phi_n(\xi)=\sum \frac{1}{2\pi}\int \Phi_n(\omega) \exp\left(i\frac{\omega}{c_n(\omega)}\xi\right)d\omega ,$$

$$\phi(\xi, \omega_0)=\sum_n P_n(\omega_0)\cos\left(\frac{\omega_0}{c_n(\omega_0)}\xi\right) ,$$

$$\rho(\xi, \omega_0)=\sum_n \frac{P_n(\omega_0)}{P(\omega_0)}\cos\left(\frac{\omega_0}{c_n(\omega_0)}\xi\right) . \qquad (22)$$

The last equation shows that the number N of components is, finite, we can in principle obtain both the percentage of power of the n'th component and the corresponding velocity from the value of $\rho(\xi, \omega_0)$ for a given ω_0 and for $(2N-1)$ different ξ's.

Finally, there may be cases in which the wave can be assumed as composed of component waves having continuously distributed velocity. In this case, introducing the velocity distribution function defined as

$$p(\omega, c)=P_n(\omega)/\Delta c_n$$

and replacing the summation by the integration in Eq. (22), we have

$$\rho(\xi, \omega)=\frac{1}{P(\omega)}\int_0^\infty p(\omega, c)\cos\left(\frac{\omega}{c(\omega)}\xi\right)dc . \qquad (23)$$

From this and using the Fourier transformation, we obtain

$$\frac{c^2 p(\omega, c)}{P(\omega)}=\frac{2}{\pi}\int_0^\infty \rho(\xi, \omega)\cos\left(\frac{\omega}{c(\omega)}\xi\right)d\xi . \qquad (24)$$

Therefore, if we find the values of $\rho(\xi,\ \omega)$ for $\xi=0\sim\infty$, we can calculate the percentage of power of component wave having the assigned velocity and frequency contained in the wave in question.

4. Two dimensional waves of a single velocity

Now let us investigate the case of two dimensional waves, in which the reasonning is quite analogous to that given above for the case of one dimensional waves, though there appear additional terms such as the direction of propagation and polarization of vibrations. At first we shall deal with those waves which are neither dispersive nor polarized.

Assuming that our waves travel with a single velocity c, we write them in the form

$$u(x,\ y,\ t)=\sum\sum A_{nm}\exp(i\rho_n x\cos\theta_m+i\rho_n y\sin\theta_m)\cos(c\rho_n t)$$
$$+\sum\sum\frac{B_{nm}}{c\rho_n}\exp(i\rho_n x\cos\theta_m+i\rho_n y\sin\theta_m)\sin(c\rho_n t)\,. \quad (25)$$

This is the solution of a two dimensional wave equation under the initial conditions that

$$\left.\begin{aligned} u(x,\ y,\ 0)&=\sum\sum A_{nm}\exp(i\rho_n x\cos\theta_m+i\rho_n y\sin\theta_m)\\ \dot{u}(x,\ y,\ 0)&=\sum\sum B_{nm}\exp(i\rho_n x\cos\theta_m+i\rho_n y\sin\theta_m)\end{aligned}\right\}. \quad (26)$$

Since $u(x,\ y,\ 0)$ and $\dot{u}(x,\ y,\ 0)$ are both real, $A_{n,m}$ and $B_{n,m}$ are the conjugate complex number of $A_{n,m+(\pi)}$ and $B_{n,m+(\pi)}$ respectively, in which (π) is a suffix defined by the relation, $\theta_{(\pi)}=\pi$.

Analogous to Eq. (5), the mean value of the absolute square of $A_{n,m}$ and that of $B_{n,m}$ are written as

$$\left.\begin{aligned} \overline{|A_{nm}|^2}&=|G^A(\rho_n,\ \theta_m)|^2\frac{\rho_n\Delta\theta_m\Delta\rho_n}{(2\pi)^2}\\ \overline{|B_{nm}|^2}&=|G^B(\rho_n,\ \theta_m)|^2\frac{\rho_n\Delta\theta_m\Delta\rho_n}{(2\pi)^2}\end{aligned}\right\}. \quad (27)$$

The spectrum density $|G(\rho,\ \theta)|^2$ in the above equation represents the amount of power carried in the waves at the initial state per unit area of the phase space which is formed by two dimensional wave numbers $\lambda=\rho\cos\theta$ and $\mu=\rho\sin\theta$.

Again corresponding to Eq. (5), we have

$$\left.\begin{aligned} \overline{A_{nm}\cdot A_{n'm'}}=0\,, \quad n \neq n',\ m \neq m' \pm (\pi) \\ \overline{B_{nm}\cdot B_{n'm'}}=0\,, \quad n \neq n',\ m \neq m' \pm (\pi) \end{aligned}\right\} \tag{28}$$

and corresponding to Eq. (6),

$$\overline{A_{nm}B_{n'm'}}=0 \tag{29}$$

for all n, m, n' and m'.

Using the above formulas we can write the spatial autocorrelation function $\phi(\xi, \eta, t)$ for the two dimensional waves in terms of their spectrum density in space as

$$\begin{aligned} \phi(\xi, \eta, t) &\equiv \overline{u(x, y, t)u(x+\xi, y+\eta, t)} \\ &= \sum\sum \frac{\rho_n \Delta\rho_n \Delta\theta_m}{(2\pi)^2} \Big\{ |G^A(\rho_n, \theta_m)|^2 \cos^2(c\rho_n t) \\ &\quad + \frac{|G^B(\rho_n, \theta_m)|^2}{c^2\rho_n^2} \sin^2(c\rho_n t) \Big\} \exp(i\rho_n \xi \cos\theta_m + i\rho_n \eta \sin\theta_m) \end{aligned}$$

From the above equation, it follows that the condition for a stationary stochastic wave of two dimensions is written as

$$\left.\begin{aligned} |G^A(\rho, \theta)|^2 = \frac{|G^B(\rho, \theta)|^2}{c^2\rho^2} \\ \text{or} \qquad\qquad \\ \omega_n^2 \overline{|A_{nm}|^2} = \overline{|B_{nm}|^2} \end{aligned}\right\}. \tag{30}$$

Introducing this into $\phi(\xi, \eta, t)$, we obtain

$$\phi(\xi, \eta, t) \equiv \phi(\xi, \eta) = \sum\sum \frac{\rho_n \Delta\rho_n \Delta\theta_m}{(2\pi)^2} |G^A(\rho_n, \theta_m)|^2 \exp(i\rho_n \xi \cos\theta_m + i\rho_n \eta \sin\theta_m)$$

Replacing the summation by the integration and dropping the suffix A we have

$$\phi(\xi, \eta) = \frac{1}{(2\pi)^2} \iint |G(\rho, \theta)|^2 \exp(i\rho\xi\cos\theta + i\rho\eta\sin\theta)\rho d\rho d\theta \tag{31}$$

and accordingly we also have by the Fourier transformation

$$|G(\rho, \theta)|^2 = \iint \phi(\xi, \eta) \exp(-i\rho\xi\cos\theta - i\rho\eta\sin\theta) d\xi d\eta \tag{32}$$

On the other hand, the spectrum density in time of the wave is written as

$$\Phi(\omega_n)=\frac{1}{4}\cdot\frac{\overline{(U_c(\omega_n))^2}+\overline{(U_s(\omega_n))^2}}{\Delta\omega_n/2\pi} \tag{33}$$

where $U_c(\omega_n)$ is the Fourier cosine coefficient of $u(x, y, t)$ with respect to t for given x and y, while $U_s(\omega_n)$ is the corresponding sine coefficient. We see in Eq. (25) that

$$\left.\begin{aligned} U_c(\omega_n)&=\sum_m A_{nm}\exp\left(i\frac{\omega_n}{c}x\cos\theta_m+i\frac{\omega_n}{c}y\sin\theta_m\right)\\ U_s(\omega_n)&=\sum_m \frac{B_{nm}}{\omega_n}\exp\left(i\frac{\omega_n}{c}x\cos\theta_m+i\frac{\omega_n}{c}y\sin\theta_m\right)\\ \omega_n&=c\rho_n\,. \end{aligned}\right\} \tag{34}$$

Using Eqs. (27), (28), (30), and (32), we can write the spectrum density $\Phi(\omega)$ in terms of the spatial autocorrelation function $\phi(\xi, \eta)$ as follows,

$$\begin{aligned}\Phi(\omega_n)&=\frac{\sum_m \overline{|A_{nm}|^2}+\overline{|B_{nm}|^2}/\omega_n^2}{4\Delta\omega_n/2\pi}\\ &=\frac{1}{4\pi c}\int_0^{2\pi}\left|G\left(\frac{\omega_n}{c},\ \theta\right)\right|^2\frac{\omega_n}{c}d\theta\\ &=\frac{1}{4\pi c}\int_0^{2\pi}\frac{\omega_n}{c}d\theta\iint\phi(\xi,\ \eta)\exp\left(-i\frac{\omega_n}{c}\xi\cos\theta-i\frac{\omega_n}{c}\eta\sin\theta\right)d\xi d\eta\ . \end{aligned} \tag{35}$$

Replacing (ξ, η) by a circular coordinate (r, ψ) defined as

$$\xi=r\cos\psi$$

$$\eta=r\sin\psi$$

and using the relation

$$\int_0^{2\pi}d\theta\exp\{-i\rho r\cos(\theta-\psi)\}=2\pi J_0(\rho r)$$

we have from Eq. (35)

$$\Phi(\omega)=\frac{1}{2c}\iint\phi(r,\ \psi)J_0(\rho r)\frac{\omega}{c}drd\psi\ . \tag{36}$$

If we introduce the azimuthal average of the spatial autocorrelation function, i.e.

$$\overline{\phi}(r)=\frac{1}{2\pi}\int\phi(r,\ \psi)d\psi \tag{37}$$

we see that a one to one correspondence exists between this function $\overline{\phi}(r)$ and the spectrum density $\Phi(\omega)$ as follows

$$\Phi(\omega)=\frac{\pi}{c^2}\omega\int_0^\infty\overline{\phi}(r)J_0\Big(\frac{\omega}{c}r\Big)rdr \tag{38}$$

$$\overline{\phi}(r)=\frac{1}{\pi}\int_0^\infty\Phi(\omega)J_0\Big(\frac{\omega}{c}r\Big)d\omega \tag{39}$$

This last equation (39) is derived by the use of the Hankel transformation. It is clear that Eq. (39) corresponds to Eq. (15) for one dimensional waves.

5. Dispersive waves of two dimensions

It will be shown in this section that Eq. (39) also holds in the case of dispersive waves without modifications except the substitution of the function $c(\omega)$ of frequency ω for the constant velocity c.

Taking the relation into account,

$$\Delta\omega_n=\Big(\frac{d\omega}{d\rho}\Big)_n\Delta\rho_n$$

we obtain

$$\Phi(\omega)=\frac{1}{4\pi}\,\frac{d\rho}{d\omega}\int_0^{2\pi}\Big|G\Big(\frac{\omega}{c},\theta\Big)\Big|^2\frac{\omega}{c}d\theta$$

corresponding to Eq. (35) of non-dispersive waves. From this and Eqs. (32) and (37), we have

$$\Phi(\omega)=\frac{\pi\omega}{c(\omega)}\,\frac{d\rho}{d\omega}\int_0^\infty\overline{\phi}(r)\,J_0\Big(\frac{\omega}{c(\omega)}r\Big)rdr.$$

Then the Hankel transformation yields the final result:

$$\overline{\phi}(r)=\int_0^\infty \frac{c(\omega)}{\pi\omega}\frac{d\omega}{d\rho}\Phi(\omega)J_0\left(\frac{\omega}{c(\omega)}r\right)\frac{\omega}{c(\omega)}\frac{d\rho}{d\omega}d\omega$$

$$=\frac{1}{\pi}\int_0^\infty \Phi(\omega)J_0\left(\frac{\omega}{c(\omega)}r\right)d\omega\ . \tag{40}$$

6. Spatial autocorrelation of filtered waves (2)

As has been mentioned in Section 3, the measurements in our method are carried out in two steps; first, the seismograph vibrations are filtered, and secondly, among filtered vibrations, the spatial autocorrelation coefficient is computed. So far as we are concerned with waves having a single velocity corresponding to a frequency ω, the azimuthally averaged autocorrelation function $\overline{\phi}(r)$ of the wave filtered by a resonator of frequency ω_0 is written from Eq. (40) as

$$\overline{\phi}(r)\equiv\overline{\phi}(r,\ \omega_0)=P(\omega_0)J_0\left(\frac{\omega_0}{c(\omega_0)}r\right) \tag{41}$$

where $P(\omega_0)$ is the same as defined by Eq. (19). In consequence, denoting the corresponding autocorrelation coefficient $\overline{\rho}(r,\ \omega_0)$, we have

$$\overline{\rho}(r,\ \omega_0)=J_0\left(\frac{\omega_0}{c(\omega_0)}r\right). \tag{42}$$

This formula clearly indicates that if one measures $\overline{\rho}(r,\ \omega_0)$ for a certain r and for various ω_0's, he can obtain the function $c(\omega_0)$, i.e. the dispersion curve of the wave for the corresponding range of frequency ω_0.

Now let us proceed to the cases in which waves are polarized, and later refer to the cases in which they are composed of partial waves having different velocities and the above procedure cannot be applied.

7. Polarization

As far as two dimensional waves propagating over a horizontal plane are concerned, it is evident that there is no polarization with respect to the vertical component of vibrations. On the other hand, the horizontal component has two typical modes of polarization; namely the vibration is confined either in the direction parallel to that of pro-

pagation, or in the direction perpendicular to that. For instance, in the case of seismic waves, *P* waves, *SV* waves, and Rayleigh waves belong to the former, while *SH* waves and Love waves belong to the latter.

In order to deal with those polarized waves, we observe the component vibration u_r parallel to and the other component u_ψ perpendicular to the direction connecting the two seismometers placed, between the vibrations of which the correlation is to be investigated. Denoting spatial autocorrelation functions for these two components as

$$\phi_r(r, \psi) \equiv \overline{u_r(x, y)u_r(x+r\cos\psi,\ y+r\sin\psi)}$$

$$\phi_\psi(r, \psi) \equiv \overline{u_\psi(x, y)u_\psi(x+r\cos\psi,\ y+r\sin\psi)}$$

we have from Eq. (31) for waves of the parallel polarization

$$\left.\begin{aligned}\phi_r(r, \psi) &= \frac{1}{(2\pi)^2}\iint \cos^2(\theta-\psi)|G(\rho, \theta)|^2 \exp\{i\rho r\cos(\theta-\psi)\}\rho d\rho d\theta \\ \phi_\psi(r, \psi) &= \frac{1}{(2\pi)^2}\iint \sin^2(\theta-\psi)|G(\rho, \theta)|^2 \exp\{i\rho r\cos(\theta-\psi)\}\rho d\rho d\theta\end{aligned}\right\} \quad (43)$$

and in the same way we have for waves of the perpendicular polarization

$$\left.\begin{aligned}\phi_r(r, \psi) &= \frac{1}{(2\pi)^2}\iint \sin^2(\theta-\psi)|G(\rho, \theta)|^2 \exp\{i\rho r\cos(\theta-\psi)\}\rho d\rho d\theta \\ \phi_\psi(r, \psi) &= \frac{1}{(2\pi)^2}\iint \cos^2(\theta-\psi)|G(\rho, \theta)|^2 \exp\{i\rho r\cos(\theta-\psi)\}\rho d\rho d\theta\end{aligned}\right\}. \quad (44)$$

The above equations show that in both cases the sum of two component autocorrelation functions

$$\phi_r(r, \psi)+\phi_\psi(r, \psi)$$

is written in the same form as Eq. (31) for non-polarized waves

$$\phi_r(r, \psi)+\phi_\psi(r, \psi) = \frac{1}{(2\pi)^2}\iint |G(\rho, \theta)|^2 \exp\{i\rho r\cos(\theta-\psi)\}\rho d\rho d\theta\,. \quad (45)$$

Thus if we know the left hand side of the above equation, we can obtain, by the use of the Fourier transformation, $|G(\rho, \theta)|^2$ which indicates the distribution of direction of wave propagation.

On the other hand, the mode of polarization is shown apparently in the azimuthally averaged autocorrelation functions;

$$\overline{\phi_r}(r)=\frac{1}{2\pi}\int\phi_r(r,\ \psi)d\psi$$

$$\overline{\phi_\psi}(r)=\frac{1}{2\pi}\int\phi_\psi(r,\ \psi)d\psi.$$

From Eq. (43) and the following relations

$$\int_0^{2\pi}\cos^2(\psi-\theta)\exp\{i\rho r\cos(\psi-\theta)\}\,d\psi=\pi\{J_0(\rho r)-J_2(\rho r)\}$$

$$\int_0^{2\pi}\sin^2(\psi-\theta)\exp\{i\rho r\cos(\psi-\theta)\}\,d\psi=\pi\{J_0(\rho r)+J_2(\rho r)\}$$

we obtain for the parallel polarization,

$$\left.\begin{aligned}\overline{\phi_r}(r)&=\frac{1}{2}\frac{1}{(2\pi)^2}\iint|G(\rho,\ \theta)|^2\{J_0(\rho r)-J_2(\rho r)\}\,\rho d\rho d\theta\\ \overline{\phi_\psi}(r)&=\frac{1}{2}\frac{1}{(2\pi)^2}\iint|G(\rho,\ \theta)|^2\{J_0(\rho r)+J_2(\rho r)\}\,\rho d\rho d\theta\end{aligned}\right\}. \tag{46}$$

In the similar way, we have for the perpendicular polarization,

$$\left.\begin{aligned}\overline{\phi_r}(r)&=\frac{1}{2}\frac{1}{(2\pi)^2}\iint|G(\rho,\ \theta)|^2\{J_0(\rho r)+J_2(\rho r)\}\,\rho d\rho d\theta\\ \overline{\phi_\psi}(r)&=\frac{1}{2}\frac{1}{(2\pi)^2}\iint|G(\rho,\ \theta)|^2\{J_0(\rho r)-J_2(\rho r)\}\,\rho d\rho d\theta\end{aligned}\right\}. \tag{47}$$

If the correlation is taken among the vibrations filtered by a resonator of frequency ω_0, we may write

$$\frac{1}{2\pi}\int|G(\rho,\ \theta)|^2\,\rho d\theta=P(\omega_0)\delta\left(\rho-\frac{\omega_0}{c(\omega_0)}\right). \tag{48}$$

Then inserting this into Eq. (46), we have the corresponding azimuthally averaged autocorrelation functions for the parallel polarization,

$$\left.\begin{aligned}\overline{\phi_r}(r,\ \omega_0)&=\frac{1}{2}P(\omega_0)\left\{J_0\left(\frac{\omega_0}{c(\omega_0)}r\right)-J_2\left(\frac{\omega_0}{c(\omega_0)}r\right)\right\}\\ \overline{\phi_\psi}(r,\ \omega_0)&=\frac{1}{2}P(\omega_0)\left\{J_0\left(\frac{\omega_0}{c(\omega_0)}r\right)+J_2\left(\frac{\omega_0}{c(\omega_0)}r\right)\right\}\end{aligned}\right\}. \tag{49}$$

Likewise we have for the perpendicular polarization,

$$\left.\begin{aligned}\overline{\phi_r}(r,\ \omega_0)&=\frac{1}{2}P(\omega_0)\left\{J_0\left(\frac{\omega_0}{c(\omega_0)}r\right)+J_2\left(\frac{\omega_0}{c(\omega_0)}r\right)\right\}\\ \overline{\phi_\psi}(r,\ \omega_0)&=\frac{1}{2}P(\omega_0)\left\{J_0\left(\frac{\omega_0}{c(\omega_0)}r\right)-J_2\left(\frac{\omega_0}{c(\omega_0)}r\right)\right\}\end{aligned}\right\}. \tag{50}$$

From the above formulas it is clear that the measurement of $\overline{\phi_r}(r,\ \omega_0)$ and $\overline{\phi_\psi}(r,\ \omega_0)$ will effectively determine the polarization of the wave.

8. Special cases

In this section we shall consider the following two special cases; (a) $|G(\rho,\ \theta)|^2$ is independent of θ, (b) $|G(\rho,\ \theta)|^2$ is zero except for $\theta=\theta_0$ and $\theta=\theta_0+\pi$. For instance, the case of microtremors will be shown in Chapter 3 to be of the former type, while seismic waves due to earthquakes may belong to the latter if observed at a point distant from their origin. We shall call the former wave an "isotropic wave" and the latter a "plane wave".

In the case of the isotropic wave, writing

$$|G(\rho,\ \theta)|^2\equiv|G(\rho)|^2\ , \tag{51}$$

we get from Eq. (31)

$$\phi(r,\ \psi)=\frac{1}{2\pi}\int_0^\infty|G(\rho)|^2J_0(\rho r)\rho d\rho\ . \tag{52}$$

Thus $\phi(r,\ \psi)$ is independent of ψ, and it is clear that in this case we can replace $\overline{\phi}(r)$ by $\phi(r,\ \psi)$ for an arbitrary ψ in the formulas obtained previously, and we need not take the average of $\phi(r,\ \psi)$ with respect to ψ. This also holds for polarized isotropic waves.

On the other hand, in the case of the plane wave, we may write

$$|G(\rho,\ \theta)|^2=|G'(\rho)|^2\delta(\theta-\theta_0) \tag{53}$$

and we have

$$\phi(r,\,\psi)=\frac{1}{2\pi}\int|G'(\rho)|^2\cos\{\rho r\cos(\psi-\theta_0)\}\rho d\rho\,. \tag{54}$$

If we observe the wave filtered by a resonator of frequency ω_0, it follows from Eqs. (48) and (53) that

$$\frac{1}{2\pi}\int|G(\rho,\,\theta)|^2\rho d\theta=|G'(\rho)|^2\rho=P(\omega_0)\delta\Big(\rho-\frac{\omega_0}{c(\omega_0)}\Big)\,. \tag{55}$$

Then the corresponding autocorrelation function $\phi(r,\,\psi,\,\omega_0)$ is written as

$$\phi(r,\,\psi,\,\omega_0)=P(\omega_0)\cos\left\{\frac{\omega_0}{c(\omega_0)}r\cos(\psi-\theta_0)\right\} \tag{56}$$

and also the corresponding autocorrelation coefficient as

$$\rho(r,\,\psi,\,\omega_0)\equiv\frac{\phi(r,\,\psi,\,\omega_0)}{\phi(0,\,\psi,\,\omega_0)}=\cos\left\{\frac{\omega_0}{c(\omega_0)}r\cos(\psi-\theta_0)\right\} \tag{57}$$

or

$$\frac{\cos(\psi-\theta_0)}{c(\omega_0)}=\frac{1}{r\omega_0}\left\{(-1)^n\,\mathrm{Cos}^{-1}\,\rho(r,\,\psi,\,\omega_0)+n\pi\right\}. \tag{58}$$

This last formula (58) shows that we can determine the velocity $c(\omega_0)$ and the angle θ_0 of the direction of propagation by measuring $\rho(r,\,\psi,\,\omega_0)$ at two different ψ's, provided the value of n is known beforehand.

Likewise, in the case of polarized plane wave, we have, for instance, for the parallel polarization

$$\left.\begin{aligned}\phi_r(r,\,\psi,\,\omega_0)&=\cos^2(\theta_0-\psi)P(\omega_0)\cos\left\{\frac{\omega_0}{c(\omega_0)}r\cos(\psi-\theta_0)\right\}\\ \phi_\psi(r,\,\psi,\,\omega_0)&=\sin^2(\theta_0-\psi)P(\omega_0)\cos\left\{\frac{\omega_0}{c(\omega_0)}r\cos(\psi-\theta_0)\right\}\end{aligned}\right\}. \tag{59}$$

In this case, although the velocity and the direction of propagation can still be known after the normalization which is needed to obtain the corresponding autocorrelation coefficient, the mode of polarization cannot be. Therefore, the polarization for an ideal plane wave is better determined by the ordinary method by investigating the amplitudes for various azimuthal angles.

Our method will, however, be effectively applied to a wave composed of two independent waves, which differ from each other in the

mode of polarization and in the velocity of propagation. The general nature of the plane stochastic waves will be given elsewhere in the future in connection with seismic waves.

9. Velocity distribution

In this section we shall deal with two dimensional waves of multiple velocities. Supposing that our waves are not polarized, and denoting a quantity related to the n'th component wave by attaching the suffix n, we write our wave in the form,

$$u = \sum_n u_n(x, y, t)\,.$$

Assuming the statistical independence among the component waves as in the case of one dimensional waves we get the following relations,

$$\phi(r, \psi) = \sum_n \phi_n(r, \psi)$$

$$\overline{\phi}(r) = \sum_n \overline{\phi}_n(r)$$

$$\overline{\phi}(r, \omega_0) = \sum_n \overline{\phi}_n(r, \omega_0) = \sum_n P_n(\omega_0) J_0\!\left(\frac{\omega_0}{c_n(\omega_0)} r\right)$$

$$\bar{\rho}(r, \omega_0) = \sum_n \frac{P_n(\omega_0)}{P(\omega_0)} J_0\!\left(\frac{\omega_0}{c_n(\omega_0)} r\right). \tag{60}$$

This last equation (60) indicates that if the number N of component waves is finite, we can obtain the velocity and the percentage of power for each component by measuring $\bar{\rho}(r, \omega_0)$ for a given ω_0 and for $(2N-1)$ different r's.

It may happen, as in the case of one dimensional waves, that the velocity of component waves is distributed continuously. For such a wave group, we define the velocity distribution function by the relation,

$$p(\omega_0, c_n)\Delta c_n = P_n(\omega_0)\,,$$

and then we can write

$$\overline{\phi}(r, \omega_0) = \int p(\omega_0, c) J_0\!\left(\frac{\omega_0}{c(\omega_0)} r\right) dc\ . \tag{61}$$

From this it follows by the use of the Hankel transformation that

$$\frac{p(\omega_0,\ c)}{P(\omega_0)}=\frac{\omega_0}{c^3}\int_0^\infty \overline{\rho}(r,\ \omega_0)J_0\!\left(\frac{\omega_0}{c(\omega_0)}r\right)rdr\ . \tag{62}$$

Thus we have the formula by which to determine the velocity distribution function from the value of $\overline{\rho}(r,\ \omega_0)$ for $r=0\sim\infty$ in the case of two dimensional waves. Eq. (62) corresponds to Eq. (24) for one dimensional waves.

In the case of the polarized wave of multiple velocities, we see from the results obtained in Section 7, that if we replace, for instance, $\overline{\phi}(r,\ \omega_0)$ by the sum of the component autocorrelation functions,

$$\overline{\phi}_r(r,\ \omega_0)+\overline{\phi}_\varphi(r,\ \omega_0)$$

every formula in this section holds unaltered.

10. Discussions and summary

The results obtained in the preceding sections indicate that the study of waves from the viewpoint of spectrum will give us additional informations which have been neglected because of the lack of proper method of analysis for the purpose. We have dealt with one dimensional stochastic waves in detail, and extended the reasoning followed there to two dimensional waves. It will be easy to proceed to the investigation of three dimensional waves, but this does not seem to be practically necessary for our measurements of waves are usually confined on a plane surface.

We shall enumerate here the principal results obtained in the present chapter.

(1) The spatial autocorrelation coefficient $\rho(\xi,\ \omega_0)$ of a one dimensional wave having a single velocity c and being filtered by a resonator of frequency ω_0 is given by the relation,

$$\rho(\xi,\ \omega_0)=\cos\left(\frac{\omega_0}{c}\xi\right). \tag{21}$$

This holds also for a dispersive wave with the substitution of $c(\omega_0)$ for the constant velocity c.

(2) If we are allowed to assume a continuous distribution of velocity in a stochastic one dimensional wave, we can obtain the velocity distribution function $p(\omega_0,\ c)$ in the form,

$$\frac{p(\omega_0,\ c)}{P(\omega_0)}=\frac{2}{\pi c^2}\int_0^\infty \rho(\xi,\ \omega_0)\cos\left\{\frac{\omega_0}{c(\omega_0)}\xi\right\}d\xi\,. \tag{24}$$

(3) In the case of a two dimensional wave having a single velocity and being not polarized, a one to one correspondence is found between the azimuthally averaged spatial autocorrelation function

$$\overline{\phi}(r)=\frac{1}{2\pi}\int_0^{2\pi}\phi(r,\ \psi)d\psi$$

and the spectrum density $\Phi(\omega)$ in time as follows,

$$\Phi(\omega)=\frac{\pi\omega}{c^2}\int_0^\infty \overline{\phi}(r)J_0\left(\frac{\omega}{c}r\right)rdr\ , \tag{38}$$

$$\overline{\phi}(r)=\frac{1}{\pi}\int_0^\infty \Phi(\omega)J_0\left(\frac{\omega}{c}r\right)d\omega\ . \tag{39}$$

(4) The azimuthally averaged spatial autocorrelation coefficient of the above wave being filtered by a resonator of frequency ω_0 is given by the relation,

$$\overline{\rho}(r,\ \omega_0)=J_0\left(\frac{\omega_0}{c}r\right)\,. \tag{42}$$

This holds also for a dispersive wave of two dimensions with the substitution of $c(\omega_0)$ for constant c.

(5) In the case of a polarized wave, we observe two component autocorrelation functions; namely, an azimuthal component ϕ_ψ and a radial one ϕ_r. It was shown that the sum of these components behaves in the same way as the autocorrelation function of a non polarized wave does. The azimuthal averages of these two ϕ's for the wave filtered by a resonator of frequency ω_0, reflect its mode of polarization and are written in the form,

$$\left.\begin{aligned}\overline{\phi}_r(r,\ \omega_0)&=\frac{1}{2}P(\omega_0)\left\{J_0\left(\frac{\omega_0}{c(\omega_0)}r\right)-J_2\left(\frac{\omega_0}{c(\omega_0)}r\right)\right\}\ ,\\ \overline{\phi}_\psi(r,\ \omega_0)&=\frac{1}{2}P(\omega_0)\left\{J_0\left(\frac{\omega_0}{c(\omega_0)}r\right)+J_2\left(\frac{\omega_0}{c(\omega_0)}r\right)\right\}\ ,\end{aligned}\right\} \tag{49}$$

for the parallel polarization. These for the perpendicular polarization are written as

$$\left.\begin{aligned}\overline{\phi}_r(r, \omega_0)&=\frac{1}{2}P(\omega_0)\left\{J_0\left(\frac{\omega_0}{c(\omega_0)}r\right)+J_2\left(\frac{\omega_0}{c(\omega_0)}r\right)\right\},\\ \overline{\phi}_\psi(r, \omega_0)&=\frac{1}{2}P(\omega_0)\left\{J_0\left(\frac{\omega_0}{c(\omega_0)}r\right)-J_2\left(\frac{\omega_0}{c(\omega_0)}r\right)\right\}.\end{aligned}\right\} \tag{50}$$

(6) The velocity distribution function for a two dimensional wave is written in the form,

$$\frac{p(\omega_0, c)}{P(\omega_0)}=\frac{\omega_0}{c^3}\int_0^\infty \overline{\rho}(r, \omega_0)J_0\left(\frac{\omega_0}{c(\omega_0)}r\right)rdr. \tag{62}$$

Chapter 2. Apparatus

Theoretical considerations in Chapter 1 have shown that the spatial autocorrelation coefficient of the filtered waves plays an important role in the spectral study of stationary stochastic waves. In order to obtain the value of the coefficients with respect to a given wave, it is necessary first to filter the vibration of every seismometer by a resonator having a certain assigned frequency, and secondly to compute the correlation coefficient for every pair of the filtered vibrations. Fig. 1 is the block diagram of an assembly of apparatus corresponding to one pair of seismometers.

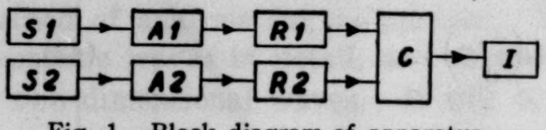

Fig. 1. Block diagram of apparatus.
S; seismometer
A; amplifier
R; resonator
C; correlation computer
I; indicator

In the study of waves from the viewpoint of "phases", the recording of vibration is essential for identifying the phases and for reading travel times. In our method, on the other hand, what we need is not the original record, but the result of the above described operations applied to them. Those operations may be carried out manually, but it should be emphasized that the troublesome labours involved in the manual operations make the application of our method practically impossible. The present study has been made possible by the automation of the operations. In fact, the theoretical studies given in Chapter 1 were initiated after the completion of a correlation computer in our laboratory, though the use of filters in our method was based on the theoretical results.

Of the elements constituting our apparatus shown in Fig. 1, seismo-

meters and amplifiers are the ordinary ones, and we need not give any detailed explanation about them. We shall describe in this chapter the details of our filter and correlation computer.

1. Filter of phase shift type

This type of resonator is rather well known in Electronics. The fundamental part of this circuit is shown in Fig. 2. If the resistance r_1 is equal to r_2, the ratio of the amplitude of output voltage to that of input voltage becomes 1/2 independent of the frequency of the input, while the phase angle shifted by the circuit depends on the frequency. This dependence is as follows; the phase angle shifted for the zero frequency is π, that for the infinite frequency is 0, while that for the frequency $f_0=1/2\pi RC$ is $\pi/2$. Therefore, if two such circuits are connected in series, the resultant phase angle shift will be nearly zero for the whole range of frequency except for the neighbourhood of $f_0=1/2\pi RC$, where the corresponding angle is nearly equal to π. Putting the resultant output into a phase inverter and putting the output of the inverter to the control grid of the first valve of the phase shift circuit result in a positive feedback for the neighbourhood of the frequency f_0 and a negative one for the else. Thus the circuit as a whole works as a resonator of frequency f_0.

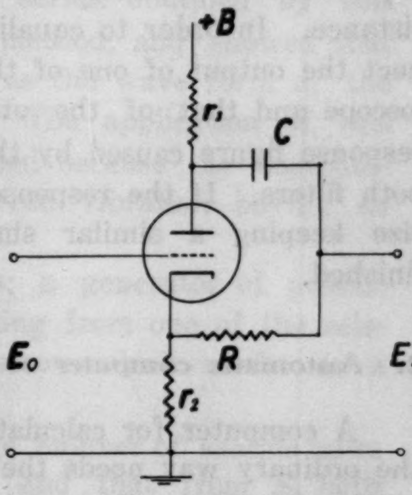

Fig. 2. Circuit for phase shift.

For the purpose of the present study we need at least two resonators having the same characteristics, and moreover their resonance frequency should cover a considerable range which depends on the nature of waves to be studied. Since microtremors due to traffic will be the first object of our study, the resonators were designed to have a frequency range covering continuously from 5 c/s to 30 c/s. The variation of resonance frequency in the resonator was made by the use of variable resistances in the phase shift circuit.

A filter of this type is much easier to construct than a filter having inductances, but the Q value attainable is rather low. In our case, stable operation for a long time was not possible at a value of Q higher

than 30.

At the time of observation, we must adjust the characteristics of the two filters in order that the resonance frequencies and Q values of both will be equal. For this purpose we are using a standard oscillator and an oscilloscope as shown in Fig. 3. At first the frequency of one of the filters is adjusted to be equal to an assigned frequency of the standard oscillator by the aid of the Lissajous' figure on the oscilloscope, and then the frequency of the other filter is adjusted to be equal to the assigned frequency in the same way. The Q value of our filter depends on the feedback constant which is controled by a variable resistance. In order to equalize the Q values of the two filters, we connect the output of one of the filters to the horizontal input of the oscilloscope and that of the other to the vertical one, and observe the response figure caused by the simultaneous application of an impulse to both filters. If the response figure on the oscilloscope diminishes in size keeping a similar shape, we regard that the adjustment is finished.

2. Automatic computer of the correlation coefficient

A computer for calculating the correlation coefficient according to the ordinary way needs the following parts; an input device such as tape or card system, arithmetic elements to make additions and multiplications, and an output device such as a printing machine or some other indicators. So far as we stick to this customary method of computation, the computing machine will become a large one, which cannot be very inexpensive. But if we use the simplified method proposed by Tomoda[3] (1956), the computer will become a very simple one.

In the method due to Tomoda, the original stochastic variable is replaced by $+1$ when it is above the mean value, and by -1 when it is below the mean value. Then the computation of the correlation coefficient in the ordinary way is applied to the resultant series of $+1$ and -1. If this value obtained is r, the true correlation coefficient ρ is deduced by the following formula,

$$\rho=\sin\frac{\pi}{2}r\ .$$

Since the mean value of the deflection of a seimometer pendulum can

3) Y. TOMODA, *Jour. Phys. Earth*, **4** (1956), 67.

be assumed as zero, we can write the above r in the form,

$$r=\frac{n_+-n_-}{n_++n_-}$$

where n_+ is the number of sample pairs for which the deflection of one of the seismometers has the same sign as that of the other, while n_- is the number of sample pairs for which their signs are opposite.

This simplified method was applied to seismograms in a correlogram analysis by Aki[4] (1956) which proved its effectiveness. Akamatu[5] (1956) compared the correlogram of a given time series obtained by this method with that obtained by the customary method, and showed that the agreement between them is satisfactory, as the wave form of the given time series is not very complicated. The application of this simplified method in the present case is justified because the computation is actually made with regard to the filtered vibration having an almost sinusoidal wave form.

The parts of our computer are as follows; a generator of pulses, circuits to compare the sign of the signal coming from one of the seismometers with that from the other, and decatron which works as a counting tube as well as an indicator.

At first we shall describe how to count the number of sample pairs for which the signal from the seismometer S_1 and that from S_2 both have the positive sign. Pulses from a generator, which is a one shot multivibrator triggered by a thyratron oscillator, play the part of sampling in the following way. If we use a frequency converting valve, e.g. 6*SA*7, having two control grids, of which one is fed by the series of pulses coming from the generator and the other by the signal coming from the seismometer S_1 as shown in Fig. 5, the output is a series of pulses as shown in Fig. 4–*c*. The height of each pulse is now proportional to the height of the signal from S_1, when the latter has the positive sign. When it is negative, no output pulses will appear. Therefore putting this series of output pulses into another one shot multivibrator, we obtain the series of pulses which appear only when the signal from S_1 has the positive sign. These pulses are now of the same height as shown in Fig. 4–*d*. Finally, if the same operation is applied to the above pulses and the signal S_2 as is done to the pulses from the generator and the signal from S_1, we have the series of pulses

4) K. Aki, *Jour. Phys. Earth*, **4** (1956), 71.
5) K. Akamatu, *ibid.*, 81.

which appear only when both the signals from S_1 and from S_2 have the positive sign as shown in Figs. 4–*e*, 4–*f* and 4–*g*.

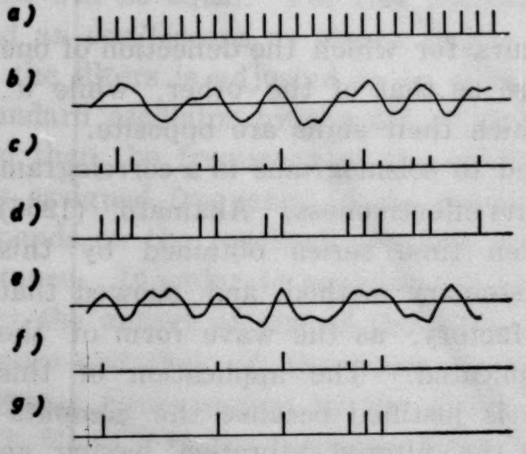

Fig. 4. Process of computation shown schematically,
a) pulses from a pulse generator,
b) signal from the seismometer 1,
c) and *d*) pulses which exist when the signal from *S*1 is positive,
e) signal from the seismometer 2,
f) and *g*) pulses which exist when the signals from both seismometers are both positive.

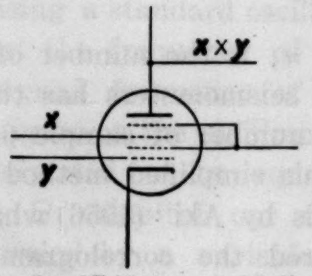

Fig. 5. 6*SA*7 as a multiplier.

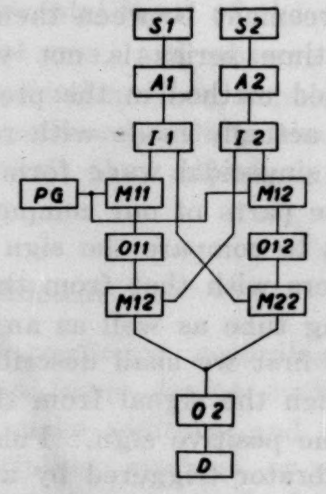

Fig. 6. Block diagram of computer.
S; seismometer
A; amplifier
I; phase inverter
M; multiplier
PG; pulse generator
O; one-shot multi-vibrator
D; decatrons

The series of pulses which appear when both of them have the negative sign will be generated in the same way as above except for the use of phase inverters applied beforehand to the signals from both seismometers. The two series of pulses thus obtained are counted in a decatron circuit, and the number n_+ of the sample pairs for which the signs of the signals from both seismometers are the same is obtained. Since we are using three decatrons in series, we can count up to one thousand. The processes above described may be understood by the block diagram in Fig. 6.

The counting of n_- is carried out in the same way as that of n_+ but with the reverse connection of the outputs of one of the inverters.

The result of counting is indicated on the decatrons. Photographs

of our computer and the decatron indicator are shown in Fig. 7 and Fig. 8.

3. Remarks

The choice of the time interval of successive pulses from the generator depends on the nature of waves to be studied. Since our primary object was microtremors of traffic origin, the time interval was taken as 1/50 second considering that the predominant period of the tremors is 1/10 second. Of course, not only the pulse interval but also the frequency range of the resonator and the characteristics of the seismometers should be appropriate to the spectral nature of the waves concerned. The whole apparatus designed for microtremors will be applied without modifications to volcanic tremors or to ground motions having rather high frequencies caused by some meteorological disturbances. On the other hand, in order to investigate waves having lower frequencies, we need some modifications of the apparatus.

As far as we are concerned with almost perfectly stationary waves, that is waves having sufficiently long durations that we can, not only obtain the correlation coefficients from large samples, but also repeat the measurement several times under the same circumstances, we need only one set of apparatus, i.e. a pair of seismometers, a pair of filters, and one correlation computer. There is, however, another important class of waves having intermediate durations, which are long enough for the computation of correlation coefficient, but nevertheless are too short for repeated measurements. To this class of waves belong some parts of the seismic waves of earthquake origin. The measurement of this latter kind of waves will be very difficult without the use of storage units such as magnetic tapes or magnetic discs.

We shall note some features of the apparatus which seem peculiar to the present method. Since a very sharp filtration is applied to the vibration, troubles with the noises in the amplifier such as caused by the hum in the power source are considerably diminished. In addition, since the correlation between the simultaneous vibrations at two points is under question, the uneven phase lag and amplification as to the frequency on the part of the seismometer and the amplifier cannot be serious matters, for the pair of seismometers and also of amplifiers are made to have identical characteristics.

Chapter 3. Microtremors

In this chapter, our method described in the preceding chapters will be applied to microtremor analyses. The microtremor studied for this purpose is believed to be caused by traffic and appears as an undesirable background noise in many precise geophysical measurements. The choice of this as our object is partly due to the handiness of its measurement as a trial application of our method but also due to the fact that the microtremor itself has formed one of the important problems in Seismology, especially in Japan.

It is well known that the characteristics of the ground are reflected more or less in its vibration whatever the origin of the vibration may be. This fact was noticed early in the beginning of this century by K. Sekiya and F. Omori who made a comparative study of seismograms recorded at Hongo and Hitotsubashi, both in Tokyo. Later, many Japanese seismologists studied ground vibrations from the view point of frequency spectrum. Among them, M. Ishimoto[6] (1937) made a systematic study both of vibrations due to earthquakes and of the background tremors, and proposed a hypothesis that the predominant period of vibration due to earthquakes coincides with that of the background tremors.

Though some negative results against the above hypothesis have been obtained by P. Byerly[7] (1947) and by K. Aki[8] (1955), the spectral study of the background tremors was succeeded in by various authors.

Y. Tomoda and K. Aki[9] (1952) made a frequency analysis by the use of a spectrometer, and confirmed the fact that vibrations having frequencies higher than 1 c/s are due to traffic. K. Kanai, T. Tanaka and K. Osada[10] (1954) made an extensive study and showed that the form of the spectral distribution of microtremors coincides with that of earthquake motions, and that it depends on the geology of the place. K. Akamatu[11] (1956) investigated the tremors observed at Hongo in more detail from the view point of correlograms in space and time.

6) M. ISHIMOTO, *Bull. Earthq. Res. Inst.*, **15** (1937), 697.
7) P. BYERLY, *Bull. Seis. Soc. Amer.*, **37** (1947), 291.
8) K. AKI, *Zisin*, [ii], **8** (1955), 99.
9) Y. TOMODA and K. AKI, *Zisin*, [ii], **5** (1952).
10) K. KANAI, T. TANAKA and K. OSADA, *Bull. Earthq. Res. Inst.*, **32** (1954), 199.
11) K. AKAMATU, *Zisin*, [ii], **9** (1956), 21.

Ishimoto's hypothesis implies a resonance phenomenon in the surface layer, and this problem has been attacked theoretically by various authors. In the following section, we shall refer to some of them assuming the hypothetical wave type of the microtremors.

1. Preliminary discussions

It will be useful to make a preliminary consideration about the wave type of the microtremors. It may be assumed that the type is one of the following four.

A. A surface wave in a narrow sense; this terminology is due to Y. Sato[12] (1954), and represents the wave having an apparent velocity along the horizontal surface which is determined if the frequency is given. If we apply our method to the wave of this type, we can obtain a definite velocity corresponding to a given frequency of the resonator by which the vibrations are filtered. And the autocorrelation function will take the form of Eq. (41), Eq. (49), or Eq. (50).

B. The vibration of a soft surface layer due to a vertically incident bodily wave such as that dealt with by R. Takahasi and K. Hirano[13] (1941); it was shown in their paper that the vibration of this type shows predominant amplitudes at the frequencies, $f=V/4H$, $3V/4H$, $5V/4H$, etc., where V is the velocity of bodily wave in the layer and H is the thickness of the layer. It will be expected in this case that the spatial autocorrelation coefficient with respect to the vibration filtered by a resonator having the predominant frequency, becomes independent of the distance r and is equal to unity.

C. The vibration of a surface layer due to an obliquely incident bodily wave which was studied for instance by G. Nishimura and T. Takayama[14] (1939); a kind of resonance phenomena is observed in this case. We assume that the microtremor belongs to this type, and consists of various vibrations resulting from waves of different incident angles. The vibration of this type is evidently not the surface wave in the narrow sense difined by Y. Sato, because the apparent velocity of this wave along the surface cannot be definite even if the frequency is given. If our method is applied to the wave of this type, a continuous distribution of velocity, that is described in Sections 3 and 9 of Chapter

12) Y. Sato, *Bull. Earthq. Res. Inst.*, **32** (1954), 161.

13) R. Takahasi and K. Hirano, *Bull. Earthq. Res. Inst.*, **19** (1941), 534.

14) G. Nishimura and K. Takayama, *Bull. Earthq. Res. Inst.*, **17** (1939), 253, 308, 319.

1, will be observed instead of definite velocities.

D. The vibration due to a periodically distributed surface disturbance such as that illustrated in the paper of K. Sezawa and K. Kanai[15] (1937); it was shown that a resonance phenomenon occurs when the frequency of vibration is equal to the solution of the characteristic equation of a surface wave for the wave length which is equal to that of the distribution of given disturbance. In this case, the form of spatial autocorrelation coefficients with respect to the vibrations filtered by resonators of various frequencies will be independent of the frequency, and will be determined by the spatial pattern of the given distrubance.

Bearing the above four types in mind and applying our correlational analyses to the microtremor at Hongo, in Tokyo, we shall be able to determine its wave type together with its several important characteristics.

2. Microtremors at Hongo

The measurement was made in the yard of the Geophysical Institute of Tokyo University, of which a map is shown in Fig. 9. In this map are shown the lines along which the spatial autocorrelation is obtained, three wooden buildings by thin line rectangles and an abandoned tennis court by a dotted line rectangle. This is the same place where K. Akamatu (1956) studied the spectrum of prevailing microtremors. The predominant frequencies of the tremors were found by her to lie at $3 \sim 4$ c/s and at $7 \sim 10$ c/s. In the present study, we shall deal with the vibrations having frequencies higher than 5 c/s, leaving the vibrations having lower frequencies including $3 \sim 4$ c/s to a later study.

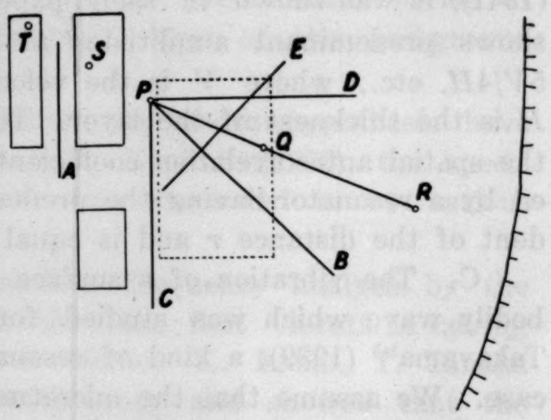

Fig. 9. Map showing lines of measurement.

Seismometers used in the present investigation are all of the moving coil type; a pair of horizontal ones having the free frequency of 10 c/s, a pair of horizontal ones of the frequency of 4.5 c/s, and a pair of vertical ones of the frequency of 4.5 c/s.

15) K. SEZAWA and K. KANAI, *Bull, Earthq. Res. Inst.*, **14** (1938), 1.

The observation of the tremors was usually made during the night time from 18h to 22h, because the daytime observation is disturbed severely by the noise due to persons walking in and around the place.

At the time of measurement, one of the pairs of seismometers is set up along the line of measurement, and the signals coming from them are sent through wires to the amplifiers placed in the laboratory to be analysed by the resonators and the correlation computer. The correlation coefficient obtained from the sampling during a short period varies notably with time, for instance, 50 second sampling yields the correlation coefficient, for a seismometer pair 20 meters apart from each other, varying from 0.5 to -0.9. Therefore a sampling time of at least five or ten minutes is needed, this corresponding to the sample size of more than five thousands.

3. Direction of propagation

Fig. 10 shows the autocorrelation coefficients measured along the lines B, C, D, and E in Fig. 9. In this measurement, horizontal seismometers having the frequency of 10 c/s are used and filtration is not applied. Since the curves in the figure differ only slightly from one another, we may regard the microtremor as being propagated in every direction, each with almost uniform power. Thus it may be allowed to replace the azimuthally averaged autocorrelation function by the autocorrelation function taken along any line having an arbitrary azimuthal angle. (See Section 8, Chapter 1.)

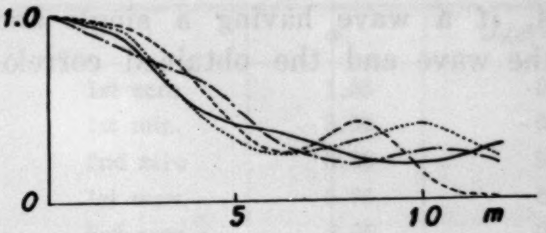

Fig. 10. Autocorrelation coefficients for various directions.

4. Horizontal heterogeneity

It was found, however, that the autocorrelation coefficient taken along a segment of a line sometimes differs significantly from that taken along another segment of the same line. An example is shown in Fig. 11, where the dotted curve represents the autocorrelation coefficient taken along the line segment PQ, and the other curve shows that taken along QR. In both cases, the horizontal seismometers are set up in such a direction as to be sensitive to the vibration which is perpendi-

cular to the line, and the signals from them are filtered by resonators of frequency 9.0 c/s. This fact evidently shows that the wave in question is not stationary in space and can not be adequately dealt with by the present method. We can, however, partly get rid of this difficulty by dealing with the wave within smaller confined areas individually. This may be justified by the fact that the above heterogeneity is due to the existence of the abandoned tennis court convered by a hard surface soil. The fatal difficulty was caused by this heterogeneity in the reduction of the velocity distribution function which was introduced in Sections 3 and 9, Chapter 1, because for its reduction the values of correlation coefficient between two seismometers reasonably apart from each other is needed.

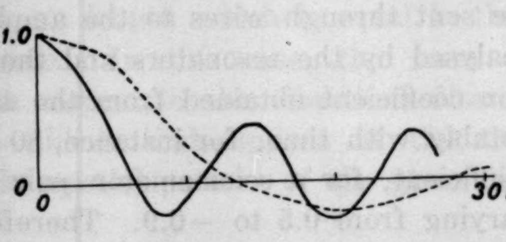

Fig. 11. Comparison of autocorrelatio coefficients measured along the lines PQ and QR.

Under this circumstance the distinction between the type A and C mentioned in Section 1 may fail to be drawn clearly. We may, however, identify the type of our wave as A, if a wave having a single and definite velocity is predominant in the wave and the obtained correlogram has a simple form.

5. Horizontal motions

Before presenting the result of measurements, we shall look back at the theoretical considerations given in Chapter 1. If a certain type of polarized wave is predominant in microtremors, the autocorrelation function with respect to the wave filtered by a resonator of frequency ω_0 will be given either in the form (49) or in the form (50), depending on the mode of polarization. Since we can assume that both $\phi_r(0, \psi)$ and $\phi_\psi(0, \psi)$ are independent of the azimuthal angle ψ in this case, we have the following autocorrelation coefficients for the parallel polarization,

$$\left.\begin{aligned}\rho_r(r, \omega_0)&=J_0\left(\frac{\omega_0}{c(\omega_0)}r\right)-J_2\left(\frac{\omega_0}{c(\omega_0)}r\right)\\ \rho_\psi(r, \omega_0)&=J_0\left(\frac{\omega_0}{c(\omega_0)}r\right)+J_2\left(\frac{\omega_0}{c(\omega_0)}r\right),\end{aligned}\right\} \qquad (63)$$

while for the perpendicular polarization,

$$\left.\begin{aligned}\rho_r(r,\ \omega_0)&=J_0\left(\frac{\omega_0}{c(\omega_0)}r\right)+J_2\left(\frac{\omega_0}{c(\omega_0)}r\right)\\ \rho_\psi(r,\ \omega_0)&=J_0\left(\frac{\omega_0}{c(\omega_0)}r\right)-J_2\left(\frac{\omega_0}{c(\omega_0)}r\right),\end{aligned}\right\} \quad (64)$$

where $\rho_r(r, \omega_0)$ and $\rho_\psi(r, \omega_0)$ are the autocorrelation coefficients for the azimuthal and radial components of vibrations respectively. In Fig. 12 the curves $J_0(x)-J_2(x)$ and $J_0(x)+J_2(x)$ are plotted. With the aid of a table of Bessel functions, the arguments giving the zero, maximum and minimum values of the above curves together with the values of the maxima and minima can be obtained as given in Table I.

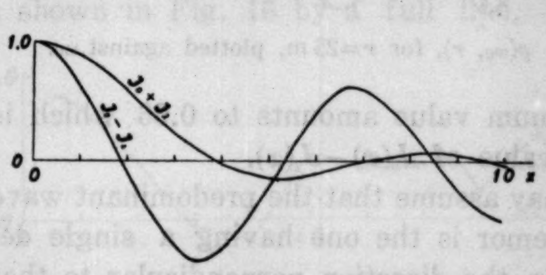

Fig. 12. Curves of $J_0(x)+J_2(x)$ and $J_0(x)-J_2(x)$.

First will be given the result of measurements along the line segment QR in the map in Fig. 9.

Table I. Arguments giving the zeros, maxima and minima.

	x	$J_0(x)-J_2(x)$	x	$J_0(x)+J_2(x)$
1st zero	1.85	0	3.9	0
1st min.	3.50	−0.85	5.1	−0.14
2nd zero	5.35	0	7.0	0
1st max.	6.75	0.62	8.5	0.07
3rd zero	8.55	0	10.0	0
2nd min.	10.1	−0.5		
4th zero	11.7	0		

The azimuthal component of autocorrelation coefficient of the horizontal motion of frequency 9 c/s along this line segment is already given by a full line curve in Fig. 11 in the preceding section. This curve resembles as a whole $J_0(x)-J_2(x)$ in Fig. 12 in form, and the values of the maxima and minima for these two are almost equal except for a notable difference in the 1st minimum value. Since the correlation coefficient is obtained in such a way that one of the pair of seismometers is fixed at the point Q, while the other is moved along QR, this difference may be attributed to the effect of the hard surface soil of the tennis court shown in Fig. 9.

If we measure the correlation coefficient for various frequencies ω_0

and for a fixed distance r, we have the result as shown in Fig. 13, where the distance is 25 meters, and the direction of vibration is perpendicular to QR. This measurement was repeated three times, each on different days but at almost the same hour. Fig. 13 shows that the autocorrelation curve is well reproducible. Also it can be seen that the first maximum of the curve appears at the frequency of 6.4 c/s, and the maximum value amounts to 0.66 which is almost equal to the corresponding value of $J_0(x)-J_2(x)$.

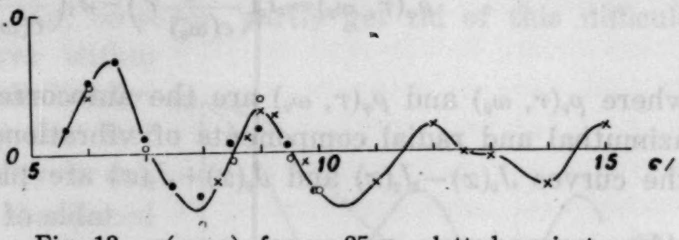

Fig. 13. $\rho(\omega_0, r)$, for r=25 m, plotted against ω_0.

These facts suggest that we may assume that the predominant wave in the horizontal motion of microtremor is the one having a single definite velocity and being polarized in the direction perpendicular to that of propagation. Then we can obtain the velocities for various frequencies by identifying the zeros, maxima and minima of the curve in Fig. 13 with those given in Table I. For instance, we have the following equation corresponding to the first maximum,

$$2\pi\cdot 6.4(\text{c/s})\cdot\frac{25(\text{m})}{C_{6.4}}=6.75\ .$$

Thus the wave velocity for the frequency 6.4 c/s is obtained as 148 m/s. The velocities for various frequencies are plotted in Fig. 17 by the mark ○.

A similar measurement is made for the seismometer pair 15 m apart from each other. The resultant autocorrelation coefficient is plotted against the frequency of resonators in Fig. 14. The wave velocities are obtained from this curve in the same way as stated in the preceding paragraph, and are plotted also in Fig. 17 by the mark ●. A good coincidence is observed between the velocity values obtained from two independent measurements as shown in Fig. 17.

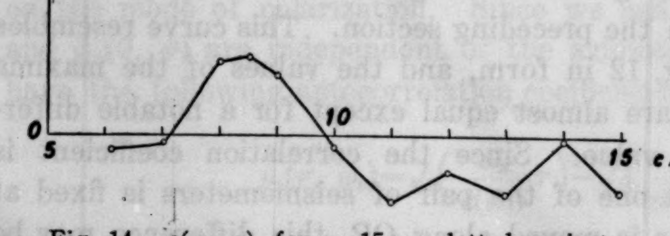

Fig. 14. $\rho(\omega_0, r)$, for r=15 m, plotted against ω_0.

Fig. 15 shows the result of a similar measurement in which the distance between the seismometers is 7.5 m. Since in this case the seismometers are placed too near the tennis court covered by hard surface soil, the departure of the autocorrelation curve from the theoretical one, $J_0(x)-J_2(x)$, is considerable, and the velocities cannot be deduced.

A similar measurement is also made about the radial component of the autocorrelation coefficient of the horizontal motion, and the result is shown in Fig. 16 by a full line, where the distance between two seismometers is 25 m. It is confirmed, by observing correlations for a fixed frequency and various distances, that the maximum which appears in Fig. 16 at the frequency of about 7.3 c/s is the first maximum. Therefore the extrapolation of the curve toward lower frequencies as in Fig. 16 is justified at least as a general trend. It is clear from the figure that the value of the first maximum is very small compared with that for the azimuthal component which is shown by a dotted line, and slightly larger than that of $J_0(x)+J_2(x)$ which is theoretically expected. Moreover, the argument giving the first maximum is evidently larger than that for the azimuthal component, strongly confirming the assumption that the horizontal motion is polarized perpendicularly. By identifying the zeros, maxima and minima of this curve with those of $J_0(x)+J_2(x)$ given in Table I, we can obtain wave velocities for various frequencies as shown in Fig. 17 by the mark ×.

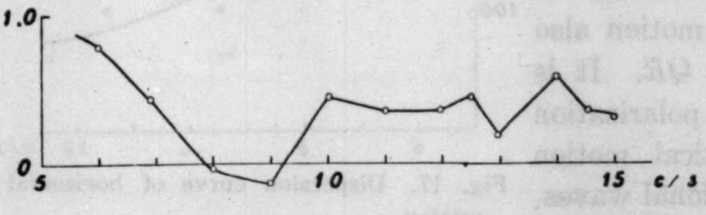

Fig. 15. $\rho(\omega_0, r)$, for $r=7.5$ m, plotted against ω_0.

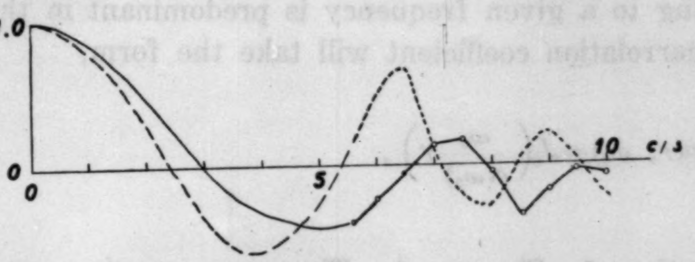

Fig. 16. Comparison of correlation curves for azimuthal and radial components.

Fig. 17 clearly indicates that all the points obtained from three independent measurements are concentrated fairly well to form a single smooth curve. This fact shows the validity of our assumption that the predominant wave in the horizontal motion of the microtremors is the one having a single definite velocity for a given frequency and being

polarized in the direction perpendicular to that of propagation. In short, the predominant wave is of Love type and the curve in Fig. 17 is its dispersion curve.

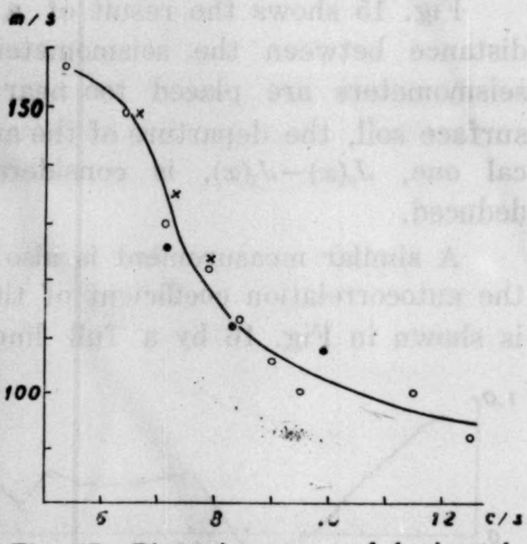

Fig. 17. Dispersion curve of horizontal motion.

6. Vertical motions

A similar measurement as applied to the horizontal motion is made about the vertical motion also along the line segment QR. It is evident that there is no polarization with respect to the vertical motion in the case of two dimensional waves. Therefore, if a wave having a definite velocity corresponding to a given frequency is predominant in the vertical motion, the autocorrelation coefficient will take the form,

$$\rho(r,\ \omega_0)=J_0\left(\frac{\omega_0}{c(\omega_0)}r\right),$$

which was derived in section 6, Chapter 1. The zeros, maxima, and minima of $J_0(x)$ are given in Table II.

The result of measurement is shown in Fig. 18, where the correlation is taken between two vertical seismometers placed along QR and

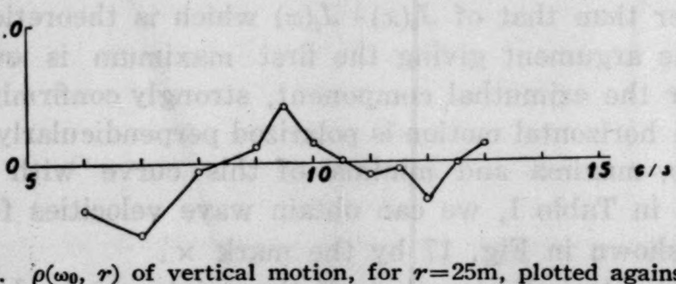

Fig. 18. $\rho(\omega_0,\ r)$ of vertical motion, for $r=25$m, plotted against ω_0.

25 m apart from each other. It is confirmed, by observing correlations for a fixed frequency and various distances, that the maximum of the correlation curve of the wave at the frequency 9.5 c/s is the first maximum, and the minimum at 7.0 c/s is the first minimum. From the

figure it can be seen that the values of the first maximum and the first minimum are almost equal to those of $J_0(x)$. Thus we may assume that a surface wave in the narrow sense is predominant in the

Table II. $J_0(x)$.

	x	$J_0(x)$		x	$J_0(x)$
1st zero	2.40	0	2nd min	10.18	−0.250
1st min.	3.83	−0.403	4th zero	11.79	0
2nd zero	5.52	0	2nd max.	13.33	+0.218
1st max.	7.01	+0.300	5th zero	14.93	0
3rd zero	8.65	0			

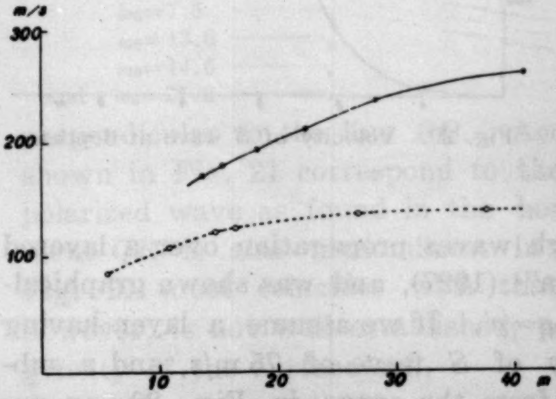

Fig. 19. Comparison of dispersion curves of vertical motion obtained from experiment and theory. (Abscissa is wave length.)

vertical motion as well as in the horizontal motion. By identifying the zeros, maxima and minima of the curve in Fig. 18 with those of $J_0(x)$, we get a dispersion curve as shown by a full line in Fig. 19.

If the vertical motion is a surface wave in the narrow sense, it is most natural to regard it as of Rayleigh type. It is remarkable that the wave velocity for the vertical motion identified as a Rayleigh wave is about twice as large as that for the horizontal motion identified as a Love wave, as indicated in Figs. 17 and 19.

7. The velocity of S wave at various depths

Recently T. Takahashi[16] (1955) studied the dispersion of Love type waves propagating over a heterogeneous medium, and gave a method of determining the structure of the medium from a given dispersion curve. According to him, if the derivatives of density and rigidity are zero at the surface, the depth z at which the velocity of S wave is equal to a given V_S can be found by the formula

$$Z(V_S)=\frac{1.11}{4\pi}V_S\int_0^{T_S}\left[\left\{\frac{V_S}{V_0(T)}\right\}^2-1\right]^{-1/2}dT$$

16) T. TAKAHASHI, *Bull. Earthq. Res. Inst.*, **33** (1955), 287.

where T is the period of wave, $V_Q(T)$ is the phase velocity of wave corresponding to a period T, and T_S is the period for which $V_Q(T)$ is equal to V_S.

Introducing the phase velocity of the horizontal motion given in Fig. 17 into the above formula, we get the variation of S wave velocity with depth as shown in Fig. 20. In this calculation, the surface values of the velocity and its derivative are assumed as 75 m/s and zero respectively. From Fig. 20 it can be seen that there is a rapid increase in velocity at depths from 2 m to 3.5 m, and above and below these depths the velocities are nearly constant respectively. This fact suggests a discontinuity of substance at the depth of about 2.7 m.

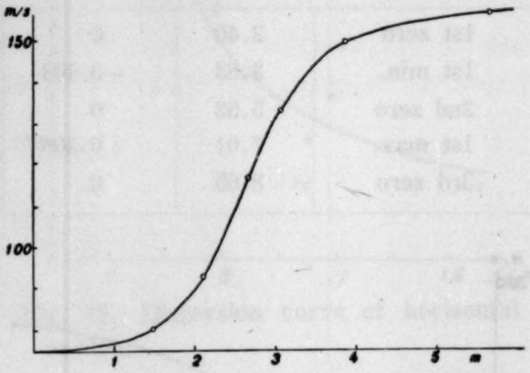

Fig. 20. Velocity of S wave at depths.

The dispersion curve of Rayleigh waves propagating over a layered surface was discussed by K. Sezawa[17] (1927), and was shown graphically in the case of $\lambda=\mu$, $\lambda'=\mu'$, and $\rho=\rho'$. If we assume a layer having thickness of 2.7 m with the velocity of S wave of 75 m/s, and a substratum with 160 m/s as suggested from the curve in Fig. 20, an application of Sezawa's result to such a structure yields a dispersion curve for Rayleigh wave as shown by a dotted line in Fig. 19. The figure shows a considerable discrepancy between the curve obtained by the measurement and that expected theoretically from the structure which is determined by the use of the dispersion curve of the Love wave.

This discrepancy may be attributed either to the difference between the velocity of the SV wave and that of the SH wave, or to a misidentification of the type of wave.

A similar phenomenon is reported in a paper by J. E. White, S. N. Heaps, and P. L. Lawrence[18] (1956) in which a surface wave identified as Rayleigh wave is shown to have group and phase velocities about twice as large as those for Love wave.

17) K. SEZAWA, *Bull. Earthq. Res. Inst.*, **3** (1927), 1~18.

18) J. E. WHITE, S. N. HEAPS, and P. L. LAWRENCE, *Geophysics*, **21** (1956), 715.

8. An example of anomalous dispersion

In this section will be given the result of measurement along the line segment PQ in the tennis court as shown in Fig. 9. As has often been mentioned previously, this place is covered by hard surface soil.

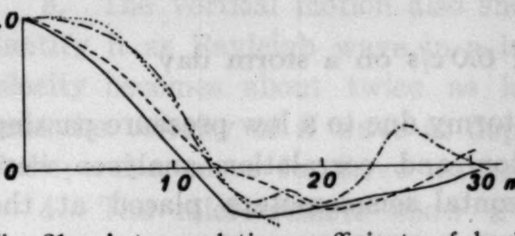

Fig. 21. Autocorrelation coefficients of horizontal motion along the line PQ for
$\omega_0=7.5$ ··········,
$\omega_0=13.6$ — — —,
$\omega_0=14.6$ - - - - - -,
and $\omega_0=21.2$ ———.

Fig. 21 indicates the autocorrelation coefficients with respect to waves filtered by resonators having frequencies 7.5, 13.6, 14.6 and 21.2 c/s. In this case the coefficients are plotted against the distance between the seismometers. The seismometers used are of horizontal type and are placed so as to be sensitive in the direction perpendicular to the line PQ. Accordingly the autocorrelation curves shown in Fig. 21 correspond to the azimuthal component. If such a polarized wave as found in the horizontal motion along the line segment QR is also predominant in this case, the form of the curves in Fig. 21 must coincides with that of $J_0(x)-J_2(x)$. This coincidence, however, is not well established, perhaps due to the horizontal heterogeneity of the surface soil.

The most striking fact revealed by this measurement is that the general trend of the curves or the distance giving their first zero is almost independent of the frequency. This fact reminds us the type D illustrated in the preliminary discussions. But to be consistent with the existence of wave of type A at a near place, it may be more natural to attribute this fact to the effect of hard surface soil and to assume an anomalous dispersion in which the wave velocity increases almost proportionally to the frequency of vibration.

The autocorrelation coefficients of vertical motions having frequencies of 7.0 and 13.6 c/s are plotted against the distance in Fig. 22. Although the curve for the frequency 13.6 c/s indicates the existence of waves having shorter wave lengths, the general trend coincides with that for the fre-

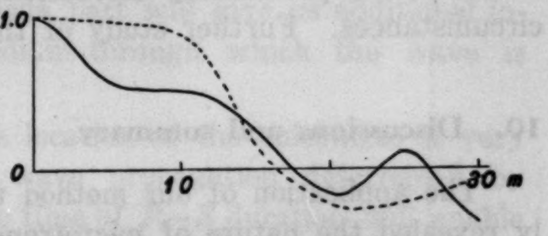

Fig. 22. Autocorrelation coefficients of vertical motion along the line PQ for
$\omega_0=13.6$ c/s ———,
and $\omega_0=7.0$ c/s - - - - - -.

quency 7.0 c/s, also showing an anomalous dispersion.

From the comparison between the curves for the horizontal motions and those for the vertical motions, it can be seen that the velocity of the latter is notably larger than that of the former, and this is the very fact observed along the line segment QR.

9. Unusual behavior of vibration of 6.0 c/s on a storm day

On March 9, 1957, when it was stormy due to a low pressure passing near the east coast of Japan, filtration and correlation analyses were applied to the vibrations of two horizontal seismometers placed at the points S and T in Fig. 9. The range of the resonator frequency was from 5.5 to 10.0 c/s. The correlation coefficients obtained are plotted in Fig. 23 against the frequency of the resonator.

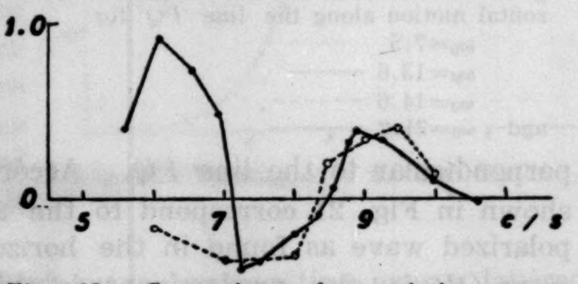

Fig. 23. Comparison of correlation curves measured on a storm day and a calm day.

The dotted curve in Fig. 23 indicates the correlation observed on a calm day. The coincidence of these two curves is fairly good in the frequency range higher than 7.5 c/s, but the value of correlation coefficient for the storm day at the frequency 6.0 c/s amounts to more than 0.9, while that for the calm day is below zero. This high value was unexpected, for the distance between seismometers is about 14 m which is long enough for a considerable decrease of correlation with respect to vibrations having higher frequencies than 5.0 c/s. Also this fact is interesting because the frequency of 6.0 c/s is just twice as large as the most predominant frequency of microtremors at this place, and it suggests to us a possibility that the vibration of type B mentioned in the preliminary discussions might be generated under some circumstances. Further study of this problem is being prepared.

10. Discussions and summary

The application of our method to the microtremors has satisfactorily revealed the nature of microtremors in the frequency range higher than 5.0 c/s, and yielded the following results.

1. In the horizontal motion of microtremors a perpendicularly po-

larized wave is predominant. Both the horizontal and vertical motions can be regarded as having respectively a single definite velocity corresponding to a given frequency.

2. Identifying the horizontal motion as Love wave, we have obtained the velocity of S wave at various depths.

3. The vertical motion also shows a definite dispersion. But if we identify it as Rayleigh wave in a layered medium, the obtained phase velocity becomes about twice as large as that expected theoretically from the velocity of S wave at depths which is determined by the use of dispersion curve for Love wave.

4. The microtremors show a marked anomalous dispersion at a place having hard surface soil.

It may be noted that the value of velocity obtained by our method is that of the phase velocity, so that the corresponding dispersion curve indicates the local structure of medium at the place of measurement. In addition, there is no such ambiguity in our method as that encountered in the determination of travel time of surface waves by the customary method.

The results obtained in this chapter strongly show the efficiency of the present method for the analyses of complicated waves. We shall note here several ways of its application to other waves appearing in Seismology.

Our method will be most effectively applied to the microseismic waves, and will clarify its wave type, the direction of propagation, and the structure of medium at the place of measurement just in the same way as in the present study of microtremors. The location of the origin of volcanic tremors is a very interesting problem in physical volcanology and can be most easily and precisely made by the direction determination by our method. In addition, the coda part of seismic waves due to an earthquake will be another important object to be studied by our method. The investigations of this coda part will give us additional informations about the structure of medium through which the wave is propagated.

Another important problem is the location of the epicentres of very small earthquakes. The direction of wave propagation determined by the present method together with the time of $P-S$ duration will enable us to locate epicentres from observations made at a single station.

11. Acknowledgment

The writer expresses his thanks to Prof. Chuji Tsuboi of the Geophysical Institute, Tokyo University for his constant guidance and encouragement as well as for his valuable suggestions made in the preparation of the manuscript. The greater part of this study was made while the writer was working at the Geophysical Institute. This work was supported in part by a Grant from the Ministry of Education.

---

22. 複雑な波動のスペクトル的研究

地震研究所 安芸敬一

ここで複雑な波動というのは，stationary stochastic wave と呼ぶべきものである．これまで地震記象は位相的な立場から主に解析されて来ているが，位相的には取扱い得ない波動も地震学の分野には数多くある．たとえば，地震波のなかの複雑な部分，脈動，常時微動，火山微動などである．こういう波動の理論模型は stationary stochastic wave と呼ぶのが適当なものであり，このような波動について，1 次元及び 2 次元の場合，その空間スペクトルと時間スペクトルの関係を求めた．

このような波の解析は，先づ sharp な filter をとおし，次に空間相関を測定するという手続きによつて最も有効に行われる．このための電子管装置を製作した．

この方法を常時微動に応用した結果次のことがわかつた．但し観測された常時微動は本郷向ケ丘のものであり．周波数範囲は 5 c/s 以上である．

1) 常時微動はあらゆる方向について殆んど一様な強さをもつている．

2) 上下動も水平動も，周波数を与えると速度が殆んど 1 つに定まる．佐藤泰夫のいう狭い意味での表面波である．

3) 上下動も水平動も分散性をもつ．

4) 水平動は主に進行方向に対し直角に振動する波から成る．つまり Love 波と見做される．

5) 分散曲線から地下の S 波の速度を高橋健人の方法によつて求めた．

6) 上下動の速度は水平動のそれの略 2 倍の大きさをもつ．この事実は White 等によつても経験されているが，理論的には不可解であると思われる．

7) 固い地表層をもつ場所で常時微動は逆分散の現象を示した．速度が殆んど周波数に比例して増大する．

Fig. 3. Resonator and its accessories.

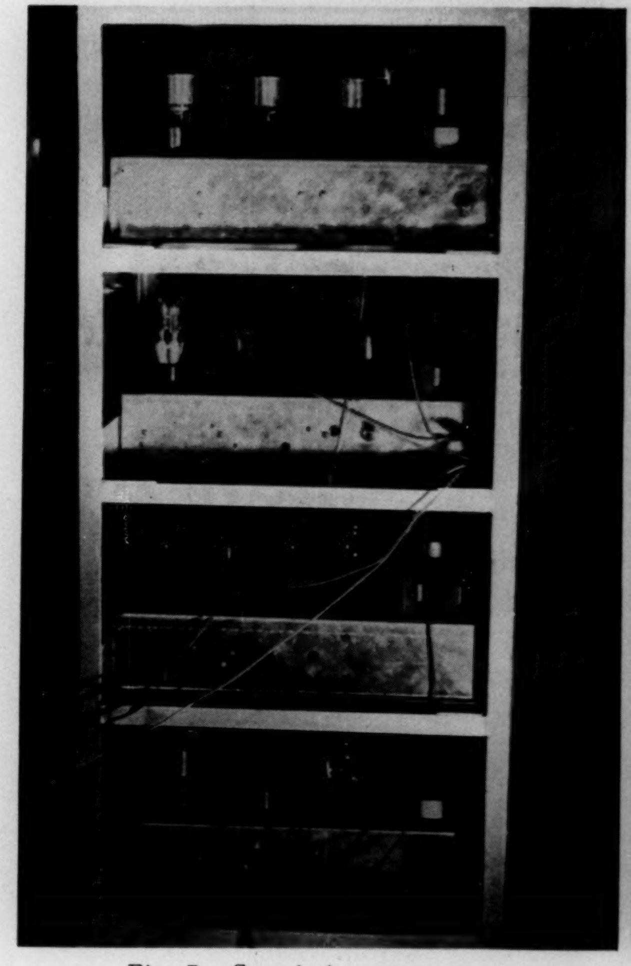

Fig. 7. Correlation computer.

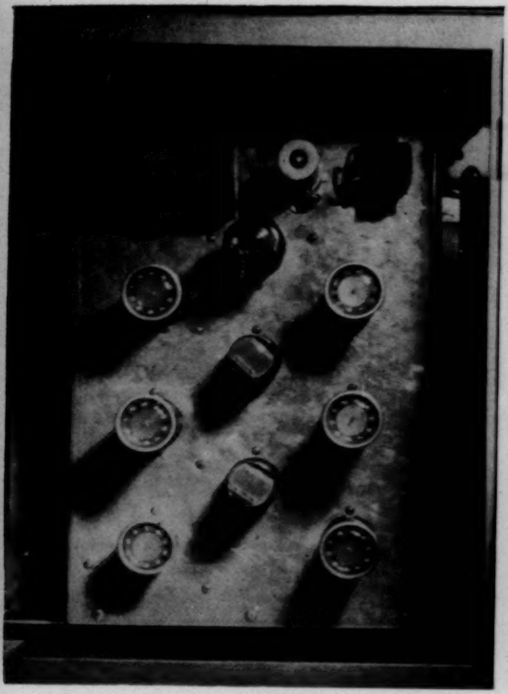

Fig. 8. Decatron indicator.

（震研彙報 第三十五号 図版 安芸）

23. *The Requisite Conditions for the Predominant Vibration of Ground.*

By Kiyoshi KANAI,

Earthquake Research Institute.

(Read July 17, 1956 and June 25, 1957.—Received June 30, 1957.)

1. Introduction

The vibrational characteristics of ground became clear from the observational studies of earthquakes and micro-tremors and theoretical studies of multiple reflections of waves, as well as from statistical studies of earthquake damage. Roughly speaking, from the results of studies, it is known that there are two kinds of spectral response type peculiar to each ground. That is to say, one type of the spectral response of ground has a predominant peak and another is irregular in shape and has a number of peaks.

The ground of the former type is considered to consist of a single layer, and the semi-empirical formula for the seismic characteristics of ground has already been studied.[1]

The ground of the latter type is considered to consist of plural layers and the present paper mainly deals with the vibrational problem of this type of ground by means of theoretical studies.

In this investigation, for simplicity, we try to examine the multiple reflection, problems of elastic waves in the layer, in which distortional waves of the purely plane type of sinusoidal infinite train are propagated vertically upwards.

The notations used in this paper are as follow: U=displacement of primary waves, U_n=resultant displacement of each layer, ρ_n=density, v_n=velocity, $\alpha_n=\rho_n v_n/\rho_{n+1}v_{n+1}$, H_n=thickness, t=time, $p=2\pi/T$, T=period of waves, $f_n=2\pi/L_n$, L_n=wave length, z=vertical axis, $q_n=pH_n/v_n$, n=number of a layer from free surface.

1) K. KANAI, *Bull. Earthq. Res. Inst.*, **35** (1957), 20.

K. KANAI, R. TAKAHASI and H. KAWASUMI, *Proc. World Conference Earthq. Engg.*, June 1956, 31–9, equation (23). *Corrigenda* to the denominator of (23). Read 0.2 for 0.1.

2. Preliminary study

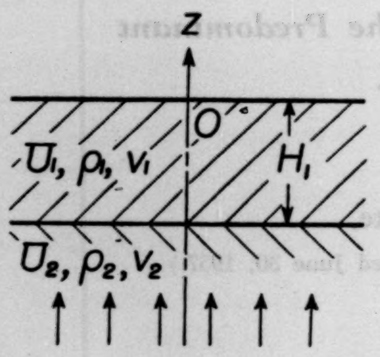

Fig. 1.

Firstly, we shall try to examine the simplest case of a single stratified layer.

If the incident waves in the lower medium be of the type expressed by the following

$$U_0 = \cos(pt - f_2 z) , \qquad (1)$$

the resultant displacement of the stratum is expressed by[2)]

$$U_1 = \frac{2\cos\left(q_1 \frac{x}{H_1}\right)\cos\{pt - \tan^{-1}(\alpha_1 \tan q_1)\}}{\sqrt{\cos^2 q_1 + \alpha_1^2 \sin^2 q_1}} . \qquad (2)$$

Then, the resultant displacement on the free surface is written by

$$|U_{1_{z=0}}| = \frac{2}{\sqrt{\cos^2 q_1 + \alpha_1^2 \sin^2 q_1}} . \qquad (2')$$

The requisite conditions for predominant vibration to appear at the ground surface may be obtained from the following equations:

$$\frac{\partial U_{1_{z=0}}}{\partial q_1} = 0 , \qquad (3)$$

and

$$\left|\frac{\partial^2 U_{1_{z=0}}}{\partial q_1^2}\right|_{q_1 = q_m} < 0 , \qquad (4)$$

in which q_m is the solution of (3).

Substituting (2′) in (3), we obtain

$$(1-\alpha_1^2)(\cos^2 q_1 + \alpha_1^2 \sin^2 q_1)^{-3/2} \cos q_1 \sin q_1 = 0 . \qquad (3')$$

The solutions of (3′) become as follow:

$$\cos q_1 = 0 , \quad \text{i.e.} \quad q_1 = (2m+1)\frac{\pi}{2} , \qquad [m = 0, 1, \cdots] \qquad (5)$$

and

2) K. SEZAWA and K. KANAI, *Bull. Earthq. Res. Inst.*, **13** (1935), 253, Equation (9).

$$\sin q_1 = 0\ , \quad \text{i.e.} \quad q_1 = (n+1)\pi\ . \quad [n=0, 1, \cdots] \tag{6}$$

The left term of (4) becomes as follow :

$$(1-\alpha_1^2)\{\cos^2 q_1(1+\sin^2 q_1) - \alpha_1^2 \sin^2 q_1(1+\cos^2 q_1)\}(\cos^2 q_1 + \alpha_1^2 \sin^2 q_1)^{-5/2}\ . \tag{7}$$

Substituting (5) in (7),

$$\alpha_1^{-3}(\alpha_1^2 - 1)\ . \tag{8}$$

Then, (8) tells us that the condition of $\alpha_1 < 1$ satisfies (4). In other words, when $\alpha_1 < 1$, that is to say, the vibrational impedance of the stratum is less than that of the subjacent medium, the maximum of the vibration amplitude at the free surface appeared at such period as $T = 4H_1/(2m+1)v_1$ and the amplitude at the surface in synchronous vibrations becomes $2/\alpha_1 (\equiv 2\rho_2 v_2/\rho_1 v_1)$ by substituting (5) in (2).

In the same way, from (4), (6), (7) and (2), we knew that, when the vibrational impedance of the stratum is higher than that of the subjacent medium, the amplitude at the surface becomes maximum at such period as $T = 2H_1/(n+1)v_1$ and the maximum amplitude at the surface is twice as large as the value of incident waves amplitude. This case has little meaning in connection with the nature of excitation of vibrations.

Now, taking only the fundamental mode of (3) into consideration, that is to say, the cases of $m=0$ in (5) and $n=0$ in (6), the amplitude distribution in the stratum can be written as shown in Figs. 2 and 3

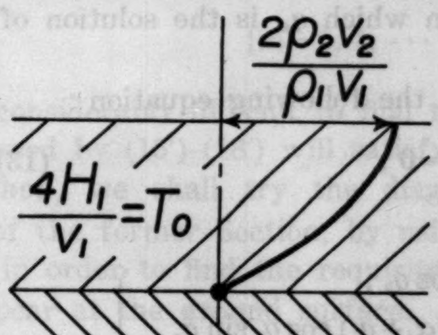

Fig. 2.

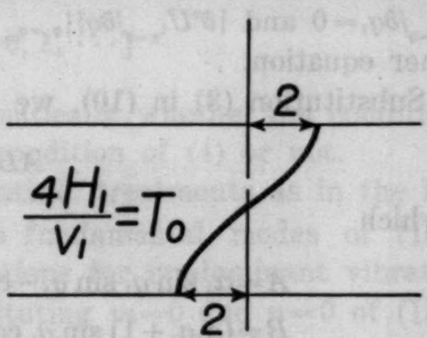

Fig. 3.

by using (2). Figs. 2 and 3 directly tell us the same conclusion which has been drawn from somewhat complicated calculation by using (4). The diagrammatical treatments like this seem to play an important part in the problem of plural stratified layers.

3. The case of two stratified layers

If the incident waves in the lowest medium be of the type:

$$U_0=\cos(pt-f_3 z), \quad (9)$$

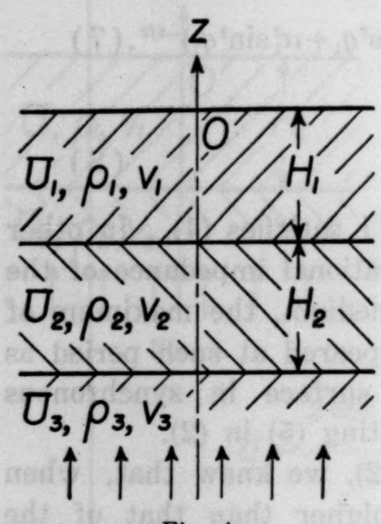

Fig. 4.

the resultant displacements in the each layer are expressed by[3)]

$$U_1=\frac{2}{\Phi}\cos q_1\frac{z}{H_1}\cos\left(pt-\tan^{-1}\frac{Q}{P}\right), \quad (10)$$

$$U_2=\frac{2}{\Phi}\left\{\cos q_1\cos q_2\left(\frac{H_1}{H_2}+\frac{z}{H_2}\right)-\alpha_1\sin q_1\sin q_2\left(\frac{H_1}{H_2}+\frac{z}{H_2}\right)\right\}\cdot\cos\left(pt-\tan^{-1}\frac{Q}{P}\right), \quad (11)$$

where

$$\left.\begin{aligned}\Phi&=\sqrt{P^2+Q^2}\,,\\ P&=\cos q_1\cos q_2-\alpha_1\sin q_1\sin q_2\,,\\ Q&=\alpha_2(\cos q_1\sin q_2+\alpha_1\sin q_1\cos q_2)\,.\end{aligned}\right\} \quad (12)$$

The requisite conditions for predominant vibration to appear at the ground surface may be obtained from (3) and (4), that is to say, $\partial U_{1_{z=0}}/\partial q_1=0$ and $|\partial^2 U_{1_{z=0}}/\partial q_1^2|_{q_1=q_m}<0$, in which q_m is the solution of the former equation.

Substitution (3) in (10), we obtain the following equation:

$$AB-CD=0\,, \quad (13)$$

in which

$$\left.\begin{aligned}A&=\alpha_1\sin q_1\sin q_2-\cos q_1\cos q_2\,,\\ B&=(\alpha_1 a_1+1)\sin q_1\cos q_2+(\alpha_1+a_1)\cos q_1\sin q_2\,,\\ C&=(\alpha_1 a_1+1)\sin q_1\sin q_2-(\alpha_1+a_1)\cos q_1\cos q_2\,,\\ D&=2\alpha_2(\alpha_1\sin q_1\cos q_2+\cos q_1\sin q_2)\,,\\ a_1&=\frac{H_2}{H_1}\cdot\frac{v_1}{v_2}\,.\end{aligned}\right\} \quad (14)$$

3) K. KANAI, *Bull. Earthq. Res. Inst.*, **30** (1952), 31. Special case of $\xi_1=0$, $\xi_2=0$, $\xi_3=0$.

It is easy to find the general solutions of (13) by looking at (14), that is to say, the following conditions make A and C zero simultaneously and then they satisfy (13):

$$\cos q_1 = 0\,, \qquad \sin q_2 = 0\,, \tag{15}$$

$$\sin q_1 = 0\,, \qquad \cos q_2 = 0\,. \tag{16}$$

By the same way, we can find that the following conditions make B and D zero simultaneously and then they satisfy (13):

$$\cos q_1 = 0\,, \qquad \cos q_2 = 0\,, \tag{17}$$

$$\sin q_1 = 0\,, \qquad \sin q_2 = 0\,. \tag{18}$$

The conditions (15)-(18) may be rewritten as follows:

$$q_1\left(\equiv \frac{2\pi H_1}{Tv_1}\right) = (2m+1)\frac{\pi}{2}\,, \quad q_2\left(\equiv \frac{2\pi H_2}{Tv_2}\right) = (n+1)\pi\,, \tag{15'}$$

$$q_1 = (m+1)\pi\,, \qquad q_2 = (2n+1)\frac{\pi}{2}\,, \tag{16'}$$

$$q_1 = (2m+1)\frac{\pi}{2}\,, \qquad q_2 = (2n+1)\frac{\pi}{2}\,, \tag{17'}$$

$$q_1 = (m+1)\pi\,, \qquad q_2 = (n+1)\pi\,. \tag{18'}$$

$$[m = 0, 1, \cdots, \quad n = 0, 1, \cdots]$$

It is considerably difficult to find mathematically whether the conditions expressed by (15′)-(18′) will satisfy the condition of (4) or not.

Then, we shall try the diagrammatical treatments as in the last part of the former Section, by using the fundamental modes of (15′)-(18′), in order to find the requisite conditions for predominant vibration to appear at the ground surface. Substituting $m=0$ and $n=0$ of (15′)-(18′) in (10) and (11), we obtain the displacement distribution in each layer as shown in Figs. 5-8. Figs. 5-7 show that, when the values of the numerator of the expressions of surface displacement are higher than those of their denominator, the predominant vibration at the ground surface will appear. On the other hand, Fig. 8 show that, this case has little meaning in connection with the nature of excitation of vibrations.

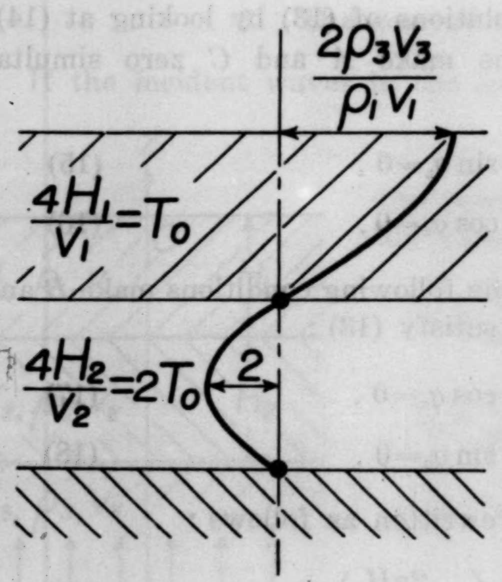

Fig. 5.

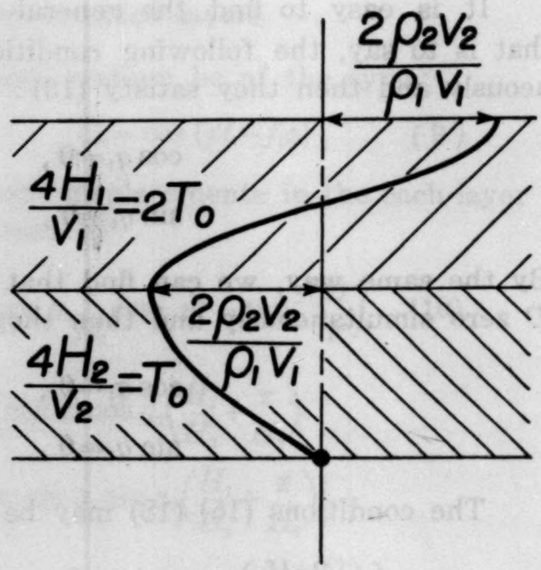

Fig. 6.

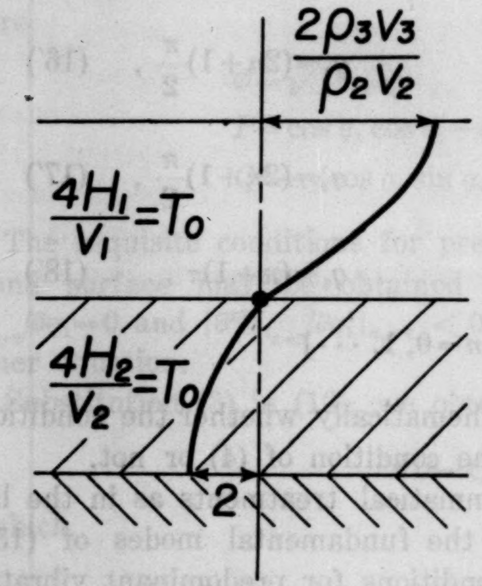

Fig. 7.

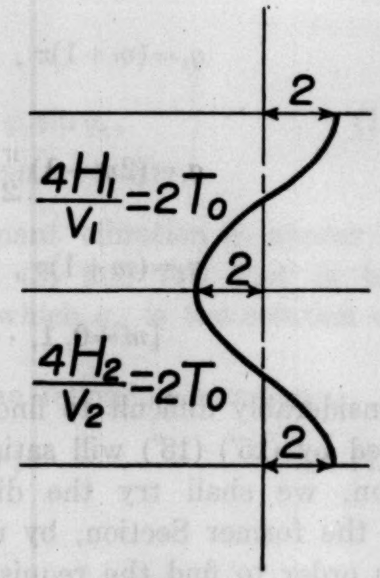

Fig. 8.

The requisite conditions for predominant vibration to be appeared at the ground surface, which may be found from these results, are enumerated as follows.

(i) In the case of $\rho_1 v_1 < \rho_3 v_3$, $T_0=4H_1/v_1$ and $H_2/H_1=2v_2/v_1$, the predominant amplitude at the surface is $2\rho_3 v_3/\rho_1 v_1$. In this case, the value of $\rho_2 v_2$ itself scarcely affects the surface amplitude. (See Fig. 5.)

(ii) In the case of $\rho_1 v_1 < \rho_2 v_2$, $T_0=4H_2/v_2$ and $H_2/H_1=v_2/2v_1$, the

predominant amplitude at the surface is $2\rho_2v_2/\rho_1v_1$. In this case, the value of ρ_3v_3 itself has no connection with the surface amplitude. (See Fig. 6.)

(iii) In the case of $\rho_2v_2<\rho_3v_3$, $T_0=4H_1/v_1$ and $H_2/H_1=v_2/v_1$, the predominant amplitude at the surface is $2\rho_3v_3/\rho_2v_2$. In this case, the value of ρ_1v_1 itself has no meaning in this problem. (See Fig. 7.)

These results may be explained by wave problem as follow: In general, since the wave reflections at the various boundaries interfere with one another, the spectral response of the amplitude of the surface is very irregular. Except in very unusual circumstances the maximum value of the peak is not large as in the case of the single layer. Otherwise, in some particular circumstances, when all the waves, being reflected at every boundaries and arriving at the free surface, are in the same phase, the surface amplitude grows up to an extremely large value.

It is a noteworthy fact that the rigidity itself of the medium of a layer among three layers scarcely affects the predominant vibration of ground surface. In other words, these results tell us that, it will be provable that the predominant vibration appears at the ground surface, even if a rigid medium exists at the superficial layer or intermediate one.

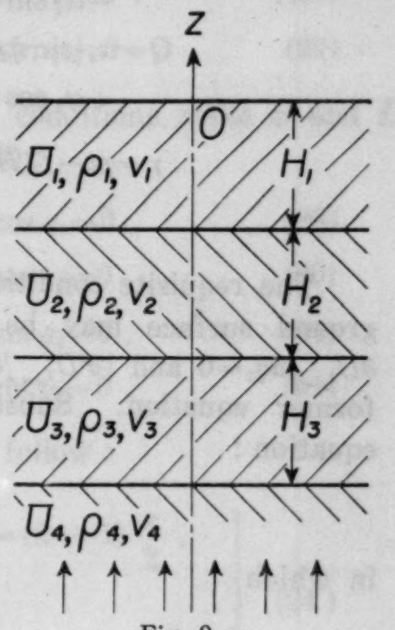

Fig. 9.

4. The case of three stratified layers

If the incident waves in the lowest medium be of the type expressed as follows

$$U_0=\cos(pt-f_4z)\,, \tag{19}$$

the resultant displacements in the each layer are expressed by[4)]

$$U_1=\frac{2}{\Phi}\cos f_1z\cos\gamma\,,$$

$$U_2=\frac{1}{\Phi}\left\{(1+\alpha_1)\cos\left(q_1-q_2\frac{z+H_1}{H_2}\right)\right.$$

$$\left.+(1-\alpha_1)\cos\left(q_1+q_2\frac{z+H_1}{H_2}\right)\right\}\cos\gamma\,,$$

4) K. KANAI and S. YOSHIZAWA, *Bull. Earthq. Res. Inst.*, **31** (1953), 275.

$$
\left.\begin{aligned}
U_3=\frac{2}{\Phi}\Big\{&(1+\alpha_1)(1+\alpha_2)\cos\left(q_1+q_2-q_3\frac{z+H_1+H_2}{H_3}\right)\\
&+(1-\alpha_1)(1+\alpha_2)\cos\left(q_1-q_2+q_3\frac{z+H_1+H_2}{H_3}\right)\\
&+(1-\alpha_1)(1-\alpha_2)\cos\left(q_1-q_2-q_3\frac{z+H_1+H_2}{H_3}\right)\\
&+(1+\alpha_1)(1-\alpha_2)\cos\left(q_1+q_2+q_3\frac{z+H_1+H_2}{H_3}\right)\Big\}\cos\gamma\,,
\end{aligned}\right\}\quad(20)
$$

where

$$
\left.\begin{aligned}
&\Phi=\sqrt{P^2+Q^2}\,,\\
&P=\cos q_3(\cos q_1\cos q_2-\alpha_1\sin q_1\sin q_2)\\
&\qquad-\alpha_2\sin q_3(\sin q_1\cos q_2+\alpha_1\cos q_1\sin q_2)\,,\\
&Q=\alpha_3\{\sin q_3(\cos q_1\cos q_2-\alpha_1\sin q_1\sin q_2)\\
&\qquad+\alpha_2\cos q_3(\cos q_1\sin q_2+\alpha_1\sin q_1\cos q_2)\}\,,\\
&\gamma=pt-f_4(H_1+H_2+H_3)-\tan^{-1}\frac{Q}{P}\,.
\end{aligned}\right\}\quad(21)
$$

The requisite conditions for predominant vibration to appear at the ground surface may be obtained from (3) and (4), that is to say, $\partial U_{1_{z=0}}/\partial q_1=0$ and $|\partial^2 U_{1_{z=0}}/\partial q_1^2|_{q_1=q_m}<0$, in which q_m are the solution of the former equation. Substituting (3) in (20), we obtain the following equation:

$$
AB+CD=0\,,\qquad(22)
$$

in which

$$
\left.\begin{aligned}
&A=\cos q_3(\cos q_1\cos q_2-\alpha_1\sin q_1\sin q_2)\\
&\qquad-\alpha_2\sin q_3(\sin q_1\cos q_2+\alpha_1\cos q_1\sin q_2)\,,\\
&B=\sin q_3\{\cos q_1\cos q_2(a_3+\alpha_2+\alpha_1\alpha_2 a_2)\\
&\qquad-\sin q_1\sin q_2(\alpha_1 a_3+\alpha_2 a_2+\alpha_1\alpha_2)\}\\
&\qquad+\cos q_3\{\sin q_1\cos q_2(1+\alpha_1 a_2+\alpha_2)\\
&\qquad+\cos q_1\sin q_2(a_2+\alpha_1+\alpha_2)\}\,,\\
&C=\cos q_3\{-(a_3+a_2\alpha_2+\alpha_1\alpha_2)\cos q_1\cos q_2\\
&\qquad+(a_3\alpha_1+a_2\alpha_1\alpha_2+\alpha_2)\sin q_1\sin q_2\}
\end{aligned}\right\}\quad(23)
$$

$$
\left.\begin{aligned}
&\quad +\sin q_3\{(\alpha_1 a_2+\alpha_1\alpha_2 a_3+1)\sin q_1\cos q_2\\
&\quad +(a_2+\alpha_2 a_3+\alpha_1)\cos q_1\sin q_2\}\ ,\\
&D=\alpha_3\{\sin q_3(\cos q_1\cos q_2-\alpha_1\sin q_1\sin q_2\\
&\quad +\alpha_2\cos q_3(\cos q_1\sin q_2+\alpha_1\sin q_1\cos q_2)\}\ ,\\
&a_2=\frac{H_2}{H_1}\frac{v_1}{v_2}\ ,\qquad a_3=\frac{H_3}{H_1}\frac{v_1}{v_3}\ .
\end{aligned}\right\}
$$

It will be able easy to find the general solutions of (22) by looking at (23), that is to say, the following conditions make A and C zero simultaneously and then they satisfy (22):

$$\cos q_1=0\ ,\quad \cos q_2=0\ ,\quad \cos q_3=0\ , \tag{24}$$

$$\cos q_1=0\ ,\quad \sin q_2=0\ ,\quad \cos q_3=0\ , \tag{25}$$

$$\cos q_1=0\ ,\quad \sin q_2=0\ ,\quad \sin q_3=0\ , \tag{26}$$

$$\cos q_1=0\ ,\quad \cos q_2=0\ ,\quad \sin q_3=0\ . \tag{27}$$

In the same way, we find that the following conditions make B and D zero simultaneously, and then they satisfy (22):

$$\sin q_1=0\ ,\quad \cos q_2=0\ ,\quad \cos q_3=0\ , \tag{28}$$

$$\sin q_1=0\ ,\quad \sin q_2=0\ ,\quad \cos q_3=0\ , \tag{29}$$

$$\sin q_1=0\ ,\quad \cos q_2=0\ ,\quad \sin q_3=0\ , \tag{30}$$

$$\sin q_1=0\ ,\quad \sin q_2=0\ ,\quad \sin q_3=0\ . \tag{31}$$

The conditions (24)-(31) may be rewritten as follow:

$$
\left.\begin{aligned}
&q_1\left(\equiv\frac{2\pi H_1}{Tv_1}\right)=(2m+1)\frac{\pi}{2}\ ,\quad q_2\left(\equiv\frac{2\pi H_2}{Tv_2}\right)=(2n+1)\frac{\pi}{2}\ ,\\
&q_3\left(\equiv\frac{2\pi H_3}{Tv_3}\right)=(2s+1)\frac{\pi}{2}\ .
\end{aligned}\right\} \tag{24'}
$$

$$q_1=(2m+1)\frac{\pi}{2}\ ,\qquad q_2=(n+1)\pi\ ,\qquad q_3=(2s+1)\frac{\pi}{2}\ , \tag{25'}$$

$$q_1=(2m+1)\frac{\pi}{2}\ ,\qquad q_2=(n+1)\pi\ ,\qquad q_3=(s+1)\pi\ , \tag{26'}$$

$$q_1=(2m+1)\frac{\pi}{2}\ ,\qquad q_2=(2n+1)\frac{\pi}{2}\ ,\qquad q_3=(s+1)\pi\ , \tag{27'}$$

$$q_1=(m+1)\pi\,,\qquad q_2=(2n+1)\frac{\pi}{2}\,,\qquad q_3=(2s+1)\frac{\pi}{2}\,,\qquad (28')$$

$$q_1=(m+1)\pi\,,\qquad q_2=(n+1)\pi\,,\qquad q_3=(2s+1)\frac{\pi}{2}\,,\qquad (29')$$

$$q_1=(m+1)\pi\,,\qquad q_2=(2n+1)\frac{\pi}{2}\,,\qquad q_3=(s+1)\pi\,,\qquad (30')$$

$$q_1=(m+1)\pi\,,\qquad q_2=(n+1)\pi\,,\qquad q_3=(s+1)\pi\,.\qquad (31')$$

$$[m=0,1,\cdots,\quad n=0,1,\cdots,\quad s=0,1,\cdots]$$

It is considerably difficult to find mathematically whether the conditions expressed by (24′)-(31′) will satisfy the condition of (4) or not.

Next, we shall try the diagrammatical treatments as in the former Section, by using the fundamental modes of (15′)-(18′), namely, $m=0$, $n=0$ and $s=0$, in order to find the requisite conditions for predominant vibration to appear at the ground surface.

Substituting (24′)-(31′) of $m=0$, $n=0$ and $s=0$ in (20), we obtain the displacement distribution in each layer as shown in Figs. 10-17.

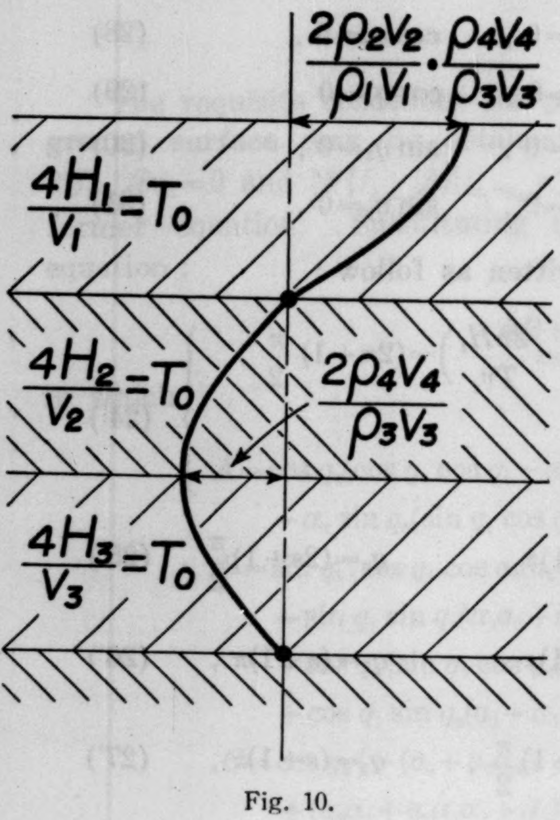

Fig. 10.

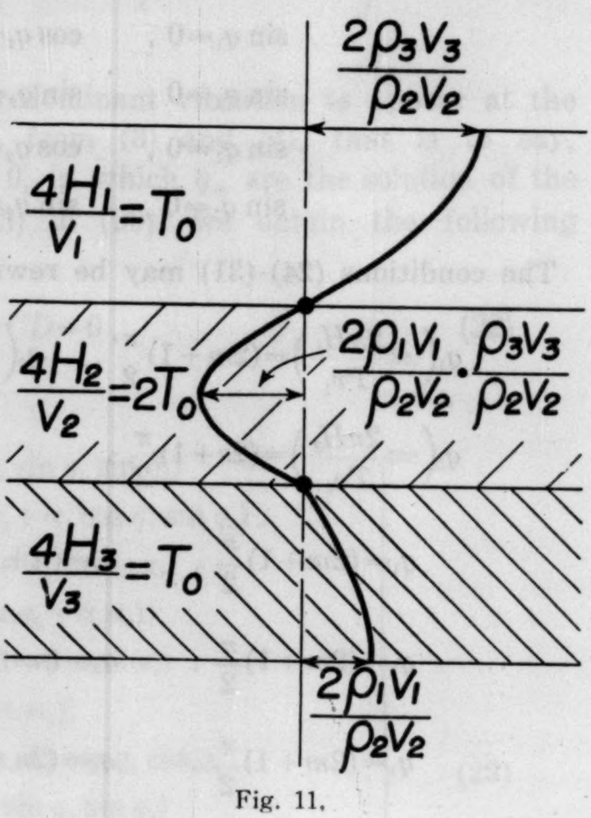

Fig. 11.

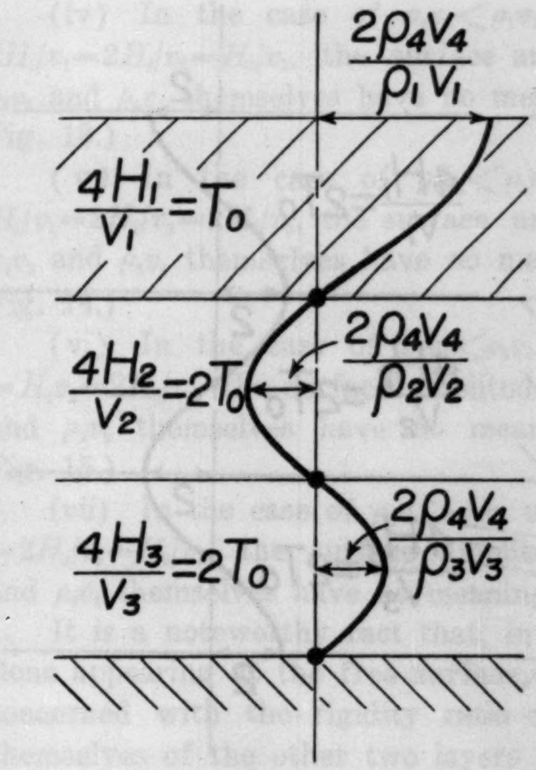

Fig. 12.

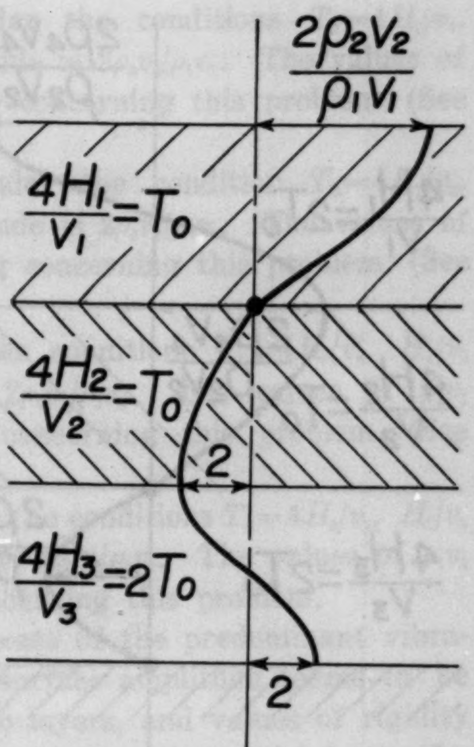

Fig. 13.

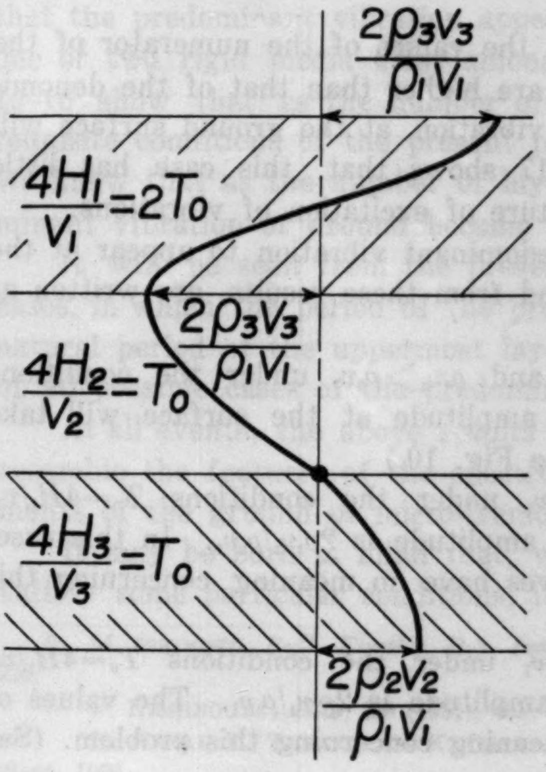

Fig. 14.

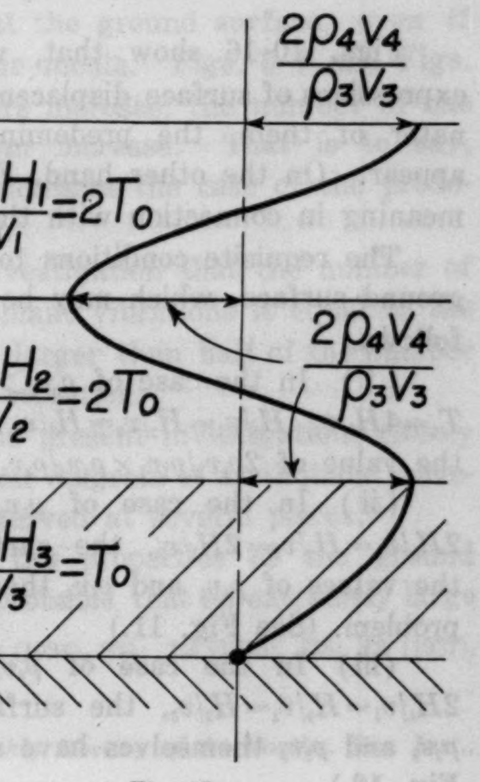

Fig. 15.

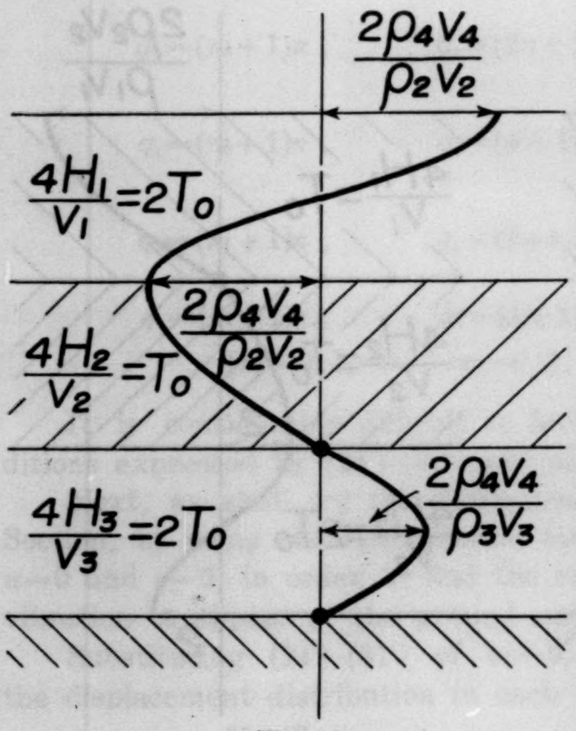

Fig. 16.

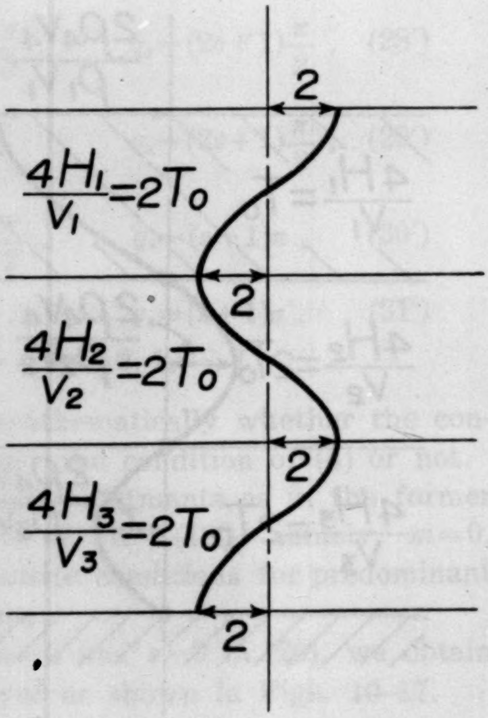

Fig. 17.

Figs. 10-16 show that, when the values of the numerator of the expressions of surface displacement are higher than that of the denominator of them, the predominant vibration at the ground surface will appear. On the other hand, Fig. 17 shows that, this case has little meaning in connection with the nature of excitation of vibrations.

The requisite conditions for predominant vibration to appear at the ground surface, which may be found from these results, are written as follows.

(i) In the case of $\rho_2 v_2 > \rho_1 v_1$ and $\rho_4 v_4 > \rho_3 v_3$ under the conditions $T_0 = 4H_1/v_1$, $H_1/v_1 = H_2/v_2 = H_3/v_3$, the amplitude at the surface will take the value of $2\rho_2 v_2/\rho_1 v_1 \times \rho_4 v_4/\rho_3 v_3$. (See Fig. 10.)

(ii) In the case of $\rho_3 v_3 > \rho_2 v_2$ under the conditions $T_0 = 4H_1/v_1$, $2H_1/v_1 = H_2/v_2 = 2H_3/v_3$, the surface amplitude is $2\rho_3 v_3/\rho_2 v_2$. In this case, the values of $\rho_1 v_1$ and $\rho_4 v_4$ themselves have no meaning concerning this problem. (See Fig. 11.)

(iii) In the case of $\rho_4 v_4 > \rho_1 v_1$ under the conditions $T_0 = 4H_1/v_1$, $2H_1/v_1 = H_2/v_2 = H_3/v_3$, the surface amplitude is $2\rho_4 v_4/\rho_1 \rho_1$. The values of $\rho_2 v_2$ and $\rho_3 v_3$ themselves have no meaning concerning this problem. (See Fig. 12.)

(iv) In the case of $\rho_2 v_2 < \rho_1 v_1$ under the conditions $T_0 = 4H_1/v_1$, $2H_1/v_1 = 2H_2/v_2 = H_3/v_3$, the surface amplitude is $2\rho_2 v_2/\rho_1 v_1$. The values of $\rho_3 v_3$ and $\rho_4 v_4$ themselves have no meaning concerning this problem. (See Fig. 13.)

(v) In the case of $\rho_3 v_3 < \rho_1 v_1$ under the condition $T_0 = 4H_2/v_2$, $H_1/v_1 = 2H_2/v_2 = 2H_3/v_3$, the surface amplitude is $2\rho_3 v_3/\rho_1 v_1$. The values of $\rho_2 v_2$ and $\rho_4 v_4$ themselves have no meaning concerning this problem. (See Fig. 14.)

(vi) In the case of $\rho_4 v_4 < \rho_3 v_3$ under conditions $T_0 = 4H_3/v_3$, $H_1/v_1 = H_2 v_2 = 2H_3/v_3$, the surface amplitude is $2\rho_4 v_4/\rho_3 v_3$. The values of $\rho_1 v_1$ and $\rho_2 v_2$ themselves have no meaning concerning this problem. (See Fig. 15.)

(vii) In the case of $\rho_4 v_4 > \rho_2 v_2$ under the conditions $T_0 = 4H_2/v_2$, $H_1/v_1 = 2H_2/v_2 = H_3/v_3$, the surface amplitude is $2\rho_4 v_4/\rho_2 v_2$. The values of $\rho_1 v_1$ and $\rho_3 v_3$ themselves have no meaning concerning this problem.

It is a noteworthy fact that, in the case of the predominant vibrations appearing at the free surface, the surface amplitude seems to be concerned with the rigidity ratio of two layers, and values of rigidity themselves of the other two layers have no connection with the predominant amplitude. These results tell us again that, it will be provable that the predominant vibration appears at the ground surface, even if one or two rigid media exist among four media. Figs. 5–7 and Figs. 10–16 show that as the number of layers increase, the number of the requisite conditions of the present problem increase. That is to say, we know that as the number of layers increases the case of the predominant vibration of ground become rarer.

It will be seen from the present investigation that the number of cases, in which the period of the predominant vibrations is equal to the natural period of the uppermost layer is larger than half of the number of all possible cases of the predominant vibration.

At all events, the above results of the present investigations closely resemble the features of the spectrogramic diagram of earthquake movements of the ground or micro-tremor observed at several places.[5)]

It may be born in mind that, when the properties of the ground satisfy some particular conditions, it is probable that an extremely large

5) M. ISHIMOTO, *Bull. Earthq. Res. Inst.*, **12** (1934), 234; **13** (1935), 438; **15** (1937), 526.

F. KISHINOUYE, *ditto*, **29** (1951), 403.

K. KANAI, T. TANAKA and K. OSADA, *Monthly Meeting of the Earthq. Res. Inst.*, (Sept. 1956).

vibration amplitude will appear at the ground surface, even if a rigid medium exists at the superficial layer or intermediate one.

In such cases, discrimination between good or bad ground considered from a vibrational point of view will sometimes differ from the statical point, namely, the bearing power of ground, etc.

The above results are one of the most important factors in the development of earthquake resistant structural design.

5. Conclusion

From the present mathematical investigations on the vibration problem of the surface layer, the following has been made clear:

(i) In general, in the case of multiple stratified layers, since the elastic wave reflections at the various boundaries interfere with one another, the spectral response of the amplitude of the surface layer is very irregular and the maximum value of the peak is not so large as in the case of the single layer.

(ii) In some particular circumstances, when all the waves being reflected at every boundary and arriving at the free surface, are in the same phase, the surface amplitudes grows up to an extremely large value.

(iii) It is probable that extremely large vibration amplitude will appear at the ground surface, even if a rigid medium exist in the superficial layer or intermediate one.

(iv) At many times, the predominant period of ground vibration coincides with the natural period of the uppermost layer.

(v) The most important conclusion of the present investigation concerning the development of earthquake resistant structural design is that the discrimination of good or bad ground from the vibrational point of view will sometimes differ from that viewed from the statical point, namely, the bearing power of ground, etc.

23. 卓越震動が現われるための地盤の条件

地震研究所 金井 清

地盤の震動が或周期で卓越する現象については，多くの験震的並びに数理的な研究が行われて来た．最近，この問題は，耐震工学上で特に注意をひき始めたようである．

自然地震並びに常時微動からみた地盤の震動性状は2つの型に大別できる．即ち 1 つの型は地盤特有な或周期の波がはつきり卓越するものであり，他の1つの型は2つ以上の卓越する周期があり，極端な場合には，その数が多くて卓越周期の言葉があてはまらない．

前者は 1 層から成る表面層の震動問題として一応の説明がつき，これについては験震的研究結果から求めた実験式に数理的検討を加えた半実験式を既に発表した．

本研究は後者の場合，即ち表面層が 2 層以上から成つている場合に，如何なる条件があれば，地表面に特別に大きな震動が誘発されるかをしらべたものである．この論文の計算法は少しも新しいものではなく，20 年も前から順々に出されたものの応用に過ぎない．

地表面の震動が特に大きくなるのは，境界面で反射して来る波が同位相になつて重り合うからであるから，層数が多くなる程，この現象の起こりにくくなる事は容易に想像できる．

しかし，多層の場合でも，各層の剛性と厚さの関係が特別な条件を満足する場合には，各境界面で反射してくる波がすべて同位相になる現象も起り得て，地表面の震動は特別に大きくなる．

しかして，最上層或は中間層に硬い層があつてもこのような条件が存在し得ることがわかつた．

即ち，この事は，震動的にみた地盤の良否と，地耐力等から見たそれとは一致しない場合があり得る事を示唆するものである．

地耐力等からは，かなり良いと推定される地盤が，地震動，常時微動からみた震動性状並びに過去の震害資料からはどうしても良いとは言えない実例がいくつかあるが，これは，恐らく本研究の結果で解釈されるものと考えられる．

vibration amplitude will appear at the ground surface, even if a rigid medium exists at the superficial layer or intermediate one.

In such cases, discrimination between good or bad ground considered from a vibrational point of view will sometimes differ from the statical point, namely, the bearing power of ground, etc.

The above results [illegible] development of earthquake resistant structural design.

Most [illegible] investigations on the vibration problem of the surface [illegible] been made [illegible]

(i) [illegible] elastic wave [illegible] the [illegible] interface with the [illegible] surface layer [illegible] very [illegible] the [illegible] value of the [illegible] in the case of [illegible]

(ii) In some particular circumstance, when all the [illegible] reflecting [illegible] and [illegible] at the [illegible] surface are in the same phase, the surface amplitudes grow up to an extremely large value.

(iii) It is probable that extremely large vibration amplitude will appear at the ground surface, even if a rigid medium exist in the superficial layer or intermediate one.

(iv) At many times, the predominant period of ground vibration coincides with the natural period of the uppermost layer.

(v) The most important conclusion of the present investigation concerning the development of earthquake resistant structural design is that the discrimination of good or bad ground from the vibrational point of view will sometimes differ from that viewed from the statical point, namely, the bearing power of ground, etc.

24. *The Nature of Seismic Origins as Inferred from Seismological and Geodetic Observations* (1).

By Keichi KASAHARA,

Earthquake Research Institute.

(Read June 26, 1956, October, 23, 1956, December 18, 1956, March 26, 1957, April 23, 1957, and June 25, 1957.
—Received June 29, 1957.)

CONTENTS.

Page

General Introduction 474

Chapter I. Spectral Analyses of Initial Motions of Seismograms........... 477

1. Introduction.. 477
2. Spectral analyses of transient wave-forms.......................... 478
3. Characteristics of seismographs and the reduction for them 481
4. Various effects of wave propagation through the earth.............. 483

Chapter II. Wave Generation from Explosion Origins 487

1. Introduction 487
2. Spectral analyses of seismograms obtained by explosion tests 488
3. Characteristics of explosion origins 492
4. Wave phenomena in the vicinity of explosion origins 495
5. Deformation of wave-forms due to the viscosity of the medium 497

Chapter III. Spectrum of Seismic Waves and Magnitude of Earthquakes.... 500

1. Introduction.. 500
2. Spectral analyses of seismograms 501
3. The M-T curve.. 503
4. The energy and the dimension of seismic origins 507
5. Further discussion on the related problems 511

Chapter IV. Analyses of Crustal Deformations Accompanied by Great Earthquakes 512

1. Introduction.. 512
2. General view of earthquakes accompanying crustal deformations 514
3. Statics of a lateral fault 516
4. Features of some actual faults 519
5. Discussion on the related problems 523
6. A lateral fault of finite length (model experiments) 526

(To be continued.)

General Introduction.

Earthquakes were thought, in ancient times, to be caused by some super-natural causes. Since those days, quite a few references have been made to those mysterious phenomena which took place abruptly causing terrible shocks on the surface of the earth. It took quite a long time until we arrived at the right understanding of the phenomena. At the end of the last century, when seismology grew up to be a branch of modern science, however, definite evidence was established that earthquakes occur in connection with elastic waves generated from a point in the earth. This was indeed the starting point of physical seismology, and thereafter, a remarkable development has taken place following this fundamental finding. Studies carried out in the past sixty years have resulted in a great store of knowledge about the nature of earthquakes.

In the earlier period of seismology, most studies on seismic waves were made under the assumption that the origin is a point in the earth. It is well-known that H. Lamb carried out successfully a theoretical work on elastic waves generated from a point laid on the surface of a homogeneous medium.[1] With his theory in mind, we could understand fairly well the most fundamental structure of seismograms. However, it was noticed that seismograms actually observed were not so simple as theoretical curves in their detailed structure. In order to account for the discrepancy between theory and observation, it was naturally required to make more complicated assumptions on the origin of earthquakes. It has also been recognized that seismic waves undergo complicated modifications while they are propagated through the actual earth. As to the influence of this sort, numbers of papers have been published, providing some knowledge about the constitution of the earth as well as about wave propagation through the medium of complicated structures. Since, however, it is beyond the scope of this paper to put much stress on problems of wave propagation, the writer is not here going to trace back the development of this side of seismology.

With the progress of observation technique, seismologists began to pay attention to remarkable facts which seemed to have an important bearing on the mechanism of earthquake origins. J. Shida was the first who noticed the fact that the push-pull distribution of initial motions is

1) H. LAMB, *Phil. Trans.*, A, **203** (1904), 1.

fairly systematic in regard to azimuths.[2] His discovery attracted attention of many seismologists, especially of those in Japan, who examined the distribution in different ways and came to the conclusion that most earthquakes were probably caused by such stress change at origins as to be interpreted with a couple of shearing forces or with a combination of compressional and tensile stresses working perpendicularly with one another.[3]

C. F. Richter initiated a study from a new standpoint in 1935. He introduced the magnitude as an indicator for the scale of earthquakes.[4] Since then not a few papers have been published by himself and B. Gutenberg as well as by other seismologists, who carried out extensive studies upon the related problems. One of the important contributions made by them was the estimation of seismic energies based on the observational results of earthquakes. Owing to the success in treatment of energy, it became possible to investigate the earthquake occurrence synthetically with various kinds of studies related to crustal deformations or to the thermal process within the earth.

Meanwhile, some seismologists came to improve the model of seismic origin which has been so far assumed as a point. The first approach to the model, in which the finite dimension was taken into consideration, was made by K. Sezawa and other theoreticians.[5] They assumed that the origin is of spherical shape in place of a point, and studied waves caused by stress changes on the surface of the sphere. According to their conclusions, forms and amplitudes of elastic waves generated from the origin concerned are given as the functions of the dimension and the rapidity of the stress change. It is also found that, if the distribution of forces at the origin is determined so as to satisfy the push-pull distribution on the earth's surface, outstanding characteristics of some deep-focus earthquakes can be interpreted satisfactorily.

We shall now turn the point of discussion to crustal deformations associated with seismic activities as obtained from geodetic observations. Many references have been made, since old days, to crustal deformations such as faults or land-upheavals occurring in the case of great

2) J. SHIDA, *Tôyô-gakugei Zasshi*, **45** (1929), 275 (in Japanese).
3) *f.i.* H. HONDA, A. MASATSUKA, and K. EMURA, *Sci. Rep., Tohoku Univ., Ser.* 5, **8** (1957), 30.
4) C. F. RICHTER, *Bull. Seis. Soc. Amer.*, **25** (1935), 1.
5) K. SEZAWA, *Bull. Earthq. Res. Inst.*, **14** (1936), 10.
H. KAWASUMI and R. YOSIYAMA, *Bull. Earthq. Res. Inst.*, **13** (1935), 496.
H. HONDA, *Geophys. Mag.*, **8** (1934), 153.
W. INOUYE, *Bull. Earthq. Res. Inst.*, **14** (1936), 582.

earthquakes. Their features come to be investigated more accurately by means of repeated precise levelling as well as triangulation over the epicentral areas. C. Tsuboi compiled the results of such observations in a voluminous paper,[6] in which he pointed out that no strain in the earth's crust exceeds a certain limit except in the vicinity of a seismic fault. As a result of his later study, he came to the conclusion that the strength of the crust was not infinitely large. It seems likely that strain energy would be accumulated in a sufficiently large volume of the crust giving rise to a great earthquake when the strain exceeds a limit. He estimated the maximum amount of energy accumulated in the crust as about 3×10^{24} c.g.s., which agreed well with the energy of seismic waves estimated for the largest earthquake that ever known.[7]

The similarity between the mode of crustal deformations and that of push-pull distribution of initial motions is sometimes noticeable. Although such a comparison is not always possible, we can see good agreement between the patterns of deformations and of push-pull distribution in the case of particular great earthquarkes, which are accompanied by typical lateral fautls.[8] These facts suggest that there would be an inseparable relation between the earth's strain and the earthquake origin.

A number of seismologists have lately reported that they found some evidence that the origin of great earthquakes seemed likely to shift successively to one direction across the hypocentral space.[9] The presumed mode of shifting is similar to that of the propagation of fractures in a brittle material. If the fact is established in future, it would also play an important *rôle* in investigating the mechanism of earthquakes.

On taking into account the possible relations between earthquakes and crustal deformations or propagation of fractures, the above-mentioned model of spherical origin seems to be too rough in order to build a unified picture of seismic origins. In case we assume another model, with which we can explain all the facts consistently, it would be accepted as more suitable than the previous one. In fact, it seems to the

6) C. TSUBOI, *Jap. Journ. Astro. Geophys.*, **10** (1933), 93.
7) C. TSUBOI, *Journ. Phys. Earth*, **4** (1956), 63.
8) *f.i.* H. HONDA, *Zishin-hadô* (1942), p. 107 (in Japanese).
9) H. BENIOFF, *Earthquakes in Kern County, Calif., 1952, Bull. 171*, Division of Mines (1955), 199.
T. USAMI, *Quart. Journ., Seismology*, **21** (1956) 1 (in Japanese).
S. KÔMURA, *Zisin (Journ. Seis. Soc. Japan)*, [ii], **9** (1957), 174 (in Japanese).

present writer that a number of seismologists are inclined to support the following idea, though detailed parts of it are still open to question. The idea is that, when a certain volume of the earth is strained to the limit of its strength, fracture-like events would take place in some part of it and the accumulated strain energy is radiated from there as seismic waves. This kind of idea seems to be similar to the well-known hypothesis of H. F. Reid,[10] though he presented his theory on the basis of very few observational facts.

We have studied, in the above, how the picture of seismic origins was improved with the progress of seismological and geodetic investigations. In spite of the investigations hitherto carried out, we are still far away from any satisfactory solution of the most fundamental question in seismology. The writer is here going to add something to the study of seismic origins by carrying out some analyses related to a revised model of origins by which we can interpret consistently the evidence obtained from both the seismological and geodetic standpoint. The final purpose of the present paper being such, the majority of the discussion will be made upon the characteritics of natural earthquakes. In addition, however, some discussion will be made on the nature of explosion origins, which will be of some use for studying the fundamental problem of seismic prospecting.

Chapter I.

Spectral Analyses of the Initial Motions of Seismograms.

1. Introduction.

We have seen in the foregoing introduction that the period or the form of seismic waves has a close relation to the condition of origins. Notwithstanding its importance, the wave-form of initial motions has not been investigated so fully as amplitudes or travel-times of seismic waves. One of the reasons that only a few studies being carried out upon the characteristics of wave-forms may probably depend on the circumstances that the ordinary method of frequency analysis can not be applied conveniently to such complicated forms which are composed of various kinds of wavelets.

Some seismologists have lately undertaken wave-form analyses by means of spectral analysers or by the auto-correlation method, which

10) H. F. REID, *Physics of the Earth*, VI (1933), p. 100.

have been developed in connection with information theory. These methods can be applied usefully to such wave-forms as are to be seen in the later part of seismograms, which are composed of stationary time series.[11] The initial part of seismograms, with which our main interest is concerned, is transient rather than stationary, so that it is necessary to find an improved method which fits our present purpose.

2. Spectral analyses of transient wave-forms.

The general feature of the initial motion is characterized by a sudden beginning of vibrations which comes after a long period of no disturbances and is followed by succeeding vibrations of complicated wave-forms. It is widely accepted by seismologists that only the first several vibrations would be important in conducting studies on the seismic origin, while the complicated vibrations lying between the initial motions and the later remarkable phases are belived to be produced secondarily by some causes such as multiple reflections and conversions during wave propagation. In order to pick up the information directly coming from the origin, the analyses should be made in such a way as to avoid undesirable influences of those vibrations.

The simplest way can be effected by cutting off the unnecessary part of the seismogram. This procedure is identical with multiplication of the original wave-form by a rectangular pulse which is 1 throughout the necessary interval of time and 0, outside it. However, the method would be less suitable than that described in the following, because the sharp cut-off of the later part, apparently constrained as a result of the multiplied step-function, would be as remarkable as the real beginning of the seismogram, so that we would have some non-real harmonic component by the procedure.[12] Such an effect would disturb our appropriate interpretation of spectrum, though we might be able to avoid such an influence by adjusting the duration of the step-function suitably for respective cases.

Let us consider that the original wave-form is expressed by $f(t)$, a part of which is to be analysed around $t=t_0$. Let $f(t)$ be multiplied by a weight function $K(t)$, which is taken temporarily as follows,

$$K(t)=e^{-c^2(t-t_0)^2/4} \quad \cdots \quad (1)$$

11) S. GOLDMAN, *Information Theory* (1953), p. 239.

12) S. GOLDMAN, *Frequency Analysis, Modulation and Noise* (1948), p. 61.

Then, we obtain a modified function $F(t)$ as,

$$F(t)=f(t)\cdot K(t)\,, \tag{2}$$

which is practically equal to $f(t)$ in the neighbourhood of $t=t_0$, but becomes different from it approaching zero when $t-t_0$ goes to $\pm\infty$ (Fig. 1). Employing a suitable value for the constant c in (1), we obtain an isolated wave-form in which are conserved well the spectral structre of the part of $f(t)$ in question. The spectrum of such an isolated wave-form can be studied by means of Fourier analysis as was shown by Y. Satô,[13] so that it is possible to replace the direct analysis of $f(t)$ by the spectral analysis of $F(t)$ as deduced from the above-mentioned procedure.

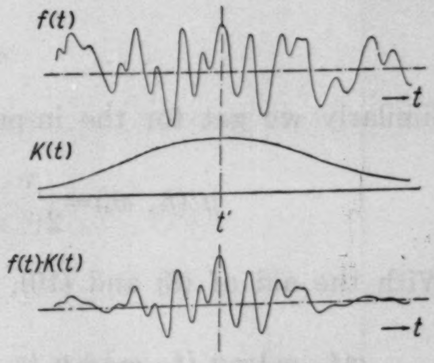

Fig. 1. Schematic view of the procedure to obtain $F(t)$ from $f(t)$.

This modification of the original function will, of course, give rise to some alteration of the result as will be examined in the following. Let $Y(\omega)$ be the frequency characteristics of an imagined linear filter, then the impulsive response of it is given as,[14]

$$B(t)=\frac{1}{2\pi}\int_{-\infty}^{+\infty} Y(\omega)\, e^{i\omega t} d\omega\ . \tag{3}$$

When $Y(\omega)$ is given as follows,

$$Y(\omega)=e^{-(\omega_0-\omega)^2/c^2}, \tag{4}$$

$B(t)$ becomes,

$$B(t)=\frac{1}{2\pi}\int_{-\infty}^{+\infty} e^{-(\omega_0-\omega)^2/c^2}\, e^{i\omega t}\, d\omega\ , \tag{5}$$

or

$$=\frac{c}{2\sqrt{\pi}}\, e^{i\omega_0 t}\, e^{-c^2t^2/4}\ . \tag{6}$$

The response of the filter to the in-put of $f(t)$ from $t=-\infty$ to $t=t_0$ is written, with the principle of superposition,[15] as follows,

13) Y. Satô, *Bull. Earthq. Res. Inst.*, **32** (1954), 259.
14) S. Goldman, *Information Theory* (1953), p. 223.

$$g_+(t_0,\ \omega_0)=\int_{-\infty}^{t_0} f(t)B(t-t_0)dt\ , \tag{7}$$

and

$$=\frac{c}{2\sqrt{\pi}}\int_0^{+\infty} f(t_0-\tau)\,e^{-c^2\tau^2/4}\,e^{i\omega_0\tau}\,d\tau\ , \tag{8}$$

where,

$$\tau=t_0-t\ . \tag{9}$$

Similarly we get for the in-put of $f(t)$ from $t=+\infty$ to $t=t_0$,

$$g_-(t_0,\ \omega_0)=\frac{c}{2\sqrt{\pi}}\int_{-\infty}^{0} f(t_0-\tau)\,e^{-c^2\tau^2/4}\,e^{i\omega_0\tau}\,d\tau\ . \tag{10}$$

With the aid of (8) and (10), we obtain,

$$g(t_0,\ \omega_0)=g_+(t_0,\ \omega_0)+g_-(t_0,\ \omega_0)=\frac{c}{2\sqrt{\pi}}\int_{-\infty}^{+\infty} f(t_0-\tau)\,e^{-c^2\tau^2/4}\,e^{i\omega_0\tau}\,d\tau\ , \tag{11}$$

which is considered as the total response of the filter to $f(t)$ with respect to the vicinity of $t=t_0$. We notice that the right-hand side of (11) is exactly the same as the Fourier transform of a function $F(t_0,\ t)$, provided that

$$F(t_0,\ t)=\frac{c}{2\sqrt{\pi}}f(t)\,e^{-c^2(t-t_0)^2/4}\ . \tag{12}$$

We know, therefore, that when the modified function $F(t)$ is subject to Fourier analysis, the result will be identical with the total response of the filter (4) to the in-put of $f(t)$ with respect to $t=t_0$. It is easily seen that Δt, the length of the effective duration of $K(t)$ in which is secured the good similarity between $f(t)$ and $F(t)$, is proportional to c, whereas $\Delta\omega$, the band-width of the imagined filter, to $1/c$ (Fig. 2). Therefore the following relation exists between the two quantities, such as,

$$|\Delta t|\cdot|\Delta\omega|\approx 1\ , \tag{13}$$

which is the principle of uncertainty in information theory.[16]

15) *ibid*. p. 224.

16) GOLDMAN, *Frequency Analysis, Modulation and Noise* (1948), p. 135.

The larger the value of c is given, the longer the interval of good similarity of $F(t)$ with $f(t)$ becomes until both the functions coincide with together perfectly, when $c=\infty$. In such a case the band-width of the filter is zero, which means the result being composed of line spectra as can be seen in ordinary Fourier analysis (Fig. 3). If $f(t)$ is stationary in its spectral structure, (11) would give the same picture of the spectrum notwithstanding the different value of c. On the contrary, an application of a different value of c to a transient wave-form would lead us to a different picture of the spectrum ; however, unless c differs exceedingly the result would not suffer from essential troubles. Accordingly it is not a difficult matter to choose the suitable value of c for studying the initial part of ordinary seismograms.

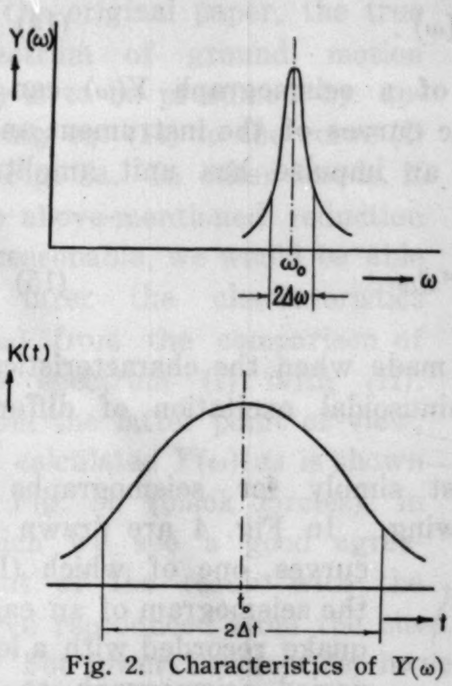

Fig. 2. Characteristics of $Y(\omega)$ and $K(t)$.

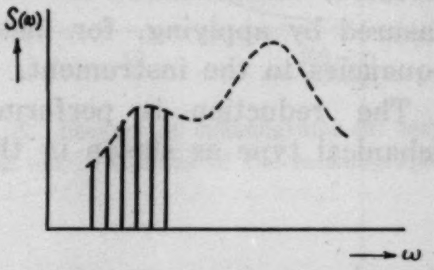

Fig. 3. Continuous spectrum and line spectrum.

3. Characteristics of seismographs and the reduction for them.

Wave-forms on seismograms do not indicate the ground motion itself but illustrate the response of a seismograph to it, so that we could not see the nature of seismic waves accurately unless we perform necessary reduction for such influences. Seismographs, including pendulums, amplifiers,[18] filters, and galvanometers, are considered as linear systems of information transmission, for which reduction can be made in the following way. Let the spectrum of recorded wave-forms and the im-

17) Y. SATÔ, *loc. cit.* 13).

18) Amplifiers with AVC circuit are non-linear, and so the seismograms recorded with such instruments can not be used for the present investigation.

pulsive response of the seismograph be $R(\omega)$ and $Y(\omega)$, respectively, then the true spectrum of ground motions is given as,[19]

$$S(\omega)=R(\omega)/Y(\omega)\ . \tag{14}$$

We know that the impulsive response of a seismograph $Y(\omega)$ can be derived from the so-called characteristic curves of the instrument under the consideration that the spectrum of an impulse has unit amplitude for all frequencies, or,

$$\delta(t)=\frac{1}{2\pi}\int_{-\infty}^{+\infty} e^{i\omega t}\,d\omega\ . \tag{15}$$

Therefore, the reduction can be easily made when the characteristics is measured by applying, for instance, sinusoidal excitation of different frequencies to the instrument.

The reduction is performed most simply for seismographs of mechanical type as shown in the following. In Fig. 4 are drawn two curves, one of which (I) is the seismogram of an earthquake recorded with a long-period seismograph at the Hongo station, Tokyo, and another (II) shows the true ground motion deduced from (I) by means of numerical integration.[20] We calculated the spectra for the two wave-forms in such a way as was shown in the last section, where c was taken

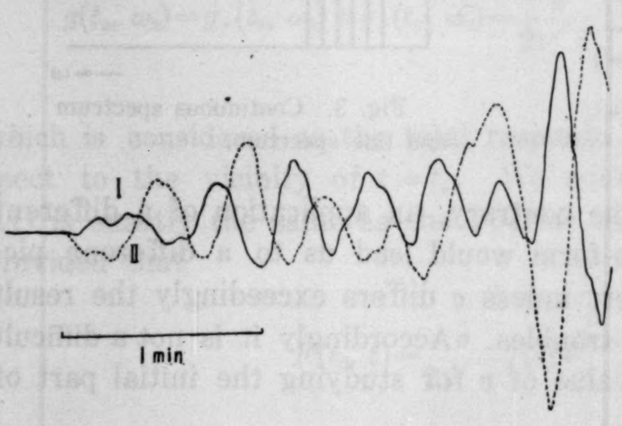

Fig. 4. Seismogram of an earthquake (I) and the true ground motion deduced from it (II), after H. Kawasumi.

19) S. GOLDMAN, *loc. cit.*, 11), p. 230.
Eq. (14) should be applied to the case in which $R(\omega)$ is given as follows,

$$R(\omega)=\int_{-\infty}^{+\infty} R(t)\,e^{-i\omega t}dt\ .$$

Multiplication of recorded wave-forms $R(t)$ by a weight function $K(t)$, however, gives a modified spectrum $R'(\omega)$ in place of $R(\omega)$, that is,

$$R'(\omega)=\int_{-\infty}^{+\infty} R(t)\cdot K(t)\,e^{-i\omega t}\,dt.$$

So that (14) will be applied to the following analyses under the assumption that

$$R'(\omega)\propto R(\omega)\ .$$

20) H. KAWASUMI, *Zisin*, **4** (1932), 71 (in Japanese).

as 0.05 $\sec^{-1}$ and 2π, 100 sec (Fig. 5a). The characteristics of the instrument concerned being given in the original paper, the true spectrum of ground motion (II) is to be presumed by applying eq. (14) to the curve (I) in Fig. 5a. In other words, if the above-mentioned reduction is reasonable, we would be able to infer the characteristics $Y(\omega)$ from the comparison of the spectrum (I) with (II). From the latter point of view, we calculated $Y(\omega)$ as is shown in Fig. 5b (black circles), in which we see a good agreement of the result with the curve reproduced from the cited paper.

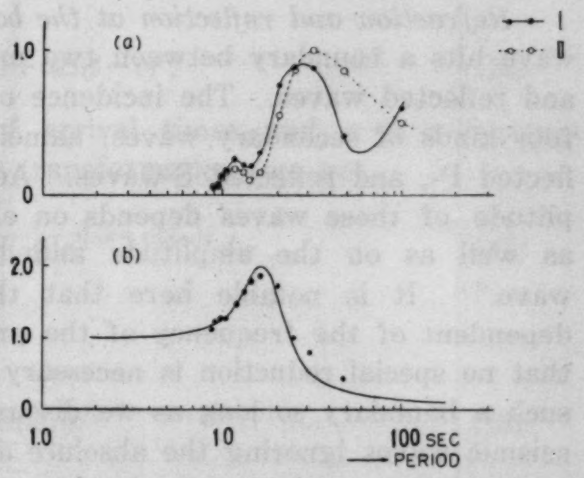

Fig. 5. Spectra of seismograms (a) and the presumed characteristics of the seismograph (b).

For lower frequencies, however, no good agreement can be seen. Such a discrepancy at lower frequencies may be attributed partly to the shift of the base line which is often adjusted during the course of numerical integration as was seen in the original paper. In reality, as will be shown in the following section, a certain shift of the base line will cause some alteration of the result, which is most remarkable for lower harmonics but becomes less for higher ones.[21]

4. Various effects of wave propagation through the earth.

Theories of wave generation, to which the following chapters will be referred, have been developed on the assumption that the medium is perfectly elastic and homogeneous. It is needless to say that such an assumption is merely the first approximation to the actual earth through which seismic waves are propagated, so that we have to examine how the wave-form is to be influenced by those complicated circumstances. The factors which cause the most remarkable alteration of wave-forms would be the layered structure of the earth as well as the viscosity of rock which forms the earth's crust. Therefore we shall, in the following, briefly discuss the influences of complicated structures within the earth,

21) *cf.* p. 486.

while discussion on the viscosity of rock will be made in later chapter in connection with explosion origins.

Refraction and reflection at the boundary of a layer. When a plane wave hits a boundary between two media, it is converted into refracted and reflected waves. The incidence of P-wave, for example, will cause four kinds of secondary waves, namely, refracted P-, refracted S-, reflected P-, and reflected S-waves. According to the theory, the amplitude of these waves depends on elastic constants of both the media as well as on the amplitude and the incident angle of the incident wave.[22] It is notable here that the amplitude of such waves is independent of the frequency of the primary wave ; so that we may infer that no special reduction is necessary for the wave propagation through such a boundary so long as we discuss only the normalized spectrum of seismic waves ignoring the absolute amplitude or the phase angle. Extending the conclusion to the free surface, we may also exclude from consideration its influence on the spectrum.

Overlapping of two different phases. It is sometimes experienced that a different phase of waves is recorded on seismograms in a very short interval of time after the inital motion. The typical case is known as the direct P-wave overlapped with a refracted one which is propagated through a high-velocity layer (Fig. 6). We had better not to use seismograms recorded under such conditions. Unforunately, however, it is not always possible to obtain records in which the direct P-wave is observed separately from other phases. Some of the following analyses being made under such circumstances, it is necessary to take the effect of the overlapping into account, though it would be difficult to perform a complete reduction for it.

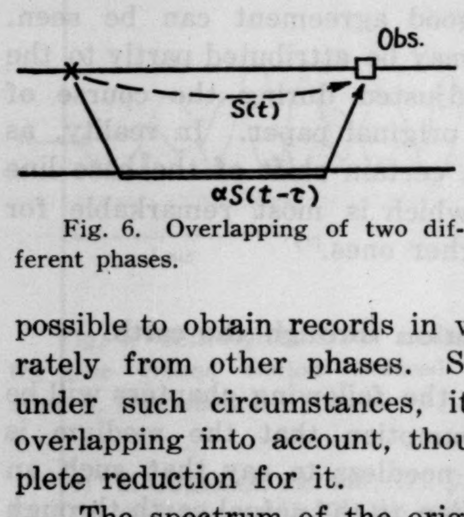

Fig. 6. Overlapping of two different phases.

The spectrum of the original wave does not greatly change when it is converted to secondary phase[23], therefore we simplify the problem to the overlapping of two different wavelets, the spectral structures of which being the same[24] (unless a special note is made, discussion in the

22) H. HONDA, *loc. cit.*, 8), p. 38.
23) *loc. cit.*, 22).
24) We assume the waves of the same structure being radiated to all the directions from the origin. The assumption would be allowed so long as the discussion is concerned with a model of spherical origin (*cf.* Chapter II and III).

following will be confined to P-waves). Let the direct wave and the refracted one be $S(t)$ and $\alpha S(t-\tau)$, respectively, then the superposition of the two becomes,

$$R(t)=S(t)+\alpha S(t-\tau)\ , \tag{16}$$

where τ denotes the difference of arrival times, and α is a constant. Applying the theorem of Fourier transformation, we get,

$$S(t)=\frac{1}{2\pi}\int_{-\infty}^{+\infty}|S(\omega)|e^{i[\omega t+\phi_s(\omega)]}\,d\omega\ , \tag{17}$$

and

$$\alpha S(t-\tau)=\frac{\alpha}{2\pi}\int_{-\infty}^{+\infty}|S(\omega)|e^{i[\omega t-\omega\tau+\phi_s(\omega)]}\,d\omega\ . \tag{18}$$

Hence the spectrum of the overlapped waves becomes as,

$$|R(\omega)|e^{i\phi_R(\omega)}=|S(\omega)|\,(1+\alpha\, e^{-i\omega\tau})\,e^{i\phi_s(\omega)}\ , \tag{19}$$

where, $\alpha e^{-i\omega\tau}$ is a function which indicates the influence of overlapping and is expressed as follows,

$$1-\alpha\leq\frac{|R(\omega)|}{|S(\omega)|}\leq 1+\alpha\ . \tag{20}$$

(20) will have the most remarkable influences on the spectrum when $\alpha=1$ and $e^{-i\omega\tau}=\pm 1$. In ordinary cases, however, such conditions would very seldom hold and the spectrum of the original wave would be subject to such a modification as shown in Fig. 7. In so far as approximate treatments of spectra are concerned, it might be allowable not to make strict reduction for the present influences.

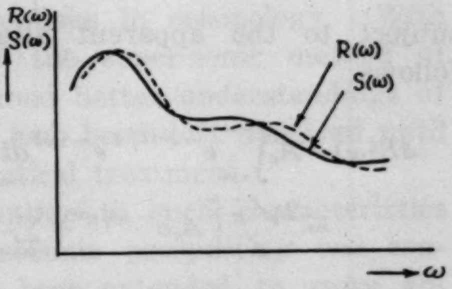

Fig. 7. Distortion of spectrum due to the overlapped phase.

Multiple reflection of waves within a surface-layer. When seismic waves are propagated into a layered medium, multiple reflection takes place there. The phenomenon is considered as the excitation of the layers by the incidence of seismic impulses. Hence the spectrum of seismic motions on the earth's surface will be given as,

$$R(\omega)=Y_2(\omega)\cdot S(\omega)\,, \tag{21}$$

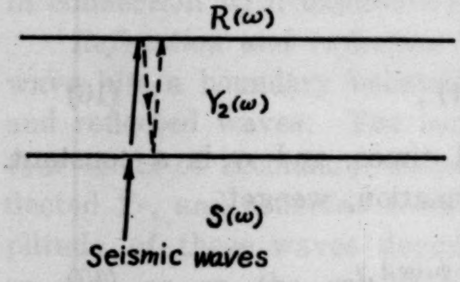

Fig. 8. Multiple-reflction of waves within a surface layer.

where, $Y_2(\omega)$ and $S(\omega)$ denote, respectively, the total response of the layers and the spectrum of the incident waves. The present phenomenon becomes more and more remarkable when the layers are subject to successive incidence of seismic waves.[25] Since, however, the main interest concerned here is the characteristics of the initial disturbances, the multiple reflection would not effect so much as in the case of later phases.

Remarks on the apparent alteration of spectra due to procedures of numerical calculation. The method of analysis proposed in the second section is based on the multiplication by a weight function, which will make some apparent alteration of spectra when the base line of the seismogram is not taken accurately. We suppose the shift of the said line to be,

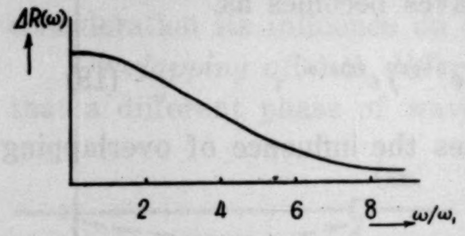

Fig. 9. Effect due to constant shift of the base line of the original seismogram ($\omega_1=c/5$).

$$\Delta R(t)=A_0+\sum_m A_m \cos\omega_m t\,. \tag{22}$$

Then the result of the analysis will be subject to the apparent alteration of spectrum which is given as follows.

$$\Delta R(\omega)=A_0\int_{-\infty}^{+\infty} e^{-c^2t^2/4}e^{-i\omega t}\,dt+\sum_m A_m\int_{-\infty}^{+\infty}\cos\omega_m t\, e^{-c^2t^2/4}e^{-i\omega t}\,dt, \tag{23}$$

$$=\frac{2\sqrt{\pi}}{c}\left[A_0 e^{-\omega^2/c^2}+\sum_m\frac{A_m}{2}\left\{e^{-(\omega-\omega_m)^2/c^2}+e^{-(\omega-\omega_m)^2/c^2}\right\}\right]. \tag{24}$$

In the case of the constant shift, for example,[26]

$$A_0\neq 0,\ A_1=A_2=\cdots=0\,, \tag{25}$$

and so we get

$$\Delta R(\omega)=\frac{2\sqrt{\pi}}{c}A_0 e^{-\omega^2/c^2}\,, \tag{26}$$

25) K. KANAI, *Bull. Earthq. Res. Inst.*, **31** (1953), 233.

26) *cf.* p. 483.

which is most remarkable for the fundamental frequency but is negligible for harmonics higher than, say, the 5th (Fig. 9). In the following chapter, however, the analyses will be so made that the predominent part of the spectrum is given by higher harmonics, in order that the above-mentioned factor would not cause great troubles in the result.

Similar treatment is also possible in order to estimate the influences of distortion of seismograms caused by the inaccuracy of seismographs.

Chapter II.
Wave Generation from Explosion Origins.

1. Introduction.

Wave generation from an explosion origin is the most fundamental procedure in seismic prospecting which accomplished remarkable progress in these ten or twenty years. The main purpose of the technique is to infer the underground structure by investigating seismic waves caused artificially. For that purpose, geophysicists introduced various kinds of advanced technique into the study, which is concerned, more or less, with the characteristics of seismic waves. In order to apply the method successfully to actual geophysical problems or to improve further such techniques, it is necessary for us to have thorough knowledge about the nature of seismic waves.

Another notable bit of progress in this field is the extended application of the technique to fundamental problems in seismology. With the aid of the technique as well as of the super-sonic method of laboratory experiment, seismologists obtained better understandings of some problems of elastic waves, which had been left unsolved until then because of the difficulties of mathematical treatment.

We need not have paid particular attention to such characteristics of wave generation so long as classical seismic prospecting was concerned; however, since its application has been extended to more advanced purposes as mentioned above, it is necessary to get more clear information about seismic waves from an explosion origin. The explosion origin is, fortunately, rather simple in its mechanism and the theoretical model of spherical origin can be applied to it more reasonably than to natural earthquakes. We shall, therefore, make analyses of seismic waves with resect to the theoretical model, and study also some physical evidence related to the nature of explosion origins.

2. Spectral analyses of seismograms obtained by explosion tests.

Seismograms fit for our purpose of studying the most fundamental mechanism of an explosion origin are those recorded with seismographs of suitable characteristics in the field of very simple underground structure. It is not always possible to get such materials for analyses, however, the writer was able to obtain the following data with the permission of the respective observers, the seismograms thus collected being considered fairly suitable for the study. The observers and the location of the field of these experiments are as follows (see also Table I).

Table I. Conditions of the field experiments.

Experiment	Charge	Depth	Rock type	Velocity	Volume of crushed rock	Distance of observation point
	kg	m		m/sec		m
A	(cap 1)	0.75	sand	250	—	8.5–10.5
B	0.28	8.5	(unknown)	4500	—	250–310
C	1.125	13	sand clay	1700	—	150–725
D	33.75	22	(unknown)	2800	— m³	
E	1,000	shallow	〃	5800	20,000	50–32,000
F	7,800	〃	igneous rock	2500	36,000	8,650–21,100
G	29,700	〃	〃	—	—	—
H	57,000	〃	〃	2500	300,000	—
I	1,000	7.1	shale	2000	(2,500)	—
J	3,500	15–20	sandstone	3300	30,000	—
K	0.45	ca. 100	green stone	7000	—	16.5
L	0.90	〃	〃	〃	—	〃
M	1.80	〃	〃	〃	—	〃
N	7.20	〃	〃	〃	—	〃
O	14.40	〃	〃	〃	—	〃

Remarks: Experiments G∼J are referred only to see the relation between the charge of explosives and the volume of crushed rock.
Rock type and velocity in the table correpond to the medium wherein the explosions were made.

A) Experiment made by the Seismic Exploration Group of Japan at Katamachi, Niigata Pref.[27)].

B) Experiment made by the Geological Survey of Japan at Honbetsu, Hokkaidô.[28)]

27) *Rep. Seis. Expolor. Group, Japan*, No. 5 (1955).
28) unpublished.

C) Experiment made by the Geological Survey of Japan at Shibazaki, Ibaraki Pref.[29].

D) Experiment made by the Geological Survey of Japan at Ikushunbetsu, Hokkaidô.[30]

E) Experiment made by the Research Group for Explosion Seismology in the Tôhoku district of Japan (shot point: Kamaisi, Iwate Pref.)[31].

F) Experiment made by the Research Group for Explosion Seismology in the Tôhoku district of Japan (shot point: Isibuti, Iwate Pref.).[32]

G and H) Experiments made by the Research Group for Explosion Seismology in the Tôhoku district of Japan (shot point: Isibuti and Kamaisi, Iwate Pref.).[33]

I and J) Experiments reported by T. Suzuki.[34]

K∼O) Experiments made by L. Obert and W. Duvall at Mt. Weather mine, Virginia.[35]

Seismograms thus selected are of fairly simple features except those from experiments E and F, which were undertaken to clarify the curstal structure of the said district. Those explosion tests on a large scale being carried out with different types of seismographs set at temporary stations, the seismograms show very different features from each other. We shall therefore trace, in detail, the procedure of getting spectra for the initial motions taking the experiment E as an example.

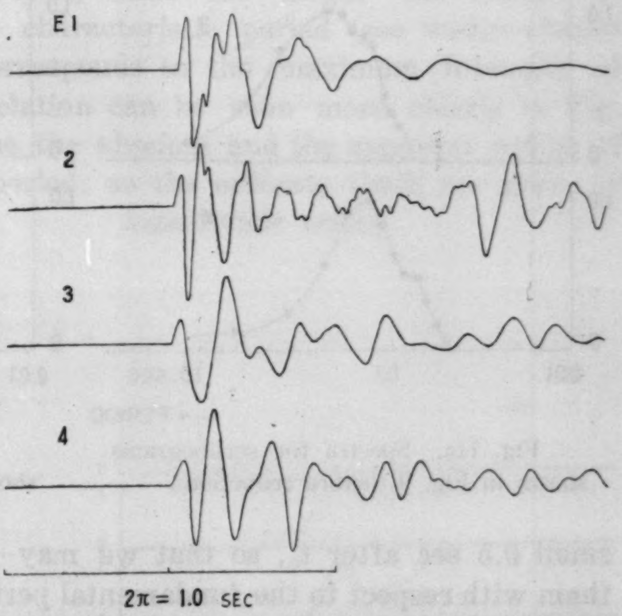

Fig. 10. Seismograms obtained by the experiment (E). Time scale of the trace (E1) is taken 3 times as large as the other three.

29) S. NAGUMO, K. MORI, and M. HAYAKAWA, *Rep., G.S.J.*, No. 164 (1955) (in Japanese).
30) unpublished.
31) unpublished.
32) Res. Group, Explos. Seis., *ibid.*, **30** (1952), 279.
33) Res. Group, Explos. Seis., *ibid.*, **29** (1951), 97; **32** (1954), 79.
34) T. SUZUKI, *Zisin*, **16** (1944), 163 (in Japanese).
35) L. OBERT and W. DUVALL, *Bureau of Mines Rep. Investigations* 4683 (1950).

Fig. 10 shows seismograms at several stations where the initial motions were recorded sufficiently large (all the traces analysed are referred to the vertical component).[36] We take the standard time of analysis t_0 at the beginning of the respective disturbances and let $f(t)$ be multiplied by $K(t)$, in which the decay constant c was given for E 2∼4 as 5 sec^{-1}. The amplitudes of $F(t)$ thus obtained become very

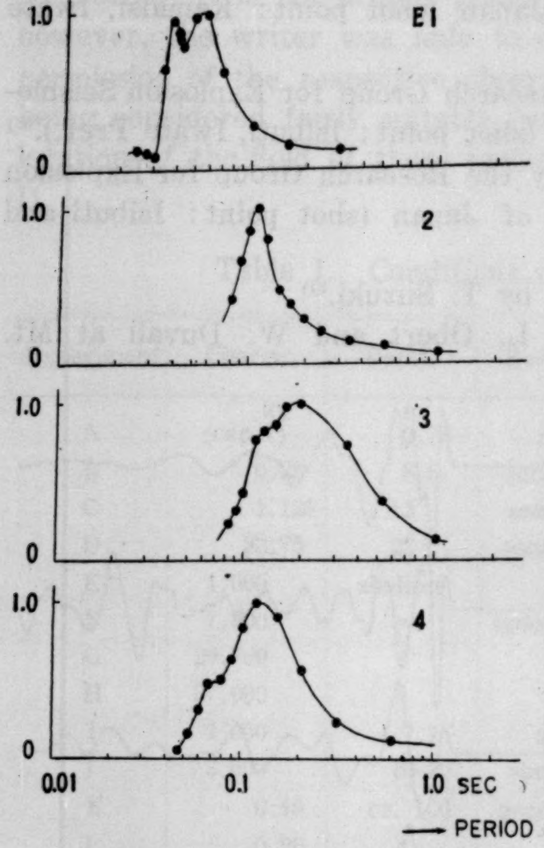

Fig. 11a. Spectra for seismograms shown in Fig. 9 (before reduction).

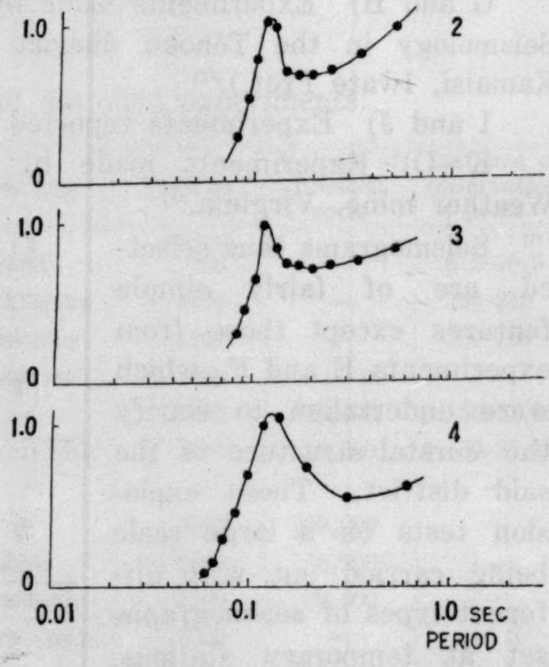

Fig. 11b. Spectra for seismograms shown in Fig. 10 (reduced).

small 0.5 sec after t_0, so that we may carry out Fourier analyses of them with respect to the fundamental period 2π taken as 1.0 sec. Fig. 11a shows the spectral intensity of each harmonic calculated in this way, where the ordinate is given in arbitrary scale.

True spectra of the ground motion can be drawn by applying the above-mentioned method of reduction to the results drawn in Fig. 11a. Spectra in Fig. 11b are the results finally obtained, which are of quite similar features to each other in spite of their dissimilarity before the reduction. This evidence leads us to an opinion that the main feature

36) Discussion will be made only about the vertical component in all the cases except those of K∼O, in which the radial strain component will be analysed.

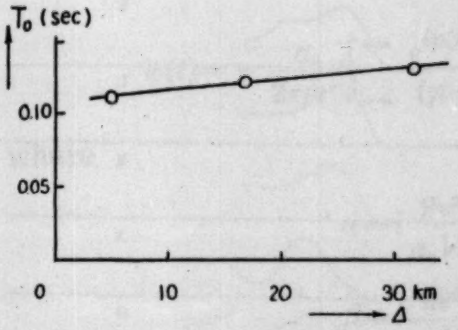

Fig. 12. Characteristic periods versus epicentral distances.

of the spectrum would not be greatly influenced by the conditions of propagation, so that we might regard it, to a certain degree of approximation, as the non-distorted information of origin's characteristics. Fig. 12 illustrates the frequency of the maximum spectral intensity plotted against the epicentral distance of stations, in which we notice that the former is approximately independent of the latter.

Seismograms of all the experiments listed in Table I are analysed in a similar way taking proper values of c and 2π for the respective cases. The spectra thus obtained are illustrated in Figs. 13 a∼d. We see in the figure a marked tendency that the larger the charge of explosives is, the longer the characteristic period (see wedge-shaped marks in the figures) which corresponds to the maximum intensity of the spectrum becomes. The relation can be seen more clearly in Fig. 16, where we take the charge as the abscissa and the apparent radius of the origin deduced from the period, as the ordinate (both are given in logarithmic scale).

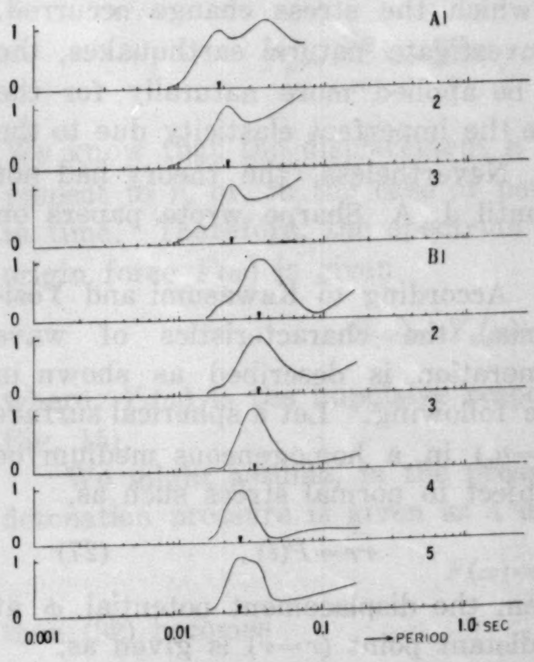

Fig. 13a. Spectra of seismograms analysed (experiments A and B).

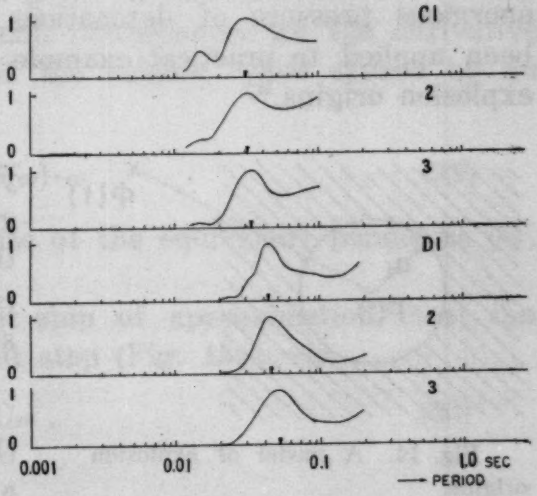

Fig. 13b. Spectra of seismograms analysed (experiments C and D).

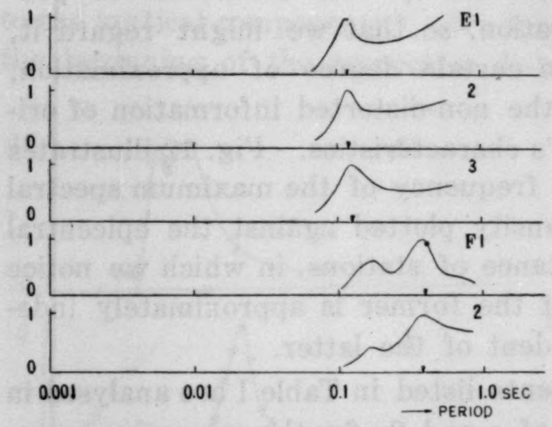

Fig. 13c. Spectra of seismograms analysed (experiments E and F).

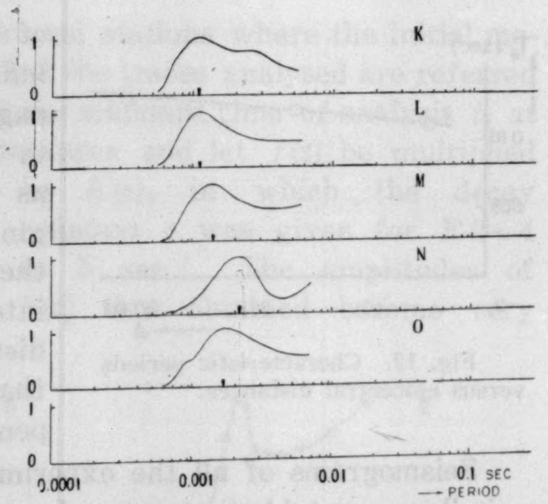

Fig. 13d. Spectra of seismograms analysed (experiments K～O).

3. Characteristics of explosion origins.

The fundamental characteristics of explosion origins can be investigated with the aid of a model of spherical origin. H. Kawasumi and R. Yosiyama studied wave generation from such a simplified origin, showing theoretically that the wave-form was given as a function of the radius of the surface on which the stress change occurred. Although their first aim was to investigate natural earthquakes, the assumptions taken by them seem to be applied more naturally for the cases of explosions provided we ignore the imperfect elasticity due to the enormous pressure of detonations. Nevertheless, the theory had not been applied to practical example until J. A. Sharpe wrote papers on explosion origins.[37)]

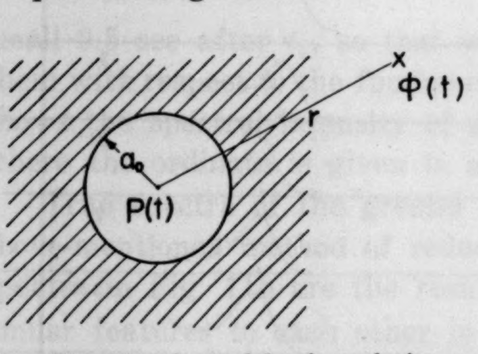

Fig. 14. A model of explosion origins.

According to Kawasumi and Yosiyama, the characteristics of wave generation is described as shown in the following. Let a spherical surface ($r=a_0$) in a homogeneous medium be subject to normal stress such as,

$$\widehat{rr}=P(t)\,, \tag{27}$$

then, the displacement potential ϕ at a distant point ($r=r$) is given as,

37) H. KAWASUMI and R. YOSIYAMA, *loc. cit.*, 5).
J. A. SHARPE, *Geophys.*, **7** (1942), 144; *ibid.*, **7** (1942), 311.

$$\phi(t) = -\frac{a_0}{2\pi\rho r}\int_{-\infty}^{+\infty}\frac{e^{ip(t-(r-a_0/V))}}{(p-\alpha)(p-\beta)}dp\int_{-\infty}^{+\infty}P(\omega)e^{-ip\omega}\,d\omega\,, \tag{28}$$

where

$$\left.\begin{aligned}\alpha &= i\frac{2v^2}{a_0V}+\frac{2v}{a_0}\sqrt{1-\left(\frac{v}{V}\right)^2}\,,\\ \beta &= i\frac{2v^2}{a_0V}-\frac{2v}{a_0}\sqrt{1-\left(\frac{v}{V}\right)^2}\,,\end{aligned}\right\} \tag{29}$$

and ρ, V, v denote density, velocities of dilatational and rotational waves, respectively. The expression for ϕ in (28) is identical with the solution for the equation of a pendulum,

$$\ddot{\theta}+2\varepsilon\dot{\theta}+n^2\theta=P(t)\,, \tag{30}$$

provided we take $\alpha=i\varepsilon+\sqrt{n^2-\varepsilon^2}$, $\beta=i\varepsilon-\sqrt{n^2-\varepsilon^2}$. The deflection of a pendulum subject to an exciting force $P(t)$ has been well investigated, with the aid of which we can study the characteristics of the model origin concerned. The curves (b) in Fig. 15 are the impulsive response of such an equivalent pendulum as is related with the conditions of the model origin in the following way.

$$T_p=\frac{2\pi}{n}=\frac{\pi a_0}{v}\,,\qquad h=\frac{\varepsilon}{n}=\frac{v}{V}\,. \tag{31}$$

We know that the displacement u is given as the derivative of ϕ with respect to r, or, in the case of periodic disturbances as the derivative in time. Therefore, the spectrum of the seismic wave caused by an origin force $F(\omega)$ is given

$$S(\omega)=Y_0(\omega)\cdot F(\omega)\cdot\omega\,, \tag{32}$$

where, $Y_0(\omega)$ is the impulsive response of the equivalent pendulum (*cf.* Fig. 15).

We might assume, in the present step of approximation, that the detonation pressure is given as a unit step (Fig. 15a), *viz.*,

$$F(\omega)=1/\omega\,, \tag{33}$$

then (32) becomes

$$S(\omega)=Y_0(\omega)\,. \tag{34}$$

Therefore, the spectrum similar with the curves in Fig. 15b will be

observed. When $Y_0(\omega)$ is known in this way, we are able to presume a_0 with the aid of (32), which is to be understood as the apparent radius of the origin concerned.

We have no accurate information about the stress change on the surface of the imagined sphere, so that we simply assume here that $f(t)$ is approximately given as a unit step-function (Fig. 15a). From the comparison of the analysed spectra (Fig. 11 and 13) with that drawn in Fig. 15b, we see a fairly good agreement between them. Under these considerations we regard T_0, which is determined for the respective spectra, as equal to the period which corresponds to the maximum intensity of the theoretical curve in the last figure. The apparent radius thus estimated is plotted against the charge of explosives in Fig. 16, wherein we see a clear tendency that $\log a_0$ increases proportionally to $\log W$. This is an evidence that is naturally understood from the standpoint of our present model. If we ignore the influences due to the different quality of explosives (*cf.* reference (43)), we obtain the following relation between W and a_0, that is

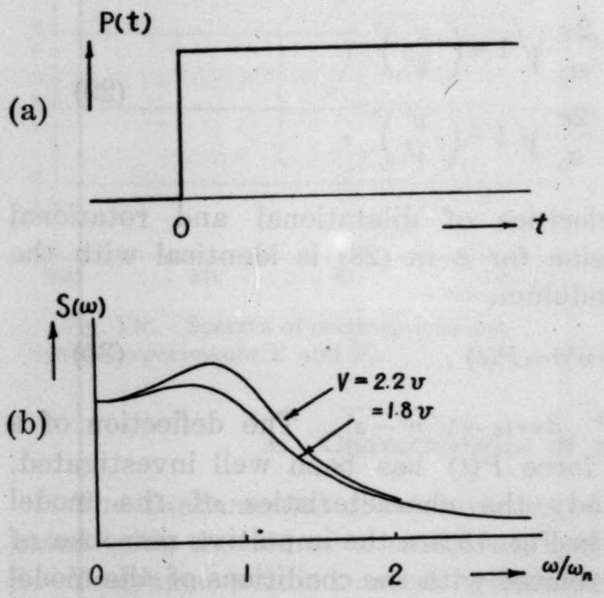

Fig. 15. Unit step-function and the spectrum of seismic waves ($\lambda=\mu$).

$$\log a_0=\alpha+\beta \log W \,, \tag{35}$$

where, $\alpha=0.52$ and $\beta=0.38$.

The next problem with which we are concerned is to clarify the actual meaning of the apparent radius deduced from the analysis. The question would be solved most simply provided the cited radius is practically equal to some observable quantity such as the average dimension of the volume in which rock is perfectly crushed by detonation pressure. a^* plotted in Fig. 16 indicates the radius of a sphere, the volume of which is equal to the total volume of crushed rock (*cf.* Table I). We notice in the figure that a^* increases together with a_0, and that the

latter is several times as large as the former. This fact suggests a close relation existing between the two quantities, which would be of essential bearing to make clear the mechanism of wave generation from an explosion origin.

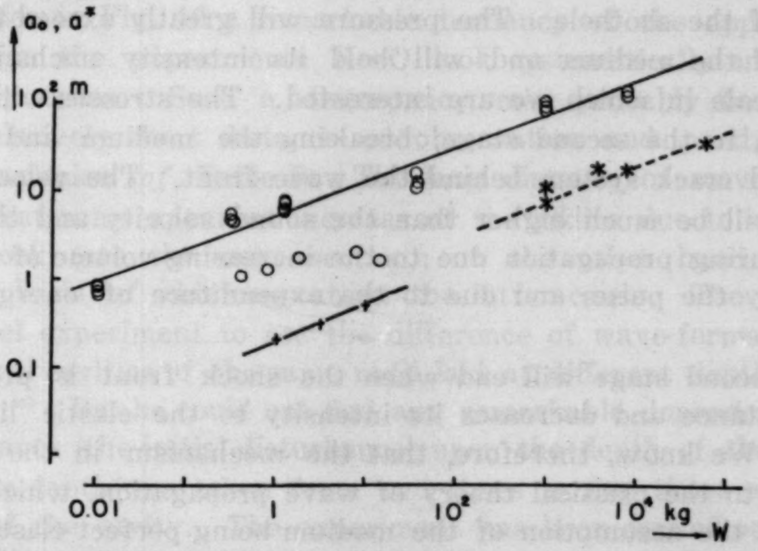

Fig. 16. Apparent radii of explosion origins (○), equivalent radii of crushed regions (*) *versus* charge of explosives. ×—×—× illustrates the relation between W and a^*, which is given by T. Murata, experimentally[38].

4. Wave phenomena in the vicinity of explosion origins.

Discussion in the previous section was made on the assumption that the medium can be regarded as perfectly elastic. This assumption would be reasonable in so far as the discussion concerns the phenomenon taking place at distant places from the origin. In the very vicinity of the origin, however, we can no more apply the assumption to the problem even if we exclude from discussion such complicated phenomena as fracture production *et al.* In such a space, the medium is subject to violent increase of high detonation pressure which causes in the medium various sorts of abnormal phenomena. The most significant one is known as the stress-strain relation being no more linear under such conditions, as a result of which we observe shock waves or plastic waves in place of elastic ones, propagating in the cited region.[39] Their characteristics being so complicated that it would be scarecely possible to obtain complete solutions for the phenomenon.

38) T. MURATA and K. TANAKA, *Journ. Industri. Explos. Soc., Japan*, **16** (1955), 32 (in Japanese).

39) H. KOLSKY, *Stress Waves in Solids* (Oxford, 1953), p. 163.

G. Morris presented, several years ago, a theory of explosion origins, in which he tentatively assumed three stages of the formation of elastic waves[40]. The first stage is explosion taking place in a borehole loaded with explosives, which results in very high compressional stresses on the wall of the shothole. The pressure will greatly exceed the ultimate strength of the medium and will hold its intensity unchanged within the time scale in which we are interested. The stresses will spread out spherically, in the second stage, breaking the medium and forming a complicated crack system behind the wave front. The velocity of propagation will be much higher than the sound velocity and the intensity will fall during propagation due to the increasing volume of the medium occupied by the pulse, and due to the expenditure of energy in crack formation.

The second stage will end when the shock front is propagated to critical distance and decreases its intensity to the elastic limit of the medium. We know, therefore, that the mechanism in the third stage is subject to the classical theory of wave propagation, which have been studied on the assumption of the medium being perfect elastic. In such a sense, direct application of Kawasumi and Yosiyama's theory to the analysis of wave-forms would probably give the cited distance as the apparent radius of the explosion origin. Morris has estimated the critial distance to be about four feet in the case of experiment with one pound charge exploded in sandstone. This value looks to be in good harmony with our own results (*cf.* Fig. 16), provided we could assume that the stress at the critical distance shows a rapid increase and a considerably long duration.

T. Okawa and others recently performed laboratory experiments of wave generation caused by explosions in large specimens made of concrete.[41] Their first aim of the study being not to get the actual proof of Morris's hypothesis, they do not give full discussion on the point whether the critical distance exists as Morris says or not; however, it is not impossible to find out an evidence for the velocity being larger than the sound velocity in the very vicinity of the origin (see Fig. 16 in their paper).

It would be impossible to get direct proof for the cited model unless we carry out accurate measurements of wave velocity at very close

40) G. MORRIS, *Geophys.*, **15** (1950), 61.

41) T. OKAWA, M. HIRAYAMA, and K. KIYOTA, *Journ. Industri. Explos. Soc., Japan*, **18** (1957), 22 (in Japanese).

points to the origin, but we might not make essential mistakes in concluding here that the apparent radius of the origin is more naturally understood as the critical distance in Morris's theory rather than the radius of the space in which rock is crushed to fine pieces (Fig. 18).

We notice in Fig. 16 a remarkable tendency of the apparent radii estimated for the experiments K∼O look systematically smaller than the ordinary cases. Such a discrepancy may probably be attributed partly to relatively short distance of observation and partly to large depth of explosion (*cf.* Table I). The long distance of wave path will cause in effect some apparent increase of the radius due to viscous property of rock (see the next section); on the other hand, we have no reliable basis of thinking about the latter cause. The writer has made a model experiment to see the difference of wave-forms generated from spherical cavities of the same radii laid at different depths beneath the surface.[42] But he could not find any remarkable dependence of the period of waves (the initial disturbance) upon the depth of the origin in so far as the depth was taken from two times to five times as large as the radius of the cavity. The experiment has been carried out in a way so as the medium to be subject to no breaking, so that it does not give the full picture of shallow explosions. It is a well known fact that the volume of crushed rock depends not only on the charge of explosives but also on the conditions of loading which includes the depth from the earth's surface. There is a reason, therefore, for presuming the explosions at great depth to be associated with relatively small dimension of origins compared with those of surface explosions, although the writer can not give any quantitative discussion on that point because of no experimental data are available at present.

5. Deformation of wave-forms due to the viscosity of the medium.

Discussion in the previous paper enables us to presume the radius of the origin two times or more larger than that of the crushed region provided we take the influence of high detonation pressure into consideration. The actually estimated radius of the origin is, however, several times as large as a^*, so that the discrepancy can not be understood only from the above-mentioned standpoint. Another sort of effect

42) K. KASAHARA, Experimental studies on the mechanism of generation of elastic waves, VI., *Monthly Meeting of E.R.I.*, (Dec. 2, 1955).

is noticed on the viscosity of rock, which have such an influence on the spectrum that they can not be disregarded. The effect has been discussed by many seismologists, and the following study will be made on the basis of N. Ricker's theory presented several years ago.[43] He has introduced an expression for the said effect in the following,

$$\chi_1 = e^{-(\omega/\omega_0)^q kx} \sin\frac{2\pi\omega}{v}(x-vt)\ , \tag{36}$$

where, χ_1 denotes a plane wave (longitudinal) of single frequency ω, and q, k are constants. ω_0 is called the cut-off frequency which characterizes the absorption in the medium. Although his treament of wave-forms were based on the functions represented by Fourier integrals, we shall deal with it from the standpoint of spectral analysis.

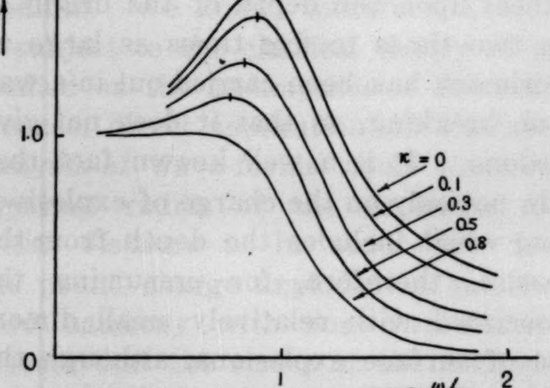

Fig. 17. Apparent increase of the characteristic period (T_0) with distance.

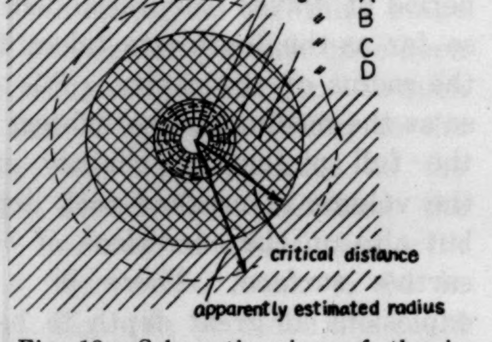

Fig. 18. Schematic view of the improved model. Region A: shothole, B: perfectly crushed rock, C: non-elastic region, D: elastic region, broken line: the apparent dimension of the origin to be estimated from the characteristic period.

Let the spectrum of the original wavelet be $S(\omega)$, then we obtain the following expression for the wave propagated to a point $x=x$, that is,

$$S'(\omega) = e^{-(\omega/\omega_0)^q kx} S(\omega)\ . \tag{37}$$

So that we can see the characteristics of the absorption effect by applying (37) to actual examples. Fig. 17 shows the effect with respect

43) N. RICKER, *Geophys.*, **15** (1950), 348. His discussion is concerned mainly with the propagation plane waves, but it is also applicable to spherical waves in so far as we only discuss the relative distortion of spectrum.

to the original spectrum referred to the model (*cf.* Fig. 15). The curves are drawn for different values of a parameter, κ, which is given as follows,

$$\kappa = kx \ , \tag{38}$$

where q was assumed as 2, tentatively.

The spectrum of the wave concerned is subject to more remarkable alteration with the increase of κ, and the predominent frequency of the spectrum becomes lower as the result. According to A. Kubotera, the value of k is $7.9 \times 10^{-7}\ \mathrm{cm}^{-1}$ for the propagation of $\overline{P}$ through the earth's crust,[44] so that κ will be as large as 0.4 for observation points 5 km apart from the shot point.[45] These conditions can be applied, for instance, to the experiments E, F, and so on, therefore we know from Fig. 19 that the characteristic period T_0 and the radius of the origin a_0 would have been estimated 40 or 50% larger in such cases. Values of κ can not be estimated for the other experiments such as A, B, C, and D, but we may assume the apparent increase of a_0 for them being of the same order. Because, in those experiments which had been carried out with smaller charges of explosive, an important *rôle* was played by higher frequencies of waves, which were subject to relatively large influences of the viscosity notwithstanding their short distances of propagation.

From the combination of the two factors that have been discussed in the above, we obtain an improved picture of explosion origins (Fig. 18). Outside the perfectly crushed region (B) exists another region (C), in which the intensity of the stress falls to the elastic limit of rock during its propagation to the critical distance ($r = a_c$). The assumption for elastic waves holds good outside the latter, so that it is not a^* but a_c that corresponds to a_0 taken in the theoretical model (Fig. 14). Elastic waves propagated from it are affected by the viscosity of rock resulting in the apparent increase of the origin's dimension as shown in the figure with a broken line. Approximated estimation of these radii concerned will result in the following relation,

$$\text{apparently estimated radius,} \quad a' = 1.5\, a_0 = 3 \sim 5\, a^* \ . \tag{39}$$

44) A. KUBOTERA, *Zisin* (*Journ. Seis. Soc. Japan*), [ii], **5** (1952), 77.
45) The ratio (ω/ω_0) in (37) is assumed as 1.

Chapter III.

Spectrum of Seismic Waves and Magnitude of Earthquakes.

1. Introduction.

A number of seismologists have pointed out the tendency that the larger the magnitude of an earthquake is, the longer the period of the seismic waves generated from the origin becomes. B. Gutenberg and C. F. Richter examined this tendency and found the relation between the magnitude M and the period of seismic waves of the maximum amplitude T to be as follows,[46]

$$\log T = -0.82 + 0.22\,M\,. \tag{40}$$

Meanwhile, some seismologists are of the opinion that the occurrence of great earthquakes might be attributed to subsequent release of strain energy in the crust, such a release being probably caused by fractures which take place when the stress exceeds the limit of strength at certain places in the crust. From this view-point, the relation between M and T is well understood, because the period of seismic waves are likely to depend on the dimensions of the origin space, whereas a large amount of strain energy can be released from the origin of large dimensions. It must be noticed, however, that the form or the period of surface waves, which are usually recorded as waves of the maximum amplitude on seismograms at distant stations, will be seriously affected by the condition of the propagation path; so that we have not been able to get a clear-cut picture of seismic origin by analysing surface waves even though complicated reduction was often made. The influences of propagation paths on forms of bodily waves, especially those of the initial P-waves, are considered to be not so serious. In order to infer the nature of seismic origins, therefore, it seems advantageous to analyse P-waves.

Recently, K. Kanai carried out analyses from this standpoint with the intention of obtaining a formula which is of practical use for determining the magnitude of an earthquake from the period of its initial motion.[47] Although the main purpose of his study was such as mentioned above, this sort of study suggests that we may infer the state of earthquake origin to a certain extent, provided appropriate analyses of

46) B. GUTENBERG and C. F. RICHTER, *Bull. Seis. Soc. Amer.*, **32** (1942), 163.
47) K. KANAI, *Bull. Earthq. Res. Inst.*, **31** (1953), 45.

P-waves are worked out. On the other hand, there have been several studies related to the density of energy accumulation in the origin space, the result of which was in good harmony with the hypothesis supposing an inseparable relation of earthquake occurrence with the mechanical strength of rock.[48] These analyses were based, however, on the dimension of seismic origins, which was deduced from the distribution of aftershocks or of crustal deformations, so that the method can not be applied to deep-focus earthquakes and others, not accompanied by such evidence. If we could analyse wave-forms and see how large the seismic origins are, the method would be applicable to all sort of earthquakes, in principle. What the writer would here like to study is an estimate of the energy accumulation around earthquake origins by applying the method of wave-form analysis. The study will be made not only for destructive earthquakes but also for deep-focus ones, as shown in the next section.

2. Spectral analyses of seismograms.

In most of the papers published so far, determination of periods of seismic waves was made on the basis of direct measurement of seismograms. The writer believes, however, that the seismic wave-form is better analysed by means of spectral analysis as we have studied in the first chapter. Seismograms used in the present analyses are those of 21 earthquakes (8 destructive in Japan area, 7 distant, 6 deep-focus), the initial motions of which were recorded large enough for the

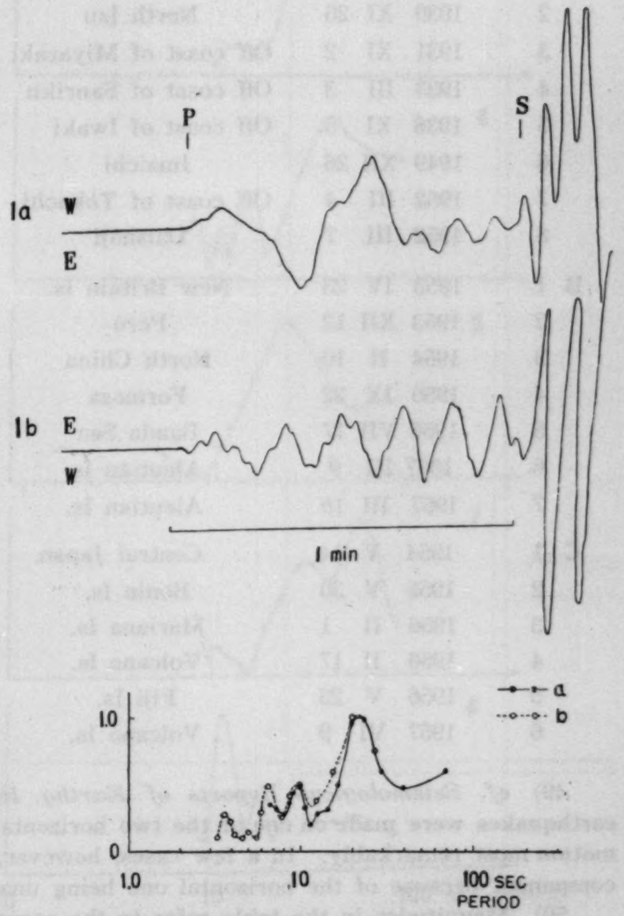

Fig. 19. Seismograms of the Tango earthquake and the spectra of their initial motions.

48) C. TSUBOI, *loc. cit.*, 7).

present purpose with long-period seismographs at the Hongo station of Tokyo University.[49] Table II shows these earthquakes together with their magnitudes reported in seismological bulletins.[50]

Fig. 19 shows the seismograms and spectra of the Tango earthquake, as an example, upon which the analyses were made for the two seismograms of EW-components recorded with instruments of different

Table II. Earthquakes with which the present chapter is concerned.

No.		Date			Epicentre	Distance from Tokyo km	Depth km	Magnitude
A	1	1927	III	7	Tango Pen.	370	—	7.4
	2	1930	XI	26	North Izu	100	—	7.0
	3	1931	XI	2	Off coast of Miyazaki	720	—	7.2
	4	1933	III	3	Off coast of Sanriku	420	—	8.5
	5	1938	XI	5	Off coast of Iwaki	250	—	7.8
	6	1949	XII	26	Imaichi	100	—	6.5
	7	1952	III	4	Off coast of Tokachi	600	—	8.2
	8	1952	III	7	Daishôji	280	—	6.5
B	1	1953	IV	23	New Britain Is.	5000	—	7.7
	2	1953	XII	12	Peru	15000	—	7.7
	3	1954	II	10	North China	(4000)	—	7.3
	4	1955	IX	22	Formosa	2400	—	(6.5)
	5	1956	VII	17	Banda Sea	4500	—	7.3
	6	1957	III	9	Aleutian Is.	4000	—	8.0
	7	1957	III	16	Aleutian Is.	4000	—	6.8
C	1	1954	V	14	Central Japan	230	250	7.0
	2	1955	V	30	Bonin Is.	1000	600	7.2
	3	1956	II	1	Mariana Is.	2500	500	6.8
	4	1956	II	17	Volcano Is.	360	200	7.3
	5	1956	V	23	Fiji Is.	6200	450	6.3
	6	1957	VI	9	Volcano Is.	360	350	6.8

49) *cf. Seismological Reports of Earthq. Res. Inst.*. Analyses of the respective earthquakes were made on one of the two horizontal components, which recorded the initial motion most remarkably. In a few cases, however, analyses were referred to the vertical component because of the horizontal one being unavailable.

50) Magnitudes in the table refer to the reports from C.M.O., Japan, or from Pasadena as well as to *Rika-nenpyô* (Annual Table of Constants, Tokyo Astronomical Observatory). When different values are reported for an earthquake, some adjustment was made.

characteristics (solid and broken lines). The results obtained for all the listed earthquakes are illustrated in Figs. 20 a∼c, in which index-numbers are given for the respective spectra so as to correspond to those in Table II.

3. The M-T curve.

To see the dependence of the period on the magnitude, the results from the previous section were plotted in Fig. 21, in which the magnitude reported for the respective earthquakes was taken as the abscissa while T_0, the period of the maximum spectral intensity, as the ordinate (*cf.* also Table IV). Data for shallow earthquakes (groups A and B) are shown with black circles whereas cross marks are used for deep-focus earthquakes (group C); besides these the results of deep-focus shocks shown in H. Honda's paper[51] are also plotted. Although his estimation of periods was made in a different way from the

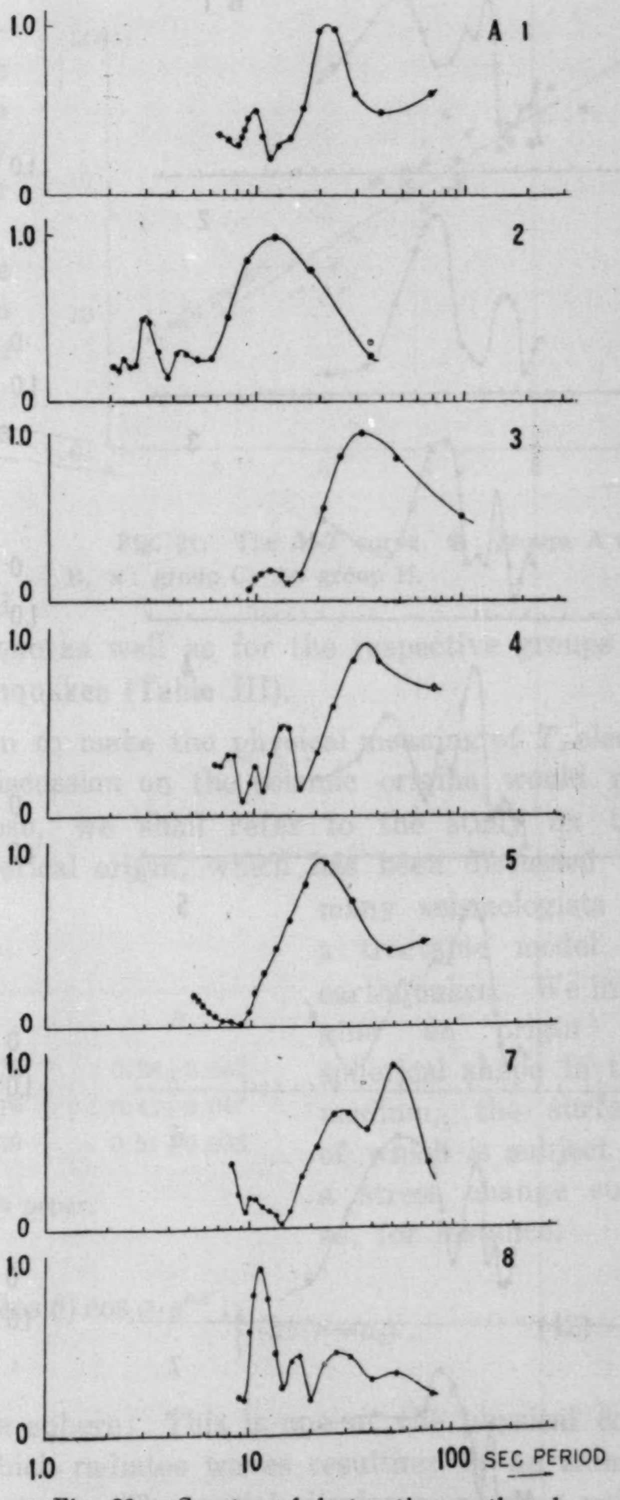

Fig. 20a. Spectra of destructive earthquakes (Japan area).

51) H. HONDA and H. ITO, *Geophys. Mag., C.M.O., Japan*, **13** (1939), 155.

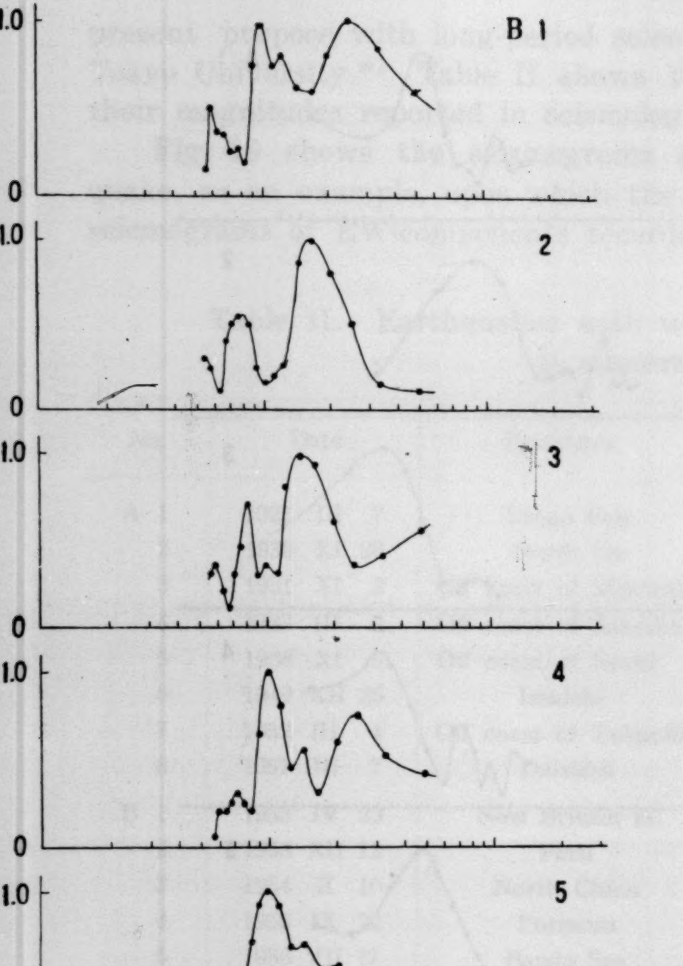

Fig. 20b. Spectra of distant earthquakes.

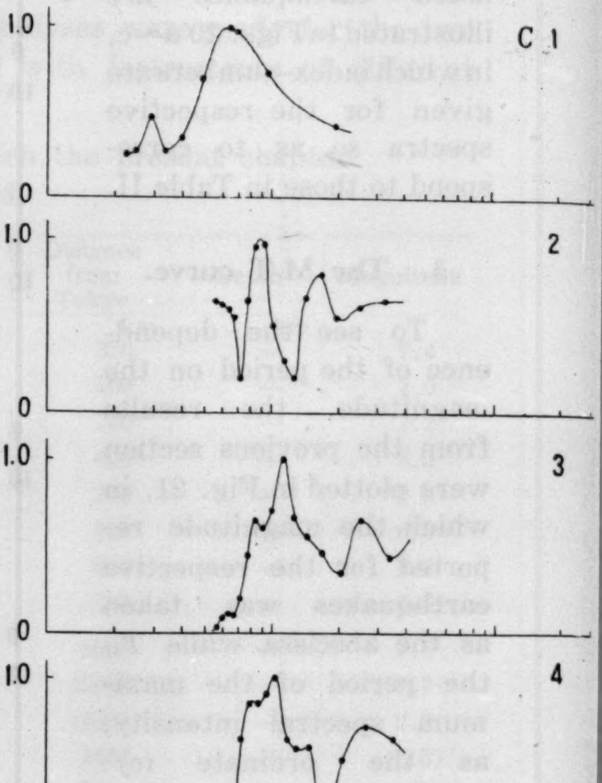

Fig. 20c. Spectra of deep-focus earthquakes.

writer's, no marked discrepancy can be seen between the general tendency for both the cases. Therefore we may use Honda's results together with group C.

In the figure, we see that there is approximately a linear relation between the magnitude and the logarithmus of T_0, so that we assume the relation, as

$$\log T_0 = \alpha + \beta M, \qquad (41)$$

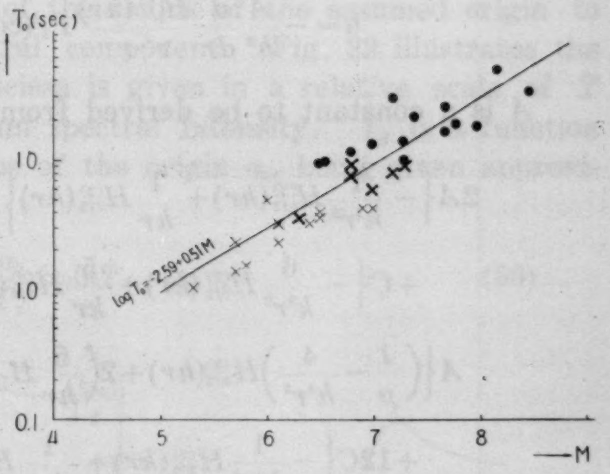

Fig. 21. The *M-T* curve. ●: groups A and B, ×: group C, ×: group H.

and calculate constants α and β, for the whole groups in one as well as for the respective groups of shallow and deep-focus earthquakes (Table III).

We are now in a position to make the physical meaning of T_0 clear, otherwise the forthcoming discussion on the seismic origins would not be useful. For that purpose, we shall refer to the study on the wave generation from a spherical origin, which has been discussed by many seismologists as a tractable model of earthquakes. We imagine an origin of spherical shape in the medium, the surface of which is subject to a stress change such as, for instance,

Table III.

Group	α	β
Shallow (A, C)	−0.78	0.28±0.042
Deep-focus (C, H*)	−2.19	0.43±0.047
Whole (A, B, C, H*)	−2.59	0.51±0.033

*) Results given in Honda's paper.

$$\left.\begin{aligned} \widehat{rr} &= FP_2^1(\cos\theta)\cos\varphi \cdot e^{i\omega t}\,, \\ \widehat{r\theta} &= \widehat{r\varphi} = 0\,, \end{aligned}\right\} (\text{at } r = a_0)\,, \qquad (42)$$

where a_0 is the radius of the sphere. This is one of the physical conditions of seismic origins, which radiates waves resulting in an azimuthal distribution of quadrant type. The radial displacement at a point $(r=r)$ due to P-waves is given by W. Inouye as follows,[52]

52) W. INOUYE, *Bull. Earthq. Res. Inst.*. **16** (1938), 599.

$$u=-\frac{A}{h^2}\frac{d}{dr}\frac{H_5^{(2)}(hr)}{\sqrt{r}}P_2^{\,1}(\cos\theta)\cos\varphi\cdot e^{i\omega t}\,. \tag{43}$$

A is a constant to be derived from the following relations, *viz.*,

$$\left.\begin{aligned}
&2A\left\{-\frac{1}{h^2r^2}H_{5/2}^{(2)}(hr)+\frac{1}{hr}H_{7/2}^{(2)}(hr)\right\}\\
&\qquad+C\left\{-\frac{6}{k^2r^2}H_{5/2}^{(2)}(kr)+\frac{5}{kr}H_{7/2}^{(2)}(kr)-H_{9/2}^{(2)}(kr)\right\}=0\,,\\
&A\left\{\left(\frac{\lambda}{\mu}-\frac{4}{h^2r^2}\right)H_{5/2}^{(2)}(hr)+2\left(\frac{5}{hr}H_{7/2}(hr)-H_{9/2}^{(2)}(hr)\right)\right\}\\
&\qquad+12C\left\{-\frac{1}{k^2r^2}H_{5/2}^{(2)}(kr)+\frac{1}{kr}H_{7/2}^{(2)}(kr)\right\}=\frac{F\sqrt{r}}{\mu}\,,
\end{aligned}\right\} \tag{44}$$

where,

$$h=\sqrt{\frac{\rho}{\lambda+2\mu}}\,\omega\,,\qquad k=\sqrt{\frac{\rho}{\mu}}\,\omega\,. \tag{45}$$

Frequency characteristics of the longitudinal wave generated from the origin being known from (43), we obtain the following function,

$$Y(\omega)=A(a_0,\ V_p,\ V_s,\ \omega)\,. \tag{46}$$

This is the spectrum of P-wave radiated from the origin when the stress change takes place impulsively (*cf.* eqs. (15) and (42)). If the stress at the origin changes as $f(t)$, the spectrum becomes,

$$R(\omega)=Y(\omega)\cdot G(\omega)\,, \tag{47}$$

where, $G(\omega)$ is given from $f(t)$ in such a way,

$$G(\omega)=\int_{-\infty}^{\infty}f(t)\,e^{i\omega t}\,dt\,, \tag{48}$$

Although we have no concrete knowledge on $f(t)$, it may be considered that the function is a unit-step, approximately, provided we assume an origin being like a fracture production. Hence,

$$G(\omega)=1/\omega\,. \tag{49}$$

Fig. 22 shows the curves for (46)[53] as well as for (49), in which the

53) *loc. cit.*, 52).

abscissa, ha_0 indicates the ratio of the radius of the assumed origin to the wave-length of each spectral component. Fig. 23 illustrates the curve for (47), in which the abscissa is given in a relative scale of T to T_0, the period of the maximum spectral intensity. T_0 is a function of the velocity V_p and the radius of the origin a_0, being given approximately as,

$$ha_0 = \frac{2\pi}{V_p} \frac{a_0}{T_0} \doteqdot 0.7 . \qquad (50)$$

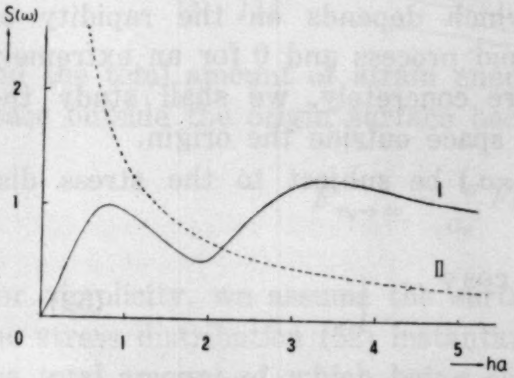

Fig. 22. Impulsive response of the spherical origin (I, after W. Inouye) and the spectrum of a unit step-function (II).

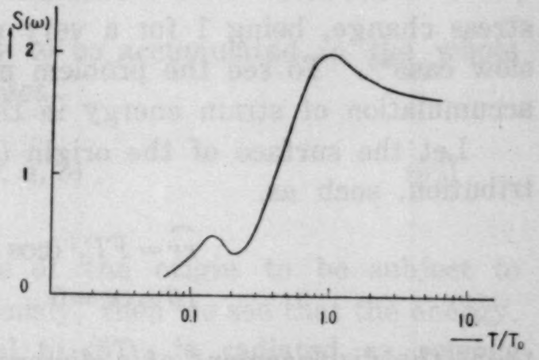

Fig. 23. Spectrum of P-wave caused by a step-like stress change in time. The period of the harmonic which corresponds to the maximum intensity is taken as T_0.

If the actual state of earthquake origins is well approximated by the above-stated model, we may expect a satisfactory agreement between the theoretical curves and those spectra shown in Figs. 20a, b, c. Although the latter is not so simple as the former, we see some similarity between them when we compare their fundamental structures. As long as the similarity is taken for granted, we can estimate the apparent radius of the respective origin referring to the assumed model. a_0 in Table IV are the values obtained from (50) assuming V_p as 6 km/sec for shallow earthquakes, while as 8 km/sec, for deep-focus ones.[54]

4. The energy and the dimension of seismic origins.

We shall turn the point of discussion to the energy accumulation in the seismic origins. The relation between the magnitude and the energy of seismic waves has been studied from various standpoints. According

54) Phase angles of spectrum can not be calculated accurately because of their uncertainty in determining $2n\pi$. So that no discussion is made on them.

to B. Gutenberg and C. F. Richter, the relation is given as follows,

$$\log E = a + bM\,, \tag{51}$$

where, for example, $a=11.8$ and $b=1.5$.[55] Therefore, when we know the volume of the space, wherein the seismic energy is accumulated effectively, the density of accumulation can be estimated.

Referring to the above-stated model of seismic origins, the total energy of radiated waves is n-times as large as the difference between the strain energy distributed, respectively, before and after the earthquake occurrence. n is a constant which depends on the rapidity of stress change, being 1 for a very rapid process and 0 for an extremely slow case[56]. To see the problem more concretely, we shall study the accumulation of strain energy in the space outside the origin.

Let the surface of the origin ($r=a_0$) be subject to the stress distribution, such as,

$$\left.\begin{aligned} \widehat{rr} &= FP_2^1(\cos\theta)\cos\varphi\,, \\ \widehat{r\theta} &= \widehat{r\varphi} = 0\,, \end{aligned}\right\} \tag{52}$$

then, the displacement of a distant point at (r,θ,φ) is given,

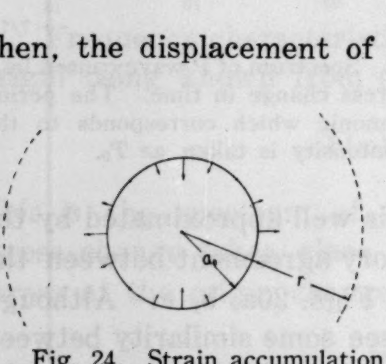

Fig. 24. Strain accumulation around a spherical origin.

$$\left.\begin{aligned} u &= \frac{a}{r^2}\sin 2\theta\cos\varphi\,, \\ v &= \frac{b}{r^2}\cos 2\theta\cos\varphi\,, \\ w &= -\frac{b}{r^2}\cos\theta\sin\varphi\,, \\ &a,\ b: \text{constants}, \end{aligned}\right\} \tag{53}$$

where, and u, v, w are the displacement in r-, θ-, and φ-directions, which satisfy the following conditions of equilibrium when $\lambda=\mu$.

$$\left.\begin{aligned} &(\lambda+2\mu)\sin\theta\frac{\partial\Delta}{\partial\theta} - 2\mu\left\{\frac{\partial\varpi_r}{\partial\varphi} - \frac{\partial}{\partial r}(r\varpi_\varphi\sin\theta)\right\} = 0\,, \\ &(\lambda+2\mu)\frac{1}{\sin\theta}\frac{\partial\Delta}{\partial\theta} - 2\mu\left\{\frac{\partial}{\partial r}(r\varpi_\theta) - \frac{\partial\varpi_r}{\partial\theta}\right\} = 0\,, \\ &(\lambda+2\mu)\,r\sin\theta\frac{\partial\Delta}{\partial r} - 2\mu\left\{\frac{\partial}{\partial\theta}(\varpi_\varphi\sin\theta) - \frac{\partial\varpi_\theta}{\partial\varphi}\right\} = 0\,. \end{aligned}\right\} \tag{54}$$

55) B. GUTENBERG and C. F. RICHTER, *Trans. Amer. Geophys. Union*, **37** (1956) 243.
56) K. SEZAWA and K. KANAI, *Bull. Earthq. Res. Inst.*, **14** (1936), 10.

The strain energy in unit volume being written as,

$$e = \frac{1}{2}\Big[(\lambda+2\mu)(e_{rr}+e_{\theta\theta}+e_{\phi\phi})^2+\mu(e_{\theta\varphi}^2+e_{\varphi r}^2+e_{r\theta}^2 - 4e_{\theta\theta}e_{\varphi\varphi}-4e_{\varphi\varphi}e_{rr}-4e_{rr}e_{\theta\theta})\Big], \tag{55}$$

we obtain the amount of the energy in a spherical shell ($a_0 \leqq r \leqq r_0$) to be,

$$E_{r_0} = \iiint er^2 \sin\theta d\theta d\varphi dr = \Big(\frac{1}{a_0^3} - \frac{1}{r_0^3}\Big)F(\mu, a, b), \tag{56}$$

and the total amount of strain energy to be accumulated in the whole space outside the origin surface becomes,

$$E_{r_0 \to \infty} = \frac{1}{a_0^3}F(\mu, a, b). \tag{57}$$

For simplicity, we assume the surface of the origin to be subject to the stress distribution (52) instantaneously, then we see that the energy, the total amount of which being equal to (57), is radiated as seismic waves. In other words, suppose the surface of the origin has been subject to the stress (52) initially and is liberated from it suddenly,[57)58)] then the strain energy that has been distributed around the surface disappears and, in place of it, seismic waves will be observed, their energy amounting equal to the strain energy disappeared. From such considerations, we may treat the dependence of E_{r_0}/E_∞ on r_0 as an indicator for the accumulation of the *seismic energy*. Fig. 25 is drawn to show the relation between E_{r_0} and r_0, both of which are given in relative scales.

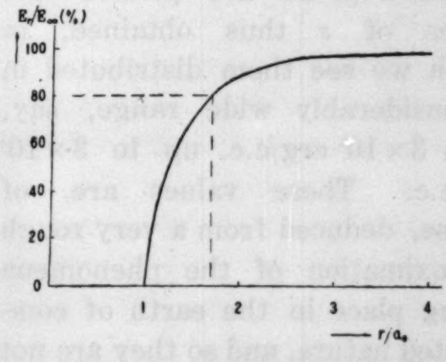

Fig. 25. Volume of a spherical shell around the origin and the energy accumulated in it.

From Fig. 25 we see, for instance, that 80% of the total energy is accumulated in the spherical shell lying between a_0 and 1.7 a_0. Although

57) K. SEZAWA and K. NAKAI, *loc. cit.*, 56).

58) This assumption is somewhat different from the ordinary model of fracture production, in which is assumed the initial stress being distributed uniformly in the medium. But we employ the above saying, here, for simplicity.

we have no other reliable evidence for justifying the above dimension as the most reasonable, we shall define it as the effective volume of the shell for energy accumulation. So far as the present definition is taken, we can study the densities of energy accumulation (mean values) in such a way,

$$\varepsilon = \frac{0.8E}{V_e}\,, \qquad (58)$$

where,

$$V_e \doteqdot \frac{4\pi}{3} a_0^3 \times 4\,. \qquad (59)$$

E is obtained by applying (51) to the respective earthquakes and V_e is known from the estimated values of a_0 with the aid of eq. (59) (*cf.* Table IV).

In Fig. 26 are plotted the values of ε thus obtained, in which we see them distributed in a considerably wide range, say, from 3×10^2 erg/c.c. up to 3×10^4 erg/c.c. These values are, of course, deduced from a very rough approximation of the phenomena taking place in the earth of complicated nature, and so they are not considered as definite ones. However, as long as we regard the estimate as order-of-magnitude one, there may be no serious mistake in the conclusions. The writer would like to note that the upper limit of the density thus obtained is approximately equal to that presented by C. Tsuboi on the basis of geodetic studies on

Table IV.

Earthquake		M	T_0 sec	a_0 km
A	1	7.4	23	16
	2	7.0	13	9
	3	7.2	30	20
	4	8.5	33	23
	5	7.8	20	14
	6	6.5	—	—
	7	8.2	50	36
	8	6.5	10	7.1
B	1	7.7	24	17
	2	7.7	18	13
	3	7.3	14	10
	4	(6.5)	9.5	6.8
	5	7.3	10	7.1
	6	8.0	19	7.4
	7	6.8	14	10
C	1	7.0	6.0	5.3
	2	7.2	8.5	7.6
	3	6.8	9.6	8.5
	4	7.3	9.6	8.5
	5	6.3	3.6	3.2
	6	6.8	9.0	8.0
H	1	6.0	4.9*	4.4
	2	6.1	3.3*	2.9
	3	5.8	1.6*	1.4
	4	6.1	1.9*	1.7
	5	6.4	3.3*	2.9
	6	7.0	4.4*	3.9
	7	6.9	4.4*	3.9
	8	6.5	4.0*	3.6
	9	6.5	3.7*	3.3
	10	5.7	2.3*	2.5
	11	5.7	1.4*	1.2
	12	5.3	1.0*	0.9

*) after H. Honda.

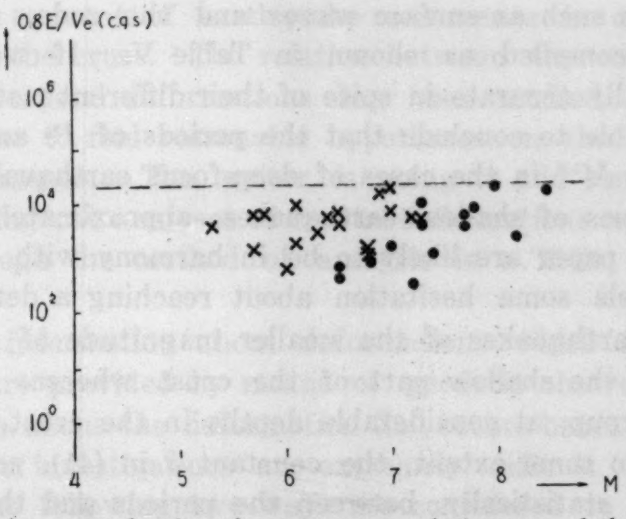

Fig. 26. Apparent density of energy accumulation around the seismic origins (●: shallow earthquakes, ×: deep-focus earthquakes).

crustal deformations.[59] It is a notable fact that, so far as the density of energy accumulation concerns, no remarkable difference of character could be found between shallow earthquakes and deep-focus ones.

5. Further discussion on the related problems.

Lastly, we shall give a short discussion of some related problems which have been left unstudied in detail in the above sections. In the third section of this chapter, a relation is given between T_0 and M (*cf.* eq. (41) and Table III). Many seismologists have studied the relation with respect to the different phases of seismic waves. Among them, however, few have made analyses on those of bodily waves, with which the present paper is concerned. Excluding the papers written

Table V.

Class of earthquakes	Remarkable shallow	Local shallow	Moderate deep-focus
P-wave		$T^3 \propto M$ [61]	$T \propto M^{0.5}$ [62]
S-wave	$T \propto M^{0.3}$ [60]	$T^3 \propto M$ [61]	$T \propto M^{0.5}$ [62]

59) C. TSUBOI, *loc. cit.*, 7).
60) K. AKI, *Zisin* (*Journ. Seis. Soc. Japan*), [ii], **8** (1955), 99 (in Japanese).
61) A. E. JONES, *Bull. Seis. Soc. Amer.*, **28** (1938), 313.
62) K. KANAI, *loc. cit.*, 47).

on later phases such as surface waves and the coda, results obtained by them are compiled as shown in Table V. If we assume these results as equally accurate in spite of their different method of analyses, we might be able to conclude that the periods of *P*- and *S*- waves are proportional to $M^{0.5}$ in the cases of deep-focus earthquakes, whereas to $M^{0.3}$, in the cases of shallow earthquakes, approximately. The results of the present paper are likely to be in harmony with them, however, the writer feels some hesitation about reaching a definite conclusion. Because, the earthquakes of the smaller magnitude of group A look to be occurred in the shallow part of the crust whereas the larger ones of the same group, at considerable depths in the crust. Such tendency might affect, to some extent, the constant β in (41), provided a certain relation exists, statistically, between the periods and the focal depths.

According to the result obtained in the fourth section, we may conclude that the mangnitude of energy radiation depends closely upon the dimension of the origin, on the surface of which the stress change occurs. In other words, even if the strain energy is accumulated in a large volume of the crust, such energy could not be released effectively, unless a sufficiently large space exists as the origin of stress release. C. Tsuboi has lately presented an opinion that an *earthquake volume* is to be taken into consideration, as an important factor in earthquake occurrence.[63] From the present standpoint, such a volume should be understood in relation to the above-mentioned space for stress release. We would have, then, a more consistent picture of earthquake occurrence, with which we could interpret the evidence shown in Fig. 21.

Chapter IV.

Analyses of Crustal Deformations Accompanied by Great Earthquakes.

1. Introduction.

Crustal deformations have been often observed at the time of great earthquakes. Although no instrumental observations have been reported about the exact time when the deformations appeared on the surface, it is widely believed that most part of the deformations were probably

63) C. TSUBOI, *loc. cit.*, 7).

produced at the moment of earthquake occurrence in consequence of stress change in the crust. The relation between the nature of great earthquakes and crustal deformations has been studied by many geophysicists in order to find reasonable hypotheses on the mechanism of earthquake occurrence. The writer is going to add something to the studies by carrying out analyses of crustal deformations accompanied by earthquakes, though the method of analysis is a little different from those studies.

Most of the information about deformations which appear on the earth's surface are provided by means of geodetic observations. Since nothing is known about the deformation that occurs beneath the surface, however, accurate investigations are extremely difficult. Under these circumstances, the following two ways are considered to be practicable from the standpoint of the theory of elasticity. They are:

a) to determine analytically possible distribution of stresses or strains on an underground horizontal plane, imagined at a certain depth in the crust, so as to satisfy the conditions of elastic equilibrium as well as the deformations observed at the surface, or,

b) to calculate the deformation on the surface on the basis of a probable model of the phenomenon (*f.i.* the stress change caused by the production of a fault), and to compare it with the results actually observed.

Taking the first way, S. Homma wrote a paper on the crustal deformations accompanied by the North-Izu earthquake of 1930.[64] Since no particular assumption was employed, his theory is to be applied to any case provided the deformation on the surface is known. However, if an earthquake occurs as a result of fracture production in an extremely strained medium, the surface newly produced will be the origin of stress change in the crust; so that, except when the fracture plane lies nearly horizontally, the result from his theory will be of little physical significance.

On the contrary, the second way can not be applied to all cases, because it requires particular assumptions to be made in the analysis. Crustal deformations are of complicated nature, in general, as have been manifested by C. Tsuboi in his paper written on the related phenomena. However, we know some examples, in them, of rather simple features, in which were observed systematic distribution of horizontal displacements on both sides of a lateral fault. For such ones

64) S. HOMMA, *Quart. Journ. Seismology, C.M.O., Japan,* **16** (1952), 57 (in Japanese).

we may take a model, which would be accepted as a probable one as long as the deformations on the earth's surface are concluded from the model to be not greatly different from the observed ones.

2. General view of earthquakes accompanying crustal deformations.

Geodetic observations that have been carried out so far show crustal deformations associated with seismic activity to be observable only in the cases of earthquakes of considerably large magnitudes. It is also noticed that the phenomenon seems not to be observed in the case of a deep-focus earthquake, even when the magnitude is large. These circumstances seem likely to suggest that the magnitude and the focal depth of an earthquake play an important *rôle* in the occurrence of crustal deformations on the earth's surface. Under such considerations, we shall try to obtain a general relation between the earthquake and the crustal deformations, taking, as examples, destructive earthquakes which took place since 1923 in the Japan area (Table VI).[65]

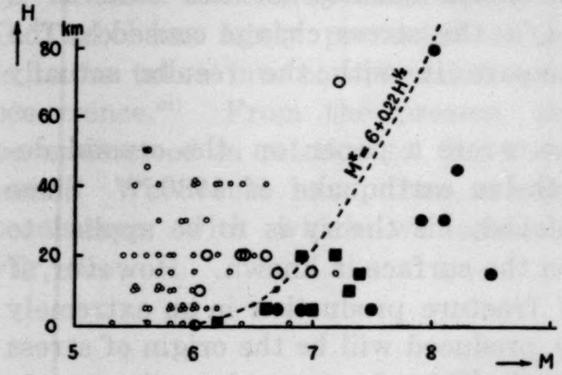

Fig. 27. Characteristics of earthquakes accompanying crustal deformations.

■ Destructive earthquake accompanying crustal deformations (push-pull distribution: A type).

● Destructive earthquake accompanying crustal deformations (push-pull distribution: B type).

○ Destructive earthquake accompanying no crustal deformations.

o Non-destructive earthquake (no crustal deformations.) (1944–1950).

We can see graphically in Fig. 27 the relation between these factors, in which the black marks are used for earthquakes which accompanied crustal deformations (earthquakes with tsunamis are included, on the assumption that such tsunamis were caused in consequence of deformations of the sea bottom), whereas empty marks, for earthquakes for which no description of such phenomena could be found. The classification refers only to several series of bulletins, and, besides this, it might be impossible for observers in the field to certify the occurrence of the phenomena to the slightest magnitude. Taking these cir-

65) *Rika-nenpyô* (Annual Table of Constants, Tokyo Astronom. Obs.), 1957.

Table VI. Destructive earthquakes and their types classified with respect to push-pull distributions, crustal deformations, and tsunamis.

No.	Date	Epicentre	M	H (km)	Push-pull distrib.	Crustal deform.	Tsunami
1	1923 IX 1	Kwantô	7.9	30	B	B	+
2	1927 III 7	Tango	7.4	14	A	A*	—
3	1927 X 27	Sekihara	5.4	—	–	+	—
4	1929 XI 20	Aritagawa	6.2	—	–	–	—
5	1930 XI 26	North-Izu	7.0	<10	A	A*	—
6	1931 IX 21	Saitama	6.7	10–20	–	–	—
7	1933 III 3	Sanriku	8.5	(15)	B	+	+
8	1933 IX 21	Noto Pen.	—	—	–	–	—
9	1935 VII 11	Shizuoka	6.6	<7	A	–	—
10	1936 II 21	Kawachi-Yamato	6.7	10	B	–	—
11	1938 I 12	Tanabe	7.0	15	–	–	—
12	1938 V 23	Iwaki	7.5	(70)	–	–	+
13	1938 XI 5	Iwaki	7.5	shallow	B	–	+
14	1939 III 20	Miyazaki	6.7	—	–	–	+
15	1939 V 1	Oga Pen.	6.9	20	A	+	+
16	1949 VII 15	Nagano	6.4	—	A	–	—
17	1941 XI 19	Miyazaki	7.0	—	–	–	+
18	1943 III 4	Tottori	6.4	20	B	–	—
19	1943 III 5	Tottori	6.4	20	B	–	—
20	1943 VIII 12	Fukushima	6.0	0	–	–	—
21	1943 IX 10	Tottori	7.3	10	A	(A)*	—
22	1943 X 13	Nagano	6.0	10	A	–	—
23	1944 XII 7	Tônankai	8.3	0–30	–	–	+
24	1945 I 13	Mikawa	6.9	0–10	B	+*	—
25	1946 XII 21	Nankaidô	8.1	30	B	B	+
26	1948 VI 28	Fukui	7.2	(20)	A	A*	—
27	1949 XII 26	Imaichi	6.5	<10	B	B	—
28	1952 III 4	Tokachi	8.2	40–50	B	–	+
29	1952 III 7	Daishôji	6.5	20	A	–	—
30	1952 VII 18	Yoshino	7.2	70	B	–	—
31	1953 XI 26	Bôsô	8.0	80	B	–	+
32	1955 X 19	Futatsui	6.2	shallow	A	+	—

Remarks.[66] Push-pull distribution A: quadrant type, B: other types.
Crustal deformation A: lateral fault type, B: other types.
+: appeared but the type was unknown, *: seismic fault,
–: no report on crustal deformations.
Tsumami +: recorded on mareograms, —: no report.

66) Classification of these types are referred to the reports published in *Bull. Earthq. Res. Inst.*, *Ken-shin Jihô* (*C.M.O.*), *Zisin*, and other bulletins.

cumstances into consideration, we still notice the evidence that crustal deformations appear in the cases of earthquakes, the magnitudes of which are greater than such a limit as is given, for instance,

$$M^* = 6 + 0.22\,H^{1/2}, \tag{60}$$

where H denotes the focal depth measured in km.

Another notable piece of evidence in Fig. 27 is seen for those earthquakes which were reported as accompanied crustal deformations of type A. All of them are of focal depths less than 30 km and showed push-pull distribution of A type. In some of them, moreover, which were accompanied by seismic falts, a remarkable similarity is noticed between the patterns of horizontal displacements and the mode of push-pull distributions.[67] These facts might be recognized as an important indication of their occurrence to be associated with strain accumulation and fracture production in the crust. Excluding detailed features of them from discussion, it does not seem difficult for us to suppose the mechanism on the basis of some simple model, and so we shall study the occurrence of the said type of crustal deformations in the following.

3. Statics of a lateral fault.

The outstanding feature of such crustal deformations as were concerned in the end of last section is characterized with a long seismic fault and the systematic distribution of horizontal displacements observed in the vicinity of the fault. In those particular cases which are often called lateral faults, deformations in the horizontal direction are more significant than those in the vertical direction, so that we might be able to interpret the phenomenon as the deformation of the medium (half-space) which is subject to uniform shear stress to the limit of strength resulting in a long fracture along the surface. Employing the present model, we shall study the phenomenon in the following (Fig. 28).

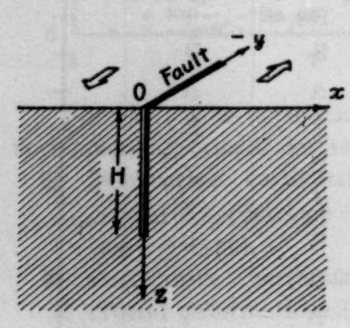

Fig. 28. Model of a lateral fault.

Let the x-, y-, and z-axes be as shown in the figure and the initial shear stress be working only on the y, z-plane. Conditions of equilibrium are given to the present system, as

67) H. HONDA, *loc. cit.*, 8).

$$\left.\begin{aligned}(\lambda+\mu)\frac{\partial}{\partial x}\Delta+\mu\left(\frac{\partial^2}{\partial x^2}+\frac{\partial^2}{\partial y^2}+\frac{\partial^2}{\partial z^2}\right)u=0\ ,\\(\lambda+\mu)\frac{\partial}{\partial y}\Delta+\mu\left(\frac{\partial^2}{\partial x^2}+\frac{\partial^2}{\partial y^2}+\frac{\partial^2}{\partial z^2}\right)v=0\ ,\\(\lambda+\mu)\frac{\partial}{\partial z}\Delta+\mu\left(\frac{\partial^2}{\partial x^2}+\frac{\partial^2}{\partial y^2}+\frac{\partial^2}{\partial z^2}\right)w=0\ ,\end{aligned}\right\}\qquad(61)$$

where,

$$\left.\begin{aligned}\Delta=\frac{\partial u}{\partial x}+\frac{\partial v}{\partial y}+\frac{\partial w}{\partial z}\ ,\\\left(\frac{\partial^2}{\partial x^2}+\frac{\partial^2}{\partial y^2}+\frac{\partial^2}{\partial z^2}\right)\Delta=0\ ,\end{aligned}\right\}\qquad(62)$$

and λ, μ, u, v, w denote the elastic constants and displacements in x-, y-, z-directions, respectively. We know that the conditions of the fault production can be replaced with a negative stress taken supplementarily so as to cancel the initial shear stress on the necessary part of the $x=0$ plane. Suppose they are given as follows,

$$X_y=\sum_m\sum_n F_{mn}\cos my\cos nz\ ,\quad (x=0)\ ,\qquad(63)$$

then the solution for (61) will become,

$$\left.\begin{aligned}u=\sum_m\sum_n A_{mn}\,U(x)\sin my\cos nz\ ,\\v=\sum_m\sum_n B_{mn}\,V(x)\cos my\cos nz\ ,\\w=\sum_m\sum_n C_{mn}\,W(x)\sin my\sin nz\ ,\end{aligned}\right\}\qquad(64)$$

wherein, the following condition for the free surface must be satisfied at $z=0$, that is,

$$X_z=Y_z=Z_z=0\ .\qquad(65)$$

The present section deals with the simplest case, in which it is assumed that the phenomenon is uniform in y-direction, or $\partial/\partial y\equiv0$. This assumption may approximately hold good for long seismic faults. The solution becomes, then,

$$\left.\begin{aligned}n=0\ ,\\v=\sum_n(B_n\cosh lx+B'_n\sinh lx)\cos nz\ ,\\w=0\ ,\end{aligned}\right\}\qquad(66)$$

where, B and B' are constants which are to be determined from physical conditions. Stress change on the $x=0$ plane is written as,

$$\left.\begin{aligned} X_y=\sum_n F_n \cos nz &=1 \quad (x=0,\ 0\leq z\leq H)\,, \\ &=0 \quad (x=0\,, \quad H<z)\,. \end{aligned}\right\} \tag{67}$$

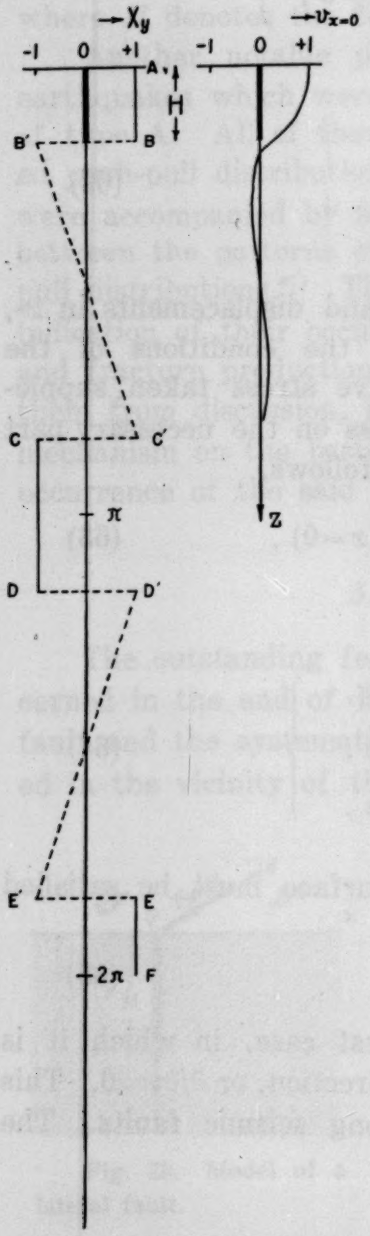

Fig. 29. Stress distribution (X_y) on the $x=0$ plane (left), and the displacement ($v_{x=0}$) caused by it (right).

While at $x=\infty$, every component of deformations must be zero, and so we finally obtain,

$$B'_n=-B_n=\frac{F_n}{\mu n}\,, \quad l=n\,. \tag{68}$$

Numerical calculation was carried out for a stress distribution as shown in Fig. 29 (left), in which the distribution for the interval of 2π is illustrated taking the depth of the fault as $H=\pi/6$. AB is the stress change which corresponds directly to the fault production, while CD is added for the convenience of numerical culculation. The latter is taken far enough from the surface so as not to disturb the stress distribution in the vicinity of the fault. Stress between B′ and C′ (broken line) represents the indirect effect coming from the space behind the fault ($x<0$). Although we have no concrete basis of presuming the distribution of the said effect, we assume it to be -1 at B′ increasing linearly with depth to be $+1$ at C′. The picture in the right half of Fig. 29 illustrates the distribution of v along the $x=0$ plane, in which no remarkable displacement can be seen in the region below the bottom of the fault; and from this result we may recognize the above-assumed distribution of B′C′ to be reasonable in the present degree of approximation. Numerical values in Table VII shows the coefficients for the stress distribution ABB′C′CDD′··· expanded into Fourier series. Putting these values in (66), we obtain the displacement in the medium which will be caused by the fault. Equi-value lines in Fig.

Table VII.

n	F_n	F_n/n
0	0	—
1	.220	.220
2	0	0
3	.838	.280
4	0	0
5	.290	.058
6	0	0
7	−.163	−.023
8	0	0
9	−.283	−.032
10	0	0
11	−.107	−.010
12	0	0
13	.080	.005
14	0	0
15	.192	.014
16	0	0
17	.097	.005
18	0	0
19	−.048	−.003
20	0	0
21	−.082	−.004
22	0	0
23	−.034	−.001
24	0	0

30 are for v, distributing in the vertical cross-section (v at $x=z=0$ is taken as 100). We see in it that the displacement is large in the vicinity of the fault getting smaller as the distance from the fault becomes large. This tendency agrees with that observed in some cases of lateral faults which will be studied in the following section. Fig. 31 is drawn for the distribution curves of v_0 on the surface taking the depth of the fault as a parameter, which shows that the larger the depth of the fault is, the smaller is the rate of decrease of v_0 with distance. Therefore, the most probable value of H can be known from the comparison of these curves with the distribution actually observed.

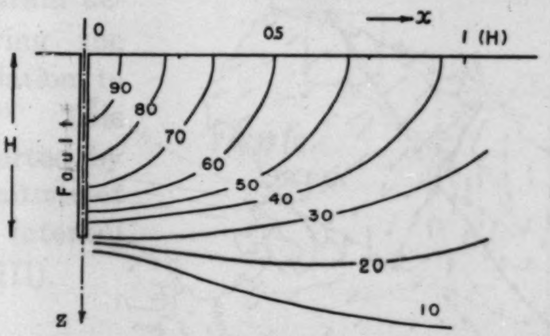

Fig. 30. Distribution of v in the vertical cross-section.

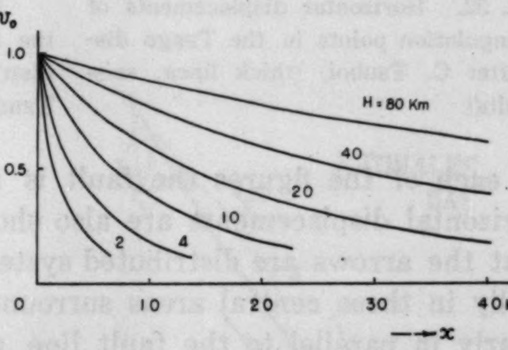

Fig. 31. Diminution of v_0 with distance (x).

4. Features of some actual faults.

Among many examples of crustal deformations, we shall develop the investigation of three typical cases, to which the present model

is likely to be reasonably applied. They are the deformations observed after the Tango earthquake (1927), the North-Izu earthquake (1930), and the California earthquake (1906), the observational results on which are illustrated in Figs. 32～34.[68)69)70)]

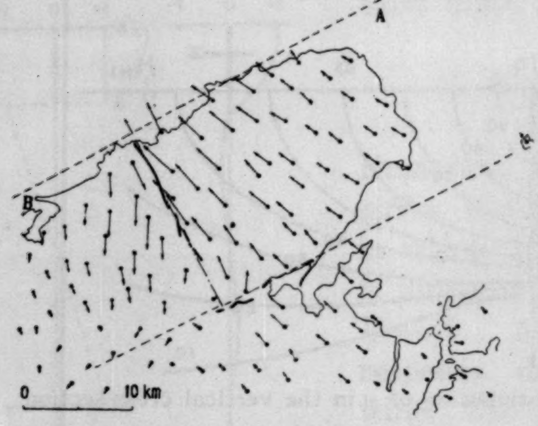

Fig. 32. Horizontal displacements of the triangulation points in the Tango district (after C. Tsuboi) (thick lines: seismic faults).

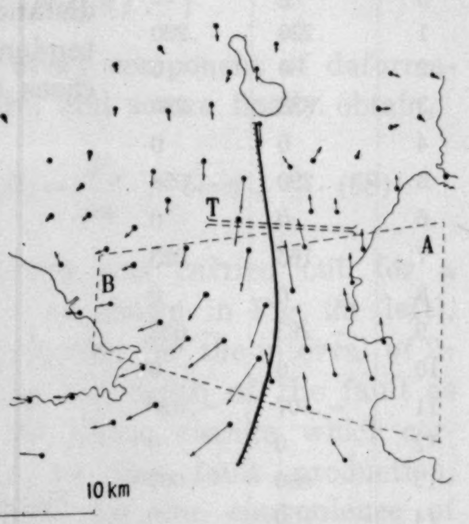

Fig. 33. Horizontal displacements of the triangulation points in the North-Izu district (after S. Yamaguti), (thick line: the Tanna fault, T: the railway tunnel).

In each of the figures the fault is shown with thick lines, while the horizontal displacements are also shown with arrows as vectors. We see that the arrows are distributed systematically around the main fault; especially in those central areas surrounded with broken lines, arrows are nearly in parallel to the fault line and are in the same tendency of diminution with distance from the fault as shown in Fig. 31. From these results we may justify to apply the theory of a simplified fault of infinite length to the said examples, provided we limit our discussion to the deformations in the central areas (faults of finite length will be studied later by means of model experiments).

Figs. 35～37 show the distribution of v_0 diminuting with distance from the faults, in which the resultant displacements observed are plotted as v_0. As they are in the direction nearly parallel to the respective faults, this simplified treatment of vectors will cause no serious troubles in the

68) C. TSUBOI, *loc. cit.*, 6).

69) S. YAMAGUTI, *Bull. Earthq. Res. Inst.*, **15** (1937), 899.

70) *Report, State Earthquake Investigation Commission, the California Earthquake of April 18, 1906*, (Carnegie Institution of Washington, 1908).

result. Before applying the theoretical curves to the plotted results, we have to remark on a peculiar aspect that the displacements on one side of the fault are systematically larger than those on the other side. Such discrepancy is most remarkable in the case of the San Andreas fault and less for the other two. The fact is thought to be caused by the development of strain accumulation in the crust during the period from the first triangulation to the earthquake occurrence.[71] This view may be somewhat supported by the relation between the magnitude of discrepancy and the time interval mentioned above (*cf.* Table VIII).

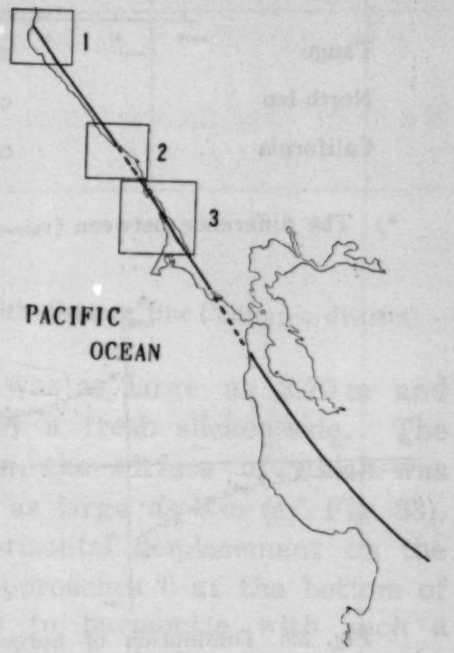

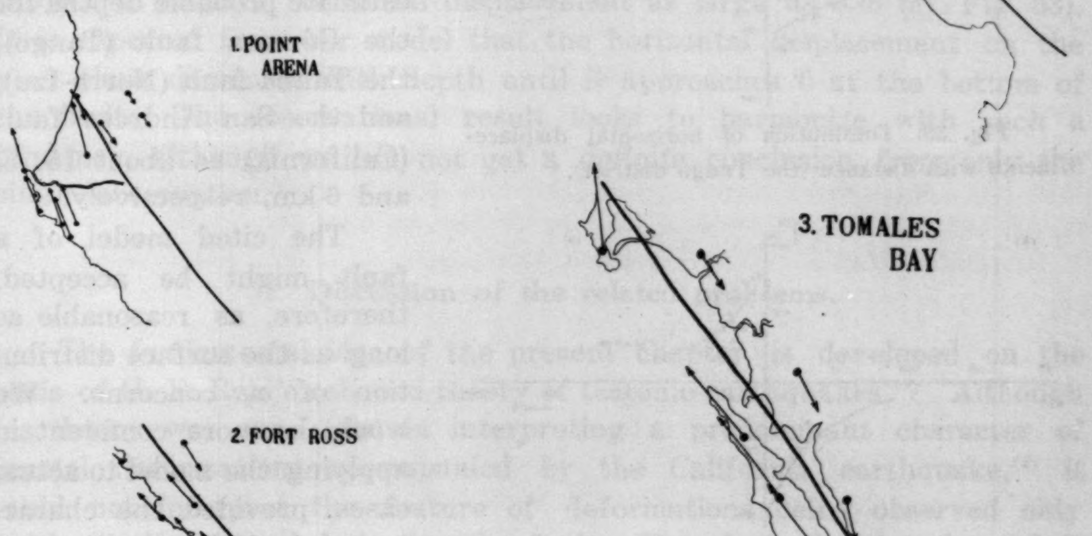

Fig. 34. Index map of the California district and horizontal displacements of the triangulation points (thick line: San Andreas fault). (After State Earthquake Investigation Commission of California Earthquake).

71) H. F. Reid, *Physics of the Earth*, VI, (1933) p. 82.

Table VIII.

Earthquake	Discrepancy between v_0 on the A-and B-sides of the fault*	Time interval between the surveys made before and after the earthquake
	cm	years
Tango	ca. 40	30
North-Izu	ca. 25	7
California	ca. 50～200	20～30

*) The difference between $(v_0)_{x=0}$ presumed respectively for A and B areas.

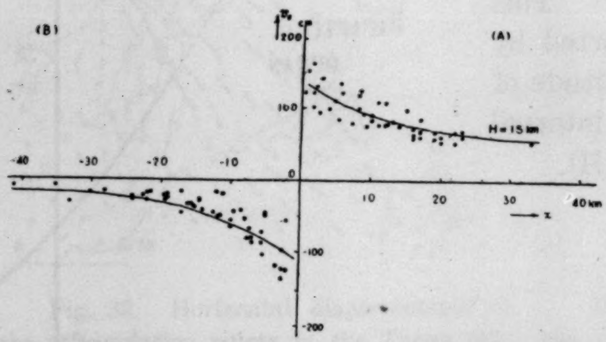

Fig. 35. Diminution of horizontal displacements with distance (the Tango district).

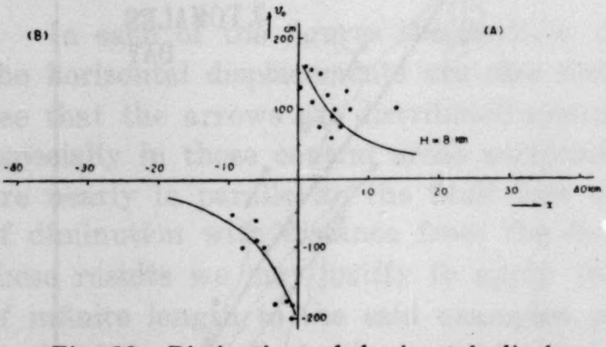

Fig. 36. Diminution of horizontal displacements with distance (the North-Izu district).

Under these considerations, we apply the curves in Fig. 31 to the observational results plotted in Figs. 35～37. We thus estimate probable depths for the Gômura fault (Tango), the Tanna fault (North-Izu), and the San Andreas fault (California) as about 15, 8, and 6 km, respectively.

The cited model of a fault might be accepted, therefore, as reasonable so long as the surface distribution of v_0 concerns. We would be more confident in applying the model to actual cases, provided the characteristics of deformation beneath the surface is observed to be in good harmony with the model (*cf.* Fig. 30). It is, of course, very difficult to get clear information about such an evidence generally. The North-Izu earthquake has furnished, however, a rare oppotunity for our studying the problem. R. Takahasi reported about his observation of a seismic fault in a drain drift of the Tanna railway tunnel, which was under construction at that time.[72] According to his paper, the displacement,

72) R. TAKAHASI, *Bull. Earthq. Res. Inst.*, **9** (1931), 435.

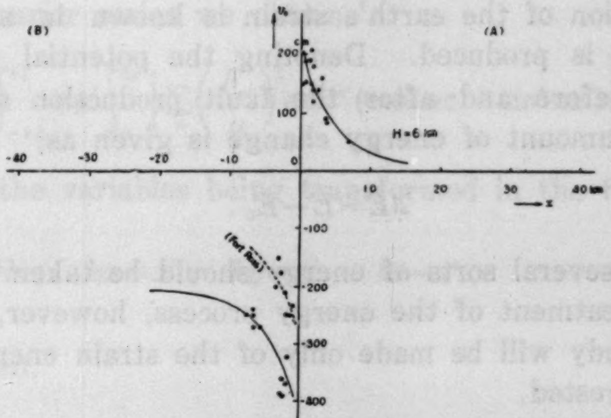

Fig. 37. Diminution of horizontal displacements with distance (the California district).

which was nearly in horizontal direction, was as large as 2.70 m and the drain tunnel was completely closed by a fresh slicken-side. The tunnel passed 160 m below the Tanna basin, the surface of which was subject to relative horizontal displacement as large as 3 m (*cf*. Fig. 33). It is expected from our model that the horizontal displacement on the $x=0$ plane decreases with depth until it approaches 0 at the bottom of the fault. The observational result looks to harmonize with such a tendency, although we can not get a definite conclusion from only the single observation.

5. Discussion of the related problems.

The fundamental idea of the present chapter is developed on the basis of H. F. Reid's rebound theory of tectonic earthquakes.[73] Although his theory was successful in interpreting a predominant character of crustal deformations accompanied by the California earthquake,[74] it could not interpret the feature of deformations being observed only in the limited area lying near the fault. This fact, that has been left as an obstacle to his theory, can be understood provided we take the model of a fault of finite depth.

It is of much interest from the geophysical standpoint to study how large an amount of energy change is caused in consequence of fault production in the crust. So far as the present theory is concerned, the

73) H. F. REID, *loc., cit.*, 10).

74) The present discussion is made only on the relation between a fault and of the earth's strain, but not made on such dynamical motion of fault production as shown in Reid's theory.

spatial distribution of the earth's strain is known in all of the space where the fault is produced. Denoting the potential energy involved in the crust before and after the fault production as E_0 and E, respectively, the amount of energy change is given as,

$$\Delta E = E - E_0 \,. \tag{69}$$

We know that several sorts of energy should be taken into account for the complete treatment of the energy process, however, in the present chapter, the study will be made only of the strain energy, in which we are mostly interested.

The expression for the energy in unit volume of the strained medium is written as,

$$e = \frac{1}{2}\Big[(\lambda+\mu)\Delta^2 + \mu(e^2_{xy} + e^2_{yz} + e^2_{zx} - 4e_{xx}e_{yy} - 4e_{yy}e_{zz} - 4e_{zz}e_{xx})\Big] \,, \tag{70}$$

where, $\Delta = e_{xx} + e_{yy} + e_{zz}$ and e_{xx}, e_{yy}, e_{zz}, e_{xy}, e_{yz}, e_{zx} denote the strain components, respectively[75]. According to our assumption on the fault production, the crust is considered to be in a strained state before the fault appears; so that we have to consider the effect of such initial strains to carry out a complete estimation of the strain energy. However, in the present step, we ignore the effect coming from them and study the most predominant feature of the energy process.

From (66) and (67) we obtain the stress component to be caused by the fault in such a way as,

$$\left.\begin{aligned} &\frac{\partial v}{\partial x} = -\sum_n \frac{F_n}{\mu} e^{-nx} \cos nz \,, \quad \frac{\partial v}{\partial z} = -\sum_n \frac{F_n}{\mu} e^{-nx} \sin nz \,, \\ &\frac{\partial u}{\partial x} = \frac{\partial u}{\partial y} = \frac{\partial u}{\partial z} = \frac{\partial v}{\partial y} = \frac{\partial w}{\partial x} = \frac{\partial w}{\partial y} = \frac{\partial w}{\partial z} = 0 \,. \end{aligned}\right\} \tag{71}$$

Therefore (70) becomes,

$$\begin{aligned} E &= \int_0^\infty dx \int_{-L}^{L} dy \int_0^h \mu\left\{\left(\frac{\partial v}{\partial x}\right)^2 + \left(\frac{\partial v}{\partial z}\right)^2\right\} dz \\ &= \int_0^\infty dx \int_{-L}^{L} dy \int_0^h \mu\left\{\left(\sum_n \frac{F_n}{\mu} e^{-nx} \cos nz\right)^2 + \left(\sum_n \frac{F_n}{\mu} e^{-nx} \sin nz\right)^2\right\} dz \,, \end{aligned} \tag{72}$$

where, h and L denote, respectively, effective values of the depth and the length of the space, in which occur the deformations. From the or-

75) A. E. H. LOVE, *The Mathematical Theory of Elasticity*, 4th ed. (1927), p. 102.

thogonality of Fourier series we obtain,

$$E=\frac{\mu}{4k}\int_0^{\infty}dx'\int_{-kL}^{kL}dy'\int_0^{2\pi}\left\{\sum_n\left(\frac{F_n}{\mu}\right)^2 e^{-2nz'}(\cos^2 nz'+\sin^2 nz')\right\}dz' , \tag{73}$$

where, we take the variables being transformed in the following way,

$$\frac{2\pi}{12H}=k , \quad kx=x' , \quad ky=y' , \quad kz=z' . \tag{74}$$

(73) becomes, then,

$$E=\frac{\pi}{2}\mu L\sum_n n\left(\frac{F_n}{\mu n}\right)^2 . \tag{75}$$

Putting numerical values in (75), we can estimate the change of strain energy. Numerical calculation was made for the cases of the Gômura fault and the Tanna fault (for the San Andreas fault, however, the energy has not been calculated, because the writer is not confident in regarding all the extent of such a long fault as homogeneous). In

Table IX.

Fault	Gômura	Tanna	San Andreas
$2L$	30 km	15 km	(400 km)
H	15 km	8 km	6 km
$(v)_{x=z=0}$	150 cm	200 cm	250 cm
$(X_y)_{x=z=0}$	3×10^7 c.g.s.	8×10^7 c.g.s.	—
E_{fault}	4×10^{22} 〃	3×10^{22} 〃	—
$E_{\text{seis.}}$	10^{23} 〃	4×10^{22} 〃	—

(μ was taken as 5×10^{11} c.g.s.).

Table IX are shown the conditions of calculation, in which H and $(v)_{x=z=0}$ are estimated from the distribution curves in Figs. 35~37, while L is assumed from the distribution of aftershocks as well as of crustal deformations reported for the respective cases. When $(v)_{x=z=0}$ is known, F_n is deduced from (66) and (68), so that we obtain $(X_z)_{x=z=0}$ and E, respectively, with the aid of (67) and (75).

We compare the strain energy E_{fault} with the energy of seismic waves $E_{\text{seis.}}$ to see that the two quantities are approximately of the same order, with each other. It must be remarked here that the

present estimation of the strain energy was made on an extremely simplified model, in which no account has been taken of other kinds of strains, such as vertical displacements, dilatations, *et al.* If we could take all the factors into consideration, the total amount of energy change would be two or three times larger than the present values.

In the last part of this section, we shall give a short description of the location of the seismic origin. According to seismological observations which concern the Tango and the North-Izu earthquakes,[76][77] the depths of origins are given as 14 km, and less than several kilometres respectively. The values are much the same as the estimated depths of faults, in the respective cases; therefore, reflecting the above-mentioned coincidence as well as the observational facts that the epicentres were determined exactly on the fault lines, we might be able to arrive at an important conclusion that the earthquakes concerned had occurred at the points in the crust, which corresponded to the bottom of the fault planes estimated from observational results of crustal deformations. The problem being of essential bearing on earthquake occurrence, we shall study it in a later chapter.

6. A lateral fault of finite length (model experiments).

We have dealt, in the foregoing sections, with the outstanding features of crustal deformations which will be caused by a simplified model of a fault of infinite length. Such an assumption has been accepted as the first approximation. For applying it to actual analyses, however, an examination should be made upon the accuracy of applying the above-mentioned model to actual faults of finite length.

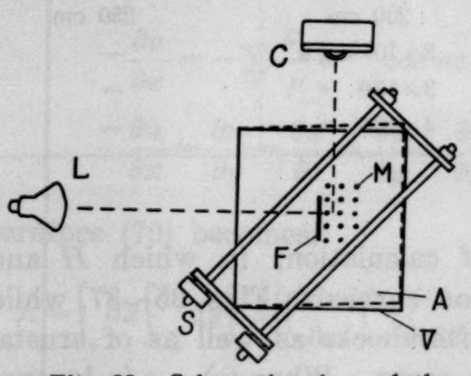

Fig. 38. Schematic view of the laboratory set. V: aluminum frame, A: block of agar-agar, S: screws, M: steel balls, L: lamp, F: cutting as a model of fault, C: camera.

It is not easy to study the problem theoretically, even though it might not be impossible; so we are going to investigate the improved model by means of model experiments. The schematic view of the laboratory set is shown in Fig. 38, where V is

76) S. KUNITOMI, *Kenshin-jihô*, **3** (1927–28), 77 (in Japanese).
77) Seismological Division, C.M.O., *ditto*, **4** (1930–31), 279 (in Japanese).

an aluminum frame (40×40×10 cm) in which is placed the medium of agar-agar solution A.[78] The frame can be deformed with screws S so as to let the medium be subject to uniform stress. On the surface of the medium numbers of steel balls M (1 mm in diameter) are distributed being illuminated brightly with a lamp L. In such a case we observe on the surface of each ball an image of the lamp, which is so fine that the displacement of each ball can be detected accurately from examination of photo records with a comparater. Figs. 39 and 40 show enlarged pictures of the records. The stress-strain relation in

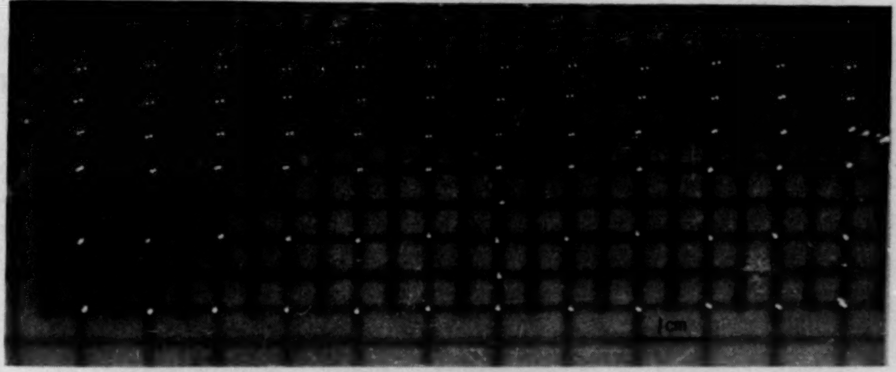

Fig. 39. Horizontal displacements (no cutting).

Fig. 40. Horizontal displacement caused by a cutting (length: 8 cm, depth: 4 cm).

the present medium is linear up to the strain being as large as 10^{-2} or more, so that all the experiments were made so as not to exceed the limit. Another consideration which is necessary for obtaining good results is to make the experiment as quickly as possible in order to avoid a trouble which might be caused by the viscous properties of the medium.

Observations were made with the medium, subject to the initial stress,

78) K. KASAHARA, *Bull. Earthq. Res. Inst.*, **30** (1952), 259.

by applying different conditions of cutting as the model of a fault.[79] An example of the observational results is illustrated in Fig. 41 which corresponds to the fault being 8 cm long and 4 cm deep. We first examine the relation of horizontal displacements *versus* distances from the fault, with respect to the features in the central part of the patterns. The distribution curves of displacements (v_0) with distance are drawn in Figs. 42 (b, c, d) which correspond, respectively, to the lengths of 4 cm, 8 cm, and 40 cm (the depth of the cutting was 4 cm for all the cases). The last case of the above-mentioned three can be regarded as practically equivalent with the fault of infinite length, and the curve shows, in fact, quite a similar feature with the theoretical one (Fig. 31) provided we take the depth as 4 cm. Such a result of good agreement is the evidence for the technique being accurate enough for the present purpose. The decay curve (c) of displacements seems to be similar to (d), whilst the curve (b) is slightly different from the above two. From the consideration that the length of the cutting is the least of the three, the difference is attributed to the influence of the fault's dimension. The difference is, however, so slight that it can be

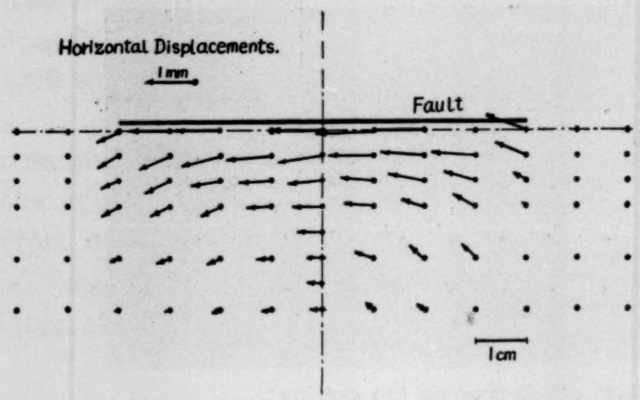

Fig. 41. Horizontal displacements caused by a cutting (length: 8 cm, depth: 4 cm).

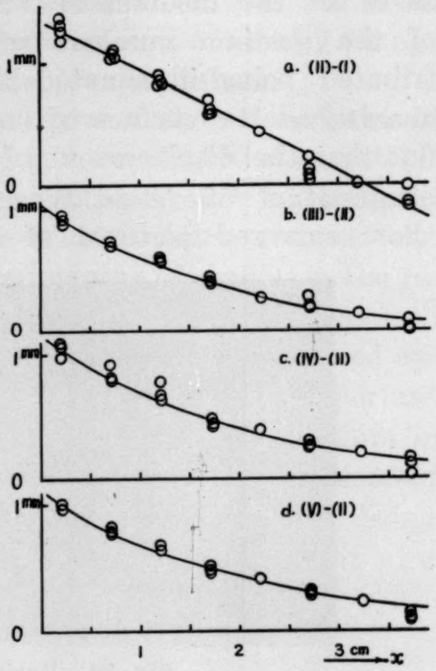

Fig. 42. Diminution of horizontal displacements with distance. (I): No stress, (II): uniform shear stress, (III): cutting (length: 4 cm, depth: 4 cm), (IV): cutting (length: 8 cm, depth: 4 cm), (V) cutting (length: 40 cm, depth: 4 cm).

79) Observations were made only for horizontal displacements, so that the following discussion is not developed about deformations in vertical direction in spite of their importance.

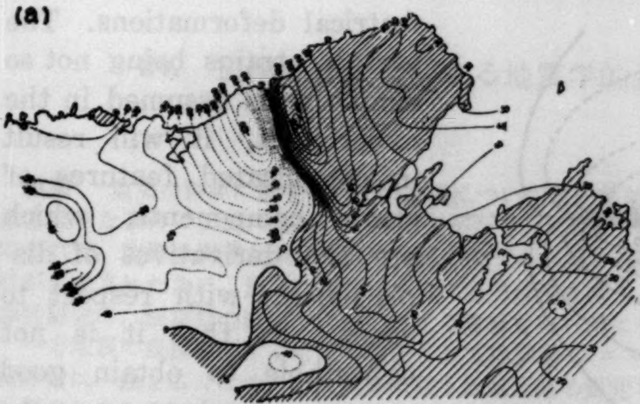

Fig. 43a. Lines of equal northward displacements (after C. Tsuboi).

Fig. 43b. Lines of equal dilatation (after C. Tsuboi).

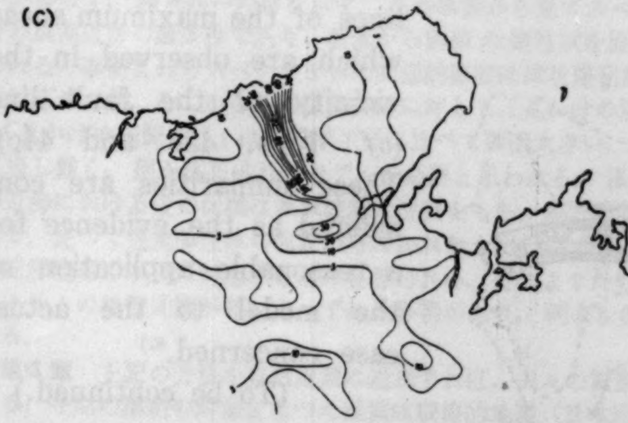

Fig. 43c. Lines of equal maximum shear (after C. Tsuboi).

detected only by careful comparison, and so long as we are concerned with the fault being not extremely shorter than its depth, we do not suffer from any fatal mistake in applying the model of infinite length to the actual case.

We remember that the proposed model has been justified only from the comparison of distribution of v_0 in the central part of the faults. In the last part of this section, we shall try another examination. When the surface's deformation is known with respect to x and y coordinates, several kinds of strain components can be deduced from the data.[80] According to C. Tsuboi's analysis, the earth's strains associated with the Tango earthquake are as shown in Figs. 43 a~c, whereas the deformations due to the model fault of 8 cm length and 4 cm depth (*cf.* Fig. 41) are also analysed to get corresponding strains. The results are drawn in Figs. 44 a~c (in relative scale), where the patterns for the area lying on the opposite side of the cutting were assumed from the condition of sym-

80) C. TSUBOI, *loc. cit.*, 6), p. 214. The Gômura fault was sinistral, whereas the present model shows a dextal fault. This difference should be taken into consideration in the following comparison.

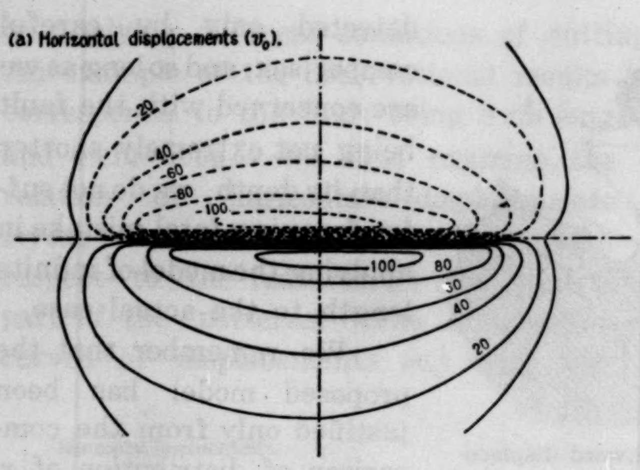

Fig. 44a.

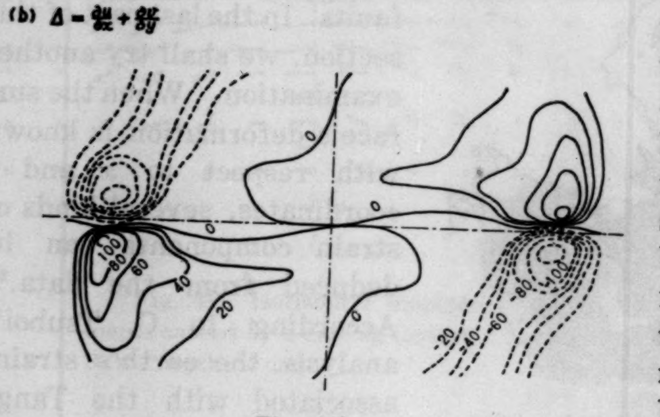

Fig. 44b.

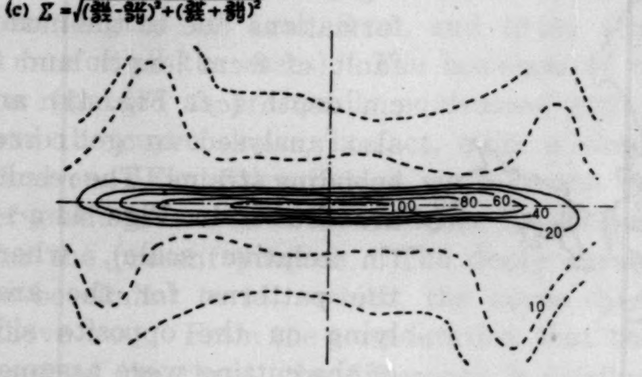

Fig. 44c.

metrical deformations. The earth's strains being not so simple as is assumed in the experiment, it will result in complicated features of strain components, which are the derivatives of displacements with respect to space. So that it is not expectable to obtain good agreements between the actual deformations and the model to their detailed features of distribution, however, we still observe some notable similarity between Tsuboi's figures and the present ones, such as, systematic distributions of positive and negative vortices of dilatations located at the extremities of the fault (*cf.* Figs. 43b and 44b), and the concentrated equi-value lines of the maximum shear which are observed in the vicinity of the fault line (*cf.* Figs. 43c and 44c). These similarities are considered as the evidence for a reasonable application of the model to the actual case concerned.[81)]

(To be continued.)

81) Poisson's ratio of the model is about 0.4, which is far larger than that of the ordinary rock. This difference will not result, however, in essential alteration of the conclusion, provided it concerns only qualitative discussion.

24. 震源の性状に関する地震学的及び測地学的研究 (一)

地震研究所 笠 原 慶 一

緒論. 地震の震源に関する研究の進展について歴史的に考察を行つた. 初期の段階においては, 最も簡単な条件の震源に基づいて諸研究がなされていたが, その後理論及び観測両面が充実されるにつれて, 次第に複雑な条件をもつ震源のモデルが用いられるようになつた. 即ち初動分布の規則性が発見された為に, 震源に作用する力にも方位性を考える必要が生まれ, 又球状震源に関する理論的研究は, 地震動の波形や周期の有する意義を明らかにした.

一方地震の規模に関する研究の成果として地震動のエネルギーを推定することが可能となり, 研究分野は一段と広くなつた. 大地震に伴う地殻変動の研究も進められ, 地殻の物理的な性状が明らかにされると共に, 地殻の一部に貯えられる弾性エネルギーが, 地震そのもののエネルギー源となる可能性も見出された.

現在これらの知識を基礎にして, 地震現象の機構に関する仮説がたてられているわけであるが, 波動論的立場から採用されている球状震源のモデルと測地学的見地から提起されているモデルとを調和させようとする研究は余り見うけられないように思われるので, 本研究の主な目的もこの点に置かれている.

第1章 地震動, 特にその初動部の波形は, 震源の性状に関する情報源として有用であるが, それを取りあつかう適当な手段がないために広範囲にわたる解析は行われなかつた.

本章においては, 原記象の波形に一つの重価函数を乗じ, その結果得られる孤立波形を初動波形の代用としてスペクトル解析する方法を提出した. このようにして得られるスペクトラムの物理的意味を考察すると共に, 地震計その他の特性を補正する方法を実例と共に示した.

更に地震波動の伝播過程においてそのスペクトル構造に変化をもたらす恐れのある2, 3の因子について, その影響の程度を簡単に調べてある.

第2章 火薬爆発による地震動発生の機構は自然地震のそれよりも簡単ではあるが, 自然地震の震源を取り扱う予備段階としても, 又地震探査技術の基礎的問題としても重要な研究対象である. そのような見地から, いろいろな薬量の爆発実験の際に得られた震動波形を解析した.

大局的に見れば, スペクトラムの最大強度に対応する周期 (特性周期) は薬量と共に増大する. 個々のスペクトラムを比較して見ると, 同一震源によるもの相互間では観測点までの距離の多少にかかわらず, 略々同一の形を示す. この事実から見てスペクトラムの形の決定に参与するのはおおむね震源近傍の諸条件であり, 前者から震源の諸性状を直接的に推定することが許されるものと思われる. 事実これらスペクトラムの共通的様相は球状爆発震源のモデルから期待されるものと容易に対応がつき, そこから各回爆発実験に対して「見かけの震源半径」が推定される.

「見かけの震源半径」は破砕域半径に比べて数倍大きい. これだけの差は実験・測定の誤差にのみは帰し難く, 何か修正されたモデルが必要と思われる. 爆発によつて生じた圧力が強大な為に, 震源近傍における歪の伝播は衝撃波的な性質をもち, ある距離において始めて弾性波的性質を示すに到る. 従つて完全弾性体の仮定から導かれた上記「見かけの震源半径」は破砕平径よりはむしろこの転移境界の半径に対応するものと思われる. それより外側においても岩石の粘弾性によつてスペクトラムの特性周期が長い方へずれる影響があり, 両者を併せ考えれば上記のくいちがいは理解される.

第3章 上記の方法を自然地震に適用すれば, 夫々の震源の大きさを近似的に推定することができる. 今回の解析の対象となつた地震は破壊的地震 (日本地域及び遠地) 並びに相当規模の大きい深発地震であり, 問題の性質上, 本郷における長週期地震計の記象を採用した.

各スペクトラムから直接読み取られる特性周期は地震の規模と共に増大する傾向がある. 球状震源のモデル (象限型) から期待される初動のスペクトル構造と上記解析結果とを比較することにより "見かけの震源の大きさ" が求められるが, その結果及び験震学的に推定される地震動のエネルギーを組み合わせて, 震源域におけるエネルギー集積の密度を計算した.

別の方面の研究から地殻内に集積する弾性エネルギー密度の上限として $3\times10^3 \sim 2\times10^4$ c.g.s. 程

度の値が結論されているが，本章で扱われた地震について見ると密度の分布範囲は $3\times10^2\sim3\times10^4$ c.g.s. であり上記の値と一致する．しかもこの分布範囲は規模の大小に無関係のように見られ，又破壊的地震と深発地震との間にも著るしい相違が見られない事実は特筆に値する．

第4章 大地震に伴う地殼変動の様相は，地震の発生機構に関する重要な情報を含んでいるものと予想される．日本地域の資料に関する概観的な調査によると地殼変動を伴つた地震はその規模がある限界値以上のものであり，その限界値は浅い地震に対しては比較的低く，震源の深いものについてはやや高い値をとるものと思われる．これらのうちある一群の地震は，特徴として震源が比較的浅く，初動分布は象限型を呈し，しかも地殼変動（断層の認められる場合が多い）の分布型は初動分布の特性と密接な関係があるように見うけられる．

このような特性をもつ地震の代表例，丹後地震その他について，解析を進めた．着目する現象のモデルとして，一様な shear 歪力の下にある半無限弾性体の表面から一定の深さまで，無限に長い断層が発生したと考える．その結果生起される弾性体の表面及び内部の変形を求めた．

表面の変形は断層に平行な水平変位で現わされるが，その変位量は断層から遠い地点程小さくなる傾向があり，実際に丹後・北伊豆・カリフォルニヤ地震の際観測された変動の様相とよく一致する．これから実際の断層の深さを推定して見ると，前記三例につきそれぞれ 15，8，6 km の値が得られた．又，われわれのモデルからは，断層をはさむ両側の相対的変位は深さと共に減少するものと予想されるが，北伊豆地震に際して丹那トンネル内で観測された変動量は地表におけるよりもやや小さく，上記の予想とも矛盾していない．

験震学的に求められた丹後・北伊豆地震の震源が上記のようにして推定される断層の底部に位置することになることは，地震の機構を考える上に極めて興味深いものがある．両者の場合について断層形成に伴う歪エネルギーを概算して見るとそれぞれ 4×10^{22} c.g.s.，3×10^{22} c.g.s. となり地震動から推定されているエネルギーと略々同等であることも判つた．

更に断層の長さが有限な場合については模型実験的手法により考察を行つた．この場合は shear の他に各種の歪成分が地表に現われるが，その断層周辺における分布は丹後地震の場合に観測された結果と類似している．又断層の長さが深さに比べて極端に短くない限り，その中央部の地表に見られる水平変動の分布は無限長断層の場合と大差ないことが判つた．（未完）

25. *Studies of Microseisms by Observations.*

By Fuyuhiko KISHINOUYE,
Earthquake Research Institute.

(Read Oct. 25, 1955 and April 24, 1956.—Received June 30, 1957.)

The period of microseisms is nearly equal everywhere in the world, and many investigations have been made, and many theories published of the origin of microseisms. But the mode of microseisms is found to be different at each place of observation, and the properties of microseisms are not known completely at present. The aim of this paper is to describe the results of various studies as materials for the theory of microseisms.

Microseisms observed at Hongo, Tokyo compared with Variations of Meteorological conditions

Microseisms were recorded every day on the first floor of the Earthquake Research Institute during the period from November 1952 till 1955, to study the annual variation of microseisms.

The observations were carried out once a day for two minutes at 11 h–12 h J. S. T., but when microseisms were large they were recorded two minutes at many times in a day.

The recording instruments used were portable mechano-optical seismographs[1] of horizontal and of vertical component. The magnification of the seismographs was usually 2000, but when microseisms became large it changed to 1000. The free-vibration period of the horizontal seismograph was set at 10 sec., and that of the vertical at 7–8 sec. At most times of recording, only the N–S component was recorded, and when amplitudes became large two horizontal components were observed, or moreover, the vertical component was added to the observation. The time marks were made at every second with an electromagnetic shutter controlled by an electric-contact clock interrupting lamp light in short time. The time marks of seismograms are important for identifying the corresponding times on records of different components or on

1) F. KISHINOUYE, *Bull. Earthq. Res. Inst.*, **20** (1942), 215–219.

records at different places.

How to express microseismic movements by numerical values is a difficulty because of their irregular variations of periods and of amplitudes. Mostly the maximum double amplitude and its period were measured to represent the condition of microseisms at the observation.

The correlations between observed amplitude and period of microseisms and meteorological conditions were studied of data at the Stations Tomisaki, Cyoshi and Onahama during the observation period. A part of the data of the investigation is shown in diagrams (Fig. 1). The variation

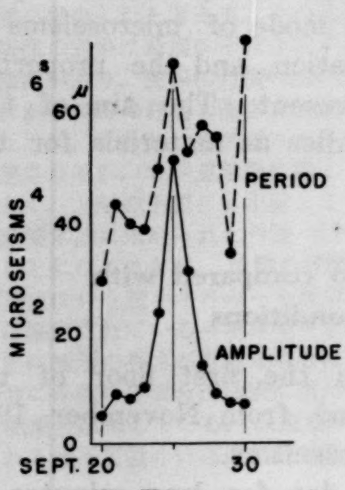

Fig. 1-a.

Fig. 1-c. Positions of the Meteorological Stations.

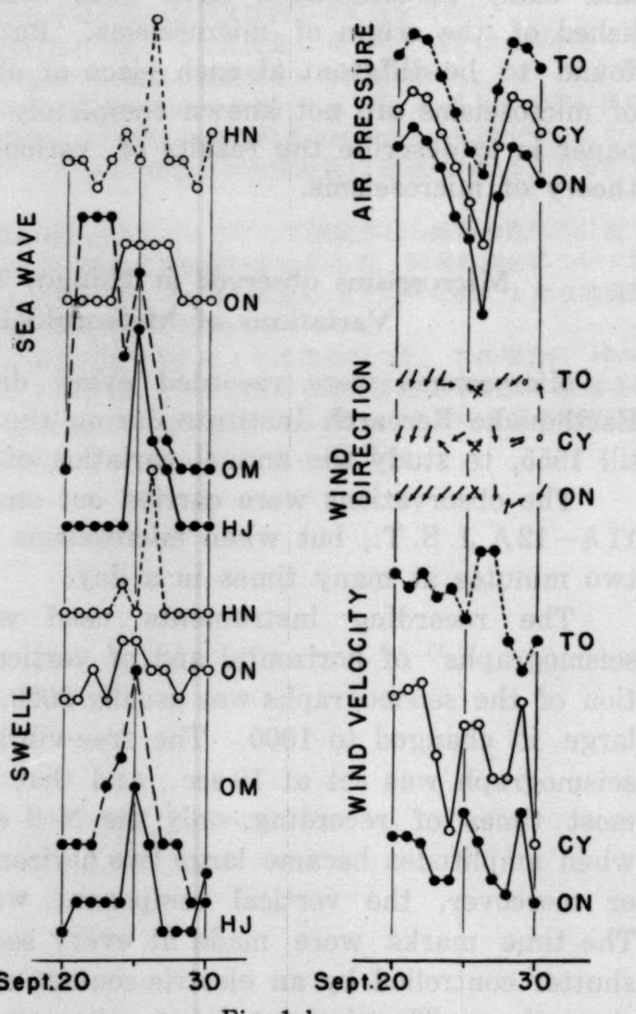

Fig. 1-b.
(The name of stations is shorten)

of microseisms was compared also with conditions of sea waves generated by wind or of swells observed at Hachijōjima, Onahama and Cyoshi.

The correlations between microseisms and the above data were found to be sometimes close and at other times not. And although the number of data was large no definite result could be obtained.

The Annual Variation of Microseisms at Hongo, Tokyo

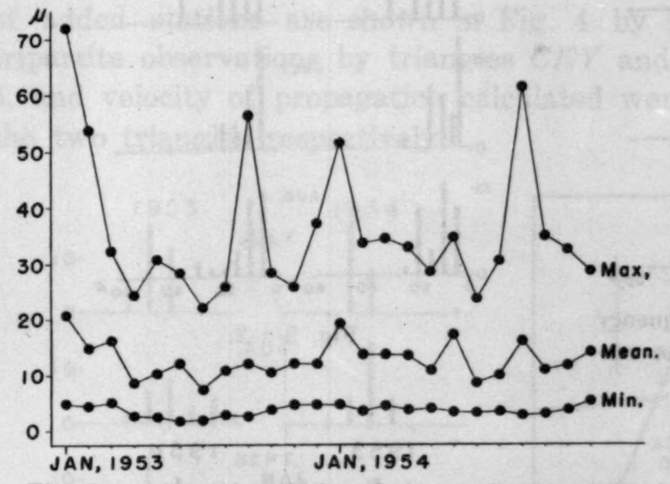

Fig. 2–a. Annual variation of the maximum amplitude in a day, (Maximum, mean and minimum values in a month of the maximum double amplitudes of each day.)

Monthly mean, maximum and minimum of period and those of double amplitude were taken from the data obtained every day in the period 1953 and 1954. The results are shown in Fig. 2 and following characteristics of microseisms were deduced: Microseisms are small in spring and large during later autumn and early winter, except in summer microseisms become very large when a typhoon passes on the sea along the eastern coast of northern Japan.

The frequency distribution of maximum amplitudes and that of periods of microseisms in every month were obtained and shown in Fig. 3.

Frequency distribution of periods at the maximum amplitude was sharp at the period 3–4 sec.

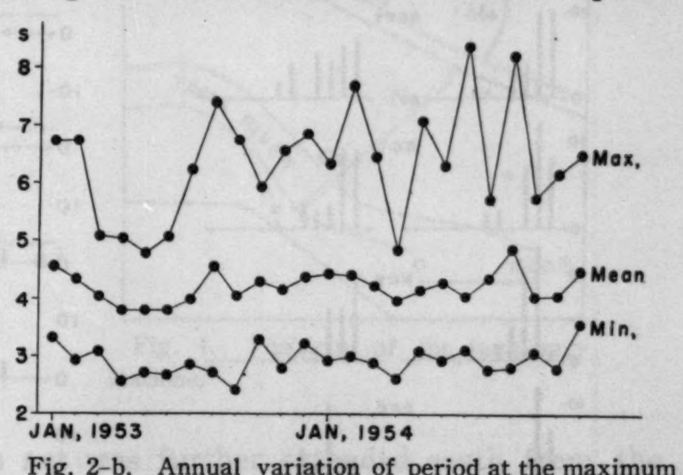

Fig. 2–b. Annual variation of period at the maximum amplitude.

Comparative Observations of Microseisms at Near Places

The results of the tripartite observations in the yard of the Tokyo Astronomical Observatory at Mitaka, Tokyo, have already been reported

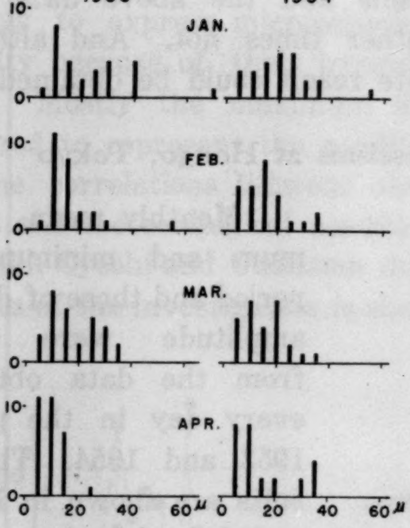

Fig. 3-a-1. Monthly frequency distribution of the maximum amplitude.

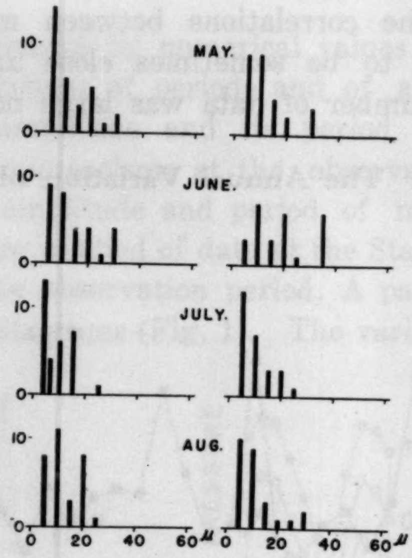

Fig. 3-a-2.

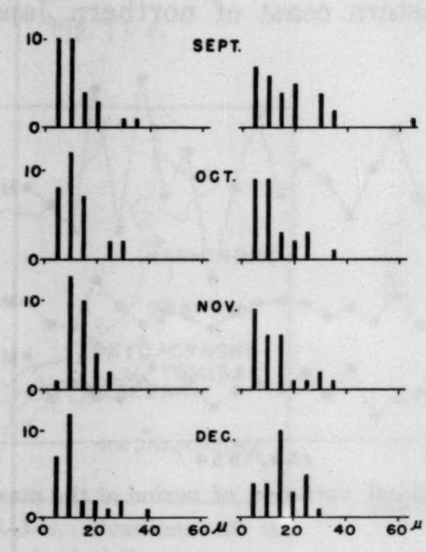

Fig. 3-a-3.

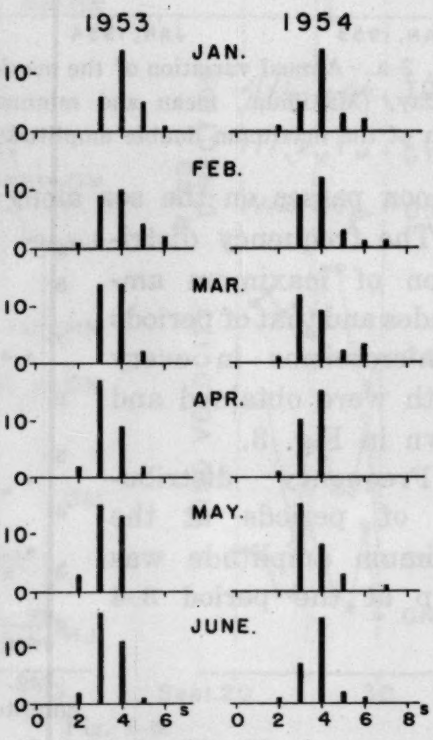

Fig. 3-b-1. Monthly frequency distribution of period at the Maximum amplitude.

in several papers. The observations were mostly at four places simultaneously to make two tripartite observations at the same time taking three stations from the four. The direction and velocity of propagation of microseisms obtained from the two tripartite stations were in accord with each other as mentioned before[2].

The observation net was extended out of the yard. The positions of added stations are shown in Fig. 4 by alphabets. The results of tripartite observations by triangles *CEY* and *CRY* are as shown in Fig. 5, and velocity of propagation calculated were 348 and 267 in m/s for the two triangles respectively.

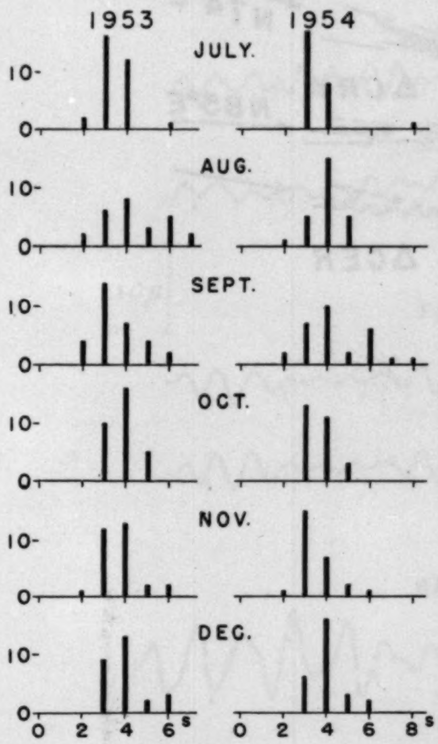

Fig. 3-b-2.

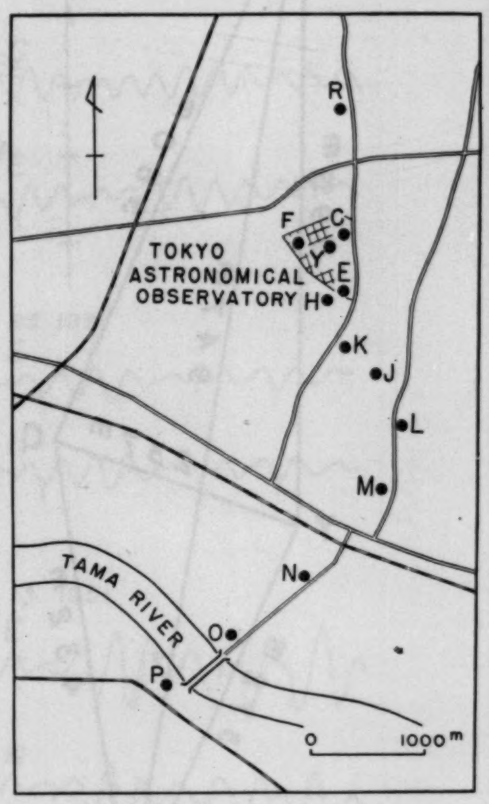

Fig. 4. Positions of the temporary stations.

In 1951 the observation net was further extended south from the observatory. Simultaneous observations at three stations were difficult, so in most cases the observations for comparison were carried out at two stations for each observation. The simultaneous record at various places are shown in Figs. 6-a, 6-b. The earth movements at the cor-

2) R. IKEGAMI and F. KISHINOUYE, *Bull. Earthq. Res. Inst.*, **29** (1951), 305-312.

responding places resemble each other closely, except between stations N and P. Then cross-correlation functions were calculated of the records at N and P. (Fig. 7).

In the investigation of microseisms, methods of harmonic analysis have been applied. Recently correlogram analysis was developed, and it was taken also in this study.

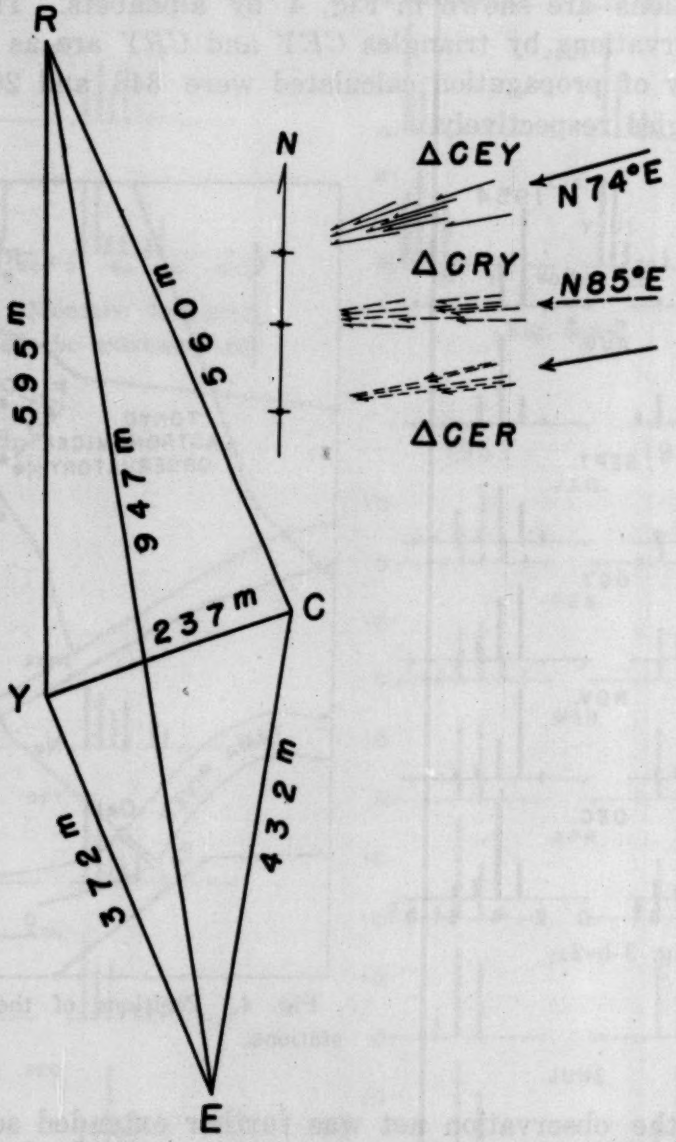

Fig. 5. Comparison of simultaneous tripartite observations.

Readings of amplitudes were made every second on the record, which was 2 minute observation, and then the values of readings were put in the mathematical expressions below. (Sometimes one half-second reading was made to check the results of the one-second readings.)

Functions of cross-correlation or autocorrelation were respectively calculated by the formulae,

$$\varphi' = \frac{1}{N} \sum_{k=1}^{N} \bar{x}_{k+j} \bar{y}_k$$

and

$$\varphi = \frac{1}{N} \sum_{k=1}^{N} \bar{x}_{k+j} \bar{x}_k .$$

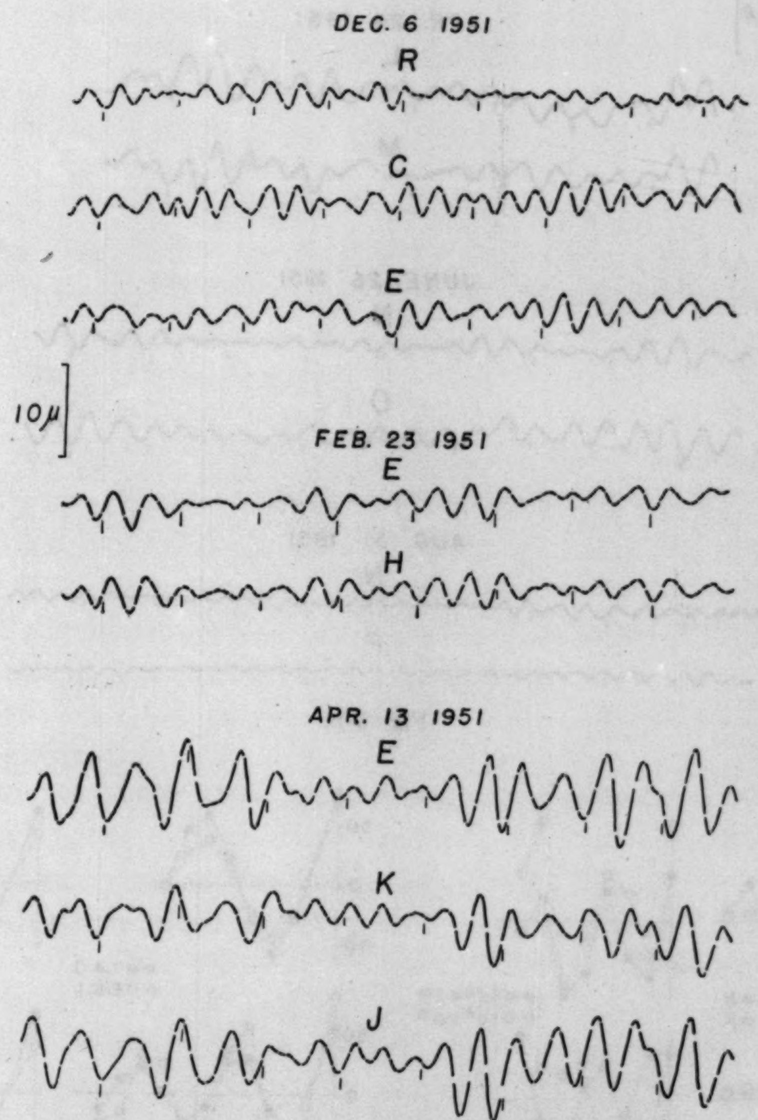

Fig. 6-a. Simultaneous observations at station on sets.

Autocorrelations between simultaneous microseisms at the Earthquake Research Institute (E.R.I.) and the Tokyo Astronomical Observatory (T.A.O.), or the Mitaka Branch of the Transportation Technical Research Insti-

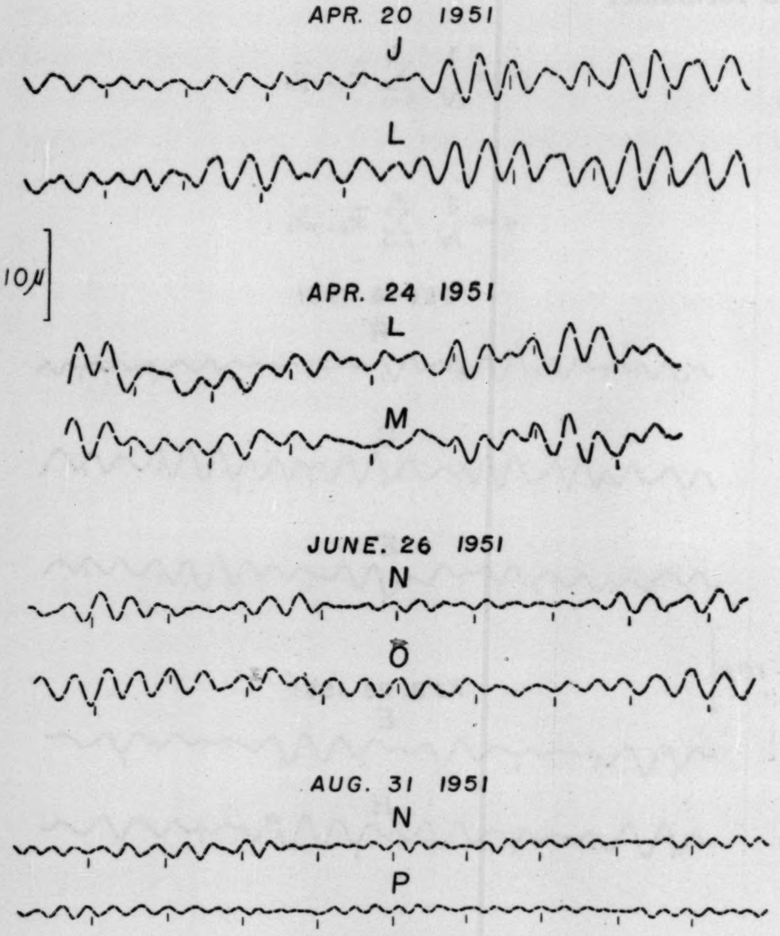

Fig. 6–b.

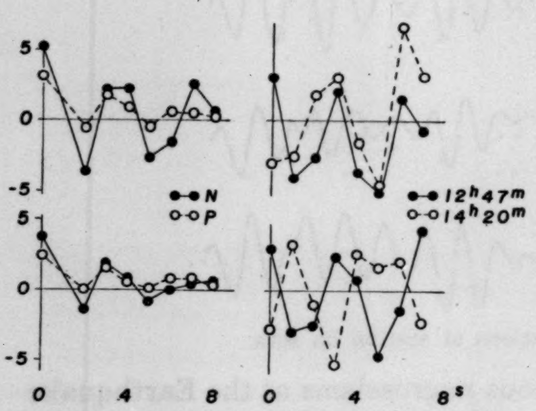

Fig. 7. Autocorrelation and cross correlation of microseisms at stations *N* and *P*.

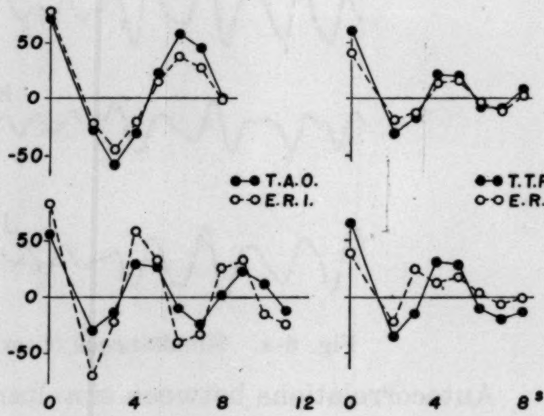

Fig. 8. Autocorrelation of microseisms simultaneous at different places.

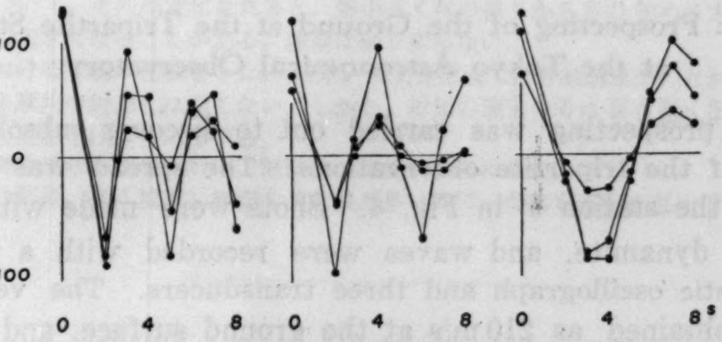

Fig. 9. Autocorrelation of microseisms at E. R. I.

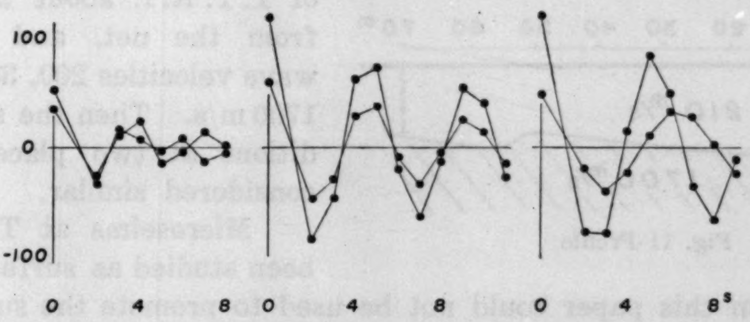

Fig. 10. Autocorrelation of microseisms at T.A.O.

tute (T.T.R.I.) were obtained. The results are shown in Fig. 8. Microseisms at the same time at these places may be equal in period.

Autocorrelation functions of microseisms at E. R. I. and T. A. O. were calculated more to know the period of microseisms there precisely (Figs. 9 and 10).

From the results, all stations from *R* southward to *O* (distance about 6 km.) may be on a block of the ground, because microseisms at those stations closely resemble. But the station beyond the River Tama moved differently from the northern side of the river. The writer was reminded of his old paper on microseisms[3] in which he supposed as land block vibrations. This consideration may have weak points in that the observations were small in number and did not include all types of microseisms there, moreover the analysed amplitudes were comparatively small, in other words "signal to noise ratio" was small, so it may be not sufficient to conclude different movement of the opposite side of the river.

---

3) F. KISHINOUYE, *Bull. Earthq. Res. Inst.*, **13** (1935), 146–154.

Seismic Prospecting of the Ground at the Tripartite Stations at the Tokyo Astronomical Observatory

Seismic prospecting was carried out to discover subsoil conditions of the net of the tripartite observations. The spread was set 70 m in North from the station Y in Fig, 4. Shots were made with less than 90 grams of dynamite, and waves were recorded with a five element electromagnetic oscillograph and three transducers. The velocity of P wave was obtained as 210 m/s at the ground surface, and 1700 m/s in the under layer. The profile of the ground deduced is shown in Fig. 11. Mr. E. Shima[4] studied the subsoil of the yard of the Mitaka Branch of T. T. R. I. about 2.5 km east from the net, and found the wave velocities 200, 300, 400 and 1700 m/s. Then the subsoil conditions at two places may be considered similar.

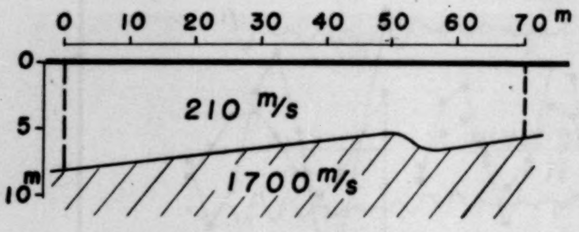

Fig. 11–Profile.

Microseims at T. A. O. had been studied as surface waves[5]. The result in this paper could not be used to promote the surface wave theory. Above studies concerning microseisms were aimed at making clear the properties of microseisms, however many questions still remain to be investigated. The writer will continue further the observational studies of microseisms.

Lastly the writer expresses his thanks to many persons who helped his studies at their desks or in field observations. Especially he thanks Mr. R. Ikegami and Miss M. Kotaka for their assistance in this investigation.

---

25. 観測による土地の脈動の研究

地震研究所 岸 上 冬 彦

土地の脈動の原因についての理論は，現在数種あつて決定的のものはない．そこで脈動について まだ多くの知られてない性質をもとめるために筆者の得た結果を研究材料として提出する．
本郷において観測した脈動と各地の気象海象と比べたが，相関のあう時とあわない時とがあつて 簡単な関係は見られなかつた．

---

4) E. SHIMA, Private communication. The prospecting described in this paper was made by the kind help of Mr. Shima, to whom the writer wishes to express his thanks.

5) R. IKEGAMI and F. KISHINOUYE, *Bull. Earthq. Res. Inst.*, **28** (1950), 118.

脈動の振幅について，その年変化を見ると，春小さく秋の終りから冬の 初めに大きい．但し夏には台風のある時に大きくなることがある．周期は余り変らない．

異なる場所における脈動の比較をした．結果，天文台附近では各観測点が，どれもよく似た 振動をしているが，多摩川の対岸とは似てない．しかし，対岸の測定の時は 都合悪く振幅が 小さかつたので，はつきりしたことは後日にゆずる．

天文台附近の弾性波地下探査を行い，脈動波の研究の参考にした．

これらの研究の結果，更に測定し観測すべき点が多いので，なおも研究を進めている．

Surface Prospecting of the [illegible] Station [illegible] Observatory

Surface prospecting was carried out in [illegible] at the end of the [illegible] from the [illegible] in Fig. [illegible] were made with less than [illegible] grams of dynamite, and waves were recorded with a five element electromagnetic oscillograph and [illegible]. The velocity of P wave was obtained as 210 m/s at the ground surface, and 1700 m/s in the under layer. The profile of the ground deduced is shown in Fig. 11. Mr. E. Shima[a] studied the subsoil of the yard of the Mitaka Branch of T.T.R.I. about 2.5 km east from the net, and found the wave velocities 200, 300, 400 and 1700 m/s. Then the subsoil conditions at two places may be considered similar.

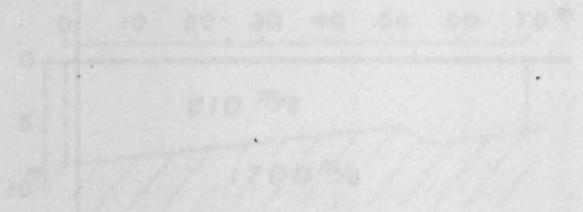

Fig. 11 Profile.

Microseisms at T.A.O. had been studied as surface waves[b]. The result in this paper could not be used to promote the surface wave theory. Above studies concerning microseisms were aimed at making clear the properties of microseisms, however many questions still remain to be investigated. The writer will continue further the observational studies of microseisms.

Lastly the writer expresses his thanks to many persons who helped his studies at their desks or in field observations. Especially he thanks Mr. N. Ikegami and Miss M. Kotaka for their assistance in this investigation.

[illegible]

[illegible]

a) E. Shima, Private communication. The prospecting described in this paper was made by the kind help of Mr. Shima to whom the writer wishes to express his thanks.

b) [illegible] and [illegible], *Bull. Earthq. Res. Inst.*, 28 (1950), [illegible].

26. *Vibration of a Building upon the Elastic Foundation.*

By Yasuo SATÔ and Rinzo YAMAGUCHI,
Earthquake Research Institute.

(Read Dec. 20, 1955 and Feb. 28, 1956.—Received June 29, 1957.)

1. Introduction

Today the oscillations of buildings are being very actively studied, and the problem of the effect of foundations is also being discussed. In these investigations, however, when the oscillations of buildings are discussed, the motion of the ground is assumed not to be affected by the buildings, while in the discussion of the foundation the existence of buildings are always neglected. It is evident, however, that such a method of investigation is not adequate. We must solve for the coupled motion of buildings and their foundations.

The calculation of such a coupled system is not easy, but fortunately I. Toriumi[1)] recently published an elaborate study, which makes it possible to obtain the result without special difficulty.

In this paper we utilize his result, consequently the assumptions adopted in his study are also assumed here: namely

1) Buildings are supposed to be circular cylinders.
2) In the problems of vertical and horizontal oscillations, the stress components are assumed to be constant within the circle of a base and vanish outside of it.
3) In the problem of rocking, the stress is proportional to x within the circle and zero outside.

We further assume, in the present paper, that the seismic waves come vertically upward and the ground motion is a pure vertical of horizontal one.

2. Notations

Notations in the paper of Toriumi are also adopted with only slight change, but many new ones are added, so all are given in this section.

1) I. TORIUMI, "Vibrations in Foundations of Machines", *Technology Reports of the Osaka University*, **5** (1955), 103.

I. TORIUMI, "Vibrations in Foundation of Machine on the Ground," *Journ. Seism. Soc., Japan*, [ii], **7** (1955), 216, (in Japanese).

A	$=2\mu\pi r_0/(f_{1H}+if_{2H})$. cf. (4.6).
A'	$=A/m_0 p^2$. cf. (4.17).
A_V, A_H	Amplitudes of incident waves vertical and horizontal respectively.
a_0	$=pr_0\sqrt{(\rho/\mu)}=pr_0/V_s=2\pi r_0/$(Wave length of S-waves).
$a_{0\text{MAX}}$	Value of a_0 that gives the maximum magnification.
B	$=(1/4)\mu\pi r_0^3/(f_{1R}+if_{2R})$. cf. (4.11).
B'	$=B/m_0 p^2 l_0^2$. cf. (4.17).
c	Magnification coefficient of a forced oscillation of a seismograph.
f_{1H}, f_{2H}	cf. (4.6). f_1 and f_2 in Toriumi's paper. (Horizontal motion)
f_{1R}, f_{2R}	cf. (4.11). id. (Rocking motion)
f_{1V}, f_{2V}	cf. (3.4). id. (Vertical motion)
h	Damping coefficient of a pendulum. $(=\varepsilon/n)$
h_{apparent}	Apparent damping coefficient of a building.
I_0	Moment of inertia of a building around its center of gravity.
k_0	Radius of gyration of a building.
l_0	Height of a building from its base to the center of gravity.
m_0	Mass of a building.
$\overline{M}_{z=0}$	Moment of a force.
n	Frequency of the free oscillation of a building.
p	Circular frequency of incident waves.
Q_H, Q_V	Horizontal and vertical force transmitted from a building to the ground.
r_0	Radius of a building.
S	$=m_0 p^2/2\pi\mu r_0$.
S_0	$=S/a_0^2=(\rho_0/\rho)\cdot(l_0/r_0)=(\rho_0/\rho)\cdot\beta$.
T_0	Period of the free oscillation of a building.
T_{MAX}	Period of the incident wave giving the maximum amplitude.
U_1	Displacement at the free surface. (Horizontal motion)
U_G	Displacement of the center of base. (Rocking motion)
U_D	Additional displacement of the center of the base caused by the existence of a building. (Horizontal motion)
U_H	Displacement of the center of gravity. (Horizontal motion)
U_R	Horizontal displacement of the center of gravity. (Rocking motion)
u	Ratio of the frequency of the free oscillation of a building and incident waves. $(=n/p)$
V_{MAX}	Maximum amplitude.

W	Displacement of the center of gravity. (Vertical motion)
W_1	Displacement of the free surface. (Vertical motion)
X	$=\mathfrak{B}_{UR}\cdot\exp(-i\vartheta_{UR})$.
Y	$=\mathfrak{B}_{\Gamma R}\cdot\exp(-i\vartheta_{\Gamma R})$.
Z	$=\mathfrak{B}_{H}\cdot\exp(-i\vartheta_{H})$.
α	$=k_0/l_0$.
β	$=l_0/r_0$.
Γ_R	Angle of inclination of a building. (Rocking motion)
γ	id. (Toriumi's notation)
ν	$=a_0(n/p)$. cf. (5.12)
λ, μ	Lamé's constants of the foundation.
ρ, ρ_0	Density of the foundation and building respectively.
ϑ_H, ϑ_V	Phase difference between the incident waves and the oscillation of the building. (Horizontal and vertical motion)
$\vartheta_{UR}, \vartheta_{\Gamma R}$	Phase difference between the incident waves and the horizontal or angular motion. (Rocking motion)
$\mathfrak{B}_H, \mathfrak{B}_V$	cf. (5.1) and (3.2).
$\mathfrak{B}_{UR}, \mathfrak{B}_{\Gamma R}$	cf. (4.2) and (4.3).

3. Vertical motion

First we consider the problem of vertical motion. Incident waves are assumed to be propagated vertically upward. The amplitude of the waves is A_V and the circular frequency is p. The method of solving this problem is briefly illustrated in Fig. 1.

The oscillation of the free surface would be, were it not for the building

$$W_1=2A_V\exp(ipt). \tag{3.1}$$

Displacement of the building caused by this wave is assumed to be

$$W=2A_V\exp(ipt)\cdot\mathfrak{B}_V\exp(-i\vartheta_V), \tag{3.2}$$

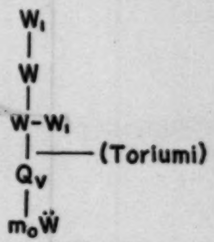

Fig. 1.

where $\mathfrak{B}_V$ and ϑ_V are both supposed to be real. Our present purpose is to obtain these two quantities as functions of material constants and of dimensions of the building.

An additional displacement caused by the existence of a building is

$$W-W_1=2A_V\exp(ipt)\cdot\{\mathfrak{B}_V\exp(-i\vartheta_V)-1\}. \tag{3.3}$$

According to Toriumi's theory, the relation between the vertical force

transmitted from the structure to the foundation and the vertical displacement of the center of the base is given by the following expression.

$$\text{force}^{2)}: \qquad -Q_V \exp(ipt)\,,$$

$$\text{displacement}: \qquad Q_V \exp(ipt)\cdot\{f_{1V}+if_{2V}\}/\mu\pi r_0. \qquad (3.4)$$

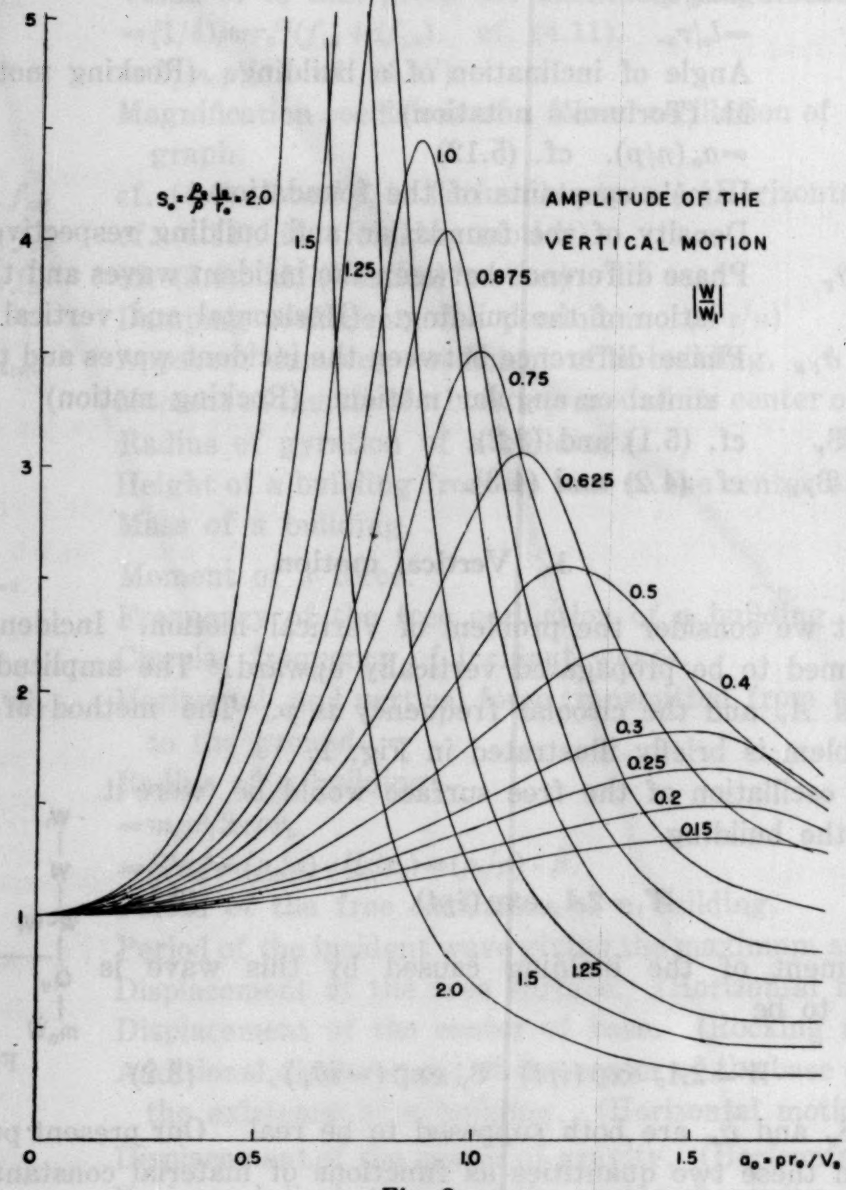

Fig. 2.

Therefore the force from the building to the foundation, corresponding to the displacement given in (3.3) is

2) His force is assumed to be plus when it acts toward the direction of $-z$.

$$-(W-W_1)\cdot\mu\pi r_0/\{f_{1V}+if_{2V}\}\ . \tag{3.5}$$

The force from the foundation to the building is

$$+(W-W_1)\cdot\mu\pi r_0/\{f_{1V}+if_{2V}\}$$
$$=2A_V\exp(ipt)\cdot\{\mathfrak{B}_V\exp(-i\vartheta_V)-1\}\cdot\mu\pi r_0/\{f_{1V}+if_{2V}\}\ . \tag{3.6}$$

This force makes the building with a mass m_0 have an acceleration $\ddot{W}$, therefore

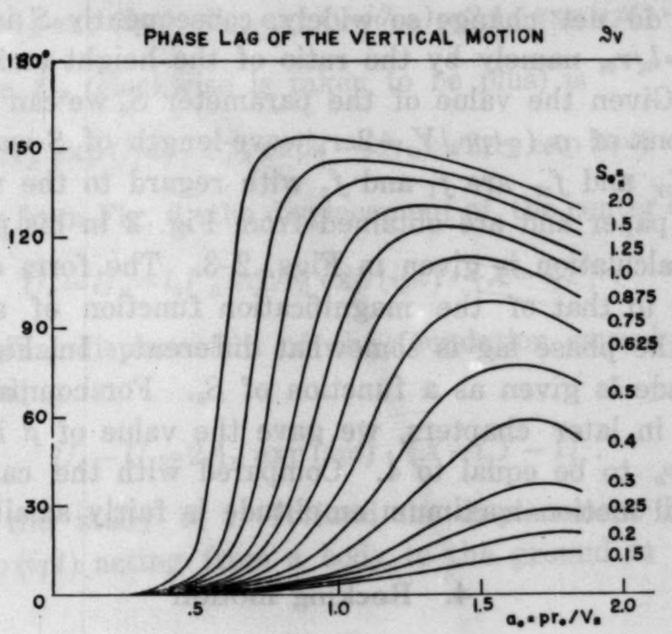

Fig. 3.

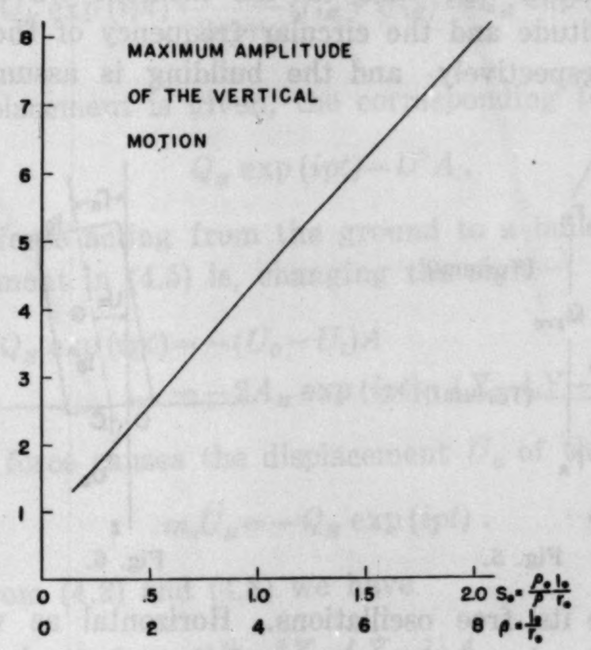

Fig. 4.

$$m\ddot{W}=m_0(-p^2)\cdot 2A_V \exp(ipt)\cdot \mathfrak{B}_V \exp(-i\vartheta_V) \tag{3.7}$$

must be equal to the expression given in (3.6).

$$\mathfrak{B}_V \exp(-i\vartheta_V)=1/[1+2S\{f_{1V}+if_{2V}\}], \tag{3.8}$$

where

$$S=m_0p^2/2\mu\pi r_0=a_0^2(\rho_0/\rho)\cdot(l_0/r_0)=a_0^2S_0\,.$$

ρ_0 and ρ do not change so widely, consequently S is chiefly determined by $\beta=l_0/r_0$, namely by the ratio of the height and the radius of a building. Given the value of the parameter S_0 we can express $\mathfrak{B}_V$ and ϑ_V as functions of $a_0\,(=pr_0/V_s=2\pi r_0/$wave-length of S-waves). In this expression, f_{1V} and f_{2V} are f_1 and f_2 with regard to the vertical motion in Toriumi's paper and are obtained from Fig. 2 in his paper. The result of our calculation is given in Figs. 2–3. The form of the curve of $\mathfrak{B}_V$ is similar to that of the magnification function of a seismograph, but that of the phase lag is somewhat different. In Fig. 4 the maximum amplitude is given as a function of S_0. For comparison with the result given in later chapters, we gave the value of β in the abscissa assuming ρ/ρ_0 to be equal to 4. Compared with the cases of rocking and horizontal motion maximum amplitude is fairly small.

4. Rocking motion

Next we consider the case of the incident waves being purely horizontal. Amplitude and the circular frequency of the incident wave are A_H and p respectively· and the building is assumed to be rigid

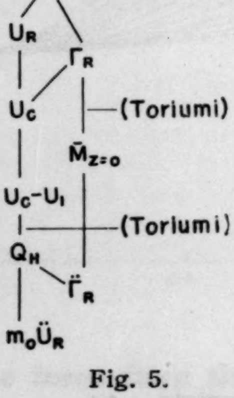

Fig. 5.

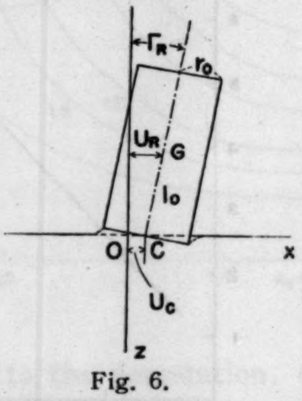

Fig. 6.

enough to ignore its free oscillations. Horizontal as well as rocking motion are considered and the scheme of the solution is given in Fig. 5.

If there were no building the oscillation at the free surface $z=0$ would be

$$U_1=2A_H \exp(ipt) . \quad (4.1)$$

Displacement of the building caused by the incidence of waves is (cf. Fig. 6)

$$U_R=2A_H \exp(ipt) \cdot \mathfrak{V}_{UR} \exp(-i\vartheta_{UR}) \equiv 2A_H \exp(ipt) \cdot X . \quad (4.2)$$

Deflection angle Γ_R (clockwise is taken to be plus) is

$$\Gamma_R=2A_H \exp(ipt) \cdot \mathfrak{V}_{\Gamma R} \exp(-i\vartheta_{\Gamma R}) \equiv 2A_H \exp(ipt) \cdot Y . \quad (4.3)$$

As is clear from Fig. 6, the displacement of the center of the base is

$$U_G=U_R-l_0\Gamma_R \equiv 2A_H \exp(ipt) \cdot \{X-l_0Y\} . \quad (4.4)$$

The additional displacement of the foundation caused by the existence of a building is

$$U_G-U_1=2A_H \exp(ipt) \cdot \{X-l_0Y-1\} . \quad (4.5)$$

According to the study of I. Toriumi the displacement U' caused by a force $Q_H \exp(ipt)$ acting from a body to the ground in the direction $+x$ is

$$U'=Q_H \exp(ipt) \cdot \frac{1}{2\pi\mu r_0}\{f_{1H}+if_{2H}\} \equiv Q_H \exp(ipt)/A . \quad (4.6)$$

If the displacement is given, the corresponding force is

$$Q_H \exp(ipt)=U'A . \quad (4.7)$$

Therefore the force acting from the ground to a building corresponding to the displacement in (4.5) is, changing the sign

$$\begin{aligned}-Q_H \exp(ipt) &= -(U_G-U_1)A \\ &= -2A_H \exp(ipt) \cdot \{X-l_0Y-1\} \cdot A . \quad (4.8)\end{aligned}$$

Since this force causes the displacement U_R of the center of gravity

$$m_0\ddot{U}_R=-Q_H \exp(ipt) . \quad (4.9)$$

Substituting from (4.2) and (4.8) we have

$$m_0p^2X=\{X-l_0Y-1\}A . \quad (4.10)$$

Next we will consider the rotational motion. We will quote again from the paper of I. Toriumi.

When the moment of the force acting from a building to the ground is given by $\bar{M}_{z=0}$ (Counter-clockwise is taken to be plus.) the angular deflection γ is

$$\gamma=\frac{4\bar{M}_{z=0}}{\pi r_0^3\mu}\exp(ipt)\cdot\{f_{1R}+if_{2R}\}\equiv\bar{M}_{z=0}\exp(ipt)/B\ . \tag{4.11}$$

This expression also gives the deflection when the moment of a force acting from the ground to a building is $\bar{M}_{z=0}$ (taking the clockwise direction plus).

If the deflection angle is given the moment of a force is

$$\bar{M}_{z=0}\exp(ipt)=\gamma B\ . \tag{4.12}$$

When the deflectional angle is expressed by Γ_R in the equation (4.3)

$$\bar{M}_{z=0}\exp(ipt)=\Gamma_R B=2A_H\exp(ipt)\cdot YB\ . \tag{4.13}$$

Then the moment of a horizontal force $-Q_H\exp(ipt)$ around the center of gravity G acting on the base of a building is

$$l_0Q_0\exp(ipt)=l_0 2A_H\exp(ipt)\cdot\{X-l_0Y-1\}A\ . \tag{4.14}$$

The angular motion Γ_R is caused by the moment expressed in (4.13) and (4.14), therefore we have

$$I_0\ddot{\Gamma}_R=\bar{M}_{z=0}\exp(ipt)+l_0Q_H\exp(ipt)\ . \tag{4.15}$$

Substituting from (4.3), (4.13) and (4.14)

$$-m_0k_0^2p^2Y=YB+l_0\{X-l_0Y-1\}A\ . \tag{4.16}$$

(4.10) and (4.16) are the simple linear equations of X and Y, so we can easily obtain the next solutions.

$$\left.\begin{aligned}l_0Y\equiv Y'&=-1\Big/\left\{\left(1-\frac{1}{A'}\right)(B'+\alpha^2)+1\right\}\\X&=(B'+\alpha^2)\Big/\left\{\left(1-\frac{1}{A'}\right)(B'+\alpha^2)+1\right\},\end{aligned}\right\} \tag{4.17}$$

where

$$A' \equiv A/m_0p^2 = 1/S(f_{1H} + if_{2H}) \,,$$
$$B' \equiv B/m_0p^2l_0^2 = 1/8\beta^2 S(f_{1R} + if_{2R}) \,,$$

and

$$\alpha^2 \equiv k_0^2/l_0^2 \,,$$
$$S = m_0p^2/2\pi\mu r_0 = a_0^2 S_0 = a_0^2 \frac{\rho_0}{\rho}\frac{l_0}{r_0} \,. \tag{4.18}$$

Introducing the relations (cf. (4.6) and (4.11).)

$$A = 2\pi\mu r_0 / \{f_{1H} + if_{2H}\} \,,$$

and

$$B = \pi\mu r_0^3 / 4\{f_{1R} + if_{2R}\} \,,$$

into the above expressions and somewhat modifying we have

$$Y' = 1 \Big/ \left[a_0^2 S_0 (f_{1H} + if_{2H})\alpha^2 + \left\{ -(1+\alpha^2) + \frac{1}{8\beta^2}\frac{f_{1H} + if_{2H}}{f_{1R} + if_{2R}} \right\} - \frac{1}{a_0^2}\frac{1}{8\beta^2 S_0 (f_{1R} + if_{2R})} \right] ,$$

$$X = -\left\{ \alpha^2 + \frac{1}{8\beta^2 a_0^2 S_0 (f_{1R} + if_{2R})} \right\} \Big/ \left[\qquad '' \qquad \right] . \tag{4.19}$$

Y' is, in a few words, a magnification coefficient of a building with regard to the rotational motion, and if the center of gravity remains unmoved

$$Y' = -1 \,. \tag{4.20}$$

X is the magnification with respect to the translation, and if the building moves with just the same motion as the foundation, the magnification proves to be

$$X = 1 \,. \tag{4.21}$$

The result of numerical calculations is given in Figs. 7–15.

Fig. 7 shows $\mathfrak{V}_{UR} = |U_R/U_1| = |X|$, namely the magnification of the displacement of the center of gravity. The parameter in this figure is $\beta = l_0/r_0$. In this calculation a simple relation $\rho_0/\rho = 1/4$ is assumed, since

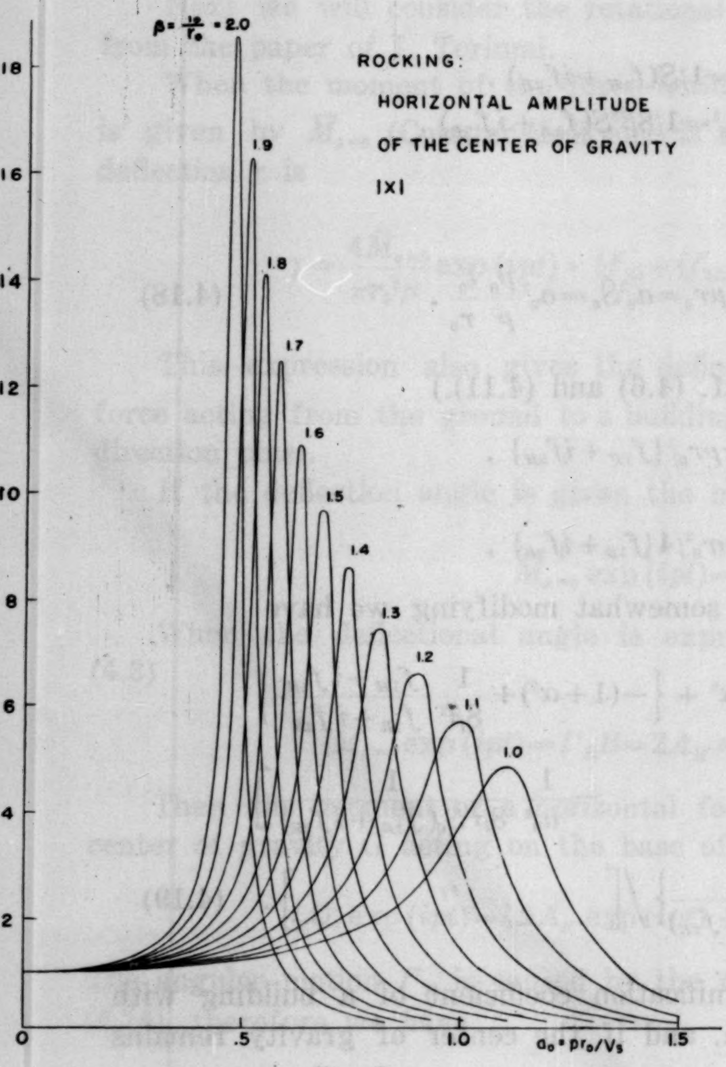

Fig. 7.

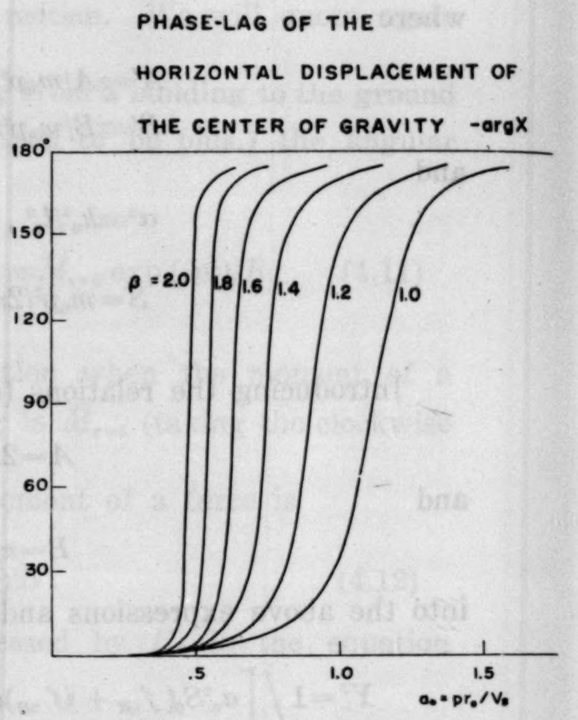

Fig. 8.

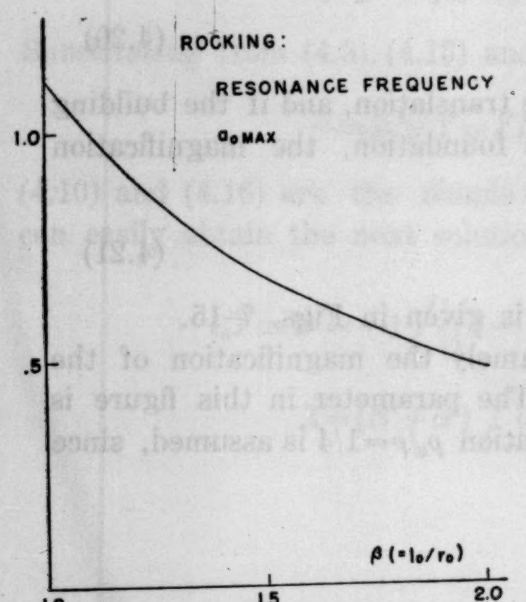

Fig. 10.

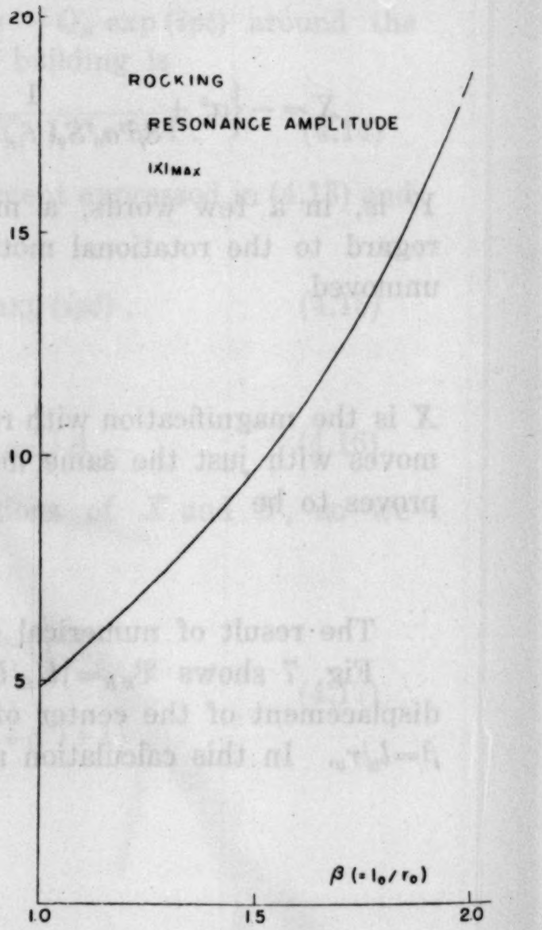

Fig. 9.

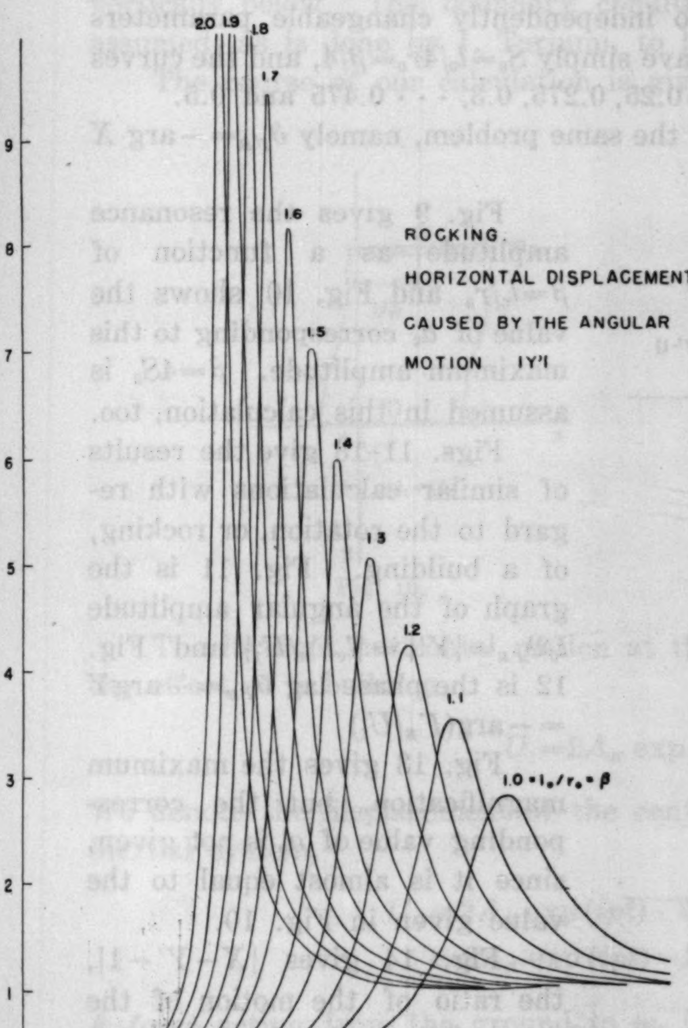

Fig. 11.

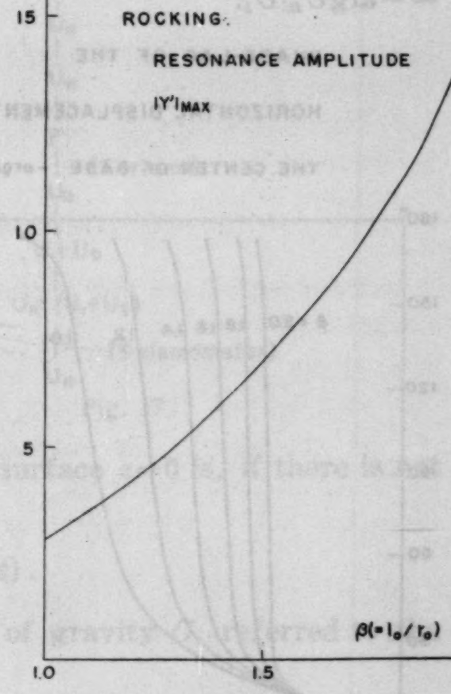

Fig. 13.

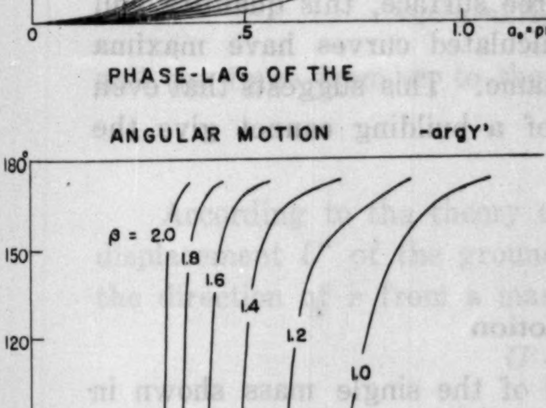

Fig. 12.

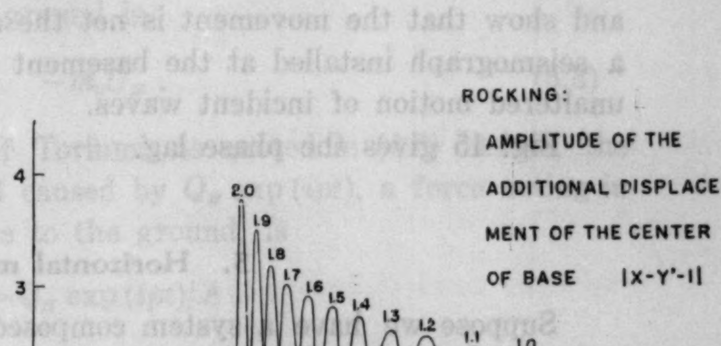

Fig. 14.

it is too complicated to have two independently changeable parameters ρ_0/ρ and l_0/r_0. From (4.18) we have simply $S_0=l_0/4r_0=\beta/4$, and the curves in the figure give the cases $S_0=0.25$, 0.275, 0.3, $\cdots$ 0.475 and 0.5.

Fig. 8 gives the phase lag of the same problem, namely $\vartheta_{UR}=-\arg X=-\arg U_R/U_1$.

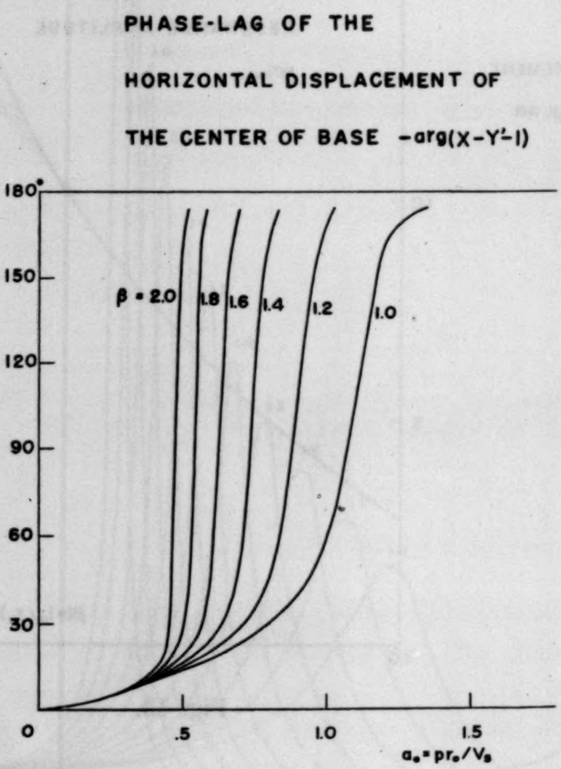

Fig. 15.

Fig. 9 gives the resonance amplitude as a function of $\beta=l_0/r_0$ and Fig. 10 shows the value of a_0 corresponding to this maximum amplitude. $\beta=4S_0$ is assumed in this calculation, too.

Figs. 11–13 give the results of similar calculations with regard to the rotation, or rocking, of a building. Fig. 11 is the graph of the angular amplitude $l_0\mathfrak{B}_{PR}=|Y'|=|l_0\Gamma_R/U_1|$ and Fig. 12 is the phase lag $\vartheta_{PR}=-\arg Y=-\arg(\Gamma_R/U_1)$

Fig. 13 gives the maximum magnification, but the corresponding value of a_0 is not given, since it is almost equal to the value given in Fig. 10.

Fig. 14 gives $|X-Y'-1|$, the ratio of the motion of the base center to that of the ground without building. If the base of a building moves exactly the same as the free surface, this quantity will become identically equal to 1, but the calculated curves have maxima and show that the movement is not the same. This suggests that even a seismograph installed at the basement of a building cannot give the unaltered motion of incident waves.

Fig. 15 gives the phase lag.

5. Horizontal motion

Suppose we have a system composed of the single mass shown in Fig. 16. We will calculate the horizontal motion corresponding to the shear vibration caused by a purely horizontal vibration incident from

vertically below. The boundary condition at the base of a building is assumed, as is done by I. Toriumi, to be X_z=const.

The course of our calculation is given in Fig. 17.

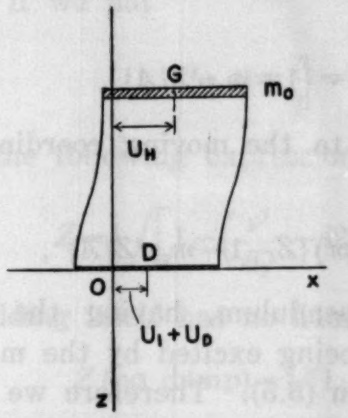

Fig. 16.

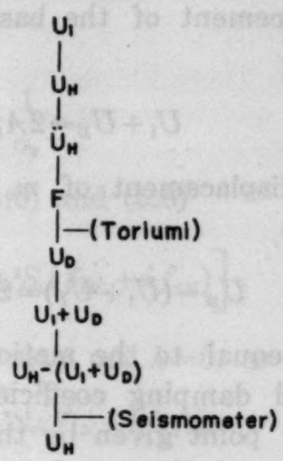

Fig. 17.

The incident horizontal motion at the surface $z=0$ is, if there is not the effect of a building,

$$U_I=2A_H \exp(ipt) .$$

We denote the displacement of the center of gravity G, referred to the inertial system,

$$U_H=2A_H \exp(ipt) \cdot \mathfrak{B}_H \exp(-i\vartheta_H)$$

$$\equiv 2A_H \exp(ipt) \cdot Z. \tag{5.1}$$

A force acting from the ground to m_0 is

$$m_0\ddot{U}_H=2A_H \exp(ipt) \cdot m_0(-p^2)Z , \tag{5.2}$$

and the force from m_0 to the ground is

$$-m_0\ddot{U}_H . \tag{5.3}$$

According to the theory of Toriumi, as quoted in (4.6) before, the displacement U' of the ground caused by $Q_H \exp(ipt)$, a force acting in the direction of x from a mass to the ground, is

$$U'=Q_H \exp(ipt)/A .$$

If, instead of $Q_H \exp(ipt)$, we put (5.3) into the above expression, we obtain that additional displacement U_D at the base center of a building,

caused by the existence of the building,

$$U_D=2A_H \exp(ipt)\cdot m_0p^2Z/A\ . \tag{5.4}$$

The displacement of the base is, adding the displacement of the free surface,

$$U_1+U_D=2A_H \exp(ipt)\cdot\{1+m_0p^2Z/A\}\ . \tag{5.5}$$

The displacement of m_0 referred to the moving coordinates given by (5.5) is

$$U_H-(U_1+U_D)=2A_H \exp(ipt)\{Z-1-m_0p^2Z/A\}\ , \tag{5.6}$$

which is equal to the motion of a pendulum, having the same free period and damping coefficient, and being excited by the motion of a supporting point given by the equation (5.5). Therefore we can apply the well-known theory of a seismograph.

If we denote the motion of the earth by x, and the displacement of a pendulum referred to moving coordinates by y, then the next equation holds, which connects x and y:

$$\frac{d^2y}{dt^2}+2\varepsilon\frac{dy}{dt}+n^2y=-\frac{d^2x}{dt^2}\ . \tag{5.7}$$

Assuming the form

$$x=x_m \exp(ipt)\ ,$$
$$y=y_m \exp(ipt)\ ,$$

we have

$$y=cx\ , \tag{5.8}$$

where $c=1/\{(u^2-1)+i2hu\}\ ,$

$$u=n/p\ ,\quad h=\varepsilon/n\ .$$

Putting $x\rightarrow U_1+U_D\ ,$

$$y\rightarrow U_H-(U_1+U_D)\ , \tag{5.9}$$

we have from (5.5) and (5.6)

$$\begin{aligned}2A_H \exp(ipt)\cdot\{Z-1-m_0p^2Z/A\}\\ =c\cdot 2A_H \exp(ipt)\cdot\{1+m_0p^2Z/A\}\ .\end{aligned} \tag{5.10}$$

Therefore

$$Z=1\Big/\left[\frac{1}{1+c}-\frac{m_0p^2}{A}\right]. \qquad (5.11)$$

Now, if we put

$$u=\frac{n}{p}=\frac{n}{a_0V_s/r_0}=\frac{1}{a_0}\nu, \qquad (5.12)$$

we have the following expression using (4.6) and (5.8)

$$Z=1\Big/\left[1-\left(\frac{\nu^2}{a_0^2}-i2h\frac{\nu}{a}\right)^{-1}-a_0^2S_0(f_{1H}+if_{2H})\right]. \qquad (5.13)$$

If the building itself has no damping, we may put $h=0$, so that

$$Z\,(\text{no damp})=1/[1-a_0^2/\nu^2-a_0^2S_0(f_{1H}+if_{2H})]. \qquad (5.14)$$

The additional displacement caused by the existence of the building is, using (5.4) and (5.13)

$$U_D=2A_H\exp(ipt)\cdot a_0^2S_0(f_{1H}+if_{2H})$$

$$\div\left[1-\left(\frac{\nu^2}{a_0^2}-i2h\frac{\nu}{a}\right)^{-1}-a_0^2S_0(f_{1H}+if_{2H})\right]. \qquad (5.15)$$

If the building itself has no damping

$$U_D=2A_H\exp(ipt)\cdot a_0^2S_0(f_{1H}+if_{2H})/[1-a_0^2/\nu^2-a_0^2S_0(f_{1H}+if_{2H})]. \qquad (5.16)$$

In the case of resonance

$$n=p \quad \text{or} \quad a_0=\nu. \qquad (5.17)$$

Introducing this relation, we have

$$U_D\,(\text{resonance})=-2A_H\exp(ipt). \qquad (5.18)$$

Therefore

$$U_1+U_D\,(\text{resonance})=0, \qquad (5.19)$$

which implies that the base center of a building does not move at all. An interesting property.

A general expression for the motion of the base is

$$U_1+U_D=2A_H\exp(ipt)\cdot\left\{1-\left(\frac{\nu^2}{a_0^2}-i2h\frac{\nu}{a_0}\right)^{-1}\right\}Z. \qquad (5.20)$$

When $h=0$

$$U_1+U_D=2A_H \exp(ipt)\cdot\{1-a_0^2/\nu^2\}\,Z\,(\text{no damp})\,. \tag{5.21}$$

The results of numerical calculations are given in Figs. 18–24.

We have now three parameters a_0, S_0 and ν. Besides there is another one h which gives the damping property inherent in the building itself. To avoid a useless complication we will assume that the building itself is without damping ($h=0$), and show, as an example, the calculation of the case $\nu^2=n^2r_0^2/(\mu/\rho)=1$.

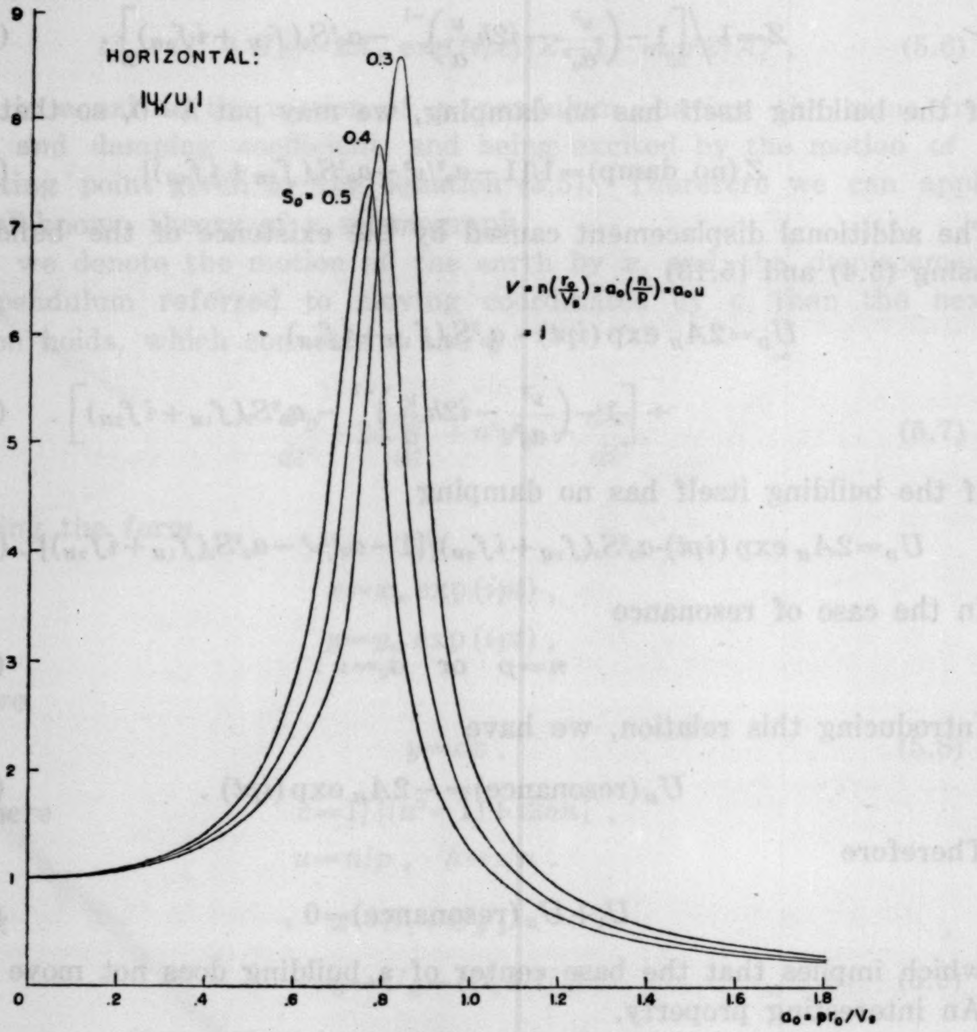

Fig. 18.

Fig. 18 gives the magnification $\mathfrak{V}_H$ with regard to the displacement of the center of gravity G (cf. (5.1)), and Fig. 19 the phase difference

ϑ_H (cf. (5.1)). Fig. 20 is the magnification with regard to the displacement of the center of the base of the building (cf. U_1+U_D in (5.5)). In this figure all the curves become zero at the point $a_0=1$, which fact was mentioned before in (5.19). The values $S_0=0.3$, 0.4 and 0.5 are adopted because, it seems, they can represent a short, medium and tall building.

Fig. 21 gives the maximum magnification. Abscissa is

$$1/\nu^2=(\mu/\rho)/n^2r_0^2\ .$$

In the case of a simple pendulum there is a relation between the maximum magnification V_{MAX} and the damping coefficient

$$V_{\text{MAX}}=1/2h\ . \qquad (5.22)$$

If we apply this relation to the above figure and calculate the apparent damping coefficient h_{apparent}, then we have the result shown in

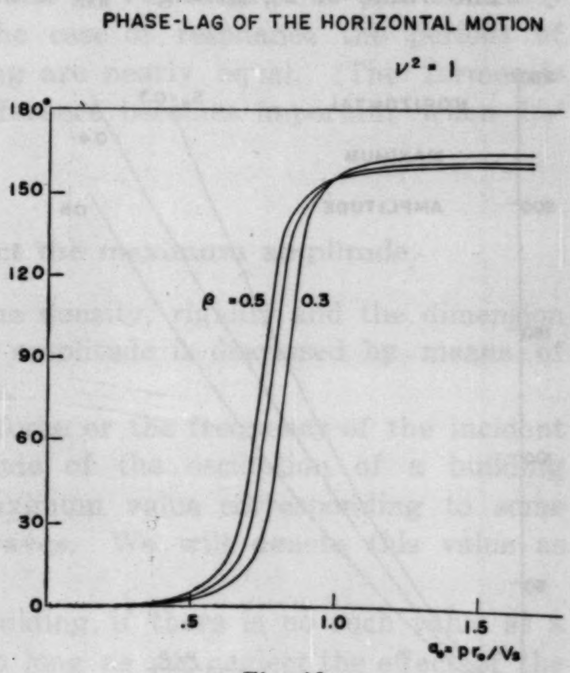

Fig. 19.

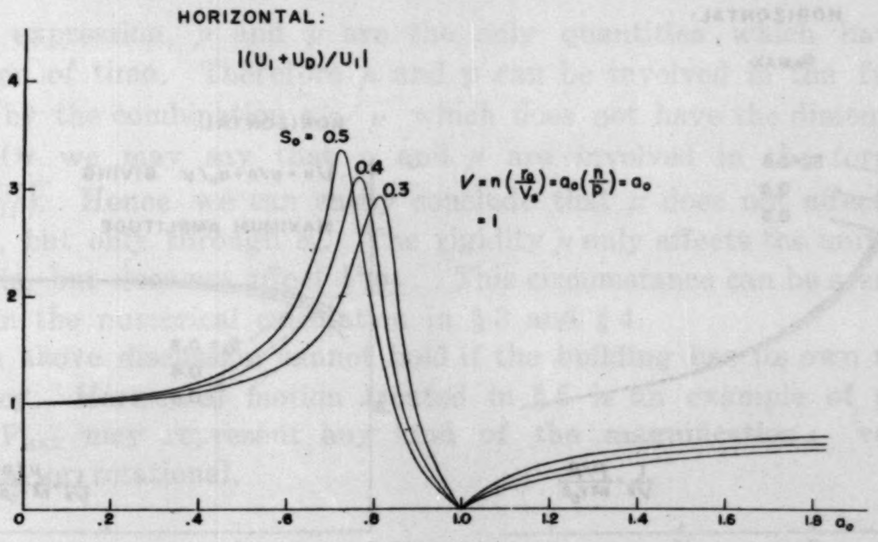

Fig. 20.

Fig. 22. This is the case when the building itself has no damping, and

h_{apparent} is caused only by the radiation of energy from the building into the elastic medium.

The value of a_0, giving V_{MAX} is shown in Fig. 23 as a function of

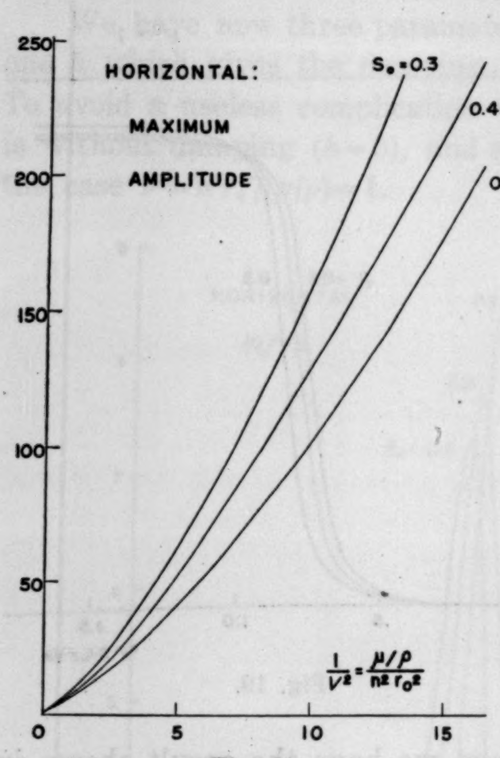

Fig. 21.

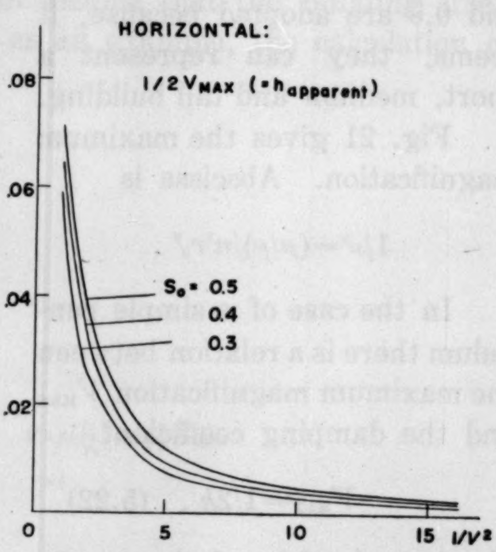

Fig. 22. The apparent damping coefficient when the building itself is without damping.

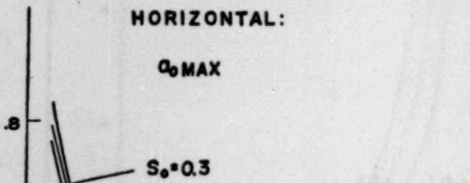

Fig. 23. The resonance frequency as a function of $1/\nu^2=(\mu/\rho)/(n^2r_0^2)$.

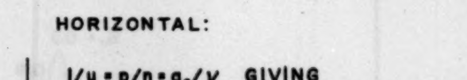

Fig. 24.

$1/\nu^2$. In a_0 and $1/\nu^2$, ρ and μ are both involved and the above figure is a little difficult to interpret, so a graph of $a_0/\nu=p/n=1/u$ is given in Fig. 24 as a function of $1/\nu^2$. When $1/\nu^2$ is large $1/u=p/n$ is nearly equal to 1. That means that in the case of resonance the periods of incident waves and of the building are nearly equal. (The former is always a little larger and the difference becomes important when $1/\nu^2$ becomes small.)

6. Elements which affect the maximum amplitude

In this section the effect of the density, rigidity and the dimension of the building on the maximum amplitude is discussed by means of the method of dimensional analysis.

If the period of the external force or the frequency of the incident seismic waves varies, the amplitude of the oscillation of a building varies accordingly and takes a maximum value corresponding to some value of the period of incident waves. We will denote this value as V_{MAX}.

As is in the case of a rigid building, if there is no such value as a natural frequency of a building, so long as we neglect the effect of the gravity, we can assume that V_{MAX} is a function of $m_0, r_0, l_0; \rho, \mu$ and p.

$$V_{MAX}=F(m_0, r_0, l_0;\ \rho, \mu;\ p)\,. \tag{6.1}$$

In this expression, μ and p are the only quantities which have the dimension of time. Therefore μ and p can be involved in the function F only by the combination $p/\sqrt{\mu}$ which does not have the dimension of time. Or we may say that p and μ are involved in the form $a_0=pr_0/\sqrt{(\mu/\rho)}$. Hence we can easily conclude that μ does not affect V_{MAX} directly, but only through a_0. The rigidity μ only affects the unit of the time axis, but does not affect V_{MAX}. This circumstance can be seen practically in the numerical calculation in § 3 and § 4.

The above discussion cannot hold if the building has its own natural frequency. Horizontal motion treated in § 5 is an example of such a case. V_{MAX} may represent any kind of the magnification: vertical, horizontal or rotational.

7. Approximate formulas giving the resonance period and the amplitudes[3]

7.1 Rocking motion

In the case of rocking motion we can find that the resonance peaks of the translation as well as rotation appear corresponding to the period given by the following approximate formula

$$T_{\text{MAX}} \doteqdot 6(l_0/V_s)\,, \qquad (7.1)$$

which is obtained from Fig. 10.

Also, using the Figs. 9, 10 and 13, we can deduce the next formula

$$|X|_{\text{MAX}} \doteqdot 5.7\, a_0^{-1.5}\,, \qquad (7.2)$$

and

$$|Y'|_{\text{MAX}} \doteqdot 3.5\, a_0^{-2}\,, \qquad (7.3)$$

which give maximum magnification factors of the displacement of the center of gravity and rotation of the building, respectively.

7.2 Horizontal motion

In a similar manner we can obtain the formulas in the case of the horizontal motion. A one-mass undamped system shows maximum response

$$|Z|_{\text{MAX}} \doteqdot 1.5\, S_0^{-1} a_0^{-3}\,, \qquad (7.4)$$

for the incident wave with a period

$$T_{\text{MAX}} \doteqdot 1.3\, a_0^{0.2} T_0 \quad (0.3 < a_0 < 0.7)\,. \qquad (7.5)$$

3) The authors owe entirely to Dr. H. Kawasumi for this section. cf. H. KAWASUMI and K. KANAI, "Vibrations of buildings in Japan, Part I. Small amplitude vibrations of actual buildings".

26. 弾性地盤上に建つ建築物の振動

地震研究所 {佐藤泰夫 山口林造

1. 建築物の振動とこれに影響を及ぼす地盤問題も昨今盛んに多くの議論を生んでゐる．然しここでは建築物と地盤とを別々に扱ふ縦来の方法を離れて，それらを一体の振動系と見做し上下動，水平動及びロッキングの夫々の場合についての振動性能を求めてみた，計算のもとになる部分は鳥海氏によつて為されたものを使用することにし，従つて建物は円柱状と考へ，更に底面での力の作用の仕方も同氏がとられた仮定——上下及び水平動の場合には円内で応力一定，外部では 0，ロッキングの時には円内では x に比例する応力，外では 0——がそのまま成立つものとする．又地震波は鉛直下方から純粋の上下又は水平動が入射するものとして計算した．

2. 記号を §2 に示す．

3. 上下動に関する考への運びは Fig. 1 に従ひその結果を Fig. 2～Fig. 3 に示す．倍率曲線としては地震計のそれに良く似たものが得られるが，位相差には多少の違ひがある．Fig. 4 には極大倍率を S_0 を変数にとつて示してあるが，後のロッキング，水平動にくらべかなり小さい．

4. ロッキングの場合の考への筋道は Fig. 5 に示す，Fig. 7 及び Fig. 8 に重心の水平変位についての倍率及び位相差を，そして Fig. 9 及び Fig. 10 に極大倍率とそれを与へる a_0 の値を示す．ここでは建物と地盤の密度の比を 1/4 にとり，従つてパラメーターは建物の縦横の比になつてゐる．

回転に関するものについては上と同様に Fig. 11 から Fig. 13 までに，但し極大を与へる a_0 は殆んど変らないから図示はしてない．

又底面中心の変位に関するものは Fig. 14 と Fig. 15 に夫々倍率と位相差を示した．これから見ても建物の地階においた地震計も猶，入射地動そのままを与へるものではないことが明瞭である．

5. 水平動に於ては Fig. 16 に示されるやうな単一質量の模型を考へて，建物の剪断振動に相当する水平動を Fig. 17 に示される筋道で計算をした．

前二節と異り複雑化をさけて建物は非減衰と仮定し，更に $\nu=1$ といふ特別な場合を採つて計算した．Fig. 18 は重心の変位に関する倍率を，Fig. 19 にその位相差を示す．Fig. 20 には建物底面の中心に関する倍率が示されてゐる．この場合 $a_0=1.0$ で曲線が凡て倍率 0 の点に集まるのは，丁度共振に相当した場合に (5.19) の式が成立することを図示してゐるのである．

Fig. 21 に極大倍率を及びそれと関聯して建物の見かけの減衰係数を Fig. 22 に示す．又極大を与へる a_0 を $1/\nu^2$ の函数として表したのが Fig. 23 である．Fig. 24 には a_0/ν，即ち建物の週期と入射波の周期との比をグラフ化してある．$1/\nu^2$ が大きくなれば，その比は殆んど 1 に等しく，つまり共振の時，建物と入射波の周期は殆んど等しいが，前者は常に後者よりも常に小さいといふことが分る．

6. 極大倍率に影響を与へる要素としては，建物が剛体と考へてよい場合のやうに，それ自身の振動数なるものが存在せず，又重力を考慮に入れない限り，m_0, r_0, l_0; ρ, μ; p がその要素と考へられる．そして次元解析の助けを借りて考へるなら，時の次元をもつものは μ 及び p のみだから，μ 及び p はただ $p/\sqrt{\mu}$ 或は $a_0=pr_0/\sqrt{\mu/\rho}$ として含まれなければならない，このことから μ の変動は a_0 を通じてのみ影響することが結論される．

7. 実用的な見地を考へて簡潔な近似式をつけ加へた．ロッキングの水平と回転，及び水平動の極大倍率は夫々 a_0 の 1.5, 2, 3 乗に逆比例してゐるといつた関係があることである．

御指導を給はつた河角広，金井清両先生に厚く御礼申し上げる．

27. *Geomagnetic Studies of Volcano Mihara. The 8th Paper.*

(*Continuous Observation of Changes in Geomagnetic Declination during the Period 1955～56*)

By Izumi YOKOYAMA,

Earthquake Research Institute.

(Read June 25, 1957.—Received June 30, 1957.)

A continuous recording of geomagnetic declination has been carried out at the western coast of Ooshima Island in order to study the relation between the changes in the geomagnetic field and the activities of Volcano Mihara on this island. The results obtained by the observation during the period from 1951 to 1954 have already been reported in this Bulletin[1]. Towards the end of 1955, a new station where a continuous recording of declination is also carried out in the same manner as station No. 37 Nomashi, was set up in the vicinity of station No. 14 Zoo on the east side of the island. The purpose of this new station No. 43 Zoo is, as mentioned in the previous paper[1], to verify that the changes at both stations on the west and east sides of the island should be in the opposite direction in relation to the activities of Volcano Mihara provided the changes are caused

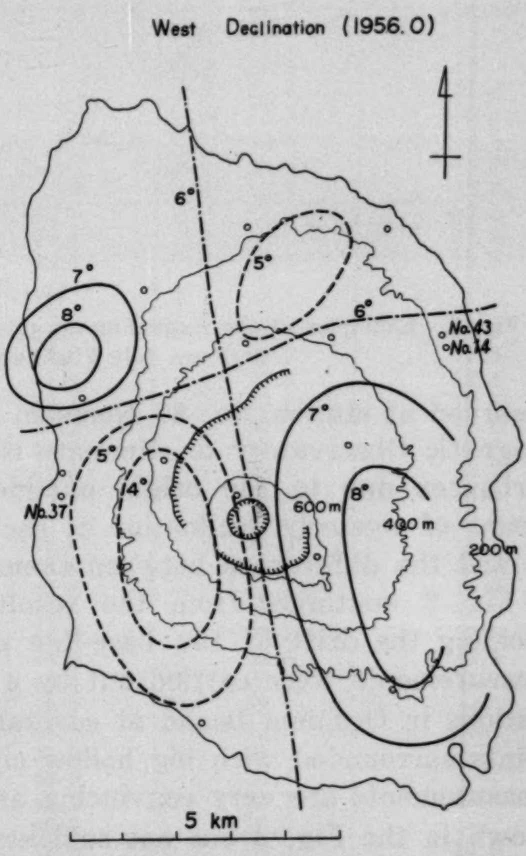

Fig. 1. The distribution of the westerly declination in Ooshima Island for 1956. 0.

1) I. YOKOYAMA, *Bull. Earthq. Res. Inst.*, **33** (1955), 251.

by the increase or decrease in magnetization of the volcano probably due to the temperature changes in its interior.

In order to examine the gradual changes associated with the volcanic activities, the hourly values are read off from the weekly records and the daily means and finally the semi-monthly means are obtained exactly in the same procedure described in the previous paper. The mean values

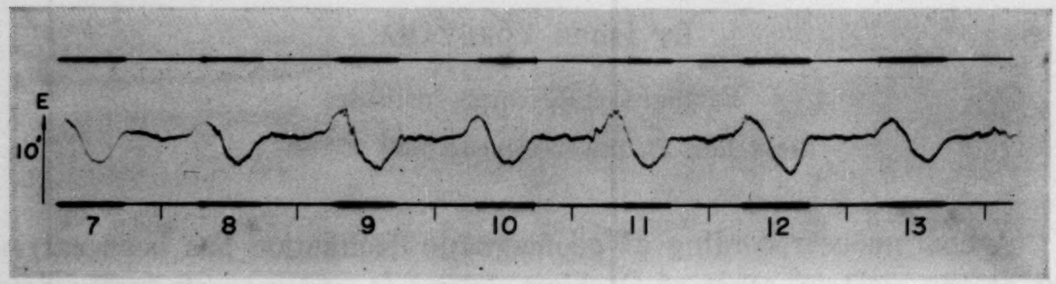

(a) Nomashi

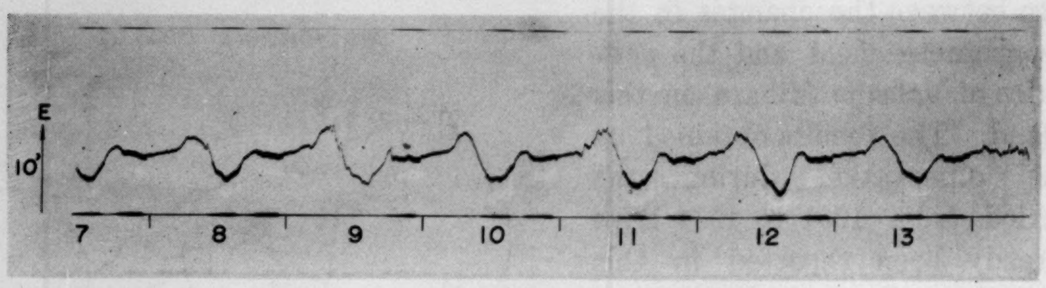

(b) Zoo

Fig. 2. Examples of the magnetogram obtained at both stations in Ooshima Island. (From July 7 to July 14, 1956 J.S.T.)

observed at station No. 37 Nomashi are compared with that of Kakioka Magnetic Observatory to eliminate the effect of transient magnetic disturbances due to the origin outside of the earth. The semi-monthly means of westerly declination at each station during the period 1955~56 and the differences between them are tabulated in Table I and shown in Fig. 3. continued from the results since 1951. For the purpose of avoiding the drift of the base-line on the magnetogram, the absolute measurements were carried out by a G.S.I. type magnetometer[2)] at both stations in Ooshima Island at several epochs which are shown by the points surrounded with big hollow circles in the figure. These absolute measurements are very convincing as to the reliability of the results shown in the Fig. 3 but not sufficient by themselves to trace the mode of the changes in detail. The surface activities of the volcano are shown in an arbitrary scale at the bottom of the figure while their quantitative expression by energy of volcanic tremors or earthquakes till 1954 are

Table I. The semi-monthly means of the westerly declination at Ooshima and Kakioka.

Period	Ooshima		Kakioka	Difference Nomashi–Kakioka
	West (Nomashi)	East (Zoo)		
1955				
Jan.	6°10′.3		6°22′.3	-12′.0
	10.6		22.5	12.0
Feb.	10.8		22.6	11.8
	10.5		22.3	11.8
Mar.	10.2		22.3	12.1
	10.0		22.3	12.4
Apr.	9.9		22.6	12.7
	9.6		22.6	13.0
May	9.3		22.7	13.4
	9.4		22.5	13.1
June	9.6		22.5	13.0
	9.5		22.6	13.2
July	9.3		22.6	13.3
	9.5		22.4	13.0
Aug.	10.6		22.7	12.0
	10.7		22.3	11.6
Sept.	10.8		22.7	11.9
	10.4		22.5	12.1
Oct.	10.5		22.6	12.0
	10.5		22.5	12.1
Nov.	10.1	8°48′.8	22.5	12.4
	10.4	48.2	23.0	12.5
Dec.	10.1	48.4	22.6	12.5
	10.0	48.1	22.3	12.3
1956				
Jan.	10.2	48.0	22.7	12.5
	10.4	48.0	22.9	12.4
Feb.	10.2	47.7	22.6	12.4
	10.4	48.1	23.0	12.6
Mar.	10.7	48.2	23.2	12.6
	10.6	48.7	23.5	12.9
Apr.	9.5	47.8	22.7	13.2
	10.6	49.4	24.0	13.4
May	9.5	48.2	23.0	13.5
	10.1	49.4	24.3	14.2
June	8.9	48.4	23.1	14.2
	9.1	48.6	23.1	14.0
July	9.2	48.5	23.1	13.9
	9.7	48.6	23.2	13.5
Aug.	9.5	48.5	22.8	13.3
	* —	48.4	23.3	—
Sept.	—	48.7	23.7	—
	—	48.1	23.3	—
Oct.	—	47.7	23.0	—
	—	48.3	23.4	—
Nov.	—	48.2	23.7	—
	—	48.2	23.6	—
Dec.	9.8	47.6	22.8	13.0
	9.6	47.2	22.7	13.2

* The cave in which the variometer had been operated collapsed by a strong typhoon in August and was reconstructed in November.

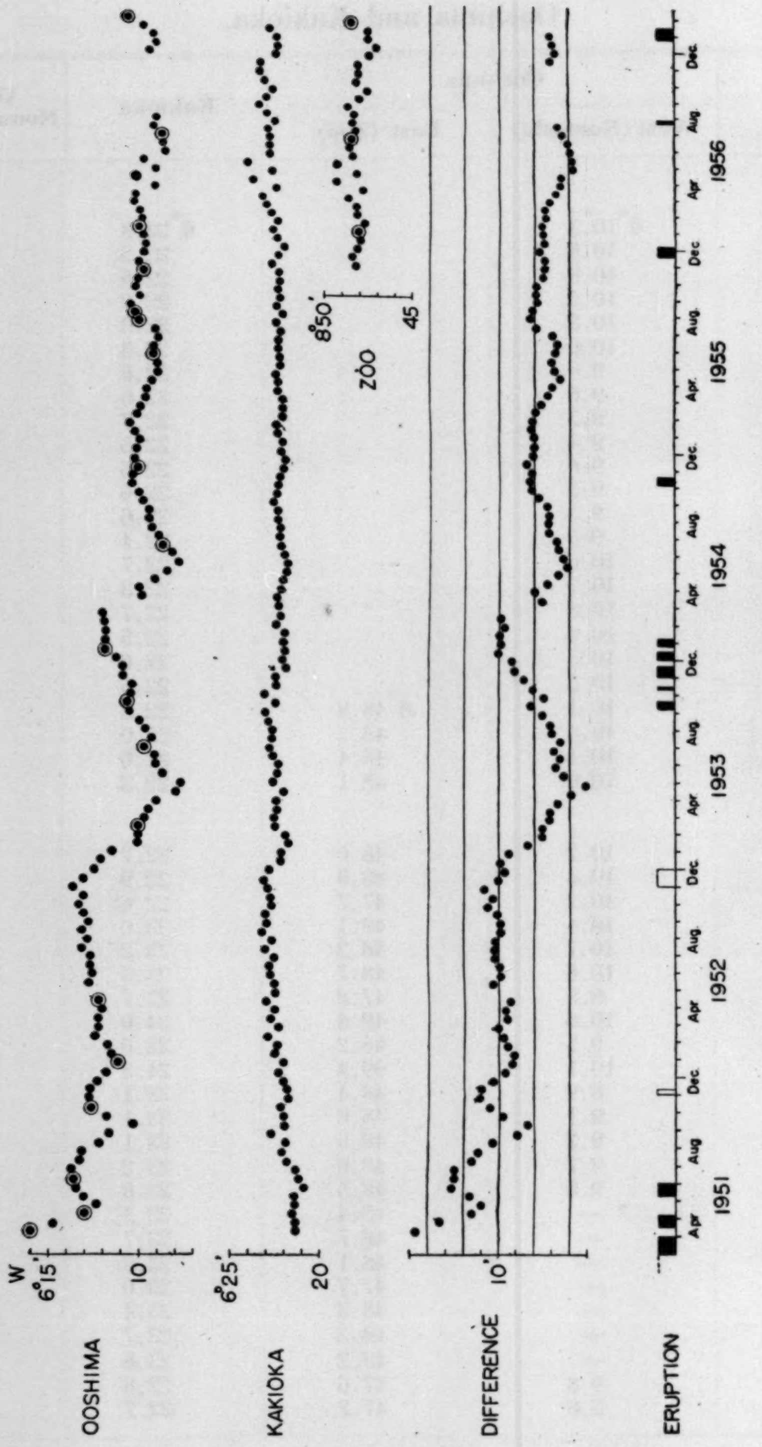

Fig. 3. The semi-monthly means of the westerly declination and activities of Volcano Mihara.

found in the writer's other papers[3]. During the period 1955~56, the minor eruptions were observed in Dec. 1955 and Aug. 1956 but no new lava was ejected in either case.

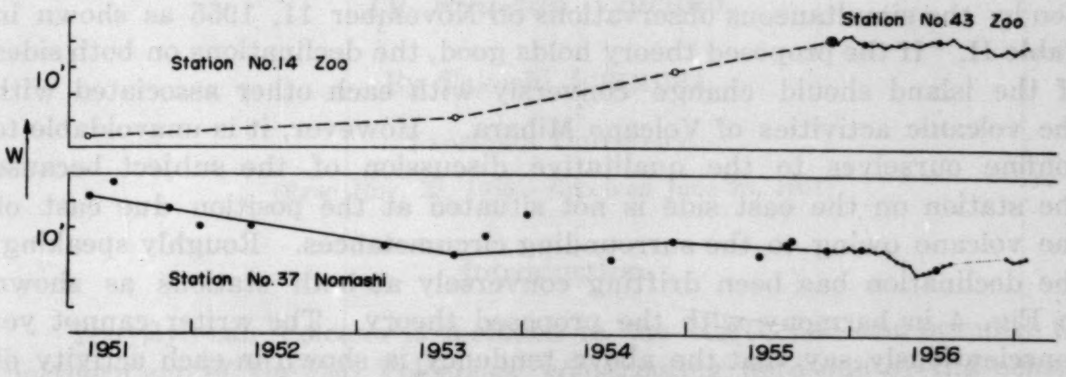

Fig. 4. The changes of the westerly declination at two stations in Ooshima Island. The hollow circles show the instant values and the black the semi-monthly means.

The result shown in Fig. 3 confirms the conclusion obtained in the previous paper that the declination at Nomashi Station tends towards the west whenever the volcano becomes active and returns eastward after the subsidence of activity. Furthermore, it is noticeable that the amplitude of undate change accompanied by the volcanic activities has decreased gradually year by year after the 1950-51 eruption and the same may be said of the activity itself. Here, the writer must refer to the annual variation seen in the figure, as a matter of fact: Unless the volcano shows the activities annually by its own mechanism, it is hard to find a valid cause for the apparently annual variation seen in the figure as far as our present knowledge in geomagnetism goes.

The contrast of modes in changes between the west and east sides of

Table II. Simultaneous observations at the stations Nos. 14 and 43 Zoo.

Time	No. 14 (Absolute Measurem.)	No. 43 (Magnetogram)	Kakioka
Nov. 11, 1955			
18*h* 33*m*	6°30′.5	8°47′.9	6°22′.6
46	30.9	48.2	22.8
19 06	30.4	47.8	22.3
21	30.8	48.1	22.8
Mean	6°30′.6	8°48′.0	6°22′.6

2) I. YOKOYAMA, *Bull. Earthq. Res. Inst.*, **31** (1953), 211.
3) I. YOKOYAMA, *Bull. Earthq. Res. Inst.*, **34** (1956), 185; **35** (1957), 75.

the island is shown in Fig. 4 where the changes at the two stations are compared with that of Kakioka. The semi-monthly means observed at the station No. 43 Zoo are connected to the instant values of the station No. 14 Zoo by the simultaneous observations on November 11, 1955 as shown in Table II. If the proposed theory holds good, the declinations on both sides of the island should change conversly with each other associated with the volcanic activities of Volcano Mihara. However, it is unavoidable to confine ourselves to the qualitative discussion of the subject because the station on the east side is not situated at the position due east of the volcano owing to the surrounding circumstances. Roughly speaking, the declination has been drifting conversely at both stations as shown in Fig. 4 in harmony with the proposed theory. The writer cannot yet conscientiously say that the above tendency is shown in each activity of the volcano comparing the results of continuous recording at both stations because no moderate activity occured these years.

Summarizing the results altogether from 1951 to 1956, we can positively say that local anomalous changes of a particular type in the geomagnetic field have taken place on Ooshima Island and may safely say that these changes are associated with the volcanic activities of Volcano Mihara in the proposed physical theory and have decayed in their amplitude with the decline of the volcanic activity after the great 1950–51 eruption.

---

27. 三原山の地球磁気学的研究 第8報
(1955～56 年間の偏角変化の連続観測)

地震研究所 横 山 泉

1950–51 年の三原山大噴火に際して，1951 年から同地において地磁気偏角の連続観測を行つているが，第6報に引続いて 1955–56 年間の観測結果を報告する．三原山の東西両側においては，火山活動に伴う偏角変化が相互に反対向きであろうことが予想されるので，55 年末から新たに東側の動物園内に連続観測所を設けた．

51 年以来の成果を概観するに，大島において地磁気の異常変化が観測されたことは確実であり，これが火山活動に関係するものであり，理論から予想されるような推移を示したと認めてよいであろう．なお，火山活動も次第に衰微を示しているが，これに伴う地磁気の異常変化の振幅も次第に減衰して，ある状態に落着くかの如くである．

28. *Geological Investigations on the Zaō Volcanoes.*
IV Ryū-zan Volcano.

By Takeshi ICHIMURA,

Yamagata University.

(Read Nov. 27, 1956.—Received June 28, 1957)

Introduction

The Ryū-zan Volcano is included in the North Zaō and occupies the northern end of the Zaō Volcanoes, constructing here one of the centers of activities which are arranged from northeast to southwest in this volcanic area. It is not so extensive as compared with the Kumano Volcano (Zaō Proper) and Byōbu Volcano[1] situated further south, but has very complicated topography and structure due to repeated eruptions and successive openings of explosion craters. Such activities are supposed to have taken place in concert with other parts of the Zaō Volcanoes. Since the present Ryū-zan Volcano is deeply dissected by subsequent erosion and is intensely destructed by explosion, it is very easy to investigate its history of volcanism which seems to be an important key point in making clear the activities of such adjoining volcanoes as Kumano and Gando.

The geological investigations of the Ryū-zan Volcano and its surrounding area were first intended by A. Takada[2] many years ago and recently by the writer's students[3]. The writer's field and laboratory works were also carried on intermittently since 1948, although he unfortunately had an accident in July of 1955, when he was attacked by a big bear on the northern flank of Ryū-zan and was severely injured. The results of these works are summarized in this paper.

Location

The Ryū-zan Volcano is situated at the southeastern corner of Yamagata City where it includes such districts as Takiyama, Zaō and

1) T. ICHIMURA, *Bull. Earthq. Res. Inst.*, **33** (1955), 593-629.
2) A. TAKADA, *Graduation Thesis, Tokyo Univ., M.S.* 1922.
3) K. SUGAI, 〃 , *Yamagata Univ., M.S.* 1955.
S. SUTŌ, 〃 , 〃 ., 〃 . 〃 .

Higashizawa. The volcanic area is not far from Yamagata and can easily be approached through several courses. For the purpose of climbing up Ryū-zan and Torikabuto-yama, the Zaō Hot Spring is, however, selected usually as its base, because there are bus roads between Yamagata or Kaminoyama and this place. Each of these summits is directly attainable from here within a short distance. To the summit of Ryū-zan, it is also accessible from Yamagata through Iwanami and Tsuchisaka or Kannō, although both courses are long and steep as compared with others.

Topographical and Geological Features of the Ryū-zan Volcano

The Ryū-zan Volcano is chiefly composed of Ryu-zan (1363.5 m.) and Torikabuto-yama (1401 m.). These two peaks rise up respectively at the northern and southern sides of the Zaō Hot Spring. They are partly forested thickly and have steep or rugged features. The eastern side of this area faces to Gando-san beyond a deep valley dissected by the Mamigasaki-gawa, whereas its western part suddenly lowers down from the steep ridge to slightly undulated table land, which passes gradually into the hilly land westwards, ending at the southern periphery of the Yamagata Basin. The northern end of the table land is bordered by liparitic or dacitic masses of Saruoka-yama, Chitose-yama and Togami-yama close to Yamagata. Of these, Chitose-yama has a beautiful conical form.

The mountainous area mentioned above is watered by the Mamigasaki-gawa, Su-kawa and their tributaries. The Mamigasaki-gawa runs northwestwards and joins such tributaries as Happō-zawa, Gando-zawa, Kote-zawa, Nabekurafudō-zawa, Hanoki-zawa, Nidari-zawa, Mizunashi-zawa, Atera-zawa, Matsudome-zawa, Ōshio-zawa, Koshio-zawa and Hime-sawa on its way. It constructs a typical alluvial fan at the end of its valley, where a part of this gentle slope is occupied by the old town of Yamagata.

The Su-kawa, on the other hand, finds its origin at the bottom of the explosion crater surrounding the Zaō Hot Spring and flows into the Su-kawa of Yamagata Basin* after it gathers the water of the Harai-gawa, Ichido-gawa, Nido-gawa, Sando-gawa and other tributaries. In the case of the Mamigasaki-gawa, the main river and tributaries are

* There is another river called the Su-kawa in the Yamagata Basin, where it runs from south to north and joins to the Mogami-gawa in the vicinity of Nagasaki.

characterized by the predominance of deep gorges with some terraces along them, but the Su-kawa valley is wide and monotonous through its course. It is believed to be due to the occurrence of granitic rocks in the former and the exposure of mud flow in the latter. Besides them, one of noticeable features is the abundance of swamp, large or small, in the area covered by mud flows. They are represented by Haryū-numa, Sanbongi-numa, Sara-numa, Sakazuki-ko, Shiginoyachi-numa and others (Fig. 1).

The area under consideration is geologically intricate, being built up of granite (granodiorite), Neogene sediments and older or younger volcanics as well as of Quaternary fluviatile or talus deposits. The younger volcanics are represented by andesite lavas or other ejecta and rest upon the eroded surface of granite and other base rocks (Fig. 2).

(1) Intrusives and extrusives before the first eruption of the Ryū-zan Volcano:—The most important rock is composed of biotite granite and hornblende biotite granite in which the former is more extensively distributed than the latter, being frequently associated with plagioliparite, felsitic rock and propylite. There are some textural varieties from coarse to fine, and some of these are more or less schistosed. Among them, fine-grained granite is mostly found at the area including the Hime-sawa, Koshio-zawa and Bōbara. In this case, it contains quartz, orthoclase, plagioclase and biotite less than 1 mm. in diameter. The coarse-grained granite is, on the other hand, seen along the Fudō-zawa and Harai-gawa. Its essential components are commonly 5 mm. or more in longer diameter, and biotite-rich varieties have a dark color.

The commonest type of granite is a medium-grained variety which is leaucocratic or melanocratic, and its specimen from the Koshio-zawa is characterized by a warm color.

Under the microscope, such various kinds of granite as mentioned above consist of quartz, orthoclase, microcline, andesine, biotite, hornblende, magnetite, zircon, allanite, apatite, pyrite, titanite in association with leucoxene, epidote, chlorite, sericite, limonite and kaoline.

Moreover, the granites exposed at the Ryū-zan volcanic area contain xenoliths with an ellipsoidal or irregular form, 10 m. or thereabouts in the maximum diameter. They are dioritic or lamprophyric, mineral components being quartz, plagioclase, green biotite, green hornblende, apatite (prismatic or acicular), pyrite, magnetite, titanite, leucoxene, sericite, epidote and chlorite. They are lithologically similar to those in the Gassan granite.

Fig. 1. Topographical map of the Ryū-zan Volcano and its vicinity.
1. Takayu explosion crater, 2. Kannō explosion crater,
3. Akakura explosion crater, 4. Suzuritaki explosion crater.

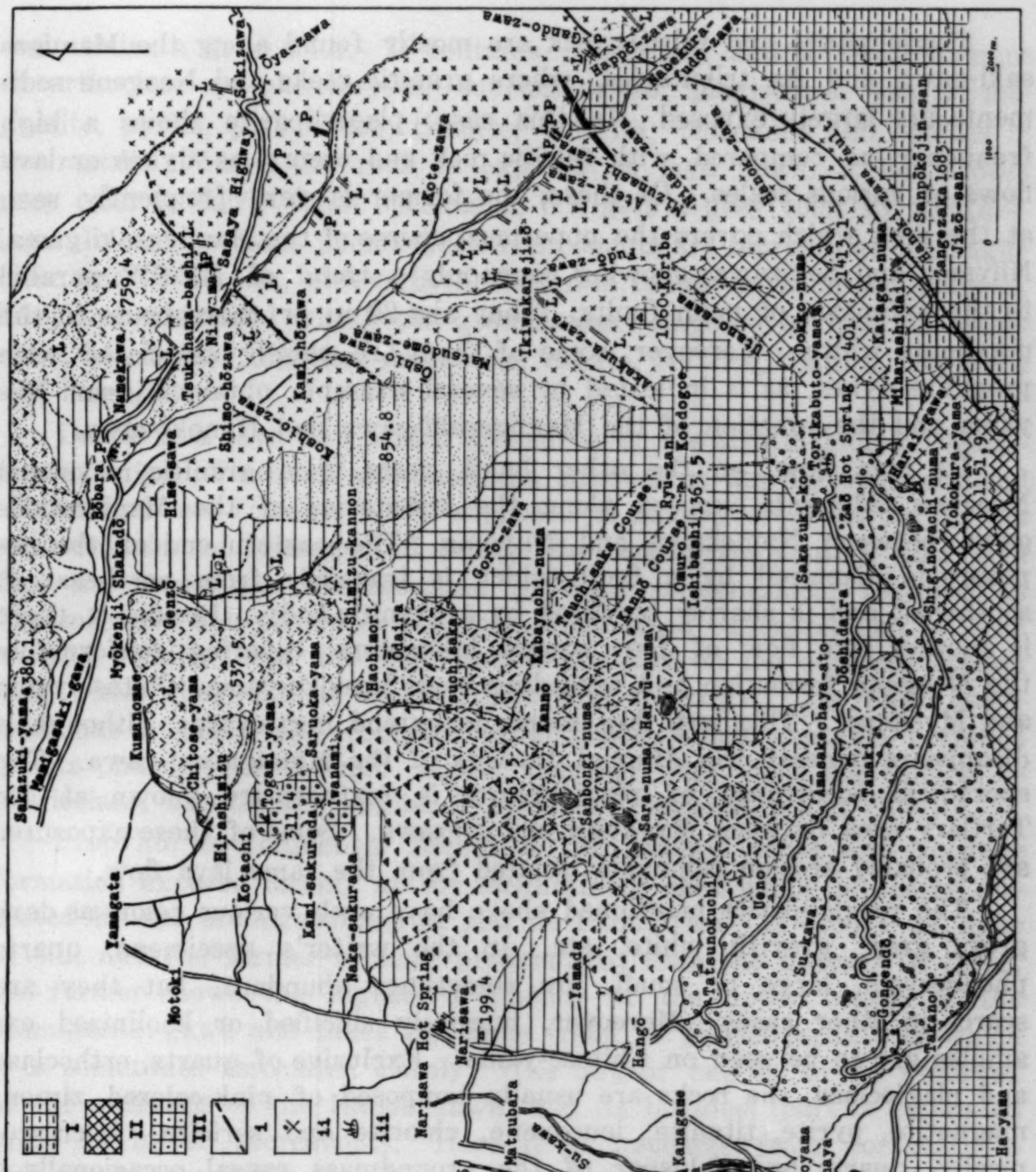

Fig. 2. Geological map of the Ryū-zan Volcano and its vicinity.
1. Quaternary fluviatile deposits, 2. Talus deposits, 3. Kannō mud flow, 4. Su-kawa mud flow, 5. Torikabuto-yama lava and mud flow, 6. Ryū-zan lava and agglomerate, 7. Dacite, 8. Plagioliparite and associated rocks, 9. Propylite, 10. Upper Tuff Formation, 11. Lower Tuff Formation, 12. Granite (granodiorite), I. Jizō-san lava (Kumano Volcano), II. Yokokura-yama lava and agglomerate, (Kumano Volcano), III. Ha-yama lava (Ha-yama Volcano) i. Fault, ii. Fossil localities, iii. Hot spring.

Plagioliparite and felsitic rock are mostly found along the Mamigasaki-gawa and its tributaries, where granitic rocks and Neogene sediments are largely exposed. In this case, plagioliparite shows a high frequency as compared with felsitic rock and occurs as dykes or lava flows of various scales. Of these, the former is very frequently seen at the area which covers the uppermost course of the Mamigasaki-gawa, Niiyama and Sekizawa, showing commonly a trend of NE-SW parallel to the extension of main faults. They are 20 m. or thereabouts in the maximum width. Moreover, some of them are closely associated with propylite dykes, as is indicated by several example obtained near Niiyama and the junction of the Mamigasaki-gawa and Hanoki-zawa.

Its lava flow, on the other hand, rests upon granitic rocks and Neogene sediments exposed along the tributaries of the Mamigasaki-gawa between Namekawa and Niiyama. The eastern end of the exposure is displaced by a fault which is traceable from northeast to southwest and is sharply bordered by a granitic body. Besides it, there is another lava flow of four square kilometers, covering conformably the Neogene formation and spreading over Saruoka-yama, Chitose-yama and Myōkenji. This lava flow seems to extend northwards, although it disappears beneath the Alluvial deposits of the Mamigasaki-gawa. The sporadical occurrence of plagioliparite is furthermore known at the Tertiary area between Myōkenji and Hōzawa. Some of these exposures are probably erosion remnants isolated from the same lava flow.

The palgioliparite mentioned above have such various colors as dark grey, grey, greyish white, etc. In the writer's specimens, quartz phenocrysts, large or small, are sometimes abundant, but they are scarce in other cases. Moreover, intensely silicified or kaolinized examples are to be seen on Chitose-yama. Exclusive of quartz, orthoclase and plagioclase, the rocks are usually composed of pink-colored zircon, magnetite, pyrite, titanite, leucoxene, chlorite and sericite. Microscopically, quartz and feldspar of the groundmass reveal occasionally a spherulitic structure.

Felsitic rock is quite similar to plagioliparite in its mode of occurrence. When the rock takes a dyke form, it cuts granitic rocks at Hōzawa and the upper course of the Mamigasaki-gawa, but its lava flow is extensively distributed on the hilly land beyond the Mamigasaki-gawa, where it is sometimes associated with plagioliparite or andesitic rock with a trachytic texture.

Injected felsitic rock is generally intensely subjected to weathering

and attains a grey color. It contains plagioclase and a small amount of orthoclase as phenocrysts, but orthoclase, plagioclase, quartz, magnetite, pyrite, pink zircon, titanite, chlorite, leucoxene and epidote in the matrix. When the rock is exposed as lava flows, it has a dark grey color in fairly fresh specimens, but gets a grey color by weathering. In such a case, phenocrystic components are represented by plagioclase and orthoclase, although the latter is found in a minor amount. They are embedded within the groundmass composed of quartz, orthoclase, plagioclase, apatite, magnetite, calcite, sericite, titanite, leucoxene and limonite.

Dacite is a lava flow which spreads over the area including Togami-yama, Onigoe, Iwanami and Sakurada situated at the northwestern end of the Ryū-zan Volcano. It is supposed to have poured out during the sedimentation of Miocene tuff beds. The erosion remnant of this lava flow are sometimes characterized by such topographical features as Togami-yama and others at present. Some good exposures can be seen on the cutting near the bus station and also on the adjacent stream bed, where they exhibit an indistinct joint structure. The fresh specimen has a black and compact groundmass which contains corroded quartz phenocrysts, 2–4 mm. across, together with such ingredients as plagioclase, hornblende, augite, hypersthene, magnetite and chlorite.

Propylite is frequently found in the granitic mass and Neogene formation exposed largely at the mountainous area which is deeply dissected by the Mamigasaki-gawa and its tributaries. It occurs as dyke or sill; and the former is more predominant than the latter. Of these, the former shows the highest frequency at the upper course of the Mamigasaki-gawa and takes the same trend as plagioliparite with which it is sometimes associated closely. The largest one is to be observed at the entrance of the Hanoki-zawa, and its broadest part is estimated to be 100 m. or thereabouts. Here it is traceable from northeast to southwest across the granitic area watered by the Mamigasaki-gawa and Happō-zawa.

There are also other remarkable exposures at Namekawa and Nii-yama as well as on the ridge just behind Hōzawa, constructing sill and dykes, large or small, in green tuff beds.

Propylite sills and dykes mentioned above are undoubtedly younger than green tuff, but there are some possibilities of older propylite which are suggested by the presence of its pebbles in the tuffaceous conglomerate. Similarly, propylite is older than plagioliparite, since the former

is found as xenolith in the latter. The rock is believed to have mostly been altered from andesite and basalt.

It is a compact rock with a dark green or yellowish green color, being composed of plagioclase, augite, pyrite, magnetite, limonite, hematite, chlorite, calcite, titanite, leucoxene and sericite. The specimen obtained from the Ōshio-zawa, on the other hand, contains some phenocrystic aggregates of chlorite, calcite, hematite, limonite, etc. They are supposed to have been changed from olivine crystals.

(2) Neogene sediments:—These sediments are largely exposed at this volcanic area, being represented by green tuff, sandy tuff, brecciated tuff, conglomerate, sandstone, siltstone and shale. They are divided into two tuff formations, upper and lower. Of these, the Lower Tuff Formation corresponds to the Yoshino Formation[4], whereas the Upper Tuff Formation is similar to the Sugarida Formation[5] in other districts.

The distribution of the Lower Tuff Formation is restricted to the eastern side of the Ryū-zan Volcano. The formation is mainly composed of green tuff beds, and its thickest part is 400 m. or thereabouts. When it rests directly upon granitic rocks, conglomerate is frequently seen at its base. It is used to pass into a brecciated tuff or green tuff upwards, being well exposed at the southeast of Genzō and along the Ōshio-zawa as well as on the river bed near Niiyama. It is rich in boulders, 1 m. in maximum diameter, and contains some pebbles of granitic rocks. Moreover, there are some green tuff beds which are characterized and complicated by the occurrence of propylite fragments and sills. Such a geological feature seems to indicate that propylite has, at least, two different ages of injection or eruption in connection with the sedimentation of green tuff.

In contrast with the formation mentioned above, the Upper Tuff Formation is distributed from north to south at the volcanic area, being intercalated with sandstone, siltstone and shale. It is estimated to be about 300 m. at the thickest part and is closely associated with lava flows of plagioliparite and felsitic rock. The sandy tuff exposed near the Narisawa Hot Spring preserves such Brachiopods as *Terebratalia tenuis*, *Terebratulina crossei*,, etc. Most of the upper tuff formation are, however, covered by ejecta and lava flows of the Ryū-zan Volcano and talus deposits. Its geological structure is, therefore, partly undetermined.

4) S. MINAKAWA, *Bull. Yamagata Univ., Nat. Sc.*, **4** (1957), 244.
5) 〃 , *op. cit.*, (1957), 245.

Since the Upper Tuff Formation was subjected to the strong disturbance, its strike and dip change from place to place. For instance, the alternate beds of black shale and sandstone exposed at Shimizu-kannon reveal a strike of N50°E and a dip of 30°NW, but the siltstone beds of Kabayachi-numa situated near the Tsuchisaka Course are N–S in strike and 50°W in dip. In the case of light green tuff beds stratified behind the Narisawa Hot Spring has a strike of N25°W, inclining 25° east-northeastwards.

(3) Lavas and ejecta from the Ryū-zan Volcano were not so frequently erupted as those of the Byōbu Volcano[6] and Aoso Volcano[7]. They are shown by the eruption of the Ryū-zan lava and agglomerate, Torikabuto-yama lava and mud flow, Su-kawa mud flow and Kannō mud flow.

(i) Ryū-zan lava (olivine two-pyroxene andesite or olivine-bearing two-pyroxene andesite) and agglomerate:—Ryū-zan is built up of the Ryū-zan lava and agglomerate which are elevated to 1363.5 m. above the sea-level at the highest point. These volcanic products rest upon the eroded surface of granitic rocks and the Neogene formation. They are covered by the Torikabuto-yama lava at the southeast and are overlain by the Kannō mud flow at the west, whereas disappears partly beneath the Su-kawa mud flow at the south. The thickest part of lava and agglomerate is estimated to be about 400 m., being well exposed at the northern side of the Zaō Hot Spring.

(ii) Torikabuto-yama lava (olivine two-pyroxene andesite or olivine bearing two-pyroxene andesite) and mud flow:—The volcanic products are exposed on Torikabuto-yama and its surrounding area, but they are found in a small extent as compared with the Ryū-zan lava and mud flow mentioned above.

The lava and agglomerate of this area rest on the surface of granite, palgioliparite, Ryū-zan lava, Yokokura-yama lava and Jizō-san lava, being partly bordered by a big fault from the last one (Fig. 8). The gently sloped area between Momiji-tōge and Zange-zaka seems to be composed of mud flow which passes possibly into the lava flow upwards.

The lava flow here is frequently cliffed, as is indicated at the northeast of Torikabuto-yama where it covers directly granite and on the western flank of the same peak. Its exposure reveals varying

6) T. ICHIMURA, *op. cit.*, (1955), 627–628.
7) 〃 , *Bull. Earthq. Res. Inst.*, **31** (1953), 147–148.

thickness from place to place, and it is about 200 m. thick in the case of the lava flow exposed on the western flank.

(iii) Su-kawa mud flow:—There are two mud flows on this volcano. One of them is the Su-kawa mud flow erupted from the explosion crater just behind the Zaō Hot Spring (Figs. 3, 4). It extends westwards further down to Shindō, Yuzaka and Kubotebara beyond the Ōu Railway Line, forming here a complicatedly undulated area with several swamps represented by Shiginoyachi-numa, Sakazuki-ko and others.

The mud flow is traceable for a distance of about 11 km. from east to west and shows varying width between 700 m. and 4000 m. Its total area is estimated to be 26 km²., and the maximum thickness is 100 m. or there-abouts along the Su-kawa where the mud flow is exposed on the Ryū-zan lava.

(iv) Kannō mud flow:—It is widely exposed at the western side of Ryū-zan, extending from Tsuchisaka to Kannō and Dōshidaira southwards (Figs. 5, 6, 7). The area of this mud flow is about 11 km². and is suddenly elevated above the Tertiary sediments with some characteristic topographical features of table land. As is indicated by the Su-kawa mud flow, it is about 100 m. in its thickest part and is noticed by the sporadical distribution of such swamp as Haryū-numa, Sanbongi-numa, Sara-numa, etc.

(v) Quaternary sediments:—They are represented by younger or older fluviatile deposits and talus deposits.

(a) Younger or older fluviatile deposits: Fluviatile deposits are accumulated along the Mamigasaki-gawa, Su-kawa and their tributaries, consisting of gravel, sand, and clay beds. The older deposits construct some terraces at the upper course of the Mamigasaki-gawa along its tributaries. There is also a remarkable fan at the lower course of the Mamigasaki-gawa.

(b) Talus deposits:—Neogene sediments are thinly covered by talus deposits on the hilly land including Monzen, Naka-sakurada, Narisawa, Yamada, Hangō, etc. They are composed of andesite blocks or fragments derived from the Kannō mud flow or other detritus.

Structure of the Ryū-zan Volcano

The Ryū-zan Volcano is a homate rising up on the northern extension of the weak zone, where the Kumano Volcano and Byōbu Volcano were borned. It is not so large as above-mentioned volcanoes, but is

very complicated in its form and structure. The present topography of this volcano depends upon the intense destruction due to repeated eruptions and explosions which took place in connection with other parts of the Zaō Volcanoes. The rugged peak of Ryū-zan was mainly resulted from these volcanic activities.

The relationship between the lava flows, agglomerates and mud flows constructing the Ryū-zan Volcano is well observed at the area surrounding the Zaō Hot Spring, along the Tsuchisaka Course and on Koedogoe as well as along the Gorō-zawa and Akakura-zawa. For instance, the lava flows exposed on the wall of explosion crater near the Zaō Hot Spring and the cliff extending southwestwards from here are piled up with an inclination of about 20°W (Fig. 3), and they are intercalated by agglomerate near the trail of Dōshidaira branching from the bus road.

The lava flow of the crater wall mentioned above seems to be more than 400 m. in its thickness. There is, however, no base rock appearing beneath this lava. The lava flow is also overlapped predominantly on the northern flank of Ryū-zan where it inclines 40°NW along the Tsuchisaka Course, but 20°NW along the Gorō-zawa. In the former case, it is intercalated by a thick agglomerate. The similar rock is found at the lowest part of the lava flow exposed along the Gorō-zawa. Moreover, the inclination of lava flow is 5°–15°E on the flank between Koedogoe and the Akakura-zawa, whereas it is 20°–30°S at Omuro and Ishibashi. These lavas and agglomerates are, therefore, inferred to have been erupted from the crater somewhere near the summit of Ryū-zan. In addition, the steep inclination of the agglomerate bed along the Tsuchisaka Course suggests that there were some disturbances at this area after repeated activities of Ryū-zan Volcano.

Such structures as observed on Ryū-zan are indistinct at its opposite side, viz., Torikabuto-yama. The volcanic products from here are, however, displaced by several faults, large or small, running from the northern side of Sanpōkōjin-san to the Hanoki-zawa and its adjoining area. In this faulting, the side of Torikabuto-yama was thrown down against the Jizō-san lava of Sanpōkōjin-san. Besides them, the Torikabuto-yama lava inclines 10°–20° southwards. It was probably caused by the local subsidence taken place in connection with the explosion of the Ryū-zan Volcano, as is shown by the Kumano-dake lava exposed largely on the wall of the Umanose explosion crater[8].

8) T. ICHIMURA, *Bull. Earthq. Res. Inst.*, **29** (1951), 330–332.

Craters

The Ryū-zan Volcano is now a destruction remnant due to repeated explosions and continuous erosions, but seems to have been a characteristic homate at the earlier stage of its activity. The structure of this volcano also suggests that it was formerly higher than the present altitude and had a large crater on its, summit. Such a crater had still kept its original form, when the Ryū-zan lava and agglomerate were erupted from here and the vicinity, although it was almost obscured later with the formation of the explosion crater surrounding the Zaō Hot Spring.

Explosion craters are well preserved mostly as compared with the pre-existing crater under consideration. They are represented by four semi-circular hollow distributed around Ryū-zan (Fig. 1).

One of these is the Takayu explosion crater which is the largest of all with a diameter of 2500 m. from northwest to southeast and has a steep wall of 250–400 m. high between Ryū-zan and Torikabuto-yama. It is the source of the Su-kawa and Su-kawa mud flow, being characterized by the presence of the Zaō Hot Spring which comes out here and there at its bottom. The crater wall here is frequently highly cliffed at the north, but there are some evidences to suggest a local subsidence at the southeast.

In connection with it, the western side of Ryū-zan is sccoped out downwards by the opening of the Kannō explosion crater. It is, however, found in an extension smaller than the Takayu explosion crater and has a diameter of 1500 m. from northeast to southwest. The original crater wall is more or less deformed and is intricately dissected by subsequent erosion (Figs. 5, 6).

The Kannō mud flow was poured out from here and spreads over the eroded surface of Neogene sediments. It constructs a gently undulated area, where Haryū-numa, Sanbongi-numa, Sara-numa and others are found.

Besides these, two subordinate explosion craters are known at the uppermost course of the Akakura-zawa and just below the summit of Ryū-zan. They are respectively named the Akakura explosion crater and Suzuritaki explosion crater by the writer. In these cases, the Akakura explosion crater opens northeastwards and is about 750 m. in diameter from northwest to southeast. It has no mud flow, and its horse-shoe-shaped hollow is well observed from the summit of Gando-san.

The Suzuritaki explosion crater seems to have exploded northwards close to the summit of Ryū-zan. It is found in very small scale, but has a sharp outline, being closely associated with the Kannō explosion crater.

Mineral Composition of Lavas and Ejecta

(1) Ryū-zan lava and agglomerate:—The Ryū-zan Volcano is mainly composed of the Ryū-zan lava and agglomerate which disappear partly beneath the Torikabuto-yama lava, Su-kawa mud flow and Kannō mud flow. They are exposed here and there at this volcanic area, particularly along the Gorō-zawa, Tsuchisaka Course and bus road of the Zaō Hot Spring as well as on the wall of the Takayu explosion crater.

The Ryū-zan lava and fragments of its agglomerate are almost olivine two-pyroxene andesite and are frequently characterized by the abundance of large plagioclase phenocrysts. They have a black or dark grey color in fresh specimens, but obtain a grey color when decomposed. There is also a reddish variety supposed to have been subjected to reheating. These rocks are compact or porous and consist of plagioclase, augite, hypersthene, olivine, magnetite, tridymite, bowlingite, chlorite and brown glass.

Among them, plagioclase is found as phenocryst or an important ingredient of the groundmass. The phenocrystic plagioclase found here ranges from labradorite to anorthite with a composition of An_{67-90} and is generally anhedral or subhedral, taking a tabular or rectangular form. The largest one examined by the writer is 2.5 cm. in longer diameter. The large phenocryst is abundantly to be seen in the lava exposed along the Gorō-zawa and Tsuchisaka Course as well as on the Takayu crater wall. As is shown by many thin sections, the crystal is distinctly or indistinctly zoned, and some of it encloses augite, magnetite and chlorite in a regular or irregular arrangement. It is also noticed that the phenocryst is often invaded by the groundmass or brown glass which resulted in the formation of a worm-eaten structu re. The turbid part is present in very low frequency and is observed at the central or peripheral part of crystal, being fringed by a narrow clear zone without any enclosure.

In the groundmass, it is more acidic and occurs as a lath-shaped or rectangular crystal, mostly 0.02 mm.—0.2 mm. long. The swarm of such a minute crystal affords a fluidal structure and pilotaxitic texture

to the groundmass.

Augite is the commonest ingredient in all specimens, but its phenocryst is absent in the thin sections of some andesites collected from the cutting of the bus road between Dōshidaira and the Zaō Hot Spring or elsewhere. This mineral is occasionally associated with hypersthene

Table I. Composition and optical characters of plagioclase, augite and hypersthene phenocrysts (measured by F. Hori)

	No. 1. (T.I. 50073104)	No. 2. (T.I. 50080106)	No. 3. (T.I. 51100802)
Plagioclase	$\alpha=1.568\pm0.002$ (n_1 min.) $\gamma=1.582\pm0.002$ (n_2 max.) An_{77-86}	$\alpha=1.564\pm0.002$ (n_1 min.) $\gamma=1.580\pm0.002$ (n_2 max.) An_{67-82}	$\alpha=1.566\pm0.002$ (n_1 min.) $\gamma=1.579\pm0.002$ (n_2 max.) An_{76-81}
Augite	$\alpha=1.694\pm0.002$ $\beta=1.703\pm0.002$ $\gamma=1.719\pm0.002$ $2V(+)=45°$ $Ca_{36}Mg_{35}Fe_{29}$	$\alpha=1.695\pm0.002$ $\beta=1.702\pm0.002$ $\gamma=1.721\pm0.002$ $2V(+)=45°$ $Ca_{36}Mg_{36}Fe_{28}$	$\alpha=1.693\pm0.002$ $\beta=1.701\pm0.002$ $\gamma=1.718\pm0.002$ $2V(+)=46°$ $Ca_{38}Mg_{36}Fe_{26}$
Hypersthene	$\gamma=1.712\pm0.002$ $2V(-)=56°$ $\rho>\nu$	$\gamma=1.707\pm0.002$ $2V(-)=60°$ $\rho>\nu$	$\gamma=1.703\pm0.002$ $2V(-)=60°$ $\rho>\nu$

	No. 4. (T.I. 55073101)	No. 5. (T.I. 56060304)
Plagioclase	$\alpha=1.568\pm0.002$ (n_1 min.) $\gamma=1.585\pm0.002$ (n_2 max.) An_{80-90}	$\alpha=1.566\pm0.002$ (n_1 min.) $\gamma=1.584\pm0.002$ (n_2 max.) An_{75-89}
Augite	$\alpha=1.689\pm0.002$ $\beta=1.692\pm0.002$ $\gamma=1.715\pm0.002$ $2V(+)=50°$ $Ca_{41}Mg_{42}Fe_{17}$	$\alpha=1.689\pm0.002$ $\beta=1.700\pm0.002$ $\gamma=1.703\pm0.002$ $2V(+)=48°$ $Ca_{40}Mg_{40}Fe_{20}$
Hypersthene	$\gamma=1.701\pm0.002$ $2V(-)=63°$ $\rho>\nu$	$\gamma=1.703\pm0.002$ $2V(-)=48°$ $\rho>\nu$

To confirm An and CaMgFe ratio the charts devised by F. Chayes [Am. Min. Bowen Volume, (1952) 95] and H.H. Hess [Am. Min. 34 (1949), 634] were respectively used.

No. 1.= The Ryū-zan lava from the summit of Ryū-zan.
No. 2.= 〃 Dōshidaira-Haryū-numa.
No. 3.= 〃 near the summit of Ryū-zan.
No. 4.= 〃 the Tsuchisaka Course.
No. 5.= 〃 the Gorō-zawa.

and forms a zonal structure together, the latter being always fringed by the former which is sometimes represented by a crystal aggregate. The extinction angle of phenocrystic augite, $Z \wedge c$, is 38°–40°. When the crystal is zoned, the inner part has a large extinction angle as compared with the periphery. It is subhedral or anhedral, and its largest one is 3.69 mm. long and 1.42 mm. across.

In the groundmass, augite is an important mineral which has a prismatic or granular form, being 0.02 mm.–0.08 mm. long or across in both cases.

The occurrence of hypersthene is restricted only to phenocryst, and its frequency is generally higher than phenocrystic augite. There are, however, several specimens almost free of this mineral, as is shown by those obtained from the southern foot of Ryū-zan and Kannō Course. It is usually a subhedral or anhedral crystal with a long prismatic habit, and the largest one is 2.43 mm. long and 0.83 mm. across. Magnetite is occasionally enclosed in it.

Olivine is not infrequently to be seen in most of thin sections, but is almost or entirely absent in the specimens from the summit of Ryū-zan, Dōshidaira-Haryū-numa, near Dōshidaira and the cutting between Dōshidaira and Zaō Hot Spring. It is commonly found as a subhedral phenocryst, the largest crystal being 3 mm. long and 1.26 mm. across. Generally, this mineral passes into bowlingite or chlorite. Such an alteration begins along the crack or periphery of the crystal and finally spreads over its whole part. Moreover, the crystal encloses magnetite, and it is sometimes fringed by skeleton crystals of the same mineral.

One of the predominant ingredients in the groundmass is magnetite which takes an octahedral or ill-defined form, generally 0.01 mm.–0.08 mm. in diameter. When the crystal has a phenocrystic size, it occurs usually as an irregular grain with the maximum diameter of 0.8 mm. On the contrary, tridymite is a mineral of negligible amount and fills up the interstices of other ingredients in the groundmass. The similar frequency is revealed by the brown glass contained in plagioclase phenocrysts.

In the lava and andesite fragments of agglomerate under consideration, xenoliths are largely represented by a rounded or subangular basaltic rock, large or small. Microscopically, they consist of basic plagioclase, augite, hypersthene, olivine, magnetite, calcite and bowlingite. These xenoliths have no sharp boundary against the groundmass.

The groundmass is an aggregate of labradorite, augite, magnetite,

tridymite and chlorite, being mostly characterized by a pilotaxitic or orthophyric texture.

(ii) Torikabuto-yama lava and mud flow:—So far as is known at present, the Torikabuto-yama lava associated with mud flow is exposed on Torikabuto-yama and at its adjacent area. In this case, The lava and fragments of mud flow are olivine two-pyroxene andesite or olivine bearing two-pyroxene andesite with a dark grey or grey or reddish color and porphyritic texture. They are, however, quite free of big plagioclase crystals which are very frequently present in the Ryū-zan lava.

Microscopically, these volcanic products are composed of plagioclase, augite, hypersthene, olivine, magnetite, quartz and xenoliths.

The most important ingredient is plagioclase which is found as phenocryst and in the groundmass. The phenocrystic plagioclase ranges from labradorite to bytownorthite with a composition of An_{51-82}. It is often rich in such enclosures as augite and magnetite. There is also a worm-eaten structure due to the invasion of the groundmass and the light brown glass. Moreover, some of it contains minute fragments of goethite, as can be seen in the specimens from Nanamagari between the Zaō Hot Spring and Dokko-numa.

The phenocrystic plagioclase of Torikabuto-yama lava is distinguishable from that of the Ryū-zan lava in its high frequency of a partly or wholly turbid part. The crystal is euhedral or subhedral, the largest one being 3.06 mm. long and 1.98 mm. across. Mostly it is well zoned with frequent occurrence of zonally enclosed augite and magnetite.

Plagioclase occurs as a lath-shaped crystal in the groundmass, where it is characterized by a fluidal arrangement. The crystal is always elongated and is commonly 0.02 mm.–0.2 mm. in length.

Augite takes a prismatic or granular form. Its phenocryst is subhedral or anhedral and has mostly a small size. Even the largest crystal is 1.56 mm. long and 0.59 mm. across. As is shown by the Ryū-zan lava, the phenocrystic augite is usually zoned with a core of hypersthene, whereas there is another case in which the latter contains the former as irregular patches elongated along c-axis of the mother crystal. It twins simply or complicatedly on (100) or (101), and its extinction angle, $Z \wedge c$, is 40° (±). The frequency of occurrence is high when compared with hypersthene.

In the groundmass, augite is granular or prismatic. It is 0.02 mm. –0.08 mm. across respectively.

The crystal of hypersthene occurs in low frequency and has a long prismatic habit. It is generally euhedral or subhedral, being 1.62 mm. long and 0.93 mm. across in the largest crystal. Magnetite is present as its enclosure.

Table II. Composition and optical characters of plagioclase, augite and hypersthene phenocrysts (measured by F. Hori).

	No. 1. (T.I. 48100301)	No. 2. (T.I. 48100302)	No. 3. (T.I. 52100603)
Plagioclase	$\alpha=1.556\pm0.002$ (n_1 min.) $\gamma=1.580\pm0.002$ (n_2 max.) An_{54-82}	$\alpha=1.555\pm0.002$ (n_1 min.) $\gamma=1.577\pm0.002$ (n_2 max.) An_{52-76}	$\alpha=1.554\pm0.002$ (n_1 min.) $\gamma=1.577\pm0.002$ (n_2 max.) An_{51-76}
Augite	$\alpha=1.685\pm0.002$ $\beta=1.694\pm0.002$ $\gamma=1.710\pm0.002$ $2V(+)=48°$ $Ca_{40}Mg_{41}Fe_{19}$	$\alpha=1.691\pm0.002$ $\beta=1.699\pm0.002$ $\gamma=1.718\pm0.002$ $2V(+)=47°$ $Ca_{38}Mg_{37}Fe_{25}$	$\alpha=1.691\pm0.002$ $\beta=1.700\pm0.002$ $\gamma=1.718\pm0.002$ $2V(+)=48°$ $Ca_{39}Mg_{36}Fe_{25}$
Hypersthene	$\gamma=1.708\pm0.002$ $2V(-)=62°$ $\rho>v$	$\gamma=1.705\pm0.002$ $2V(-)=58°$ $\rho>v$	$\gamma=1.702\pm0.002$ $2V(-)=65°$ $\rho>v$

To confirm An and CaMgFe ratio the charts devised by F. Chayes and H. H. Hess were respectively used.

No. 1=The Torikabuto-yama lava from the north of Dokko-numa.
No. 2= 〃 near the summit of Torikabuto-yama.
No. 3= 〃 near Miharashidai.

Olivine is always known only as phenocryst. Its frequency varies in different thin sections. It is conspicuously present in some of them, but is almost or wholly absent in others. The olivine-less example is seen in the specimens collected along the trail between Utanosawa and Fudō-taki. The olivine crystal is commonly anhedral and is sometimes surrounded by the aggregate of augite. It alters partly into goethite or bowlingite and contains magnetite.

Magnetite is a very common mineral in the groundmass, but it is not so abundant as that of the Ryū-zan lava. The octahedral or granular crystal is mostly 0.01 mm.–0.08 mm. in diameter. In the largest one, it is 0.5 mm.

Quartz is a xenocryst with low frequency. It is, however, contained in almost all thin sections. The crystal has a rounded form due to the magmatic corrosion and is occasionally fringed by augite. The

largest crystal is 1 mm. (±) in diameter. Besides the ingredients mentioned above, brown glass rarely fills up the interstices of lath-shaped plagioclase and augite in the groundmass.

Xenolith is contained in every thin section and is used to have a distinct border against the mother rock. It is a basaltic rock consisting of plagioclase, augite, magnetite, as well as of olivine.

The groundmass is constructed by plagioclase, augite, magnetite and brown glass. Of these ingredients, plagioclase reveals remarkably a fluidal arrangement. The pilotaxitic or hyalopilitic texture is also to be seen.

(iii) Andesite fragments of the Su-kawa mud flow:—Andesite fragments of this mud flow were almost supplied from the Ryū-zan lava and Torikabuto-yama lava. They are, therefore, composed of olivine two-pyroxene andesite and olivine-bearing two-pyroxene andesite. These andesite fragments have the same mineral compositions and textures as those of the lavas already mentioned.

(iv) Andesite fragments of the Kannō mud flow:—The Ryū-zan lava is the source of the andesite fragments in the Kannō mud flow. These fragments are thus represented by olivine two-pyroxene andesite or olivine-bearing two-pyroxene andesite which is closely associated with a small amount of two-pyroxene andesite. Most of these are remarkably porphyritic with the abundance of phenocrystic plagioclase. In the vicinity of Kannō, the writer collected some specimens characterized by the frequent occurrence of large plagioclase. As is shown by the Ryū-zan lava, such a phenocrystic plagioclase ranges from labradorite to anorthite, euhedral or subhedral, having frequently a worm-eaten structure and being sometimes traversed by veinlets of the light brown glass. In this case, augite, magnetite and goethite as well as chlorite are also found as its enclosures. Moreover, some of it is well zoned and slightly turbid. Minute lath-shaped plagioclase is always a predominant ingredient in the groundmass and constructs a pilotaxitic texture together with augite and magnetite.

The similarities between the andesite fragments of the Kannō mud flow and Ryū-zan lava are equally confirmed on augite and hypersthene in which the latter is usually fringed by the former. The same may be said of olivine crystal, although its frequency is variable in different specimens. Olivine occurs only as phenocryst and is generally less than augite or hypersthene in its amount, but there is an abnormal example in the specimens obtained on the hill about 500 m. north of Kannō and

along the Tsuchisaka Course, where it contains noticeably this mineral as compared with augite and hypersthene. When such a crystal is subjected to the alteration, it passes partly or wholly into bowlingite. Besides these, most of octahedral or ill-defined crystals of magnetite are scattered over the groundmass. In addition, brown glass and basaltic xenolith are seen in some specimens.

History of Volcanic Activities

The Ryū-zan Volcano rises up on the eroded surface of biotite granite or hornblende biotite granite (granodiorite) and overlying Neogene sediments exposed together with such extrusives as plagioliparite, felsitic rock, dacite and propylite. Its volcanism took place on the extension of a weak zone between the Kumano Volcano and Byōbu Volcano with a trend of NW–SE. It seems to have violently been repeated as is indicated by the distribution of various volcanic products.

In the first activity, the Ryū-zan lava are believed to have poured out from the pre-existing crater. Mostly, it flowed westwards down to Dōshidaira on the one hand and Tsuchisaka or Ōdaira on the other. There were also intermittent ejections of agglomerate during its activity. The Ryū-zan lava is, therefore, intercalated with agglomerate here and there. The main body of the volcano is supposed to have been built up at this time. It was probably a homate.

After its formation, the eruption of the Torikabuto-yama lava happened at the southeastern side of the pre-existing crater or on the neighbouring flank. Thus, the lava flow constructed Torikabuto-yama and furthermore extended to the adjacent area, where it covered the Ryū-zan lava and the granite. The lava exposed here is undoubtedly associated with mud flow, but the exact relationship has not yet been confirmed, although the extension of these volcanic products are topographically traceable.

Other remarkable activities resulted in the formation of such explosion craters as Takayu and Kannō which were repeatedly followed by the eruption of the Su-kawa mud flow and Kannō mud flow. They began with the opening of the Takayu explosion crater by which the central part of the volcano was blown off, and the crater lost its original form. In connection with it, the Su-kawa mud flow poured out from this explosion crater opened southwestwards and buried the bottom of the Su-kawa valley, having spread down to Kubotebara, Shindō and

Yuzaka.

The Kannō explosion crater was formed a little later, and the northwestern side of Ryū-zan was largely broken down with the eruption of the Kannō mud flow at its bottom. The mud flow here extends westwards or southwards. It covers the Su-kawa mud flow, Ryū-zan lava or its agglomerate and Neogene sediments at the area including Hachimori, Ōdaira, Tsuchisaka, Kannō, Sanbongi-numa, Dōshidaira, etc. They were succeeded by the explosion taken place at the uppermost course of the Akakura-zawa and near the summit of Ryū-zan. These craters were probably opened at the final stage of activities.

The present Ryū-zan Volcano is, therefore, a destruction remnant in which its original altitude was lowered to some extent, and it remains traces of its former activities only in the frequency of acidic hot spring comming up through the crater bottom.

In such cases, the activities took place in concert with those of the Kumano Volcano and Byōbu Volcano. Among them, the lavas and ejecta from the Ryū-zan Volcano are found in a complicated relationship to the Jizō-san lava and Yokokura-yama lava of the Kumano Volcano. Moreover, it can be said that the activities of the Ryū-zan Volcano are likely to have ceased earlier than the Kumano Volcano, although there are still some questions for the Gando Volcano located beyond the Mamigasaki-gawa.

Summary

(i) The Ryū-zan Volcano is located at the northern end of the Zaō Volcanoes and rests upon the eroded surface of base rocks composed of granite (granodiorite) and Neogene sediments as well as such extrusives as plagioliparite, propylite, etc. It is now built up of Ryū-zan and Torikabuto-yama, but is only a destruction remnant of the original volcano.

(ii) Volcanic products are represented by the Ryū-zan lava and agglomerate, Torikabuto-yama lava and mud flow, Su-kawa mud flow and Kannō mud flow. Of these, the Ryū-zan lava, Su-kawa mud flow and Kannō mud flow are extensively exposed.

(iii) The Ryū-zan lava and its agglomerate erupted probably from the pre-existing crater subjected later to the remarkable deformation due to explosion. The Su-kawa mud flow poured out from the Takayu explosion crater formed at the position of pre-existing crater, whereas

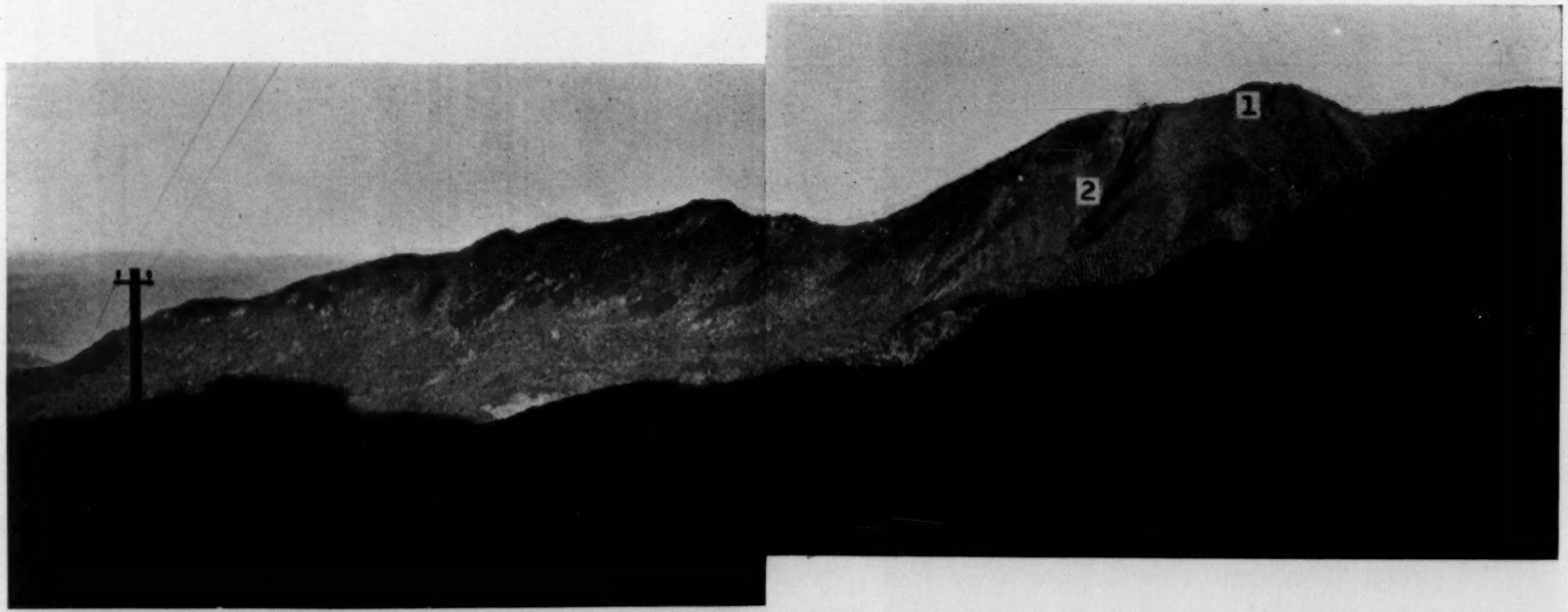

Fig. 3. The northwestern wall of the Takayu explosion crater viewed from Nanamagari between the Zaō Hot Spring and Dokko-numa. The lava flow exposed on the southern extension of this wall inclines 20° westwards. 1=The summit of Ryū-zan, 2=Crater wall.

(震研彙報 第三十五号 図版 市村)

Fig. 4. The southeastern wall of the Takayu explosion crater viewed from Sakazuki-ko which is found on the Su-kawa mud flow. 1=Torikabuto-yama, 2=Sanpōkōjin-san, 3=Jizō-san.

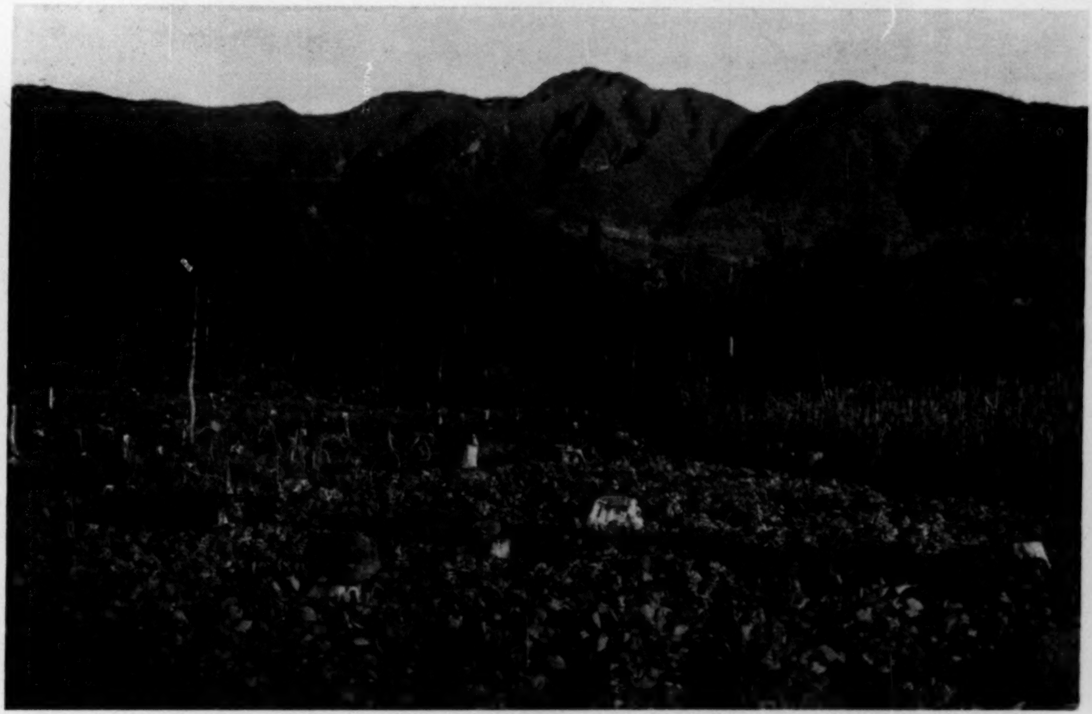

Fig. 5. The northwestern side of Ryū-zan where the Kannō explosion crater was opened northwestwards. The Kannō mud flow poured out from here, and its topographical feature is partly shown in the foreground of this picture.

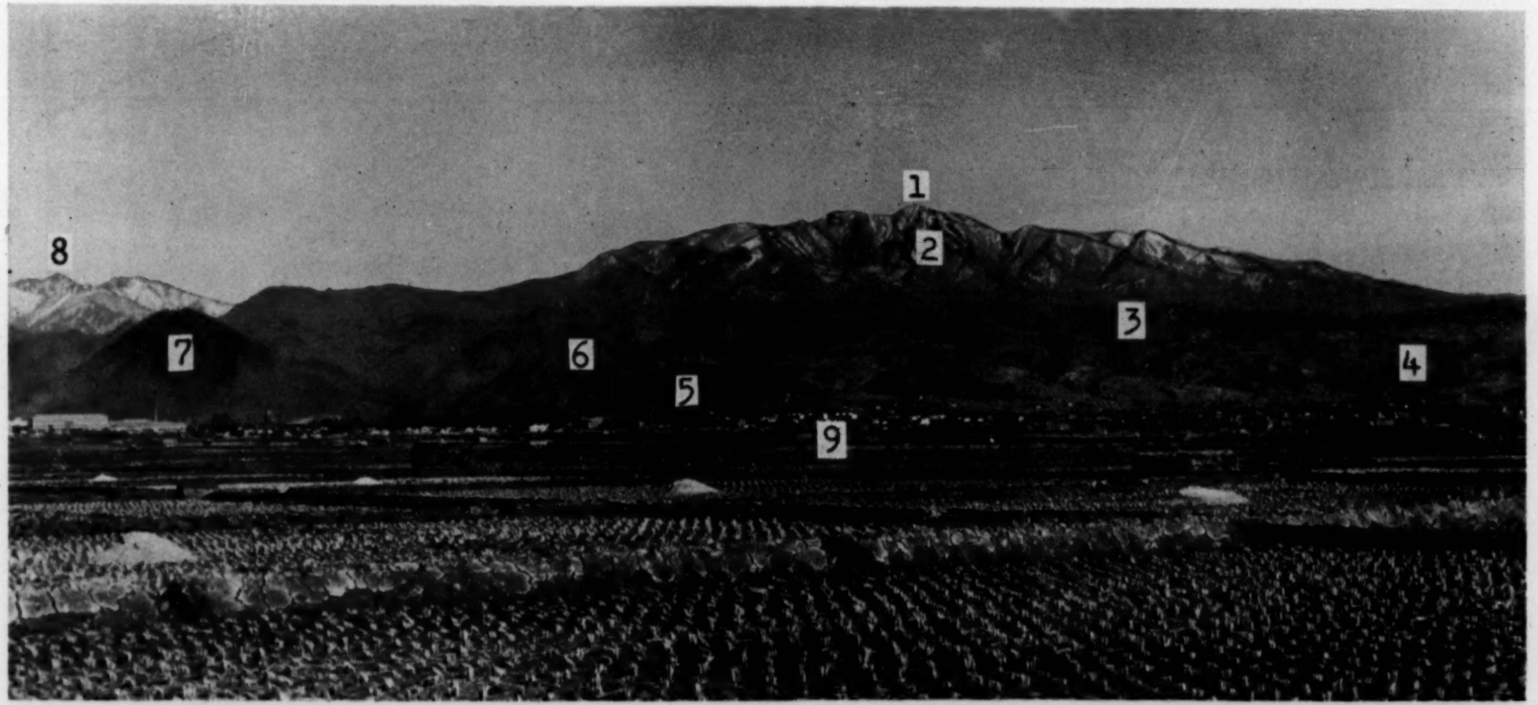

Fig. 6. Ryū-zan viewed from near Iizuka. 1=The summit of Ryū-zan, 2=Kannō explosion crater, 3=The Kannō mud flow resting upon the Neogene formation, 4=The Neogene formation, 5=Togami-yama (dacite), 6=Saruoka-yama (plagioliparite), 7=Chitose-yama (plagioliparite), 8=Gando-san, 9=Yamagata.

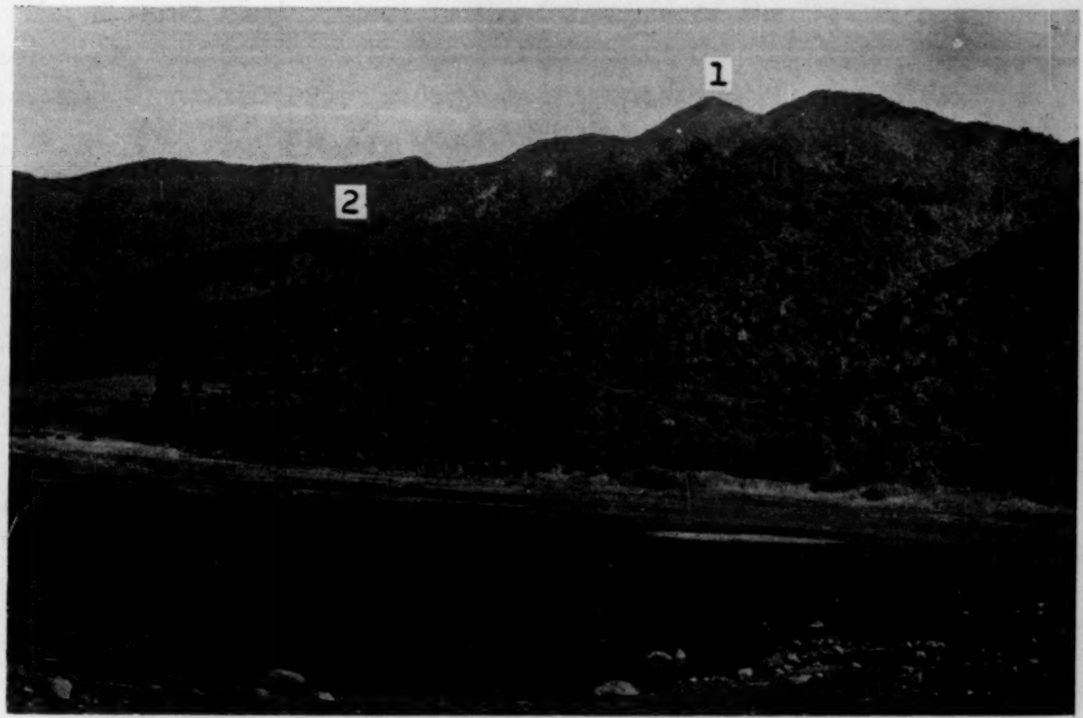

Fig. 7. Haryū-numa on the Kannō mud flow. The Kannō explosion crater is seen in the background. 1=The summit of Ryū-san, 2=A part of crater wall.

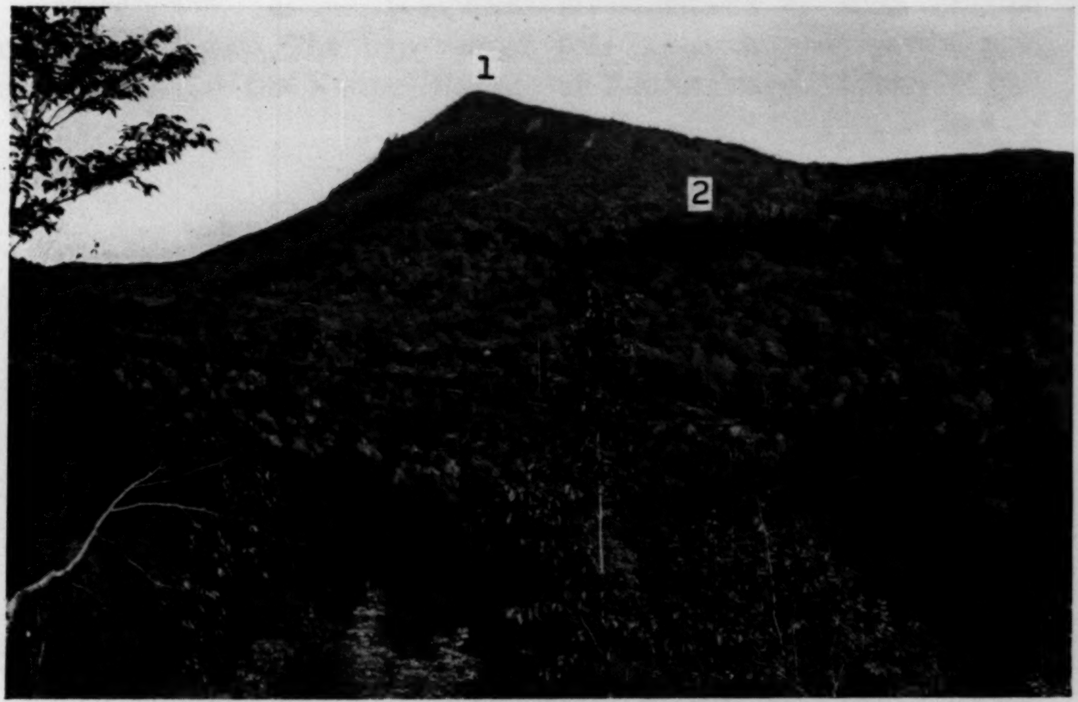

Fig. 8. Sanpōkōjin-san with a fault scarp at its northern side. The gently sloped area is built up of the Mud flow associated with the Torikabuto-yama lava and is displaced down against the Jizō-san lava exposed on Sanpōkōjin-san. The Hanoki-zawa fault runs along the northern foot of this peak and Jizō-san. 1=Sanpōkōjin-san, 2=Zangezaka.

(震研彙報 第三十五号 図版 市村)

the Kannō mud flow ejected in the formation of the Kannō explosion crater. In connection with these activities, the Akakura explosion crater and Suzuritaki explosion crater were opened. The present topography of the Ryū-zan Volcano, therefore, depends on such eruptions and explosions as well as on the subsequent erosions.

(iv) The activities of the Ryū-zan Volcano are likely to have successively repeated in the pre-historic time in concert with other parts of the Zaō Volcanoes. The first activity is supposed to have started in the beginning of the Quaternary, as can be inferred from those of the Aoso Volcano and Byōbu Volcano. There is, however, still no exact evidence to confirm the relationship between the Ryū-zan Volcano and Gando Volcano rising up within a short distance, although they erupted on the eroded surface of similar base rocks.

Acknowledgements

The writer wishes to express his appreciation to Dr. N. Nasu, Dr. H. Tsuya and Mr. T. Watanabe whose kindness facilitated greatly his field and laboratory works. Thanks are also due to Mr. F. Hori for his co-operation in the petrographical investigations of lavas erupted from this volcano. The expense of this research was partly paid from the fund for the Natural Science of Educationary Ministry.

---

28. 蔵王火山の地質学的研究 (第 4 報)

山形大学 市 村 毅

蔵王火山群の北端には竜山火山がある．この火山は竜山と鳥兜山とよりなり，花崗岩（花崗閃緑岩），新第三系，これ等を貫く火山岩または新第三系に伴う各種熔岩などを基盤岩として，その上に盛上り，火山体は竜山熔岩（橄欖石複輝石安山岩または含橄欖石複輝石安山岩）及びその集塊岩，鳥兜山熔岩（橄欖石複輝石安山岩または含橄欖石複輝石安山岩）及びその泥流，酢川泥流，神尾泥流などにより構成されている．

火山活動は，竜山熔岩及び集塊岩の噴出に始まり，竜山火山の主要なる部分は，このとき築き上げられたものと思われる．これに続いて，鳥兜山熔岩や泥流が旧噴火口の南東側或は側面から供給され，その後，高湯爆裂火口，神尾爆裂火口が生ずるに当つて，酢川泥流と神尾泥流とを順次に流出したもののようである。その他，赤倉爆裂火口や硯滝爆裂火口も引続き生じたが，これらには，泥流を伴わない。こうした相次ぐ爆発と爆裂火口生成のために，竜山火山は破壊されて旧態を失い，現在見られるような山容を呈するに至つたのである．竜山火山の活動は，隣接する熊野火山や屏風火山などのそれらと第四紀に入つてから，相呼応して行かれたものであり，有史以後の活動は，知られていない．活動の名残りとしては，高湯爆裂火口底から，蔵王温泉に見られるように，強酸性の温泉が多量に湧出している．

the Kannô mud flow ejected in the formation of the Kannô explosion crater. In connection with these activities, the Akakura explosion crater and Suzuritaki explosion crater were opened. The present topography of the Ryû-zan Volcano, therefore, depends on such eruptions and explosions as well as on the subsequent erosions.

(iv) The activities of the Ryû-zan Volcano are likely to have successively repeated in the pre-historic time in concert with other parts of the Zaô Volcanoes. The first activity is supposed to have started in the beginning of the Quaternary, as can be inferred from those of the Aoso Volcano and Byobu Volcano. There is, however, still no exact evidence to confirm the relationship between the Ryû-zan Volcano and Gandô Volcano rising up within a short distance, although they erupted on the eroded surface of similar base rocks.

Acknowledgements

The writer wishes to express his appreciation to Dr. N. Nasu, Dr. H. Tsuya and Mr. T. Watanabe whose kindness facilitated greatly his field and laboratory works. Thanks are also due to Mr. F. Hori for his co-operation in the petrographical investigations of lavas erupted from this volcano. The expense of this research was partly paid from the fund for the Natural Science of Educationary Ministry.

23. 蔵王火山の地質学的研究（第4報）

山形大學　市　村　　毅

[illegible]

[illegible]

29. *Seven-Channel Triggered Magnetic Tape Recorder for Routine Seismic Observations.*

By Syun'itiro OMOTE and Yoshio YAMAZAKI,

Earthquake Research Institute.

(Read 18, Dec., 1956—Received June 30, 1957)

1. Introduction

A new equipment for recording earthquake motions by means of a magnetic tape recorder named MATS–1 was completed some four years ago. Since then routine seismic observations by means of this tape recorder equipment has been made continuously with success and fairly satisfactory records of earthquakes have been accumulated.

As will be seen in the previous paper[1] the equipment then constructed was a machine having only one component. Needless to say it is preferable, or even necessary, to have a three-component seismograph for recording a complete set of seismic signals. And the first type recorder seismograph MATS–1 was not very satisfactory in that it had only one channel. We were anxious to have a multi-channelled seismograph of a magnetic tape recorder system. By the benefit of the institutional research fund awarded to our Institute by the Ministry of Education, we were able to have a chance to construct multi-channelled one. A seven-channel magnetic tape recorder seismograph MATS–2 for routine use was constructed and put in operation recently. The characteristics of this machine will be described here somewhat in detail.

2. General construction of the equipment

In order to make the explanation simple the construction and the works of the respective unit devices are concentrated in Table I and illustrated schematically in the block diagram in Fig. 1. The appearance of the whole equipment is shown in Fig. 2.

Ground vibrations due to seismic shocks are converted into a signal voltage through a seismometer and the signal voltage is connected to the

1) S. OMOTE, S. MIYAMURA and Y. YAMAZAKI, *Bull. Earthq. Res. Inst.*, **33** (1955), 397.

Table I. Constructions and works of each unit.

Unit	Electric power controller	Preamplifier	Direct-coupled amplifier	Modulation unit	Demodulation unit
Construction	1. AC 100-volt switch. 2. Cut-off relay for main power. 3. Alarm circuit in the case of emergency.	1. 12AX7. 2. Connection tester of the seismometer line. 3. Input tester terminal.	1. 12AT7, 12AX7.	1. 6J6, 12AU7.	1. 12AX7, 6AU6, 12AU7×2.
Works	1. On and off of the main power line. 2. Automatic cut-off of the main power line when (1) the tape is broken, (2) some troubles took place in any part of the power unit, (3) the voltage of the power line dropped below 80 volts.	Amplification of output voltage from a seismometer.	Amplification of output voltage from the preamplifier.	Pulse width modulation. Carrier frequency is 800 cps. Fluctuation is less than 0.8 cps.	Demodulation of the modulated seismic signal.
Channel	1	7	7	7	7
Type		CR-coupled low frequency amplification.	Cascode type connection.	Pulse width modulated system.	
Gain		28 db.	37 db.	Maximum modulation is attained at 80% of total width	90 db.
Input		Non-distortion range 50 μV–1.3 mV at the full gain (10 cps).	±D.C. 30 mV. (maximum)	±D.C. 7.0 V.	235 μV.
Output current		±D.C. 50 μA–1.3 mA.	±D.C. 0.51 mA.	±D.C. 0.7 mA.	±D.C. 0.78 mA.
Remarks					

Unit	Amplifier for preservation magnetic tape recorder	Regulator unit for recordings	Oscillograph	Magnetic tape recorder with loop tape	Preservation tape recorder
Construction	1. 12AU7, ½12AU7.	1. Trigger circuit. 2. Delay circuit for recording time regulation. 3. Counter. 4. Test button.	1. Galvanometer, 100 cps. 2. recording camera. 3. Tuning fork 100 cps.	1. Recording heads of 4 traces; 2 banks. 2. Play back heads of 4 traces; 2 banks. 3. Erasing head connected with 30 KC oscillator. (5Y3, 6V2×2) 4. Contact relay that alarms tape break.	1–3, The same to the left column.
Works	Applies the pulse width modulated signals on to the recording head of the preservation magnetic tape recorder.	1. To make start the recording motors. 2. To regulate the time during which the recording are performed. 3. To indicate the number of recorded earthquakes. 4. To monitor the works of the every parts.	Photographed on a bromide paper.	1. Recording. 2. Playing back. 3. Erasing.	1. Recording.
Channel	7	1	13	1	1
Type	CR-coupled amplification.	C-R coupled low freq. amplification Delay circuit by charge and discharge system.	Electromagnetic damping.	Tape width; 1/2 inch endless tape; speed 7.5 in/sec. Wow less than 0.3%.	Wind up system.
Gain	20 db (variable).	80 db (variable).	5.5×10^{-5} A/mm.		
Input	3.5 V			Input to the recording head is 14.0 V.	
Output	14.0 V	AC 100 V		Output from the play back head is 235 μV. Tape noise; ca.50 μV.	
Remarks			paper speed; 30 mm/sec.	S/N; 38–40 db.	

input of the preamplifier. From there it is led to the main amplifier before reaching the modulation unit. The square waves of a symmetric

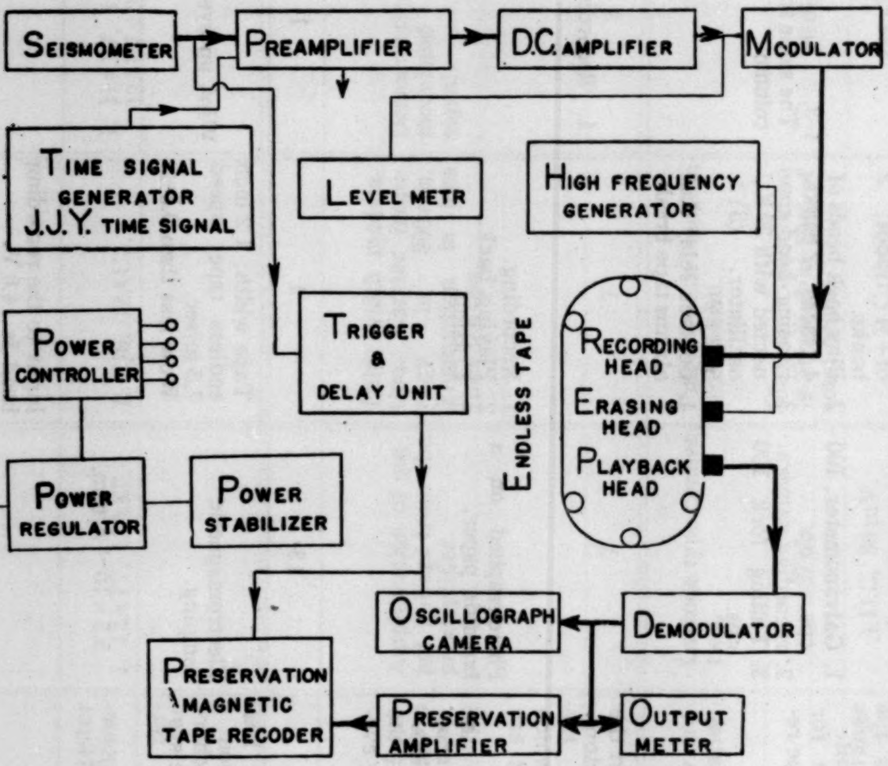

Fig. 1. Block diagrams of the equipment.

type generated by a pulse generator with a frequency of 800 cps are used as carrier waves for modulation. When modulation takes place the width of the pulse of the square carrier waves is changed by the output from the main amplifier which is connected to the original seismic signals, in such a way as the positive information signal causes the positive current pulses to decrease, and likewise the negative information signal causes the negative current pulses to decrease. The amount of change in width depends upon the amplitude of the seismic signal, a large amplitude signal causing the width to vary greatly. When the high frequency information signal is applied the width of the pulses is changed at a high rate of repetition depending upon the modulation frequency, the time rate of changing of the pulse width is regulated by the frequency of the input waves.

This pulse width modulated seismic signal is subjected to additional stages of gain, and then connected to the recording head, where it is

recorded on the magnetic tape running with the constant speed of 7.5 inches per second. The tape is endless, i.e. in loop form. The seismic signal recorded on the tape reaches the playback head 40 seconds later after having passed over the recording head. The output voltage taken out of the playback head is divided into two. One part is lead to the oscillograph after passing through the demodulator, where the pulse width modulated seismic signal is demodulated into the original signal of low frequency. These low frequency seismic waves cause the galvanometer in the recording oscillograph to vibrate and the seismic curves are photographed on the bromide paper. The other part of the output voltage from the playback head is led to the recording head of the preservation magnetic tape recorder after passing through an amplifier, and here seismic waves are recorded on the magnetized tape. The erasing head is placed immediately before the recording head so that all the information recorded on the tape will be erased completely and the tape supplied to the recording head will always be a clean one. The erasing is effected by the high frequency current of 30 KC applied to the erasing head. In this way the endless tape goes round continuously.

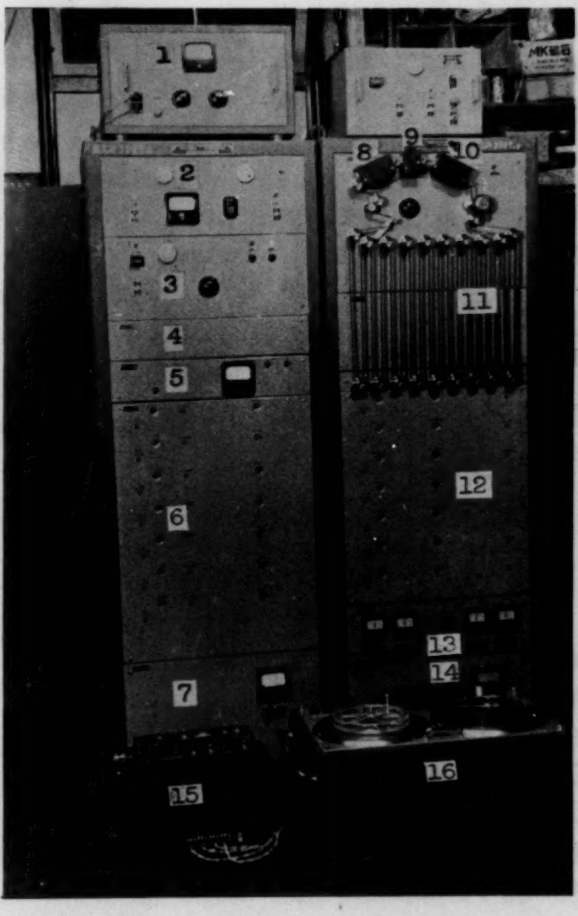

Fig. 2. 1. Preamplifier. 2. Power controller 3. Recording time controller. 4. Trigger unit. 5. Level meter. 6. D.C. Amplifier and modulator. 7. Power unit. 8. Playback head. 9. Erasing head. 10. Recording head. 11. Endless tape. 12. Demodulator. 13. Output meter. 14. Power unit. 15. Recording oscillograph. 16. Preservation magnetic tape recorder.

Besides these devices several additional units are necessary, including a trigger circuit which makes start the recording oscillograph and the preservation magnetic tape recorder as soon as earthquake motions

arrived at the place where the seismometers are installed. There is also a reset circuit in order to stop the operation of the oscillograph and the preservation tape recorder when the seismic vibration of the ground has died away and then to reset everything for the next recording. Some other accessories are also attached, such as time-marking devices for the accurate commencement time of the earthquake motions, stabilization circuits for the power supply, a level meter to indicate input level, a counter device that announces the number of earthquakes registered on the recording equipments, an alarm device that announces the occurrence of troubles in any part of the equipments, and the relay mechanism that cuts off the power source in the case of emergency.

3. Details of the unit devices

a) *Preamplifier*. The seismic signal is taken from a seismometer and connected to the input of the preamplifier. From there it goes on to the direct-coupled amplifier. In the preamplifier two stages of the CR-coupled system are employed. The gain of the two amplifier stages is changeable, the maximum being 28 db. The tubes used are 12AX7. The amplification looks rather low considering the large number of the tubes used. This is due to the fact that the amplified voltage is lowered to 50 : 1 at the last stage in order to make it match better with the impedance of the direct-coupled amplifier.

In the pannel of the preamplifier there are also housed the test terminals used for adjusting the amplification and the tester circuit that checks the continuation of seismometer lines.

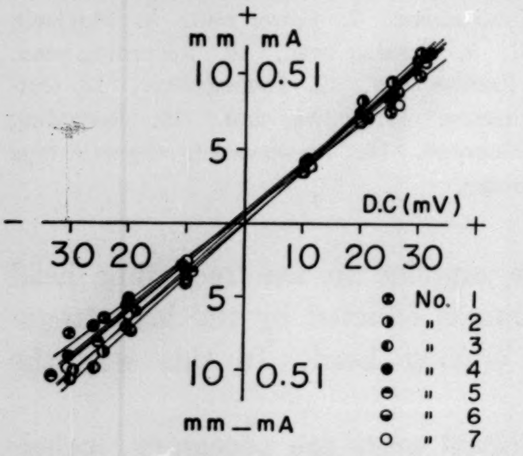

Fig. 3. Characteristic curves of direct-coupled amplifier, that indicate input voltage and output current relations.

b) *Direct-coupled amplifier*. The second unit is a direct-coupled amplifier. For the purpose of getting a good signal-to-noise ratio a Cascord system is employed. The maximum gain obtainable is as high as 37 db. The output signals from the preamplifier are amplified by a tube 12AT7 (V_1). The voltage due to R–8 is applied to the first grid of

12AX7 (V_2), by which the amplitudes of the pulse voltage generated in the R12 are regulated. The gain of the D.C. amplifier fluctuates with the fluctuations of the line voltages of the power line. This disadvantage, however, in practice only slightly affects the gain of the diret-coupled amplifier, provided the commercial 100-volt AC current is well stabilized. The characterstic curves of the direct-coupled amplifier units are shown in Fig. 3 with respect to each of the seven channels.

c) *Modulator*. As is well known the frequency of earthquake waves is so extraordinarily low that signal voltages from the seismometer will not be recorded directly on the magnetic tape. In order to overcome this difficulty a modulation system is introduced. In the former equipment a frequency modulated system was employed, while, in the present equipment the pulse width modulated system (PWM) was employed. The PWM has advantages over other types of modulation system in that:

(1) It works in good stability.

(2) Electric circuits are simple.

(3) The tape speed needs not be held so uniform as in the FM system.

However, it also has disadvantages in that: (1) the connecting part of the loop magnetic tape leaves a distinct mark on the seismic record and (2) a somewhat higher tape speed is required than that of other modulation system. As long as the FM system is employed, the fluctuation of 0.5% in the tape speed produces the change of cycles by 2–3% in the carrier waves of 800 cps. Namely, in the FM system the output is directry proportional to the velocity of the recording medium such as tape, so the tape velocity must be kept at a strictly uniform rate in order to have a good signal-to-noise ratio. In the case of PWM no such strict uniformity in the tape velocity is demanded.

In a pulse width modulated system, as in the other types of modulation, the fluctuation in the center frequency of the carrier waves presents a serious problem with respect to the accuracy of the recorded seismic signals. In our equipment, however, this fluctuation is successfully reduced to as low as 0.1%. The tape speed, from all these considerations, was determined to be as 7.5 inches per second.

As will be seen in the circuit diagrams in Figs. 4–a and b, the output voltage of the 800 cps generated by the Hartlay oscillator is amplified beyound its saturation point and is clipped. It then passes to the differentiation transformer where the pulses are differentiated. These

differentiated pulses are fed in parallel to the second grid of 12AX7 (V_2) of the respective modulation units of the seven channels. In such a man-

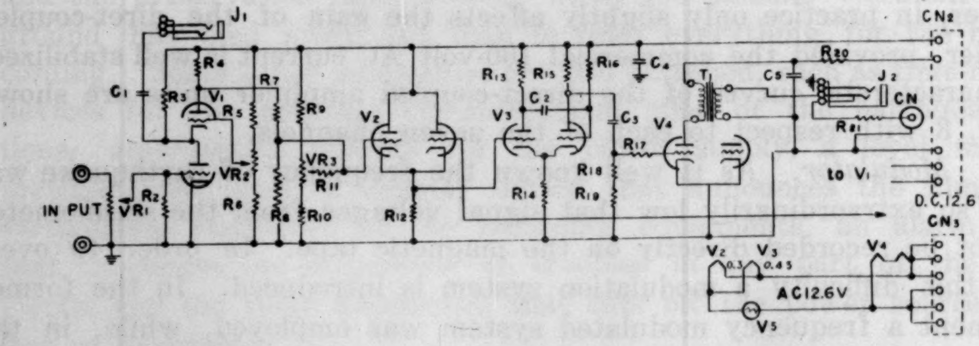

Fig. 4-a. Circuit diagrams of amplifier and modulator.

ner the carrier waves of a regular square form generated in the respective modulation units of the seven channels are controlled by a single source of pulses.

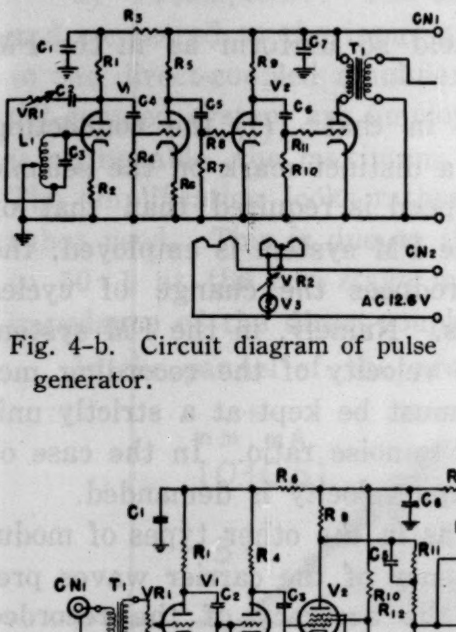

Fig. 4-b. Circuit diagram of pulse generator.

The differentiated pulses fed to the second grid of 12AX7 (V_2) are here mixed with the seismic signal from the output of the D.C. amplifier. The pulse voltage drops between the two ends of the resistor R12 regulate the tube 6J6 (V_3) and the voltage of the square wave type in 800 cps is formed between the two ends of the resistances, R18-R19.

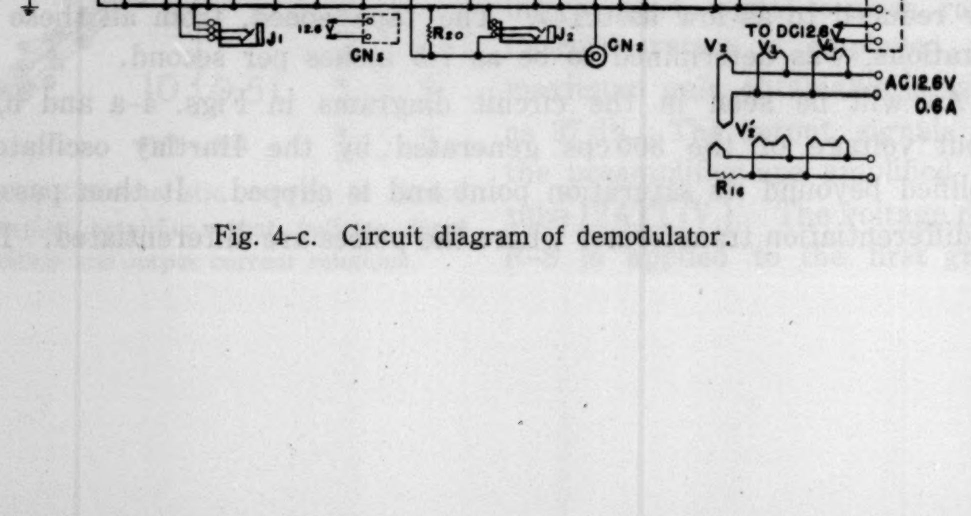

Fig. 4-c. Circuit diagram of demodulator.

Then the pulse-width modulated signals are amplified in their current through the left hand side of the 12AU7 (V_4). These pulses of current are coupled to the recording head through the output transformer connected to the plate of 12AU7 (V_4). The maximum amplitude to be recorded without any distortion modulates the width of the pulse to the depth of 80% of the original width. The non-distortion input voltage to be modulated is 1.2 mV at 10 cps with the full gain of the preamplifier. Modulation and demodulation characteristic curve of a channel is depicted in Fig. 5. In the figure input voltage to the first grid of the direct-coupled amplifier is related to the output current from the demodulator. In preparing the figure the output from the modulator is directly connected to the input of the demodulator, skipping over the units including the magnetic heads and magnetic tape.

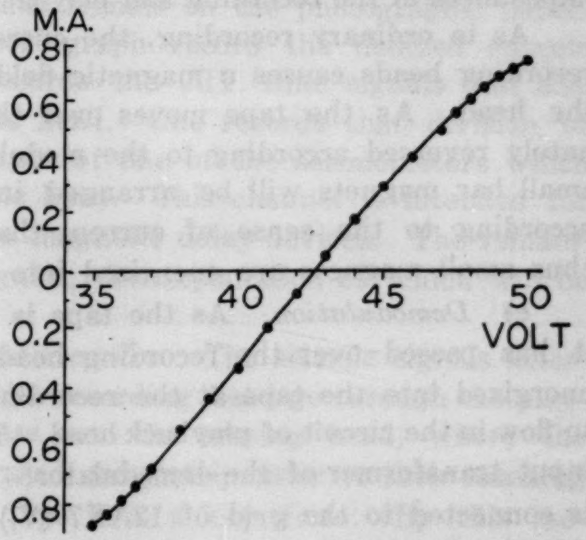

Fig. 5. Modulation and demodulation characteristic curve of a channel. Abssissa in a input voltage to a modulator. Ordinate is the output current from a demodulator. (In this figure the modulator and the demodulator are connected directly, without passing through the magnetic tape.)

d) *Head assembly.* As to the recording head, seven-track units have been designed for a 1/2 inch tape. Two banks of heads are used with four heads per bank, which gives the total number of seven information channels, as the fourth head of the second bank is not used for recording. In order to minimize the cross-talk between the heads, the tracks of the four heads of the second bank are made to fit in the gaps between the tracks of the four heads of the first bank. The seven playback heads are arranged in the same way as the recording heads, namely, they consist of two banks of four heads each and the distance between the two banks of playback heads is adjusted to be the same as that between the recording heads as far as is possible. In practice, however, there is apt to remain some slight difference between the two distances of the respective two banks. This difference, however, can be calibrated very accurately beforehand so that no errors will result

from the arrangement of the banks in calculating the commencement time of seismic signals. The background noise due to the magnetic tape tends to be loud at the tracks on the extreme outer sides of the tape. However, as will be seen in Fig. 10, the tape noise due to the extreme outer tracks disturbs the seismic records only slightly. The impedances of the recording and playback heads are 50 ohms at 1000 cps.

As in ordinary recording, the current passing through the magnetic recording heads causes a magnetic field to be produced in the gap of the head. As the tape moves over the head and the current is alternately reversed according to the modulated pulses applied to the head, small bar magnets will be arranged into the tape in regular directions according to the sense of current that passes through the head, and thus small magnets are energized into the recording tape.

e) *Demodulation.* As the tape is again run over the heads, after it has passed over the recording heads, the magnets which have been energized into the tape at the recording head cause an electric current to flow in the circuit of playback head. This current is then coupled to the input transformer of the demodulator. The secondary of the transformer is connected to the grid of 12AX7 (V_1) and then passes into the 6AU6 (V_2).

In this process, the weak current of blunt square waves from the playback head, being amplified and clipped, becomes free from the wave distortion, and reproduces the same current pulses which are applied to the magnetic recording heads. The gain of the amplifier of this part must be made very large, say 90 db, since the output current from the playback head is very small. In the next stage, as will be seen in the demodulation wiring diagram in Fig. 4–c, these modulated seismic signals are put into the resistance-condenser differentiator. The output signal from this differentiator is than applied to the bistable multivibrator. The signal is then applied to a filter, by which the 800 cps pulses are filtered out; the residue is the original seismic signal. The demodulated and reproduced seismic signal is then applied to a galvanometer of the recording oscillograph.

As has been mentioned, the demodulation circuit is designed to create a high gain so that specially designed shieldings are needed on the input transformer of the unit in order to prevent the ham inductions from outside. For the purpose of checking, there is a jack on each channel leading to a cathode-ray oscillograph, provided it is desired to have a monitor of the output waveforms from the demodulator.

f) *Recording oscillograph.* The demodulated low frequency seismic signals are led to a recording oscillograph of 13 channels. The frequency and the sensitivity of the galvanometer used are 100 cps and 5.5×10^{-5} A/mm respectively. The electric motor that drives the bromide paper in the recording camera is triggered by the seismic pulse and the camera records the seismic signals on the photographic paper. Six of the 13 channels of the oscillograph record the delayed seismic signals mentioned above, one records the JJY time signals that also have passed through the magnetic head. One records that division of the seismic signals from the output of one of the seismometers which did not pass through the magnetic head. This channel is intended for checking the distortion due to the magnetic delay devices. The remaining five channels are for time signals, the explanation of which will be given later.

g) *Preservation magnetic tape recorder.* The seismic signals energized into the magnetic tape at the recording head go through the playback head and a moment later pass onto the erasing head, where the seismic signals in the tape are erased completely prior to their reaching the recording head again, as the tape is in a loop form. By this mechanism the recording head is always supplied with a clean tape. In order to have the seismic signals permanently in the form of recorded magnetic tape it is necessary to have another magnetic tape recoder machine exclusively for the preservation of magnetic tape.

As already stated in the preceding paragraph (e), after the seismic signals are taken out of the playback head and freed from wave distortions, a part of the current pulse of modulated waves are shunted to the amplifier circuit for the preservation magnetic tape recorder unit. The amplified current of the pulse width modulated seismic signals are then applied to the recording head of the preservation unit.

The mechanism by which the recording is made on a preservation magnetic tape is the same as that of the recording part of the endless tape. In this part too an erasing head is placed directly before the recording one. The driving mechanism of the preservation tape is the wind-up system, not the endless system. In this case too special care must be taken for the geometrical configurations of the relative position of the two banks of magnetic heads. In practice, careful calibrations on the time difference of the two different banks will eliminate any remarkable error in the reading of the seismic phases. The operation of this part is controlled in the same way as with the recording oscillograph. The starting

of the winding up of the tape reel is triggered by the seismic pulse, and its stopping is effected by the function of the control unit.

h) *Delay unit*. The memorizing capacity, one of the greatest advantages of the magnetic tape recorder seismograph, is attained by the recording of seismic signals on the magnetic tape. The length of the time during which the memory capacity will last is controlled by the delay unit. In this delay unit the delay time is given by the running time of the tape from the recording head to the playback head. In the former equipment, MATS-1, there was a special storing box of magnetic tape prepared for the purpose of giving a long delay time. In the present equipment, however, on the one hand, the tape is twice as broad as the former one and, on the other hand, the tape speed too is twice as fast as that of the former one, so that the storing box is no longer applicable. For the purpose of elongating the running course of the endless tape, as will be seen in Fig. 2, a simpler but surer mechanism consisting of twelve rollers is employed. By this mechanism we can have the delay time of forty seconds successfully. In such a mechanism the rotation friction of the rollers must be made extremely small in order to have the tape run smoothly.

There may be varying opinions as to what is the proper length of the delay time. The driving of the motor of the recording camera of the oscillograph and of that of the preservation magnetic recoder, reaches its full force less than a few seconds after the trigger circuit is closed. The delay time might be made very short, provided the trigger starts exactly at the beginning of the P waves of seismic signals. However, as is well known, the beginning of the P is in some cases so small in amplitude that if we adjust the trigger level so high as to be sensitive enough to catch it, a false start may frequently be caused by the ground noises that are so common especially in large cities. In order to avoid this confusion it would be safe so to design the trigger circuit that it will start at the beginning of the large S phase. For this reason the delay time should be made longer than the P–S time of the earthquakes to be recorded. In designing this equipment we at first aimed at recording near-by earthquakes and chose a delay time of about 40 seconds. It will not be difficult to elongate the delay time by more than 50% by adjusting the locations of one or two rollers.

i) *Control unit*.

(i) Trigger amplifier. The input voltage to the trigger amplifier is derived from a seismometer installed side by side with the recording seismo-

meters. As soon as the input voltage from the trigger seismometer exceeds some definit level, a pulse is sent out from this amplifier (Fig. 6).

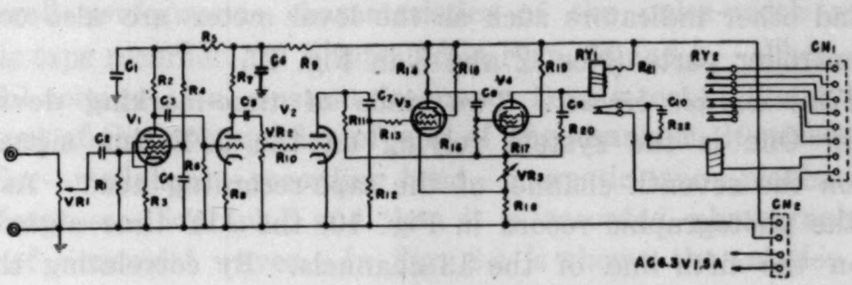

Fig. 6. Trigger circuit diagram.

In order to avoid the false starting due to ground noises the trigger level is carefully adjusted. With respect to the seismometer used, the input level that makes the trigger start is adjusted at about 3 mV, at 10 cps, namely, 0.5 gals at 10 cps of ground accelerations (Fig. 7). The electric pulse issuing from the trigger amplifier puts the following circuits into action: (1) It makes the electric circuit of the motor that drives the recording camera of the oscillograph close. (2) It makes the circuit of the driving unit of the preservation magnetic recorder close. (3) It makes the electric circuit of the recording time controller close. (4) It makes the counter and alarm circuits close.

(ii) Recording time controller circuit. This unit controls the time during which the recording camera and the preservation magnetic tape recorder are in full operation. The output pulse from the trigger amplifier makes start the delay circuit consisting of the tubes, the circuits consisting of the mechanical relays, and the combinations of these circuits, and as a result of such operation the driving of the motors of the camera and of the tape recorder are made to stop automatically. The operation time is adjusted at 1, 2, 3 and 4 minutes respectively. As soon as the recording is completed the whole equipment is reset for the next recording.

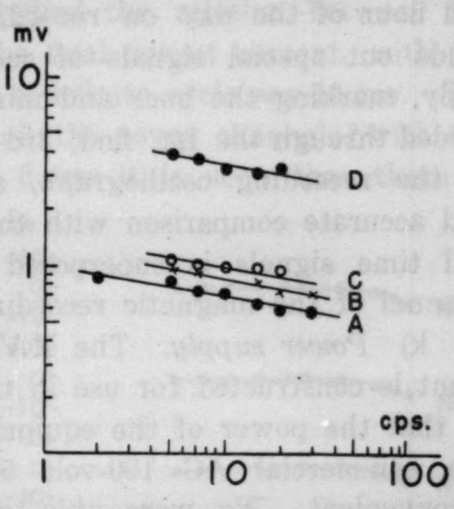

Fig. 7. Diagram indicating the trigger level. Indicator points the graduation D; No. 4, C; No. 6, B; No. 8, A; No. 10 (maximum sensitivity).

(iii) Auxiliary devices. Besides these units mentioned above, some auxiliary devices such as the counter for the number of recorded earthquakes and other indicators such as the level meter are also contained in the controller parts (Nos. 2 and 3 in Fig. 2).

j) *Time marker circuit*. Two kinds of time-marking devices are employed. One is the system relying on the JJY time signals fixed directly on the seventh channel of the tape-recording head. As will be seen in the photographic record in Fig. 10, the JJY time signal is recorded on the fifth line of the 13 channels. By correlating this time signal line with the lines of seismic waves recorded side by side on the same paper, it is easy to have the accurate commencement time of the recorded earthquake with reference to the second. There is no knowing, however, what minute and what hour of the day this second mark or even the minute mark due to the JJY time signal left on the record represents, since it is only for three or four minutes that seismic recordings usually last. For the purpose of giving the standard minute and hour of the day on record, a standard clock is employed which sends out special signals of seconds, minutes, and even hours unceasingly, marking the hour and minute of the day. These marks are recorded through the 1st, 2nd, 3rd and 4th channels of the galvanometers of the recording oscillograph, and, at the same time, to give a good and accurate comparison with the time mark of JJY, a part of this special time signals is superposed to the JJY time mark on the seventh channel of the magnetic recording head.

k) *Power supply*. The MATS-2 type magnetic tape recorder equipment is constructed for use in the routine observation of earthquakes, so that the power of the equipment needs to be supplied entirely from the commercial AC 100-volt 50 cps, for otherwise it would be very inconvenient. We were able to overcome successfully every disadvantage originating from the use of the AC 100-volt, such as fluctuations of the voltage of the source power, the residual ripples which are apt to remain on the rectified heater current of the tubes etc. by some means or other.

When the main switch of the power supply is closed artificially, all the circuits are closed one by one automatically in due order and all the conditions are automatically fulfilled for the next recording of seismic signals, as long as the power is supplied. These processes are shown in Table I.

4. Overall characteristics

Overall performance characteristics of the pulse-width modulated magnetic tape recorder are illustrated in Figs. 8a and b. When a known sinusoidal voltage of a constant frequency from a test oscillator is applied to an input of the preamplifier of one of the channels, it passes through "amplifier—modulator—recording head—magnetic tape—playback head—demodulator—oscillograph" and then it is recorded photographically in a form of sinusoidal waves. In Fig. 8-a is shown the relation between the input voltage and the recorded amplitude of the sinusoidal waves with respect to different frequencies. From this figure we see that the difference in the frequencies exerts little effect on the output amplitude within the range from 14 to 50 cps, while for higher frequencies it appears that the sensitivity begins to decrease. With respect to any other of the seven channels, as will be seen in Fig. 8-b, a like curve is to be obtained.

Then in the next place has been studied the relation between the input current and the amplitude of the final output current, with the frequency of the input signals fixed at a definite cycle say 14 cps. The relation has been studied with each of the seven channels, with the result illustrated in Fig. 9. From the figure it is seen that there is

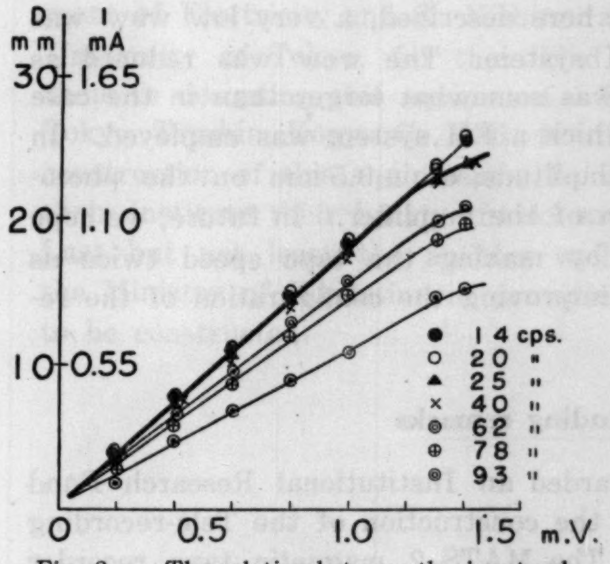

Fig. 8-a. The relation between the input voltage and the recorded amplitude with respect to different frequencies.

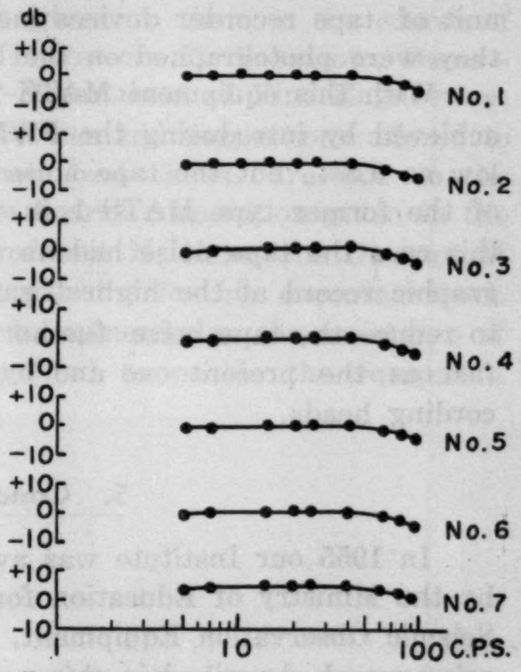

Fig. 8-b. Over-all frequency characteristics.

some difference 20% at the maximum, in the sensitivity of the seven channels. This difference, however, seems to originate not from any system of the magnetic tape recorder, namely modulation, magnetic tape, or demodulation parts, but from the difference of sensitivity or of frequency characteristics of galvanometers.

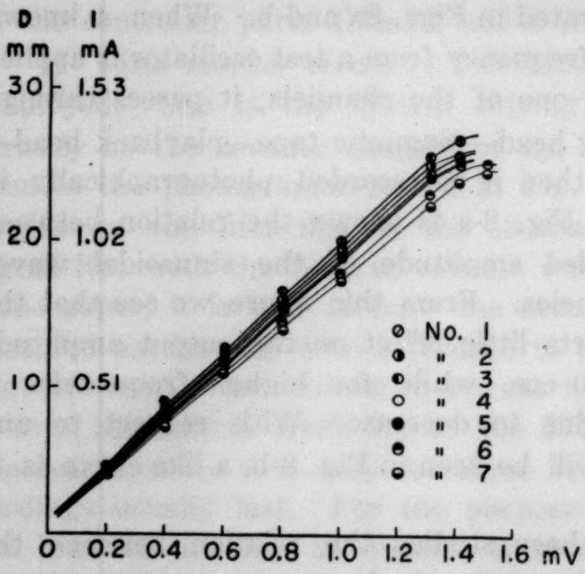

Fig. 9. Relation between the input voltage and the recorded amplitude of different channels at a fixed cycle, 14 cps.

As the examples, the records of a test oscillator and of ground noises photographed on a bromide paper are reproduced respectively in Fig. 10 a, b, as the final product of the magnetic rape recorder equipment. In preparing the records, the output voltage from a test oscillator and a seismometer due to ground noises were applied in parallel to the inputs of the preamplifier of the seven channels, and then the input signals were passed through every unit of tape recorder devices including the magnetic tape, and finally they were photographed on the bromide papers.

With this equipment MATS–2 here described, a very low wow was achieved by introducing the PWM system. The wow was reduced as low as 0.3%, but the tape noise was somewhat larger than in the case of the former type MATS–1, in which a FM system was employed. In this case the tape noise had an amplitude of ± 0.5 mm on the photographic record at the highest gain of the amplifier. In future, we hope to reduce the tape noise further by making the tape speed twice as fast as the present one and by improving the configuration of the recording heads.

5. Concluding remarks

In 1955 our Institute was awarded an Institutional Research Fund by the Ministry of Education for the construction of the Tele-recording Seismic Observation Equipment. The MATS–2 magnetic tape recorder seismograph described in this paper has been constructed as a recording part of the said equipment. The wireless part was constructed by

Miyamura and others[2] as reported in the preceding Bulletin.

By means of this MATS-2 the behaviour of the ground vibration due to seismic shocks is now recorded through six seismometers. The seismometers are now installed so as to register the earth movement in terms of three components at two different locations.

The photographic record to be obtained by the MATS-2 has a great advantage over other types of seismic records in that the paper speed is more than ten times as fast as in ordinary types of seismometers, while the consumption of bromide paper is only as little as one-tenth or even one-hundredth of the amount consumed on other typed.

The seismic signal recorded on tape will be of unlimited usefulness. It is permanently available in the same live electrical form in which it was recorded. A played-back record coupled with a filtering circuit will be especially advantageous for the further analysis of seismic waves. Moreover the reproducible seismic signals recorded on a magnetic tape will be found ready for repeated analyses by whatever new analytical techniques that may be evolved in future.

6. Acknowledgement

The authors wish to express their gratitude to Assistant Professor S. Miyamura for his earnest support given to them in the course of this study. Thanks are also due to Professors H. Sakamoto, Department of Electricity and G. Nishimura, Department of Fine Engneering, University of Tokyo, for their kind advices and suggestions offered to them in designing this equipment. Their best thanks are due to the Tokyo Tsushin Kogyo Co. Ltd. for the hearty cooperation given in the construction of this equipment. To Professor N. Nasu, the Director of their Institute their hearty thanks are also due for his encouragement. Last but not least the authors wish to acknowledge the assistance of the Ministry of Education in providing fund to enable the equipment to be constructed.

2) S. Miyamura and M. Tsujiura, *Bull. Earthq. Res. Inst.*, **35** (1957), 381.

29. 磁気テープ利用遅延記録方式による 7 素子地震動常時観測装置

地震研究所 表 俊一郎
山崎良雄

磁気録音テープを利用する遅延記録方式地震動常時観測装置はすでに数年前に試作せられ，今日迄観測がつづけられてきた．しかしこの時は 1 成分のみの記録装置であつたために実際の地震観測装置としては極めて不充分なものであつた．今回機会を得て 7 素子による磁気テープ遅延記録方式による地震動常時観測装置を完成したのでここにその概略を報告した．本機の構成は第 1 図の blockdiagram 及び第 I 表に見る通りである．前回のものとくらべ改良された主な点は (1) channel 数を 7 とした．(2) channel の数が増加したのでテープ幅を 1/2 吋とした．(3) 前回には変調方式として周波数変調を用いたが今回はパルス幅変調をとりいれることとした．(4) テープ送り速度を 7.5 吋/秒と前回より早くした．(5) 刻時装置を改良し正確な発震時が記録せられるようにした．等である．テープの幅が大きくなり，又 speed も早くなつたので遅延時間を長くすることには困難が伴つた．前回のように箱の内にためる方式は利用できなくなつたので沢山のローラーを用い，テープの走行距離を延長させるようにした．現在は遅延時間 40 秒で運転されているが，この機構でも 1 分位迄遅延時間を延長することは容易である．

常時観測を目標とするので電源には全て 100 volt 交流を利用している．従つて電源電圧の変動等により妨害せられないよう充分注意して構成されているばかりでなく，運転中に発生するかも知れない種々の故障に対してはそれぞれ警報又は自動停止装置が働作するようになされている．

録音ヘッド相互の cross-talk はほとんど認められない．PWM を採用したのでテープ回転ムラによる影響もきわめて少ない．しかし全体として tape noise による影響は前回の 1 成分のものより少し大きいようである．

本機は完成してからまだ日が浅いが故障なく観測がつづけられている．

オシログラフに記録される地震動の paper-speed は 30 mm/sec であるので地震動の解析には大きな利用が期待される．paper-speed が早いにもかかわらず記録が遅延方式であるのでブロマイド紙の消費は極めて少なくてすむのも本機の大きな特徴の 1 つである．なお，テープとして保存される地震動記録は今後ますます利用の途がひらかれることと期待せられる．

昭和 30 年文部省機関研究費として本所に「無線式無人地震計による精密地震観測法の研究」の費用が交附せられた．この研究において無線搬送による地震動電送部分は宮村その他により研究が行われ，すでに本所彙報に報告せられている．本機はこの機関研究の記録部分として製作せられたものである．

本装置の開発にあたつては東京通信工業株式会社の労力に負うところが多いので特にしるして感謝の意を表したい．また本所宮村助教授からあたえられた援助に対して厚く感謝する．本機の経費は文部省機関研究費に負うものであり，当局に厚く感謝の意を表したい．なお，本機関研究を遂行するにあたり有益な助言をあたへられた東京大学工学部西村源六郎教授，坂本捷房教授に感謝を捧げる．終りに本研究に対し終始支持と激励とをあたえられた那須所長に感謝する．

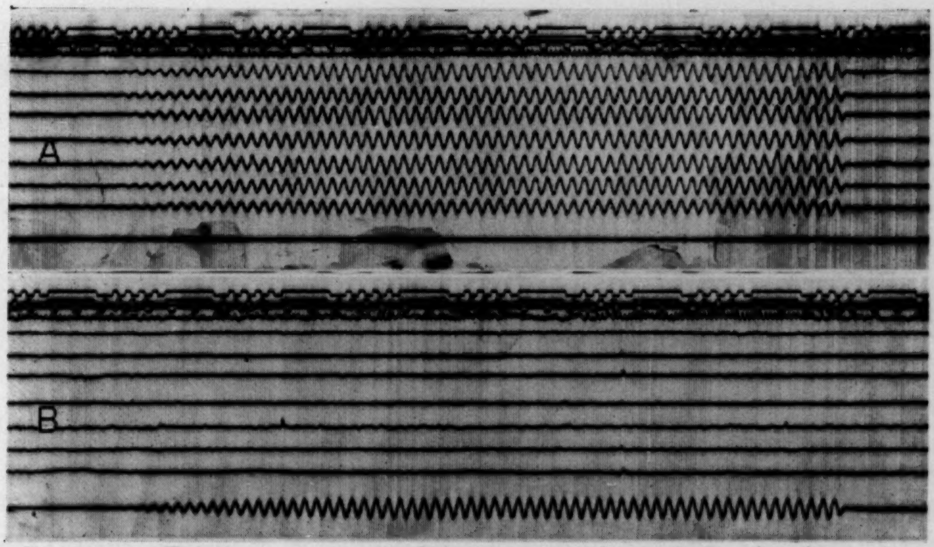

Fig. 10-a. Fidelity test record of the tape recorder system. An alternating voltage is applied in paralell to the seismometer terminal of respective seven channel. (1/4 the actual)

A; a record passing through the entire units, including the magnetic delay unit.

B; a direct record through the amplifier without passing through the magnetict tape. (B is recorded on a bromide paper 1.2 m ahead to A)

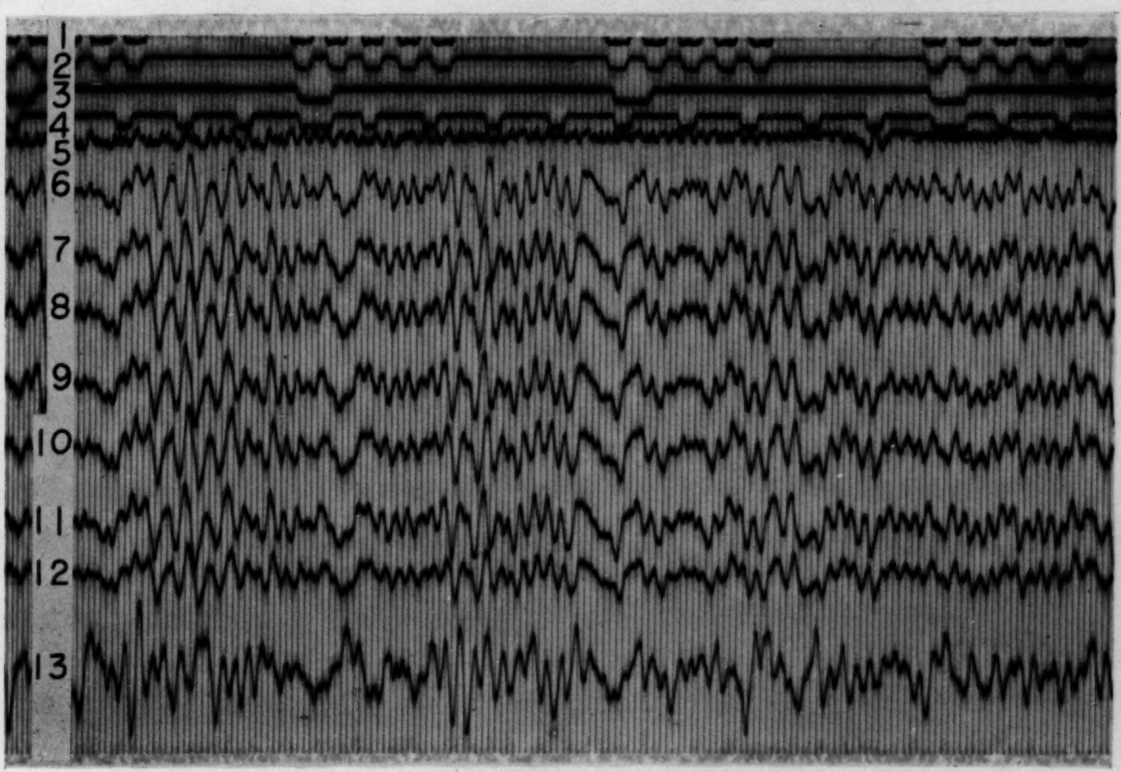

Fig. 10-b. An example of a record of the ground noise. The output voltage from a seismometer is fed in paralell to the seven channels of the magnetic tape recorder. (2/3 the actual)

Traces 1–4; time marks for second, minute and hour.
5; time mark from JJY time signal.
6–12; records of ground noise.
13; a direct record of ground noise, skipping the magnetic tape unit.

30. *Earthquake Observations in Kawasaki and Turumi Areas and the Seismic Qualities of the Ground.* (*Part II*).

By Syun'itiro OMOTE, Shauzow KOMAKI
and Naoyoshi KOBAYASHI,

Earthquake Research Institute.

(Read May 28, 1957.—Received June 30, 1957)

1. Introduction

In our previous paper[1)] we analyzed the seismograms obtained at nine observation stations in the Kawasaki and Turumi regions, a short distance to the south of the Tokyo area, and discussed the seismic qualities of the ground of nine locations where the seismometers were installed. In grading the seismic qualities of the ground of the respective locations, the vibration characteristic of the Keio Station, station S*, was used as the standard. Referring to this standard station the relative seismic qualities of the ground of the other stations were described.

In the course of our analysis of the seismographic records obtained at the respective stations, we came to the conclusion that station S probably recorded a somewhat larger amplitude because of the high cliff of some 30 meters, near the edge of which the station was situated. In order to give reasonable correction to the amplitude of station S, we hoped to change the standard station from S to another standing on ground with better conditions.

On the other hand, as we stated in the previous paper, the studies of the connection between ground vibration and seismic destruction have mainly been developed in the Tokyo area where many seismic observations had been carried out. In discussing the seismic quality of the ground of these locations, their vibration characteristics were compared with that of the Hongo location where our Institute stands, and by doing so the relative grade of the seismic quality of the locations in the Tokyo area was described. For the purpose of giving wider application to our former study, it is intended in this paper to attempt a

1) S. OMOTE, S. KOMAKI and N. KOBAYASHI, *Bull. Earthq. Res. Inst.*, **34** (1956), 335.
* In the present paper, S stands for the Keio High School instead of S-1 used in the previous paper.

comparison between the vibration characteristics of the Kawasaki and Turumi stations and that of the Hongo observation station, station H*.

The seismic observations at the Hongo station were carried out in the same way as in the Kawasaki and Turumi areas, using the same type of the seismometer to register the same component of the earth vibration and covering the same observation period. Though the commencement of the seismic observation by means of the said seismometer was somewhat later than had been expected, at station H, we could have many seismic records for making a comparative study in relation to those of our previous study. Such seismic records were laid at our disposal by the courtesy of the Observation Branch of our Institute. The present report is the result of interpretations studied with these records.

2. Period interpretations

Of the twelve earthquakes analyzed in detail in our previous paper, three earthquakes, Nos. 10, 36 and 38, were recorded at station H. The histograms due to the vibration periods of these earthquakes are illustrated in Fig. 1. From these were calculated such factors and predominant periods as were defined in the previous paper. These are; the sharpness factor $s_H(N/2)$, the flatness factor $f_H(N/2)$, the predominant period $T_H(N/2)$ due to the larger waves, the predominant period $T_H(A)$ due to the summed-up amplitudes, and the predominant period $T_H(W)$ due to the weighted frequencies. In them the suffix H represents the values of station H.

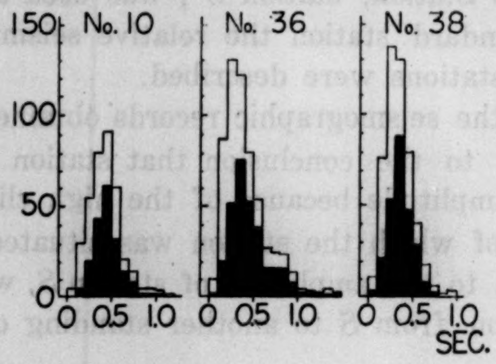

Fig. 1. Frequency histograms whose class interval is 0.1 sec.
White column: Histograms due to all waves.
Black column: Histograms due to larger waves.

The ratio of the value of station S to that of station H is computed with regard to each of these factors and predominant periods. The product is worked out of this ratio and the corresponding characteristic ratios of the respective stations in the Kawasaki and Turumi areas due to station S with the results shown in Table I–a. By this the standard is transfered from station S to station H. The figures in each column in

* H stands for Hongo.

Table I.

a. Characteristic ratios of the seismic quality of the ground.

	H	*S*	*S*-9	*S*-2	*S*-3	*S*-4	*S*-7	*S*-5	*S*-6	*S*-8
S(*N*/2)	1	1.01	1.96	3.06	3.56	3.67	5.28	5.17	4.32	4.13
F(*N*/2)	1	1.14	1.16	1.32	1.60	1.50	1.87	2.00	1.97	1.62
T(*N*/2)	1	1.10	0.94	1.36	1.45	1.61	1.55	1.64	1.68	2.01
T(*A*)	1	1.00	1.08	1.28	1.28	1.30	1.35	1.48	1.38	1.68
T(*W*)	1	1.18	1.18	1.62	1.53	1.65	1.62	1.70	1.68	2.17

b. Orders of characteristic ratios.

	H	*S*	*S*-9	*S*-2	*S*-3	*S*-4	*S*-7	*S*-5	*S*-6	*S*-8
S(*N*/2)	1	2	3	4	5	6	10	9	8	7
F(*N*/2)	1	2	3	4	6	5	8	10	9	7
T(*N*/2)	2	3	1	4	5	7	6	8	9	10
T(*A*)	1	2	3	5	4	6	7	9	8	10
T(*W*)	1	3	2	5	4	7	6	9	8	10

Table I-a have been numbered in order from small to large in Table I-b with respect to each item. Looking at Table I we find that all the characteristic ratios of stations *S* and *S*-9, representing the best seismic quality, have the values of nearly unity. This fact shows that the seismic qualities of these locations are to be ranked at the same grade as station *H*, or at only a slightly inferior grade.

3. Amplitude interpretations

In order to make clear the relationship between the two stations as to the summed-up amplitude, the sums of the amplitudes of all the waves that fall into the respective class intervals of periods were made out in the form

$$A_i = \sum_p a_{i,p} ,$$

where A_i is the summed-up amplitude of the *i*'th class and a_p the element amplitude in the *i*'th class. The summed-up amplitude A_i due to station *S*, denoted here as $A_{S,i}$, was divided by the value of the summed-up amplitude of the corresponding class intervals $A_{H,i}$, of station *H*. The running averages of these ratios were calculated as to every three numbers adjoining in order. The averaged ratios are plotted to the

respective class periods as will be seen in Fig. 2. The larger circle in the figure represents the ratio where the numbers of waves in the denominator is greater than one half of the average number of waves per class. The medium circle represents the ratio where the number of waves in the denominator falls between one half and a quarter of the average number of waves per class. The smaller circle represents the ratio where the number of waves in the denominator is smaller than a quarter of the average number of waves per class. Therefore, it may be said that the smaller circles represent a value less reliable than the larger circles. Looking at Fig. 2, we notice that the amplitude ratios are only slightly bigger than unity with respect to each earthquake throughout the class intervals, and the mean value of these reliable ratios marked by the larger circles is 1.60. Though in some cases there are a few circles representing somewhat larger values than unity in the range longer than 0.6 sec., they are marked by smaller circles that show a low reliability.

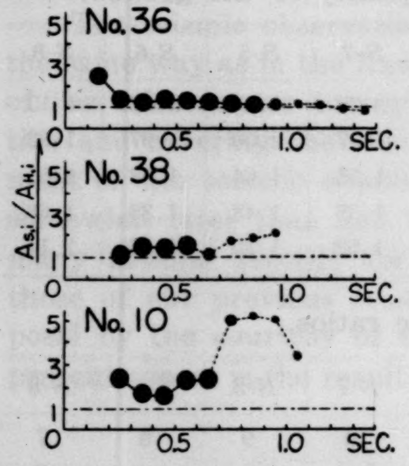

Fig. 2. Period characteristics of summed-up amplitude ratio.

In our previous paper it was noticed that the values of the maximum amplitude ratio of the stations, calculated with station S as the standard did not exceed 2 even in the stations considered to stand on very soft ground. On the other hand, referring to the studies made in the Tokyo area, it is expected that the values of the ratio of the stations which stand on very soft ground are greater than 2. It is one of the purposes of this paper to make clear whether or not station S has recorded too large a maximum amplitude in relation to its firm ground.

Now, the maximum amplitudes at two stations, S and H, were compared with those of eleven earthquakes, Nos. 9, 10, 29, 30, 36, 38, 39, 42, 43, 44 and 54. As a result of the calculation we had the mean value of the ratios of the maximum amplitudes, as

$$A_S/A_H = 1.57 \pm 0.18 ,$$

where A_S is the maximum amplitude of station S and A_H is that of H. It is noticed that this value is nearly equal to that mean value 1.60, calculated from Fig. 2.

Table II. Relation between the maximum amplitude ratio and the thickness of alluvium.

a. Station in Kawasaki and Turumi areas.

Observation station	*S*	*S*-9	*S*-2	*S*-3	*S*-4	*S*-7	*S*-5	*S*-6	*S*-8
Maximum amplitude ratio	1.57	1.05	1.38	2.18	1.62	2.24	2.50	3.09	2.80
Thickness of alluvium (m)	0	5	35	40	45	45	45	70	45

b. Stations in Tokyo area.

Observation station	Sumida	Oshima	Komatsugawa	Higashi-shinozaki
Maximum amplitude ratio	1.62	2.46	2.68	2.90
Thickness of alluvium (m)	30	45	50	66

In our previous paper, maximum amplitude ratios of the respective eight observation stations were calculated with the maximum amplitude of station *S* as the standard. In order to transfer the standard station from *S* to *H*, the figures of the maximum amplitude ratios which were already laboured out in the former paper were multiplied by the value 1.57 obtained above. The relation between these ratios and the thickness of the alluvium at each station is shown in Table II-a and in Fig. 3 with solid circles.

In the period from 1952 to 1954 Miyamura[2] carried out seismic observations at four locations in down-town Tokyo as well as at the Hongo station, using six seismometers with different periods. From his data on the maximum amplitudes and periods recorded by these seismometers, we picked up such amplitudes as were recorded by

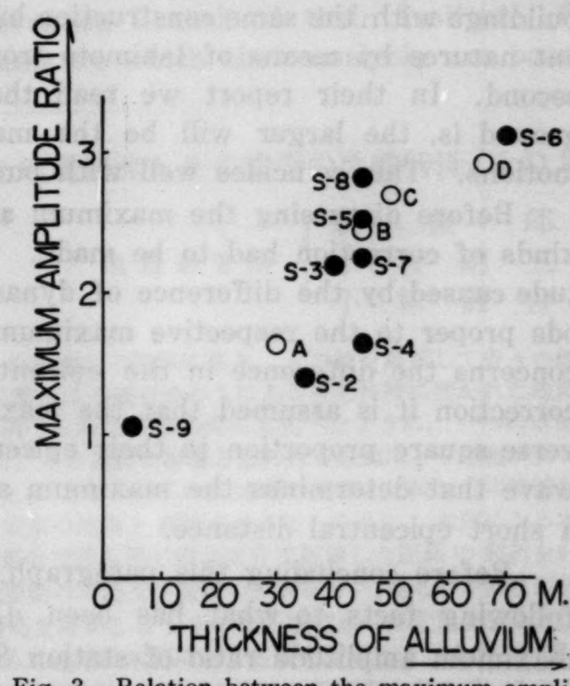

Fig. 3. Relation between the maximum amplitude ratio and the thickness of alluvium.

A: Sumida. C: Komatsugawa.
B: Oshima. D: Higashi-shinozaki.

2) S. Miyamura, *Bull. Earthq. Res. Inst.*, **33** (1955), 512.

Ishimoto tromometers having the oscillation period of one second, and we computed the ratios of the maximum amplitudes of the down-town stations to that of the up-town Hongo station. These maximum amplitude ratios of the stations too were related to the thickness of alluvium[3] at the respective stations in Table II–b and in Fig. 3, with the open circles.

In this figure we can compare the ground conditions of the stations distributed in the Kawasaki and Turumi areas with those of the Tokyo area. Looking carefully at Fig. 3, we notice that the ground conditions of the 1st group of stations in the Kawasaki and Turumi areas, including S and S–9, resemble closely in seismic quality that of station H standing in up-town Tokyo, those of the 2nd group, including S-2, S–3 and S–4, that of the Sumida station in the Tokyo area, and lastly that those of the 3rd group, S–5, S–6, S–7 and S–8, are in good accord with those of such stations as Oshima, Komatsugawa and Higashi-shinozaki, which stand in down-town Tokyo.

Kanai and others[4] made some observations of earthquakes in many buildings with the same construction but standing on the ground of different natures by means of Ishimoto tromometers having a period of one second. In their report we read that the smaller the regidity of the ground is, the larger will be the maximum amplitude of earthquake motions. This coincides well with our result.

Before discussing the maximum amplitude in this paragraph, two kinds of correction had to be made. One is the correction of the amplitude caused by the difference of dynamic magnification due to the periods proper to the respective maximum amplitudes. The other correction concerns the difference in the epicentral distances. In practising this correction it is assumed that the maximum amplitudes decrease in inverse square proportion to their epicentral distances[5] because it is the S wave that determines the maximum amplitude of the earthquakes with a short epicentral distance.

Before concluding this paragraph, it will be of some use to add the following facts to what has been discussed above. One is that the maximum amplitude ratio of station S to station H is smaller than unity as regards earthquakes with the epicentres off the east coast of Honsyu

3) S. OMOTE, *Bull. Earthq. Res. Inst.*, **33** (1955), 479.
4) K. KANAI, T. SUZUKI and S. YOSHIZAWA, *ibid.*, **34** (1956), 61.
5) H. KAWASUMI, *Bull. Earthq. Res. Inst.*, **30** (1952), 319.
C. TSUBOI, *Journ. Phys. Earth*, **5** (1957), 1.

Island of Japan. Another is that the maximum amplitude ratio of station *S* to station *H* is extremely large, 4.05 in the case of earthquake No. 11, with the epicentre in the vicinity of Titibu City in the western mountaineous part of the Kwanto District.

4. Conclusions

Judging from the period and amplitude interpretations studied above, the following results will be summarized.

The stations belonging to the 1st group in the previous paper, *S* and *S*-9 have a seismic quality similar to that of station *H* located in the up-town of Tokyo. The 2nd group including *S*-2, *S*-3 and *S*-4 have a seismic quality similar to that of Sumida station. The 3rd group including *S*-5, *S*-6, *S*-7 and *S*-8 have a seismic quality similar to those of Oshima, Komatsugawa and Higashi-shinozaki stations in the downtown of Tokyo.

The authors wish to express their indebtedness to Professor Takahiro Hagiwara, the Chief of the Observation Branch of their Institute, for the use of the original seismograms on which their analysis was based.

---

30. 川崎鶴見地域9ヶ所で行つた地震観測とその場所の地盤特性(その2)

地震研究所 表 俊一郎
小牧昭三
小林直吉

我々はさきに川崎鶴見地区9ヶ所に置かれた地震計の記録に基き，その波を解析して各々の地震計の置かれた場所の地盤特性を調べた．その際には洪積台地の上にある慶応高校に置かれた地震計の記録を基準として他の観測点の震動特性が調べられた．その時にも述べたように，一つには基準点とした慶応高校が約30mの崖の上にあつて，その崖縁の影響と思われる原因により振幅が少し大きく出すぎるように思われる傾向が見えること，もう一つには，本郷の記録と比較して川崎鶴見地域の地盤をすでにかなりよく調べられている東京の地盤と関連させることの為に，本郷にある本研究所に於て，川崎鶴見地域で用いたと同じ地震計で而も同じ南北成分で観測した記録の解析を行つた．本郷で観測された地震の記録について地震動の周期及び振幅の解析を行い，慶応の周期及び振幅とそれぞれ比を求めることによつて，先に慶応を基準として求めた各観測点の特性比及び最大振幅比を本郷を基準としたものに書き直した，因みに慶応の本郷に対する最大振幅比は，1.57±0.18である．更に宮村は昭和27年−29年に本郷と東京下町とに於て地震の比較観測を行つているので，そのdataを用いて，本郷に対する下町各点の最大振幅比を求めた．このようにして川崎鶴見地域の各観測点と東京下町の各観測点とを関連づけることができた．これらの解析結果につき考察を行い，次のような結論を得た．即ち前に第1群に選定された慶応及びキリンビールは本郷と同様な地盤特性を示し，第2群に属する東芝，味の素，市場は隅田に第3群の鋼管，森永，港湾，埠頭は大島，小松川 東篠崎に対応することが解つた．

Island of Japan. Another is that the maximum amplitude ratio of station S-6 to station H is extremely large, 4.05 in the case of earthquake No. 11 with the epicentre in the vicinity of Itoigawa City in the western mountaineous part of the Kanagawa District.

4. Conclusions

Judging from the period and amplitude investigations treated above, the following results will be summarized.

The stations belonging to the 1st group in the previous paragraph and S-9 have a seismic quality similar to that of station H located in the up-town of Tokyo. The 2nd group including S-2, S-3 and S-4 have a seismic quality similar to that of Sumida station. The 3rd group including S-5, S-6, S-7 and S-8 have a seismic quality similar to those of Oshima, Komatsugawa and Higashi-shinozaki stations in the down-town of Tokyo.

The authors wish to express their indebtedness to Professor Takahiro Hagiwara, the Chief of the Observation Branch of their Institute, for the use of the original seismograms on which their analyses were based.

30. [illegible]

[illegible]

31. 浅間火山前掛山の鏡鉄鉱について

地震研究所 { 南 英一
小 坂 丈 予

(昭和 32 年 6 月 25 日発表—昭和 32 年 6 月 30 日受理)

浅間火山火口西方約 0.5 km, 内側外輪山の前掛山カルデラ崖の内壁にある裂罅状の水蒸気孔に赤鉄鉱 (Hematite) が美麗な結晶をなして産することは古くから知られている[1),2)] (第 1 図).

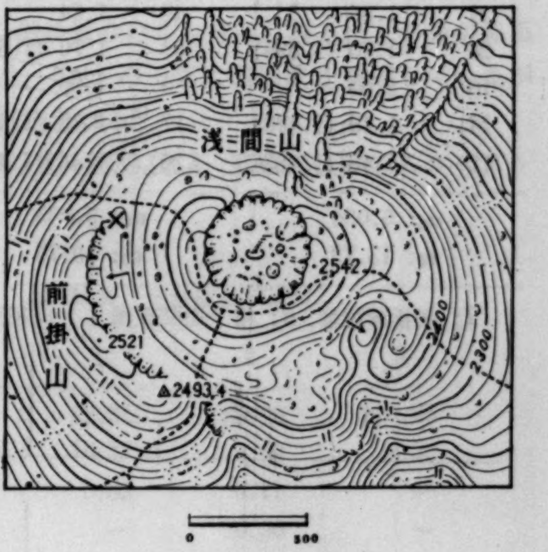

第 1 図 浅間山火口附近
×・・・鏡鉄鉱産地

産状は約 50°C の水蒸気を弱く噴出する複輝石安山岩 (前掛山屏風岩熔岩) の割目の内側に鱗片状の結晶として密生している (第 2 図). その大きさは直径約 3～5 mm, 厚さ 0.2～0.5 mm の六角板状, 鋼灰色, 金属光沢を有するもので鏡鉄鉱 (Specular iron) とも呼ばれ得るものである (第 3 図). しかしその微粉末は暗赤色を呈している.

本試料を東大理学部地質学教室にある X 線ガイガースペクトロメータにより鉄対陰極で測定した粉末廻折像, 及び当研究所に於て撮影したクロム対陰極による X 線粉末写真の結果とから得られた値を綜合して第 I 表に示した. 比較のため理学部鉱物学教室所蔵の岡山県真庭郡川上村の玄武岩の空隙中に産する大きな赤鉄鉱の結晶をも測定した. それによるとこの浅間山産の鏡鉄鉱は赤鉄鉱のほか少量の磁鉄鉱をも含んでいることが判明した[3)]. 第 I 表には参考のために既に報告されている純粋の Fe_2O_3 (赤鉄鉱), Fe_3O_4 (磁鉄鉱) の測定値[4)] をも併せて示したが, その格子面間隔及び廻折線強度は夫々よく一致している. 第 I 表の値を図示したのが第 4 図である. 次にこの赤鉄鉱の格子定数をやや正確に求めるため, 試料に標準となる純粋の金属珪素をまぜて補正を行いながら測定をくりかえした. 得られた値は第 I 表の ( ) の内に示す. その結果から計算した格子

1) 津屋弘逵 地理学 **2** (1934), 1291.
2) 八木貞助 浅間火山 (1936), 197.
3) 磁鉄鉱の廻折線は赤鉄鉱のそれと重複するものが多いので, 多量の赤鉄鉱中に混在している少量の磁鉄鉱の検出は困難であるが, この場合は 2.09 Å の廻折線の現出から磁鉄鉱の存在を確認した.
4) A.S.T.M., *X-Ray Powder Diffraction Card-Indices.*

第 I 表　X 線 粉 末 廻 折 線 表

浅間山産		川上村産		Fe_2O_3			Fe_3O_4	
I	*d* Å	*I*	*d* Å	*hkl*	*I*	*d* Å	*I*	*d* Å
							6	4.85
26	3.69	28	3.68	102	28	3.68		
13	2.99						28	2.97
66	2.71 (2.698)	100	2.70 (2.699)	104	100	2.69		
61	2.52 (2.517)	53	2.53 (2.518)	110	75	2.51	100	2.53
6	2.44						11	2.42
22	2.21 (2.205)	20	2.21 (2.208)	113	18	2.20		
5	2.09						32	2.10
21	1.85	49	1.84	114	63	1.84		
26	1.70 (1.694)	58	1.70 (1.695)	116	63	1.69	16	1.71
10	1.60	9	1.60	212	13	1.60	64	1.61
14	1.49 (1.486)	17	1.49 (1.485)	214	50	1.485	80	1.483
17	1.46 (1.453)	16	1.46 (1.452)	300	50	1.452		
a_0: 5.034		a_0: 5.033		a_0: 5.028				
c_0: 13.73		c_0: 13.75		c_0: 13.73				

I: 廻折線強度, *d*: 格子面間距離 ( ) は補正値, *hkl*: 格子面指数.

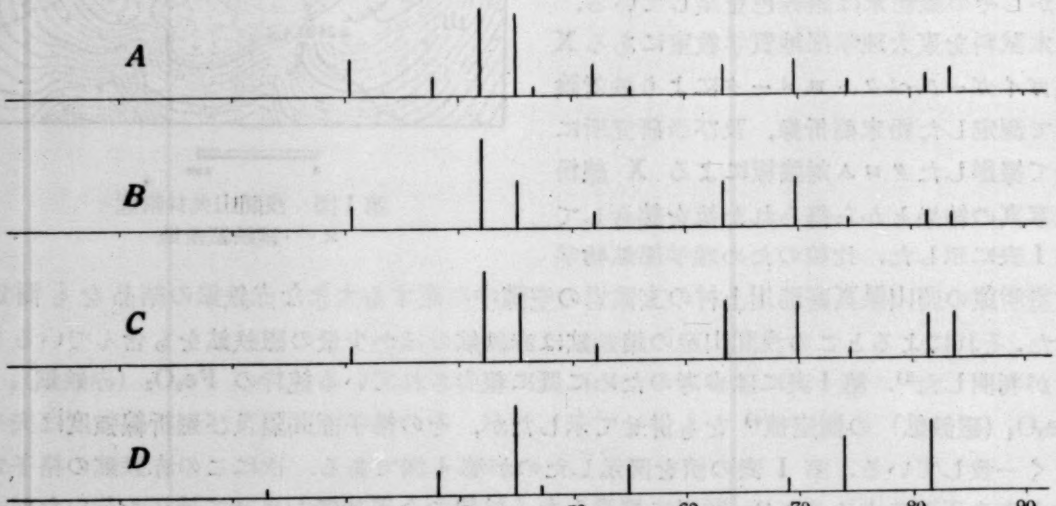

第4図　X 線粉末廻折図　A: 浅間山産, B: 川上村産, C: Fe_2O_3, D: Fe_3O_4
数字は Fe 対陰極による廻折角 (2θ) の度数である.

定数は $a_0=5.034$ Å, $c_0=13.73$ Å であり純粋の Fe_2O_3[5] の値とよく一致した. 併せて行つた川上村産の試料の結果もほぼ同じであつた. また廻折線相互の強度比から, 試料中の

5) A. N. and H. WINCHEL, *Elements of Optical Mineralogy* (1951).

赤鉄鉱と磁鉄鉱の含有量比を求め，化学分析の結果との比較をこころみたが，この方法によつては磁鉄鉱中に赤鉄鉱が少量混入している場合は比較的容易に行うことができるが，その逆の時はその量比の算定が行いにくく，従つて正確な値を求めることは困難であつた[6].

筆者等が行つた化学分析の結果を第II表に示す．試料は湯煎上で濃塩酸と加熱して分解し，とけない部分を不溶残渣とした．また FeO 測定のためには特にその分解に注意を払い，炭酸ソーダを加えて塩酸で分解する方法[7]，及び弗化水素，硫酸を用いる分解法の両者を行つてみた．鉄の測定は過マンガン酸カリによる滴定で行い，Reinhardt 法により，塩化物の処理を行つた．また総鉄の測定に際しての還元には塩化第一錫を用いた．分析の結果は大部分が酸化鉄よりなり，不純物は比較的少なかつた．含有する FeO は X 線によりその存在を確められた磁鉄鉱による部分もあるが，本試料について東大理学部地球物理学教室で行われた熱磁気分析の結果からは，磁鉄鉱の存在を確認し得るほどの量が見出されず，従つて磁鉄鉱の量はそれほど多くなく，FeO の一部は磁鉄鉱を構成しているがその大部分は赤鉄鉱中に含まれているものと推定される[8].

また弧光分析により錫の 3262.32 Å，2863.32 Å，2839.98 Å，2706.51 Å の各スペクト

第II表　前掛山産鏡鉄鉱化学成分

	Wt. %
Fe_2O_3	92.54
FeO	2.13
SiO_2**	2.66
TiO_2	0.42
MgO	0.38
CaO	0.05
H_2O-	0.00
H_2O+*	0.67
不溶残渣	0.61
計	100.46

* 灼熱減量より求めたもので FeO の補正を施した．
** SiO_2 は主として表面に附着した不純物によるものと考えられる．

第III表　赤鉄鉱化学成分

	1	2	3
Fe_2O_3	92.91	95.90	90.26
FeO	6.17	4.50	2.36
MgO	0.82	0.11	—
CaO	—	0.36	—
P_2O_5	—	0.056	—
MnO	—	—	—
H_2O	—	0.25	—
灼熱減量	—	—	4.25
	99.90	100.78	96.87

(1) C. F. Rammelsberg, Vesuvio 火山産[9].
(2) 高壮吉，岩手県仙人鉱山産[10].
(3) 木野崎吉郎，朝鮮黄海道載寧産[10].

6) 註 4) と同様の理由による．
7) A. Stock und U. A. Stähler, *Praktikum der quantitativen anorganischen Analyse*, 4. Auf., (1930), 57.
8) 但しこの試料は棒磁石には吸引される．

ル線を明らかに検出することが出来たが，川上村産のものについては殆んど検出し得なかつた．

赤鉄鉱の従来の分析資料中に往々かなりの量の FeO を含んでいるものがあり，例えば Vesuvio 火山産の赤鉄鉱などは 6.17% の FeO を含有している．第3表は今までに発表された赤鉄鉱の分析結果の 2〜3 の例を示す[9),10)]．

なを Vesuvio 火山の噴気孔にともなつて産する赤鉄鉱の成因については，$FeCl_3$ ガス及び水蒸気が高温に於て

$$2FeCl_3+3H_2O \rightleftarrows Fe_2O_3+6HCl$$

の如き可逆反応を生ずるといわれているが[11)]，現在の前掛山噴気孔は温度も低く且つその水蒸気中には塩素はほとんど検出されず[12)]，その成因については疑問の点が多い．この赤鉄鉱の結晶の生成が現在も徐々に行われつつあるという可能性はむしろ少く，この噴気孔が過去において現在より更に活発な時代に，今よりも高温で且つ塩化ガスに富んだ状態で出来たものではないかと思われるが，また一方合成の赤鉄鉱は鉄を含む固相と水蒸気のみの作用でも出来ることが知られているから，その確実な成因については今後の研究にまたなければならない．

以上要するに浅間火山前掛山噴気孔に産する鏡鉄鉱は若干の磁鉄鉱を含むほかは，比較的不純物の少い，また格子定数からみてもごく普通の赤鉄鉱である．

終りにわれわれの X 線測定に協力せられた本学理学部鉱物学教室の村岡久志氏，及び熱磁気変化の測定を行われた同地球物理学教室の秋本俊一氏にお礼申上げる．

---

31. On the Specular Iron from Mt. Maekake, Volcano Asama.

Eiiti MINAMI and Joyo OSSAKA,

Earthquake Research Institute.

We present here a report on the results of X-ray analyses and chemical analyses of the specular iron (hematite) produced in a steam vent of Mt. Maekake, the inner somma of Volcano Asama.

The X-ray analyses showed us the presence of minor quantities of magnetite besides hematite, and the measurement after accurate correction by mixing silicon as a standard proved that the hematite is of the quite common variety with lattice constants a_0: 5.034 Å and c_0: 13.73 Å.

The result of the chemical analyses is, in weight percentage; Fe_2O_3: 92.54, FeO: 2.13, SiO_2: 2.66, TiO_2: 0.42, MgO: 0.38, CaO: 0.05, H_2O-: 0.00, H_2O+: 0.67, insoluble residue

---

9) F. ZAMBONINI, ***Mineralogia Vesuviana*** (1936), 64.
10) Z. HARADA, ***Jour. Faculty Sci. Hokkaido Uuiv.***, IV-**3** (1936), 248.
11) F. ZAMBONINI, 前出.
12) 野口喜三雄 日化誌 **59** (1938), 902.

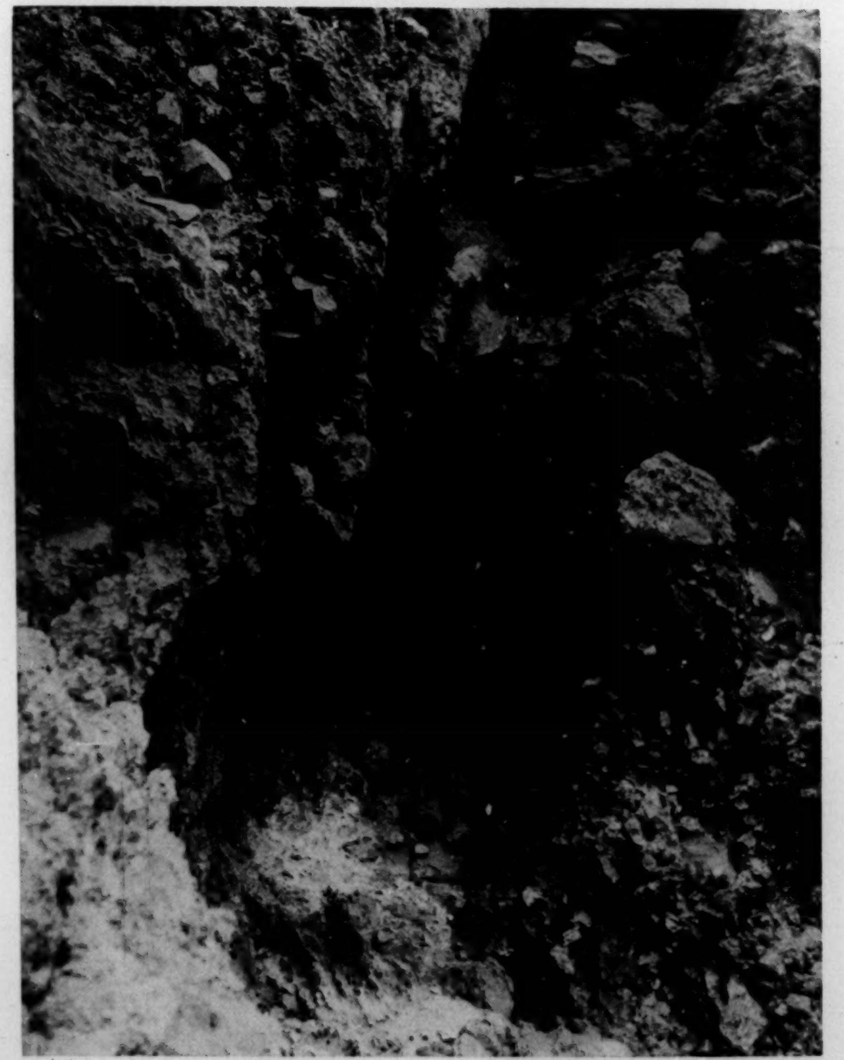

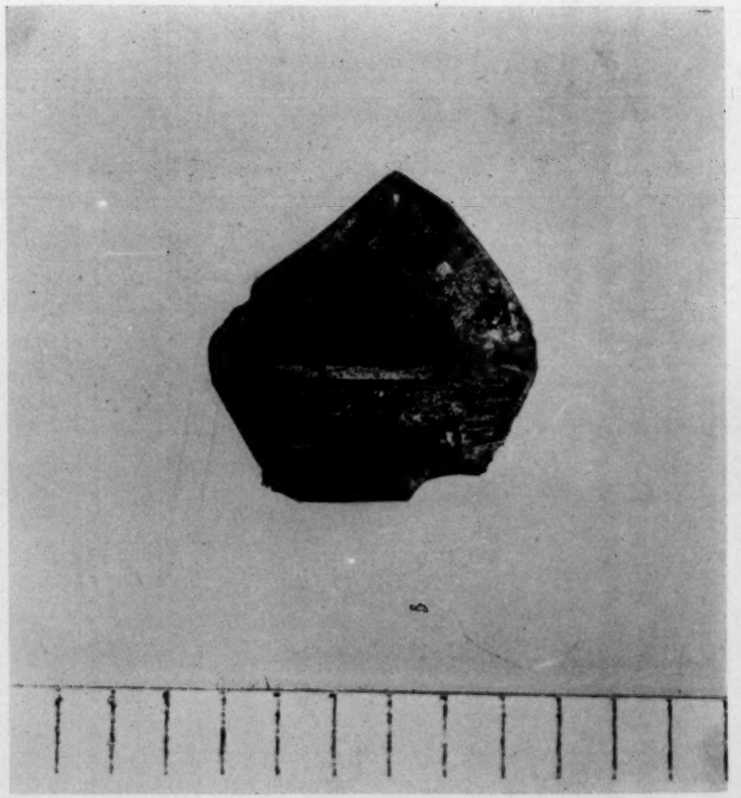

第3図 鏡鉄鉱の単結晶 (1 目盛: 1 mm)

← 第2図 前掛山噴気孔，中央暗黒の裂罅内側に鏡鉄鉱が密集して附着している.

1.61 and the total being 100.46%. From the FeO content also, we can assume the existence of magnetite in this sample. The spectrochemical analysis shows minor quantity of Sn.

The steam vent which produces this iron oxide crystals has at present, a low temperature and is very poor in other gas contents, and therefore the origin of the formation of this mineral here is not yet clear.

1.51 and the total being 100.19%. From the FeO content also, we can assume the existence of magnetite in this sample. The spectrochemical analysis shows minor quantity of Cu.

The steam-vent which produced this iron oxide crystals has, at present, a low temperature and is very poor in water and contents, and therefore the origin of the formation of this mineral here is not yet clear.

昭和32年11月30日印刷
昭和32年12月5日發行

東京都文京區本富士町一番地
東京大學構内
編纂兼
發行者　東京大學地震研究所

東京都千代田區富士見町一丁目十番地
印刷者　笠井康頼

東京都千代田區富士見町一丁目十番地
印刷所　株式會社　國際文献印刷社

賣捌所
東京都中央區日本橋通二丁目六番地
丸善株式會社

Sold by
Maruzen Co., Ltd.,
Nihonbashi-dôri, Chûô-ku, Tôkyô.
Price of this copy: 616 Yen. (Postage exclusive.)

BULLETIN OF

THE EARTHQUAKE RESEARCH INSTITUTE

UNIVERSITY OF TOKYO

Vol. XXXV, Part 3. September, 1957.

Contents.

Papers and Reports.

Page

22. K. AKI, Space and Time Spectra of Stationary Stochastic Waves, with Special Reference to Microtremors. (in English) 415
23. K. KANAI, The Requisite Conditions for the Predominant Vibration of Ground. (in English) 457
24. K. KASAHARA, The Nature of Seismic Origins as Inferred from Seismological and Geodetic Observations (1). (in English) 473
25. F. KISHINOUYE, Studies of Microseisms by Observations. (in English) 533
26. Y. SATÔ and R. YAMAGUCHI, Vibration of a Building upon the Elastic Foundation. (in English) 545
27. I. YOKOYAMA, Geomagnetic Studies of Volcano Mihara. The 8th Paper. (Continuous Observation of Changes in Geomagnetic Declination during the Period 1955~56). (in English) 567
28. T. ICHIMURA, Geological Investigations on the Zaō Volcanoes. IV Ryū-zan Volcano. (in English) 573
29. S. OMOTE and Y. YAMAZAKI, Seven-Channel Triggered Magnetic Tape Recorder for Routine Seismic Observations. (in English) 595
30. S. OMOTE, S. KOMAKI and N. KOBAYASHI, Earthquake Observations in Kawasaki and Turumi Areas and the Seismic Qualities of the Ground. (Part II). (in English) 613
31. E. MINAMI and J. OSSAKA, On the Specular Iron from Mt. Maekake, Volcano Asama. (in Japanese) 621

(For the papers written in Japanese or in occidental languages, the abstracts are given in occidental languages or in Japanese respectively.)

BULLETIN OF THE EARTHQUAKE RESEARCH INSTITUTE,
UNIVERSITY OF TOKYO. Vol. XXXV, Part 4. December, 1957.

東京大學
地震研究所彙報

第 35 號　第 4 册

昭和 32 年 12 月

目　次

論文及報告

頁

32. P波S波の速度比に就いて（英文）……………………………吉山良一 627
33. 地球核を通る地震波に対する磁場の影響（英文）…………………行武　毅 641

所　報
索　引

(The titles in occidental languages are given on the back cover.)

本彙報ハ年4回 (但シ第1號ヨリ第6號マデハ不定期ニ，第7號ハ3冊トシテ發行セリ)，彙報別冊ハ不定期ニ發行ス.

本彙報掲載ノ論文及ビ報告ノ内容ニ關シテハ著者ノミニ其責任アルモノトス.

本彙報ニ關スル照會通信ハ東京大學地震研究所長ヘ宛テラレタシ.

The Bulletin is published quarterly. (Vols. I–VI were published at irregular intervals and Vol. VII consisted of three parts.)

Supplementary Volume is published at irregular interval.

The authors of the papers alone are responsible for the statements and opinions contained in their respective papers.

All communications relating to this Bulletin should be addressed to the Director of the Earthquake Research Institute, University of Tokyo.

32. *The Ratio of the Velocity of P and S Waves.*

By Ryoichi YOSHIYAMA,

Earthquake Research Institute.

(Read Feb. 26, 1957.—Received Sept. 30, 1957.)

1. Introduction

In a previous paper[1], "Magnitude of the hypocentral region of an earthquake" was estimated from a time-distance curve analysis of seismic waves, and its seismological significance was studied in connection with earthquake energy to give a quantitative and seismometrical definition of the "hypocentral region of an earthquake." Practically, the estimate is greatly affected by the assumed values of V_P/V_S, the velocity ratio of the P and S waves, in the calculation. Therefore, and also from the following view point, the ratio is studied in this paper. So far, structures of the earthcrust were studied and classified in relation to the velocity of seismic waves, chiefly of P waves. While the determination of velocity is only made slowly, because of local difference and local complexity of the structure as classified from P-wave velocity: it is as yet difficult to find out a resolute seismological meaning of such a classification. Thereupon the velocity ratio of P and S wave, being directly related to the Poisson's ratio, comes to our attention as another measure of the classification. If the result here obtained, which implies an abrupt increase of the ratio V_P/V_S (to 1.78 from 1.67 in the earthcrust) at the Mohorovičić boundary, while nothing remarkable at any other boundary in the crust, be ascertained by further investigation, another geophysical significance will be added to the Mohorovičić boundary.

In due course, a method of examining the accuracies of the observed arrival time of P wave in Japan is presented.

2. Formula of calculation

The velocity ratio V_P/V_S is computed directly from a diagram of P–S interval (τ) against arrival time (T) of P, a linear relation between the two being presumed by many authors. Of course, strictly speaking,

1) R. YOSHIYAMA, "The Hypocentral Region of Earthquakes," *Bull. Seism. Soc. Am.*, **39** (1949), 187–188; **43** (1953), 153–158.

V_P/V_S should be computed from the respective analysis of time-distance curve of P and S waves. The method herein adopted is somewhat an expedient one to get a mean estimate of V_P/V_S, and, for that purpose, will be superior to the above mentioned strict method, because local complex structure only slightly affects the T–τ diagram to be computed: theoretically, if the ratio V_P/V_S is constant, the linear relation between T and τ is not affected at all either by the local difference of the velocity, or by the topographical or geological differences among the observatories, which give much trouble in the time-distance curve analysis. Putting,

$$V_P/V_S=1+\frac{1}{a} \tag{1}$$

where a is a certain constant, we get

$$a\tau+b=T \tag{2}$$

where b means the time when $\tau=0$, and, being denoted by T_0', was distinguished by the writer in the previous paper from the origin time, T_0, of P in the time-distance curve analysis.

The formula (2) being linear, and only two quantities being unknown, calculation of V_P/V_S, is far easier than the analysis of a time-distance curve. Assuming one a-value in several earthquakes, b being particular to each, and taking all the equations of observations of the form of (2) together in one scheme of the least square calculation, we can raise the accuracy of the computed a. According to the writer's rough estimation heretofore obtained, V_P/V_S in the earthcrust is 1.66∼1.70, while that below the Moho.-boundary is larger than 1.77.

In the following, studies of shallow focus earthquakes with the observations at short distances will give the V_P/V_S in the earthcrust, while those of deep-seated ones that below the Moho.-boundary. As to the shallow focus earthquake, particularly in Japan, observations of sufficiently high accuracy are difficult to obtain, because small earthquakes, which would otherwise give a distinct P and S phase, are not observed across sufficient distances owing to the short-coming of magnification of seismograph; on the other hand, P and S phase of a large earthquake are too complicated to be duly identified owing to the complicated earthquake mechanism.

3. Shallow focus earthquakes in Japan (1)

To avoid an undercrustal effect, calculation based on short distance

observations, that is, observations of as small a P–S interval (τ) as possible is advisable, while, to get sufficient accuracy in the calculation by the T–τ diagram, we must have for each earthquake a sufficient number, some four or five at least, of observations distributed over some range of τ in the T–τ diagram. The extent of the range, or, in other words, the upper limit of τ to be adopted in the calculation, and the requisite number of observations for each earthquake should be determined taking the accuracy of observations into consideration.

In the Kinki district of Japan, shallow focus earthquakes arise frequently and geographical distribution of observatories are favourable for observation of these earthquakes. Therefore, eight shallow focus earthquakes in this area in 1953 and 1954, tabulated in Table I, are first

Table I.

Earthq. No.	Date	Epicentre		Depth
		N	E	km
1	Sept. 18, 1953	33°48′	135°36′	10
2	Oct. 8, 1953	33 48	135 06	20
3	Nov. 7, 1953	34 42	136 24	10
4	Mar. 22, 1954	34 12	135 12	10
5	Apr. 20, 1954	35 12	135 30	10
6	Apr. 26, 1954	36 00	136 18	10~20
7	June 24, 1954	35 24	135 45	10~20
8	Oct. 25, 1954	34 54	134 54	Shallow

(*from Seism. Bull. Centr. Meteor. Obs. Japan*)

studied. In the seismological Bulletin of the Central Meteorological Observatory (Japan) are reported the arrival times and the P–S intervals of these earthquakes except earthquake No. 8, about which the writer requested information as to observations.

There being nine unknown quantities, one a and eight b, the a-value common to the eight earthquakes was calculated based on 72 observations in all, in which the largest τ is 17 sec, with the result that $a=1.395$ and $V_P/V_S=1.72$.

However, the standard deviation of a single observation of arrival time reached 1.3 sec. Moreover, the upper-limit of τ as large as 17 sec, adopted in the above calculation, to get a sufficient number of observations for a required accuracy of calculation, is too large to study the earthcrust, because, in the time-distance curve of P, some undercrustal effect is apparent already at a distance of 100 km, where P–S interval

is perhaps not more than 14 sec. And, by the writer's asking each observatory for the reexamination of the seismograms, it was ascertained that, as regards the earthquakes, No. 1, 2, 3, 4 and 7, many observations were unsatisfactory, partly because of the conditions of the observatories, and partly because of an undiscernible P and S phases. As to the earthquakes, No. 5, 6 and 8, some of the observations were revised and are given in the Table II, III and IV, and, on these three

Table II. Earthq. No. 5; $T_z=13^h13^m30^s$ J.S.T.

Obs.	Δ km	T sec	τ sec	$\varepsilon_T(\tau)$ sec	$\varepsilon_T(\Delta)$ sec
Kyoto	30.7	6.0	3.2	+0.13	−0.97
Maizuru	29.8	7.9	4.4	+0.22	+1.08
Kobe*	64.2	11.6	8.0	−1.49*	−0.77
Nara	64.9	12.0	7.0	+0.41	−0.53
Osaka	61.0	12.0	7.5	−0.34	+0.16
Toyooka	71.2	13.9	8.9	−0.54	+0.33
Hikone	68.5	14.0	9.2	−0.90	+0.78
Himeji	83.4	16.3	9.9	+0.35	+0.62
Kameyama	96.2	17.1	10.3	+0.55	−0.87
Wakayama	111.6	19.2	12.0	+0.09	−1.61
Tsu	106.2	19.5	11.8	+0.69	−0.25
Sumoto	109.9	19.8	12.9	−0.66	−0.66

$a=1.504$, $b_5=+1.06$ sec.

Table III. Earthq. No. 6; $T_z=05^h20^m22^s$ J.S.T.

Obs.	Δ km	T sec	τ sec	$\varepsilon_T(\tau)$ sec	$\varepsilon_T(\Delta)$ sec
Fukui*	7.4	3.5	1.8	+2.58*	+2.09
Tsuruga	44.2	6.4	4.9	+0.82	+0.24
Ibukiyama	68.8	9.2	8.0	−1.04	−1.17
Gifu	78.8	11.6	9.1	−0.29	−0.52
Takayama*	87.1	11.8	13.8	−7.16*	−1.72
Hikone	81.6	13.1	9.4	+0.75	+0.45
Maizuru	101.8	16.9	12.4	+0.04	+0.73
Nagoya	110.4	18.1	13.4	−0.26	+0.49
Kyoto	120.6	18.3	13.6	−0.36	−1.27
Kameyama*	126.7	19.3	15.2	−1.77*	−1.35
Toyama	111.9	20.5	14.6	+0.34	+2.54

$a=1.504$, $b_6=-1.79$ sec.

Table IV. Earthq. No. 8; $T_z=20^h22^m46^s$ J.S.T.

Obs.	$\varDelta$	T	τ	$\varepsilon_T(\tau)$	$\varepsilon_T(\varDelta)$
	km	sec	sec	sec	sec
Himeji	19.1	3.5	3.7	−1.04	±0.00
Kobe	34.0	5.7	4.6	−0.04	+0.37
Sumoto	59.2	10.8	7.6	+0.40	+1.21
Toyooka	70.7	11.1	8.3	−0.36	−0.20
Osaka	63.5	11.5	7.8	+0.80	+1.40
Wakayama	76.2	13.5	9.5	+0.24	+0.97
Kyoto*	77.1	15.1	8.8	+2.81*	+2.75
Takamatsu	100.1	16.8	11.8	+0.08	−0.13
Hikone	129.5	20.4	14.3	−0.08	−1.21

$a=1.504$, $b_8=-1.03$ sec.

earthquakes, the following was computed. For convenience of tabulation and calculation, arrival time (T) of P are measured from a certain arbitrary time, which is denoted by T_z and is given at the top of each table. From these observations of T and τ, except five observations (Kobe in No. 5; Fukui, Takayama and Kameyama in No. 6; Kyoto in No. 8), a, common to the three earthquakes, and three b are calculated.

The results are that

$$a=1.504\,, \qquad \text{i.e.} \quad V_P/V_S=1.665\,,$$

$$b_5=+1.06\ \text{sec}\,, \qquad b_6=-1.79\ \text{sec}\,, \qquad b_8=-1.03\ \text{sec},$$

residuals (obs.-cal.) of T being calculated and denoted by $\varepsilon_T(\tau)$,

$$\sum_{27} \varepsilon_T^2(\tau)=7.62\ \text{sec}^2$$

excluding the five observations stated above.

The standard deviation of a single observation of T is 0.6 sec and the standard deviation of a is 0.03, so that V_P/V_S is 1.65∼1.68. The resulting T–τ diagram of the three earthquakes is

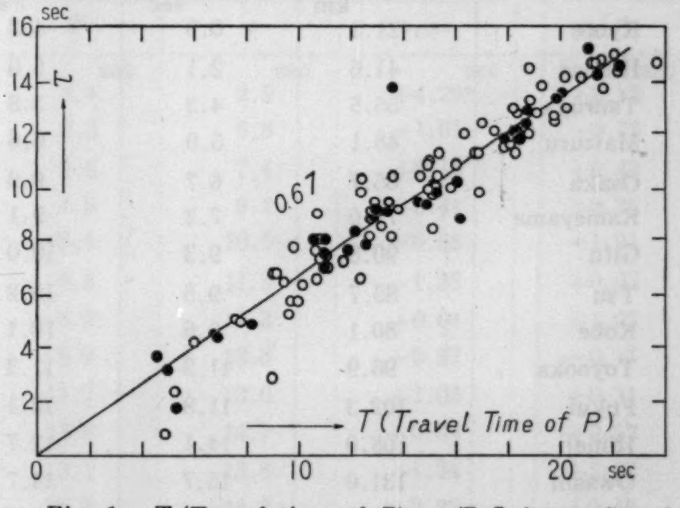

Fig. 1. T (Travel time of P)∼τ (P–S interval) relation of the earthquakes in the Kinki district, origin time of P being assumed at the time when $\tau=0$. And ●··Earthq. No. 5, 6, 8; ○··Earthq. No. 9∼14.

shown in Fig. 1 by filled-up circles ●; open circles ○ in the same figure are concerned with the six earthquakes studied in the following paragraph.

4. Shallow focus earthquakes in Japan (2)

In the above calculation, from a somewhat presumptive consideration by the writer of the accuracy of each observation, only three earthquakes of the eight were available. Therefore, six more earthquakes in the same district, given in Table V, were studied. The arrival times

Table V.

Earthq. No.	Date	Epicentre N	Epicentre E	Depth
				km
9	Nov. 24, 1953	35°12′	135°48′	20
10	Dec. 21, 1954	35 06	135 42	20
11	Feb. 13, 1955	33 54	135 12	10
12	Feb. 17, 1955	36 00	136 18	20~30
13	Nov. 4, 1955	34 42	136 06	60
14	Nov. 17, 1955	33 57	135 33	20

(*from Seism. Bull. Centr. Meteor. Obs. Japan*)

Table VI. Earthq. No. 9; $T_z=14^h53^m19^s$ J.S.T.

Obs.	Δ	T	τ	$\varepsilon_T(\tau)$	$\varepsilon_T(\Delta)$
	km	sec	sec	sec	sec
Kyoto	21.3	0.3	4.2	−0.25	+1.43
Hikone	41.6	2.1	5.0	+0.37	+0.14
Tsuruga	55.5	4.3	5.8	+1.38	+0.01
Maizuru	48.1	5.0	6.6	+0.90	+2.06
Osaka	65.7	6.7	9.9	−2.28	+0.71
Kameyama	72.0	7.2	9.1	−0.59	+0.17
Gifu	90.8	9.3	10.0	+0.17	−1.06
Tsu	85.7	9.5	10.2	+0.08	+0.02
Kobe	80.1	9.6	10.1	+0.33	+1.17
Toyooka	96.9	11.2	11.3	+0.15	−0.23
Fukui	102.3	11.8	12.1	−0.43	−0.50
Himeji	108.0	14.1	12.7	+0.98	+0.72
Owashi	131.0	15.7	14.7	−0.37	−1.79
Wakayama	121.9	15.9	14.8	−0.32	+0.02
Sumoto	125.4	16.4	15.0	−0.12	−0.03

$a=1.478$, $b_9=-5.66$ sec.

Table VII. Earthq. No. 10; $T_z=19^h32^m07^s$ J.S.T.

Obs.	Δ	T	τ	$\varepsilon_T(\tau)$	$\varepsilon_T(\Delta)$
	km	sec	sec	sec	sec
Kyoto*	9.6	−3.3	0.8	+3.72*	+1.50
Hikone	54.5	0.9	6.8	−0.95	−0.66
Osaka	52.2	1.2	6.5	−0.21	+0.13
Nara	47.9	1.4	5.3	+1.76	+1.00
Maizuru	50.0	1.9	6.4	+0.64	+1.17
Kobe	65.9	2.8	7.0	+0.65	−0.65
Ibukiyama	69.7	4.2	10.4	−2.97	+0.09
Tsuruga	69.6	5.3	8.1	+1.53	+1.19
Kameyama	75.1	5.6	9.2	+0.20	+0.58
Tsu	86.6	6.9	9.8	+0.61	−0.21
Himeji	95.6	7.6	10.1	+0.87	−1.11
Wakayama	107.7	8.1	12.0	−1.44	−2.74
Toyooka	93.8	8.7	9.9	+2.26	+0.35
Sumoto	111.0	8.8	12.4	−1.33	−2.58
Gifu	102.7	10.0	13.0	−1.02	+0.05
Owashi	123.4	11.1	13.9	−1.25	−2.43
Nagoya	115.4	12.6	14.2	−0.19	+0.51
Fukui	116.0	14.0	14.4	+0.91	+1.73

$a=1.478$, $b_{10}=-8.20$ sec.

Table VIII. Earthq. No. 11; $T_z=02^h27^m48^s$ J.S.T.

Obs.	Δ	T	τ	$\varepsilon_T(\tau)$	$\varepsilon_T(\Delta)$
	km	sec	sec	sec	sec
Wakayama*	37.2	0.4	2.9	+4.29*	+2.12
Sumoto	54.8	0.5	6.8	−1.01	−0.72
Tokushima	59.8	2.5	7.4	+0.11	+0.42
Shionomisaki	72.2	4.5	9.1	−0.41	+0.35
Owashi	94.0	6.1	10.5	−0.88	−1.91
Kobe	87.0	6.8	11.3	−1.36	+0.03
Osaka	88.8	8.2	11.3	+0.04	+1.07
Nara	104.7	9.8	12.8	−0.57	−0.17
Himeji	113.4	11.7	13.0	+1.03	+0.31
Murotomisaki	118.2	12.8	14.7	−0.39	+0.52
Takamatsu	115.6	13.1	13.8	+1.24	+1.17
Kyoto	133.4	15.4	14.7	+2.22	+0.43

$a=1.478$, $b_{11}=-8.54$ sec.

Table IX. Earthq. No. 12; $T_z = 17^h06^m16^s$ J.S.T.

Obs.	Δ	T	τ	$\varepsilon_T(\tau)$	$\varepsilon_T(\Delta)$
	km	sec	sec	sec	sec
Fukui	8.0	0.5	2.4	+1.67	+1.97
Tsuruga	44.4	2.8	5.1	−0.02	−0.43
Ibukiyama	68.5	7.6	6.6	+2.56	+0.16
Gifu	79.5	8.0	8.8	−0.29	−1.37
Hikone	81.4	8.4	8.5	+0.55	−1.13
Kanazawa	69.3	8.7	9.5	−0.63	+1.26
Takayama	87.0	10.2	10.9	−1.20	−0.39
Maizuru	101.7	13.1	11.5	+0.82	−0.14
Nagoya	111.0	14.1	13.3	−0.84	−0.76
Kyoto	120.2	14.1	14.5	−2.62	−2.36

$a = 1.478$, $b_{12} = -4.72$ sec.

Table X. Earthq. No. 13; $T_z = 08^h32^m42^s$ J.S.T.

Obs.	Δ	T	τ	$\varepsilon_T(\tau)$
	km	sec	sec	sec
Nara	24.2	0.9	5.8	+1.11
Tsu	37.9	1.0	7.7	−1.60
Hikone	64.4	1.9	9.0	−2.62
Kyoto	48.5	2.0	8.0	−1.05
Kameyama	37.2	2.9	7.2	+1.03
Osaka	52.0	3.9	8.1	+0.70
Owashi	70.9	4.8	10.5	−1.94
Kobe	83.4	6.5	10.5	−0.24
Nagoya	94.4	9.3	11.6	+0.93
Gifu	98.6	9.3	11.9	+0.49
Tsuruga	105.5	9.4	12.0	+0.45
Wakayama	99.5	9.5	11.3	+1.57
Maizuru	107.3	10.0	12.0	+1.04
Sumoto	115.1	10.3	12.8	+0.16

$a = 1.478$, $b_{13} = -8.78$ sec.

of P and P–S intervals, reported in the Seismological Bulletin of the Central Meteorological Observatory, are given in the Tables VI to XI, T being measured from a certain arbitrary time T_z and were used in the calculation without any revision in this case, but two observations, Kyoto and Wakayama, denoted by *, are omitted. The results of the calculation based on these 75 observations for the six earthquakes are that

Table XI. Earthq. No. 14; $T_s = 03^h 53^m 08^s$ J.S.T.

Obs.	Δ	T	τ	$\varepsilon_T(\tau)$	$\varepsilon_T(\Delta)$
	km	sec	sec	sec	sec
Shionomisaki	59.0	0.4	7.6	−0.64	+0.14
Owashi	61.2	0.6	7.3	−0.01	+0.01
Sumoto	72.2	2.7	9.5	−1.15	+0.20
Kobe	88.2	4.8	11.0	−1.27	−0.50
Osaka	77·7	4.9	8.4	+2.67	+1.36
Tokushima	89.9	5.8	10.9	−0.12	+0.15
Kyoto	119.5	9.6	12.5	+1.31	−1.39
Kameyama	130.8	10.0	14.2	−0.80	−2.96

$a = 1.478$, $b_{14} = -10.19$ sec.

$$a = 1.478 \pm 0.05 \text{ (M.E.)}, \qquad \text{i.e.} \quad V_P/V_S = 1.676,$$

$$b_9 = -5.66 \text{ sec}, \quad b_{10} = -8.20 \text{ sec}, \quad b_{11} = -8.54 \text{ sec},$$

$$b_{12} = -4.72 \text{ sec}, \quad b_{13} = -8.78 \text{ sec}, \quad b_{14} = -10.19 \text{ sec},$$

$$\sum_{75} \varepsilon_T^2(\tau) = 105.50 \text{ sec}^2 .$$

The standard deviation of a single observation of arrival time T is 1.2 sec and that of the calculated a is 0.05, therefore V_P/V_S is estimated between 1.70∼1.65. The T–τ diagram, T being measured from each "b", of the six earthquakes is given by open circles in Fig. 1. That V_P/V_S is about 1.68 is also concluded from a calculation based on 102 observations of 11 earthquakes which occured in swarm in Tokusima and Kooti Prefecture of the Sikoku district in 1955, Fig. 2 being the T–τ diagram of these earthquakes, but the mean of $\varepsilon_T(\tau)$ is as large as 1.8 sec; the dispersion of observations are too large to study in more detail. Since the effect of the inner part, whose V_P/V_S is no less than 1.78 as shown later on, increases the apparent V_P/V_S of the earthcrust, 1.67 may be perhaps

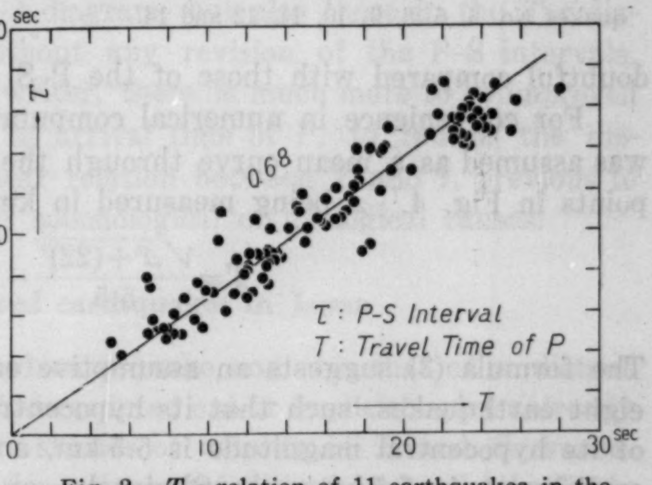

Fig. 2. T–τ relation of 11 earthquakes in the Sikoku district in 1955.

the most probable value thereof. Results of a computation with the seven earthquakes studied in the "Velocities of P at short distances"[2] by Dr. C. F. Richter gives also $V_P/V_S \doteqdot 1.67$, provided the observations whose P–S intervals are less than 8 sec are used.

5. Some remarks on the accuracies of observations

Fig. 3 is the time-distance relation of the above studied eight earthquakes in the Kinki district, the earthquake No. 13, since clearly deeper focussed than the others, being excluded. The time when $\tau=0$, which is given by respective "b", is adopted for the origin time of each earthquake. In the figure, not only the observed travel time of P, given in the tables and measured of course from "b", but also $a\tau$, that is, calculated travel time from the P–S intervals are plotted. In this way, if not always advisable, observations of S are added to the computation of the P-wave velocity, when the accuracies of observations of arrival times are doubtful compared with those of the P–S intervals.

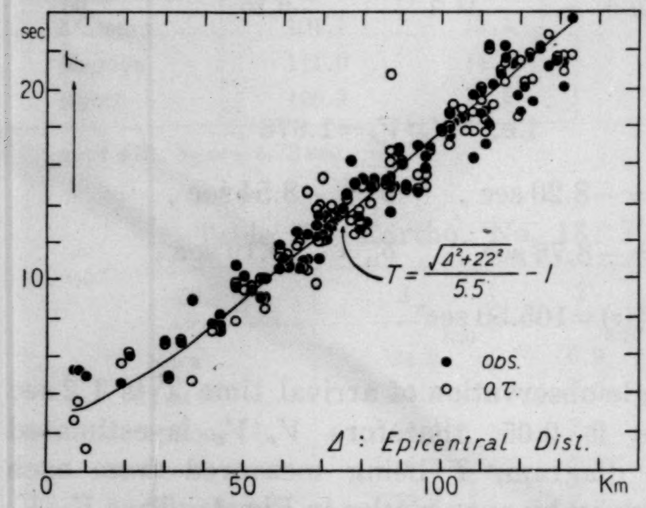

Fig. 3. Time-distance relation of the earthquakes No. 5, 6, 8, 9, 10, 11, 12 and 14.

For convenience in numerical computation, the following expression was assumed as a mean curve through the all, observed and calculated, points in Fig. 4. Δ being measured in km,

$$T=\frac{\sqrt{\Delta^2+(22)^2}}{5.5}-1 \text{ sec.} \qquad (3)$$

The formula (3) suggests an assumptive earthquake as a mean of the eight earthquakes, such that its hypocentral depth is 22 km, while radius of its hypocentral magnitude is 5.5 km, and the P-wave velocity in the earth-crust is 5.5 km/sec. Obviously, even to determine the P-wave velocity, too dispersive are the observations, but it does no matter in

2) C. F. RICHTER, "Velocities of P at short distances," *Bull, Seism. Soc. Am.*, **40** (1950), 281–289.

the present study whether these, plausible to the writer, implications are appropriate or not.

The last column $\varepsilon_T(\Delta)$ of the tables give the residuals of the observed T, measured of course from "b", from the calculated ones by the formula (3), that is

$$\varepsilon_T(\Delta) = (\text{"}T\text{" in the Table-}b) - (T \text{ cal. by (3)}) .$$

Thus we have two kind of residuals of observed arrival time of P, respectively denoted by $\varepsilon_T(\tau)$ and $\varepsilon_T(\Delta)$, one from the T–τ diagram, and the other from the T–Δ diagram. And the correlation between the two are illustrated in Fig. 4.

In Fig. 4, most of the observations are within a range of $|\varepsilon_T(\tau)| \leqslant 1$ sec and $|\varepsilon_T(\Delta)| \leqslant 1$ sec, and, as far as these points are concerned, any significant correlations between $\varepsilon_T(\tau)$ and $\varepsilon_T(\Delta)$ are not observed. On the other hand, for the observations whose $\varepsilon_T(\tau)$ or $\varepsilon_T(\Delta)$ is large, we can clearly see a positive correlation; that is, if we assume some corrections to the arrival time, not only the dispersions in the T–Δ diagram, but also those in the T–τ diagram, decrease altogether without any revision of the P–S intervals. Consequently it seems to the writer, there is much more to be improved in the observation, especially, of arrival time of P, to reduce the dispersions from the assumed linear relation between T and τ, previous to attributing them to some other seismological or geological causes.

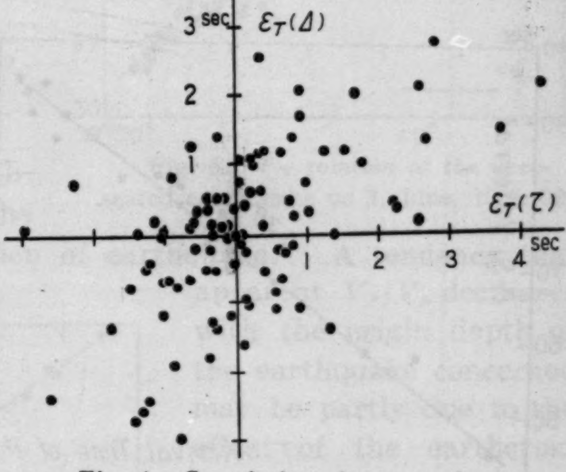

Fig. 4. Correlations between the two kind of residuals.

6. Deep-seated earthquakes in Japan

That $d\tau/dT$ of a deep-seated earthquake and also that of a distant earthquake are about 0.8 has been pointed out or implicitly given already by some senior authors in their studies of velocity of P and S waves. In this paper, $(d\tau/dT)$ of the three deep-seated earthquakes in the Table XII was computed, time-distance curve and earthquake mechanism of these earthquakes being long before thoroughly investigated by Kawasumi, the writer and others. Especially as regards earthquake No. 15,

Table XII.

Earthq. No.	Date	Origin time	Epicentre		Depth
		h m s	N	E	km
15	Feb. 20, 1931	5 33 24.0	44°29′	135°45′	325
16	June 3, 1929	6 38 36.1	34 20	137 08	353
17	June 2, 1931	11 37 52.3	35 55	137 23	240

Kawasumi and the writer[3)] studied its earthquake mechanism and time-distance curve of P in some detail based on world wide observations. Fig. 5 is the T–τ diagram of the earthquake.

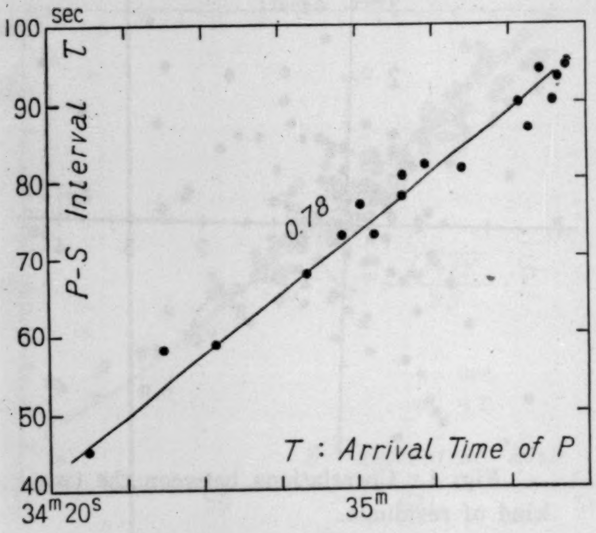

Fig. 5. T–τ relation of the deep-seated earthquake on 20, Feb., 1931.

According to the results of studies of earthquake mechanism, one of the four "nodal points of S wave" of this earthquake, where original S wave from the origin would not be observed theoretically at all, is close to Aomori in Japan.

Since the observations of P–S interval at observatories near the nodal points would be naturally inaccurate, observations at Aomori and some other observatories near the nodal point are not used. And also excluded are the observations at epicentral distances much greater than the inflexion point, $\Delta_i \doteqdot 7°$, of the time distance curve of P wave. In the T–τ diagram, Fig. 5, 18 points are plotted, but observation of arrival time at Haboro seems unreliable. Then the results of the calculation based on 17 points are,

$$a=1.280\pm 0.05 \text{ (M.E.)}\,, \qquad \text{i.e. } V_P/V_S=1.781\,,$$

$$b=26.5 \text{ sec}\pm 4 \text{ sec}\,.$$

Fig. 6 is the T–τ diagram of the earthquake No. 16 in which 49 points are plotted; 10 observations, Tsu, Shionomisaki and etc., whose residuals

3) H. KAWASUMI and R. YOSHIYAMA, "On the Deep-seated Earthquake of Feb. 20, 1931" [in Japanese], *Zisin* (*Jour. Seism. Soc. Japan*), **6** (1934), 415, "On the Mechanism of a Deep-seated Eapthquake", *Proc. Imp. Acad. Japan*, **10** (1934), 345-348.

are greater than 5 sec, being excluded. And the results of computation with 29 points whose residuals are smaller than 2 sec are,

$a=1.270$, i.e. $V_P/V_S=1.787$,

$b=37.4$ sec.

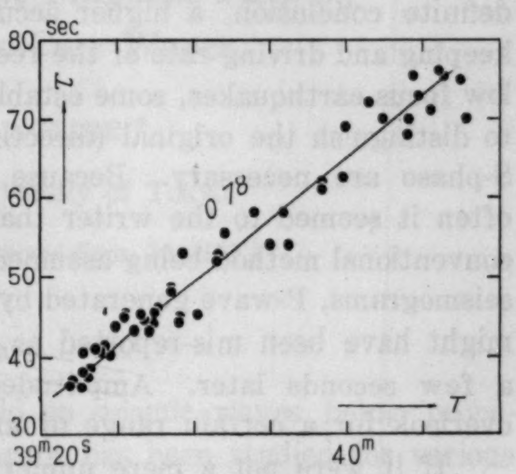

Fig. 6. T-τ relation of the deep-seated earthquake on 3, June, 1929.

Fig. 7 is the T-τ diagram of the earthquake No. 17. Calculations with 24 points out of 33 points in the figure gives a result that

$a=1.291$, i.e. $V_P/V_S=1.774$,

$b=53.5$ sec.

The results of b of these three earthquakes were already used in the studies of the "Hypocentral region of earthquake." A tendency that apparent V_P/V_S decreases with the origin depth of the earthquake concerned may be partly due to the effect of the earthcrust whose V_P/V_S is not greater than 1.68. However, some actual increase of V_P/V_S towards the inner part of the earth may be also expected.

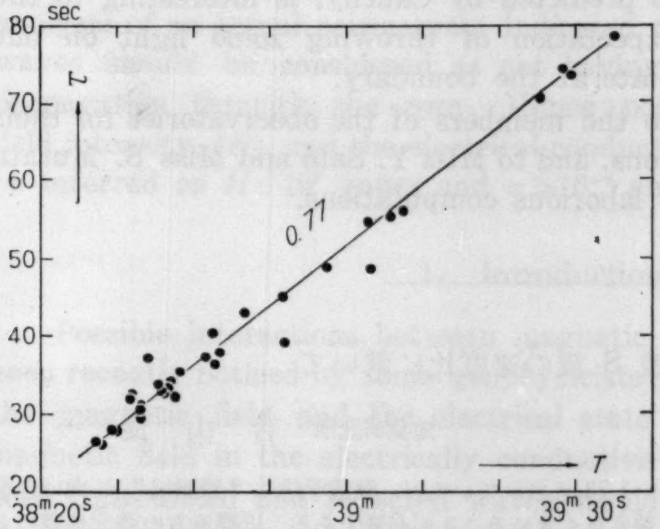

Fig. 7. T-τ relation of the deep-seated earthquake on 2, June, 1931.

7. Concluding remarks and acknowledgement

It is clear that in the earthcrust V_P/V_S is not much greater than 1.67 and that of inner part is about 1.78, the corresponding Poisson's ratio being 0.22 and 0.27 respectively. Since the T-τ diagrams and the T-Δ diagrams of the shallow focus earthquakes, for the range of distance $\Delta=130$ km$\sim$200 km, are extremely dispersive, presumed abrupt (in practical saying) increase of V_P/V_S at the Moho.-boundary was not confirmed in this paper. However, if the increase of

V_P/V_S is gradual, the apparent V_P/V_S of the deep focus earthquake, for example No. 17, will be far less than that here obtained. To get a more definite conclusion, a higher accuracy of observations, as regards time-keeping and driving rate of the recording drum, and, especially for shallow focus earthquakes, some established seismological and practical method to distinguish the original (directly coming from the earthquake centre) S-phase are necessary. Because, in the course of these studies, very often it seemed to the writer that, the incidence of S wave following a conventional method being assumed at a certain "remarkable phase" in the seismograms, P-wave generated by S wave at some inner-crustal boundary might have been mis-reported as the original S wave which comes out a few seconds later. Amplitudes of these P waves are too large to overlook for a certain range of angle of incidence of the S-wave.

If it were not a mere numerical appearance resulting from the calculation, accuracies of which are yet unsatisfactory, the fact that the Poisson's ratio of the two media, bounded by the Moho.-boundary, is almost equally larger in the one and less in the other than the generally adopted value of 0.25 predicted by Cauchy, is interesting to the writer, and leads to the expectation of throwing some light on our knowledge of the physical state at the boundary.

The writer is grateful to the members of the observatories for their kind information of observations, and to Miss Y. Satô and Miss S. Murata for their assistance in these laborious computations.

---

32. P 波 S 波の速度比に就いて

地震研究所 吉 山 良 一

P 波と S 波の速度比は半ば習慣的に 1.73 とされているが，験震学的に“震源域”の大いさを計算するためにはこの比の値をも少し精度高くきめることが必要である．近畿地方の浅発地震によつて計算した結果，地殻内ではこの比が 1.73 よりは明かに小さく 1.67 に近く，深発地震で調査した結果,内部では 1.78 に近いのではないかと思われる．アメリカに於ける近地地震観測からも同地に於けるこの比の値は矢張り 1.67 に近く推定され，地殻内に於ける P波の速度が日本とアメリカに於いて，少くとも今迄のところ可成り異つているらしいことに比べて面白い一致である．即ち速度比が速度そのものよりも地殻とそれから内部の性質のちがいを一層端的に示しているものとすれば，モホロビチック不連続面の性質を明かにするために，或はまた，その辺りに最も多く地震が発生することをも考え合せて，この比の調査は冒頭の目的以外にも更にくわしく行わねばならぬと思われる．そのためには，装置の面からも，また複雑な地震記象の中から S 波をはつきり検出するための基本的な技術の面からも観測の精度を高める必要がある．

---

33. *The Influence of the Magnetic Field on Spectra of Seismic Core Waves.*

By Takesi YUKUTAKE,*

Graduate School, University of Tokyo.

(Read Sept. 24, 1957.—Received Sept. 30, 1957.)

Summary

The influence of the magnetic field on seismic waves being propagated in the electrically conductive core has been studied for various values of magnetic field intensity and electrical conductivity. It has resulted in knowledge that seismic waves passing through the core are not affected by the magnetic field unless the field intensity exceeds 10^6 gauss or the electrical conductivity is smaller than 10^{-8} emu. The spectral analyses of an actual seismogram indicated that the spectrum of seismic waves should be considered as not having been changed owing to the propagation through the core. Hence possible limits of the magnetic field intensity, (H), and the electrical conductivity, (σ), in the core would be inferred as $H<10^7$ gauss and $\sigma>10^{-8}$ emu.

1. Introduction

Possible interactions between magnetic field and seismic waves have been recently noticed by some geophysicists in the hope of investigating the magnetic field and the electrical state in the earth's core. If the magnetic field in the electrically conductive core were strong enough, both transmitted and reflected waves would be strongly affected by the electromagnetic force associated with magneto-hydrodynamic or magneto-elastic couplings between motions and magnetic fields. From the fact that *ScS* waves do not seem to be affected by magneto-hydrodynamic waves which will be generated in the electrical conductor permeated by magnetic flux, Rikitake[1] has determined the possible limit or range of the magnetic field intensity (H) and the electrical conductivity (σ) in the core. His results are $H<10^4$ gauss and $10^{-8}<\sigma<10^{-5}$ emu. Al-

* Communicated by T. Rikitake.

1) T. RIKITAKE, *Bull. Earthq. Res. Inst.*, **30** (1952), 191-205.

though the details have not yet been published, Hide and Runcorn[2] have also obtained $H<10^6$ gauss from the study of electro-magnetic damping of P wave within the earth.

Some attempts based on solid or liquid state physics have been also made in order to estimate the electrical conductivity in the core as accurately as possible. Elsasser has obtained $\sigma=1.3\times10^{-5}$ emu from a calculation under the assumption that the core is composed of metallic iron under high pressure and high temperature. Meanwhile, Bullard has reached $\sigma=1\times10^{-6}$ emu by taking into account the pressure and temperature variations empirically determined in the earth.

In this paper the writer studies the characteristics of core waves by applying spectral analyses to various phases of seismic waves observed at Tokyo on the occasion of a particular earthquake that occurred in the Atlantic near Argentina. On the basis of the study, the writer also considers the possibility of inferring the possible range of the intensity of the magnetic field and the electrical conductivity in the earth's core. Although no exact results are obtained, the possible range suggested by the present study is almost the same as those given by Rikitake, Hide and Runcorn.

2. Theory

As has been studied in an electrically conductive fluid, motions in an elastic conductor permeated by magnetic flux are affected by so-called Lorentz force. When elastic waves are propagated through a magnetic field, the velocity and the amplitude of waves are to be modified by couplings between motions and fields. If it is supposed that there were an extraordinarily strong field in the core which is highly conductive, frequency characteristics of seismic core waves might become different from those of the waves which do not pass through the core. By comparing the core waves, for example P' waves, with the other phase, PP, we might be able to obtain some information about the intensity of the magnetic field in the core.

The equation of motion when elastic waves are progagated through an elastic conductor placed in a magnetic field has been studied by Knopoff[4]. He has applied his theory to the longitudinal waves passing through the core which is assumed to occupy a region only in which

2) R. HIDE, *Physics and Chemistry of the Earth*, *vol.* **1** (Pergamon Press, 1956), p. 116.

4) L. KNOPOFF, *Jour. Geophys. Res.*, **60** (1955), 441–456.

the magnetic fluxes are confined and outside which no magnetic flux exists. He concluded that the attenuation of seismic waves caused by the magnetic field is not significant and the interaction with the magnetic field is not an important mechanism in the propagation of seismic waves through the earth's core even for considerably high values of the intensity of the magnetic field and the conductivity. But Knopoff's assumption that the fluxes terminate at the boundary does not seem to fit the condition in the core. In this paper the writer will adopt some different model as the earth's core, that is, only the electrical conductivity is discontinuous at the boundary and the intensity of the magnetic field is constant everywhere.

Combining the following, the fundamental equation is obtained; one is the principal equation of elasticity and the other that of electromagnetic force,

$$\frac{\partial^2 \boldsymbol{U}}{\partial t^2}=\alpha^2 \text{ grad div } \boldsymbol{U}-\beta^2 \text{ rot rot } \boldsymbol{U}+\frac{\boldsymbol{F}}{\rho}\,, \tag{1}$$

$$\boldsymbol{F}=[\sigma(\boldsymbol{E}+\boldsymbol{v}\times\boldsymbol{B})]\times\boldsymbol{B}\,, \tag{2}$$

where α and β are the velocity of the longitudinal and the transverse waves. ρ and σ denote density and electrical conductivity respectively, $\boldsymbol{E}$ and $\boldsymbol{B}$ are the electric field and the magnetic induction, $\boldsymbol{U}(u_x, u_y, u_z)$ the displacement vector, $\boldsymbol{v}$ is the velocity, i.e. $\partial \boldsymbol{U}/\partial t$, and $\boldsymbol{F}$ represents the body force, the electromagnetic force in this case, exerting on the elastic body. With the aid of Maxwell's equations, $\boldsymbol{F}$ may be expressed in terms of $\boldsymbol{v}$ and $\boldsymbol{B}$, as follows;

$$\left(\nabla^2-\sigma\mu\frac{\partial}{\partial t}\right)\boldsymbol{F}=-\sigma\{\text{rot rot}(\boldsymbol{v}\times\boldsymbol{B})\}\times\boldsymbol{B}\,, \tag{3}$$

where μ is magnetic permeability. When the magnetic field is located in y-direction, substituting (1) into (3), the following equations will be obtained,

$$\left(\frac{\partial^2}{\partial z^2}-\sigma\mu\frac{\partial}{\partial t}\right)\left(\beta^2\frac{\partial^2}{\partial z^2}-\frac{\partial^2}{\partial t^2}\right)u_x=0\,, \tag{4}$$

$$\left(\frac{\partial^2}{\partial z^2}-\sigma\mu\frac{\partial}{\partial t}\right)\left(\beta^2\frac{\partial^2}{\partial z^2}-\frac{\partial^2}{\partial t^2}\right)u_y=0\,, \tag{5}$$

$$\left(\frac{\partial^2}{\partial z^2}-\sigma\mu\frac{\partial}{\partial t}\right)\left(\alpha^2\frac{\partial^2}{\partial z^2}-\frac{\partial^2}{\partial t^2}\right)u_z=\frac{\sigma B_y^2}{\rho}\frac{\partial^2 u_z}{\partial z^2\partial t}\,. \tag{6}$$

For the compressional plane waves

$$u_z = Ae^{ip(t-z/c)}, \tag{7}$$

which are propagated in z-direction, equation (6) becomes

$$\left(\frac{p^2}{c^2}+ip\sigma\mu\right)\left(p^2-\frac{\alpha^2 p^2}{c^2}\right)=ip\frac{\sigma B^2}{\rho}\frac{p^2}{c^2}. \tag{8}$$

According to Knopoff's expression, (8) and its solution are written as follows;

$$(c^2-\alpha^2)(c^2-iV_e^2)=c^2V_h^2, \tag{9}$$

$$2c^2=V_h^2+\alpha^2+iV_e^2\pm\sqrt{(V_h^2+\alpha^2+iV_e^2)^2-4iV_e^2\alpha^2}, \tag{10}$$

where V_h is the phase velocity of magneto-hydrodynamic waves, that is,

$$V_h=\frac{B}{\sqrt{\rho\mu}}, \tag{11}$$

and

$$V_e=\sqrt{\frac{p}{\mu\sigma}}. \tag{12}$$

In the case of $V_h^2 \ll \alpha^2$, the roots of equation (10) can be expressed in a simpler form,

$$C_1\approx\alpha\left\{1+\frac{V_h^2}{2(\alpha^2-iV_e^2)}\right\}, \tag{13}$$

$$C_2\approx i^{1/2}V_e\left\{1-\frac{V_h^2}{2(\alpha^2-iV_e^2)}\right\}. \tag{14}$$

On the other hand, if $V_e^2 \ll \alpha^2$, they will be approximated in somewhat different form,

$$C_1'\approx\sqrt{\alpha^2+V_h^2}\left\{1+\frac{iV_e^2V_h^2}{2(\alpha^2+V_h^2)^2}\right\}, \tag{15}$$

$$C_2'\approx i^{1/2}\frac{V_e}{\sqrt{1+\dfrac{V_h^2}{\alpha^2}}}. \tag{16}$$

From (13), (14), (15) and (16) it is obvious that the waves in the electrical conductor are attenuated owing to the existence of the magnetic field. For the waves whose velocities are C_1, C_2, C'_1 and C'_2, the attenuation factors are expressed respectively as follows;

$$C_1: \quad \exp\left[-pd\frac{V_h^2V_e^2}{2\alpha^5\left(1+\frac{V_h^2}{\alpha^2}+\frac{V_e^4}{\alpha^4}\right)}\right] \tag{17}$$

$$C_2: \quad \exp\left[-\frac{pd}{\sqrt{2}\,V_e}\left\{1+\frac{(\alpha^2-V_e^2)V_h^2}{2\alpha^4\left(1-\frac{V_h^2}{\alpha^2}+\frac{V_e^4}{\alpha^4}\right)}\right\}\right] \tag{18}$$

$$C'_1: \quad \exp\left[-pd\frac{V_h^2V_e^2}{2(\alpha^2+V_h^2)^{5/2}}\right]$$

$$=\exp\left[-p^2d\frac{B^2}{2\mu^2\rho\sigma\left(\alpha^2+\frac{B^2}{\rho\mu}\right)^{5/2}}\right] \tag{19}$$

$$C'_2: \quad \exp\left[-\frac{pd}{V_e}\sqrt{\frac{1}{2}\left(1+\frac{V_h^2}{\alpha^2}\right)}\right]$$

$$=\exp\left[-d\sqrt{\frac{\mu\sigma p}{2}\left(1+\frac{B^2}{\alpha^2\mu\rho}\right)}\right] \tag{20}$$

The second type wave specified by C_2 or C'_2 is the rapidly attenuative wave. The depth of penetration δ where the amplitude of the wave diminishes to as small as $1/e$ of that of the incident one becomes,

$$\delta \doteqdot \left\{\frac{2}{\mu\sigma p}\times\frac{1}{1+\frac{B^2}{\alpha^2\mu\rho}}\right\}^{1/2} \tag{21}$$

for the wave C'_2. As for the first type wave C_1 or C'_1, the attenuation is not so remarkable as for the second type wave, but the stronger the magnetic field intensity grows or the lower the electrical conductivity becomes, the more notable the attenuation will become.

Now let us consider an infinitely extended slab of an elastic conductor bounded by the planes $z=0$ and $z=d$. Outside this region the

conductivity is zero everywhere. The compressional plane wave being propagated in z-direction yields at the boundary $z=0$ two modes of oscillation. One has the velocity of the ordinary elastic wave type C_1, and the other is the wave attenuating rapidly in the conductive region. These excited waves likewise produce two modes of waves at the other boundary $z=d$, so that four types of waves are in the slab. These four waves, together with the incident, refracted and reflected waves in the non-conducting region, should satisfy the following conditions at the boundary:

1) the displacements due to these waves are continuous,
2) the tangential component of the magnetic field is continuous,
3) the total stress composed of the mechanical stress and the electromagnetic stress is continuous.

Now that the intensity of the toroidal field in the core which has no radial component is inferred to be much stronger than that of the poloidal field[5], the seismic waves being propagated in the radial direction are nearly perpendicular to the field. In the calculation below we shall take as actual a model as possible.

When the magnetic field $(1/\mu)\boldsymbol{B}(=\boldsymbol{H})$ is parallel to the boundary and perpendicular to the direction of propagation of the wave, we can easily derive the following relation in the electric conductor from Maxwell's equations.

$$\left(\frac{\partial}{\partial t}-\frac{1}{\sigma\mu}\nabla^2\right)\boldsymbol{b}=\mathrm{rot}\left(\frac{\partial \boldsymbol{U}}{\partial t}\times \boldsymbol{B}\right), \tag{22}$$

where $\boldsymbol{b}$ is the induced magnetic flux density. Assuming

$$\boldsymbol{b}=\begin{pmatrix}0\\ b_y\\ 0\end{pmatrix}=\begin{pmatrix}0\\ Se^{ip(t-z/c_i)}\\ 0\end{pmatrix}, \tag{23}$$

the solution of (22) is obtained as follows,

$$b_y=\frac{-\dfrac{p}{c_i}BA_i}{i-\dfrac{1}{\sigma\mu}\dfrac{p}{c_i}}\,e^{ip(t-z/c_i)}, \tag{24}$$

5) E. C. BULLARD and H. GELLMAN, *Phil. Trans. Roy. Soc. London, A*, **247** (1954), 213-278.

where A_l is the amplitude of the compressional wave. To satisfy the boundary condition the total sum of these additive magnetic induction must be zero across the boundaries, because the magnetic induction $\boldsymbol{B}$ is constant everywhere and does not change with the time.

As mentioned above, the total stress consists of two kinds, the elastic stress and the electromagnetic one, which are in general represented by a tensor (T_{ij}). In this case it is sufficient only to satisfy the condition of continuity of the component T_{zz}, the conditions for the other components being automatically satisfied provided the condition for the component T_{zz} is fulfilled. T_{zz} is written as

$$T_{zz}=\rho\alpha^2\frac{\partial u_z}{\partial z}-\frac{1}{2\mu}(B+b_y)^2. \tag{25}$$

The first term of this equation represents the elastic stress and the second Maxwell's stress due to the magnetic field. The value of the second term being continuous at the boundaries, because the tangential component of the magnetic field does not change there, so that we see that we have only to bring the first term into question. On taking into account the continuity conditions of the quantities calculated in (24) and (25) together with the continuity of the displacements at the boundaries $z=0$ and $z=d$, we have six equations to be solved.

From these equations the ratio K of the amplitude of the transmitted wave to that of the incident one is obtained as follows;

$$K=\frac{4q_2(q_1r_2-q_2r_1)e^{ip(d/\alpha)}}{\{q_2(r_1-1)-q_1(r_2+1)\}^2e^{-ip(d/c_1)}-\{q_2(r_1+1)-q_1(r_2+1)\}^2e^{ip(d/c_1)}}, \tag{26}$$

where

$$q_k=\frac{\dfrac{p}{c_k}}{i-\dfrac{V_e^2}{c_k^2}}, \tag{27}$$

$$r=\frac{\alpha}{c_k}. \tag{28}$$

In the course of the derivation of the transmission coefficient K, the writer assumed that the waves (specified by the velocity C_2), which are

generated at one side of the boundaries, are attenuated so strongly that they have practically no effects upon the other boundary. The assumption will be justified by the fact that the depth of penetration of these waves is very small and will never reach the opposite boundary if the width of the conductive region is wide. In reality the earth's core is so large that the depth of penetration δ given in (21) is negligibly small compared with the dimension of the core, so that the above-stated assumption could safely be adopted.

Although we do not know any accurate values of the intensity of the magnetic field and the electrical conductivity in the core, it has been presumed that the magnetic field intensity is less than 10^3 gauss[6]), and the electrical conductivity is $10^{-8}<\sigma<10^{-5}$ emu[7]) from various points of view. In the calculation, it will be assumed that the velocity of seismic waves is 10 km/sec, the density $\rho=10$ g/cm^3, the permeability $\mu=1$ cgs emu, and the diameter of the core is 7000 km. With these values we see that the velocity of the magneto-hydrodynamic wave V_h is less than 1 m/sec, hence it will be allowable to make use of the approximations (13) and (14). Then the transmission coefficient will be approximately written as

$$K \doteqdot \frac{1}{1+\dfrac{2}{r_2}} \exp\left[ip\frac{d}{\alpha}\left(1+\frac{\alpha}{c_1}\right)\right]. \tag{29}$$

From this the following equation will be derived for $\sigma=10^{-6}$ emu.

$$|K|^2 \doteqdot \frac{1}{1+2\sqrt{\dfrac{1}{T}}\times 10^{-3}+\dfrac{2}{T}\times 10^{-6}}, \tag{30}$$

where T is the period of the seismic wave and $p=2\pi/T$. As a consequence it may be concluded that seismic waves having periods longer than 1 sec would be little affected by the magnetic field the intensity of which is less than 10^3 gauss.

By taking the product of the complex conjugate in (26), we can obtain the following real function for the transmission coefficient,

$$|K|^2=\frac{C}{A-B\cos\left(\dfrac{2\pi}{T}\dfrac{d}{c_1}+\theta\right)}, \tag{31}$$

6) E. C. BULLARD and H. GELLMAN, *loc. cit.*, 5).
7) T. RIKITAKE, *loc. cit.*, 1).

where A, B and C are all real-positive. Although A, B and C are the functions of period, they vary little provided the variation of period is not very large, while the cosine-term is subject to oscillations with small changes in the period. Accordingly we may regard A, B and C as constants comparing with the cosine-term in a small range of period and the transmission coefficient K takes the value between $K_{\min}$ and $K_{\max}$.

$$\frac{C}{A+B} \leqq |K|^2 \leqq \frac{C}{A-B} \tag{32}$$

Table I. Mean values of square of transmission coefficient; K_0^2.

T (sec.)	B (gauss) \ σ (emu)	10^{-9}	10^{-8}	10^{-5}	10^{-2}	10
10	10^3	0.980	0.994	1.000	1.000	1.000
	10^4	0.980	0.994	1.000	1.000	1.000
	10^5	0.980	0.994	1.000	1.000	1.000
	10^6	0.980	0.994	1.000	1.000	1.000
	10^7	0.948	0.949	0.957	0.957	0.957
4	10^3	0.969	0.990	1.000	1.000	1.000
	10^5	0.969	0.990	1.000	1.000	1.000
	10^6	0.970	0.990	1.000	1.000	1.000
	10^7	0.978	0.955	0.957	0.957	0.957

Table II. Minimum values of square of transmission coefficient; $K^2_{\min}$.

T (sec.)	B (gauss) \ σ (emu)	10^{-9}	10^{-8}	10^{-5}	10^{-2}	10
10	10^3	0.980	0.994	1.000	1.000	1.000
	10^4	0.980	0.994	1.000	1.000	1.000
	10^5	0.980	0.994	1.000	1.000	1.000
	10^6	0.980	0.994	1.000	1.000	1.000
	10^7	0.941	0.916	0.918	0.918	0.918
4	10^3	0.969	0.990	1.000	1.000	1.000
	10^5	0.969	0.990	1.000	1.000	1.000
	10^6	0.970	0.990	1.000	1.000	1.000
	10^7	0.934	0.916	0.918	0.918	0.918

Table III. Maximum values of square of transmission coefficient; K^2_{max}.

T (sec.)	B (gauss) \ σ (emu)	10^{-9}	10^{-8}	10^{-5}	10^{-2}	10
10	10^3	0.980	0.994	1.000	1.000	1.000
	10^4	0.980	0.994	1.000	1.000	1.000
	10^5	0.980	0.994	1.000	1.000	1.000
	10^6	0.981	0.994	1.000	1.000	1.000
	10^7	0.995	0.996	0.999	0.999	0.999
4	10^3	0.970	0.990	1.000	1.000	1.000
	10^5	0.970	0.990	1.000	1.000	1.000
	10^6	0.970	0.990	1.000	1.000	1.000
	10^7	1.026	0.998	1.000	1.000	1.000

Table I, II and III show these K_0, K_{min} and K_{max} respectively, where K_0 represents the transmission coefficient in case of the sinusoidal term being zero, that is to say, $K_0=C/A$. In Fig. 1 the relation between the transmission coefficient K_0 and the electrical conductivity is shown taking the intensity of the magnetic field as the parameter, and in Fig. 2 the relation between K_0 and the magnetic field is also shown by taking the conductivity as the parameter.

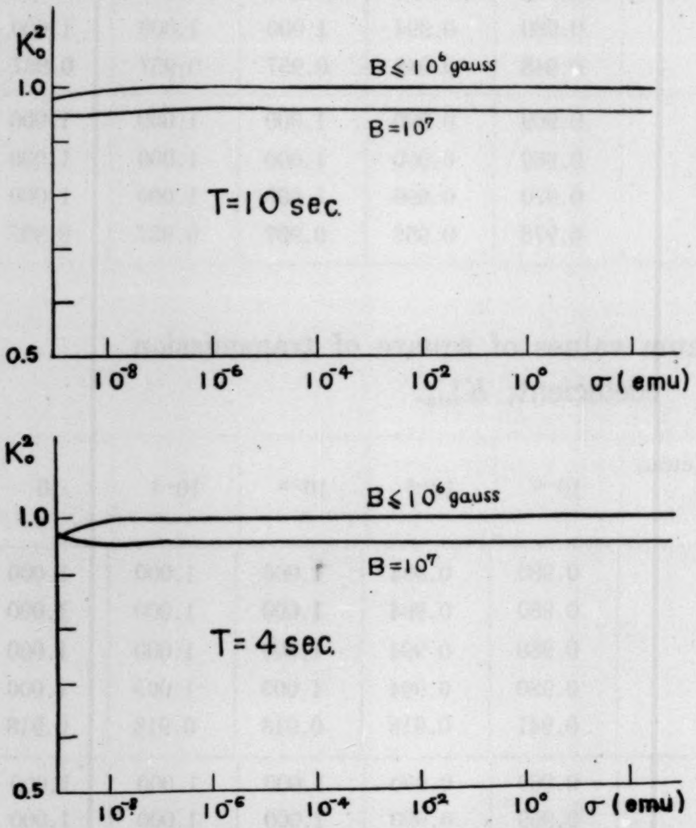

Fig. 1. Relation between the transmission coefficient (K_0) and the electrical conductivity (σ) for $T=10$ sec. and 4 sec.

From these it might well be said that the intensity of the magnetic field should exceed 10^6 gauss in order to have a significant influence upon the seismic waves passing

through the core and that the electrical conductivity would not show any effect as long as it takes a value larger than 10^{-8} emu.

3. Spectral analyses of core waves.

It has been so far believed that predominating periods of seismic core waves cover a range roughly from $T=1$ to 5 sec., though, as far as the writer knows, no detailed analysis has been carried out. In this context, the writer would here like to analyse a seismogram of a distant earthquake as one example of the records of core waves. Since only one seismogram is available, the reliability of the results will not be very great. However, this sort of study would serve to make clear the differences, if any, between the properties of core waves from those of the other waves such as propagated in the mantle. Since no detailed study has been published yet, it would be also of interest to investigate the characteristics of core waves by means of spectral analysis.

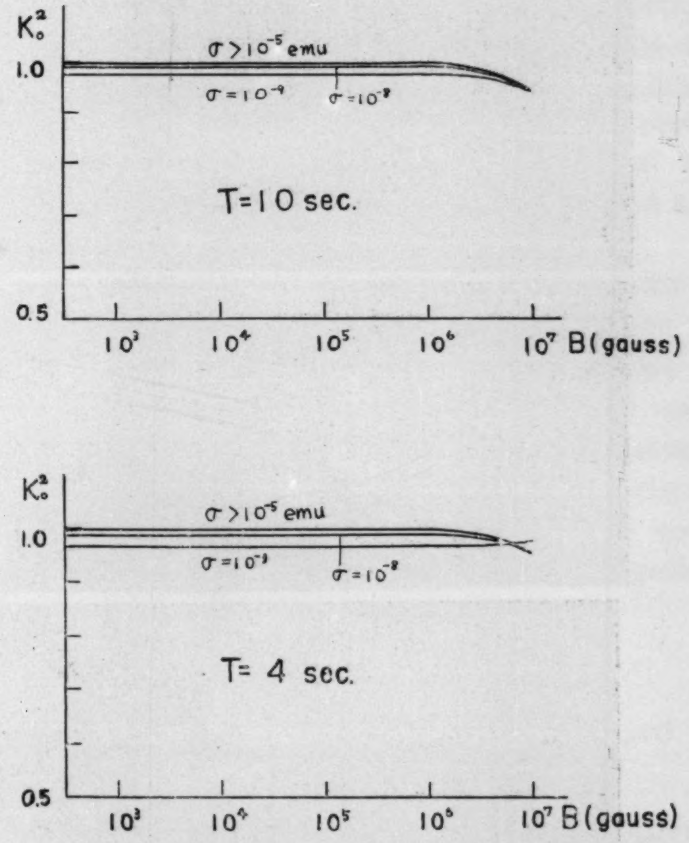

Fig. 2. Relation between the transmission coefficient (K_0) and the magnetic field (B) for $T=10$ sec. and 4 sec.

The earthquake taken up here occurred near South Georgia Island (the epicenter was at 29.5°W, 54°S) at $12^h47^m05^s$ (GMT) on June 27th, 1929 and its magnitude was $M=7.8$. Seismograms used for the analyses are those obtained at Hongô station with Ewing's vertical seismograph ($T=10.8$ sec., $h^2=0.05$) and Oomori's horizontal one ($T=31.1$ sec., $h^2=0.11$) (Fig. 3, Fig. 4). The amplitude spectra of this earthquake was computed in accordance with Kasahara's method[8]. The results are shown

8) K. KASAHARA, *Bull. Earthq. Res. Inst.*, **35** (1957), 473–532.

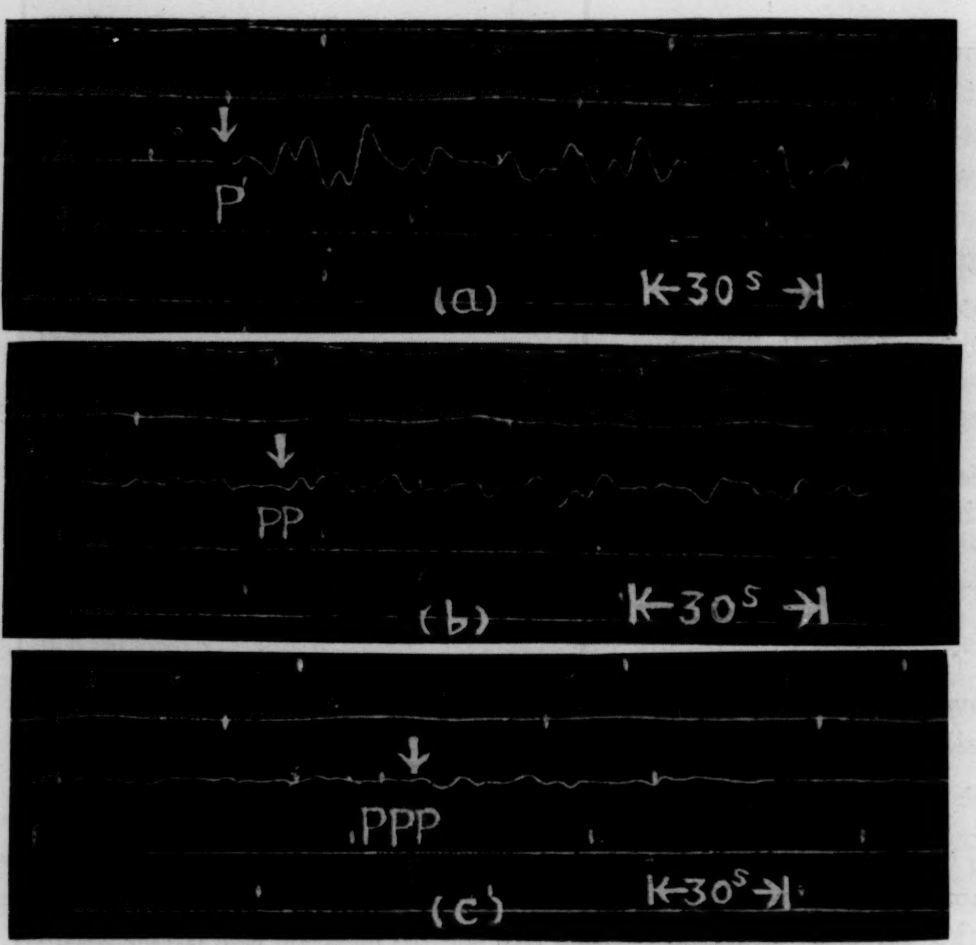

Fig. 3. Seismograms used for analyses of the vertical components: (a) *P'* wave, (b) *PP* wave, (c) *PPP* wave.

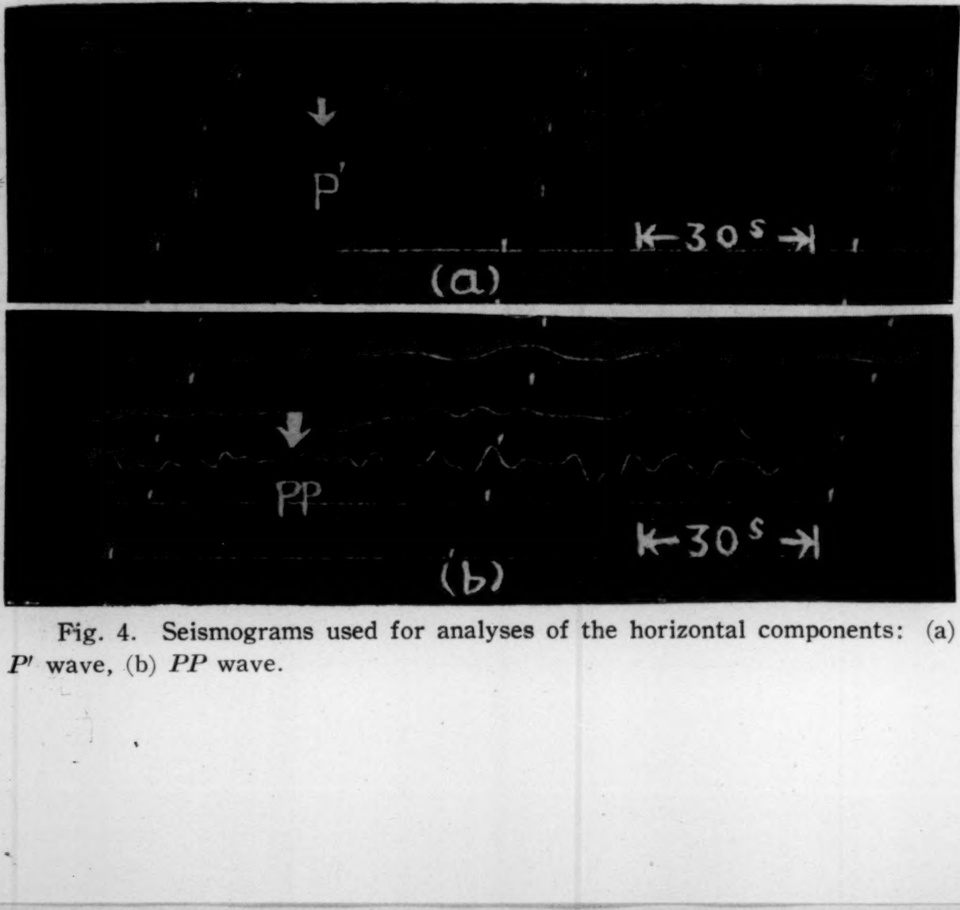

Fig. 4. Seismograms used for analyses of the horizontal components: (a) *P'* wave, (b) *PP* wave.

in Fig. 5 and Fig. 6 in which, as a matter of course, the corrections for alteration of spectra due to the characteristics of seismographs are made. In this case P' wave seems to have the maxima of the amplitude at about $T=2.2$, 4 and 10 sec., while it does not seem that the short period waves are predominating in particular. It may rather be said that the waves around $T=10$ sec. are most predominating for P' as we can also see in the other phases such as *PP*.

In order to study the characteristics of P' wave, it is necessary to depict the idealized spectrum of the longitudinal wave that can be regarded as the one which would travel along the same path as that of P' without being affected by the core and to compare it with the spectrum of P' wave itself. For the purpose, *PP* or *PPP* which are propagated through the mantle of the earth and recorded on the same seismogram would serve to take the place of such a virtual wave. The spectra of *PP* and *PPP* waves are also shown in Fig. 5 and Fig. 6 together with that of P'. As for the up and down component of the seismogram which seems to give more precise information about the longitudinal waves than the horizontal component, the amplitude of *PP* is smaller than that of P' wave on the whole, and moreover the amplitude of *PPP* is smaller than that of *PP*. In addition to these differences that can be seen in the amplitude ratio, the periods of maximum amplitude of *PPP* seem to have shifted from those of *PP*, a similar tendency being also observed between P' and *PP*. From these facts it is apparent that on reflection of seismic waves at the earth's surface, their spectra are likely to be transformed by some unknown mechanism; the amplitude is diminished and the period is some what lengthened. Therefore the spectra of *PP* and *PPP* are not to be used by themselves as the standard of comparison and the spectrum corrected for the effect of reflection is now required.

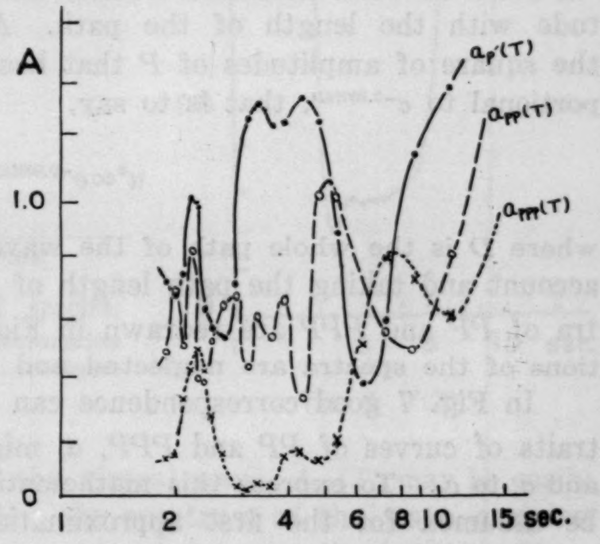

Fig. 5. The amplitude spectra of the vertical component: $a_{p'}(T)$ is the spectrum of P' wave, $a_{pp}(T)$ that of *PP* wave, $a_{ppp}(T)$ that of *PPP* wave: ordinate in arbitrary unit.

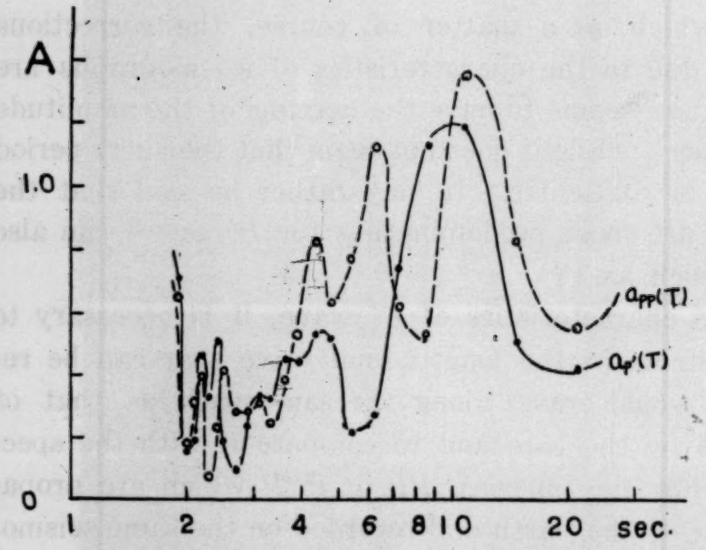

Fig. 6. The amplitude spectra of the horizontal component: $a_{P'}(T)$ is the spectrum of P' wave, $a_{pp}(T)$ is that of *PP* wave: ordinate in arbitrary unit.

It is assumed here that the every reflection has the same influence upon the amplitude spectra of seismic waves. The effect of reflection would be surmised from the appearence of the spectra of *PP* and *PPP*, though by what mechanism it is exerted on the seismic waves are unknown. Before proceeding further, we must pay attention to the attenuation of amplitude with the length of the path. According to Gutenberg's study[9] the square of amplitudes of *P* that has travelled in the mantle is proportional to $e^{-0.00012D}$, that is to say,

$$u^2 \propto e^{-0.00012D} ,$$

where *D* is the whole path of the waves. Taking this absorption into account and taking the path length of P' as a unit of length, the spectra of *PP* and *PPP* are redrawn in Fig. 7, in which the small fluctuations of the spectra are neglected and the curves are smoothed.

In Fig. 7 good correspondence can be seen between the individual traits of curves of *PP* and *PPP*, a_1 might be transferred to a_2, b_1 to b_2 and c_1 to c_2. To express this mathematically, the following relation will be assumed for the first approximation between the spectrum of *PP*, $A_{PP}(T)$ and that of *PPP*, $A_{PPP}(T)$,

$$A_{PPP}(T+kT)=f(T)\cdot A_{PP}(T) , \tag{33}$$

where $f(T)$ is the operator of real function which represents the characteristics of reflection. As the value of k

$$k=0.2$$

9) B. GUTENBERG, *Bull. Seis. Soc. Amer.*, **35** (1945), 57–69.

is obtained from Fig. 7. Fig. 8 shows the function $f(T)$ as calculated numerically. If the same relation as in the expression (33) is also taken for granted between the spectra of *PP* and the virtual wave suffering no effect of reflection, namely,

$$A_{PP}(T+kT)=f(T)\cdot A_{OP}(T) \tag{34}$$

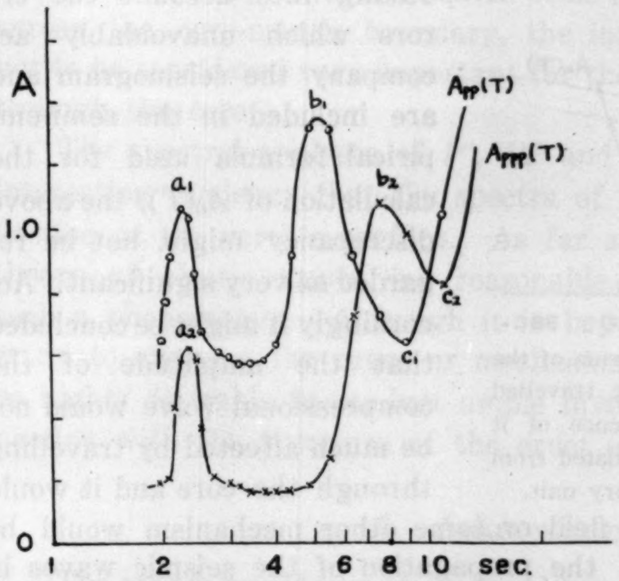

Fig. 7. The corrected curves of spectra, $A_{pp}(T)$ and $A_{ppp}(T)$, for the effect of absorption due to the difference of the path length: ordinate in arbitrary unit.

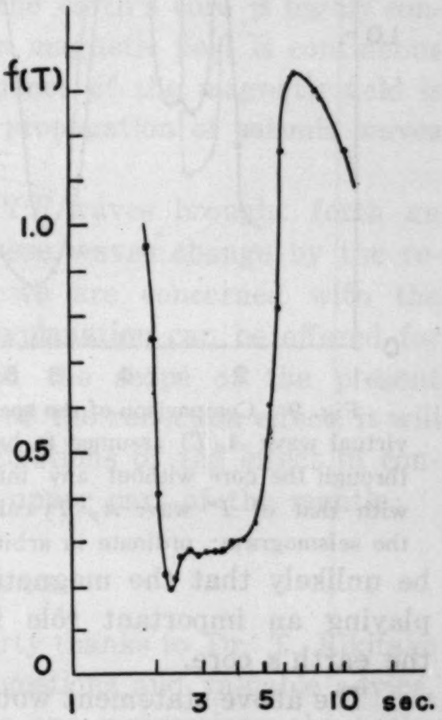

Fig. 8. $f(T)$

where $A_{OP}(T)$ is the spectrum of the virtual wave, $A_{OP}(T)$ may be easily calculated. $A_{OP}(T)$ thus obtained is the spectrum of the wave arriving at the surface with the same angle of incidence with that of *PP*. Since the amplitude of the seismic wave differs also on account of the difference of the angle of incidence and the epicentral distance, the spectrum of the virtual wave $A_0(T)$ is not the same as $A_{OP}(T)$. For this reason amplitude ratio of *P'* to *PP* is calculated to become 0.375 at $\Delta=155°$ by Dana[10]. Taking it into account, $A_0(T)$, the standard spectrum of the longitudinal wave assumed to have passed through the core without any influence of it is obtained in Fig. 9.

10) S. W. DANA, *Bull. Seis. Soc. Amer.*, **35** (1945), 27–35.

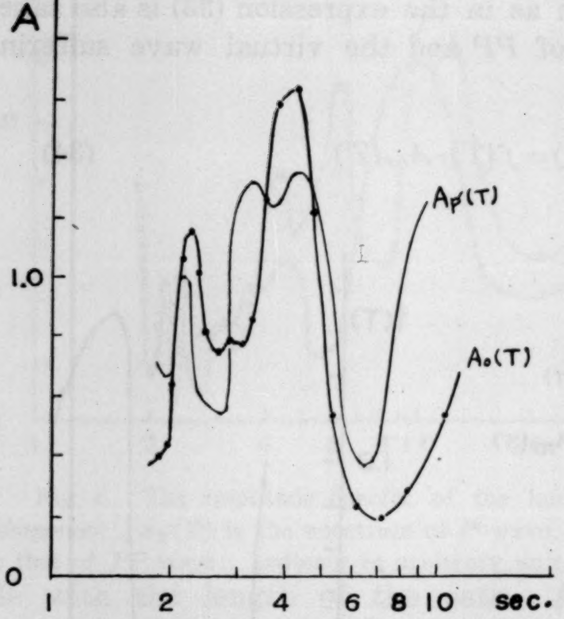

Fig. 9. Comparison of the spectrum of the virtual wave $A_0(T)$ assumed to have travelled through the core without any influence of it with that of P' wave $A_{P'}(T)$ calculated from the seismogram: ordinate in arbitrary unit.

In Fig. 9 it will be noticed that the periods of maximum or minimum amplitude of $A_0(T)$ curve agree with those of $A_{P'}(T)$ curve fairly well, which is the curve of P' wave, though some discrepancy can be seen in the value of the amplitude. Taking into account the errors which unavoidably accompany the seismogram and are included in the semi-empirical formula used for the calculation of $A_0(T)$, the above discrepancy might not be regarded as very significant. Accordingly it might be concluded that the amplitude of the compressional wave would not be much affected by travelling through the core and it would be unlikely that the magnetic field or some other mechanism would be playing an important rôle in the propagation of the seismic waves in the earth's core.

The above statement would be also supported by Gutenberg's study[11]. He has investigated the absorption of the seismic waves in the core using $P'P'$ and P, as well as in the mantle, and obtained almost the same absorbing factor as in the mantle. This means that the core would be exerting no significant influence upon the propagation of seismic waves.

4. Concluding remarks

As stated before, if the core waves were subject to some remarkable modification owing to the propagation through the core, the physical state in the core would be brought to light partly. The results of analysis of core waves, however, have clarified that there seems to be no effect of travelling through the core, if any, there must be little. According to the calculation of interactions between seismic waves and

11) B. GUTENBERG, *loc. cit.*, 9).

magnetic field, as shown in Fig. 1 and Fig. 2 the amplitude ratio of the transmitted wave to the incident one is not affected unless the intensity of the magnetic field exceeds 10^6 gauss, or the electrical conductivity is smaller than 10^{-8} emu. Therefore as a limit of the magnetic field intensity and the electrical conductivity in the core $H<10^7$ gauss and $\sigma>10^{-8}$ emu could be safely adopted. As for the conductivity the above value has agreed with the lower limit obtained by Rikitake.

Also in case of using the model that the earth's core is highly conductive comparing with the mantle while the magnetic field is continuous across the core-mantle boundary, the influence of the magnetic field is not to be considered very important for the propagation of seismic waves through the core.

The spectral analyses of P', PP and PPP waves brought forth an interesting tendency that the spectra of these waves change by the reflection at the earth's surface. As far as we are concerned with the theory of elastic waves, no reasonable explanation can be offered for such a phenomenon. Although it is beyond the scope of the present study to examine the cause or mechanism of the reflection effect, it will be highly desirable to conduct ample investigations of the effect in connection with the structure of the crust or upper part of the mantle.

5. Acknowledgments

The writer would like to express his hearty thanks to Dr. T. Rikitake who has given him numerous helpful suggestions and valuable advice, and to Mr. K. Kasahara for his kind advice and instructions about the spectral analysis of seismic waves. He also wishes to thank Messrs. I. Yokoyama and S. Uyeda for their incessant encouragement and counsels in the course of this study.

33. 地球核を通る地震波に対する磁場の影響

東京大学大学院
地球物理学課程　行　武　毅

最近，地震波と地球磁場との相互作用を利用して地球核内の磁場や電気伝導度を求める試みが二三なされてきた．核内においてトロイダル磁場はポロイダル磁場より遙かに強い磁場を作つていると推定されるので，核と同程度の厚さを持つ電気伝導体中を磁場に垂直に伝播する地震波に対して，磁場の強さと電気伝導度をパラメーターとして透過係数を求めた．その結果，地震波に対する磁場の影響は殆んどないが，磁場の強さが 10^6 gauss を越えるか，電気伝導度が 10^{-8} emu より小さくなれば僅かに振幅の減少が期待される．

従来 P′ 波の振幅は短周期において卓越していると考えられていたが，アルゼンチン沖に起つた一つの地震をスペクトル分析によつて調べた結果，核を通過したために生じたと推定される地震波の特性は認められないことがわかつた．このことより，核内磁場の上限および電気伝導度の下限として，10^7 gauss, 10^{-8} emu，という値が得られる．

なお P′ 波の特性を求める際に併せて得られた PP, PPP 波のスペクトルをみると，何に起因するかは不明であるが，地表面の反射によつて地震波は振幅が著しく減衰し，卓越周期がのばされているという興味ある事実が認められた．

——所　報——

◎談話会記事

第 346 回談話会（昭和 32 年 7 月 16 日）

1. 岩盤上の鉄筋コンクリート造建物に於ける地震観測結果　金井清・鈴木富三郎
2. 桜島火山活動に伴う諸現象の綜合観測（桜島綜合研究代表者）　水上武
3. 桜島火山の活動に伴う火山地震　水上武・茂木清夫・平賀士郎・宮崎務
4. 桜島に於ける火山性微小地震の数例　茂木清夫
5. 桜島に於ける微動測定（地表と井戸底の比較）　田中貞二・平賀士郎
6. 桜島及びその周辺に於ける土地の伸縮観測結果及びその解析　下鶴大輔・後藤賢一
7. 桜島及び鹿児島湾岸の水準測量　岡田惇

第 347 回談話会（昭和 32 年 9 月 24 日）

1. 地球核をとおる地震波に対する磁場の影響　行武毅（力武所員紹介）
2. 大島と川奈との間に起つた群発地震について　横山泉
3. 破壊に関するグリフイスの仮説と大小地震の相似性　安芸敬一
4. 電磁脈動計　岸上冬彦・渡辺義夫

追加　三原火山におけるガス組成の変化と火山活動　南英一・野口喜三雄・神谷宏

第 348 回談話会（昭和 32 年 10 月 22 日）

1. 1894 年の庄内地震の研究　岸上冬彦
2. 弾性地盤上に建つ構造物の剪断振動　佐藤泰夫・山口林造
3. 浅間山火口附近の硼酸鉱物について（予報）　野口喜三雄・島誠
4. 浅間火山の鉄質沈澱物の研究（第 1 報）　小坂丈予

第 349 回談話会（昭和 32 年 11 月 26 日）

1. 自然地震動初動部の解析（第 3 報）辷り破壊による地震動　笠原慶一
2. 大地震に伴う地殻変動の特性（第 3 報）丹後地震の震源モデル　笠原慶一
3. 活動褶曲としての新潟平野の沈降　宮村摂三
4. 建物の振動とその等価回路　嶋悦三

5. 日本に於ける地磁気短周期変化の異常 (第 7 報)　力武常次・横山泉・上田誠也・行武毅・中川英子

6. 東海村砂地で行つた地震探査　表俊一郎・山崎良雄・小牧昭三・小林直吉・真島秀泰

7. 砂丘地域における常時微動　金井清・田中貞二・長田甲斐男

8. 地震動の大きさと周期との関係 (補遺)　金井清

9. 強震の研究 (序報)　金井清

第 350 回談話会 (昭和 32 年 12 月 17 日)

1. 佐久間ダム湛水による土地変形の観測 (続報)　萩原尊礼・笠原慶一・山田重平・斎藤貞夫・岡田惇

2. 岩盤上の鉄筋コンクリート造建物における地震観測結果 (続報)　金井清・鈴木富三郎

3. 砂丘地域における地震動の観測結果 (第 1 報)　金井清・田中貞二・鈴木富三郎

4. 地震時の建物振動における建物地下部分の影響　金井清

Index to Vol. XXXV.

Page

AKI, K., (22) Space and Time Spectra of Stationary Stochastic Waves, with Special Reference to Microtremors. (in English) 415

AOKI, K. and ICHIMURA, T., (5) Some Geological Considerations of the Neogene Sediments Exposed at the Western Margin of the Yamagata Basin. (in English) 47

FUKUDA, T.; MORIMOTO, R. and OSSAKA, J., (18) Geology of Imaichi District with Special Reference to the Earthquake of Dec. 26, 1949 (III). (in English) 359

HUZITA, K.; MORIMOTO, R. and KASAMA, T., (4) Cenozoic Volcanism in the Southwestern Japan with Special Reference to the History of the Setouchi (Inland Sea) Geologic Province. (in English) ... 35

ICHIMURA, T., (28) Geological Investigations on the Zaō Volcanoes. IV Ryū-zan Volcano. (in English) 573

ICHIMURA, T. and AOKI, K., (5) Some Geological Considerations of the Neogene Sediments Exposed at the Western Margin of the Yamagata Basin. (in English) 47

KANAI, K., (16) Semi-empirical Formula for the Seismic Characteristics of the Ground. (in English) 309

KANAI, K., (23) The Requisite Conditions for the Predominant Vibration of Ground. (in English) 457

KANAI, K.; TANAKA, T. and OSADA, K., (8) Measurement of the Micro-tremor. II. (Tokyo Metropolis.) (in Japanese) 109

KANAI, K.; TANAKA, T. and OSADA, K., (9) Measurement of the Micro-tremor. III. (Yokohama City.) (in Japanese) 135

KANAI, K.; NASU, N.; TANAKA, T. and OSADA, K., (10) Measurement of the Micro-tremor. IV. (Sakata and Tsuruoka.) (in Japanese). 149

KANAI, K.; KAWASUMI, H.; TANAKA, T. and OSADA, K., (11) Measurement of the Micro-tremor. V. (Osaka City.) (in Japanese) 163

KANAI, K.; TANAKA, T.; MORISHITA, T. and NAKAGAWA, K., (12) Measurement of the Micro-tremor. VI. (Ichinomiya City, Aichi Prefecture.) (in Japanese) 181

KANAI, K.; TANAKA, T. and OSADA, K., (13) Measurement of the Micro-tremor. VII. (Kawasaki City.) (in Japanese) 191

KASAHARA, K., (24) The Nature of Seismic Origins as Inferred from Seismological and Geodetic Observations (1). (in English) 473

KASAMA, T.; MORIMOTO, R. and HUZITA, K., (4) Cenozoic Volcanism in the Southwestern Japan with Special Reference to the History

of the Setouchi (Inland Sea) Geologic Province. (in English) ... 35
KAWASUMI, H.; KANAI, K.; TANAKA, T. and OSADA, K., (11) Measurement of the Micro-tremor. V. (Osaka City.) (in Japanese) 163
KISHINOUYE, F., (19) Phase Lag of Vibrations of Buildings Excited by a Vibrator. (in English) 377
KISHINOUYE, F., (25) Studies of Microseisms by Observations. (in English) 533
KOBAYASHI, N.; OMOTE, S. and KOMAKI, S., (30) Earthquake Observations in Kawasaki and Turumi Areas and the Seismic Qualities of the Ground. (Part II). (in English) 613
KOMAKI, S.; OMOTE, S. and KOBAYASHI, N., (30) Earthquake Observations in Kawasaki and Turumi Areas and the Seismic Qualities of the Ground. (Part II). (in English) 613
MINAMI, E. and OSSAKA, J., (31) On the Specular Iron from Mt. Maekake, Volcano Asama. (in Japanese) 621
MINAMI, E.; OSSAKA, J.; MURAI, I. and TSUYA, H., (21) Studies on the Spring and Underground Waters in Volcano Asama and its Vicinity (1)—Chemical Compositions of the Spring and Underground Waters in the Zyabori River Valley and its Neighbourhood—(in Japanese) 395
MIYAMURA, S. and TSUJIURA, M., (20) UHF Multi-channel Radio Telerecording Seismograph. Part I. (in Japanese) 381
MORIMOTO, R.; HUZITA, K. and KASAMA, T., (4) Cenozoic Volcanism in the Southwestern Japan with Special Reference to the History of the Setouchi (Inland Sea) Geologic Province. (in English) ... 35
MORIMOTO, R.; OSSAKA, J. and FUKUDA, T., (18) Geology of Imaichi District with Special Reference to the Earthquake of Dec. 26, 1949 (III). (in English) 359
MORISHITA, T.; KANAI, K.; TANAKA, T. and NAKAGAWA, K., (12) Measurement of the Micro-tremor. VI. (Ichinomiya City, Aichi Prefecture.) (in Japanese) 181
MURAI, I.; OSSAKA, J.; Minami, E. and TSUYA, H., (21) Studies on the Spring and Underground Waters in Volcano Asama and its Vicinity (1)—Chemical Compositions of the Spring and Underground Waters in the Zyabori River Valley and its Neighbourhood—(in Japanese) 395
NAKAGAWA, K.; KANAI, K.; TANAKA, T. and MORISHITA, T., (12) Measurement of the Micro-tremor. VI. (Ichinomiya City, Aichi Prefecture.) (in Japanese) 181

NASU, N.; KANAI, K.; TANAKA, T. and OSADA, K., (10) Measurement of the Micro-tremor. IV. (Sakata and Tsuruoka.) (in Japanese) 149

OMOTE, S. and YAMAZAKI, Y., (29) Seven-Channel Triggered Magnetic Tape Recorder for Routine Seismic Observations. (in English) .. 595

OMOTE, S.; KOMAKI, S. and KOBAYASHI, N., (30) Earthquake Observations in Kawasaki and Turumi Areas and the Seismic Qualities of the Ground. (Part II). (in English) 613

OOBA, S., (14) Study of the Relation between the Subsoil Conditions and the Distribution of the Damage Percentage of Wooden Dwelling Houses in the Province of Tōtōmi in the case of the Tōnankai Earthquake of December 7th, 1944. (in Japanese) 201

OSADA, K.; KANAI, K. and TANAKA, T., (8) Measurement of the Micro-tremor. II. (Tokyo Metropolis.) (in Japanese) 109

OSADA, K.; KANAI, K. and TANAKA, T., (9) Measurement of the Micro-tremore. III. (Yokohama City.) (in Japanese) 135

OSADA, K.; KANAI, K.; NASU, N. and TANAKA, T., (10) Measurement of the Micro-tremor. IV. (Sakata and Tsuruoka.) (in Japanese). 149

OSADA, K.; KANAI, K.; KAWASUMI, H. and TANAKA, T., (11) Measurement of the Micro-tremor. V. (Osaka City.) (in Japanese) 163

OSADA, K.; KANAI, K. and TANAKA, T., (13) Measurement of the Micro-tremor. VII. (Kawasaki City.) (in Japanese) 191

OSSAKA, J.; MORIMOTO, R. and FUKUDA, T., (18) Geology of Imaichi District with Special Reference to the Earthquake of Dec. 26, 1949 (III). (in English) 359

OSSAKA, J.; MURAI, I.; MINAMI, E. and TSUYA, H., (21) Studies on the Spring and Underground Waters in Volcano Asama and its Vicinity (1)—Chemical Compositions of the Spring and Underground Waters in the Zyabori River Valley and its Neighbourhood—(in Japanese) 395

OSSAKA, J. and MINAMI, E., (31) On the Specular Iron from Mt. Maekake, Volcano Asama. (in Japanese) 621

RIKITAKE, T. and SATO, S., (2) The Geomagnetic D_{st} Field of the Magnetic Storm on June 18–19, 1936. (in English) 7

SATO, S. and RIKITAKE, T., (2) The Geomagnetic D_{st} Field of the Magnetic Storm on June 18–19, 1936. (in English) 7

SATÔ, Y., (1) Study on Surface Waves XIII. Nomograph for the Phase Velocity of Love-Waves in Doubly Stratified Medium. (in English) 1

SATÔ, Y. and YAMAGUCHI, R., (26) Vibration of a Building upon the Elastic Foundation. (in English) 545
TAJIMA, H. and YOKOYAMA, I., (3) A Gravity Survey on Volcano Mihara, Ooshima Island by Means of a Worden Gravimeter. (in English) 23
TAKAHASHI, T., (15) The Dispersion of Rayleigh Waves in Heterogeneous Media. (in English) 297
TANAKA, T.; KANAI, K. and OSADA, K., (8) Measurement of the Micro-tremor. II. (Tokyo Metropolis.) (in Japanese) 109
TANAKA, T.; KANAI, K. and OSADA, K., (9) Measurement of the Micro-tremor. III. (Yokohama City.) (in Japanese) 135
TANAKA, T.; KANAI, K.; NASU, N. and OSADA, K., (10) Measurement of the Micro-tremor. IV. (Sakata and Tsuruoka.) (in Japanese) 149
TANAKA, T.; KANAI, K.; KAWASUMI, H. and OSADA, K., (11) Measurement of the Micro-tremor. V. (Osaka City.) (in Japanese) 163
TANAKA, T.; KANAI, K.; MORISHITA, T. and NAKAGAWA, K., (12) Measurement of the Micro-tremor. VI. (Ichinomiya City, Aichi Prefecture.) (in Japanese) 181
TANAKA, T.; KANAI, K. and OSADA, K., (13) Measurement of the Micro-tremor. VII. (Kawasaki City.) (in Japanese) 191
TSUJIURA, M. and MIYAMURA, S., (20) UHF Multi-channel Radio Tele-recording Seismograph. Part I. (in Japanese) 381
TSUYA, H.; OSSAKA, J.; MURAI, I. and MINAMI, E., (21) Studies on the Spring and Underground Waters in Volcano Asama and its Vicinity (1)—Chemical Compositions of the Spring and Underground Waters in the Zyabori River Valley and its Neighbourhood—(in Japanese) 395
YAMAGUCHI, R. and SATO, Y., (26) Vibration of a Building upon the Elastic Foundation. (in English) 545
YAMAZAKI, Y. and OMOTE, S., (29) Seven-Channel Triggered Magnetic Tape Recorder for Routine Seismic Observations. (in English) . . 595
YOKOYAMA, I., (6) Energetics in Active Volcanoes. 2nd Paper. (in English) 75
YOKOYAMA, I., (7) Energetics in Active Volcanoes. 3rd Paper. (in English) 99
YOKOYAMA, I., (17) Geomagnetic Anomaly on Volcanoes with Relation to Their Subterranean Structure. (in English) 327
YOKOYAMA, I., (27) Geomagnetic Studies of Volcano Mihara. The 8th

Paper. (Continuous Observation of Changes in Geomagnetic Declination during the Period 1955–56). (in English) 567
YOKOYAMA, I. and TAJIMA, H., (3) A Gravity Survey on Volcano Mihara, Ooshima Island by Means of a Worden Gravimeter. (in English) 23
YOSHIYAMA, R., (32) The Ratio of the Velocity of P and S Waves. (in English) 627
YUKUTAKE, T., (33) The Influence of the Magnetic Field on Spectra of Seismic Core Waves. (in English) 641

ix

Paper. (Continuous Observation of Changes in Geomagnetic Declination during the Period 1959–61). (in English) 595

YOKOYAMA, I. and TAJIMA, H., (37) A Gravity Survey on Volcano Mihara, Ooshima Island by Means of a Worden Gravimeter. (in English) 24

YOSHIYAMA, R., (32) The Ratio of the Velocity of P and S Waves. (in English) 637

YUKUTAKE, T., (33) The Influence of the Magnetic Field on Spectra of Seismic Core Waves. (in English) 640

索 引 第35号

頁

安芸敬一 (22) 複雑な波動のスペクトル的研究 (英文) 415

青木和子・市村 毅 (5) 山形盆地西縁の新第三紀堆積岩に関する地質学的考察 (英文) 47

福田知子・森本良平・小坂丈予 (18) 今市地震地域の地質 (3) (英文) 359

藤田和夫・森本良平・笠間太郎 (4) 瀬戸内地質区を中心とした西南日本の新生代火山活動 (英文) 35

市村 毅 (28) 蔵王火山の地質学的研究 (第4報) (英文) 573

市村 毅・青木和子 (5) 山形盆地西縁の新第三紀堆積岩に関する地質学的考察 (英文) 47

金井 清 (16) 地盤の震動特性に関する半実験式 (英文) 309

金井 清 (23) 卓越震動が現われるための地盤の条件 (英文) 457

金井 清・田中貞二・長田甲斐男 (8) 常時微動の測定結果 第2報 (東京都内III) (邦文) 109

金井 清・田中貞二・長田甲斐男 (9) 常時微動の測定結果 第3報 (横浜市内) (邦文) 135

金井 清・那須信治・田中貞二・長田甲斐男 (10) 常時微動の測定結果 第4報 (庄内地方) (邦文) 149

金井 清・河角 広・田中貞二・長田甲斐男 (11) 常時微動の測定結果 第5報 (大阪市内) (邦文) 163

金井 清・田中貞二・森下利三・中川恭次 (12) 常時微動の測定結果 第6報 (一宮市内) (邦文) 181

金井 清・田中貞二・長田甲斐男 (13) 常時微動の測定結果 第7報 (川崎市内) (邦文) 191

笠原慶一 (24) 震源の性状に関する地震学的及び測地学的研究 (一) (英文) 473

笠間太郎・森本良平・藤田和夫 (4) 瀬戸内地質区を中心とした西南日本の新生代火山活動 (英文) 35

河角 広・金井 清・田中貞二・長田甲斐男 (11) 常時微動の測定結果 第5報 (大阪市内) (邦文) 163

岸上冬彦 (19) 起振機による建物の振動の位相差測定 (英文) 377

岸上冬彦 (25) 観測による土地の脈動の研究 (英文) 533

小林直吉・表 俊一郎・小牧昭三 (30) 川崎鶴見地域9ヶ所で行つた地震観測とその場所の地盤特性 (その2) (英文) 613

小牧昭三・表 俊一郎・小林直吉 (30) 川崎鶴見地域9ヶ所で行つた地震観測と

その場所の地盤特性（その 2）（英文）………………………………… 613
南　英一・小坂丈予　(31)　浅間火山前掛山の鏡鉄鉱について（邦文）………… 621
南　英一・小坂丈予・村井　勇・津屋弘逵　(21)　浅間火山及びその周辺地域の湧水並びに地下水の研究（第1報）——蛇堀川溪谷及びその附近の湧水並びに地下水の化学成分——（邦文）…………………………………… 395
宮村摂三・辻浦　賢　(20)　超短波多重遠隔記録地震計（第1報）（邦文）……… 381
森本良平・藤田和夫・笠間太郎　(4)　瀬戸内地質区を中心とした西南日本の新生代火山活動（英文）………………………………………… 35
森本良平・小坂丈予・福田知子　(18)　今市地震地域の地質 (3)（英文）……… 359
森下利三・金井　清・田中貞二・中川恭次　(12)　常時微動の測定結果 第6報（一宮市内）（邦文）…………………………………………… 181
村井　勇・小坂丈予・南　英一・津屋弘逵　(21)　浅間火山及びその周辺地域の湧水並びに地下水の研究（第1報）——蛇堀川溪谷及びその附近の湧水並びに地下水の化学成分——（邦文）…………………………………… 395
中川恭次・金井　清・田中貞二・森下利三　(12)　常時微動の測定結果 第6報（一宮市内）（邦文）…………………………………………… 181
那須信治・金井　清・田中貞二・長田甲斐男　(10)　常時微動の測定結果 第4報（庄内地方）（邦文）…………………………………………… 149
表　俊一郎・山崎良雄　(29)　磁気テープ利用遅延記録方式による7素子地震動常時観測装置（英文）…………………………………………… 595
表　俊一郎・小牧昭三・小林直吉　(30)　川崎鶴見地域9ヶ所で行つた地震観測とその場所の地盤特性（その 2）（英文）………………………………… 613
大庭正八　(14)　1944年12月7日東南海地震に見られた遠江地方の家屋被害分布と地盤との関係（邦文）………………………………………… 201
長田甲斐男・金井　清・田中貞二　(8)　常時微動の測定結果 第2報（東京都内III）（邦文）…………………………………………………… 109
長田甲斐男・金井　清・田中貞二　(9)　常時微動の測定結果 第3報（横浜市内）（邦文）………………………………………………………… 135
長田甲斐男・金井　清・那須信治・田中貞二　(10)　常時微動の測定結果 第4報（庄内地方）（邦文）…………………………………………… 149
長田甲斐男・金井　清・河角　広・田中貞二　(11)　常時微動の測定結果 第5報（大阪市内）（邦文）…………………………………………… 163
長田甲斐男・金井　清・田中貞二　(13)　常時微動の測定結果 第7報（川崎市内）（邦文）………………………………………………………… 191
小坂丈予・森本良平・福田知子　(18)　今市地震地域の地質 (3)（英文）……… 359
小坂丈予・村井　勇・南　英一・津屋弘逵　(21)　浅間火山及びその周辺地域の湧

水並びに地下水の研究（第1報）——蛇堀川渓谷及びその附近の湧水並びに地下水の化学成分——（邦文）........ 395
小坂丈予・南　英一　(31)　浅間火山前掛山の鏡鉄鉱について（邦文）........ 621
力武常次・佐藤節子　(2)　1936年6月18日～19日の磁気嵐の D_{st} 場（英文）.... 7
佐藤節子・力武常次　(2)　1936年6月18日～19日の磁気嵐の D_{st} 場（英文）.... 7
佐藤泰夫　(1)　表面波の研究 XIII. 二つの表面層をもつ媒質内を伝わるラブ波の位相速度を求める計算図表（英文）........ 1
佐藤泰夫・山口林造　(26)　弾性地盤上に建つ建築物の振動（英文）........ 545
田島広一・横山　泉　(3)　ウォルドン重力計による伊豆大島の重力測量（英文）.. 23
高橋健人　(15)　不均質媒質内の Rayleigh 波の分散（英文）........ 297
田中貞二・金井　清・長田甲斐男　(8)　常時微動の測定結果 第2報（東京都内 III)（邦文）........ 109
田中貞二・金井　清・長田甲斐男　(9)　常時微動の測定結果 第3報（横浜市内）（邦文）........ 135
田中貞二・金井　清・那須信治・長田甲斐男　(10)　常時微動の測定結果 第4報（庄内地方）（邦文）........ 149
田中貞二・金井　清・河角　広・長田甲斐男　(11)　常時微動の測定結果 第5報（大阪市内）（邦文）........ 163
田中貞二・金井　清・森下利三・中川恭次　(12)　常時微動の測定結果 第6報（一宮市内）（邦文）........ 181
田中貞二・金井　清・長田甲斐男　(13)　常時微動の測定結果 第7報（川崎市内）（邦文）........ 191
辻浦　賢・宮村摂三　(20)　超短波多重遠隔記録地震計（第1報）（邦文）........ 381
津屋弘逵・小坂丈予・村井　勇・南　英一　(21)　浅間火山及びその周辺地域の湧水並びに地下水の研究（第1報）——蛇堀川渓谷及びその附近の湧水並びに地下水の化学成分——（邦文）........ 395
山口林造・佐藤泰夫　(26)　弾性地盤上に建つ建築物の振動（英文）........ 545
山崎良雄・表　俊一郎　(29)　磁気テープ利用遅延記録方式による7素子地震動常時観測装置（英文）........ 595
横山　泉　(6)　火山活動エネルギー（第2報）I. 大島三原山の 1950～52 年間の活動について II. 日本及びインドネシヤの諸火山の活動例について（英文）........ 75
横山　泉　(7)　火山活動のエネルギー（第3報）（英文）........ 99
横山　泉　(17)　火山地域における地磁気異常と地下構造（英文）........ 327
横山　泉　(27)　三原山の地球磁気学的研究 第8報 (1955～56 年間の偏角変化の連続観測)（英文）........ 567

横山　泉・田島広一　(3)　ウォルドン重力計による伊豆大島の重力測量（英文）……………………………………………………… 23
吉山良一　(32)　P 波 S 波の速度比に就いて（英文）…………………………… 627
行武　毅　(33)　地球核を通る地震波に対する磁場の影響（英文）……………… 641

BULLETIN

OF THE

EARTHQUAKE RESEARCH INSTITUTE

UNIVERSITY OF TOKYO

VOL. XXXV

1957

東京大学

地震研究所彙報

第 35 號

昭和 32 年

CONTENTS.

Vol. XXXV.

Part 1. March, 1957.

Papers and Reports.

Page

1. Y. SATÔ, Study on Surface Waves XIII. Nomograph for the Phase Velocity of Love-Waves in Doubly Stratified Medium. (in English) 1
2. T. RIKITAKE and S. SATO, The Geomagnetic D_{st} Field of the Magnetic Storm on June 18–19, 1936. (in English) 7
3. I. YOKOYAMA and H. TAJIMA, A Gravity Survey on Volcano Mihara, Ooshima Island by Means of a Worden Gravimeter. (in English) 23
4. R. MORIMOTO, K. HUZITA and T. KASAMA, Cenozoic Volcanism in the Southwestern Japan with Special Reference to the History of the Setouchi (Inland Sea) Geologic Province. (in English) 35
5. T. ICHIMURA and K. AOKI, Some Geological Considerations of the Neogene Sediments Exposed at the Western Margin of the Yamagata Basin. (in English) 47
6. I. YOKOYAMA, Energetics in Active Volcanoes. 2nd Paper. (in English) 75
7. I. YOKOYAMA, Energetics in Active Volcanoes. 3rd Paper. (in English) 99
8. K. KANAI, T. TANAKA and K. OSADA, Measurement of the Micro-tremor. II. (Tokyo Metropolis.) (in Japanese) 109
9. K. KANAI, T. TANAKA and K. OSADA, Measurement of the Micro-tremor. III. (Yokohama City.) (in Japanese) 135
10. K. KANAI, N. NASU, T. TANAKA and K. OSADA, Measurement of the Micro-tremor. IV. (Sakata and Tsuruoka.) (in Japanese) 149
11. K. KANAI, H. KAWASUMI, T. TANAKA and K. OSADA, Measurement of the Micro-tremor. V. (Osaka City.) (in Japanese). 163
12. K. KANAI, T. TANAKA, T. MORISHITA and K. NAKAGAWA,

Measurement of the Micro-tremor. VI. (Ichinomiya City, Aichi Prefecture.) (in Japanese) 181
13. K. KANAI, T. TANAKA and K. OSADA, Measurement of the Micro-tremor. VII. (Kawasaki City.) (in Japanese) 191
14. S. OOBA, Study of the Relation between the Subsoil Conditions and the Distribution of the Damage Percentage of Wooden Dwelling Houses in the Province of Tōtōmi in the case of the Tōnankai Earthquake of December 7th, 1944. (in Japanese) 201

Part 2. June, 1957.

15. T. TAKAHASHI, The Dispersion of Rayleigh Waves in Heterogeneous Media. (in English) 297
16. K. KANAI, Semi-empirical Formula for the Seismic Characteristics of the Ground. (in English) 309
17. I. YOKOYAMA, Geomagnetic Anomaly on Volcanoes with Relation to Their Subterranean Structure. (in English) 327
18. R. MORIMOTO, J. OSSAKA and T. FUKUDA, Geology of Imaichi District with Special Reference to the Earthquake of Dec. 26, 1949 (III). (in English) 359
19. F. KISHINOUYE, Phase Lag of Vibrations of Buildings Excited by a Vibrator. (in English) 377
20. S. MIYAMURA and M. TSUJIURA, UHF Multi-channel Radio Tele-recording Seismograph. Part I. (in Japanese) 381
21. J. OSSAKA, I. MURAI, E. MINAMI and H. TSUYA, Studies on the Spring and Underground Waters in Volcano Asama and its Vicinity (1) —Chemical Compositions of the Spring and Underground Waters in the Zyabori River Valley and its Neighbourhood— (in Japanese) 395

Part 3. September, 1957.

22. K. AKI, Space and Time Spectra of Stationary Stochastic Waves, with Special Reference to Microtremors. (in English). 415
23. K. KANAI, The Requisite Conditions for the Predominant Vibration of Ground. (in English) 457
24. K. KASAHARA, The Nature of Seismic Origins as Inferred from Seismological and Geodetic Observations (1). (in English) ... 473

25. F. KISHINOUYE, Studies of Microseisms by Observations. (in English) 533
26. Y. SATÔ and R. YAMAGUCHI, Vibration of a Building upon the Elastic Foundation. (in English) 545
27. I. YOKOYAMA, Geomagnetic Studies of Volcano Mihara. The 8th Paper. (Continuous Observation of Changes in Geomagnetic Declination during the Period 1955~56). (in English) . 567
28. T. ICHIMURA, Geological Investigations on the Zaō Volcanoes. IV Ryū-zan Volcano. (in English) 573
29. S. OMOTE and Y. YAMAZAKI, Seven-Channel Triggered Magnetic Tape Recorder for Routine Seismic Observations. (in English). 595
30. S. OMOTE, S. KOMAKI and N. KOBAYASHI, Earthquake Observations in Kawasaki and Turumi Areas and the Seismic Qualities of the Ground. (Part II). (in English) 613
31. E. MINAMI and J. OSSAKA, On the Specular Iron from Mt. Maekake, Volcano Asama. (in Japanese) 621

Part 4. December, 1957.

32. R. YOSHIYAMA, The Ratio of the Velocity of P and S Waves. (in English) 627
33. T. YUKUTAKE, The Influence of the Magnetic Field on Spectra of Seismic Core Waves. (in English) 641

目　次

第 35 號

第 1 冊　昭和 32 年 3 月

論文及報告

			頁
1.	表面波の研究 XIII. 二つの表面層をもつ媒質内を伝わるラブ波の位相速度を求める計算図表 (英文)	佐藤泰夫	1
2.	1936 年 6 月 18 日～19 日の磁気嵐の D_{st} 場 (英文)	力武常次 佐藤節子	7
3.	ウォルドン重力計による伊豆大島の重力測量 (英文)	横山泉 田島広一	23
4.	瀬戸内地質区を中心とした西南日本の新生代火山活動 (英文)	森本良平 藤田和夫 笠間太郎	35
5.	山形盆地西縁の新第三紀堆積岩に関する地質学的考察 (英文)	市村毅 青木和子	47
6.	火山活動のエネルギー (第 2 報) I. 大島三原山の 1950～52 年間の活動について II. 日本及びインドネシヤの諸火山の活動例について (英文)	横山泉	75
7.	火山活動のエネルギー (第 3 報) (英文)	横山泉	99
8.	常時微動の測定結果 第 2 報 (東京都内 III) (邦文)	金井清 田中貞二 長田甲斐男	109
9.	常時微動の測定結果 第 3 報 (横浜市内) (邦文)	金井清 田中貞二 長田甲斐男	135
10.	常時微動の測定結果 第 4 報 (庄内地方) (邦文)	金井清 那須信治 田中貞二 長田甲斐男	149
11.	常時微動の測定結果 第 5 報 (大阪市内) (邦文)	金井清 河角広 田中貞二 長田甲斐男	163
12.	常時微動の測定結果 第 6 報 (一宮市内) (邦文)	金井清 田中貞二 森下利三 中川恭次	181
13.	常時微動の測定結果 第 7 報 (川崎市内) (邦文)	金井清 田中貞二 長田甲斐男	191
14.	1944 年 12 月 7 日東南海地震に見られた遠江地方の家屋被害分布と地盤との関係 (邦文)	大庭正八	201

第 2 冊　昭和 32 年 6 月

			頁
15.	不均質媒質内の Rayleigh 波の分散 (英文)	高橋健人	297
16.	地盤の震動特性に関する半実験式 (英文)	金井清	309
17.	火山地域における地磁気異常と地下構造 (英文)	横山泉	327
18.	今市地震地域の地質 (3) (英文)	森本良平 小坂丈予 福田知子	359
19.	起振機による建物の振動の位相差測定 (英文)	岸上冬彦	377
20.	超短波多重遠隔記録地震計 (第 1 報) (邦文)	宮村摂三 辻浦賢	381
21.	浅間火山及びその周辺地域の湧水並びに地下水の研究 (第 1 報)—蛇堀川渓谷及びその附近の湧水並びに地下水化学成分 (邦文)	小坂丈予 村井勇 南英一 津屋弘逵	395

第 3 冊　昭和 32 年 9 月

22.	複雑な波動のスペクトル的研究 (英文)	安芸敬一	415
23.	卓越震動が現われるための地盤の条件 (英文)	金井清	457
24.	震源の性状に関する地震学的及び測地学的研究 (一) (英文)	笠原慶一	473
25.	観測による土地の脈動の研究 (英文)	岸上冬彦	533
26.	弾性地盤上に建つ建築物の振動 (英文)	佐藤泰夫 山口林造	545
27.	三原山の地球磁気学的研究 第 8 報 (1955～56 年間の偏角変化の連続観測) (英文)	横山泉	567
28.	蔵王火山の地質学的研究 (第 4 報) (英文)	市村毅	573
29.	磁気テープ利用遅延記録方式による 7 素子地震動常時観測装置 (英文)	表俊一郎 山崎良雄	595
30.	川崎鶴見地域 9 ヶ所で行つた地震観測とその場所の地盤特性 (その 2) (英文)	表俊一郎 小牧昭三 小林直吉	613
31.	浅間火山前掛山の鏡鉄鉱について (邦文)	南英一 小坂丈予	621

第 4 冊　昭和 32 年 12 月

32.	P 波 S 波の速度比に就いて (英文)	吉山良一	627
33.	地球核を通る地震波に対する磁場の影響 (英文)	行武毅	641

昭和33年3月15日印刷
昭和33年3月20日發行

東京都文京區本富士町一番地
東京大學構内
編纂兼
發行者　東京大學地震研究所

東京都千代田區富士見町一丁目十番地
印刷者　笠井康頼

東京都千代田區富士見町一丁目十番地
印刷所　株式會社　國際文献印刷社

賣捌所
東京都中央區日本橋通二丁目六番地
丸善株式會社

Sold by
Maruzen Co., Ltd.,
Nihonbashi-dôri, Chûô-ku, Tôkyô.
Price of this copy: 145 Yen. (Postage exclusive.)

BULLETIN OF

THE EARTHQUAKE RESEARCH INSTITUTE

UNIVERSITY OF TOKYO

Vol. XXXV, Part 4. December, 1957.

Contents.

Papers and Reports.

Page

32. R. YOSHIYAMA, The Ratio of the Velocity of P and S Waves. (in English).. 627

33. T. YUKUTAKE, The Influence of the Magnetic Field on Spectra of Seismic Core Waves. (in English) 641

Institute Notes.

Index.

(For the papers written in Japanese or in occidental languages, the abstracts are given in occidental languages or in Japanese respectively.)